

Vol. 23, No. 2, June, 2024

ISSN (Print): 0972-6268; ISSN (Online) : 2395-3454

NATURE ENVIRONMENT & POLLUTION TECHNOLOGY

*A Multidisciplinary, International Journal
on Diverse Aspects of Environment*



Technoscience Publications

website: www.neptjournal.com



Technoscience Publications

A-504, Bliss Avenue, Balewadi,
Opp. SKP Campus, Pune-411 045
Maharashtra, India

www.neptjournal.com

Nature Environment and Pollution Technology (An International Quarterly Scientific Research Journal)

EDITORS

Dr. P. K. Goel (Chief Editor)

Former Head, Deptt. of Pollution Studies
Y. C. College of Science, Vidyannagar
Karad-415 124, Maharashtra, India

Dr. K. P. Sharma (Honorary Editor)

Former Professor, Deptt. of Botany
University of Rajasthan
Jaipur-302 004, India

Executive Editor : Mrs. Apurva Goel, C-102, Building No. 12, Swarna CGHS,
Beverly Park, Kanakia, Mira Road (E) (Thane) Mumbai-401107,
Maharashtra, India

Published by : Mrs. T. P. Goel, Technoscience Publications, A-504, Bliss Avenue,
Balewadi, Pune-411 045, Maharashtra, India

E-mail : contact@neptjournal.com; operations@neptjournal.com

INSTRUCTIONS TO AUTHORS

Scope of the Journal

The Journal publishes original research/review papers covering almost all aspects of environment like monitoring, control and management of air, water, soil and noise pollution; solid waste management; industrial hygiene and occupational health hazards; biomedical aspects of pollution; conservation and management of resources; environmental laws and legal aspects of pollution; toxicology; radiation and recycling etc. Reports of important events, environmental news, environmental highlights and book reviews are also published in the journal.

Format of Manuscript

- The manuscript (mss) should be typed in double space leaving wide margins on both the sides.
- First page of mss should contain only the title of the paper, name(s) of author(s) and name and address of Organization(s) where the work has been carried out along with the affiliation of the authors.

Continued on back inner cover...

Nature Environment and Pollution Technology

Vol. 23, No. (2), June 2024

CONTENTS

1. **V. F. Salahalden, M. A. Shareef and Q. A. M. Al Nuaimy**, Assessment of Deposited Red Clay Soil in Kirkuk City Using Remote Sensing Data and GIS Techniques 591-604
2. **Md. Mesbah Uddin Bhuiyan, Md. Anwar Hossain Bhuiyan, Md. Saiful Islam and Umma Sabira**, Petrography and Diagenesis of Thin-Bed Reservoirs from the Eastern Folded Belt of Bangladesh 605-618
3. **Chatla Subbarayudu and Mohan Kubendiran**, A Comprehensive Survey on Machine Learning and Deep Learning Techniques for Crop Disease Prediction in Smart Agriculture 619-632
4. **A. Kumar, G. Mukherjee and S. Gupta**, Role of Biotechnology and Genetic Engineering in Bioremediation of Cadmium Pollution 633-648
5. **Le Zhang, Ying Chen, Huan Zhang, Yabin Jin, Zhe Shen and Gending Duan**, Application of Membrane Separation Technology in Electroplating Wastewater Treatment and Resource Recovery: A Review 649-665
6. **Siriorn Boonyawanich, Peerada Prommeenate, Sukunya Oaew, Wantanasak Suksong, Nipon Pisutpaisal and Saowaluck Haosagul**, Detection of Sulfur Oxidizing Bacteria to Oxidize Hydrogen Sulfide in Biogas from Pig Farm by NGS and DNA Microarray Technique 667-677
7. **Shipa Rani Dey, Prasann Kumar and Joginder Singh**, Total Soluble Protein Mediated Morphological Traits in Mustard Treated with Thiourea and Salicylic Acid 679-694
8. **M. V. Vincy and R. Brilliant**, Assessing Riparian Floristic Diversity and Vegetation Dynamics in the Vamanapuram River Basin, Kerala: A Comprehensive Analysis 695-710
9. **Alfredo Ricardo Zárate Valencia and Antonio Alfonso Rodríguez Rosales**, Application of Random Forest in a Predictive Model of PM10 Particles in Mexico City 711-724
10. **Sukjallin Ryntathieng, Meguovilie Sachu and Mayashree B. Syiem**, Response and Tolerance of Cyanobacterial Exopolysaccharides to Rice Field Herbicide 2,4-D 725-734
11. **T. R. Sundararaman, M. Millicent Mabel and G. Carlin Geor Malar**, A Novel Coal-Associated Soil as an Effective Adsorbent for Reactive Blue Dye Removal 735-746
12. **Manisha Parashar and Gaurav Mudgal**, The Prostrate Spurge-isolated PGPB Endophytes, EP1-AS, and EP1-BM That Can Tolerate High Levels of Salinity and Heavy Metals and Allow Wheat Growth Under These Stressors 747-759
13. **Jyoti Sarwan, Jagadeesh Chandra Bose†, Shivam Kumar, Shruti Singh Bhargav, Sharad Kumar Dixit, Muskan Sharma, Komal Mittal, Gurmeet Kumar and Nazim Uddin**, Biodegradation of Cellulosic Wastes and Deinking of Colored Paper with Isolated Novel Cellulolytic Bacteria 761-773
14. **Moufid. Hebbache, N. Zenati, N. Belahcene and D. Messadi**, Impact of Hydraulic Developments on the Quality of Surface Water in the Mafragh Watershed, El Tarf, Algeria 775-783
15. **Kiran Bishnoi, Pushpa Rani, Minakshi Karwal and Narsi R. Bishnoi**, PAHs Biodegradation by Locally Isolated Phanerochaete chrysosporium and Penicillium citrinum from Liquid and Spiked Soil 785-795
16. **Manika Kohli and Vinakshi Grover**, Sustainable Water Conservation and Management Practices: A Perception Survey of the Farmers of Haryana, India 797-810
17. **Siriorn Boonyawanich, Peerada Prommeenate, Sukunya Oaew, Nipon Pisutpaisal and Saowaluck Haosagul**, Hydrogen Sulfide Oxidizing Microbiome in Biogas-Stream Fed Biofilter in Palm Oil Factory 811-818
18. **Salma El Majaty, Abdellatif Touzani and Youssef Kasseh**, Circular Economy as an Important Lever to Reduce Greenhouse Gas Emissions: Case of an Electricity Distribution Company in Morocco 819-828
19. **Sriroop Chaudhuri and Mimi Roy**, Moss Bags as Active Biomonitors of Air Pollution: Current State of Understanding, Applications and Concerns 829-841
20. **Govindaraju, T. Y. Vinutha, C. J. Rakesh, S. Lokanath and A. Kishor Kumar**, Surface Runoff Estimation Using SCS-CN Method for Kurumballi Sub-watershed in Shivamogga District, Karnataka, India 843-854
21. **S. Bintariningtyas, T. Mulyaningsih and Y. Purwaningsih**, Coal Mining and MSME: Is it Mutually Beneficial? 855-862
22. **J. B. M. Seeletse, N. A. Ndukwe and J. P. H. van Wyk**, Temperature-related Saccharification of Delignified Sawdust Materials from the Lagos Lagoon in Nigeria 863-874
23. **A. K. Shukla, I. Ahmad, S. K. Jain and M. K. Verma**, Assessment of Continuous Growth of Glacial Lakes in the Teesta River Basin Using Semi-Automated Geospatial Approach 875-886
24. **R. Ravikiran, G. Raghu and B. Praveen**, Elucidating Mycotoxin-Producing Aspergillus Species in River Water: An Advanced Molecular Diagnostic Study for the Assessment of Ecological Health and Contamination Risk 887-898
25. **Jaris Veneros, Llandercita Cuchca Ramos, Malluri Goñas, Eli Morales, Erick Auquiñivín-Silva, Manuel Oliva and Ligia García**, Seasonal Variability of Water Quality for Human Consumption in the Tilacancha Conduction System, Amazonas, Peru 899-909
26. **Le Zhang, Jin Hu, Longlong Yan, Si Chen, Yabin Jin, Huan Zhang, Zhe Shen and Tao Yu**, Study on the Technology of Ultrasonic, Chemical and Mechanical Combined Treatment of Oilfield Aging Oil 911-922
27. **Nilofar Saifi and Bandana Jha**, An Overview of Solid Waste Management Practices in Pune, Maharashtra, India 923-934
28. **R. Karthik, Ramya Ranjan Behera, Uday Shankar, Priyadarshi Patnaik and Rudra Prakash Pradhan**, Transforming Energy Access: The Role of Micro Solar Dome in Providing Clean Energy Lighting in Rural India 935-946

29. **A. K. Prodjosantoso, Y. Febriadi, A. R. P. Utami and M. P. Utomo**, The Stabilization of Copper and Cadmium in The Hydrated CaO-CuO-SiO₂ and CaO-CdO-SiO₂ Composites 947-957
30. **Arularasi Thenarasu, Mee Kin Chai, Yeong Hwang Tan, Ling Shing Wong, Ranjithkumar Rajamani and Sinouvassane Djearamane**, Study of *Chlorella vulgaris* from Different Growth Phases as Biosensor for Detection of Titanium and Silver Nanoparticles in Water 959-969
31. **Srikanth Satish Kumar Darapu and Sai Kumar Vindula**, Assessment of the Swelling Behavior of NaOH-Contaminated Red Earth in the Visakhapatnam Region of India Using X-ray Diffraction Analysis 971-978
32. **Vandana Saxena, Ashish Kumar Singh, Atul Srivastava and Anushree Srivastava**, Eco-Engineered Low-Cost Carbosorbent Derived from Biodegradable Domestic Waste for Efficient Total Chromium Removal from Aqueous Environment: Spectroscopic and Adsorption Study 979-989
33. **K. M. P. I. Jayathilake, P.M. Manage and F. S Idroos**, Invasive Aquatic Plants as Potential Sustainable Feedstocks for Biochar Production and as an Innovative Approach for Wastewater Treatment 991-1005
34. **M. A. López-Ramírez, O. P. Castellanos-Onorio, F. Lango-Reynoso, M. del R. Castañeda-Chávez, J. Montoya-Mendoza, M. Díaz-González and B. Ortiz-Muñiz**, Evaluation of an Electrocoagulation Process Modified by Fenton Reagent 1007-1016
35. **R. Sathiyi Priya and U. Rahamathunnisa**, A Comprehensive Study of Remote Sensing Technology for Agriculture Crop Monitoring 1017-1027
36. **Anuradha Sharma and Sakshi Manhas**, Forensic Identification and Isolation of Pathogenic Bacteria From Raw Vegetables and Fruits 1029-1034
37. **Christsam Joy S. Jasje-Santander and Ian Dominic F. Tabañag**, Statistical Performance of Gridded Rainfall Datasets Over Ungauged Jalaur River Basin, Philippines 1035-1045
38. **R. M. H. H. Jayarathne, A. R. Nihmiya, A. H. L. R. Nilmini and P. K. D. D. P. Pitigala**, Fabrication of Tin and Zinc Gas Diffusion Electrodes for Electrochemical Reduction of Carbon Dioxide 1047-1055
39. **S. Sathish, A. Saravanan, R. Suresh, K. Saranya, R. Sarweswaran, G. Balaji and S. Seralathan**, Experimental Analysis of Anaerobic Co-digestion: Potential of Fruit Wastes 1057-1063
40. **Pushpa Rani, Chhotu Ram, Arti Yadav, Deepak Kumar Yadav, Kiran Bishnoi and Narsi Ram Bishnoi**, Comparative Analysis of Various Seed Sludges for Biohydrogen Production from Alkaline Pretreated Rice Straw 1065-1073
41. **Ishar, Paulina Taba and Fahrudin**, Effectiveness of Activated Carbon from Nutmeg Shell (*Myristica fragrans*) Waste as Adsorbent for Metal Ions Pb(II) and Cu(II) in Liquid Waste 1075-1083
42. **Mewgef El Ezza dite Hanane Djieh Cheikh Med Fadel, B. A. Dick, E. C. S'Id, M. B. Ammar, Ould Sidi Y. M., L. S. Mohamed, Mohamed Iemine Yehdih and Mohamed Fekhaoui**, The Effect of Senegal River Irrigation Water Quality on Soil Salinization: A Study of the Main Canal of the M'Pourie Plain in Mauritania 1085-1093
43. **Sugata Datta, Abhishek Chauhan, Anuj Ranjan, Abul Hasan Sardar, Hardeep Singh Tuli, Seema Ramniwas, Moyad Shahwan, Ujjawal Sharma and Tanu Jindal**, A Comparative Review on Bisphenol A Sources, Environmental Levels, Migration, and Health Impacts in India and Global Context 1095-1104
44. **Megha Chauhan and Deepali Rani Sahoo**, Towards a Greener Tomorrow: Exploring the Potential of AI, Blockchain, and IoT in Sustainable Development 1105-1113
45. **E. A. Enoguanbhor, G.O. Chukwurah, E. C. Enoguanbhor, M.O. Isimah, A. E. O. Kosun, N. I. Ewurum and Eike Albrecht**, Underlying Anthropogenic Driving Factors of Forest Landscape Degradation in the Kilimanjaro World Heritage Site, Tanzania Using Survey-based Data 1115-1122
46. **Didi Nuryadin, Mohammad Nurcholis, Gita Astyka Rahmanda and Indra Wahyu Pratama**, Optimization of Aviation Biofuel Development as Sustainable Energy Through Simulation of System Dynamics Modeling 1123-1131
47. **Anita, Mahiya Kulsoom, Aneet Kumar Yadav, Monu Kumar, Kamla Pat Raw, Satguru Prasad and Narendra Kumar**, Accumulation and Translocation of Heavy Metals in *Hibiscus cannabinus* Grown in Tannery Sludge Amended Soil 1133-1139
48. **Md. Al Amin and Md. Tanvir Ahmed**, Beachgoers' Knowledge, Perceptions, and Willingness to Pay for Sustainable Waste Management in Kuakata Sea Beach, Bangladesh 1141-1150
49. **Wisam Alawadi, Ayman Alak Hassan and Ammar Dakhil**, Evaluation of Grid-Based Aridity Indices in Classifying Aridity Zones in Iraq 1151-1160
50. **Priyanka Devi and Prasann Kumar**, Alleviation of Different Climatic Conditions by Foliar Application of Salicylic Acid and Sodium Nitroprusside and Their Interactive Effects on Pigments and Sugar Content of Maize Under Different Sowing Dates 1161-1166
51. **Michael Otu, Brian F. I. Anyatang, Bassey Kooffreh and Rose Ohiana Ugbe**, An Appraisal of the Legal Frameworks and Policy Shift in the Nigerian Energy Sector 1167-1174
52. **E. B. Ogbuene, A. M. Oroke, C. T. Eze, E. Etuk, O. G. Aloh, F. E. Achoru, J. C. Ogbuka, O. J. Okolo, A. V. Ozorme, C. J. Ibekwe, C. A. Eze and S. Akatakpo**, Heavy Metal Concentration in Fish Species *Clarias gariepinus* (Catfish) and *Oreochromis niloticus* (Nile Tilapia) from Anambra River, Nigeria 1175-1182
53. **José L. Ramos-Tejeda, José A. Valeriano-Zapana and Nilton B. Rojas-Briceño**, Presence of Heavy Metals in Purple Crab (*Platyxanthus orbigny*) Tissues in Southern Peru 1183-1188
54. **Zaid Raad Abbas, Aqeel Mohammed Majeed Al-Ezee, Sawsan Hassan Authman and Maan Abdul Azeez Shafeeq**, The Passive Environmental Effect of the Fungicide Benomyl on Soil Promoting Bacteria and Concentration of Some Important Soil Elements 1189-1194
55. **Rery Novio, Sri Mariya, Widya Prarikeslan and Sophia Aulia Ramon**, Study of Temporal Dynamics of Urban Heat Island Surface in Padang West Sumatra, Indonesia 1195-1200
56. **E. E. Salman, A. M. Akol, J. S. Abdel Hamza and Ahmed Samir Naje**, Implementation of the AquaCrop Model for Forecasting the Effects of Climate Change on Water Consumption and Potato Yield Under Various Irrigation Techniques 1201-1207
57. **P. N. Muonye and C. C. Nnaji**, Enhanced Natural Attenuation Technique, Edaphic and Microbiological Changes in Oil-Impacted Soil of Odhiaje Community, Rivers State 1209-1220

**The Journal
Is
Currently
Abstracted
and
Indexed
In:**

WorldCat (OCLC)

British Library

Connect Journals (India)

Indian Science

JournalSeek

Research Bible (Japan)

SHERPA/RoMEO

Directory of Science

AGRIS (UN-FAO)

Ulrich's (Refereed) database

NAAS Rating 2024 = 5.33

CNKI Scholar (China National Knowledge Infrastructure)

Scopus Cite Score (2022) 0.90

Scopus®, SJR (2023) 0.204

Index Copernicus (2022) = 128.35

Indian Science Abstracts, New Delhi, India

Chemical Abstracts, U.S.A.

Pollution Abstracts, U.S.A.

Elsevier Bibliographic Databases

Paryavaran Abstract, New Delhi, India

Zoological Records

CAB Abstracts, U.K.

Electronic Social and Science Citation Index (ESSCI)

Indian Citation Index (ICI)

CrossRef (DOI)

EBSCO: Environment Index™

ProQuest, U.K.

Google Scholar

DOAJ

Zetoc

J-Gate

Environment Abstract, U.S.A.

Centre for Research Libraries

Elektronische Zeitschriftenbibliothek (EZB)

CSA: Environmental Sciences and Pollution Management

Access to Global Online Research in Agriculture (AGORA)

Present in UGC-CARE List (Group II)

UDL-EDGE (Malaysia) Products like i-Journals, i-Focus and i-Future

NATURE ENVIRONMENT AND POLLUTION TECHNOLOGY

EDITORS

Dr. P. K. Goel (Chief Editor)

Former Head, Deptt. of Pollution Studies
Yashwantrao Chavan College of Science
Vidyanagar, Karad-415124
Maharashtra, India

Dr. K. P. Sharma (Honorary Editor)

Former Professor, Ecology Lab, Deptt. of Botany
University of Rajasthan
Jaipur-302004, India
Rajasthan, India

Executive Editor: Mrs. Apurva Goel (Bachelor of Engineering; Masters in Environment) C-102, Building No.12, Swarna CGHS, Beverly Park, Kanakia, Mira Road (E) (Thane) Mumbai-401107, Maharashtra, India
(E-mail: operations@neptjournal.com)

Business Manager: Mrs. Tara P. Goel, Technoscience Publications, A-504, Bliss Avenue, Balewadi, Pune-411045, Maharashtra, India (E-mail: contact@neptjournal.com)

EDITORIAL ADVISORY BOARD

1. **Dr. Saikat Kumar Basu**, Deptt. of Biological Sciences, University of Lethbridge, Lethbridge AB, Alberta, Canada
2. **Dr. Elsayed Elsayed Hafez**, Plant Protection and Biomolecular Diagnosis Department, Arid Lands Cultivation Research Institute (ALCRI), Alexandria, Egypt
3. **Dr. Tri Nguyen-Quang**, Department of Engineering Agricultural Campus, Dalhousie University, Canada
4. **Dr. Sang-Bing Tsai**, Wuyi University Business School, Wuyishan, China
5. **Dr. Zawawi Bin Daud**, Faculty of Civil and Environmental Engg., Universiti Tun Hussein Onn, Malaysia, Johor, Malaysia
6. **Dr. B. Akbar John**, School of Industrial Technology, Universiti Sains Malaysia (USM), Penang, Malaysia
7. **Dr. C. Stella**, Centre for Agro Marine Research, Sethubhaskara Agricultural College and Research Foundation, Visalayankottai, Karaikudi, T.N., India
8. **Dr. G.R. Pathade**, Krishna Institute of Allied Scinces, Krishna Vishwa Vidyapeeth, Karad, Maharashtra, India
9. **Dr. Amit Arora**, Department of Chemical Engineering, National Institute of Technology (NIT), Hamirpur, H.P., India
10. **Prof. Riccardo Buccolieri**, Deptt. of Atmospheric Physics, University of Salento, Dipartimentodi Scienzee Tecnologie Biologicheed Ambientali, Laboratory of Micrometeorology, Lecce, Italy
11. **Dr. Tai-Shung Chung**, Graduate Institute of Applied Science and Technology, National Taiwan University of Science and Technology, Taipei, Taiwan
12. **Dr. Abdeltif Amrane**, Technological Institute of Rennes, University of Rennes, France
13. **Dr. Giuseppe Ciaburro**, Dept. of Architecture and Industrial Design, Università degli Studi, Della Campania, Italy
14. **Dr. A.B. Gupta**, Dept. of Civil Engineering, Malviya National Institute of Technology (MNIT), Jaipur, India
15. **Claudio M. Amescua García**, Department of Publications Centro de Ciencias dela Atmósfera, Universidad Nacional Autónoma de México
16. **Alexander B. Ruchin**, Joint Directorate of the Mordovia State Nature Reserve and National Park, Saransk 430005, Russia
17. **Wei (Welsh) Wang**, State Key Lab of Environmental and Biological Analysis, Hong Kong Baptist University, Hong Kong



Assessment of Deposited Red Clay Soil in Kirkuk City Using Remote Sensing Data and GIS Techniques

V. F. Salahalden†, M. A. Shareef and Q. A. M. Al Nuaimy

Surveying, Engineering Technical College-Kirkuk, Northern Technical University, Mosul, Iraq

†Corresponding author: V. F. Salahalden; veyan.farhad @ntu.edu.iq

Nat. Env. & Poll. Tech.
Website: www.neptjournal.com

Received: 06-09-2023

Revised: 01-11-2023

Accepted: 09-11-2023

Key Words:

Red clay soil

Remote sensing

GIS

IDW

Linear regression model

ABSTRACT

This study investigates the physical characteristics of red clay using the IDW approach and linear regression modeling in an area of 268.12 km², focusing on Kirkuk, Bor, and Jambor structures. Through the analysis of 52 soil samples and the integration of laboratory data with IDW and regression results, several significant findings have emerged. The IDW method combined with linear regression proves to be a cost-effective and efficient approach for obtaining soil property data and generating accurate digital maps of red clay's physical features. The Silt concentration exhibits a wide range, while the gravel content remains relatively low, indicating the predominance of silt in the soil composition. Analysis of Atterberg limits reveals the soil's behavior and consistency in response to moisture, with the plasticity index generally falling within the low to medium range due to the considerable silt content in most soil samples. The linear regression model highlights positive correlations between the liquid limit, plastic limit, and plasticity index. Moderately positive relationships exist between the liquid limit and clay content, as well as a weak positive association between the liquid limit and specific gravity. Dry density, on the other hand, shows no significant correlation with other physical variables, suggesting its independence from the measured parameters. The plastic limit demonstrates a stronger relationship with the clay content compared to the liquid limit. Additionally, weak positive correlations are found between the liquid limit, plastic limit, and specific gravity and water content, indicating the influence of moisture on these parameters. Furthermore, gravel exhibits a moderate positive correlation with sand and silt concentrations, while a strong positive correlation is observed between sand and silt contents, underscoring their close association with the soil composition.

INTRODUCTION

In the field of soil science, the formation of “red clay,” an insoluble clay mineral, occurs through the weathering of rocks in the Earth's crust under wet and warm weather conditions (Yang et al. 2020a, Zhang et al. 2020). Soil, which comprises physical and chemical properties, mineral particles, organic components, air, and water, plays a vital role in the natural environment (Taqi et al. 2016). The particle size distribution of soil is an important physical property and is typically categorized into three fractions: clay (0.002 mm), silt (0.002-0.02 mm), and sand (>0.02 mm) (Fongaro et al. 2018).

Traditional soil surveys provide valuable information on the physical and chemical characteristics of soil at the component level, enabling the creation of maps that illustrate the spatial distribution of these characteristics across different locations (Zhu et al. 2010). However, mapping soil properties can be challenging in areas with low agricultural potential, and conventional

soil survey methods can be time-consuming and expensive, particularly in remote regions (Shareef & Hasan 2020).

Many techniques have been proposed in recent decades to estimate various soil parameters using remote sensing data (Mohamed et al. 2020). In addition to providing information about the spatiotemporal variations in soil, remote sensing (RS) and GIS techniques offer dependable alternatives to older approaches that can cover large areas (Akumu et al. 2015, Jaber et al. 2022, Mezaal & Pradhan 2018, Mezaal et al. 2018, 2017a, 2017b, Shafri, et al. 2017, Sahbeni et al. 2023). RS provides spatial and integrated images of land attributes, enabling a comprehensive understanding of the landscape. By combining multispectral high-resolution data with digital image processing methods, remote sensing can enhance the identification of lithology and geological formations (Martins & Gadiga 2015).

Moreover, remote sensing data can serve as supporting variables for predicting surface soil texture across geographic

areas with the collection of a limited number of soil samples (Liao et al. 2013). Regression analysis models and geostatistical approaches are commonly used to estimate soil properties from RS data (da Silva Chagas et al. 2016, Sridevy et al. 2023). Geographic information systems (GIS) are employed to organize, analyze, and store the extracted information in databases. GIS also facilitates the modeling and mapping of soil properties by utilizing interpolation methods to depict the spatial distribution of the data (Maarez et al. 2022). GIS is used to model and map soil properties and the location distribution of the extracted data using interpolation methods (Akumu et al. 2015).

However, factors such as soil heterogeneity, interpolation method, and sampling can influence the quality of maps generated through geostatistical techniques (Shareef et al. 2020). Spatial interpolation techniques, which consider the actual locations of sample data points, are widely employed to produce maps by quantifying assessments for researched parameters across various positions. These techniques involve the weighted averaging of surrounding data points (Raheem et al. 2022, 2023, Raheem & Omar 2021). Collecting soil data is crucial for addressing queries related to natural hazards, land management, and reconstruction (Buenemann et al. 2023)

Given the absence of a precise map indicating the physical characteristics and distribution of Kirkuk's red clay, this study utilized GIS-based linear regression models

to assess and map the physical characteristics of red clay. However, due to time constraints and the unpredictable nature of soil deposits, gathering and interpreting data on soil physical parameters with high precision is challenging. Hence, the primary objective of this study is to identify the most reliable correlations among indicators of clay soil properties, employing the ordinary least squares method to describe these relationships.

MATERIAL AND METHODS

Location and Geologic Setting of the Study Area

The research site is located in the northern part of Iraq, specifically within a longitude range of $44^{\circ} 00'$ to $44^{\circ} 50'$ E and a latitude range of $35^{\circ} 10'$ to $35^{\circ} 40'$ N (Fig. 1). The study area covers a substantial area of 268.12 km² and encompasses the Fatha and Injana formations. The climate in this region can be characterized as semiarid and Mediterranean, with hot and dry summers and cold winters. The majority of rainfall occurs between December and March, while the summer months experience little to no precipitation (Muhaimed & Al-Hedny 2013).

Topography and Geology of the Study Area

The city of Kirkuk is situated in the hilly northern part of the Kirkuk Plain, with an elevation ranging from 340 to 360 meters above sea level. The Kirkuk structure, also known as

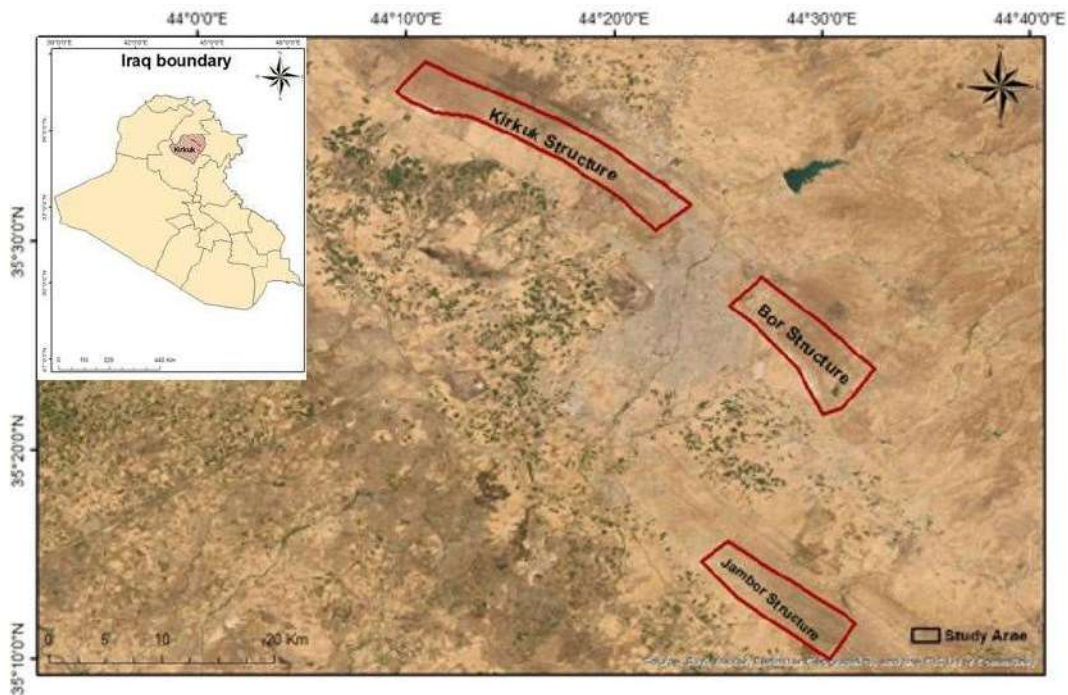


Fig. 1: Location map of the study area.

Baba Dome, marks the northern edge of the plain, while the Hamrin structure delineates the eastern edge. The western and northern margins are outlined by the Hamrin structure and the lower Zap River, respectively (Buday 1980).

During the Pliocene epoch, significant tectonic movements led to the formation of various structures in the region, including Kirkuk, Bia-Hassan, Khabaze, Jambur, and Hamrin, as well as a broad syncline represented by the Kirkuk-Hawija plain. The erosion caused by the rocks in the highest areas between these structures resulted in the deposition of eroded materials from higher grounds to lower areas (Jassim & Goff 2006). In Kirkuk, the earliest rocks belong to the Fatha Formation, which originated in the middle Miocene. This formation consists of gypsum, red claystone, and green marl, overlain by sandstone and red claystone from the Injana Formation, which dates back to the Upper Miocene (Al-Naqib 1959).

The research region is predominantly flat, with some variations in elevation primarily concentrated in the southwestern corner. The presence of anticlines such as Bor, Jambor, and Kirkuk indicates that the high terrain resulted from structural forces. The elevation in the surveyed area ranges from 500 meters above sea level in the northeast

to 200 meters above sea level in the southwest (Jabbar 2015). The Fatha Formation, originating from the middle Miocene epoch, is exposed in the study area. It comprises thick gypsum layers alternating with reddish-brown or green claystone, marl, or limestone, with a thickness range of 100 to 200 meters (Jabbar 2015). The Injana Formation, composed of thin-bedded calcareous sandstone, red and green mudstone, and siltstone, was formed later in the Miocene period (Alhirmizy 2015).

Methods

The methodology employed in this study encompasses field measurements, satellite data analysis, and the application of geographic information systems (GIS) techniques. Specifically, inverse distance weighting (IDW) and a linear regression model were utilized to investigate the distribution of red clay and various physical properties of the soil. The physical properties considered in this analysis include soil texture, Atterberg limits, specific gravity, dry density, and water content. A graphical representation of the overall methodology can be found in Fig. 2.

Field measurements and soil analysis: A total of fifty-two soil sampling sites were selected within the Bor, Jambor, and

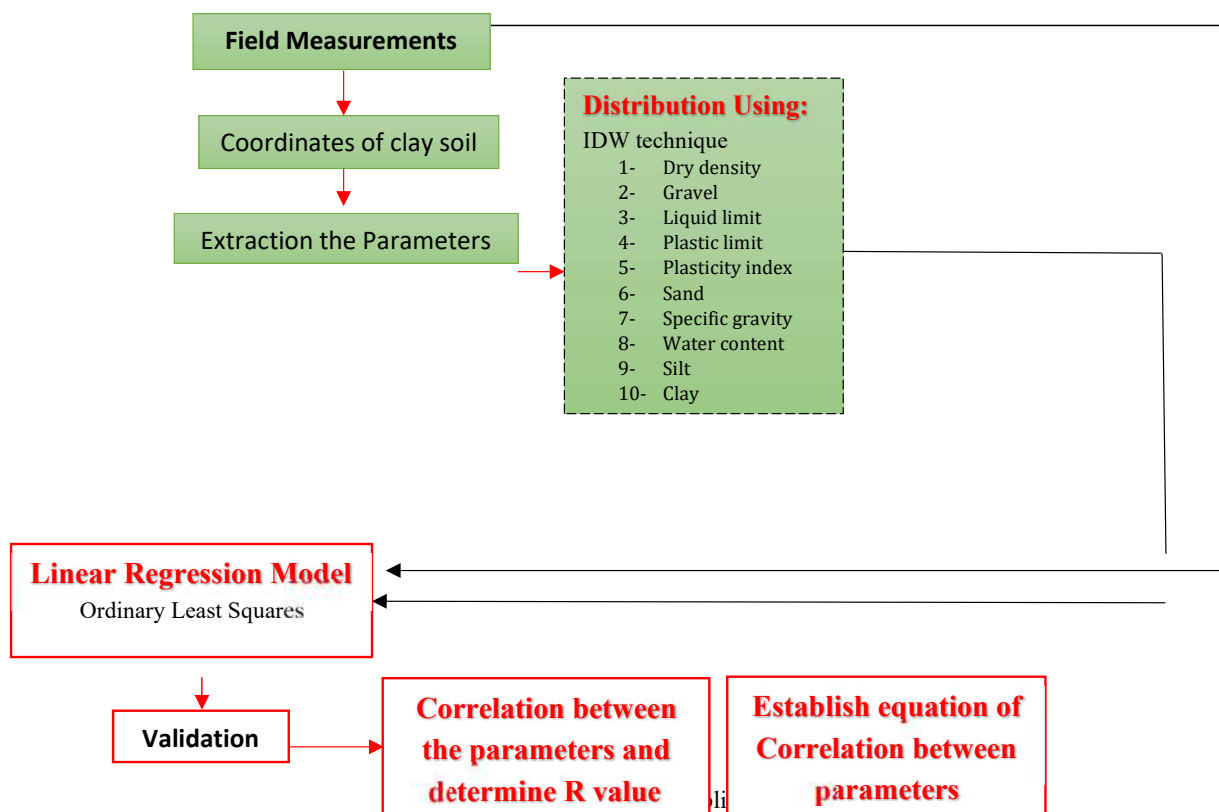


Fig. 2: Flow chart of the applied method.

Kirkuk structures, which are part of the Fatha and Injana Formations. The precise coordinates of these sites were determined using a portable GPS device with an accuracy of ± 3.6 . For the analysis of soil properties, an HS-5001EZ moisture-density meter was employed to measure the dry density and water content. At each sampling site, soil samples were collected at a depth of 30 cm after removing the topsoil layer. These samples were then air-dried before being transported to the laboratory for further analysis.

In the laboratory, the soil samples underwent various tests to determine their physical properties. The Atterberg limits, which include the liquid limit (LL) and plastic limit (PL), were determined using the Casagrande three-point approach. The specific gravity of the soil was measured, and the percentages of sand, silt, and clay in the soil were determined using hydrometers. The liquid limits were calculated based on the 3-millimeter diameter of the soil thread during the testing for plastic limits (Zolfaghari et al. 2015). All measurements and analyses were conducted following the standards set by the American Society for Testing and Materials (ASTM)

Inverse distance weighted: Geostatistics is a statistical branch that specializes in the analysis of spatial distribution and variability (Shit et al. 2016, Yadav et al. 2023). In this study, the spatial patterns of various physical properties of red clay were described using interpolated maps created through the inverse distance weighted (IDW) method (Belief 2018, Ratshiedana et al. 2023). The IDW interpolation approach was utilized to predict the values of unmeasured sites or unsampled locations (Shit et al. 2016). Geographers often employ the IDW interpolation technique to fill in data gaps, where it uses a weighted combination of nearby sample points to estimate values in grid cells. The closer the data points are to the target location, the greater their influence on the estimation process (Nistor et al. 2020, Zhang et al. 2020).

To determine the unknown value, $Z(X)$, at a specific position X , the following equations, Eq. 1 and Eq. 2, were employed:

$$Z(X) = \sum_{i=1}^n W_i Z(X_i), \quad \dots(1)$$

where n represents the monitoring station, $Z(X)$ represents the value at the sampled sites, and W_i represents the weight of X_i , which is defined as:

$$W_i = \frac{\frac{1}{d_j^k}}{\left(\sum_{i=1}^n \frac{1}{d_j^k}\right)} \quad \dots(2)$$

where d_i is the horizontal distance between the interpolation points and the observed positions, and k is the distance power (Yang et al. 2020b).

Linear Regression Model

Simple regression analysis is a statistical tool that explores the relationships between dependent and independent variables by employing various regression models, including linear regression, exponential regression, logarithmic regression, polynomial regression, and power regression models (Eskandari et al. 2023, Shahien & Ogila 2022). The assessment of regression relationships often involves the use of Pearson's correlation coefficient. By calculating Pearson's correlation coefficient (R), we can evaluate the strength and direction of the association between two variables. In the matrix plot, we observed strong correlations ($R = 0.68$), moderate correlations ($R = 0.36-0.67$), and weak correlations ($R = -0.35$) between the variables (Shahien & Ogila 2022).

The function of linear regression is given in Eq. 3:

$$Y = A + BX + \mathcal{E} \text{ (Shareef et al. 2014)} \quad \dots(3)$$

Where Y is the dependent variable, X is the independent variable, A is the intercept, B is the slope, and \mathcal{E} is the error term.

RESULTS AND DISCUSSION

Field measurements of soil were conducted at 52 selected locations within the city of Kirkuk, specifically in three sections: the Bor, Jambor, and Kirkuk structures. The HS-5001EZ moisture-density gauge was utilized for this purpose.

Laboratory and Statistical Analysis

Particle size analysis: Upon conducting a specific size analysis of the fifty-two soil samples, it was observed that the percentage of gravel was generally low across most samples, ranging from 0 to 4 percent. However, there was one site in the Kirkuk structure's Injana Formation where the percentage of gravel was notably higher at 16.3 percent. On average, the gravel content was 0.49 percent in the Injana Formation and slightly higher at 0.66 percent in the Fatha Formation.

The results for sand content varied from 0 to 30 percent, with two locations in the Injana Formation exhibiting higher percentages of 42 and 61 percent. In contrast, the average sand content in the Fatha Formation was 7.5 percent, slightly lower than the average of 8.9 percent in the Injana Formation. Silt, on the other hand, predominated in the vast majority of the soil samples, although specific percentages were not provided in the given information.

Atterberg limits: The Atterberg limits were used to determine the boundary between different physical states of sediments. The findings of the Atterberg limits analysis revealed that the liquid limit ranged from 18 to 43%, with an average of 30.17%. Within the Jambor structure, the Fatha Formation exhibited the highest percentage of liquid limit,

while the Injana Formation showed the lowest percentage. Specifically, in the Fatha Formation, the liquid limit ranged from 27 to 43%, with an average of 31.88 percent, whereas in the Injana Formation, it ranged from 18 to 34.8%, with an average of 30.42%. These results indicate that samples from the Fatha Formation generally had a higher liquid limit compared to samples from the Injana Formation.

The plastic limit, representing the moisture content at which soil transitions from a plastic to a semisolid state, ranged from 16 to 22%, with an average of 19%. Notably, there was a small difference in the plastic limit between the Fatha Formation (average of 19.46%) and the Injana

Formation (average of 19.35%).

The plasticity index, which is the difference between the liquid limit and the plastic limit, varied from 2 to 21%. The majority of the samples exhibited a plasticity index ranging from 5 to 20%, indicating a transition from low plasticity to medium plasticity. It is worth noting that the presence of a significant percentage of silt in most soil samples contributed to the plasticity index falling within the low to medium range.

Partial Analysis of the Soil Using IDW

Using the IDW approach, the spatial distribution of physical properties was examined, leading to the identification of five

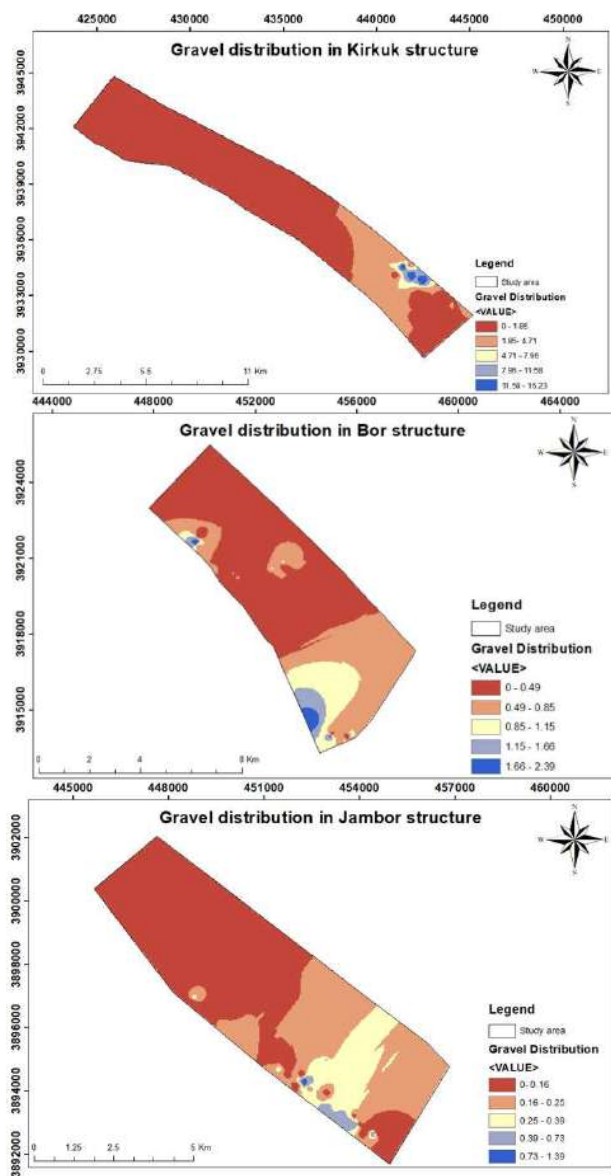


Fig. 3: IDW representation of gravel.

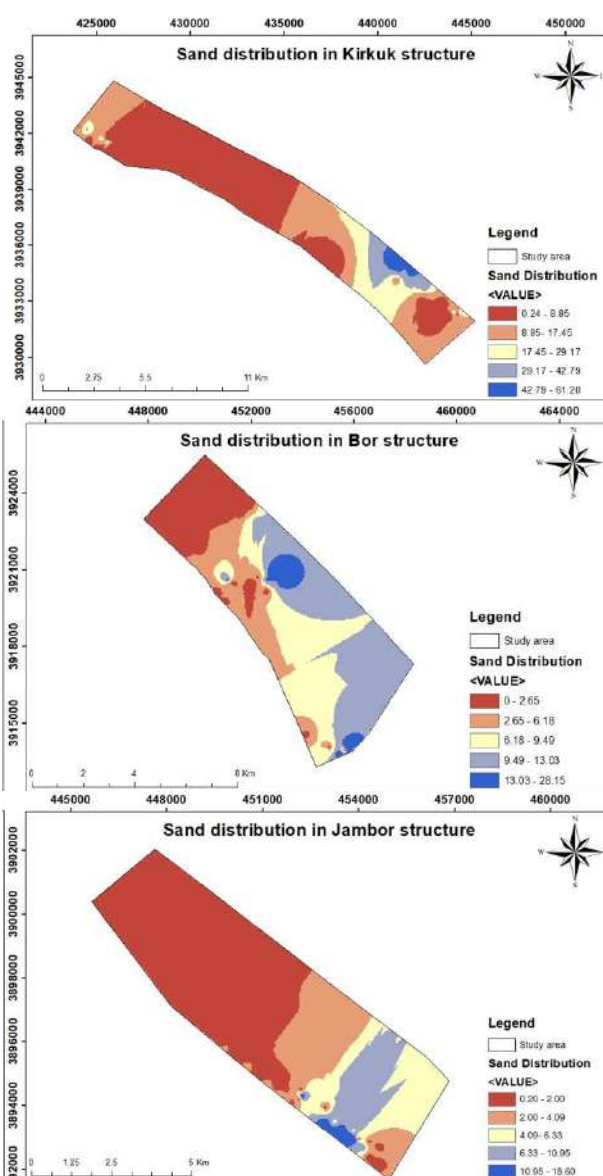


Fig. 4: IDW representation of sand.

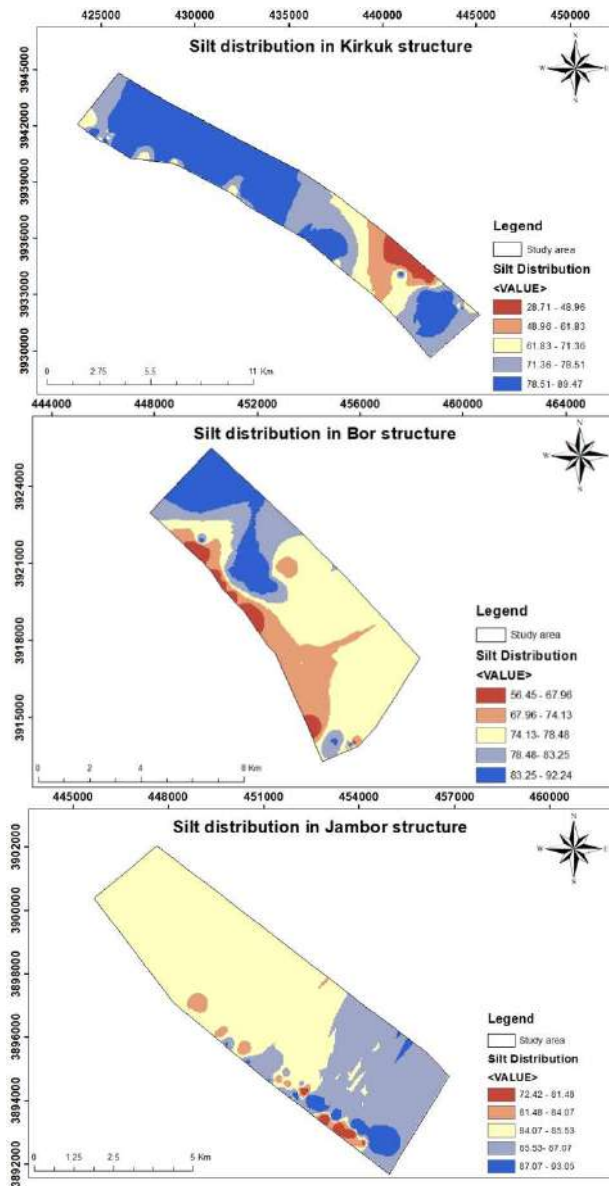


Fig. 5: IDW representation of silt.

distinct regions: very low, low, medium, high, and very high. Higher-proportion regions are represented in blue, while lower-proportion regions are depicted in red. The study area was divided into three sections: Kirkuk structure, Bor structure, and Jambor structure. Kirkuk structure (ranging from 28.71 to 89.47%), Bor structure (ranging from 56.45 to 92.24%), and Jambor structure (ranging from 72.42 to 93.05%), as depicted in Fig. 5, were all found to contain a comparatively high proportion of silt. Fig. 3 provides insights into the distribution of gravel percentages across the three sections, showing a range of 0 to 16.23% in the Kirkuk

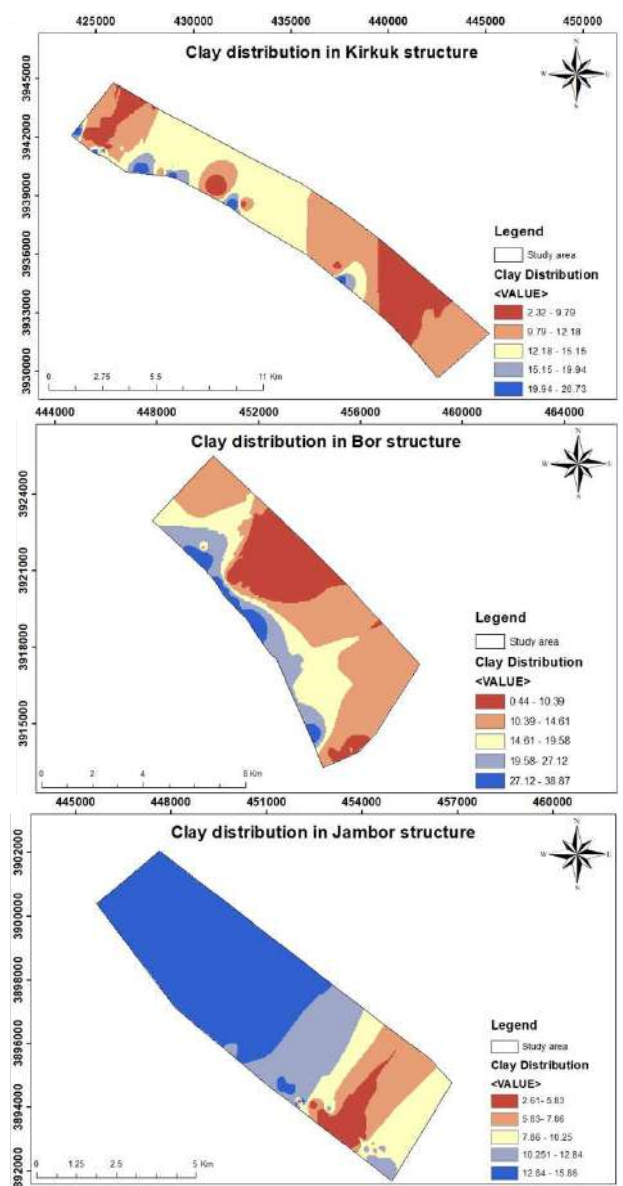


Fig. 6: IDW representation of clay.

structure, 0 to 2.39% in the Bor structure, and 0 to 1.39% in the Jambor structure.

Similarly, Fig. 4 showcases the variation in sand percentages, with the Kirkuk structure ranging from 0.24 to 61.20%, the Bor structure ranging from 0.0 to 28.15%, and the Jambor structure ranging from 0.2 to 18.6%. The percentage of clay is depicted in Fig. 6, revealing a range of 2.32 to 26.73% in the Kirkuk structure, 0.44 to 38.87% in the Bor structure, and 2.61 to 15.86% in the Jambor structure. Field measurements utilizing an HS-5001EZ moisture-density gauge were conducted to determine the dry density

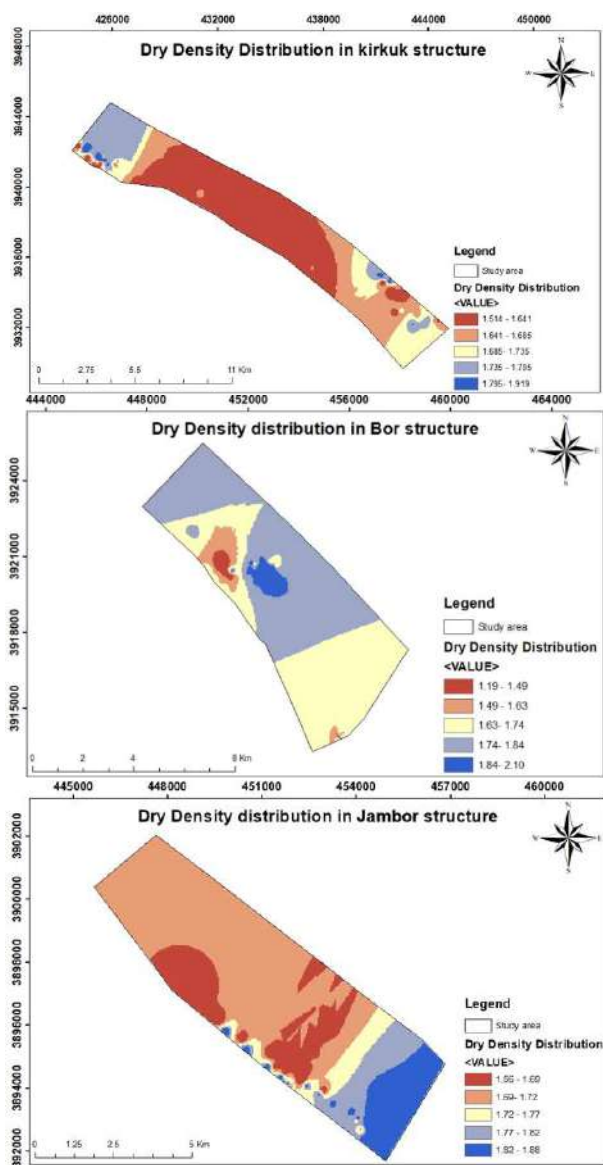


Fig. 7: IDW representation of dry density.

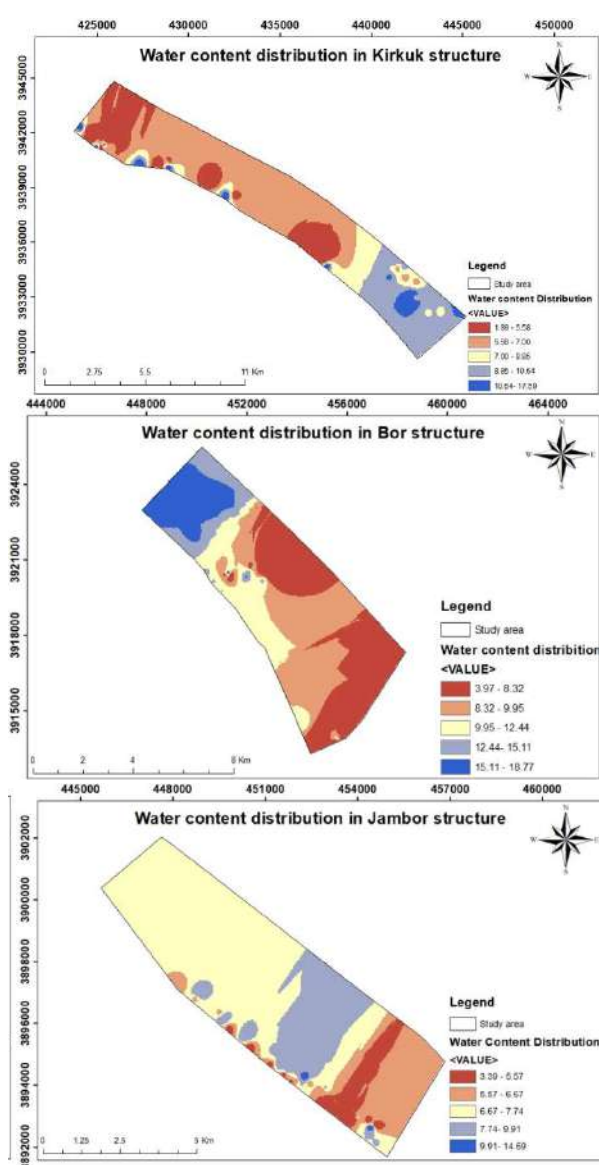


Fig. 8: IDW representation of water content.

Table 1: The root mean squared error (RMSE) and R^2 for maps.

Physical properties	Kirkuk hills		Bor mountain		Jambor hills	
	RMSE	R^2	RMSE	R^2	RMSE	R^2
Water Content	0.078	0.825	0.087	0.815	0.066	0.83
Dry density	0.015	0.891	0.0054	0.858	0.0033	0.92
Liquid Limit	0.29	0.765	0.098	0.8	0.15	0.79
Plastic Limit	0.16	0.78	0.047	0.858	0.044	0.863
Specific gravity	0.022	0.884	0.0044	0.92	0.00096	0.945
Gravel	0.038	0.865	0.012	0.9	0.028	0.877
Sand	0.123	0.793	0.093	0.81	0.079	0.82
Silt	0.21	0.775	0.059	0.85	0.113	0.798
Clay	0.065	0.841	0.046	0.86	0.059	0.85

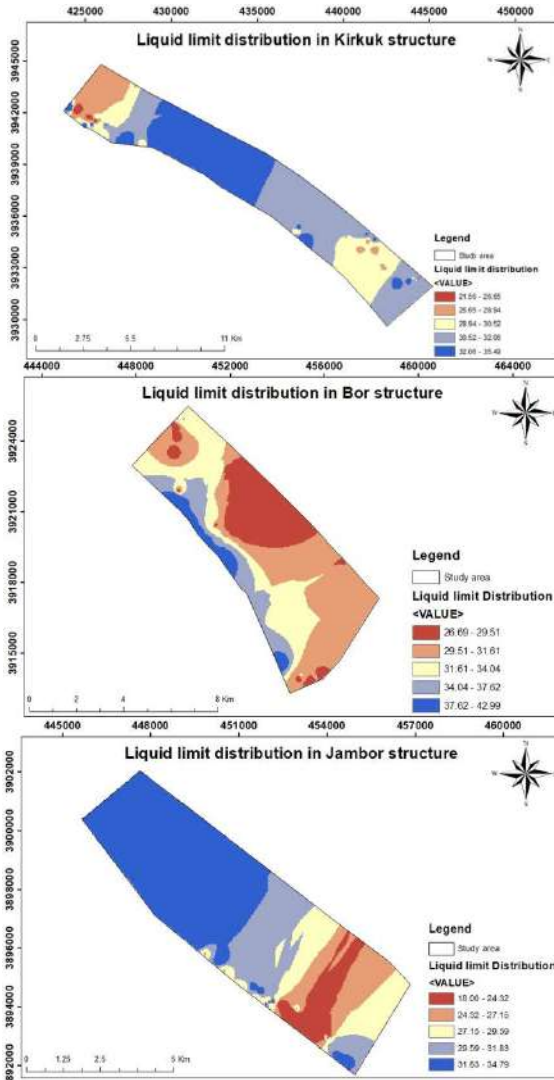


Fig. 9: IDW representation of liquid limit.

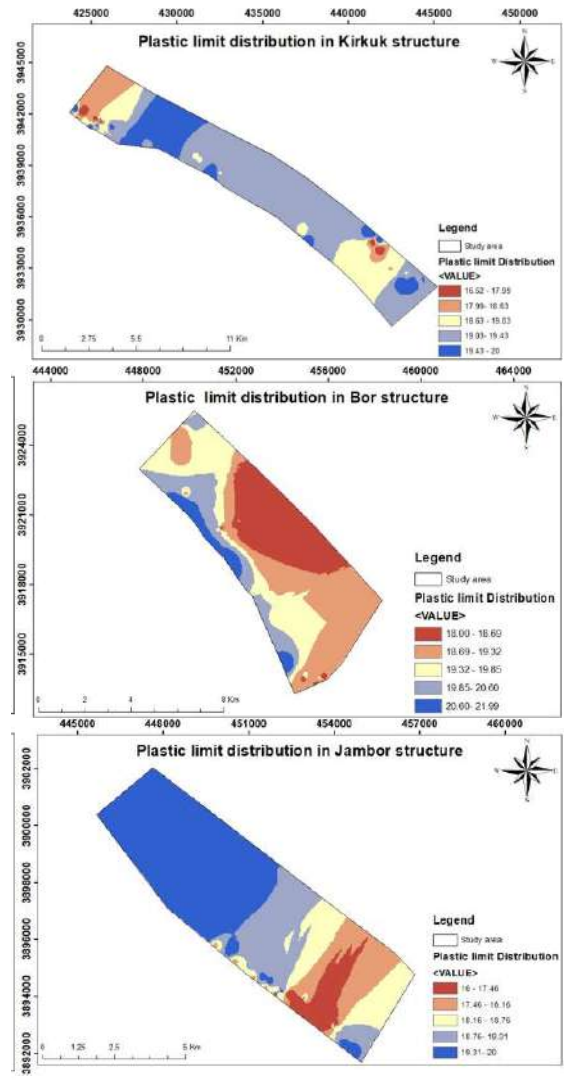


Fig. 10: IDW representation of plastic limit.

Table 2: Relationship between the physical properties of red clay.

	Water content	Dry Density	Liquid Limit	Plastic Limit	Plasticity index	specific gravity	Gravel	sand	silt	clay
Water content	1									
Dry Density	0.06	1								
Liquid Limit	0.112	0.08	1							
Plastic Limit	0.12	0.08	0.94	1						
Plasticity index	0.09	0.07	0.99	0.89	1					
specific gravity	0.151	0.012	0.102	0.006	0.009	1				
Gravel	0.003	0.013	0.00007	0.00005	0.0002	0.01	1			
sand	0.007	0.001	0.04	0.03	0.036	0.018	0.33	1		
silt	0.002	0.006	0.03	0.03	0.031	0.0013	0.45	0.81	1	
clay	0.09	0.003	0.58	0.495	0.596	0.151	0.005	0.07	0.02	1

and water content, as shown in Fig. 7 and Fig. 8, respectively. Dry density values ranged from 1.51 to 1.92 g.m⁻³, in the Kirkuk structure, 1.19 to 2.10 g.m⁻³ in the Bor structure, and 1.56 to 1.88 g.m⁻³ in the Jambor structure.

Water content varied between 1.89 and 17.59% in the Kirkuk structure, 3.97 and 18.77% in the Bor structure, and 3.39 and 14.69% in the Jambor structure. Fig. 9, 10, and 11 show the range of Atterberg limits in the soil analysis. Fig. 9 provides insights into the liquid limit, which spans from 18 to 43. Fig. 10 presents the plastic limit, ranging from 16 to 22. The plasticity index, displayed in Fig. 11, varies from 4 to 21. It is worth noting that a substantial proportion of soil samples contain silt, resulting in a plasticity index that predominantly falls within the low to medium range.

Validation and Model Generation

To validate the accuracy of the physical property maps

generated using the IDW method for red clay, a validation process was conducted. A subset of 30% of the soil samples was utilized to compare the field measurements with the values estimated by the IDW interpolation. Table 1 provides the Root Mean Square Error (RMSE) values for the various physical properties assessed during the validation process. Choosing an interpolation method depends on the size of the data present in a study area. Different interpolation methods were applied to choose the best method and apply it to producing maps of the physical and chemical properties of red clay. The accuracy of the maps was calculated by applying the root mean square. The IDW method was the most accurate and appropriate method to produce maps. R^2 of the IDW ranged between 0.74 and 0.92, while R^2 .

A linear regression model was employed to establish connections and characterize the physical characteristics

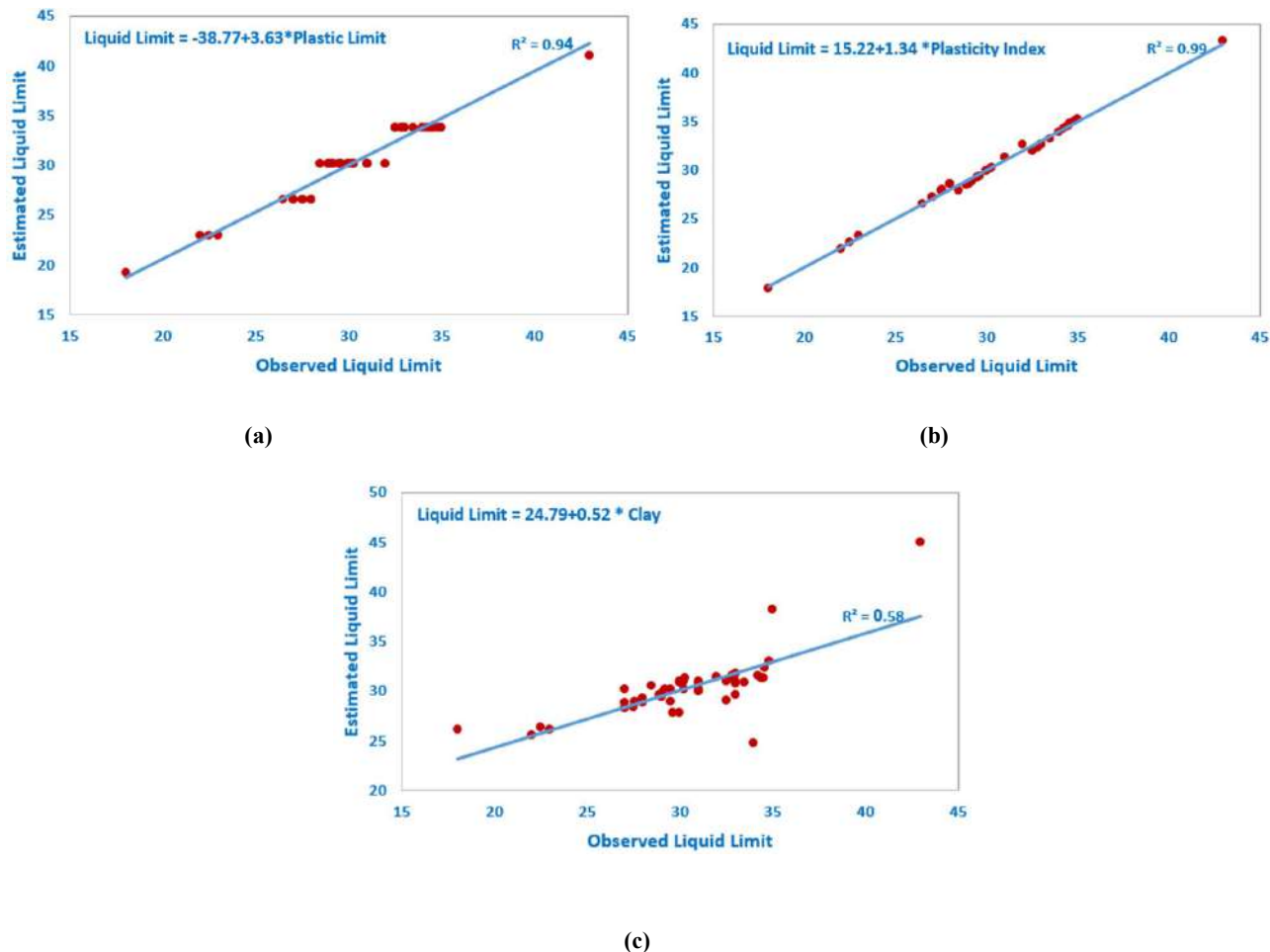


Fig. 11: Correlation Liquid Limit with (a) Plastic Limit, (b) Plasticity Index, and (c) Clay.

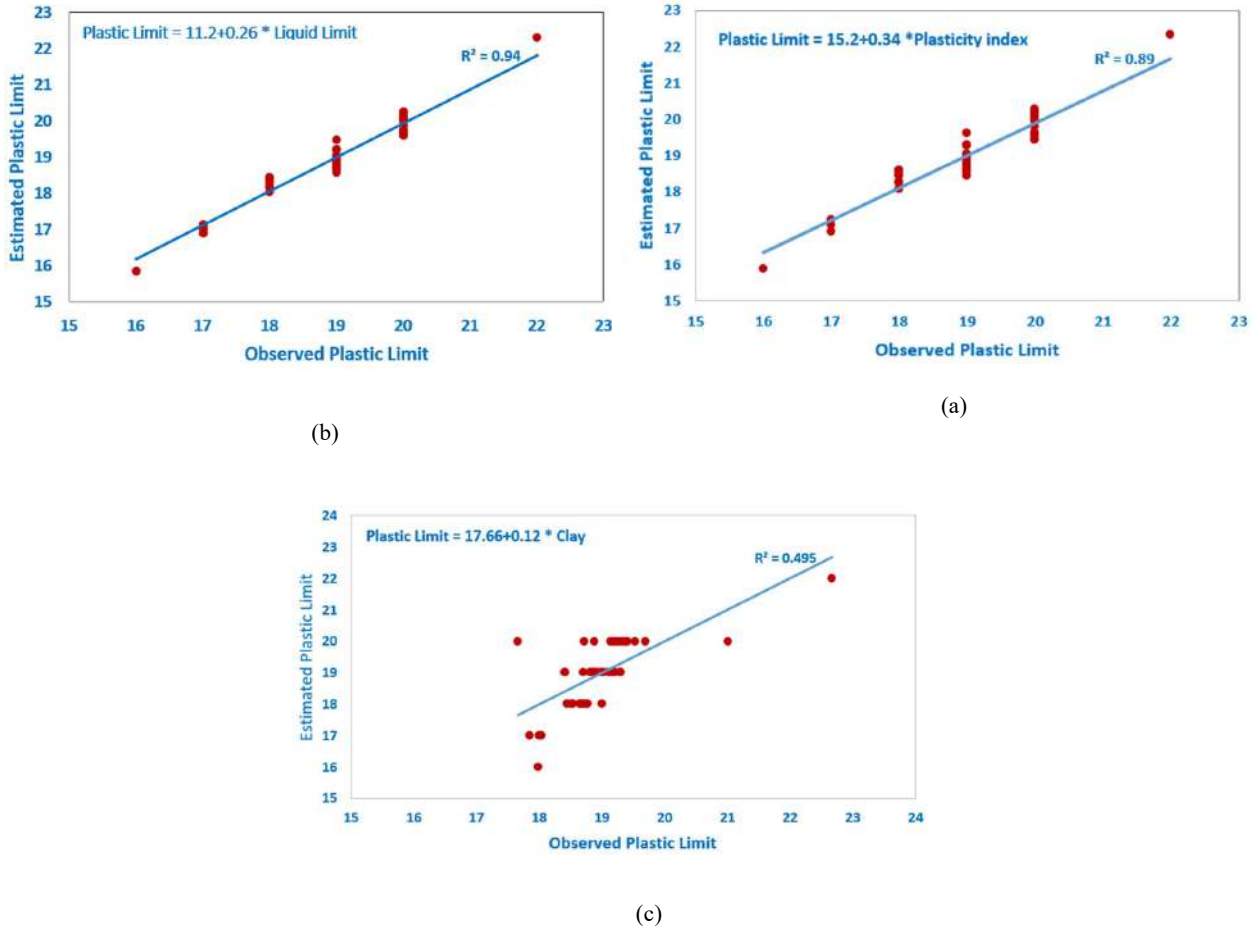


Fig. 12: Correlation of Plastic Limit with (a) Liquid limit, (b) Plasticity Index, and (c) Clay.

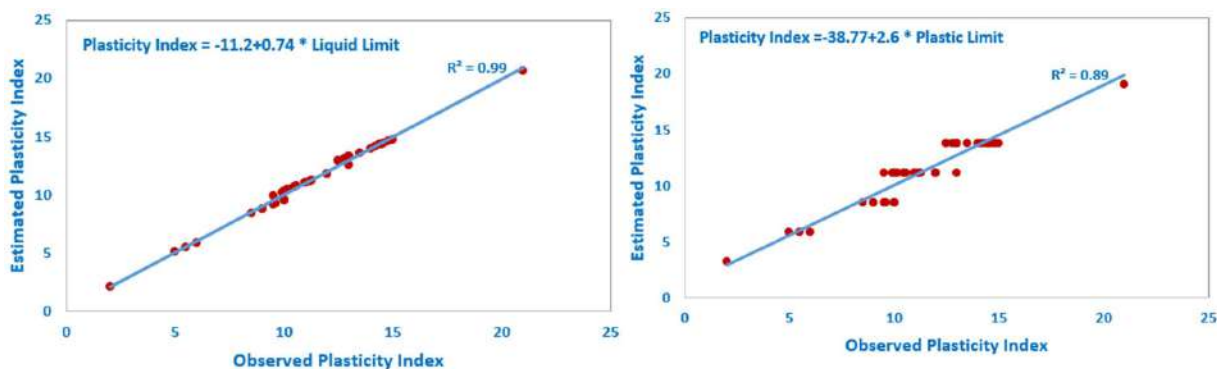
of red clay. The relationships between various soil properties, including soil texture (gravel, sand, silt, and clay), Atterberg limits (liquid limit, plastic limit, and plasticity index), water content, dry density, and specific gravity, were examined. The correlation analysis results are presented in Table 2.

The correlation analysis revealed a weak positive association between water content and liquid limit, plastic limit, and specific gravity, with correlation coefficients of 0.12, 0.120, and 0.151, respectively. However, no significant relationship was observed between dry density and the other parameters.

Regarding the liquid limit, a strong positive correlation was found with the plastic limit and plasticity index (0.94 and 0.99, respectively), a moderately positive correlation with clay content (0.58), and a weak positive correlation with specific gravity (0.102). The plastic limit exhibited a moderately significant association with clay content (0.495),

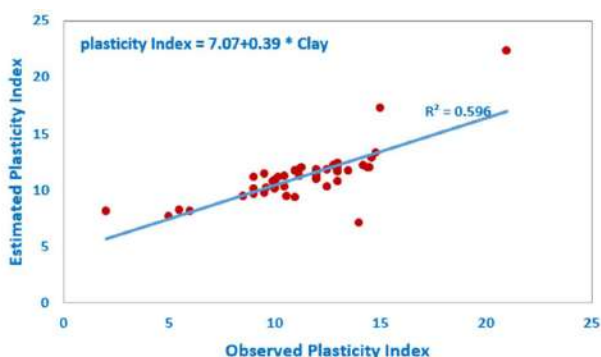
while a high positive correlation was observed between the plasticity index and plastic limit (0.89). Furthermore, an intermediate positive association (0.596) was found between the plasticity index and clay percentage. The clay content showed only a slight positive correlation with specific gravity (0.151). Gravel displayed a moderately favorable association with sand (0.33) and silt (0.45), which is a common trend. Notably, a strong positive correlation (0.81) was identified between sand and silt percentages. The correlations between liquid limit, plastic limit, and plasticity index exhibit a direct and ideal correlation. The logical nature of these interactions arises from their dependence on common elements, such as clay content.

Figs. 11 to 16 display examples of correlation coefficients and regression equations obtained through the linear regression model. These figures, calculated using ArcMap software, demonstrate the relationships between the investigated soil parameters. The correlation coefficients,



(a)

(b)



(c)

Fig. 13: Correlation of Plasticity Index with (a) Liquid limit, (b) Plastic Limit, and (c) Clay.

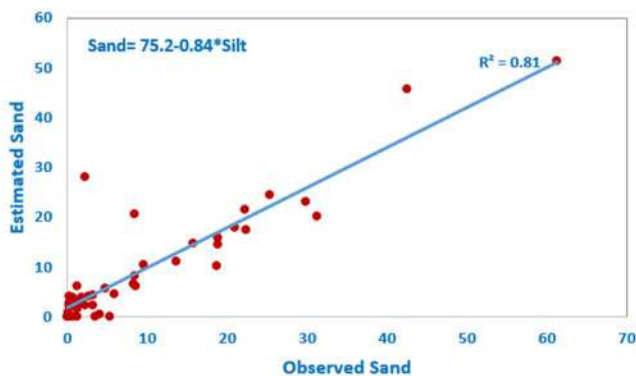


Fig. 14: Correlation of sand with silt.

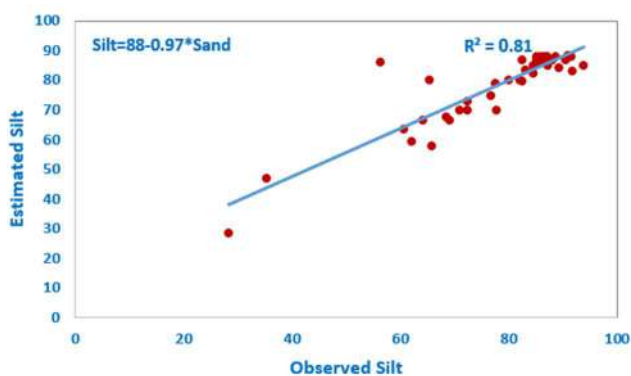


Fig. 15: Correlation of silt with sand.

represented by the R-value, indicate the strength and direction of the associations. The empirical regression equations derived from the model offer initial insights into the characteristics of the studied variables.

CONCLUSION

The analysis of red clay’s physical parameters using the IDW approach and linear regression modeling, covering an area of 268.12 km2 and three different structures (Kirkuk,

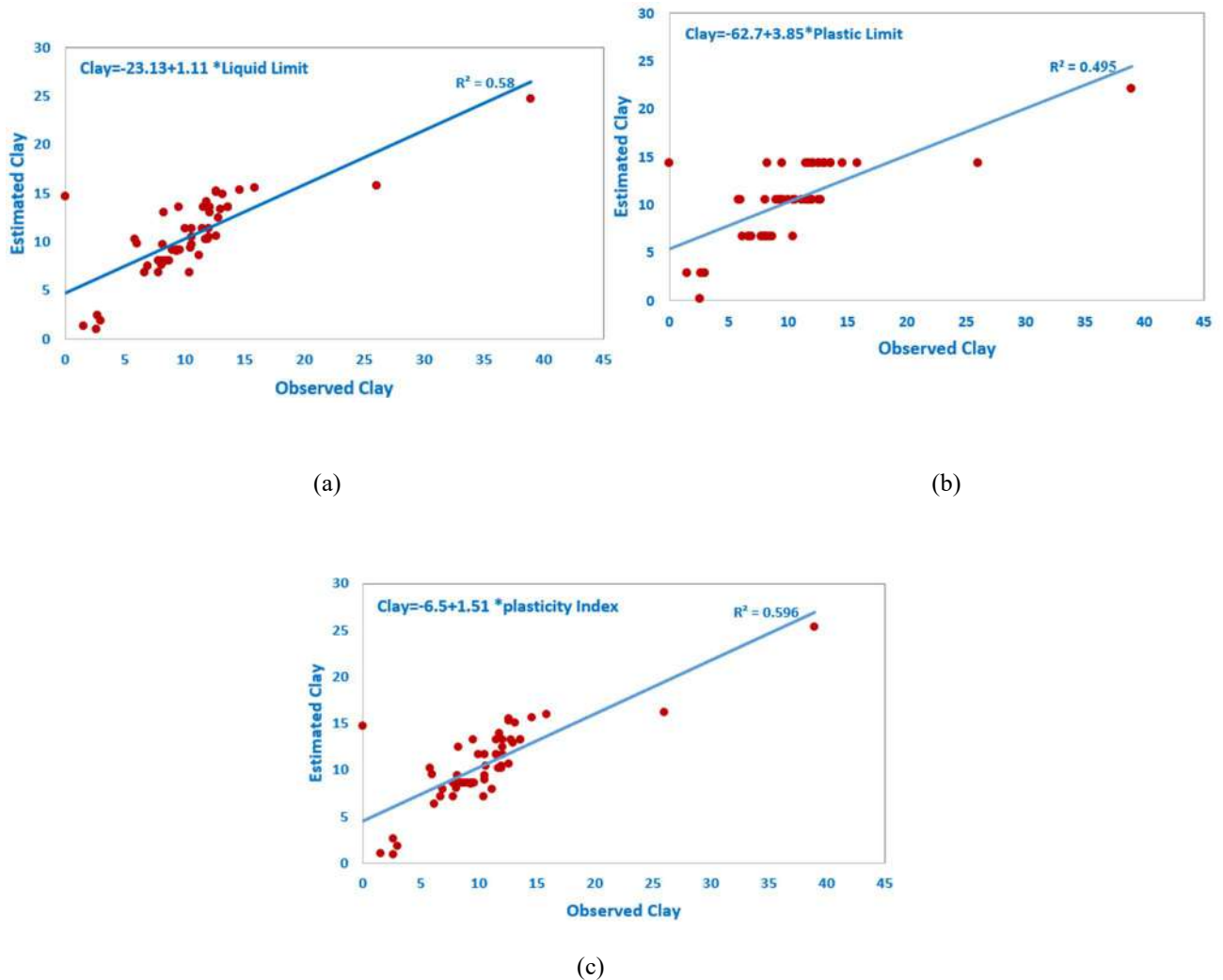


Fig. 16: Correlation of Clay with (1) Liquid limit, (2) Plastic Limit, and (c) Plasticity Index.

Bor, and Jambor), has yielded significant insights into the characteristics of the soil. By examining soil samples from 52 locations and combining laboratory data with IDW and regression results, several key findings have emerged.

First, the IDW method coupled with linear regression has proven to be a rapid, cost-effective, and reliable approach for obtaining soil property data. This approach enables the creation of accurate digital maps of red clay's physical features. Regarding the soil texture analysis, silt concentration exhibited the widest range, varying from 28.56% to 92.28%. On the other hand, gravel content was found to be relatively low, ranging from 0% to 16.03%. These findings highlight the dominance of silt in the soil composition.

The field measurements conducted using the HS-5001EZ

moisture-density gauge revealed water content ranging from 2.24% to 18.8%, while dry density values ranged from 1.19 to 2.12. These results provide insights into the soil's moisture characteristics and density distribution across the study area.

The analysis of Atterberg limits demonstrated a range of 21 to 43 for the liquid limit and 16 to 22 for the plastic limit. These limits indicate the soil's consistency and behavior in response to moisture content. Furthermore, the plasticity index, reflecting the soil's plasticity, fell within the low to medium range due to the significant percentage of silt present in most soil samples.

The linear regression model revealed positive correlations between the liquid limit, plastic limit, and plasticity index, with Pearson's correlation coefficients of 0.94 and 0.99, respectively. Additionally, the liquid limit displayed a

moderately positive relationship with clay content ($R = 0.58$) and a weak positive association with specific gravity ($R^2 = 0.12$). The plastic limit and plasticity index exhibited a positive correlation with clay concentration ($R^2 = 0.495$ and $R^2 = 0.596$, respectively).

Interestingly, no correlation was found between dry density and other physical variables, suggesting that dry density is independent of the measured parameters. Furthermore, a stronger relationship was observed between clay content and the plastic limit compared to the liquid limit. Moreover, the liquid limit, plastic limit, and specific gravity were all weakly positively correlated with water content, indicating the influence of moisture on these parameters.

Last, gravel showed a moderate positive correlation with sand and silt concentrations. Additionally, a strong positive correlation ($R^2 = 0.81$) was observed between sand and silt contents, indicating their close association with the soil composition.

In summary, the comprehensive analysis of red clay's physical properties using the IDW method and linear regression modeling has provided valuable insights into the soil's characteristics. These findings enhance our understanding of the soil composition, moisture characteristics, and behavior, contributing to effective soil management and land-use planning in the study area.

REFERENCES

- Akumu, C., Johnson, J., Etheridge, D., Uhlig, P., Woods, M., Pitt, D. and McMurray, S. 2015. GIS-fuzzy logic-based approach in modeling soil texture: using parts of the Clay Belt and Hornepayne region in Ontario Canada as a case study. *Geoderma*, 239: 13-24.
- Al-Naqib, K.M. 1959. Geology of Southern Area of Kirkuk Liwa, Iraq. General Secretariat of the League of Arab States, Cairo, Egypt.
- Alhirmizy, S. 2015. Automatic mapping of lineaments using shaded relief images derived from Digital Elevation Model (DEM) in Kirkuk Northeast Iraq. *Int. J. Sci. Res.*, 4(5): 2228-2233.
- Belief, E. 2018. GIS based spatial modeling to mapping and estimation relative risk of different diseases using inverse distance weighting (IDW) interpolation algorithm and evidential belief function (EBF) (Case study: Minor Part of Kirkuk City, Iraq). *Int. J. Eng. Technol.*, 7(4.37): 185-191.
- Buday, T. 1980. The Regional Geology of Iraq: Stratigraphy and Paleogeography. Dar El-Kutib Publication House, University of Mosul, Baghdad, p. p445.
- Buenemann, M., Coetzee, M.E., Kutuahupira, J., Maynard, J.J. and Herrick, J.E. 2023. Errors in soil maps: The need for better on-site estimates and soil map predictions. *PLoS One*, 18(1): e0270176.
- da Silva Chagas, C., de Carvalho Junior, W., Bhering, S.B. and Calderano Filho, B. 2016. Spatial prediction of soil surface texture in a semiarid region using random forest and multiple linear regressions. *Catena*, 139: 232-240.
- Eskandari, M., Zeinadini, A., Seyedmohammadi, J. and Navidi, M. 2023. Estimating quantity of date yield using soil properties by regression and artificial neural network. *Commun. Soil Sci. Plant Anal.*, 54(1): 36-47.
- Fongaro, C.T., Demattê, J.A., Rizzo, R., Lucas Safanelli, J., Mendes, W. d. S., Dotto, A.C., Vicente, L.E., Franceschini, M.H. and Ustin, S.L. 2018. Improvement of clay and sand quantification based on a novel approach with a focus on multispectral satellite images. *Remote Sens.*, 10(10): 1555.
- Jabbar, M.F.A. 2015. Geomorphology and Morphometry of Segmented Kirkuk Alluvial Fan, Northern Iraq. *Iraqi Bull. Geol. Min.*, 11(2): 27-43.
- Jaber, H.S., Shareef, M.A. and Merzah, Z.F. 2022. Object-based approaches for land use-land cover classification using high resolution quick bird satellite imagery (a case study: Kerbela, Iraq). *Geod. Cartogr.*, 48(2): 85-91-85-91.
- Jassim, S.Z. and Goff, J.C. 2006. Geology of Iraq. DOLIN, sro, distributed by Geological Society of London.
- Liao, K., Xu, S., Wu, J. and Zhu, Q. 2013. Spatial estimation of surface soil texture using remote sensing data. *Soil Sci. Plant Nutr.*, 59(4): 488-500.
- Maarez, H.G., Jaber, H.S. and Shareef, M.A. 2022. Utilization of Geographic Information System for hydrological analyses: A case study of Karbala province, Iraq. *Iraqi J. Sci.*, 4118-4130.
- Martins, A.K. and Gadiga, B.L. 2015. Satellite remote sensing for mineral deposit assessment of clay in Mubi Local Government Area of Adamawa State, Nigeria. *Geosci.*, 5(1): 26-30.
- Mezaal, M.R. and Pradhan, B. 2018. An improved algorithm for identifying shallow and deep-seated landslides in dense tropical forest from airborne laser scanning data. *Catena*, 167: 147-159.
- Mezaal, M.R., Pradhan, B. and Rizeei, H.M. 2018. Improving landslide detection from airborne laser scanning data using optimized Dempster-Shafer. *Remote Sens.*, 10(7): 1029.
- Mezaal, M.R., Pradhan, B., Sameen, M.I., Mohd Shafri, H.Z. and Yusoff, Z.M. 2017a. Optimized neural architecture for automatic landslide detection from high-resolution airborne laser scanning data. *Appl. Sci.*, 7(7): 730.
- Mezaal, M.R., Pradhan, B., Shafri, H.Z.M. and Yusoff, Z.M. 2017b. Automatic landslide detection using Dempster-Shafer theory from LiDAR-derived data and orthophotos. *Geomat., Nat. Hazards Risk*, 8(2): 1935-1954.
- Mohamed, E., Ali, A., El-Shirbeny, M., Abutaleb, K. and Shaddad, S.M. 2020. Mapping soil moisture and their correlation with crop pattern using remotely sensed data in arid regions. *Egypt. J. Remote Sens. Space Sci.*, 23(3): 347-353.
- Muhaimeed, A.S. and Al-Hedny, S. 2013. Evaluation of long-term vegetation trends for northeastern Iraq: Mosul, Kirkuk, and Salah al-Din. *IOSR J. Agric. Veter. Sci.*, 5(2): 67-76.
- Nistor, M.M., Rahardjo, H., Satyanaga, A., Hao, K.Z., Xiaosheng, Q. and Sham, A.W.L. 2020. Investigation of groundwater table distribution using borehole piezometer data interpolation: Case study of Singapore. *Eng. Geol.*, 271: 105590.
- Raheem, A.M., Naser, I.J., Ibrahim, M.O. and Omar, N.Q. 2023. Inverse distance weighted (IDW) and kriging approaches integrated with linear single and multi-regression models to assess particular physical-consolidation soil properties for Kirkuk city. *Model. Earth Syst. Environ.*, 72: 4080.
- Raheem, A.M. and Omar, N.Q. 2021. Investigation of distinctive physico-chemical soil correlations for Kirkuk city using spatial analysis technique incorporated with statistical modeling. *Int. J. Geo-Eng.*, 12(1): 1-21.
- Raheem, A.M., Omar, N.Q., Naser, I.J. and Ibrahim, M.O. 2022. GIS implementation and statistical analysis for significant characteristics of Kirkuk soil. *J. Mech. Behav. Mater.*, 31(1): 691-700.
- Ratshiedana, P.E., Abd Elbasit, M.A., Adam, E., Chirima, J.G., Liu, G. and Economon, E.B. 2023. Determination of soil electrical conductivity and moisture on different soil layers using electromagnetic techniques in irrigated arid environments in South Africa. *Water*, 15(10): 1911.
- Sahbeni, G., Ngabire, M., Musyimi, P.K. and Székely, B. 2023. Challenges and opportunities in remote sensing for soil salinization mapping and

- monitoring: A review. *Remote Sens.*, 15(10): 2540.
- Shahien, M. and Ogila, W.A. 2022. Prediction of geotechnical properties of deltaic clays by using regression analysis models. *Egypt. J. Pure Appl. Sci.*, 59(2): 36-62.
- Shareef, M., Hassan, N., Hasan, S. and Khenchaf, A. 2020. Integration of sentinel-1A and sentinel-2b data for land use and land cover mapping of the Kirkuk Governorate, Iraq. *Int. J. Geoinform.*, 16(3).
- Shareef, M.A. and Hasan, S.F. 2020. Characterization and estimation of date palm trees in an urban area using GIS-based least-squares model and minimum noise fraction images. *J. Ecol. Eng.*, 21(6).
- Shareef, M.A., Toumi, A. and Khenchaf, A. 2014. Estimation of water quality parameters using the regression model with fuzzy k-means clustering. *Int. J. Adv. Comput. Sci. Appl.*, 5(6).
- Shit, P.K., Bhunia, G.S. and Maiti, R. 2016. Spatial analysis of soil properties using GIS based geostatistics models. *Model. Earth Syst. Environ.*, 2(2): 1-6.
- Sridevy, S., Raj, M.N., Kumaresan, P., Balakrishnan, N., Tilak, M., Raj, J. and Rani, P. 2023. Mapping of soil properties using machine learning techniques. *Int. J. Environ. Clim. Change*, 13(8): 684-700.
- Taqi, A.H., Al Nuaimy, Q.A. and Karem, G.A. 2016. Study of the properties of soil in Kirkuk, Iraq. *J. Radiat. Res. Appl. Sci.*, 9(3): 259-265.
- Yadav, T., Singh, Y., Yadav, S.S., Singh, A. and Patel, T. 2023. Spatial variability in soil properties, delineation site-specific management division based on soil fertility using fuzzy clustering in Gwalior, Madhya Pradesh, India. *Int. J. Plant Soil Sci.*, 35(6): 49-78.
- Yang, L., Kaisheng, C., Mengfei, L. and Yingchao, W. 2020a. Study on failure of red clay slopes with different gradients under dry and wet cycles. *Bull. Eng. Geol. Environ.*, 79(9): 4609-4624.
- Yang, W., Zhao, Y., Wang, D., Wu, H., Lin, A. and He, L. 2020b. Using principal components analysis and IDW interpolation to determine spatial and temporal changes of surface water quality of Xin'anjiang river in Huangshan, China. *Int. J. Environ. Res. Public Health*, 17(8): 2942.
- Zhang, Y., Pu, S., Li, R.Y.M. and Zhang, J. 2020. Microscopic and mechanical properties of undisturbed and remoulded red clay from Guiyang, China. *Sci. Rep.*, 10(1): 1-14.
- Zhu, A.-X., Qi, F., Moore, A. and Burt, J.E. 2010. Prediction of soil properties using fuzzy membership values. *Geoderma*, 158(3-4): 199-206.
- Zolfaghari, Z., Mosaddeghi, M. and Ayoubi, S. 2015. ANN-based pedotransfer and soil spatial prediction functions for predicting Atterberg consistency limits and indices from easily available properties at the watershed scale in western Iran. *Soil Use Manage.*, 31(1): 142-154.



Petrography and Diagenesis of Thin-Bed Reservoirs from the Eastern Folded Belt of Bangladesh

Md. Mesbah Uddin Bhuiyan*† , Md. Anwar Hossain Bhuiyan**, Md. Saiful Islam*  and Umma Sabira* 

*Department of Oceanography, Noakhali Science and Technology University, Noakhali-3814, Bangladesh

**Department of Geology, University of Dhaka, Dhaka-1000, Bangladesh

†Corresponding author: Md. Mesbah Uddin Bhuiyan; mesbah.ocn@nstu.edu.bd

Nat. Env. & Poll. Tech.
Website: www.neptjournal.com

Received: 05-10-2023

Revised: 10-11-2023

Accepted: 17-11-2023

Key Words:

Thin-bed reservoir

Petrography

Diagenesis

Unconventional hydrocarbons

Energy resources

ABSTRACT

The main purpose of the study is to identify the thin-bed reservoirs of the Eastern Folded Belt (Sylhet and Bandarban) and characterize them with diligence. A detailed qualitative and quantitative analysis has been carried out. It is based on thin-section petrographic analyses of sandstone samples. These samples are from the reservoir horizons of the Sylhet region and Bandarban region fields. The purpose of this analysis is to characterize the textural and mineralogical properties.

Additionally, it aims to evaluate the post-depositional diagenetic changes. The results obtained from the field and laboratory analysis are studied extensively to characterize the thin-bed reservoirs. Samples from the Sylhet area are medium-coarse-grained, fairly sorted, tight packing, submature-mature sublithic characteristics. Contrarily, samples from the Bandarban region are mature-submature sublithic arenites, which are fine-medium-grained, moderately well-sorted, and moderately loosely packed. Despite the similarity of the detrital elements (quartz, feldspar, lithic grains, mica, etc.) in the two areas, silica cementation is more frequent in Sylhet region samples than early carbonate cementation in Bandarban region samples. Comparatively speaking, the sediments in the Sylhet region are more compact than those in the Bandarban region. The most important outcome of this study is that the thin bed of the unconventional reservoir and the conventional reservoir are in close proximity. The Thin-bed reservoir units of the Eastern Folded Belt are found to be medium to fine-grained and well sorted, with frequent alteration of sand-shale with the prevalence of parallel bedded sandstone. Average porosity is 4% to 12%, and pore spaces are interconnected. So, the permeability rate is good enough to flow the hydrocarbon through these pore spaces.

Most importantly, the thin bed and tight reservoir (average porosity 4% to 12%, but pore spaces are not interconnected) are not more prominent than 1 meter or 2 meters. Subsequently, though the vertical thickness is not so high, they keep up a momentous tirelessness of horizontal progression. On the contrary, at whatever point it comes to a conventional reservoir, the vertical thickness is higher than that of the unconventional reservoir. But their lateral persistence is not as long as unconventional ones.

INTRODUCTION

Bangladesh, a country with finite energy resources, has predominantly relied on natural gas as its primary energy source since 1990. The nation is presently undergoing a profound energy crisis. There is widespread concern regarding the potential depletion of natural gas reserves within 10 years or slightly longer, considering the projected annual increase in gas demand exceeding 5 percent. Since 2005, a notable scarcity of gas has been observed, primarily attributed to escalating gas demand surpassing the available supply (Islam & Lupin 2020). In the geographical expanse encompassing Bangladesh's central and eastern regions, particularly the northeastern Sylhet basin, the focus of exploration endeavors has been terrestrial investigations

(Rahman & Faupl 2003). The East Delta Hill Tract province in Bangladesh is a relatively uncharted territory within hydrocarbon provinces (Islam & Lupin 2020, Khan et al. 2018, Rahman & Faupl 2003).

Nevertheless, a comprehensive analysis of the factors contributing to the depletion of the exploratory well in the Sitakund anticline has failed to yield a coherent and scientifically substantiated explanation. Despite the considerable endeavors invested in the Chittagong Hill Tracts region, the outcomes have been lacking in cumulative or descriptive attributes. The Chittagong Hill Tracts of Bangladesh have garnered considerable attention from oil and gas companies due to the existence of anticlinal structures such as the Sitakund anticline, Sitapahar anticline,

Bandarban anticline, and Teknaf anticline (Connelly et al. 2019, Islam & Lupin 2020). As a result, the region has become a focal point for drilling activities by various companies in the oil and gas industry. The exploration efforts in the Chittagong Hill Tracts have thus far been limited to conventional anticlinal formations. An alternative methodology for exploration endeavors could potentially center on investigating unconventional and stratigraphic traps. The identification of these entities presents a challenge due to their lack of association with any specific fold structure. Instead, their presence is determined by the natural lithological changes, commonly referred to as facies variations, within the underlying rock strata (Connelly et al. 2019, Johnson & Nur Alam 1991, Rahman & Faupl 2003).

The Sylhet Basin, located in the north-eastern part of the Bengal Basin, has been examined in numerous geological studies (Alam et al. 2003, Johnson & Nur Alam 1991, Shamsuddin & Khan 1991). The stratigraphic succession was primarily established by lithologic correlation with sections in neighboring Assam and north-eastern India (Khan et al. 2010). The Bandarban structure lies in the middle zone of the folded part of the Chittagong hill tracts. Sedimentation in this part of the Bengal Basin was controlled by the collision of the Indian plate with the Burmese and the Tibetan plates and by the uplift and erosion of the Himalayan and Indo-Burma mountain ranges (Alam et al. 2003). The stratigraphic succession of the Chittagong-Tripura Folded Belt (CTFB) is of a Neogene age, starting with the basal Surma Group, which is overlain by the Tipam and Dupi Tila sandstones, respectively. The Surma Group of the Bengal Basin is the result of a major delta pro-gradation since the beginning of Neogene times (Miocene). It is thought to have been characterized by repetitive transgressive and regressive phases that resulted from subsidence as well as relative sea-level changes (Rahman & Faupl 2003).

In geology, the expression “thin beds” pertains to specific sedimentary layers or rock strata that exhibit a reduced thickness compared to the surrounding rock formations. The thickness of these thin beds exhibits a considerable range, spanning from a few millimeters to several centimeters. The differentiation of certain strata from their surrounding counterparts can be attributed to their unique characteristics, including but not limited to mineral composition, sedimentary structures, and chromatic properties (Bhuiyan & Hossain 2020). The observed stratification exhibits a series of slender layers, which may encompass a diverse range of sedimentary materials such as sand, silt, clay, or other analogous substances (Bhuiyan & Hossain 2020).

Thin-bed reservoirs present unique opportunities and challenges within hydrocarbon exploration and reservoir engineering. Thin bed reservoirs exhibit inherent diversity

due to multiple layers with distinct characteristics. The spatial distribution of porosity and permeability within geological layers can vary due to these strata’s heterogeneous composition, particle size, and depositional attributes (Ehrenberg 1993). These properties play a crucial role in facilitating the storage and movement of fluids within the subsurface environment. The fluid flow in thin-bed reservoirs is a complex phenomenon primarily attributed to the intricate interactions among the different layers. The efficacy of a reservoir characterized by thin beds is contingent upon the interconnectivity of its pore spaces, the existence of seals to impede fluid flow, and the overall permeability distribution across the layers (Bhuiyan & Hossain 2020, Ehrenberg 1993).

The reservoir horizons of the Sylhet and Bandarban fields exhibit variations in depth, thereby implying potential disparities in their petrographic and diagenetic characteristics. Reservoir characterization and field development necessitate precisely identifying variations in texture, mineralogy, and diagenetic alterations within the reservoir horizons of the two fields under investigation (Akter et al. 2023, Johnson & Nur Alam 1991, Khan et al. 2018). The present study aims to comprehensively analyze and compare reservoir horizons within the domains of petrography and diagenesis. The primary objectives of this study are to identify and analyze post-depositional diagenetic alterations in sandstone reservoirs, assess their impact on reservoir qualities, categorize the sandstones, and characterize the textural and mineralogical attributes of sandstone samples obtained from the Sylhet and Bandarban fields. By achieving these objectives, a comprehensive understanding of the diagenetic processes and their effects on reservoir properties can be obtained, contributing to the overall knowledge of sandstone reservoir systems (Akter et al. 2023, Ehrenberg 1990, Hossain et al. 2020, Johnson & Nur Alam 1991, Khan et al. 2018, Rahman & Faupl 2003).

The primary objective of this current investigation is to thoroughly analyze and assess the sandstones found within the Surma Group. This research aims to achieve two specific goals: i) to identify and thoroughly describe the thin-bed reservoirs present within the Surma Group sandstones, and ii) to elucidate the post-depositional diagenetic alterations that have occurred and their subsequent impact on the properties of these reservoirs.

MATERIALS AND METHODS

Field Investigation

To facilitate the objectives of the current investigation, an extensive fieldwork campaign was conducted in various road cuts and stream sections located within the Sylhet Trough and Bandarban district.

Sylhet

The Jaintiapur area, situated in the Sylhet district, has been selected as one of the study sites for investigation. It is geographically positioned between latitudes 25° 05' N to 25° 11' N and longitudes 92° 00' E to 92° 11' 15'' E (Fig. 1). For field investigation, three specific sections within the Jaintiapur area have been chosen.

The Shari River section is approximately 12 km south of Jaintiapur Thana and stretches from Sharighat to Tetulghat, near the border of India. This investigation is characterized by fault-controlled features observed along the river's meandering course. The lithology of this section consists of alternating bluish shale and yellowish sandstone, with intermittent calcareous sandstone bands.

The Tetulghat section primarily represents a stream-cut area that offers a highly advantageous view of the underlying sediments belonging to the Surma Group. The present section exhibits a remarkable sequence of alternating bluish-grey shale, silty shale, sandy shale, yellowish-brown sandstone, mudstone, and calcareous sandstone interbeds. Unconventional reservoirs, specifically thin beds, and tight reservoirs, are predominantly observed within this sub-section.

The examination of Nayagang River cut sections provides an opportunity for conducting field-based research aimed at the identification and assessment of unconventional reservoirs. The Naya Gang section exhibits a noteworthy sequence consisting of heterolithic beds, fine-grained sandstones with parallel lamination, and sandstones with trough cross-bedding. The bottom portion of the succession exhibits sedimentary structures such as laminated and trough crossbedding, which are indicative of conventional reservoirs. These features have been selected for a comparison analysis with unconventional reservoirs.

Bandarban

The Bandarban Anticline is a region of interest situated in the Bandarban district. It is geographically located between latitudes 22°05' N to 22°13' N and longitudes 92°08' E to 92°15' E. For field inquiry, four specific parts within the Bandarban area were selected.

The Sangu River section encompasses conventional and unconventional reservoirs and subsurface geological formations containing hydrocarbon resources. This section observes a prominent sandstone unit of considerable thickness, which is subsequently covered by a series of

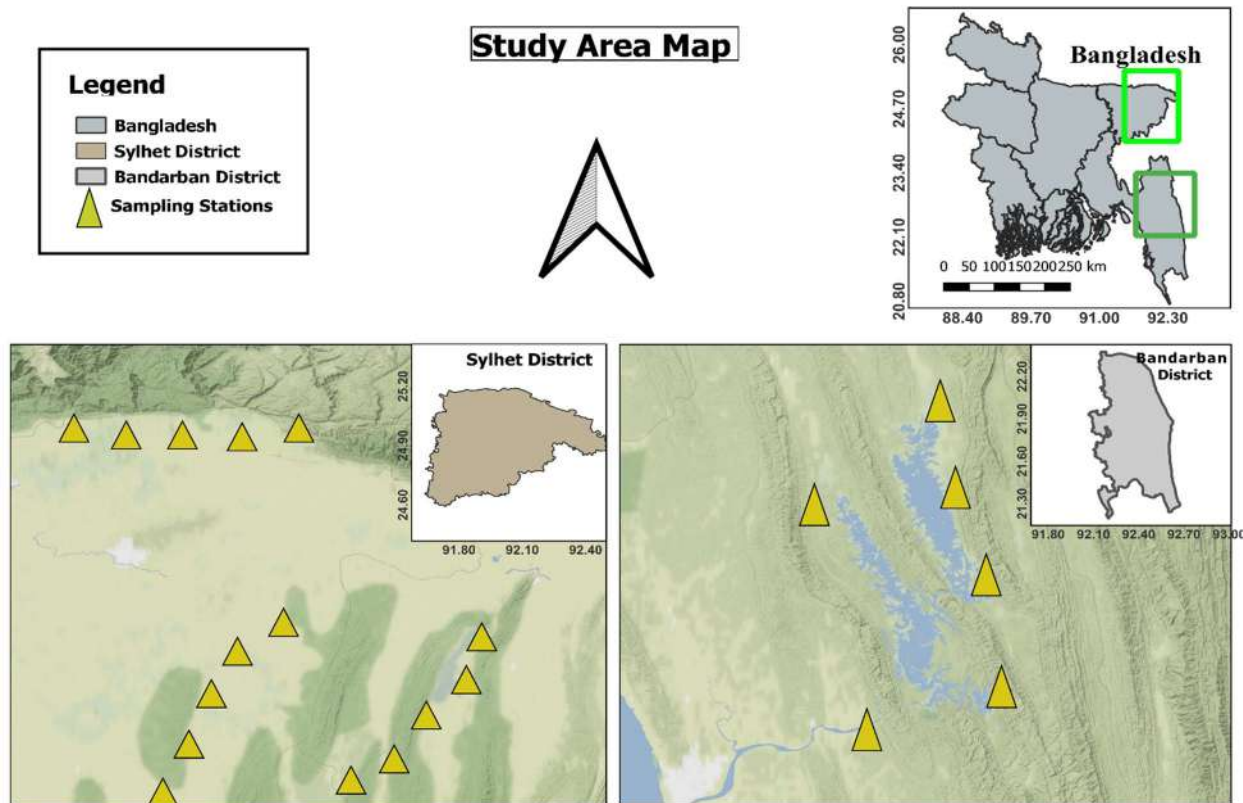


Fig. 1: Study area map showing sampling locations both in Sylhet region and Bandarban region.

heterolithic beds. These beds exhibit an intertidal sequence characterized by flaser, wavy, and lenticular bedding structures.

Bonopropat channel sand section is situated approximately 2 kilometers in the southwest direction from the town of Bandarban. The examination of sedimentary structures presented in this particular section, in conjunction with the associated facies assemblage, provides an advantageous opportunity to investigate the distinctive attributes of the unconventional reservoir.

The Shoilopropat section is situated approximately 5 kilometers to the south of Bandarban town. The Shoilopropat section is characterized by a remarkable sequence of hetero-lithic beds, comprising thin-bedded play, exhibiting alternating sandstone and shale layers.

Rupali Jhorna section is approximately 8 kilometres in the southwest direction from the urban center of Bandarban. This succession is characterized by a prominent sandstone unit at its base, followed by heterolithic beds.

Laboratory Analysis

The samples that were chosen for analysis were observed to be in either a loose or moderately indurated state. The impregnation process was deemed crucial for the successful preparation of each sample. Subsequent procedures were executed following the impregnation process to facilitate the production of thin sections.

Preparation of Standard Thin Section

At first, slabs were cut with a knife, and the prepared slabs were washed with water and acetone to remove gases. Araldite resin and Araldite hardener were mixed 1:1 and diluted with toluene to increase viscosity (30% glue, 70% toluene). After submerging the samples in it for 3 days, the solution penetrated them. The indurated samples were then heated in an oven at 40°C temperature for 2 days to increase their rigidity. One side of the impregnated slab was polished on a coarse grinding lap and a glass plate until smooth and flat. Then, this was mounted on a clean microscope slide, applying Araldite glue (resin: hardener = 1:1) on the polished surface. The sample's free face was ground on a coarse lap until light could pass through. The rock sample's thickness was tested regularly using a polarising microscope until it reached 0.03 mm. After adding Canada balsam to the heated rock slide, a thin coverslip was applied.

Staining

The requisite solution was prepared by dissolving 0.1 grams of Alizarin Red S in 100 milliliters of 0.2% hydrochloric acid (HCl). The experimental procedure involved the immersion

of precisely one-half of the slide into the designated solution for 2-3 minutes. Subsequently, the slide underwent a thorough washing process using distilled water. In the context of mineralogy, it has been observed that calcite exhibits a distinctive red coloration upon staining, whereas dolomite, on the other hand, does not manifest any discernible reaction.

Thin Section Petrography

The present study involved implementing a comprehensive qualitative and quantitative analysis, employing the esteemed Research Petrographic Microscope (LEICA), specifically the DM750P model. The images were captured utilizing the LEICA ICC50E module, seamlessly integrated with the microscope apparatus.

SEM

The 7600F is a state-of-the-art field-emission scanning electron microscope (FE-SEM) designed to visualize and image objects at the nanoscale level. A series of images were captured using the JEOL JSM-7600F scanning electron microscope (SEM) equipped with a backscattered electron detector operated at the Department of Nanomaterials and Ceramic Engineering (NCE), Bangladesh University of Engineering and Technology (BUET), Dhaka.

RESULTS AND DISCUSSION

Texture

Based on visual comparisons to a reference slide, the analysis of grain size estimations in thin slices suggests that the Bhuban sandstone generally exhibits a finer-grained nature in comparison to the Bokabil sandstone. There is observable evidence of a progressive increase in grain size, consistent with the overall geological and sedimentological evolution of the Bengal Basin. This evolution is characterized by a gradual shallowing of the deltaic basin, leading to the dominance of the fluvial system at the uppermost level. The findings of the study suggest that a majority of the grains exhibit subangular to subrounded shapes, as well as subspherical to subprismoidal forms.

Based on the findings of this investigation, it has been determined that the sandstones within the Surma Group exhibit a high degree of sorting, ranging from well to very well sorted. The collected data reveals that among the total number of samples analyzed, 61% exhibit a well-sorted nature. Furthermore, 22% of the samples demonstrate a very well-sorted characteristic. Additionally, 11% of the samples fall within the range of being classified as well as very well sorted. Lastly, a minor proportion of 6% of the samples display a moderate level of sorting (Fig. 2).

The majority of the collected samples exhibit a matrix composition ranging from 1% to 4%, with only a limited number of specimens being entirely devoid of any matrix material. The analysis of grain size, sorting, and matrix composition in the sandstone samples indicates a predominance of texturally mature and clean characteristics.

Porosity

The quantification of thin section porosity was conducted through a visual comparative analysis for every individual sample. The findings consistently demonstrated that thin section porosity values were consistently lower than those obtained through porosimeter analysis, exhibiting an average disparity of 13.5 percent (Fig. 3).

The findings of the current investigation demonstrate that the porosity of thin-bed reservoirs within the Bhuban formation exhibits a range of 4 to 12% when analyzed using thin-section techniques. The findings of this investigation

demonstrate a discernible pattern in the porosity values observed within the samples obtained from the Bhuban Formation. Specifically, it is observed that the porosity values exhibit a decreasing trend up to a certain depth, followed by a subsequent increase to a significant extent at greater depths.

Detrital Components

The detrital components observed in this study are the by-products resulting from the disintegration and decomposition processes of pre-existing rocks, including igneous, metamorphic, and sedimentary rocks (Fig. 4 & 5). These components are subsequently deposited within the basin following varying durations of transportation via water and/or wind mechanisms.

Detrital Framework Grains

The detrital framework grains found within sandstone

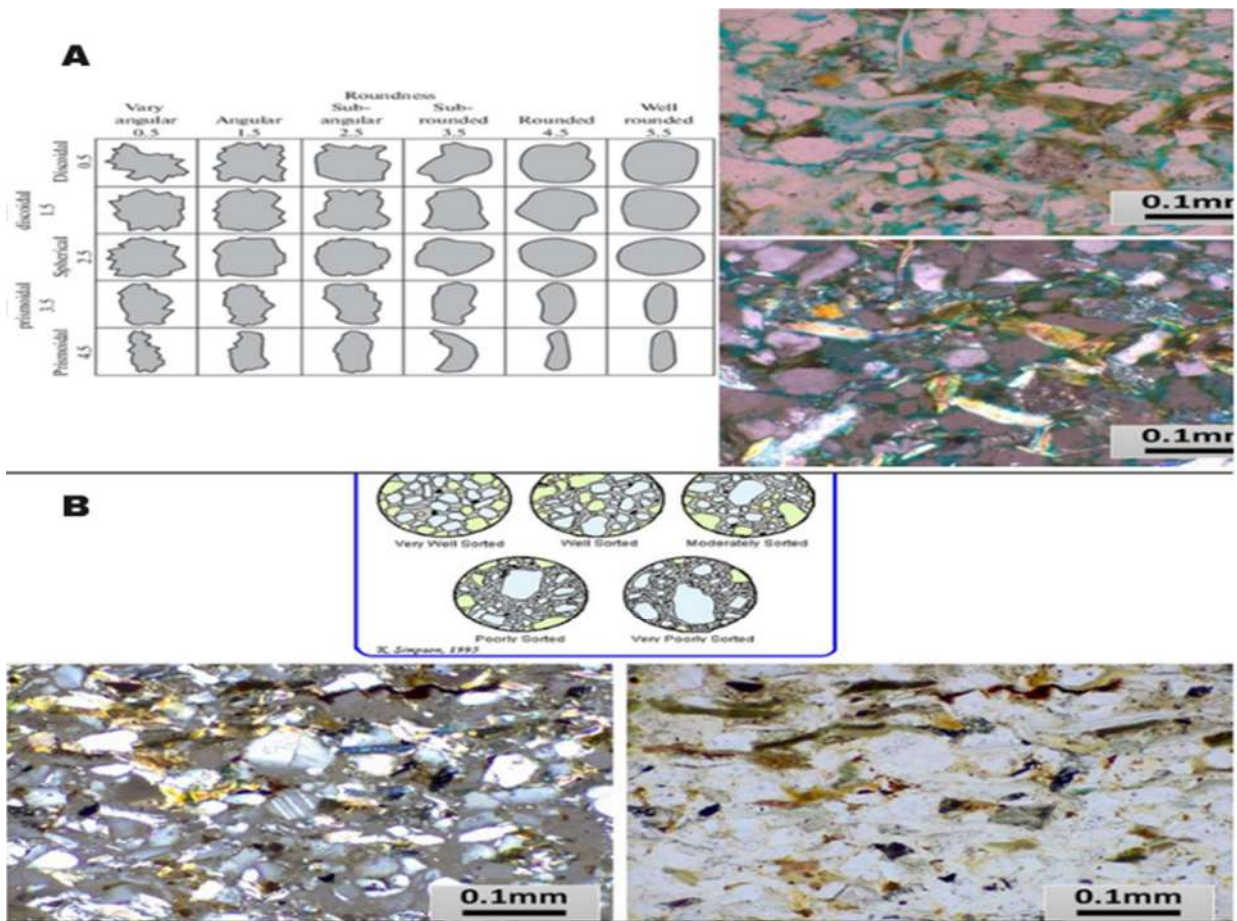


Fig. 2: A visual comparison chart for estimating roundness and sphericity (after Power 1982), subangular to subrounded and Subspherical (A), well to very well sorted (B).

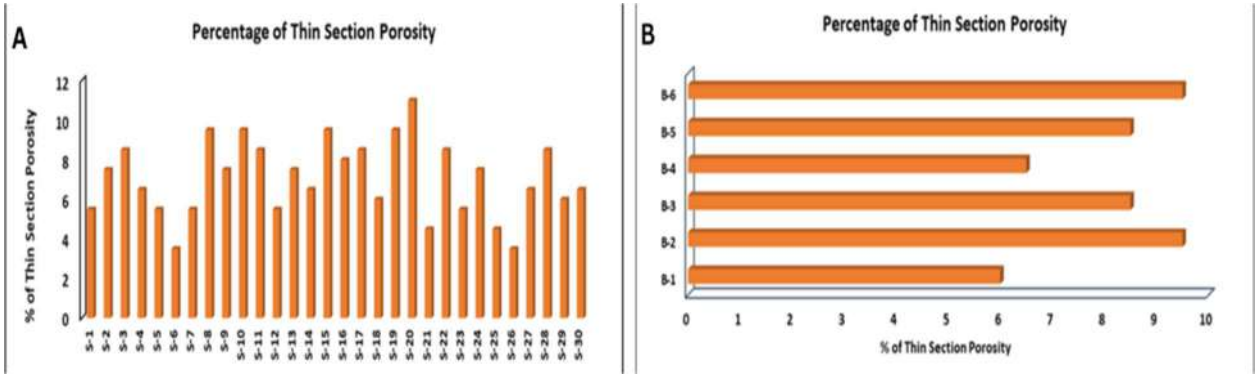


Fig. 3: Percentage of thin section porosity at Sylhet region (A) and Bandarban region (B).

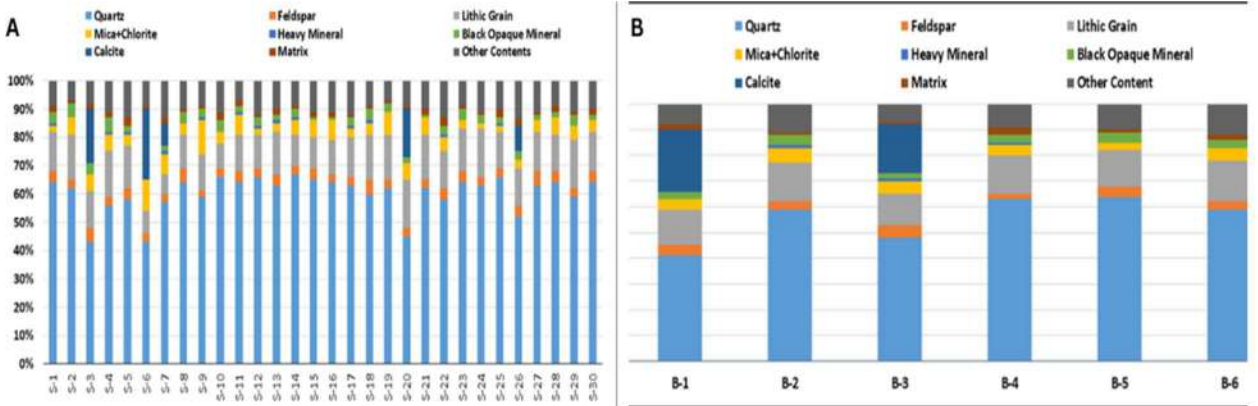


Fig. 4: Mineralogical composition from Sylhet region (A) and Bandarban region (B).

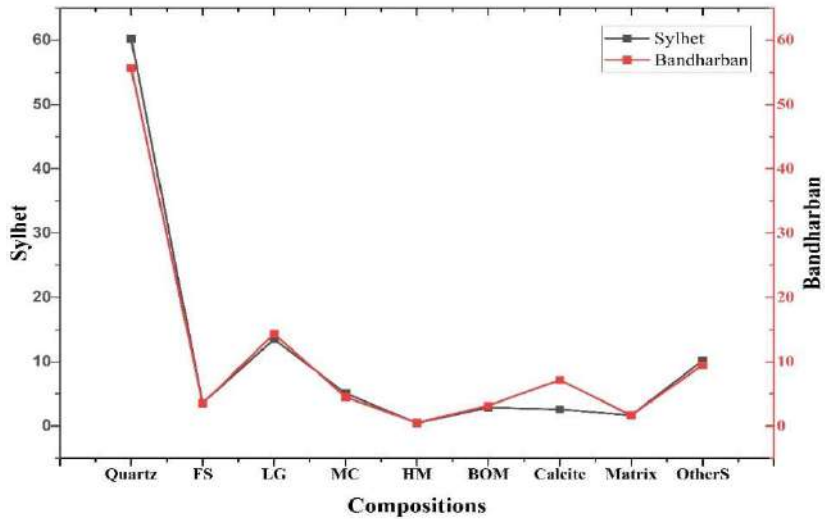


Fig. 5: Comparison of Thin section petrographic data (mineralogical composition, including Quartz, FS=Feldspar, LG=Lithic Grain, MC=Mica+Chlorite, HM=Heavy Mineral, BOM=Black Opaque Mineral).

Table 1: Framework of grains in the studied samples from Sylhet region and Bandarban Region.

Major	Minor	Minor Accessories
Quartz	Chlorite	Non-opaque heavy minerals
Feldspar	Mica Muscovite	Dark opaque grains
Lithic Grains	Biotite	Organic matters

deposits consist of sand-sized particles that can be classified as either monomineralic or polymineralic. Monomineralic grains, such as quartz, feldspars, and mica, are composed of a single mineral species. On the other hand, polymineralic grains, known as lithic grains, are comprised of multiple mineral species (Table 1).

Quartz, as determined through meticulous analysis, has been identified as the predominant constituent within the sandstone samples under investigation. The mineral quartz is primarily found in two forms: monocrystalline grains, which can be either strained or unstrained, and polycrystalline grains (Fig. 6).

Siltstone fragments are commonly encountered lithic grains of sedimentary origin, typically comprised of silt-sized quartz, feldspars, mica, and various other constituents, which are held together by a clay-rich matrix or alternative cementing agents. The lithic types mentioned herein are frequently encountered and account for a range of 5% to 20% in terms of the overall lithic grain composition (Fig. 6).

Cherts exhibit a dominant composition of quartz, with the occurrence of larger quartz crystals as well as minor impurities. The present study focuses on the characterization

of ubiquitous rock fragments, which are found to constitute a significant proportion ranging from 1% to 7% of the overall lithic grains.

Quartz-mica aggregates potentially originate from igneous sources. These grains consist primarily of quartz and mica minerals, lacking any discernible preferred planar fabric. The lithic grains under consideration in this study are found to comprise a range of 1% to 6% of the overall sample (Fig. 6).

The present study investigates the relative abundance of lithic grains within the sample, specifically focusing on a subset of grains categorized as “types of grains.” These particular grains are found to comprise a range of 4% to 13% of the total lithic grain population.

Among the detrital framework grains of sandstone, feldspars hold significant importance alongside quartz and lithic grains. Our findings reveal that feldspars account for a range of 0 to 3% and 1% to 4% in these sandstone formations. The sandstone samples under investigation exhibit the coexistence of both potassium and plagioclase feldspars (Fig. 6).

Chlorite, a prevalent detrital mineral, has been observed in abundance within the sandstone samples under investigation. The observed phenomenon manifests as substantial detrital flakes measuring between 0.2 and 0.5 mm in size. These flakes frequently exhibit splayed-out ends and are distinguished by their distinct green hue and pronounced pleochroism (Fig. 6 K-L).

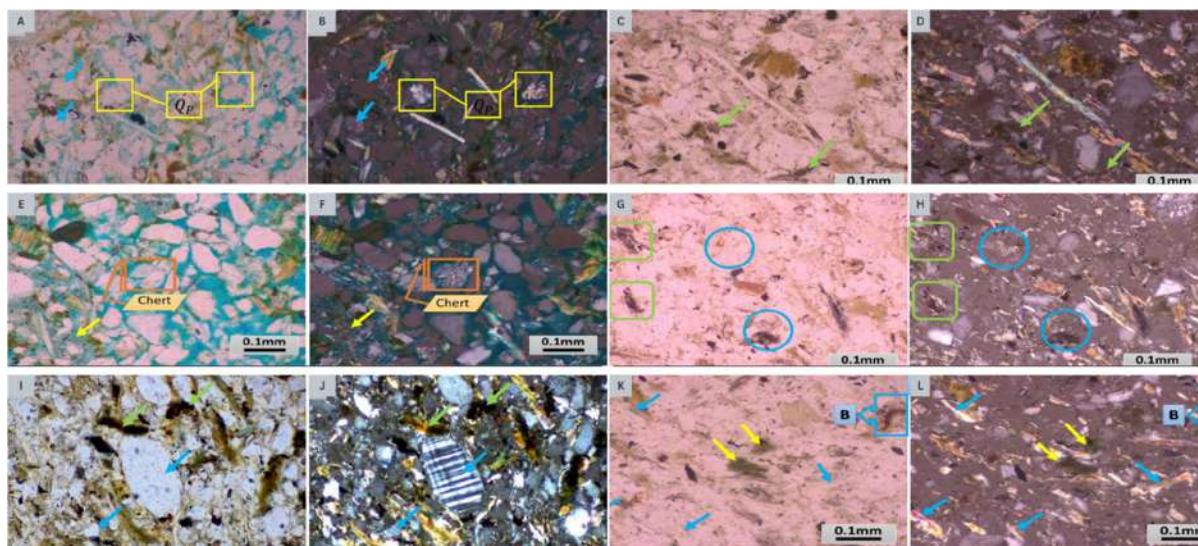


Fig. 6: A-B: Monocrystalline quartz (blue arrow) and polycrystalline quartz (yellow box); C-D: Siltstone fragments (green arrow), E-F: Chert (orange box) and matrix (yellow arrow); G-H: Quartz-mica aggregates (green box) and chert (blue circle); I-J: Feldspar (blue arrow) and organic matter (green arrow); K-L: Chlorite (yellow arrow), muscovite (blue arrow) and biotite (blue box).

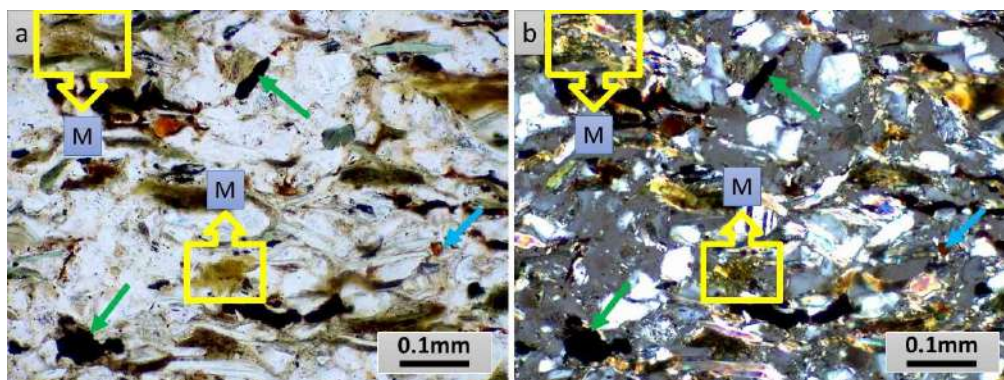


Fig. 7: Heavy minerals (blue arrow), indeterminate (green arrow) and matrix (yellow box).

The present investigation employs thin-section petrographic analysis to examine the occurrence of muscovite and biotite as detrital flakes, characterized by frequently observed splayed-out ends (Fig. 6). The relative abundance of muscovite is typically greater in comparison to biotite. Chlorite and mica, two distinct mineral species, are collectively classified as monocrystalline phyllosilicates within the realm of mineralogy. The sandstones of the Bhuban Formation exhibit a notable presence of constituents ranging from 2% to 11% within thin-bed reservoirs.

Various categories of dense minerals are present in small quantities as subordinate sedimentary particles, collectively comprising a range of 0 to 3% of the overall constituents of the rock. The assemblage of heavy minerals comprises various mineral species, such as garnet, zircon, tourmaline, epidote, rutile, Kyanite sillimanite, hornblende, augite, and other unidentified black opaque grains (Fig. 7). The observed range of black opaque grains spans from 0% to 3% of the total rock constituents.

The matrix comprises fine clastic mineral particles that are interstitial to the framework grains and are deposited concurrently with the supporting grains. The analysis of point count data reveals that the overall matrix content is consistently low, with a majority of the samples exhibiting levels below 4%.

The identification of the mineralogy within the matrix is challenging due to its exceptionally fine-grained composition. The identified constituents of the specimens under investigation are confirmed to be quartz and clay minerals, specifically kaolinite, illite, and chlorite (Fig. 7).

In certain instances, the pseudo matrix exhibits similarities to the matrix. The identification of pseudomatrix can be accomplished through the application of specific criteria, as established by Dickinson in 1970 (Dickinson 1970).

Authigenic Components

The presence of authigenic kaolinites has been exclusively observed within the lower segment of the Bhuban formation sequence. The findings from scanning electron microscopy (SEM) analysis and eye estimation techniques reveal that the presence of authigenic kaolinite in the rock composition is limited to a range of 0.1% to 2%. Two distinct modes of occurrence have been duly acknowledged in the scientific literature. The first mode, referred to as pore-filling kaolinites, is characterized by the absence of any discernible association with precursor minerals (Fig. 8). These kaolinites are observed to occupy discrete pore spaces within well-sorted sandstones. In the context of thin sections, the observed specimens exhibit a colorless appearance when examined under plane-polarized light. Furthermore, their birefringence, as determined under a 20X Nicols microscope, is found to be relatively low. The composition of these specimens primarily consists of particles of kaolinite, with an average size in the range of several microns.

The assemblage of authigenic non-clay minerals in the studied geological formation encompasses various mineral species, such as quartz, ferroan calcite, and siderite, among others. The aforementioned phenomena manifest themselves in the form of substances that fill the pores and replace the grains. The presence of authigenic quartz, specifically in the form of quartz overgrowths, has been identified as a prevalent diagenetic mineral within the Bhuban sandstones located in the Eastern folded belt of Bangladesh. The presence of quartz overgrowth cement in thin-bed reservoir sandstones is observed to range from 0 to 1% and 1% to 4% of the overall rock composition (Fig. 9).

Quartz overgrowths within thin sections, when observed through the conventional polarizing microscope, can be identified based on two distinct characteristics. Firstly, the presence of a “dust line” demarcating the boundary between the detrital grain nuclei and the overgrowths serves

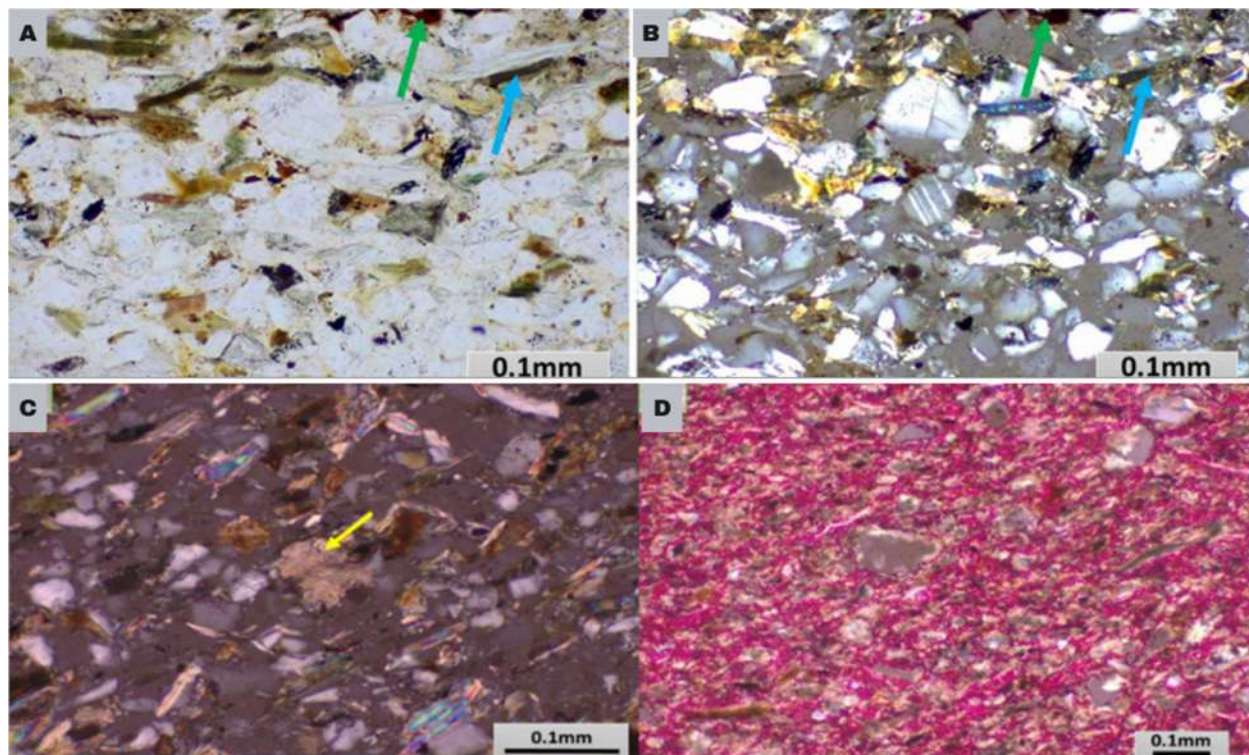


Fig. 8: A-B: Pore-filling grain (green arrow) and chlorite rim (blue arrow); C-D: Isolated pore-filling calcite (yellow arrow).

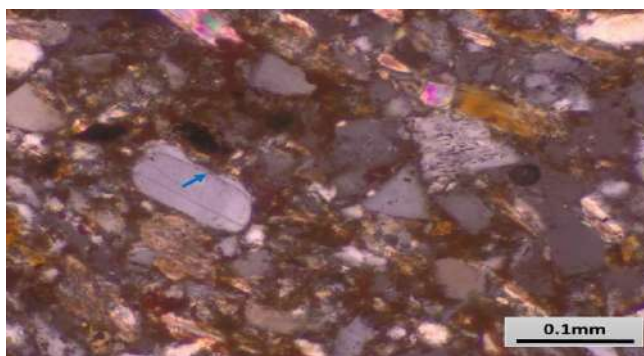


Fig. 9: Photomicrograph of quartz overgrowth.

as a reliable indicator. Alternatively, the identification can be made by observing the well-formed crystal faces of the overgrowths, which exhibit a distinctive morphology (Fig. 9). The formation of dust lines is a prevalent phenomenon attributed to the presence of a delicate layer of illite clay, characterized by its discernible high birefringence. In addition to the presence of clay films or coatings, the occurrence of dust lines is frequently observed due to the formation of various impurities between the overgrowths and nuclei.

Calcite cement, an extensively prevalent authigenic mineral, has been observed within the sandstones of the

Surma Group in the Eastern folded belt of Bangladesh. The petrographic examination of calcite cement reveals its colorless appearance, variable relief under plane light, and rhombohedral cleavages. The Bhuban sandstones exhibit a variable calcite cement content, ranging from 0% to 26% of the overall rock composition. The presence of calcite cement within geological formations manifests in two distinct forms: i) as isolated pore-filling and replacive Fe-calcite cement and ii) as poikilotopic ferroan calcite.

Isolated pore-filling and replacive Fe-calcite cement: The prevalent forms of calcite cement within the Surma sandstones (Fig. 8) encompass the infilling of isolated pore spaces by

ferroan calcite cement, as well as the replacement of detrital grains by calcite cement. In the present study, it has been observed that calcite predominantly undergoes replacement in the marginal region of detrital grains. However, it is noteworthy that certain samples exhibit extensive grain replacement, leading to a substantial augmentation in the proportion of ferroan calcite. Specifically, the content of ferroan calcite has been found to range from 17% to 35% of the overall constituents of the rock.

Poikilotopic ferroan calcite: The occurrence of poikilotopic ferroan calcite cement is limited to a small number of samples, wherein it fills the pore spaces, resulting in a complete reduction of both porosity and permeability to a value of zero (Fig. 8). Through the SEM method, it has been determined that poikilotopic calcite cement accounts for approximately 35% to 41% of the overall rock components. These crystals exhibit a euhedral morphology and display a size range spanning from 0.5 mm to over 1.0 mm. The phenomenon of poikilotopic cement crystallization has been proposed to involve the expansion of intergranular space, leading to subsequent rearrangements in the packing of detrital grains and an increase in the separation between these grains (Dapples 1971).

Classification and Nomenclature of the Studied Sandstone Samples

By the established criterion, it has been determined that all specimens under examination exhibit a matrix content of less than 15%. Consequently, these specimens have been initially categorized as clean sands or arenites. The proportions of quartz, feldspars, and lithic grains were recalculated to yield a total of 100% (Fig. 10).

Diagenesis

The term diagenesis encompasses a comprehensive array of physical, physico-chemical, and chemical processes that occur after sediment burial. The sediments undergo diagenetic alterations after their burial, resulting in their transformation into lithified rocks. The diagenetic alterations in the composition and texture of sediments give rise to the modification of the reservoir properties of sandstones.

Diagenetic Processes

The Surma Group of sediments is primarily characterized by a nearly equal distribution of alternating sandstones and shales, accompanied by lesser amounts of siltstones and minimal conglomerates. The sandstone formations, which consist of both detrital and authigenic constituents, predominantly exhibit characteristics of fine-grained and well-sorted arenites, with a minor presence of matrix material ranging from 0 to 4%. The diagenesis of Surma sandstones in the Eastern folded belt structure is characterized by notable alterations like grain contacts and the deformation of soft lithic grains.

Compaction

The initial diagenetic process that exerts an influence on sand deposits shortly after their deposition and subsequent burial beneath the sediment-water interface is known as compaction. The overburden pressure experienced by sediments primarily drives this process. The observed phenomenon exhibits a positive correlation between its intensity and the depth of burial.

The initial reaction of compaction entails the reconfiguration of detrital grains, commonly referred

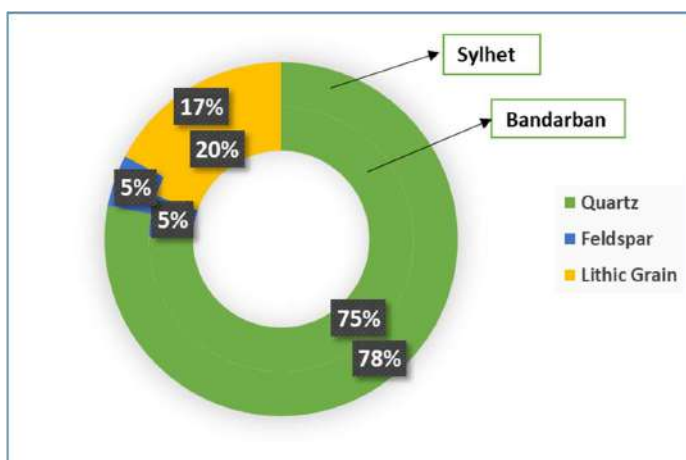


Fig. 10: Relative abundance of Quartz, Feldspar, and Lithic grains (recalculated to 100%).

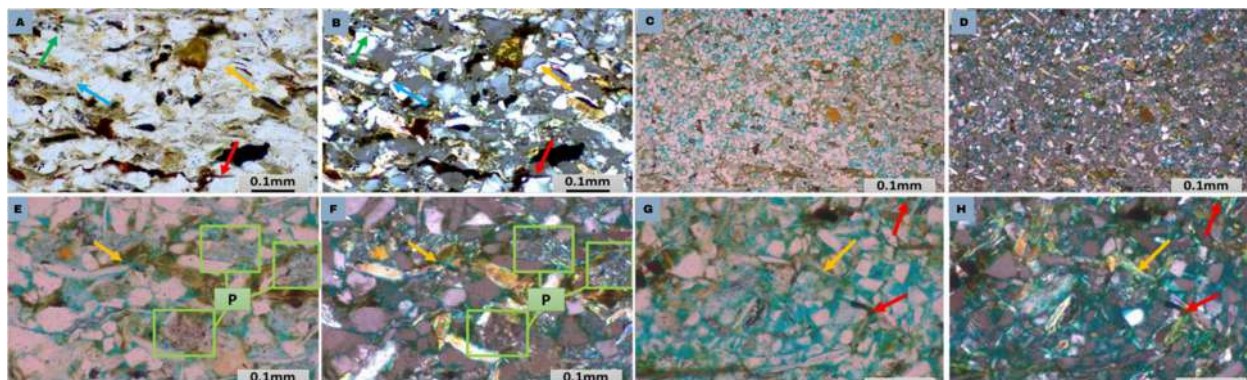


Fig. 11: A-B: Concavo convex (orange arrow), grain coating (red arrow), point contact (blue arrow) and suture contact concavo (green arrow); C-D: Pseudomatrix and mica fracturing; E-F: Pseudomatrix (green box) and mica fracturing (orange arrow); G-H: Gentle bending (orange arrow), grain fracturing and tight packing (red arrow).

to as packing readjustment. This phenomenon leads to a more densely packed arrangement of grains (Fig. 11). The readjustment is characterized by alterations like grain contacts. Initially, at shallow depths, the contacts between grains are primarily point contacts. However, as the depth increases, these contacts gradually transform into elongated, concavo-convex, and sutured contacts (Fig. 11).

Ductile or labile grains, including shale, claystone, siltstone, phyllite, schist fragments, and others, play a significant role as constituents within Surma sandstones. These sandstones undergo permanent deformation as a result of compression from neighboring rigid grains in response to the applied overburden pressure. The process of compression frequently results in the displacement of pliable lithic particles into neighboring pore spaces, causing them to undergo significant deformation and adopt the characteristics of an interstitial matrix, commonly known as a pseudo-matrix (Fig. 11).

The occurrence of flexural deformation in mica and chlorite minerals, as well as the propensity for brittle fracture in feldspar, lithic grains, and heavy minerals, is a prevalent phenomenon observed within the Surma Sandstone formation. The phenomenon of mica bending is observed to vary in response to the magnitude of overburden stress. However, under more substantial overburden stress, mica undergoes more pronounced bending, resulting in a distinctive zigzag shape. In such cases, the bending may be accompanied by fracturing (Fig. 11). Feldspars exhibit a higher degree of susceptibility toward fracturing (Fig. 11). This fracturing phenomenon primarily occurs along the cleavage planes of feldspars. However, it is worth noting that fracturing is also a prevalent occurrence in brittle lithic grains (Fig. 11).

Pressure Solution

The phenomenon of pressure solution entails the dissolution of mineral grains occurring at the precise locations where they come into contact under the influence of external stress. This process leads to the formation of densely packed grains and subsequently enhances the compaction of the surrounding rocks. Within the Surma Sandstones, the dominant mineral implicated in pressure solution phenomena is quartz. As a secondary process, quartz overgrowths have precipitated from the fluid residing within the pore spaces. The investigation of pressure solution phenomena within the current geological sequence has primarily focused on the Bhuban Formation. At the same time, its significance within the BokaBil Formation appears to be comparatively less pronounced. The aforementioned phenomenon represents a significant contributor to the formation of quartz overgrowth cement.

Cementation

The process of cementation, which involves the chemical precipitation of authigenic minerals from subsurface pore fluids, is a significant phenomenon in geological formations. These minerals, commonly referred to as authigenic minerals or cement, play a crucial role in the consolidation and alteration of sedimentary rocks. The examined samples have exhibited the presence of various cementing minerals, including silica in the form of quartz overgrowth, ferroan calcite, chlorite, kaolinite, illite, and siderite. The presence of cementitious materials is observed consistently across the entire sequence, with occasional occurrences limited to specific horizons.

The occurrence of secondary enlargement of quartz grains, specifically in the form of quartz overgrowths, has

been extensively documented in the sandstone samples under investigation. These overgrowths are commonly observed in abundance within the lower section of the sequence, while their presence is relatively scarce in the upper portion. The presence of more sophisticated forms of quartz overgrowths (Fig. 9) in the lower portion of the sequence indicates a significant flow of pore water enriched with silica throughout the corresponding sedimentary layers.

The phenomenon of silicate replacement by calcite and the dissolution of feldspars have been observed in numerous samples. The present study reveals compelling evidence about the phenomenon of silicate replacement within calcareous sandstones, as well as the dissolution of feldspars, predominantly observed in the lower portion of the investigated strata. It is important to note that these occurrences are limited to specific horizons within the geological formation under examination.

The prevalence of calcite cement is the predominant diagenetic characteristic observed in the examined specimens. The calcite cement present in the studied sample exhibits a ferroan composition, indicating the presence of iron within its mineral structure. The cementation process has effectively occupied all pore spaces, resulting in a complete reduction of both porosity and permeability to an absolute minimum. The present study investigates a specific form of cementation characterized by the loose arrangement of particles, colloquially referred to as “floating” grains, and the absence of compactional features and most diagenetic minerals. The phenomenon of calcite generation of this particular type has been observed in a limited number of samples (Fig. 12).

Authigenic chlorites, specifically chlorite rims and pore-filling chlorites, have been identified as prevalent diagenetic minerals in the sandstone samples examined (Fig. 12).

These chlorites manifest as grain-coating chlorites and pore-filling chlorites and have been observed across a wide range of sandstone specimens. The presence of alternative chlorite cement has been observed, albeit infrequently. The presence of chlorite rims has been observed to exert an indirect influence on the preservation of porosity through the inhibition of quartz overgrowth growth. The mechanisms responsible for the generation of these enigmatic features, characterized by their delicate occurrence and intricate textural associations with detrital grains and diagenetic minerals, remain elusive.

The final diagenetic phase observed in Early Miocene sandstones, specifically in the lower portion of the sequence, is the cementation by kaolinite. The prevalence of pore-filling kaolinite (Fig. 12) surpasses that of in situ alteration kaolinite. However, it is worth noting that the impact of kaolinite precipitation on porosity is comparatively less significant when compared to the effects of Fe calcite or quartz cementation.

The presence of authigenic illite, a diagenetic mineral, was observed in the sandstone samples. In terms of volumetric considerations, its impact on reservoir properties is relatively inconsequential. However, it assumes a catalytic role in facilitating pressure solution (Fig. 12) of quartz grains, which serves as a prominent mechanism for the formation of quartz overgrowth cement.

Replacement

The Surma sequence typically exhibits the replacement of silicates, such as quartz and feldspars, as well as certain lithic grains. The predominant replacive agents observed in this study are primarily composed of calcite, with a lesser extent of chlorite. The phenomenon of replacement has been observed to manifest primarily through the following

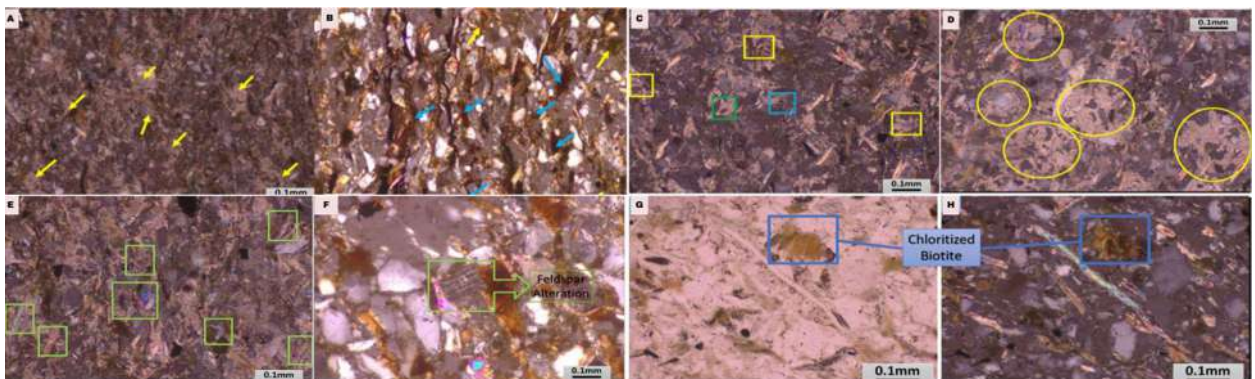


Fig. 12: A-B: Calcite and chlorite cementation (yellow arrow), kaolinite/illite cementation (blue arrow); C-D: Feldspar replacement by calcite (blue box), remnant quartz (green box), corroded grain and quartz replacement by calcite (yellow box), quartz grains replacement by calcite (yellow circle); E-F: Mica replacement by calcite (green box) and feldspar alteration along the cleavage plane (green arrow); G-H: Chloritized biotite (blue box)..

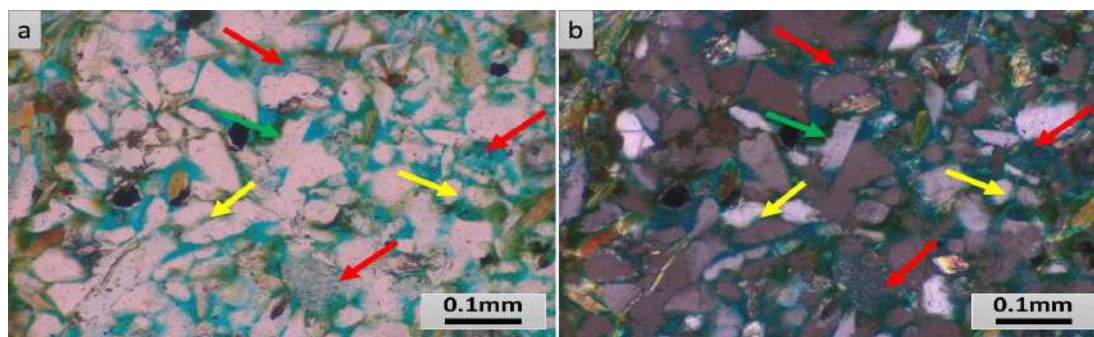


Fig. 13: Dissolution of quartz (yellow arrow), dissolution of feldspar (green arrow) and dissolution of lithic grains (red arrow).

modalities: a) Corroded replacement, characterized by the presence of corroded and crenulated grain boundaries. Quartz predominantly serves as the substituting agent, wherein it undergoes replacement by calcite (Fig. 12). b) Skeletal Remnants: The presence of skeletal grains is noted after the process of replacement. The phenomenon of skeletal replacement has predominantly been observed in feldspars and lithic grains. The replacement of feldspar grains occurs specifically along the cleavage planes or areas of weakness, while the lithic grains' siliceous component undergoes replacement by calcite (Fig. 12). c) Remnant Replacement: A minuscule fraction of detrital grains, such as quartz or feldspars, has been observed to persist as remnant grains after the replacement process. The presence of calcite cement in the vicinity of remnant grains is a commonly observed phenomenon. Multiple remnants exhibit consistent extinction properties that resemble the individual components of a singular grain (Fig. 12).

The process of biotite alteration, resulting in the formation of chlorite, is commonly referred to as chloritized biotite. Chloritized biotite (Fig. 12) exhibits distinctive characteristics, including a laminar morphology and a brown hue with a discernible greenish undertone.

Alteration

The present study has yielded compelling evidence of discernible alteration within the examined sandstone samples. The petrographic evidence about alteration exhibits a degree of ambiguity, as observed in instances where a grain possessing the characteristic geometry of a precursor mineral, such as feldspar, is found to be comprised of novel minerals, specifically small aggregates or filaments of kaolinite.

The alteration of feldspar and biotite minerals has been observed and documented (Fig. 12). The present investigation has revealed the occurrence of both partial and complete alterations within the examined sandstone specimens. Within the realm of feldspars, it has been

observed that plagioclase and orthoclase feldspars exhibit a higher degree of susceptibility to alteration when compared to their microcline counterparts.

Dissolution

The phenomenon of dissolution of soluble constituents in sandstones, whether completely or partially, has been documented in select samples of the Early Miocene sequence within the Eastern folded belt structure. The aforementioned process has induced the formation of secondary porosity within the sandstone formations, thereby leading to a general augmentation in the overall porosity of said rocks (Fig. 13). The dissolution of various materials, including feldspars, lithic grains, and ferroan calcite cement, has been observed and documented. In certain specimens, the dissolution of constituents within the rock matrix is observed to occur at a significant magnitude, resulting in the development of porosity. This porosity, attributed to dissolution processes, accounts for approximately 35% to 40% of the overall porosity exhibited by the rock samples under investigation.

CONCLUSION

The petrographic investigations were carried out quantitatively and qualitatively on thin layers of the sandstone samples from the Sylhet and Bandarban regions. The sediments in Sylhet samples are submature-mature, densely packed, subangular-subrounded, poorly sorted, and of medium-coarse grain size. Contrarily, Bandarban samples are mature-sub mature, moderately-loosely packed sediments with fine-medium-grained, subangular-subrounded, moderate-well sorted, and these characteristics. The sandstones in both fields are quartz arenites that are subarkosic and mostly made of quartz, feldspar, mica, lithic grains, clay, and other authigenic minerals other than clay. The field study demonstrates that thin beds are fine to medium-grained (sometimes very fine-grained), sub-angular to sub-rounded, and well-sorted. Frequent change of sand-shale with the predominance of

parallel bedded sandstone is observed. Both inner-granular and intra-granular, along with the pore canal, are the recognizable proof observed from laboratory analysis. The average porosity ranges from 4% to 12%, most of which are interconnected. The pore spaces within the tight reservoir are not interconnected despite a considerable amount of pore spaces (average porosity 4% - 8%) there. Here, the permeability is very low.

On the other hand, conventional reservoirs are medium to fine-grained, well-sorted, and contain an average porosity of 10% to 20%, most of which are connected. The foremost imperative disclosure made from this study is that the thin beds of the unconventional and conventional reservoirs have similar pro-perm values. The most vital difference is that the thickness of the thin bed and tight reservoir is not more than 1 or 2 meters. Along these lines, even though the vertical thickness is not so high, they keep up an extensive lateral persistence. Therefore, thin-bed reservoirs might be considered as good as conventional ones. Bangladesh is facing an impending energy crisis. To reduce the dependency on the conventional reservoir, serious steps have to be focused on an unconventional reservoir, particularly a thin-bed reservoir.

ACKNOWLEDGEMENTS

We are especially grateful to the Department of Nanomaterials and Ceramic Engineering (NCE), Bangladesh University of Engineering and Technology (BUET), for the SEM analysis of our samples collected from the fieldwork. We acknowledge the field assistance received from the residents of the study areas as well as the colleagues from the University of Dhaka and Noakhali Science and Technology University for their dedicated and sincere support. We would like to thank both the laboratories of the Department of Geology, University of Dhaka, and the Department of Oceanography, Noakhali Science and Technology University.

REFERENCES

Akter, M., Rahman, M.J.J., Ma, M., Hossain, D. and Khanam, F. 2023. Depositional and diagenetic controls on reservoir quality of Neogene Surma Group from Srikail Gas Field, Bengal Basin, Bangladesh. *Minerals*, 13(2): 283. DOI: 10.3390/min13020283

- Alam, M., Alam, M.M., Curray, J.R., Chowdhury, M.L.R. and Gani, M.R. 2003. An overview of the sedimentary geology of the Bengal Basin in relation to the regional tectonic framework and basin-fill history. *Sed. Geol.*, 155(3-4): 179-208. DOI: 10.1016/S0037-0738(02)00180-X
- Bhuiyan, A.H. and Hossain, S. 2020. Petrographic characterization and diagenetic evaluation of reservoir sandstones from Smørbukk and Heidrun fields, offshore Norway. *J. Nat. Gas Geosci.*, 5(1): 11-20. DOI: 10.1016/j.jnggs.2019.12.001
- Connelly, D.P., Sikder, A.M. and Presser, J.L.B. 2019. Tectonic Evolution of Eastern Folded Belt of Bangladesh The Massive Australian Precambrian-Cambrian Impact Structure (MAPCIS) part one. February 1992.
- Dickinson, W.R. 1970. *Fins. J. Sediment. Petrol.*, 40(2): 695-707.
- Dapples, E.C. 1971. Physical classification of carbonate cement in quartzose sandstones. *SEPM J. Sed. Res.*, 41(1): 1865. DOI: 10.1306/74d72220-2b21-11d7-8648000102c1865d
- Ehrenberg, S.N. 1990. Relationship between diagenesis and reservoir quality in sandstones of the Garn. *Am. Assoc. Petrol. Geol. Bull.*, 74(10): 1538-1558.
- Ehrenberg, S.N. 1993. Porosity. *AAPG Bull.*, 77(7): 1260-1286.
- Hossain, M.S., Xiao, W., Khan, M.S.H., Chowdhury, K.R. and Ao, S. 2020. Geodynamic model and tectono-structural framework of the Bengal Basin and its surroundings. *J. Maps*, 16(2): 445-458. DOI: 10.1080/17445647.2020.1770136
- Islam, M.R. and Lupin, J.H. 2020. A Review on Hydrocarbon Prospectivity in Chittagong Hill Tracts and Adjacent Area. *Open J. Geol.*, 10(2): 187-212. DOI: 10.4236/ojg.2020.102011
- Johnson, S.Y. and Nur Alam, A.M. 1991. Sedimentation and tectonics of the Sylhet trough, Bangladesh. *Geol. Soc. Am. Bull.*, 103(11): 1513-1527. DOI: 10.1130/0016-7606(1991)103<1513:SATOTS>2.3.CO;2
- Khan, M.S.H., Hossain, M.S. and Uddin, M.A. 2018. Geology and active tectonics of the Lalmai Hills, Bangladesh: An overview from Chittagong Tripura Fold Belt perspective. *J. Geol. Soc. India*, 92(6): 713-720. DOI: 10.1007/s12594-018-1093-5
- Khan, S., Rehman, S., Zeb Khan, A., Khan, M.A. and Shah, M.T. 2010. Soil and vegetables enrichment with heavy metals vegetalegical sources in Gilgit, northern Pakistan. *Ecotoxicol. Environ. Saf.*, 73(7): 1820-1827. DOI: 10.1016/j.ecoenv.2010.08.016
- Rahman, M.J.J. and Faupl, P. 2003. The composition of the subsurface Neogene shales of the Surma group from the Sylhet Trough, Bengal Basin, Bangladesh. *Sed. Geol.*, 155(3-4): 407-417. DOI: 10.1016/S0037-0738(02)00190-2
- Shamsuddin, A.H.M. and Khan, S.I. 1991. Geochemical criteria of migration of natural gases in the Miocene sediments of the Bengal Foredeep, Bangladesh. *J. Southeast Asian Earth Sci.*, 5(1-4): 89-100. DOI: 10.1016/0743-9547(91)90016-Q

ORCID DETAILS OF THE AUTHORS

Md. Mesbah Uddin Bhuiyan: <https://orcid.org/0000-0001-9315-732X>
 Md. Saiful Islam: <https://orcid.org/0000-0002-4333-8787>
 Umma Sabira: <https://orcid.org/0009-0003-1278-6784>



A Comprehensive Survey on Machine Learning and Deep Learning Techniques for Crop Disease Prediction in Smart Agriculture

Chatla Subbarayudu and Mohan Kubendiran†

*School of Computer Science and Engineering, Vellore Institute of Technology, Vellore 632014, India

†Corresponding author: Mohan Kubendiran; mohan.k@vit.ac.in

Nat. Env. & Poll. Tech.
Website: www.neptjournal.com

Received: 14-08-2023

Revised: 04-10-2023

Accepted: 13-10-2023

Key Words:

Crop disease prediction
Feature extraction
Machine learning
Smart agriculture
Deep learning

ABSTRACT

Diseases caused by bacteria, fungi, and viruses are a problem for many crops. Farmers have challenges when trying to evaluate their crops daily by manual inspection across all forms of agriculture. Also, it is difficult to assess the crops since they are affected by various environmental factors and predators. These challenges can be addressed by employing crop disease detection approaches using artificial intelligence-based machine learning and deep learning techniques. This paper provides a comprehensive survey of various techniques utilized for crop disease prediction based on machine learning and deep learning approaches. This literature review summarises the contributions of a wide range of research works to the field of crop disease prediction, highlighting their commonalities and differences, parameters, and performance indicators. Further, to evaluate, a case study has been presented on how the paradigm shift will lead us to the design of an efficient learning model for crop disease prediction. It also identifies the gaps in knowledge that are supposed to be addressed to forge a path forward in research. From the survey conducted, it is apparent that the deep learning technique shows high efficiency over the machine learning approaches, thereby preventing crop loss.

INTRODUCTION

Advancements in Information and Communication Technologies (ICT) and the Internet of Things (IoT) have revolutionized the agricultural industry by shaping the traditional method of farming in a smarter way to maximize yield and increase food production (Fountas et al. 2015). Smart farming involves the coagulation of different technologies, namely wireless sensors connected to the Internet of Things, robotics, artificial intelligence, and cloud computing (Wolfert et al. 2017). Agriculture plays a vital role in promoting the growth and economy of a country. In India, agriculture plays a significant role in meeting the expanded food demand raised by the population. However, crops are prone to diseases due to various fungi, bacteria, and viruses (Vishnoi et al. 2021). Crops infected by these disease-causing organisms are supposed to be detected and treated in time (Chen et al. 2020a). If they are left undetected, it may dwindle food production. This may also worsen the food supply chain, which degrades the performance of agricultural activity (Li et al. 2021). The traditional methods of manual inspection are not conducive, even for small-scale farmers.

Food loss per year accounts for nearly 37%, which has to be substantially reduced (Tiwari et al. 2021). This also

results in financial losses for the farmers. Traditionally, farmers rely on suggestions from experts when samples of infected crops are taken as specimens or a personal visit is needed. This process is tedious since it requires finding an expert and supervision. Sometimes, the findings may not be reliable or effective (Bera et al. 2019). Therefore, it is essential to detect and treat crop diseases precisely. This challenge motivates the researchers to design an automatic, reliable, and efficient method to detect crop diseases (Hang et al. 2019). To assist in the process of detecting and classifying crop diseases, image processing techniques play a prominent role. The image processing technique involves different stages, namely acquisition, pre-processing, segmentation, feature extraction, selection, and classification. The major advantage of image processing techniques involves the use of threshold methods, region methods, and color detection to diagnose and detect crop diseases (Ganatra et al. 2018). Most of the techniques face limitations in accuracy, which need to be improved. The major problem with utilizing these techniques is the manual generation of feature parameters that are supposed to be alleviated (Yuan et al. 2021). Several researchers and academicians have contributed a lot to identifying and classifying crop diseases. Some of the commonly used artificial

intelligence-based approaches are machine learning and deep learning.

The most popular technique used for crop disease detection is the convolutional neural network. More than machine-learning models, deep learning acts as a state-of-the-art technology. The major advantages of using convolutional neural networks are zero human supervision, automatic feature extraction, high accuracy, less computation, and handling large datasets (Khan et al. 2021). Building an automated recognition system benefits amateurs and professional experts in identifying the conditions of the crop by its appearance and features while determining the disease. Various methods based on perception, non-linearity, and configurations have been surveyed. This survey provides a comprehensive review of crop diseases utilizing machine learning and deep learning techniques. It focuses on the type of crop, datasets, models utilized, and performance parameters for classification. The work also involves the classification of several image-processing algorithms that perform crop disease detection and classification.

Motivation

Crop yield is mainly affected by several environmental factors or pathogens. Timely diagnosis and detection of crop diseases can provide protection, thereby reducing the food and financial losses incurred. Hence, it is essential to design a methodology that would detect, predict, or forecast crop diseases. When faced with a wide variety of datasets, parameters, hardware configurations, and experimental conditions, it can be challenging to select the most appropriate model to use for machine learning, deep learning, or artificial intelligence research. Therefore, researchers need to conduct a comprehensive analysis to identify a reliable model for data processing, prediction, and categorization of crop diseases. This motivates us to carry out an extensive survey corresponding to crop disease detection and prediction based on machine and deep learning techniques that have been proposed.

Major Contributions

The main aim of this survey is to carry out a comprehensive analysis of machine learning and deep learning techniques utilized for crop disease prediction. The major contributions of this survey are as follows:

- To identify various types of image segmentation methods that act as a base for detecting and classifying crop disease.
- A comparative analysis with a summary and insights into various techniques applied to various crops are presented.

- Performance investigations based on various methods of machine and deep learning techniques are performed.
- Research gaps and case studies have been presented that would shed light on how the learning approach would lead us into the future.

Organization of the Survey

This survey has been organized as follows: Section 1 defines the introduction; Section 2 provides the classification of machine learning and deep learning techniques utilized for agricultural crop diseases; Section 3 provides the performance investigations in terms of parameters and models on crop disease prediction using machine and deep learning techniques; section 4 provides the case studies to evaluate the survey and presents the research gaps; and section 5 provides the conclusion and the future scope.

PAST STUDIES

Computer Vision

Computer vision can be described as the coagulation of various techniques to obtain, process, scrutinize, and gain insights from complex, high-dimensional data (Jähne et al. 1999). Computer vision involves signal processing, image processing, and pattern recognition. One of the major important processes of image processing involves image segmentation. To analyze and detect crop diseases, images are scanned, and the regions that are affected are segmented for further processing (Kaur et al. 2014). Images are segmented into various parts based on features such as pixel intensity, color, and texture. Image segmentation techniques can be broadly classified into edge-based segmentation, region-based segmentation, and hybrid segmentation (Zaitoun et al. 2015). Some of the important image segmentation-based approaches utilized in both machine and deep learning techniques are classified along with their advantages and limitations in Table 1.

Classification of Machine Learning Models for Crop Disease Prediction

Agriculture has become a hot spot for research since it has been influenced by the use of modern technologies like IoT, Artificial Intelligence (AI), and cyber connectivity (Tamsekar et al. 2019). Smart Agriculture offers the utilization of high-end applications by way of data acquisition obtained from multiple sources, namely sensors, cameras, robots, and drones. Machine learning techniques have opened a wide arena of opportunities that offer applications based on analyzing various features and constraints, giving rise to an insight that would rectify traditional problems like manual

Table 1: Classification of crop disease segmentation approaches.

Image Segmentation Approaches	Advantages	Limitations
Region-based Segmentation (Singh et al. 2019)	Enables us to select among the automated and collective images. Provides a trustworthy performance.	Consumes huge amounts of memory and storage
Edge-based Segmentation (Badage et al. 2018)	It is good for images to have better contrast between objects	Inadequate in case of faulty detection or with a huge number of edges
Threshold-based Segmentation (Singh et al. 2017)	Robust and less cost topologically Suitable for real-time scenarios	Highly sensitive to noise.
Clustering-based Segmentation (Zhang et al. 2019)	Divides images into homogenous regions utilized for real-time problems to be solved.	Produces clusters of similar sizes
Watershed-based Segmentation (Yu et al. 2023)	Output is reliable	Involves highly complex gradient computation
Neural Network-based Segmentation (Senthilk et al. 2009)	Utilized for making decisions Accuracy is high	Training is highly difficult

inspection, fault diagnosis, disease detection, the severity of disease, and prediction. This section provides a classification of traditional methods of machine learning that have been applied to various crop diseases.

Singh and Kaur (2019) proposed plant disease detection based on region-based segmentation and a KNN classifier. Their methodology utilized the Grey-Level Co-occurrence Matrix (GLCM) technique to analyze textural features, achieving 97% accuracy in detecting leaf miners, mosaic viruses, and whiteflies in plant leaves. Chopda et al. (2018) developed a plant disease detection model for cotton crops using a decision tree classifier. Sharma et al. (2018) introduced an artificial neural network-based approach for predicting potato late blight disease based on weather parameters, achieving an accuracy of 90%. Gadekallu et al.

(2021) proposed a novel principal component analysis whale optimization-based neural network model for classifying tomato plant diseases using the GPU. Their model achieved a training accuracy of 99% and a testing accuracy of 86%. Rumpf et al., (2010) proposed early identification and classification of sugar beet diseases based on support vector machines and spectral vegetation significance, achieving an accuracy of 97%. However, their methodology suffered from target class overlap. Bhatia et al. (2020) presented a powdery mildew disease prediction model using the hybrid support vector machine logistic regression model, with an accuracy of 92.37%. Still, they indicated the need for further performance improvement. Nababan et al. (2018) developed a disease detection system for oil palm using a Naive Bayes classifier based on expert system technology, achieving an

Table 2: Comparative analysis of machine learning models utilized for crop disease prediction.

Author	Machine Learning Model	Merits	Demerits
(Gadekallu et al. 2021)	PCA-Whale Optimization Algorithm (WOA)	Dimensionality has been greatly reduced	Their model considers only the linear relationship between the data
(Geetha et al. 2020)	Random Forest (RF)	Since it uses a bagging technique the accuracy and reliable	Training time for the dataset is quite high
(Resti et al. 2022)	Multimodal Naïve Bayes (MNB) and KNN	Easy to implement	The success rate of MNB and KNN highly depends on data
(Hatuwal et al. 2020)	Convolutional Neural Network (CNN)	Performs multiclass classification	Suffers from repeated training of data which possess high computation time.
(Kaur et al. 2020)	Support Vector Machine (SVM) &	Reduces redundancy and improves accuracy	Fewer features are considered
Chaudhari et al. 2020)	K-means Clustering and Support Vector Machine (SVM)	Identifies the symptom-wise banana leaf diseases	Accuracy has to be improved
(Dang-Ngoc et al. 2021)	Hierarchical Support Vector Machine (HSVM)	Diseased main leaf regions are segmented automatically	Low quantity Dataset
(Mojumdar et al. 2021)	K-means clustering, GLCM & Support Vector Machine (SVM)	Extracted features will determine and classify healthy or sick using SVM	Classification Accuracy needs to be improved
(Nirmal et al. 2022)	Support Vector Model	Distinguishes healthy and unhealthy leaves effectively	Utilized fewer samples of data, which needs to be improved

accuracy rate of 80%. However, precision improvement was identified as a major disadvantage. Geetha et al. (2020) proposed an effective crop prediction model based on a random forest algorithm that does not require large datasets for classification.

Chauhan & Deepika (2020) introduced a maize disease detection system using a random forest classification algorithm for three variants of diseases. Their model achieved an accuracy of 80.68% but exhibited limitations in handling large datasets effectively. Resti et al. (2022) proposed a corn plant disease and pest detection system using multimodal Naive Bayes and a k-nearest neighbor classifier. Their work achieved an accuracy of 99.54% for KNN and 92.72% for MNB, but heavily depended on the size and quantity of the data. Hatuwal et al. (2020) presented a plant disease detection system using convolutional neural networks with features extracted using the Haralick texture feature algorithm. Their CNN model achieved a higher accuracy of 97.89% compared to conventional approaches like random forest, support vector machine, and k-nearest neighbors but suffered from repeated training and high computation time. Table 2 provides a comparative analysis of machine learning models for various crops, including their advantages and limitations.

Comparative Analysis of Deep Learning Models on Crop Disease Prediction

Deep learning is a subcategory of machine learning that follows the exact functioning of the human brain. Deep learning trains itself based on the artificial neural network model (Kaur et al. 2021). Typically, it can be described as a multi-layer perceptron that consists of layers that are hidden and can perform feature extraction and find its relevance to gain data insights (Shinde & Shah. 2018). The major advantage of the deep learning model is that it performs feature extraction automatically for classification (Sarangi et al. 2021). It performs many levels of training in a hierarchical order. The most widely used methodology for deep learning models is convolutional neural networks (Li et al. 2021). This model can be used to process large amounts of heterogeneous data. It includes three types of activation functions, namely sigmoid, tanH, softmax, and ReLu functions (Dhar et al. 2021). The model consists of a convolution layer, a pooling layer, a fully connected layer, and a drop-out layer. It is composed of three layers, namely the input, hidden, and output layers (Sarwinda et al. 2021). This section provides a comparative analysis of various works carried out by researchers based on deep-learning models for crop disease prediction.

The paddy crop disease detection and classification system proposed by Haridasan et al. (2023) uses deep

learning. The system they developed had a 91.45% success rate in classifying data. However, overfitting of the data occurred in the tuning parameter. Arun Malik et al. (2022) designed and evaluated a hybrid method for detecting sunflower leaf disease by using a deep-learning approach. Their model achieved an accuracy of 89.2%. Due to unorganized data, high computation time was exhibited.

A deep-learning architecture based on generative adversarial networks was suggested by Habin Jin et al. (2022) to identify diseases in grape leaves with an accuracy of 86.36%. However, their model suffered from class imbalance, which needed a data augmentation technique. Upadhyay & Kumar (2022) created a rice plant disease detection system based on a convolutional neural network approach with an accuracy of 99.7%. The major advantage was that it efficiently processed huge datasets, and hence, no manual feature extraction method was required.

Feng Jiang et al. (2020) created a deep learning model based on a support vector machine and convolutional neural networks for detecting four kinds of rice leaf diseases. They achieved a high accuracy of 96.8%. However, CNN suffered from problems such as optimal neurons and low data samples. Yun Zhao et al. (2022) proposed a plant disease classification model based on the fusion of the inception and residual structures and an embedded attention mechanism called RIC-Net. It achieved an accuracy of 99.55% by detecting diseases in corn, potatoes, and tomatoes. However, their proposed methodology had to be tested by using real-time datasets, which should be large.

Using an enhanced DenseNet (DenseNet Network), Jiang et al. (2023) proposed a rice disease deep detection model with a 99.4% average classification accuracy. Using a conditional generative adversarial network (C-GAN), Amreen et al. (2021) presented a deep-learning approach to tomato plant disease detection by creating synthetic images of tomato plant leaves with an accuracy of 99.51 percent. The main benefit of their approach was that overfitting was eliminated through the use of C-GAN for data augmentation. However, the generator and the discriminator competed with each other, making the training unstable and slow.

To detect plant diseases with thermal images, Bhakta et al. (2023) developed a novel modified deep convolutional neural network. To lessen the computational burden and the overfitting issue in the case of a short dataset, they proposed using three convolutional layers. Their approach had a 97.5% success rate. To evaluate the efficacy of their model, it must be applied to a sizable data set. Using a convolutional neural network on mobile devices hosted in a Platform-as-a-Service (PaaS) cloud, Lanjewar & Panchbhai (2023) developed a method for predicting the presence of disease in tea leaves.

The accuracy of their model was 100 percent. A key issue was the need to append healthy tea leaf data within the dataset.

Ozguven & Adem (2019) came up with the automatic detection and classification of leaf spot disease in sugar beet using the deep learning model and achieved an accuracy of 95.48%. However, accuracy needed to be improved further. Xu et al. (2023) came up with a deep-learning model for wheat leaf disease identification. Their methodology was experimented with using the wheat data obtained from the Henan Province of China. Their methodology achieved a classification accuracy of 98.83%; however, the number of samples utilized was not comprehensive.

Noah Bevers et al. (2022) created a transfer learning-based convolutional neural network for soybean plant disease detection with an accuracy of 96.8%. However, their methodology suffered from the omission of data-augmented images, which diminished the overall performance. A rE-GoogLeNet convolutional neural network model for detecting rice leaf diseases in the wild was proposed by Le Yang et al. (2023). Their methodology achieved an accuracy rate of 99.58%, which was a 1.72% improvement over the GoogLeNet model. However, the major drawback was that their model was computationally more intensive.

For accurate sugarcane leaf disease diagnosis, Li et al. (2022) presented a lightweight vision transformer based on shuffle convolution with an accuracy of 98.84%. For accurate diagnosis of grape leaf disease and pests, Lu et al. (2022) proposed a ghost-convolution enlightened transformer hybrid model with an accuracy of 98.14 percent. However,

processing the limited data required by the model was laborious.

Lamba et al. (2023) presented a new hybrid model (GCL) based on a network structure. The GCL combined the generative adversarial network (GAN) with a convolutional neural network (CNN) and a long short-term memory network (LSTM) for dataset segmentation. Their methodology achieved an accuracy of 97%. However, the major drawback was that it used very limited data for classification. A hybrid classification model based on modified feature-weighted fuzzy clustering (MFWFC) was proposed by Senthilkumar and Prabhusundhar (2023). Their model achieved an accuracy of 93.57%. However, there were too many classification algorithms used in the system, making it excessively complicated.

Zhang et al. (2023) proposed using multi-channel automatic orientation recurrent attention networks for tomato leaf disease detection. Their model achieved an accuracy of 96.47% with the PlantVillage dataset. However, their model posed limitations since they used small datasets. Using a refined swin transformer and a limited data set, Wang et al. (2022) presented a method for the practical recognition of cucumber leaf diseases. Their methodology achieved an accuracy of 98.97%. However, training time was quite high. Singh et al. (2023) came up with a novel framework for potato leaf disease detection using a deep learning model and achieved an accuracy of 97.2%. The major advantage of their proposed methodology was that it was computationally fast since an additional transition layer was added. However,

Table 3: Comparative analysis of deep learning models utilized for crop disease prediction.

Author	Deep Learning Model	Merits	Demerits
(Haridasan et al. 2023)	SVM, CNN	It is efficient since the dataset contains more dimensions	Classification accuracy needed to be improved
(Haibin Jin et al. 2022)	GANs	Multi-feature fusion mechanism captures the fine-grained features	Model suffers from class imbalance
(Jiang et al. 2023)	DenseNet + Adabound Algorithm + Channel Attention (Squeeze and Extraction)	A variety of features are considered for the classification	Computational time is quite high
(Amreen et al. 2021)	Conditional Generative Adversarial Networks	Prevented the problem of overfitting	Training the model becomes unstable and slow.
(Bhakta et al. 2023)	Modified Deep CNN + Thermal Imaging	Reduces the computation overhead and overfitting	The model has to be validated using large datasets
(Lanjewar & Panchbhai 2023)	CNN + PaaS Cloud	Reduces the computation overhead and overfitting	The dataset is not perfect since healthy tea leaves are not included.
(Noah Bevers et al. 2022)	Transfer Learning + CNN	Transfer learning boosted the performance of the CNN	Omitted Large Features that are highly needed.
(Senthilkumar et al. 2023)	Hybrid Classifier Model	Handles dynamic arrival of data	Design is complex
(Mahum et al. 2023)	Densely Connected Convolutional Neural Network – 201	Complexity is reduced by decreasing parameters.	Their method has to be evaluated by using large datasets.

their model suffered from an overfitting problem. Mahum et al. (2023) proposed a cotton leaf disease detection system using deep neural networks. Their proposed methodology achieved an accuracy of 99.37%. However, it suffered from weak learning when explicit regularisation was explained, which was one of the major drawbacks. Table 3 provides a comparative analysis of deep-learning models for crop disease prediction.

PERFORMANCE EVALUATION OF VARIOUS WORKS OF MACHINE LEARNING AND DEEP LEARNING TECHNIQUES ON CROP DISEASE PREDICTION

This section gives a summary and insights into the results of a performance evaluation of the parameters used in machine learning and deep learning models for crop disease detection. Table 4 provides a comparative analysis of machine learning models utilized for crop disease prediction.

Summary and Insights on Machine Learning Models on Crop Disease Prediction

Most of the machine learning utilized for crop disease prediction involves the use of Support vector machines (Rumpf et al.2010, Bhatia et al. 2020, Kaur et al. 2020, Chaudhari et al. 2020, Orin et al. 2021, Dang et al. 2021, Genitha et al. 2019, Mojumdar et al. 2021, Nirmal et al. 2022, Kilaru et al. 2021, Mohanty et al. 2022), the K-Nearest

Neighbour algorithm (Singh et al. 2019, Resti et al. 2022), the Decision Tree (Chopda et al. 2018), the Artificial Neural Network (Sharma et al. 2018), the Random Forest algorithm (Geetha et al. 2020, Chauhan et al. 2021), and Naive Bayes (Resti et al. 2022, Hatuwal et al. 2020). Among these methods, the support vector machine is more utilized since it addresses misclassifications. In the case of a large number of properly labeled items in a dataset, supervised learning algorithms such as SVM followed by KNN perform better by yielding a good result. These two algorithms succeeded then and there with the use of a random forest algorithm. The utilization of neural network-based optimization methods outperforms all the above-mentioned algorithms in terms of accuracy, precision, recall, and F1 scores. For potato crops, works based on KNN and ANN can be used.

Among these, KNN performs at par with an accuracy of 97%. The major difference between KNN and ANN is the number of points selected or the number of data or features selected for classification. Random forest algorithm performs much better than SVM since it accepts the data as they are, whereas SVM considers the distance between the data or the feature. The accuracy of the random forest algorithm is similar to that of the SVM. The training time taken by the random forest is comparatively lower than that of the SVM.

Performance Evaluation of Deep Learning Models on Crop Disease Prediction

Table 4: Performance evaluation of machine learning models on crop disease prediction.

Reference	Machine Learning Model/Algorithm	Dataset	Crop/Plant	Tool	Performance Metric and Result
(Singh & Kaur 2019)	Grey Level Co-occurrence Matrix (GLCM)-Texture Analysis; K-means Clustering-Region based Segmentation; KNN Classifier for disease prediction	PlantVillage Dataset	Potato leaves	MATLAB	Accuracy 97%
(Bhatia et al. 2018)	SVM-Noise Removal using Adaptive Sampling Noise Reduction (ANR) method; Logistic Regression-Classification.	Tomato Powdery Mildew Disease (TPMD) dataset	Tomato	R Studio 1.1.463	Accuracy-92.37%
(Chauhan & Deepika 2021)	Label finding, Gradient Calculation, random forest classifier	Corn Dataset	Maize	Python, Pandas Package	Accuracy-80.68%
(Hatuwal et al. 2020)	Haralick Texture Feature Algorithm, Convolution Kernel, Max Pooling, ReLu	Kaggle PlantVillage Dataset	Apple, cherry, Grape, Peach, Pepper, Strawberry	Google Colab	Accuracy-97.89%
(Kaur et al. 2020)	SVM, Decision Tree, NB, KNN	Citrus disease dataset	Citrus	MATLAB (R 2019)	Accuracy 90.4%
(Kilaru et al. 2021)	YOLO + Discrete Wavelet Transform + SVM, DarkNet Architecture	Kaggle PlantVillage Dataset	Maize	Matlab	SVM and its variants perform much better
(Mohanty et al. 2022)	Histogram of Oriented Gradients (HOG), Logistic Regression, Support Vector Machine, Random Forest	Kaggle PlantVillage Dataset	Tomato	Numpy, Open CV	Accuracy-73%

This section provides a performance evaluation of deep-learning models for crop disease prediction. For deep learning, from the standpoint of recognition accuracy, it has gone beyond finding the correlation and inter-class and intra-class correlation between the datasets. Some of the deep learning models involve transfer learning, reinforcement learning, and so on. Table 5 provides a comparative analysis of the deep-learning models utilized for crop disease prediction.

Summary and Insights on Deep Learning Models on Crop Disease Prediction Convolutional Neural Network

In CNN, the number of parameters to learn and the computation time are reduced. Also, the number of features generated gets summed up and is robust (Haridasan et al. 2023). To identify complex features, several layers of convolution with distinct kernel sizes can be utilized (Arun Malik et al. 2022). The Otsu-based thresholding technique is highly efficient since it facilitates effective noise removal,

thereby benefiting automatic feature extraction, which reduces the computational overhead (Upadhyay & Kumar 2022). The degradation problem caused by an increase in the network depth between the convolutional layers of a residual structure in Inception-based convolutional neural networks with an incorporated modified convolutional block attention module (CBAM) (Yun Zhao et al. 2022) has been solved. Too many parameters, a huge model size, and a lengthy training period are problems that the Inception architecture aims to address. Because of this, the network architecture can autonomously choose superior characteristics, simplifying network parameters and computations.

DenseNet

The combination of DenseNet and the channel attention mechanism squeeze-and-excitation helps us to strengthen the features that are favorable while rejecting the unfavourable ones (Jiang et al. 2023). The use of DenseNet with more transition layers reduces the computation time taken for training the model. The utilization of Softmax functions

Table 5: Comparative analysis of deep learning models utilized for crop disease prediction.

Reference	Deep Learning Model/ Algorithm	Dataset	Crop/Plant	Tool	Performance Metric and Result
(Haibin et al. 2022)	VGG16 and InceptionV1	Plant Village public dataset	Grape	TensorFlow; CuDNN Computational Library	Accuracy of VGG16 and InceptionV1 achieve 96.13%
(Jiang et al. 2023)	DenseNet network (DenseNet), Adabound algorithm	Public dataset	Rice	Pytorch	The average CA 99.4%
(Bhakta et al. 2023)	VGG-16, VGG-19, Resnet50 and Resnet101,svm,LR	Open environment	Plant disease	Python with Keras; TensorFlow	95% accuracy and high precision 97.5%
(Lanjewar & Panchbhai 2023)	ResNet50, Xception, and NASNetMobile	Mendeley data website	Tea leaf	Python	Recognition accuracy is 100%
(Xu et al. 2023)	VGG-19, ZFNet, GoogLeNet, Inception-V4	Open-source databases	Wheat leaf	Keras 2.2.4 Frame, TensorFlow GPU 1.14.0; python 3.7; CuDNN 7.0	The overall CA was 98.83%, and the maximum testing accuracy was 99.95%
(Le Yang et al. 2023)	rE-GoogLeNet convolutional neural network	Public dataset PlantVillage	Rice leaf	TensorFlow 2.3 Python 3.7	Accuracy-99.58%
(Li et al. 2023)	Shuffle-convolution-based lightweight vision transformer	public dataset Plant Village,	Sugarcane leaf diseases	PyTorch 1.10	Accuracy-98.84%
(Lamba et al.2023)	LSTM + CNN + GAN	Mendeley, Kaggle, UCI, and GitHub	Paddy diseases	Google Colab	Accuracy-97%
(Wang et al. 2022)	Swin Transformer and GAN	Chinese dataset	Cucumber	Anaconda framework-PyTorch 1.7.0	Accuracy-98.97%
(Singh et al. 2023)	CNN	Google images	Cotton	Python 3.10.9, libraries: OpenCV, Keras, Tensorflow, Numpy, Matplotlib	Accuracy-99.39%
(Mahum et al. 2023)	DenseNet-201	Plant Village Dataset	Potato leaf	Python framework with Keras v0.1.1 library	Accuracy -97.2%

benefits multi-class cataloging. However, the class imbalance problem can be solved by using data augmentation or oversampling of data (Mahum et al. 2023). Utilization of conditional generative adversarial networks along with the DenseNet121 model generates synthetic images that yield high accuracy.

Transfer Learning Methods

The combination of VGG-16 and MobileNet (Arun Malik et al. 2022), which is an ensemble model, yields more accuracy and eradicates the traditional problems of learning like overfitting, gradient problems, huge data processing, and

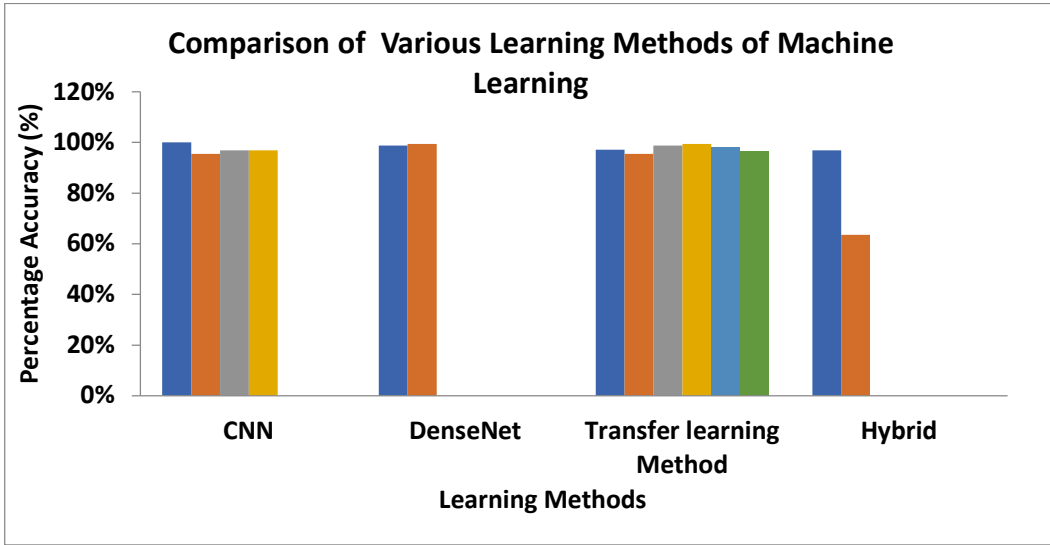


Fig. 1: Comparison of various machine learning strategies.

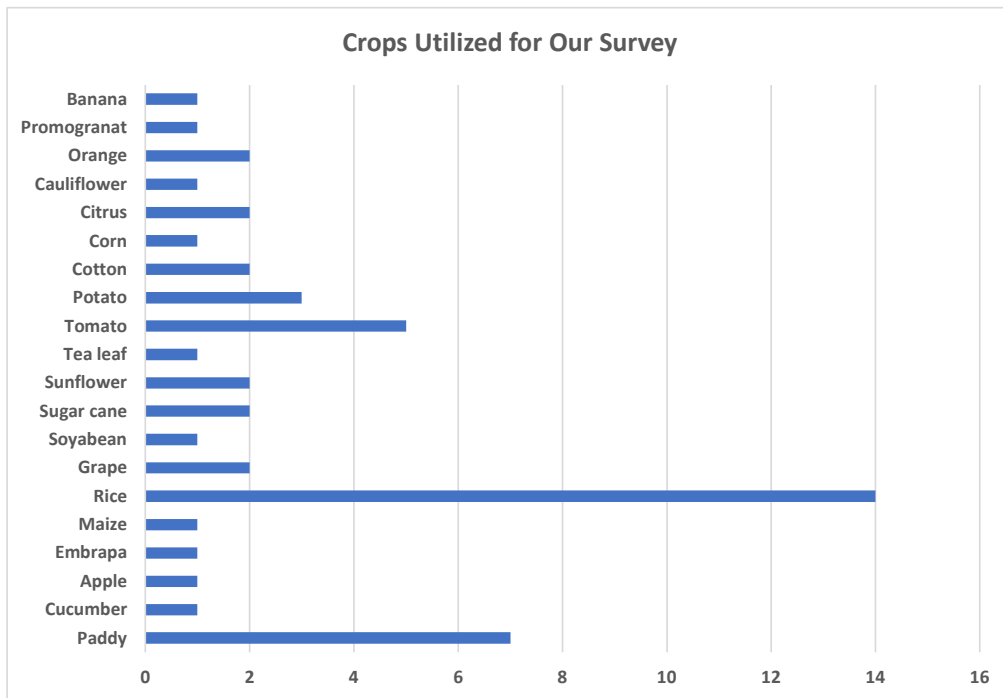


Fig. 2: Crops utilized for our survey.

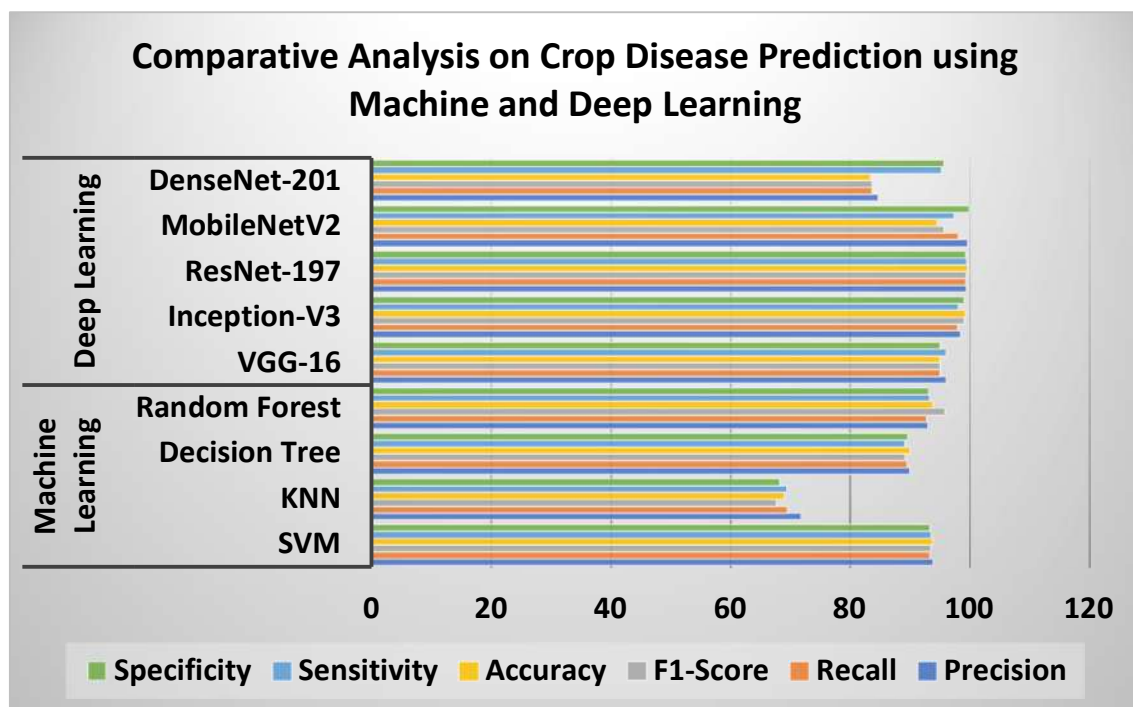


Fig. 3: Comparative analysis of crop disease prediction using machine and deep learning models.

less training time. Similarly, the combination of VGG-16 and Inception V1 provides a higher accuracy of 96.13% (Haibin et al. 2022). GANs are highly attractive to researchers due to the following reasons: 1) They can process huge datasets. 2) Different numbers of parameters and computation sizes can be varied. 3) Hyperparameter selection is easy, and it can be used for multiple-tuning training, which consumes very little time. The work proposed by (Xu et al. 2023) has made a great impact and contains a coagulation of two parallel CNNs. It consists of a residual channel attention block (RCAB), a feedback block (FB), elliptic metric learning (EML), and CNN, achieving a higher accuracy of 99.95%. The major use of EML is that it can be used to distinguish and alleviate recurring features. To extract the deep semantic features of an image, transformer-based deep learning models can be adapted. Images with low resolution and complex backgrounds can use these transformer-based approaches for disease detection. The horizontal patching of features from the low-level to the high-level convolution layer is an example of how the combination of convolution and transformer makes deep semantic feature extraction possible (Lu et al. 2022). An asymptotic non-local means algorithm and a multi-channel automatic orientation recurrent attention network (Zhang et al. 2023) can be used together to get rid of background noise and pull out useful information for diagnosing and classifying diseases. The approach is effective at pinpointing infected areas and

determining disease variance across and within population groups.

Hybrid Methods

A combination of CNN, GANs, and LSTM performs better; however, an increase in the dataset and the generation of new images for feature extraction are computationally difficult (Lamba et al. 2023). The hybrid classifier model (Senthilkumar & Prabhushundhar 2023) provides a great achievement in meeting the goals of increasing the size of the dataset, the training time taken by the model, and the size of the window utilized for pre-processing. This can be used for prediction. Deep CNN: DCNN models, namely ResNet50, Xception, and NASNetMobile, achieved 100% accuracy (Lanjewar & Panchbhai 2023). Fig. 1 provides a comparative analysis of different types of methodologies for machine learning strategies. Fig. 2 provides a comparison of the various crops utilized for our survey. Fig. 3 provides the comparison analysis of crop disease prediction classification accuracy based on deep and machine learning models.

CASE STUDIES

Due to the advancements of technology, IoT, or machine intelligence, has been made viable, thereby connecting physical objects to the internet and facilitating aid for farmers.

This section also provides an analysis of different scenarios that can be solved by using deep learning techniques.

Scenario 1: *Among all the models surveyed, provide a comparative analysis of the accuracy of various machine and deep learning models based on different crop diseases. From the analysis, please provide an overview and comment on its efficiency.*

Answer: Fig. 4 provides a comparative analysis of various machine and deep learning models developed for various crop diseases.

From Fig. 4, it is apparent that more than the machine learning models, deep learning models outperform. Of all the models surveyed, it is identified that VGG19 (Xu et al. 2023) has been applied for disease detection on cotton crops, providing an accuracy of 100%. NASNetMobile (Lanjewar & Panchbhai 2023) provides an accuracy of at most 99%. NASNetMobile has been applied for tea leaf disease detection. From the Fig., it is identified that RESNET employed in NASNetMobile provides the highest accuracy along with the VGG19 model. Of the remaining DenseNet models (Jiang et al. 2023, Noah et al. 2022), RESNET152V2 (Singh et al. 2023) provides the highest accuracy of more than 99%. These approaches can be utilised to test other crop diseases such as maize, cotton, jute, fruits, and vegetables.

Scenario 2: *India is the largest exporter of the commercial crop ‘cotton.’ Cotton suffers from a wide variety of diseases,*

which degrade the growth of the farmer’s economies of the farmers. Is there any model that possibly detects and classifies, giving a classification accuracy of, at most, 100% performance? The model developed should be able to process a large amount of data.

Answer: By collecting a large number of data from the agricultural department in Salem, Tamil Nadu. A dataset has been processed by using data transformation, data cleaning, data reduction, and data processing steps.

It is then fed into the model of RESNET152V2, which is a transfer learning model consisting of a data augmentation pattern classification with more than 22 types of diseases. Their proposed model (Singh et al. 2023) has utilized three convolutional hidden layers that can be used to identify cotton diseases through four different feature labels. The architecture of the proposed model is depicted in Fig. 5. The model can achieve a classification accuracy of 99.39%. Their proposed model consists of an input layer where the cotton leaves are fed as input, which is then processed to obtain an RGB image. This is then fed into the convolution layer, which consists of a leaky reactivation layer unit along with the max pooling function, which contains a dimensionality reduction from 128×128 dimensions to 126×126 , 63×63 , and 30×30 dimensions, which then gets connected to the fully connected layer of 64 features, and finally, the 22 classes of features can be obtained.

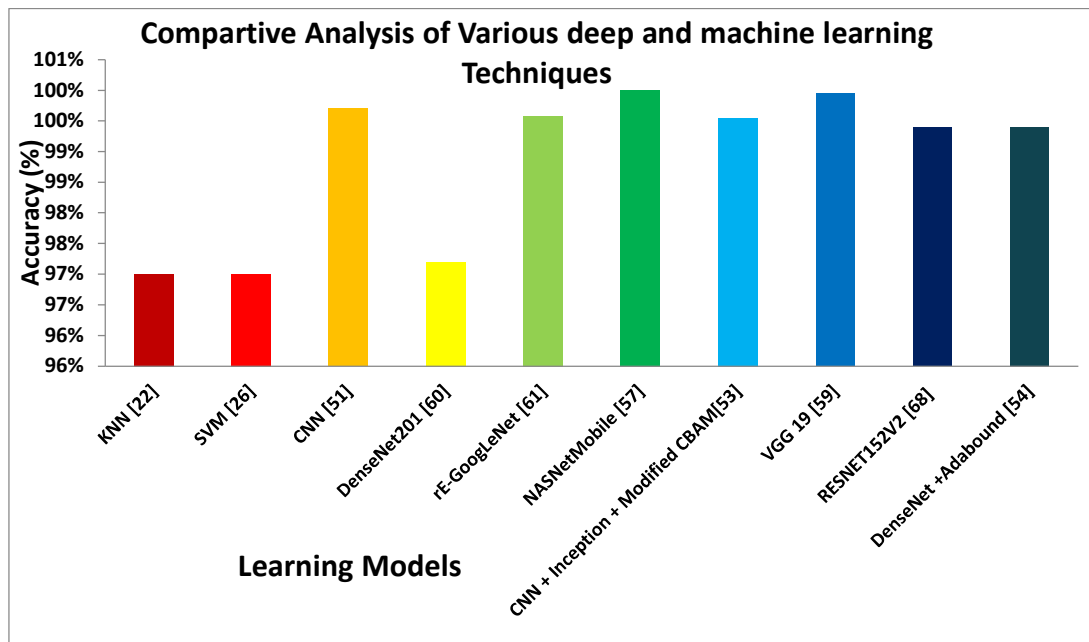


Fig. 4: Comparative analysis of various machine and deep learning models.

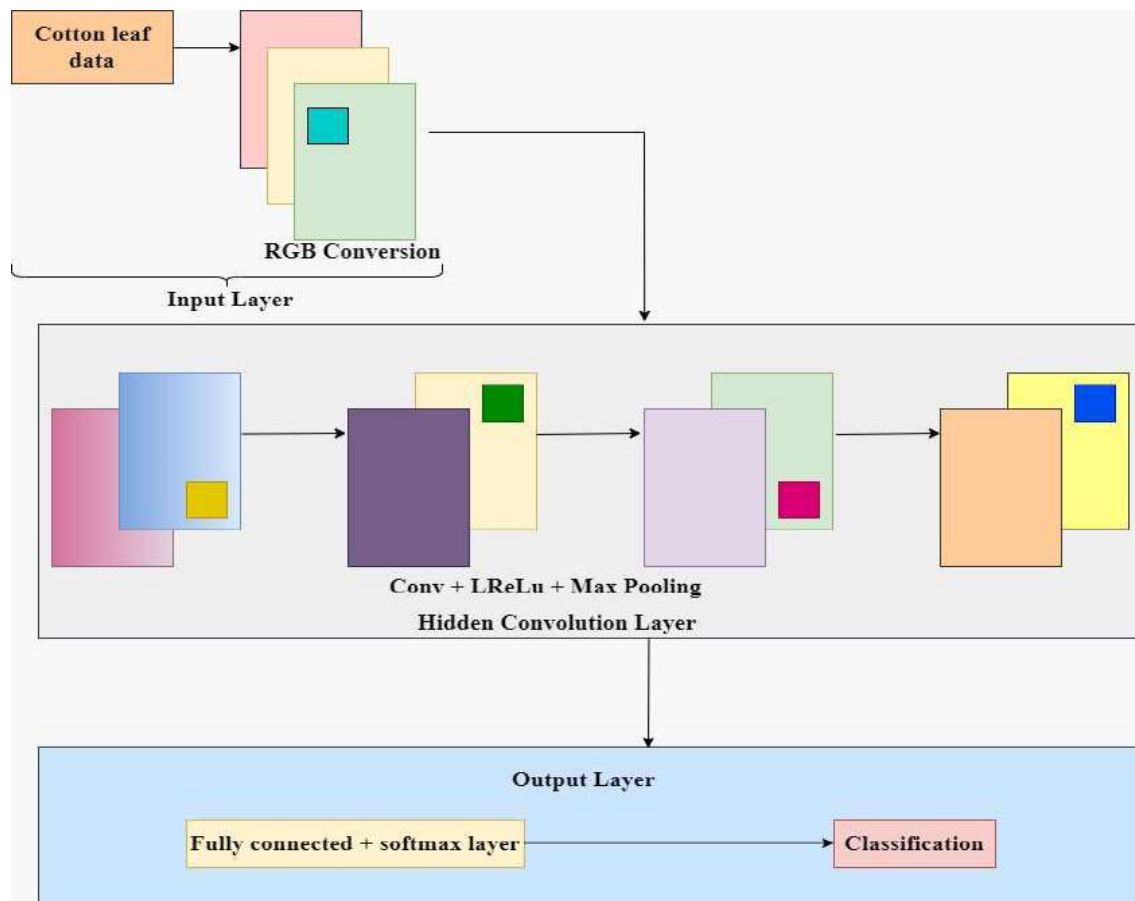


Fig. 5: Deep learning model case study for the scenario.

Table 6: Comparison of Deep Learning Models based on precision, size, and speed.

Model	Precision	Size	Speed
VGG16 + Inception (Haibin et al. 2022)	96.13%	240 MB	60FPS
C-GAN (Amreen et al. 2021)	99.10%	180MB	120FPS
LSTM + CNN + GAN (Lamba et al. 2023)	97%	58MB	210FPS
YOLO-MobileNetv3 (Maski et al. 2021)	98.39%	11.52MB	244FPS
YOLOv4 (Liu et al. 2020)	95%	236MB	62FPS
Tiny-YOLOv4 (Bochkovskiy et al. 2020)	96.71%	33.4MB	220FPS
YOLO-Fastest (Redmon et al. 2018)	92.38%	1.3MB	230FPS

Scenario 3: Viruses that affect papaya cause a ringspot on its leaves, which has to be detected. Hence, to reduce the damage, what are the hybrid methods that can provide the most classification with higher accuracy? The major requirements are speed and data size.

Answer: The major requirement of the deep learning model is that it has to alleviate the problem of overfitting due to the huge size of the data. Hence, a based architecture, along with

the concept of bounding box approaches, increases the speed and supports huge data sizes. Hence, YOLO with NCNN can process 236 megabits of data. Some of the hybrid models that can handle large data sets are given in Table 6 as follows:

Scenario 4: How to address the problems of image resolution; class imbalance, and insufficient data size while designing a learning model for crop disease identification and classification?

Answer: To address the problem of image resolution or faded image classifications, conditional generative adversarial networks can be utilized (Amreen et al. 2021). C-GANs provide synthetic images, which help in classification and accuracy. To address the problem of class imbalance, data augmentation approaches like position and color augmentation can be utilized (Bhakta et al. 2023). To achieve better performance DenseNet architecture or YOLO backbone architectures can be utilised to improve classification accuracy.

RESEARCH GAPS AND INSIGHTS

1. Utilization of seasonal and geographical data for crop yield estimation based on GIS technology is yet to be investigated (Haridasan et al. 2023).
2. Automatic feature extraction-based techniques have to be developed (Upadhyay & Kumar 2022).
3. To address the problem of overfitting while making a model to learn, it is necessary to devise a new data augmentation technique that would cater to various needs (Singh et al. 2023).
4. While training a model, the inter-class and intra-class similarities can cause confusion, which is supposed to be addressed (Yun Zhao et al. 2022).
5. Investigation on faster-RCNN and Updated-RCNN-based deep learning models that are supposed to be investigated against various crops for disease detection has not been explored yet (Ozguven & Adem 2019).
6. Severity assessment, along with disease detection, is an area that is supposed to be explored (Jiang et al. 2023).
7. Base model architectures and frozen-core training approaches in the case of transfer learning approaches are yet to be explored and investigated.
8. To prevent the network model from the problem of overfitting conditional generative adversarial network (C-GAN) is utilized as a data augmentation technique that can enhance the size of the dataset (Amreen et al. 2021).
9. Segmentation-based lightweight-based model to address crop disease detection and its severity is an emerging area (Li et al. 2023).
10. Recognition of multiple diseases on a single leaf is supposed to be investigated further (Wang et al. 2022).

CONCLUSION AND FUTURE WORK

In this paper, several works by various authors on machine learning and deep learning techniques for crop prediction

are surveyed. A comparative analysis based on performance parameters, type of model, datasets, and tools for crop disease detection catering to various requirements is investigated. Research gaps have been identified concerning various machine learning models and different learning methods. Moreover, a comparison table of various learning strategies has been formulated, which acts as a backbone for future researchers.

Future work should involve federated learning-based deep learning models that can be applied to the detection, prediction, and classification of crop diseases. Neural Architecture Search Network Mobile searches for the best possible algorithm, which has to be utilized for modeling an effective learning technique. Multi-scale feature extraction techniques to enhance the process of feature extraction will provide efficient detection of the diseased images. Deep CNN-based models can provide more stability and reliability for better performance results. Deep Convolutional Extreme Learning Machine models (DC-ELM) improve training speed by removing convergence and alleviating the requirement for multiple iterations to change the hidden layer weights. Devising the best optimizer according to the requirements provides an improvement in the performance of the classifier.

REFERENCES

- Abbas, A., Jain, S., Gour, M. and Vankudothu, S. 2021. Tomato plant disease detection using transfer learning with C-GAN synthetic images. *Comput. Electron. Agric.*, 187: 0168. <https://doi.org/10.1016/j.compag.2021.106279>
- Arun Malik, A., Vaidya, G., Jagota, V., Eswaran, S., Sirohi, A., Batra, I., Rakhra, M. and Evans Asenso. 2022. Design and evaluation of a hybrid technique for detecting sunflower leaf disease using a deep learning approach. *J. Food Qual.*, 20: 700.
- Badage, A. 2018. Crop disease detection using machine learning: Indian agriculture. *Int. Res. J. Eng. Technol.*, 5(9): 866-869.
- Bera, T., Das, A., Sil, J. and Das, A.K. 2019. A survey on rice plant disease identification using image processing and data mining techniques. *Technologies*, 365–376. https://doi.org/10.1007/978-981-13-1501-5_31
- Bhakta, I., Phadikar, S., Majumder, K., Mukherjee, H. and Sau, A. 2023. A novel plant disease prediction model based on thermal images using modified deep convolutional neural network. *Precision Agric.*, 24(1): 23-39. <https://doi.org/10.1007/s11119-022-09927-x>
- Bhatia, A., Chug, A. and Singh, A.P. 2020. Hybrid SVM-LR classifier for powdery mildew disease prediction in tomato plants. 7th Int. Conf. Signal Process. Integr. Networks (SPIN), pp. 218–223. *IEEE Publ.* <https://doi.org/10.1109/SPIN48934.2020.9071202>
- Bochkovskiy, A., Wang, C.Y. and Liao, H.Y.M. 2020. Yolov4: Optimal speed and accuracy of object detection. *arXiv*, 2: 109.
- Chaudhari, V. and Patil, M. 2020. Banana leaf disease detection using K-means clustering and Feature extraction techniques. In *Int. Conf. Adv. Comput. Commun. Mater. (ICACCM)*, 2020 (pp. 126-130. *IEEE Publ.* <https://doi.org/10.1109/ICACCM50413.2020.9212816>
- Chauhan, M. and Deepika, S. 2021. Detection of maize disease using random forest classification algorithm. *Turk. J. Comput. Math. Educ.*, 12: 715-720.

- Chen, J., Zhang, D. and Nanekaran, Y.A. 2020a. Identifying plant diseases using deep transfer learning and enhanced lightweight network. *Multimedia Tools Appl.*, 79(41-42): 31497-31515. <https://doi.org/10.1007/s11042-020-09669-w>
- Chopda, J., Raveshiya, H., Nakum, S. and Nakrani, V. 2018. Cotton crop disease detection using decision tree classifier. *Int. Conf. Smart City Emerg. Technol.*, 1112: 85371. <https://doi.org/10.1109/ICSCET.2018.8537336>
- Dang-Ngoc, H., Cao, T.N.M. and Dang-Nguyen, C. 2021. Citrus leaf disease detection and classification using hierarchical support vector machine. *Electr. Electron. Eng.*, 21: 69-74. <https://doi.org/10.1109/ISEE51682.2021.9418680>
- Dhar, P., Dutta, S. and Mukherjee, V. 2021. Cross-wavelet assisted convolution neural network (AlexNet) approach for phonocardiogram signals classification. *Biomed. Signal Process. Control*, 63: 102142. <https://doi.org/10.1016/j.bspc.2020.102142>
- Feng Jiang, F., Lu, Y., Chen, Y., Cai, D. and Li, G. 2020. Image recognition of four rice leaf diseases based on deep learning and support vector machine. *Comput. Electron. Agric.*, 179: 2020.105824. <https://doi.org/10.1016/j.compag.2020.105824>
- Fountas, S., Carli, G., Sørensen, C. G., Tsiropoulos, Z., Cavalaris, C., Vatsanidou, A., Liakos, B., Canavari, M., Wiebensohn, J. and Tisserye, B.A. 2015. Farm management information systems: Current situation and future perspectives. *Comput. Electron. Agric.*, 115: 40-50. <https://doi.org/10.1016/j.compag.2015.05.011>
- Gadekallu, T.R., Rajput, D.S., Reddy, M.P.K., Lakshmana, K., Bhattacharya, S., Singh, S., Jolfaei, A. and Alazab, M. 2021. A novel PCA-whale optimization-based deep neural network model for classification of tomato plant diseases using GPU. *J. Real-Time Image Process.*, 18(4): 1383-1396. <https://doi.org/10.1007/s11554-020-00987-8>
- Ganatra, N. and Patel, A. 2018. A survey on disease detection and classification of agriculture products using image processing and machine learning. *Int. J. Comput. Appl.*, 180(13): 1-13.
- Geetha, V., Punitha, A., Abarna, M., Akshaya, M., Illakiya, S. and Janani, A. P. 2020. An effective crop prediction using a random forest algorithm. In *Int. Conf. System, Comput., Autom. Networking (ICSCAN)*, 2020, pp. 1-5. *IEEE Publ.* <https://doi.org/10.1109/ICSCAN49426.2020.9262311>
- Genitha, C., Dhinesh, E. and Jagan, A. 2019. Detection of leaf disease using principal component analysis and linear support vector machine. *Adv. Comput.*, 11: 350-355. <https://doi.org/10.1109/ICoAC48765.2019.246866>
- Jin, H., Li, Y., Qi, J., Feng, J., Tian, D. and Mu, W. 2022. GrapeGAN: Unsupervised image enhancement for improved grape leaf disease recognition. *Comput. Electron. Agric.*, 198: 2022.107055. <https://doi.org/10.1016/j.compag.2022.107055>
- Hang, J., Zhang, D., Chen, P., Zhang, J. and Wang, B. 2019. Classification of plant leaf diseases based on improved convolutional neural network. *Sensors*, 19(19): 4161. <https://doi.org/10.3390/s19194161>
- Haridasan, A., Thomas, J. and Raj, E.D. 2023. Deep learning system for paddy plant disease detection and classification. *Environ. Monit. Assess.*, 195(1): 120.
- Hatuwal, B.K., Shakya, A. and Joshi, B. 2020. Plant leaf disease recognition using random forest, KNN, pp. 13-19. SVM and CNN.
- Jähne, B., Haussecker, H. and Geissler, P. Eds.. 1999. *Handbook of computer vision and applications*, 2. Academic Press.
- Jiang, M., Feng, C., Fang, X., Huang, Q., Zhang, C. and Shi, X. 2023. Rice disease identification method based on attention mechanism and deep dense network. *Electronics*, 12(3): 508. <https://doi.org/10.3390/electronics12030508>
- Kaur, A., Guleria, K. and Kumar Trivedi, N.K. 2021. Feature selection in machine learning: Methods and comparison. *Adv. Comput. Innov. Technol. Eng.*, 21: 789-795. <https://doi.org/10.1109/ICACITE51222.2021.9404623>
- Kaur, B., Sharma, T., Goyal, B. and Dogra, A. 2020. A Genetic Algorithm based Feature Optimization method for Citrus HLB Disease Detection using Machine Learning. *Smart Syst. Invent. Technol.*, 32: 1052-1057. <https://doi.org/10.1109/ICSSIT48917.2020.9214107>
- Kaur, D. and Kaur, Y. 2014. Various image segmentation techniques: A review. *Int. J. Comput. Sci. Mobile Comput.*, 3(5): 809-814.
- Khan, R.U., Khan, K., Albattah, W. and Qamar, A.M. 2021. Image-based detection of plant diseases: From classical machine learning to the deep learning journey. *Wireless Commun. Mobile Comput.*, 1: 1-13. <https://doi.org/10.1155/2021/5541859>
- Kilaru, R. and Raju, K.M. 2021. Prediction of maize leaf disease detection to improve crop yield using machine learning based models. *Comput. Sci. Technol.*, 17: 212-217. <https://doi.org/10.1109/ICRTCST54752.2022.9782023>
- Lamba, S., Baliyan, A. and Kukreja, V. 2023. A novel GCL hybrid classification model for paddy diseases. *Int. J. Inf. Technol.*, 15(2): 1127-1136. <https://doi.org/10.1007/s41870-022-01094-6>
- Lanjewar, M.G. and Panchbhai, K.G. 2023. Convolutional neural network based tea leaf disease prediction system on smart phone using paas cloud. *Neural. Comput. Appl.*, 35(3): 2755-2771. <https://doi.org/10.1007/s00521-022-07743-y>
- Le Yang, X.Y., Zhang, S., Long, H., Zhang, H., Xu, S. and Liao, Y. 2023. GoogLeNet based on residual network and attention mechanism identification of rice leaf diseases. *Comput. Electron. Agric.*, 320: 107543.
- Li, L., Zhang, S. and Wang, B. 2021. Apple leaf disease identification with a small and imbalanced dataset based on lightweight convolutional networks. *Sensors*, 22(1): 173. <https://doi.org/10.3390/s22010173>
- Li, S., Wang, L., Li, J. and Yao, Y. 2021. Image classification algorithm based on improved AlexNet. In *J. Phys. Conf. Ser.*, 1813: 012051.
- Li, X., Li, X., Zhang, S., Zhang, G., Zhang, Muqing, & Shang, H. 2023. SLViT: Shuffle-convolution-based lightweight vision transformer for effective diagnosis of sugarcane leaf diseases. *J. King Saud Univ. Comput. Inf. Sci.*, 35(6): 101401. <https://doi.org/10.1016/j.jksuci.2022.09.013>
- Liu, J. and Wang, X. 2020. Tomato diseases and pests detection based on improved Yolo V3 convolutional neural network. *Front. Plant Sci.*, 11: 898. <https://doi.org/10.3389/fpls.2020.00898>
- Lu, X., Yang, R., Zhou, J., Jiao, J., Liu, F., Liu, Y., Su, B. and Gu, P. 2022. A hybrid model of ghost-convolution enlightened transformer for effective diagnosis of grape leaf disease and pest. *J. King Saud Univ. Comput. Inf. Sci.*, 34(5): 1755-1767. <https://doi.org/10.1016/j.jksuci.2022.03.006>
- Mahum, R., Haris, M., Zaib-Un-Nisa, M., Muhammad, A., Falak, S.K., Muhammad, S., Saipunizam, M. and Iskander, T. 2023. A novel framework for potato leaf disease detection using an efficient deep learning model. *Hum. Ecol. Risk Assess. Int. J.*, 29(2): 303-326.
- Maski, P. and Thondiyath, A. 2021. Plant disease detection using advanced deep learning algorithms: A case study of papaya ring spot disease. *Vision Comput.*, 47: 49-54. <https://doi.org/10.1109/ICIVC52351.2021.9526944>
- Mohanty, R., Wankhede, P., Singh, D. and Vakhare, P. 2022. Tomato plant leaves disease detection using machine learning. *Appl. Artif. Intell. Comput.*, 311: 544-549, 2022. <https://doi.org/10.1109/ICAIC53929.2022.9793302>
- Mojumdar, M.U. and Chakraborty, N.R. 2021. Orange and Orange leaves diseases detection using Computerized Techniques. *Comput. Commun. Networking Technol.*, 62: 1-4. <https://doi.org/10.1109/ICCCNT51525.2021.9579964>
- Nababan, M., Laia, Y., Sitanggang, Delima, Sihombing, O., Indra, E., Siregar, S., Purba, W. and Mancur, R. 2018. The diagnosis of oil palm disease using Naive Bayes Method based on Expert System Technology. *J. Phys. Conf. Ser.*, 1007(1): 012015. <https://doi.org/10.1088/1742-6596/1007/1/012015>
- Nirmal, M.D., Jadhav, P. and Pawar, S. 2022. Pomegranate leaf disease classification using feature extraction and machine learning.

- Smart Electron. Commun., 11: 619-626. <https://doi.org/10.1109/ICOSE54921.2022.9951907>
- Noah Bevers, N., Sikora, E. J. and Hardy, N.B. 2022. Soybean disease identification using original field images and transfer learning with convolutional neural networks. *Comput. Electron. Agric.*, 203: 107449. <https://doi.org/10.1016/j.compag.2022.107449>
- Orin, T.Y., Mojumdar, M.U., Siddiquee, S. M. T. and Chakraborty, N. R. 2021. Cauliflower leaf disease detection using computerized techniques. *Comput., Commun. Autom.*, 218: 730-733. <https://doi.org/10.1109/ICCCA52192.2021.9666437>
- Metin, O.M. and Adem, K. 2019. Automatic detection and classification of leaf spot disease in sugar beet using deep learning algorithms. *Physica Part A*, 2019: 122537.
- Redmon, J. and Farhadi, A. 2018. Yolov3: An incremental improvement. *arXiv*, 027: 67.
- Resti, Y., Irsan, C., Putri, M. T., Yani, I., Ansyori, A. and Suprihatin, B. 2022. Identification of corn plant diseases and pests based on digital images using multinomial naïve Bayes and K-nearest neighbor. *Sci. Technol. Indonesia*, 7(1): 29-35. <https://doi.org/10.26554/sti.2022.7.1.29-35>
- Rumpf, T., Mahlein, A.K., Steiner, U., Oerke, E.C., Dehne, H.W. and Plümer, L. 2010. Early detection and classification of plant diseases with support vector machines based on hyperspectral reflectance. *Comput. Electron. Agric.*, 74(1): 91-99. <https://doi.org/10.1016/j.compag.2010.06.009>
- Sarangi, P. K., Guleria, K., Prasad, D. and Verma, D.K. 2021. Stock movement prediction using neuro-genetic hybrid approach and impact on growth trend due to COVID-19. *Int. J. Networking Virtual Organisations*, 25(3/4): 333-352. <https://doi.org/10.1504/IJNVO.2021.120172>
- Sarwinda, D., Paradisa, R.H., Bustamam, A. and Anggia, P. 2021. Deep learning in image classification using residual network (ResNet) variants for detection of colorectal cancer. In *Procedia Comput. Sci. 5th Int. Conf. Comput. Sci. Comput. Intell.*, 179: 423-431. <https://doi.org/10.1016/j.procs.2021.01.025>
- Senthilk, N. and Rajesh, R. 2009. Edge detection techniques for image segmentation- A survey of soft computing approaches. *Int. J. Recent Trends Eng. Technol.*, 1(2): 250-254.
- Senthilkumar, T.P. and Prabh Sundhar, P. 2023. Prediction of rice disease using modified feature-weighted fuzzy clustering (MFWFC) based segmentation and hybrid classification model. *Int. J. Syst. Assur. Eng. Manag.*, 15: 131-148 <https://doi.org/10.1007/s13198-022-01835-7>
- Sharma, P., Singh, B.K. and Singh, R.P. 2018. Prediction of potato late blight disease based upon weather parameters using artificial neural network approach. *Comput. Commun. Networking Technol.*, 3: 1-13. <https://doi.org/10.1109/ICCCNT.2018.8494024>
- Shinde, P. P. and Shah, S. 2018. A review of machine learning and deep learning applications. In *2018 Fourth International Conference on Computing Communication Control and Automation (ICCUBEA)* (pp. 1-6). IEEE.
- Singh, J. and Kaur, H. 2019. Plant disease detection based on region-based segmentation and KNN classifier. In *Proceedings of the International Conference on ISMAC in Computational Vision and Bio-Engineering 2018 (ISMAC-CVB)*, pp. 1667-1675. Springer International Publishing.
- Singh, J. and Kaur, H. 2019. Plant disease detection based on region-based segmentation and KNN classifier. In *Proceedings of the International Conference on ISMAC in Computational Vision and Bio-Engineering 2018 (ISMAC-CVB)*, pp. 1667-1675. Springer International Publishing.
- Singh, P., Singh, P., Farooq, U. 2023. CottonLeafNet: cotton plant leaf disease detection using deep neural networks. *Multimed Tools Appl.* (2023).
- Singh, V. and Misra, A. K. 2017. Detection of plant leaf diseases using image segmentation and soft computing techniques. *Information processing in Agriculture*, 4(1): 41-49.
- Tamsekar, P., Deshmukh, N., Bhalchandra, P., Kulkarni, G., Hambarde, K. and Husen, S. 2019. Comparative analysis of supervised machine learning algorithms for GIS-based crop selection prediction model. In *Computing and Network Sustainability: Proceedings of IRSCNS 2018*.
- Tiwari, V., Joshi, R. C. and Dutta, M. K. 2021. Dense convolutional neural networks based multiclass plant disease detection and classification using leaf images. *Ecological Informatics*, 63: 101289.
- Upadhyay, S.K., Kumar. 2022. A novel approach for rice plant diseases classification with deep convolutional neural network. *Int. j. inf. tecnol.*, 14: 185-199.
- Vishnoi, V. K., Kumar, K. and Kumar, B. 2021. Plant disease detection using computational intelligence and image processing. *J. Plant Dis. Prot.*, 128(1): 19-53.
- Wang Fengyi, Yuan Rao, Qing Luo, Xiu Jin, Zhaohui Jiang, Wu Zhang, Shaowen Li. 2022. Practical cucumber leaf disease recognition using improved Swin Transformer and small sample size, *Computers and Electronics in Agriculture*, 107163.
- Wolfert, S., Ge, L., Verdouw, C. and Bogaardt, M. J. 2017. Big data in smart farming—a review. *Agricultural systems*, 153: 69-80.
- Xu, Laixiang, Bingxu Cao, Fengjie Zhao, Shiyuan Ning, Peng Xu, Wenbo Zhang, Xiangguan Hou. 2023. Wheat leaf disease identification based on deep learning algorithms, *Physiological and Molecular Plant Pathology*, 101940.
- Yu, Y., Wang, C., Fu, Q., Kou, R., Huang, F., Yang, B. and Gao, M. 2023. Techniques and challenges of image segmentation: A review. *Electronics*, 12(5): 1199.
- Yuan, Y., Chen, L., Wu, H. and Li, L. 2021. Advanced agricultural disease image recognition technologies: A review. *Inf. Process. Agric.*, 19: 534-546.
- Yun Zhao, Cheng Sun, Xing Xu, Jiagui Chen. 2022. RIC-Net: A plant disease classification model based on the fusion of Inception and residual structure and embedded attention mechanism, *Computers and Electronics in Agriculture*, 2021.106644.
- Zaitoun, Nida M., and Musbah J. Aqel. 2015. Survey on image segmentation techniques. *Procedia Computer Science*, 797-806.
- Zhang Yukai, Shuangjie Huang, Guoxiong Zhou, Yahui Hu, Liu Jun Li. 2023. Identification of tomato leaf diseases based on multi-channel automatic orientation recurrent attention network, *Computers and Electronics in Agriculture*, 205: 107605.
- Zhang, S., You, Z. and Wu, X. 2019. Plant disease leaf image segmentation based on superpixel clustering and EM algorithm. *Neural Computing and Applications*, 31: 1225-1232.



Role of Biotechnology and Genetic Engineering in Bioremediation of Cadmium Pollution

A. Kumar*† , G. Mukherjee*  and S. Gupta** 

*University Institute of Biotechnology, Chandigarh University, Gharuan, Punjab, India

**Department of Microbiology, Mata Gujri College, Fatehgarh Sahib, Punjab, India

†Corresponding author: A. Kumar; abhijitgupta.biotech@cumail.in

Nat. Env. & Poll. Tech.
Website: www.neptjournal.com

Received: 24-08-2023

Revised: 01-11-2023

Accepted: 02-11-2023

Key Words:

Bioremediation

Heavy metals

Cadmium

Anthropogenic

Environmental pollution

ABSTRACT

Cadmium (Cd) is ubiquitous and an unessential trace element existing in the environment. Anthropogenic activities and applications of synthetic phosphate fertilizers greatly enhance the concentration of Cadmium in the environment, which proves to be carcinogenic. The long-term effects of heavy metals contamination on plants and animals have recently become a major public health concern. Thanks to the application of science and technology, new environmental initiatives can have a lower environmental impact significantly. The role of microbes is very well known and must be considered as potential pollutant removers. Microbial flora can remove heavy metals and oil from contaminated soil and water. In comparison to conventional techniques, bioremediation itself proved to be a more potent technique because the established mechanisms render it ineffective. Biotechnological advancements are inherently harmful to the environment because they have the potential to reduce metal pollution. Pollutants in the environment can be effectively removed using bioremediation. Both native and introduced species can thrive in a microorganism-friendly environment.

INTRODUCTION

Currently, environmentalists are mainly worried about changes to biogeochemical cycles caused by the wide range of organic and inorganic contaminants generated by human activities (Vara et al. 2003). As industrialization spread, countries used a variety of remediation techniques for dealing with newly created pollution problems. Heavy metals are among the most pernicious of these environmental hazards. When compared to other organic contaminants like pesticides or petroleum by-products, heavy metals have a far longer half-life in nature. Because of this, the existence of heavy metals is cause for serious alarm. Variable quantities of heavy metals have increased over time alongside the expansion of the global economy, leading to environmental damage (Han et al. 2002). The presence of heavy metals severely harms all living things in the environment. Both the water supply itself and biomagnification can be a cause of heavy metal contamination. Air pollution is another potential cause of heavy metal contamination in mining regions (Santona et al. 2006). The Love Canal catastrophe at the American Niagara Falls (Fletcher 2002) described the devastating impact of heavy metals on the local human and animal population. There are now a number of traditional technologies in use for the elimination of heavy metals, but each has significant

drawbacks, including a high initial investment and ongoing maintenance. In the process of removing heavy metals from the soil, beneficial soil components are also damaged by the chemical technique. Aside from the obvious health risks, chemical procedures produce a lot of slurry at a high cost per person (Hinchman et al. 1996).

Heavy metals can be classified as “essential” or “toxic.” Heavy metals such as Zn, Fe, Mn, and Cu are required for plant growth, whereas molybdenum, cobalt, and nickel are required for microbial cell maintenance. Some heavy metals, such as cadmium, lead, mercury, arsenic, and chromium, are harmful to plants, humans, and the microbial population and hence pose a risk to crops even in low quantities. Because these metals interfere with vital biological processes (photosynthesis, protein synthesis), plant development and productivity are hampered (Hall 2002). Cd causes Itai Itai, renal, and bone problems, but heavy metals, in general, cause cancer in humans (WHO 2007). Human actions and natural processes both have a role in the genesis of these heavy metals in the ground (weathering of rocks). Human activity includes but is not limited to, the extraction and processing of minerals and metals for use in manufacturing and everyday life. Human activity has resulted in a hundred times more Pb, Cd, and Zn emissions than those from natural causes.

Heavy metal contamination can be traced back to mining activities. Since their dangerous effects endanger human health, biodiversity, and ecosystems, they warrant severe environmental concern (Navarro et al. 2008).

The industrial revolution is directly responsible for the enormous growth in the prevalence of hazardous substances in the environment. Toxin build-up in the food chain has a negative influence on human health (Chaffei et al. 2004). Increasing concentrations of cadmium have a huge impact on the environment due to its toxicity and carcinogenicity. Human activities such as fertilizer application, sewage sludge disposal, and industrial waste disposal on land have all contributed to Cd accumulation (Naidu et al. 1997). As a result, Cd concentrations in food crops have increased. As a result, it alters the normal macronutrient-micronutrient ratio, slowing plant development. A range of cellular activities is affected when plants are exposed to even trace quantities of Cd (Hall 2002). Human health may suffer as a result of the rapid absorption of Cd from enriched soil by many crop species, resulting in high food consumption (Tripathi et al. 2005, Rani et al. 2008).

Furthermore, multiple Faisalabad businesses were discovered to be releasing effluent with high amounts of Cd, resulting in an increase of more than 200% in the amount of Cd observed in the land that was irrigated with this wastewater (Hussain et al. 2010). Plants serve as a key entrance point from the soil because they absorb it and then convey it to animals and people (Cheng et al. 2006). This heavy metal typically inhibits the growth of plants, decreases the availability of nutrients, and hampers the mechanism of absorption by plants (Ramon et al. 2003, Jun-yu et al. 2008). Even minute quantities of Cd in plants impact several biological processes (Hall 2002). Because Cd exposure reduces gas exchange reactions (photosynthesis and transpiration rates), plant growth is hampered (Januskaitiene et al. 2010, Wang et al. 2009, Ekmekçi et al. 2008, Wu et al. 2007, Sun et al. 2008).

Heavy metals in soil can be removed using different procedures. These procedures are depicted in Fig. 1. Biological methods have various advantages over physical and chemical approaches, including low cost, great efficiency, universal adoption, little environmental impact, and adaptability (it can be employed both ex- and in-situ). Gadd (2000) effectively used bacterial procedures to mobilize and immobilize heavy metals via different mechanisms such as biotransformation, complexation, sorption, sequestration, and other mechanisms. In recent years, the use of microbial technology to reduce toxic waste has grown in favor (Radhika et al. 2006). Park et al. (2008) reported the precipitation of Cd with sulfide by the activities of sulfate-reducing bacteria and

achieved 99.7% results. According to Hadi and Bano, 2010 inoculating lead-polluted soil with diazotrophs dramatically boosted dry maize biomass. If plants are exposed to high amounts of Cd, the bacterial inoculants may aid in their growth. Plant growth-promoting bacteria can help mitigate the negative effects of environmental pressures such as salt, flooding, and metal stresses (Mayak et al. 2004, Grichko & Glick 2001, Burd et al. 1998).

Moreover, bacteria may serve as a disease defense for plants (Wang et al. 2000). *Beta vulgaris*'s capacity to extract/accumulate Cd was greatly enhanced after being inoculated with Cd-tolerant bacteria like *Staphylococcus pasteurii* and *Agrobacterium tumefaciens* (Chen et al. 2013). When used for phytostabilization, plants with high Cd tolerance and root-holding capacity are ideal (Zhang et al. 2012). Strict crop species selection can boost plant metal stress resistance, although many soil microorganisms can also survive in metal-poor environments (Aleem et al. 2003). The uptake of Cd by the metal hyperaccumulator *Salix caprea* was reduced due to the presence of *Burkholderia* sp. bacteria in the rhizosphere, as reported by Kuffner et al. (2010). The bacterial strains show promise as inoculants to boost plant development even when exposed to hazardous levels of Cd in the soil.

Processes like global warming, depletion of the ozone layer, degradation of soil and water bodies via organic and inorganic activities, and other concerned environmental oddities have recently confronted humanity. These pose a threat to the world's existing biota because of the harm they can do to food supplies and human and animal health. Heavy metal pollution, in particular, is a major problem all over the world because of the harm it does to the environment and human health when it accumulates in the food chain. This review compiles expert opinions on the global concentration of Cd, the causes and consequences of Cd pollution, and new approaches to bioremediating Cd.

HEAVY METALS

Phipps (1981) has developed the most widely used and well-known definition of heavy metals. Heavy metals are defined as those with an atomic number greater than 20 and a specific gravity of less than 5 g cm³. The production and utilization of several goods necessitate the use of heavy metals. Heavy metals are further categorized into -

- a) **Essential/Non-Toxic:** All forms of life, whether plants, animals, or microorganisms, they are benefitted greatly from the presence of these essential metals, even in trace amounts. Iron (Fe), molybdenum (Mo), and manganese (Mn) are all required by all cells in the human body,

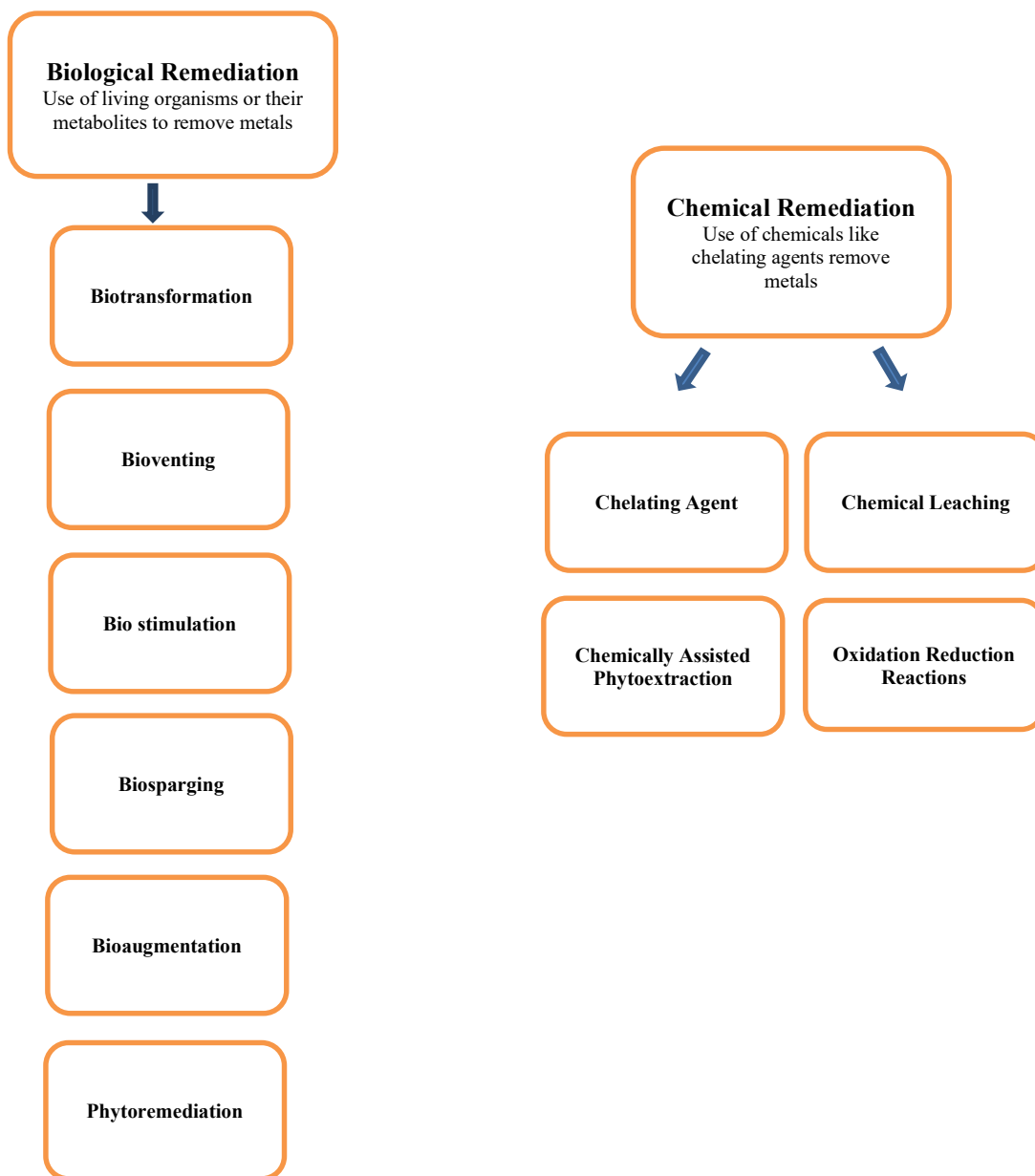


Fig. 1: General approaches used for metal remediation.

while animals require selenium (Se). Nickel (Ni), zinc (Zn), cobalt (Co), copper (Cu), and vanadium (V) are examples of heavy metals that are essential for life but also poisonous to cells (Meharg 2005).

- b) **Toxic/Non-Essential:** These heavy metals are hazardous to any species that come into contact with them, even at minute concentrations, and yet they serve no biological purpose. Some examples of such metals are lead (Pb), cadmium (Cd), arsenic (As), mercury (Hg), and chromium (Cr) (Sun et al. 2001).

CADMIUM

At 4°C, Cd has a specific gravity that is about 8.65 times that of water. Natural cadmium is always bound to zinc; it never occurs by itself. It is mostly manufactured as a waste product during the smelting of zinc, lead, and copper ores. Although greenockite (CdS) is less well-known than zinc mineral sphalerite (ZnS), it is an extremely important mineral in its own right (Thomas 1992). Cd is found in the crust of the Earth at low concentrations (0.1 to 0.5 ppm) but in many different places. Approximately 5-110 ng L⁻¹ of Cd has been

found in ocean water, with the majority of this concentration being deposited in marine phosphates (Morrow 2001). Emitted through both natural and human-caused processes, Cd is most commonly found in the environment due to its use in Ni-Cd batteries, paint, electroplating, and solar cells, as represented in Fig. 2 (ATSDR 2008).

CADMIUM POLLUTION

Heavy Cd contamination threatens the South and Southeast of the globe (Luo et al. 2012). Heavy metal pollution of China's agricultural soil has affected almost 20 million hectares, which might slow the country's food production (Wei & Chen 2001). Due to water scarcity, industrial effluents are increasingly being used for agricultural crop irrigation, contributing to soil contamination with hazardous metals (Luo et al. 2010). Cd is easily absorbed by living things due to its mobility and accumulation in the soil-plant system. While it serves no known biological purpose and is highly harmful to plants, animals, and humans (Lehoczky et al. 2000). The concentration of Cd, Ni, Cr, Zn, and Pb in urban soil was found to be higher than the allowable limit of surface soils (3 mg.kg^{-1} soil) in a study by Malik et al. 2010, who argued for the urgent need for extensive baseline investigations of geographical distribution and remediation of heavy metals. Soil Cd limits vary by country, with Chinese limits set at 0.6 mg.kg^{-1} (ESPA 2005), Dutch limits at 0.8-5 (Iram et al. 2012), and Indian limits at 3-6 mg.kg^{-1} (ESPA 2005). (Awashthi 2000).

Shah Alam River is polluted by the trash from numerous factories in the textile, paper, ghee, tannery, sugar mill, and distillery sectors (Khan et al. 2010). In the Shah Alam River,

the Cd concentration was observed to be ten times higher than the limit set by the WHO. Heavy metals (Cd, Cr, Co, Cu) were also shown to be polluting the Ravi River sediments by Rauf et al. (2009). Concentrations of Cd ranged from 0.99 to 3.17 micrograms per gram of dry matter. Metals like this accumulate in river sediments and then pollute the land above them. Kashif et al. (2009) studied heavy metal pollution in the Hudiara drain that runs near the Hudiara village in the region of Lahore in Pakistan. Due to the introduction of unknown polluted waste into the sewer, the metal pollution index increased. The accumulation of these metals in the food chain raises concerns about their potential hazard to human health.

Heavy metal contamination was also found in the municipal sewage water of Sargodha, Pakistan, as reported by Ahmad et al. (2011). Canola growth was stunted due to the high concentrations of Cd, Cr, and Pb in the wastewater. Rehman et al. (2008) analyzed the metal content of three industrial areas in Pakistan: Peshawar, Gujranwala, and Huripur. Industrial effluents with high concentrations of heavy metals are commonly utilized for irrigation by the local indigenous population, according to the paper. Crops that are subjected to this method absorb the metals, which then make their way into the human food supply. Another study used flame atomic absorption spectrometry to look for metal pollution in dust and soil samples obtained from several locations along the Islamabad Expressway (FAAS). Heavy metal buildup varied along the Expressway, although Cd was discovered at levels as high as 51 mg.kg^{-1} . Heavy metal pollution has increased as a result of urbanization, making its measurement essential (Faiz et al. 2009). In their study of 44

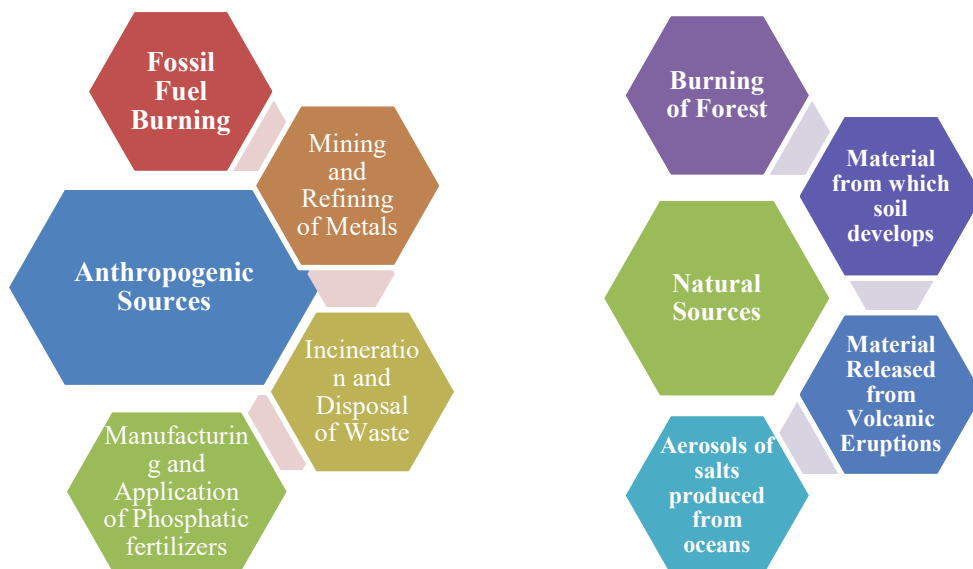


Fig. 2: Sources of cadmium.

samples, Ahmed et al. (2007) found that the Cd concentration in the blood of jewelers was $398\ 183\ \mu\text{g}\ 100\ \text{mL}^{-1}$, whereas the Cd concentration in the blood of automobile workers was $768\ 180\ \mu\text{g}\ 100\ \text{mL}^{-1}$. Cd levels were within WHO's tolerable range, but prolonged exposure could be harmful to those working in the jewelry and auto industries.

CADMIUM CONTAMINATION AND OTHER HEAVY METALS

Heavy metal contamination in agricultural soils and crops is receiving increased attention in the south and southeast Asian countries like Pakistan, India, Bangladesh, China, Japan, Malaysia, and Indonesia due to their impact on human health, which will hamper the further life processes in these regions. Enhanced heavy metal contamination in northeast China's Phaeozem due to human and industrial activities was observed by Guo & Zhuo (2006). The accumulation of four metals (Pb, Cd, Zn, and Cu) was investigated, and a spectrum of heavy metal concentrations in soil was recorded (10-62, 0.01-3, 40-248, and 10-51 $\text{mg}\cdot\text{kg}^{-1}$ soil, respectively). Previous data led them to believe that Cd, among other heavy metals, posed a unique environmental risk to the local area. Soil Cd is frequently found alongside Zinc, particularly in Zn and Cu ores. Plants may take up and translocate Cd as a result of a zinc deficiency (Koleli et al. 2004). In addition to raising Fe content, exogenous Cd treatment increased P, K, and Mn accumulation in wheat roots by limiting their transfer to the shoot (Zhang et al. 2002). Cd exchangeable percentages in soil were much greater than Cu and Pb exchangeable percentages. Cd was thought to be the most mobile element in the soil, making it easily available to crops and increasing the possibility that it would end up in human food sources. As a result, Cd pollution in agricultural soils became the region's top priority (Xiong et al. 2003). Cadmium (Cd) is a very poisonous metal that ranks eighth on the list of the most harmful elements, according to the US Environmental Protection Agency's (EPA) national priority list (HazDat 2008). Using edible crop components as metal accumulators causes spoilage, which limits food availability (Xiong et al. 2003). As previously discussed, Cd concentrations in soil and industrial effluent have exceeded the permissible level; nevertheless, the impacts of this increase on crop development, plant physiology, and biochemical properties have not been adequately examined.

PHYSIOCHEMICAL METHODS FOR REMEDIATION

Physical Methods

On-site remediation: It mainly involves the separation of contaminated soil from the uncontaminated one. But this procedure is not complete itself, it requires many further

engineering measures (Herrero et al. 2005). With the help of this technique, we can create hindrances for the other contaminates in a specified area (Zheng & Wang 2002). We can use this technique when other methods are not economically feasible. Subsurface barriers are employed in this technique to remove the contaminated water from the soil which will help in the prevention of surface water and groundwater flow. The flow of uncontaminated water can be prevented from contamination after the utilization of these subsurface barriers (Zhu et al. 2012). Barriers can be used in the form of upstream, downstream, or surrounding the contaminated site. We can use these barriers in combination with the system where capping arrangements can be done properly which helps in maintaining the isolation of contaminated soil, and infiltration of contaminated water can also be restricted.

Off-site remediation: Before 1984, this method was commonly used for the remediation of contaminants from the soil. In this technique, the soil which is full of contamination can be replaced by uncontaminated soil. By doing so, it is going to enhance the efficiency of soil which will help in further dilution of the concentration of heavy metals (Khalid et al. 2017). This technique can be employed in 2 ways: 1. Soil spading 2. Importing new soil to the site.

Chemical Methods

Soil washing: This is one of the widely considered methods of soil remediation. In this technique, different washing agents, such as inorganic, organic chelating agents, and surfactants, can be used. This technique also known as soil leaching or chemical extraction helps in the mobilization of organic and inorganic contaminants towards groundwater. A wide variety of reagents and chemicals can be utilized, such as EDTA, organic acids, cyclodextrins, and surfactants. Chelate EDDS was used for the chemical extraction of Zn and Pb (Hauser et al. 2005). Coal ash has become a popular material for the extraction of heavy metals. EDTA is well known for the effective removal of cationic metals rather than anionic metals. The soil wash method was developed for cadmium-contaminated paddy fields (Kimura et al. 2007). He performed it in three steps: (1) treating the soil with calcium chloride solution, (2) Eliminating Cd and CaCl_2 by washing of treated soil with H_2O , and (3) using of wastewater treatment system on site. The average cadmium concentration by two-thirds was reduced in rice grains. Soil fertility was affected but can be corrected afterward with this technique.

Immobilization techniques: This technique helps in the confinement of heavy metals with the help of immobilizing agents. Processes like adsorption, precipitation, and

complexation have been employed. Immobilizing agents, which are organic and inorganic, can be used for the immobilization of heavy metals in contaminated soil (Shahid et al. 2013, Austruy et al. 2014, Ashraf et al. 2016). Heavy metals can get immobilized on solid surfaces, which helps reduce the bioavailability in soil. Various organic agents and amendments are widely used in this technique such as biosolids and animal manures. Organic agents such as biosolids have both positive and negative kind of impacts on this process. Positive impact means they are going to act as the best adsorbent for the stabilization of heavy metals in soil (Venegas et al. 2015, Shakoor et al. 2015). A negative impact was also reported for these organic agents (Cele & Maboeta 2016). The reagent di-ammonium phosphate was studied to be more efficient for stabilizing Cd and Zn in soil (Khan et al. 2015). Metals can easily form complexes with organic components (Shahid et al. 2013). Organic contents of the soil were increased by doing organic amendments (Bolan et al. 2014). Cellulose, lignin proteins, lipids, simple sugars, hemicellulose, and starch can form complexes with metals (Niazi et al., 2017).

BIOREMEDIATION

Pollutants that are either organic or inorganic can be reduced to lower concentrations by using microbes, plants, or their metabolites. In the event of large volumes of effluents containing complex organic matter and low metal contamination, conventional Physico-chemical approaches for metal remediation are both prohibitively expensive and inappropriate. When the use of pure biosorption metal removal is not possible, a well-chosen consortium of metal-resistant cells in growth can guarantee improved removal by bio-precipitation, biosorption, and ongoing metabolic uptake of metals following physical adsorption (Gadd 2004). Researchers have recently discovered that bacteria, yeast, and fungi isolated from polluted environments may effectively scavenge metals. Some bacterial strains have a high tolerance for different metals, making them ideal for the simultaneous removal of those metals from wastes (Park et al. 2008). Everything is ready for metal collecting to be applied to growing microbial cells that are resistant to metals.

BIO-AUGMENTATION

This subfield of bioremediation involves the external application of microorganisms that have been previously

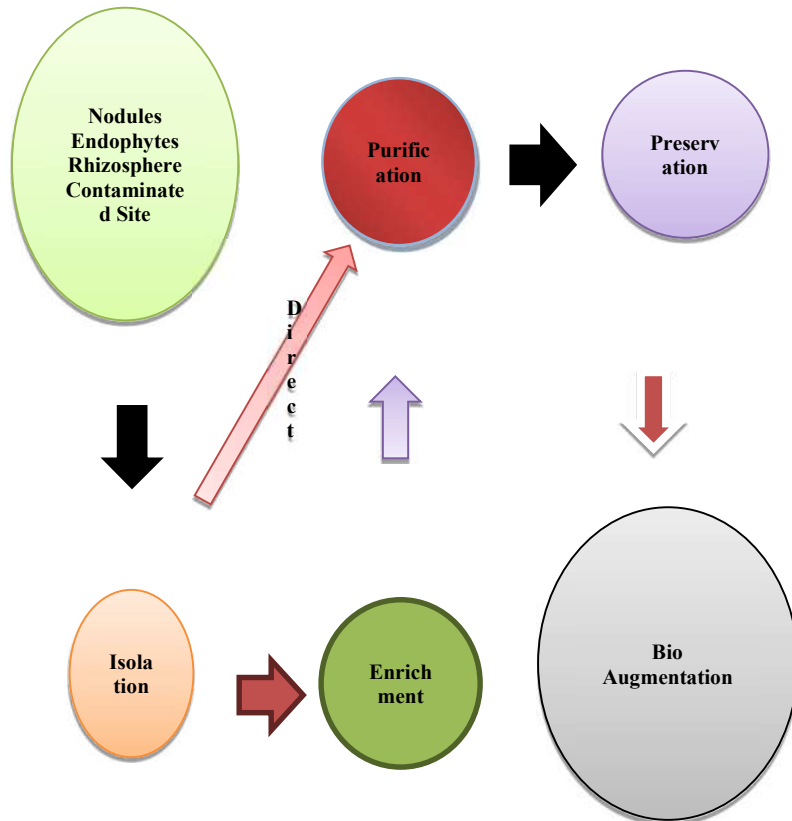


Fig 3: Schematic diagram of isolation and inoculation of microbes from source to end user.

isolated from their native environments (such as the rhizosphere, nodules, and polluted areas), purified, and enriched in a controlled laboratory setting (Fig. 3). The goal of introducing new microorganisms from outside the host organism is to increase the abundance of beneficial microorganisms in a given area. The toxicity of metals makes them an obstacle to the growth of microorganisms in both soil and water. What this means is that bio-stimulation or increasing a targeted population of microorganisms in a polluted place is necessary for decontamination (bio-augmentation). Some researchers have isolated bacteria from polluted places and then enriched them to be more effective against that particular pollutant (Kuffner et al. 2010) before applying them there. Inhibiting bacterial development, cadmium is a powerful metal (Prapagdee & Watcharamusik 2009). Cd-resistant strains were obtained from several contaminated locations and tested for Cd scavenging in a range of environmental settings by many researchers. Soil contaminated with metals may be more habitable for bacteria with a high tolerance for the elements. Heavy metal resistance, the mobilization or immobilization of metals in soil, and metal uptake by plants have all been studied extensively and found to correlate well (Kuffner et al. 2008, Gadd 2000, Aleem 2003).

PHYTOREMEDIATION

Phytoremediation refers to the practice of using plants to remove and bind to pollutants. The phytoextraction of Cd from soil using three plant species was conducted with and without inoculation. The uptake and buildup of Cd in the plant's foliage from calcareous soil were dramatically enhanced by bacterial inoculation. Cd buildup in plants was inversely associated with a decrease in plant fresh weight. It was shown that under inoculation conditions, *Amaranthus retroflexus* accumulated the most Cd of any crop tested (including sunflowers and alfalfa) (Motesharezadeh et al. 2010). The potential for metal extraction by four bacterial species isolated from a radish plant (Chen et al. 2010). Improvements in both growth and Cd extraction from the soil to various plant sections were observed after bacterial inoculation. The inoculated bacteria produced siderophores, IAA, ACC-deaminase (inhibit ethylene synthesis), and solubilized inorganic P, all of which contributed to the enhanced growth. Microbial activity in soil increased cadmium's solubility and mobility, making it easier for the radish to absorb. Getting metals out of contaminated soil is a complicated process that relies heavily on bacteria. *Pseudomonas* and *Bacillus*, two common bacteria, increased Cd extraction from polluted soil by 58% to 104%, respectively. For the aforementioned bacterial strains,

tomato cadmium absorption was increased by 92.1-113.0 percent compared to the non-inoculated control group (He et al. 2009).

Vegetables high in chlorophyll are less likely to contain metals than other vegetables. Two leafy vegetables were studied for their sensitivity to Cd stress and reported negative effects by Liu et al. (2007). Both plants absorbed significant amounts of Cd through their root cell walls, while *Brassica pekinensis* had larger Cd concentrations in their shoot. Protein levels rose in response to Cd stress and were associated positively with soluble Cd. Plants' metal accumulation is influenced by the metals' solubility, mobility, and velocity of transfer from the soil to the roots (Kumar et al. 2009). Vetches had the most metal uptake, while lufa had the lowest. In addition, heavy metals like Cd accumulate more in the leaves of vegetables than in the roots. Evidence was presented that vegetables have the potential to function as a hyperaccumulator for in-situ metals cleanup. Higher biomass and greater Cd extraction from polluted soil were observed in *Solanum nigrum* (Ji et al. 2011). Double-cropping this crop in contaminated soil was shown to dramatically lower Cd levels in field trials. These qualities are what made the *Solanum nigrum* a viable option for metal extraction.

The accumulation of Cd at higher trophic levels of the food chain has made the worldwide problem of remediating Cd-contaminated soil even more pressing. The ability of Cd hyperaccumulators to withstand and take up considerable quantities of heavy metal from soils makes them an interesting study subject. Species of plants vary in their ability to hyperaccumulate Cd. Since Cd has weak affinities with soil ligands, it can be readily taken up by the plant's roots and then distributed throughout the rest of the plant's aerial parts (Sanit'a Di Toppi & Gabbrielli 1999), pH, temperature, the content of Cd in media, and the concentration of other components are all responsible for plant remediation of Cd (Yang et al. 1998). Species of plants have been identified as Cd hyperaccumulators due to their ability to store up to 105 mg.g⁻¹ Cd in their shoot dry weight (Baker & Brooks 1989).

Cd hyperaccumulation in *Thlaspi caerulescens* was first documented in the early 1990s. The first signs of Cd toxicity in *T. caerulescens* appeared at a concentration of 200 M, indicating a substantially higher tolerance to the metal. Cd was notably concentrated in the shoots of *T. caerulescens*, suggesting that it was translocated from the solution to the upper parts of the plant (Brown et al. 1994). The *T. caerulescens* hairy root culture also demonstrated Cd remediation from an aqueous solution (Nedelkoska & Doran, 2000). "These findings verified the

use of *T. caerulea* as a hyperaccumulating plant for the removal of Cd contamination. Two species, *A. halleri* and *T. caerulea*, were observed to hyperaccumulate Cd in addition to Zn (Cosoio et al. 2004). Cadmium of *A. halleri* was found in the mesophyll of leaves (Kupper et al. 2004). However, *T. caerulea* and *A. halleri* were discovered to be low-biomass plants that could not adapt to a wide variety of environments. As a result, several alternatives to *T. caerulea* and *A. halleri* were recommended, including *Calamagrostis epigejos*, *Sedum* species, *Brassica* species, and *Solanum nigrum* (Lehmann & Rebele 2004, Sun et al. 2009, Wei et al. 2006, Xiao et al. 2017, Li et al. 2018, Quartacci et al. 2006, Sheng & Xia 2006, Liu et al. 2011). *C. epigejos* grows quickly, even in poor, sandy soils or wet, marshy areas, and it can withstand harsh weather and high winds. Cd uptake was investigated, and limited root-to-shoot transfer was detected; this suggests that the plant can provide greater ecological value through phytostabilization than through phytoextraction, thanks to its high tolerance for heavy metals (Lehmann & Rebele 2004).

As well as Cu and Zn, *S. nigrum* has been found to accumulate significant amounts of Cd (Wei et al. 2005). There was also a study that looked at how EDTA affected Cd absorption by *S. nigrum*. It was reported that only a small dose of EDTA (0.1 g.kg⁻¹) in soil could successfully promote phytoextraction of Cd. Still, a large dose (0.5 g.kg⁻¹) harmed plant growth and reduced biomass, rendering the phytoremediation approach less efficient (Sun et al. 2009). The ability of *S. nigrum* to enter a blooming stage has been investigated in a subsequent study (Wei et al. 2006). Collectively, these investigations demonstrate that *S. nigrum* significantly accumulates high levels of Cd and contributes to the regulation of pollution in Cd-contaminated soils. *Sedum alfredii*, another plant, also showed considerable promise for Cd clean-up. This research demonstrated that exposure to high Zn concentrations results in elevated Cd levels (Xiong et al. 2004). As Cd and Zn concentrations rise, the amount of both metals found in leaves and stems rises as well. This finding confirmed that *S. alfredii* functions as a hyperaccumulator of Cd and Zn. Soil DC supply and additions like humic acid and compost increased Cd extraction by *S. alfredii* by a factor of 2 (Xiao et al. 2017). By decreasing ion mobility in contaminated soil, *S. plumbizincicola*, another species, has been shown to increase Cd and Zn content when EDTA is added (Li et al. 2018).

Phytoextraction of Cd from the large-sized plant *Brassica juncea* (Indian mustard) was found to be on par with that from *T. caerulea*. Unlike a Cd-sensitive species, *B. juncea* plants can withstand high levels of Cd stress (Quartacci et al. 2006). Lipid alterations in the cell membranes of *B. napus*

were seen with direct exposure to cadmium, suggesting that this species of *Brassica* is more resistant to Cd than its relatives (Sheng & Xia 2006). It was discovered that six different kinds of the plant *B. pekinensis*, often known as Chinese cabbage, were able to extract a large quantity of Cd from soil (Liu et al. 2011).

More effective soil plants for Cd clean-up have been the subject of hydroponic system research. Arundo donax's phytoremediation capability was investigated through experiments in both soil and hydroponic systems. Because both the Bio Concentration Factor (BCF) and the Translocation Factor (TF) were greater than 1, the authors concluded that Cd was taken up significantly more efficiently in the hydroponic system than in soil cultures but that high exposure to Cd caused the plant to exhibit antioxidant stress (Khankhane et al. 2017). Garlic (*Allium sativum*) grown in a hydroponic system has been shown to accumulate high levels of cadmium (Cd) in its bulb, shoot, and root, proving that garlic has the potential to remove Cd from its solution and store it there. Increases in Cd²⁺ concentration increase the quantity of Cd in garlic roots. Researchers observed that the plant extracted Cd at a rate 1826 times higher than the control but that only a trace amount of Cd is accumulated in garlic bulbs and shoots. (Jiang et al. 2001). Growing *Bidens pilosa* on soil resulted in 405.91 mg.kg⁻¹ of Cd accumulation in its shoots while growing it in nutrient solution resulted in 1651.68 mg.kg⁻¹ (Dai et al. 2017). There are a few species of hydroponics plants that are hyperaccumulators of Cd, and they include *Coronopus didymus* and *Abelmoschus manihot* (Sidhu et al. 2017). In *C. didymus*, TF is more efficacious than BCF. *A. manihot*'s BCF values were found to be more than the reference value, and its TF values were also greater than 1 after being treated with Cd at 15-60 mg.kg⁻¹ (Wu et al. 2018). Superoxide anion amount, hydrogen peroxide content, and antioxidative activities were all shown to rise in both the roots and the shoots, all of which helped with the detoxification process (Sidhu et al. 2017, Wu et al. 2018). Because of this, *C. didymus* and *A. manihot* can be used as Cd hyperaccumulators to clear Cd from working-field environments.

MECHANISMS OF CADMIUM REMOVAL

Soil contamination can occur when any pollutant, organic or inorganic, comes into contact with soil components (Fig. 4). But when heavy metals are bound to the organic matter and microbial cells in the soil, they are not destroyed. They can only be released slowly, limiting their bioavailability to plants.

Biosorption

Metals can be bound to the surface of cells without expending

any energy (passive biosorption) or to the inside of cells at the cost of energy (active biosorption) by the use of functional groups and proteins (Das et al. 2008, Goyal et al. 2003). Metals can be physically adsorbed on the surface of microorganisms and organic molecules in a quick process known as passive biosorption. In contrast, the more involved process of active biosorption might take a while. Biosorption is essential for both live and dead biomass. However, bioaccumulation is unique to the living organisms.

Biosorption is a complex process that is regulated by various factors such as temperature, pH, biosorbent concentration, and presence of contaminants. With the rise in the concentration of contaminants, biosorption tends to decrease. In this technique, the amount of biosorbent also plays an important role, which restricts the sorption process by bringing conformational changes in binding sites within the biosorbent (Das et al. 2008). The biosorption of Cd can be affected by temperature, pH, and time, which researchers have already reported. In general, it is the notion that with each degree rise in temperature increases the rate of reaction of the biosorption process by 10 times. Temperature factor plays a partial role in this process. When it is in the range of 25-30°C, the adsorption of cadmium occurs (Zeng et al. 2010), while at the range of 20-35°C, the biosorption process is not affected (Aksu et al. 1992). The influence of pH on the bioavailability of metals in the solution has been reported, which in turn affects the functioning of the carboxyl group. At higher pH, this carboxyl group gets activated and reduces metal availability by sorption-precipitation mechanisms (Kratochvil & Volesky 1998).

Microbial biomass as biosorbent: Heavy metals can be absorbed by microbes thanks to the presence of different functional groups. Cell walls are mostly composed of cellulose in algae, chitin and chitosan in fungi, and peptidoglycan in bacteria. These chemicals have a negative charge on microbial surfaces because of the presence of carboxyl, sulfhydryl, and sulfate functional groups (Das et al. 2008). To effectively bind positively charged metals, these active sites are required to be negative in charge. Cadmium can get adsorbed on the microbial and plant biomass by occupying active sites. pH influences the charges in soil. Acidic soils carry a positive charge, while basic soils carry a negative charge. In this case, the interaction between soil-metal and microbe would be a sandwiched kind of reaction for metals like cadmium. Soil health can be improved by the addition of organic matter, which provides negative charges to the particles that help in metal sorption by physical adsorption or ion exchange mechanisms. Metal bioremediation has been linked to a wide variety of tolerance and resistance mechanisms (Giotta et al. 2006).

Biosorption of Cd was effective for the photosynthetic bacterial species such as *Rhodobacter* and *Rhodovulum* depending upon their growth conditions, whether it is dark or light under aerobic and anaerobic processes. It was reported by Watanabe et al in 2003 that *Rhodovulum* species had a maximum adsorption capacity of Cd in aerobic dark $K_f= 17.44$ and $K_f= 1.27$ for anaerobic light growing conditions. Biological strains were used for the biosorption of cadmium since concentrations were discovered to be too high for safety (Abou Zeid et al. 2009). Biosorption of Cd

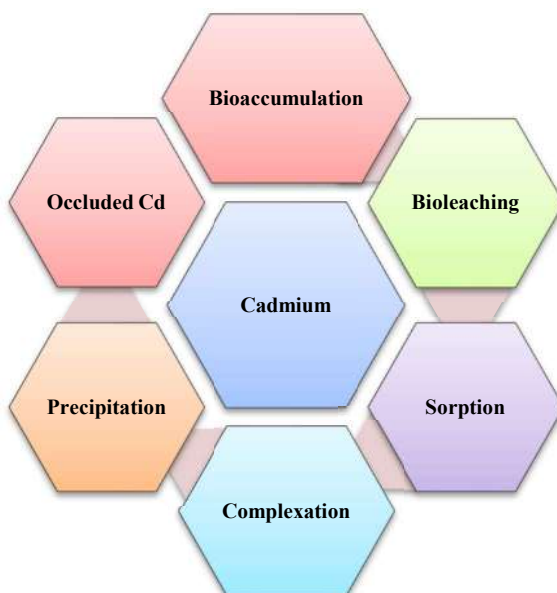


Fig. 4: Interactions of cadmium in soil.

by *Pseudomonas mendocina* proved efficient. Studying the optimal conditions for Cd uptake, researchers found that 2.5 ppm Cd, pH 7, and 30 °C were optimal. Different bacterial species, as described by Kumar et al. (2010), have been shown to reduce the stressors of numerous metals by a process called biosorption. *Aspergillus niger* reduced Cd stress by 50%, whereas *Pseudomonas* was the most effective metal-removal bacteria.

There was a positive association between Cd depletion and protein synthesis, suggesting that the protein generated

by the implanted microorganisms plays a major role in Cd removal (Chovanova et al. 2004). Even though bacteria are abundant in soil and play a key part in biosorption, fungi efficiently adsorbed metals on their surface because of their higher biomass. Biosorption of Cd, Cu, and Pb by fungal cells was highly efficient. The results of the study's biosorption of metals were best explained by the Langmuir model. Dried fungal biomass was shown to be the most effective at absorbing heavy metals at a pH of 6. (Say et al. 2001). Yeast's ability to biosorb metals via cell

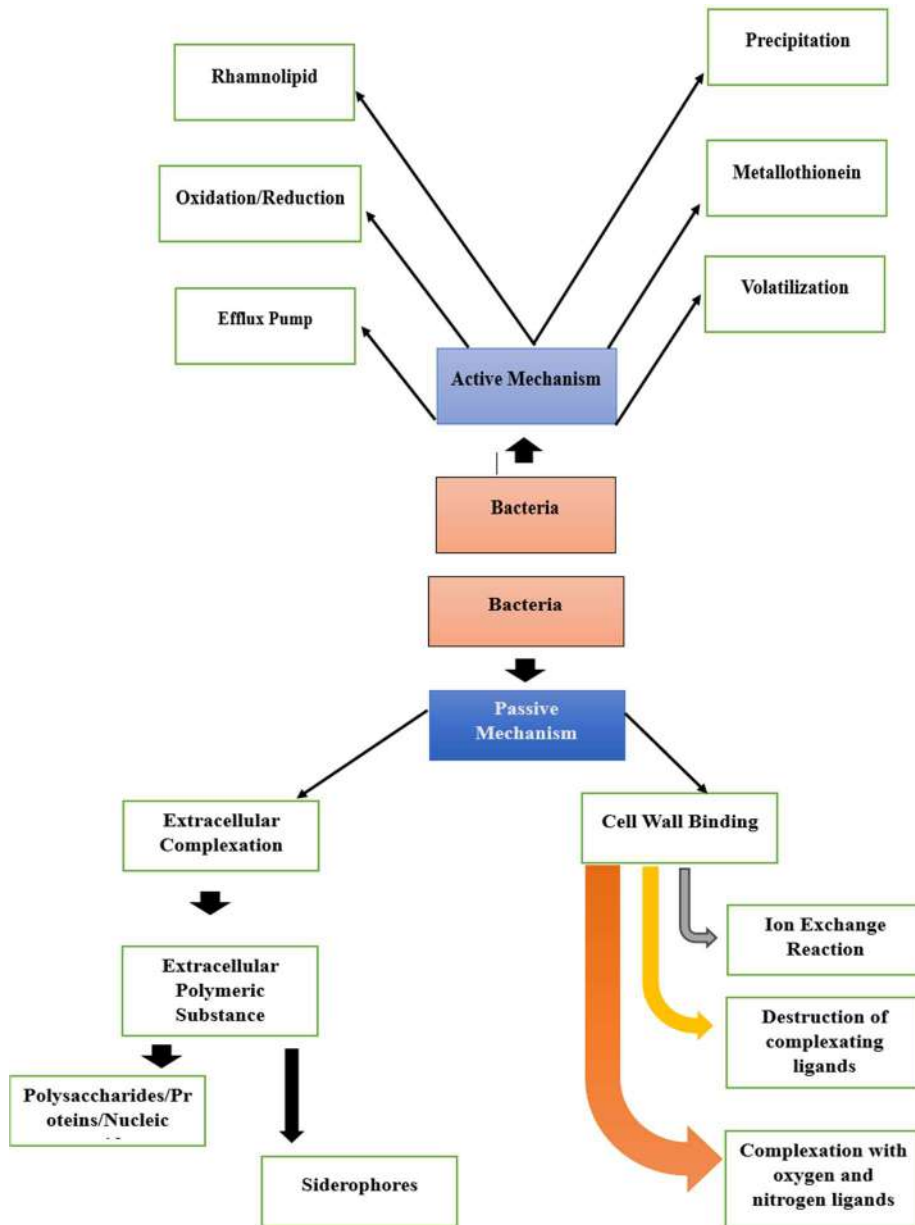


Fig. 5: General cadmium resistance mechanisms operating in bacteria.

surface adsorption was crucial. Cd uptake by exponentially growing yeast was greatest when inoculated at 30 degrees Celsius (Anagnostopoulos et al. 2010). The growth of *Rhodobacters phaeoides* was studied by Bai et al. (2008) to learn more about the kinetic characteristics and mechanism of Cd removal. With an R2 value between 0.9790 and 0.9916, the second-order equation was used to fit the data on the elimination process. In addition, bio-precipitation as Cd sulfide was revealed to be the primary route for Cd elimination, with bio-sorption only playing a secondary role.

Bio-precipitation

The precipitation mechanism could be used to get rid of cadmium. When there are more carbonates, phosphates, and sulfides in the soil (Wang et al. 2002, 2001), chemical precipitation is a major contribution. When bacteria exist that can hydrolyze the aforementioned chemicals and release the appropriate anions for metal precipitation, bio-precipitation becomes the most common method. As a result of the widespread interest in the recently published study on metal precipitation by microbial manipulation, other investigations on the topic have been reported (Seetharam et al. 2009, Diels et al. 2006, Wang et al. 2001, 2002, Sharma et al. 2000, Bang et al. 2000). Metals are removed via bio-precipitation after being reduced in concentration via sulfate reduction, which is aided by the use of a variety of organic waste as a carbon source for SRB (Diels et al. 2006). It was discovered that *Pseudomonas aeruginosa* was responsible for the removal of Cd from hydrothermal vents through precipitation; the bacteria hydrolyzed thiosulfate, releasing sulfide ions that interacted with Cd to create cadmium sulfide precipitates (Wang et al. 2002).

MECHANISM OF CADMIUM RESISTANCE IN BACTERIA

For the detoxification of cadmium and other heavy metals, eukaryotic microorganisms exhibit a special mechanism that binds with polythiols. The presence of plasmids in bacteria promotes resistance against heavy metals. Resistance mechanisms in bacteria against cadmium employ various mechanisms, which are as follows (Fig. 5).

Efflux Mechanisms

A number of efflux mechanisms have been studied so far. The presence of integrated membrane proteins in the efflux system helps in the protrusion of contaminants from inside of the microbes into the environment. A very well-known efflux mechanism has been reported in *S. aureus* (Andersen 2015). With the advancements in the field of bioinformatics maximum number of efflux pump proteins were identified

in *S. aureus*, which were encoded by either plasmids or chromosomes (Schindler et al. 2015). These efflux pumps were further categorized into 5 different families.

- 1) the resistance-nodulation-division (RND) superfamily,
- 2) the ATP binding cassette (ABC) superfamily,
- 3) the multidrug and toxin extrusion (MATE) family,
- 4) the small multidrug resistance (SMR) family, and
- 5) the major facilitator superfamily

There are various RND transporters, like the AcrAB–TolC complex and the MexBA–OrpM complex, which are present in *E. Coli* and *P. aeruginosa*. Both are gram-negative. With these transporters, periplasmic adaptor proteins, transmembrane pumps, and the outer membrane channels were also present, which helps in the efflux of metals. Gram-negative bacteria that possess RND transporters are responsible for the resistance against multidrug. Protein AcrB, which is present in *E. Coli*, has a homologous protein that was identified in the *S. aureus* named FarE, which is also a part of the RND efflux system. Thus, the resistance against metals in *S. aureus* was identified due to the presence of FarE when it combines with fatty acids, which act as the substrates (Alnaseri et al. 2015).

Alcaligenes eutrophus strain CH34 was found in sediments or soils with a content of heavy metals. This strain grows at the expense of a variety of organic substrates with the exclusion of sugars, oxidative metabolism, facultative chemolithotrophy, and the presence of megaplasmids conferring resistance towards heavy metals (Collard et al. 1993). Plasmid pMOL 30 is responsible for the resistance towards Cd^{2+} , Co^{2+} , Cu^{2+} , Zn^{2+} , Hg^{2+} and Ti^{2+} (Diels & Mergeay 1990). In this plasmid, the CZC gene cluster ensures resistance to these metals. This gene cluster includes the operon (structural genes), upstream of which a regulatory region is located. When compared with the sequences of corresponding putative proteins, the strongly hydrophilic *czcA* emerges as a transmembrane protein, which ensures a cation/protein antiporter efflux. In association with *czcB* and *czcC*, *czcA* allows the efflux of heavy metal ions. A cadmium-resistant micro-organism identified as an *Azomonas agilis* PY101 has been isolated from a contaminated stream, which accumulated high levels of cadmium by the formation of cadmium sulfide in the cell (You et al. 1996, You & Park 1998).

Enzymes responsible for the impermeability of bacterial cell walls to the cadmium: Cadmium makes its way into the cell as a toxic substrate of zinc and manganese transport systems, which are present in Gram-negative and Gram-positive bacteria. Both transport systems are

encoded by chromosomes (Filice et al. 2016). The concept of impermeability was best shown in *B. Subtilis*, which is associated with chromosomal mutations. As a result of these mutations, the entry of cadmium is restricted by membranes of the transport system (Zheng et al. 2016).

Enzymes catalyze the biotransformation of cadmium into non-toxic forms: For the remediation of heavy metals many organisms, such as bacteria and fungi, employ different strategies of detoxification processes. During the detoxification process, changes in the valence state of organometallic metals or compounds occur (Dixit 2015). This biotransformation results in valency change, which further results in the production of less volatile and toxic compounds. For example, there is the reduction of mercury ions into metallic mercury and the oxidation of arsenite to arsenate. In comparison to other heavy metals, the actual mechanism required for the conversion of cadmium to Cd^0 is still unknown (Guo et al. 2016). Methylation is a widely used and most common detoxification mechanism that results in the transformation of metals into their organometallic compounds. Mercury and lead are metals that can undergo methylation, which produces free metal forms that are less toxic than the actual ones, such as methyl mercury and dimethyl mercury are more toxic than mercury. Methylated products form volatile compounds following chemical and microbial degradation mechanisms. There is only one report that showed the biotransformation of cadmium and lead (Pavic' et al. 2015).

Cadmium ions binding: Metallothionine, metallo chaperons, cell wall components (exopolysaccharides), surface factors, and their binding to intracellular binding proteins provide an important strategy for bacterial species to combat cadmium-increasing concentrations. In *Arthobacter viscosus* and *Klebsiella aerogenes*, cadmium can bind with the capsular surface, while in other bacteria, cadmium binds to insoluble cell-bound $CdHPO_4$ (Coelho et al. 2015). The binding potential of intracellular binding proteins helps in the sequestration and storage of nutrients, which enhances the resistance potential. Small cysteine-rich proteins such as metallothionines can bind with Cd^{2+} (Naik & Dubey 2017). The presence of this small cysteine-rich protein, metallothionine, helps in the reduction of the concentration of free ions in the cytoplasm and cytoplasmic metal cation binding proteins.

CONCLUSION

Bioremediation is an important part of environmental clean-up because it allows metals like lead, mercury, and cadmium to be removed without releasing harmful pollutants. Bioremediation occurs when contaminants and essential

supplements are degraded by microorganisms such as nitrogen, phosphorus, and trace components. Treatment of degraded wastewater and soil has proven to be an affordable option in comparison to other clean-up methods and pollution control technologies. To develop new methods of cleaning up polluted areas, collaborative efforts are required. Microorganisms are essential for the preservation of natural resources and environmental management. Even though fungi, algae, and protists can all help remove persistent pollutants, more research is needed to determine the best microbial genetic and expression system so that these agents can be the most effective bioremediators in the future.

REFERENCES

- Abou Zeid, A.A., Hassanein, W.A., Salama, H.M. and Fahd, G.A.A. 2009. Biosorption of some heavy metal ions using bacterial species isolated from agriculture waste water drains in Egypt. *J. Appl. Sci. Res.*, 5: 372-383.
- Ahmad, K., Ejaz, A., Azam, M., Khan, Z.I., Ashraf, M., Al-Qurainy, F., Fardous, A., Gondal, S., Bayat, A.R. and Valeem, E.E. 2011. Lead, cadmium and chromium contents of canola irrigated with sewage water. *Pak. J. Bot.*, 43: 1403-1410.
- Ahmed, S., Ikram, N., Shan, U.A and Ayyub, A. 2007. Heavy metal exposure; jewelers and automobile workers. *Professional Med. J.*, 14: 398-402.
- Aksu, Z., Sag, Y. and Kutsal, T. 1992. The biosorption of copper by *C. vulgaris* and *Z. ramigera*. *Environ. Technol.*, 13: 579-586.
- Aleem, A., Isar, J. and Malik, A. 2003. Impact of long-term application of industrial wastewater on the emergence of resistance traits in *Azotobacter chroococcum* isolated from rhizospheric soil. *Bioresour. Technol.*, 86(1): 7-13.
- Alnaseri, H., Arsic, B., Schneider, J.E., Kaiser, J.C., Scinocca, Z.C., Heinrichs, D.E. and McGavin, M.J. 2015. Inducible expression of resistance nodulation-division-type efflux pump in *Staphylococcus aureus* provides resistance to linoleic and arachidonic acids. *J. Bacteriol.*, 197:1893-1905.
- Anagnostopoulos, V.A., Symeopoulos, B.D. and Soupioni, M.J. 2010. Effect of growth conditions on biosorption of cadmium and copper by yeast cells. *Global NEST J.*, 12: 288-295.
- Andersen, J.L. 2015. Multidrug efflux pumps from Enterobacteriaceae, *Vibrio cholerae*, and *Staphylococcus aureus* bacterial food pathogens. *Int. J. Environ. Res. Public Health*, 12:1487-1547.
- Ashraf, A., Bibi, I., Niazi, N.K., Ok, Y.S., Murtaza, G., Shahid, M., Kunhikrishnan, A., Li, D. and Mahmood, T. 2016. Chromium (VI) sorption efficiency of acid-activated banana peel over organo-montmorillonite in aqueous solutions. *Int. J. Phytoremed.*, 19(7): 605-613.
- ATSDR. 2008. Draft Toxicology Profile for Cadmium by the Agency for Toxic Substances and Disease Registry. US Department of Health and Human Services, Public Health Service, p.265.
- Austruy, A., Shahid, M., Xiong, T., Castrec, M., Payre, V., Niazi, N.K., Sabir, M. and Dumat, C. 2014. Mechanisms of metal-phosphates formation in the rhizosphere soils of pea and tomato: environmental and sanitary consequences. *J. Soils Sed.*, 14(4): 666-678.
- Awashthi, S.K. 2000. Prevention of Food Adulteration Act No. 37 of 1954: Central and State Rules as Amended for 1999. Ashoka Law House, New Delhi, India.
- Bai, H.J., Zhang, Z.M., Yang, G.E. and Li, B.Z. 2008. Bioremediation of cadmium by growing *Rhodobactersphaeroides*: Kinetic characteristic and mechanism studies. *Bioresour. Technol.*, 99: 7716-7722.

- Baker, A. and Brooks, R. 1989. Terrestrial higher plants hyperaccumulate metallic elements. A review of their distribution, ecology, and phytochemistry. *Biorecovery*, 1(2): 81-126.
- Bang, S.W., Clark, D.S. and Keasling, J.D. 2000. Cadmium, lead, and zinc removal by expression of the thiosulfate reductase gene from *Salmonella typhimurium* in *Escherichia coli*. *Biotechnol. Lett.*, 22: 1331-1335.
- Beolchini, F., Dell'Anno, A., Fonti, V., Rocchetti, L., Ubaldini, S., Vegliò, F. and Danovaro, R. 2008. Bioleaching as a bioremediation strategy for dredged sediments polluted by heavy metals. *Europ. Bioremed. Conf.*, 07: 601.
- Bolan, N., Kunhikrishnan, A., Thangarajan, R., Kumpiene, J., Park, J., Makino, T., Kirkham, M.B. and Scheckel, K. 2014. Remediation of heavy metal(loid) contaminated soils – To mobilize or to immobilize? *J. Hazard. Mater.*, 266: 141-166.
- Brown S. L., Chaney, R. L., Angle, J. S. and Baker, A. J.M. 1994. Phytoremediation potential of *Thlaspi caerulescens* and bladder campion for zinc- and cadmium-contaminated soil. *J. Environ. Qual.*, 23(6): 1151-1157.
- Burd, G.I., Dixon, D.G. and Glick, B.R. 1998. A plant growth-promoting bacterium that decreases nickel toxicity in plant seedlings. *Appl. Environ. Microbiol.*, 64: 3663-3668.
- Cele, E.N. and Maboeta, M. 2016. A greenhouse trial to investigate the ameliorative properties of biosolids and plants on physicochemical conditions of iron ore tailings: Implications for an iron ore mine site remediation. *J. Environ. Manag.*, 165: 167-174.
- Chaffei, C., Pageau, K., Suzuki, A., Gouia, H., Ghorbal, H.M. and Daubresse, C.M. 2004. Cadmium toxicity induced changes in nitrogen management in *Lycopersicon esculentum*, leading to a metabolic safeguard through an amino acid storage strategy. *Plant Cell Physiol.*, 45: 1681-1693.
- Chen, L., S. Luo, X. Xiao, H. Guo, J. Chen, Y. Wan, B. Li, T. Xu, Q. Xi, C. Rao, C. Liu and G. Zeng. 2010. Application of plant growth-promoting endophytes (PGPE) isolated from *Solanum nigrum* L. for phytoextraction of Cd-polluted soils. *Appl. Soil Ecol.*, 46: 383-389.
- Chen, S., Chao, L., Sun, L. and Sun, T. 2013. Effects of bacteria on cadmium bioaccumulation in the cadmium hyperaccumulator plant *Beta vulgaris* var. *Cicla* L. *Int. J. Phytorem.*, 15: 477-487.
- Cheng, F.M., Zhao, N.C., Xu, H.M., Li, Y., Zhang, W.F., Zhu, Z.W. and Chen, M.X. 2006. Cadmium and lead contamination in japonica rice grains and its variation among the different locations in southeast China. *Sci. Total Environ.*, 359: 156-166.
- Chovanova, K., Sladekova, D., Kme, V., Proksova, M., Harichova, J., Puskarova, A., Polek, B. and Ferianc, P. 2004. Identification and characterization of eight cadmium-resistant bacterial isolates from a cadmium-contaminated sewage sludge. *Biol. Bratislava.*, 59: 817-827.
- Coelho, L.M., Rezende, H.C., Coelho, L.M., de Sousa, P.A., Melo, D.F. and Coelho, N.M. 2015. Bioremediation of polluted waters using microorganisms. In: N Shiomi (ed) *Agricultural and biological sciences. Adv. Bioremed. Wastewater Pollut. Soil*, 11: 514.
- Collard, J.M., Provoost, A., Taghavi, S. and Mergeay, M. 1993. A new type of *Alcaligenes eutrophus* CH34 zinc resistance generated by mutations affecting the regulation of the *cnr* cobalt nickel resistance system. *J. Bacteriol.*, 175: 779-784.
- Cosio, C., Martinoia, E. and Keller, C. 2004. Hyperaccumulation of cadmium and zinc in *Thlaspi caerulescens* and *Arabidopsis halleri* at the leaf cellular level. *Plant Physiol.*, 134: 716-725.
- Dai, H., Wei, S., Twardowska, I., Han, R. and Xu, L. 2017. Hyperaccumulating potential of *Bidens pilosa* L. for Cd and elucidation of its translocation behavior based on cell membrane permeability. *Environ. Sci. Pollut. Res.*, 24(29): 23161-23167.
- Das, N., Vimala, R. and Karthika, P. 2008. Biosorption of heavy metals. An overview. *Ind. J. Biotechnol.*, 7: 159-169.
- Diels, L. and Mergeay, M. 1990. DNA probe mediated detection of resistance bacteria from soils highly polluted by heavy metals. *Appl. Environ. Microbiol.*, 56: 1485-1491.
- Diels, L., Geets, J., Dejonghe, W., Van Roy, S., Vanbroekhoven, K., Szewczyk, A. and Malina, G. 2006. Heavy metal immobilization in groundwater by in situ bioprecipitation: Comments and Questions about efficiency and sustainability of the process. *Soils Sed. Water Energy*, 11: 99-112.
- Dixit, R. 2015. Bioremediation of heavy metals from soil and aquatic environment: an overview of principles and criteria of fundamental processes. *Sustainability*, 7: 2189-2212.
- Ekmekçi, Y., Tanyolaç, D. and Ayhan, B. 2008. Effects of cadmium on antioxidant enzyme and photosynthetic activities in leaves of two maize cultivars. *Plant Physiol.*, 165: 600-611.
- Faiz, Y., Tufail, M., Javed, M.T., Chaudhry, M.M. and Siddique, N. 2009. Road dust pollution of Cd, Cu, Ni, Pb, and Zn along Islamabad Expressway, Pakistan. *Microchem. J.*, 92: 186-192.
- Filice, F.P., Li, M.S., Henderson, J.D. and Ding, Z. 2016. Mapping Cd²⁺-induced membrane permeability changes of single live cells by means of scanning electrochemical microscopy. *Anal Chim Acta*, 12: 101. doi: 10.1016/j.aca.2015.12.027
- Fletcher, T. 2002. Neighborhood change at Love Canal: Contamination, evacuation, and resettlement. *Land Use Policy*, 1 311-323.
- Gadd, G.M. 2000. Bioremediation potential of microbial mechanisms of metal mobilization and immobilization. *Curr. Opin. Biotechnol.*, 11: 271-279.
- Gadd, G.M. 2004. Microbial influence on metal mobility and application for bioremediation. *Geoderma*, 122: 109-119
- Giotta, L., Agostiano, A., Italiano, F., Milano, F. and Trotta, M. 2006. Heavy metal ions influence the photosynthetic growth of Rhodobactersphaeroides. *Chemosphere*, 62: 1490-1499.
- Goyal, N., Jain, S.C. and Banerjee, U.C. 2003. Comparative studies on the adsorption of heavy metals. *Adv. Environ. Technol.*, 7: 311-319.
- Grichko, V.P. and Glick, B.R. 2001. Amelioration of flooding stress by ACC deaminase-containing plant growth-promoting bacteria. *Plant Physiol. Biochem.*, 39: 11-17.
- Guo, G.L. and Zhou, Q.X. 2006. Evaluation of heavy metal contamination in Phaeozem of northeast China. *Environ. Geochem. Health*, 28: 331-340.
- Guo, S., Yao, Y., Zuo, L., Shi, W., Gao, N. and Xu, H. 2016. Enhancement of tolerance of *Ganoderma lucidum* to cadmium by nitric oxide. *J Basic Microbiol.*, 56: 36-43.
- Hall, J.L. 2002. Cellular mechanisms for heavy metals detoxification and tolerance. *J. Exp. Bot.*, 53: 1-11.
- Han, F.X., Banin, A. and Y. Su. 2002. Industrial age anthropogenic inputs of heavy metals into the pedosphere. *Naturwissenschaften*, 89(11): 497-504.
- Hauser, L., Tandy, S., Schulin, R. and Nowack, B. 2005. Column extraction of heavy metals from soils using the biodegradable chelating Agent EDDS. *Environ. Sci. Technol.*, 39(17): 6819-6824.
- HazDat. 2008. Cadmium. HazDat Database: ATSDR's Hazardous Substance Release and Health Effects Database. Atlanta, GA: Agency for Toxic Substances and Disease Registry. <http://www.atsdr.cdc.gov/hazdat.html>.
- He, L.Y., Chen, Z.J., Ren, G.D., Zhang, Y.F., Qian, M. and Sheng, X.F. 2009. Increased cadmium and lead uptake of a cadmium hyperaccumulator tomato by cadmium-resistant bacteria. *Ecotoxicol. Environ. Saf.*, 72: 1343-1348.
- Herrero, R., Lodeiro, P., Rey-Castro, C., Vilarinho, T. and Sastre de Vicente, M.E. 2005. Removal of inorganic mercury from aqueous solutions by biomass of the marine macroalga *Cystoseira baccata*. *Water Res.*, 39(14): 3199-3210.
- Hinchman, R.R., Negri, M.C. and Gatliff, E.G. 1996. Phytoremediation: Using green plants to clean up contaminated soil, groundwater, and wastewater. *J. Hazard. Waste Manag.*, 96: 1-13.

- Hussain, A., Murtaza, G., Ghafoor, A., Basra, S.M.A., Qadir, M. and Sabir, M. 2010. Cadmium contamination of soils and crops by long-term use of raw effluent, ground, and canal waters in agricultural lands. *Int. J. Agric. Biol.*, 12: 851-856.
- Iram, S., Ahmad, I. and Akhtar, S. 2012. Distribution of heavy metals in periurban agricultural areas soils. *J. Chem. Soc. Pak.*, 34:861-869.
- Jan, S., Werner, H., Gerald, F.F. and Douwe, V.S. 2002. Molecular characterization of cadmium resistance in *Streptococcus thermophilus* strain 4134: an example of lateral gene transfer. *Appl. Environ. Microbiol.*, 68: 5508-5516.
- Januskaitiene, I. 2010. Impact of low concentration of cadmium on photosynthesis and growth of pea and barley. *Environ. Res. Engin. Manag.*, 3: 24-29.
- Ji, P., Sun, T., Song, Y., Ackland, M.L. and Liu, Y. 2011. Strategies for enhancing the phytoremediation of cadmium-contaminated agricultural soils by *Solanum nigrum* L. *Environ. Pollut.*, 159: 762-768.
- Jiang, W., D. Liu and Hou, W. 2001. Hyperaccumulation of cadmium by roots, bulbs, and shoots of garlic. *Bioresour. Technol.*, 76(1): 9-13.
- Jun-Yu, H., Yan-fang, R., Cheng, Z. and De-an, J. 2008. Effects of cadmium stress on seed germination, seedling growth, and seed amylase activities in rice (*Oryza sativa*). *Rice Sci.*, 15: 319-325.
- Kupper, H., Lombi, E., Zhao, F.J. and McGrath, S.P. 2000. Cellular compartmentation of cadmium and zinc in relation to other elements in the hyperaccumulator *Arabidopsis halleri*. *Planta*, 212(1): 75-84.
- Kashif, S.R., Akram, M., Yaseen, M. and Ali, S. 2009. Studies on heavy metals status and their uptake by vegetables in adjoining areas of Hudaira drain in Lahore. *Soil Environ.*, 28: 7-12.
- Khalid, S., Shahid, M., Niazi, N.K., Murtaza, B., Bibi, I. and Dumat, C. 2017. A comparison of technologies for remediation of heavy metal contaminated soils. *J. Geochem. Explor.*, 182: 247-268.
- Khan, M.A., Chattha, M.R., Farooq, K., Jawed, M.A., Farooq, M., Imran, M., Iftkhar, M. and Kasana, M.I. 2015. Effect of farmyard manure levels and NPK applications on the pea plant growth, pod yield, and quality. *Life Sci. Int. J.*, 9: 3178-3181.
- Khan, T., Muhammad, S., Khan, B. and Khan, H. 2010. Investigating levels of selected heavy metals in surface water of Shah Alam River, Khyber Pakhtunkhwa. *J. Himalayan Earth Sci.*, 43: 48-49.
- Khankhane, P.J., Tabassum, A. and Patel, A. 2017. Cadmium tolerance and its enhanced accumulation potential of *Arundo donax* by EDTA. *J. Environ. Biol.*, 38(2): 327-334.
- Kimura, T., Takase, K. and Tanaka, S. 2007. The concentration of copper and a copper-EDTA complex at the pH junction formed in soil by an electrokinetic remediation process. *J. Hazard. Mater.*, 143(3): 668-672.
- Koleli, N., Eker, S. and Cakmak, I. 2004. Effect of zinc supply on cadmium toxicity in durum and bread wheat grown in zinc-deficient soil. *Environ. Pollut.*, 131: 453-459.
- Kratochvil, D. and Volesky, B. 1998. Advances in the biosorption of heavy metals. *Tibtech*, 16: 291-300.
- Kuffner, M., De Maria, S., Puschenreiter, M., Fallmann, K., Wieshammer, G., Gorfer, M., Strauss, J., Rivelli, A.R. and Sessitsch, A. 2010. Culturable bacteria from Zn- and Cd-accumulating *Salix caprea* with differential effects on plant growth and heavy metal availability. *J. Appl. Microbiol.*, 108: 1471-1484.
- Kuffner, M., Puschenreiter, M., Wieshammer, G., Gorfer, M. and Sessitsch, A. 2008. Rhizosphere bacteria affect the growth and metal uptake of heavy metal accumulating willows. *Plant Soil*, 304: 35-44.
- Kumar, A., Bisht, B.S. and Joshi, V.D. 2010. Biosorption of heavy metals by four acclimated microbial species, *Bacillus* spp., *Pseudomonas* spp., *Staphylococcus* spp. and *Aspergillus niger*. *J. Biol. Environ. Sci.*, 4: 97-108.
- Kumar, J.I.N., Soni, H., Kumar, R.N. and Bhatt, I. 2009. Hyperaccumulation and mobility of heavy metals in vegetable crops in India. *J. Agri. Environ.*, 10: 29-38.
- Lehmann, C. and Rebele, F. 2004. Assessing the potential for cadmium phytoremediation with *Calamagrostis epigejos*: A pot experiment. *Int. J. Phytoremed.*, 6(2): 169-183.
- Lehoczky, E., Marth, P., Szabados, I. and Szomolanyi, A. 2000. The cadmium uptake by lettuce on contaminated soils as influenced by liming. *Commun. Soil Sci. Plant Analy.*, 31: 2433-2438.
- Liu, C.P., Shen, Z.G. and Li, X.D. 2007. Accumulation and detoxification of cadmium in *Brassica pekinensis* and *B. chinensis*. *Biologia Plantarum*, 51: 116-120.
- Liu, W., Zhou, Q., Zhang, Z., Hua, T., and Cai, Z. 2011. Evaluation of cadmium phytoremediation potential in Chinese cabbage cultivars. *J. Agric. Food Chem.*, 59(15): 8324-8330.
- Lu, R.K., Shi, Z.Y. and Xiong, L.M. 1992. Cadmium contents of rock phosphates and phosphate fertilizers of China and their effects on the ecological environment. *Acta Pedol. Sinica*, 29: 150-157
- Luo, X., Yu, S., Zhu, Y. and Li, X. 2012. Trace metal contamination in urban soils of China. *Sci. Total Environ.*, 421: 17-30.
- Malik, R.N., Jadoon, W.A. and Husain, S.Z. 2010. Metal contamination of surface soils of industrial city Sialkot, Pakistan: A multivariate and GIS approach. *Environ. Geochem. Health*, 32: 179-191.
- Mayak, S., Tirosht, T. and Glick, B.R. 2004. Plant growth-promoting bacteria that confer resistance in tomato plants to salt stress. *Plant Physiol. Biochem.*, 42: 565-572.
- Meharg, A.A. 2005. Mechanisms of plant resistance to metal and metalloid ions and potential biotechnological applications. *Plant Soil*, 274: 163-174.
- Morrow, H. 2001. Cadmium and Cadmium Alloys. John Wiley & Sons, Inc., NY, pp. 471-507
- Motesharezadeh, B., Savaghebi-Firoozabadi, G.R., Hosseini, H.M. and Alikhani, H.A. 2010. Study of the enhanced phytoextraction of cadmium in a calcareous soil. *Int. J. Environ. Res.*, 4: 525-532.
- Naidu, R., Kookana, R.S., Sumner, M.E., Harter, R.D. and Tiller, K.G. 1997. Cadmium sorption and transport in variable charge soils: A review. *J. Environ. Qual.*, 26: 602-617.
- Naik, M.M. and Dubey, S. 2017. Lead- and Mercury-Resistant Marine Bacteria and Their Application in Lead and Mercury Bioremediation. Springer, Berlin, pp. 29-40.
- Navarro, M.C., Pérez-Sirvent, C., Martínez-Sánchez, M.J., Vidal, J., Tovar, P.J. and Bech, J., 2008. Abandoned mine site as a source of contamination by heavy metals: a case study in a semi-arid zone. *J. Geochem. Explor.*, 96: 183-193.
- Nedelkoska T.V. and Doran P.M. 2000. Hyperaccumulation of cadmium by hairy roots of *Thlaspi caerulescens*. *Biotechnol. Bioeng.*, 67(5): 607-615.
- Niazi, N.K., Bibi, I., Fatimah, A., Shahid, M., Javed, M.T., Wang, H., Ok, Y.S., Bashir, S., Murtaza, B., Saqib, Z.A. and Shakoor, M.B. 2017. Phosphate-assisted phytoremediation of arsenic by *Brassica napus* and *Brassica juncea*: Morphological and physiological response. *Int. J. Phytoreme.*, 19(7): 670-678.
- Park, Y.J., Koa, J.J., Yun, S.L., Lee, E.Y., Kim, S.J., Kang, S.W., Lee, B.C. and Kim, S.K. 2008. Enhancement of bioremediation by *Ralstoniasp. HM-1* in sediment polluted by Cd and Zn. *Bioresour. Technol.*, 99: 7458-7463.
- Pavić, A., Ilić-Tomić, T., Pačevski, A., Nedeljković, T., Vasiljević, B. and Morić, I. 2015. Diversity and biodeteriorative potential of bacterial isolates from deteriorated modern combined-technique canvas painting. *Int. Biodeterior. Biodegrad.*, 97: 40-50.
- Phipps, D.A. 1981. Chemistry and Biochemistry of Trace Metals in Biological Systems. In N.W. Lepp. (ed.) *Effect of Heavy Metal Pollution on Plants*. Barking, UK, pp. 1-54.
- Prapagee, B. and Watcharamusik, A. 2009. Adaptive and cross-protective responses against cadmium and zinc toxicity in cadmium-resistant bacterium isolated from a zinc mine. *Braz. J. Microbiol.*, 40: 838-845.

- Quartacci, M.F., Argilla, A., Baker, A.J.M and Navari-Izzo, F. 2006. Phytoextraction of metals from a multiply contaminated soil by Indian mustard. *Chemosphere*, 63(6): 918-925.
- Radhika, V., Subramanian. S. and Natarajan. K.A. 2006. Bioremediation of zinc using *Desulfotomaculum nigrificans*: Bioprecipitation and characterization studies. *Water Res.*, 40: 3628-3636.
- Ramon, O., Vazquez, E., Fernandez, M., Felipe, M. and Zornoza, P. 2003. Cadmium stress in white lupine: Effects on nodule structure and functioning. *Plant Physiol.*, 161: 911-919.
- Rani, A., Shouche, Y.S. and Goel, R. 2008. Declination of copper toxicity in pigeon pea and soil system by growth-promoting *Proteus vulgaris* KNP3 strain. *Curr. Microbiol.*, 57: 78-82.
- Rani, A., Souche, Y.S. and Goel, R. 2009. Comparative assessment of in situ bioremediation potential of cadmium resistant acidophilic *Pseudomonas putida* 62BN and alkalophilic *Pseudomonas monteilii* 97AN strains on soybean. *Inter. Biodeter. Biodeg.*, 63: 62-66.
- Rauf, A., Javed, M., Ubaidullah, M. and Abdullah, S. 2009. Assessment of heavy metals in sediments of the river Ravi, Pakistan. *Inter. J. Agri. Biol.*, 11: 197-200.
- Rehman, W., Zeb Noor, N.A. and Nawaz, M. 2008. Heavy metal pollution assessment in various industries of Pakistan. *Environ. Geol.*, 55: 353-358.
- Sanit'a Di Toppi, L. and Gabbrielli, R. 1999. Response to cadmium in higher plants. *Environ. Exper. Bot.*, 41(2): 105-130.
- Santona, L., Castaldi, P. and Melis, P. 2006. Evaluation of the interaction mechanisms between red muds and heavy metals. *J. Hazrad. Mater.*, 136(2): 324-329.
- Say, R., Denizli, A. and Arcoa, M.Y. 2001. Biosorption of cadmium (II), lead (II), and copper (II) with the filamentous fungus *Phanerochaete chrysosporium*. *Bioresour. Technol.*, 76: 67-70.
- Schindler, B.D., Frempong-Manso, E., DeMarco, C.E., Kosmidis, C., Matta, V., Seo, S.M. and Kaatz, G.W. 2015. Analyses of multidrug efflux pump-like proteins encoded on the *Staphylococcus aureus* chromosome. *Antimicrob. Agents Chemother.*, 59: 747-748.
- Seetharam, C., Soundarajan, S., Udas, A.C., Rao, A.S. and Apte, S.K. 2009. Lyophilized, non-viable, recombinant *E. coli* cells for cadmium bioprecipitation and recovery. *Process Biochem.*, 44: 246-250.
- Shahid, M., Austruy, A., Echevarria, G., Arshad, M., Sanaulah, M., Aslam, M., Nadeem, M., Nasim, W. and Dumat, C. 2013. EDTA-enhanced phytoremediation of heavy metals: A review. *Soil Sed. Contam. Int. J.*, 23(4): 389-416.
- Shahid, M., Xiong, T., Masood, N., Leveque, T., Quenea, K., Austruy, A., Foucault, Y. and Dumat, C. 2013. Influence of plant species and phosphorus amendments on metal speciation and bioavailability in a smelter impacted soil: a case study of food-chain contamination. *J. Soils Sed.*, 14(4): 655-665.
- Shakoor, M., Niazi, N., Bibi, I., Rahman, M., Naidu, R., Dong, Z., Shahid, M. and Arshad, M. 2015. Unraveling health risk and speciation of arsenic from groundwater in rural areas of Punjab, Pakistan. *Int. J. Environ. Res. Public Health*, 12(10): 12371-12390.
- Sharma, P.K., Balkwill, D.L., Frenkel, A. and Vairavamurthy, M.A. 2000. A new *Klebsiella planticola* strain (Cd-1) grows anaerobically at high cadmium concentrations and precipitates cadmium sulfide. *Appl. Environ. Microbiol.*, 66: 3083-3087.
- Sheng, X. and Xia, J. 2006. Improvement of rape (*Brassica napus*) plant growth and cadmium uptake by cadmium-resistant bacteria. *Chemosphere*, 64(6): 1036-1042.
- Sidhu, G.P.S., Singh, H.P., Batish, D.R., and Kohli, R.K. 2017. Tolerance and hyperaccumulation of cadmium by a wild, unpalatable herb *Coronopus didymus* (L.) Sm. (Brassicaceae). *Ecotoxicol. Environ. Saf.*, 135: 209-215.
- Singh, P. and Cameotra, S.S. 2004. Enhancement of metal bioremediation by use of microbial surfactants. *Biochem. Biophys. Res. Commun.*, 319: 291-297.
- Sun, B., Zhao, F.J., Lombi, E. and McGrath, S.P. 2001. Leaching of heavy metals from contaminated soils using EDTA. *Environ. Pollut.*, 113:111-120
- Sun, Y., Zhou, Q. and Diao, C. 2008. Effects of cadmium and arsenic on growth and metal accumulation of Cd-hyperaccumulator *Solanum nigrum* L. *Bioresour. Technol.*, 99: 1103-1110.
- Sun, Y., Zhou, Q., Wang, L. and Liu, W. 2009. The influence of different growth stages and dosage of EDTA on Cd uptake and accumulation in Cd-hyperaccumulator (*Solanum nigrum* L.). *Bull. Environ. Contam. Toxicol.*, 82(3): 348-353.
- Thomas, O.L. 1992. Cadmium from Minerals Year book Volume 1. Metals and Minerals, U.S. Bureau of Mines, pp. 271-276.
- Tripathi, M., Munot. H.P., Souche. Y., Meyer. J.M. and Goel, R. 2005. Isolation and functional characterization of siderophore producing lead and cadmium resistant *Pseudomonas putida* KNP9. *Curr. Microbiol.*, 50: 233-237.
- Vara, P., Narasimha, M. and de Oliveira Freitas, H.M. 2003. Metal hyperaccumulation in plants: Biodiversity prospecting for phytoremediation technology. *Electr. J. Biotechnol.*, 6(3): 285-321.
- Venegas, A., Rigol, A. and Vidal, M. 2015. Viability of organic wastes and biochars as amendments for the remediation of heavy metal-contaminated soils. *Chemosphere*, 119: 190-198.
- Wang, C., Knill, E., Glick, B.R. and Defago, G. 2000. Effect of transferring 1-aminocyclopropane-1-carboxylic acid (ACC) deaminase genes into *Pseudomonas fluorescens* strain CH40 and its gacA derivative CHA96 on their growth-promoting and disease-suppressive capacities. *Can. J. Microbiol.*, 46: 898-907.
- Wang, C.L., Lum, A.M., Ozuna, S.C., Clark, D.S. and Keasling, J.D. 2001. Aerobic sulfide production and cadmium precipitation by *Escherichia coli* expressing the *Treponema denticola* cysteine desulfhydrase gene. *Appl. Microbiol. Biotechnol.*, 56: 425-430.
- Wang, C.L., Ozuna, S.C., Clark, D.S. and Keasling, J.D. 2002. A deep-sea hydrothermal vent isolate, *Pseudomonas aeruginosa* CW961, requires thiosulfate for Cd²⁺ tolerance and precipitation. *Biotechnol. Lett.*, 24: 637-641.
- Wang, H., Zhao, S.C., Liu, R.L., Zhou, W. and Jin, J.Y. 2009. Changes of photosynthetic activities of maize (*Zea mays* L.) seedlings in response to cadmium stress. *Photosynthetica*, 47: 277-283.
- Wei, C.Y. and Chen, T.B. 2001. Hyperaccumulators and phytoremediation of heavy metal contaminated soil: A review of studies in China and abroad. *Acta Ecologica Sinica*, 21: 1196-1203.
- Wei, S., Zhou, Q., and Koval, P.V. 2006. Flowering stage characteristics of cadmium hyperaccumulator *Solanum nigrum* L. and their significance to phytoremediation. *Sci. Tot. Environ.*, 369(1-3): 441-446.
- Wei, S., Zhou, Q., Wang, X., Zhang, K., Guo, G. and Ma, L. Q. 2005. A newly-discovered Cd-hyperaccumulator *Solanum nigrum* L. *Chinese Sci. Bull.*, 50(1): 33-38.
- World Health Organization (WHO). 2007. Health risks of heavy metals from long-range transboundary air pollution. World Health Organization, Regional Office for Europe, Copenhagen, Denmark, pp. 1-129.
- Wu, F., Zhang, G., Dominy, P., Wu, H. and Bachir, D.M.L. 2007. Differences in yield components and kernel Cd accumulation in response to Cd toxicity in four barley genotypes. *Chemosphere*, 70: 83-92.
- Xiao, W., Li, X. and Ye, D. 2017. Enhancement of Cd phytoextraction by hyperaccumulator *Sedum alfredii* using electrical field and organic amendments. *Environ. Sci. Pollut. Res.*, 24(5): 5060-5067.
- Xiong, X., Allinson, G., Stagnitti, F. and Peterson, J. 2003. Metal contamination of soils in the Shenyang Zhangshi irrigation area. *Bull. Environ. Contam. Toxicol.*, 70: 935-941.
- Xiong, Y.H., Yang, X. E., Ye, Z.Q. and He, Z. L. 2004. Characteristics of cadmium uptake and accumulation by two contrasting ecotypes of *Sedum alfredii* Hance. *J. Environ. Sci. Health Part A Hazard. Subs. Environ. Eng.*, 39(11-12): 2925-2940.

- Yang, M.G., Lin, X.Y. and Yang, X. E. 1998. Impact of Cd on growth and nutrient accumulation of different plant species. *Chin. J. Appl. Ecol.*, 9(1): 89-94.
- You, K.M. and Park, Y.K. 1998. Cd²⁺ removal by *Azomonas agilis* PY101, cadmium accumulating strain in continuous aerobic culture. *J. Microbiol.*, 36: 159-163.
- You, K.M., Lee, J.H., Kim, J.H., Hah, N.J., Lee, Y.N. and Park, Y.K. 1996. Cd²⁺ removal by *Azomonas agilis* PY101, cadmium accumulating strain in continuous aerobic culture. *J. Microbiol.*, 34: 289-293.
- Zeng, Q., Cheng, J.S., Tang, L.H., Liu, X.F., Liu, Y.Z., Li, J.H. and Jiang, J.H. 2010. Self-assembled graphene-enzyme hierarchical nanostructures for electrochemical biosensing. *Adv. Func. Mat.*, 20: 3366-3372.
- Zhang, G., Fukami, M. and Sekimoto, H. 2002. Influence of cadmium on mineral concentrations and yield components in wheat genotypes differing in Cd tolerance at the seedling stage. *Field Crops Res.*, 77: 93-98.
- Zhang, S., Li, T., Huang, H., Zou, T., Zhang, X., Yu, H., Zheng, Z. and Wang, Y. 2012. Cd accumulation and phytostabilization potential of dominant plants surrounding mining tailings. *Environ. Sci. Pollut., Res. Int.*, 9: 3879-3888.
- Zheng, C. and Wang, P.P. 2002. A Field demonstration of the simulation-optimization approach for remediation system design. *Ground Water*, 40(3): 258-266.
- Zheng, L., Abhyankar, W., Ouwering, N., Dekker, H.L., van Veen, H. and Van der Wel, N.N. 2016. The *Bacillus subtilis* spore inner membrane proteome. *J. Proteome Res.*, 17: 976. doi:10.1021/acs.jproteome.5b00976.
- Zhu, L., Ding, W., Feng, L., Kong, Y., Xu, J. and Xu, X. 2012. Isolation of aerobic denitrifiers and characterization for their potential application in the bioremediation of oligotrophic ecosystems. *Bioresour. Technol.*, 108: 1-7.

ORCID DETAILS OF THE AUTHORS

A. Kumar: <https://orcid.org/0000-0003-1069-2234>

G. Mukherjee: <https://orcid.org/0000-0003-2835-9317>

S. Gupta: <https://orcid.org/0000-0001-7723-4487>



Application of Membrane Separation Technology in Electroplating Wastewater Treatment and Resource Recovery: A Review

Le Zhang*[†], Ying Chen**, Huan Zhang***, Yabin Jin*, Zhe Shen* and Gending Duan*

*The Institute of Energy and Architecture, Xi'an Aeronautical Institute, Xi'an 710077, PR of China

**Shaanxi LvYuan Testing Technology Co. Ltd., Xi'an 710116, PR of China

***College of Chemistry and Material, Weinan Normal University, Weinan 714099, PR China

[†]Corresponding author: Le Zhang; zl_202106011@163.com

Nat. Env. & Poll. Tech.
Website: www.neptjournal.com

Received: 09-10-2023

Revised: 16-11-2023

Accepted: 17-11-2023

Key Words:

Electroplating wastewater
Heavy metals
Treatment
Membrane technology
Hybrid process

ABSTRACT

The rapid development of industry has led to the generation of a large amount of electroplating wastewater. The direct discharge of untreated electroplating wastewater may lead to the formation of toxic metal-organic complexes, which is a challenging problem for human health and the living environment of organisms. Due to the high solubility of heavy metals in aquatic environments and their easy absorption by organisms, effective treatment of electroplating wastewater is of great significance. The ultimate goal of electroplating wastewater treatment should be to recover metals and water from electroplating wastewater. In indoor experiments, pilot tests, and industrial applications of electroplating wastewater treatment, membrane treatment technology commonly used in wastewater terminal treatment has attracted great attention. Membrane treatment technology seems to be the most promising method for removing heavy metals and organic pollutants from electroplating wastewater. This article reviews the membrane treatment technologies for electroplating wastewater, introduces the advantages and disadvantages of various membranes in the treatment of electroplating wastewater, the removal efficiency of pollutant types, and their comparison. The focus is on the treatment effects of nano-filtration membrane, ultra-filtration membrane, micro-filtration membrane, reverse osmosis membrane, ceramic membrane, biofilm, etc., on electroplating wastewater. Compared with a single treatment method, the combination of different processes shows higher efficiency in removing various pollutants.

INTRODUCTION

With the rapid development of society and the economy and the continuous improvement of urbanization, water pollution has become increasingly severe, and water resources are in serious shortage (Güven et al. 2022). Strengthening sewage treatment and protecting water resources to achieve sustainable development is an essential and urgent task (Maulin et al. 2022). In recent years, the increasingly mature membrane separation technology has been widely used in industrial wastewater and domestic sewage purification, applied water treatment, seawater desalination, brackish water desalination, and other water treatment fields. This is due to its numerous advantages, such as excellent separation effects, energy-saving, and environmentally friendly nature, a simple process, convenient operation, and a small footprint (Sm et al. 2022, Ahmed et al. 2022).

Membrane separation technology uses a selectively permeable membrane made of special organic or inorganic materials, driven by external energy or a chemical potential

difference, to separate, grade, purify, and concentrate mixtures (Ibrar et al. 2022). As membrane separation technology develops, new membrane materials have become a focal point and area of significant research interest (Manetti & Tomei 2022). The research and development of new membrane materials mainly include nano-fiber membrane-supported polymer composite membranes, organic-inorganic hybrid membranes, and inorganic membranes (Rodenburg et al. 2022). Membrane separation technology can be categorized according to pore size and filtration accuracy into the following types: micro-filtration (MF), ultra-filtration (UF), nano-filtration (NF), reverse osmosis (RO), and electro dialysis (ED) (Malhas et al. 2022).

The research demonstrated that a PET nanofiber membrane was prepared using electrostatic spinning. This PET nanofiber membrane was then used as a substrate and coated with crosslinked chitosan (Mansor et al. 2021). Subsequently, interfacial polymerization of m-phenylenediamine (MPD) and trimethylene chloride (TMC) was carried out to create a nanofibril polyamide

composite reverse osmosis membrane (Khan & Boddu 2021). The membrane's rejection rate for a 2 g.L⁻¹ sodium chloride solution reached 92%, with a corresponding flux of 21 g/(m².h), showcasing good interception performance that can satisfy the requirements for high-purity water. Other studies have indicated that chemical bonding between organic and inorganic materials can be achieved through molecular design and surface modification of organosilicon materials and inorganic nanomaterials. This results in the pervaporation of organic compounds with excellent flux, selectivity, solvent resistance, and stability. At 50°C, the flux of a 5% ethanol aqueous solution is greater than 1000 g/(m².h), and at 70°C, the separation factor for a 1% butanol solution exceeds 70, with a flux of more than 1300 g/(m².h) (Ahin 2021).

In recent years, besides focusing on membrane materials research, some experts and scholars have made progress in studying membrane wastewater treatment technology. It has been reported that a biofilm reactor is created by combining biological treatment and membrane separation technology (Salgot & Folch 2018, Biniiaz et al. 2019). With pore sizes ranging from 0.03 to 0.2 μm, the membrane exhibits a high-efficiency interception and separation effect. As microorganisms are entirely retained within the reactor, pollutants can be efficiently degraded and separated, resulting in high-quality water (Biniiaz et al. 2019).

The micro-filtration combined technologies of coagulation-micro-filtration, adsorption-micro-filtration, and precipitation-micro-filtration can effectively play the

advantages of dissolved salts, adsorbents, precipitators, and micro-filtration membranes, strengthen the separation effect and effectively reduce membrane pollution (Rahimpour et al. 2019). The research shows that the integrated technology of membrane filtration and adsorption can control the flow rate and time of stock solution entering the membrane module, adjust the solute concentration of the concentration difference polarization layer, and extract and derive the concentrated solution of the concentration difference polarization layer in time, and solve the two significant problems of concentration difference polarization and membrane pollution at the same time (Damtie et al. 2018, Leonzio 2017)

At present, membrane treatment technology is widely used in sewage treatment. Despite the many research achievements in electroplating wastewater treatment, there are fewer instances of membrane treatment technology implemented in industrial applications (Cho et al. 2018). Electroplating wastewater is characterized by an overly complex composition, increasing discharge year by year, and progressively high pollutant concentrations, posing a significant challenge to adequate environmental protection (Silva et al. 2017). Chemical precipitation technology is commonly used for treating electroplating wastewater (Fig. 1) (Ozokwelu et al. 2017). However, due to the addition of numerous chemicals during the treatment process, the treated wastewater's salinity increases significantly, severely affecting the biodegradability of wastewater in the later stages of the process. At the same time, many

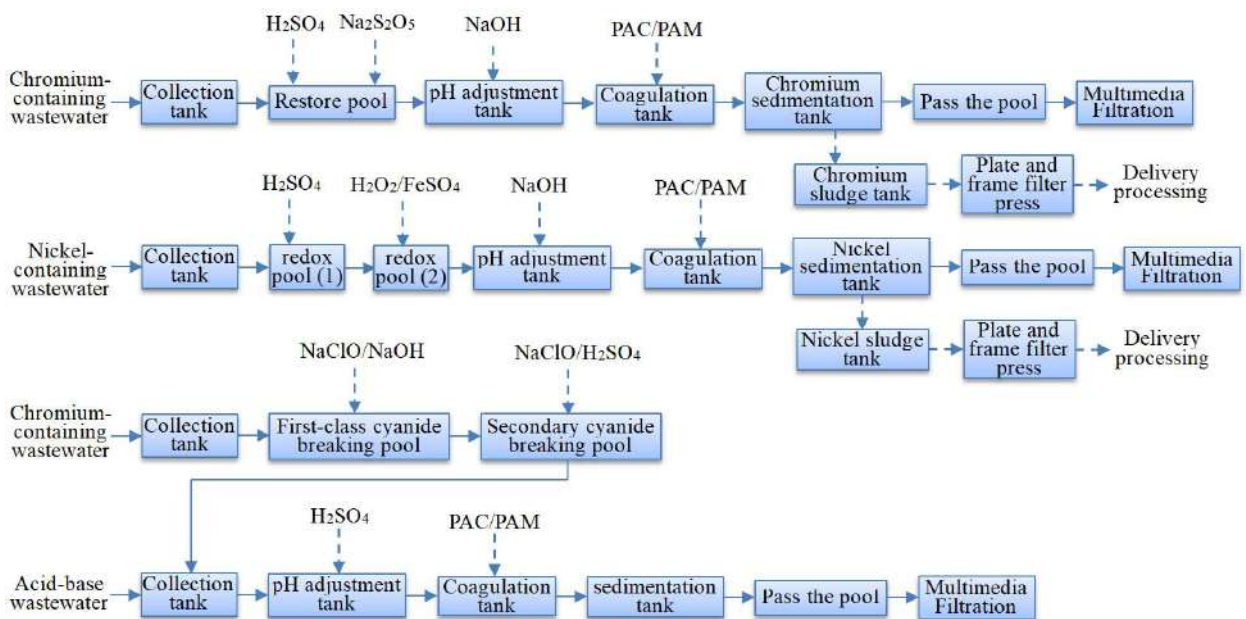


Fig. 1: Several common electroplating wastewater chemical treatment processes.

heavy metals are lost from the wastewater, and substances such as ammonia, nitrogen, and total phosphorus become challenging to remove in subsequent processes (Hosseini et al. 2017). Moreover, the treatment process generates a considerable amount of sludge, which results in a low reuse rate of reclaimed water and significantly increased reuse costs (Noah et al. 2016, Babilas & Dydo 2018). The latest “Emission Standard of Electroplating Pollutants” (GB21900-2008), implemented in our country in 2008, sets higher requirements for the discharge concentration limits of heavy metals and other related indicators in electroplating wastewater. Therefore, adopting more environmentally friendly production processes and advanced wastewater treatment technologies that meet these requirements is essential for solving the problem of up-to-standard discharge of electroplating wastewater (Hoslett et al. 2018).

Due to its excellent treatment effects and robust adaptability, membrane treatment technology has emerged as an advanced method for the harmless and efficient treatment of electroplating wastewater (Al-Saydeh et al. 2017, Akar et al. 2021). The typical membrane filtration process is illustrated in Fig. 2, where large particle contaminants accumulate on the surface while smaller particles either pass through the membrane pores or remain within them. Applying membrane treatment technology for electroplating wastewater results in a wastewater reduction treatment process (Sur & Mukhopadhyay 2018, Wen et al. 2018). In this process, the amount of chemicals added is minimal. Following pretreatment of the wastewater, it directly enters the membrane element for concentration. The final effluent meets the requirements for reuse, and the concentrated wastewater can be recycled. Consequently, the volume of wastewater requiring discharge is significantly reduced, along with sludge production, leading to decreased treatment costs (Wen et al. 2018).

A large number of practices using membrane separation technology to treat industrial electroplating wastewater have

shown that different membrane properties have different requirements for the ability to separate water quality and treatment. For example, composite membranes, porous membranes, and exchange membranes are mainly treated with non-organic ions, bacteria, and inorganic ions. Electroplating wastewater is rich in a large amount of heavy metals and contains many anions that are harmful to human health. At the same time, the acidity and alkalinity of the wastewater are also different from normal water quality. Therefore, solving some impurities in the wastewater and reusing industrial wastewater to obtain useful substances cannot be done without the use of membrane separation technology.

This article aims to summarize the application research of membrane treatment technology for electroplating wastewater and theoretically analyze the treatment effects and development prospects of nano-filtration membrane, ultra-filtration membrane, micro-filtration membrane, reverse osmosis membrane, ceramic membrane, biofilm, etc., on electroplating wastewater. At the same time, it considers the technical defects and potential problems that membrane treatment technology may face in the electroplating wastewater treatment process.

CHARACTERISTICS AND HAZARDS OF ELECTROPLATING WASTEWATER

Characteristics

Sources of electroplating wastewater: waste electroplating solution, washing wastewater during equipment maintenance, wastewater from washing workshops, cleaning water for electroplating parts, condensed water formed by condensation of ventilation equipment, seepage or leaking water from aqueducts, and various bath liquids during improper operation and drained wastewater (Akar et al. 2021).

Due to the different requirements of each plating piece, the relevant technical conditions, such as the electroplating

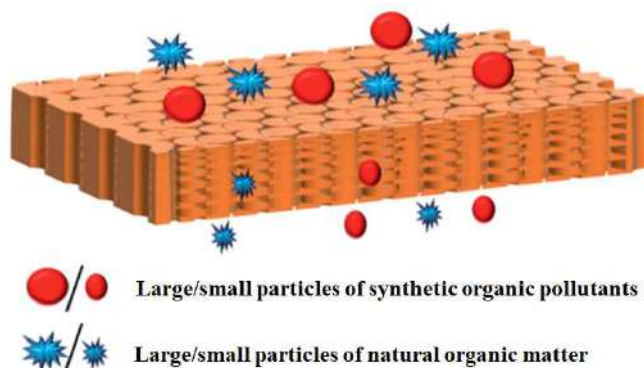


Fig. 2: The usual membrane filtration process.

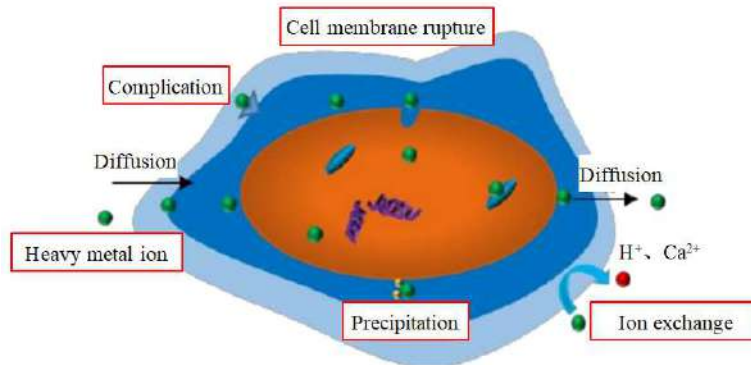


Fig. 3: Toxicity mechanism of heavy metal ions on cells.

solution and coating layer selected during electroplating, are also different, so the formed electroplating wastewater contains a wide variety of pollutants and significant differences between components (Albergamo et al. 2019). In addition to many heavy metal ions, wastewater contains various citric acids, surfactants, cyanide, etc (Akar et al. 2021, Albergamo et al. 2019).

Hazards

The electroplating industry will produce a large amount of electroplating wastewater in production. Such wastewater contains heavy metal ions such as chromium, copper, nickel, cadmium, zinc, and more toxic compounds such as cyanide (Mohagheghian et al. 2018). Once these toxic and refractory substances enter the natural environment, they will exist in nature for a long time. They can eventually be enriched in animals and plants through the food chain in the ecological cycle and even eventually in the human body at the top of the food chain. It can destroy the cells and tissues of the human body (Fig. 3) (Takuma et al. 2018). Symptoms such as poisoning, cancer, aberration, and mutation that lead human body will bring great harm and impact human beings and the social environment (Mohagheghian et al. 2018).

Therefore, before treating electroplating wastewater, the source, type, and pollution degree of pollutants in the wastewater should be identified first to be recovered and treated safely and effectively. All electroplating wastewater can be recovered by strictly controlling the discharge content of pollutants. Discharge up to the standard to protect the environment so that wastewater pollution will not cause harm to society and human health (Sur & Mukhopadhyay 2018, Abdel & Alseroury 2019).

CURRENT SITUATION AND PROBLEMS OF TREATMENT OF ELECTROPLATING WASTEWATER

The treatment process of electroplating wastewater mainly includes four parts: pretreatment, comprehensive treatment,

membrane treatment, and evaporation treatment (Koby et al. 2017). The pretreatment stage of wastewater generally follows the principles of classified collection and qualitative treatment. For example, the pretreatment of wastewater containing cyanide adopts the alkaline chlorination method, the pretreatment of wastewater containing chromium adopts the sulfite reduction method, and the pretreatment of wastewater containing nickel, cadmium, and copper. The pretreatment of wastewater, such as zinc, adopts the chemical precipitation or ion exchange method, and the pretreatment of acid-base wastewater adopts the neutralization method (Castel & Favre 2018, Hackbarth et al. 2016). After pretreatment, all kinds of wastewater will enter the comprehensive treatment stage. In the comprehensive treatment stage, technologies such as physicochemical and biochemical treatment are used to remove different pollutants, such as organic matter, ammonia nitrogen, and total nitrogen, so that the effluent meets the influent requirements of membrane treatment. In the membrane treatment section, the multi-stage and multi-stage combined membrane process concentrates and reduces the amount of wastewater (Hedayati et al. 2017). The high salinity membrane system produces water and evaporative condensate water, which is recycled back to production to achieve zero discharge of electroplating wastewater (John et al. 2016).

Due to the complex composition of electroplating wastewater, difficult control of composition, significant variation in water quality, and intense pollution, the current treatment of electroplating wastewater has the following problems (Hackbarth et al. 2016).

Unreasonable Classification

Although electroplating wastewater generally follows the principles of classified collection and qualitative treatment, its classification is unreasonable due to its wide variety. With the application of various new technologies, new processes, and new materials in the modern electroplating

industry, the pollutants in electroplating wastewater have become increasingly complex. Currently, the classification of electroplating wastewater in my country needs to be clarified and unreasonable. Some areas are divided into 3 to 5 categories. Some areas even reach more than ten categories, which makes the treatment and reuse of electroplating wastewater more complex, and the treatment cost rises (John et al. 2016, Hackbarth et al. 2016).

Lower Reuse Rate of Electroplating Wastewater Treatment

Driven by cleaner production, the recycling rate of electroplating wastewater has been dramatically improved, especially with new technologies such as membrane treatment, nano-filtration, and ion exchange, which have also improved the level of electroplating wastewater treatment (Scarazzato et al. 2017, Van 2018). However, on the whole,

the recycling rate of electroplating wastewater in my country is low, especially since the treatment of the organic matter in electroplating wastewater could be better. Although modern electroplating wastewater treatment and reuse technology has made significant progress in the treatment of metal ions, the stability of the wastewater treatment and reuse device could be better. It is challenging to meet the requirements of industrialized sewage standards (Quiton et al. 2022).

Lower Rate of Reuse Up to Standard of Electroplating Wastewater Treatment

With the promulgation and implementation of a series of rules and regulations, such as the “Emission Standard of Electroplating Pollutants” and “Emission Standard of Electroplating Water Pollutants,” the discharge of electroplating pollutants has made significant progress compared with the original (Zhang et al. 2018). However,

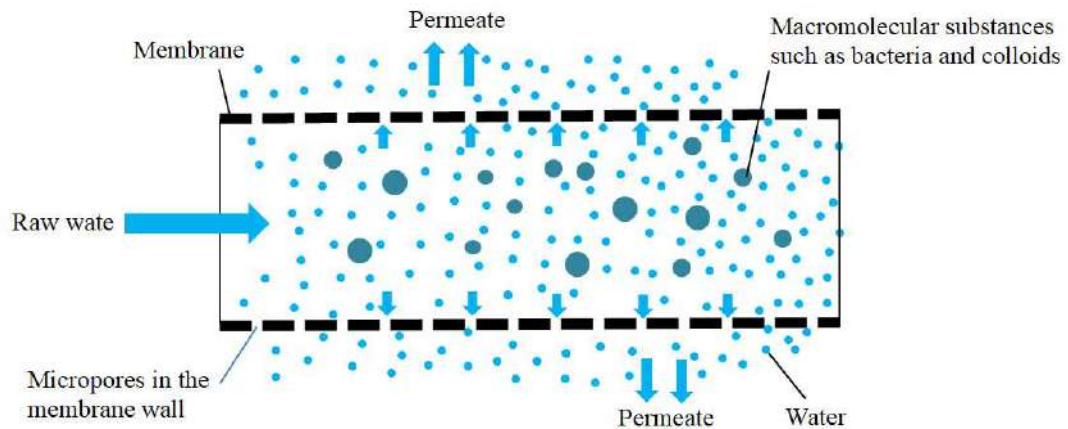


Fig. 4: Membrane separation process principle.

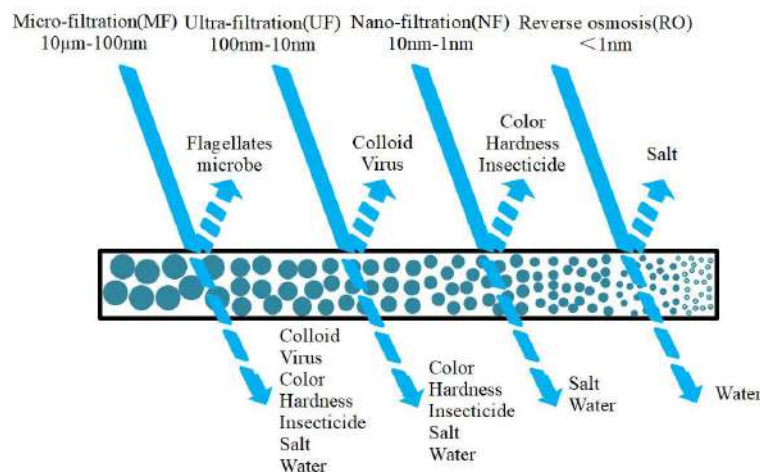


Fig. 5: The filtration process of several common filter membranes.

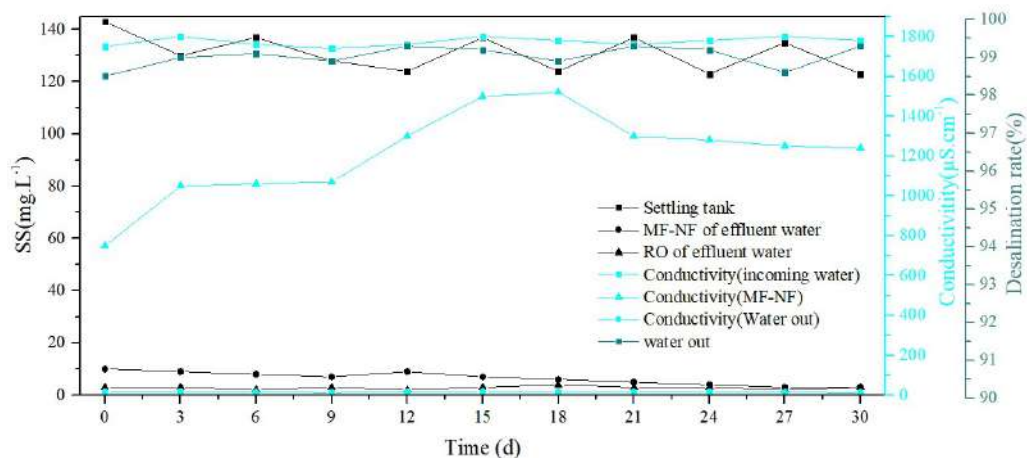


Fig. 6: Effect of membrane treatment system on conductivity, desalination, and SS removal.

many enterprises' electroplating wastewater treatment processes and equipment still need to be improved to meet the standard requirements (Fonseca et al. 2018). For treatment and reuse, defining different treatment water qualities based on the required water quality for reclaimed water reuse may be more meaningful than blindly pursuing sewage standards. Therefore, many enterprises and scholars have also begun to consider reusing the reclaimed water from electroplating wastewater treatment, which may greatly reduce operating treatment costs (Zhang et al. 2018, Van 2018).

Membrane Treatment Technology

The membrane treatment technology of electroplating wastewater uses a membrane with selective permeability to separate the solute and the solvent (Fig. 4), the solute and the solvent (water) in the solution under the action of a particular external driving force, to achieve the purpose of purification, concentration, and purification (Fonseca et al. 2018, Van 2018). When the driving force is concentration difference plus chemical reaction, the membrane process is liquid membrane separation; when the driving force is the potential difference, the membrane separation process is electrodialysis; when the driving force is a pressure difference, the membrane separation process is micro-filtration, ultra-filtration, reverse osmosis, nano-filtration (Moslehyani et al. 2019, Park et al. 2018).

The characteristics of membrane treatment technology include separation effects reaching the nanometer level, low process energy consumption, easy maintenance and high reliability of equipment, small equipment footprint, and no introduction of other chemical substances in the material being treated during the process, preventing secondary pollution (Bankole et al. 2017, Ahsan & Imteaz 2019).

In recent years, with the development of electroplating wastewater membrane treatment technology and new discharge standards, a single membrane treatment technology can no longer fulfill the current requirements for electroplating wastewater treatment. As a result, more methods or process combinations are employed in integrated forms to treat electroplating wastewater (Ahsan & Imteaz 2019, Lakhotia et al. 2019). The mainstream membrane treatment technologies include nano-filtration, ultra-filtration, micro-filtration, reverse osmosis, ceramic, and biological membranes. The filtration processes of several standard filter membranes are illustrated in Fig. 5.

Nano-filtration Membrane

Nano-filtration is a membrane separation technology between ultra-filtration and reverse osmosis. The pore size is generally 10 to 1 nm. It is a functional semipermeable membrane that allows solvent molecules or some low molecular weight solutes or low valent ions to pass the membrane (Lakhotia et al. 2019). The molecular weight of it intercepts organic matter is about 150-500, the ability to intercept soluble salt is between 2-98%, and the desalination of monovalent anion salt solution is lower than that of high-valent anion salt solution (Ahmadi et al. 2017, Yan et al. 2018).

Park et al. (2018) used an integrated membrane treatment technology of micro-filtration, nano-filtration, and reverse osmosis to treat electroplating wastewater. The results show that when the COD_{Cr} value range of electroplating wastewater inlet is between 100-150 mg.L⁻¹, the COD_{Cr} of the water sample in the return water storage tank has decreased to below 10 mg.L⁻¹ after being treated by the integrated membrane system (Yan et al. 2018). Although the water quality of the inlet system fluctuates due to the

partial interception effect of the integrated membrane on COD_{Cr}, the COD_{Cr} value of the return water storage tank can be stabilized below 10 mg.L⁻¹, and the COD_{Cr} removal rate can reach about 95% (He et al. 2019, Ya et al. 2018). This shows that the integrated membrane system has certain advantages in COD_{Cr} treatment. The average removal rate of SS reached 97.1%, and the desalination rate reached 98% (Fig. 6), meeting the standards for electroplating wastewater reuse.

Gündoğdu et al. (2019) used ultra-filtration, nano-filtration, and reverse osmosis technology to establish a pilot-scale platform for electroplating wastewater treatment. The experimental results show that this technology can concentrate nickel ions in nickel-containing electroplating wastewater 8-10 times and produce water. Through the subsequent supplementary processes such as alkali neutralization and ion exchange, the conductivity of the produced water can reach below 2 μS.cm⁻¹, the heavy metal indicators are not detected, and the TOC is less than 5 mg.L⁻¹ (Ya et al. 2018, Hegoburu et al. 2020). Hegoburu et al. (2020) conducted a cross-flow filtration experiment on electroplating wastewater with a new pH-stabilized nano-filtration membrane. The results showed that the new pH-stabilized nano-filtration membrane could remove about 75% of heavy metals when treating acidic electroplating wastewater.

In summary, it can be seen that under the combined process treatment of electroplating wastewater, the heavy metal ions in the water can be significantly reduced, the removal rate of COD_{Cr} in the water can reach 95%, the removal rate of SS can reach 97.1%, the desalination rate can reach 98%, and the conductivity of the effluent can reach 2 μS.cm⁻¹, TOC is below 5 mg.L⁻¹, meeting the standards for electroplating wastewater reuse.

Ultrafiltration Membrane

Ultra-filtration membrane is a membrane process between micro-filtration and nano-filtration, and the membrane pore size is between 100 nm and 10 nm (Chew et al. 2018). The ultra-filtration membrane sieving process is driven by the pressure difference on both sides of the membrane, and the ultra-filtration membrane is used as the filter medium. Only water and small molecular substances are allowed to pass through to become permeate. In contrast, substances in the raw solution whose volume is larger than the pore size of the membrane surface are trapped on the liquid inlet side of the membrane and become the concentrated solution, thus realizing the purification, separation, and concentration of the raw solution (Totaro et al. 2017, Zhu et al. 2018).

Shen et al. (2019) used the “chemical precipitation-tubular ultra-filtration” combined process to treat copper and total phosphorus in pyrophosphate copper-plating wastewater. The results showed that the dosage of calcium hydroxide was 1.25 g.L⁻¹, the stirring time was 24 min, and when the stirring speed was 150 rpm, the operating pressure was 0.15 MPa (Zhu et al. 2018). The flow rate on the membrane surface was 2.5 m.s⁻¹, the stable flux of the membrane was about 700 L/(m².h), and the mass concentration of copper in the effluent was stable between 0.2 and 0.3 mg.L⁻¹, the mass concentration of total phosphorus is stable between 0.2 and 0.4 mg.L⁻¹, all of which meet the requirements of effluent standards (Fig. 7) (Oden & Sari-Erkan 2018, Chen et al. 2018).

Sabeen et al. (2019) used the loading flocculation-ultra-filtration -reverse osmosis process to treat printed circuit board (PCB) wastewater containing high concentrations of heavy metal ions. When the dosage is 1.0 mg.L⁻¹, and the stirring speed is 250 r.min⁻¹, the experimental results show

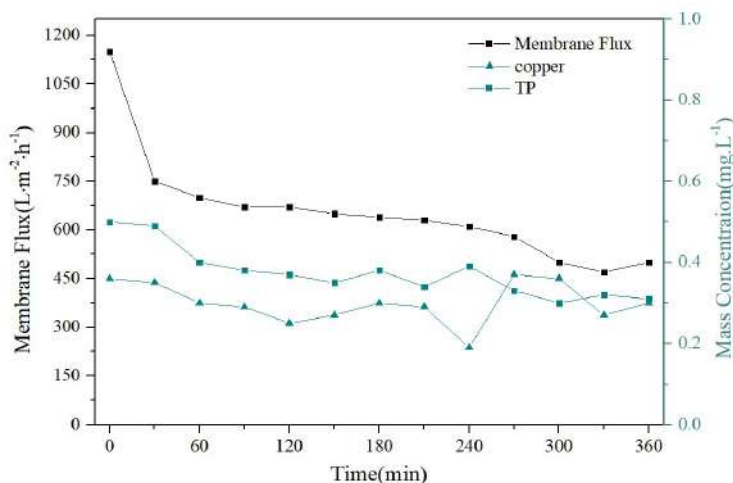


Fig. 7: Membrane flux and effluent quality under continuous operation.

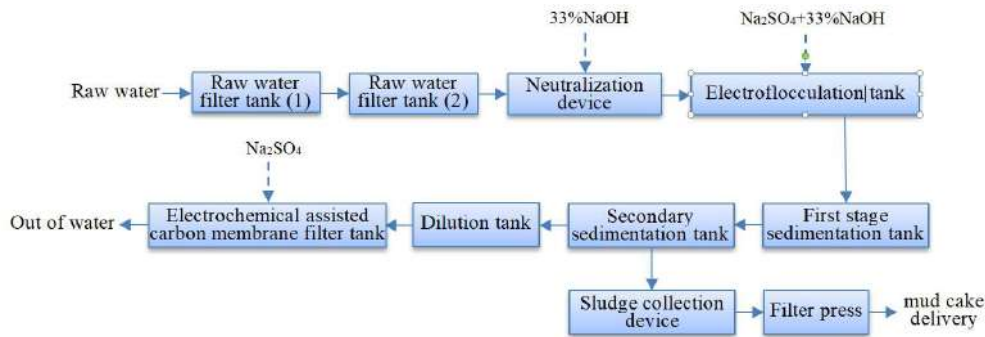


Fig. 8: Electroplating wastewater treatment process.

that the Cu^{2+} and Ni^{2+} concentrations in the effluent are 0.025 mg.L^{-1} and 0.022 mg.L^{-1} , and the removal rates are 90.7% and 90.1%, the highest desalination rate can reach 97.6% (Tezcan et al. 2017).

In summary, it can be seen that when using ultrafiltration membranes to treat electroplating wastewater, it is generally necessary to combine other processes for treatment, such as chemical precipitation tube ultrafiltration process, loaded flocculation ultrafiltration reverse osmosis process, etc. The treatment effect of electroplating wastewater using a single ultrafiltration membrane is poor, especially for the removal of heavy metals, which is very limited. However, when the combined process is used to treat electroplating wastewater, when the operating conditions are suitable, the heavy metal ions in the water will be greatly removed, and the desalination rate is also high. The treated wastewater is easy to reach the effluent standard.

Micro-filtration Membrane

The micro-filtration membrane can retain particles between 10 and $0.1 \mu\text{m}$, allowing macromolecules and dissolved solids (inorganic salts) to pass through while retaining suspended solids, bacteria, and large molecular weight colloids (Chen et al. 2018).

Chowdhury et al. (2018) employed an electrochemically assisted carbon membrane for removing organic matter in electroplating wastewater. The process flow is illustrated in Fig. 8 (Bhateria & Dhaka 2017, Thamaraiselvan et al. 2018). Experimental results demonstrated that the effluent's COD content was 54 mg.L^{-1} , and the effluent's Zn^{2+} concentration and COD index met the standard for electroplating pollutant discharge.

Li et al. (2023) conducted an industrial treatment test on electroplating wastewater using a combination of acid-base neutralization precipitation, membrane separation, facultative membrane bioreactor, and reverse osmosis processes. The results demonstrate that the process is feasible and stable, with

effective treatment outcomes (Thamaraiselvan et al. 2018, Aslam et al. 2018). The treatment effects of each process section are presented in Table 1 (Kim et al. 2018). Without adding coagulants and flocculants, the effluent consistently meets the electroplating pollutant discharge standards requirements. Simultaneously, heavy metal resources, such as Cu and Ni in the sludge, can be recovered, significantly reducing the costs of chemicals and sludge disposal. The treatment cost per ton of wastewater is approximately 19.1 Yuan, offering economic and environmental benefits (Aslam et al. 2018).

At present, the dual membrane method MF+RO is the most mainstream method for treating electroplating wastewater using membrane separation. The ion retention rate of RO membrane is generally higher than 96% under normal working conditions, which electroplating enterprises highly favor. However, due to the susceptibility of RO membranes to various pollution factors and their high requirements for influent water, direct passage through RO membranes can easily cause membrane blockage, which limits the efficiency and service life of the entire membrane system in treating and reusing electroplating wastewater. So, in the front end of the RO membrane system, an MF membrane system is used to pre-treat the influent water of the reverse osmosis membrane so that the wastewater meets the influent requirements of the reverse osmosis membrane. After that, it is pressurized to remove heavy metal ions through the reverse osmosis membrane system, which can better achieve the expected treatment and reuse effect.

Reverse Osmosis Membrane

Reverse osmosis, also referred to as hyperfiltration, features a membrane structure with a thin, dense layer ($0.1\text{-}1.0 \mu\text{m}$) on the surface and a porous support layer ($100\text{-}200 \mu\text{m}$) beneath the surface layer (Badruzzaman et al. 2019). This membrane separation operation uses pressure difference as the driving force to separate the solvent from the solution. Pressure is applied to the feed liquid on one side of the

Table 1: Treatment effect of each process section.

Process unit	Influent concentration [mg.L ⁻¹]					Effluent concentration [mg.L ⁻¹]					Removal rate (%)
	COD _{Cr}	Total Cyanide (CN)	Total nickel	Total copper	Total Silver	COD _{Cr}	Total Cyanide (CN)	Total nickel	Total copper	Total Silver	
Nickel-containing wastewater pre-separation system	40	-	25	-	-	39	-	5	-	-	2.5(COD) 80(Total nickel)
Nickel-containing wastewater membrane separation system	39	-	5	-	-	38	-	0.5	-	-	2.6(COD) 90(Total nickel)
Acid copper wastewater pre-separation system	15	-	-	100	-	14	-	-	5	-	6.7(COD) 95(Total copper)
Acid copper wastewater membrane separation system	14	-	-	5	-	13	-	-	0.5	-	7.1(COD) 90(Total copper)
Silver-containing wastewater membrane separation system	250	25	-	-	40	240	0.3	-	-	3	4(COD),98.8(CN) 92.5(Total silver)
Silver-containing wastewater ion exchange system	240	0.3	-	-	3	236	0.3	-	-	0.01	1.7(COD),0(CN) 99.7(Total silver)
Cyanide-containing wastewater pre-separation system	250	25	-	60	-	240	2	-	4	-	4(COD),92(CN) 93.3(Total copper)
Cyanide-containing wastewater membrane separation system	240	2	-	4	-	236	0.3	-	0.5	-	1.7(COD),85(CN) 87.5(Total copper)
Biochemical treatment system	208	0.06	0.07	0.1	0.0005	40	0.06	0.07	0.1	0.0005	80.8(COD),0(CN), 0(Total nickel),0(Total copper), 0(Total silver)
RO system concentrate	40	0.06	0.07	0.1	0.0005	66.7	0.1	0.12	0.17	0.0008	-
Emission limit [mg.L ⁻¹]	-	-	-	-	-	80	0.3	0.5	0.5	0.3	-

membrane; when the pressure surpasses its osmotic pressure, the solvent will permeate against the natural flow direction. Reverse osmosis occurs on the membrane's low-pressure side, while concentration occurs on the high-pressure side (Qin et al. 2019, Senusi et al. 2018).

Sanmartino et al. (2017) designed a chemical pretreatment reverse osmosis membrane and evaporative crystallization process to treat electroplating wastewater based on the water quality and quantity characteristics. Following the project's stable operation, the mass concentration of

Cr⁶⁺ in the pretreatment system effluent can be as low as 0.13 mg.L⁻¹, producing approximately 225 tons of recycled water daily with a conductivity of 424 $\mu\text{S.cm}^{-1}$ (Table 2) (Senusi et al. 2018, Rathna et al. 2019). The treatment cost per ton of wastewater is about 9.7 Yuan, offering good economic benefits, stable system operation, and a high degree of automation, ultimately achieving zero discharge of electroplating wastewater (Rathna et al. 2019, Abdel-Fatah 2018).

Fujioka et al. (2018) analyzed the source and content

Table 2: Pretreated effluent.

	pH	7.5	8.0	7.0	7.5	7.5
Pretreatment system effluent	Cr ⁶⁺ [mg.L ⁻¹]	0.19	0.15	0.16	0.16	0.13
	CN[mg.L ⁻¹]	0.21	0.17	0.19	0.15	0.14
Reuse system effluent	Water production [m ³ .h ⁻¹]	25.5	24.7	25.0	25.3	25.5
	Conductivity [$\mu\text{S.cm}^{-1}$]	562	643	424	513	438
	TDS[mg.L ⁻¹]	525	589	467	534	307

of wastewater from enterprises, applied chemical methods to treat various types of wastewater containing chromium, nickel, and cyanide, and used reverse osmosis membrane separation technology to reuse backwater (Rajoria et al. 2021). The controller controls the wastewater treatment center system of automatic dosing of each treatment unit. The operation process is stable and controllable, and the real-time operation data can be directly transmitted to the environmental protection management department, which meets the requirements of clean production and realizes the purpose of energy saving and emission reduction of the enterprise (Mokhtar et al. 2018, Giwa et al. 2019).

In summary, due to the mature development of reverse osmosis membrane equipment and technology, the treatment effect of electroplating wastewater by reverse osmosis membrane is good, especially for the removal rate of heavy metals and TDS in water. The TDS removal rate is stable at over 94%, and the cost of wastewater treatment is also low. This indicates that reverse osmosis is a key step in removing heavy metals and TDS in electroplating wastewater. However, during normal operation of reverse osmosis cleaning conditions, the membrane inside the reverse osmosis component may be contaminated by inorganic salt scale, microorganisms, colloidal particles, and insoluble organic substances. These pollutants deposit on the surface of the membrane, resulting in a decrease or simultaneous deterioration of the standardized production water flow rate and system desalination rate. Timely cleaning is necessary.

Ceramic Membrane

The ceramic membrane separation process is a “cross-flow

filtration” form of fluid separation process: the raw material liquid flows at high speed inside the membrane tube, and under pressure driving, the clarified permeate containing small molecular components penetrates the membrane vertically outward. The turbid concentrated solution containing large molecular components is intercepted by the membrane, thereby achieving the purpose of separation, concentration, and purification of the fluid (Giwa et al. 2019, Abdel-Fatah 2018).

Samaei et al. (2018) treated electroplating wastewater with electro-flocculation and ceramic membrane in small and pilot-scale experiments. The results of electro-flocculation and ceramic membrane experiments in pilot-scale experiments are shown in Fig. 9 (Tao et al. 2022, Zsirai et al. 2018, Davoodbeygi et al. 2023). The test results show that the optimum pH value of the ceramic membrane for treating electroplating wastewater is 10-10.5, and the optimum operating pressure is 3 MPa. This method has a good removal effect on chromium, nickel, copper, and zinc (Zsirai et al. 2018). The removal rate has reached more than 95%, and the final effluent complies with the discharge standard in “Emission Standard of Electroplating Pollutants.”

Davoodbeygi et al. (2023) constructed a Fenton oxidation-activated carbon adsorption-ceramic membrane filtration coupling process. The results showed that this technology’s removal rate of COD and TOC was stable at about 29.6% and 18.0%, and the removal rate of turbidity reached more than 84.3% (Dharupaneedi et al. 2019). After treatment, the concentrations of COD and TOC in the effluent are less than 52.1 mg.L^{-1} and 18.0 mg.L^{-1} , and the turbidity of the effluent is far less than 0.5 NTU (Fig. 10) (Zhang et al. 2018).

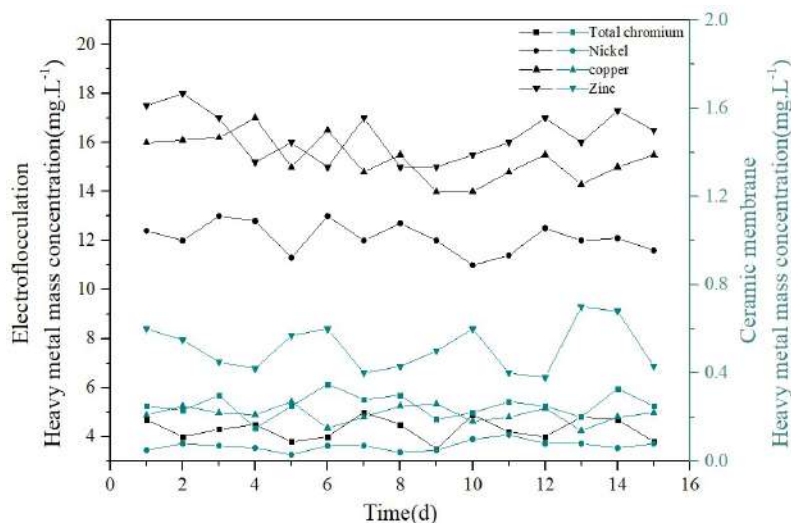


Fig. 9: Pilot test of electro-flocculation and Ceramic membrane pilot test.

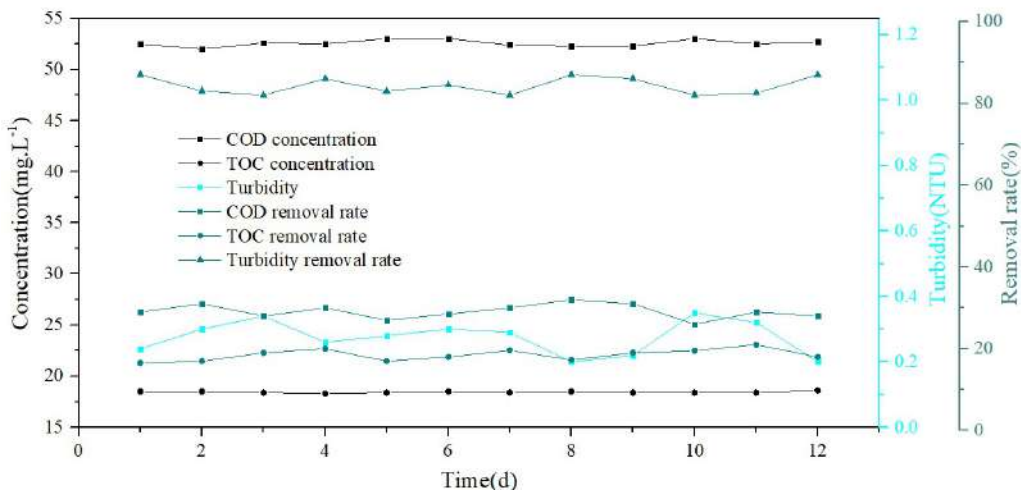


Fig. 10: Concentration and removal rate of COD, TOC, and turbidity.

Wang (2018) used ceramic membrane, reverse osmosis, and multi-effect evaporation technology to reduce the content of hexavalent chromium in the effluent to 0.01 mg.L⁻¹, the content of nickel to 0.11 mg.L⁻¹, and the content of iron to 0.28 mg.L⁻¹, the manganese content was reduced to 0.08 mg.L⁻¹, the COD and TDS in the effluent were reduced to 8.5 mg.L⁻¹ and 136 mg.L⁻¹, the turbidity of the effluent was reduced to 0.3 NTU (Table 3) (Nidhi et al. 2019, Bai et al. 2019, Bhateria & Dhaka 2017). It complies with the cooling water reuse standard in the “Design Specification for Urban Sewage Reuse,” The reverse osmosis concentrated water is evaporated by a high-efficiency evaporator, realizing zero discharge of electroplating wastewater treatment (Bhateria & Dhaka 2017).

Bukhari et al. (2017) used silicon carbide flat membranes to treat electroplating wastewater. The results show that silicon carbide flat membrane has good acid and alkali, oil, and corrosion resistance and can effectively reduce suspended solids and some organic matter in electroplating wastewater (Pronk et al. 2019). The removal rate of suspended solids and turbidity is as high as 99%, and the flat membrane effectively removes COD while reducing operating costs (Zhao et al. 2019).

In summary, it can be seen that when using ceramic membranes to treat electroplating wastewater, it is generally

necessary to combine other processes for treatment, such as electrocoagulation and ceramic membrane processes, Fenton oxidation activated carbon adsorption ceramic membrane filtration coupling process, ceramic membrane reverse osmosis multi-effect evaporation process, silicon carbide flat membrane, etc. When a single ceramic membrane is used to treat electroplating wastewater, the effluent quality is greatly affected by the reaction pH value, and its treatment effect is very limited. However, when combined processes are used to treat electroplating wastewater, most of the heavy metals such as hexavalent chromium, nickel, iron, and manganese in the effluent are removed, and the COD and turbidity in the effluent are also greatly reduced.

Biofilm Membrane

Biofilm treatment technology is a method of organic sewage treatment using microorganisms (i.e., biofilms) attached to the surface of particular solid objects (Desmond et al. 2018).

Rahman et al. (2021) used the micro-electrolysis-DMBR process to treat electroplating wastewater. The removal rates of hexavalent chromium and nickel were 99.34% and 99.14%, the removal rates of COD and ammonia nitrogen were 94.75% and 90.22% (Fig. 11), and the effluent reached “Emission Standards for Electroplating Pollutants”

Table 3: Effluent quality of ceramic membrane and first stage reverse osmosis process.

Project	pH	Turbidity (NTU)	Chroma (time)	[mg.L ⁻¹]						
				COD	NH ₃ -N	TDS	Iron	Chromium	Nickel	Manganese
Ceramic membrane effluent	7.8	0.3	0.2	70.5	0.066	3412	0.25	0.01	0.05	0.09
Reverse osmosis effluent	7.7	n.d.	n.d.	8.5	0.012	136	n.d.	n.d.	0.01	n.d.

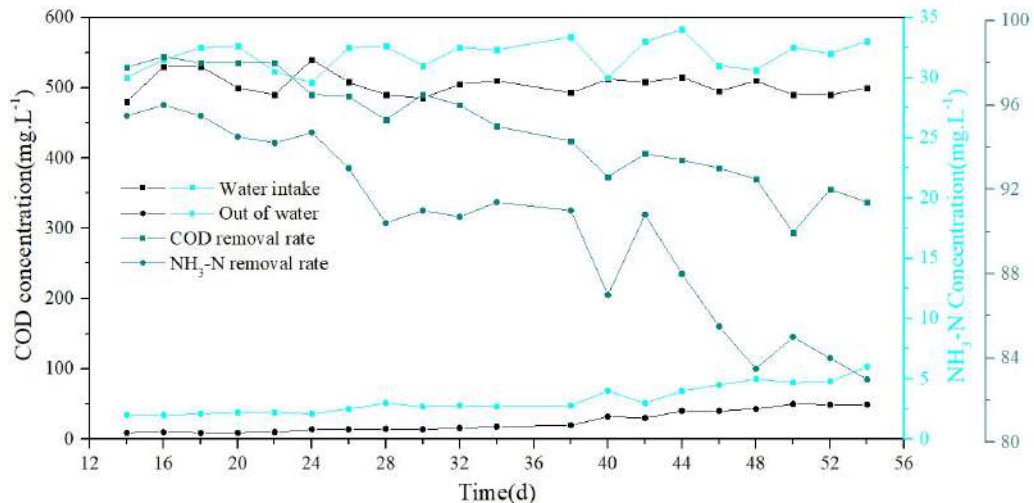


Fig. 11: Removal of COD and NH₃-N in Micro electrolysis-DMBR.

(GB21900-2008) (Guan et al. 2017).

Xiong et al. (2023) used a green emulsion liquid film to recover zinc from electroplating water. The experimental conditions were that the pH value of the environment was 3.8, the volume content of surfactant was 4%, the equivalent concentration of the internal phase was 1.61 N, and the concentration of zinc was 3.8 (Noah et al. 2018, Bratovcic et al. 2022). When the concentration is 742 mg.L⁻¹, the emulsion volume ratio of the external phase is 0.94, and the carrier concentration is 8.9%, the maximum recovery rate of zinc can reach 97.4%. Z Rujia (2020) added a sedimentation tank at the MBR tank's front end during the electroplating wastewater treatment system transformation, which alleviated the problem of membrane blockage. The system can maintain stable operation for at least 24 h after online backwashing. After three weeks of operation, the comprehensive wastewater MBR The daily average fluxes of MBR and mixed wastewater are 12.56 L/(m².h) and 10.49 L/(m².h), respectively, and the average daily running time of 21 h can meet the requirements of treated water volume and discharge water quality (Goswami et al. 2019, Sari Erkan et al. 2018).

Li-Kun et al. (2018) used the suspended carrier composite MBR process (HMBR) to run in parallel with the normal MBR process, represented by heavy metal ions Cu²⁺, Ni²⁺, and Cr (VI). They focused on the electroplating synthesis of the two processes under the impact of different concentrations of heavy metals (Tan et al. 2019, Bortoluzzi et al. 2017). The effect of wastewater efficiency and microbial activity, as well as the control effect of carrier intervention on membrane fouling and the impact on the diversity of microbial populations, the experimental results show that

under the impact of Cu²⁺, Ni²⁺, Cr(VI) concentrations of 5-30 mg.L⁻¹, HMBR the removal rate of COD and NH₃-N by the process is over 60% and 40%, while the removal rate of COD and NH₃-N by the standard MBR process is over 30% and 15% (Fig. 12) (Wang & Wang 2019). Rajasimman et al. (2021) applied biological methods to treat zinc-nickel alloy electroplating wastewater. The COD removal rate could reach 91.45%.

In summary, the treatment of electroplating wastewater by biofilm mainly relies on artificially cultivated composite functional bacteria, which have electrostatic adsorption, enzyme catalytic conversion, complexation, flocculation, co-precipitation, and pH buffering effects. The outer shell of microbial functional bacteria carries a certain negative charge and is easy to absorb metal ions with positive charges. The bacterial micelles themselves have strong biological flocculation, which can adsorb and chelate heavy metals on their surface. Functional bacteria first reduce Cr⁶⁺ in wastewater to Cr³⁺, and then Cr³⁺, zinc, nickel, copper, and lead plasma are adsorbed and synthesized into clusters by the bacteria. After solid-liquid separation, the wastewater is discharged or reused to meet the standards, while heavy metal ions precipitate into sludge.

In summary, membrane treatment technology for electroplating wastewater has been extensively employed in laboratory experiments, pilot tests, and industrial applications. The most widely used membrane treatments include nano-filtration membranes, ultra-filtration membranes, micro-filtration membranes, reverse osmosis membranes, ceramic membranes, and biological membranes. For treating electroplating wastewater, nano-filtration membranes can achieve an average removal rate of 97.1% for suspended

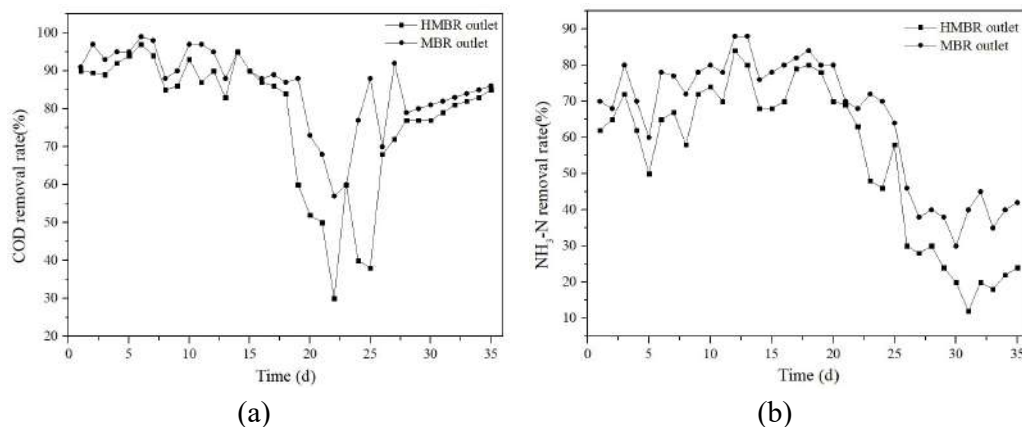


Fig. 12: (a) COD removal effect of HMBR and MBR processes at each stage; (b) NH₃-N removal effect of HMBR and MBR processes at each stage.

solids, a desalination rate of 98%, reduce effluent turbidity to below 0.1 NTU, attain a conductivity of below 2 $\mu\text{S}\cdot\text{cm}^{-1}$ for the produced water, achieve a TOC of less than 5 $\text{mg}\cdot\text{L}^{-1}$, and remove approximately 75% of heavy metals in wastewater. When ultra-filtration membranes treat electroplating wastewater, the total phosphorus concentration in the effluent remains stable between 0.2 and 0.4 $\text{mg}\cdot\text{L}^{-1}$. The Cu^{2+} and Ni^{2+} concentrations in the effluent can be reduced to 0.025 $\text{mg}\cdot\text{L}^{-1}$ and 0.022 $\text{mg}\cdot\text{L}^{-1}$, respectively, with removal rates reaching 90.7% and 90.1%, and the highest desalination rate of effluent can reach 97.6%. When micro-filtration membranes treat electroplating wastewater, the COD content of the effluent can be reduced to 54 $\text{mg}\cdot\text{L}^{-1}$. The effluent's Zn^{2+} concentration and COD index meet the emission standards, and the water treatment cost per ton is approximately 19.1 Yuan. When reverse osmosis membranes treat electroplating wastewater, the mass concentration of Cr^{6+} in the effluent can be as low as 0.13 $\text{mg}\cdot\text{L}^{-1}$, producing about 225 tons of recycled water daily with a conductivity of 424 $\mu\text{S}\cdot\text{cm}^{-1}$, and the water treatment cost per ton is around 9.7 Yuan. When ceramic membranes treat electroplating wastewater, hexavalent chromium, nickel, iron, and manganese in the effluent are reduced to 0.01 $\text{mg}\cdot\text{L}^{-1}$, 0.11 $\text{mg}\cdot\text{L}^{-1}$, 0.28 $\text{mg}\cdot\text{L}^{-1}$, and 0.08 $\text{mg}\cdot\text{L}^{-1}$, respectively. The COD and TDS in the effluent are reduced to 8.5 $\text{mg}\cdot\text{L}^{-1}$ and 136 $\text{mg}\cdot\text{L}^{-1}$, the effluent turbidity is reduced to 0.3 NTU, and the removal rate of suspended solids and turbidity reaches as high as 99%. When biofilm treats electroplating wastewater, hexavalent chromium and nickel removal rates reach 99.34% and 99.14%. COD and ammonia nitrogen removal rates reach 94.75% and 90.22%, and the effluent meets discharge requirements. Simultaneously, the maximum zinc recovery rate can reach 97.4%.

When using membrane treatment technology to treat electroplating wastewater, the effluent quality is better than

traditional processes, with strong impact resistance, and can significantly reduce the concentration of pollutants. However, it also has certain drawbacks, such as high membrane cost, easy occurrence of membrane pollution, and high energy consumption. Therefore, the future development of membrane treatment technology in the field of electroplating wastewater treatment must focus on the research and development of membrane materials while formulating a series of feasible laws and regulations and treated standards, standardizing the management of the electroplating wastewater treatment industry, and deepening research and innovation of technology.

CONCLUSIONS AND FUTURE PERSPECTIVES

Membrane treatment technology is currently the predominant approach in electroplating wastewater treatment and plays a crucial role in the overall process. This paper outlines four prospects for the advancement of membrane treatment technology for electroplating wastewater:

- (1) As the electroplating industry continues to develop, the complexity of electroplating wastewater increases. Developing more scientific, safe, and reasonable classification and treatment methods is essential. Electroplating wastewater should be divided into categories based on specific physical or chemical properties, and appropriate treatment processes should be designed accordingly. Combining various membrane processes for different treatment methods can enhance the overall efficiency of wastewater treatment.
- (2) The high salt content of electroplating wastewater poses a challenge, as it can lead to membrane fouling during treatment. Although physicochemical methods are employed in the pretreatment stage to reduce salt

content, finding rapid, safe, and environmentally friendly solutions to prevent membrane clogging remains a significant challenge.

- (3) Different types of electroplating wastewater should be treated with various membranes according to their primary components and characteristics. Establishing a relationship between wastewater types and membrane selection can lead to more effective and reasonable treatment approaches.
- (4) At present, the membrane treatment technology for electroplating wastewater mainly focuses on the direct removal of heavy metals, thereby transferring pollutants and waste resources. However, there is little research on the classification and recovery of heavy metals in wastewater after membrane technology treatment. Membrane treatment technology should be used to concentrate and collect heavy metals and other pollutants in electroplating wastewater and then further classify and recover heavy metals from the concentrated wastewater, thereby promoting resource recovery and sustainable development.
- (5) The development direction of membrane separation technology will be more green and environmentally friendly. In the process of treating electroplating wastewater, physical methods are mainly used to collect and concentrate heavy metal ions in the wastewater, which can increase the recovery rate of metal ions. Whether it is aerospace research, land construction, or domestic exploration, membrane separation technology is indispensable. In today's society, various countries are striving to improve their membrane separation technology capabilities. From biofilms to polymer membranes and liquid membranes, membrane separation technology research has become a high-tech research type.
- (6) Membrane technology in the field of electroplating wastewater treatment will soon become a cutting-edge topic of key development at home and abroad. Therefore, higher requirements have been put forward for membrane materials, especially to manufacture membrane materials that are suitable for the environmental protection industry with high strength, long lifespan, pollution resistance, and high throughput. The research on membrane separation technology is also advancing day by day. With the increasing improvement of regulations and standards, the continuous maturity of membrane technology, and the continuous reduction of costs, membrane technology will appear to be more advanced in technology and more widely used in applications.

ACKNOWLEDGEMENT

The present work is sponsored by the Science Foundation of Shaanxi Province of China (No.2022JQ-327), the Special Scientific Research Program of the Education Department of Shaanxi Province (No.22JK0425) and the school-level fund project of Xi'an Aeronautical University (No. 2021KY1203).

List of abbreviations

Nano-filtration	NF
Ultra-filtration	UF
Micro-filtration	MF
Reverse osmosis	RO
Electrodialysis	ED
Polyethylene terephthalate	PET
M-phenylenediamine	MPD
Trimethylene chloride	TMC
Polyacrylamide	PAM
Polyaluminum chloride	PAC
Nanometer	Nm
Chemical oxygen demand	COD
Suspended matter	SS
Total organic carbon	TOC
Total phosphorus	TP
Printed circuit board	PCB
Total Cyanide	CN
Total dissolved solids	TDS
Nephelometric Turbidity Units	NTU
No detection	n.d.
Dynamic membrane bio-reactor	DMBR
Membrane Bio-Reactor	MBR
Hybrid membrane bioreactor	HMBR

REFERENCES

- Abdel, W.R. and Alseroury, F.A. 2019. Wastewater treatment: a case study of the electronics manufacturing industry. *Int. J. Environ. Sci. Technol.*, 16(1): 47-58.
- Abdel-Fatah, M.A. 2018. Nanofiltration systems and applications in wastewater treatment: Review article. *Ain Shams Eng. J.*, 9(4): 3077-3092.
- Ahin, D. 2021. Forward Osmosis Membrane Technology in Wastewater Treatment. *Osmotically Driven Membrane Processes*. Intech Open, UK.
- Ahmadi, M., Jorfi, S., Kujlu, R., Ghafari, S., Darvishi Cheshmeh Soltani, R. and Jaafarzadeh Haghhighifard, N. 2017. A novel salt-tolerant bacterial consortium for biodegradation of saline and recalcitrant petrochemical wastewater. *J. Environ. Manage.*, 191(12): 198-208.
- Ahmed, S.F., Mehejabin, F., Momtahn, A., Tasannum, N., Faria, N.T., Mofijur, M., Hoang, A.T., Vo, D. and Mahlia, T. 2022. Strategies to improve membrane performance in wastewater treatment. *Chemosphere*, 306: 135527. DOI: 10.1016/j.chemosphere.2022.135527

- Ahsan, A. and Imteaz, M. 2019. 14 - Nanofiltration Membrane Technology Providing Quality Drinking Water. In: Nanotechnology in Water and Wastewater Treatment. Elsevier, 12(5): 291-295.
- Akar, S., Lorestani, B., Sobhanardakani, S., Cheraghi, M. and Moradi, O. 2021. Removal of Ni(II) and Cr(VI) ions from electroplating wastewater using ferrous sulfate. *Kurdistan Univ. Med. Sci.*, (2): 435-439.
- Albergamo, V., Blankert, B., Cornelissen, E.R., Hofs, B., Knibbe, W., van der Meer, W. and de Voogt, P. 2019. Removal of polar organic micropollutants by pilot-scale reverse osmosis drinking water treatment. *Water Res.*, 148(9): 535-545.
- Al-Saydeh, S.A., El-Naas, M.H. and Zaidi, S.J. 2017. Copper removal from industrial wastewater: A comprehensive review. *J. Ind. Eng. Chem.*, 56(9): 35-44.
- Aslam, M., Ahmad, R. and Kim, J. 2018. Recent developments in biofouling control in membrane bioreactors for domestic wastewater treatment. *Sep. Purif. Technol.*, 206(9): 297-315.
- Babilas, D. and Dydo, P. 2018. Selective zinc recovery from electroplating wastewaters by electrodialysis enhanced with complex formation. *Sep. Purif. Technol.*, 192(6): 419-428.
- Badruzzaman, M., Voutchkov, N., Weinrich, L. and Jacangelo, J.G. 2019. Selection of pretreatment technologies for seawater reverse osmosis plants: A review. *Desalination*, 449(12): 78-91.
- Bai, D., Wang, X., Huo, D., Ying, Q., Wang, N. and Xia, B. 2019. Coprecipitation Preparation of Cu/Zn/Al-Hydroxalcalite-Like Compound for Copper Removal from Electroplating Wastewater. *J. Chem.*, 20(3): 1-9.
- Bankole, M.T., Abdulkareem, A.S., Tijani, J.O., Ochigbo, S.S., Afolabi, A.S. and Roos, W.D. 2017. Chemical oxygen demand removal from electroplating wastewater by purified and polymer-functionalized carbon nanotube adsorbents. *Water Resour. Ind.*, 18(15): 33-50.
- Bhateria, R. and Dhaka, R. 2017. Impact of electroplating effluent on growth of *Triticum aestivum* and *Hordeum vulgare*. *Environ. Technol. Innovation*, 8(9): 389-398.
- Bhateria, R. and Dhaka, R. 2017. Impact of electroplating effluent on growth of *Triticum aestivum* and *Hordeum vulgare*. *Environ. Technol. Innov.*, 8(6): 389-398.
- Biniat, P., Torabi Ardekani, N., Makarem, M.A. and Rahimpour, M.R. 2019. Water and wastewater treatment systems by novel integrated membrane distillation (MD). *Chem. Eng.*, 3(1): 8-12.
- Bortoluzzi, A.C., Faitão, J.A., Di Luccio, M., Dallago, R.M., Steffens, J., Zabet, G.L. and Tres, M.V. 2017. Dairy wastewater treatment using integrated membrane systems. *J. Environ. Chem. Eng.*, 5(5): 4819-4827.
- Bratovic, A., Buksek, H. and Helix-Nielsen, C. 2022. Concentrating hexavalent chromium electroplating wastewater for recovery and reuse by forward osmosis using underground brine as draw solution. *Chem. Eng. J.*, 13(7): 431-435.
- Bukhari, S.Z.A., Ha, J., Lee, J. and Song, I. 2017. Fabrication and optimization of a clay-bonded SiC flat tubular membrane support for microfiltration applications. *Ceram. Int.*, 43(10): 7736-7742.
- Castel, C. and Favre, E. 2018. Membrane separations and energy efficiency. *J. Membr. Sci.*, 548(12): 345-357.
- Chen, Q., Xu, W. and Ge, Q. 2018. Novel Multicharge Hydroacid Complexes That Effectively Remove Heavy Metal Ions from Water in Forward Osmosis Processes. *Environ. Sci. Technol.*, 52(7): 4464-4471.
- Chew, C.M., Aroua, M.K. and Hussain, M.A. 2018. Advanced process control for ultrafiltration membrane water treatment system. *J. Cleaner Prod.*, 179(5): 63-80.
- Cho, H., Choi, Y. and Lee, S. 2018. Effect of pretreatment and operating conditions on the performance of membrane distillation for the treatment of shale gas wastewater. *Desalination*, 437(9): 195-209.
- Chowdhury, Z.Z., Pal, K., Sagadevan, S., Yehye, W.A., Johan, R.B., Shah, S.T., Adebese, A., Ali, M.E., Islam, M.S. and Rafique, R.F. 2018. Electrochemically active carbon nanotube (CNT) membrane filter for desalination and water purification. In: *Emerging Technologies for Sustainable Desalination Handbook*. Butterworth-Heinemann, 45(3): 333-363.
- Damtie, M.M., Kim, B., Woo, Y.C. and Choi, J. 2018. Membrane distillation for industrial wastewater treatment: Studying the effects of membrane parameters on the wetting performance. *Chemosphere*, 206(3): 793-801.
- Davoodbeygi, Y., Askari, M., Salehi, E. and Kheirieh, S. 2023. A review on hybrid membrane-adsorption systems for intensified water and wastewater treatment: Process configurations, separation targets, and materials applied. *J. Environ. Manage.*, 335: 117577.
- Desmond, P., Morgenroth, E. and Derlon, N. 2018. Physical structure determines compression of membrane biofilms during gravity-driven membrane (GDM) ultrafiltration. *Water Res.*, 143(13): 539-549.
- Dharupaneedi, S.P., Nataraj, S.K., Nadagouda, M., Reddy, K.R., Shukla, S.S. and Aminabhavi, T.M. 2019. Membrane-based separation of potential emerging pollutants. *Sep. Purif. Technol.*, 210(9): 850-866.
- Fonseca Couto, C., Lange, L.C. and Santos Amaral, M.C. 2018. A critical review on membrane separation processes applied to remove pharmaceutically active compounds from water and wastewater. *J. Water Process Eng.*, 26(2): 156-175.
- Fujioka, T., Ishida, K.P., Shintani, T. and Kodamatani, H. 2018. High rejection reverse osmosis membrane for removal of N-nitrosamines and their precursors. *Water Res.*, 131(4): 45-51.
- Giwa, A., Ahmed, M. and Hasan, S.W. 2019. Polymers for Membrane Filtration in Water Purification. In: *Polymeric Materials for Clean Water*. Cham: Springer International Publishing, 6(2): 167-190.
- Goswami, L., Kumar, R.V., Pakshirajan, K. and Pugazhenthii, G. 2019. A novel integrated biodegradation—microfiltration system for sustainable wastewater treatment and energy recovery. *J. Hazard. Mater.*, 365(3): 707-715.
- Guan, W., Tian, S., Cao, D., Chen, Y. and Zhao, X. 2017. Electrooxidation of nickel-ammonia complexes and simultaneous electrodeposition recovery of nickel from practical nickel-electroplating rinse wastewater. *Electrochim. Acta*, 246(17): 1230-1236.
- Gündoğdu, M., Jarma, Y.A., Kabay, N., Pek, T.Ö. and Yüksel, M. 2019. Integration of MBR with NF/RO processes for industrial wastewater reclamation and water reuse-effect of membrane type on product water quality. *J. Water Process Eng.*, 100574 : (14)29.
- Güven, H., Ersahin, M.E. and Ozgun, H. 2022. Energy self-sufficiency in wastewater treatment plants: perspectives, challenges, and opportunities. *Clean Energy Resour. Recov.*, 3(8): 105-122. DOI: 10.1016/j.cerrev.2022.100206
- Hackbarth, F.V., Maass, D., de Souza, A.A.U., Vilar, V.J.P. and de Souza, S.M.A.G. 2016. Removal of hexavalent chromium from electroplating wastewaters using marine macroalga *Pelvetia canaliculata* as a natural electron donor. *Chem. Eng. J.*, 290(13): 477-489.
- He, D., Cao, Z., Zhang, G., Zeng, L., Li, Q. and Guan, W. 2019. Recovery of nickel from electroplating wastewater with a new extractant. *Chem. Papers*, 73(3): 583-589.
- Hedayati, M.A., Hazrati, H., Sargolzaei, J. and Shayegan, J. 2017. Assessing and simulation of membrane technology for modifying starchy wastewater treatment. *Appl. Water Sci.*, 7(6): 2753-2765.
- Hegoburu, I., Zedda, K.L. and Velizarov, S. 2020. Treatment of Electroplating Wastewater Using NF pH-Stable Membranes: Characterization and Application. *Membranes*, 10(12): 399-401.
- Hoslett, J., Massara, T.M., Malamis, S., Ahmad, D., van den Boogaert, I., Katsou, E., Ahmad, B., Ghazal, H., Simons, S., Wrobel, L. and Jouhara, H. 2018. Surface water filtration using granular media and membranes: A review. *Sci. Total Environ.*, 6(39): 1268-1282.
- Hosseini, S.S., Nazif, A., Alaei Shahmirzadi, M.A. and Ortiz, I. 2017. Fabrication, tuning and optimization of poly (acrilonitrile) nanofiltration membranes for effective nickel and chromium removal from electroplating wastewater. *Sep. Purif. Technol.*, 187(12): 46-59.
- Ibrar, I., Yadav, S., Naji, O., Alanezi, A.A., Ghaffour, N., Deon, S., Subbiah, S. and Altaee, A. 2022. Development in forward Osmosis-

- Membrane distillation hybrid system for wastewater treatment. *Sep. Purif. Technol.*, 12(28): 286-290.
- John, M., Heuss-Aßbichler, S., Ullrich, A. and Rettenwander, D. 2016. Purification of heavy metal loaded wastewater from electroplating industry under synthesis of delafossite (ABO₂) by "Lt-delafossite process". *Water Res.*, 100(9): 98-104.
- Khan, A.A. and Boddu, S. 2021. Hybrid membrane process: an emerging and promising technique toward industrial wastewater treatment. *Membrane-Based Hyb. Process. Wastewater Treat.*, 5(12):345-349.
- Kim, S., Chu, K.H., Al-Hamadani, Y.A.J., Park, C.M., Jang, M., Kim, D., Yu, M., Heo, J. and Yoon, Y. 2018. Removal of contaminants of emerging concern by membranes in water and wastewater: A review. *Chem. Eng. J.*, 335(5): 896-914.
- Kobyas, M., Demirbas, E., Ozyonar, F., Sirtbas, G. and Gengec, E. 2017. Treatments of alkaline non-cyanide, alkaline cyanide and acidic zinc electroplating wastewaters by electrocoagulation. *Process Saf. Environ. Prot.*, 105(2): 373-385.
- Lakhotia, S.R., Mukhopadhyay, M. and Kumari, P. 2019. Iron oxide (FeO) nanoparticles embedded thin-film nanocomposite nanofiltration (NF) membrane for water treatment. *Sep. Purif. Technol.*, 211(5): 98-107.
- Leonzio, G. 2017. Optimization of column distillation in a wastewater treatment plant. *J. Environ. Chem. Eng.*, 5(6): 5732-5745.
- Li, S., Dai, M. and Ali, I. 2023. Recovery of nickel from actual electroplating wastewater by integrated electrodeposition with adsorption pretreatment technique. *Trans. Inst. Chem. Eng., Process Saf. Environ. Prot., Part B*.
- Li-Kun, W., Guang-Zhi, H., Li-Ming, S. U. Xin-Ying, Z. Zhi-Qiang, X. Zhi. 2018. Efficiency of electroplating wastewater treatment by suspended carrier integrated with MBR technology. *China Environmental Science*, 38(7): 2490-2497.
- Malhas, R., Ghafoori, S. and Omar, M. 2022. Application of ultrafiltration membrane-embedded activated carbon-filter in Kuwait wastewater treatment in comparison with a conventional method. *Desal. Water Treat.*, 6(24): 246-250.
- Manetti, M. and Tomei, M.C. 2022. Extractive polymeric membrane bioreactors for industrial wastewater treatment: Theory and practice. *Trans. Inst. Chem. Eng. Process Saf. Environ. Prot. Part B*, 5(16): 162-165.
- Mansor, E.S.A.E. 2021. Tight ultrafiltration polyethersulfone membrane for cheese whey wastewater treatment. *Chem. Eng. J.*, 407(1):123-125.
- Maulin, S., Steve, P. and Rodriguez, C. 2022. Emerging and innovative technologies for water and wastewater treatment. *Lett. Appl. Microbiol.*, 75(4): 700-705. DOI: 10.1111/lam.13644
- Mohagheghian, A., Ayagh, K., Godini, K. and Shirzad-Siboni, M. 2018. Photocatalytic reduction of Cr(VI) from synthetic, real drinking waters and electroplating wastewater by synthesized amino-functionalized Fe₃O₄-WO₃ nanoparticles by visible light. *J. Ind. Eng. Chem.*, 59(10): 169-183.
- Mokhtar, M., Dickson, S.E., Kim, Y. and Mekky, W. 2018. Preparation and characterization of ion selective membrane and its application for Cu²⁺ removal. *J. Ind. Eng. Chem.*, 60(13): 475-484.
- Moslehiani, A., Ismail, A.F., Matsuura, T., Rahman, M.A. and Goh, P.S. 2019. Chapter 3 - Recent Progresses of Ultrafiltration (UF) Membranes and Processes in Water Treatment. In: *Membrane Separation Principles and Applications*. Elsevier, 8(12): 85-110.
- Nidhi Maalige, R., Aruchamy, K., Mahto, A., Sharma, V., Deepika, D., Mondal, D. and Nataraj, S.K. 2019. Low operating pressure nanofiltration membrane with functionalized natural nanoclay as antifouling and flux promoting agent. *Chem. Eng. J.*, 358(16): 821-830.
- Noah, N.F.M., Jusoh, N., Othman, N., Sulaiman, R.N.R. and Parker, N.A.M.K. 2018. Development of stable green emulsion liquid membrane process via liquid-liquid extraction to treat real chromium from rinse electroplating wastewater. *J. Ind. Eng. Chem.*, 66(6): 231-241.
- Noah, N.F.M., Othman, N. and Jusoh, N. 2016. Highly selective transport of palladium from electroplating wastewater using emulsion liquid membrane process. *J. Taiwan Inst. Chem. Eng.*, 64(9): 134-141.
- Oden, M.K. and Sari-Erkan, H. 2018. Treatment of metal plating wastewater using iron electrode by electrocoagulation process: Optimization and process performance. *Process Saf. Environ. Prot.*, 119(8): 207-217.
- Ozokwelu, D., Zhang, S., Okafor, O.C., Cheng, W. and Litombe, N. 2017. Chapter 5 - Separation Science and Technology. In: *Novel Catalytic and Separation Processes Based on Ionic Liquids*. Amsterdam: Elsevier, 9(2): 193-202.
- Park, J.W., Lee, Y.J., Meyer, A.S., Douterelo, I. and Maeng, S.K. 2018. Bacterial growth through microfiltration membranes and NOM characteristics in an MF-RO integrated membrane system: Lab-scale and full-scale studies. *Water Res.*, 144(4): 36-45.
- Pronk, W., Ding, A., Morgenroth, E., Derlon, N., Desmond, P., Burkhardt, M., Wu, B. and Fane, A.G. 2019. Gravity-driven membrane filtration for water and wastewater treatment: A review. *Water Res.*, 149(5): 553-565.
- Qin, M., Deshmukh, A., Epsztein, R., Patel, S.K., Owoseni, O.M., Walker, W.S. and Elimelech, M. 2019. Comparison of energy consumption in desalination by capacitive deionization and reverse osmosis. *Desalination*, 455(7): 100-114.
- Quiton, K.G.N., Huang, Y. and Lu, M. 2022. Recovery of cobalt and copper from single- and co-contaminated simulated electroplating wastewater via carbonate and hydroxide precipitation. *Sustainable Environ. Res.*, 32(1): 345-349.
- Rahimpour, M.R., Kazerooni, N.M. and Parhoudeh, M. 2019. Chapter 8 - Water Treatment by Renewable Energy-Driven Membrane Distillation. In: Basile, A., Cassano, A., Figoli, A. (Eds.), *Current Trends and Future Developments on (Bio-) Membranes*, Elsevier, 179-211.
- Rahman, M.L., Sarjadi, M.S., Arshad, S.E., Musta, B., Abdullah, M.H., Sarkar, S.M. and O'Reilly, E.J. 2021. Toxic metal ions removal from electroplating wastewater using polymer chelating ligands. *Curr. Anal. Chem.*, 9(5): 17-20.
- Rajasimman, M., Rajamohan, N. and Sujatha, S. 2021. Recovery of Zinc from Electroplating Wastewater Using Green Emulsion Liquid Membrane. IWA Publishing, London
- Rajoria, S., Vashishtha, M. and Sangal, V.K. 2021. Review on the treatment of electroplating industry wastewater by electrochemical methods. *Mater. Today: Proc.*, 47(9): 1472-1479.
- Rathna, R., Nakkeeran, E. and Varjani, S. 2019. Realistic Advancement in Engineered Osmosis for Water Treatment. In: *Water and Wastewater Treatment Technologies*. Singapore: Springer Singapore, 23(12): 187-207.
- Rodenburg, L.A., Hermanson, M.R. and Sumner, A.L. 2022. Effect of membrane filtration on the fate of polychlorinated biphenyls in wastewater treatment. *Chemosphere*, 287(Pt 3): 132335. DOI: 10.1016/j.chemosphere.2021.132335
- Rujia, Z. 2020. Improvement of Sedimentation - MBR for electroplating wastewater treatment. *China Resour. Compreh. Utiliz.*, 38(5): 202-204.
- Sabeen, A.H., Kamaruddin, S.N.B. and Noor, Z.Z. 2019. Environmental impacts assessment of industrial wastewater treatment system using electrodeless nickel plating and life cycle assessment approaches. *Int. J. Environ. Sci. Technol.*, 16(7): 3171-3182.
- Salgot, M. and Folch, M. 2018. Wastewater treatment and water reuse. *Curr. Opin. Environ. Sci. Health*, 2(8): 64-74.
- Samaei, S.M., Gato-Trinidad, S. and Altaee, A. 2018. The application of pressure-driven ceramic membrane technology for the treatment of industrial wastewaters - A review. *Sep. Purif. Technol.*, 200(15): 198-220.
- Sanmartino, J.A., Khayet, M., García-Payo, M.C., El-Bakouri, H. and Riaza, A. 2017. Treatment of reverse osmosis brine by direct contact membrane distillation: Chemical pretreatment approach. *Desalination*, 420(12): 79-90.
- Sari Erkan, H., Bakaraki Turan, N. and Önkal Engin, G. 2018. Membrane Bioreactors for Wastewater Treatment. Elsevier, The Netherlands,

pp.151-200.

- Scarazzato, T., Panossian, Z., Tenório, J.A.S., Pérez-Herranz, V. and Espinosa, D.C.R. 2017. A review of cleaner production in electroplating industries using electrodialysis. *J. Cleaner Prod.*, 168(15): 1590-1602.
- Senusi, F., Shahadat, M., Ismail, S. and Hamid, S.A. 2018. Recent Advancement in Membrane Technology for Water Purification. In: *Modern Age Environmental Problems and their Remediation*. Cham: Springer International Publishing, 45(9): 147-167.
- Shen, Y., Yang, D., Wu, Y., Zhang, H. and Zhang, X. 2019. Operation mode of a step-feed anoxic/oxic process with distribution of carbon source from anaerobic zone on nutrient removal and microbial properties. *Sci. Rep.*, 9(1): 1153.
- Silva, L.L.S., Sales, J.C.S., Campos, J.C., Bila, D.M. and Fonseca, F.V. 2017. Advanced oxidative processes and membrane separation for micropollutant removal from biotreated domestic wastewater. *Environ. Sci. Pollut. Res.*, 24(7): 6329-6338.
- Sm, A., Rps, A., Pkr, B. and Apd, A. 2022. Membrane bioreactor (MBR) as an advanced wastewater treatment technology for removal of synthetic microplastics. *Dev. Wastewater Treat. Res. Process.*, 4(22): 45-60.
- Sur, D.H. and Mukhopadhyay, M. 2018. Process parametric study for COD removal of electroplating industry effluent. *3 Biotech.*, 8(2): 84.
- Takuma, Y., Sugimori, H. ando, E., Mizumoto, K. and Tahara, K. 2018. Comparison of the environmental impact of the conventional nickel electroplating and the new nickel electroplating. *Int. J. Life Cycle Assess.*, 23(8): 1609-1623.
- Tan, X., Acquah, I., Liu, H., Li, W. and Tan, S. 2019. A critical review on saline wastewater treatment by membrane bioreactor (MBR) from a microbial perspective. *Chemosphere*, 220(3): 1150-1162.
- Tao, X., Hu, X., Wen, Z., Ming, Y., Li, J., Liu, Y. and Chen, R. 2022. Highly efficient Cr(VI) removal from industrial electroplating wastewater over Bi₂S₃ nanostructures prepared by dual sulfur-precursors: Insights on the promotion effect of sulfate ions. *J. Hazard. Mater.*, 424(12): 127423.
- Tezcan, U., Onpeker, S.E. and Ozel, E. 2017. The treatment of chromium containing wastewater using electrocoagulation and the production of ceramic pigments from the resulting sludge. *J. Environ. Manage.*, 200(3): 196-203.
- Thamaraiselvan, C., Michael, N. and Oren, Y. 2018. Selective Separation of Dyes and Brine Recovery from Textile Wastewater by Nanofiltration Membranes. *Chem. Eng. Technol.*, 41(2): 185-293.
- Totaro, M., Valentini, P., Casini, B., Miccoli, M., Costa, A.L. and Baggiani, A. 2017. Experimental comparison of point-of-use filters for drinking water ultrafiltration. *J. Hosp. Infect.*, 96(2): 172-176.
- Van der Bruggen, B. 2018. Chapter 2 - Microfiltration, ultrafiltration, nanofiltration, reverse osmosis, and forward osmosis. In: *Fundamental Modelling of Membrane Systems*, Elsevier, 4(12): 25-70.
- Wang, P. 2018. A brief analysis of the practical application of ultrafiltration membrane technology in water treatment projects. *Hunan Agricultural Machinery*, 45(6): 180-185.
- Wang, Y. and Wang, R. 2019. Reverse Osmosis Membrane Separation Technology. In: *Membrane Separation Principles and Applications*, Elsevier, The Netherlands.
- Wen, Q., Wang, Q., Li, X., Chen, Z., Tang, Y. and Zhang, C. 2018. Enhanced organics and Cu²⁺ removal in electroplating wastewater by bioaugmentation. *Chemosphere*, 212(8): 476-485.
- Xiong, W., Yang, M., Wang, J., Wang, H., Zhao, P., Li, Z., Liu, B., Kong, X., Duan, H. and Zhao, Y. 2023. Removal, recycle and reutilization of multiple heavy metal ions from electroplating wastewater using super-stable mineralizer Ca-based layered double hydroxides. *Chem. Eng. Sci.*, 23(3): 145-149.
- Ya, V., Guillou, E.L., Chen, Y., Yu, J., Choo, K., Chuang, S., Lee, S. and Li, C. 2018. Scrap iron packed in a Ti mesh cage as a sacrificial anode for electrochemical Cr(VI) reduction to treat electroplating wastewater. *J. Taiwan Inst. Chem. Eng.*, 87(9): 91-97.
- Yan, X., Zhu, C., Huang, B., Yan, Q. and Zhang, G. 2018. Enhanced nitrogen removal from electroplating tail wastewater through two-staged anoxic-oxic (A/O) process. *Bioresour. Technol.*, 247(7): 157-164.
- Zhang, Y., Bian, T., Zhang, Y., Zheng, X. and Li, Z. 2018. Chelation resin efficient removal of Cu(II), Cr(III), Ni(II) in electroplating wastewater. *Fullerenes, Nanotubes Carbon Nanostruct.*, 26(11): 765-776.
- Zhang, Y., Wei, S., Hu, Y. and Sun, S. 2018. Membrane technology in wastewater treatment enhanced by functional nanomaterials. *J. Cleaner Prod.*, 197(12): 339-348.
- Zhao, R., Zhou, Z., Zhao, X. and Jing, G. 2019. Enhanced Cr(VI) removal from simulated electroplating rinse wastewater by amino-functionalized vermiculite-supported nanoscale zero-valent iron. *Chemosphere*, 218(9): 458-467.
- Zhu, J., Jin, Q. and Dongming, L. 2018. Investigation of two integrated membrane systems for the reuse of electroplating wastewater. *Water Environ. J.*, 32(2): 267-275.
- Zsirai, T., Qiblawey, H., Buzatu, P., Al-Marri, M. and Judd, S.J. 2018. Cleaning of ceramic membranes for produced water filtration. *J. Pet. Sci. Eng.*, 166(15): 283-289.



Detection of Sulfur Oxidizing Bacteria to Oxidize Hydrogen Sulfide in Biogas from Pig Farm by NGS and DNA Microarray Technique

Siriorn Boonyawanich*, Peerada Prommeenate***, Sukunya Oaew***, Wantanasak Suksong****, Nipon Pisutpaisal**(**) and Saowaluck Haosagul**† 

*Department of Agro-Industrial, Food and Environment Technology, Faculty of Applied Science, King Mongkut's University of Technology North Bangkok, Bangkok, Thailand

**Biosensor and Bioelectronics Technology Centre, King Mongkut's University of Technology North Bangkok, Bangkok, 10800, Thailand

***Biochemical Engineering and System Biology Research Group, National Center for Genetic Engineering and Biotechnology, National Science and Technology Development Agency at King Mongkut's University of Technology Thonburi, Bang Khun Thian, Bangkok, 10150, Thailand

****School of Bioresources and Technology, King Mongkut's University of Technology Thonburi, Bangkok 10150, Thailand.

†Corresponding author: Saowaluck Haosagul; h_saowaluck@hotmail.com

Nat. Env. & Poll. Tech.
Website: www.neptjournal.com

Received: 07-08-2023

Revised: 30-09-2023

Accepted: 10-10-2023

Key Words:

Hydrogen sulphide
Biogas
Sulfur oxidizing bacteria
Pig farm
Microarray

ABSTRACT

A high concentration of hydrogen sulfide (H₂S) released from pig farming is one of the major environmental problems affecting surrounding communities. In modern pig farms, the bioscrubber is used to eliminate H₂S, which is found to be driven mainly by the sulfur-oxidizing bacteria (SOB) community. Therefore, in this study, molecular biology techniques such as next-generation sequencing (NGS) and DNA microarray are proposed to study the linkage between enzyme activity and the abundance of the SOB community. The starting sludge (SFP1) and recirculating sludge (SFP2) samples were collected from the bioscrubber reactor in the pig farm. The abundance of microbial populations between the two sampling sites was considered together with the gene expression results of both *soxABXYZ* and *fccAB*. Based on the NGS analysis, the members of phylum Proteobacteria such as *Halothiobacillus*, *Acidithiobacillus*, *Thiothrix*, *Novosphingobium*, *Sulfuricurvum*, *Sulfurovum*, *Sulfurimonas*, *Acinetobacter*, *Thiobacillus*, *Magnetospirillum*, *Arcobacter*, and *Paracoccus* were predominantly found in SFP2. The presence of Cyanobacteria in SFP pig farms is associated with increased biogas yields. The microarray results showed that the expression of *soxAXBYZ* and *fccAB* genes involved in the oxidation of sulfide to sulfate was increased in *Halothiobacillus*, *Paracoccus*, *Acidithiobacillus*, *Magnetospirillum*, *Sphingobium*, *Thiobacillus*, *Sulfuricurvum*, *Sulfuricurvum*, *Arcobacter*, and *Thiothrix*. Both NGS and DNA microarray data supported the functional roles of SOB in odor elimination and the oxidation of H₂S through the function of *soxABXYZ* and *fccAB*. The results also identified the key microbes for H₂S odor treatment, which can be utilized to monitor the stability of biological treatment systems and the toxicity of sulfide minerals by oxidation.

INTRODUCTION

Next Generation Sequencing (NGS) is a nucleotide sequencing technology used to study the genetic variation associated with microbial traits using the highly variable regions within the conserved regions of 16S rRNA-encoded genes to identify phylogenetic relationships among prokaryotes (Gupta et al. 2019). NGS is a rapidly advancing technology that provides high throughput sequencing data, which can be further analyzed for sample identity (Besser et al. 2018). NGS can be applied in many research areas,

including epigenetics, genetic variation discovery, genetic diversity, population validation, microbial community, and gene expression level. This technique is currently used for studying the microbial community structure and function of genes in environmental samples (Roh et al. 2010). DNA microarray also uses genome sequence information to analyze the structure and function of thousands of genes at a time. The microarray technique relies on hybridization between DNA targets and probes, which are specific to each position on the genome or chromosome. Microarray holds DNA probes that recognize other ssDNA from tested

samples. DNA microarray has been successfully applied to analyze functional microbial communities in various conditions (Roh et al. 2010) and monitor the function and cohabitation of hundreds to thousands of microbial populations at the same time.

DNA microarrays and NGS technologies are now being applied in microbial ecology studies as tools for the advanced understanding of the role of microorganisms in various environments (Roh et al. 2010). Microarrays for microbial detection can be divided into four different types: functional gene arrays (FGAs), community genome arrays (CGAs), phylogenetic oligonucleotide arrays (POAs), and metagenomics arrays (MGA), based on represented gene type on the array (Gentry & Zhou 2006). CGA arrays from the whole genomic DNA of 12 pure culture species were successfully used to detect and identify species of bacteria in acid mine drainage and bioleaching systems (Chen et al. 2009). The relative abundance of marine sediments involved in the nitrogen cycle genes (*amoA*, *nirS*, and *nirK*) was also analyzed by FGAs arrays (Wu et al. 2001). The *soxB*, *sqr*, and *dsrA* genes were used to classify the abundance and diversity of sulfur-oxidizing bacteria in the Pearl River water. *Dechloromonas*, *Limnohabitans*, *Paracoccus*, *Sulfuritalea*, *Sulfitobacter*, and *Thiobacillus* are the dominant SOB for *soxB* (Luo et al. 2018). The diversity and distribution of *fccAB* and *soxXYZB* genes related to sulfur oxidation in 75 strains of *Thioalkalivibrio*, a group of haloalkaliphilic and chemolithoautotrophic SOB from soda lakes, were reported by Berben et al. (2019). *Paracoccus Versutus CMI* was identified by the *soxB* gene for H₂S removal efficiency up to 100% from biogas in the laboratory-scale system (Jirachaisakdeacha et al. 2020). Haosagul et al. (2021) designed a hybrid microarray covering both the whole genome sequences and specific gene regions (*soxAXBYZ* and *fccAB*) to identify the activity of sulfur-oxidizing bacterial strains that oxidize H₂S in biogas. However, the diversity of microbes is also changed according to time and environmental conditions. Thus, the combined study using microarray data and 16S rRNA analysis will provide comprehensive data for the role of microorganisms in their various environments. This research aims to study the functional role of SOB via the linkage between enzyme activity and the abundance of SOB in the bioscrubber system for treating H₂S in the biogas of pig farms using NGS and microarray techniques.

MATERIALS AND METHODS

Microbial Samples

Fresh pig manure was used as the starting sludge in wastewater treatment systems to produce biogas on the SFP farm. The treatment sludge will then be fed into

the bioscrubber as a substrate for SOB. The inlet H₂S concentration was 2,365±152 ppm, and the outlet H₂S was 20±5 ppm. This average concentration was measured in real time by a GFM416 biogas analyzer (Gas Data, England). The starting sludge (SFP1) was immobilized on the biofilter media in the form of biofilms to absorb dissolved hydrogen sulfide gas and cell survival. Water consisting of essential nutrients (pH 7) was constantly sprayed from top to bottom of the bioscrubber to maintain moisture for SOB in the system coupled with approximately 1.5±0.5% (v/v) in opposite directions of aeration. The biotreatment system has been operated until the H₂S removal efficiency is stable at 99%, which indicates the presence of product accumulations in the form of sulfate or sulfur. However, some loose sludge from the biofilm layer could be suspended along with the recirculating water in the system and settled at the bottom of the bioscrubber tank. Therefore, the settled sludge samples were collected as recirculating sludge (SFP2) for analysis of both functional genes and diversity of bacteria in comparison with the SFP1 sampling point. Both SFP1 and SFP2 sludge samples were transferred to clean tubes and centrifuged at 14,000 g (MX-301, Japan) for 15 min and stored in the freezer at -20°C before the genomic DNA extraction.

Genomic DNA Extraction for NGS Analysis

The starting sludge (SFP1) and recirculating sludge (SFP2) were defrosted at room temperature before use. SFP1 and SFP2 sludge were lysed in DNA extraction buffer and lysozyme (10 mg.L⁻¹) at a ratio of 1:1, followed by shaking at 180 rpm at 37°C for 60 min. Next, the other DNA binding proteins were released by adding 100 µL sodium dodecyl sulfate and incubated at 65°C for 30 min. DNA was precipitated with isopropanol (0.6 volume) and rinsed with ice-cold ethanol. Then, the DNA pellet was dissolved in the elution buffer, as described in Haosagul et al. (2020). The quality of gDNA was measured by NanoDrop™ 1000 Spectrophotometer (Thermo Scientific). The gDNA was prepared for NGS analysis based on the Illumina HiSeq 2500 platform according to the company's instruction using the specific primer named 515F-806R that targeted to V4 region of the 16S rRNA gene. The PCR amplification steps were described in Haosagul et al. (2021).

Microbial Community Study Using 16S rRNA Sequencing

The DNA extracts from SFP1 and SFP2 sludge were prepared into a library that could be processed in an Illumina HiSeq 2500 sequencing platform. In brief, the 16S rRNA gene segments for the PCR process were amplified using a primer set of 515F 5'-GTGCCAGCMGCCGCGGTAA-3'

and 806R 5'-GGACTACHVHHHTWTCTAAT-3' for targeting the V4 hypervariable regions. The data analysis was conducted with QIIME2 (v.2020.8). Pair-end reads obtained from the HiSeq 2500 sequencing platform were merged, filtered, and quality-controlled to gain the clean sequences with the QIIME2-DADA2 plugin. The clean sequences were clustered into the amplicon sequence variant (ASV) table at the 97% similarity level (Bolyen et al. 2019). Phylogenetic taxonomy assignment was achieved using the Silva database version 138 classifier. PICRUSt2 (Phylogenetic investigation of communities by reconstruction of unobserved states) was utilized to predict the potential function of microbial communities via marker gene sequencing profiles. PICRUSt2 analysis was applied to predict the potential Kyoto Encyclopedia of Genes and Genomes (KEGG) metabolic pathways by 16S rRNA data (Douglas et al. 2020).

Microarray Construction and Probe Designed

In brief, for probe design, a comparative genomic hybridization (CGH) microarray consisting of 61,788 probes was prepared on a glass slide. Each spot was a synthetic oligonucleotide of 60 bp/probe, which covered a list of SOB genera (42,248 probes) and other genera (NSOB) that were detected on SFP1 and SFP2 samples of bioscrubber from SFP pig farm by NGS technique. The genome sequences and genes related to sulfide oxidation (*soxAXBYZ* and *fccAB*) of each SOB species were obtained from the National Center for Biotechnology Information (NCBI) database and the Pathosystems Resource Integration Center (PATRIC) database for microarray probe design, according to the manufacturer instruction (Agilent Technologies 2019).

DNA Preparation for CGH Microarray

Fresh sludge from two sampling sites (SFP1 and SFP2) of bioscrubber from the SFP pig farm was collected and centrifugation at 10,000 g (MX-301, Japan) for 10 min. Total genomic DNAs (gDNA) from fresh sludge were extracted from the sludge pellet using a sodium dodecyl sulfate (SDS)-based DNA extraction method (Haosagul et al. 2020). Then, 20–40 µl of RNase A (10 mg/ml) was added and incubated at 37°C for one hour, followed by incubation at 65°C for 40 min. The GenepHlow™ Gel/PCR Kits purified the gDNA samples. The DNA intactness and molecular weight for each sample were checked using 0.8% (w/v) agarose gel electrophoresis. NanoDrop 2000 UV-VIS Spectrophotometer was primarily applied to measure the purity of gDNA at A_{260}/A_{280} and A_{260}/A_{230} . The values of A_{260}/A_{280} and A_{260}/A_{230} of purified gDNA should be ≥ 1.8 and ≥ 1.0 , respectively. A Qubit dsDNA BR Assay Kit then assayed the extracted dsDNA sample. The calculation of yield and dsDNA

concentration were calculated according to Eq. 1 and Eq. 2 (Agilent Technologies 2019).

$$\text{dsDNA concentration} = \text{QF value} \times (200/\text{y}) \quad \dots(1)$$

where,

QF value = the value given by the Qubit Fluorometer

y = the volume of the sample added to the assay tube.

Yield (µg) =

$$\frac{\text{gDNA concentration (ng/}\mu\text{L)} \times \text{sample volume (}\mu\text{L)}}{1000 \text{ ng/}\mu\text{g}} \quad \dots(2)$$

The gDNA with good quality was applied further for the gDNA labeling step. In brief, gDNA was purified using the reaction purification column provided by the SureTag Complete DNA Labeling Kit and SureTag DNA Labeling Kit. The DNA Labeling Kit contained Cyanine3 (Cy3) and Cyanine5 (Cy5) dyes that were used to label recirculating sludge (SFP2) and starting sludge (SFP1), respectively. The specific activity was calculated according to Eq. 3 (Agilent Technologies 2019).

$$\text{Specific Activity (pmol dyes/}\mu\text{g gDNA)} = \frac{\text{pmol per } \mu\text{L of dye}}{\mu\text{g per } \mu\text{L gDNA}} \quad \dots(3)$$

Hybridization of labeled DNA fragments from both samples (SFP1 and SFP2) and probes were performed on the CGH microarray slide for 24 hr at 65°C with agitation at 20 rpm in an Agilent hybridization oven. Unbound DNA was washed off with buffer 1 for 5 min at room temperature and washed once with buffer 2 for 1 min at 37°C. The microarray slide was analyzed for the signal intensity of each spot by the Agilent High-Resolution Microarray Scanner (C-model). The signal intensity of 61,278 probes was calculated into log₂ ratios of SFP2/SFP1. QC metrics from the microarray set, such as background noise, signal intensity, signal-to-noise, reproducibility, and DLRS (Derivative Log₂ Ratio Standard Deviation), are criteria for signal quality analysis and indicate processing errors.

RESULTS AND DISCUSSION

Quantity and Quality of gDNA

The gDNA of starting sludge (SFP1) and recirculating sludge (SFP2) from the SFP pig farm was successfully extracted. Double-stranded DNA concentrations of SFP1 and SFP2 were found in the range of 44–418 ng/µl. SFP samples had the A_{260}/A_{280} ratio of ≥ 1.8 and the A_{260}/A_{230} ratio of ≥ 1.0 (Table 1). These results confirmed the quality and quantity of both samples before they were submitted to 16S rRNA sequencing using the Illumina HiSeq 2500 platform in the next step.

Table 1: Double-stranded DNA concentration.

No.	Sample Name	Description	A_{260}/A_{280}	A_{260}/A_{230}	Qubit Concentration
1	SFP1	Starting sludge-Pig farm	1.76	1.21	418.0
2	SFP2	Recirculating sludge-Pig farm	1.92	1.95	43.6

Microbial Community of SOB Detected by NGS Analysis

The abundance of microbial community was analyzed from the 16S rRNA sequencing (based on the V4 region). A total of 28 phyla were classified from the starting sludge (SFP1) and recirculating sludge (SFP2) of a full-scale bioscrubber from SFP farms. The top three most abundant phyla detected in the SFP farm were Proteobacteria, Cyanobacteria, and Actinobacteria. The community structure of these three species was markedly changed according to H_2S eradication between SFP1 and SFP2. Before the elimination of H_2S (SFP1), Cyanobacteria, Actinobacteria, and Proteobacteria were among the top 3 most abundant phyla, with a relative abundance of 25.56%, 25.46%, and 25.33%, respectively. During the H_2S removal, the community structure changed dramatically. Proteobacteria replaced Actinobacteria with 12.95% relative abundance, which accounted for 39.79% of the total relative abundance in SFP2 (Fig. 1A). The relative abundance of Cyanobacteria was observed to be stable between

the SFP1 (25.56%) and SFP2 (25.87%). Cyanobacteria have been found in the wastewater treatment of pig farms, biogas slurry, and bioenergy production (Lu et al. 2020, Stewart et al. 2011). Especially *Synechococcus elongatus*, which can increase intracellular sucrose accumulation, leading to increased yields of both biohydrogen and biomethane (Vayenos et al. 2020, Samiotis et al. 2021). The presence of cyanobacteria in both collecting points indicated their function in the wastewater treatment of pig manure. In the class level, Betaproteobacteria (13.69-26.08%), unidentified Cyanobacteria (25.31-25.52%), and Gammaproteobacteria (3.91-6.22%) were three dominant members within phylum Proteobacteria and Cyanobacteria (Fig. 1B), which increased more than 50% of the relative abundance when collected as SFP1 to SFP2. At the order level, Burkholderiales (21.53%) has increased over 45% of the total relative abundance in SFP2 samples (Fig. 1C). Meanwhile, Thiotrichales (185-fold) was fast-growing and increasing inside the bioscrubber tank (SFP2) when compared to the starter point (SFP1). These members have been shown to play an important role

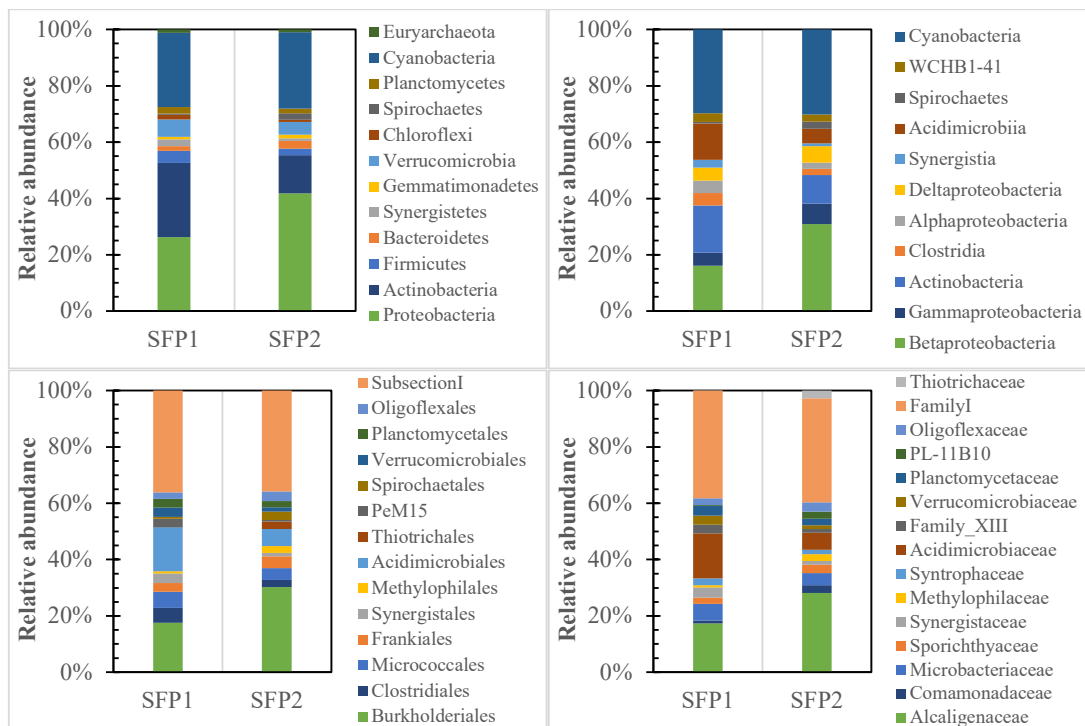


Fig. 1: Phylum (A), class (B), order (C), and family (D) levels showed the microbial dynamics during the starting sludge (SFP1) and recirculating sludge (SFP2) collected from a bioscrubber in the pig farm.

Table 2: Microbial diversity and gene expression related to eliminating H₂S in biogas.

Genus	SFP1 (%)	SFP2 (%)	Growth (%)	<i>soxABXYZ</i>	<i>fccAB</i>	Classified
<i>Novosphingobium</i>	0.315	0.344	0.030	D	ND	SOB
<i>Gemmatimonas</i>	0.289	0.493	0.204	D	ND	SOB
<i>Sphingobium</i>	0.027	0.032	0.006	D	D	SOB
<i>Acinetobacter</i>	0.018	0.060	0.042	D	ND	SOB
<i>Sulfurovum</i>	0.016	0.063	0.047	ND	D	SOB
<i>Sulfurimonas</i>	0.010	0.056	0.046	D	D	SOB
<i>Syntrophomonas</i>	0.010	0.018	0.008	ND	D	SOB
<i>Sulfuricurvum</i>	0.009	0.336	0.327	D	D	SOB
<i>Thiothrix</i>	0.007	1.853	1.846	D	D	SOB
<i>Arcobacter</i>	0.002	0.020	0.018	D	D	SOB
<i>Paracoccus</i>	0.002	0.005	0.003	D	D	SOB
<i>Acidithiobacillus</i>	0.001	0.498	0.497	D	D	SOB
<i>Halothiobacillus</i>	0.001	0.015	0.014	ND	D	SOB
<i>Magnetospirillum</i>	0.000	0.017	0.017	D	D	SOB
<i>Thiobacillus</i>	0.000	0.009	0.009	D	D	SOB
<i>Synechococcus</i>	20.953	23.248	2.295	ND	ND	NSOB
<i>MWH-UniP1_aquatic_group</i>	10.008	18.791	8.782	ND	ND	NSOB
<i>CL500-29_marine_group</i>	9.734	3.502	-6.232	ND	ND	NSOB
<i>Candidatus_Aquiluna</i>	1.670	2.068	0.398	ND	ND	NSOB
<i>Alsobacter</i>	1.093	0.150	-0.943	ND	ND	NSOB
<i>Desulfomonile</i>	0.977	0.261	-0.716	ND	ND	NSOB
<i>Ilumatobacter</i>	0.822	0.684	-0.138	ND	ND	NSOB
<i>Acidibacter</i>	0.806	1.312	0.505	ND	ND	NSOB
<i>Thiolamprobum</i>	0.718	0.523	-0.195	ND	ND	NSOB
<i>Rhodopirellula</i>	0.706	0.361	-0.345	ND	ND	NSOB
<i>Aeromicrobium</i>	0.668	0.730	0.062	ND	ND	NSOB
<i>Pirellula</i>	0.612	0.221	-0.390	ND	ND	NSOB
<i>Methanospirillum</i>	0.563	0.521	-0.042	ND	ND	NSOB
<i>Syntrophus</i>	0.421	0.108	-0.313	ND	ND	NSOB
<i>Methanosaeta</i>	0.403	0.129	-0.274	ND	ND	NSOB
<i>Roseiflexus</i>	0.280	0.262	-0.018	ND	ND	NSOB
<i>Dinghuibacter</i>	0.255	0.194	-0.061	ND	ND	NSOB
<i>Syntrophorhabdus</i>	0.198	0.518	0.320	ND	ND	NSOB
<i>Alpinimonas</i>	0.197	0.193	-0.005	ND	ND	NSOB
<i>Aminivibrio</i>	0.175	0.113	-0.063	ND	ND	NSOB
<i>Ignavibacterium</i>	0.172	0.507	0.335	ND	ND	NSOB
<i>Peredibacter</i>	0.125	0.270	0.145	ND	ND	NSOB
<i>Smithella</i>	0.122	0.393	0.271	ND	ND	NSOB
<i>vadinBC27_wastewater-sludge_group</i>	0.121	0.303	0.182	ND	ND	NSOB
<i>Hydrogenophaga</i>	0.108	0.462	0.354	ND	D	NSOB
<i>Luteolibacter</i>	0.071	0.211	0.140	ND	ND	NSOB
<i>Opitutus</i>	0.062	0.176	0.114	ND	ND	NSOB
<i>Ferrovibrio</i>	0.059	0.217	0.158	ND	ND	NSOB
<i>Mesotoga</i>	0.019	0.058	0.039	ND	ND	NSOB
<i>Sphaerochaeta</i>	0.014	0.053	0.039	ND	ND	NSOB

D=Detected, ND=Not Detected, % represent the signal intensity of the sulfide oxidation gene of the SOB genus.

in the degradation of H₂S in biogas from pig farms (Dubinina et al. 2011, Xu et al. 2020, Xu et al. 2021). On the other hand, the relative abundance of CL500-29 marine group bacteria, which belonged to the family Acidimicrobiaceae, was found to be decreasing. In contrast, the representatives of the family Alcaligenaceae, FamilyI, Thiotrichaceae, and Comamonadaceae were increased in the bioscrubber tank (Fig. 1D). These results strongly support functional roles in the oxidation of H₂S of FamilyI, Comamonadaceae, and Alcaligenaceae as discussed in the previous study (Kerstens et al. 2006, Wang et al. 2018, Li et al. 2020, Flood et al. 2021). These members were found to be predominant in the pig gut microbiota. More details on functional pig gut microbiota were reported by Wylensek et al. (2020). The member of Proteobacteria and Cyanobacteria (e.g., *Thiothrix*, *Synechococcus*, *Sulfuricurvum*) plays an important role in the elimination of H₂S, which was increased when H₂S decreased (Table 2).

At the genus level, a total of 45 genera were revealed, with a relative abundance of $\geq 0.015\%$. The coexistence genera in the bioscrubber tank of the SFP pig farm is shown in Table 2. The bacterial communities of *Synechococcus*, *MWH-UniP1_aquatic_group*, *CL500-29_marine_group*, *Thiothrix*, and *Sulfuricurvum* were mainly detected in both SFP1 and SFP2. However, the differences in the relative abundance between the two collecting points might be related to cell multiplication and gene expression associated with sulfide treatment (Stewart et al. 2011, Dong et al. 2017). In particular, the genera *Thiothrix*, *Sulfuricurvum*, and *Acidithiobacillus* in SFP2 revealed the expression of 16S rRNA genes, sulfur oxidation gene (*soxAXBYZ*), and flavocytochrome c sulfide dehydrogenase (*fccAB*) genes during H₂S removal (Friedrich et al. 2005, Hong et al. 2013, Dong et al. 2017) which also correlated with the relative abundance in the sample.

Functional Gene Predicted by PICRUSt2 and Correlation with Microbial Community

Functional gene prediction was performed using PICRUSt2 based on 16S rRNA data of SFP1 and SFP2. In total, 7,429 genes of SFP1 and SFP2 were assigned to 434 functional KEGG pathways. All genes were mapped to different KEGG pathways. Only the functional genes/pathways involved in sulfide oxidizing bacteria were focused on in this study. The functional gene prediction revealed the metabolism of sulfide oxidizing bacteria, which is involved in the super pathway of sulfate-sulfur assimilation, cysteine biosynthesis, sulfate reduction I (assimilatory), and sulfur oxidation (*Acidianus ambivalens*) with gene abundance of 0.50%, 0.44%, and 0.07% in SFP1, respectively, and 0.47%, 0.40%, and 0.13% in SFP2, respectively. Several numbers of predicted genes

were assigned to several KEGG categories that related to protein degradation (reduction of sulfate to H₂S). Based on the presented gene involved in the sulfate assimilation reduction pathway (SO₄⁻²), which incorporates sulfur to amino acids and the sulfide (S²⁻) assimilation to remove sulfur from biogas (Treu et al. 2018), it can be hypothesized that the microbial community of SFP1 and SFP2 has the potential ability in chemotrophic desulfurization.

The metabolic pathways involved in organic sulfur metabolism shown in Fig. 2 might play an important role in the bioscrubber system. The sulfide oxidizing bacteria have complex sulfur metabolism for the oxidizing and/or reducing sulfurs of various oxidation states. Flavocytochrome c sulfide dehydrogenase (*fccAB*) is one of the central enzymes in the respiratory chain of sulfur-oxidizing bacteria. This enzyme catalyzes the oxidation of sulfide and polysulfide ions to molecular sulfur, together with electron transfer to cytochrome c (Tikhonova et al. 2021). In this study, the predicted gene abundance of flavocytochrome c sulfide dehydrogenase (*fccB*) [EC:1.8.2.3] was increased from 0.01% in SFP1 to 0.02% in SFP2, which corresponded to an increase of sulfide oxidizing bacteria in Class Betaproteobacteria (0.261%) and Gammaproteobacteria (0.062%) of SFP2. Grim et al. (2021) also found that genes encoding for sulfide oxidation via flavocytochrome c sulfide dehydrogenase (*fcc*) were observed in both Betaproteobacteria and Gammaproteobacteria. Additionally, genes for chemolithotrophic thiosulfate oxidation via the Sox pathway (Lu-Kelly–Friedrich pathway) were observed in this study. Thiosulfate is directly oxidized to sulfate without forming any free intermediate. A complex multienzyme system involved in the complete oxidation of thiosulfate composed of *soxA*; L-cysteine S-thiosulfotransferase [EC:2.8.5.2], *soxX*; L-cysteine S-thiosulfotransferase [EC:2.8.5.2], *soxY*; sulfur-oxidizing protein, *soxZ*; sulfur-oxidizing protein and *soxB*; S-sulfosulfanyl-L-cysteine sulfohydrolase [EC:3.1.6.20] (Alam et al. 2021). In SFP2, gene abundances for *soxA*, *soxX*, *soxY*, *soxZ*, and *soxB* were 0.02%, 0.019%, 0.025%, 0.021%, and 0.019%, respectively, and 0.01%, 0.01%, 0.014%, 0.012% and 0.01%, respectively, for SFP1. Increasing Sox gene abundances in SFP2 support the assumption that the Sox gene was presented in chemotrophic species that form sulfur globules during thiosulfate oxidation (*Thiothrix*, *Beggiatoa*, and *Thiobacillus*) (Meyer et al. 2007). The relative abundances of *Thiothrix* (1.85%), *Acidithiobacillus* (0.49%), and *Thiobacillus* (0.009%) suggest that sulfur-oxidizing bacteria were dominant in SFP2 over SFP1. The presence of these SOBs in the SFP2 microbial community could be related to high activity in bioscrubber, which was also reported by Tilahun et al. (2018) and Alinezhad et al. (2019). The

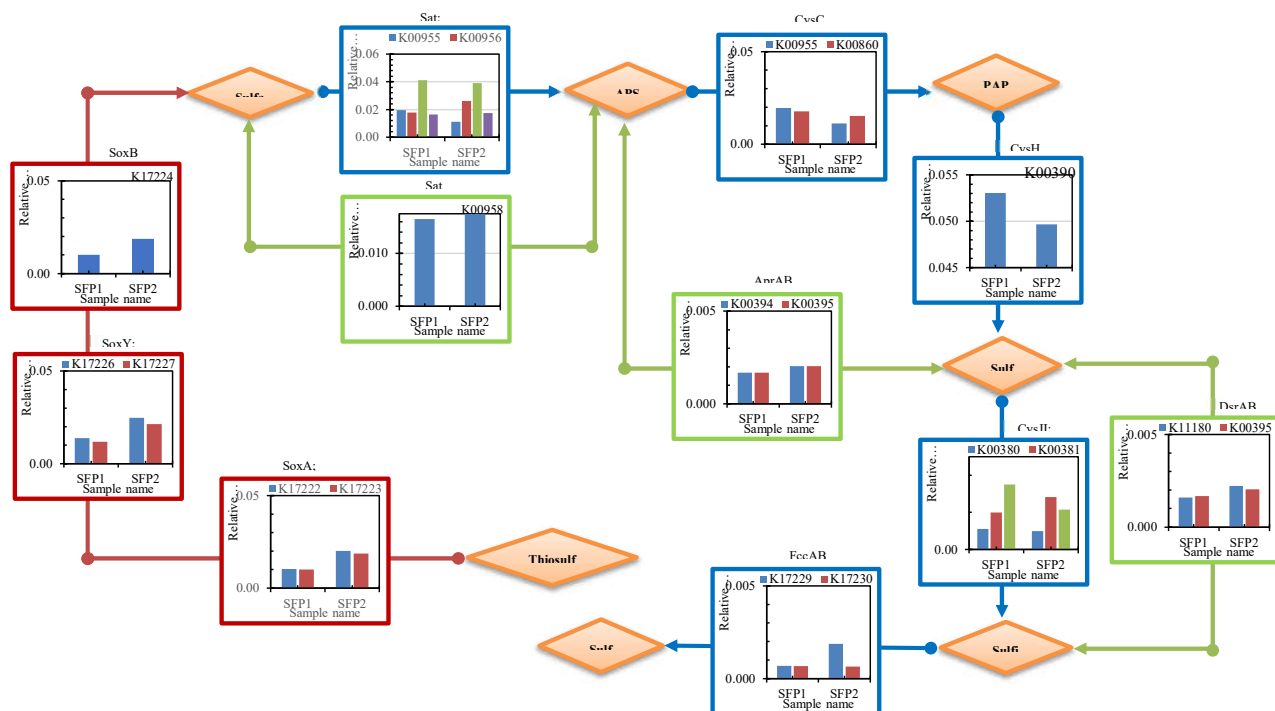
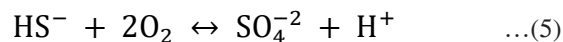
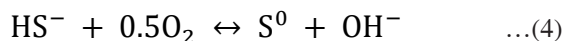


Fig. 2: Metabolic pathways of organic sulfur compounds play an important role in the bioscrubber. The assimilatory pathway [MD: M00176] (blue arrows), dissimilatory pathway [MD: M00596] (green arrows), and sulfur oxidation pathway [MD: M00595] (red arrows) were plotted with K number of microbial communities detected on starting sludge (SFP1) and recirculating sludge (SFP2).

reaction of H_2S oxidation occurring in SOB was shown in Eq. 4 and Eq. 5 (Tilahun et al. 2018). However, the route of H_2S oxidation depended on oxygen concentration, i.e., oxidation to elemental sulfur (S^0) or sulfate occurred under oxygen-limiting and non-limiting conditions, respectively.



Abundance of SOB Detected on DNA Microarray

In this study, DNA microarrays containing a total of 61,278 probes for specific genes that drive the process of sulfide oxidation by the SOB community have successfully been constructed. The abundance of sulfur-oxidizing bacteria (SOB) was detected in both starting sludge (SFP1) and recirculating sludge (SFP2), as shown in Fig. 3. The main sulfide oxidizing bacteria in the SFP2 belonged to the phyla Proteobacteria (23.95%) and Cyanobacteria (23.25%) (Fig. 3A), while the dominant phyla in SFP1 was a member of Euryarchaeota (0.40%) (Fig. 3B). Proteobacteria was previously reported as the main phylum with H_2S eliminating the potential for biogas production. This phylum is composed of various genera such as *Acidithiobacillus*, *Thiothrix*, *Novosphingobium*, *Sulfurovum*, *Acinetobacter*, *Thiobacillus*,

Magnetospirillum, and *Arcobacter* (Kodama et al. 2004, Hong et al. 2013, Haosagul et al. 2020). The three most abundant phyla detected by the NGS technique (Proteobacteria, Cyanobacteria, and Actinobacteria) had slightly different SOB communities compared to the DNA microarray technique. Probes specific for Proteobacteria and Cyanobacteria on the microarray were more prominent and diverse at the genus level than the NGS analysis technique. Moreover, the members of the genus belonging to phylum Actinobacteria and Euryarchaeota were detected in both techniques. Still, they did not play a key role in H_2S elimination due to only the 16S rRNA gene was expressed (Narihiro et al. 2008).

The top 40 strains of sulfur-oxidizing bacteria based on different protein expressions of sulfide oxidation between SFP1 and SFP2 are shown in Table 3. SOB communities in SFP2 were dominated by *Halothiobacillus hydrothermalis* strain DSM 7121, *Paracoccus denitrificans* JCM 21484, *Paracoccus alkenifer* strain DSM 11593, *Paracoccus pantotrophus* J40, *Paracoccus versutus* DSM 582, *Acidithiobacillus* sp. SH, *Halothiobacillus* sp. 39-53-45, *Magnetospirillum magnetotacticum* MS-1. The expression of the sulfur oxidation gene (*soxAXBYZ*) that oxidized thiosulfate to sulfate [EC:2.8.5.2; EC:3.1.6.20] had been increased in these genera.

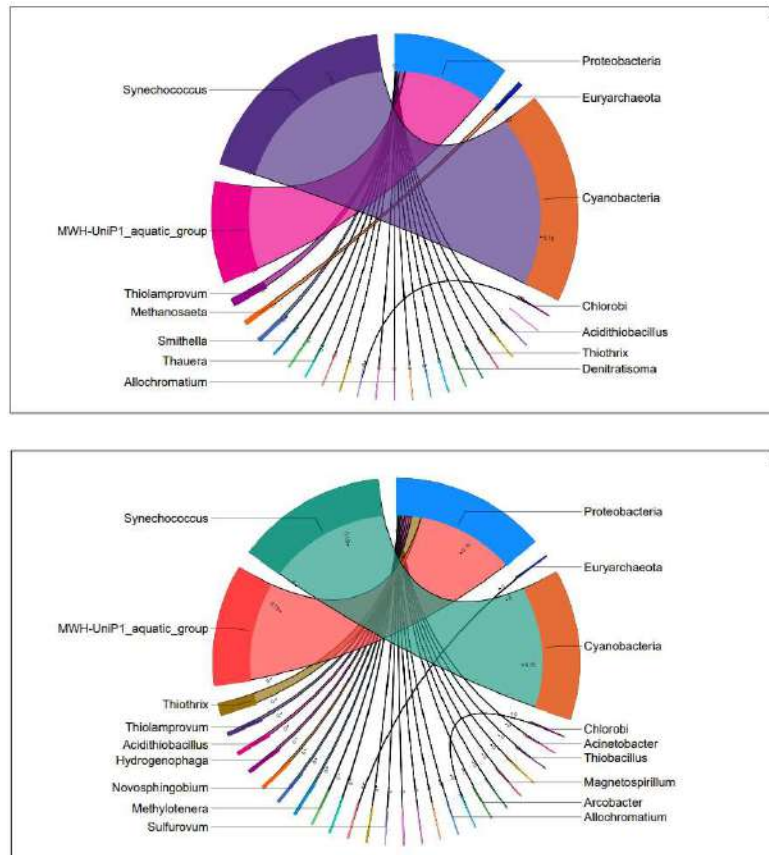


Fig. 3: Relative abundance of sulfur-oxidizing bacteria of starting sludge (SFP1) (A) and recirculating sludge (SFP2) (B) fed into bioscrubber, which was detected on a DNA microarray.

In addition, the dominant strains including *Sphingobium japonicum* UT26S, *Thiobacillus denitrificans* strain UBA4768, *Paracoccus* sp. UBA3880, *Thiobacillus denitrificans* strain UBA4768, *Sulfuricurvum* sp. UBA5598, *Sulfuricurvum* sp. MLSB, *Arcobacter cryaerophilus* strain LMG 10229, *Hydrogenophaga flava* NBRC 102514, *Paracoccus denitrificans* strain DSM 413, and *Thiothrix lacustris* strain A8; have sulfide oxidation genes (*fccAB*) [EC:1.8.2.3] for *in vitro* oxidation of H_2S with cytochrome c molecules as electron acceptors (Zhou et al. 2015). The final product of sulfide oxidation is elemental sulfur (Gregersen et al. 2011, Zhou et al. 2015). Moreover, non-sulfur oxidizing bacteria (NSOB) like *Sphaerochaeta pleomorpha* str. grapes and *Mesotoga prima* MesG1.Ag.4.2 were also increased in SFP2. Although *Sphaerochaeta pleomorpha* cannot use thiosulfate or sulfide, it reduces Fe^{3+} to Fe^{2+} in the glucose-supplemented medium (Ritalahti et al. 2012). On the other hand, *Mesotoga* was associated with high COD removal efficiency and high CH_4 yield. This genus was one of the significant members of waste sludge (Shin et al. 2019). For these reasons, both types of

NSOBs were presented as the SOB strains under the same condition.

CONCLUSIONS

This research has successfully identified sulfur-oxidizing bacteria (SOB) communities that play an important role in the biological elimination of H_2S (~2,300 ppm) in biogas production of the pig farm based on NGS and microarray techniques. The members of phyla Proteobacteria and Cyanobacteria including *Acidithiobacillus*, *Thiothrix*, *Novosphingobium*, *Sulfuricurvum*, *Sulfurovum*, *Sulfurimonas*, *Acinetobacter*, *Thiobacillus*, *Magnetospirillum*, *Arcobacter*, *Paracoccus*, and *Synechococcus* were all shown to express the H_2S functional involvement of SOB in odor removal and H_2S oxidation via *soxABXYZ* and *fccAB*. These findings not only uncovered the crucial microorganisms for H_2S odor treatment but may also be used to track the reliability of biological treatment systems and the toxicity of sulfide minerals through oxidation. Moreover, the key microbes in this study can be further applied for biogas quality improvement by H_2S reduction in the future.

Table 3: Microarray expression results showed the abundance of SOB species based on sulfide oxidation protein.

Genome ID	Genome Name	Avg. Log 2 Ratio (Cy3/Cy5)	Protein Expression				SOB/NSOB
			SFP2.SFP1	SoxXA	SoxYZ	SoxB	
AFRZ01000001.1	<i>Sulfurimonas gotlandica</i> GD1	-0.1973	D	D	D	D	SOB
AJ294325.1	<i>Halothiobacillus hydrothermalis</i> strain DSM 7121	0.6745	ND	ND	D	ND	SOB
AJ294332.1	<i>Halothiobacillus neapolitanus</i> strain DSM 581T	-0.2024	ND	ND	D	ND	SOB
AP010803.1	<i>Sphingobium japonicum</i> UT26S	0.1509	ND	ND	ND	D	SOB
BBFH01000969.1	<i>Paracoccus denitrificans</i> JCM 21484	0.5292	D	D	D	ND	SOB
CP003155.1	<i>Sphaerochaeta pleomorpha</i> str. Grapes	0.8403	ND	ND	ND	ND	NSOB
CP003532.1	<i>Mesotoga prima</i> MesG1.Ag.4.2	2.1989	ND	ND	ND	ND	NSOB
DCWD01000005.1	<i>Thiobacillus denitrificans</i> strain UBA2171	0.5991	ND	ND	ND	D	SOB
DGGG01000247.1	<i>Paracoccus</i> sp. UBA3880	0.5394	ND	ND	ND	D	SOB
DHHQ01000013.1	<i>Thiobacillus denitrificans</i> strain UBA4768	0.6037	ND	ND	ND	D	SOB
DILG01000074.1	<i>Sulfuricurvum</i> sp. UBA5598	0.1277	ND	ND	ND	D	SOB
FNXG01000003.1	<i>Paracoccus alkenifer</i> strain DSM 11593	0.8909	ND	D	ND	ND	SOB
JAEM01000011.1	<i>Paracoccus pantotrophus</i> J46	0.6060	ND	D	ND	ND	SOB
JAGK01000007.1	<i>Paracoccus pantotrophus</i> J40	0.6208	ND	D	ND	ND	SOB
JQGL01000140.1	<i>Sulfuricurvum</i> sp. MLSB	0.2709	ND	ND	ND	D	SOB
JRKO01000033.1	<i>Paracoccus versutus</i> DSM 582	0.5789	ND	D	ND	ND	SOB
LNTC01000035.1	<i>Arcobacter cryaerophilus</i> strain AZT-1	-0.5250	ND	ND	ND	D	SOB
LRUS01000073.1	<i>Arcobacter cryaerophilus</i> strain L399	-0.4044	ND	ND	ND	D	SOB
LRUT01000068.1	<i>Arcobacter cryaerophilus</i> strain L400	-0.5188	ND	ND	ND	D	SOB
LRUU01000074.1	<i>Arcobacter cryaerophilus</i> strain L401	-0.2732	ND	ND	ND	D	SOB
LRUV01000056.1	<i>Arcobacter cryaerophilus</i> strain L406	-0.5123	ND	ND	ND	D	SOB
MIBP01000017.1	<i>Sulfuricurvum</i> sp. RIFCSPHIGO2	-0.8204	ND	ND	ND	D	SOB
MTEJ01000680.1	<i>Thiothrix lacustris</i> strain A8	0.0522	D	ND	ND	ND	SOB
MTEJ01000720.1	<i>Thiothrix lacustris</i> strain A8	0.5289	ND	ND	ND	D	SOB
MXAV01000010.1	<i>Acidithiobacillus</i> sp. SH	0.1522	D	D	D	ND	SOB
NCFS01000047.1	<i>Halothiobacillus</i> sp. 35-54-62	0.5356	ND	ND	D	ND	SOB
NCHH01000032.1	<i>Sulfuricurvum</i> sp. 24-42-5	-0.3833	ND	D	ND	ND	SOB
NCJI01000088.1	<i>Halothiobacillus</i> sp. 39-53-45	1.5084	ND	D	ND	ND	SOB
NXGD01000002.1	<i>Arcobacter cryaerophilus</i> strain LMG 10229	0.2472	ND	ND	ND	D	SOB
NXGJ01000010.1	<i>Arcobacter cryaerophilus</i> strain LMG 9861	-0.2068	ND	ND	ND	D	SOB
NXGK01000016.1	<i>Arcobacter cryaerophilus</i> strain LMG 24291	-0.4705	ND	ND	ND	D	SOB
NZ_AAAP01000572.1	<i>Magnetospirillum magnetotacticum</i> MS-1	0.6233	ND	D	ND	ND	SOB
NZ_BCTF01000035.1	<i>Hydrogenophaga flava</i> NBRC 102514	0.5581	ND	ND	ND	D	SOB
NZ_BCTF01000067.1	<i>Hydrogenophaga flava</i> NBRC 102514	-1.0481	ND	ND	ND	D	SOB
NZ_CGIH01000043.1	<i>Syntrophomonas zehnderi</i> OL-4	-0.2280	ND	ND	ND	D	SOB
NZ_FNEA01000052.1	<i>Paracoccus denitrificans</i> strain DSM 413	0.5429	ND	ND	ND	D	SOB
NZ_FNEA01000064.1	<i>Paracoccus denitrificans</i> strain DSM 413	0.6220	ND	ND	ND	D	SOB
NZ_FNEA01000070.1	<i>Paracoccus denitrificans</i> strain DSM 413	0.9407	ND	ND	ND	D	SOB
NZ_FNXG01000001.1	<i>Paracoccus alkenifer</i> strain DSM 11593	0.2015	D	D	D	ND	SOB
NZ_FOYK01000064.1	<i>Paracoccus denitrificans</i> strain DSM 415	0.5959	ND	ND	ND	D	SOB

ACKNOWLEDGEMENTS

This research was funded by the Research and Researchers for Industries (Grant No. PHD60I0028) and King Mongkut's University of Technology North Bangkok, Thailand (KMUTNB-64-KNOW-37).

REFERENCES

- Agilent Technologies. 2019. Agilent oligonucleotide array-based CGH for genomic DNA analysis-enzymatic labeling for blood, cells, or tissues (with a high throughput option) protocol. Agilent Technologies, Inc, USA., <https://www.agilent.com/cs/library/usermanuals/public/GEN-MAN-G4410-90010.pdf>
- Alam, M., Fernandes, S., Mandal, S., Rameez, M.J., Bhattacharya, S., Peketi, A. and Ghosh, W. 2021. 34S enrichment as a signature of thiosulfate oxidation in the Proteobacteria. *FEMS Microbiol. Lett.*, 368: fnab073.
- Alinezhad, E., Haghghi, M., Rahmani, F., Keshizadeh, H., Abdi, M. and Naddafi, K. 2019. Technical and economic investigation of chemical scrubber and bio-filtration in the removal of H₂S and NH₃ from the wastewater treatment plant. *J. Environ. Manage.*, 241: 32-43.
- Berben, T., Overmars, L., Sorokin, D.Y. and Muyzer, G. 2019. Diversity and distribution of sulfur oxidation-related genes in Thioalkalivibrio, a genus of chemolithoautotrophic and haloalkaliphilic sulfur-oxidizing bacteria. *Front. Microbiol.*, 10: 160.
- Besser, J., Carleton, H.A., Gerner-Smidt, P., Lindsey, R.L. and Trees, E. 2018. Next-generation sequencing technologies and their application to the study and control of bacterial infections. *Clin. Microbiol. Infect.*, 24: 335-341.
- Bolyen, E., Rideout, J.R., Dillon, M.R., Bokulich, N.A., Abnet, C.C., Al-Ghalith, G.A. and Caporaso, J.G. 2019. Reproducible, interactive, scalable, and extensible microbiome data science using QIIME 2. *Nat. Biotechnol.*, 37: 852-857.
- Chen, Q., Yin, H., Luo, H., Xie, M., Qiu, G. and Liu, X. 2009. Micro-array based whole-genome hybridization for detection of microorganisms in acid mine drainage and bioleaching systems. *Hydrometallurgy*, 95: 96-103.
- Dong, Q., Shi, H. and Liu, Y. 2017. Microbial character related sulfur cycle under dynamic environmental factors based on the microbial population analysis in the sewerage system. *Front. Microbiol.*, 8: 64.
- Douglas, G.M., Maffei, V.J., Zaneveld, J.R., Yurgel, S.N., Brown, J.R., Taylor, C.M. and Langille, M.G. 2020. PICRUSt2 for prediction of metagenome functions. *Nat. Biotechnol.*, 38: 685-688.
- Dubinina, G., Grabovich, M., Leshcheva, N., Rainey, F.A. and Gavrish, E. 2011. Spirochaetaperfilievii sp. nov., an oxygen-tolerant, sulfide-oxidizing, sulfur- and thiosulfate-reducing spirochaete isolated from a saline spring. *Int. J. Syst. Evol. Microbiol.*, 61: 110-117.
- Flood, B.E., Louw, D.C., Van der Plas, A.K. and Bailey, J.V. 2021. Giant sulfur bacteria (Beggiatoaceae) from sediments underlying the Benguela upwelling system host diverse microbiomes. *PLoS One*, 16: e0258124.
- Friedrich, C.G., Bardischewsky, F., Rother, D., Quentmeier, A. and Fischer, J. 2005. Prokaryotic sulfur oxidation. *Curr. Opin. Microbiol.*, 8: 253-259.
- Gentry, T.J. and Jizhong, Z. 2006. *Microarray-based microbial identification and characterization*. Adv. Tech. Diagnostic Microbiol., Springer, Boston, MA, p. 276-290.
- Gregersen, L.H., Bryant, D. A. and Frigaard, N.U. 2011. Mechanisms and evolution of oxidative sulfur metabolism in green sulfur bacteria. *Front. Microbiol.*, 2: 116.
- Grim, S.L., Voorhies, A.A., Biddanda, B.A., Jain, S., Nold, S.C., Green, R. and Dick, G.J. 2021. Omics-Inferred Partitioning and Expression of Diverse Biogeochemical Functions in a Low-O₂ Cyanobacterial Mat Community. *Msystems*, 6: e01042-21.
- Gupta, S., Mortensen, M.S., Schjørring, S., Trivedi, U., Vestergaard, G., Stokholm, J. and Sørensen, S.J. 2019. Amplicon sequencing provides more accurate microbiome information in healthy children compared to culturing. *Commun. Biol.*, 2: 1-7.
- Haosagul, S., Oaew, S., Prommeenate, P., Sawasdee, V. and Pisutpaisal, N. 2021. DNA microarray for detection and identification of sulfur-oxidizing bacteria in Biogas Clean-up System. *Energy Rep.*, 7: 559-568.
- Haosagul, S., Prommeenate, P., Hobbs, G. and Pisutpaisal, N. 2020. Sulfide-oxidizing bacteria community in full-scale bioscrubber treating H₂S in biogas from swine anaerobic digester. *Renew. Energy*, 150: 973-980.
- Hong, P.Y., Yannarell, A.C., Dai, Q., Ekizoglu, M. and Mackie, R. I. 2013. Monitoring the perturbation of soil and groundwater microbial communities due to pig production activities. *Appl. Environ. Microbiol.*, 79: 2620-2629.
- Jirachaisakdeacha, D., Kumdhitahutsawakul, L., Pholchan, P., Kantha, U., Pathom-Aree, W. and Bovonsombut, S. 2020. Hydrogen Sulfide Removal from Biogas Using Immobilized Sulfur Oxidizing Bacterium *Paracoccus versutus* CM1 in Biofilters. *Chiang Mai J. Sci.*, 47: 872-886.
- Kersters, K., de Vos, P., Gillis, M., Swings, J. and Vandamme, P. 2006. Introduction to the Proteobacteria. *The Prokaryotes: A Handbook on the Biology of Bacteria*, 3rd, Dworkin M, Falkow S, Rosenberg E, Schleifer K & Stackebrandt E, eds.
- Kodama, Y. and Watanabe, K. 2004. *Sulfuricurvum kujiense* gen. nov., sp. nov., a facultatively anaerobic, chemolithoautotrophic, sulfur-oxidizing bacterium isolated from an underground crude oil storage cavity. *Int. J. Syst. Evol. Microbiol.*, 54: 2297-2300.
- Li, Y., Wang, X., Wang, X.Q., Wang, J. and Zhao, J. 2020. Life-long dynamics of the swine gut microbiome and their implications in probiotics development and food safety. *Gut Microbes*, 11: 1824-1832.
- Lu, Y., Zhuo, C., Li, Y., Li, H., Yang, M., Xu, D. and He, H. 2020. Evaluation of filamentous heterocystous cyanobacteria for integrated pig-farm biogas slurry treatment and bioenergy production. *Bioresour. Technol.*, 297: 122418.
- Luo, J., Tan, X., Liu, K. and Lin, W. 2018. Survey of sulfur-oxidizing bacterial community in the Pearl River water using soxB, sqr, and dsrA as molecular biomarkers. *3 Biotech*, 8: 1-12.
- Meyer, B., Imhoff, J.F. and Kuever, J. 2007. Molecular analysis of the distribution and phylogeny of the soxB gene among sulfur-oxidizing bacteria—the evolution of the Sox sulfur oxidation enzyme system. *Environ. Microbiol.*, 9: 2957-2977.
- Narihiro, T., Terada, T., Kikuchi, K., Iguchi, A., Ikeda, M., Yamauchi, T. and Sekiguchi, Y. 2008. Comparative analysis of bacterial and archaeal communities in methanogenic sludge granules from upflow anaerobic sludge blanket reactors treating various food-processing, high-strength organic wastewaters. *Microbes Environ.*, 24: 88-96.
- Ritalahti, K.M., Justicia-Leon, S.D., Cusick, K.D., Ramos-Hernandez, N., Rubin, M., Dornbush, J. and Löffler, F.E. 2012. *Sphaerochaeta globosa* gen. nov., sp. nov. and *Sphaerochaeta pleomorpha* sp. nov., free-living, spherical spirochaetes. *Int. J. Syst. Evol. Microbiol.*, 62: 210-216.
- Roh, S.W., Abell, G.C., Kim, K.H., Nam, Y.D. and Bae, J.W. 2010. Comparing microarrays and next-generation sequencing technologies for microbial ecology research. *Trends Biotechnol.*, 28: 291-299.
- Samiotis, G., Ziagova, M.G. and Amanatidou, E. 2021. Wastewater Substrate Disinfection for Application of *Synechococcus Elongatus* PCC 7942 Cultivation as Tertiary Treatment. <https://doi.org/10.21203/rs.3.rs-1067481/v1> (2021) (preprint).
- Shin, J., Cho, S.K., Lee, J., Hwang, K., Chung, J.W., Jang, H.N. and Shin, S.G. 2019. Performance and microbial community dynamics in anaerobic digestion of waste activated sludge: Impact of immigration. *Energies*, 12: 573.
- Stewart, F., Dmytrenko, O., DeLong, E. and Cavanaugh, C. 2011. Metatranscriptomic analysis of sulfur oxidation genes in the endosymbiont of *Solemya velum*. *Front. Microbiol.*, 2: 134.

- Tikhonova, T.V., Lilina, A.V., Osipov, E.M., Shipkov, N.S., Dergousova, N.I., Kulikova, O. G. and Popov, V. O. 2021. Catalytic properties of flavocytochrome c sulfide dehydrogenase from Haloalkaliphilic bacterium *Thioalkalivibrio paradoxus*. *Biochemistry*, 86: 361-369.
- Tilahun, E., Sahinkaya, E. and Çalli, B. 2018. A hybrid membrane gas absorption and bio-oxidation process for the removal of hydrogen sulfide from biogas, *International Biodeter. Biodegrad.*, 127: 69-76.
- Treu, L., Campanaro, S., Kougias, P.G., Sartori, C., Bassani, I. and Angelidaki, I. 2018. Hydrogen-fueled microbial pathways in biogas upgrading systems revealed by genome-centric metagenomics, *Front. Microbiol.*, 9: 1079.
- Vayenos, D., Romanos, G.E., Papageorgiou, G.C. and Stamatakis, K. 2020. *Synechococcus elongatus* PCC7942: A cyanobacterium cell factory for producing useful chemicals and fuels under abiotic stress conditions, *Photosynth. Res.*, 146: 235-245.
- Wang, R., Zhang, J., Liu, J., Yu, D., Zhong, H., Wang, Y. and Wei, Y. 2018. Effects of chlortetracycline, Cu and their combination on the performance and microbial community dynamics in swine manure anaerobic digestion. *J. Environ. Sci.*, 67: 206-215.
- Wu, L., Thompson, D. K., Li, G., Hurt, R.A., Tiedje, J.M. and Zhou, J. 2001. Development and evaluation of functional gene arrays for detection of selected genes in the environment, *Appl. Environ. Microbiol.*, 67: 5780-5790.
- Wylensek, D., Hitch, T.C., Riedel, T., Afrizal, A., Kumar, N., Wortmann, E. and Clavel, T. 2020. A collection of bacterial isolates from the pig intestine reveals functional and taxonomic diversity, *Nat. Commun.*, 11: 1-26.
- Xu, J., Xie, G., Li, X., Wen, X., Cao, Z., Ma, B. and Wu, Y. 2021. Sodium butyrate reduces ammonia and hydrogen sulfide emissions by regulating bacterial community balance in swine cecal content in vitro, *Ecotoxicol. Environ. Saf.*, 226: 112827.
- Xu, M., Zhou, H., Yang, X., Angelidaki, I. and Zhang, Y. 2020. Sulfide restrains the growth of *Methylocapsa acidophilus*, converting renewable biogas to single-cell protein. *Water Res.*, 184: 116138.
- Zhou, Q., Liang, H., Yang, S. and Jiang, X. 2015. The removal of hydrogen sulfide from biogas in a microaerobic biotrickling filter using polypropylene carrier as packing material, *Appl. Biochem. Biotechnol.*, 175: 3763-3777.

ORCID DETAILS OF THE AUTHORS

Saowaluck Haosagul: <https://orcid.org/0000-0002-9448-5840>



Total Soluble Protein Mediated Morphological Traits in Mustard Treated with Thiourea and Salicylic Acid

Shipa Rani Dey*, Prasann Kumar*† and Joginder Singh**

*Department of Agronomy, School of Agriculture, Lovely Professional University, Phagwara-144411, Punjab, India

**Department of Botany, Nagaland University, Nagaland, India

†Corresponding author: Prasann Kumar; prasann0659@gmail.com

Nat. Env. & Poll. Tech.
Website: www.neptjournal.com

Received: 04-08-2023

Revised: 12-10-2023

Accepted: 14-10-2023

Key Words:

Thiourea
Salicylic acid
Morphological traits
Leaf area
Total soluble protein

ABSTRACT

The total soluble protein-mediated morphological traits in mustard treated with Thiourea and Salicylic acid were investigated. In addition, it tested the hypothesis that the growth regulator salicylic acid protects the photosynthetic apparatus by up-regulating morphological traits. Under natural environmental conditions, seeds were sown in the field, and seed emergence was recorded. For three days after the 15-day stage, plants in the area were treated with thiourea and salicylic acid and allowed to grow for 90 days. Plants were harvested to assess various morphological traits. A follow-up application of SA and Thiourea plants improved plant height, leaf area, internodal length, leaf number, and accelerated plant activity. The up-regulation of morphological traits may have occurred in SA and Thiourea-mediated plants. After treatments, the level of total soluble protein was estimated in the leaves at proposed day intervals.

INTRODUCTION

The continuous quest for sustainable agricultural practices and the mitigation of various biotic and abiotic stresses has driven significant research toward understanding the intricate interplay between plant physiology and exogenous agents (More et al. 2023; Sangwan et al. 2015; Vioratti Telles de Moura et al. 2023). Among the numerous signaling molecules and compounds that have emerged as promising candidates in this context, thiourea (TU) and salicylic acid (SA) have garnered considerable attention. These chemical elicitors are known to modulate plant responses, leading to enhanced tolerance against environmental challenges and improved growth patterns. These topics have always been under constant investigation and development because SA also plays a role in stress tolerance and the metabolic reprogramming of plants during biotic and abiotic stress responses. Mustard (*Brassica* sp.) is a vital oilseed crop with widespread global cultivation and economic significance. As mustard plants are exposed to many environmental factors, including pathogenic attacks, temperature fluctuations, and soil nutrient availability, unraveling the underlying mechanisms that govern their response to stressors is crucial for developing efficient strategies to enhance crop productivity and yield. Total Soluble Proteins (TSPs)

mediate various physiological processes as critical players in signal transduction pathways and regulatory networks. The abundance and composition of TSPs within plant tissues are essential indicators of the plant's health and stress responsiveness (Kaya et al. 2023; Nabizade et al. 2023). This study aims to investigate the impact of Thiourea and Salicylic Acid treatments on mustard plants and the consequential alterations in Total Soluble Protein levels. By examining the morphological traits, growth patterns, and biochemical responses, this research sheds light on the intricate relationship between these chemical elicitors and mustard plants at the protein level. Depending on its concentration, mode of application, and plant type, it regulates plants' photosynthesis, water relations, and metabolic aspects. Moreover, SA is also involved in various developmental processes, such as floral induction, root initiation, and senescence, and is a significant component of hormone-derived signaling pathways. Besides leaf structure, it also affects stomatal closure, chlorophyll, rubisco activity, and ribulose biphosphate carboxylase activity. In addition, SA also plays a critical role in plant defense, as it is involved in the induction of systemic acquired resistance by triggering the expression of pathogenesis-related (PR) genes. SA also confers tolerance to various abiotic stresses through ion exclusion and comparison, osmotic adjustments, lipid

peroxidation reduction, synthesis of protein kinases (SIPK), and regulation of the oxidative system. By regulating the oxidative system, SA helps stabilize the plant's internal environment and protects it from further damage caused by external stresses (Ashraf et al. 2016; Nazar et al. 2015). Seedling growth of *Hedysarum coronarium* is facilitated by SA priming. Many studies have examined salicylic acid's response to abiotic stresses, such as salt, Cu, Cd, and Hg. However, little is known about salicylic acid's response to increasing Mn levels in *Brassica juncea*. The present study thus aimed to investigate the effects of Mn on the photosynthetic apparatus, plant growth, and the response of salicylic acid to Mn on antioxidant enzymes and Osmo protectants in mustard plants. Increasing crop productivity is significant in today's agricultural production. It is achieved through improved crop varieties, better irrigation systems, and the broader use of fertilizers and pesticides. By increasing the number of crops produced, farmers can feed more people at a lower cost, making food more accessible and affordable. In an earlier study, foliar application of thiourea (TU, a non-physiological thiol-based ROS scavenger) increased stress tolerance and yield of different crops. Additionally, using thiourea helps to increase the stress tolerance of crops, reducing the amount of crop loss that farmers experience due to harsh weather conditions. It helps them to produce higher yields and better quality food for their customers. The application of TU enhances the efficiency of PSI and PSII photosystems and vegetative growth. Thiourea helps to reduce the amount of oxidative stress on the crops, which can damage the crop and reduce yields. The crop can withstand harsh weather conditions and produce higher yields by reducing oxidative stress. Additionally, thiourea helps to increase photosynthesis efficiency, which allows the crop to use more energy from the sun for growth. The investigation is expected to yield crucial insights into the mechanisms through which Thiourea and Salicylic Acid influence mustard plants' TSPs, consequently influencing their growth, development, and stress tolerance. Furthermore, the findings from this study could pave the way for harnessing the potential of these elicitors as eco-friendly and sustainable alternatives to traditional agricultural practices, fostering improved crop resilience and productivity in mustard and potentially other crop species (Hasanuzzaman et al. 2022; Islam et al. 2023; Tanveer et al. 2023). Exploring Total Soluble Protein-mediated morphological traits in mustard plants subjected to Thiourea and Salicylic Acid treatments holds promise for broadening our understanding of plant stress responses and providing innovative agricultural advancements. By bridging the gap between molecular signaling and physiological outcomes, this research contributes to the ongoing efforts to create resilient agricultural systems that meet the challenges

of a changing environment and ensure food security for the growing global population.

MATERIALS AND METHODS

Salicylic Acid Preparation

Salicylic acid (SA) was procured from Sigma Aldrich Chemicals Pvt. Ltd., India. SA solutions were prepared by dissolving the required quantity (300 ppm) (approximately Rec.) of SA in 5 ml of ethanol in 100 mL volumetric flasks, and the final volume was made up according to the mark by using Double Distilled Water as a solvent.

Source of Sulfur

Thiourea ($\text{CH}_4\text{N}_2\text{S}$) (1000 ppm) (Rec.) was used as a sulfur (S) source. The required S concentrations were prepared by dissolving the requisite amount in DDW.

Biological Material

Brassica seeds were obtained from Punjab Agricultural University, Punjab. The healthy-looking and uniform-size seeds were surface sterilized with 1% sodium hypochlorite solution for 5 min, followed by repeated washing with double distilled water (DDW).

Treatment Pattern

A field trial was conducted under a randomized block design at Lovely Professional University, Phagwara, Punjab. Field preparation and sowing of brassica seeds were performed according to the recommended package and practices for the Punjab region by the Indian Council of Agricultural Research. A total of twelve treatments and three replications were conducted in this study. The following were the treatments: T0- Control, T1- Sulfur Recommended, T2- Salicylic Acid Recommended, T3- Sulfur (Rec) + Salicylic acid (Recommended), T4- Sulfur (Reco+1/2th of Rec) + Salicylic acid (Recommended), T5- Sulfur (Rec) + Salicylic acid (Reco+1/2th of Rec), T6- Sulfur (Reco-1/2th of Rec) + Salicylic acid (Recommended), T7- Sulfur (Rec) + Salicylic acid (Reco-1/2th of Rec), T8- Sulfur (Reco-1/2th of Rec) + Salicylic acid (Double of Rec), T9- Sulfur (Double of Rec) + Salicylic acid (Reco-1/2th of Rec), T10- Sulfur (Double of Rec) + Salicylic acid (Double of Rec), T11- Sulfur (Reco-1/2th of Rec) + Salicylic acid (Reco-1/2th of Rec)

Each plant's foliage was sprinkled three times with salicylic acid (SA) and thiourea (TU) solution. The sprayer's nozzle was adjusted to pump out approximately one mL (approx.) in each sprinkle. As a result, 3 mL of SA + TU solution was applied to each plant's foliage. The 30th, 60th, and 90th days of growth were conducted throughout all

the observations. The assays were repeated three times to confirm the results.

Statistical Analysis

Statistical data analysis was carried out, and the mean and the standard deviation (SD) were calculated. Analysis of variance (ANOVA) and Test of Homogeneity (DMRT) were performed on the data using SPSS (ver. 22.0 Inc., USA) to determine the least significant difference (LSD) for significant data to identify differences in the mean of the treatment. The treatment means were separated by LSD test. Data are presented as mean \pm SD ($n = 12$). Factorial analysis of FTIR spectra was performed.

Morphological Traits

Periodic observations were done in mustard to assess the effects of the provided treatments concerning morphological attributes analysis. Five plants were tagged and marked from each treatment plot for periodical observation and assessment.

Plant height: At an interval of 30 days, the height of the mustard plants was measured with a ruler. All five tagged plants from each treatment plot were measured for height, and their average value was considered for each treatment.

Leaf area: After selecting a healthy plant from each plot, the leaves were counted and separated. Then, a leaf area meter was used to measure the area. The total leaf area is the sum of individual leaf areas. The leaf area measurement was done at 30-day intervals.

Analysis of Functional Groups Through FTIR

FTIR was used to analyze the compound's functional group following the protocol by Chamberlain et al. (1969). Fourier Transform Infrared Spectroscopy (FTIR) is a powerful analytical technique used to identify and characterize the functional groups in a wide range of organic and inorganic compounds. FTIR spectroscopy is based on measuring the absorption of infrared radiation by molecules sensitive to the functional groups' vibrational modes. As a part of the FTIR analysis, dried powders of each plant material were used. A dried extract powder of 10 mg was encapsulated in a pellet of 100 mg KBr to prepare translucent sample discs from the KBr pellet. Each powder sample of each plant specimen was loaded into an FTIR spectroscope (Shimadzu, IR Affinity 1, Japan), with a range of scans from 400 to 4000 cm^{-1} with a resolution of 4 cm^{-1} . This protocol outlines the step-by-step procedure for analyzing functional groups using FTIR.

Materials:

1. FTIR spectrometer

2. Sample holder (e.g., potassium bromide (KBr) pellets or attenuated total reflection (ATR) accessory)
3. Pestle and mortar (if using KBr pellets)
4. Sample preparation tools (spatula, glass slides, etc.)
5. IR-grade KBr (if using KBr pellets)
6. Samples with known functional groups for calibration

Procedure:

1. Sample Preparation
 - a. Grind Method (KBr Pellets): i. Thoroughly clean the pestle and mortar to avoid contamination between samples. ii. Prepare a small amount of KBr powder and the sample to be analyzed. iii. Mix the sample and KBr powder in a 1:100 ratio (sample: KBr) and grind them together gently to form a homogenous mixture. iv. Use a pellet press to compress the mixture into a thin, transparent pellet.
 - b. ATR Method: i. Place a drop of the sample directly onto the ATR crystal or attach the sample using a suitable method (e.g., double-sided tape). ii. Spread the sample evenly on the ATR crystal to ensure good contact.
2. FTIR Instrument Setup
 - a. Power on the FTIR spectrometer and allow it to warm up for the specified time. b. Before starting the analysis, calibrate the instrument using the appropriate background spectrum (e.g., air or pure solvent).
3. Data Acquisition
 - a. For KBr Pellet Method: i. Place the prepared KBr pellet in the sample holder of the FTIR spectrometer. ii. Set the appropriate measurement parameters, such as resolution and scanning range (typically 4000-400 cm^{-1}). iii. Acquire the background spectrum using a clean KBr pellet in the same holder. iv. Measure the sample spectrum by subtracting the background spectrum from the sample spectrum.
 - b. For ATR Method: i. Place the sample on the ATR crystal and ensure proper alignment. ii. Set the appropriate measurement parameters as in step 3a. iii. Acquire the background spectrum using clean ATR crystal or double-sided tape without any sample. iv. Measure the sample spectrum by subtracting the background spectrum from the sample spectrum.
4. Data Analysis
 - a. Save the obtained FTIR spectra for further analysis. b. Identify the characteristic peaks corresponding to different functional groups by comparing them with

reference spectra or databases. c. Assign the peaks to the specific functional groups present in the sample.

5. Interpretation and Reporting

- Interpret the results, identifying the functional groups present in the sample based on the peak assignments.
- Prepare a report summarizing the findings and discussing the implications of the identified functional groups.

Note: It is essential to follow appropriate safety measures and guidelines while handling samples and using the FTIR spectrometer. Ensure proper disposal of specimens and cleaning of equipment after the analysis.

Determination of Protein in Mustard Leaves After Treatment

Analyzing protein content in plant tissues is paramount in understanding the physiological responses and metabolic changes induced by various treatments. Mustard leaves (*Brassica* spp.) serve as a model system for investigating the effects of external agents on protein levels due to their rapid growth and diverse biochemical responses. The Lowry method, a widely used colorimetric assay, is well-established for quantifying protein concentrations and offers high sensitivity and reproducibility. This protocol outlines the step-by-step procedure for determining protein content in mustard leaves after treatment using the Lowry method.

Materials:

- Mustard leaves samples (treated and untreated)
- Liquid nitrogen (for snap-freezing the leaves)
- Extraction buffer (e.g., Tris-HCl or phosphate buffer with protease inhibitors)
- Homogenizer (mechanical or ultrasonic)
- Centrifuge
- Bovine Serum Albumin (BSA) standard solution (1 mg.mL⁻¹)
- Lowry reagents: a. Folin-Ciocalteu reagent b. 2% sodium carbonate solution c. 1% copper sulfate solution d. Distilled water
- Cuvettes or microplates for colorimetric measurements
- Spectrophotometer capable of measuring absorbance at 750 nm

Procedure:

- Sample Collection and Preparation
 - Harvest mustard leaves from treated and untreated plants at a similar growth stage.
 - Quickly immerse the leaves in liquid nitrogen to snap-freeze them

and preserve the protein content. c. Store the frozen samples at -80°C until further processing.

2. Protein Extraction

- Prepare the extraction buffer by dissolving protease inhibitors in the chosen buffer according to the manufacturer's instructions.
- Weigh the frozen mustard leaves and transfer them to a pre-cooled homogenizer.
- Add the extraction buffer to the leaves in a ratio of 1:10 (w/v).
- Homogenize the mixture on ice until a uniform and homogenous suspension is obtained.
- Centrifuge the homogenate at a suitable speed (e.g., 10,000 x g) and temperature (4°C) to pellet cellular debris.
- Transfer the supernatant (protein extract) to a new tube and keep it on ice.

3. Protein Quantification using the Lowry Method

- Prepare a standard curve using the BSA standard solution. Dilute the BSA standard solution to create a series of known concentrations (e.g., 0, 25, 50, 75, and 100 µg.mL⁻¹).
- Add 100 µL of each standard solution and 100 µL of the protein extract to separate cuvettes or wells in a microplate.
- Add 1 mL of the Lowry reagent (Folin-Ciocalteu) to each cuvette or well and mix gently but thoroughly.
- Incubate the cuvettes or microplate at room temperature for 30 minutes, protected from direct light.

4. Colorimetric Measurement

- After the incubation period, measure the absorbance of each sample at 750 nm using a spectrophotometer.
- Ensure the spectrophotometer is blanked using a blank sample (containing all reagents except the protein extract).

5. Protein Concentration Calculation

- Plot the absorbance values of the BSA standards against their corresponding concentrations to create a standard curve.
- Determine the protein concentration of the mustard leaf extract samples from the standard curve using their respective absorbance values.

6. Data Analysis and Interpretation

- Calculate the treated and untreated samples' mean protein concentration and standard deviation.
- Perform statistical analysis, if applicable, to assess the significance of the observed differences.

The Lowry method provides a reliable and sensitive means of quantifying protein content in mustard leaves after treatment. By following this protocol, researchers can assess the impact of various treatments on protein levels,

gaining valuable insights into the physiological responses of mustard plants to different external agents. The obtained data can contribute to a deeper understanding of the molecular mechanisms underlying stress responses, ultimately aiding the development of strategies to enhance crop resilience and productivity.

RESULTS AND DISCUSSION

Plant Height

Concerning control, the plant height was maximum in T2 at 30 days after sowing. In treatment T11, its maximum height was 60, 90, and 120 DAS. The 30 days older plant shows the maximum height in treatment T2, concerning control (T0). In contrast, the plant height in T2 reached its maximum at 30 DAS compared to the control. Nevertheless, later on, the height was significantly higher than the maximum at 60, 90 and 120 DAS (Fig. 1). The role of salicylic acid in the development and growth of the plant has essential physiological functions, including enhancing the plant's ability to survive and respond to any conditions (biotic or abiotic) by enhancing the resistance of the plant to System Acquired Resistance (SAR) by stimulating or changing the internal environment in the plant. Salicylic acid involves many biological processes, including growth and development, photosynthesis, and stress response. It is believed to act as a signal molecule and can induce the production of other compounds that can help the plant respond to stress and increase its tolerance. It can also help the plant produce more defense compounds to ward off pests and diseases. In contrast, sulfur generally makes plants grow taller. Sulfur also helps to increase the production of chlorophyll, which is necessary for photosynthesis (Barman & Kundu 2023; Li et al. 2023; Wang et al. 2024). It also helps to improve the uptake of minerals and increases the plant's overall health. Sulfur encourages cell division and increases elongation and expansion in plants. There was an analysis of the interaction on plant height in T11 in which it was observed that when sulfur and salicylic acid were applied to the foliar in the appropriate amounts at half the rate of the recommendation, the plant height was observed to be elevated as well as the internodal length elongation. This is because sulfur helps in the production of hormones that boost the growth of plants. It also aids in absorbing other essential nutrients such as nitrogen, potassium, and phosphorus. In addition, the presence of sulfur can help to reduce the amount of stress the plant experiences, which leads to an increase in overall health and vigor. A combination of the two interventions was effective after 60, 90, and 120 days. On the other hand, salicylic acid was found to be effective only for plants 30 days older (Fig. 1). The impact of Total Soluble Protein

(TSP) on plant height in mustard treated with Thiourea (TU) and Salicylic Acid (SA) is a subject of significant interest in plant physiology and agricultural research. TSPs are crucial in various physiological processes, including growth and development, as they are involved in signal transduction, enzymatic activities, and stress responses. Understanding how these chemical elicitors (TU and SA) affect TSP levels and subsequently influence plant height in mustard plants can provide valuable insights into their growth-regulatory mechanisms and potential agricultural applications. Increased TSP levels in mustard plants treated with TU and SA may positively influence plant growth and development, enhancing plant height. TSPs are essential components in cell division, elongation, and differentiation, contributing to overall plant height. Elevated TSP levels may stimulate the synthesis of growth-related proteins, such as kinases and transcription factors, leading to accelerated cell elongation and promoting taller plant stature. TU and SA treatments can enhance enzyme activity in nutrient uptake and assimilation, thus increasing nutrient availability for growth processes. As TSPs regulate enzyme activities, higher TSP levels may improve nutrient utilization, increasing plant biomass and taller plants. TU and SA induce systemic acquired resistance (SAR) and priming responses, enabling mustard plants to cope better with biotic and abiotic stresses (Kaya et al. 2020; Parashar et al. 2014; Pirasteh-Anosheh et al. 2023). Higher TSP levels may contribute to synthesizing stress-responsive proteins, such as chaperones and defense-related proteins, thus enhancing stress tolerance and supporting uninterrupted growth, even under challenging environmental conditions. TU and SA treatments can influence hormone signaling pathways, including auxins, cytokinins, and gibberellins, directly impacting plant height. TSPs can modulate the biosynthesis and signaling of these hormones, leading to altered growth patterns and increased plant height. TSPs are involved in cell wall biosynthesis and remodeling, crucial for cell elongation and growth. Higher TSP levels may lead to modified cell wall composition, allowing increased cell expansion and, consequently, taller plant height in mustard. Elevated TSP levels may impact gene expression patterns, particularly those related to growth and developmental processes. TU and SA treatments can activate or repress specific genes involved in plant height regulation, and TSPs can potentially act as mediators in this process. The impact of Total Soluble Protein-mediated plant height in mustard plants treated with Thiourea and Salicylic Acid highlights the complex interplay between chemical elicitors, TSP levels, and growth-regulatory mechanisms. Combining TU and SA treatments may result in higher TSP content, enhancing growth, stress tolerance, and overall plant height in mustard. This knowledge can be harnessed to develop innovative

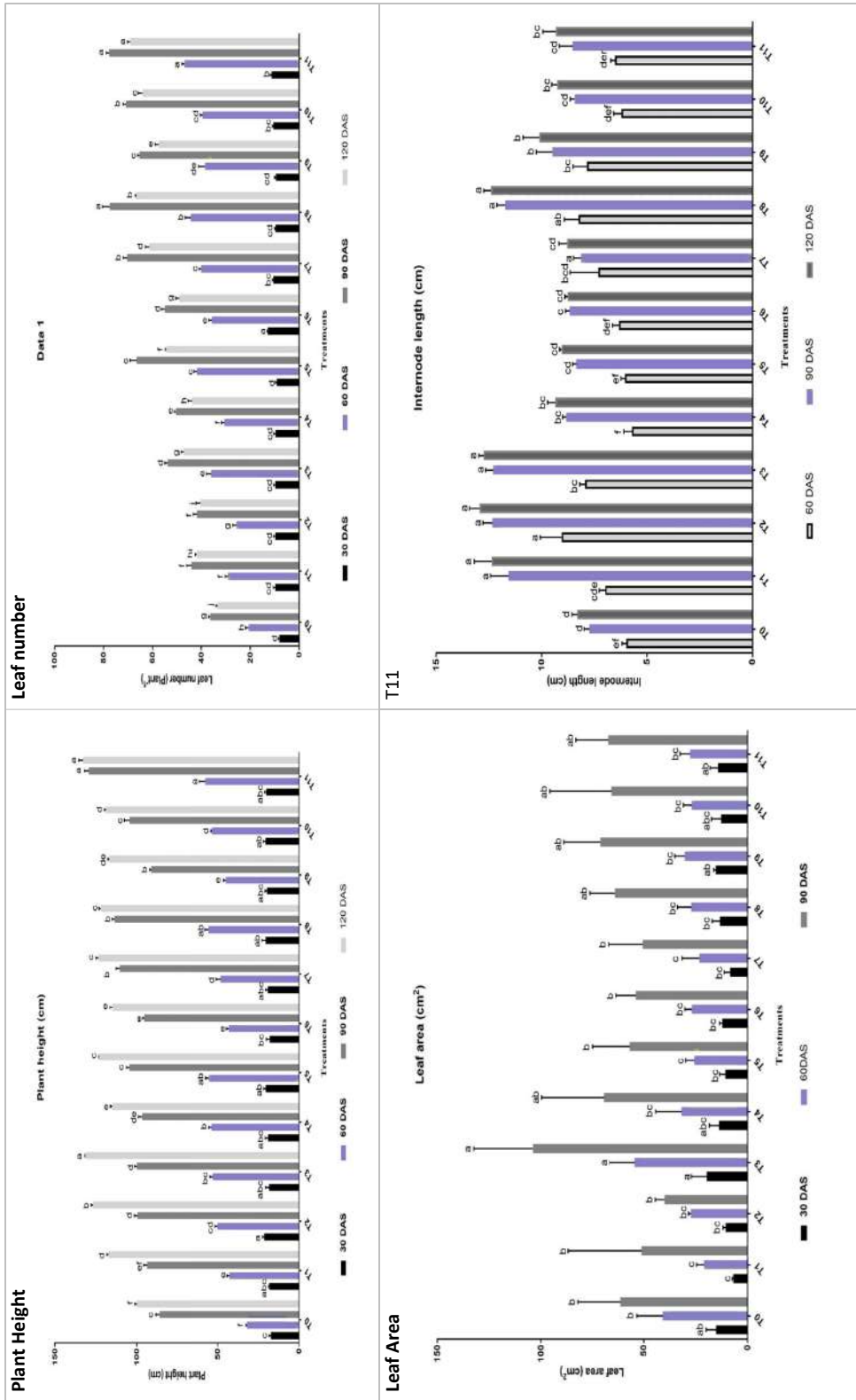


Fig. 1: Comparison of plant height, leaf number, leaf area, and internodal length of mustard crops under different treatments.

strategies for enhancing crop productivity and resilience, contributing to sustainable agricultural practices in the face of changing environmental conditions. Further research is essential to fully elucidate the molecular mechanisms involved in this intriguing phenomenon and its potential applications in crop improvement (Chakma et al. 2021; Panthi et al. 2024; Thepbandit et al. 2023).

Leaf Number

Concerning control, Sulfur (Recommended-1/2th of Rec) + Salicylic acid (Recommended) shows maximum leaf production at 30 days. However, at 60, 90, and 120 days, T11- Sulfur (Reco-1/2th of Rec) + Salicylic acid (Reco-1/2th of Rec) showed the highest number of leaves. In addition to interacting with plant nutrient S, SA interacts with phytohormones, polyamines, nitric oxide, and other nutrients. SA can also control the expression of specific genes, regulate the activity of enzymes, and induce resistance to certain diseases. In addition, SA is involved in plant acclimation to various environmental changes. Numerous reports report that S coordinated studies on auxins, gibberellins, cytokinins, abscisic acid, brassinosteroids, ethylene, nitric oxide, and salicylic acid in plants. These hormones affect plant growth, development, and stress response to environmental stimuli. SA has also been shown to improve plant stress tolerance and yield. The interaction between SA and nutrient S and other phytohormones contributed significantly to plant growth, metabolism, and stress tolerance. Salicylic acid (SA) interacts with other phytohormones and nutrients to transfer environmental signals to the plant cells. It helps plants to perceive environmental stimuli and activate the appropriate responses, such as growth and stress tolerance. The interaction between SA and other nutrients and phytohormones has improved plant growth and stress tolerance and increased yields. Higher GR activity and exogenous SA can result in a higher concentration of S/Cys-GSH. It helps to reduce oxidative damage to the plant and increases its tolerance to environmental stress. In addition, SA can improve the efficiency of photosynthesis and the absorption of other essential nutrients, leading to increased plant growth and productivity. An SA-mediated increase in GSH contents is due to increased ATP-S activity, serine acetyltransferase activity (SAT), and S and Cys contents. SA can also increase the expression of genes associated with photosynthesis and nutrient absorption, leading to more efficient photosynthesis and nutrient uptake (Devi et al. 2023; Hayat et al. 2012; Huang et al. 2024). In addition, SA can regulate the activity of enzymes in synthesizing glutathione (GSH) and other compounds, which increases GSH content and helps protect the plant from environmental stresses. Finally, SA regulates sulfotransferase (SOT12)

and S-nitrosylation, which are essential for proper SA homeostasis and signaling (Fig. 1). The impact of Total Soluble Protein (TSP) on leaf number in mustard (*Brassica* spp.) treated with Thiourea (TU) and Salicylic Acid (SA) is an essential aspect of plant physiology and agricultural research. Enhanced Leaf Primordia Initiation and Proliferation: Increased TSP levels in mustard plants treated with TU and SA may promote the initiation and proliferation of leaf primordia. TSPs are involved in cell division and differentiation processes, critical for forming leaf primordia during early plant development. Higher TSP content can enhance the number of leaf primordia, ultimately increasing the total leaf number. TU and SA treatments can influence hormonal signaling pathways, including those of auxins, cytokinins, and gibberellins, which are crucial regulators of leaf development. TSPs can modulate the biosynthesis and signaling of these hormones, affecting leaf initiation and expansion. Altered hormonal balance may lead to changes in leaf meristem activity, affecting leaf number in mustard plants. TU and SA treatments can induce stress-responsive genes and signaling pathways, increasing stress tolerance in mustard plants. Higher TSP levels may contribute to the synthesis of stress-related proteins, enhancing plant resilience and facilitating leaf development even under adverse conditions. TSPs are vital in photosynthesis and carbon and nitrogen assimilation in plant tissues. Increased TSP content may positively impact photosynthetic rates and assimilate allocation to developing leaves, promoting leaf expansion and the formation of additional leaves. TSPs are involved in cell wall biosynthesis and remodeling, crucial for cell elongation and expansion during leaf growth. Higher TSP levels can lead to modified cell wall composition, facilitating increased cell elongation and ultimately contributing to more extensive and abundant leaves. Elevated TSP levels may impact gene expression patterns during leaf development (Ali et al. 2014; Ayyaz et al. 2022; Darvizheh et al. 2019). TU and SA treatments can influence gene expression in leaf initiation and expansion, and TSPs may act as mediators in this process. The impact of Total Soluble Protein-mediated leaf number in mustard plants treated with Thiourea and Salicylic Acid highlights the complex interactions between chemical elicitors, TSP levels, and leaf development processes. Combining TU and SA treatments may result in higher TSP content, promoting leaf primordia initiation, expansion, and resilience, ultimately increasing the mustard plants' total number. This knowledge can be applied to develop innovative strategies for enhancing leaf development and crop productivity, contributing to sustainable agricultural practices and improved yield in mustard and potentially other crop species. Further research is needed to fully elucidate the molecular mechanisms involved in this phenomenon and

its potential implications for crop improvement and stress tolerance.

Leaf Area

Concerning Control (To), the leaf area increased most at the combined dose of recommended sulfur and salicylic acid (T3) throughout the observation period. SA interacts with several prohormones, polyamines, nitric oxide, and plant nutrient sulfur. SA mediates the regulation of a wide range of physiological processes, such as growth, development, and stress responses. SA also protects plants from pathogens and other environmental stresses. SA is essential for plant growth and development. SA also interacts with different plant nutrients. SA is a key signaling molecule in plant stress responses, and its production is induced in response to a wide variety of environmental and biotic stimuli. SA is also involved in gene expression regulation and is crucial in abiotic stress responses (Jain et al. 2020; Wang et al. 2024; Zhou et al. 2024). In several reports, sulfur has coordinated studies on phytohormones in plants, such as auxins, gibberellins, cytokinins, abscisic acid, brassinosteroids, ethylene, nitric oxide, and salicylic acid. SA has been demonstrated to regulate various physiological processes, such as photosynthesis, root growth, and flowering. It has also been shown to play a role in plant defense against biotic and abiotic stressors. Furthermore, SA has been studied for its potential beneficial effects on plant growth and development. Salicylic acid (SA) is a hormone naturally present in plants. It has been shown to act as a signaling molecule, triggering a cascade of responses to help the plant better adapt to stressors. It includes regulating gene expression, triggering the production of defense compounds, and stimulating the growth of new cells. Additionally, SA and other phytohormones and S play a significant role in plant growth, metabolism, and stress tolerance. SA has been found to significantly affect plant hormones, such as gibberellic acid and auxin, which can lead to enhanced plant growth and development. SA has been found to regulate the expression of specific genes and proteins involved in stress response, defence mechanisms, and growth and development. It also plays a role in activating specific metabolic pathways and can modulate the levels of certain hormones, such as gibberellin acid and auxin. This makes it essential in plant development, growth, and stress tolerance. SA has also regulated cell wall development, essential for plant structure and stress tolerance (Fig. 1).

The impact of Total Soluble Protein (TSP) on leaf area in mustard (*Brassica* spp.) treated with Thiourea (TU) and Salicylic Acid (SA) is a crucial aspect of plant physiology and agricultural research. Leaf area is an essential trait that directly influences a plant's photosynthesis, transpiration,

and overall biomass production capacity. Understanding how TU and SA treatments affect TSP levels and subsequently influence leaf area in mustard plants can provide valuable insights into the underlying mechanisms and potential applications for enhancing crop productivity (Conversa et al. 2024; Islam et al. 2023; Khan et al. 2023; Zulfikar et al. 2023). Increased TSP levels in mustard plants treated with TU and SA may positively impact photosynthetic efficiency, leading to a more extensive leaf area. TSPs are essential components of the photosynthetic apparatus, playing a pivotal role in light harvesting, electron transport, and carbon fixation. Higher TSP content can enhance the photosynthetic capacity of mustard leaves, resulting in increased leaf area to capture more sunlight and assimilate carbon dioxide. Improved Stomatal Regulation: TU and SA treatments can influence behavior and regulate stomatal density and size.

TSPs may mediate the expression of genes involved in stomatal development and function. Enhanced stomatal regulation can affect water loss through transpiration, potentially leading to larger leaves with efficient water-use strategies. TSPs are critical in cell wall biosynthesis and remodelling, directly impacting cell expansion and differentiation. Higher TSP levels can increase cell division and expansion, contributing to larger leaf areas in mustard plants. TU and SA treatments can modulate hormonal signaling pathways, including auxins, cytokinin, and gibberellins, essential leaf growth regulators. TSPs may be involved in hormonal crosstalk and response, influencing leaf area through hormonal regulation (Ghassemi-Golezani et al. 2020; Ghassemi-Golezani & Farhangi-Abriz 2018; Huang et al. 2024; Shohani et al. 2023). TU and SA treatments can induce stress-responsive genes and signaling pathways, increasing stress tolerance in mustard plants. Higher TSP levels may contribute to synthesizing stress-related proteins, promoting better leaf health and expansion, even under challenging environmental conditions. Elevated TSP levels may impact gene expression patterns during leaf development. TU and SA treatments can influence gene expression in leaf expansion and differentiation, and TSPs may act as mediators in this process. The impact of Total Soluble Protein-mediated leaf area in mustard plants treated with Thiourea and Salicylic Acid underscores the complex interactions between chemical elicitors, TSP levels, and leaf development processes (Akhter et al. 2023; Haghghi et al. 2023; Hundare et al. 2022; SOOD et al. 2013). Combining TU and SA treatments may result in higher TSP content, promoting photosynthetic efficiency, stomatal regulation, cell expansion, and stress tolerance, contributing to increased leaf area in mustard plants. This knowledge can be harnessed to develop innovative strategies for enhancing leaf development and crop productivity, contributing to

sustainable agricultural practices and improved yield in mustard and potentially other crop species. Further research is needed to fully elucidate the molecular mechanisms involved in this phenomenon and its potential implications for crop improvement and stress resilience.

Internodal Length

A maximum internodal length was found in treatment T2 compared to control (T0) at all the observation dates, such as 30, 60, and 90 days after treatment. This suggests that the treatment T2 was effective in increasing the internodal length of the plants compared to the control. The longer internodal length indicates that the treatment T2 successfully promoted better plant growth and development. Besides its role in the growth and development of plants, salicylic acid also plays a fundamental physiological role in plants. Salicylic acid involves various physiological processes, including photosynthesis, respiration, and stomatal closure. It is also known to be a signaling molecule and can trigger systemic acquired resistance in plants. By increasing the levels of salicylic acid, the treatment T2 improved the growth and development of the plants, as evidenced by the increased internodal length. It justifies the observation that salicylic acid plays a fundamental physiological role in plants. This signaling molecule triggers a defense response that helps the plant protect itself from disease. It also helps to regulate the growth and development of the plant, as evidenced by the increased internodal length in the plants treated with the T2 treatment. It suggests that salicylic acid is vital to plants' health and well-being. It includes enhancing the plant's ability to survive and respond to stress conditions (biotic or abiotic) by improving its resistance to System Acquired Resistance (SAR) by stimulating or changing its internal environment to amplify its ability to withstand and respond to stress conditions (biotic or abiotic). By activating the salicylic acid pathway, research has shown that it increases the production of antioxidants and other defence-related compounds which help the plant to better cope with environmental stressors, such as drought, cold, or pests (Bano et al. 2023; Cheng et al. 2020; Farhangi-Abriz et al. 2019; Idrees et al. 2013; Sangwan et al. 2015). In addition, salicylic acid has also been found to reduce the symptoms of diseases caused by fungi, bacteria, and viruses. It is generally believed that sulfur, in contrast to nitrogen, tends to increase the height of plants. When used as a fertilizer, sulfur helps increase chlorophyll production, essential for photosynthesis. It improves the plant's health and allows it to withstand environmental stressors. Hence, it has been found that plants treated with sulfur tend to have higher yields and be more resistant to diseases. There is evidence that sulfur promotes cell division and elongation and stimulates the expansion of cells in plants. Sulfur helps

to increase the availability of essential micro-nutrients, such as phosphorus and calcium, which also aids in plant growth. It also helps to increase the production of certain enzymes, which can increase rates of photosynthesis. Additionally, sulfur helps increase the availability of nitrogen, which is vital for synthesizing proteins and other essential compounds in the plant. When salicylic acid was applied to the foliage at the prescribed rate and in the recommended quantity in T2, an interaction analysis revealed that the average internodal length and the amount of salicylic acid applied to the foliage increased. This suggests that the application of salicylic acid and the availability of sulfur in the soil may play an important role in the synthesis of proteins and other essential compounds in the plant, leading to an increase in the average internodal length and overall growth. After 30, 60, 90, and 120 days of intervention, the intervention was effective. The results showed that the application of salicylic acid and the increased availability of sulfur in the soil positively affected the synthesis of proteins, increasing the internodal length of the plant and its overall growth. This suggests that salicylic acid and sulfur can be essential in plant development (Ahmad et al. 2011; Ali 2021; Ali et al. 2024; Ghahremani et al. 2023; Khalid et al. 2023; Osama et al. 2019).

FTIR Spectroscopy in Combination with Principle Component Analysis

The FTIR spectroscopy was performed on a leaf sample for the treatments T2, T3, and T11, as well as the control T0, to determine the effect of each treatment. FTIR spectroscopy involves the measurement of the infrared spectrum of a sample, which helps to identify the functional groups present in the sample. The effects of each treatment can be determined by comparing the ranges of the different treatments and the control. Results showed significant differences between the treatments and the control. There is no other reason this particular treatment was chosen besides the morphological output produced on the plants after these treatments have been applied. This morphological output is associated with a significant increase in the productivity of the plants. It is also believed that the treatment helps prevent disease and insect infestations. Therefore, it is the most effective and economical way of achieving the desired results. The spectral peak under different treatments is observed in Fig. 2. The results show that the spectral peak behavior is affected by the treatments. The figure also shows that the spectral peak increases with increasing treatments. It can be concluded that the treatments significantly impact the spectral peak behaviour (Devi et al. 2023; Dey et al. 2023; Hidangmayum et al. 2023; Kumar et al. 2023; Sharma et al. 2023; Sharma et al. 2023). As shown in Fig. 2, different types of functional groups are stimulated and affected after

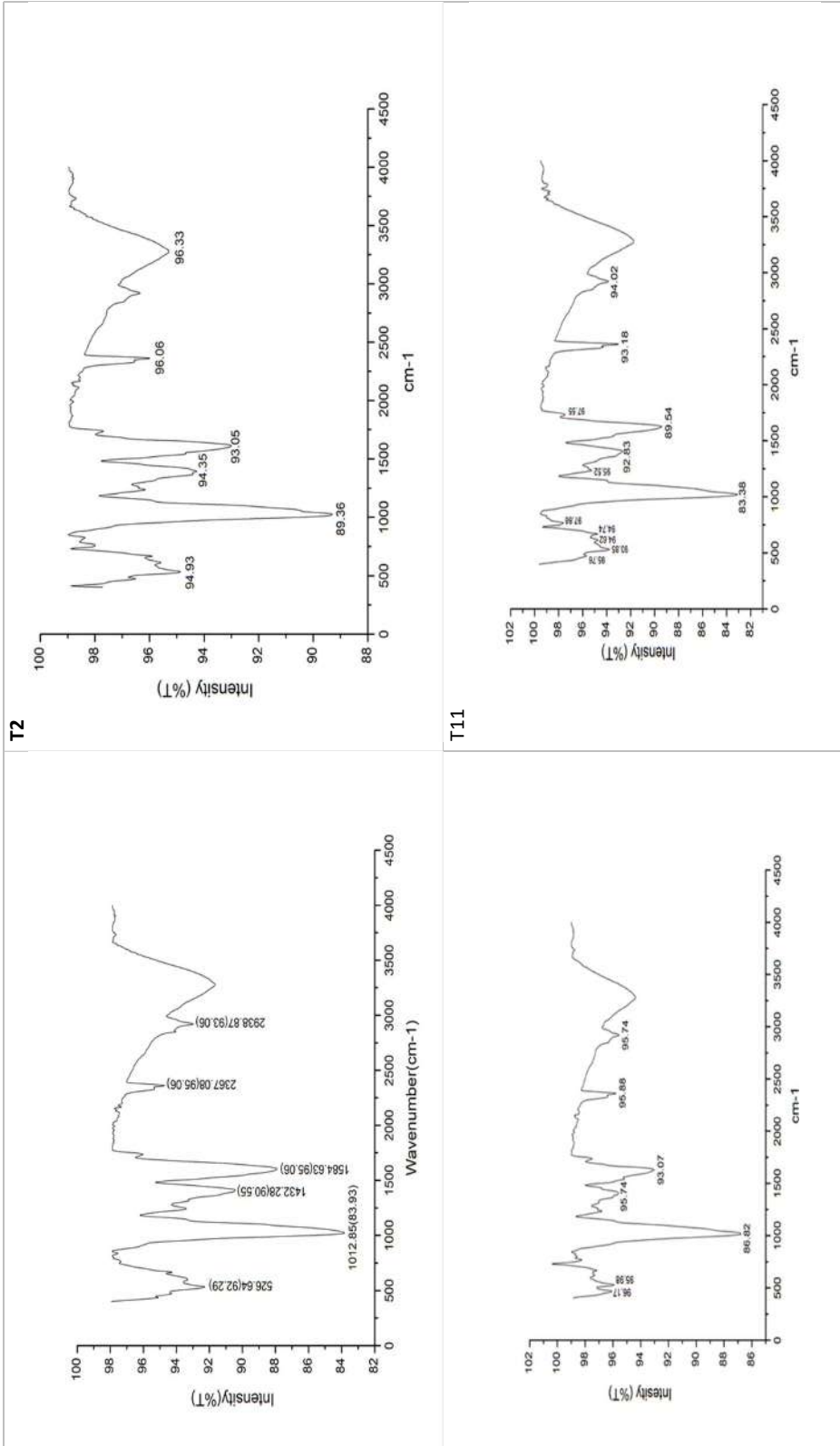


Fig. 2. Analysis of FTIR spectral patterns of leaves samples that were treated with a variety of treatments.

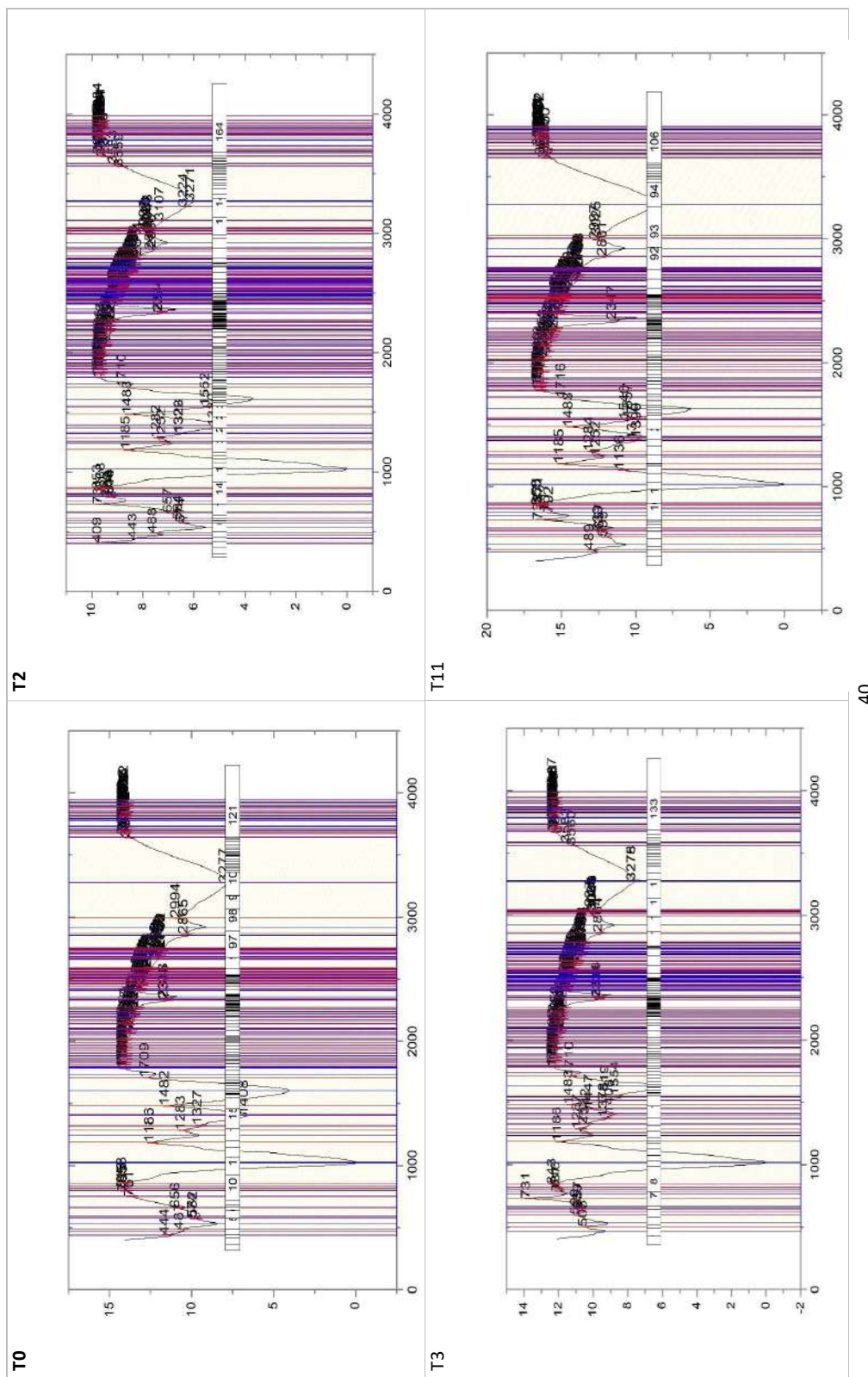


Fig. 3: The number of peaks obtained during FTIR analysis as a result of different treatments.

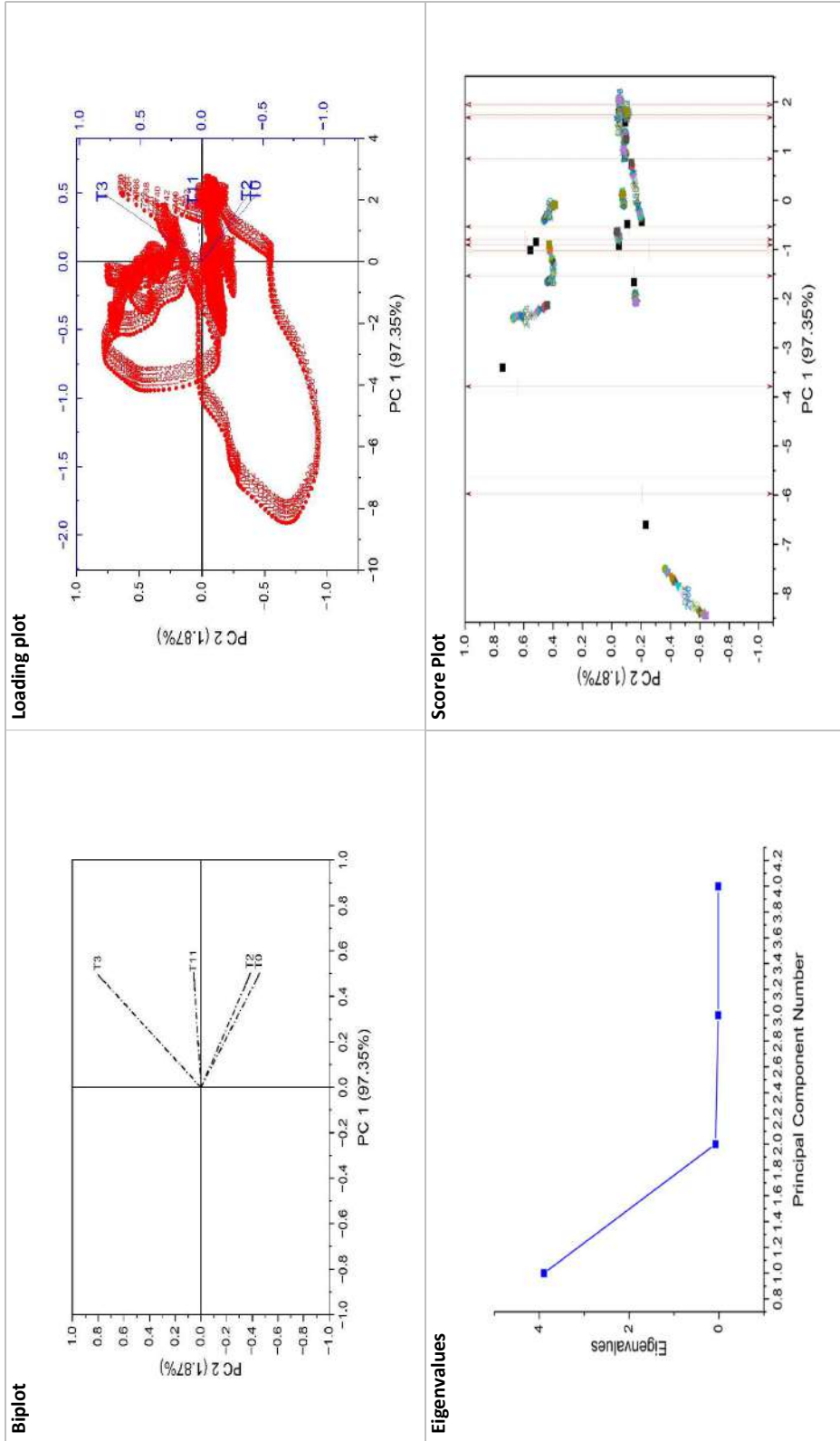


Fig. 4: A PCA analysis was carried out to analyze the FTIR spectra of mustard crops under different treatments.

treatment is applied. The results show that the functional groups were activated differently depending on the type of treatment used. All the treatments effectively started functional groups and influenced spectral peak behavior. As a result, plants that undergo such changes have differences in the types of metabolites in their cells. It leads to changes in the physical and chemical properties of the plants, affecting their growth and development. Such changes directly impact the yield and quality of the produce.

According to the peak analysis results, there were 121 peaks in T0o (Control), whereas there were 164 peaks in T2(164), 133 peaks in T3(133), and 106 peaks in T11(106) (Fig. 3). Most peaks were observed in T2 and T3, while the least was in T11. The peaks in the different time frames represented varying levels of activity. Interestingly, the peak numbers for T11 were lower than the other time frames. It suggests that the activity in T11 was lower than in the different time frames, and the lower peak numbers could indicate this.

Additionally, the varying peak numbers in the different time frames could be attributed to the different activity levels present in each time frame. A threshold value of % height was used to select the peaks, and when this threshold value was subtracted from the constant value of Y, the peaks were selected. The peak values were used to calculate the area under the curve. The area under the curve was then used to calculate the total amount of substance in the sample. This data was then used to determine the concentration of the substance in the sample. The threshold value was selected based on an analysis of the data and was used to identify the points on the graph where the substance was present in the most significant amount. The peaks were identified by subtracting this threshold value from the constant value of Y, and the area under the curve was calculated. This area was then used to determine the concentration of the substance in the sample, which allowed for a more precise measurement than would have been possible without the threshold value (Devi & Kumar 2023a, 2023b; Kumar et al. 2023; Sharma et al. 2023; Sharma et al. 2023; Sinam et al. 2023; Upadhyay et al. 2023).

Using the principal component analysis method, we calculated the factorial. The results showed that the principal component analysis could accurately capture the underlying structure of the T0, T2, T3, and T11 data. The factorial explained a large portion of the variance in the data, indicating that the method was successful. In Graph 4, we have shown the different analyses conducted. The analysis results provide a clear insight into the data structure and its relationships. We can conclude that the principal component analysis is an effective method of data analysis. Using the

biplots graph, we were able to determine the distribution of PC1 (97.35%) and PC2 (1.87%) of treatments T0, T2, T3, and T11 in the different quadrants (Q1, Q2, Q3, and Q4). We also identified the most influential variables that significantly impacted the analysis results. The biplot graph was an effective tool for visualizing the data and understanding the relationships between the variables (here, the variables are % Transmittance and wavelength under T0, T2, T3, and T11). The observation also indicated a similarity in treatment. The biplot graph showed that the treatments were clustered in one quadrant, indicating similar effects on the data. It also showed the most influential variables, which were the ones that had the most substantial impact on the outcome of the analysis. It enabled us to understand better the relationships between the variables and the treatments, which helped us make better decisions and interpret the data. During the analysis, one of the essential eigenvalues (0 to 4) (Fig. 4) was calculated, and its distribution was nicely presented. This eigenvalue was used to measure the variance in the data explained by each variable (Principal component number from 0.8 to 4.2) (Fig. 4). By understanding this, researchers could identify which variables influenced the analysis outcome most, allowing them to make better decisions and interpret the data. According to Fig. 4, there is a score plot and a scattered plot based on the analysis of FTIR spectra between % T and wavelength after analyzing FTIR spectra. After treatments, there was a clear difference in outcomes. By analyzing the FTIR spectra, researchers could identify how different variables, such as wavelength, interacted with each other and which variables had the most influence on the outcome (Devi et al. 2023; Devi et al. 2023; Dey et al. 2023; Kumari et al. 2023; Saini et al. 2023). The score and scatter plots in Fig. 4 illustrate the differences in outcomes after treatments. This allowed researchers to make more informed decisions and interpretations of the data. A representation of the loading point of data under PC1 (97.35%) and PC2 (1.87%) can be found in Fig. 4.

Estimation of Proteins in mustard leaves

The detailed table of protein content under the treatment of TU and SA has been represented in another paper by the same author.

CONCLUSION

As a result of the SA application coupled with thiourea, mustard morphological characteristics were enhanced. Additionally, it increases the plant's performance by improving the morphological attributes of mustard. As a result of the spectral changes in the spectrum, it can be concluded that both compounds change the internal metabolites of the

plant and boost its growth and development. In most of the parameters, the treatment T11 [500 ppm Thiourea + 150 ppm Salicylic Acid] was mainly effective on all the days of the treatment. However, as far as the T2 and T3 treatments are concerned, they are most effective during the first months of the plant's growth and development.

ACKNOWLEDGMENT

The authors would like to thank the Department of Agronomy, School of Agriculture, Lovely Professional University, Phagwara, Punjab, India, for providing them with constant moral support and assistance during the research period.

REFERENCES

- Ahmad, P., Nabi, G. and Ashraf, M. 2011. Cadmium-induced oxidative damage in mustard [*Brassica juncea* (L.) Czern. & Coss.] plants can be alleviated by salicylic acid. *South African Journal of Botany*, 77(1): 36–44. <https://doi.org/https://doi.org/10.1016/j.sajb.2010.05.003>
- Akhter, N., Noreen, A., Saifullah, S., Noman, A., Shahnaz, M. M., Letuma, P. M., Kausar, A., Siddique, M., Hashem, M., Alamri, S., Al-zoubi, O. M., Saleem, M., Khalid, N. and Aqeel, M. 2023. Salt ion mediated changes in biochemical and anatomical characteristics of *Brassica napus* can be countered with *Moringa* Leaf extract. *South African Journal of Botany*, 156: 352–364. <https://doi.org/https://doi.org/10.1016/j.sajb.2023.03.040>
- Ali, B. 2021. Salicylic acid: An efficient elicitor of secondary metabolite production in plants. *Biocatalysis and Agricultural Biotechnology*, 31: 101884. <https://doi.org/https://doi.org/10.1016/j.bcab.2020.101884>
- Ali, B., Xu, X., Gill, R. A., Yang, S., Ali, S., Tahir, M. and Zhou, W. 2014. Promotive role of 5-aminolevulinic acid on mineral nutrients and antioxidative defense system under lead toxicity in *Brassica napus*. *Industrial Crops and Products*, 52: 617–626. <https://doi.org/https://doi.org/10.1016/j.indcrop.2013.11.033>
- Ali, S., Bai, Y., Zhang, J., Zada, S., Khan, N., Hu, Z. and Tang, Y. 2024. Discovering Nature's shield: Metabolomic insights into green zinc oxide nanoparticles Safeguarding *Brassica parachinensis* L. from cadmium stress. *Plant Physiology and Biochemistry*, 206: 108126. <https://doi.org/https://doi.org/10.1016/j.plaphy.2023.108126>
- Ashraf, R., Sultana, B., Iqbal, M. and Mushtaq, M. 2016. Variation in biochemical and antioxidant attributes of *Raphanus sativus* in response to foliar application of plant leaf extracts as plant growth regulator. *Journal of Genetic Engineering and Biotechnology*, 14(1): 1–8. <https://doi.org/https://doi.org/10.1016/j.jgeb.2016.08.003>
- Ayyaz, A., Fang, R., Ma, J., Hannan, F., Huang, Q., Athar, H.-R., Sun, Y., Javed, M., Ali, S., Zhou, W. and Farooq, M. A. 2022. Calcium nanoparticles (Ca-NPs) improve drought stress tolerance in *Brassica napus* by modulating the photosystem II, nutrient acquisition and antioxidant performance. *NanoImpact*, 28: 100423. <https://doi.org/https://doi.org/10.1016/j.impact.2022.100423>
- Bano, K., Kumar, B., Tenguria, R. K., Alsahli, A. A. and Chen, Y. 2023. Salicylic acid and sulfur synergism ameliorates arsenic toxicity in *Brassica napus* through regulating carbohydrate accumulation and ethylene production. *South African Journal of Botany*, 160: 246–259. <https://doi.org/https://doi.org/10.1016/j.sajb.2023.07.017>
- Barman, F. and Kundu, R. 2023. Foliar application of selenium affecting pollen viability, grain chalkiness, and transporter genes in cadmium accumulating rice cultivar: A pot study. *Chemosphere*, 313: 137538. <https://doi.org/https://doi.org/10.1016/j.chemosphere.2022.137538>
- Chakma, R., Biswas, A., Saekong, P., Ullah, H. and Datta, A. 2021. Foliar application and seed priming of salicylic acid affect growth, fruit yield, and quality of grape tomato under drought stress. *Scientia Horticulturae*, 280: 109904. <https://doi.org/https://doi.org/10.1016/j.scienta.2021.109904>
- Cheng, X., Fang, T., Zhao, E., Zheng, B., Huang, B., An, Y. and Zhou, P. 2020. Protective roles of salicylic acid in maintaining integrity and functions of photosynthetic photosystems for alfalfa (*Medicago sativa* L.) tolerance to aluminum toxicity. *Plant Physiology and Biochemistry*, 155: 570–578. <https://doi.org/https://doi.org/10.1016/j.plaphy.2020.08.028>
- Conversa, G., Pacifico, S., La Rotonda, P., Lazzizzera, C., Bonasia, A. and Elia, A. 2024. Foliar application of natural zeolites affects the growth and productivity of processing tomato. *European Journal of Agronomy*, 154: 127100. <https://doi.org/https://doi.org/10.1016/j.eja.2024.127100>
- Darvizheh, H., Zahedi, M., Abbaszadeh, B. and Razzmoo, J. 2019. Changes in some antioxidant enzymes and physiological indices of purple coneflower (*Echinacea purpurea* L.) in response to water deficit and foliar application of salicylic acid and spermine under field condition. *Scientia Horticulturae*, 247: 390–399. <https://doi.org/https://doi.org/10.1016/j.scienta.2018.12.037>
- Devi, K., Bakshi, P., Kour, J., Dhiman, S., Ibrahim, M., Bhardwaj, T., Khanna, K., Madaan, I., Ohri, P., Mir, B. A., Sirhindi, G. and Bhardwaj, R. 2023. Chapter 8 - Role of salicylic acid in the regulation of physiological and molecular aspects of plants under abiotic stress (A. Sharma, S. Pandey, R. Bhardwaj, B. Zheng and D. K. B. T.-T. R. of G. R. and P. in O. E. S. Tripathi (eds.); pp. 175–196). Academic Press. <https://doi.org/https://doi.org/10.1016/B978-0-323-98332-7.00001-9>
- Devi, P., Dey, S. R. and Kumar, P. 2023. Integration of water resources management in rural areas. In: *Water Resources Management for Rural Development: Challenges and Mitigation*, pp. 139–152. Elsevier. <https://doi.org/10.1016/B978-0-443-18778-0.00013-1>
- Devi, P., Dey, S. R., Saini, L., Kumar, P., Panigrahi, S. and Dwivedi, P. 2023. Toward Sustainable Agriculture: Strategies Involving Phytoprotectants Against Reactive Oxygen Species. In: *Reactive Oxygen Species: Prospects in Plant Metabolism*, pp. 229–247. Springer Nature. https://doi.org/10.1007/978-981-19-9794-5_13
- Devi, P. and Kumar, P. 2023a. Effect of microbial oxidative enzymes on soil health. In *Microbial Oxidative Enzymes: Biotechnological Applications*, pp. 37–61. De Gruyter. <https://doi.org/10.1515/9783111062235-003>
- Devi, P. and Kumar, P. 2023b. Role of oxidative enzymes in the alleviation of oxidative stress in plant system. In: *Microbial Oxidative Enzymes: Biotechnological Applications*, pp. 109–128. De Gruyter. <https://doi.org/10.1515/9783111062235-006>
- Devi, P., Kumar, P., Sharma, K. and Singh, J. 2023. Is there a relationship between myconanotechnology and sustainable development? In: *Myconanotechnology and Application of Nanoparticles in Biology: Fundamental Concepts, Mechanism and Industrial Applications*, pp. 175–207. Elsevier. <https://doi.org/10.1016/B978-0-443-15262-7.00009-7>
- Dey, S. R., Devi, P., & Kumar, P. 2023. Organic contaminants in aquatic environments: sources and impact assessment. In: *Metal Organic Frameworks for Wastewater Contaminant Removal*, pp. 299–317. Wiley. <https://www.scopus.com/inward/record.uri?eid=2-s2.0-85174103623&partnerID=40&md5=dbfb41dc5474b67aaaca5dec64c73718>
- Dey, S. R., Sharma, M. and Kumar, P. 2023. Effects and responses of chromium on plants. In: *Environmental Science and Engineering: Vol. Part F1975* pp. 385–427. Springer Science and Business Media Deutschland GmbH. https://doi.org/10.1007/978-3-031-44029-8_14
- Farhangi-Abraz, S., Alae, T. and Tavasolee, A. 2019. Salicylic acid but not jasmonic acid improved canola root response to salinity stress. *Rhizosphere*, 9: 69–71. <https://doi.org/https://doi.org/10.1016/j.rhisph.2018.11.009>

- Ghahremani, Z., Alizadeh, B., Barzegar, T., Nikbakht, J., Ranjbar, M. E. and Nezamdoost, D. 2023. The mechanism of enhancing drought tolerance threshold of pepper plant treated with putrescine and salicylic acid. *Plant Stress*, 9: 100199. <https://doi.org/https://doi.org/10.1016/j.stress.2023.100199>
- Ghassemi-Golezani, K. and Farhangi-Abri, S. 2018. Foliar sprays of salicylic acid and jasmonic acid stimulate H⁺-ATPase activity of tonoplast, nutrient uptake and salt tolerance of soybean. *Ecotoxicology and Environmental Safety*, 166: 18–25. <https://doi.org/https://doi.org/10.1016/j.ecoenv.2018.09.059>
- Ghassemi-Golezani, K., Hassanzadeh, N., Shakiba, M.-R. and Esmailpour, B. 2020. Exogenous salicylic acid and 24-epi-brassinolide improve antioxidant capacity and secondary metabolites of *Brassica nigra*. *Biocatalysis and Agricultural Biotechnology*, 26: 101636. <https://doi.org/https://doi.org/10.1016/j.cbab.2020.101636>
- Haghighi, M., Khosravi, S., Sehar, S. and Shamsi, I. H. 2023. Foliar-sprayed calcium-tryptophan mediated improvement in physio-biochemical attributes and nutritional profile of salt stressed *Brassica oleracea* var. *italica*. *Scientia Horticulturae*, 307: 111529. <https://doi.org/https://doi.org/10.1016/j.scienta.2022.111529>
- Hasanuzzaman, M., Ahmed, N., Saha, T., Rahman, M., Rahman, K., Alam, M. M., Rohman, M. M. and Nahar, K. 2022. Exogenous salicylic acid and kinetin modulate reactive oxygen species metabolism and glyoxalase system to confer waterlogging stress tolerance in soybean (*Glycine max* L.). *Plant Stress*, 3: 100057. <https://doi.org/https://doi.org/10.1016/j.stress.2022.100057>
- Hayat, S., Maheshwari, P., Wani, A. S., Irfan, M., Alyemeni, M. N. and Ahmad, A. 2012. Comparative effect of 28 homobrassinolide and salicylic acid in the amelioration of NaCl stress in *Brassica juncea* L. *Plant Physiology and Biochemistry*, 53: 61–68. <https://doi.org/https://doi.org/10.1016/j.plaphy.2012.01.011>
- Hidangmayum, A., Dwivedi, P., Kumar, P. and Upadhyay, S. K. 2023. Seed priming and foliar application of chitosan ameliorate drought stress responses in mungbean genotypes through modulation of morpho-physiological attributes and increased antioxidative defense mechanism. *Journal of Plant Growth Regulation*, 42(10): 6137–6154. <https://doi.org/10.1007/s00344-022-10792-1>
- Huang, Q., Ayyaz, A., Farooq, M. A., Zhang, K., Chen, W., Hannan, F., Sun, Y., Shahzad, K., Ali, B. and Zhou, W. 2024. Silicon dioxide nanoparticles enhance plant growth, photosynthetic performance, and antioxidants defence machinery through suppressing chromium uptake in *Brassica napus* L. *Environmental Pollution*, 342: 123013. <https://doi.org/https://doi.org/10.1016/j.envpol.2023.123013>
- Huang, Y., Wang, H., Tang, G., Zhou, Z., Zhang, X., Liu, Y., Yan, G., Wang, J., Hu, G., Xiao, J., Yan, W. and Cao, Y. 2024. Fabrication of pH-responsive nanoparticles for co-delivery of fungicide and salicylic acid with synergistic antifungal activity. *Journal of Cleaner Production*, 451: 142093. <https://doi.org/https://doi.org/10.1016/j.jclepro.2024.142093>
- Hundare, A., Joshi, V. and Joshi, N. 2022. Salicylic acid attenuates salinity-induced growth inhibition in in vitro raised ginger (*Zingiber officinale* Roscoe) plantlets by regulating ionic balance and antioxidative system. *Plant Stress*, 4: 100070. <https://doi.org/https://doi.org/10.1016/j.stress.2022.100070>
- Idrees, M., Naeem, M., Aftab, T., Khan, M. M. A. and Moinuddin. 2013. Salicylic acid restrains nickel toxicity, improves antioxidant defence system and enhances the production of anticancer alkaloids in *Catharanthus roseus* (L.). *Journal of Hazardous Materials*, 252–253: 367–374. <https://doi.org/https://doi.org/10.1016/j.jhazmat.2013.03.005>
- Islam, S., Mohammad, F., Siddiqui, M. H. and Kalaji, H. M. 2023. Salicylic acid and trehalose attenuate salt toxicity in *Brassica juncea* L. by activating the stress defense mechanism. *Environmental Pollution*, 326: 121467.
- Islam, S., Shah, S. H., Corpas, F. J., Alamri, S. and Mohammad, F. 2023. Plant growth regulators mediated mitigation of salt-induced toxicities in mustard (*Brassica juncea* L.) by modifying the inherent defense system. *Plant Physiology and Biochemistry*, 196: 1002–1018. <https://doi.org/https://doi.org/10.1016/j.plaphy.2023.02.053>
- Jain, P., Farooq, B., Lamba, S. and Koul, B. 2020. Foliar spray of *Moringa oleifera* Lam. leaf extracts (MLE) enhances the stevioside, zeatin and mineral contents in *Stevia rebaudiana* Betoni. *South African Journal of Botany*, 132: 249–257. <https://doi.org/https://doi.org/10.1016/j.sajb.2020.03.026>
- Kaya, C., Ashraf, M., Alyemeni, M. N., Corpas, F. J. and Ahmad, P. 2020. Salicylic acid-induced nitric oxide enhances arsenic toxicity tolerance in maize plants by upregulating the ascorbate-glutathione cycle and glyoxalase system. *Journal of Hazardous Materials*, 399: 123020. <https://doi.org/https://doi.org/10.1016/j.jhazmat.2020.123020>
- Kaya, C., Ugurlar, F., Ashraf, M., Alyemeni, M. N. and Ahmad, P. 2023. Exploring the synergistic effects of melatonin and salicylic acid in enhancing drought stress tolerance in tomato plants through fine-tuning oxidative-nitrosative processes and methylglyoxal metabolism. *Scientia Horticulturae*, 321: 112368. <https://doi.org/https://doi.org/10.1016/j.scienta.2023.112368>
- Khalid, M. F., Elezz, A. A., Jawaid, M. Z. and Ahmed, T. 2023. Salicylic acid restricts mercury translocation by activating strong antioxidant defense mechanisms in sweet pepper (*Capsicum annum* L.). *Environmental Technology & Innovation*, 32: 103283. <https://doi.org/https://doi.org/10.1016/j.eti.2023.103283>
- Khan, M. M. A., Afreen, R., Quasar, N., Khanam, N. and Uddin, M. 2023. Steam-mediated foliar application of catechol and plant growth regulators enhances the growth attributes, photosynthesis, and essential oil production of lemongrass [*Cymbopogon flexuosus* (Steud.) Wats]. *Biocatalysis and Agricultural Biotechnology*, 48: 102638. <https://doi.org/https://doi.org/10.1016/j.cbab.2023.102638>
- Kumar, P., Latha, D. H. and Singh, J. 2023. Rhizoremediation of organic emerging soil contaminants: Green technology. In: *Clean Technologies Toward a Sustainable Future: Physicochemical, Biochemical and Biotechnological Approaches*, pp. 211–229. IWA Publishing. https://doi.org/10.2166/9781789063783_0211
- Kumar, P., Saini, L., & Sharma, M. 2023. Assessment of the phytochemical constituents and metabolites in the medicinal plants and herbal medicine used in the treatment and management of respiratory diseases. In: *Reference Series in Phytochemistry*, Vol. 2023. Springer Science and Business Media B.V. https://doi.org/10.1007/978-3-031-21973-3_19-1
- Kumari, P., Kumar, P. and Singh, J. 2023. Toxic contamination of aquatic habitat and its remediation. In: *Spatial Modeling of Environmental Pollution and Ecological Risk*, pp. 209–220. Elsevier. <https://doi.org/10.1016/B978-0-323-95282-8.00021-3>
- Li, Y., Wu, Y., Tang, Z., Xiao, X., Gao, X., Qiao, Y., Ma, J., Hu, L. and Yu, J. 2023. Exogenous brassinosteroid alleviates calcium deficiency induced tip-burn by regulating calcium transport in *Brassica rapa* L. ssp. *pekinensis*. *Ecotoxicology and Environmental Safety*, 251: 114534. <https://doi.org/https://doi.org/10.1016/j.ecoenv.2023.114534>
- More, S. J., Ravi, V., Sreekumar, J., Suresh Kumar, J. and Raju, S. 2023. Exogenous application of calcium chloride, 6-Benzyladenine and salicylic acid modulates morpho-physiological and tuber yield responses of sweet potato exposed to heat stress. *South African Journal of Botany*, 155: 60–78. <https://doi.org/https://doi.org/10.1016/j.sajb.2023.02.004>
- Nabizade, M., Astarai, A. R., Lakzian, A. and Taheri, M. al-R. 2023. *Pseudomonas putida* and salicylic acid key players: Impact on arsenic phytotoxicity of quinoa under soil salinity stress. *Biocatalysis and Agricultural Biotechnology*, 53: 102898. <https://doi.org/https://doi.org/10.1016/j.cbab.2023.102898>
- Nazar, R., Umar, S., Khan, N. A. and Sareer, O. 2015. Salicylic acid supplementation improves photosynthesis and growth in mustard through changes in proline accumulation and ethylene formation under drought stress. *South African Journal of Botany*, 98: 84–94.

- Osama, S., El Sherei, M., Al-Mahdy, D. A., Bishr, M. and Salama, O. 2019. Effect of Salicylic acid foliar spraying on growth parameters, β -pyrones, phenolic content and radical scavenging activity of drought stressed Ammi visnaga L. plant. *Industrial Crops and Products*, 134: 1–10. <https://doi.org/https://doi.org/10.1016/j.indcrop.2019.03.035>
- Panthi, U., McCallum, B., Kovalchuk, I., Rampitsch, C., Badea, A., Yao, Z. and Bilichak, A. (2024). Foliar application of plant-derived peptides decreases the severity of leaf rust (*Puccinia triticina*) infection in bread wheat (*Triticum aestivum* L.). *Journal of Genetic Engineering and Biotechnology*, 22(1): 100357. <https://doi.org/https://doi.org/10.1016/j.jgeb.2024.100357>
- Parashar, A., Yusuf, M., Fariduddin, Q. and Ahmad, A. 2014. Salicylic acid enhances antioxidant system in Brassica juncea grown under different levels of manganese. *International Journal of Biological Macromolecules*, 70: 551–558. <https://doi.org/https://doi.org/10.1016/j.ijbiomac.2014.07.014>
- Pirasteh-Anosheh, H., Rahimpour, B., Mohammadi, H., Ranjbar, G. and Race, M. 2023. Chapter 9 - Induced salinity tolerance by salicylic acid through physiological manipulations (M. Ozturk, R. A. Bhat, M. Ashraf, F. M. P. Tonelli, B. T. Unal, & G. H. B. T.-P. and S. R. S. M. Dar (eds.); pp. 99–109. Academic Press. <https://doi.org/https://doi.org/10.1016/B978-0-323-91883-1.00017-6>
- Saini, L., Sharma, K. and Kumar, P. 2023. Water efficiency in agriculture as a vital approach toward water management in rural areas. In: *Water Resources Management for Rural Development: Challenges and Mitigation*, pp. 127–138. Elsevier. <https://doi.org/10.1016/B978-0-443-18778-0.00020-9>
- Sangwan, P., Kumar, V., Gulati, D. and Joshi, U. N. 2015. Interactive effects of salicylic acid on enzymes of nitrogen metabolism in clusterbean (*Cyamopsis tetragonoloba* L.) under chromium(VI) toxicity. *Biocatalysis and Agricultural Biotechnology*, 4(3): 309–314. <https://doi.org/https://doi.org/10.1016/j.bcab.2015.06.001>
- Sharma, K., Devi, P., Dey, S. R. and Kumar, P. 2023. Mercury phytovolatilization: an overview of the mechanism and mitigation. In: *Role of Green Chemistry in Ecosystem Restoration to Achieve Environmental Sustainability*, pp. 325–331. Elsevier. <https://doi.org/10.1016/B978-0-443-15291-7.00031-6>
- Sharma, K., Devi, P. and Kumar, P. 2023. Metal-organic frameworks for wastewater contaminants removal. In: *Metal Organic Frameworks for Wastewater Contaminant Removal*, pp. 95–117. Wiley.
- Sharma, K., Devi, P., Kumar, P., Dey, A. and Dwivedi, P. 2023. Hazardous phytotoxic nature of reactive oxygen species in agriculture. In: *Reactive Oxygen Species: Prospects in Plant Metabolism*, pp. 135–146. Springer Nature. https://doi.org/10.1007/978-981-19-9794-5_8
- Sharma, M., Dey, S. R. and Kumar, P. 2023. Antioxidant Defence: a key mechanism of chromium tolerance. In: *Environmental Science and Engineering: F1975*: 91–116. Springer Science and Business Media Deutschland GmbH. https://doi.org/10.1007/978-3-031-44029-8_5
- Shohani, F., Hosseinin Sarghein, S. and Fazeli, A. 2023. Simultaneous application of salicylic acid and silicon in aerial parts of *Scrophularia striata* L. in response to drought stress. *Plant Physiology and Biochemistry*, 202: 107936. <https://doi.org/https://doi.org/10.1016/j.plaphy.2023.107936>
- Sinam, V., Kumar, P. and Singh, J. 2023. Bioremediation and ecorestoration strategies of aquatic environment. In: *Spatial Modeling of Environmental Pollution and Ecological Risk*, pp. 483–499. Elsevier. <https://doi.org/10.1016/B978-0-323-95282-8.00025-0>
- Sood, N., Sohal, B. S. and Lore, J. S. 2013. Foliar application of benzothiadiazole and salicylic acid to combat sheath blight disease of rice. *Rice Science*, 20(5): 349–355. [https://doi.org/https://doi.org/10.1016/S1672-6308\(13\)60155-9](https://doi.org/https://doi.org/10.1016/S1672-6308(13)60155-9)
- Tanveer, S., Akhtar, N., Ilyas, N., Sayyed, R. Z., Fitriatin, B. N., Perveen, K. and Bukhari, N. A. 2023. Interactive effects of *Pseudomonas putida* and salicylic acid for mitigating drought tolerance in canola (*Brassica napus* L.). *Heliyon*, 9(3): e14193. <https://doi.org/https://doi.org/10.1016/j.heliyon.2023.e14193>
- Thepbandit, W., Papathoti, N. K., Daddam, J. R., Hoang, N. H., Le Thanh, T., Saengchan, C., and Buensanteai, K. 2023. In vitro and in silico studies of salicylic acid on systemic induced resistance against bacterial leaf blight disease and enhancement of crop yield. *Journal of Integrative Agriculture*, 22(1): 170–184. <https://doi.org/https://doi.org/10.1016/j.jia.2022.08.112>
- Upadhyay, S. K., Devi, P., Kumar, V., Pathak, H. K., Kumar, P., Rajput, V. D. and Dwivedi, P. 2023. Efficient removal of total arsenic (As₃+As₅) from contaminated water by novel strategies mediated iron and plant extract activated waste flowers of marigold. *Chemosphere*, 313: 137551. <https://doi.org/https://doi.org/10.1016/j.chemosphere.2022.137551>
- Vioratti Telles de Moura, O., Luiz Louro Berbara, R., França de Oliveira Torchia, D., Fernanda Oliveira Da Silva, H., Augusto van Tol de Castro, T., Carlos Huertas Tavares, O., Fernandes Rodrigues, N., Zonta, E., Azevedo Santos, L. and Calderín García, A. 2023. Humic foliar application as sustainable technology for improving the growth, yield, and abiotic stress protection of agricultural crops. A review. *Journal of the Saudi Society of Agricultural Sciences*. <https://doi.org/https://doi.org/10.1016/j.jssas.2023.05.001>
- Wang, Q., Zhou, Q., Feng, Y. and Yang, X. 2024. Foliar application protected vegetable against poisonous element cadmium and mitigated human health risks. *Science of The Total Environment*, 926: 171915. <https://doi.org/https://doi.org/10.1016/j.scitotenv.2024.171915>
- Wang, S.Y., Jiang, Y.H., Chen, X., Herrera-Balandrano, D. D., Simoes, M. F., Shi, X.C. and Laborda, P. 2024. Biocontrol strategies for the management of *Sclerotinia sclerotiorum* in Brassica species: A review. *Physiological and Molecular Plant Pathology*, 130: 102239. <https://doi.org/https://doi.org/10.1016/j.pmp.2024.102239>
- Zhou, Q., Li, X., Zheng, X., Zhang, X., Jiang, Y. and Shen, H. 2024. Metabolomics reveals the phytotoxicity mechanisms of foliar spinach exposed to bulk and nano sizes of PbCO₃. *Journal of Hazardous Materials*, 465: 133097. <https://doi.org/https://doi.org/10.1016/j.jhazmat.2023.133097>
- Zulfikar, F., Moosa, A., Ferrante, A., Nafees, M., Darras, A., Nazir, M. M., AlShaqqaa, M. A. and Elsaid, F. G. 2023. Melatonin and salicylic acid synergistically improve arsenic induced oxidative stress tolerance in ornamental sword lily. *Scientia Horticulturae*, 322: 112389. <https://doi.org/https://doi.org/10.1016/j.scienta.2023.112389>



Assessing Riparian Floristic Diversity and Vegetation Dynamics in the Vamanapuram River Basin, Kerala: A Comprehensive Analysis

M. V. Vincy*[†] and R. Brilliant**

*Department of Microbiology and Biochemistry, St. Berchmans College, Changanacherry, Kerala, India

**Department of Environmental Sciences, St. John's College, Anchal, Kerala, India

†Corresponding author: M. V. Vincy; vincybrilliant@gmail.com

Nat. Env. & Poll. Tech.
Website: www.neptjournal.com

Received: 01-08-2023

Revised: 12-10-2023

Accepted: 14-10-2023

Key Words:

Vamanapuram river basin
Random sampling
Phytodiversity
Importance value index
Similarity index

ABSTRACT

The Vamanapuram River Basin (VRB) is home to a diverse range of plant species, including 152 distinct species from 50 botanical families. Poaceae, Leguminosae, Araceae, and Aseraceae are the most abundant, with 13 species. Euphorbiaceae, Acanthaceae, Apocynaceae, and Rubiaceae also contribute to the biodiversity hotspots. The VRB's vegetation profile is characterized by a dynamic interplay of plant forms and ecological niches, with 74 herbs, 30 shrubs, 12 grasses, 1 liana, and 35 towering trees. The Poaceae family thrives in this environment due to hydrological factors. The sampling sites P6 and P5 exhibit high relative frequency and density, with key species like *Macaranga peltata*, *Ficus hispida*, and *Swietenia macrophylla*. Diversity indices like the Shannon-Wiener diversity index reaffirm the VRB's tropical forest character. Beta-diversity patterns reveal unique plant species distribution dynamics among different panchayaths, emphasizing their ecological complexities. The study emphasizes the demand for specialized management and conservation techniques in this environmentally active region.

INTRODUCTION

The Western Ghats recognized as one of the planet's "hotspots" of biological diversity and a UNESCO World Heritage Site (Myers et al. 2000), stand as a global emblem of biodiversity and endemism (Daniels & Vencatesan 2008). Within this ecological treasure trove, the Western Ghats river basin boasts a wealth of riparian flora, encompassing a diverse array of plant species. These riparian zones, bridging terrestrial and aquatic systems, hold pivotal roles in ecosystem functionality and human well-being (Davis et al. 2006, Holmquist et al. 2011, Jonsson et al. 2017).

Streams and riparian zones serve as vital conduits for the movement of organisms across different landscapes, acting as dispersal routes for both terrestrial and aquatic species (Ament et al. 2014, Bennett et al. 2014, Tonkin et al. 2018). Renowned for their richness, dynamism, and complexity, riparian habitats represent some of the most diverse and intricate ecosystems on Earth yet remain exquisitely sensitive to environmental shifts (Naiman & Decamps 1997). These zones are the linchpin of river and stream ecosystems, nurturing essential functions such as the decomposition of organic matter, nutrient cycling, biological indicators of pollution, and the sustenance of ecological food chains (Holmquist et al. 2011, Jonsson et al. 2017).

Furthermore, riparian vegetation offers shading, influences water temperatures and light, impacts nutrient cycling, and stabilizes banks (Gregory et al. 1991, Naiman et al. 1993, 2000, 2010, Tang & Montgomery 1995, Prach et al. 2001, Hood & Naiman 2000).

Despite their ecological significance, rivers continue to be harnessed and controlled to meet the growing demands for energy, irrigation, water supply, and flood control driven by burgeoning human populations, rapid urbanization, and expanding industrial and commercial activities (Nilsson 2005, Lehner et al. 2011). In metropolitan areas, riparian vegetation often faces alteration or loss due to ecological disturbances within riverine watersheds (Morley & Karr 2002, Moore & Palmer 2005). The hydrological cycle, a lifeline for downstream human activities, is significantly impacted by agricultural practices, urbanization, river flow modifications, overexploitation, climate change, biological invasions (Singh et al. 2021), biodiversity depletion (Sultana et al. 2014), and stream pollution (Bere & Mangadze 2014, Schultz et al. 2004, Anbumozhi et al. 2005, Flores-Díaz et al. 2018).

Floral diversity, regardless of habitat type, remains essential for sustaining life on Earth (Cunningham et al. 2015), offering crucial insights for the identification and utilization of plant resources. A comprehensive

understanding of this subject forms the foundation for both fundamental and applied research. The southern region of the Western Ghats, characterized by its remarkable diversity of endemic species and floristic composition, stands at the forefront of these efforts. Given the current and anticipated scenarios of declining river health and global environmental changes, there is an urgent call for an integrated approach to riparian zone management (Singh et al. 2021). Close to water bodies, there often exists variation in plant species composition (Scalley et al. 2009), making the maintenance and conservation of riparian areas pivotal contributors to landscape diversity (Sabo et al. 2005).

The objective of this study is to identify and quantify plant species within the riparian zones of the Vamanapuram River Basin. It seeks to assess ecosystem health and monitor the dynamic changes in vegetation. The insights gleaned from this study hold the potential to inform conservation strategies, guide land management practices, promote habitat preservation and restoration, and support sustainable approaches while unraveling intricate ecological relationships within this critical ecosystem.

Study Area

The study area for the present research, the Vamanapuram River Basin (VRB), boasts a vast catchment area spanning 742.34 sq. km, situated within the geographical coordinates of 8°34'30" to 8°49'38" N latitudes and 76°43'47" to 77°12'08" E longitudes (Fig. 1). Originating from Chemmunji Mottai in the Western Ghats, approximately 1,717 m above mean sea level (msl), this 81-kilometer-long river gracefully flows into the Anjengo Lake within the coastal strand plains of Thiruvananthapuram district (Gopal et al. 2014). The VRB's northern boundary is marked by the Kallada River, while the Karamana River defines its southern limits, with the Ithikara River flowing between the Kallada and Vamanapuram rivers. For administrative and analytical purposes, the Vamanapuram watershed is further divided into 30 sub-watersheds and 52 micro watersheds (John & Brema 2018).

Physiographically, the VRB can be broadly categorized into three distinct zones. The first zone, characterized as the highland on the eastern side, ranges from 1,717 to 76 meters above msl. The second zone, known as the midland, lies between the lowland and highland areas, extending from 76 to 7.6 meters above msl. Lastly, the third zone, the lowland, occupies the western side and spans from 7.6 meters above msl to msl itself (Anon 1986). This area is a part of the midland terrain of the state, featuring lateritic uplands with undulating topography and intermittent valleys, as previously documented (Ajin et al. 2013).

The climatic conditions prevailing in this region are typical of a tropical monsoon climate, characterized by the southwest (SW) monsoon season, which occurs from June to September, and the northeast (NE) monsoon season, prevailing from November to February (Joi & Nair 2014).

The Western Ghats, encompassing the VRB, are renowned for their remarkable floral diversity. Nearly 5800 species of flowering plants have been meticulously documented in the Western Ghats, with an astonishing 56 genera and 2100 species being endemic to this region (http://wgbis.ces.iisc.ernet.in/biodiversity/sahyadri_enews/newsletter/issue38/article/index.htm). The evergreen forests within the Western Ghats harbor an exceptionally high percentage of species that are exclusively native to this region, with an estimated 1,500 endemic plant species (MacKinnon & MacKinnon 1986). Notably, among the evergreen tree species found here, 56% are endemic, solidifying the Western Ghats' status as one of the world's biodiversity hotspots (Myers 1988).

The Vamanapuram River Basin faces significant environmental challenges, with 87% of surface water samples exhibiting marginal water quality and 13% displaying poor quality. High *E. coli* counts and heavy nickel pollution are prevalent, exacerbated by sewage effluents and agricultural activities downstream (Nandakumar 2015). The ecosystem has been transformed by human intervention, with natural components like forests and water bodies being reduced and man-made components like plantations and roads emerging settlements (Gopal et al. 2018). River sediments show elevated iron and manganese concentrations and trace elements in sediment samples are higher than in water samples. These findings highlight the complex environmental challenges faced by the basin (Nair & Kumar 2019).

MATERIALS AND METHODS

Sampling and Data Collection

The comprehensive assessment of riparian floristic diversity and vegetation dynamics in the Vamanapuram River Basin was conducted for one year (2021-2022). The research design encompassed the strategic selection of six panchayaths labeled as P1 to P6, determined through extensive field surveys. Within each of these six panchayaths, a total of five distinct sites were carefully chosen for sampling. The vegetation study entailed meticulous fieldwork involving systematic placement of quadrats to capture the intricacies of the plant community. For the comprehensive evaluation of tree species, 10 × 10 m quadrats were established, whereas shrubs were examined within 5 × 5 m quadrats. Additionally, 1 × 1 m quadrats were designated for the assessment of herbaceous vegetation. The selection of

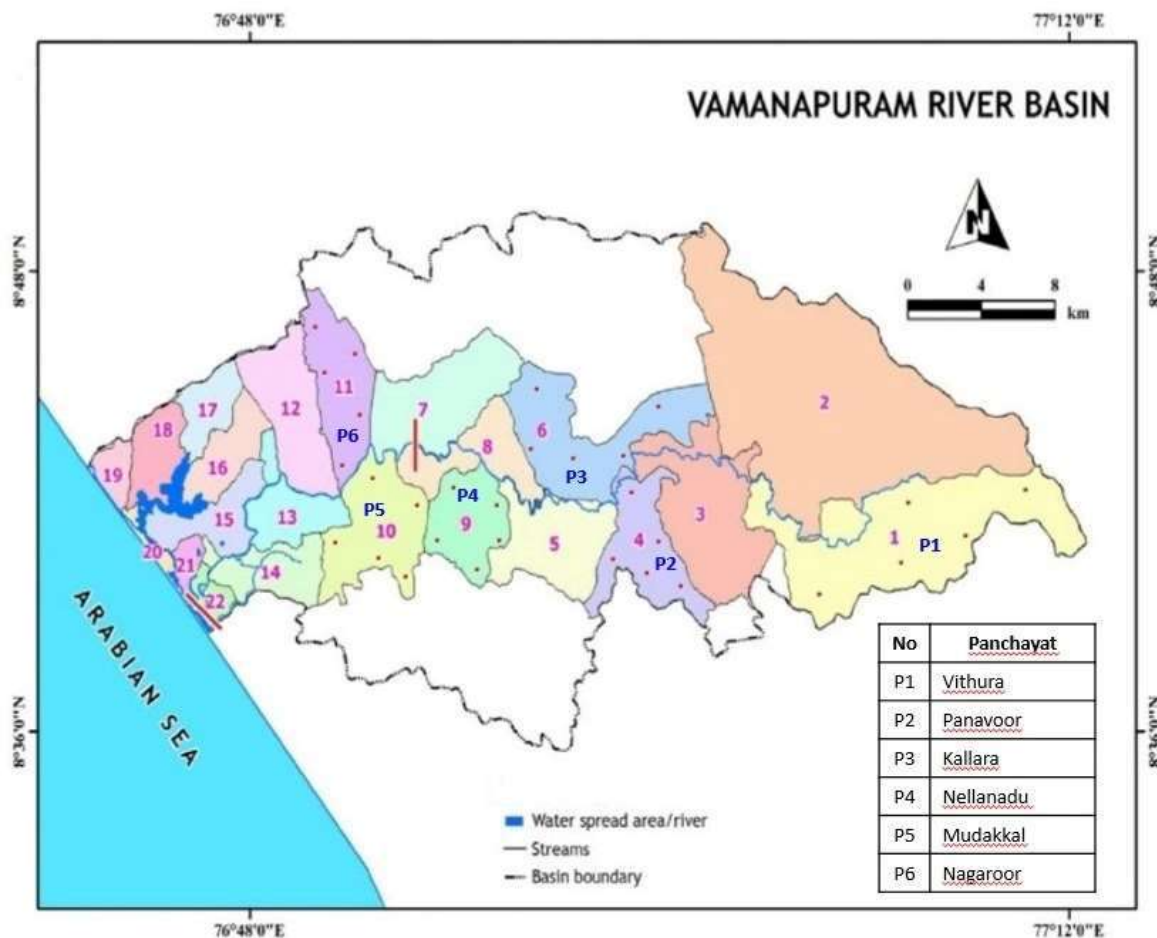


Fig. 1: Sampling sites of six locations of the Vamanapuram River Basin (Gopal et al. 2014).

sampling panchayaths within each site was randomized to ensure unbiased representation.

In the assessment of tree species, specific attention was given to enumerating the various species present within each 10×10 m quadrat. Additionally, the girth at breast height (gbh), situated at a standardized height of 1.37 m from the ground, was meticulously recorded for each tree, following the methodology established by Vincy et al. (2015). To derive meaningful analytical insights from the collected data, the approach outlined by Curtis & McIntosh (1950) was adopted. This methodology enabled the computation of crucial analytical parameters, including density, frequency, abundance, basal cover, and importance value (IV). The calculation of IV, a key determinant of species significance, adhered to the methodology outlined by Curtis (1959). This involved the summation of relative density, relative frequency, and relative dominance to establish the overall importance value for each species.

Biodiversity Indices

In the present study, a comprehensive suite of biodiversity indices was employed to unravel the intricacies of this unique ecosystem, guided by established methodologies (Danoff-Burg & Xu 2006). The Biodiversity Calculator was used to measure species diversity using Shannon's index (H'), which includes both abundance and evenness of species distribution (Danoff-Burg & Xu 2006). In addition to evaluating species richness (S), the evenness of species ($H'E$) using the same tool was also computed, as endorsed by Omoro et al. (2010).

The quest to unravel the similarities between species led us to Jaccard's index (Krebs 1989), offering insights into the shared botanical tapestry within the basin. Beyond these measures, a spectrum of univariate indices was meticulously scrutinized to illuminate different facets of biodiversity within the Vamanapuram River Basin. This array included the Shannon-Wiener diversity index (H') (Shannon & Weaver 1963), Margalef's species richness

(d) (Margalef 1968), Menhinick's Diversity Index (DMn) (Menhinick 1964), Pielou's evenness (J') (Pielou 1975), Simpson dominance (D) (Simpson 1949), Gini Coefficient (Damgaard & Weiner 2000), Berger-Parker Dominance Index (Magurran 1988, 2004, Morris et al. 2014), Buzas & Gibson's Index (Krebs & Berteaux 2006), and Fisher's alpha diversity index (Hammond & Pokorný 2020), each providing a unique lens through which to view the basin's ecological intricacies.

The Family Importance Value Index (FIV) was calculated by merging species with similar importance values (IVI) to gain a deeper understanding of their relative importance (Bano et al. 2017, Pereki et al. 2013). An analysis of variance was performed by one-way ANOVA among the six panchayaths within the Vamanapuram River Basin to determine density, frequency, and abundance. To unveil intricate interrelationships among these diversity indices, a correlation matrix was meticulously computed.

Similarity indices helped us understand the interspecific dynamics within plant communities. Both the Sorensen similarity index (Sorensen 1948, Nath et al. 2005) and the Jaccard similarity index (Magurran 2004) were instrumental in quantifying and comparing the resemblances among plant species. In the realm of beta diversity, the Sørensen Dissimilarity Index (β_{sor}) and Jaccard Dissimilarity Index (β_{jac}) were deployed to uncover and evaluate the differences in species composition across various sites. The Vamanapuram River Basin's distinctive plant assemblages were evaluated using these indices.

RESULTS AND DISCUSSION

Floristic Diversity

This comprehensive analysis includes methodologies designed to ensure sustainable protection of biodiversity, a crucial aspect of ecosystem health (Devi et al. 2014). Over a rigorous three-year period, an extensive phytosociological examination and an in-depth floristic study were conducted across six panchayaths situated within the Vamanapuram River Basin.

The floral composition serves as a valuable marker in the present investigation. It provides insights into the presence of diverse environmental elements that contribute to both inter- and intra-specific variations across a spectrum of endogenous environments (Amber et al. 2019). In recent years, many scholars have published floristic checklists of local plants (Peng et al. 2018, Leishangthem & Singh 2018, Ullah et al. 2020, Sahoo et al. 2020, Ghafari et al. 2020, Ao et al. 2021, Hodge et al. 2022, Zibtseva et al. 2022), providing insight into the rich botanical diversity within the region.

It is worth noting that the selected research location within the Vamanapuram River Basin possesses immense potential for nurturing a diverse array of plant species. This potential is attributed to the region's multifaceted topographic characteristics and microhabitats, which collectively contribute to the flourishing of rich and varied plant biodiversity.

Vegetation Profile and Community Structure

A comprehensive exploration of the basin's vegetation profile and community structure reveals a tapestry of remarkable richness, underscored by meticulous documentation (Table 1). A total of 152 distinct species were identified in this study, each belonging to one of 50 botanical families, thus encapsulating the rich floral tapestry of the basin. Among these families, several emerged as veritable hotspots of species diversity. Notably, Poaceae stood out with an impressive array of 13 distinct species, closely followed by Leguminosae with 12 species, Araceae with 10, and Asteraceae with 9. Additionally, Euphorbiaceae and Acanthaceae contributed 7 species each, while Apocynaceae showcased 6 unique species. Rubiaceae and Malvaceae held their own with 5 species each, adding further richness to the basin's botanical mosaic.

The distinctive vegetation profile of VRB reveals a dynamic interplay of plant forms and ecological niches. Within this profile, a diverse assemblage unfolds, featuring 74 herbs (48.68%), 30 shrubs (19.74%), 12 grasses (7.89%), 1 liana (0.66%), and 35 towering trees (23.03%) (Fig. 2). This diversity is a testament to the basin's intricate ecological dynamics, shaped in part by its periodic floodplain disturbances and the prevalence of wetland characteristics. It is noteworthy that members of the Poaceae family have particularly thrived in this unique vegetation profile. This phenomenon can be attributed to the basin's hydrological characteristics, as illuminated by Cherullipadi and Paul (2016).

As demonstrated by the species composition (Fig. 3), a pattern reminiscent of many river basins in Kerala emerges, with plants dominating the landscape, followed by trees and shrubs. This trend resonates with findings in other river basins within the state, such as Pamba (Paul & George 2010), Meenachil (Vincy et al. 2015), and Bharathappuzha (Cherullipadi & Paul 2016). A plausible explanation for the prominence of herbs and the relatively lower abundance of shrubs and climbers may be linked to seasonal clearings in plantations and agricultural areas, a phenomenon documented by Cherullipadi and Paul (2016).

Importance Value (IV)

The Importance Value (IV) calculation has proven to be a

Table 1: List of species and their families.

No.	Species	Family	Habit
1.	<i>Acacia auriculiformis</i> Benth.	Leguminosae	Tree
2.	<i>Acmella calva</i> (DC.) R.K.Jansen	Compositae	Herb
3.	<i>Acorus calamus</i> L.	Acoraceae	Herb
4.	<i>Adenanthera pavonina</i> L.	Leguminosae	Tree
5.	<i>Adiantum hispidulum</i> Sw.	Pteridaceae	Herb
6.	<i>Adiantum pedatum</i> L.	Pteridaceae	Herb
7.	<i>Aerva lanata</i> (L.) Juss.	Amaranthaceae	Herb
8.	<i>Aeschynomene indica</i> L.	Leguminosae	Herb
9.	<i>Aganosma cymosa</i> (Roxb.) G.Don	Apocynaceae	Liana
10.	<i>Ageratum conyzoides</i> (L.) L.	Asteraceae	Herb
11.	<i>Albizia chinensis</i> (Osbeck) Merr.	Leguminosae	Tree
12.	<i>Alloteropsis cimicina</i> (L.) Stapf	Poaceae	Grass
13.	<i>Alstonia scholaris</i> (L.) R. Br.	Apocynaceae	Tree
14.	<i>Alternanthera bettzickiana</i> (Regel) G.Nicholson	Amaranthaceae	Herb
15.	<i>Alternanthera sessilis</i> (L.) R.Br. ex DC.	Amaranthaceae	Herb
16.	<i>Amorphophallus paeoniifolius</i> (Dennst.) Nicolson	Araceae	Herb
17.	<i>Anacardium occidentale</i> L.	Anacardiaceae	Tree
18.	<i>Annona reticulata</i> L.	Annonaceae	Tree
19.	<i>Areca catechu</i> L.	Arecaceae	Tree
20.	<i>Artocarpus hirsutus</i> Lam.	Moraceae	Tree
21.	<i>Artocarpus heterophyllus</i> Lam.	Moraceae	Tree
22.	<i>Asystasia coromandeliana</i> Nees	Acanthaceae	Herb
23.	<i>Averrhoa bilimbi</i> L.	Oxalidaceae	Tree
24.	<i>Axonopus compressus</i> (Sw.) P.Beauv.	Poaceae	Grass
25.	<i>Azadirachta indica</i> A.Juss.	Meliaceae	Tree
26.	<i>Biophytum sensitivum</i> (L.) DC.	Oxalidaceae	Herb
27.	<i>Boerhavia diffusa</i> L.	Nyctaginaceae	Herb
28.	<i>Brachiaria ramosa</i> (L.) Stapf	Poaceae	Grass
29.	<i>Bridelia retusa</i> (L.) A.Juss.	Phyllanthaceae	Tree
30.	<i>Caladium bicolor</i> (Aiton) Vent.	Araceae	Herb
31.	<i>Calotropis gigantea</i> (L.) Dryand.	Apocynaceae	Shrub
32.	<i>Canscora diffusa</i> (Vahl) R.Br. ex Roem. & Schult.	Gentianaceae	Herb
33.	<i>Capsicum frutescens</i> L.	Solanaceae	Herb
34.	<i>Carica papaya</i> L.	Caricaceae	Tree
35.	<i>Caryota urens</i> L.	Arecaceae	Tree
36.	<i>Cassia alata</i> L.	Leguminosae	Herb

Table Cont....

No.	Species	Family	Habit
37.	<i>Catharanthus roseus</i> (L.) G.Don	Apocynaceae	Herb
38.	<i>Ceiba pentandra</i> (L.) Gaertn.	Malvaceae	Tree
39.	<i>Centella asiatica</i> (L.) Urb.	Apiaceae	Herb
40.	<i>Centrosema molle</i> Benth.	Leguminosae	Herb
41.	<i>Chromolaena odorata</i> (L.) R.M.King & H.Rob.	Compositae	Shrub
42.	<i>Chrysothemis pulchella</i> (Donn ex Sims) Decne.	Gesneriaceae	Herb
43.	<i>Cinnamomum verum</i> J.Presl	Lauraceae	Tree
44.	<i>Cleome rutidosperma</i> DC.	Cleomaceae	Herb
45.	<i>Cleome viscosa</i> L.	Capparidaceae	Herb
46.	<i>Clerodendrum infortunatum</i> L.	Lamiaceae	Shrub
47.	<i>Clidemia hirta</i> (L.) D. Don	Melastomataceae	Shrub
48.	<i>Cocos nucifera</i> L.	Araceae	Tree
49.	<i>Coffea arabica</i> L.	Rubiaceae	Shrub
50.	<i>Colocasia antiquorum</i> Schott	Araceae	Herb
51.	<i>Colocasia esculenta</i> (L.) Schott	Araceae	Herb
52.	<i>Commelina diffusa</i> Burm.f.	Commelinaceae	Herb
53.	<i>Costus speciosus</i> (J.Koenig) Sm.	Costaceae	Herb
54.	<i>Couroupita guianensis</i> Aubl.	Lecythidaceae	Tree
55.	<i>Crotalaria striata</i> DC.	Leguminosae	Herb
56.	<i>Cyclea peltata</i> (Lam.) Hook.f. & Thomson (Lam.) Hook. f. & Thoms.	Menispermaceae	Shrub
57.	<i>Cynodon dactylon</i> (L.) Pers.	Poaceae	Grass
58.	<i>Cyperus compressus</i> L.	Cyperaceae	Herb
59.	<i>Cyperus pangorei</i> Rottb.	Cyperaceae	Herb
60.	<i>Cyperus tenuispica</i> Steud.	Cyperaceae	Herb
61.	<i>Datura stramonium</i> L.	Solanaceae	Herb
62.	<i>Desmodium triflorum</i> (L.) DC.	Leguminosae	Herb
63.	<i>Dieffenbachia seguine</i> (Jacq.) Schott	Araceae	Herb
64.	<i>Eclipta prostrata</i> (L.) L.	Asteraceae	Herb
65.	<i>Eichhornia crassipes</i> (Mart.) Solms	Pontederiaceae	Herb
66.	<i>Elephantopus scaber</i> L.	Asteraceae	Herb
67.	<i>Emilia sonchifolia</i> (L.) DC. ex DC.	Asteraceae	Herb
68.	<i>Eragrostis unioides</i> (Retz.) Nees ex Steud.	Poaceae	Herb
69.	<i>Ficus hispida</i> L.f.	Moraceae	Tree
70.	<i>Ficus racemosa</i> L.	Moraceae	Tree
71.	<i>Heliotropium indicum</i> L.	Boraginaceae	Herb
72.	<i>Hemigraphis colorata</i> W.Bull	Acanthaceae	Herb
73.	<i>Hevea brasiliensis</i> (Willd. ex A.Juss.) Müll.Arg.	Euphorbiaceae	Tree

Table Cont....

No.	Species	Family	Habit
74.	<i>Hewittia malabarica</i> (L.) Suresh	Convolvulaceae	Herb
75.	<i>Hibiscus furcatus</i> Roxb.	Malvaceae	Shrub
76.	<i>Hibiscus hispidissimus</i> Griff.	Malvaceae	Shrub
77.	<i>Hygrophila ringens</i> (L.) R. Br. ex Spreng.	Acanthaceae	Herb
78.	<i>Hygrophila schulli</i> M.R.Almeida & S.M.Almeida	Acanthaceae	Herb
79.	<i>Hygroryza aristata</i> (Retz.) Nees ex Wight & Arn.	Poaceae	Grass
80.	<i>Hyptis suaveolens</i> (L.) Poit.	Lamiaceae	Herb
81.	<i>Ipomoea aquatica</i> Forssk.	Convolvulaceae	Shrub
82.	<i>Ipomoea triloba</i> L.	Convolvulaceae	Shrub
83.	<i>Ixora coccinea</i> L.	Rubiaceae	Shrub
84.	<i>Justicia adhatoda</i> L.	Acanthaceae	Shrub
85.	<i>Kirganelia reticulata</i> (Poir.) Baill.	Euphorbiaceae	Shrub
86.	<i>Kyllinga nemoralis</i> (J.R.Forst. & G.Forst.) Dandy ex Hutch. & Dalziel	Cyperaceae	Shrub
87.	<i>Lagenandra nairii</i> Ramam. & Rajan	Araceae	Herb
88.	<i>Lagenandra toxicaria</i> Dalzell	Araceae	Herb
89.	<i>Lantana camara</i> L.	Verbenaceae	Shrub
90.	<i>Leersia hexandra</i> Sw.	Poaceae	Grass
91.	<i>Leucas aspera</i> (Willd.) Link	Lamiaceae	Herb
92.	<i>Loranthus macrantherus</i> (Eichler) Hemsl.	Loranthaceae	Herb
93.	<i>Ludwigia hyssopifolia</i> (G.Don) Exell	Onagraceae	Herb
94.	<i>Macaranga peltata</i> (Roxb.) Muell.-Arg.	Euphorbiaceae	Tree
95.	<i>Mangifera indica</i> L.	Anacardiaceae	Tree
96.	<i>Manihot esculenta</i> Crantz	Euphorbiaceae	Shrub
97.	<i>Melastoma malabathricum</i> L.	Melastomataceae	Shrub
98.	<i>Merremia tridentata</i> (L.) Hallier f.	Convolvulaceae	Herb
99.	<i>Mikania micrantha</i> Kunth	Asteraceae	Herb
100.	<i>Mimosa pudica</i> L.	Leguminosae	Shrub
101.	<i>Mimosa diplotricha</i> Sauvalle	Leguminosae	Shrub
102.	<i>Mitracarpus verticillatus</i> (Schumach. & Thonn.) Vatke	Rubiaceae	Herb
103.	<i>Mukia maderaspatana</i> (L.) M.Roem.	Cucurbitaceae	Herb
104.	<i>Murdannia loriformis</i> (Hassk.) R.S.Rao & Kammathy	Commelinaceae	Herb
105.	<i>Musa paradisiaca</i> L.	Musaceae	Herb
106.	<i>Ocimum sanctum</i> L.	Lamiaceae	Herb
107.	<i>Oplismenus hirtellus</i> (L.) P.Beauv.	Poaceae	Grass
108.	<i>Oxalis corniculata</i> L.	Oxalidaceae	Herb
109.	<i>Pachystachys coccinea</i> (Aubl.) Nees	Acanthaceae	Shrub

Table Cont....

No.	Species	Family	Habit
110.	<i>Passiflora foetida</i> L.	Passifloraceae	Shrub
111.	<i>Pennisetum polystachion</i> (L.) Schult.	Poaceae	Grass
112.	<i>Phyllanthus amarus</i> Schum. & Thonn.	Phyllanthaceae	Herb
113.	<i>Phyllanthus emblica</i> L.	Phyllanthaceae	Tree
114.	<i>Physalis minima</i> L.	Solanaceae	Herb
115.	<i>Piper nigrum</i> L.	Piperaceae	Herb
116.	<i>Pothos scandens</i> L.	Araceae	Herb
117.	<i>Psidium guajava</i> L.	Myrtaceae	Tree
118.	<i>Psychotria curviflora</i> Wall.	Rubiaceae	Herb
119.	<i>Pueraria phaseoloides</i> (Roxb.) Benth.	Leguminosae	Shrub
120.	<i>Ricinus communis</i> L.	Euphorbiaceae	Shrub
121.	<i>Ruellia prostrata</i> Poir.	Acanthaceae	Herb
122.	<i>Saccharum spontaneum</i> L.	Poaceae	Grass
123.	<i>Sauropus androgynus</i> (L.) Merr.	Phyllanthaceae	Shrub
124.	<i>Sebastiania chamaelea</i> (Linn.) Müll. Arg.	Euphorbiaceae	Herb
125.	<i>Setaria barbata</i> (Lam.) Kunth	Poaceae	Grass
126.	<i>Setaria pumila</i> (Poir.) Roem. & Schult.	Poaceae	Grass
127.	<i>Sida cordifolia</i> L.	Malvaceae	Shrub
128.	<i>Solanum torvum</i> Sw.	Solanaceae	Shrub
129.	<i>Spermacoce ocymoides</i> Burm.f.	Rubiaceae	Herb
130.	<i>Spilanthes acmella</i> (L.) L.	Asteraceae	Herb
131.	<i>Spirodela polyrrhiza</i> (L.) Schleid.	Araceae	Herb
132.	<i>Stachytarpheta indica</i> (L.) Vahl	Verbenaceae	Shrub
133.	<i>Swietenia macrophylla</i> King	Meliaceae	Tree
134.	<i>Swietenia mahagoni</i> (L.) Jacq.	Meliaceae	Tree
135.	<i>Synedrella nodiflora</i> (L.) Gaertn	Asteraceae	Herb
136.	<i>Syngonium podophyllum</i> Schott	Araceae	Herb
137.	<i>Syzygium chavaran</i> (Bour.) Gamble	Myrtaceae	Tree
138.	<i>Syzygium cumini</i> (L.) Skeels	Myrtaceae	Tree
139.	<i>Syzygium samarangense</i> (Blume) Merr. & L.M.Perry	Myrtaceae	Tree
140.	<i>Tabernaemontana alternifolia</i> L.	Apocynaceae	Tree
141.	<i>Tamarindus indica</i> L.	Leguminosae	Tree
142.	<i>Terminalia paniculata</i> Roth	Combretaceae	Tree
143.	<i>Terminalia arjuna</i> (Roxb. ex DC.) Wight & Arn.	Combretaceae	Tree
144.	<i>Tragia involucrata</i> L.	Euphorbiaceae	Herb
145.	<i>Tridax procumbens</i> L.	Asteraceae	Herb
146.	<i>Urena lobata</i> L.	Malvaceae	Shrub

Table Cont....

No.	Species	Family	Habit
147.	<i>Vetiveria zizanioides</i> (L.) Nash	Poaceae	Grass
148.	<i>Wattakaka volubilis</i> (L. f.) Stapf	Apocynaceae	Shrub
149.	<i>Wedelia chinensis</i> (Osbeck) Merr.	Asteraceae	Herb
150.	<i>Zingiber zerumbet</i> (L.) Roscoe ex Sm.	Zingiberaceae	Herb
151.	<i>Ziziphus oenopolia</i> (L.) Mill. (L.) Mill.	Rhamnaceae	Shrub
152.	<i>Ziziphus rugosa</i> Lam.	Rhamnaceae	Tree

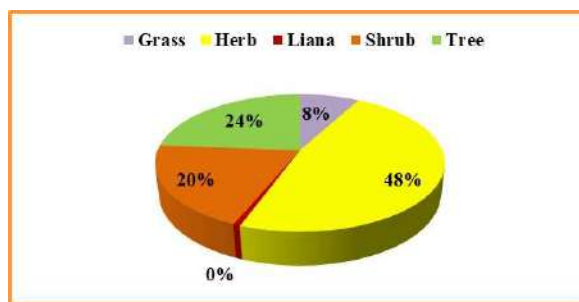


Fig. 2: Vegetation profile of Vamanapuram River Basin.



Fig. 3: Floristic composition.

crucial tool for understanding species’ ecological significance across different vegetation types, a methodology aligned with the findings of Vincy et al. (2015). The analytical framework involved computing both the relative frequency and relative density of all species observed across the six panchayaths. It is noteworthy that P6 exhibited notably high relative frequency, while P5 emerged with the highest relative density, shedding light on the distinctive ecological dynamics of these regions (Table 2).

Many tree species stood out with impressively high Importance Values (IVs) when we focused on their botanical exemplars. Notably, *Macaranga peltata*, *Ficus hispida*, and *Swietenia macrophylla* exhibited the most robust IVs within this category (Table 3). Their impressive Relative Importance Value Index (RIVI) scores further underscored

their ecological prominence, with *Macaranga peltata* leading the way with a score of 10.68, followed closely by *Ficus hispida* (10.57) and *Swietenia macrophylla* (8.31) (Table 3).

Table 2: Herbs, grass, shrubs, and trees of six panchayaths.

	F	D	A	RF	RD
P1	764	25.96	190.97	329.26	99.98
P2	633.32	21.66	196.39	284.87	100.03
P3	612.57	19.13	172.67	257.69	99.25
P4	541.72	18.07	177.89	236.36	99.94
P5	652.25	22.09	316.01	227.48	100.04
P6	637.51	22.94	186.83	337.83	100.02

Table 3: IVI and RIVI for tree species.

Tree species	GBH	TBA	IVI	RIVI
<i>Acacia auriculiformis</i> Benth.	279.46	6.12	1.92	0.64
<i>Adenanthera pavonina</i> L.	1139.82	102.02	6.21	2.07
<i>Albizia chinensis</i> (Osbeck) Merr.	172.7	2.34	5.31	1.77
<i>Alstonia scholaris</i> (L.) R. Br.	1227.74	118.33	13.82	4.61
<i>Anacardium occidentale</i> L.	1073.88	90.53	4.3	1.43
<i>Annona reticulata</i> L.	266.9	5.59	2.63	0.88
<i>Areca catechu</i> L.	1067.6	89.47	2.77	0.92
<i>Artocarpus heterophyllus</i> Lam.	3111.74	760.11	16.46	5.49
<i>Artocarpus hirsutus</i> Lam.	361.1	10.24	4.27	1.42
<i>Averrhoa bilimbi</i> L.	69.08	0.37	2.5	0.83
<i>Azadirachta indica</i> A.Juss.	78.5	0.48	9.1	3.03
<i>Bridelia retusa</i> (L.) A.Juss.	109.9	0.95	7.68	2.56
<i>Carica papaya</i> L.	204.1	3.27	1.09	0.36
<i>Caryota urens</i> L.	2885.66	653.67	16.11	5.37
<i>Ceiba pentandra</i> (L.) Gaertn.	1099	94.81	2.83	0.94
<i>Cinnamomum verum</i> J.Presl	335.98	8.86	1.34	0.45
<i>Cocos nucifera</i> L.	960.84	72.47	4.94	1.65
<i>Couroupita guianensis</i> Aubl.	439.6	15.17	3.13	1.04
<i>Ficus hispida</i> L.f.	1318.8	136.53	31.71	10.57
<i>Ficus racemosa</i> L.	376.8	11.15	7.96	2.65
<i>Hevea brasiliensis</i> (Willd. ex A.Juss.) Müll.Arg.	7096.4	3953.17	15.34	5.11
<i>Macaranga peltata</i> (Roxb.) Muell.-Arg.	4314.36	1461.18	32.05	10.68
<i>Mangifera indica</i> L.	1943.66	296.56	7.33	2.44
<i>Phyllanthus emblica</i> L.	471	17.41	1.61	0.54
<i>Psidium guajava</i> L.	282.6	6.27	2.63	0.88
<i>Swietenia macrophylla</i> King	6744.72	3571.06	24.93	8.31
<i>Swietenia mahagoni</i> (L.) Jacq.	4804.2	1811.81	15.74	5.25
<i>Syzygium chavarana</i> (Bourd.) Gamble	78.5	0.48	2.23	0.74
<i>Syzygium cumini</i> (L.) Skeels	408.2	13.08	1.49	0.5
<i>Syzygium samarangense</i> (Blume) Merr. & L.M.Perry	47.1	0.17	0.78	0.26
<i>Tabernaemontana alternifolia</i> L.	134.706	1.42	11.38	3.79
<i>Tamarindus indica</i> L.	1296.82	132.02	4.61	1.54
<i>Terminalia arjuna</i> (Roxb. ex DC.) Wight & Arn.	3501.1	962.23	9.73	3.24
<i>Terminalia paniculata</i> Roth	3579.6	1005.86	8.36	2.79
<i>Ziziphus rugosa</i> Lam.	36.424	0.104	6.14	2.05

Intriguing patterns of family-level Importance Value (FIV) emerged as well, shedding light on the collective ecological significance of plant families within the basin. Moraceae emerged as a standout with a notably high FIV of 60.4, followed by Meliaceae (49.77), Malvaceae (43.67), and Euphorbiaceae (47.39) (Fig. 4). These findings accentuate

the invaluable role played by these families in shaping the basin's unique ecological fabric.

The Importance of Value Index calculations, encapsulating a species' ecological relevance within this ecosystem, holds profound implications for species conservation and management strategies. Those species manifesting lower

Table 4: ANOVA of F, D, A.

	F	p-value
P1	74.17	< 0.00001
P2	74.76	
P3	117.19	
P4	95.7	
P5	62.43	
P6	52.95	

IVI values warrant heightened attention and protective measures, an imperative underscored by Kacholi (2013). Furthermore, our meticulous analysis, as supported by one-way ANOVA results (Table 4), has brought to light significant differences among the six panchayaths in terms of species frequency, density, and abundance. These variations underscore the intricacies of the basin's ecological tapestry and further underscore the need for tailored conservation and management strategies to safeguard its biodiversity.

Species Diversity, Concentration of Dominance and Evenness

The Shannon-Wiener diversity index values exhibited a range from 3.42 to 3.78 across the studied panchayaths (Table 5). Notably, Panchayaths 5 (P5) and 1 (P1) recorded the highest diversity index values. It is noteworthy that these values align with the diversity index range reported for tropical forests in India, as documented by Singh et al. (1984), which spans from 0.83 to 4.1. This convergence underscores the tropical forest character of the Vamanapuram River Basin. However, it is essential to emphasize that the quantification of diversity based solely on species richness or density provides only a partial view of the intricate diversity patterns, which can vary depending on the measurement method, as elucidated by Gotelli & Colwell (2001).

Moving on to Simpson's index of diversity, the values ranged from 0.96 (P6) to 0.97 (P1-P5), while Simpson's reciprocal index ranged from 25 (P6) to 33.33 (P1-P5). The concentration of dominance (Cd) showed variation, ranging from 0.03 (P1-P4) to 0.05 (P6) (Table 5). This range of Cd values observed in the present study aligns well with the reported range for tropical forests, as documented by Knight (1975), with an average Cd value of 0.06. Further, Cd levels in India's tropical forests have been reported to vary from 0.21 to 0.92, consistent with the findings of Parthasarathy et al. (1992) and Visalakshi (1995).

Moreover, the analysis encompassed additional diversity indices, each shedding light on distinct facets of ecological richness. The Menhinick's Diversity Index spanned from 2.22 (P6) to 2.93 (P5), the Margalef Richness Index ranged from 8.08 (P6) to 10.43 (P5), and the Gini Coefficient exhibited variation from 0.31 (P4) to 0.49 (P2). The Berger-Parker Dominance Index spanned from 0.05 (P14) to 0.15 (P6), while the Buzas and Gibson's Index ranged from 0.06 (P2, P3, P5) to 0.07 (P1, P4, and P6). Furthermore, the Fisher's alpha diversity index showcased a range from 14.09 (P6) to 20.21 (P5), and the Pielou's Evenness Index displayed a variation from 0.86 (P2) to 0.94 (P4) (Table 5).

The concentration of dominance exhibited noteworthy correlations, with Simpson's index (0.88) and Berger-Parker Dominance Index (0.96), as revealed by the correlation matrix computed for the diversity indices. Additionally, Menhinick's Diversity Index and Margalef Richness Index exhibited a robust association (0.9), with both demonstrating a strong correlation with Fisher's Alpha Diversity Index (0.96 and 0.99, respectively) (Table 6).

Similarity Indices

The complexities of similarity indices were investigated as part of a comprehensive study to better understand how different panchayaths interact with different plants (Kiran

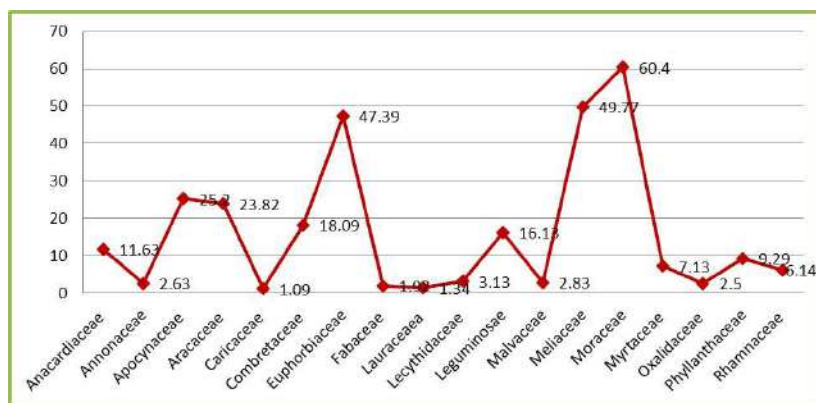


Fig. 4: FIV of families of tree species.

Table 5: Alpha diversity.

	P1	P2	P3	P4	P5	P6
Simpson's index	0.03	0.03	0.03	0.03	0.03	0.04
Simpson's index of diversity	0.97	0.97	0.97	0.97	0.97	0.96
Simpson's reciprocal index	33.33	33.33	33.33	33.33	33.33	25
Concentration of dominance	0.03	0.03	0.03	0.03	0.04	0.05
Heterogeneity	1.004	0.97	0.97	0.99	1.004	1.019
Menhinick's Diversity Index	2.28	2.33	2.66	2.6	2.93	2.22
Margalef Richness Index	8.8	8.32	9.14	8.73	10.43	8.08
Gini Coefficient	0.46	0.49	0.42	0.31	0.38	0.46
Berger-Parker Dominance Index	0.05	0.08	0.06	0.06	0.12	0.15
Buzas & Gibson's Index	0.07	0.06	0.06	0.07	0.06	0.07
Fisher's alpha diversity index	15.41	14.77	17.16	16.27	20.21	14.09
Shannon-Wiener index (H)	3.78	3.42	3.66	3.75	3.78	3.45
Pielou's Evenness Index	0.93	0.86	0.91	0.94	0.9	0.87

Table 6: Correlation of diversity indices.

	D	SDI	1/D	Cd	H	DMn	MRI	Gc	d	S	S _D	H'	E
D	1	-1	-1	0.88	0.64	0.51-	0.49-	0.3	0.78	0.45	0.5-	0.56-	-0.49
SDI		1	1	-0.88	-0.64	0.51	0.49	-0.3	-0.78	0.45-	0.5	0.56	0.49
1/D			1	-0.88	-0.64	0.51	0.49	-0.3	-0.78	0.45-	0.5	0.56	0.49
Cd				1	0.76	0.12-	0.5-	0.14	0.96	0.22	-0.06	0.35-	-0.49
H					1	0.18-	0.03	-0.04	0.62	0.63	-0.04	0.15	0.04
DMn						1	0.9	-0.66	-0.02	-0.55	0.96	0.59	0.32
MRI							1	-0.44	0.03	0.5-	0.99	0.69	0.3
Gc								1	0.17	-0.17	-0.53	-0.64	-0.68
d									1	0	0.03	-0.44	-0.64
S										1	-0.53	0.13	0.4
S _D											1	0.66	0.31
H'												1	0.89
E													1

et al. 2015). The concept of beta-diversity, hinging on the number of shared species between two assemblages, unveiled distinct patterns of plant species distribution. It was reported that P1 had 58 species of plants, whereas P2 had 54. Surprisingly, P1 and P2 shared a total of 28 plant species. However, P2 harbored 26 unique plant species not found in P1, while P1 held 30 distinct plant species absent in P2.

The landscapes of P5 and P6 featured 66 and 52 plant species, respectively. Remarkably, P5 and P6 exhibited

a shared roster of 30 plant species, attaining a Sorensen similarity index of 50.86%. These findings underscored the unique ecological dynamics within the basin, as certain panchayaths showcased a higher degree of plant species overlap. However, it is crucial to note that only specific comparisons yielded Sorensen's similarity indices above the 50% threshold. These comparisons, encompassing P1 and P2, P1 and P5, P1 and P6, and P5 and P6, unveiled values exceeding 50% for plant species similarity, providing valuable insights into the basin's ecological affinities.

Table 7: Similarity indices.

	Coefficient of Jaccard, S%					Coefficient of Sorensen, K%					
	P2	P3	P4	P5	P6	P2	P3	P4	P5	P6	
P1	20	11.45	16.91	20	21.98	P1	50	25.86	40.71	50	56.36
P2	0	13.84	18.05	18.37	18.46	P2	0	32.14	44.04	45	45.28
P3		0	13.08	13.89	13.39	P3		0	30.09	32.26	30.91
P4			0	16.55	13.71	P4			0	39.67	31.78
P5				0	20.27	P5				0	50.85

In contrast, none of the panchayaths exhibited values above 50% in terms of the Jaccard similarity index for plant species. Notably, P1 and P6 showed the highest value of 21.98%, closely followed by P5 and P6, with 20.27%. Conversely, P1 and P3 exhibited the lowest similarity, with a figure of 11.4%. P1, housing 58 plant species, showcased a 31-species overlap with P6, which held 52 species. Furthermore, P1 listed 27 plant species unobserved in P6, while P6 featured 21 species yet to be discovered in P1.

Table 7 presents a comprehensive overview of Sorensen's similarity indices across the six panchayaths. Beta diversity assessments, aligning with the methodology proposed by Ariyo (2007) and Ariyo et al. (2013), unveiled a range of Sorensen's similarity indices, ranging from 56.36% to 25.86%. Notably, P1 and P6 exhibited the highest similarity indices at 56.36%, followed by P5 and P6, P1 and P2, and P1 and P5, all hovering around the 50% mark. Conversely, P4 and P5, P3 and P5, P3 and P4, and P3 and P6 displayed lower similarity indices of 39.67%, 32.26%, 30.09%, and 30.91%, respectively. The comparison between P1 and P3 yielded the lowest similarity index at 25.86%. This striking variation in similarity indices underlines the unique ecological contexts of these panchayaths.

Dissimilarity Indices

Specifically, panchayaths P1 and P3 exhibited a pronounced dissimilarity index of 74.14%, marking a stark departure from the similarity indices observed earlier in Table 8. The dissimilarity indices for panchayath pairs, such as P2 and P3, P3 and P5, P4 and P5, and P3 and P6, showcased values ranging from 67.86% to 60.33%. P1 and P4, meanwhile, exhibited a dissimilarity score of 59.29%, while P1 and P6 registered the lowest dissimilarity value at 43.64%. These dissimilarity indices highlight the diversity of plant communities within the basin, reflecting the varying compositions of plant species.

To contextualize these findings, it is worth noting that different plant communities, based on their degree of similarity, can be amalgamated to form associations of distinct plant species. Researchers such as Chao et al.

(2006, 2008) and Muller-Dumbois & Ellenberg (1974) have classified groups with less than 65% similarity as distinct entities. This variability in similarity indices is indicative of the fluctuating competitive capacities of seedlings, contingent upon the ever-changing prospects for regeneration, which in turn are influenced by the fluctuating floristic and structural compositions from one community to another (Barker & Kirkpatrick 1994). The numerous edaphic and microclimatic factors that diverge across different tropical forest types exert significant impacts on recruitment, growth, and survival, as elucidated by Augspurger (1984). A higher similarity index value, conversely, signifies relatively homogenous environmental conditions, while a lower value signifies pronounced variability, according to Ekta (2012).

The UPGMA algorithm was employed to construct a dendrogram that aids in hierarchical clustering to unravel the complex patterns of similarity and dissimilarity (Odum 1969). This dendrogram not only enables the analysis of the degree of similarity between VRB sites in percentage but also reveals the natural groupings of species across different sites. The dendrogram vividly portrays that locations within the same groupings exhibit significantly greater similarity than those in dissimilar groups. It further highlights the organic clustering and relatedness of P4 and P6, as well as P1 and P3. These dendrogram-based insights provide a visual representation of the degree of similarity among various VRB locations, as showcased in Fig. 5.

Statistical Analysis of Beta Diversity

Table 8: Dissimilarity Indices.

	P2	P3	P4	P5	P6
P1	50	74.14	59.29	50	43.64
P2	0	67.86	55.96	55	54.72
P3		0	69.91	67.74	60.09
P4			0	60.33	68.22
P5				0	49.15
P6					0

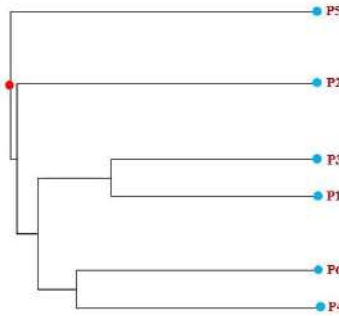


Fig. 5: Dendrogram.

Statistical analysis of beta diversity showed higher dissimilarity indices ($\sum X^2 = 189350.65$, $\sigma = 108.17$) concerning Jaccard ($\sum X^2 = 507.47$, $\sigma = 8.23$) and Sorensen similarity indices ($\sum X^2 = 4853.68$, $\sigma = 14.71$) (Table 9). One Way ANOVA analysis showed a significant difference in beta diversity ($F = 10.76$, $p = 0.003$) (Table 10).

CONCLUSION

The Vamanapuram River Basin (VRB) is home to 152 plant species from 50 different botanical families, revealing its rich biodiversity and intricate ecological dynamics. The basin is home to 13 species of Poaceae, 12 species of Leguminosae, 10 species of Araceae, and 9 species of Asteraceae. The vegetation profile includes 74 herbs, 30 shrubs, 12 grasses, 1 liana, and 35 towering trees, displaying a dynamic mix of plant forms and ecological niches. Wetland characteristics and periodic disturbances of floodplains influence this diversity, promoting the proliferation of Poaceae. Many key plant species were found to be ecologically dominant, including *Macaranga peltata*, *Ficus hispida*, and *Swietenia*

Table 9: Statistical analysis of beta diversity.

	Jaccard	Sorensen	Dissimilarity	Total
$\sum X$	31.86	150.44	886.05	1068.35
Mean	5.31	25.07	147.68	59.35
$\sum X^2$	507.47	4853.68	189350.65	194711.8
Std.Dev.	8.23	14.71	108.17	87.88

Table 10: One Way ANOVA of beta diversity.

Source	SS	df	MS	F	p-value
Between-treatments	71379.24	2	35689.62	$F = 10.76$	0.003
Within-treatments	59923.25	15	3994.88		
Error	33164.61	10	3316.46		

macrophylla. Diversity indices, including Shannon-Wiener, show a high degree of diversity in P5 and P1. Conserving and managing VRB's biodiversity and ecological dynamics is highly important, highlighting the need for customized conservation and management strategies. Having a better understanding of VRB's unique flora and how ecosystem-based conservation and management are crucial to the region's sustainability.

REFERENCES

- Ajin, R., Krishnamurthy, R.R., Jayaprakash, M. and Vinod, P.G. 2013. Flood hazard assessment of Vamanapuram River Basin, Kerala, India: An approach using remote sensing & GIS techniques. *Adv. Appl. Sci. Res.*, 4(3): 263-274.
- Amber, K., Khan, K.R., Shah, A.H., Farooq, M., Lodhi, M.H. and Shah, G.M. 2019. A comprehensive survey of floristic diversity evaluating the role of institutional gardening in the conservation of plant biodiversity. *Int. J. Biosci.*, 14(3): 325-39.
- Ament, R., Callahan, R., McClure, M., Reuling, M. and Tabor, G. 2014. *Wildlife Connectivity: Fundamentals for Conservation Action*, Center for Large Landscape Conserv., Bozeman, Montana. <https://doi.org/10.13140/RG.2.1.3958.0561>
- Anbumozhi, V., Radhakrishnan, J. and Yamaji, E. 2005. Impact of riparian buffer zones on water quality and associated management considerations. *Ecol. Eng.*, 24: 517-523.
- Anon. 1986. *Gazetteer of India, Kerala State Gazetteer*. Govt. of Kerala, Thiruvananthapuram.
- Ao, A., Changkija, S. and Tripathi, S.K. 2021. Stand structure, community composition, and tree species diversity of sub-tropical forest of Nagaland, Northeast India. *Trop. Ecol.*, 62(4): 549-62.
- Ariyo, O.C. 2007. *Economic Botany Survey of International Institute of Tropical Agriculture (IITA) Forest, Ibadan, Nigeria*. Dissertation Department of Forestry and Wildlife Management, Federal University of Agriculture, Abeokuta, Ogun State, Nigeria, p. 61.
- Ariyo, O.C., Oluwalana, S.A., Faleyimu, O.I. and Ariyo, M.O. 2013. Assessment of vegetation structural diversity and similarity index of IITA forest reserve in Ibadan, Oyo state, Nigeria. *Agrosearch*, 12(2): 135-157.
- Bano, M., Ahmed, B., Urfan, M. and Ansari, M. 2017. Ecological studies on some herbs and shrubs of the Paniyali range of Kotdwara region, Uttarakhand, India. 2. 2455-541X.
- Barker, P.C.J. and Kirkpatrick, J.B. 1994. *Phyllocladus asplenifolius*: Variability in the population structure, the regeneration niche and dispersion patterns in Tasmanian forests. *Aust. J. Bot.*, 42(2): 163-190.
- Bennett, A.F., Nimmo, D.G. and Radford, J.Q. 2014. Riparian vegetation

- has disproportionate benefits for the landscape-scale conservation of woodland birds in highly modified environments. *J. Appl. Ecol.*, 51: 514-523.
- Bere, T. and Mangadze, T. 2014. Diatom communities in streams draining urban areas: community structure in relation to environmental variables. *Trop. Ecol.*, 55: 271-281.
- Chao, A., Chazdon, R.L., Colwell, R.K. and Shen, T.J. 2006. Abundance-based similarity indices and their estimation when there are unseen species in samples. *Biometrics*, 62: 361-371.
- Chao, K.J., Phillips, O.L. and Baker, T.R. 2008. Wood density and stocks of coarse woody debris in a north-western Amazonian landscape. *Can. J. For. Res.*, 38: 795-825.
- Cherullipadi, L.B. and Paul, J. 2016. Diversity of herbaceous riparian flora in the lower stretch of Bharathappuzha River, Kerala. *S. Indian J. Biol. Sci.*, 2: 191. 10.22205/sijbs/2016/v2/i1/100392.
- Cunningham, S.C., Nally, R.M., Baker, P.J., Cavagnaro, T.R., Beringer, J., Thomson, J.R. and Thompson, R.M. 2015. Balancing the environmental benefits of reforestation in agricultural regions. *Perspect. Pl. Ecol. Evol. Syst.*, 17(4): 301-317.
- Curtis, J.T. 1959. *The Vegetation of Wisconsin, an Ordination of Plant Communities*. Wisconsin Press, Madison.
- Curtis, J.T. and McIntosh, R.P. 1950. The interrelations of certain analytic and synthetic phytosociological characters. *Ecology*, 31: 434-455.
- Damgaard, C. and Weiner, J. 2000. Describing size inequality in plant size or fecundity. *Ecology*, 81: 1139-1142.
- Daniels, R.J.R. and Vencatesan, J. 2008. *Western Ghats*. Rupa and Company, New Delhi, p. 180.
- Danoff-Burg, J. and Xu, C. 2006. Biodiversity Calculator. http://www.columbia.edu/itc/cerc/danoff-burg/MBD_Links.html
- Davis, C.A., Austin, J.E. and Buhl, D.A. 2006. Factors influencing soil invertebrate communities in riparian grasslands of the Central Platte River Floodplains. *Wetlands*, 26(2): 438-454.
- Devi, K.B., Singh, H.B. and Gupta, A. 2014. Life forms in the Hill forest of Manipur, Northeast India. *J. Agroecol. Nat. Resour. Manag.*, 1(1): 7-13.
- Ekta, S. 2012. Comparative analysis of diversity and similarity indices with special relevance to vegetation around sewage drains. *World Acad. Sci. Eng. Technol.*, 6(9): 735-737.
- Flores-Díaz, A.C., Chacón, A.Q., Bistrain, R.P., Ramírez, M.I. and Larrazábal, A. 2018. Community-based monitoring in response to local concerns: Creating usable knowledge for water management in rural land. *Water*, 10: 542.
- Ghafari, S., Ghorbani, A., Moameri, M., Mostafazadeh, R., Bidarlord, M. and Kakehmami, A. 2020. Floristic diversity and distribution patterns along an elevational gradient in the northern part of the Ardabil Province Rangelands, Iran. *Mountain Res. Dev.*, 40(1): R37.
- Gopal, V.V., Dhanya, G. and Joseph, S. 2018. Anthropogenic interventions of the riparian track of Vamanapuram River Basin, South Kerala. *J. Eco-Biol.*, 35(1): 28-39.
- Gopal, V.V., Ravinesh, R., Joseph, S. and Kumar, A.B. 2014. Terrain exploration of a seventh order stream in Attingal municipality- a case study of Vamanapuram River Basin, Southern Kerala. *India J. Aquat. Biol. Fish.*, 2: 859-865.
- Gotelli, N.J. and Colwell, R.K. 2001. Quantifying biodiversity: procedures and pitfalls in the measurement and comparison of species richness. *Ecol. Lett.*, 4(4): 379-391.
- Gregory, S.V., Swanson, F.J., McKee, W.A. and Cummins, K.W. 1991. An ecosystem perspective of riparian zones: focus on links between land and water. *Bioscience*, 41(8): 540-551.
- Hammond, M.E. and Pokorný, R. 2020. Diversity of tree species in gap regeneration under tropical moist semi-deciduous forest: an example from Bia Tano forest reserve. *Diversity*, 12(8): 301.
- Hodge, B.C., Pendleton, D.E., Ganley, L.C., O'Brien, O., Kraus, S.D., Quintana-Rizzo, E. and Redfern, J.V. 2022. Identifying predictors of species diversity to guide designation of marine protected areas. *Conserv. Sci. Pract.*, 4(5): e12665.
- Holmquist, J.G., Jones, J.R., Schmidt-Gengenbach, J., Peirotti, L.F. and Love, J.P. 2011. Terrestrial and aquatic macroinvertebrate assemblages as a function of wetland type across a mountain landscape. *Arctic, Antarctic Alp Res.*, 43(4): 568-584.
- Hood, W.G. and Naiman, R.J. 2000. Vulnerability of riparian zones to invasion by exotic vascular plants. *Plant Ecol.*, 148: 105-114.
- John, A.S. and Brema, J. 2018. Development of a Rainfall-Runoff Model for Vamanapuram River Basin. *Int. J. Appl. Eng. Res.*, 13(5): 2831-2837.
- Joji, V.S. and Nair, A.S.K. 2014. Terrain characteristics and longitudinal, land use and land cover profiles behavior—a case study from Vamanapuram river basin, southern Kerala, India. *Arab J. Geosci.*, 7: 1351-1361.
- Jonsson, M., Burrows, R.M. and Lidman, J. 2017. Land use influences macroinvertebrate community composition in boreal headwaters through altered stream conditions. *Ambio*, 46(3): 311-323.
- Kacholi, D. 2013. Floristic composition, diversity, and structure of the Kimboza forest in Morogoro region, Tanzania. *J. Educ. Humanit. Sci.*, 2(2): 84-95.
- Kiran, M., Rahees N., Vishal V. and Vidyasagar K. 2015. Floristic diversity and structural dynamics of mangroves in the northwest coast of Kerala, India. *J. Plant Dev. Sci.*, 7(7): 549-553.
- Knight, D.H. 1975. A phytosociological analysis of species-rich tropical forest on Barro Colorado Island, Panama. *Ecol. Monogr.*, 45(3): 259-284.
- Krebs, C.J. 1989. *Ecological Methodology*. Harper and Row Publishers, New York, p. 550.
- Krebs, C.J. and Berteaux, D. 2006. Problems and pitfalls in relating climate variability to population dynamics. *Climate Res.*, 32: 143-149.
- Lehner, B., Liermann, C.R., Revenga, C., Vörösmarty, C., Fekete, B.M., Crouzet, P., Doell, P., Endejan, M., Frenken, K., Magome, J., Nilsson, C., Robertson, J., Rödel, R., Sindorf, N. and Wisser, D. 2011. High-resolution mapping of the world's reservoirs and dams for sustainable river-flow management. *Front. Ecol. Environ.*, 9(9): 494-502.
- Leishangthem, D. and Singh, M.R. 2018. Tree Diversity, Distribution and Population Structure of a Riparian Forest from Certain Zones along the Dikhu River in Nagaland, India. *J. Forest Environ. Sci.*, 34(1): 31-45.
- MacKinnon, J. and MacKinnon, K. 1986. *Review of Protected Areas System in the Indo-Malayan Realm*. IUCN, Gland, Switzerland.
- Magurran, A. 1988. *Ecological Diversity and its Measurement*. Princeton University Press, Princeton.
- Magurran, A.E. 2004. *Measuring Biological Diversity*. Blackwell Publishers, Oxford, UK, p. 256.
- Margalef, R. 1968. *Perspective in Ecological Theory*. University of Chicago Press, Chicago.
- Menhinick, E.F. 1964. A comparison of some species diversity indices applied to samples of field insects. *Ecology*, 45: 858-862.
- Moore, A.A. and Palmer, M.A. 2005. Invertebrate biodiversity in agricultural and urban headwater streams: implications for conservation and management. *Ecol. Appl.*, 15: 1169-77.
- Morley, S.A. and Karr, J.R. 2002. Assessing and restoring the health of urban streams in the Puget Sound Basin. *Conserv. Biol.*, 16: 1498-509.
- Morris E.K., Caruso T., Buscot F., Fischer M., Hancock C., Maier T.S., Meiners T., Müller C., Obermaier E., Prati D. and Socher S.A. 2014. Choosing and using diversity indices: insights for ecological applications from the German Biodiversity Exploratories. *Ecol. Evol.*, 4(18): 3514-24.
- Muller – Dumbois, D. and Ellenberg, H. 1974. *Aims and Methods of Vegetation Ecology*. Wiley, New York, NY.
- Myers, N. 1988. Threatened biotas: "hotspots" in tropical forests. *Environment*, 8: 1-20.
- Myers, N., Mittermeier R.A., Mittermeier C.G., da Fonseca G.A.B. and Kent J. 2000. Biodiversity hotspots for conservation priorities. *Nature*, 403: 853-858.

- Naiman, R.J. and Décamps, H. 1997. The ecology of interfaces: riparian zones. *Annu. Rev. Ecol. Syst.*, 28(102): 621-658.
- Naiman, R.J., Bilby, R.E. and Bisson, P.A. 2000. Riparian ecology and management in the Pacific coastal rain forest. *Bioscience*, 50: 996.
- Naiman, R.J., Decamps, H. and McClain, M.E. 2010. *Riparia: ecology, conservation, and management of streamside communities*. Academic Press. 421 p.
- Naiman, R.J., Decamps, H. and Pollock, M. 1993. The role of riparian corridors in maintaining regional biodiversity. *Ecol. Appl.*, 3: 209-212.
- Nair, V.M. and Kumar, R.B.B. 2019. Assessment of heavy metal concentration in river sediments along Vamanapuram River Basin, South Kerala, India. *Nat. Environ. Pollut. Technol.*, 18(2): 593-597.
- Nandakumar, K. 2015. Poor Water Quality in Five River Basins in State. <https://www.thehindu.com/news/national/kerala/poor-water-quality-in-five-river-basins-in-state/>
- Nath, P.C., Arunachalam, A., Khan, M.L., Arunachalam K. and Barbhuiya, A.R. 2005. Vegetation analysis and tree population structure of tropical wet evergreen forests in and around Namdapha National Park, northeast India. *Biodivers. Conserv.*, 14(9): 2109-2135.
- Nilsson, C. 2005. Fragmentation and flow regulation of the world's large river systems. *Science*, 308: 405-408.
- Odum, E.P. 1969. The strategy of ecosystem development. *Science*, 164: 262-270.
- Omoró, L.M.A., Pellikka P.K.E. and Rogers, P.C. 2010. Tree species diversity, richness, and similarity between exotic and indigenous forests in the cloud forests of Eastern Arc Mountains, Taita Hills, Kenya. *J. For. Res.*, 21(3): 255-264.
- Parthasarathy, N., Kinbal, V. and Kumar, L.P. 1992. Plant Species Diversity and Human Impact in the Tropical Wet Evergreen Forests of Southern Western Ghats. Indo-French Workshop on tropical forest ecosystem: Nov. 1992. *Nat. Funct. Anth. Impact. French Inst., Pondichery*.
- Paul, J. and George, K.V. 2010. Studies on riverine flora of Pamba river basin, Kerala. *Nat. Prec.*, <https://doi.org/10.1038/npre.2010.5135.1>
- Peng, Y., Fan, M., Song, J. and Cui, T., Li, R. 2018. Assessment of plant species diversity based on hyperspectral indices at a fine scale. *Sci. Rep.*, 8: 4776. DOI:10.1038/s41598-018-23136-5
- Pereki, H., Wala, K., Thiel-Clemen, T., Bessike, M.P.B., Zida, M., Dourma, M., Batawila, K. and Akpagana, K. 2013. Woody species diversity and important value indices in dense, dry forests in Abdoulaye Wildlife Reserve (Togo, West Africa). *Int. J. Biodivers. Conserv.*, 5(6): 358-366.
- Pielou, E.C. 1975. *Ecological diversity*. Wiley, New York.
- Prach, K., Bartha, S., Joyce, C.B., Pysěk, P., van Diggelen, R. and Wiegleb, G. 2001. The role of spontaneous vegetation succession in ecosystem restoration: a perspective. *Appl. Veget. Sci.*, 4: 111-114.
- Sabo, J.L., Sponseller, R., Dixon, M., Gade, K., Harms, T., Heffernan, J., Jani, A., Katz, G., Soykan, C., Watts, J. and Welter, J. 2005. Riparian zones increase regional species richness by harboring different, not more, species. *Ecol.*, 86: 56-62.
- Sahoo, T., Acharya, L. and Panda, P.C. 2020. Structure and composition of tree species in tropical moist deciduous forests of Eastern Ghats of Odisha, India, in response to human-induced disturbances. *Environ. Sustain.*, 3: 69-82.
- Scalley, T.H., Crowl, T.A. and Thompson, J. 2009. Tree species distributions in relation to stream distance in a mid-montane wet forest, Puerto Rico. *Caribbean J. Sci.*, 45: 52-63.
- Schultz, R.C., Isenhardt, T.M., Simpkins, W.W. and Colletti, J.P. 2004. Riparian forest buffers in agroecosystems - lessons learned from the Bear Creek Watershed, central Iowa, USA. *Agrofor. Syst.*, 61: 35-50.
- Shannon, C.E. and Weaver, W. 1963. *The Math. Theory of Comm.* University of Illinois Press, USA, Urbana.
- Simpson, E.H. 1949. Measurement of diversity. *Nature*, 163: 688.
- Singh, J.S., Rawat Y.S. and Chaturvedi, O.P. 1984. Replacement of oak forest with pine in the Himalayas affects the nitrogen cycle. *Nature*, 311: 54-56.
- Singh, R., Tiwari A.K. and Singh, G.S. 2021. Managing riparian zones for river health improvement: an integrated approach. *Landsc. Ecol. Eng.*, 17: 195-223.
- Sørensen, T.A. 1948. A Method of Establishing Groups of Equal Amplitude in Plant Sociology Based on Similarity of Species Content, and Its Application to Analyses of the Vegetation on Danish Commons. I kommission hos E. Munksgaard, Copenhagen, Denmark.
- Sultana, A., Hussain, M.S. and Rathore, D.K. 2014. Diversity of tree vegetation of Rajasthan, India. *Trop. Ecol.*, 55: 403-410.
- Tang, S. and Montgomery, D. 1995. Riparian buffers and potentially unstable ground. *Environ. Manage.*, 19: 741-749.
- Tonkin, J.D., Altermatt, F., Finn, D., Heino, J., Olden, J.D., Pauls S.U. and Lytle, D.A. 2018. The role of dispersal in river network metacommunities: patterns, processes, and pathways. *Freshw. Biol.*, 63: 141-163.
- Ullah, S., Zaman, M., Jiaqi, L., Khan, Y., Ullah, S. and Gang, T. 2020. Quantifying the Estimation and Abundance of Plant Diversity of Shigar Valley, Gilgit-Baltistan. *Pak. J. Plant Pathol. Microbiol.*, 11: 522.
- Vincy, M.V., Brilliant, R., Paul, J. and Pradeepkumar, A.P. 2015. Comparison of riparian species diversity between the main river channel and subwatersheds of Meenachil river basin, Kerala, Southern India. *Braz. J. Bot.*, 38: 81-98.
- Visalakshi, N. 1995. Vegetation analysis of two tropical dry evergreen forests in southern India. *Trop. Ecol.*, 36: 117-127.
- Zibtseva, O. 2022. Tree species biodiversity in small Ukrainian towns. *Ekológia (Bratislava) - J. Inst. Landscape Ecol., Slovak Acad. Sci.*, 41(2): 161-171.

ORCID DETAILS OF THE AUTHORS

M. V. Vincy: <https://orcid.org/0000-0002-0731-5238>

R. Brilliant: <https://orcid.org/0000-0001-9267-6830>



Application of Random Forest in a Predictive Model of PM₁₀ Particles in Mexico City

Alfredo Ricardo Zárate Valencia*†  and Antonio Alfonso Rodríguez Rosales** 

*Doctorado en Ciencias Ambientales, Universidad Autónoma de Guerrero, 39070, México

**Instituto de Ciencias Aplicadas y Tecnología, Universidad Nacional Autónoma de México, 04510, México

†Corresponding author: Alfredo Ricardo Zárate Valencia; azaratev@hotmail.com

Nat. Env. & Poll. Tech.
Website: www.neptjournal.com

Received: 09-08-2023

Revised: 14-10-2023

Accepted: 16-10-2023

Key Words:

Predictive model
Air pollution
Random forest
Monitoring
PM₁₀ particles

ABSTRACT

Over time, predictive models tend to become more accurate but also more complex, thus achieving better predictive accuracy. When the data is improved by increasing its quantity and availability, the models are also better, which implies that the data must be processed to filter and adapt it for initial analysis and then modeling. This work aims to apply the Random Forest model to predict PM₁₀ particles. For this purpose, data were obtained from environmental monitoring stations in Mexico City, which operates 29 stations of which 12 belong to the State of Mexico. The pollutants analyzed were CO carbon monoxide, NO nitrogen oxide, and PM₁₀ particulate matter equal to or less than 10 µg.m⁻³, NO_x nitrogen oxide, NO₂ nitrogen dioxide, SO₂ sulfur dioxide, O₃ ozone, and PM_{2.5} particulate matter equal to or less than 2.5 µg.m⁻³. The result was that when calculating the certainty of our model, we have a value of 80.40% when calculating the deviation from the mean, using 15 reference variables.

INTRODUCTION

Air pollution is a global problem. The World Health Organization estimates that 90% of people breathe polluted air (WHO 2019). Consequently, around seven million deaths are attributed to air pollution (WHO 2014). Several organizations are focusing on evaluating pollution indicators, considering the characteristics of each place (Perevochtchikova 2013).

One of the primary air pollutants is ozone (O₃), a gas of three oxygen atoms in the upper atmosphere and at the surface level. At the surface level, the latter becomes hazardous to people's health (Liu et al. 2018). For example, industrial and vehicle emissions are considered the primary precursor sources of ozone (EPA 2021). It should be noted that wind is a significant factor in pollutant dispersion; its speed and direction are linked to pollutant concentration, and the more wind, the less pollutant concentration (Biancofiore et al. 2015).

Poor air quality is a public health problem for large cities with high population concentrations, and these air pollutant emissions are generated by motor vehicles and factories (Perevochtchikova 2009). Our case study was conducted in Mexico City, Latin America's largest city. For this reason,

the Federal and Local governments have taken care to have monitoring stations and record in databases all records of the primary pollutants on average per hour, through the guidelines and supervision of the INECC (National Institute of Ecology and Climate Change) with the operation of the DMA (Directorate of Atmospheric Monitoring) of Mexico City. Under this premise, the data generated can be used for monitoring and data science analysis to make inferences about the behavior of pollutants, which is the case here.

The data recorded in different industries and applications such as monitoring (in just one year, the DMA is more than 6 million records), which is why they have to be analyzed to look for behaviors and opportunities to improve processes and inferences, for which it is necessary to have computational tools of Data Science; otherwise, it would be almost impossible (Provost & Fawcett 2013). Big Data is about analyzing vast amounts of data, and we can divide it into two parts: the technology (Hadoop, Spark, etc.) and the platform architecture (Gonzalez Diaz 2017). With Big Data tools, any analysis would take a long time, and the relevance would be adequate.

The application of Data Science in environmental and specifically air quality monitoring has been worked on, e.g.,

Kurt and Oktay applied Airpol, a real-time forecasting system using PHP programming language, MySQL database, and MATLAB for the inferential statistics part (Kurt & Oktay 2010). It acquires data from different sources and stores them in a single central database. In retrospect, systems for predicting pollutant behaviors were treated as black boxes, where the system was not understood. It was challenging to understand the relationships of the variables and thus not know why things happened (Mohan & Kandya 2011); nowadays, analysts need to understand these relationships.

Sertel et al. (2012) integrated remote sensing, geostatistical, and spatial analysis methods. They looked at the relationship between transport, land use, and air quality (Sertel et al. 2012), i.e., they studied data from different sources to improve their results. Essentially, four types of models are used to predict $PM_{2.5}$ concentrations: regression, artificial intelligence, time series, and chemical transport (Zhou et al. 2014). Zhou et al. (2014) used EMD (Empirical Mode Decomposition), which was initially developed to study ocean waves but is now also applied in nature and social science studies.

Zhang & Yuan (2015) implemented a distributed random forest algorithm using Spark to create a predictive air quality model using actual meteorological data in Beijing (Zhang & Yuan 2015). In the same year, Anaya Díaz (2015) took meteorological data and an air quality index collected over four years in Valledupar, Colombia (Anaya Díaz 2015), using clustering techniques to estimate air quality with the application of data mining techniques. Hsieh et al. proposed an entropy-minimizing model to suggest locations for new monitoring stations using air quality data in Beijing by constructing i-layer graphs that reflect temporal correlations. In contrast, the data connections remain identical (Hsieh et al. 2015).

Data mining allows to analysis of air quality using analytical methods when scientific methods do not exist; in that sense, Soh et al. propose a predictive system for air quality using ST-DNN (Shape-Tailored Deep Neural Networks) to predict $PM_{2.5}$ 48 hours in advance (Soh et al. 2016). Also, Li et al. (2016) applied to predict air quality deep learning approach, applying a regional data treatment as a spatiotemporal process that considers spatial and temporal correlations of data to predict the air quality of all monitoring stations simultaneously with seasonal stability (Li et al. 2016), which recognizes and applies seasonal behavior in analysis and predictions.

Wang et al. (2017) categorized the main pollutant forecasting models as deterministic, statistical, and hybrid models (Wang et al. 2017). They proposed a hybrid model based on the ELM (Extreme Learning Machines) model

optimized by the DE (Differential Evolution) algorithm, managing to forecast random, irregular, and non-stationary data series. Alongside model improvements, Bellinger et al. recognize that advances in technology and lower prices for computing power in computers allow for measuring and storing different variables related to the environment (Bellinger et al. 2017), coupled with data from resources such as social networks, give a new perspective to environmental health analysis. Also, in 2017, Mahajan set out to develop a stable model with a real-time implementation (Mahajan et al. 2017), for which they used an ARIMA (Autoregressive Integrated Moving Average) model and an NNAR (Neural Network Autoregression) model to predict $PM_{2.5}$ levels in four regions of Taiwan with a total of 557 monitoring stations. In a more recent publication, Soh et al. propose this time to analyze the spatiotemporal patterns of particulate matter (PM) in Taiwan by developing a PM probability map with its patterns per day. It is a method that uses dynamic time warping and analyses the temporal similarity between multiple stations and their performance (Soh et al. 2017).

Zhu (2018) highlighted the importance of regional meteorological conditions as essential data to be considered in a predictive model for pollutants such as O_3 , as they found that in Chicago, the concentration of that pollutant is more sensitive to air temperature, wind speed, and direction, relative humidity, incoming solar radiation and cloudiness (Zhu et al. 2018). Gao also conducts model studies to predict the behavior of O_3 (most studies are based on PM). They use a few climate parameters as predictors, and the application of the Monte Carlo method to study the uncertainty of the ANN (Artificial Neural Networks) model is highlighted (Gao et al. 2018). In a study, Amado and de la Cruz (2018) built predictive models that relate the values of a prototype that makes sensor readings and relates them to the air quality index (Amado & De la Cruz 2018), together with Bayesian models, allowing them to obtain an accuracy of up to 99 % in their tests.

In an article published by Rybarczyk & Zalakeviciute (2018), they infer that forecasting is less accurate than estimation and justify the use of more demanding methods, such as Deep Learning, to predict hours or even days in advance the concentration of a pollutant (Rybarczyk & Zalakeviciute 2018). Based on the above, it seems that data analysis for predicting pollutant concentrations has been applied sparingly. Still, one also has to consider the application of the model to be developed and the experience of the implementers. In the same period, when evaluating various models, Roy et al. (2018) suggest that the Multivariate Adaptive Regression Splines (MARS) model has a better description of the data set and a higher prediction

compared to the Random Forest (RF) and the Classification and Regression Tree (CRT) (Roy et al. 2018).

Regarding accuracy again, Zhang et al. (2019) noted that until 2019, pollutant concentration prediction methods needed to effectively use existing Big Data to extract the temporal and statistical characteristics of the data (Zhang et al. 2019), resulting in limited model accuracy. Another article highlights that it is highly recommended to compare different models, such as ANN, PLS (Partial Least Squares), RFR, and MLR, when choosing which one would be the most suitable (Wei et al. 2019) and obtain the best model by averaging the results of different models. Having contributed to Big Data, more and more governments are publishing their data on their portals to stimulate its use in applications that serve their citizens (Buenadicha et al. 2019). Commercial industries are also embracing Big Data by using innovative techniques that have extracted demographic, socioeconomic, and consumer behavioral data for forecasting and analysis (Tan et al. 2020). Lim and his team presented a complementary option, mobile sampling, that improves the spatial granularity of Land Use Regression (LUR) models by deploying low-cost sensors that could improve and modernize how air pollution is measured (Lim et al. 2019). Also, Yuchi et al. (2019) showed that when measuring indoor PM_{2.5} concentrations, MLR (multiple linear regression) and RFR (random forest regression) models obtain similar results in a heavily polluted environment by using a small number of variables (Yuchi et al. 2019).

We will now look at two proposals for predicting pollutant concentrations using Air Quality Indices (AQI) (which use a combination of measured pollutants for their integration). The first is presented by Lino-Ramirez et al., which is a real-time system that monitors environmental variables from several points and makes a prediction of the behavior of those variables (Lino-Ramirez et al. 2019). It was applied in Guanajuato, Mexico, and predicts air quality according to an established traffic light. In the second case, three learning models were applied to predict the PM_{2.5} air level using data from the CPCB (Central Pollution Control Board) using more than three years of data resulting in an air quality index for the Delhi NCR region (Sihag et al. 2019). Camí Núñez highlights in his article that applied measurements such as the two previous ones are used to trigger different anti-pollution protocols and should be able to forecast pollutant concentrations sometime in advance to be timely (Camí Núñez 2020).

Next, we want to point out that, over time, predictive models tend to become more accurate but also more complex, indeed, based on the experience of previous model developments. Zhou et al. (2020), for example, in his model

made measurements at different seasons in four cities in the Yangtze River Delta with five prevalent forecasting tools, including SFGM (Seasonal Fractional-order Grey Model), SGM (Seasonal Grey Model), LSSVM (Least Squares Model) and LSSVM (Least Squares Squared Model), and LSSVM (Least Squares Squared Model), LSSVM (Least Squares Support Vector Machine), SARIMA (Seasonal Auto-regress Integrated Moving Average) and BPNN (Back Propagation Neural Network), with a considerable improvement of the prediction accuracy of seasonal air quality changes (Zhou et al. 2020). By increasing and thus enriching the data available for modeling, Pinto et al. (2020) proposed introducing data on traffic patterns (speed, intensity) and emissions generated by vehicle emission models (Pinto et al. 2020).

Another study on Delhi NCR done by Yadava & Agarwal (2020) to predict the level of PM_{2.5} in the air applied three models: LSTM (Long Short-Term Memory), Auto-regression, and SVM (Vector Machine) to test which of the models is the most suitable, using the data from the CPCB (Central Pollution Control Board) website (Yadava & Agarwal 2020).

Already Harbola et al. (2021) introduced the Air Quality Temporal Analyser (AQTA), which is a system with visual analysis of air quality data that allows the use of visualization techniques that visually display anomalies and correlations of correlated trends through an interactive, non-directed search (Harbola et al. 2021).

Neural networks rely on data, which generally comes from ground-based monitoring stations, so their coverage is limited to the number of stations installed. To overcome this limitation, Lightstone et al., through a deep neural network (DNN), combine spatial Kriging interpolation with additional local source variables by interpolating the measured PM_{2.5} concentrations across locations without monitoring stations installed (Lightstone et al. 2021).

MATERIALS AND METHODS

For our research, which is based on developing a predictive model, we have followed the steps suggested by some authors, such as (Herman et al. 2013), who propose four stages for model development (acquire, prepare, analyze, and act) and we complement it with what is suggested by (Provost & Fawcett 2013), who propose six stages (understanding the business, understanding the data, data preparation, modeling, evaluation and model development).

Fig. 1 shows the methodology we followed for our research. In step 1 of Data Access and Understanding, we seek to know the most reliable sources of data and understand how they were recorded and the formats of

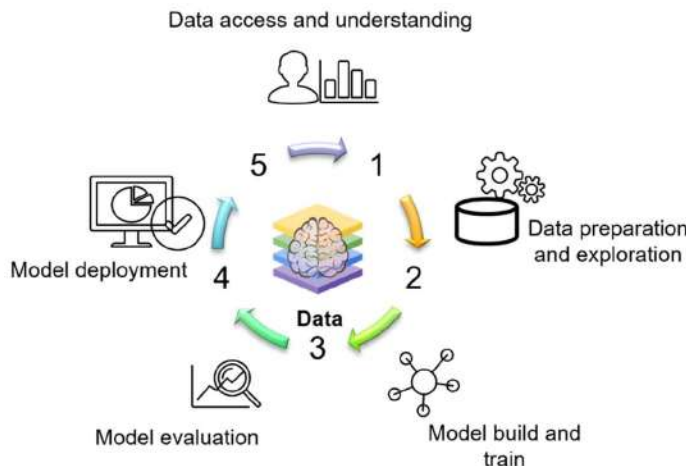


Fig. 1: Methodology followed for the research.

the data provided. Step 2 aims to review the records, eliminate incomplete or erroneous records, set nulls to a value if applicable, and prepare the data in a suitable format for modeling. In step 3, we separate data to train, review, evaluate, and apply the model (Random Forest in our case).

The 4th step allows us to evaluate the model against the actual data left for that case and to see the degree of certainty of our model.

Important note: A discussion will occur at each stage since data were analyzed at each step and further data were generated.

Data Access and Understanding

In Mexico, the INECC (National Institute of Ecology and Climate Change) dictates how data from pollutant concentration monitoring should be recorded in a database. All state or municipal governments in the republic that wish to monitor air quality for official purposes must adhere to these guidelines. For example, for each pollutant being monitored, the hourly average is recorded for each hour, starting from hour 0 to hour 23 of each day. Flags are added to indicate whether the recorded data is correct or inconsistent and is therefore invalidated.

In Mexico City and the metropolitan area, the official body that records pollutant concentrations and indicates air quality is the DMA (Atmospheric Monitoring Directorate), which depends on the SEDEMA (Ministry of the Environment) of the Mexico City Government, and operates 29 monitoring stations, 12 of which belong to the State of Mexico.

Fig. 2 shows Mexico City framed by a line and the surrounding municipalities of the State of Mexico, which

make up the Metropolitan Area. Each point refers to the locations of the monitoring stations.

The names of the monitoring stations are listed in Table 1. The records accessed are grouped by monitoring station, date and hourly average and by each pollutant, with the inclusion of flags as shown in Table 2. For example, the first record shows that it belongs to station 243, on 25 December 2020, to the hourly average 01 of the pollutant NO, which has the status of validated with a 1, and its record value of NO (nitric oxide), is 0.001 ppm.

Table 1: Some air quality monitoring stations in the CDMX metropolitan area.

Station ID	Short_name	Name	Municipality	Entity
242	AJM	Ajusco Medio	Tlalpan	CDMX
243	ATI	Atizapán	Atizapán de Zaragoza	Estado de México
300	BJU	Benito Juarez	Benito Juárez	CDMX
244	CAM	Camarones	Azcapotzalco	CDMX
245	CCA	Centro de Ciencias de la Atmósfera	Coyoacán	CDMX
246	CHO	Chalco	Chalco	Estado de México
248	CUA	Cuajimalpa	Cuajimalpa de Morelos	CDMX
249	CUT	Cuautitlán	Tepotztlán	Estado de México
250	FAC	FES Acatlán	Naucalpan de Juárez	Estado de México
431	FAR	FES Aragón	Nezahualcóyotl	Estado de México

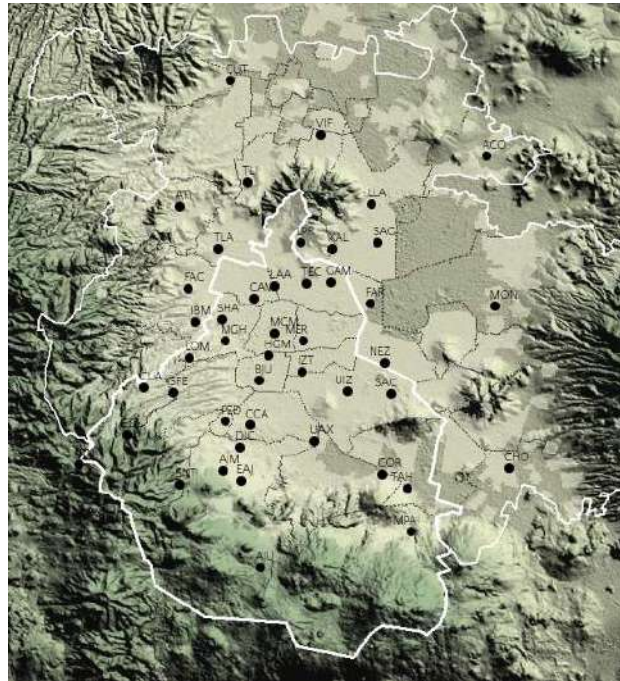


Fig. 2: Location of monitoring stations for reference only taken from the site <http://www.aire.cdmx.gob.mx/>.

Table 2 Example of pollutant records as submitted.

Station ID	Date	Time	Parameter	Validate	Value_act
243	2020-12-25	1	NO	1	0.001
243	2020-12-26	1	NO	1	0.001
243	2020-12-31	1	NO	1	0
243	2020-01-02	1	NO ₂	0	0
243	2020-01-03	1	NO ₂	1	0.003

In the field “Parameter,” the pollutant is recorded; in “Validate,” a 1 if the data is correct and 0 if it is not, and in “Value_act,” the concentration data is recorded on that date and at that time in each station.

Table 3: Pollutant records converted to fields.

FECHA	HORA	CO	NO	PM ₁₀	NOx	NO ₂	SO ₂	O ₃	PM _{2.5}
03/01/2020	8	0.4	0.001	5	0.008	0.007	0.001	0.032	2
03/01/2020	9	0.5	0.004	9	0.014	0.01	0.001	0.03	4
03/01/2020	10	0.7	0.012	8	0.03	0.018	0.001	0.025	1
03/01/2020	11	0.7	0.012	17	0.032	0.019	0.001	0.029	4
03/01/2020	12	0.8	0.015	13	0.039	0.024	0.001	0.032	3
03/01/2020	13	0.6	0.005	39	0.018	0.013	0.001	0.044	21
03/01/2020	14	0.6	0.003	17	0.014	0.011	0.001	0.048	8
03/01/2020	15	0.6	0.003	25	0.014	0.011	0.001	0.054	9

Data Preparation and Exploration

Because the analysis of the data requires that all pollutants be found in the same record, it was necessary to “pivot” the records for each pollutant (CO carbon monoxide, NO nitrogen oxide, PM₁₀ particulate matter equal to or less than 10 $\mu\text{g}\cdot\text{m}^{-3}$, NOx nitrogen oxide, NO₂ nitrogen dioxide, SO₂ sulfur dioxide, O₃ ozone, and PM_{2.5} particulate matter equal to or less than 2.5 $\mu\text{g}\cdot\text{m}^{-3}$), so that each was a field in the table and is shown in Table 3.

The INECC has established specific pollutants (referred to as “Criteria”; see Table 4 for more information) for the Mexican territory. It is precisely those pollutants that we must measure, according to INECC parameters, to

Table 4: Criteria pollutants and their allowable concentrations.

Pollutant	Concentration		Exposure time
	[ppm]	[$\mu\text{g}\cdot\text{m}^{-3}$]	
Ozone (O ₃) NOM-020-SSA1-1993	0.11	216	1 h
	0.06		8 h
Carbon monoxide (CO) NOM-021-SSA1-1993	11	12.595	8 h
Lead (Pb) NOM-026-SSa1-1993	n/a	1.5	Quarterly
Sulfur dioxide (SO ₂) NOM-022-SSA1-1993	0.13	341	24 h
Nitrogen dioxide (NO ₂) NOM-023-SSA1-1993	0.21	395	1 h
Total Suspended Particles (TSP) NOM-025-SSA1-1993	n/a	120	24 h
		50	Annual
PM ₁₀	n/a	65	24 h
		15	Annual
PM _{2.5}	n/a	1.5	24 h
			Annual

determine whether the air quality we breathe is satisfactory or not.

Below, weather data is aggregated by date and time for temperature, wind speed and direction, precipitation, humidity, and pressure, which were

obtained from the Mexican National Meteorological Service.

Seasonal Analysis of PM₁₀

Our first analysis looks for any seasonality of the PM₁₀ variable. It contrasts it with some climatic variables that might be related, such as wind speed, precipitation, humidity, and temperature. When we performed this analysis, we found inconsistent data at the stations Benito Juárez, Cuautitlán, Gustavo A. Madero, and Iztacalco. Since missing values for one or more fields affect the model, these stations have been removed from our study.

For this purpose, we have averaged the monthly values of the mentioned variables using the open-source programming language R (CRAN 2022), as the basis for all our research. In each case, if appropriate, we will show snippets of the code we have used. The computer equipment is a 7th-generation Intel Core i7 laptop with 16 GB of RAM.

Fig. 3 aimed to see if there was a relationship between PM₁₀ and some meteorological variables affecting its concentration or measurement, such as wind speed, precipitation, humidity, and temperature (Dung et al. 2019). According to the monthly averages plotted, we can observe that PM₁₀ has its highest measurements at the beginning and end of the year and its lowest point in August. However, we

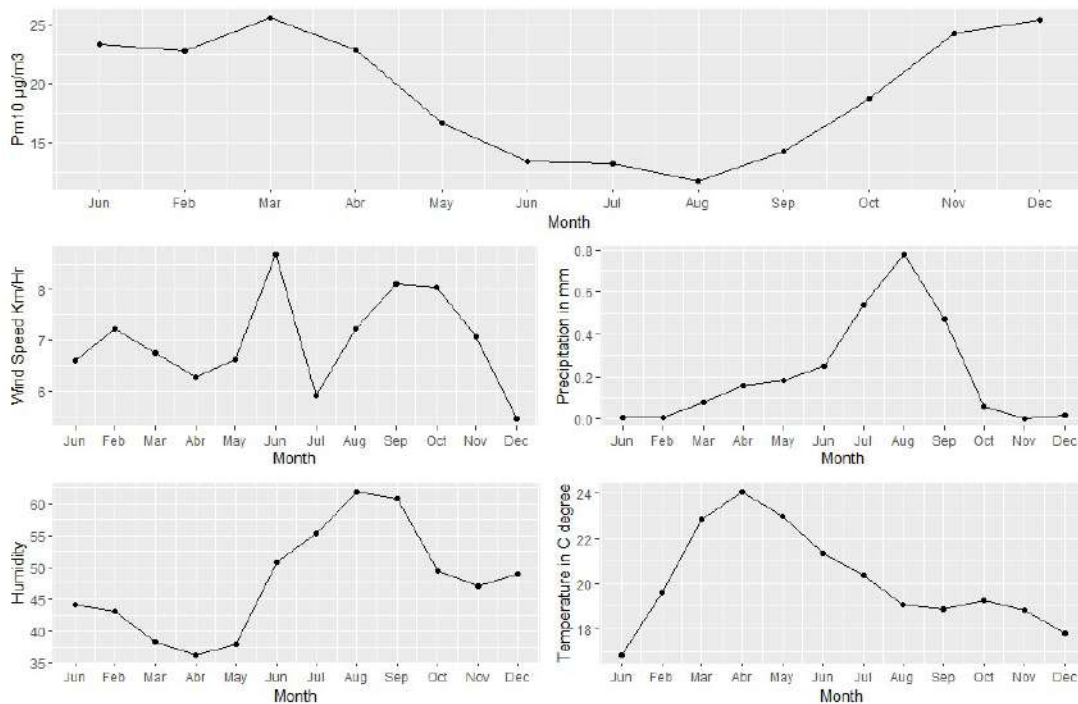


Fig. 3: Monthly comparison of 2020 PM₁₀ and some meteorological indicators.

cannot observe a similar behavior derived from the monthly averages, for example, for velocity, which has the highest values in June, September, and October, very different

compared to particulate matter. The cases of temperature and humidity also show no relationship with PM₁₀. An inverse relationship can be seen in the case of precipitation, which

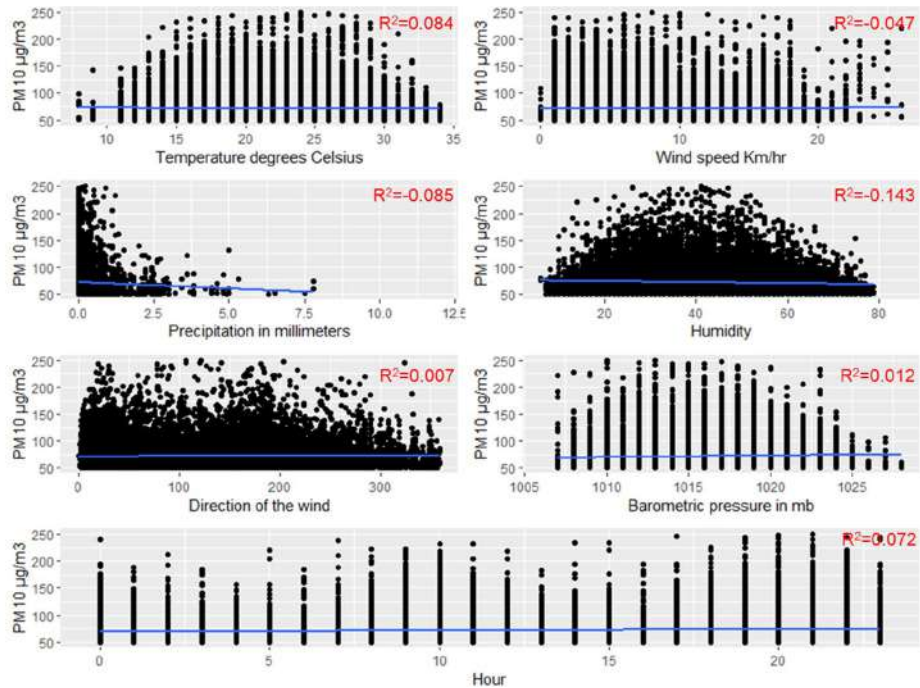


Fig. 4: Correlation of PM₁₀ with meteorological variables.

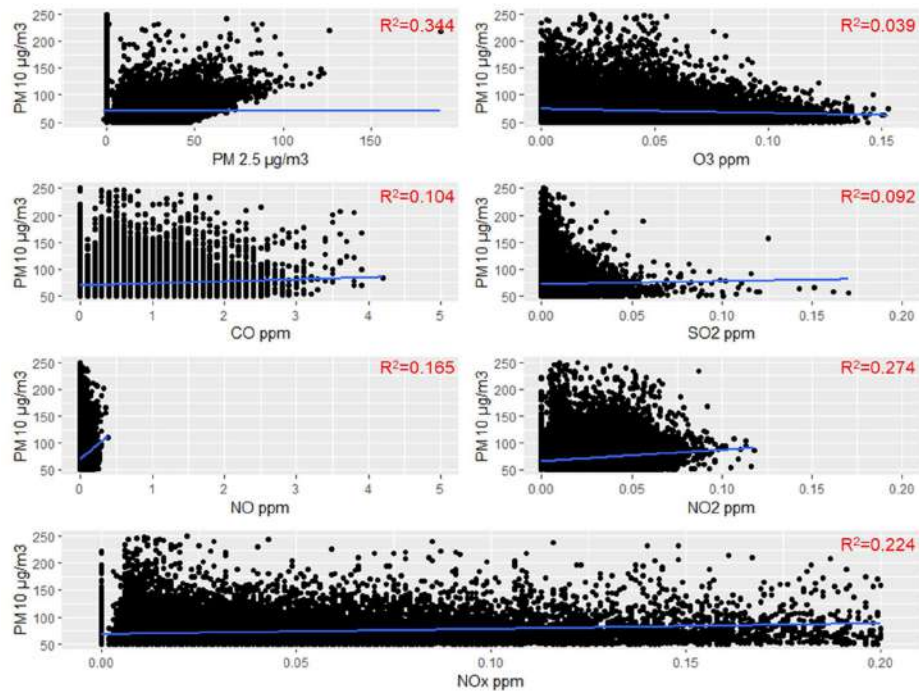


Fig. 5: Correlation of PM₁₀ and other pollutants.

has its highest values in August, in contrast to PM_{10} , and its lowest values at the beginning and end of the year.

In this first exploration, the observations present certain behaviors that allow us to verify that precipitation has a specific correlation with PM_{10} . However, we performed a correlation analysis and plotted the results in Figs. 4 & 5 for a more accurate analysis.

Correlation of Independent Variables

To carry out the analysis, we calculated the covariance and correlation of the variables involved using a linear regression model using the Pearson method and the coefficient of determination R^2 .

Fig. 4 shows the correlations between PM_{10} and meteorological variables such as temperature, wind speed, precipitation, humidity, wind direction, barometric pressure, and time of day (time is plotted in this item for the practicality of graphical presentation).

The highest correlation is found in unfavorable humidity, i.e., the more humidity, the less PM_{10} with an R^2 value of -0.143; the next most important are precipitation with -0.085 and temperature with 0.084. The others have even lower values.

The exact process was performed in Fig. 5 for the other pollutants for which data are available, such as $PM_{2.5}$, O_3 , CO , SO_2 , NO , NO_2 , and NO_x .

The highest coefficients are $PM_{2.5}$ with 0.344, NO_2 with 0.274, NO_x with 0.224, NO with 0.165, CO with 0.104, SO_2 with 0.092, and O_3 with 0.039.

Although there is no conclusive data at this exploration stage, there is a correlation of meteorological variables in which humidity is inverse and the highest. In the case of pollutant variables, the highest value is $PM_{2.5}$.

There is no single indirect variable that is decisive. However, the set of all of them will define the behavior of PM_{10} , and their modeling will be subject to this characteristic of our study data.

Model Construction and Training

Based on the experience of other research, such as Deshmukh's (Deshmukh & Gulhane 2016), we think that to develop a well-founded predictive model, a cluster analysis is necessary, which allows us to group similar objects, in our case, monitoring stations to see if some of them have similar behaviors or rather, similar measurements and group them so that perhaps, we have not one but several models according to the number of clusters found.

In our research, the function `fviz_nbclust` belonging to the R language package "factoextra" (cran.r-project.org 2022) was used to determine the optimal number of clusters. The k-means clustering minimizer aims to minimize the total variation within clusters or the total sum of squares within the cluster. That value is required to be the minimum. This function also plots the results using the so-called "elbow" method, using the "silhouette" method that calculates the average of the observations for different values of k. The optimal number of k is the highest over the range of k.

In Fig. 6, the highest number is found in cluster 2 (the elbow), indicating 2 clusters of monitoring stations. To

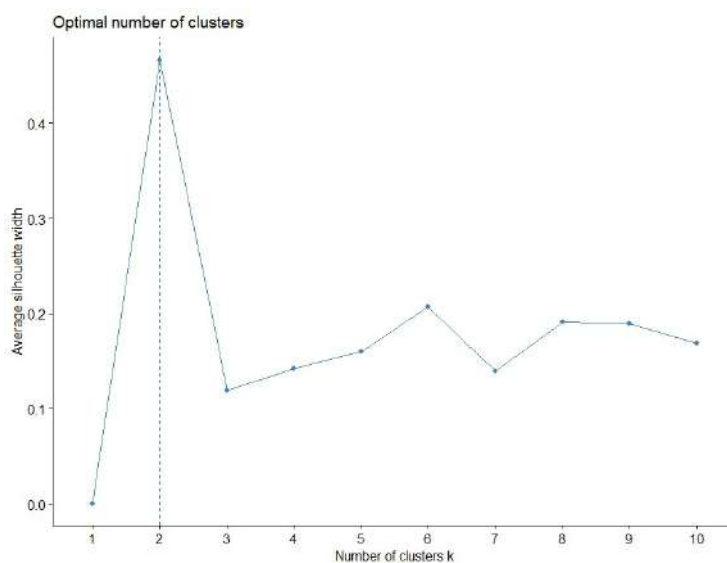


Fig. 6: Optimal number of clusters.

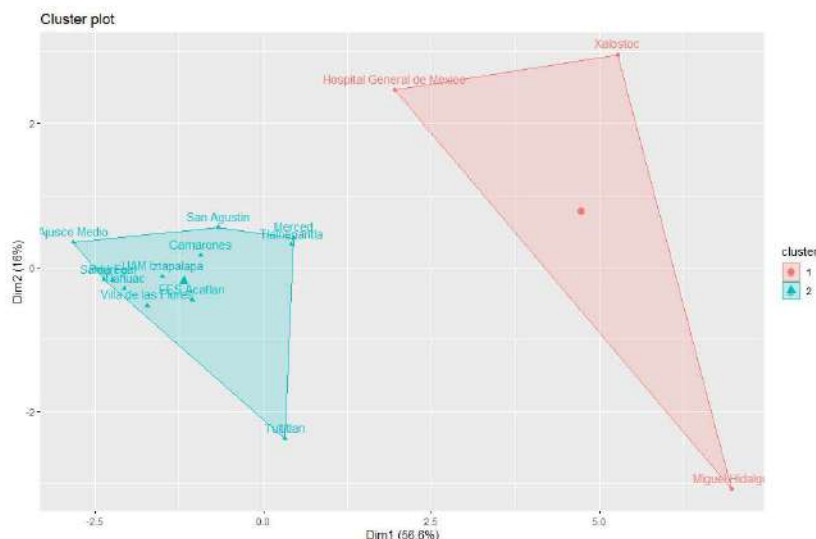


Fig. 7: Grouping of monitoring stations.

locate which stations belong to which block (clustering) by Euclidean distances, we use the function `kmeans` (`df`, `centers = 2`, `nstart = 25`), also included in the “factoextra” package, to which we parameterize the number of centroids in 2 (the value obtained above) and the other value of `nstart` indicates the number of random initial partitions, a minimum value of 25 is suggested. This function uses, by default, the Hartigan and Wong algorithm.

The “factoextra” function `fviz_cluster(model_k1, data = df)` plots the clustering results as shown in Fig. 7.

Dim1 and Dim2 shown on the axes are the new variables derived from the calculations derived from the principal component analysis process; % indicates the data’s variability, i.e., Dim1 represents 50.2% variability and Dim2 14.6%. Three of the 16 stations are from Cluster 1: Hospital General de México, Xalostoc, and Miguel Hidalgo, and the other 13 are grouped in Cluster 2.

The Method Selected for Our Model

A suitable method for classification and prediction is decision trees, but they have a different level of predictive accuracy than other methods and are not very robust (James et al. 2017). By aggregating multiple trees, methods such as bagging and random forest significantly improve their performance.

In our case, we have decided to use the random forest method as we consider it meets our requirements of having an excellent predictive performance and excellent libraries in R. For its implementation, we have chosen the “ranger” package, which is a speedy implementation of random forest

(Alvear 2018), in this site is also proposed a method for its application of which we follow some steps.

We have also based the application of random forest on what is proposed by the website “Decision trees, random forest, gradient boosting and C5.0” (Joaquín Amat 2020), which we found to be correct and very similar to other sites proposed by other data science experts.

The first part is to find the number of trees needed. However, this is not a critical parameter; it can improve the resulting model, especially regarding the computational resources used.

Using the validation with Out-of-Bag error (root mean squared error) in Fig. 8, we can see that the number of suggested trees is 381. It is important to note that this process can take up to 5 hours using our laptop.

Now, we implement the k-cross-validation (root mean squared error) to have another parameter regarding the number of trees we get.

When k-cross validation is used, the number of trees suggested is 391. As can be seen, the values in both cases are very similar, and for our case, we rounded the total number of trees to be used to 400.

Another important parameter is “mtry,” which is the number of variables or predictors randomly sampled as candidates in each split. As in the tree number process, we validated them against “oob” and k-cross with the following results.

Fig. 10 shows that the value for mtry is 10 after the values of oob train rmse stabilize.

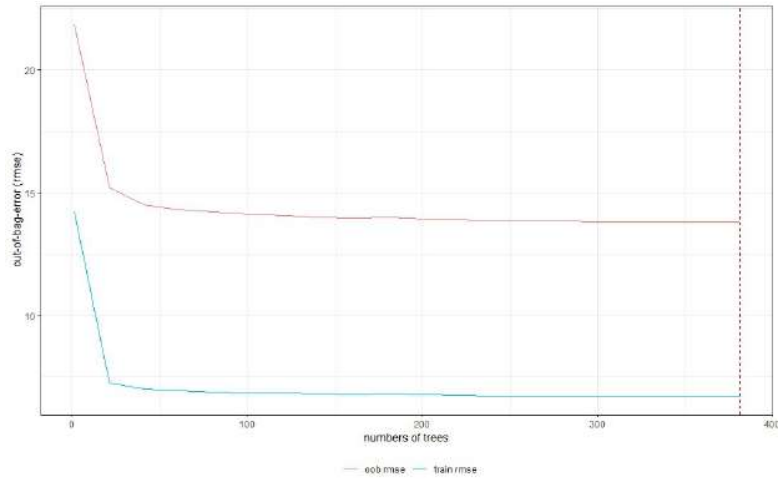


Fig. 8: Evolution of out-of-bag error vs. number of trees.

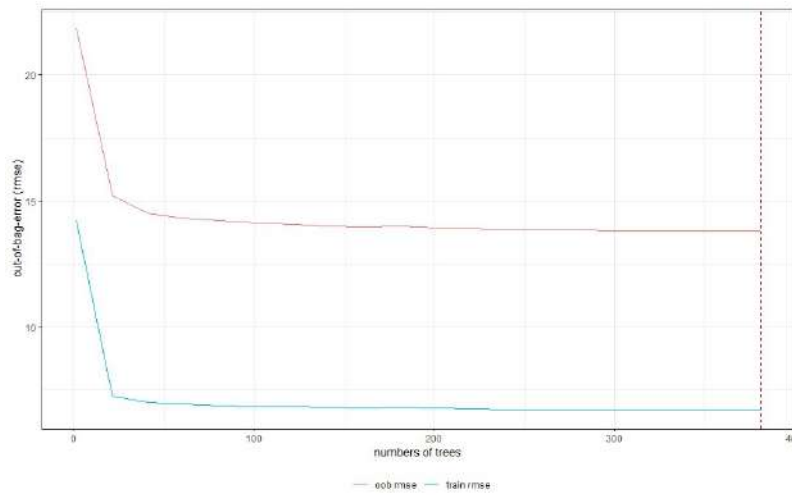


Fig. 9: Validation using kcross-validation (root mean squared error).

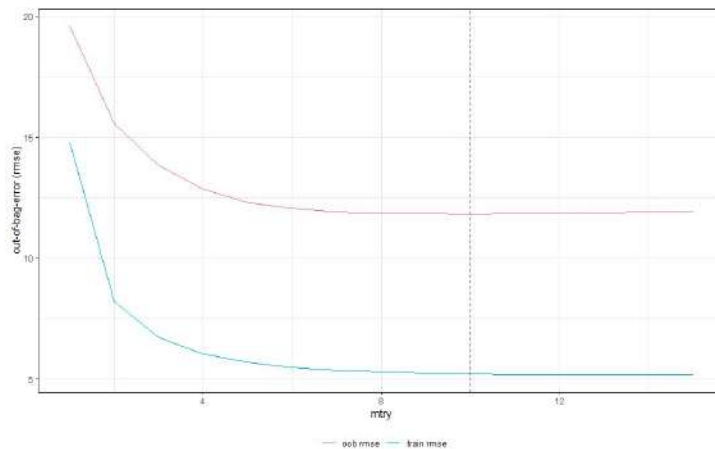


Fig. 10: Validation using out-of-bag error and mtry.

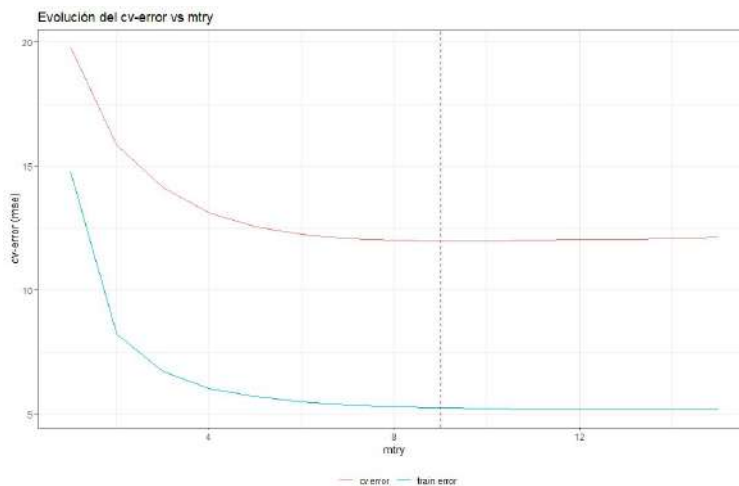


Fig. 11: Validation using kcross-validation and mtry.

When cv-error is used, mtry has a value of 9, as shown in Fig. 11, which infers that mtry will be between 9 and 10 in the model to be developed.

Grid Search

Understanding the individual behavior of the parameters is important to develop a good model. Still, it is better to analyze all of them as a whole because each one interacts with the others. So, it is better to perform a grid search or random search analysis, which we will do next.

The parameters when interacting with each other after applying the grid search are as follows (record 1): num trees 600, mtry is 9, max depth is 20, and oob is 11.9.

Now, we do a grid search based on cross-validation.

The results are consistent as they are num three 600, mtry is 9, max depth is 20, and with an average estimator

of 12.1, which are the best parameters for the model and its final training.

RESULTS AND DISCUSSION

To obtain the final model, we use the existing parameters, train the model with test data, and then apply the model with the test data to validate the results and estimate how close the estimated data is to the predicted data.

Based on the model developed, what would be the expected results, what is its level of certainty, and is it feasible to operate in real-time?

In the model with the optimized parameters where we use training data against another sample for the test, we have, on average, a difference of $9.67 \mu\text{g}\cdot\text{m}^{-3}$ from the actual PM₁₀ value.

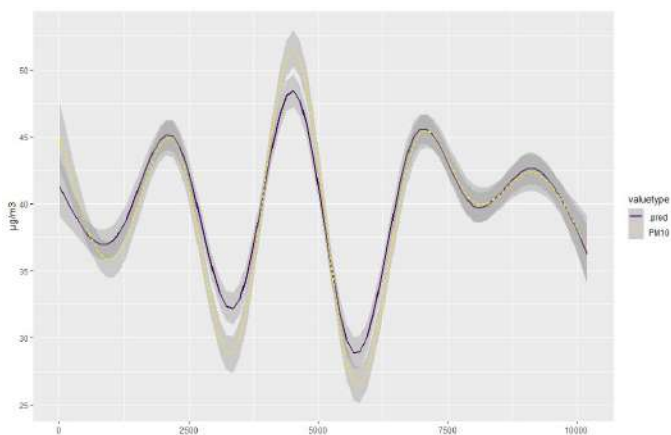


Fig. 12: Trend lines of predicted vs. actual PM₁₀ values.

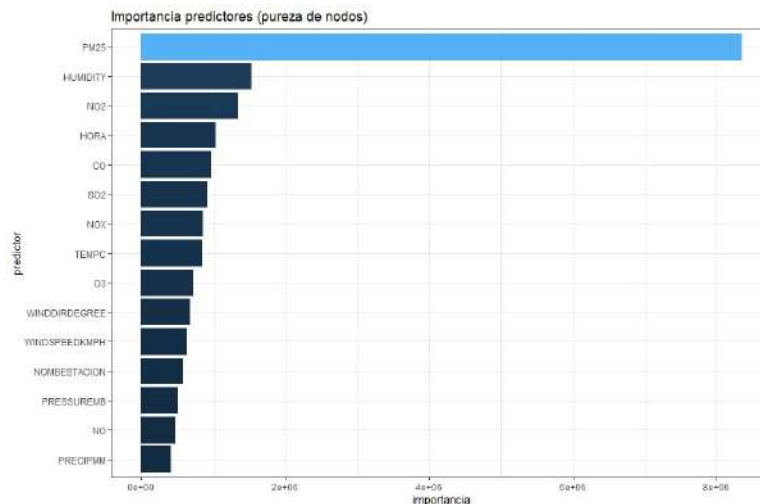


Fig. 13: Importance of predictors.

When calculating the certainty of our model, we have a value of 80.40 % certainty by calculating the deviation from the mean. This calculation is obtained by calculating the differences of the absolute differences between the calculated and actual PM_{10} values of each element, then dividing that value by each actual value multiplied by 100; the mean is then calculated and subtracted from 100%, as shown in the code above.

However, whether a model with a certainty of 80.4% is acceptable depends on what we are looking for with the model. For example, our model clearly shows trends very close to the actual, as shown in Fig. 12.

The number of predictors to be analyzed is 15, and having a certainty level of 80.4% is quite acceptable in light of the results obtained in models with even fewer variables to be analyzed.

Fig. 13 shows the predictors in the degree of importance from highest to lowest, with $PM_{2.5}$ standing out as the most important predictor, followed by relative humidity, which is a known correlation.

PM_{10} and $PM_{2.5}$ have a well-studied correlation, which is verified in our analysis. Notably, in fourth place, the importance of time is found, which we assume has to do with the peak hours of vehicular traffic, although, in Fig. 4, no such relationship is apparent.

CONCLUSIONS

It is feasible to apply Random Forest to model the behavior of air pollutants, in our case, to predict PM_{10} particles based on 15 predictors, including pollutants and climate measurements. These complex models involve a lot of database work before modeling.

A fundamental first step is selecting valid data from one or more tables in different records of the pollutant database and processing it to be analyzed in a model. Generally, there are not wrong models but incorrect or badly processed data. In this sense, we have found records where, for example, $PM_{2.5}$ values are almost 0 and PM_{10} values above $20 \mu\text{g}\cdot\text{m}^{-3}$, a fact that caught our attention because of the known correlation between these pollutants, which should be between 40% and 60% and impacts on the accuracy of the model. Then clustering, measuring, and selecting the parameters to be used in the model is also crucial.

As a recommendation, which we hope to make in a forthcoming study, it is fascinating to apply an analysis of the data now and model it using neural networks and thus be able to contrast these results with those obtained in our study.

REFERENCES

- Alvear, J.O. 2018. Decision Trees and Random Forest. Retrieved from <https://bookdown.org/content/2031/ensambladores-random-forest-parte-ii.html> (accessed date 24 July 2022).
- Amado, T.M. and De la Cruz, J.C. 2018. Development of Machine Learning-based Predictive Models for Air Quality Monitoring and Characterization. Proceedings of TENCON 2018. IEEE Region 10 Conference, pp. 668-672. <https://doi.org/10.1109/TENCON.2018.8650518>
- Anaya Díaz, J.J. 2015. Prototype System for Estimating the Behavior of the Air Quality Index Using Computational Learning Techniques. National University of Colombia, Bogotá.
- Pinto, J.A., Kumar, P., Alonso, M.F., Andreão, W.L., Pedruzzi, R., dos Santos, F.S. and de Almeida Albuquerque, T.T. 2020. Traffic data in air quality modeling: A review of key variables, improvements in results, open problems and challenges in current research. Atmos. Pollut. Res., 11(3): 454-468. <https://doi.org/10.1016/j.apr.2019.11.018>
- Bellinger, C., Shazan, M., Zaïane, O. and Osornio-Vargas, A. 2017. A systematic review of data mining and machine learning for air pollution

- epidemiology. *BMC Public Health*, 17: 907. <https://doi.org/10.1186/s12889-017-4914-3>
- Biancofiore, F., Verdecchia, M., Di Carlo, P., Tomassetti, B., Aruffo, E., Busilacchio, M. and Colangeli, C. 2015. Analysis of surface ozone using a recurrent neural network. *Sci. Total Environ.*, 514: 379-387. <https://doi.org/10.1016/j.scitotenv.2015.01.106>
- Buenadicha, C., Galdon, G., Hermosilla, M.P., Loewe, D. and Pombo, C. 2019. Why it matters and how to make fair use of data in a digital world IDB. *Ethical Data Management*.
- Camí Núñez, V., 2020 Estimation of air quality in Galicia using machine-learning techniques. Open University of Catalonia, Catalonia.
- CRAN. 2022 Factoextra: Extract and Visualize the Results of Multivariate Data Analyses. [En línea] Retrieved from <https://cran.r-project.org/web/packages/factoextra/readme/README.html> (accessed date 24 July 2022).
- Deshmukh, M.A. and Gulhane, R.A. 2016. Importance of clustering in data mining. *Int. J. Sci. Eng. Res.*, 7(12): 54.
- Dung, N.A., Son, D.H., Hanh, N.T.D. and Tri, D.Q. 2019. Effect of meteorological factors on PM10 concentration in Hanoi, Vietnam. *J. Geosci. Environ. Protect.*, 7(11): 138.
- EPA. 2021. Environmental Protection Agency. Retrieved from <https://www.epa.gov/ground-level-ozone-pollution/ground-level-ozone-basics> (accessed date October 15, 2021).
- Gao, M., Yin, L. and Ning, J. 2018. Artificial neural network model for ozone concentration estimation and Monte Carlo analysis. *Atmos. Environ.*, 184: 129-139.
- Gonzalez Diaz, I. 2017. Big Data for CEOs and Marketing Directors: How to master Big Data Analytics in 5 weeks for managers. Independently Published. <https://doi.org/10.1016/j.atmosenv.2018.03.027>
- Harbola, S., Koch, S., Ertl, T. and Coors, V. 2021. Air quality temporal analyzer: Interactive temporal analyses with visual predictive assessments. *The Eurograph. Assoc.*, 12: 45-50. <https://doi.org/10.2312/envirvis.20211083>
- Herman, M., Rivera, S., Mills, S., Sullivan, J., Guerra, P., Cosmas, A., Farris, D. and Kohlwey, M. 2013. *The Field Guide to Data Science*.
- Hsieh, H.P., Lin, S.D. and Zheng, Y. 2015. Inferring air quality for station location recommendation based on urban big data. *Knowl. Discov. Data Mining*, 16: 437-446. <https://doi.org/10.1145/2783258.2783344>
- Joaquín Amat, R. 2020. Decision Trees, Random Forest, Gradient Boosting, and C5.0. Available at https://rpubs.com/Joaquin_AR/255596 (Accessed date 18 September 2022).
- Kurt, A. and Oktay, A.B. 2010. Forecasting air pollutant indicator levels with geographic models 3 days in advance using neural networks. *Expert Syst. with Appl.*, 37: 7986-7992. <https://doi.org/10.1016/j.eswa.2010.05.093>
- Lightstone, S., Gross, B., Moshary, F. and Castillo, P. 2021. Development and assessment of spatially continuous predictive algorithms for fine particulate matter in New York State. *Atmosphere*, 12(3): 315. <https://doi.org/10.3390/atmos12030315>
- Lim, C.C., Kim, H., Vilcassim, M.R., Thurston, G.D., Gordon, T., Chen, L.C. and Kim, S.Y. 2019. Mapping urban air quality using mobile sampling with low-cost sensors and machine learning in Seoul, South Korea. *Environ. Int.*, 131: 105022. <https://doi.org/10.1016/j.envint.2019.105022>
- Lino-Ramírez, C., Bautista-Sánchez, R. and Bombela-Jiménez, S.P. 2019. Use of a real-time system for the prediction of air pollution. *Res. Comp. Sci.*, 148: 441-453.
- Liu, H., Liu, S., Xue, B., Lv, Z., Meng, Z., Yang, X. and He, K. 2018. Ground-level ozone pollution and its health impacts in China. *Atmos. Environ.*, 173: 223-230. <https://doi.org/10.1016/j.atmosenv.2017.11.014>
- Li, X., Peng, L., Hu, Y., Shao, J. and Chi, T. 2016. Deep learning architecture for air quality predictions. *Environ. Sci. Pollut. Res.*, 23: 22408-22417.
- Mahajan, S., Liu, H.M., Tsai, T.C. and Chen, L.J. 2018. Improving the accuracy and efficiency of PM_{2.5} forecast service using cluster-based hybrid neural network model. *IEEE Access*, 6: 19193-19204. <https://doi.org/10.1109/ACCESS.2018.2820164>
- Mohan, M. and Kandy, A. 2011. An evaluation and comparison of the various statistical and deterministic techniques for forecasting the concentration of criteria air pollutants. *Int. J. Environ. Pollut.*, 44(1-4): 96-105. <https://doi.org/10.1504/IJEP.2011.038407>
- Perevochtchikova, M. 2009. The current situation of environmental monitoring systems in the metropolitan area. *Estud. Demogr. Urban.*, 24: 513-547.
- Perevochtchikova, M. 2013. Ambient impact assessment of the importance of environmental indicators. *Manag. Pub. Policy*, 22: 283-312.
- Provost, F. and Fawcett, T. 2013. *Data Science for Business*. O'Reilly, Sebastopol, CA.
- Roy, S. S., Pratyush, C. and Barna, C. 2018. Predicting ozone layer concentration using multivariate adaptive regression splines, random forest, and classification and regression tree. *Inorg. Chem. Commun.*, 144: 109895.
- Rybarczyk, Y. and Zalakeviciute, R. 2018. Machine learning approaches for outdoor air quality modeling: A systematic review. *Appl. Sci.*, 8(25): 2570. <https://doi.org/10.3390/app8122570>
- Sertel, E., Demirel, H. and Kaya, S. 2012. Predictive mapping of air pollutants: A spatial approach. *Inorg. Chem. Commun.*, 17.
- Sihag, P., Kumar, V., Afghan, F. R., Pandhiani, S. M. and Keshavarzi, A. 2019. Predictive modeling of PM 2.5 using soft computing techniques: case study-Faridabad, Haryana, India. *Air Qual. Atmos. Health*, 12: 1511-1520.
- Soh, P. W., Chang, J. W. and Huang, J. W. 2018. Adaptive deep learning-based air quality prediction model using the most relevant spatial-temporal relations. *IEEE Access*, 6: 38186-38199. <https://doi.org/10.1109/ACCESS.2018.2849820>
- Soh, P.W., Chen, K.H., Huang, J.W. and Chu, H.J. 2017. Spatial-temporal pattern analysis and prediction of air quality in Taiwan. *Inorg. Chem. Commun.*, 11: 1-6. <https://doi.org/10.1109/UMEDIA.2017.8074094>
- Tan, M., Hatf, E., Taghipour, D., Vyas, K., Kharrazi, H., Gottlieb, L. and Weiner, J. 2020. Including social and behavioral determinants in predictive models: trends, challenges, and opportunities. *JMIR Med. Inform.*, 8(9): e18084. <https://doi.org/10.2196/18084>
- Wang, D., Wei, S., Luo, H., Yue, C. and Grunder, O. 2017. A novel hybrid model for air quality index forecasting based on a two-phase decomposition technique and modified extreme learning machine. *Sci. Total Environ.*, 580: 719-733. <https://doi.org/10.1016/j.scitotenv.2016.12.018>
- Wei, W., Ramalho, O., Malingre, L., Sivanantham, S., Little, J.C. and Mandin, C. 2019. Machine learning and statistical models for predicting indoor air quality. *Indoor Air*, 29(5): 704-726. <https://doi.org/10.1111/ina.12580>
- World Health Organization (WHO). 2014. Million Premature Death Annually Linked to Air Pollution. Retrieved from <https://www.who.int/news/item/25-03-2014-7-million-premature-deaths-annually-linked-to-air-pollution> (Access date 20 October 2021).
- World Health Organization (WHO). 2019. Out of 10 People Worldwide Breathe Polluted Air, But More Countries Are Taking Action. Retrieved from <https://www.who.int/es/news/item/02-05-2018-9-out-of-10-people-worldwide-breathe-polluted-air-but-more-countries-are-taking-action> (Accessed date 20 October 2021).
- Yadav, S. 2020. Predictive Model for Analyzing PM 2.5 Level Of Air. In *Proceedings of the Int. Conf. Innov. Comp. Commun.*, 15: 295. <https://dx.doi.org/10.2139/ssrn.3562955>
- Yuchi, W., Gombojav, E., Boldbaatar, B., Galsuren, J., Enkhmaa, S., Beejin, B. and Allen, R. W. 2019. Evaluation of random forest regression and multiple linear regression for predicting indoor fine particulate matter concentrations in a highly polluted city. *Environ. Pollut.*, 245: 746-753. <https://doi.org/10.1016/j.envpol.2018.11.034>

- Zhang, C. and Yuan, D. 2015. Fast Fine-Grained Air Quality Index Level Prediction Using Random Forest Algorithm on Cluster Computing of Spark. *IEEE*, pp. 929-934. <https://doi.org/10.1109/UIC-ATC-ScalCom-CBDCCom-IoP.2015.177>.
- Zhang, Y., Wang, Y., Gao, M., Ma, Q., Zhao, J., Zhang, R. and Huang, L. 2019. A predictive data feature exploration-based air quality prediction approach. *IEEE Access*, 7, pp 30732-30743. <https://doi.org/10.1109/ACCESS.2019.2897754>.
- Zhou, Q., Jiang, H., Wang, J. and Zhou, J. 2014. A hybrid model for PM2.5 forecasting based on ensemble empirical mode decomposition and a general regression neural network. *Sci. Total Environ.*, 496: 264-274. <https://doi.org/10.1016/j.scitotenv.2014.07.051>.
- Zhou, W., Wu, X., Ding, S. and Cheng, Y. 2020. Predictive analysis of the air quality indicators in the Yangtze River Delta in China: An application of a novel seasonal grey model. *Sci. Total Environ.*, 748: 141428. <https://doi.org/10.1016/j.scitotenv.2020.141428>.
- Zhu, D., Cai, C., Yang, T. and Zhou, X. 2018. A machine learning approach for air quality prediction: Model regularization and optimization. *Big Data Cogn. Comput.*, 2(1): 5. <https://doi.org/10.3390/bdcc2010005>.

ORCID DETAILS OF THE AUTHORS

Alfredo Ricardo Zárate Valencia: <https://orcid.org/0000-0002-9584-4593>

Antonio Alfonso Rodríguez Rosales: <https://orcid.org/0000-0002-2889-075X>



Response and Tolerance of Cyanobacterial Exopolysaccharides to Rice Field Herbicide 2,4-D

Sukjailin Ryntathieng, Meguovilie Sachu and Mayashree B. Syiem†

Department of Biochemistry, North-Eastern Hill University, Shillong-793022, Meghalaya, India

†Corresponding author: Mayashree B. Syiem; mayashreesyiem@yahoo.co.in

Nat. Env. & Poll. Tech.
Website: www.neptjournal.com

Received: 18-10-2023

Revised: 21-12-2023

Accepted: 27-12-2023

Key Words:

Herbicide
Cyanobacteria
Exopolysaccharide
Biomass
Bio-flocculation
SEM

ABSTRACT

This study aimed to check how herbicide 2,4-dichlorophenoxyacetic acid (2,4-D) affects the production of EPS and its composition, growth, and biomass, as well as morphology in a cyanobacterial species isolated from a rice field in Meghalaya, India. Compared to the control cells, the growth of the organism measured in terms of chlorophyll concentration increased after being exposed to 10 and 20 ppm 2,4-D. However, cultures treated with 30 and 40 ppm experienced a decrease in their growth. Likewise, the biomass content of the organism experienced a minuscule increase in content upon exposure to 10 and 20 ppm 2,4-D but was compromised upon exposure to higher doses. When exposed to 10 ppm, the total EPS content, which includes the RPS and CPS content, showed a substantial increase. Maximum EPS production was seen at 20 ppm 2,4-D. However, exposure to 30 and 40 ppm 2,4-D, EPS production in the organism experienced a significant reduction, respectively. All components of EPS, such as uronic acid, neutral sugar, and proteins, individually showed an increase in 10 and 20 ppm 2, 4-D. A similar trend was seen in the organism's bio-flocculating activity, which increased when exposed to 10 and 20 ppm, respectively. However, this activity in cells exposed to 30 and 40 ppm 2,4-D was severely reduced. Not only the content of EPS but the rate of EPS production was also enhanced in lower concentrations of 2,4-D. Although exposure to 30 ppm 2,4-D, the rate of EPS production was not significantly compromised, 40 ppm exposure adversely affected the rate of EPS production. Furthermore, visualization using scanning electron microscopy revealed the morphological changes induced by the herbicide 2,4-D.

INTRODUCTION

The most ubiquitous photosynthetic microorganisms in nature are cyanobacteria (Frigaard 2018). They generate their energy from photosynthesis and avail their nitrogen requirement through nitrogen fixation. Thus, they have the most simple nutritional requirements from the environment. This allows them to adapt to a broad range of environments, from marine to terrestrial ecosystems (Zahra et al. 2020). These organisms have received a lot of attention in recent years due to their potential applications in biotechnology. They are employed in aquaculture, bioremediation, fertilizers, and synthesis of secondary metabolites, including exopolysaccharides, vitamins, toxins, enzymes, and medicines (Abed et al. 2009).

Cyanobacteria are known to produce significant amounts of extracellular polymeric substances or exopolysaccharides (EPS), comprised of polysaccharides, lipids, and proteins in the form of heteropolymer-like lipopolysaccharides or glycoproteins (Decho 1990, Mishra 2020, Singh et al. 2019). These EPS can either stay connected to the cell surface as

sheaths, pellets, or slimes, or they can be discharged as released polysaccharides into the environment (Pereira et al. 2011). The synthesis and production of EPS by cyanobacteria are correlated to the ability of these organisms to survive in unfavorable and stressful conditions. Its synthesis helps create a microenvironment that is structurally stable and hydrated and provides chemical and physical defense from biotic and abiotic stress factors (Parwani et al. 2021). EPS produced by cyanobacteria is a type of biopolymer that favors the formation of complex microbial communities called biofilms, where they serve key structural and defensive roles (Rossi & De Philippis 2015). Also, the cyanobacterial EPSs produced promote the formation of microbial associations under stressed or hostile environments. Several important elements influence cyanobacterial EPS production. Two examples are energy availability and the C/N ratio (De Philippis & Vincenzini 1998, Rossi & Philippis 2015). Other key elements that influence cyanobacterial EPS synthesis include nutrient level as well as growth conditions like light intensity, salinity, and temperature (Rossi & De Philippis 2015).

Structurally, cyanobacterial EPS have a complex nature and are primarily due to the presence of proteins, uronic acids (glucuronic and galacturonic acid), pyruvic acid, and *O*-methyl, *O*-acetyl, and sulfate groups (Ozturk et al. 2010). The presence of a significant amount of uronic acids contributes to the anionic and sticky nature of the exopolysaccharides. Also, substantial amounts of neutral sugars such as xylose, arabinose, mannose, and glucose are found in EPS, where glucose is the most common sugar and accounts for a large amount of the EPS composition (Plude et al. 1991, Rossi & De Philippis 2016). Owing to their structural complexity, cyanobacterial EPSs have many possible potential applications, including biofloculants, bioadhesives, soil conditioners, biopolymers, biofilms formation, food supplements, in bioremediation, and useful as medicinally important bioactive compounds (Singh et al. 2019).

Bacteria are the main removal/degradation agents for environmental toxins such as herbicides, pesticides, insecticides, and different petroleum hydrocarbons, among which some of these chemicals can be used as the sole source of carbon and energy (Fuller & Scow 1997). Several studies have looked at the impact of pesticides, especially herbicides, on exopolysaccharide synthesis (Ahmad & Khan 2012, Sultan et al. 2019, Shahid & Khan 2022). In the literature, it has been seen that herbicides like 2,4-D affect the generation of EPS in several species. However, there is very little information in the literature about anthropogenic variables affecting EPS production in cyanobacteria, such as excessive herbicide use in agricultural fields. As a result, the goal of this study is to see how the herbicide 2,4-D (10, 20, 30, and 40 ppm) affects exopolysaccharide (EPS) synthesis in the cyanobacterium *Nostoc muscorum* Meg 1.

MATERIALS AND METHODS

Growth Conditions

Nostoc muscorum Meg 1, a cyanobacterium used in the present study, was previously isolated by Ahad et al. (2017). The culture was grown in BG-11₀ media (pH 7.5) and maintained in a culture room under continuous light at a photon fluence rate of 50 $\mu\text{mol}\cdot\text{m}^{-2}\cdot\text{s}^{-1}$ and a temperature of $25 \pm 2^\circ\text{C}$ (Rippka et al. 1979).

2,4-D Treatment

Different concentrations of 2,4-D, such as 10, 20, 30, and 40 ppm, were prepared from a 2,4-D stock solution (300 ppm). To evaluate the effect of the herbicide 2,4-D on various parameters, the cultures were incubated with the herbicide for 7 days.

Chlorophyll *a* Content

The organism's growth was checked by a rise in chlorophyll-*a* concentration, as described by Mackinney (1941). Three mL of culture was centrifuged for three min at 2500 g. The supernatant was discarded, and 3 mL of methanol was added to the pellet and left overnight for chlorophyll extraction. After the incubation period, the solution was centrifuged at 2500 g. A spectrophotometer was used to measure the absorbance of the supernatant at 663 nm. The concentration of chlorophyll-*a* was determined using the formula:

$$\text{Chlorophyll-}a \text{ (}\mu\text{g}\cdot\text{mL}^{-1}\text{)} = \text{Absorbance at 663 nm} \times 12.63$$

Biomass Content

The biomass content was determined by placing 3 mL of culture in pre-weighed filter sheets and drying them in a hot air oven at 45°C until they reached a constant weight. The filter papers were weighed again with a weighing balance, and the difference was calculated as the biomass's true weight. The dry weight of the whole biomass content was expressed in grams (g).

Extraction of Exopolysaccharide

The EPS was extracted using the procedures of Cérantola et al. (2000) and Chi et al. (2007). Cell cultures were centrifuged at 10,000 g for 10 min at 4°C after 30 days of incubation. The supernatant, which contains the released polysaccharide (RPS), was collected for extraction. For Capsular or cell-bound polysaccharides (CPS) extraction, 5 mL of 0.05% NaCl, pre-heated at 60°C , was added to the pellet and incubated in a hot water bath at 60°C for 30 min. The mixture was then centrifuged for 30 min at 10,000 rpm, and the supernatant was collected. An equivalent amount of 96% ethanol was added to the supernatant separately and incubated at -20°C for 72 h. After incubation, the precipitate was centrifuged at 10,000 rpm for 30 min at 4°C and rinsed thrice with 96% ethanol. The final precipitate was dissolved in 1 mL of distilled water and stored at -20°C for further experiments.

Determination of the Polysaccharide Content

Using glucose as a reference standard, the carbohydrate content of extracellular polysaccharides was calculated using the Phenol-Sulphuric acid method described by Dubois et al. (1956).

Released polysaccharide (RPS) content: 200 μL of an extract solution was mixed with 200 μL of 5% phenol and 1000 μL of concentrated sulphuric acid. The tubes were vigorously agitated before being immersed in a boiling water bath for 5 min and then cooled before being left at room temperature for 30

min. The absorbance was spectrophotometrically measured at 492 nm.

Capsular polysaccharide (CPS) content: An extract solution (200 μL) was mixed with 5% phenol (200 μL) and concentrated sulphuric acid (500 μL), and the tubes were vigorously agitated before being immersed in a boiling water bath for 5 min and cooled before being left at room temperature for 30 min. The absorbance was spectrophotometrically measured at 492 nm.

Total polysaccharide content: Total polysaccharide content was obtained by calculating the sum of RPS and CPS content for its control and treated cultures.

Exopolysaccharide Components

Uronic acid content: 1.2 mL sodium tetraborate was added to 200 μL of the sample, and the mixture was vortexed before being treated in a hot water bath for 5 min at 100°C. It was then chilled in an ice bath. After that, 20 μL of m-hydroxy diphenyl reagent was added, mixed thoroughly, and allowed to stand for 5 min (Blumenkrantz & Asboe-Hansen 1973) before reading absorbance at 520 nm. D-glucuronic acid was used as standard (5-50 $\mu\text{g}/\text{mL}$).

Neutral sugar content: The neutral sugar content was estimated using Roe's (1955) method. 4 mL of anthrone reagent was added to 200 μL of extracted solution and carefully mixed. After 10 min of incubation in a boiling water bath, the mixture was chilled, and absorbance was measured at 630 nm. D-glucose was used as standard (10-100 $\mu\text{g}/\text{mL}$).

Protein content: Bradford's (1976) technique was used to estimate protein levels. 200 μL of an extracted solution was mixed with 3 mL of Bradford reagent. It was then incubated in the dark for 5 min, and the absorbance of the solution was read at 595 nm. BSA solution was used as standard (10-100 $\mu\text{g}\cdot\text{mL}^{-1}$).

Bioflocculating Activity

Cell culture was centrifuged for 5 min at 2900 x g. 0.5 mL of the EPS-containing supernatant was then diluted with 4.25 mL of 0.5 N acetic acid and 0.25 mL of Alcian Blue dye preparation (Alcian Blue 8 GX (1 $\text{mg}\cdot\text{mL}^{-1}$) in 0.5 N acetic acid). It was then incubated for 30 min at room temperature before being centrifuged for 10 min at 2900 x g. The supernatant was spectrophotometrically read at 610 nm. Alcian Blue and acetic acid are used in the reference assays with no EPS added.

$$\text{Flocculating activity} = \{(B - A)/B\} \times 100\%$$

where A and B are the absorbance values at 610 nm of sample and control, respectively (Kurane et al. 1994).

Rate of EPS Production

To check the rate of the production of EPS of the organism, the increase or decrease in EPS during that period was divided by the increase or decrease in biomass content during that period.

Scanning Electron Microscopy (SEM)

To check the morphological changes in the organism, control, and treated cultures were first centrifuged, and 4% glutaraldehyde in phosphate buffer was added to the pellet, followed by incubation at 4°C for 24 h. Next, the samples were washed in 0.1 % sodium cacodylate buffer three times (15 min each) and then dehydrated in acetone (20% – 100%) at 4°C at an interval of 15 min each. The dehydrated samples were mounted on brass stubs, followed by gold coating before viewing under SEM (JSM, 6360, JEOL, Japan).

Statistical Analysis

All experiments were performed in triplicate, and the data were presented as mean \pm standard deviation. GraphPad Prism 5 Software was used to do a one-way analysis of variance (ANOVA) to check the significant differences between the control and treated cultures (Dunnett test).

RESULTS AND DISCUSSION

Effect of 2,4-D on Growth (Chlorophyll Content and Biomass)

Fig. 1a shows the chlorophyll content of *Nostoc muscorum* Meg1 after exposure to 2,4-D (10, 20, 30, and 40 ppm). Exposure to 10 and 20 ppm 2,4-D, the chlorophyll content was increased by 20% ($p < 0.01$) and 1.7%, respectively, compared to their control cells. However, cultures treated with 30 and 40 ppm 2,4-D, 27%, and 84.46% ($p < 0.01$) reduction were observed. Similarly, biomass content was significantly enhanced by 12.1% upon 10 ppm exposure ($p < 0.05$). The increase in biomass output was just 4.3%, with no significant differences observed in cultures exposed to 20 ppm 2,4-D. Upon exposure to 30 and 40 ppm, there was a drastic reduction in biomass production by 21.5% and 42.13%, respectively, with a significant value of $p < 0.001$, as shown in Fig. 1b.

Effect of 2,4-D on Exopolysaccharide (EPS) Content and Rate of EPS Production

In the control culture, the total EPS content of the organism was found to be 114.6 $\mu\text{g}/\text{mL}$, out of which 90.6 $\mu\text{g}\cdot\text{mL}^{-1}$ is the released polysaccharide (RPS) and 23.9 $\mu\text{g}\cdot\text{mL}^{-1}$ is the capsular/bound polysaccharide (CPS). These values for control were taken as 100% to check the organism's reaction

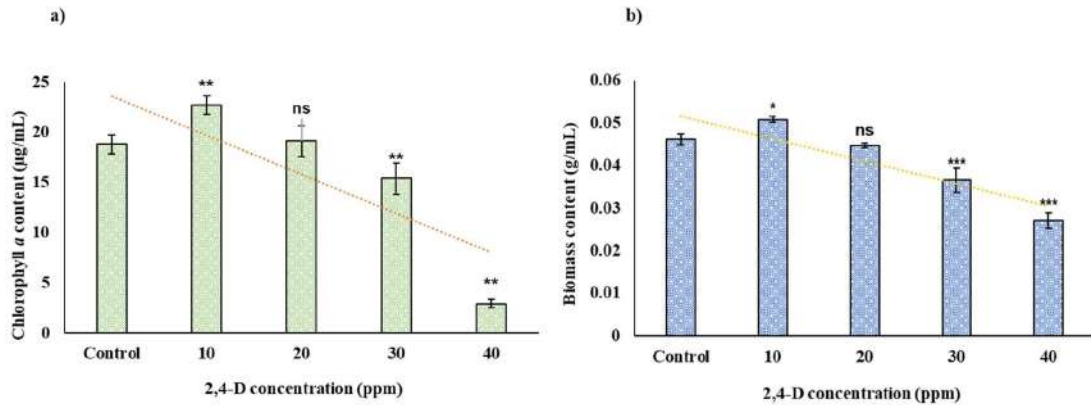


Fig. 1: Effect of 2,4-D herbicide on (a) chlorophyll content and (b) biomass content. All values are in mean \pm standard deviation (N = 3), with asterisks (* p < 0.05, ** p < 0.01, and *** p < 0.001) above the histogram bars indicating significance in differences between control and 2,4-D treated cells.

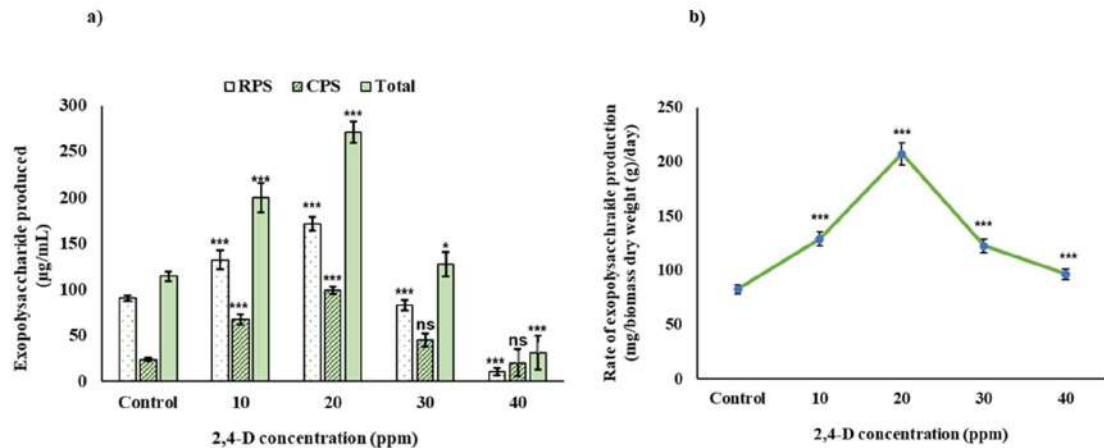


Fig. 2: Effect of 2,4-D on (a) EPS content and (b) rate of exopolysaccharide production. All values are in mean \pm standard deviation (N = 3), with asterisks (* p < 0.05, ** p < 0.01, and *** p < 0.001) above the histogram bars indicating significance in differences between control and 2,4-D treated cells.

to 2,4-D at various concentrations in terms of percentage outcomes. At 10 ppm, the total EPS content was increased by 74.17%, in RPS by 45.6%, and in CPS by 182.5%. At 20 ppm, the concentration was increased by 136% (total), 89.16% (RPS), and 315.8% (CPS). At 30 ppm, there is a reduction in the total EPS and also in RPS content by 28%. Nevertheless, the CPS content was still inclined by as much as 42%. The effect on EPS content upon exposure to 40 ppm 2,4-D was drastically affected. The total EPS content was reduced by 64%. In addition, 66% and 56% reductions were detected for RPS and CPS (Fig. 2a). Furthermore, the rate of EPS production observed an increase of 58% and 144% upon exposure to 10 and 20 ppm 2,4-D. The increase in EPS production was still evident in 30 ppm 2,4-D (48%) and 16% in 40 ppm as compared to control (Fig. 2b).

Effect of 2,4-D on Uronic Acid, Neutral Sugar, and Protein Content

Cultures exposed to 10 and 20 ppm 2,4-D showed an increase in the total uronic acid content by 46% and 98.3%, respectively, as compared to the control (Fig. 3a). Although there was an increase of 11.8% in the content of the uronic acid even at 30 ppm 2,4-D exposure, the concentration of uronic acid was reduced by 22% in the presence of 40 ppm 2,4-D (p < 0.05).

There was an increase in the neutral sugar content by 10.3%, 41.7%, and 15.1% at 10, 20, and 30 ppm 2,4-D, respectively. However, a significant (p < 0.05) decrease of 29.4% has been recorded at exposure to 40 ppm 2,4-D in comparison to the control (Fig. 3b). Furthermore, the protein content of the extracted EPS treated with 10 ppm 2,4-D

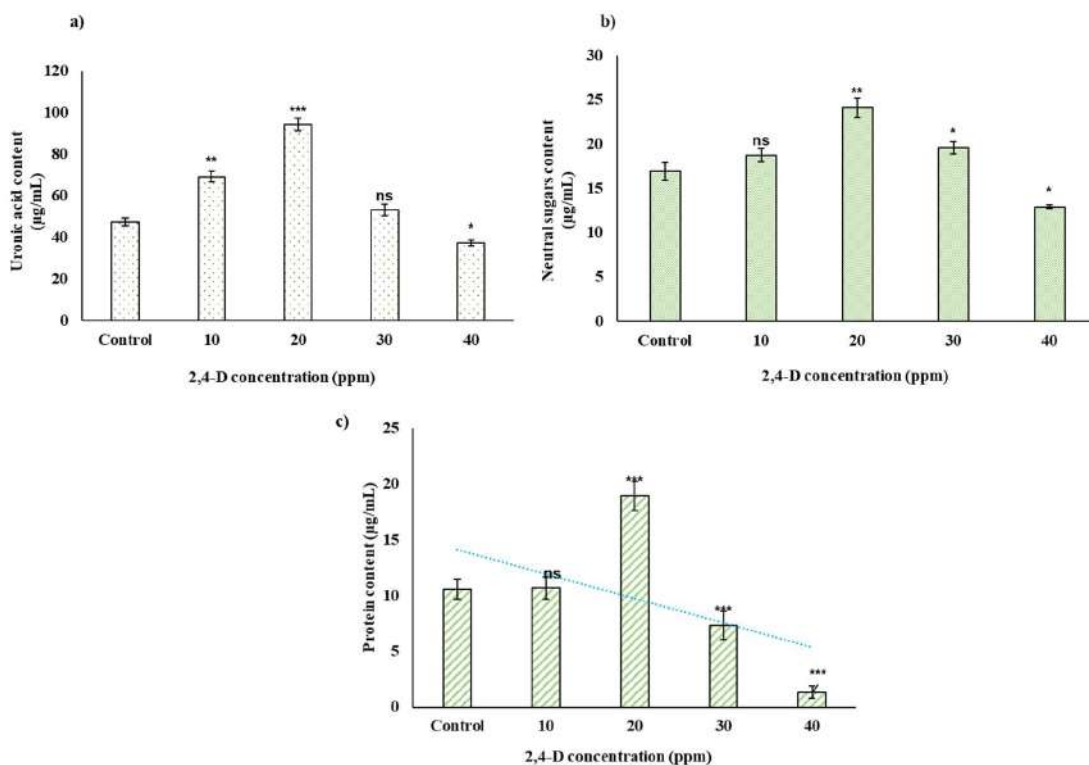


Fig. 3: Effect of 2,4-D on (a) Uronic acid content, (b) neutral sugar content, and (c) protein content. All values are in mean \pm standard deviation (N = 3), with asterisks (* p < 0.05, ** p < 0.01, and *** p < 0.001) above the histogram bars indicating significance in differences between control and 2,4-D treated cells.

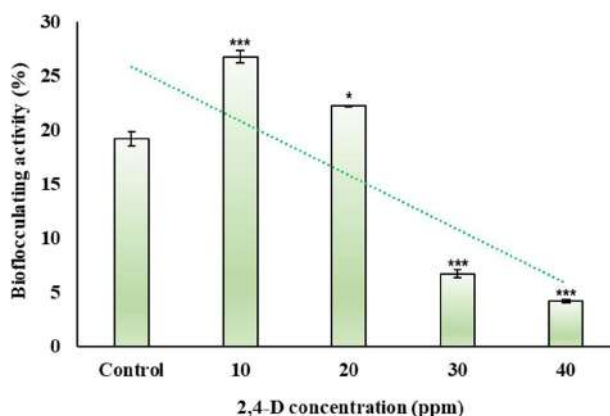


Fig. 4: Effect of 2,4-D on the bio-flocculating activity of *Nostoc muscorum* Meg 1. All values are in mean \pm standard deviation (N = 3), with asterisks (* p < 0.05, ** p < 0.01, and *** p < 0.001) above the histogram bars indicating significance in differences between control and 2,4-D treated cells.

observed an insignificant increase by just < 1%, but extreme rise in the protein content was observed by as much as > 78% in culture treated with 20 ppm 2,4-D. At 30 and 40 ppm, the protein content showed a significant reduction (p < 0.001) by ~ 30 and 87%, respectively (Fig. 3c).

Effect of 2,4-D on Bio-flocculating Activity

There was an increase in the bio-flocculating activity

compared to control upon exposure to 10 and 20 ppm 2,4-D by 39.5% (p < 0.001) and 15.8% (p < 0.05). In contrast, the bio-flocculating activity was significantly reduced by 65.1% and 78.2% (p < 0.001) upon exposure to 30 and 40 ppm (Fig. 4).

Effect of 2,4-D Stress on the Morphology of the Organism

The morphological changes of *Nostoc muscorum* Meg, 1

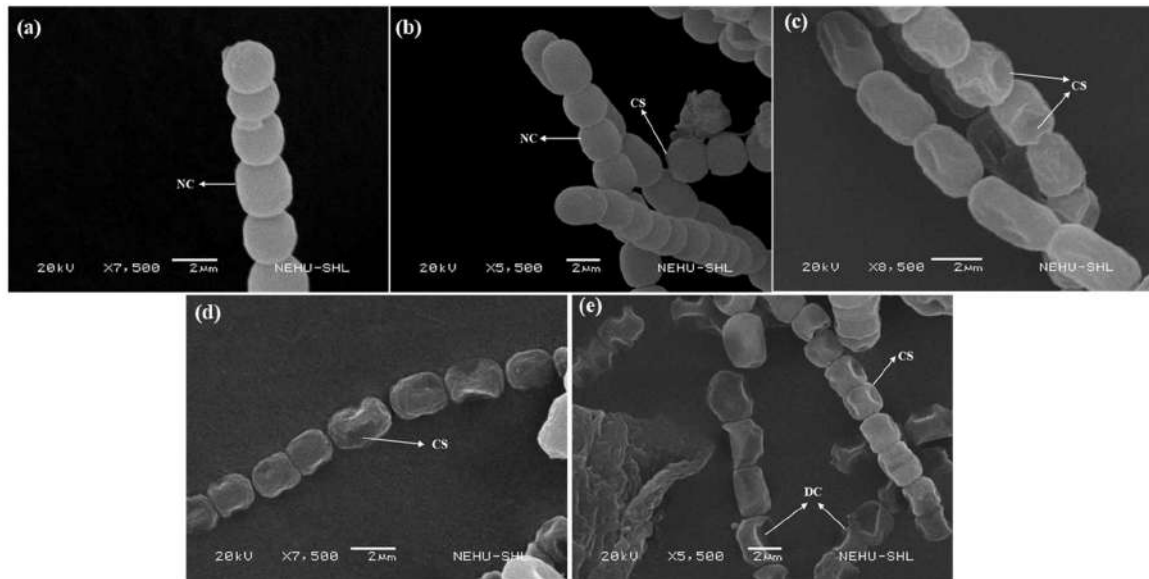


Fig. 5: Effect of 2,4-D on the morphology of *Nostoc muscorum* Meg 1. (a) Control and under-treatment of 2,4-D (b) 10 ppm (c) 20 ppm (d) 30 ppm (d) 40 ppm. NC: Normal cell; CS: Cell shrinkage; DC: Deformed cell.

under 2,4-D stress, were visualized under SEM. Control cultures showed healthy cells with intact filaments (Fig. 5a). At 10 ppm 2,4-D, the cells were intact, but minor shrinkages of the cells were seen (Fig. 5b). A much higher percentage of cell shrinkage was observed with increased 2,4-D doses (20 and 30 ppm) (Fig. 5c and 5d). However, at 40 ppm, cells were distorted and severely deformed (Fig. 5e).

Discussion

Environmental contamination and its remediation have recently gained a lot of worldwide attention (Ali et al. 2019). Agrochemical contaminations such as pesticide/herbicide from pesticide manufacturing plants, wastewater recharge facilities (wells or basins), and waste disposal sites are some substantial sources of environmental pollution (Pérez-Lucas et al. 2018). As a result, it is critical to find ways to reduce these agrochemicals from polluted areas to ensure that environmental pollution is regulated (Pavlidis & Tsihrintzis 2018). On the other hand, chemical and physical procedures for eliminating toxic agrochemical compounds are non-specific, costly, and environmentally unfriendly (Bala et al. 2022). As a result, finding suitable bioremediation processes and technologies based on microbial sources becomes critical. In this context, the usage of exopolysaccharides as bio-flocculants is one of the probable bioremediation possibilities in wastewater treatment since they are eco-friendly, non-toxic, and biodegradable.

Even though cyanobacteria can be used as an excellent tool for bioremediation of agrochemical pollution due to its

bio-flocculating activity, an excessive and non-standardized amount of polluting chemicals such as pesticides and herbicides may impede the organism's ability to bio-remediate (Gouveia et al. 2019). Furthermore, pesticides have been found to harm cyanobacterial growth, production, and biomass when applied in a continuous and unstandardized dose (Sachu et al. 2021).

In the present study, the herbicide 2,4-D was seen to negatively affect the growth of the cyanobacterium *Nostoc muscorum* Meg 1 at concentrations above 30 ppm (Fig. 1). The effect of the herbicide on growth could be due to changes in pigment synthesizing enzymes or by bringing changes such as photochemical activity and/or disruption of the light-harvesting complexes (Kalaji et al. 2016, Székács 2021). The prominent change seen when cultures were exposed to lesser doses of 2,4-D (< 20 ppm) was an increase in growth compared to control cells. This observation finds its explanation in the publication by Bellinaso et al. (2003), where it was suggested that physiological changes that occur in the organisms following exposure to lower limits of stress cause microbial metabolism to develop an alternative metabolic pathway to avoid a biochemical reaction that is hindered by stressors such as herbicides or due to the hormetic effect where the organism increases its metabolic activities to overcome such immediate adverse exposure (Sachu et al. 2021).

Excess synthesis of exopolysaccharides could be one of the reasons which provide protection against environmental stress like herbicides in soils (Ahemad & Khan 2012). In the present study, the total EPS content, as well as the RPS

and CPS contents, experienced a significant upsurge ($p < 0.001$) in their contents upon exposure to 10 and 20 ppm, respectively, where the highest EPS production was observed at 20 ppm {136% (total), 89.14% (RPS) and 315.8% (CPS)}. An increase in the contents of EPS may be because these extracellular polysaccharides are thought to present barriers to compounds such as xenobiotics and prevent their access to the organism by forming biofilms and inhibiting membrane fusion (Rossi & De Phillippis 2015, Tiwari et al. 2019). However, with an increase in the concentration of 2,4-D (30 and 40 ppm), the synthesis of EPS was affected. It was found to be more severe at 40 ppm, where the total EPS content was cut by 72.7%, with reductions of 88.2% and 31.5% for RPS and CPS, respectively, in comparison to control (Fig. 2a). Its reduction might be because herbicide-membrane contact causes the outer protective polysaccharide layer to be destroyed, which results in a decrease in EPS content (Tiwari & Prasad 2022). Following this, it was found that the rate of production of exopolysaccharide showed a similar trend in which maximum production of EPS was found at 20 ppm. This can be attributed to the fact that the herbicide at this concentration may have been perceived as a toxic threat that, in turn, resulted in the induction of EPS synthesis in the cyanobacterium. This is an example of a hormetic response by the organism when lower concentrations of a toxic substance like 2,4-D were present in its surroundings. Ahemad and Khan (2010) have already explained this phenomenon that excess EPS generation is most likely to provide the microorganisms with additional protection while they exist in stressful environments. The reduction in the rate of EPS production at higher doses of exposure seen in the study reiterated that the metabolic activities leading to the production of EPS were severely compromised during chronic exposure to the herbicide.

The compositions of EPS, such as neutral sugars, uronic acids, and proteins (glycoproteins) produced by the organism, were also affected in a similar fashion under herbicide stress. The presence of uronic acids in EPS as one of its components is significant as the negatively charged uronic acids give EPS its anionic property. Due to this anionic nature, it gives the whole macromolecule a sticky texture. Additionally, it gives EPS its ability to bind positively charged ions. This distinguishing property is advantageous in bioremediation (Bender et al. 1994, Pereira et al. 2011). Similar conclusions were reported by Redmile-Gordon et al. (2014).

An upsurge was seen in the neutral sugar concentration up to an exposure to 30 ppm 2,4-D and above, which it declined (Fig. 3b). Costa et al. (2018) and Liu et al. (2019) pointed out that neutral sugars play an essential role in the formation of microbial aggregates. Further, neutral sugars represent intracellular carbon flux that is critical for the generation

of cell energy and other molecular composites required for microbial growth. As a result, changes in this carbohydrate storage may have an impact on a variety of cell activities, including carbon fixation (Mesquita et al. 2021).

It has been pointed out that the presence of soluble proteins in the exopolysaccharide might be because of the trapped exoenzymes in the EPS matrix (Frølund et al. 1996, Kaplan Can et al. 2019). Several researchers have also reported the presence of tightly-linked peptide-sugar moieties in cyanobacterial exopolysaccharides (Panoff et al. 1988, Tiwari et al. 2020). Its presence provides varying degrees of hydrophobicity, which significantly contributes to the emulsifying property of the EPS (Alvarez et al. 2021). Protein content present in EPS helps to bind to surfaces where EPS and protein adhesins are involved in the primary steps of microbial adhesions to surfaces (Costa et al. 2018). The changes in EPS composition under 2,4-D stress may have been due to alterations in the protein content observed in the present study. This explanation has also been put forward by Donot et al. in 2012.

The increase in the exopolysaccharide's bio-flocculating activity in lower concentrations of 2,4-D (39.5% ↑ in 10 ppm) indicated that the increase in uronic acid content positively aided the flocculation mechanism (Khangembam et al. 2016).

The compromised level in all the parameters studied under higher doses of 2,4-D exposure was reflected in the biomass content of the organism. This finding was similar to the reports of Galhano et al. (2009) and Shen et al. (2009), who showed that excessive doses of herbicide could result in lessened biomass content of cyanobacteria. The inference of the present study is that the reduced EPS content registered in the study could be because of (1) compromised synthesis of EPS itself and/or (2) due to a reduction in biomass production that indirectly affected EPS production. The entire morphology of the cells was affected by the presence of 2,4-D was visible under SEM. Further, with the progressive increase in the concentration of 2,4-D, these effects were seen to be concurrently amplified, indicating that the higher doses of 2,4-D had severe consequences on the cells themselves, thus compromising their ability to mount any defense against such exposures. The schematic representation of the effect of herbicide on *Nostoc muscorum* Meg 1 is shown in Fig. 6

CONCLUSION

The outcome of this study undoubtedly established the toxic nature of unstandardized doses of 2,4-D. That 2,4-D at concentrations greater than 20 ppm can impair the production of various EPS components such as neutral sugars, uronic acids, and proteins, thereby severely restricting viable EPS synthesis was also established. The toxicity of 2,4-D was

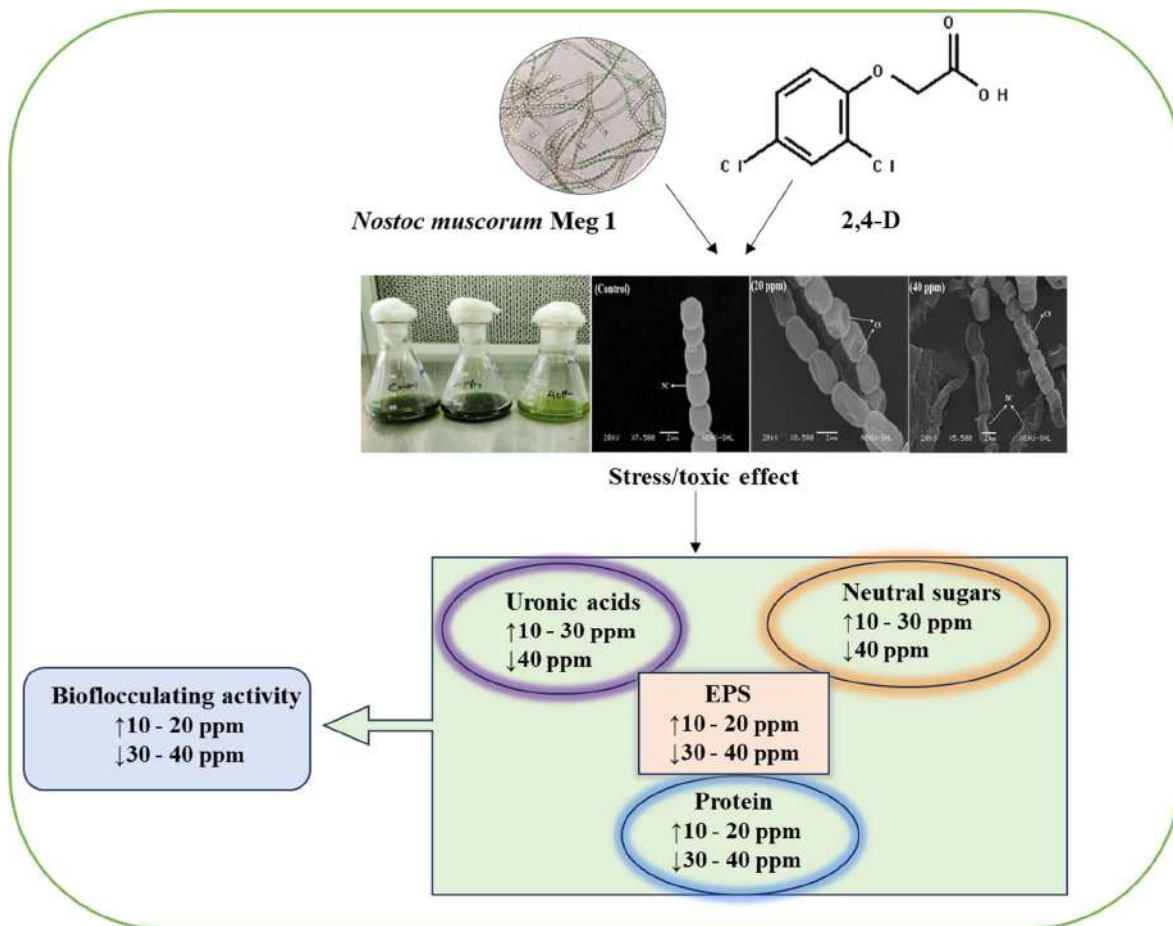


Fig. 6: Schematic representation of the effect of herbicide on *Nostoc muscorum* Meg 1.

such that at higher concentrations, it could penetrate the EPS barrier and affect the cellular metabolism, leading to reduced biomass production. However, looking further in the better part of this study, we found that when 2,4-D is present at low concentrations, the EPS production is stimulated, and the organism could mitigate the threat of 2,4-D at the EPS level itself without exposing the cells to this harmful herbicide.

ACKNOWLEDGMENT

The authors would like to acknowledge the University Grants Commission (UGC) Government of India for granting a fellowship under CSIR-NET-JRF and National Fellowship for Higher Studies of ST students being implemented by the Ministry of Tribal Affairs, SAIF (SEM) NEHU.

REFERENCES

- Abed, R.M., Dobretsov, S. and Sudesh, K. 2009. Applications of cyanobacteria in biotechnology. *J. Appl. Microbiol.*, 106(1): 1-12.
- Ahad, R.I.A., Goswami, S. and Syiem, M. B. 2017. Biosorption and equilibrium isotherms study of cadmium removal by *Nostoc muscorum* Meg 1: morphological, physiological and biochemical alterations. *3 Biotech.*, 7: 1-12.
- Ahemad, M. and Khan, M.S. 2010. Growth promotion and protection of lentils (*Lens esculenta*) against herbicide stress by *Rhizobium* species. *Ann. Microbiol.*, 60: 735-745.
- Ahemad, M. and Khan, M.S. 2012. Evaluation of plant-growth-promoting activities of rhizobacterium *Pseudomonas putida* under herbicide stress. *Ann. Microbiol.*, 62(4): 1531-1540.
- Ali, H., Khan, E. and Ilahi, I. 2019. Environmental chemistry and ecotoxicology of hazardous heavy metals: environmental persistence, toxicity, and bioaccumulation. *J. Chem.*, 2: 1-14.
- Alvarez, X., Alves, A., Ribeiro, M.P., Lazzari, M., Coutinho, P. and Otero, A. 2021. Biochemical characterization of *Nostoc* sp. exopolysaccharides and evaluation of potential use in wound healing. *Carbohydr. Polym.*, 254: 117303.
- Bala, S., Garg, D., Thirumalesh, B.V., Sharma, M., Sridhar, K., Inbaraj, B.S. and Tripathi, M. 2022. Recent strategies for bioremediation of emerging pollutants: A review for a green and sustainable environment. *Toxics*, 10(8): 484.
- Bellinaso, M.D.L., Greer, C.W., Peralba, M.D.C., Henriques, J.A.P. and Gaylarde, C.C. 2003. Biodegradation of the herbicide trifluralin by bacteria isolated from soil. *FEMS Microbiol. Ecol.*, 43(2): 191-194.
- Bender, J., Rodriguez-Eaton, S., Ekanemesang, U.M. and Phillips, P. 1994.

- Characterization of metal-binding biofloculants produced by the cyanobacterial component of mixed microbial mats. *Appl. Environ. Microbiol.*, 60(7): 2311-2315.
- Blumenkrantz, N. and Asboe-Hansen, G. 1973. A new method for the quantitative determination of uronic acids. *Anal Biochem.*, 54(2): 484-489.
- Bradford, M.M. 1976. A rapid and sensitive method for the quantitation of microgram quantities of protein utilizing the principle of protein-dye binding. *Anal. Biochem.*, 72: 248-254.
- Cérantola, S., Bounéry, J.D., Segonds, C., Marty, N. and Montrozier, H. 2000. Exopolysaccharide production by mucoid and non-mucoid strains of *Burkholderia cepacia*. *FEMS Microbiol Lett.*, 185(2): 243-246.
- Chi, Z., Su, C.D. and Lu, W.D. 2007. A new exopolysaccharide produced by marine *Cyanothece* sp. 113. *Bioresour. Technol.*, 98(6): 1329-1332.
- Costa, O.Y., Raaijmakers, J.M. and Kuramae, E.E. 2018. Microbial extracellular polymeric substances: ecological function and impact on soil aggregation. *Front Microbiol.*, 9: 1636.
- De Philippis, R. and Vincenzini, M. 1998. Exocellular polysaccharides from cyanobacteria and their possible applications. *FEMS Microbiol. Rev.*, 22(3): 151-175.
- Decho, A.W. 1990. Microbial exopolymer secretions in ocean environments: Their role(s) in food webs and marine processes. *Oceanogr. Mar. Biol.*, 28: 73-153.
- Donot, F., Fontana, A., Baccou, J. C. and Schorr-Galindo, S. 2012. Microbial exopolysaccharides: main examples of synthesis, excretion, genetics, and extraction. *Carbohydr. Polym.*, 87(2): 951-962.
- DuBois, M., Gilles, K.A., Hamilton, J.K., Rebers, P.T. and Smith, F. 1956. Colorimetric method for determination of sugars and related substances. *Anal. Chem.*, 28(3): 350-356.
- Frigaard, N.U. 2018. Sugar and Sugar Alcohol Production in Genetically Modified Cyanobacteria. In *Genetically Engineered Foods*. Academic Press, Cambridge, MA, pp. 31-47.
- Frølund, B., Palmgren, R., Keiding, K. and Nielsen, P.H. 1996. Extraction of extracellular polymers from activated sludge using a cation exchange resin. *Water Res.*, 30(8): 1749-1758.
- Fuller, M.E. and Scow, K.M. 1997. Lack of capsular exopolymer effects on the biodegradation of organic compounds by *Pseudomonas* sp. strains JS1 and JS150. *Microb. Ecol.*, 34: 248-253.
- Galhano, V., Peixoto, F., Gomes-Laranjo, J. and Fernandez-Valiente, E. 2009. Differential effects of bentazon and molinate on *Anabaena cylindrica*, an autochthonous cyanobacterium of Portuguese rice field agro-ecosystems. *Water Air Soil Pollut.*, 197: 211-222.
- Gouveia, D., Almunia, C., Cogne, Y., Pible, O., Degli-Esposti, D., Salvador, A. and Armengaud, J. 2019. Ecotoxicoproteomics: A decade of progress in our understanding of anthropogenic impact on the environment. *J. Proteomics*, 198: 66-77.
- Kalaji, H.M., Jajoo, A., Oukarroum, A., Brestic, M., Zivcak, M., Samborska, I.A. and Ladle, R.J. 2016. Chlorophyll fluorescence is a tool to monitor the physiological status of plants under abiotic stress conditions. *Acta Physiol. Plant*, 38: 1-11.
- Kaplan Can, H., Gurbuz, F. and Odabaşı, M. 2019. Partial characterization of cyanobacterial extracellular polymeric substances for aquatic ecosystems. *Aquat. Ecol.*, 53: 431-440.
- Khangembam, R., Tiwari, O.N. and Kalita, M.C. 2016. Production of exopolysaccharides by the cyanobacterium *Anabaena* sp. BTA992 and application as biofloculants. *J. Appl. Biol. Biotechnol.*, 4(1): 008-011.
- Kurane, R., Hatamochi, K., Kakuno, T., Kiyohara, M., Kawaguchi, K., Mizuno, Y. and Taniguchi, Y. 1994. Purification and characterization of lipid biofloculant produced by *Rhodococcus erythropolis*. *Biosci. Biotechnol. Biochem.*, 58(11): 1977-1982.
- Liu, C., Jia, J., Ma, T. and Feng, X. 2019. Origin and distribution of neutral sugars in soils. *Chin. J. Plant Ecol.*, 43(4): 284-295.
- Mackinney, G. 1941. Absorption of light by chlorophyll solutions. *J. Biol. Chem.*, 140(2): 315-322.
- Mesquita, A.F., Gonçalves, F.J., Rocha, C.P., Marques, J.C. and Gonçalves, A.M. 2021. Biochemical effects of two pesticides in three different temperature scenarios on the diatom *Thalassiosira weissflogii*. *Processes*, 1247 : (7)9.
- Mishra, P. 2020. Cyanobacterial Exopolysaccharide as Natural Sources for Food Packaging Applications. Springer, Singapore, pp. 171-184
- Ozturk, S., Aslim, B. and Suludere, Z. 2010. Cadmium (II) sequestration characteristics by two isolates of *Synechocystis* sp. in terms of exopolysaccharide (EPS) production and monomer composition. *Bioresour. Technol.*, 101(24): 9742-9748.
- Panoff, J. M., Priem, B., Morvan, H. and Joset, F. 1988. Sulphated exopolysaccharides are produced by two unicellular strains of cyanobacteria, *Synechocystis* PCC 6803 and 6714. *Arch. Microbiol.*, 150: 558-563.
- Parwani, L., Bhatt, M. and Singh, J. 2021. Potential biotechnological applications of cyanobacterial exopolysaccharides. *Braz. Arch. Biol. Technol.*, 64: e21200401.
- Pavlidis, G. and Tsihrintzis, V.A. 2018. Environmental benefits and control of pollution to surface water and groundwater by agroforestry systems: a review. *Water Resour. Manag.*, 32: 1-29.
- Pereira, S., Micheletti, E., Zille, A., Santos, A., Moradas-Ferreira, P., Tamagnini, P. and De Philippis, R. 2011. Using extracellular polymeric substances (EPS)-producing cyanobacteria for the bioremediation of heavy metals: Do cations compete for the EPS functional groups and also accumulate inside the cell? *Microbiology*, 157(2): 451-458.
- Pérez-Lucas, G., Vela, N., El Aatik, A. and Navarro, S. 2019. Environmental Risk of Groundwater Pollution by Pesticide Leaching Through the Soil Profile: Pesticides-Use and Misuse and Their Impact in the Environment. *IntechOpen Publishers*, NY, pp. 1-28.
- Plude, J.L., Parker, D.L., Schommer, O.J., Timmerman, R.J., Hagstrom, S.A., Joers, J.M. and Hnasko, R. 1991. Chemical characterization of polysaccharide from the slime layer of the cyanobacterium *Microcystis flos-aquae* C3-40. *Appl. Environ. Microbiol.*, 57(6): 1696-1700.
- Redmile-Gordon, M.A., Brookes, P.C., Evershed, R.P., Goulding, K.W.T. and Hirsch, P.R. 2014. Measuring the soil-microbial interface: extraction of extracellular polymeric substances (EPS) from soil biofilms. *Soil Biol. Biochem.*, 72: 163-171.
- Rippka, R., Deruelles, J., Waterbury, J.B., Herdman, M. and Stanier, R.Y. 1979. Generic assignments, strain histories, and properties of pure cultures of cyanobacteria. *Microbiology*, 111(1): 1-61.
- Roe, J.H. 1955. The determination of sugar in the blood and spinal fluid with anthrone reagent. *J. Biol. Chem.*, 212: 335-343.
- Rossi, F. and De Philippis, R. 2015. Role of cyanobacterial exopolysaccharides in phototrophic biofilms and complex microbial mats. *Life*, 5(2): 1218-1238.
- Rossi, F. and De Philippis, R. 2016. Exocellular Polysaccharides in Microalgae and Cyanobacteria: Chemical Features, Role, and Enzymes and Genes Involved in Their Biosynthesis: The Physiology of Microalgae. Springer, Singapore, pp. 565-590.
- Sachu, M., Kynshi, B.L., and Syiem, M.B. 2021. Herbicide monuron mediated alterations in carbon and nitrogen fixation in the cyanobacterium *Nostoc muscorum* Meg 1. *J. Appl. Phycol.*, 33(4): 2209-2220.
- Shahid, M. and Khan, M.S. 2022. Ecotoxicological implications of residual pesticides to beneficial soil bacteria: A review. *Pestic. Biochem. Physiol.*, 188: 105272.
- Shen, J., DiTommaso, A., Shen, M., Lu, W. and Li, Z. 2009. Molecular basis for differential metabolic responses to monosulfuron in three nitrogen-fixing cyanobacteria. *Weed Sci.*, 57(2): 133-141.
- Singh, S., Kant, C., Yadav, R.K., Reddy, Y.P. and Abraham, G. 2019. Cyanobacterial Exopolysaccharides: Composition, Biosynthesis, and Biotechnological Applications. Academic Press, Cambridge, MA, pp. 347-358.
- Sultan, M., Waheed, S., Ali, U., Sweetman, A.J., Jones, K.C. and Malik, R.N. 2019. Insight into the occurrence, profile and spatial distribution

- of organochlorine pesticides in soils of solid waste dumping sites of Pakistan: Influence of soil properties and implications for environmental fate. *Ecotoxicol. Environ. Saf.*, 170: 195-204.
- Székács, A. 2021. *Herbicide Mode of Action*. Elsevier, The Netherlands, pp. 41-86.
- Tiwari, O.N., Muthuraj, M., Bhunia, B., Bandyopadhyay, T.K., Annapurna, K., Sahu, M. and Indrama, T. 2020. Biosynthesis, purification, and structure-property relationships of new cyanobacterial exopolysaccharides. *Polym. Test*, 89: 106592.
- Tiwari, S. and Prasad, S.M. 2022. Exogenous application of phytohormones modulates pesticide-induced injury in two rice field cyanobacteria: Toxicity alleviation by up-regulation of the ascorbate-glutathione cycle. *Plant Stress*, 3: 100046.
- Tiwari, S., Parihar, P., Patel, A., Singh, R. and Prasad, S.M. 2019. *Metals in Cyanobacteria: Physiological and Molecular Regulation*. Academic Press, Cambridge, MA, pp. 261-276.
- Zahra, Z., Choo, D.H., Lee, H. and Parveen, A. 2020. *Cyanobacteria: Review of current potentials and applications*. *Environments*, 7(2): 13.

ORCID DETAILS OF THE AUTHORS

Mayashree B Syiem: <https://orcid.org/0000-0001-5954-3892>



A Novel Coal-Associated Soil as an Effective Adsorbent for Reactive Blue Dye Removal

T. R. Sundararaman*†, M. Millicent Mabel** and G. Carlin Geor Malar**

*Department of Chemical Engineering, Rajalakshmi Engineering College, Thandalam, Chennai-602105, India

**Department of Biotechnology, Rajalakshmi Engineering College, Thandalam, Chennai-602105, India

†Corresponding author: T. R. Sundararaman; sundararaman.tr@rajalakshmi.edu.in

Nat. Env. & Poll. Tech.
Website: www.neptjournal.com

Received: 29-07-2023

Revised: 12-09-2023

Accepted: 11-10-2023

Key Words:

Coal
Soil
Reactive blue
Adsorbent
Dye

ABSTRACT

The project aims to remove reactive blue dye from the effluent of textile industries by utilizing coal-associated soil as an adsorbent, as it possesses effective physical properties and distinguishing characteristics. In comparison to other separation techniques, the adsorption method is the most effective, cost-effective, and straightforward. A batch adsorption investigation was carried out to examine the various adsorption-influencing factors, including solution pH, adsorbent dosage, contact time, temperature, and dye concentration. Contact time of 30 min, an adsorbent dosage of 10g.100 mL⁻¹, a solution pH of 7, a temperature of 30°C, and an initial dye concentration of 100 mg.L⁻¹ were found to be optimal for dye adsorption. Using two distinct kinetic models, the evaluation of kinetic studies revealed that the pseudo-second-order provided the greatest fit, with a higher R² value than the pseudo-first-order. The thermodynamic parameters Gibbs free energy (ΔG°), entropy (ΔS°), and enthalpy (ΔH°) indicated that the current adsorption system was exothermic and spontaneous. Further study of the adsorption isotherm revealed that the Langmuir isotherm model provided the best fit, with an R² value of 0.977%.

INTRODUCTION

Water contamination or pollution results from the discharge of industrial effluents and the continuous, excessive use of fertilizers and pesticides in agricultural fields (Mahvi et al. 2011, Malakootian et al. 2013). The degradation of the water quality that results in water contamination or pollution is brought on by the discharge of industrial effluents and the continued excessive use of fertilizers and pesticides in agricultural areas (Sharifpour et al. 2018, Javid et al. 2020). Freshwater demand is rising rapidly as it is heavily contaminated by the textile, leather, paper, and cosmetic industries (Muthulingam et al. 2018). Every year, a wide range of synthetic dyes are manufactured and used in industry (Malar et al. 2023). The dyeing process loses 50% of its reactive colors to effluents (Amin & Blackburn 2015). Reactive dyes are pigments with reactive groups that can make covalent connections between the dye's carbon atom and the OH-, NH-, or SH groups in fiber (Zhao et al. 2022). They are assemblages of hues that establish covalent bonds with fibers and become components of the fiber itself. When they engage chemically with the molecules of the fiber, covalent bonds are formed.

One example of a reactive dye is reactive blue 4. With the molecular formula C₂₃H₁₂C₁₂N₆Na₂O₈S₂, reactive blue 4 has an anthraquinone molecular structure (Epoloto et al.

2005). The molecular weight of reactive blue 4 is 637.43. The dye is dark blue and also comes in powder form. This dye is often used to color cotton, nylon, and other textiles. Also, reactive dyes directly contaminate the ecosystem and cause different carcinogenic or mutagenesis diseases in living beings (Berradi et al. 2019). Hence, removing reactive dyes from and other effluents before they enter natural water bodies is environmentally significant. As reactive dyes prevent light trapping for photosynthesis, plants are also harmed (Bae et al. 2006).

Textile manufacturing produces the most wastewater in the environment, which has intense color, highly variable pH, high chemical oxygen demand, and toxicity. Reactive dye dyes cotton, wool, and polyamide filters in textiles. Most reactive dyes do not bind to textiles (Lellis et al. 2019). Reactive dyes are non-degradable in aerobic biological treatment systems, leaving persistent colors in effluents. Many biological and chemical methods have been developed to remove dyes from aqueous-colored effluents and lessen their ecological impact (Adane et al. 2021). But traditional methods cannot purify textile industry wastewater of colored effluents.

Adsorption is a surface phenomenon that is the result of complex interactions between the three constituents: the adsorbent, the adsorbate, and the wastewater, which may

be effluent, a synthetic solution, or water (Seenuvasan et al. 2021). The separation is based on the selective adsorption of pollutants by an adsorbent, i.e., thermodynamic and/or kinetic selectivity, as a result of particular interactions between the surface of the adsorbent material and the pollutants adsorbed. The affinity between the adsorbent and the adsorbate is the primary interaction factor affecting adsorption in this ternary system (Rapo & Tonk 2021). The carbon in coal comprises mesoporous components that are effective for adsorbing dye molecules from industrial or aqueous effluents, and these oxides have active sites. Hence, the soil associated with coal also contains significant amounts of carbon in addition to the mineral oxides (Baocheng et al. 2008, Tarkwa et al. 2019, Astuti et al. 2019).

In this study, the removal of reactive blue dye is expected using the coal-associated soil as an effective adsorbent. The batch adsorption study was performed with optimized parameters, including pH, temperature, contact time, adsorbent dosage, and dye concentration. The adsorption mechanism was validated through isotherm and kinetic studies.

MATERIALS AND METHODS

Preparation of Adsorbent

Coal-associated soil was collected from the Mannargudi Coalfield, Tamil Nadu, India. The soil was washed with water and then dried at room temperature to remove any dust particles. To get the ideal adsorbent for the dye removal, the dried soil samples were sieved through a mesh sieve. Using FTIR (Perkin Elmer spectrum RX 1) and SEM (Zeiss FESEM SIGMA VP03-04 MODEL) spectroscopy, coal-associated soil was qualitatively analyzed both before and after adsorption. The characteristics of the collected coal-associated soil were estimated as follows: pH: 2.8, organic matter content: 29.90%, silica content: 32.13%, alumina content: 1.12%, and iron oxide content: 1.97%.

Preparation of Adsorbate

Reactive Blue 4 dye ($C_{23}H_{14}C_{12}N_6O_8S_2$, molecular weight is 637.43) was purchased from Sigma Aldrich Pvt. Ltd. Adding 1g of reactive blue dye to 1L of water made the Reactive Blue 4 dye standard solution. To get different concentrations of dye solution, ranging from 10 mg.L⁻¹ to 100 mg.L⁻¹, the standard solution was diluted with distilled water. Reactive blue dye was discovered to have a maximum wavelength (max) of 580 nm (Dutta et al. 2021). Reactive blue dye was analyzed colorimetrically to quantify the concentration of the dye in the solution both before and after adsorption.

Batch Adsorption Studies

Adsorption experiments were carried out in batches

for various adsorption-influencing parameters such as temperature, solution pH (2 to 10), initial reactive blue dye concentration (50 to 250 mg.L⁻¹), contact time (10 to 50 min), and adsorbent dosage (6 to 14 g.100 mL⁻¹). The batch adsorption experiments for each parameter study were carried out by varying the respective parameters while keeping the other parameters constant.

To 100 mL of working solution, a suitable amount of adsorbent was added and agitated in a rotary shaker at 100 rpm to ensure efficient adsorption. At a specified time interval, the samples were collected and centrifuged at 2000 rpm for 10 min to distinguish the solution and the adsorbent. The supernatant was collected, and the percentage removal of reactive blue dye from the aqueous solution was calculated by measuring absorbance at 580 nm with a colorimeter. Using Eqn. (1), the percentage removal of reactive blue dye was calculated.

$$\% \text{ Removal} = \frac{C_i - C_f}{C_i} \times 100 \quad \dots(1)$$

Where C_i and C_f are the initial and final concentrations of dye (mg/L).

Isotherm and Kinetics Studies

The isothermal study aids in identifying the interface mechanism between coal-associated soil and reactive blue dye. At various adsorbate concentrations (50-250 mg.L⁻¹), adsorption isotherm investigations were conducted. The optimal amount of adsorbent was added to 100 mL of the working solution and kept in the rotary shaker for the allotted period. The samples were taken after the specified time interval and centrifuged at 2000 rpm for 10 min, and the absorbance was measured at 580 nm. The equilibrium adsorption capacity of the coal-associated soil was calculated by Eqn. (2).

$$q_e = \frac{(C_i - C_e)V}{m} \quad \dots(2)$$

where q_e is the equilibrium adsorption capacity (mg/g), C_i and C_e are the initial and final concentrations of dye (mg.L⁻¹), V is the volume of reactive dye solution (L), and m is the weight of adsorbent used (g). Langmuir and Freundlich's isotherms were performed with the equilibrium data using MATLAB R2016a software.

The rate of adsorption was elucidated using the adsorption kinetics study. By stirring the flasks containing 100 mL of various dye solution concentrations (ranging from 50 mg.L⁻¹ to 250 mg.L⁻¹) and the necessary amount of adsorbent, kinetic studies were carried out. The samples were collected every 5 min and centrifuged. Eqn. (3) was used to calculate the amount of reactive blue dye that has

been removed from coal-associated soil over specific time intervals.

$$q_t = \frac{(C_i - C_t)V}{m} \quad \dots(3)$$

Where q_t is the equilibrium adsorption capacity (mg/g), C_i is the initial concentration of dye (mg/L), C_t is the concentration of dye at different time intervals (mg.L⁻¹), V is the volume of reactive dye solution (L), and m is the weight of adsorbent used (g). Similar to the isotherm studies, the kinetic parameters were found using MATLAB R2016a software.

Thermodynamic Study

The experimental study investigated the thermodynamic aspects of the adsorption process between a reactive blue dye and coal-associated soil. The experiments were conducted at various temperatures ranging from 30°C to 50°C. A 250 mL Erlenmeyer flask was used, containing 100 mL of the dye solution and 10 g of soil. The thermodynamic parameters, including Gibbs free energy (ΔG° , KJ.mol⁻¹), enthalpy change (ΔH° , KJ/mol), and entropy change (ΔS° , J/mol), were determined using Eqns. (4) and (5):

$$\Delta G^\circ = -RT \ln K_d \quad \dots(4)$$

$$K_d = \frac{q_e}{C_e} \quad \dots(5)$$

Where K_d is the equilibrium constant, q_e is the equilibrium adsorption capacity (mg/g), C_e is the equilibrium concentration (mg.L⁻¹), and R is the gas constant (8.314 J mol⁻¹ K⁻¹).

RESULTS AND DISCUSSION

Characterization Studies of the Adsorbent

SEM analysis: SEM analysis was used to examine the adsorbent's porous characteristics and surface structure. The SEM analysis of coal-associated soil before and after the dye adsorption is shown in Fig. 1(a & b). Before adsorption, a rough, porous structure with higher voids was observed (Fig. 1(a)), and the enhanced surface area with irregular and linked pores, which are crucial for the effective adsorption of reactive blue dye molecules, was also exhibited. Following the adsorption of the dye, the formation of the agglomeration was evident in Fig. 1(b). As a result, the agglomerates and disappeared pores with a smooth surface support the dye's adsorption to coal-associated soil.

FTIR analysis: FTIR analysis was performed before and after adsorption of the dye and is shown in Fig. 2. A high signal at 2954.52 cm⁻¹ indicates that alkanes stretch the C-H bond before adsorption (Malar et al. 2019). The presence of additional functional groups, such as aromatic ring stretching, aliphatic, and aromatic phosphate compounds, is indicated by the absorption peaks at 1620.40 cm⁻¹, 1011.97 cm⁻¹, and 927.84 cm⁻¹. The silicone group and the primary amine (C-N) broadening are related to the strong peak at 1054.21 cm⁻¹. The FTIR examination of coal-associated soil suggests that alcohol and amine groups may form covalent connections prior to adsorption, forming a matrix structure that would make it simpler to remove the coal.

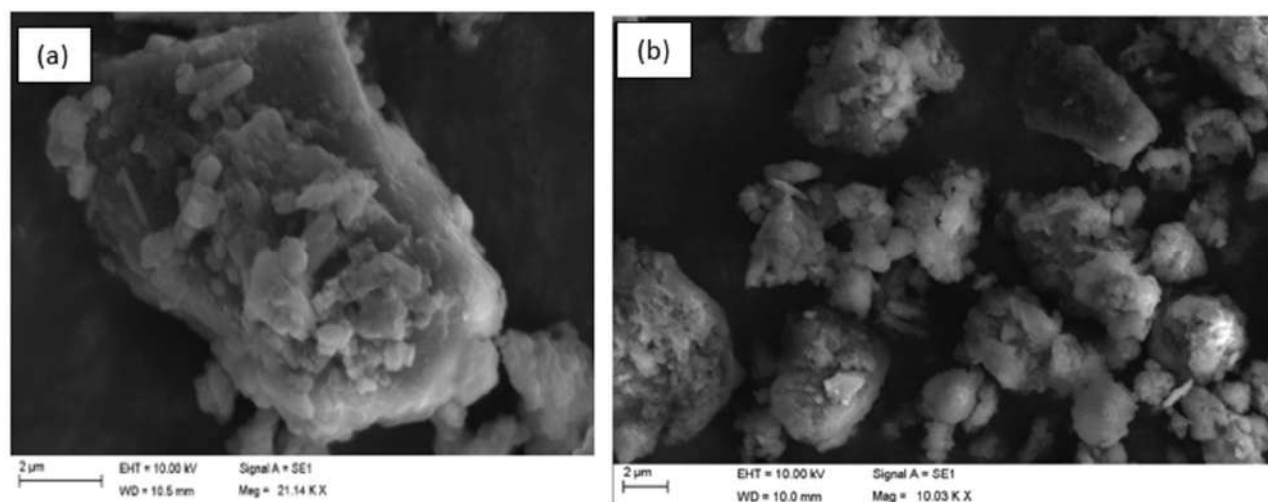


Fig. 1: Electron Micrographs of coal-associated soil (a) before and (b) after adsorption.

Effect of pH

In a batch adsorption experiment, the pH of a dye solution was varied from 2.0 to 10.0 while keeping other parameters constant. The results, shown in Fig. 3, demonstrate that the percentage removal of the dye increased gradually as the pH shifted from acidic to neutral (El-Nemr et al. 2020). Equilibrium adsorption occurred at neutral pH due to the dye's neutral nature. However, beyond neutral pH, the percentage removal decreased. The highest removal of the dye was observed at pH 7.0 (neutral).

Effect of Contact Time

In a batch study, the effect of contact time on the removal of reactive blue dye using coal-associated soil as the adsorbent was investigated. The dye concentration was 100 mg.L^{-1} , the pH was maintained at 7, and the adsorbent dosage was 10 g. The sample was agitated in an orbital shaker at 100 rpm, and samples were collected at 10-minute intervals. Fig. 4 revealed that the removal of reactive blue dye increased from 10 min to 30 min. The initial adsorption rate was high, likely due to the availability of more active sites. However, once equilibrium was reached, no further adsorption occurred (Zhang 2023). The highest percentage removal of the dye onto coal-associated soil was observed at a contact time of 30 mins.

Effect of Adsorbent Dosage

In the batch adsorption experiment, the impact of adsorbent dosage on the removal of reactive blue dye was investigated while keeping other parameters constant. The dosage of the adsorbent was varied from 6 g to 14 g, and as demonstrated in Fig. 5, lower adsorbent dosages resulted in lower percentage removal of the dye. This can be attributed to the limited availability of active sites on the surface of the coal-associated soil. However, as the adsorbent dosage increased, the percentage removal of the dye also increased due to the greater number of active sites provided by the soil. Beyond an adsorbent dosage of 10 g, there was no significant increase in dye removal due to factors such as low driving force, saturation of active sites, and insufficient dye presence in the solution. Therefore, the optimum adsorbent dosage for the removal of reactive blue dye was determined to be $10 \text{ g.}100 \text{ mL}^{-1}$.

Effect of Initial Dye Concentration

In a batch adsorption experiment, the impact of initial dye concentration on the adsorption of reactive blue dye onto coal-associated soil was examined. The experiment involved different reactive blue concentrations ranging from 50 mg.L^{-1} to 250 mg.L^{-1} (Fig. 6). It was observed that as the dye concentration increased, the adsorption of reactive

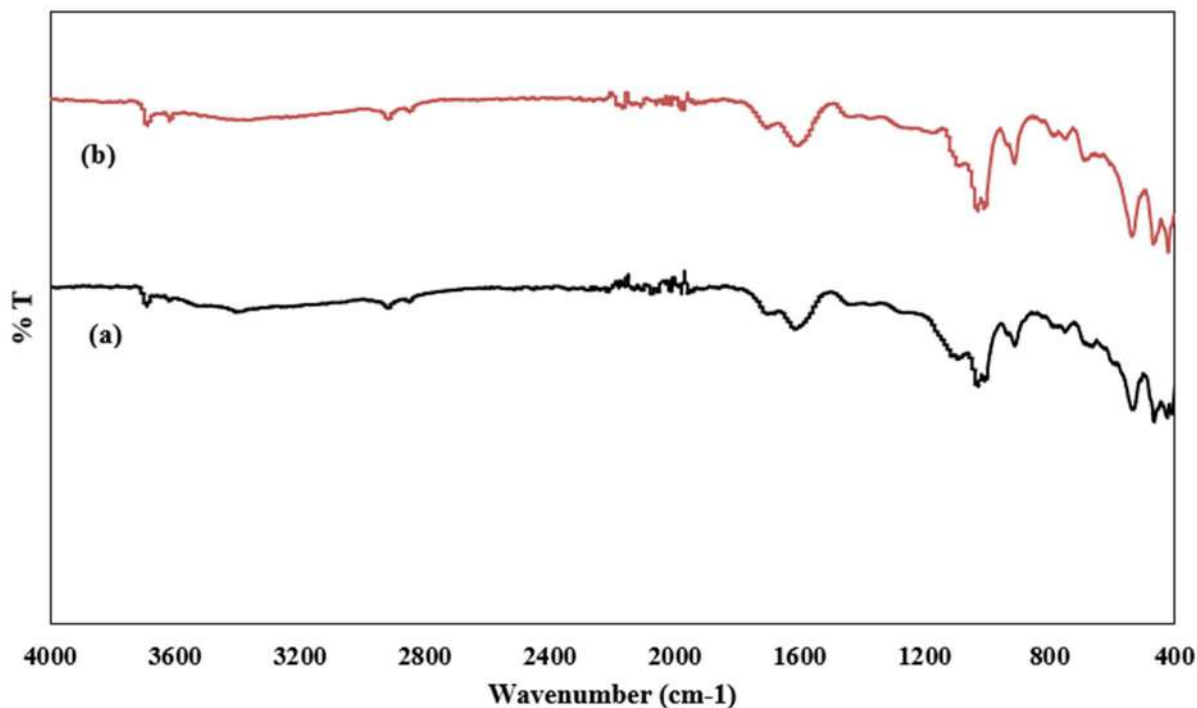


Fig. 2. FT-IR Spectrum of coal-associated soil (a) before and (b) after adsorption.

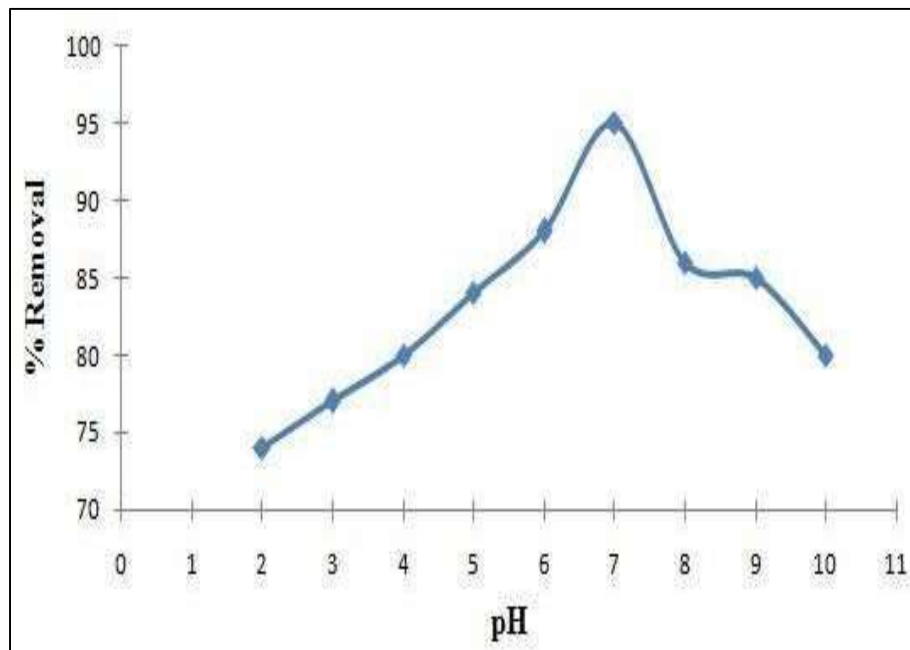


Fig. 3: Effect of pH on adsorption.

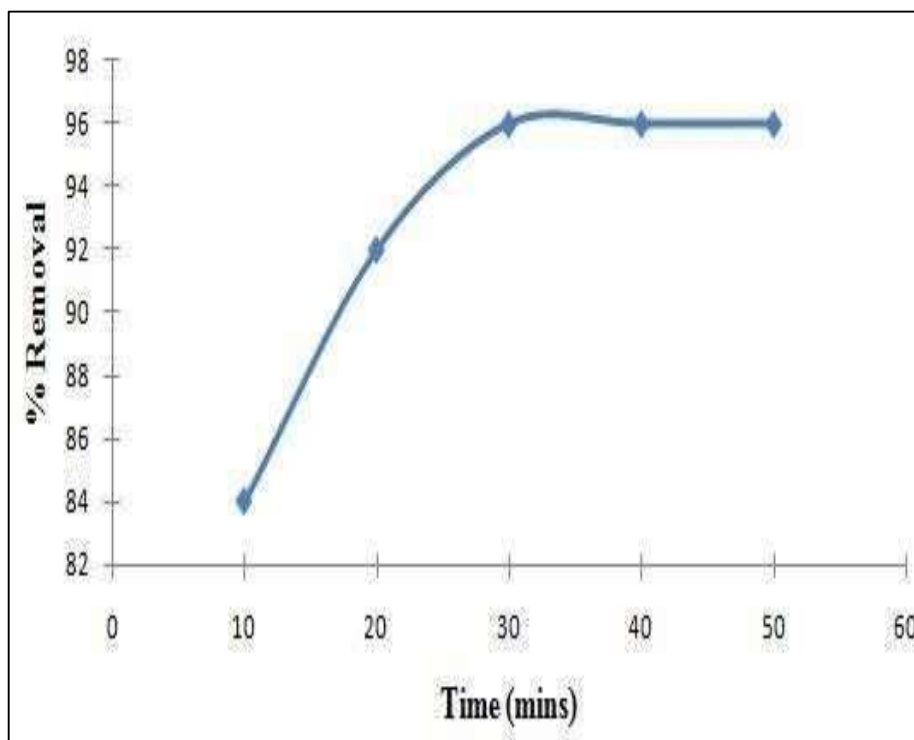


Fig. 4: Effect of contact time in adsorption.

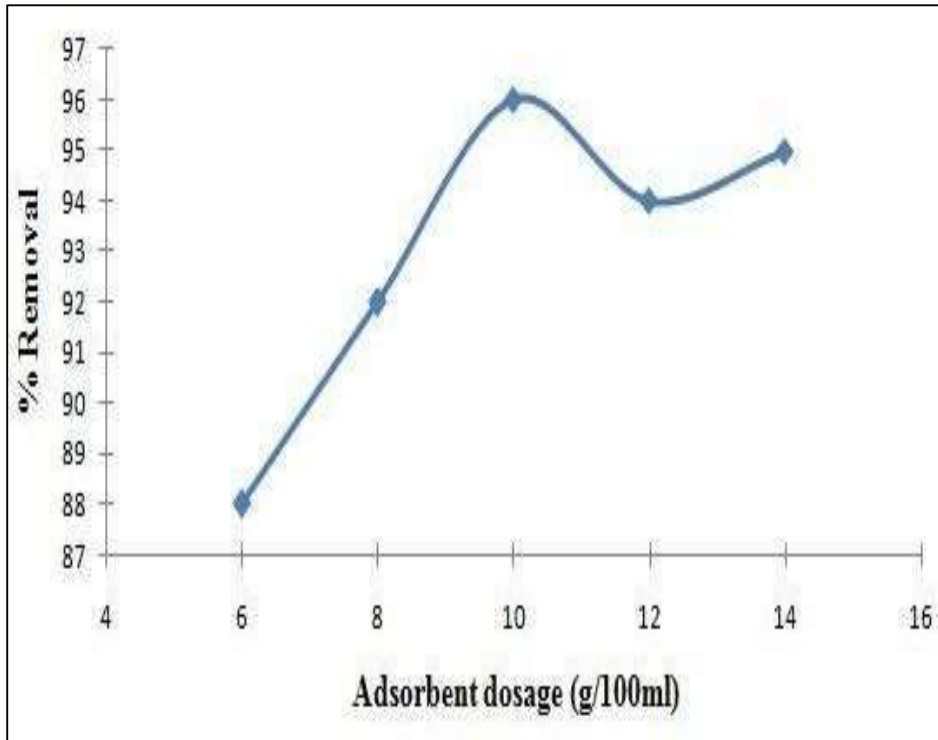


Fig. 5: Effect of Adsorbent dosage in adsorption.

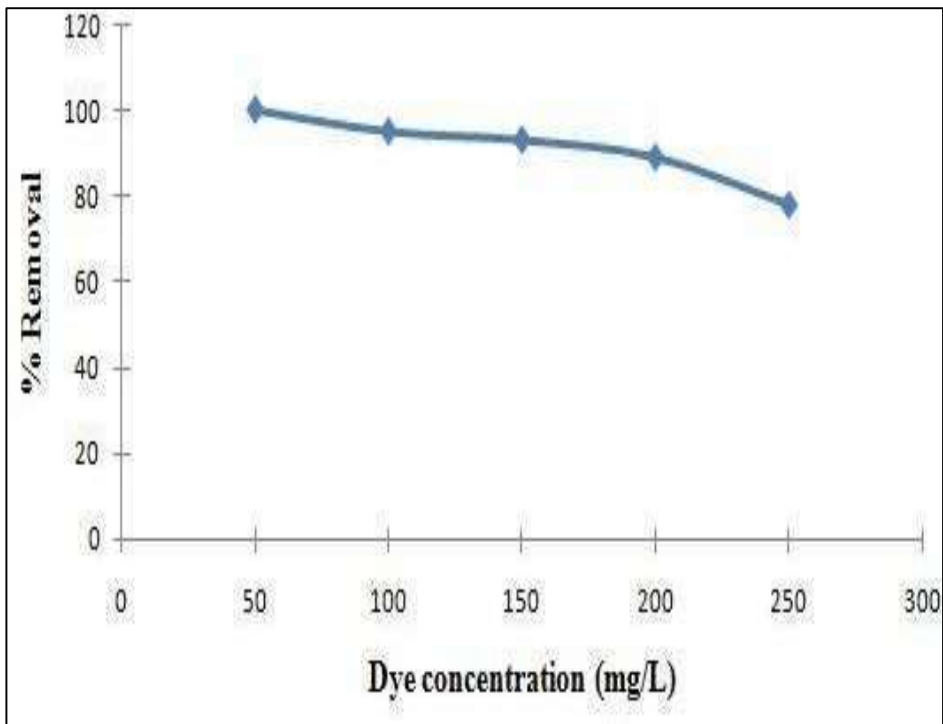


Fig. 6: Effect of Initial Dye Concentration in adsorption.

blue dye decreased. This decrease can be attributed to the limited availability of active sites on the soil's surface at higher dye concentrations, resulting in a reduced percentage removal of dye. Consequently, the optimal dye concentration for effective adsorption was determined to be 100 mg.L⁻¹.

Effect of Temperature

In a batch adsorption experiment, the impact of temperature on the removal of reactive blue dye using coal-associated soil as the adsorbent was investigated. The experiment involved three different temperatures (303K, 313K, 323K) while keeping other parameters constant. Fig. 7 depicts the effect of temperature on the dye removal. It was observed that as the temperature increased, the removal of reactive blue dye decreased. This can be attributed to the weakening of the attractive forces between the dye and the soil at higher temperatures. The results suggest that the adsorption process

was exothermic, and the optimal temperature for efficient removal of reactive blue dye was determined to be 303K.

Adsorption Kinetics Studies

An adsorption kinetic experiment was conducted using coal-associated soil as the adsorbent to investigate the rate of reactive blue dye removal from an aqueous solution. The experiment involved varying the initial dye concentration (50 mg.L⁻¹ to 250 mg.L⁻¹) and contact time (5 mins to 30 mins) while keeping the adsorbent dosage at 10 g and temperature at 303K.

Two adsorption kinetic models were used, and Table 1 presents the calculated rate constants (k_1 , k_2), correlation coefficients (R^2), and adsorption capacities (q_e) for each model. The rate constant for pseudo-second-order kinetics decreased with increasing dye concentration, indicating competition for active sites on the soil's surface. Pseudo-

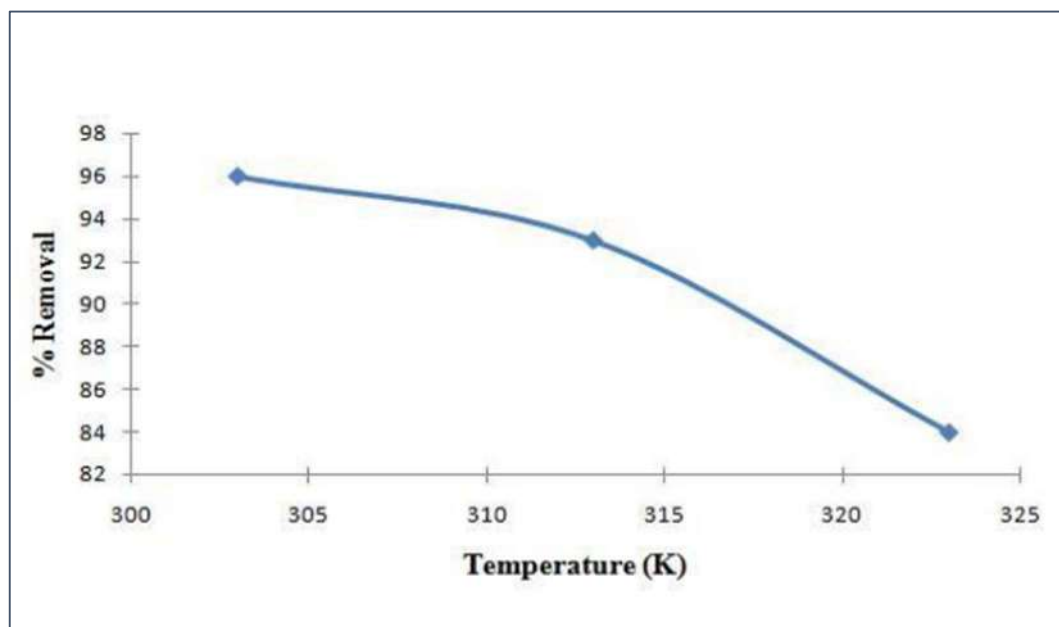


Fig. 7: Effect of temperature on adsorption.

Table 1: Kinetic fit for the adsorption of reactive blue dye onto coal-associated soil.

C_o [mg.L ⁻¹]	Exp q_e [mg.g ⁻¹]	Pseudo first order			Pseudo second order		
		Calc q_e [mg.g ⁻¹]	k_1 (min ⁻¹)	R^2	Calc q_e [mg.g ⁻¹]	k_2 (g.mg ⁻¹ .min ⁻¹)	R^2
50	0.50	0.183	-0.0035	0.966	0.523	1.002	0.999
100	0.98	1.203	-0.0054	0.874	1.526	0.044	0.777
150	1.46	1.877	-0.0052	0.932	1.976	0.052	0.941
200	1.86	2.181	-0.0052	0.890	2.227	0.075	0.988
250	2.20	3.346	-0.0063	0.949	2.597	0.073	0.998

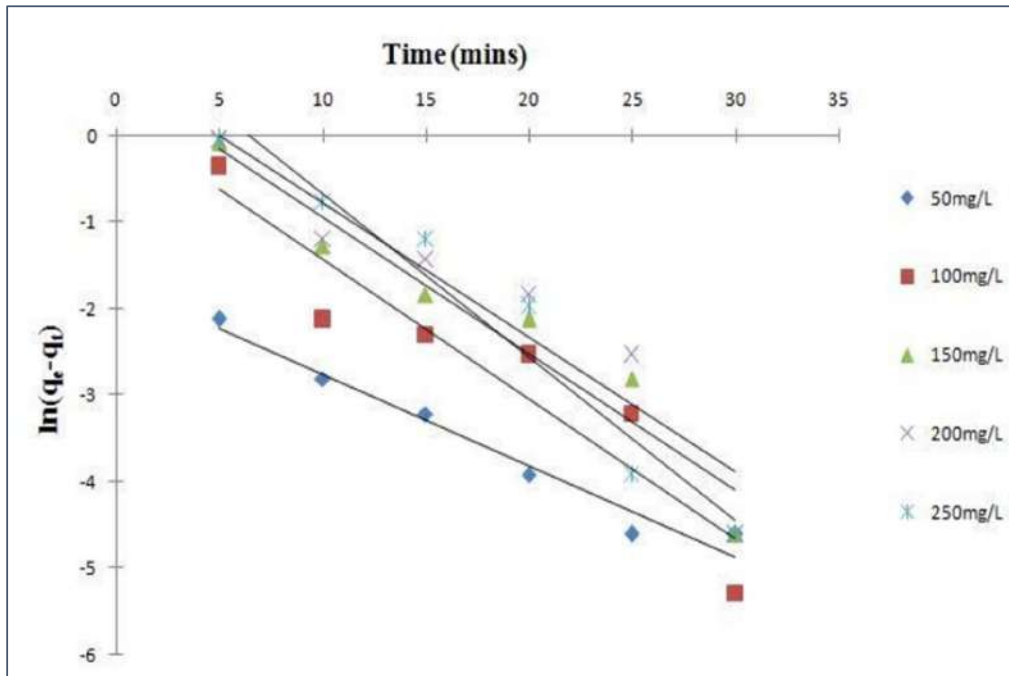


Fig. 8: Pseudo-first-order kinetic fit for the adsorption of reactive blue dye onto coal-associated soil.

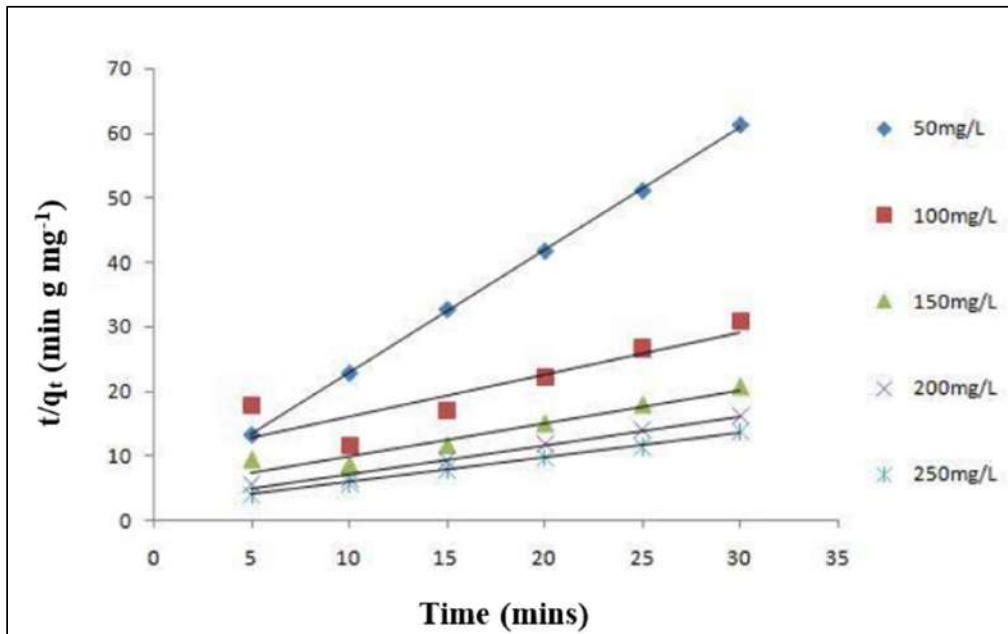


Fig. 9: Pseudo-second-order kinetic fit for the adsorption of reactive blue dye onto coal-associated soil.

first-order kinetics exhibited irregular values, as illustrated in Fig. 8. By comparing the experimental and calculated equilibrium adsorption capacities, it was determined that the pseudo-second-order kinetic model (Fig. 9) provided a better fit, supported by higher R^2 values. Hence, the pseudo-

second-order model was considered the best fit for this adsorption process.

Adsorption Isotherm Studies

To gain insights into the adsorption mechanism between

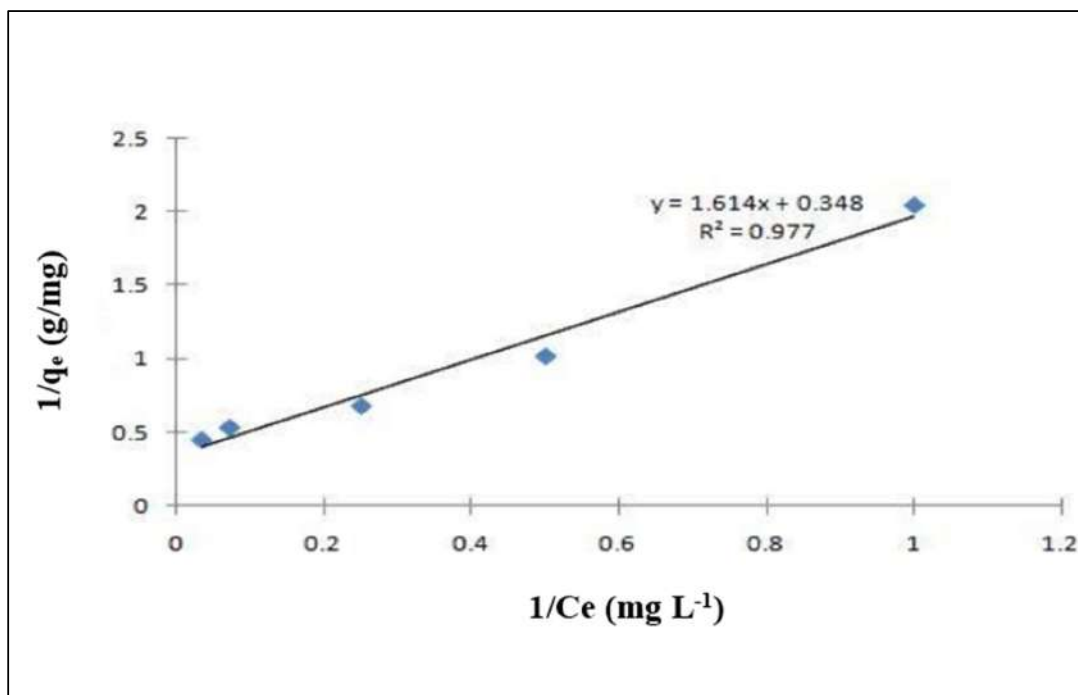


Fig. 10: Langmuir isotherm fit for the adsorption of reactive blue dye onto coal-associated soil.

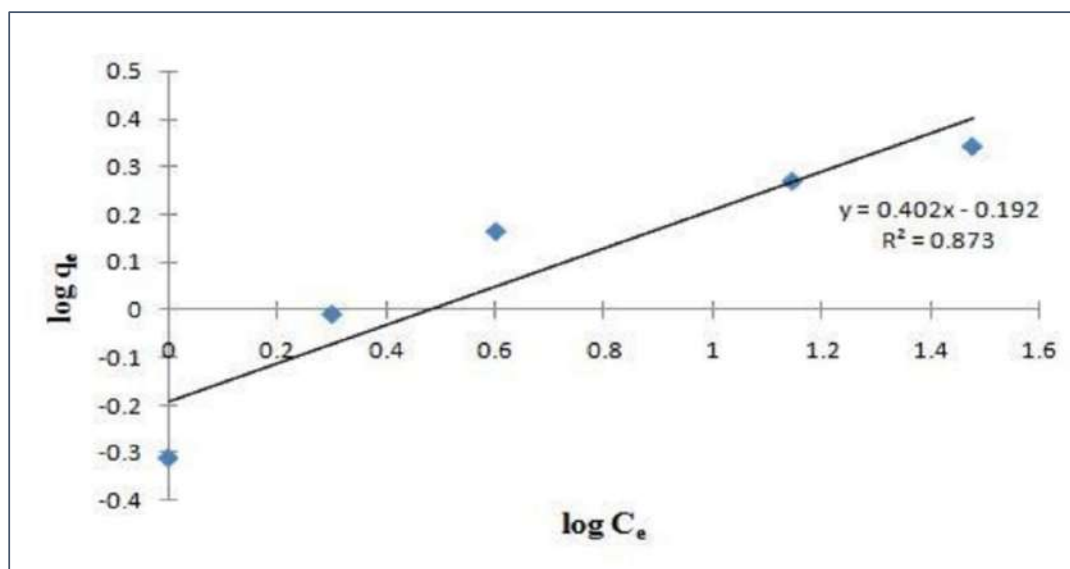


Fig. 11: Freundlich isotherm fit for the adsorption of reactive blue dye onto coal-associated soil.

reactive blue dye and coal-associated soil, an isothermal study was conducted. Adsorption isotherm analysis was performed at equilibrium using two different models: Langmuir and Freundlich adsorption isotherm models. These two-parameter models aimed to determine the maximum adsorption capacity of the coal-associated soil. The

adsorption isotherm study results are depicted in Fig. 10 and Fig. 11, showcasing the Langmuir and Freundlich adsorption isotherm plots, respectively. By employing nonlinear equations of different isotherm models and utilizing the experimental data, adsorption isotherm parameters such as correlation coefficients (R^2) and maximum monolayer

Table 2: Isotherm fit for the adsorption of reactive blue dye onto coal-associated soil.

Adsorption isotherm models	Parameters	Values	R ²
Langmuir	q _{max} [mg.g ⁻¹]	2.8735	0.977
	K _L [L.mg ⁻¹]	0.2156	
Freundlich	K _F [(mg.g ⁻¹)(L.mg ⁻¹) ^(1/n)]	0.8253	0.873
	n [g.L ⁻¹]	2.4875	

adsorption capacity (q_{max}) were calculated and presented in Table 2.

The analysis revealed that the Langmuir isotherm model exhibited the best fit for the removal of reactive blue dye by coal-associated soil. This conclusion was supported by the higher correlation coefficient (R²) value compared to the Freundlich isotherm model. Thus, the Langmuir adsorption isotherm model, describing the adsorption process as a monolayer and homogeneous in nature, was identified as the most suitable model for explaining the

adsorption behavior of reactive blue dye onto coal-associated soil.

Thermodynamic Studies

A thermodynamic study was conducted to gain insights into the adsorption behavior of reactive blue dye onto coal-associated soil, focusing on the randomness, spontaneity, and nature of the process. The thermodynamic parameters, including Gibbs free energy (ΔG°), change in entropy (ΔS°) and change in enthalpy (ΔH°), were calculated from the

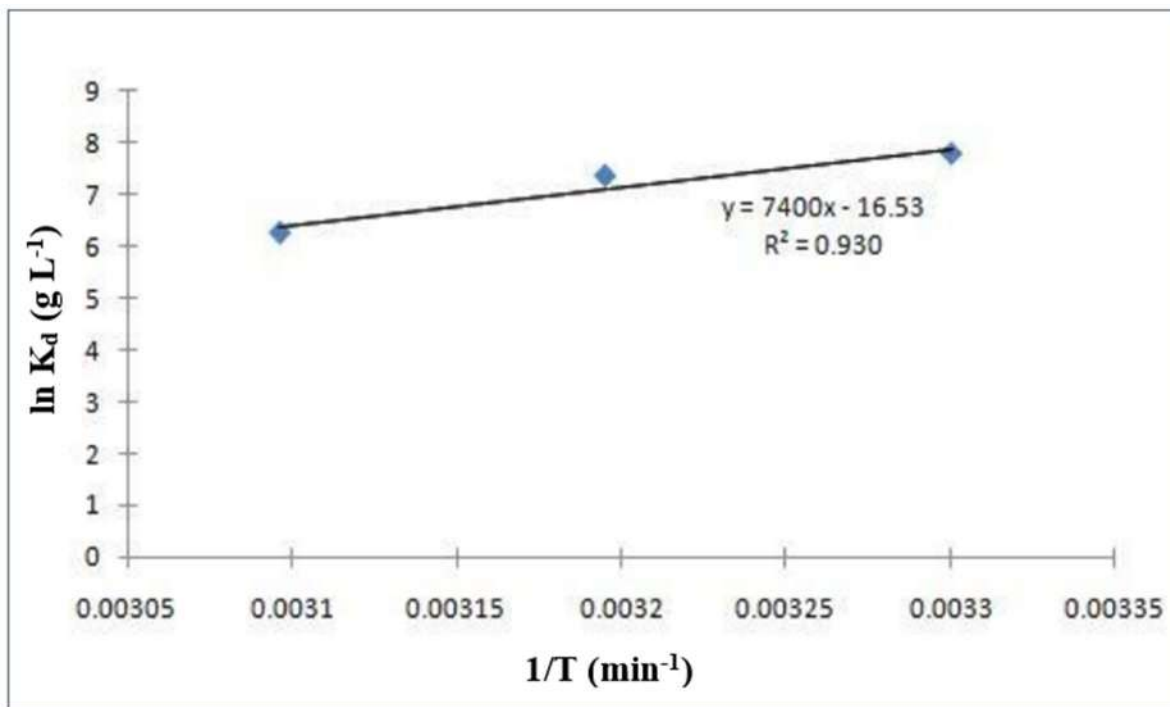


Fig. 12. Thermodynamic parameters for the adsorption of reactive blue dye onto coal-associated soil.

Table 3: Thermodynamic parameters for the adsorption of reactive blue dye onto coal-associated soil.

Concentration of dye [mg.L ⁻¹]	Temperature [°C]	ΔH° [KJ.mol ⁻¹]	ΔS° [J.mol ⁻¹]	ΔG° [KJ.mol ⁻¹]
100	30	-61.523	-137.43	-19.586
	40			-19.121
	50			-16.797

Table 4: Comparison of Various adsorbents used in Reactive Blue Dye Adsorption.

S.No.	Dye	Adsorbent	Kinetic Model Fitted	Isotherm Fitted	References
1.	RB 13	White Iraqi Kaolin clay	-	Langmuir	Baqir and Halbus (2014)
2.	RB	Natural and Modified Wheat Straw	Pseudo-second-order	Freundlich	Mousa and Taha (2015)
3.	RB 222	Industrial waste sludge	Second-order	Freundlich	Gunes and Kaygusuz (2013)
4.	RB 221	Chitosan Glycan	Pseudo-second-order	Langmuir	Chiu et al. (2018)
5.	RB 4	Lemon Peel Bead	Pseudo-second-order	Freundlich	Praipipat et al. (2022)
6.	RB 13	Fe ₃ O ₄ loaded Chitin	Pseudo-second-order	Langmuir	Gautam et al. (2020)
7.	RB 4	Coal-associated soil	Pseudo-second-order	Langmuir	This Study

graph plotted between $\ln K_d$ and $1/T$, as shown in Fig. 12. The results of the thermodynamic parameters are presented in Table 3. It was observed that the negative value of change in entropy (ΔS°) indicated that the adsorption process was driven by enthalpy. Furthermore, the negative value of change in enthalpy (ΔH°) suggested that the process was exothermic, while the negative value of Gibbs free energy (ΔG°) indicated that the adsorption of reactive blue dye onto coal-associated soil was spontaneous and feasible. Table 4 shows the comparison of various literature that reported the adsorption of reactive blue dye using various adsorbents.

CONCLUSION

The coal-associated soil used in this study is readily available and cost-effective, making it a promising adsorbent for removing Reactive blue dye. Through batch adsorption experiments, various important parameters were optimized, including adsorbent dosage ($10\text{g.}100\text{mL}^{-1}$), temperature (30°C), pH (7.0), contact time (30 mins), and initial dye concentration (100 mg.L^{-1}). The Langmuir isotherm model effectively described the adsorption of Reactive blue dye onto coal-associated soil, suggesting a monolayer adsorption mechanism. The kinetics of the process were best represented by the pseudo-second-order model, indicating a chemical nature of adsorption. Thermodynamic analysis confirmed that the adsorption process was exothermic, feasible, and spontaneous. Based on these findings, this study demonstrates the potential of coal-associated soil as a favorable and economically viable adsorbent for the removal of toxic dyes from wastewater.

REFERENCES

- Adane, T., Adugna, A.T. and Alemayehu, E. 2021. Textile industry effluent treatment techniques. *J. Chem.*, 53: 144.
- Amin M.N. and Blackburn R.S. 2015. Sustainable chemistry method to improve the wash-off process of reactive dyes on cotton, *ACS Sustain. Chem. Eng.*, 3(4): 725-732.
- Astuti, W., Chafidz, A., Wahyuni, E.T., Prasetya, A., Bendiyasa, I.M. and Abasaed A.E. 2019. Methyl violet dye removal using coal fly ash (CFA) as a dual-site adsorbent. *J. Environ. Chem. Eng.*, 7(5): 103262.
- Bae, J.S., Freeman, H.S. and Kim, S.D. 2006. Influences of new azo dyes to the aquatic ecosystem. *Fiber Polym.*, 7: 30-35.
- Baocheng, Q., Zhou, J., Xiang, X., Zheng, C., Zhao, Z. and Zhou, X. 2008. Adsorption behavior of Azo Dye C. I. Acid Red 14 in aqueous solution on surface soils. *J. Environ. Sci.*, 20(6): 704-709.
- Baqir, S.J. and Halbus, A.F. 2014. Removal of reactive blue dye from wastewater by adsorption on white Iraqi kaolin clay. *JUBPAS*, 22(7): 1947-1956.
- Berradi, M., Hsissou, R., Khudhair, M., Assouag, M., Cherkaoui, O., El Bachiri, A. and El Harfi, A. 2019. Textile finishing dyes and their impact on aquatic environments. *Heliyon*, 5(11): e02711.
- Chiu, C.W., Wu, M.T., Lee, J.C.M. and Cheng, T.Y. 2018. Isothermal adsorption properties for the adsorption and removal of reactive blue 221 dye from aqueous solutions by cross-linked β -chitosan glycan as acid-resistant adsorbent. *Polymers*, 10: 1328.
- Dutta, S., Gupta, B., Srivastava, S.K. and Gupta, A.K. 2021. Recent advances on the removal of dyes from wastewater using various adsorbents: a critical review. *Mater. Adv.*, 2: 4497-4531.
- El-Nemr, M.A., Abdelmonem, N.M., Ismail, I.M.A., Ragab, S. and El-Nemr, A. 2020. The efficient removal of the hazardous azo dye acid orange 7 from water using modified biochar from pea-peels. *Desal. Water Treat.*, 203: 327-355.
- Epoloto, W.J., Lee, Y.H., Bottomley, L.A. and Pavlostathis, S.G. 2005. Characterization of the textile anthraquinone dye reactive blue 4. *Dyes Pigm.*, 67(1): 35-46.
- Gautam, D., Say, L. and Hooda, S. 2020. Fe₃O₄ loaded chitin: A promising nano adsorbent for reactive blue 13 dye. *Environ. Adv.*, 2: 100014.
- Gunes, E. and Kaygusuz, T. 2015. Adsorption of Reactive Blue 222 onto an industrial solid waste included Al(III) hydroxide: pH, ionic strength, isotherms, and kinetics studies. *Desal. Water Treat.* 53(9), 2510-2517
- Javid, N., Honarmandrad, Z. and Malakootian, M. 2020. Ciprofloxacin removal from aqueous solutions by ozonation with calcium peroxide. *Desal. Water Treat.*, 174: 178-185.
- Lellis, B., Favaro-Polonio, C.Z., Pamphile, J.A. and Polonio, J.C. 2019. Effects of textile dyes on health and the environment and bioremediation potential of living organisms. *Biotechnol. Res. Innov.*, 3(2): 275-290.
- Mahvi, A.H., Malakootian, M. and Heidari, M.R. 2011. Comparison of polyaluminum silicate chloride and electrocoagulation process in natural organic matter removal from surface water in Ghochan, Iran. *J. Water Chem. Tech.*, 33(6): 377-385.
- Malakootian, M., Radhakrishna, N., Mazandarany, M.P. and Hossaini, H. 2013. Bacterial-aerosol mission from wastewater treatment plant. *Desal. Water Treat.*, 51: 4478-4488.
- Malar, C.G., Sathya, K., Rajalakshmi, S. and Rajalakshmi, P. 2023. A critical analysis of the nanotechnology-based approach in textile wastewater treatment. *Nanotechnol. Environ. Engg.*, 8: 535-548.
- Malar, C.G., Seenivasan, M. and Kumar, K.S. 2019. Adsorption of nickel ions by surface modified magnetite nanoparticles: Kinetics study. *J Environ. Biol.*, 40: 748-752.
- Mousa, K.M. and Taha, A.H. 2015. Adsorption of reactive blue dye onto

- natural and modified wheat straw. *J. Chem. Eng. Process. Technol.*, 6: 1000260.
- Muthulingam, S., Suganthi, J.R.G., Gopalakrishnan, S., Malar, G.C.G., Priya, M.E. and Kumar, M.A. 2018. Effective utilization of crustacean shells for preparing chitosan composite beads: applications in ameliorating the biosorption of an endocrine disrupting heavy metal. *Desal. Water Treat.*, 121: 28-35.
- Praipipat, P., Ngamsurach, P. and Prasongdee, V. 2022. Comparative reactive blue 4 dye removal by lemon peel bead doping with iron(III) oxide-hydroxide and zinc oxide. *ACS Omega*, 7: 41744-41758.
- Rapo, E. and Tonk, S. 2021. Factors affecting synthetic dye adsorption, desorption studies: A review of results from the last five years (2017-2021). *Molecules*, 26(17): 5419.
- Seenuvasan, M., Malar, C.G. and Growther, L. 2021. Production of a biopolymer film from biological wastes and its statistical analysis. *Biores. Technol. Rep.*, 13: 100610.
- Sharifpour, H., Javid, N. and Malakootian, M. 2018. Investigation of single-walled carbon nanotubes in the removal of Penicillin G (Benzyl penicillin sodium) from aqueous environments. *Desal. Water Treat.*, 124: 248-255.
- Tarkwa, B., Acayanka, E. and Jiang, B. 2019. Highly efficient degradation of azo dye Orange G using laterite soil as catalyst under irradiation of non-thermal plasma, *Appl. Catal. B: Environ.*, 246: 211-220.
- Zhang, X. 2023. Study on the adsorption properties of Cr(VI) by biochar with different treatments. *Nat. Environ. Pollut. Technol.* 22: 1563-1569.
- Zhao, C., Shi, R., Li, S., Li, P., Zhang, X. and Tong, G. 2022. Synthesis and properties of novel reactive dyes comprising acyl fluoride group on cotton fabrics. *Molecules*, 27(13): 4147.



The Prostrate Spurge-isolated PGPB Endophytes, EP1-AS, and EP1-BM That Can Tolerate High Levels of Salinity and Heavy Metals and Allow Wheat Growth Under These Stressors

Manisha Parashar† and Gaurav Mudgal

University Institute of Biotechnology, Chandigarh University, Mohali 140413, Punjab, India

†Corresponding author: Manisha Parashar; nishuparashar78@gmail.com

Nat. Env. & Poll. Tech.
Website: www.neptjournal.com

Received: 17-10-2023
Revised: 22-12-2023
Accepted: 24-12-2023

Key Words:

Salinity
Heavy metals
Wheat
Plant growth promoting bacteria

ABSTRACT

This research investigates the potential of two Plant Growth-Promoting Bacteria (PGPB) strains, EP1-AS and EP1-BM, isolated from the halophyte *Euphorbia prostrata*, to enhance plant growth and provide abiotic stress resilience. The study addresses the urgent need for sustainable agricultural practices in the face of challenges like soil salinization and heavy metal contamination. The investigation comprehensively analyzes the heavy metal and salt tolerance of the PGPB strains, revealing their potential applications in promoting plant growth under adverse environmental conditions. The research further explores the impact of these PGPB strains on wheat plants subjected to varying concentrations of heavy metals and salts. Results indicate that both PGPB strains, especially EP1-BM, exhibit significant tolerance to heavy metals and salt stress. EP1-BM demonstrates remarkable resilience even under high concentrations of these stressors. The study extends its findings to in vitro testing on wheat plants, revealing the positive influence of PGPB strains on germination, shoot length, and root length in the presence of salt and heavy metals. This research underscores the significance of understanding plant-microbe interactions, particularly in the context of promoting sustainable agriculture in challenging environments. The identified resilience of PGPB strains, especially EP1-BM, suggests their potential application as bio-remediators and plant growth promoters in soils affected by salinity and heavy metal stress. The promising results observed will be followed-up field trials. They will highlight the translational potential of these PGPB strains, offering a novel avenue for developing biofertilizer formulations with a cautious approach to safety concerns. Overall, this study contributes valuable insights into harnessing the untapped potential of resilient plants and their associated microbial communities for sustainable agriculture. It addresses key global challenges outlined by the United Nations Sustainable Development Goals.

INTRODUCTION

A confluence of environmental challenges, encompassing pollution, the impact of coronaviruses, and the far-reaching consequences of climate change, has compounded recent global economic meltdowns. Among the environmental stressors, pollution from heavy metals and salinity has emerged as a substantial threat, exerting diverse and complex pressures on economic stability. Heavy metal pollution, often stemming from industrial processes, not only disrupts ecosystems but also imposes significant economic burdens (Vinayak 2020a, 2020b, Sharma 2021, Mudgal et al. 2021). Contaminated water sources, soil degradation, and compromised agricultural productivity lead to escalating cleanup costs, increased healthcare expenditures, and disruptions in global food supply chains. Industries reliant on pristine water resources encounter heightened

operational challenges, intensifying economic strain. Salinity, exacerbated by climate change and suboptimal agricultural practices, presents an additional economic menace. Soil salinization negatively impacts crop yields, contributing to reduced agricultural output and escalating food prices.

Moreover, salinity-induced deterioration of infrastructure, especially in coastal regions, entails increased maintenance costs and undermines the durability of structures. Adding to the economic complexity, the ongoing challenges posed by coronaviruses have disrupted global trade, supply chains, and labor markets (Kaur & Mudgal 2021). This pandemic has underscored the intricate interplay between economic vulnerabilities and environmental stressors, emphasizing the imperative of comprehensive strategies to address concurrent threats. Climate change, characterized

by an uptick in extreme weather events, further amplifies economic risks worldwide. Rising sea levels, more intense storms, and shifting precipitation patterns contribute to increased infrastructure damage, surging insurance claims, and challenges for industries reliant on climate-sensitive resources. Amidst these challenges, biotechnological initiatives have emerged as promising avenues for relief. Innovations in biotechnology offer potential solutions for remediating heavy metal pollution, improving soil salinity tolerance in crops, and even contributing to medical advancements for pandemic preparedness (Kaur & Mudgal 2021). Harnessing biotechnological tools allows for targeted interventions, fostering resilience and sustainable practices in the face of multifaceted economic and environmental threats. The escalating threats of soil salinization, heavy metal contamination, and other environmental challenges pose a substantial risk to agricultural productivity, thereby imperiling global food security. Conventional agricultural methodologies often prove inadequate in mitigating these challenges, necessitating the exploration of sustainable and ecologically sound alternatives. Recent years have witnessed a burgeoning interest in harnessing the potential of Plant Growth-Promoting Bacteria (PGPB) to augment plant growth and confer resistance against abiotic stressors.

Spurges, belonging to the expansive Euphorbiaceae family of flowering plants, exhibit a global distribution and are distinguished by their milky sap and diverse morphologies (Webster 1967). With numerous species employed in traditional medicine and some extensively scrutinized for their biological and biochemical attributes (Pascal 2017), spurges have recently garnered increased significance in the realms of biology and biotechnology. Their potential applications span diverse fields, encompassing medicine, agriculture, and industry. Extensive studies on the biology of spurges have unveiled a repertoire of bioactive molecules, including alkaloids, flavonoids, terpenoids, and phenolic compounds (Akdad et al. 2022). These compounds exhibit multifaceted biological activities such as anti-inflammatory, anti-oxidant, and anti-cancer properties (Singh 2021). Notably, certain spurges have been investigated for their prowess in bioremediation, contributing to environmental sustainability (Jeevanandam 2021). The field of spurge biotechnology has witnessed substantial progress, with genetic engineering techniques harnessed to modify plants for bioremediation purposes. Certain spurges also serve as valuable models for delving deeper into plant biology and biochemistry (Chan, Crabtree et al. 2010). For instance, *Euphorbia lathyris* has been instrumental in studying plant hormones (Sivakumaran & Hall 1978, Mingo-Castel 1984), while *Euphorbia milii* has contributed to the understanding of plant stress responses (Khaksar et al. 2016). Beyond their

role in bioremediation, spurges have exhibited potential applications in medicine. Some species display anti-cancer and anti-inflammatory activities, aligning with their traditional medicinal use for various ailments (Salatino et al. 2007).

Moreover, spurges have attracted attention for their potential role in biofuel production, with certain species possessing high triglyceride levels suitable as an energy source (Linfang et al. 2021, Srivastava & Soni 2019). The dynamic landscape of spurge biology and biotechnology underscores the breadth of their potential applications across various domains. Future research endeavors should delve deeper into understanding the molecular mechanisms of these plants to unlock their full potential and further elucidate their applications in diverse fields.

Our work culture themes over exploring various hardy, succulent and resilient plants and their interaction with the microbial communities and anticipating the research outcomes to translate into enhancement of crop productivity under various stressors (Ramamoorthy et al. 2009, Siva et al. 2009, Mudgal & Mudgal 2011, Mudgal et al. 2011, Kaur & Mudgal 2020a, 2020b, Parashar 2020a, 2020b, Vinayak 2020, 2021, Kaur & Mudgal 2021, Sharma 2021, Mudgal et al. 2021, 2011, Kaur et al. 2022, 2023a, 2023b, Parashar et al. 2023, Saeed et al. 2023).

Of the many Euphorbias, *Euphorbia prostrata*, a halophyte plant renowned for its robustness in adverse environmental conditions, has become a focal point of investigation (Webster 1967, Dubyna et al. 2022, Unde & Kumar 2022). The ramifications of salinity and heavy metal pollution on plant growth are profound, impacting nutrient uptake, water balance, cellular homeostasis, and various physiological processes. PGPB emerges as a promising solution to alleviate these stressors, leveraging mechanisms such as phytohormone production, nutrient solubilization, and the regulation of stress-responsive genes. Expanding our understanding of the distinctive traits exhibited by PGPB isolates derived from *Euphorbia prostrata* holds immense potential. This insight can serve as a foundation for evaluating their efficacy as biotechnological tools, offering solutions to bolster sustainable agriculture in challenging environmental conditions. The exploration of PGPB isolates, in conjunction with the resilience showcased by halophytes like *Euphorbia prostrata*, represents a strategic approach to advancing agricultural practices that align with environmental sustainability and global food security imperatives.

In a preceding investigation (Parashar et al. 2023), we successfully isolated two co-culturable bacterial endophytes, EP1-AS and EP1-BM, originating from the stem internodal segments of *Euphorbia prostrata*, a succulent member of

the Euphorbiaceae family. Employing a comprehensive approach involving morphological, biochemical, and molecular analyses, we identified these strains as novel members of Enterobacteriaceae, specifically *Lelliottia amnigena*. Both isolates exhibited substantial plant growth promotion (PGP) potentials during rigorous assays. EP1-BM manifested as swiftly expanding swarms, while EP1-AS exhibited growth in the form of rounded colonies on nutrient agar. The PGP effects of these isolates were substantiated through meticulous in vitro and ex-vitro seed-priming treatments with wheat and tomato seeds. Remarkably, these treatments resulted in significantly elevated seed germination rates and noteworthy enhancements in morphometric and physiological aspects of plant growth. The validation extended into field trials, where both EP1-AS and EP1-BM demonstrated commendable yields in wheat grain and tomato fruit harvests. This groundbreaking study represents the pioneering exploration of PGPB endophytes within *Euphorbia prostrata*, shedding light on their potential contributions to enhancing agricultural productivity. The results underscore the significance of these novel bacterial strains in promoting sustainable plant growth and heralding a promising avenue in the context of plant-microbe interactions and agroecological practices.

The present study seeks to explore the potential of the above two PGPB endophytes isolated from a sandmat spurge in enhancing plant survival and physiological growth under the effect of salinity and exposure to various heavy metals.

MATERIALS AND METHODS

Culturing Bacterial Endophytes EP1-AS and EP1-BM

Two PGPB endophytic bacteria, EP1-AS and EP1-BM, were isolated from *Euphorbia prostrata* and characterized for their PGP profiles previously (Parashar et al. 2023). Each was revived from a glycerol stock to raise pure colonies over ampicillin-supplemented nutrient agar (NA) plates with conditions specified previously. From a single colony for each, a 17 hrs old pure culture with an overnight cell density of $\geq 10^9$ CFU/ml was inoculated in 100ml of Nutrient Broth (NB) and incubated, was incubated at 37°C with orbital shaking at 200 rpm overnight. For a control, *Escherichia coli* was used at a similar inoculum size. All chemicals and reagents were of research grade (Himedia, Mumbai, India).

Measuring Heavy Metals and Salt Tolerance of EP1-AS and EP1-BM

The susceptibility of bacterial strains to four distinct heavy

metal salts viz., sodium arsenite (NaAsO_2), lead nitrate [$\text{Pb}(\text{NO}_3)_2$], chromium trioxide (CrO_3), cadmium sulfate (CdSO_4) was evaluated in accordance with Washington's (1980) agar dilution methodology (Washington 1980). Stock solutions of the following heavy metal salts were prepped and filtered through a 0.22 μm Millipore filter to guarantee sterility. For each heavy metal concentration (200 ppm, 500 ppm, 700 ppm, and 1000 ppm), respectively, each salt was added to the autoclaved 30 mL of NB agar medium and incubated at a temperature of 37°C. Likewise, to create salt stress, stock solutions of different salt concentrations (1%, 2%, 3%, 4%, and 5%) were prepared and filtered through the same Millipore filter as used in the former. Later, the stocks were added to an autoclaved NB medium at a temperature of 37°C. Visual observations were scored based on the growth of new streaks. For a control, *Escherichia coli* was used at a similar inoculum size. All chemicals and reagents were of research grade (Himedia, Mumbai, India).

Surface Sterilization and Seed Priming of Wheat Seeds

Wheat seeds of a variety named UNNAT PBW 343 were procured from a local shop in Mohali Punjab) and were surface sterilized with 70% ethanol and flash treatment of mercuric chloride for 10 seconds, along with three later washes of sterile distilled water. Surface sterilized 20 wheat seeds each for EP1-AS, EP1-BM, and control sets were primed with 17 hrs old fresh inoculum ($\geq 10^9$ CFU. mL^{-1}) of EP1-AS and EP1-BM prepared in NB media and were kept in overnight incubation. For control sets, the seeds were put overnight only in sterile NB media.

Preparation of Setup for Experiment

For the experimental setup, 15 EP1-AS, EP1-BM primed seeds, and unprimed control seeds were placed on tissue paper wetted with the 15 mL of desired concentration of heavy metals and salt and placed on a plastic petri dish. 15 mL of prepped stocks for each concentration were poured onto tissue paper containing prepped seeds. Separate independent trials were run each for salt and heavy metal stress treatments according to the desired concentration (ppm) applied every 5 days. Observations were recorded every 2 days for germination, root, and shoot length. The control treatment sets were avoided with seed treatments with endophytes, but the same was replaced with plain NB.

Statistical Analyses and Data Presentation

All experiments were done thrice with three or more replicates per trial for each variable. Data in graphs showed the average of the or more trials with averaged replicates, and standard errors were depicted with error bars inferring

standard deviations from the mean values. Pictures in the figures were representative seedlings for the observed trends in each of the treatment trials shown with a scale bar for clarity and measurable distinguishments. Graphs were prepared in MS Excel, along with pictures in figures assembled and adjusted using MS PowerPoint.

RESULTS AND DISCUSSION

The EP1-AS and EP1-BM Isolates

Both the novel *L. amnigena* isolates were previously characterized at our end (Parashar et al. 2023). In brief, as before, the isolates showed up as peculiar off-white bacterial growth when revived over nutrient agar (NA) plates with ampicillin. These bacteria were later tested under treatment in liquid suspension media with various stressors.

EP1-AS and EP1-BM Tolerating High Salt and Heavy Metal Levels in Culture Media

Salinity tolerance of EPI-AS and EPI-BM: Table 1 shows the effect of various salt concentrations on the growth of the two bacterial isolates. Upon elevating the salt concentration to 2%, both the control and EP1-AS strains exhibited mild growth, whereas EP1-BM demonstrated robust growth, indicating its exceptional tolerance to elevated salt levels. At 3% salt concentration, the control and EP1-AS maintained moderate growth, while EP1-BM sustained vigorous growth, underscoring its remarkable ability to thrive in highly saline environments. Upon further escalation to 4% salt concentration, the control exhibited no growth, signifying its sensitivity to heightened salinity. In contrast, both EP1-AS and EP1-BM strains displayed moderate growth, indicating their capacity to endure this salt concentration. Notably, at a 5% salt concentration, neither the control nor EP1-AS strains exhibited any growth, revealing their susceptibility to elevated salinity. In stark contrast, EP1-BM exhibited exceptional growth, showcasing its outstanding salt tolerance, even in the face of heightened salinity. These findings underscore the significance of EP1-BM as a potential candidate for enhancing salt tolerance in crops subjected to saline conditions. The robust growth exhibited by EP1-BM, particularly at higher salt concentrations, positions it as a promising microbial ally in mitigating the adverse effects of salinity on plant growth.

Further exploration into the molecular mechanisms underlying EP1-BM's exceptional salt tolerance could unveil valuable insights for developing biotechnological interventions aimed at improving crop resilience in saline environments. The identified differential responses among EP1-AS, EP1-BM, and the control also emphasize the

Table 1: Two PGPB endophyte strains (EP1-AS and EP1-BM) and a control bacterium (*Escherichia coli*) were tested at various salt concentrations (1% to 5%). The bacterial growth response was scored as follows: “++++”: abundant growth; “+++”: moderate growth; “++” lower than moderate” and “-”: no visible growth.

	Salinity (%)				
	1	2	3	4	5
Control	++	+	+	-	-
EP1-AS	++++	+++	+++	++	-
EP1-BM	++++	++++	++++	+++	++

intricate interplay between endophytic bacteria and plant host EP in coping with environmental stressors. These insights pave the way for future investigations into harnessing the potential of endophytes, such as EP1-BM, for sustainable agricultural practices in salt-affected regions.

Heavy metals tolerance of bacterial endophytes: Table 2 summarizes the effect of all the heavy metals on the growth of the two EP endophytes seen in plate assays:

Sodium arsenite ($NaAsO_2$): At 200 ppm of sodium arsenite, both the control and AS strains displayed moderate growth, signifying their tolerance to the elevated concentration. However, EP1-BM exhibited remarkable growth (++) , showcasing its resilience even at this lower concentration. Upon increasing the concentration to 500 ppm, EP1-AS and the control both exhibited moderate growth (+), whereas EP1-BM displayed significant growth (++) , highlighting its exceptional tolerance to higher concentrations. At 1000 ppm of sodium, both the control and EP1-AS strains showed no growth (-), indicating their sensitivity to extreme levels of the heavy metal. In contrast, EP1-BM continued to exhibit remarkable growth (++) , demonstrating its remarkable ability to withstand even the highest concentrations of sodium arsenite.

Lead nitrate [$Pb(NO_3)_2$]: At a concentration of 200 ppm of lead nitrate, the control displayed moderate growth (+), indicating its tolerance to the high concentration of the heavy metal. Both EP1-AS and EP1-BM strains exhibited remarkable growth (+++), showcasing their resistance to lead nitrate. Upon increasing the concentration to 500 ppm, the control and EP1-AS strains both exhibited moderate growth (+), indicating their tolerance to higher levels of lead nitrate. EP1-BM also showed abundant growth (+), demonstrating its resilience to higher concentrations of lead. At 700 ppm, the control did not show any growth (-), suggesting its susceptibility to the high concentration. At 1000 ppm, both EP1-AS and EP1-BM strains exhibited growth (+), demonstrating their tolerance to even higher levels of lead nitrate.

Chromium trioxide (CrO_3): The control was sensitive to chromium trioxide and failed to survive at concentrations

ranging from 200 ppm to 1000 ppm. EP1-AS tolerated concentrations up to 500 ppm, displaying visible growth, while EP1-BM tolerated up to 1000 ppm, showing remarkably visible growth.

Cadmium sulphate ($CdSO_4$): The control was non-responsive to all cadmium sulfate concentrations ranging from 200 to 1000 ppm. In contrast, EP1-AS tolerated up to 700 ppm of this heavy metal, and EP1-BM showed visible growth even at 1000 ppm.

In summary, the results reveal distinct levels of salt and heavy metal tolerance among the bacterial strains. While the control demonstrated sensitivity to increasing concentrations, both EP1-AS and EP1-BM displayed robust resistance to higher salinity and heavy metal stress, with EP1-BM emerging as the more resistant strain. This suggests that EP1-BM holds potential as a bio-remediator and agronomist in environments with salinity and heavy metal stress. This invites further exploration into EP1-BM's stress response mechanisms and its role as a plant growth promoter in salt-damaged agricultural soils. Moreover, the specific tolerance exhibited by EP1-BM to lead, chromium, and cadmium positions it as a promising candidate for biotechnological applications aimed at mitigating heavy metal contamination in crops and soils.

Table 2: Two PGPB endophyte strains (EP1-AS and EP1-BM) and a control bacteria (*Escherichia coli*) were tested at various heavy metal concentrations in plate assay, inferring growth as streaks. The bacterial growth response was scored as follows: “+++”: abundant growth; “++”: moderate growth; and “-”: no visible growth.

	Concentrations (ppm)			
	200	500	700	1000
<i>Sodium arsenite</i>				
Control	+	+	-	-
EP1-AS	++	++	+	+
EP1-BM	+++	+++	++	+
<i>Lead nitrate</i>				
Control	++	+	-	-
EP1-AS	+++	++	++	+
EP1-BM	+++	++	++	++
<i>Chromium trioxide</i>				
Control	-	-	-	-
EP1-AS	+	+	-	-
EP1-BM	++	+	+	+
<i>Cadmium Sulphate</i>				
Control	-	-	-	-
EP1-AS	+	+	+	-
EP1-BM	+	+	+	+

EP1-AS and EP1-BM Priming Restores Wheat Seedling Growth Under High Salinity

The PGPB endophytes isolated from EP displayed a remarkable and promising impact on wheat seed treatments over time, particularly when compared to untreated controls. This emphasizes their potential plant growth-promoting (PGP) attributes, which align with the findings from previous biochemical PGP assays conducted in earlier research. In the current study, we examined the influence of salt on seeds treated/untreated with EP1-AS/EP1-BM in three distinct trials.

Untreated wheat seeds in the control group exhibited visibly compromised development as salt concentration increased (Fig. 1a), consistent with observations in the existing literature. However, priming seeds with either EP1-AS/EP1-BM endophytes significantly rescued seed germination, especially in the presence of 100 mM onwards up to 200 mM salt concentration, compared to control untreated seed lots (Fig. 1a). Notably, even at the highest salinity of 300 mM, BM maintained superior germinating seedling growth compared to AS, while controls without EP1-AS/EP1-BM treatment showed negligible propagules in any seed germination trials (Fig. 1a). Moreover, control plants demonstrated tolerance up to only 200 mM salinity with limited shoot growth, beyond which, at 250 and 300 mM, shoot growth was impeded (Fig. 1b). In contrast, EP1-AS and EP1-BM bacterized seeds exhibited increased tolerance to elevated salinity compared to control seeds. This tolerance is further supported by the maintenance of root length and vigor (Fig. 1c and 1d). Among the three, EP1-BM exhibited a stronger response in rescuing wheat seeds under higher salt stress compared to EP1-AS and the control. This suggests that the bacterization of wheat seeds with EP1-AS and, more prominently, with EP1-BM enhances tolerance against salinity.

From a perspective standpoint, these results underscore the potential application of EP1-BM as a valuable resource in enhancing crop resilience to salinity stress. EP1-BM, exhibiting a stronger response in rescuing wheat seeds under higher salt stress, holds promise for sustainable agriculture in saline environments. Further research avenues could explore the molecular mechanisms underlying the differential responses of EP1-AS and EP1-BM, providing insights into optimizing plant-endophyte interactions. Long-term investigations into the impacts of bacterization on crop productivity and soil health could contribute to more comprehensive and applicable outcomes in the field of agriculture, aligning with the global pursuit of sustainable development goals.

EP1-AS and EP1-BM Priming Restores Wheat Seedling Growth Under High Heavy Metal Concentrations

As for salinity stress, we tested the effect of EP1-AS/EP1-BM bacterization over wheat under stress from four selected heavy metal salts as well, namely, sodium arsenite,

lead nitrate, cadmium sulfate, and chromium trioxide. In the case of sodium arsenite and lead nitrate (Fig. 2 and Fig. 3), the EP1-AS/EP1-BM untreated controls showed a drastic decrease in the emergence of propagules with time and in the overall number of seeds responding with germination as surmised from the effects at 200 ppm and

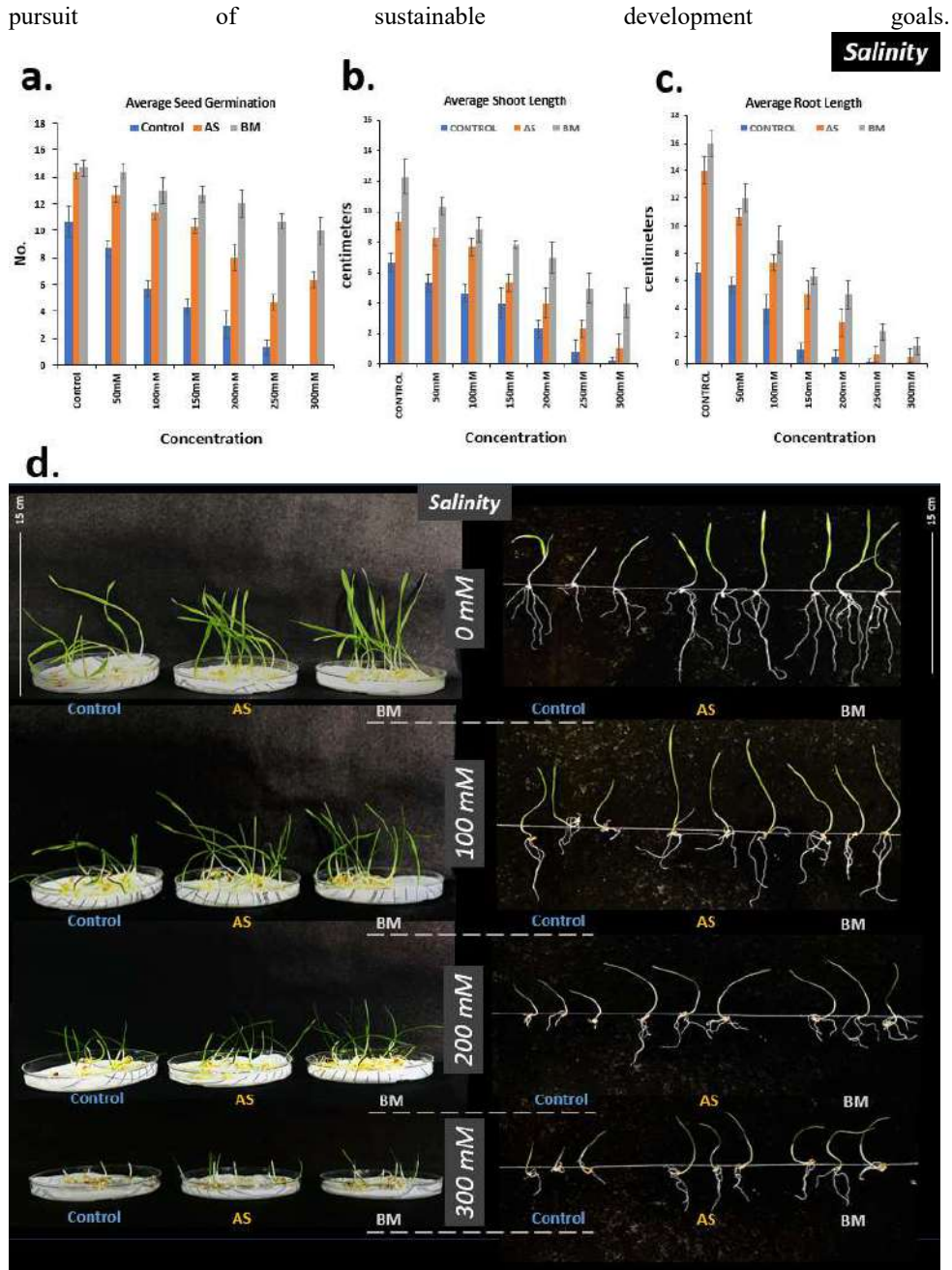


Fig. 1: Effect of seed bacterization treatments with EP1-AS and EP1-BM under various levels of salinity. Here, the parameters shown are a) average germination from 20 wheat seeds per replicate per trial, b) shoot length development, and c) root length development. The results represent the averaged outcomes of three independent trials. In d), scale bars represent the lengths of seedlings under different variables.

500 ppm of these heavy metals. However, lead nitrate seems more affecting with much higher detrimentally over wheat seedling emergence, which seemed almost abrogated under 700 ppm and 1000 ppm. Under seed treatments with EP1-AS/EP1-BM, however, germination was normalized and

rescued at all levels of increased heavy metal concentrations (Fig. 2a and 3a). This rescue feature was always seen more significantly improved with BM-treated seed lots compared to EP1-AS treated lots. However, if we see the shoot growth statistics (Fig. 2b and 3b), the productive seedling growth

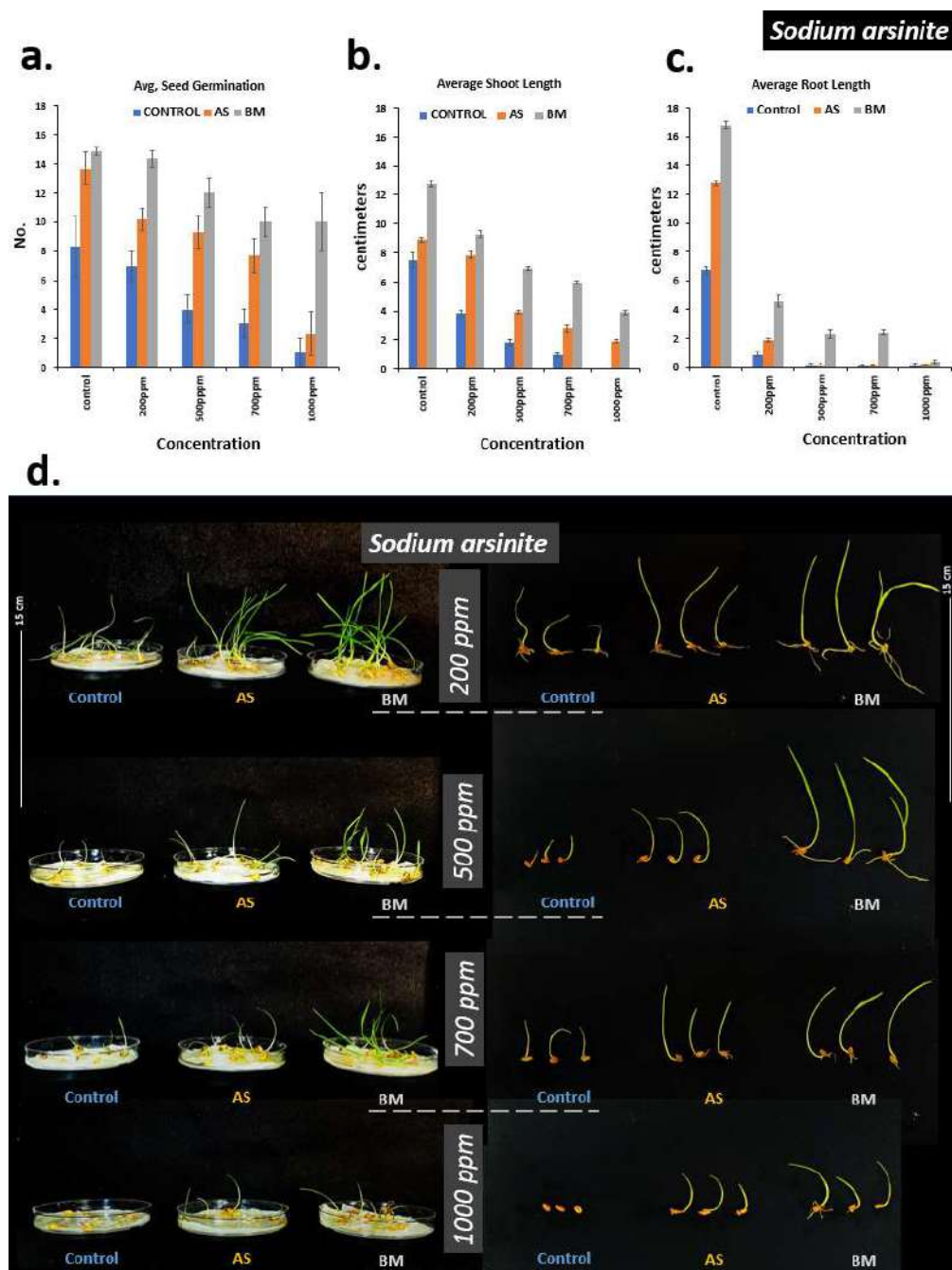


Fig. 2: Effect of seed bacterization treatments with EP1-AS and EP1-BM under various levels of the heavy metal sodium arsenite. Here, the parameters shown are a) average germination from 20 wheat seeds per replicate per trial, b) shoot length development, and c) root length development. The results represent the averaged outcomes of three independent trials. In d), scale bars represent the lengths of seedlings under different variables.

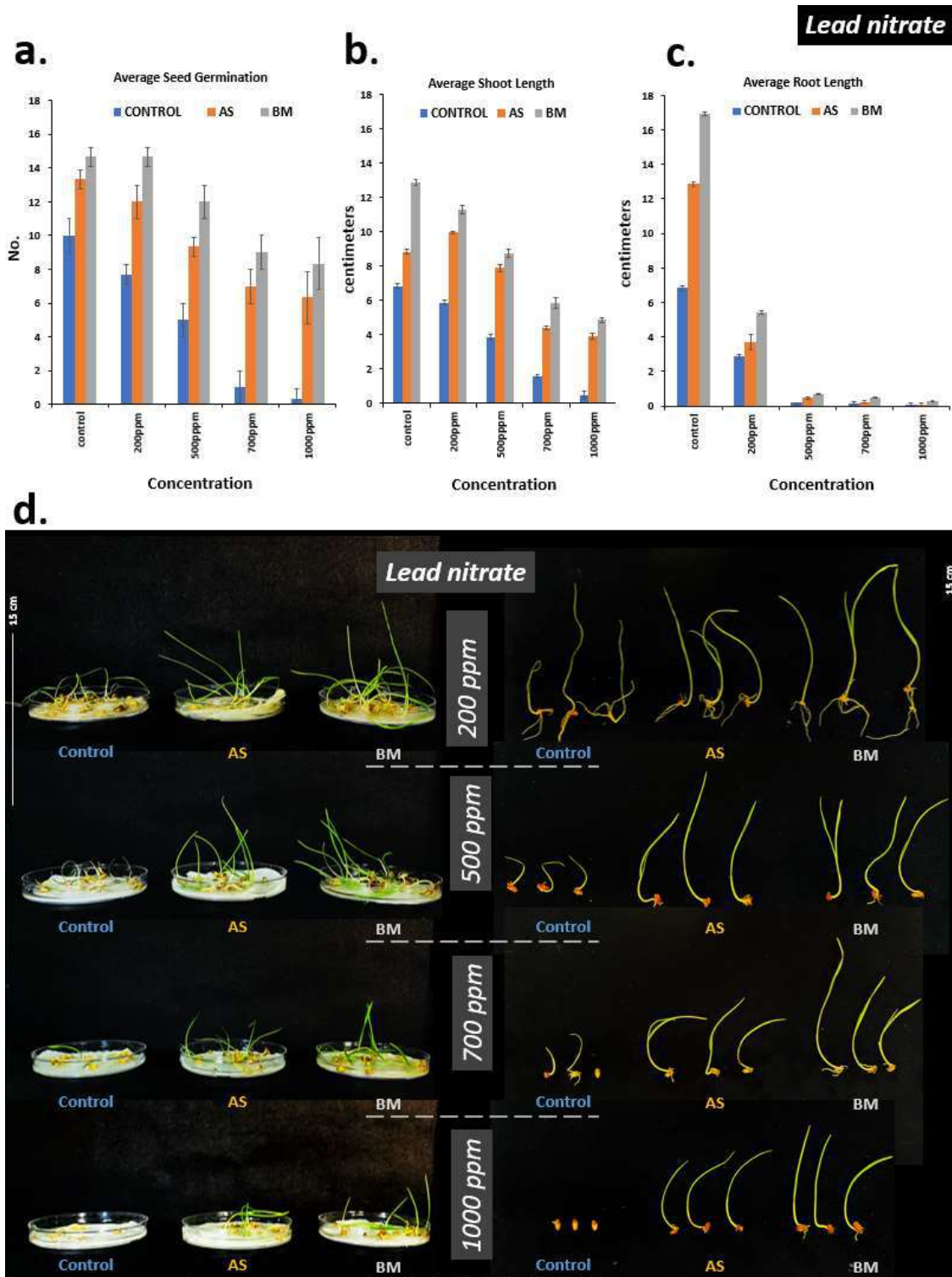


Fig. 3: Effect of seed bacterization treatments with EP1-AS and EP1-BM under various levels of the heavy metal lead nitrate. Here, the parameters shown are **a)** average germination from 20 wheat seeds per replicate per trial, **b)** shoot length development, and **c)** root length development. The results represent the averaged outcomes of three independent trials. In **d)**, scale bars represent the lengths of seedlings under different variables.

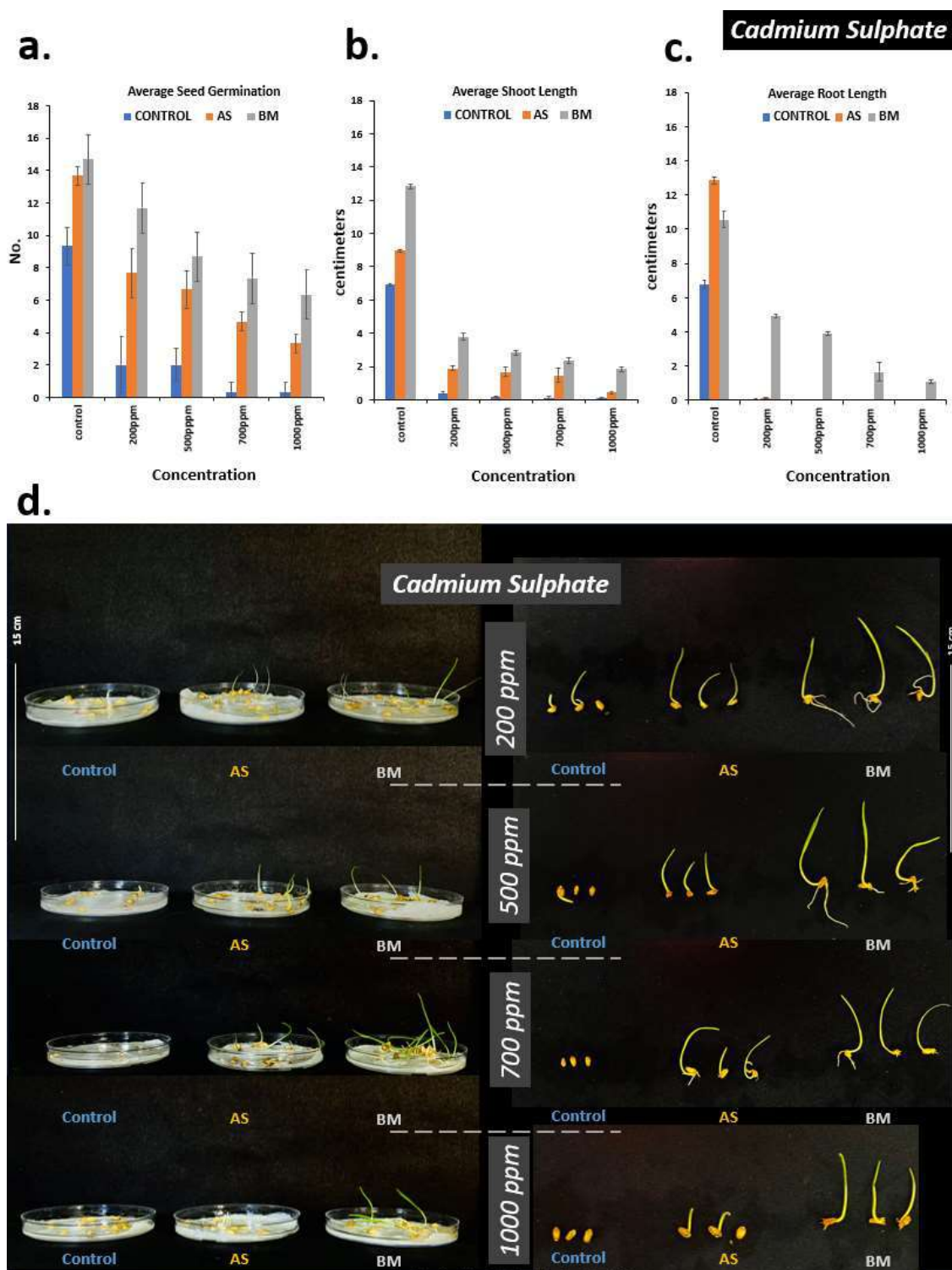


Fig. 4: Effect of seed bacterization treatments with EP1-AS and EP1-BM under various levels of the heavy metal Cadmium sulfate. Here, the parameters shown are a) average germination from 20 wheat seeds per replicate per trial, b) shoot length development, and c) root length development. The results represent the averaged outcomes of three independent trials. In d), scale bars represent the lengths of seedlings under different variables.

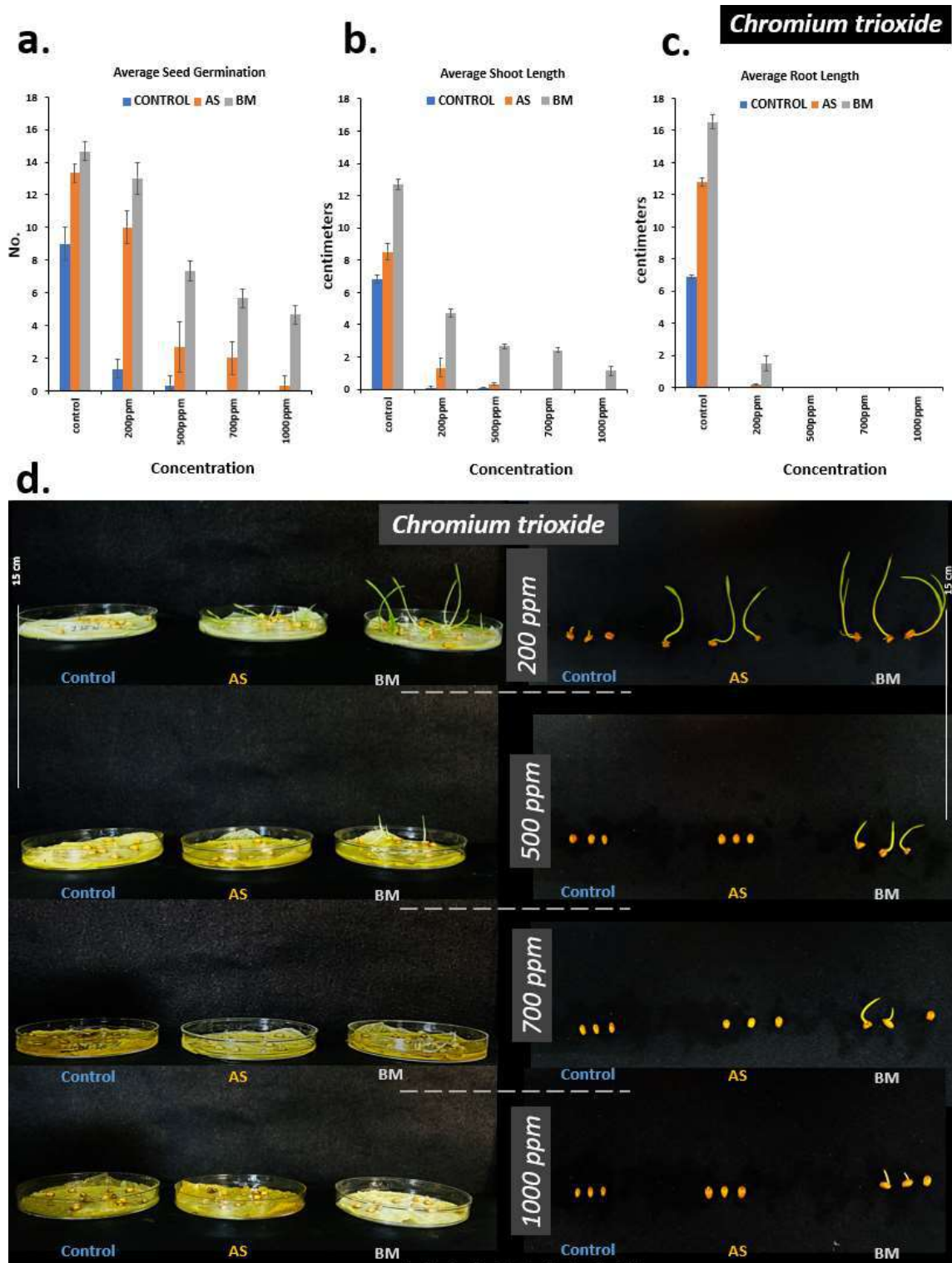


Fig. 5: Effect of seed bacterization treatments with EP1-AS and EP1-BM under various levels of the heavy metal chromium trioxide. Here, the parameters shown are a) average germination from 20 wheat seeds per replicate per trial, b) shoot length development, and c) root length development. The results represent the averaged outcomes of three independent trials. In d), scale bars represent the lengths of seedlings under different variables.

feature was only more prominent within the case with lead nitrate.

In contrast, in the case of sodium arsenite, the seedling shoot was observed to be more badly impacted, resulting in a very low length, which is easily differentiated under observations at 500 mM of either of these two heavy metals. This detrimentally also reflected well with seedlings' root development with comparatively much lower lengths at 200 mM itself for sodium arsenite than for lead nitrate (Fig. 2c and 3c). Beyond 200 mM, however, root growth was negligible and ceased completely in the case of either heavy metal. EP1-AS/EP1-BM treatments, however, could remarkably and significantly rescue the root growth in both cases of heavy metals, of which BM specifically and appreciably could hold much better root length even at 500 ppm and 700 ppm of sodium arsenite (Fig 2c) but for lead nitrate could only do better at 200 mM concentration (Fig 3c). The visual observation representations of the seedlings equated with the above results (Fig. 2d and 3d).

Effects with cadmium sulfate and chromium trioxide were more decrementing for the wheat seedling development (Fig. 4 and 5). In brief, control EP1-AS/EP1-BM untreated seed lots showed abrupt ceasing of germination at 200 ppm of either heavy metal such that only some 10 to 20% germination could be seen, especially at 500 ppm for chromium trioxide showed negligible seedling emergence compared to cadmium which still showed the emergence of the percentage as also in 200 ppm (Fig. 4a and 5a). Hence, comparatively, chromium trioxide seemed more problematic to seed germination success than cadmium sulfate. EP1-AS and EP1-BM treatments, however, seemed to enhance the germination profiles of seeds under treatments, but still, they can't be called, leading to productive germination. This is because shoot and root developments were badly impacted at any of the tested levels of heavy metals (Fig. 4b, 4c and 5b, 5c). Seedling shoot and root developments can also be seen and documented (Fig. 4d and 5d). EP1-BM as can be seen, maintained a higher rescuing ability for the shoot and root development in all levels of both the heavy metal.

Excess ions, such as sodium and chloride, can accumulate in plant tissues, disrupting crucial physiological processes (Malik et al. 2020). High salt concentrations compete with essential nutrients like potassium, calcium, and magnesium for plant roots. Similarly, heavy metals, even at low concentrations, can be toxic to plants and disrupt cellular processes, leading to oxidative stress (Asati et al. 2016). For instance, metals like cadmium inhibit photosynthesis, which is crucial for plant growth. The severity of these effects depends on factors like the type and concentration of salts or heavy metals, plant species, soil type, and environmental

conditions. Plant species exhibit varying tolerance to salt and heavy metal stress, with some better adapted to such conditions.

The coexistence of two environmental pollutants, salt and heavy metals, significantly impacts plant development and growth. In wheat seedlings, salt stress at concentrations of 100 mM can decrease shoot length due to physiological changes like osmosis, ion imbalance, and oxidative stress, hindering cell division and elongation. Heavy metal pollution also detrimentally affects wheat seedling growth by impeding nutrient uptake, protein transport, and essential molecule synthesis, resulting in various growth defects (Bharti & Sharma 2022). The damage caused by salt and heavy metals depends on factors such as concentration, exposure duration, and genotype.

Salt stress disrupts cell osmotic equilibrium, causing cell shrinkage and death. Heavy metal pollution reduces root length by impairing water and nutrient uptake, damaging cell membranes, and generating free radicals that damage DNA and cellular proteins. The extent of root length reduction depends on pollutant concentration, exposure duration, and plant genetics. Understanding these complex interactions is crucial for developing strategies to mitigate the adverse impacts of salt and heavy metal stress on plant growth and overall health.

Within the domain of stress biology, ground-dwelling spurge have emerged as resilient species, displaying remarkable adaptability to challenging environmental conditions such as arid landscapes, saline soils, and polluted sites. From a biotechnological standpoint, these plants have become central subjects in translational research, particularly for applications in phytoremediation, bioenergy production, and phytomedicines. Our research is dedicated to uncovering the potential of endophytic microbial communities associated with robust succulent plants, with a specific emphasis on ground-dwelling spurge within the Euphorbiaceae family. This exploration led to the isolation of two distinct *Lelliotia* *amnigena* isolates, EP1-AS and EP1-BM, from internodal explants of the sandmat spurge, *Euphorbia prostrata*. Despite initial suspicions of contamination, these isolates demonstrated noteworthy plant-growth-promoting (PGP) properties, resulting in enhanced growth and productivity in wheat and tomato crops under *ex vitro* conditions. Notably, the EP1-BM isolate exhibited more pronounced PGP effects, further heightened through seed-priming treatments, showcasing improved *in vitro* plant regeneration efficiency in their latex-bearing spurge host. This enhancement extended to key physiological parameters, including chlorophylls, carotenoids, phenols, and flavonoids, signifying a holistic improvement in plant stress resilience and physiological vigor.

The promising results observed in *ex vitro* trials prompted an extended assessment through field testing, affirming the ability of EP1-AS and EP1-BM isolates to enhance crop productivity in wheat and tomato. While *L. amnigena* strains have been associated with pathogenesis in specific contexts, their general limited virulence factors suggest potential safety in practical applications. As we contemplate translating our PGPB findings into practical use, a cautious approach to pathogenesis and toxicity profiling is essential. Our innovative strategy involving cell-free spent supernatants of EP1-AS and EP1-BM isolates offers a novel avenue for developing biofertilizer formulations while addressing safety concerns. Importantly, our investigation has sparked intriguing inquiries regarding the colonization, dissemination, and endophytic potential of *Lelliotia* spp. in cultivated plants. The intricate interplay between these bacteria and their hosts, combined with the exploration of translational opportunities, emphasizes the need for rigorous and comprehensive research.

In our upcoming endeavors, we are expanding on this foundation, delving into the relationship between these isolates and their potential to enhance salt tolerance and heavy metal tolerance in crops, particularly focusing on wheat. By continuing to unravel the bioprospects from resilient plants and their associated microbial communities, we aim to pioneer sustainable agriculture and tap into the untapped potential of these often underestimated and robust plant species. These translational research endeavors are especially critical considering the global zero-hunger target by 2030 amidst the looming challenges of climate change and the broader Sustainable Development Goals (SDGs) outlined by the United Nations Organization (UNO).

CONCLUSION

In conclusion, this research article delves into the evaluation of Plant Growth-Promoting Bacteria (PGPB) strains EP1-AS and EP1-BM, isolated from the halophyte *Euphorbia Prostrata*, for their potential to enhance plant growth and provide abiotic stress resilience. The study addresses the pressing need for sustainable agricultural practices in the face of challenges like soil salinization and heavy metal contamination. The investigation involves a comprehensive analysis of the heavy metal and salt tolerance of the PGPB strains, shedding light on their potential applications in promoting plant growth under adverse environmental conditions. The research further explores the impact of these PGPB strains on wheat plants subjected to varying concentrations of heavy metals and salts. Results indicate that both PGPB strains, especially EP1-BM, exhibit significant tolerance to heavy metals and salt stress. EP1-BM demonstrates remarkable resilience even under high

concentrations of these stressors. The study extends its findings to *in vitro* testing on wheat plants, revealing the positive influence of PGPB strains on germination, shoot length, and root length in the presence of salt and heavy metals.

The research underscores the significance of understanding plant-microbe interactions, particularly in the context of promoting sustainable agriculture in challenging environments. The identified resilience of PGPB strains, especially EP1-BM, suggests their potential application as bio-remediators and plant growth promoters in soils affected by salinity and heavy metal stress.

ACKNOWLEDGMENTS

The authors would like to acknowledge the support provided by UIBT, Chandigarh University, for infrastructure and for registering MP as pre-doctoral students under the able supervision of GM, who runs an in-house theme of research, ‘Exploring Resilient Life’ at UIBT, Chandigarh University. Further, the works in the manuscript could not have been realized successfully without the services of the other laboratory members with GM and laboratory support staff throughout UIBT, who are equally to be thanked. The institutes, however, had no role in shaping the manuscript and/or in the decision to publish it.

DATA AVAILABILITY

The homologs of the 16S rRNA gene sequences corresponding to the EP1-AS and EP1-BM isolates have been securely deposited in the GenBank database hosted by the National Center for Biotechnology Information (NCBI), with accession numbers OR342320 and OR342321, respectively. In adherence to transparency and scientific openness, the corresponding authors commit to providing any raw data that underpins the findings of this article. Interested parties are invited to formally request access to the data, and such requests will be accommodated promptly and without undue reservation. This commitment ensures the accessibility and reproducibility of the study’s results, fostering a collaborative and accountable approach to scientific research.

REFERENCES

- Amtaghri, S., Akdad, M., Slaoui, M. and Eddouks, M. 2022. Traditional uses, pharmacological, and phytochemical studies of *Euphorbia*: A review. *Curr. Top. Med. Chem.*, 22: 1553-1570.
- Asati, A. 2016. Effect of heavy metals on plants: An overview. *Int. J. Appl. Innov. Eng. Manag.*, 5(3): 56-66.
- Bharti, R. and Sharma, R. 2022. Effect of heavy metals: An overview. *Mater. Today Proceed.*, 51: 880-885.
- Chan, A.P., Crabtree, J., Zhao, Q., Lorenzi, H., Orvis, J., Puiu, D., Melake-Berhan, A., Jones, K.M., Redman, J., Chen, G., Cahoon, E.B., Gedil, M., Stanke, M., Haas, B.J., Wortman, J.R., Fraser-Liggett, C.M., Ravel,

- J. and Rabinowicz, P.D. 2010. Draft genome sequence of the oilseed species *Ricinus communis*. *Nature Biotechnol.*, 28: 951-956
- Chaudhary, P., Singh, D., Swapnil, P., Meena, M. and Janmeda, P. 2023. *Euphorbia nerifolia* (Indian Spurge Tree): A plant of multiple biological and pharmacological activities. *Sustainability*, 15: 1225
- Dubyna, D.V., Ennan, A.A.A., Dziuba, T.P., Vakarenko, L.P., Shykhalieva, G.M. and Kiryushkina, H.M. 2022. Anthropogenic transformations of vegetation in the Kuyalnik estuary valley (Ukraine, Odesa District). *Diversity*, 14: 1115.
- Linfang, H., Shilin, C. and Meihua, Y. 2012. *Euphorbia hirta* (Feiyangcao): A review on its ethnopharmacology, phytochemistry and pharmacology. *J. Med. Plants Res.*, 6: 5176-5185
- Jeevanandam, J. 2021. Biosynthesized metal nanoparticles in bioremediation. *Bioremediation*, 5: 126-161.
- Kaur, J., Dhar, S.K., Chauhan, A., Yadav, S., Mudgal, G., Lyudmila, A., Atuchin, V. and Abdi, G. 2023a. GC-MS validated phytochemical up-leveling with in vitro-raised *Sansevieria trifasciata*. *Current Plant Biology*, 35-36: 100308
- Kaur, J. and Mudgal, G. 2020a. An efficient protocol for micropropagation of small-flowered bugleweed. *Plant Cell Biology and Molecular Biology*, 5: 16-22.
- Kaur, J. and Mudgal, G. 2020b. Phytochemistry and pharmacological assets of *Ziziphus Juazeiro-Mart*: A review. *Plant Cell Biol. Mol. Biol.*, 16: 112-126.
- Kaur, J. and Mudgal, G. 2021. An efficient and quick protocol for in vitro multiplication of snake plant, *Sansevieria trifasciata* var. *laurenti*. *Plant Cell, Tissue and Organ Culture*, 147: 405-411.
- Kaur, J., Mudgal, G., Chand, K., Singh, G.B., Perveen, K., Bukhari, N.A., Debnath, S., Mohan, T.C., Charukesi, R. and Singh, G. 2022. An exopolysaccharide-producing novel *Agrobacterium pusense* strain JAS1 isolated from a snake plant enhances plant growth and soil water retention. *Sci. Rep.*, 12: 21330
- Kaur, J., Mudgal, G., Negi, A., Tamang, J., Singh, S., Singh, G.B., Bose K., J.C., Debnath, S., Wadaan, M.A., Farooq Khan, M., Ruokolainen, J. and Kesari, K.K. 2023b. Reactive Black-5, Congo red, and methyl orange: Chemical degradation of azo-dyes by *Agrobacterium*. *Water*, 15: 1664
- Kaur, J. 2020. Genetic Transformation of *Olea europaea* (Olive). for folate biofortification. *Plant Cell Biol. Mol. Biol.*, 16: 72-82.
- Khaksar, G., Siswanto, D., Treesubuntorn, C. and Thiravetyan, P. 2016. *Euphorbia milii*-endophytic bacteria interactions affect the hormonal levels of the native host differently under various airborne pollutants. *Mol. Plant Micro. Interact.*, 29: 663-673
- Malik, A., Butt, T.A., Naqvi, S.T.A., Yousaf, S., Qureshi, M.K., Zafar, M.I., Farooq, G., Nawaz, I. and Iqbal, M. 2020. Lead tolerant endophyte *Trametes hirsuta* improved the growth and lead accumulation in the vegetative parts of *Triticum aestivum* L. *Heliyon*, 6: e04188.
- Mingo-Castel, A. 1984. Hormonal effects on phyllotaxis of *Euphorbia lathyris* L. *Botan. Mag.*, 97: 171-178.
- Mudgal, G., Kaur, J., Chand, K., Parashar, M., Dhar, S.K., Singh, G.B. and Gururani, M.A. 2022. Mitigating the mistletoe menace: Biotechnological and smart management approaches. *Biology*, 11: 1664
- Mudgal, G. 2021. *The Antioxidant Arsenal against COVID-19*. Springer International Publishing, Cham, Germany, pp. 327-357.
- Mudgal, G. and Mudgal, B. 2011. Evidence for the unusual choice of host and haustoria by *Dendrophthoe falcata* (L.f. Ettingsh), a leafy mistletoe. *Arch. Phytopathol. Plant Protect.*, 44: 186-190.
- Mudgal, G., Mudgal, B., Gururani, M.A. and Jelli, V. 2011. *Pseudaulacaspis cockerelli* (Cooley, hyperparasitizing *Dendrophthoe falcata* (L.f.) Ettingsh. *Arch. Phytopathol. Plant Protect.*, 44: 282-286.
- Parashar, M., Dhar, S.K., Kaur, J., Chauhan, A., Tamang, J., Singh, G.B., Lyudmila, A., Perveen, K., Khan, F., Bukhari, N.A., Mudgal, G. and Gururani, M.A. 2023. chapters 2 Novel plant-growth-promoting *Lelliottia amnigena* isolates from *Euphorbia prostrata* Aiton enhance the overall productivity of wheat and tomato. *Plants*, 12: 3081
- Parashar, M., Mudgal, G. and Jaspreet, K. 2020a. Phytochemical profiling, antimicrobial and antioxidant activities on leaves extract of *Murraya koenigii*. *Plant Cell Biol. Mol. Biol.*, 303-313.
- Parashar, M., Mudgal, G. and Sharma, S. 2020b. Bioremediation using green approaches with *Euphorbia prostrata*: A review. *Plant Cell Biol. Mol. Biol.*, 21: 127-135.
- Pascal, O.A. 2017. A review of the ethnomedical uses, phytochemistry, and pharmacology of the *Euphorbia* genus. *J. Pharm. Innov.*, 6: 1, 34.
- Ramamoorthy, S., Mudgal, G., Rajesh, D., Nawaz Khan, F., Vijayakumar, V. and Rajasekaran, C. 2009. Characterization of novel pH indicator of natural dye *Oldenlandia umbellata* L. *Natural Prod. Res.*, 23: 1210-1217.
- Saeed, T., Khan, T.A., Ahmad, A., Yusuf, M., Kappachery, S., Fariduddin, Q., Mudgal, G. and Gururani, M.A. 2023. Exploring the effects of selenium and brassinosteroids on photosynthesis and protein expression patterns in tomato plants under low temperatures. *Plants*, 12: 3351.
- Salatino, A., Salatino, M.L.F. and Negri, G. 2007. Traditional uses, chemistry, and pharmacology of *Croton* species (Euphorbiaceae). *J. Brazil. Chem. Soc.*, 18: 11-33.
- Sharma, A. 2021. *Toxicity with Waste-Generated Ionizing Radiations: Blunders Behind the Scenes*. Free Radical Biology and Environmental Toxicity. Springer International Publishing, Cham, Germany, pp. 305-325.
- Singh, G.B. 2021. *Molecular Communications Between Plants and Microbes*. Plant-Microbial Interactions and Smart Agricultural Biotechnology. CRC Press, Boca Raton, USA, pp. 147-184.
- Siva, R., Rajasekaran, C. and Mudgal, G. 2009. Induction of somatic embryogenesis and organogenesis in *Oldenlandia umbellata* L., a dye-yielding medicinal plant *Plant Cell Biol. Mol. Biol.*, 98: 205-211.
- Sivakumaran, S. and Hall, M.A. 1978. Effects of age and water stress on endogenous levels of plant growth regulators in *Euphorbia lathyris* L. *J. Exper. Bot.*, 29: 195-205.
- Srivastava, R. and Soni, N. 2019. An updated review on the phytopharmacological profile of *Euphorbia tithymaloides* (L). *Poit. Pharma Innov. J.*, 8: 109-115.
- Unde, S. and Kumar, S.R. 2022. Phytoremediation potentials of some ornamental plants: A review. *Adv. Innov. Res.*, 85: 14-20.
- Vinayak, A. 2020. Waste to energy: Sustainable bioremediation approach for renewable energy. *Plant Cell Biol. Mol. Biol.*, 11: 292-302.
- Vinayak, A. 2021. *Environment Persistent Free Radicals: Long-Lived Particles*. Free Radical Biology and Environmental Toxicity. Springer International Publishing, Cham, Germany, pp. 1-19.
- Washington, J. 1980. Dilution susceptibility test: Agar and macro-broth dilution procedures. *Am. Soc. for Microbiol.*, 11: 2461.
- Webster, G.L. 1967. The genera of Euphorbiaceae in the southeastern United States [concl.]. *J. Arnold Arboretum*, 48: 363-430.



Biodegradation of Cellulosic Wastes and Deinking of Colored Paper with Isolated Novel Cellulolytic Bacteria

Jyoti Sarwan , Jagadeesh Chandra Bose† , Shivam Kumar, Shruti Singh Bhargav, Sharad Kumar Dixit, Muskan Sharma, Komal Mittal, Gurmeet Kumar and Nazim Uddin

University Institute of Biotechnology, Chandigarh University, Mohali-140413, Punjab, India

†Corresponding author: Jagadeesh Chandra Bose; jcbouseuibtlab@gmail.com

Nat. Env. & Poll. Tech.
Website: www.neptjournal.com

Received: 16-11-2023

Revised: 19-12-2023

Accepted: 27-12-2023

Key Words:

Cellulases

Bioethanol

Bacillus paramycooides

Deinking

Endoglucanases

ABSTRACT

Biofuels are the cheapest source of energy, and the continuous decline of traditional sources of energy with the increasing population leads to looking for alternatives to reduce the consumption of traditional sources of energy. Bioethanol production from lignocellulosic wastes and cellulosic wastes is not a new approach for fuel production but a cheap and accessible way for the production of fuel. *Bacillus* is one of the major species that can act as a source of diversified enzymes. In this study, it was emphasized on screening and isolation of a novel, characterization, and best catalytic action on both celluloses and proteins in the presence of different carbon and nitrogen sources. It was observed the effective catalytic breakdown of cellulose with the crude enzyme to glucose allowed for fermentation with *Saccharomyces*, ultimately leading to the generation of alcohol. The study aims to isolate the microbes that can produce cellulases and enzymes and could be used for biodegradation to produce ethanol in the reaction. The maximum enzyme activity was achieved at 3.112 UI with optimized pH and temperature, and the maximum conversion of sugars into alcohol was about 70% in the newspaper, cartons, colored paper, and disposable paper cups. An essential observation was the decolorization of the origami craft paper within 24 hours. The study was involved in enhancing the maximum Enzyme activity of cellulases from different cellulosic raw materials. Hence, it was achieved by JCB strain, optimization of pH, temperature, and acids for the biodegradation. The presence of peaks at 3200 and 2900 was a confirmation of ethanol bonds in the biodegradation reaction mixtures.

INTRODUCTION

The increasing demand for fuel and dependency on fossil fuels leads to the search for alternatives for energy (Sun et al. 2022). Within the global energy industry, fossil fuels stand out as a pivotal non-renewable resource. They played a crucial role in driving the Industrial Revolution and fostering technical, social, and economic progress. However, the excessive reliance on these non-renewable fuels in industrial and transportation processes has led to environmental pollution. The combustion of fossil fuels releases greenhouse gases, contributing to climate change and global warming. Moreover, the rapid depletion of fossil fuel reservoirs due to over-exploitation emphasizes the urgent need to explore alternative, renewable energy sources to address future energy challenges. In response to this dilemma, lignocellulosic biofuels emerge as a promising alternative energy source capable of replacing fossil fuels. Lignocellulosic biofuels, derived from flexible ligninolytic microbes, offer a sustainable solution by converting

lignocellulosic biomass (LCB) and biological waste into energy fuels. This approach presents a significant opportunity to mitigate the pressing issue of environmental pollution caused by fossil fuel use. By harnessing the potential of lignocellulosic biofuels, we can pave the way for a more sustainable and eco-friendly energy future (Rath et al. 2022). Bioethanol has piqued the interest of researchers in recent decades due to its versatility in applications such as hydrogen generation, pharmaceuticals, and fuel. Cellulosic ethanol is routinely produced from lignocellulosic biomass via pre-treatment, enzymatic saccharification, and fermentation. However, the refractory nature of lignocellulosic biomass inhibits enzyme accessibility, making conversion into fermentable sugars and bioethanol more challenging. Many straw biomass resources in China have been squandered and cannot be efficiently utilized (Xian et al. 2022). Renewable biofuels such as biodiesel, bioethanol, and biobutanol are long-term solutions to the depletion of fossil fuels. Plant biomass is a sustainable feedstock for their production, which is degraded to sugars with the help of microbe-derived

enzymes, followed by microbial conversion of those sugars to biofuels. Given their global need, more attempts have been made to produce them on a big scale, which is ultimately leading to breakthrough research in biomass energy (Sartaj et al. 2022). The bulk of the world's energy demand is fulfilled by fast-depleting fossil fuels, which are also environmentally harmful. With rising global energy consumption, the price of fossil fuels significantly rises every quarter. As a result, there is an urgent need for an alternative that not only meets energy demand but is also clean and renewable. Various renewable feedstocks, mainly lignocellulosic biomass, are fermented by microorganisms to create biofuel and other bio-based platform chemicals (Sahoo et al. 2023). In countries with a large agricultural population, like India and other Asian nations, improper handling of biowaste can seriously contaminate the environment. The most obvious, economical, and ecologically friendly method will be microbial waste degradation, as most biowaste can be readily broken down by many microbial communities and successfully converted into less toxic or hazardous forms. Certain bacteria target plant-based celluloses, which are the primary structural element of most plant cells, by producing cellulases. Several energy-dense derivatives are produced by this process, including glucose, cellobiohydrolase, and others, which may be used to make bioethanol. Enzymes called cellulases hydrolyze glucose's polymeric structure, which is found in the majority of waste products derived from plants (Bose & Sarwan 2023). The shift to biomass valorization by biorefineries, including the composition of the biomass (cellulose, hemicellulose, and lignin if it is lignocellulosic material; humidity level, distribution of triglycerides and fatty acids, concentration of sugars if wet wastes), the classification of biorefineries (from first to fourth generation), the target products that can be produced (ethanol, biodiesel, methane, hydrogen), and the process technologies (biochemical, chemical, or thermochemical) used for biomass transformation (Giuliano 2023). The deinking process of the cellulosic wastes remains in the sewage treatment, deinking of the colored paper can lead to the eco-friendly approach to the wastewater treatment. Similarly, during the deinking process of the recycling paper, chemical methods are used for deinking the colored paper. Therefore, using cellulolytic bacteria is helpful as a cost-effective and nontoxic method for deinking the colored paper. Several examples of effective protease-producing *Bacilli* strains in the bacterial community are *B. amyloliquifaciens*, *B. subtilis*, and *B. licheniformis*, besides other bacterial species known as *Staphylococcus*, *Pseudomonas*, *Serratia*, *Alcaligenes*, *Vibrio*, *Brevibacterium*, *Flavobacterium* and *Halobacterium* (Sarwan & Bose 2022). The main aim of this study is to isolate and characterize novel bacterial strains from soil and to determine their ability to produce cellulase

and protease enzymes and their potential for degradation of various bio-waste (Sarwan & Bose 2021, 2022, Sarwan et al. 2021, Sharma et al. 2023) Therefore using the novel cellulolytic bacteria for the degradation of cellulosic wastes and deinking of colored paper can be used as a cheap and nature-friendly approach for the degradation and energy production.

MATERIALS AND METHODS

Sample Collection for the Isolation of the Cellulase-Producing Microorganisms

Different soil samples were collected with gloves and kept in sterilized polybags. Collected soil samples were brought into the lab. The soil samples were serially diluted in the (v/w) 1g in 99 mL of distilled water. For the isolation of cellulolytic microbes, CMC media was prepared by using 1% CMC, 0.01g $MnSO_2$, 0.01g $MgSO_4$, 0.01g K_2HPO_4 , 0.01g KH_2PO_4 in total volume of 100 mL in Erlenmeyer flask (Darwesh et al. 2020). Media constituents were mixed thoroughly, pH was maintained from 6.7-7.2, and plates were incubated for 48 h at 37°C. Pure cultures were obtained with the streaking method.

Visualization of Cellulase Enzyme Activity with Congo Red Assay

The plates were made with the mentioned CMC agar and flooded with Congo red solution after the incubation of 48 h of the cultures. Congo red was used as aqueous Congo red of 1% in 100 mL of distilled water and treated for 15 minutes on the plates. After the treatment of Congo red to the plates, the plates were treated with NaCl solution for 10 minutes. Clear zones on the plates were showing cellulolytic activity in isolated microbe (Saleh et al. 2023).

Enzymatic Assay of Cellulases by Microbes

Subculturing bacteria in the Luria broth culture medium with cellulose and 50 mM of citrate buffer at pH 5 was used for the enzymatic test, which was then incubated for 48 h at 140 rpm in a shaking incubator. After centrifuging for 15 min at 40°C at 10,000 ×g, the supernatant was recovered. After treating the 0.2 mL supernatant with CMC, phosphate buffer was added to bring the pH down to 6.5. Using the 3,5-dinitric salicylic acid (DNS) technique, the total reducing sugars were determined and compared to the glucose standard curve (Islam 2019, Shanmugapriya et al. 2012). One unit of enzyme activity denoted as U/mL, can be used to further describe the enzyme activity of microbial enzymes. The amount of enzyme involved in this activity is measured in units of 1 u mol of reducing sugar released per minute (Asem

et al. 2017, Zeng et al. 2016). Using the Lowry method and a colorimetric technique with Folin reagent, determine the free amino acid content of a given sample (Islam et al. 2019, Mothe & Sultanpuram 2016, Singhanian et al. 2018). One mol of reducing sugar is released each minute by the amount of enzyme involved in this enzyme activity. The equation used to determine enzyme activity.

$$\text{Enzyme Activity (U/mL)} = \frac{\mu\text{g of glucose released} \times 1000}{\text{Mol. of glucose} \times \text{incubation time}}$$

Determination of Different Cellulases in Isolated Microbes

Exoglucanases: For determination of the presence of exoglucanase activity in the microbial cells, the cells were treated with a solution of 1% avicel dissolved in 50 mM of citrate or phosphate buffer of the total volume of 400 μL , and pH was adjusted 5 -5.5. 0.5 mL of crude enzyme mixture was incubated at 50°C for 1 h in a water bath. For termination of the reaction, the mixture was instantly kept in an ice bath. The reaction mixture was centrifuged at 10000 rpm for 10 min at 40°C. After collecting the 0.5 mL of supernatant added 0.5 mL of sulphuric acid and 1% phenol in it. The presence of free-reducing sugar was determined with the DNS method on a UV-Vis Spectrophotometer at 450nm and compared with the glucose standard curve(K & Sarwan, 2023b)

Endoglucanases: For determination of the endoglucanase activity in the isolated microbes was analyzed with 1% soluble cellulose by maintaining pH 6.7 with phosphate buffer in 1mL of crude enzyme and incubated for 2 h at 50°C in a water bath. The supernatant was collected for centrifuge at 10000rpm for 6 min, and enzyme assay was calculated with the DNS method on spectrophotometric readings (Nguyen & Hoang 2020).

β -Glycosidases

For determination of the beta glycosidases enzyme activity, 0.5mL of the crude enzyme was mixed with 1% cellobiose/ lactose in 100 mL by adjusting pH at 6 in 50mM phosphate buffer for 2 h at 40°C in a shaking incubator. The mixture was centrifuged at 10,000 rpm, and the supernatant was collected for DNS assay on UV –A visible spectrophotometer at 450nm.

Lignin Peroxidases: To perform the assay, 1mL of culture broth from each isolate was placed in Eppendorf tubes, and the culture broths were subjected to centrifugation at 4°C and 7000 rpm in a cooling centrifuge. Given that lignin peroxidase is extracellular, the supernatant from each centrifuge tube containing the enzyme was collected for

further analysis. For the enzyme test, a reaction mixture was prepared by combining 1 mL of 50 mM sodium potassium tartrate (pH 4) buffer with 0.1 mL of a 0.1 mM H_2O_2 inducer. This solution was supplemented with 32 μM methylene blue, and 10 μL of the enzyme supernatant was added to initiate the reaction. To serve as a control, a separate test tube was prepared by adding 10 μL of distilled water to the aforementioned reaction mixture in lieu of the enzyme supernatant. The assessment of enzyme activity was based on the observed % decolorization of the methylene blue dye. This experimental design allows for the evaluation of LiP's demethylation capabilities under specified conditions, providing valuable insights into its enzymatic activity. (Rath et al. 2022). The final test solution was incubated at room temperature for 1 hour before the absorbance was measured using a UV-Vis spectrophotometer.

Identification of the Isolated Microbes

Microscopic identification was done of the isolated microbes. The isolate that exhibited the largest hydrolytic zone indicating the highest enzyme activity compared to the other isolates, was chosen for 16s RNA ribotyping sequencing. The 16s RNA sequencing was conducted using universal primers. The forward primer used was 926-(3' AAA CTC AAA GGA ATT GAC GG 5'), while the reverse primers used were -518-(5' ATT ACC GCG GCT GCT GG 3') and 1100-(5' TTG CGC TCG TTG 3') (Carvalho et al. 2021, Rashid et al. 2022). Phylogenetic analysis of the isolated microbes. With the obtained Fasta sequence files of the isolated microbes, the FASTA sequences were aligned in the Nucleotide blast of the NCBI site and found most similar microbes and again aligned with multiple sequence sites. The construction of a phylogenetic tree was performed using the MegaX software. This involved comparing the detected isolate with a set of neighbor-joining organisms and determining the degree of similarity between them (Carvalho et al. 2021)

Biodegradation of Wastes for Utilization in Bioethanol Production

The aim of the select different cellulosic wastes to be degraded with cellulolytic microbe and utilization of the reducing sugars with yeast. There were different cellulosic wastes taken including newspaper, colored paper, cartons, and paper cups. These four wastes were added to the MSM mentioned above medium, and cellulosic wastes were utilized to make reducing sugars as the sole of carbon. Therefore, various cellulosic substrates were successfully utilized in minimum essential medium, and the presence of reducing sugars was observed with the DNS method. The process of biodegradation involved – chopping down different cellulosic or lignocellulosic wastes into fine pieces

and added into the minimum essential medium with w/v in 100 mL of distilled water each. The medium was autoclaved at 121 and 15 psi pressure for 20 min. After cooling down of the medium, in the LAF hood, crude enzyme 0.5 mL was inoculated and kept for incubation at 34°C for 24 h-114 h. The determination of the reducing sugars released by crude enzyme was calculated with three different parameters: first was the traditional method DNS, second was the refractometer, and third was the glucometer. A glucometer is a device that can be used as a biosensor in human blood and biological reactions. The amount of sugar mg.dL^{-1} in the glucometer can be converted into mg.mL^{-1} . Once the monitoring of reducing sugars was done, the inoculation of yeast cells was performed. The local baker's yeast was purchased from the bakery and activated with a sugar solution for 24 h at 28°C. The inoculum of activated yeast cells of 100 μL was then procured into the reaction mixture. The reaction mixture was analyzed with different parameters from 0 h to 114 h, like sugars, pH, alcohol, and cell growth

(Ega et al. 2020, Deka et al. 2013, Dadwal & Satyanarayana 2020).

Estimation of Alcohol with Potassium Dichromate Method

The presence of ethanol content was estimated with the potassium dichromate method and a standard curve of ethanol was prepared. Estimation of acid production with pH paper- the production of acids in the reaction was observed from time to time with litmus paper and a pH meter.

Effect of Different Parameters on Biodegradation

There were four different parameters taken to optimize the best possible cell growth, enzyme activity, and biodegradation in the reaction mixture. These parameters were as follows: Obviously, the pH of the mixture and different sets were taken in triplicates to enhance maximum cell growth and enzyme activity. Different temperature sets from lowest to highest range 15 degrees C to 60 degrees

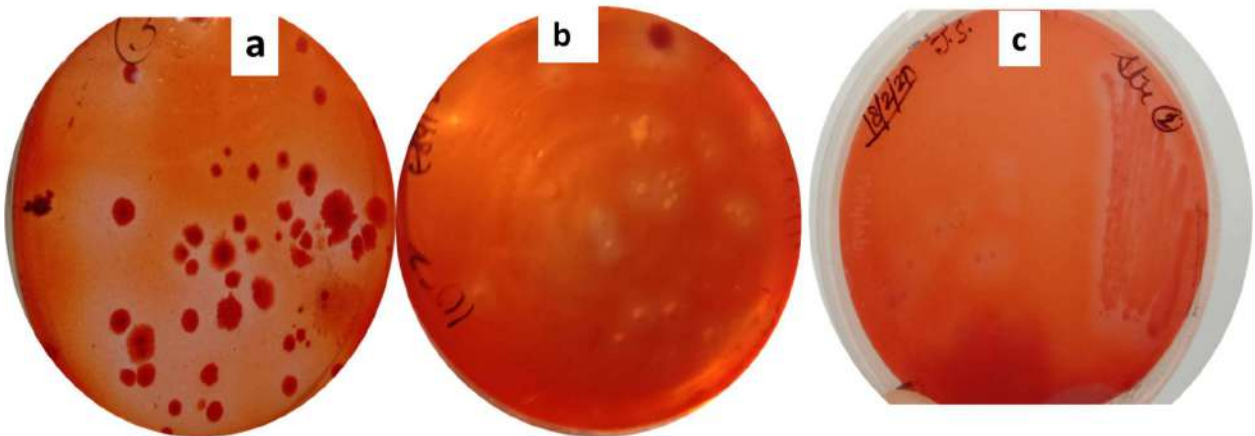


Fig. 1: An illustration of screening of cellulases producing microbes a), b), and c) describes the zone of clearance on CMC agar plates.

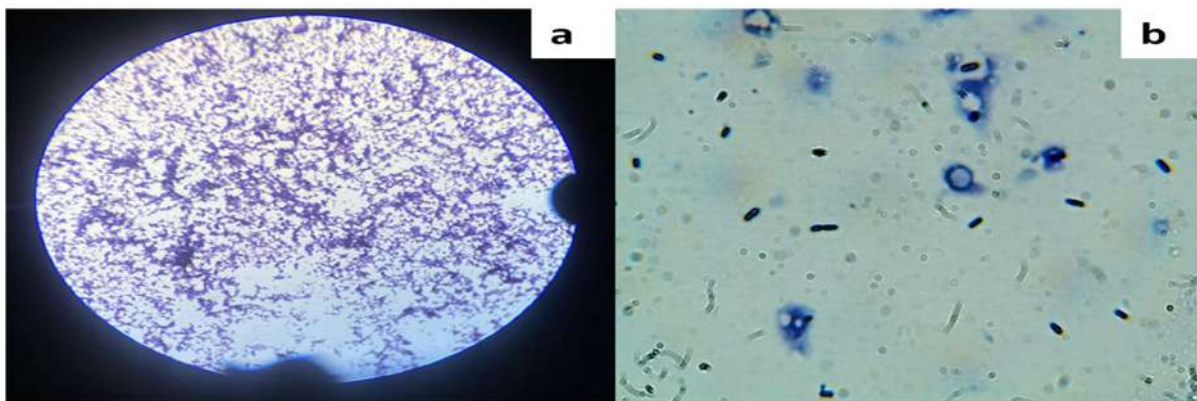


Fig. 2: Microscopic studies of isolated bacteria under a) compound microscope and b) Metzer Vision Plus-5000 microscope.

Celsius. Similarly, there were different pH ranges taken from pH 4 -12 (Yaya et al. 2021, Restuhadi & Silaturahmi 2019, Zeng et al. 2016, Liggieri et al. 2009). Effect of inoculum size from 0.1mL to 2mL and different concentrations of the cellulosic wastes or substrate were also determined to achieve the maximum degradation (Rojas et al. 2009). At last, for every optimization parameter, the DNS assay was done.

RESULTS AND DISCUSSION

During the isolation process, the soil samples were collected from the sites where cellulosic wastes were discarded. The isolation procedure was done with sterile conditions. The screening of various microorganisms was done with a nutrient agar (Himedia) medium, and there were 10 microbes selected for the isolation process. Isolates were purified with the streaking method and further screening. Screening of cellulase enzymes was done with CMC media plates, and the hollow zone appearance was an indication of the utilization of cellulose in the medium by the microbes. Screening of cellulases-producing bacteria among 10 microbes with similar zones of clearance was further analyzed with cellulases assay. After qualitative analysis of cellulases, microscopy studies were performed with gram staining (Bose & Sarwan 2023), and the colonies of microbes were observed under two different microscopes. Fig. 1 describes the screening of cellulases-producing microbes with a zone of inhibition on CMC agar plates. One picture was captured in a light microscope, and another was observed

under Metzer Vision plus-5000 under a 100x lens. With microscopic studies, it was revealed that isolated microbes were gram-positive, elongated, and more similar to bacilli as well as IMVIC tests of the isolated microbes revealed gram-positive and bacillus family of bacteria. Fig. 2 describes the microscopic studies of isolated bacteria under a compound microscope and Metzer under 100x resolution. Fig. 1 describes 3 different strains with higher and lower cellulase activity: JCA, JCB, and JCC.

A bacterial strain was identified – with 96% similarity to *Bacillus paramycooides*, and the phylogenetic tree was built with the software MegaX. Neighbor-joining method opted to identify closely related species with *Bacillus paramycooides*. Fig. 3. showing phylogenetic analysis and relation with neighbor-joining species (Carvalho et al. 2021). The Data was submitted to NCBI and got an accession number in Genebank with ON150894 (Thakur et al. 2019, Sarwan & Bose 2021, 2022, Ganesan et al. 2021).

Fig. 2 describes the fact that after the isolation of cellulases-producing enzyme microbes, morphological studies were performed on the isolated strain of the microbes. With morphological studies, it was gram-positive, bacilli-structured, and bead-like bacteria under the microscope. Other studies revealed that it was catalases negative, Simmon citrate positive, IMVIC positive strain and sent for further genomic sequencing. During isolation among 10 isolates, 3 isolates were giving similar cellulase activities. They were named JCA, JCB, and JCC. The JCB giving maximum enzyme activity was 2.901 UI (Bose & Sarwan 2023b).

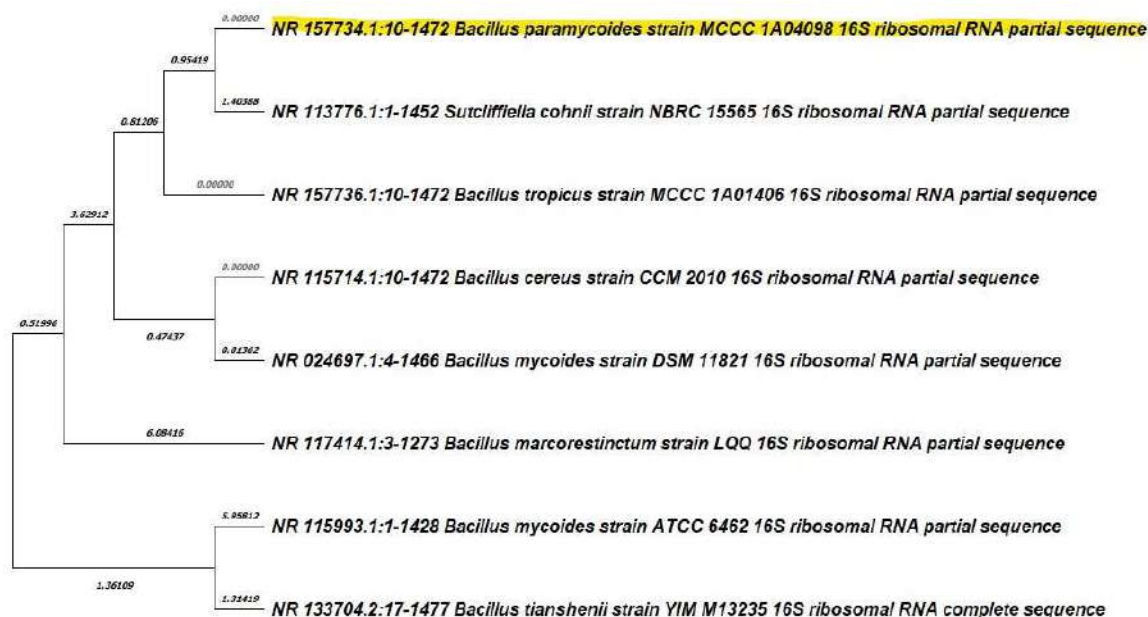


Fig. 3: Phylogenetic tree of isolated bacterial strain.

Fig. 3 illustrates the similar neighbor species. During the construction of the phylogenetic tree from the NCBI nucleotide blast, there was the presence of numerous fumigates- unidentified species. Therefore, the authors recognized with most similar strains and made a phylogenetic tree with Mega X software.

Figs. 4 and 5 describe the effect of pH and temperature on different factors of cells like cell growth. The growth

curve of bacteria was maximum achieved, giving 1.209 spectrophotometric readings after 48 h at 37°C and pH 7.8. Similarly, enzyme activity was 2.98 UI at the same temperature and pH, biodegradation, called ethanol production, was maximum achieved at pH 8 and temperature 34°C was 60-70% according to ethanol standard. Figs. 6 and 7 showing the maximum activity was found in 1mL of inoculum, and 1.5 g of substrate concentration was 2.189 UI and 3.156 UI.

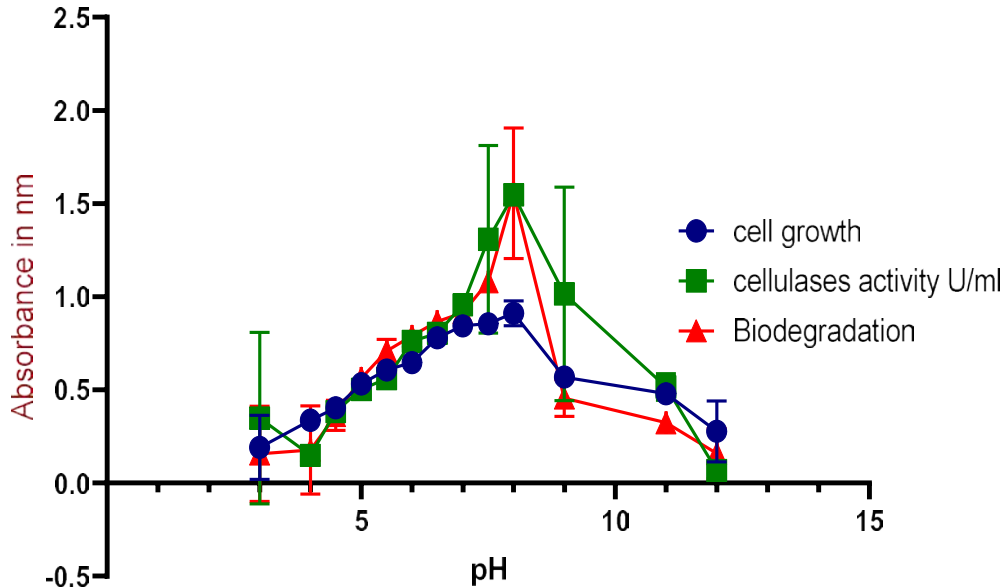


Fig. 4: Optimization of pH for maximum cell growth, cellulase activity, and biodegradation.

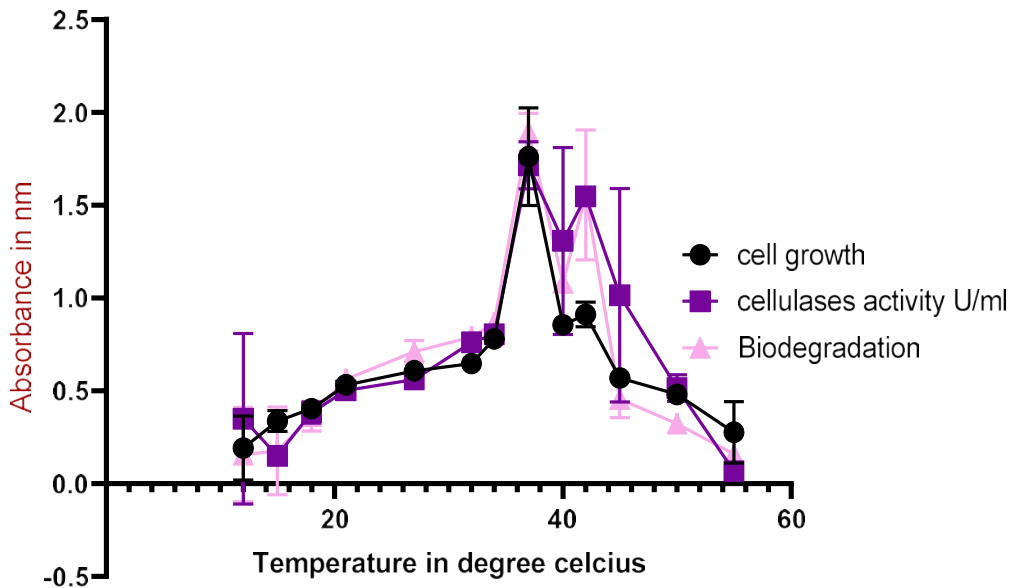


Fig. 5: Optimization of Temperature for achieving maximum cell growth, cellulase activity, and biodegradation.

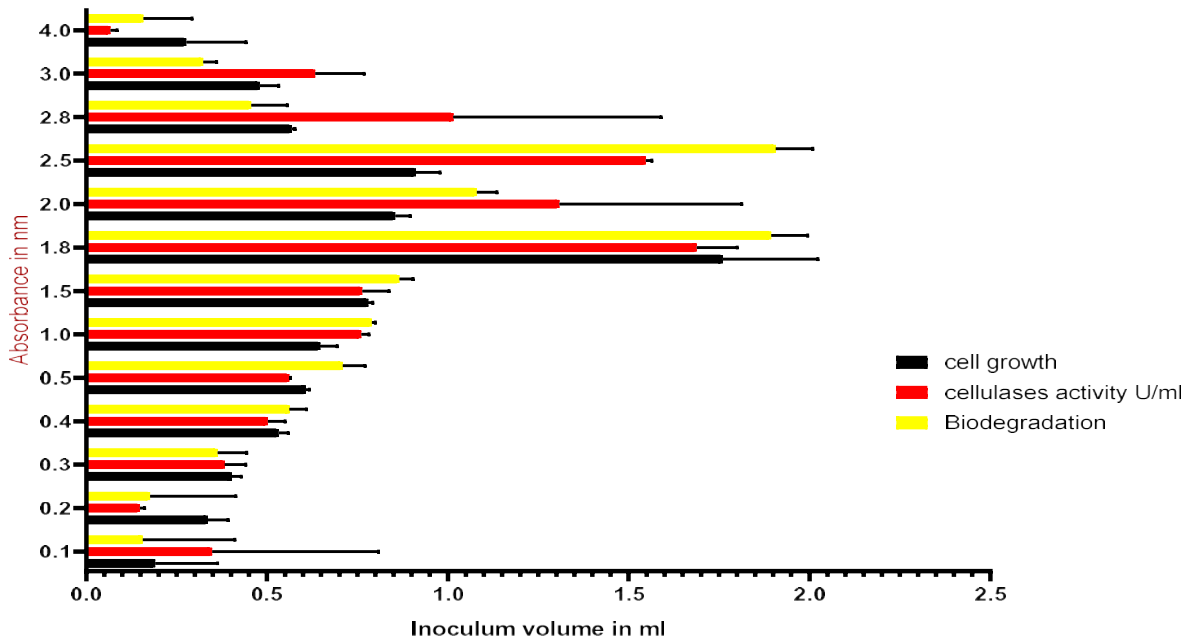


Fig. 6: The effect of inoculum size on cellulases, cell growth, and biodegradation.

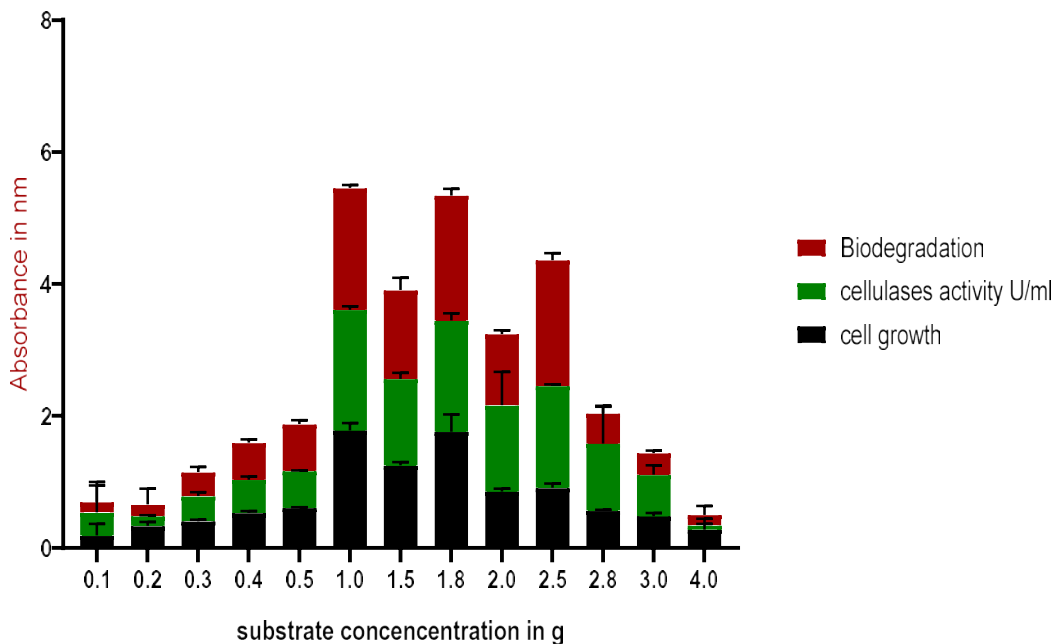


Fig. 7: Representing the effect of substrate concentration on enzyme activity.

Fig. 8 describes the list of various cellulosic wastes for biodegradation. Before being used as a substrate, they were finely chopped. Next, Fig. 9 describes the evaluation of sugar during biodegradation. During cellulase activity, sugars were released and calculated. Still, when reducing sugars were completely utilized, the amount of free reducing

sugars decreased, but again, inoculation of the yeasts cells, the sugar release was observed as in Fig. 4 (Fu et al. 2022). Among all four cellulosic wastes, Newspapers are called NPS, Paper cups as PCS, Cartons CTS, and Purple paper PPS. Per the studies, paper cups were not as disposable as they claim, it takes at least 15 days to

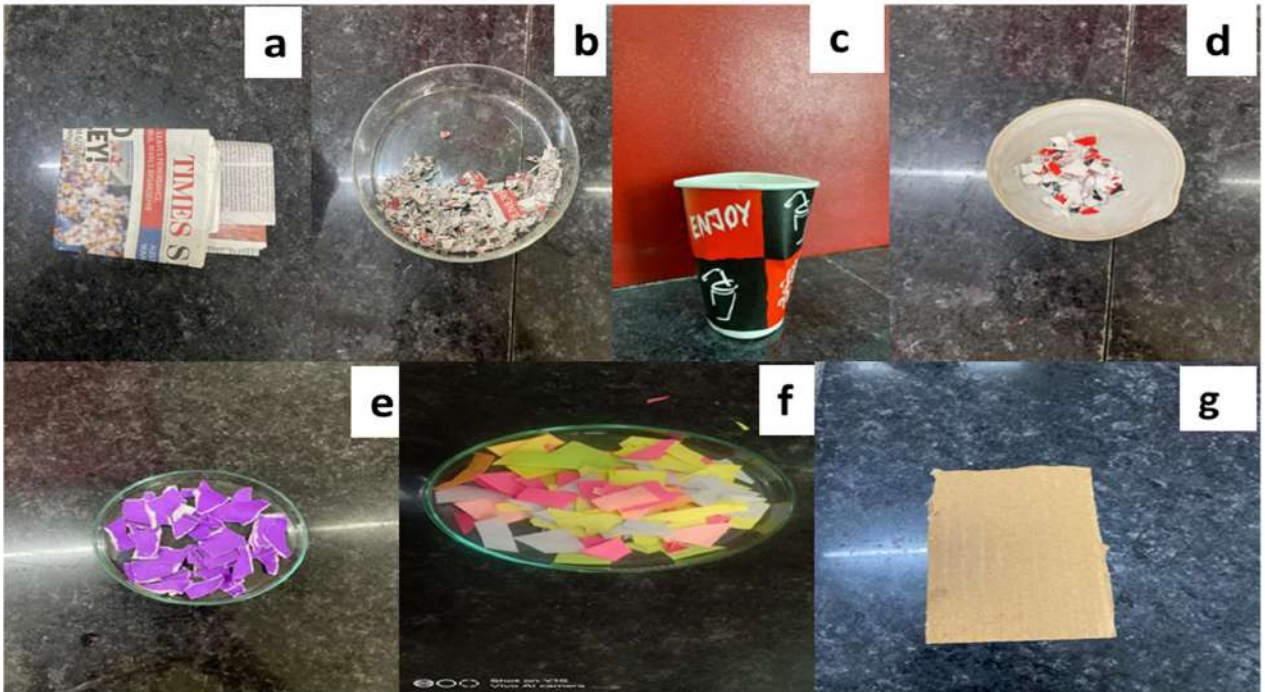


Fig. 8: Different cellululosic substrates for biodegradation.

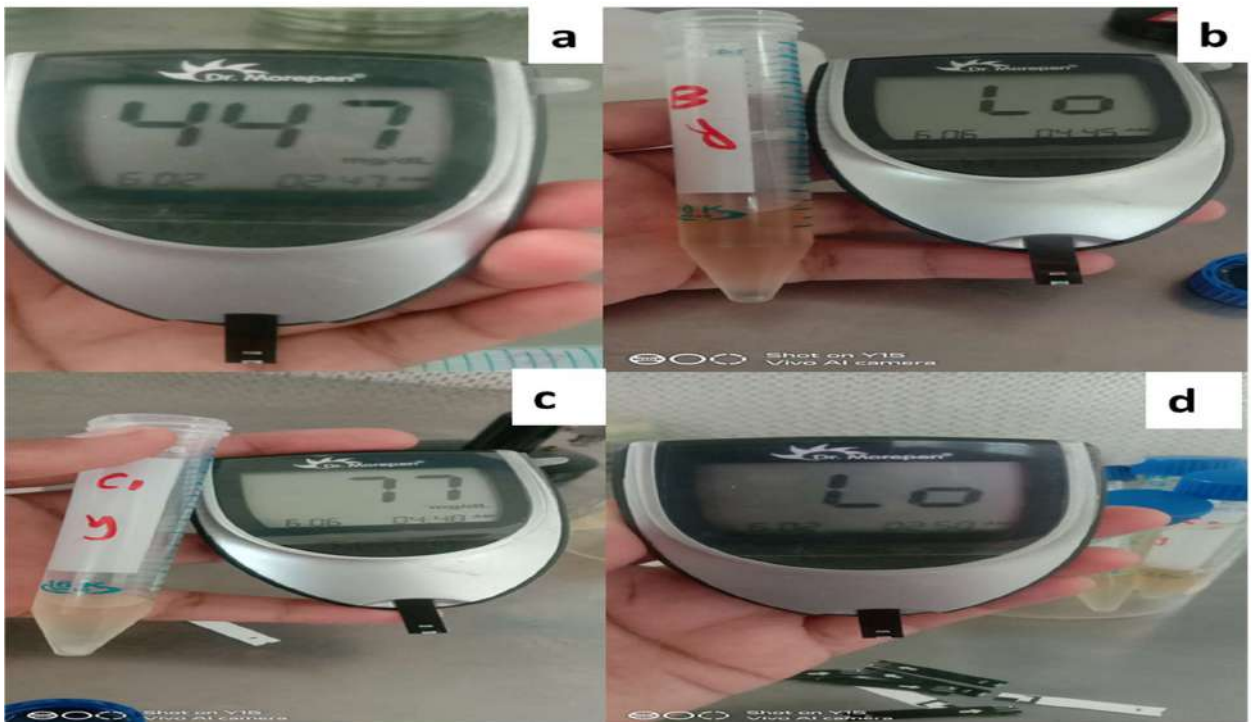


Fig. 9: Evaluating sugar molecules released during fermentation.

the degradation of Paper cups. The maximum alcohol produced by NPS, CTS, and PPS was 70-80% as the ethanol

standard curve, but the lowest in PCS was 30% (Darwesh et al. 2020)

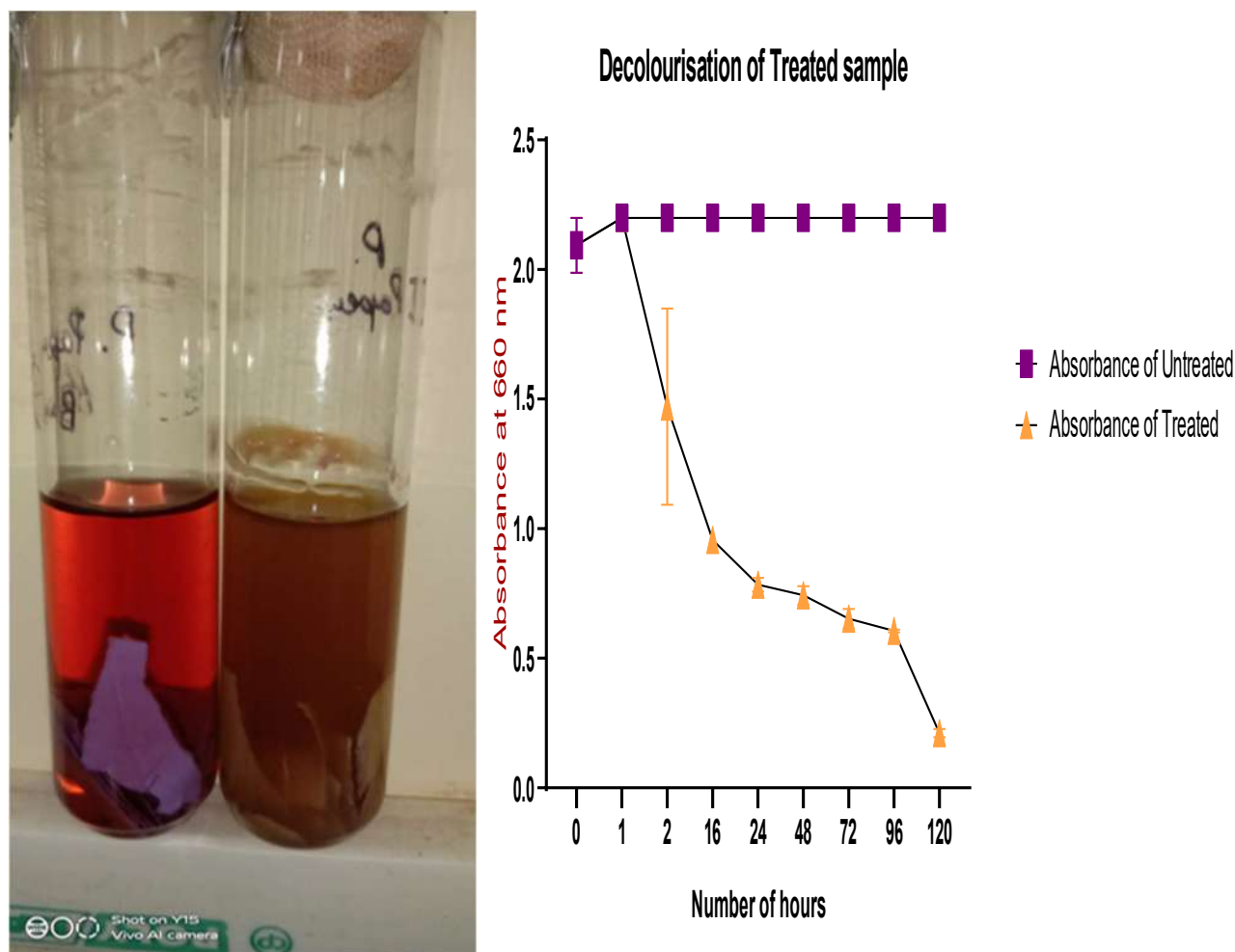


Fig. 10: The degradation and decolorization of colored craft paper with h.

Fig. 10 shows the unexpected decolorization of colored paper as PPS and Fig. 10 shows the decolorization of the PPS with control. The paper dye was unknown for the study; therefore, the spectrum of UV-visible spectrophotometer at 660 nm of both control and treated samples. The treated sample contained an isolated strain for biodegradation (Boonchuay et al. 2021) (Gea et al. 2023), but it was able to reduce colored dye from the sample. The formula for decolorization is $\frac{\text{absorbance control} - \text{absorbance sample}}{\text{absorbance control}} \times 100 = 100$ after 7 days (Rath et al. 2022) for complete decolorization. In the last section of the study, the ethanol bonds were confirmed with FTIR spectroscopy in all four samples. Table 1 describes the different bonds present in the samples, and Fig. 11 compares four samples with ethanol standard peaks in FTIR.

FTIR Interpretation

X- AXIS (Infrared Spectrum): The horizontal axis, also

known as the x-axis, illustrates the infrared spectrum by plotting the intensity of the spectrum. The peaks observed, referred to as absorbance bands, align with the distinct vibrations of sample atoms when exposed to the infrared region of the electromagnetic spectrum. The wave number on the infrared spectrum is typically plotted within the range of 400 to 4000 cm^{-1} . Table 1 expresses different bonds present in the sample for the confirmation of the biodegradation from cellulose to ethanol. Therefore, the peaks detected on 3200, 2900, and 900 identify the presence of alcohols in the biodegradation. All the samples were giving 0.8 optical density in the biodegradation, confirming the 70-80% alcohol produced during the fermentation. The methylene blue control gave 0.812 absorbance, and the sample gave 0.234, describing 50%-60% decolorization. Y-AXIS (Absorbance/Transmittance Percentage): The vertical axis, or y-axis, represents the level of infrared light either transmitted through or absorbed by the sample

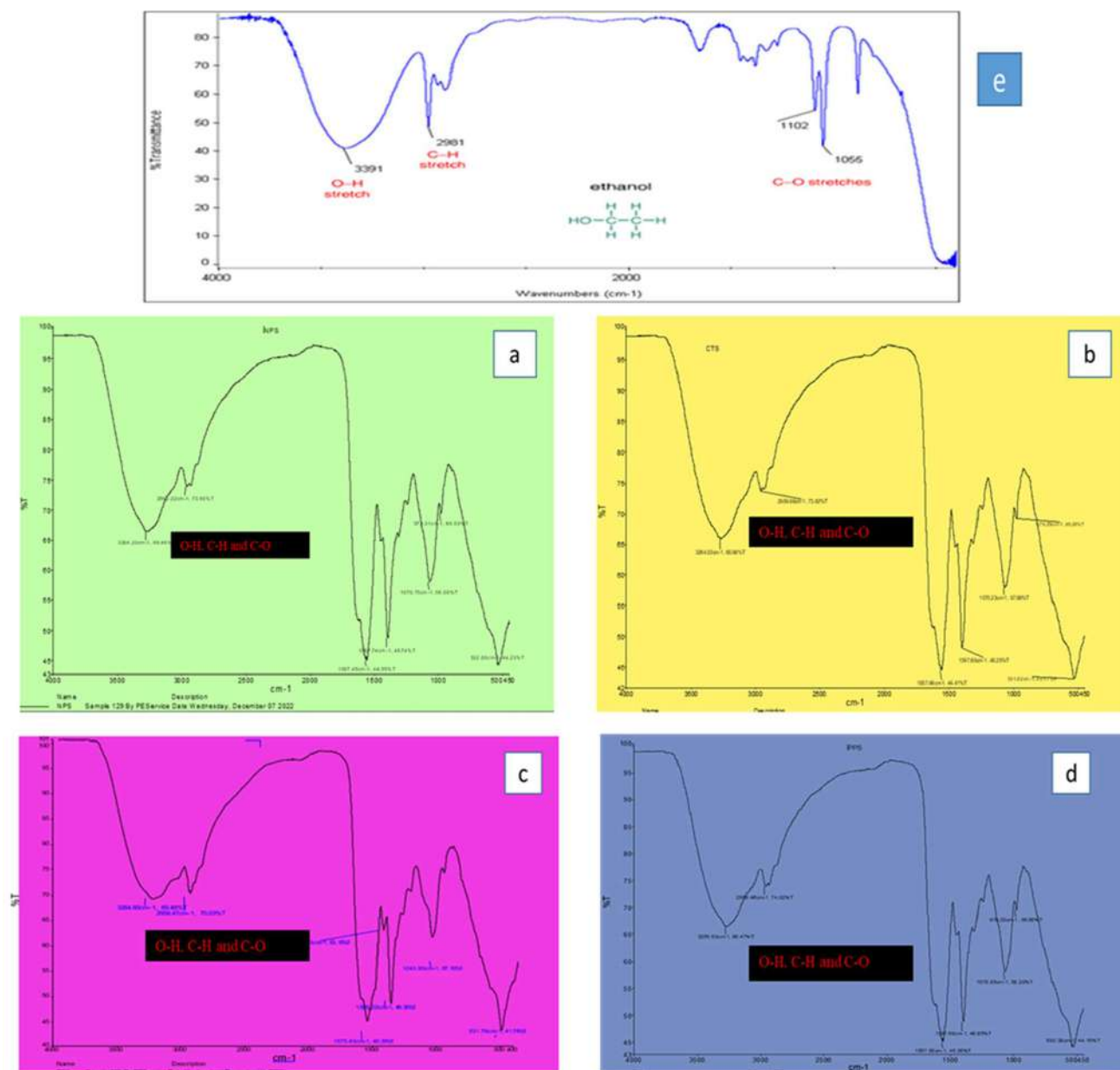


Fig. 11: FTIR bond confirmation of alcohol in the biodegradation process.

material under analysis. This axis provides a measure of the absorbance or transmittance percentage, offering insights into how the sample interacts with infrared radiation (Anjos et al. 2015, Campos, 2015, Gantumur et al. 2023).

CONCLUSIONS

According to the research, microbial enzymes are the cheapest source for biodegradation and if they can provide optimum pH and temperature, they can provide the maximum

degradation. In this study authors have tried to explain different evaluation strategies for biodegradation. During the process of biodegradation, the acid produced continues till the end of the process. Cell growth is also affected in the medium, increasing or decreasing the pH and temperature of the medium. Inoculum size and substrate concentration can also impact cell growth, ethanol production, and cellulase activity. This study also concluding ethanol production from the various cellulosic wastes and the isolated microorganism similar to *Bacillus paramycoides*

Table 1: Expressing the FTIR bond's presence in biodegradation.

Sample name	Wavenumber [cm ⁻¹]	Functional group expected
NPS and PPS	3264.20	Hydroxyl group H bonded O-H stretch
	2960.22	Methyl C-H asym./sym. stretch
	1557.49	Primary amine N-H bend, secondary amine >N-H bend,
	1397.74	Phenol or tertiary alcohol O-H bend, organic sulfate, ammonium ion
	1070.75	Cyclic ether, C-O stretch, primary amine C-N stretch, skeletal C-C vibrations (Adiani et al. 2022)
	978.31	Vinyl C-H (out of plane) bend (Sidi-Yacoub et al. 2019) (Hamden et al. 2022, Landari et al. 2018, Hirphaye 2022, Ana et al. 2021)
PCS	3264.85	Normal or polymeric O-H Stretch Hydroxyl group H bonded
	2958.47	Methyl C-H Asymmetric Symmetric Stretch
	1399.22	Phenol or Tertiary Alcohol, O-H Bend, organic sulfate, ammonium ion (Sindhu et al. 2012, Akhabue et al. 2019, Imamura et al. 2008, Aging & Munajad, 2018)
CTS	3264.80	Normal or polymeric O-H Stretch Hydroxyl group H bonded
	2959.66	Methyl C-H Asymmetrical and Symmetrical Stretch
	1557.46	Carboxylate (Carboxylic acid salts)
	1070.23	Aromatic Ethers, Cyclic ether, C-O stretch, primary amine C-N stretch, skeletal C-C vibrations
	1397.60	Organic Sulfates Phenol organic sulfate, ammonium ion (Rios-Corripio et al. 2011, Sindhu et al. 2010, Aging & Munajad, 2018, Bayu et al. 2019)

can completely decolorize the colored origami craft paper with a shorter time of 24 h, as well as laccases activity was observed. Therefore, more studies can be done in the same direction to explore more utilization of the bacillus strain. Hence, the novel cellulolytic bacteria are successfully biodegrading the cellulosic wastes and help provide the sugars for bioethanol production. The process of deinking during the recycling process of the paper wastes requires lots of water and chemicals for the deinking and recycling process. However, the process of degradation with novel cellulolytic bacteria is quite cheap and eco-friendly approach to saving the environment. With the greater shift from relying on natural resources to bioethanol and biodiesel, the novel cellulolytic bacteria can work efficiently, reduce the risk of environmental pollution, and serve as an important industrial enzyme.

REFERENCES

Adiani, V., Gupta, S. and Variyar, P.S. 2022. FTIR-based rapid microbial quality estimation of fresh-cut jackfruit *Artocarpus heterophyllus* bulbs. *J. Food Meas. Charact.*, 16(3): 1944-1951. <https://doi.org/10.1007/s11694-022-01312-6>

Aging, T. and Munajad, A. 2018. Fourier transform infrared FTIR spectroscopy analysis of transformer paper in mineral oil-paper composite insulation under accelerated. *Energies*, 11(2): 364. <https://doi.org/10.3390/en11020364>

Akhabue, C.E., Otoikhian, K.S., Adeniyi, A.G. and Ighalo, J.O. 2019. Effect of dilute acid pre-treatment on the functional complexes and surface morphology of wood sawdust for bioethanol production process modeling and biofuels production. *Int. Mater. Congr.*, 12: 719. <https://www.researchgate.net/publication/337946719>

Ana, L., Santiago, R., Malvar, R.A. and Mart, D. 2021. FTIR screening to elucidate compositional differences in maize recombinant inbred lines with contrasting saccharification efficiency yields. *Agronomy*, 11(6): 1130.

Anjos, O., Campos, M.G., Ruiz, P.C. and Antunes, P. 2015. Application

of FTIR-ATR spectroscopy to the quantification of sugar in honey. *Food Chem.*, 169: 218-223. <https://doi.org/10.1016/j.foodchem.2014.07.138>

Asem, D., Leo, V. V., Passari, A. K., Tonsing, M. V., Joshi, J. B., Uthandi, S., Hashem, A., Abd-Aillah, E. F. and Singh, B. P. 2017. Evaluation of gastrointestinal bacterial population for the production of holocellulose enzymes for biomass deconstruction. *PLoS ONE*, 12(10): 1-17. <https://doi.org/10.1371/journal.pone.0186355>

Bayu, A., Nandiyanto, D., Oktiani, R. and Ragadhita, R. 2019.. How to read and interpret FTIR spectroscopy of organic material. *Indon. J. Sci. Technol.*, 1: 97-118.

Boonchuay, P., Techapun, C., Leksawasdi, N., Seesuriyachan, P., Hanmoungjai, P., Watanabe, M., Srisupa, S. and Chaiyaso, T. 2021. Bioethanol production from cellulose-rich corncob residue by the thermotolerant *saccharomyces cerevisiae* TC-5. *J. Fungi*, 7(7): 547 <https://doi.org/10.3390/jof7070547>

Bose, J.C. and Sarwan, J. 2023. Multi-enzymatic degradation potential against wastes by the novel isolate of *Bacillus*. *Biomass Convers. Biorefinery*, 7: 4620. <https://doi.org/10.1007/s13399-023-04620-z>

Campos, M.G. 2015. Application of FTIR-ATR spectroscopy to the quantification of sugar in honey Application of FTIR-ATR spectroscopy to the quantification of sugar in honey. *J. Food Chem.*, 7: 138.

Carvalho, J.K., Panatta, A.A.S., Silveira, M.A.D., Tav, C., Johann, S., Rodrigues, M.L.F. and Martins, C.V.B. 2021. Yeasts isolated from a lotic continental environment in Brazil show the potential to produce amylase, cellulase, and protease. *Biotechnol. Rep.*, 30: e00630. <https://doi.org/10.1016/j.btre.2021.e00630>

Dadwal, A., Sharma, S. and Satyanarayana, T. 2020. Progress in ameliorating beneficial characteristics of microbial cellulases by genetic engineering approaches for cellulose saccharification. *Front. Microbiol.*, 11: 1-18. <https://doi.org/10.3389/fmicb.2020.01387>

Darwesh, O.M., El-Maraghy, S.H., Abdel-Rahman, H.M. and Zaghloul, R.A. 2020. Improvement of paper waste conversion to bioethanol using novel cellulose-degrading fungal isolate. *Fuel*, 262: 651. <https://doi.org/10.1016/j.fuel.2019.116518>

Deka, D., Das, S.P., Sahoo, N., Das, D., Jawed, M., Goyal, D. and Goyal, A. 2013. Enhanced cellulase production from *Bacillus subtilis* by optimizing physical parameters for bioethanol production. *Biotechnology*, 2: 1-11. <https://doi.org/10.5402/2013/965310>

Dini, I.R., Restuhadi, F. and Silaturahmi, K. 2019. The effect of

- purification on Snail (*Achatina fulica*) cellulase enzyme characteristic. IOP Conf. Ser. Earth and Environ. Sci., 250(1): 356-370. <https://doi.org/10.1088/1755-1315/250/1/012051>
- Ega, S.L., Drendel, G., Petrovski, S., Egidi, E., Franks, A.E. and Muddada, S. 2020. Comparative analysis of structural variations due to genome shuffling of *Bacillus Subtilis* vs15 for improved cellulase production. Int. J. Mol. Sci., 21(4): 1299. <https://doi.org/10.3390/ijms21041299>
- Fu, Y., Gao, H., Yu, H., Yang, Q., Peng, H., Liu, P., Li, Y., Hu, Z., Zhang, R., Li, J., Qi, Z., Wang, L., Peng, L. and Wang, Y. 2022. Specific lignin and cellulose depolymerization of sugarcane bagasse for maximum bioethanol production under optimal chemical fertilizer pretreatment with hemicellulose retention and liquid recycling. Renew. Energy, 200: 1371-1381. <https://doi.org/10.1016/j.renene.2022.10.049>
- Ganesan, M., Remitha, M.V, Muniraj, I. and Uthandi, S. 2021. Thermophilic cellulase for biomass deconstruction Thermophilic cellulase for biomass deconstruction. Int. Environ. J., 56: 684-692.
- Gantumur, M.A., Sukhbaatar, N., Shi, R., Hu, J., Bilawal, A., Qayum, A., Tian, B., Jiang, Z. and Hou, J. 2023. Structural, functional, and physicochemical characterization of fermented whey protein concentrates recovered from various fermented-distilled whey. Food Hydrocoll., 135: 108130. <https://doi.org/10.1016/j.foodhyd.2022.108130>
- Gea, S., Bulan, R., Zaidar, E., Piliang, A. F., Oktari, N., Rahayu, S., Hutapea, Y. A. and Sari, R. M. (2023). Ultrasound pretreatment and enzymatic deinking by using bacterial cellulases from rice husk. J. Wood Chem. Technol., 43(3): 117-128. <https://doi.org/10.1080/02773813.2023.2190594>
- Giuliano, A. 2023. The Transition of Scientific Research from Biomass-to-Energy/Biofuels to Biomass-to-Biochemicals in a Biorefinery Systems Framework. Energies, 16(5), 4-7. <https://doi.org/10.3390/en16052261>
- Hamden, Z., El-ghoul, Y., Alminderej, F.M. and Saleh, S.M. 2022. High-quality bioethanol and vinegar production from Saudi Arabia date : Characterization and evaluation of their value and antioxidant efficiency. Environ. Technol., 1: 6-9.
- Hirphaye, B.Y. 2022. Bio-ethanol production potential of Water Hyacinth (*Eichhornia crassipes*) as alternative energy feedstocks. Genes, 14: 1-17.
- Imamura, K., Ohyama, K., Yokoyama, T., Maruyama, Y., Imanaka, H. and Interscience, W. 2008. Temperature scanning FTIR analysis of interactions between sugar and polymer additive in amorphous sugar-polymer mixtures. J. Polym. Sugar, 97(1): 519-528. <https://doi.org/10.1002/jps>
- Islam, F. 2019. Isolation and characterization of cellulase-producing bacteria from sugar industry waste. Am. J. BioSci., 7(1): 16. <https://doi.org/10.11648/j.ajbio.20190701.13>
- Islam, M., Sarkar, P. K., Mohiuddin, A. K. M. and Suzaudula, M. 2019. Optimization of fermentation condition for cellulase enzyme production from *Bacillus* sp. Malay. J. Halal Res., 2(2): 19-24. <https://doi.org/10.2478/mjhr-2019-0009>
- Landari, H., Roudjane, M., Messaddeq, Y. and Miled, A. 2018. Pseudo-continuous flow FTIR system for glucose, fructose, and sucrose identification in the mid-IR range. MI, 14: 1-18. <https://doi.org/10.3390/mi9100517>
- Liggieri, C., Obregón, W., Trejo, S. and Priolo, N. 2009. Biochemical analysis of a papain-like protease isolated from the latex of *Asclepias curassavica* L. Acta Biochim. Biophys. Sin., 41(2): 154-162. <https://doi.org/10.1093/abbs/gmn018>
- Mothe, T. and Sultanpuram, V.R. 2016. Production, purification, and characterization of a thermotolerant alkaline serine protease from a novel species *Bacillus caseinilyticus*. 3 Biotech., 6(1): 1-10. <https://doi.org/10.1007/s13205-016-0377-y>
- Nguyen, B.L. and Hoang, A.T.P. 2020. Screening of cellulolytic actinomycetes for decomposition of agricultural waste. Chem. Eng. Trans., 78: 283-288. <https://doi.org/10.3303/CET2078048>
- Rashid, A., Mirza, S.A., Keating, C., Ali, S. and Campos, L.C. 2022. Indigenous *Bacillus paramycooides* spp. and *Alcaligenes faecalis*: a sustainable solution for bioremediation of hospital wastewater. Environ. Technol., 43(12): 1903-1916. <https://doi.org/10.1080/09593330.2020.1858180>
- Rath, S., Paul, M., Behera, H. K. and Thatoi, H. 2022. Response surface methodology mediated optimization of Lignin peroxidase from *Bacillus mycooides* isolated from SimLipal Biosphere Reserve, Odisha, India. Journal of Genetic Engineering and Biotechnology, 20(1). <https://doi.org/10.1186/s43141-021-00284-2>
- Rios-Corripio, M. A., Rios-Leal, E., Rojas-López, M. and Delgado-Macuil, R. 2011. FTIR characterization of Mexican honey and its adulteration with sugar syrups by using chemometric methods. J. Phy. Conf. Ser., 274(1): 12098. <https://doi.org/10.1088/1742-6596/274/1/012098>
- Rojas, J.A., Cruz, C., Mikán, J.F., Villalba, L.S., Cepero de García, M.C. and Restrepo, S. 2009. Isoenzyme characterization of proteases and amylases and partial purification of proteases from filamentous fungi causing biodeterioration of industrial paper. Int. Biodeter. Biodegrad., 63(2): 169-175. <https://doi.org/10.1016/j.ibiod.2008.07.009>
- Sahoo, A., Das, P.K., Patra, S. and Veeranki, V.D. 2023. Engineered yeasts for the production of biofuel and platform chemicals. Adv. Biotechnol. Biofuels Sustain., 5: 411
- Saleh, A.K., Salama, A., Badawy, A.S., Diab, M.A. and El-Gendi, H. 2023. Paper sludge saccharification for batch and fed-batch production of bacterial cellulose decorated with magnetite for dye decolorization by experimental design. Cellulose, 45: 546.
- Sartaj, K., Patel, A., Matsakas, L. and Prasad, R. 2022. Unraveling metagenomics approach for microbial biofuel production. Genes, 13(11): 1942.
- Sarwan, J. and Bose, J.C. 2021. Importance of microbial cellulases and their industrial applications. Ann. Roman. Soc. Cell Biol., 25(1): 3568-3575.
- Sarwan, J. and Bose, J.C. 2022. Role of isolates of bacillus species for biodegradation of multiple contaminants. Ann. Roman. Soc. Cell Biol., 1(2): 292-298.
- Sarwan, J., Pandey, P. and Bose, J.C. 2021. Proteases immobilization and pharmacological aspects of matrix metalloproteinases. Ann. Roman. Soc. Cell Biol., 25(1): 3604-3615.
- Shanmugapriya, K., Saravana, P.S. and Manoharan, M. 2012. Isolation, screening, and partial purification of cellulase from cellulase-producing bacteria. Int. J. Adv. Biotechnol. Res., 3(1): 509-514.
- Sharma, H., Rana, N., Sarwan, J., Bose, J.C., Devi, M. and Chugh, R. 2023. Nano-material for wastewater treatment. Mater. Today: Proceed., 15: 258. <https://doi.org/10.1016/j.matpr.2023.02.258>
- Sidi-Yacoub, B., Oudghiri, F., Belkadi, M. and Rodríguez-Barroso, R. 2019. Characterization of lignocellulosic components in exhausted sugar beet pulp waste by TG/FTIR analysis. J. Thermal Anal. Calorimet., 138(2): 1801-1809. <https://doi.org/10.1007/s10973-019-08179-8>
- Sindhu, R., Binod, P. and Ansari, R. 2012. Organosolvent pretreatment and enzymatic hydrolysis of rice straw for the production of bioethanol. Cellulose, 27: 473-483.
- Sindhu, R., Binod, P. and Satyanagalakshmi, K. 2010. Formic acid is a potential pretreatment agent for the conversion of sugarcane bagasse to bioethanol. Cellulose, 26: 121-139.
- Singhania, S., Ansari, R., Neekhra, N. and Saini, A. 2018. Isolation, identification, and screening of alkaline protease from thermophilic fungal species of Raipur. Int. J. Life-Sci. Sci. Res., 4(2): 1627-1633. <https://doi.org/10.21276/ijlssr.2018.4.2.1>
- Sun, W., Li, X., Zhao, J. and Qin, Y. 2022. Pretreatment strategies to enhance enzymatic hydrolysis and cellulosic ethanol production for biorefinery of corn stover. Int. J. Mol. Sci., 23(21): <https://doi.org/10.3390/ijms232113163>
- Thakur, N., Goyal, M., Sharma, S. and Kumar, D. 2019. Industrial Applications and Approaches Used in Strain Improvement Proteases. Springer, Cham

Xian, X., Fang, L., Zhou, Y., Li, B., Zheng, X., Liu, Y. and Lin, X. 2022. Integrated bioprocess for cellulosic ethanol production from wheat straw: new ternary deep-eutectic-solvent pretreatment, enzymatic saccharification, and fermentation. *Fermentation*, 8(8): 371.

Yaya, A. Gimba, Abubakar Idris, Abdullahi Hassan and Opeyemi N. Hassan 2021. Isolation and optimization of the fermentation condition of cellulolytic microbial isolates from cassava wastewater. *GSC Biological and Pharmaceutical Sciences*, 14(1): 011-017. <https://doi.org/10.30574/gscbps.2021.14.1.0421>

Zeng, R., Yin, X.Y., Ruan, T., Hu, Q., Hou, Y.L., Zuo, Z.Y., Huang, H. and Yang, Z.H. 2016. A novel cellulase produced by a newly isolated *Trichoderma virens*. *Bioengineering*, 3(2): 1-9. <https://doi.org/10.3390/bioengineering3020013>

ORCID DETAILS OF THE AUTHORS

Jyoti Sarwan: <https://orcid.org/0000-0002-9805-2129>

Jagadeesh Chandra Bose: <https://orcid.org/0000-0002-4181-9675>



Impact of Hydraulic Developments on the Quality of Surface Water in the Mafragh Watershed, El Tarf, Algeria

Moufid. Hebbache*, N. Zenati**† , N. Belahcene*** and D. Messadi*

*Department of Chemistry, Bdji Mokhtar University, Annaba, Algeria

**Laboratory Science and Technology of Water and Environment, Souk Ahras University, Souk Ahras, Algeria

***Laboratory of Life Sciences and Technologies, Souk Ahras University, Souk Ahras, Algeria

†Corresponding author: Zenati Nouredine; zenati_nouredine@yahoo.fr

Nat. Env. & Poll. Tech.
Website: www.neptjournal.com

Received: 28-07-2023

Revised: 13-09-2023

Accepted: 19-09-2023

Key Words:

Dam

Hydraulic development

Wadi

Water quality index

ABSTRACT

The wadis are environments of great ecological and economic importance. They are the seat of several hydraulic developments. The latter disrupts the functioning of the wadi in different ways. They modify their hydrological regime, disrupt the ecological conditions upstream and downstream of the reservoir, reduce the self-purification capacities, and modify the processes of erosion and solid transport. It is in this perspective that we have carried out a study of the impact of hydraulic installations on the quality of the waters of the Mafragh watershed. The hydrographic network of the watershed receives the wastewater discharged by the localities and by the industries located along these rivers. This wastewater contributes to the degradation of the water quality of the wadis. The spatio-temporal variation of the water quality index showed a good quality at the level of the dams, while at the level of the sites, which are located downstream, the quality generally varies between bad and very bad during the study period.

INTRODUCTION

The Wadis are environments of great ecological and economic importance. They are the seat of intense human activity and hydraulic developments leading to spills of various types of pollutants, which disrupt the natural functioning of these ecosystems (Amiard 1989, Bryan & Langston 1992).

Several research studies around the world (Cheggour 1988, Dahbi 1989, Jarvie et al. 2003, Baran et al. 2007, Duh et al. 2008, Bharti & Katyal 2011, Manjusha et al. 2013, Sharma et al. 2014, Satish Chandra 2017) have shown the effect of hydraulic developments and anthropogenic discharges on the degradation of the physico-chemical quality of water in watercourses.

In the Algerian wadis, several authors have highlighted such contaminations (Debieche et al. 2003, Benrabah et al. 2013, Zenati 2010, Zenati et al. 2013, Bougherira et al. 2014, Bellazi et al. 2020) which are due to domestic and industrial activities. The Mafragh watershed, one of the most temperate and watered regions of Eastern Algeria, breathes through only one outlet, which is the Mafragh wadi. The construction of the dams was responsible for reducing the effects of flooding in the watershed. The expansion of urban and industrial areas has caused significant environmental consequences in terms of surface water pollution.

Several indexes of the physico-chemical quality of water have been developed and used in different countries around the world, such as France (MESD & Water Agencies 2003), Spain (Queralt 1982, Fernandez-Alaez et al. 1992) Canada, (Provencher & Lamontagne 1979, Hebert 1997, 2005), the United States (Otto 1978), Mexico (Alvarez 2006), etc.

The methodology followed in our study is to use the water quality index (WQI) of the Canadian Council of Ministers of the Environment (CCME) to provide a mathematical framework for assessing ambient water quality conditions regarding water quality objectives. It offers a high degree of flexibility design in terms of the type and number of variables to be measured, the study period, and the type of water body examined (watercourse, section, lake, etc.).

MATERIALS AND METHODS

Study Area

The Mafragh watershed is located in the extreme northeast of Algeria (Fig. 1), which is part of the Constantine coastal basins from where the definition of the Constantine-East coastal basin appropriated it. This basin, which has longitudes ranging from 7°45' to 8°45' East and latitudes ranging from 36°20' to 36°55' north, does not encompass the entire area of El Tarf state.

It is drained by two important watercourses, wadi Bounamoussa to the west and Wadi El Kebir East to the east. They converge towards the marsh (more than 8,900 ha) called the MeKhada tide and reach the sea through a single outlet, wadi Mafragh.

Wadi Bounamoussa originated under the name of Wadi El Kebir at Koudiat Ben Ahmed (1729 m). The confluence of Wadi El Kebir and Wadi Bouhadjar gives birth to Wadi Bounamoussa. It drains a watershed of 1,135 km². It receives tributaries such as Wadi Sudan, wadi Guerriah, and the Chabet El Erg to its confluence with Wadi El Kebir East. A dam is built on this wadi, intended to satisfy the demand for water for the city of Annaba, for industry, and the irrigated perimeter of Bounamoussa.

The second wadi, El Kebir East, has its upper course formed by three wadis: two in Tunisia, the Kebir proper and the Ballauta, and an Algerian Oued Bougous. Their confluence is located in the small pre-coastal plain of Mexena. It drains a watershed of (1685 km²). Two Mexa and Bougous dams are built on this wadi intended for the supply of drinking water for the two states of El Tarf and Annaba.

In the plain of El Tarf, wadi El Kebir East receives Wadi Guergour and Wadi Bouhalloufa, including a dam under construction with a capacity of 50 hm³ and Wadi Boulathan. In the northeast, it receives wadi Messida. In the dune massif of Bouteldja, wadi El Kebir East receives three tributaries: wadi Bourdim, wadi Bouglez, and Wadi El Bahaim. These tributaries play an important role in surface flow and the supply and drainage of groundwater.

The hydrographic network draining the region is the subject of 4 studies for the construction of dams, allowing

the satisfaction of water needs of all sectors for the two states of El Tarf and Annaba. The projected dams have a lower capacity with 52 hm³ at the Bougous dam, 20 hm³/year at the Boulatane dam, 20 hm³ at the Guergour dam, and 65 hm³ at the Bounamoussa dam2.

The study region, by its agricultural vocation and its soil-climatic conditions, is an important agricultural pole in eastern Algeria. The cultivation practices identified are market gardening, industrial, grain farming, fodder, and tree crops, as well as pastoral farming.

Industry in the region occupies a less important place in the socio-economic development. It is dominated by small and medium-sized food industries characterized mainly by tomato paste.

Geological studies carried out by Joleaud (1936), Villa (1980), and Marre (1992) show the existence of two large sets:

The set of coastal plains is characterized by recent quaternary sediments, which constitute the bottom of this tectonic depression, and Numidian sandstones, which constitute the summits, the most important of which are located around the town of Daghoussa.

The allochthonous Sets of units constitute:

- Mauritanian flyschs, which are mainly composed of alternating clay and calcareous clay banks. They cover small areas upstream from El Kebir East.
- Massylian flysch is formed mainly by marls and clays with very thin sandstone and limestone banks. They are exposed in the various places of the mountain of Cheffia.

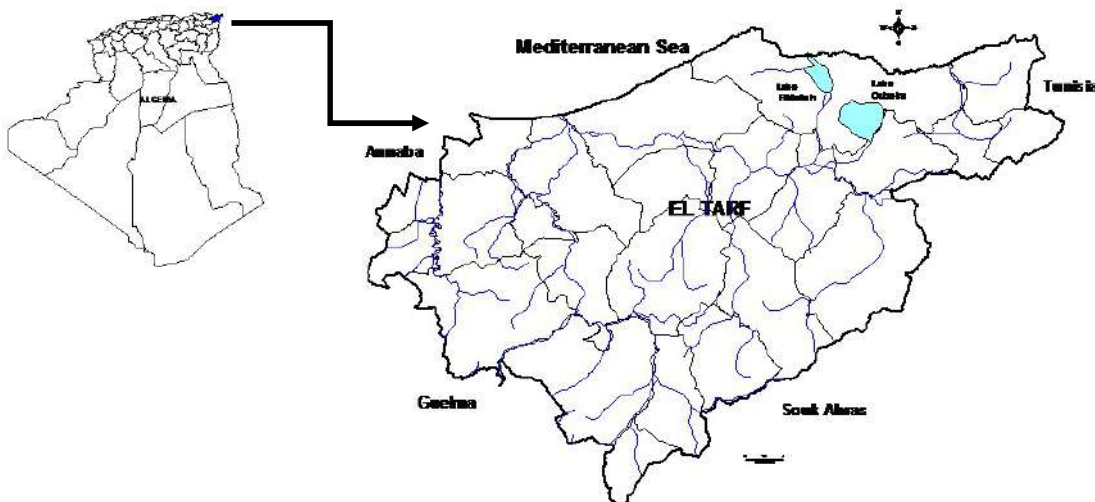


Fig. 1: Map of the location of the study area.

- The Numidian aquifer constitutes the southern relief of the watershed. This series is composed of Numidian sandstones, sub-Numidian clays, and supra-Numidian clays.

The general evolution of the climate in the region is characterized by a dry climate in September and October. Whereas, from November to April the climate is humid throughout the region. In May, the climate becomes dry to very dry. In June, it is very dry. The situation deteriorates further in July and August. The climate is then hyperarid in the majority of the stations.

Sample and Analysis

We assessed the level of water quality in the hydrographic network of the Mafragh watershed, which receives several discharges, based on a spatio-temporal sampling protocol covering the year 2017 and 11 sampling sites, namely (Fig. 2):

- Mexa Dam (D1),
- Cheffia Dam (D2),
- Wadi El Kebir East (S1, S5 et S6),
- Wadi Gourgour (S2),
- Wadi Bouhalloufa (S3),
- Wadi Boullathan (S4),
- Wadi Bounamoussa (S7 and S8),
- Wadi Mafragh (S9).

During the water sample collection campaigns, we respected the sampling standards “filtration (0.45 µm filter),

acidification (5 mL HCl or HNO₃) and storage (4°C)” (AFNOR/T91E).

The physico-chemical parameters (pH, temperature, conductivity) are measured in situ using a multi-parameter WTW device (multi 340i / SET). The analysis of the chemical elements was carried out by volumetry (Cl⁻), atomic absorption with flame, and colorimetry.

Methodology

The Canadian Council of Ministers of the Environment (CCME) Water Quality Index (WQI) provides a mathematical framework for assessing ambient water quality conditions regarding specific objectives. It offers great flexibility in terms of the type and number of variables to be measured, the period of study, and the type of water body examined (watercourse, section, lake, etc.).

The calculation of the IQE Indexis:

$$IQE = 100 - \left(\frac{\sqrt{F_1^2 + F_2^2 + F_3^2}}{1.732} \right) \dots(1)$$

The calculation of the index is based on three terms:

Scope (F1) - number of variables non-conforming with water quality recommendations;

Frequency (F2) - number of times where these recommendations are not followed; and the amplitude (F3) - deviation of the non-conforming measurements compared to the corresponding recommendations.

The division of these terms by 1.732 comes from the fact that each of the three factors that make up the index can

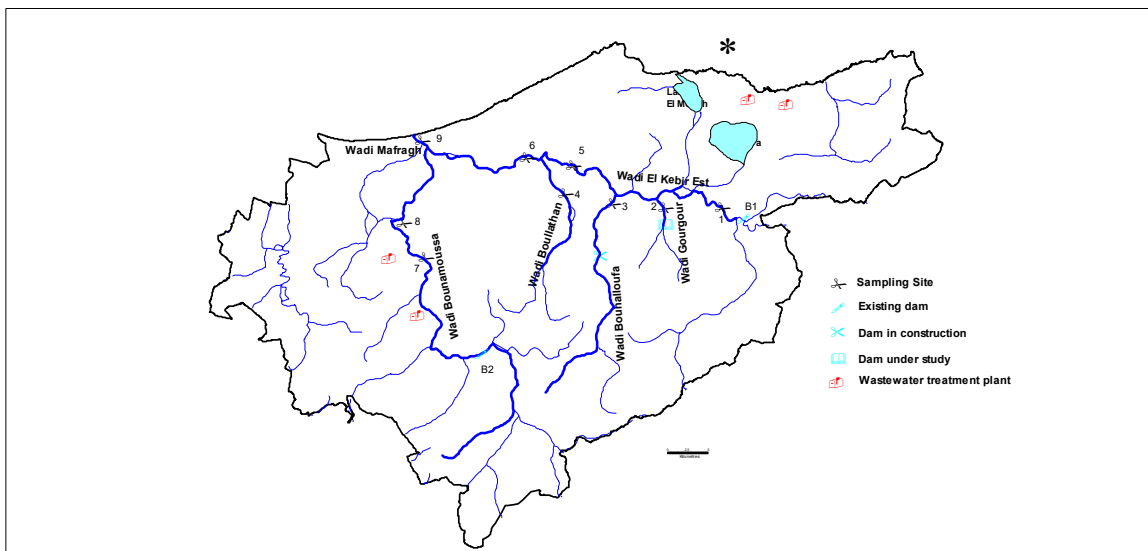


Fig. 2: Map of location of sites.

reach the value of 100. The maximum length is, therefore:

$$\sqrt{100^2 + 100^2 + 100^2} = \sqrt{30\,000} = 173.2 \quad \dots(2)$$

This division by 1,732 has the effect of reducing the maximum length to 100. The index produces a value which is between 0 and 100. The higher the number, the better the quality of water.

Explanation of Each of the Index Terms

First of all, the term F1 (range) represents the percentage of parameters of which at least one measurement is non-conforming with the corresponding recommendation during the study period:

$$F_1 = \left(\frac{\text{number of nonconforming parameters}}{\text{total number of deparameters}} \right) \times 100 \quad \dots(3)$$

Then, the term F2 (frequency) represents the percentage of analytical results non-conforming with the recommendations.

$$F_2 = \left(\frac{\text{number of nonconforming results}}{\text{total number of results}} \right) \times 100 \quad \dots(4)$$

Finally, the term F3 (amplitude) represents the gap between the non-conforming analytical results and the recommendations to which they relate. The term F3 is an asymptotic function that brings the normalized sum of the deviation coefficients (nsdc) compared to the recommendations within a range of values from 0 to 100.

$$F_3 = \left(\frac{\text{nsdc}}{0.01 * \text{nsdc} + 0.01} \right) \quad \dots(5)$$

To calculate the overall degree of nonconformity, add the gap coefficients of the nonconforming analytical results and divide this sum by the total number of analytical results. This variable is called the normalized sum of the deviation coefficients (nsdc).

$$\text{nsdc} = \left(\frac{\sum_i \text{gap coefficient } i}{\text{total number of results}} \right) \quad \dots(6)$$

To determine the gap coefficient, we have three possibilities:

- If the result should not exceed the recommendation:

$$\text{Gap coefficient } i = \left(\frac{\text{nonconforming result } i}{\text{Recommendation } i} \right) - 1 \quad \dots(7)$$

If the result should not be inferior to the recommendation:

$$\text{Gap coefficient } i = \left(\frac{\text{Recommendation } i}{\text{nonconforming result } i} \right) - 1 \quad \dots(8)$$

- If the recommendation is null (equal to zero):

Gap coefficient i = nonconforming results

RESULTS AND DISCUSSION

Hydrochemical Typology of Waters

The surface waters of the Mafragh watershed contain several chemical facies, among them calcium bicarbonate, sodium chloride, sodium bicarbonate, calcium chloride, and potassium bicarbonate facies. However, the calcium bicarbonate facies remain the most dominant. In detail, these waters are distributed between two hydrochemical poles:

- A calcium bicarbonate pole. It is the most dominant facies. It characterizes almost all of the surface waters, with a percentage of 72% of the total sum of the samples.
- A calcium and sodium chloride pole:
 - The calcium chloride facies are the second facies from the point of view of importance. It corresponds to 14% of the total sum of the samples. It is recorded at Wadi El Kebir East and its tributaries.
 - The sodium chloride facies are observed only at the level of Wadi Mafragh.

With the exception of station 9 of Wadi Mafragh, where the influence of the sea and the marshy zone on the concentrations of major elements has been noted, the other stations are under the influence of discharges of domestic and industrial wastewater record values of conductivity and major ion contents less high compared to that of wadi Mafragh (Table 1).

In order to establish a relationship between the different physico-chemical parameters and to better assess the effect of hydraulic developments and anthropogenic discharges on the water quality of the Mafragh watershed. The statistical processing of the principal component analysis and the analysis of variance was carried out on 9 sites and 12 variables: Conductivity, T, pH, Ca^{2+} , Mg^{2+} , Na^+ , K^+ , TAC, SO_4^{2-} , and Cl^- . NO_3^- and NO_2^- .

Data processing by PCA, using as variables the T°, pH, Conductivity, Ca^{2+} , Mg^{2+} , Na^+ , K^+ , Cl^- , SO_4^{2-} , NO_3^- , NO_2^- and TAC; and as noted, the 79 samples taken from the 9 sites prospected on the hydrographic network of the Mafragh watershed, reveal several axes. The first two express the maximum of the variance (56.43%). The information given by axis 1 corresponds to 31.6% of the variance, and axis 2 represents 24.83% (Fig. 3).

The distribution of physico-chemical variables according to the F1-F2 plan presented on the positive side of the F1 axis a positive correlation with the conductivity, Cl^- , Na^+ , SO_4^{2-} , Ca^{2+} , and Mg^{2+} . This axis reflects a combination of indigenous ions and elements reflecting the mineralization of waters linked to anthropogenic activities. Moreover, the anthropic effect on these sites is noted by their high levels of descriptors of anthropization (Cl^- , Ca^{2+} , and Na^+), as underlined by Mary (1999) and Gouiadia (2008) in New Caledonia and Algeria, respectively.

Table 1: Mean and extended values of the measured physico-chemical parameters.

		T	pH	Cond	TAC	Cl ⁻	NO ₂ ⁻	NO ₃ ⁻	Na ⁺	K ⁺	Ca ²⁺	Mg ²⁺	SO ₄ ²⁻
Site1	Max	26,06	8,10	889,00	145,00	53,16	5,20	25,00	64,38	105,60	113,11	17,77	104,32
	Min	10,59	7,13	443,00	100,00	13,41	0,01	0,00	3,36	4,32	25,99	9,93	29,31
	Moy	19,18	7,53	686,45	127,36	38,89	1,92	6,35	24,28	32,28	59,57	12,71	49,34
Site2	Max	22,50	7,55	1049,00	330,00	547,20	74,00	13,00	54,23	85,95	88,51	65,34	90,05
	Min	10,67	7,18	508,00	150,00	39,87	4,50	2,40	1,84	6,14	27,81	11,66	58,77
	Moy	15,43	7,40	891,43	223,00	218,13	18,33	7,17	14,16	53,97	65,33	23,56	68,48
Site3	Max	22,21	7,83	772,00	241,00	443,00	4,00	33,00	56,98	86,25	94,54	50,05	69,34
	Min	9,90	7,30	248,00	107,00	22,15	0,05	1,35	2,52	4,56	29,35	10,71	22,34
	Moy	14,92	7,50	568,57	164,14	161,19	2,41	8,11	17,43	49,96	62,83	19,94	44,57
Site4	Max	22,86	7,87	941,00	300,00	115,00	7,00	38,00	117,92	90,31	134,26	21,17	59,31
	Min	9,97	7,10	442,00	97,00	31,31	0,07	2,20	2,52	6,64	29,35	10,71	27,55
	Moy	15,48	7,44	828,71	190,04	73,84	4,07	10,97	37,39	56,31	70,73	15,52	39,25
Site5	Max	26,89	7,66	2223,00	240,00	443,00	5,10	47,00	373,19	86,04	128,24	36,53	210,30
	Min	9,83	6,86	522,00	80,00	66,45	0,00	0,10	5,82	9,08	38,30	10,18	26,38
	Moy	15,93	7,25	1307,86	161,63	173,52	2,40	9,27	100,95	48,61	83,92	18,73	102,49
Site6	Max	24,71	7,80	817,00	213,00	133,14	13,00	13,00	178,32	91,55	79,77	18,95	55,44
	Min	10,69	7,20	380,00	101,00	13,29	0,00	0,20	4,08	6,13	28,44	10,48	19,41
	Moy	15,92	7,46	659,00	154,29	85,49	3,71	4,68	38,05	50,92	63,48	13,07	36,01
Site7	Max	26,85	7,95	826,00	171,00	70,21	4,50	16,33	79,35	71,40	109,21	20,55	59,23
	Min	10,03	7,45	449,00	60,00	22,15	0,01	0,88	1,78	5,96	23,93	9,36	25,24
	Moy	19,15	7,72	663,09	131,23	54,79	1,30	7,93	37,54	29,36	65,20	15,53	43,28
Site8	Max	26,55	8,03	826,00	161,00	80,30	4,00	19,35	80,25	93,74	101,24	29,32	60,24
	Min	9,33	7,30	430,00	60,00	17,73	0,00	0,50	3,53	6,25	39,26	10,08	22,14
	Moy	19,04	7,68	632,45	125,01	59,21	1,19	8,39	41,34	36,90	70,36	18,61	46,21
Site9	Max	26,21	8,05	7780,00	256,00	2000,41	4,20	40,87	1998,36	95,04	290,46	139,92	143,06
	Min	11,15	7,38	473,00	100,00	48,73	0,11	0,00	4,15	10,03	42,78	10,89	56,37
	Moy	19,63	7,68	4701,00	207,39	1232,44	1,61	13,95	1136,17	45,68	172,39	63,69	123,11

According to axis F2, the variables most correlated to this main component are NO₂⁻, K⁺, NO₃⁻ and T. This axis F2 reflects the impact of agriculture and the discharge of wastewater on certain watercourses like El Kebir East at site 00, wadi Guergour and Bouhalloufa.

Since other variables (TAC and pH) are close to the center of the factorial plan, their correlation is certainly not very strong. These variables are probably better explained by other main components, other than F1 and F2.

An ascending hierarchical classification made from individuals in a sampling cycle made it possible to complete the information from the CPA and to classify the sites into two groups. Two main groups are identified in Fig. 4.

The first group represents waters with very strong mineralization with very high Na⁺ and Cl⁻ values, taken from Oued Mafragh. It is the most loaded with dissolved

mineralization. It reflects the polluting load contained in the waters of the two Wadis of Bounamoussa and El Kebir East and the effect of the Mekhada marsh and the sea on the increase in the concentration of these two chemical ions.

High levels of HCO₃⁻ mark the second group and Ca²⁺. It is the water taken from the rest of the sampling sites. These high levels reflect wastewater discharges and leaching of carbonate rocks.

The typology highlighted by the CPA and the CAH is linked to the contributions of mineral elements by anthropogenic activities of varying intensity depending on the sites is a natural mineralization process linked to water-rock contact and to the through fall phenomena. Indeed, the station under strong anthropic and geological influence records the highest values of conductivity and major ion contents. It is the Mafragh wadi station high in Cl⁻ and Na⁺ are explained by the geology of the region (Mekhada

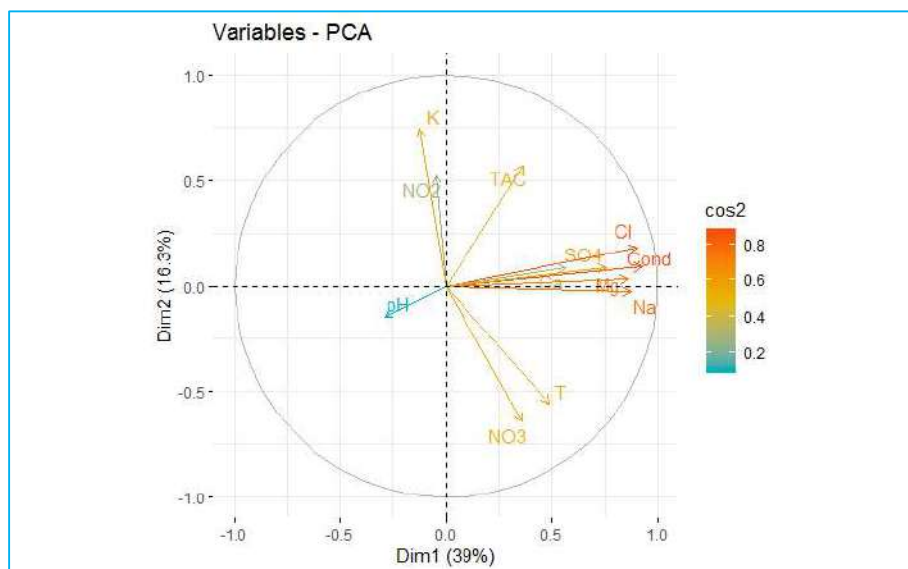


Fig. 3: Correlation circle of physico-chemical variables.

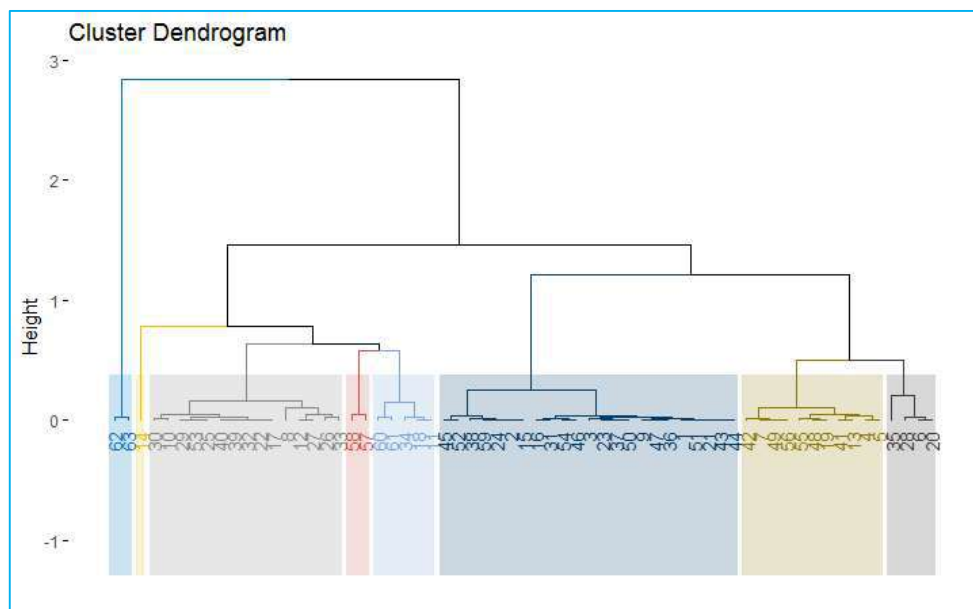


Fig. 4: Hierarchical classification of individuals

marsh), the contribution of discharges by the two wadis of Bounamoussa and El Kebir east and the sea.

In order to test the spatial effect and the temporal effect, the two-factor analysis of variance (Friedman test), carried out on the physico-chemical parameters of the waters of the Mafragh watershed, reveals significant differences ($P < 0, 05$) between stations (Table 2) for the contents of calcium, sodium, sulfate, chloride, complete alkaline titer, and conductivity.

Comparison of the variances by the same test does not reveal significant differences in the magnesium, nitrite, nitrate, and potassium content between seasons ($P \geq 0.05$).

Spatio-Temporal Variation of the Water Quality Index

In order to be able to follow the evolution of water quality at the scale of the Mafragh watershed, a calculation of the water quality index for all of the watershed sites monitored during 2017 has been realized. With regard to the two Mexa

Table 2: Comparison of the parameters according to the two factors “site” and “time”.

	T	pH	Cond	TAC	Cl ⁻	NO ₂ ⁻	NO ₃ ⁻	Na ⁺	K ⁺	Ca ²⁺	Mg ²⁺	SO ₄ ²⁻
p	1	0.036	8.1 10 ⁻⁷	0.0055	4.1 10 ⁻⁷	0.027	0.88	0.00021	0.98	0.00087	0.011	4.2 10 ⁻⁸

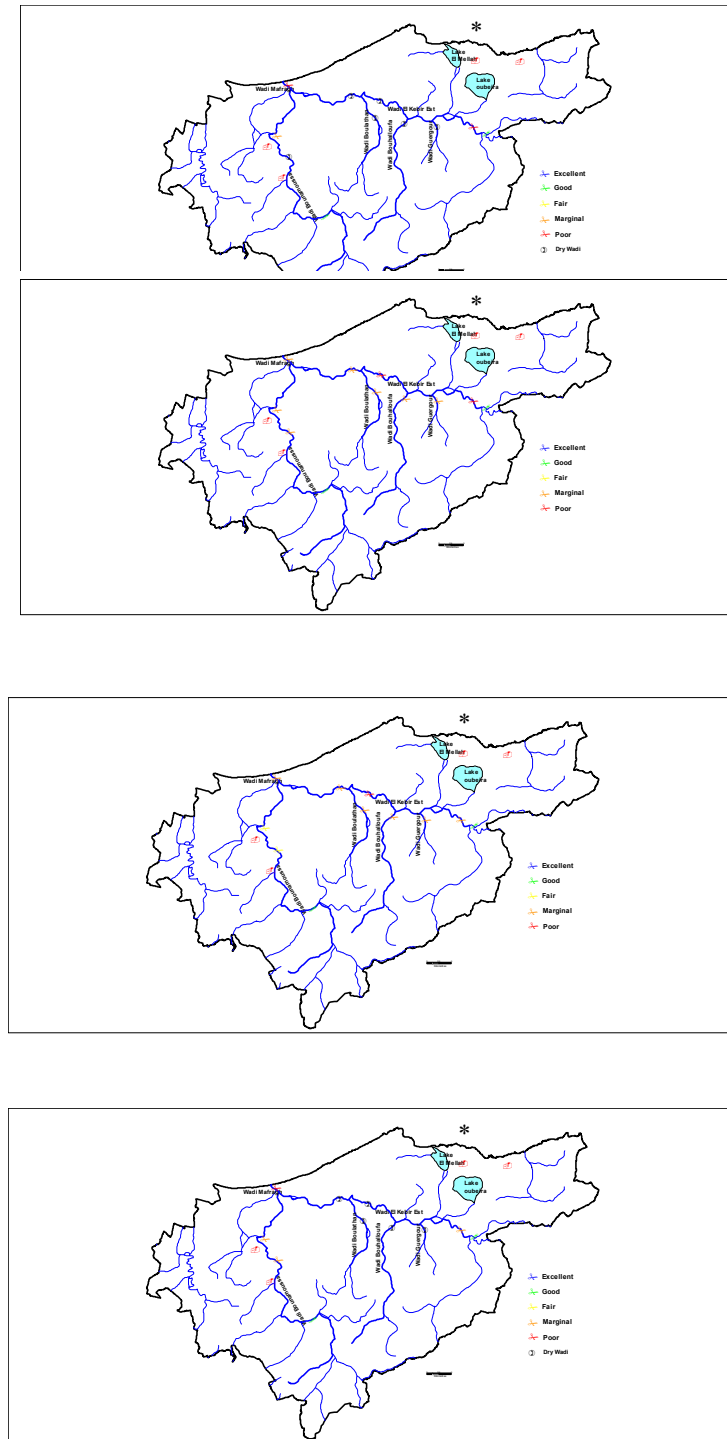


Fig. 5: Evolution of the water quality index.

and Cheffia dams, the time evolution of the overall quality shows that during 2017 a good quality. As for the level of the 9 sites (Fig. 5), the majority of the watercourses show very poor to poor quality.

During the spring, the quality showed a clear (fair) improvement in Oued Bounamoussa, in particular by the water releases from the Cheffia dam for farmers. These have greatly reduced the concentration of pollutants by diluting wadi water, increasing their flow rates and thus promoting their purification against the various polluting substances.

This quality deteriorated further during the summer and autumn at the level of watercourses due to a strong disturbance by anthropic activities and the drought that marked the summer period. The analysis of the minimum and maximum values of the physico-chemical quality parameters studied and the values of the surface water quality index at the level of the site during the period 2017 allows us to show large amplitudes of variations both spatially and temporally within the same site.

CONCLUSION

The deterioration in the water quality of the Mafragh watershed is mainly linked to upstream hydraulic developments and the absence of wastewater treatment plants. The sites studied reveal a multitude of impacts threatening the quality of the water (wastewater discharges without prior treatment).

The analysis of the physicochemical data obtained with regard to Algerian surface water quality standards indicates the quality of the majority of stations in the watershed is poor to very poor. This is explained by the fact that the water courses of this basin have an intermittent flow. They have black, mineralized water with very high salinity levels at Wadi Mafragh. Indeed, upstream hydraulic development does not ensure a continuous renewal of water and a dilution of pollutants in the water.

REFERENCES

Alvarez, A. 2006. Water quality index in the Amajac river basin, Hidalgo, Mexico: Diagnosis and Prediction, 75: 71-83.

Amiard-Triquet, C. 1989. Bioaccumulation and relative harmfulness of some metal pollutants to marine species. *Bull. Ecol. Technol.*, 20(2): 129-151.

Baran, N., Mouvet, C. and Négrel, Ph. 2007. Hydrodynamic and geochemical constraints on pesticide concentrations in the groundwater of an agricultural catchment (Brévilles, France). *Environ. Pollut.*, 148: 729-738.

Bellazi, M. A., Zenati, N., Belahcene, N., Samer, F., Berredjem, Y. and Gheid, A. 2020. Spatio-Temporal Variability of Water Pollution in the Watershed of Wadi Echaref, Sedrata, Algeria. *Pollut. Res.*, 39: S20-S27.

Benrabah, S., Bousnoubra, H., Kherici, N. and Cote, M. 2013. Characterization of the water quality of the West Kebir wadi (Northeast Algeria). *Rev. Sci. Technol. Synth.*, 26: 30-39.

Bharti, N. and Katyal, D. 2011. Water quality indices used for surface water vulnerability assessment. *Int. J. Environ. Sci.*, 2(1): 154-173.

Bougherira, N., Hani, A., Djabri, L., Toumi, F., Chaffai, H., Haied, N., Nechem, D. and Sedrati, N. 2014. Impact of urban and industrial wastewater on surface and groundwater, in the region of Annaba (Algérie). *Energy Procedia*, 50: 692-701.

Bryan, G.W. and Langston, W. J. 1992. Bioavailability, accumulation, and effects of heavy metals in sediments with special reference to united estuary. *Environ. Pollut.*, 76: 89-131.

Cheggour, M. 1988. Contribution to the study of a paralic environment: The Bouregreg estuary (Moroccan Atlantic coast)- global ecological conditions and study of metallic contamination. Thesis, Takadoum-Rabat, p. 337.

Dahbi, N. 1989. Contribution to the Study of a Paralic Environment: The Bouregreg Estuary (Moroccan Atlantic coast): Hydrology, Hydrodynamics, and Metallic Pollution. Thesis, Takadoum-Rabat, p. 150.

Debieche, T.H., Mania, J. and Mudry, J. 2003. Species and mobility of phosphorus and nitrogen in a wadi-aquifer relationship. *J. Afr. Earth Sci.*, 37: 47-57.

Duh, J.D., Shandas, V., Chang, H. and George, L.A. 2008. Rates of urbanization and the resiliency of air and water quality. *Sci. Total Environ.*, 400(1-3): 238-256.

Fernandez-Alaez, C., Fernandez-Aleaz, M. and Becares, E. 1992. Use of two chemical indices (ICG and ISQA) in determining the water quality of several Spanish rivers. *Appl. Hydroecol.*, 4: 37-47.

Gouaïdia, L. 2008. Influence of lithology and climatic conditions on the variation of the physico-chemical parameters of the water of a water table in a semi-arid zone, case of the water table of Meskiana, Northeast Algeria. Doctoral Thesis, hydrogeology option. Badji Mokhtar Annaba University.

Jarvie, H.P., Neal, C., Withers, P.J.A., Robinson, A. and Salter, N. 2003. Nutrient water quality of the Wye catchment, UK: exploring patterns and fluxes using the environment agency data archives. *Hydrol. Earth Syst. Sci.*, 7(5): 722-743.

Joleaud, L. 1936. Étude géologique de la région de Bône et de Lacalle... Imp. La Typo-litho & J. Carbonel.

Manjusha, B., Prakash, K., Abhijit, B., Sheetal, Manisha, B. and Bholay, A.D. 2013. Water quality assessment of the River Godavari, A Ramkund, Nashik, (Maharashtra), India. *Int. J. Eng. Sci.*, 2(2): 64-68.

Ministry of Ecology and Sustainable Development and Water Agency. 2003. Evaluation and Water Quality System for Watercourses (SEQ-Eau), Evaluation Grid, version 2.

Marre, A. 1992. The Algerian Oriental Tell from Collo to the Tunisian border. Geomorphological Study, Vol. 1 and 2. O.P.U. Alger; Algeria.

Mary, N. 1999. Physico-Chemical and Biological Characterizations of New Caledonia's Rivers, Proposal of a Biotic Index Based on the Study of Benthic Macroinvertebrates. Doctoral Thesis, University of the Pacific, Stockton, CA, USA.

Otto, W. 1978. Water Quality Index: A Survey of Indexes used in the United States, Environmental Monitoring Series, EPA.-600/4-78-005, 1, 28.

Provencher, M. and Lamontagne, M.P. 1979. A Method for Establishing a Water Quality Index for Different Uses (IQE). Environmental Protection Services, Montreal, Quebec, Canada

Queralt, R. 1982. The quality of the waters in the rivers, *Water Technol.*, 4: 449-457

Satish Chandra, D. 2017. Estimation of water quality index by weighted arithmetic water quality index method: A model study. *Int. J. Civ. Eng. Technol.*, 8(4): 1215-1222.

Sharma, M.K., Jain, C.K. and Singh, O. 2014. Characterization of point sources and water quality assessment of River Hindon Using water quality Index. *J. Indian Water Resour. Soc.*, 34(1) : p53-64.

Villa, J.M. 1980. The Alpine Chain of Eastern Algeria and the Algerian-Tunisian Borders. State Thesis. University, Toulouse, p. 665.

Zenati, N. 2010. Pollution of the Aquatic Environment: Diagnosis and Proposal, Annaba Region. Doctoral Thesis. Department of Geology, Badji Mokhtar Annaba University, p 289.

Zenati, N., Messadi, D. and Belahcene, N. 2013. Effect of the rejection

of the Annaba steel plant on the environmental objectives of Oued Meboudja. Algeria. *Water and Health*, 6: 1-7.

ORCID DETAILS OF THE AUTHORS

N. Zenati: <https://orcid.org/0000-0002-1096-559X>



PAHs Biodegradation by Locally Isolated *Phanerochaete chrysosporium* and *Penicillium citrinum* from Liquid and Spiked Soil

Kiran Bishnoi^{*(**)}†, Pushpa Rani^{*}, Minakshi Karwal^{***} and Narsi R. Bishnoi^{*}

^{*}Department of Environmental Science and Engineering, Guru Jambheshwar University of Science & Technology, Hisar-125001, Haryana, India

^{**}Department of Environmental Studies, Govt. College for Women, Hisar-125001, Haryana, India

^{***}Department of Applied Sciences, KIET Group of Institutions, Delhi-NCR, Ghaziabad-201206, U.P., India

†Corresponding author: K. Bishnoi; kiranbishnoi@gmail.com

Nat. Env. & Poll. Tech.
Website: www.neptjournal.com

Received: 23-08-2023

Revised: 29-10-2023

Accepted: 01-11-2023

Key Words:

Biodegradation

Phenanthrene

Polycyclic aromatic hydrocarbons

Phanerochaete chrysosporium

Penicillium citrinum

ABSTRACT

In the present study, biodegradation of polycyclic aromatic hydrocarbons (PAHs) was examined using two fungal strains, namely *P. chrysosporium* and *P. citrinum*, isolated from locally contaminated soil. These two fungal strains were compared based on degradation properties under standardized conditions (pH 7.0, temperature 30°C, carbon source yeast extract) using PAH sole and a mixture of five different PAHs. In liquid media, PAH degradation was higher as compared to spiked soil by *P. chrysosporium*, followed by *P. citrinum*. In liquid culture, maximum degradation was 96.13% phenanthrene, 86.34% fluoranthene, 72.75% pyrene, 52.25% chrysene, and 40.16% benzo(a)pyrene by *P. chrysosporium*. PAH degradation in spiked soil was 78.5% phenanthrene, 65.91% fluoranthene, 61.73% pyrene, 48.2% chrysene, and 26.82% benzo(a)pyrene within 28 days by *P. chrysosporium*. Both local fungal isolates showed potential for degradation of PAHs alone and in PAH mixtures.

INTRODUCTION

Unorganised and unmanaged expansion activities pose a severe threat to the environment by introducing harmful chemicals/ substances into the environment like polycyclic aromatic hydrocarbons (PAHs). PAHs are a large group of organic compounds having two or more fused aromatic rings, mainly having C and H atoms (Jacques et al. 2008, Bright et al. 2023). More than 500 different PAHs are present in the environment, but US EPA listed 16 PAHs under the ‘‘priority pollutants’’ category (US EPA 2002), many of which are well-known as mutagens, carcinogens, and teratogens (Abdel-Shafy & Mansour 2016). Both natural and anthropogenic sources are responsible for their wide distribution in the environment. Due to their bioaccumulation tendency, they enter the food chain. Natural sources include fires (forest and grassland), volcanic eruptions, oil seeps, exudates from trees, etc. (Babu et al. 2019). Anthropogenic sources include residential heating, burning (coal and wood), coal gasification and liquefying plants, carbon black, coal-tar pitch and asphalt production, coke and aluminum production, petroleum refineries, vehicular emissions and incineration of municipal waste (Abdel-Shafy & Mansour 2016, Alekseev

& Abakumov 2021). PAHs are widely dispersed at various levels in soils, river water and sediments, groundwater, and atmosphere (Bishnoi et al. 2009, Malik et al. 2010, Masih et al. 2010, Gupta & Kumar 2020). Some PAHs have also been found in fruits and vegetables in trace amounts, which may have been transferred from air and soil during cultivation or transportation and storage (Bishnoi et al. 2006, Paris et al. 2018).

Due to their boundless occurrence and health effects, it has become a need of the hour to carry out remediation of PAHs. Different types of physical, chemical, and biological methods can be used for PAH remediation. While PAHs may undergo adsorption, chemical oxidation, photolysis, and volatilization, neutralization by microbial activities is the primary process affecting the persistence of PAHs in contaminated sites (Ghosal et al. 2016, Thacharodi et al. 2023). Bioremediation of PAHs is considered an efficient, economical, versatile, and ecologically acceptable treatment. Both fungi and bacteria can metabolize different types of PAHs, but their pathways for degradation are different. Many recent studies reported several bacteria and filamentous fungal species having the capability for

mineralization or degradation of PAHs (Liu et al. 2017, Gu et al. 2021). Bioremediation using fungi-based technology, renowned as mycoremediation, is gaining more attention for the degradation of PAHs. Different fungal strains such as *Phanerochaete chrysosporium*, *Trichoderma harzianum*, *Pleuroyos ostreatus*, *Trametes versicolor*, *Cunninghamella elegans*, *Aspergillus niger* and *Penicillium janthinellum* can degrade a variety of PAHs to polar compounds (Kadri et al. 2017, Al-Hawash et al. 2018, Etim et al. 2022). Most of the studies on fungal strains for PAH degradation are divided into ligninolytic and non-ligninolytic fungi. Improving this microbial-based bioremediation technique includes the exploration of new strains capable of wide spectrum degradation of PAHs and optimization of influencing factors affecting degradation rate (Singh & Tiwary 2017, Ibrahim et al. 2018).

The degradation of individual PAHs by pure and mixed microbial communities has been studied by several researchers (Zhong et al. 2011, Sonwani et al. 2019). However, contaminated sites are generally occupied with complex mixtures of PAHs, and the degradation rate and extent of degradation for individual PAHs vary depending on the presence of other hydrocarbons (Sawulski et al. 2015). To be implemented as a remediation technology, mycoremediation has to degrade a mixture of PAHs from the contaminated site.

Phenanthrene was chosen as a model compound for studying the degradation process, as it is a frequently occurring and abundant PAH pollutant. The present study aims at screening the fungal strains isolated from PAH-contaminated sites and optimizing the degradation of some frequently occurring and abundant PAHs with the isolated strains.

MATERIALS AND METHODS

Culture Medium

A basal salt media (BSM) (Saraswathy & Hallberg 2002) along with a 0.01% mixture of five PAHs (phenanthrene, acenaphthene, anthracene, fluoranthene, and pyrene) as carbon source, were used for enrichment. Rose Bengal Agar (RBA) Medium ($\text{g}\cdot\text{L}^{-1}$): dextrose, 10; peptone, 5; $\text{MgSO}_4\cdot 7\text{H}_2\text{O}$, 0.5; K_2HPO_4 , 1.0; Rose Bengal, 0.033; and streptomycin, 0.033 and agar 2% was used for fungus growth on Petri plates. Potato Dextrose Agar (PDA) slants were used for maintaining fungal strains at 4°C.

Isolation of PAHs Degrading Fungal Strains

Fifty soil samples were collected from different contaminated sites like highways, refineries, and sewage-irrigated soil from Panipat, Hisar, and Faridabad cities of Haryana, India,

for isolation of fungal strains. The soil sample (10 g) was mixed with deionized water (100 mL) and placed in a shaker (120 rpm) overnight at 28°C in 250 mL Erlenmeyer flasks. After that, the supernatant (5 mL) was added to BSM plus trace element solution (45 mL) in 250 mL Erlenmeyer flasks amended with 0.01 % phenanthrene and was shaken for five days at 28°C and 120 rpm in shaker cum-incubator. The inoculum (10%) from previous experiments was taken and subcultured in the same medium for the enrichment process. The enrichment action was repeated for 3 months and the next three months in a 0.01% mixture of five PAHs (phenanthrene, acenaphthene, anthracene, fluoranthene, and pyrene). The 0.1 mL culture of 10-fold diluted PAHs enriched culture was spread on RBA plates supplemented with streptomycin ($0.033 \text{ g}\cdot\text{L}^{-1}$) and incubated for 5 days at 28°C. The fungal colonies grown on plates were purified by repeated striking methods. A total of 23 fungal strains were isolated. Among all the isolates, 10 fungal strains were selected for further study, deepening upon their growth ability on agar medium containing a mixture of five PAHs.

Preparation of Fungal Inocula

Fungal inocula used for degradation experiments were prepared by growing the respective fungal isolate on PDA slants for 7-10 days. Following sufficient growth, 10 mL of sterilized distilled water was pipetted into a slant and gently agitated to suspend the spores. The spore suspension was then used to inoculate 100 mL sterile BSM media in a 250 mL conical flask incubated for 48 hours at 30°C at 120 rpm. After 48 hours of incubation in an incubator shaker, the mycelial pellets formed were filtered through Whatman #1 filter paper and washed twice using sterilized distilled water. Before inoculation, mycelium was homogenized with the help of a magnetic stirrer. 1 mL of homogenized mycelial suspensions ($1.0 \text{ g}\cdot\text{L}^{-1}$ wet biomass) was used as inoculum for further study.

Screening of Fungal Strains

Fungal strains were screened for the selection of efficient fungus based on oven-dry weight at 60°C and percent degradation of PAH in BSM media after 7 days of incubation time. Out of 10, two fungal strains were screened, namely *Phanerochaete chrysosporium* (isolated from Panipat refinery soil) and *Penicillium citrinum* (isolated from sewage irrigated soil contaminated with PAHs, Hisar) identified from Microbial Type Culture Collection (MTCC), Institute of Microbial Technology, Chandigarh and Indian Agricultural Research Institute (IARI), New Delhi, respectively, based on their best performance.

Experimental Design for Optimization Study

Experiments were carried out in 25 mL Erlenmeyer flasks

having 9 mL of sterilized (autoclaving at 15 psi and 121°C for 20 min) Basal Salt medium plus 1 mL mycelial suspension (1.0 g.L⁻¹ wet biomass) pre-culture fungal inoculums agitated at 120 rpm in BOD cum incubator shaker. Culture conditions and standardization of various parameters (pH, temperature, phenanthrene concentration, and time) were studied. Based on the screening experiment, selected fungal strains were further studied at different pH (5.0, 6.0, 7.0, 8.0, and 9.0), temperature (20°C, 30°C and 40°C), phenanthrene concentration (50, 100, 150, and 200 ppm) and time (7, 14, 21 and 28 days). To see the effect of carbon sources on the degradation of PAH under optimized conditions, three different carbon sources were used (yeast extract, peptone, and glucose at 5 g.L⁻¹).

Biodegradation Study of PAHs Mixture

Liquid medium: Biodegradation experiments were carried out in 25 mL Erlenmeyer flasks having 9.0 mL sterilized basal salts medium with 5 g.L⁻¹ yeast extract (BSMY) and 1 mL of homogenized mycelial suspensions (1.0 g.L⁻¹ wet biomass) containing combination of five different PAH (200 ppm phenanthrene, 100 ppm of fluoranthene and pyrene, and 50 ppm of chrysene and benzo(a)pyrene).

Spiked soil: Bioremediation experiments (in triplicate) were performed in Erlenmeyer flasks (100 mL) having 10 g of sterilized agricultural soil (unexposed to PAHs) samples. The soil was spiked with a solution containing a range of PAHs in hexane to give a final soil concentration of 100 mg.kg⁻¹ for fluoranthene and pyrene, 200 mg.kg⁻¹ for phenanthrene, and 50 mg.kg⁻¹ for chrysene and benzo(a)pyrene. The spiked soil was placed in a fume hood for 2 hours for evaporation of hexane. 9 mL BSMY medium containing 1 mL homogenized mycelial suspensions (1.0 g.L⁻¹ wet biomass) added in 10 g spiked soil. Microcosms were incubated at 30°C with pH 7.0 in the dark for 28 days at 70% humidity in the humidity cabinet.

All three flasks were analyzed at 0, 7, 14, 21 and 28 days. Results were expressed as means. The standard deviation was less than 2% of the mean.

Quantification of PAHs

PAH extraction of both samples (liquid and soil) were carried out by adding hexane (20 mL) to each flask, which was kept in a BOD cum incubator shaker at 4°C and 120 rpm for 4 h. After that, the samples were placed in an ultrasonicator (Trans-sonic) for 15 min for two times for proper separation of the organic phase from the aqueous phase. The organic phase sample was cleaned up using chromatography to remove impurities and, after that, concentrated on the rotary evaporator (JSGW) two times with hexane. After that, the sample was centrifuged for 10 min at 10000 rpm and

filtrated with syringe filters (0.45µm). High-performance liquid chromatography (HPLC Water 600) equipped with UV-detector and C-18 column was used for the analysis of samples. The mobile phase used was an acetonitrile-water mixture (75:25) with a maintained flow rate of 1.0 mL.min⁻¹. The sample (20 µL) was injected into the column through a sample loop. The concentration of PAH was calculated by comparing peak areas of the sample chromatogram and standard chromatogram (Bishnoi et al. 2008).

The Concentration of PAH (ppm):

$$= \frac{\text{Peak Area of Chromatogram of the Sample}}{\text{Peak Area of Chromatogram of Standard PAH Compound}} \times \text{Concentration of Standard PAH Compound}$$

Biodegradation efficiency was calculated as:

$$\text{Biodegradation efficiency (\%)} = \frac{(C_0 - C_e)}{C_0} \times 100$$

Where C₀ is the initial concentration of PAHs (mg.kg⁻¹); C_e is the residual concentration of PAHs (mg.kg⁻¹).

RESULTS AND DISCUSSION

Isolation and Screening

Among 23 fungal isolates, 10 (coded F1, F2, F3...F10) were selected for further screening in BSM medium with 50 ppm phenanthrene concentration after 7 days incubation period. Independent of fungi species, studied for phenanthrene degradation and mycelial growth to check their best performance. Enzymatic activities were also studied for the selection of fungal strains (data not shown). Among 10 fungal strains, the maximum degradation of phenanthrene was 17.56% and 10.23% with *P. chrysosporium* (F2) and *P. citrinum* (F5), respectively (Fig. 1). The highest mycelial growth was also obtained with these two isolates 5.73 g.L⁻¹ and 6.42 g.L⁻¹. Maximum degradation of phenanthrene was found with *P. chrysosporium* fungal strain. Still, dry-weight fungal biomass was found to be maximized in the *P. citrinum* strain (Fig. 1). Some other fungal strains showed high dry-weight biomass but less percent degradation. This showed that there is no direct correlation between percent degradation and biomass weight. Quintero et al. (2008) observed a similar effect with the degradation of hexachlorocyclohexane (HCH) isomers on white rot fungi. In this study, the mycelial growth of *P. chrysosporium* was higher than *Bjerkandera adusta* in the presence of HCH isomers, but the degradation rate was high with *B. adusta*.

Effect of Environmental Factors on Phenanthrene Degradation

Environmental factors like pH, temperature, initial dose

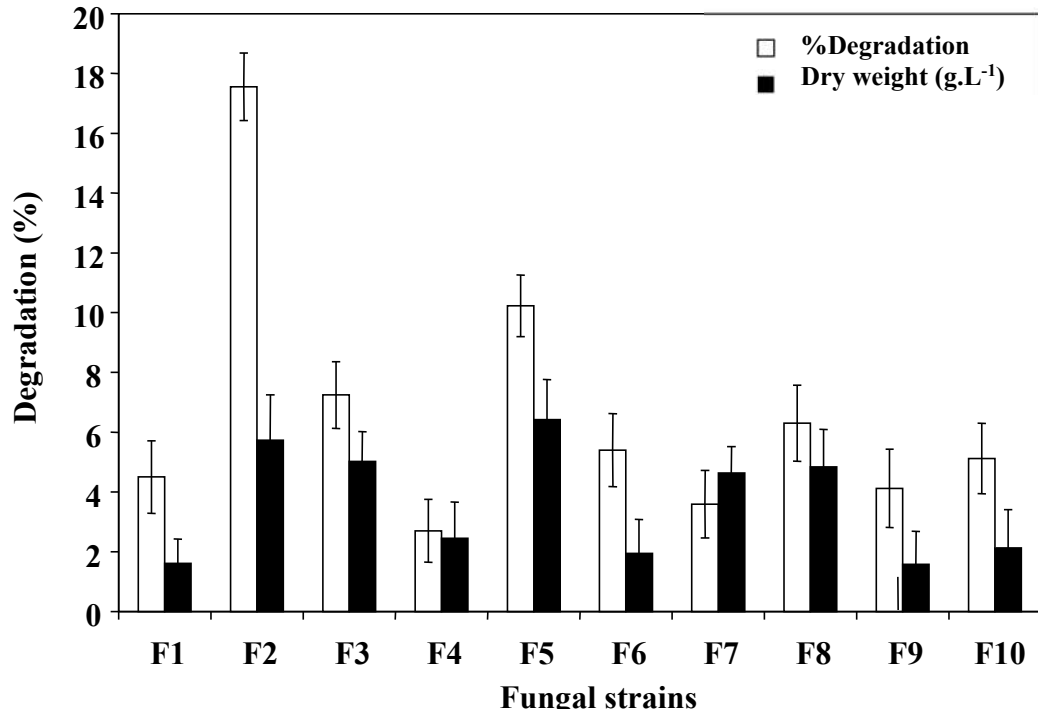


Fig. 1: Comparison of percent degradation and dry weight during degradation of phenanthrene with 10 isolates.

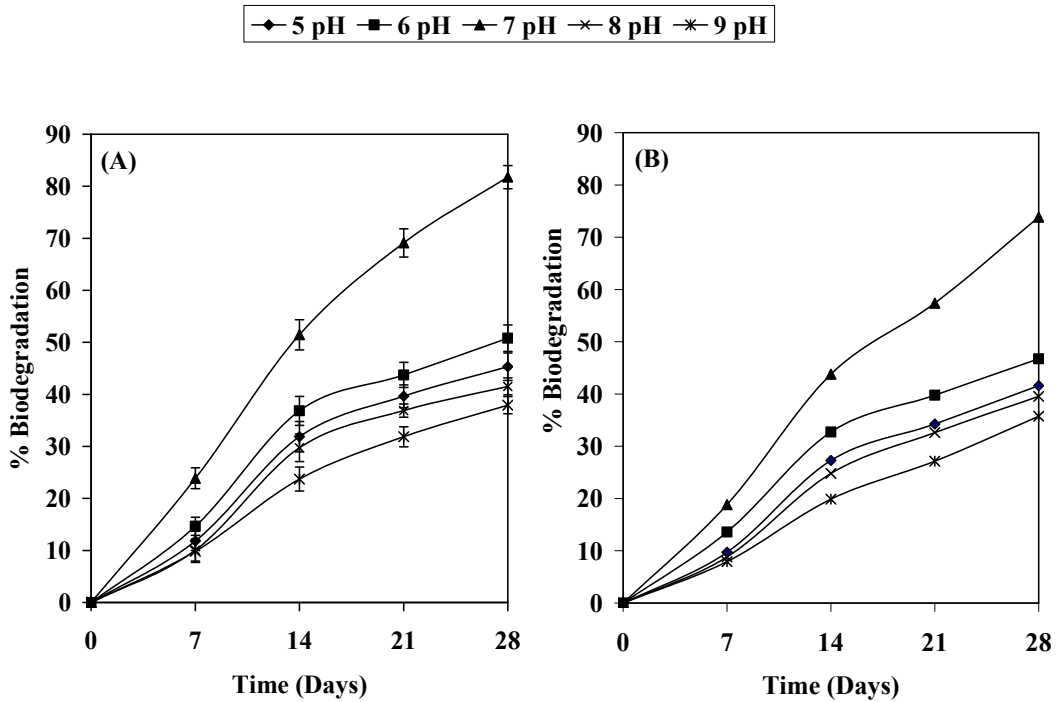


Fig. 2: Effect of different pH values on biodegradation of phenanthrene by (A) *P. chrysosporium* and (B) *P. citrinum* (50 ppm).

of PAHs, type of fungal strain, etc., play a critical role in the degradation of these recalcitrant toxic compounds (Shankhwar & Paliwal 2021). A series of experiments were conducted with both the fungal strains to test phenanthrene degradation at various pHs from 5.0 to 9.0 and temperatures ranging from 20°C to 40°C. The phenanthrene degradation increased with an increase in pH from 5.0 to 7.0 and again decreased with a further increase in pH from 7.0 to 9.0. Maximum degradation of PAH was observed at pH 7.0 by both fungal strains (Fig. 2). The optimal temperature for degradation of phenanthrene was observed at 30°C (Fig. 3), whereas biodegradation efficiency decreased as temperature increased or decreased. Temperature is a crucial factor in the bioavailability of PAH molecules (Okere & Semple 2012). The increased temperature decreased oxygen solubility, which led to a reduction in the metabolic activity of aerobic microbes. Optimal conditions for both the fungal strains were determined to be 30°C and pH 7.0. Microbial activity was slower with an increase or decrease in temperature up to its optimal value. It was also found that the phenanthrene concentration was 78.54 % and 74.8 % with *P. chrysosporium* and *P. citrinum*, respectively, at 50 ppm concentration, but at 200 ppm concentration, the rate of degradation was low (Fig. 4), which slightly differs from the report of Ting et al. (2011). The higher concentration of PAHs results in

a reduced degradation rate due to the increased toxicity of PAH metabolites, and microbial community growth is affected due to an increase in toxicity (Bishnoi et al. 2008, Qi et al. 2017). Adverse environmental conditions (like pH and temperature) may reduce the biodegradation by microbes (Wang et al. 2016).

Effects of Carbon Sources on the Degradation of Phenanthrene

The carbon source is required for microbial growth, and due to the toxicity of PAHs, additional carbon sources must be provided. Fungi can co-metabolize different PAHs in the presence of carbon sources (Shankhwar & Paliwal 2021). In the present study, three carbon sources- yeast extract, glucose, and peptone were compared for their effect on microbial growth (Fig. 5). Phenanthrene degradation was 44.82%, 79.79%, 94.44%, and 100% with *P. chrysosporium* (Fig. 5 A) and 36.48%, 67.41 %, 87.24% and 94.82% with *P. citrinum* (Fig. 5 B) at 7, 14, 21 and 28 days, respectively, in presence of yeast extract (5 g.L⁻¹). The yeast extract supported more degradation as compared to other carbon sources studied as shown in Fig. 5. A similar finding was observed by Mineki et al. (2015) using yeast extract for the transformation of PAHs in soil. They also noticed similar outcomes when additional carbon substrates, such as lactose, sucrose, and yeast extract,

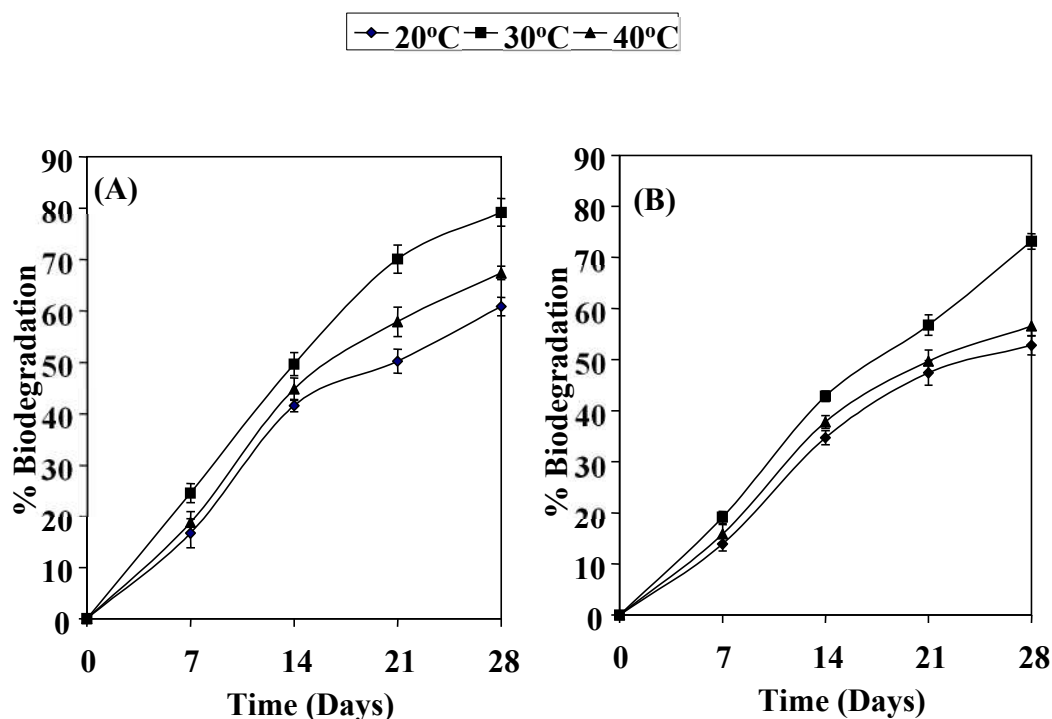


Fig. 3: Effect of different temperatures on biodegradation of phenanthrene by (A) *P. chrysosporium* and (B) *P. citrinum* (50 ppm).

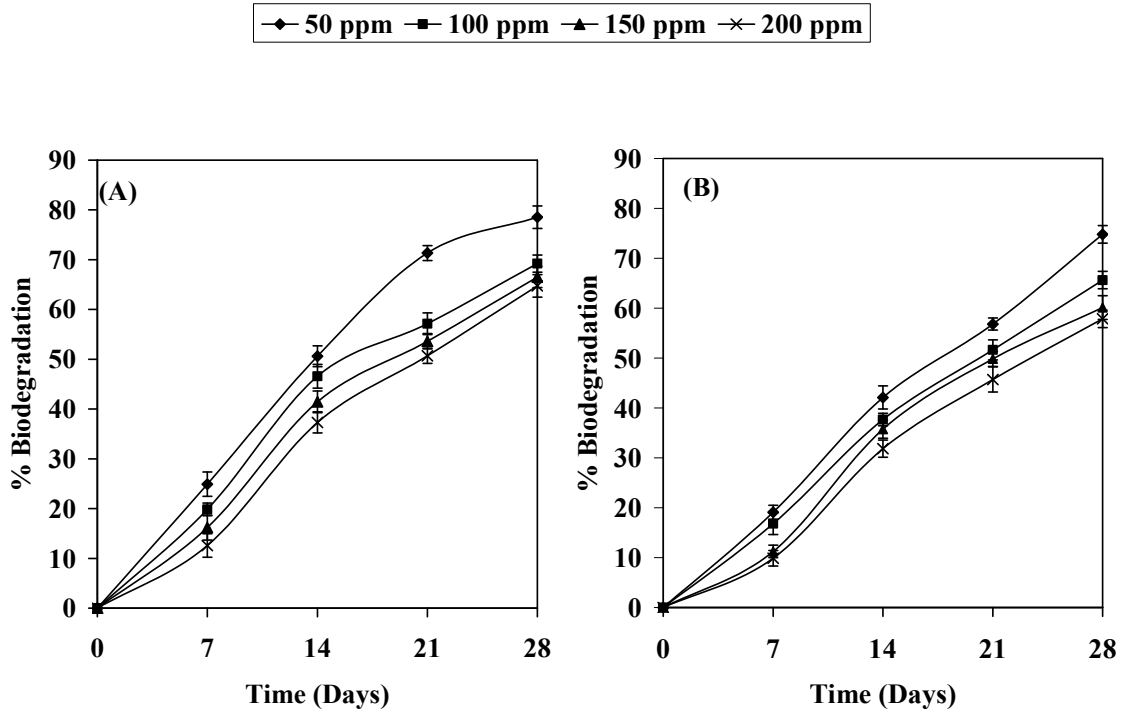


Fig. 4: Effect of different concentrations of phenanthrene on biodegradation of phenanthrene by (A) *P. chrysosporium* and (B) *P. citrinum*.

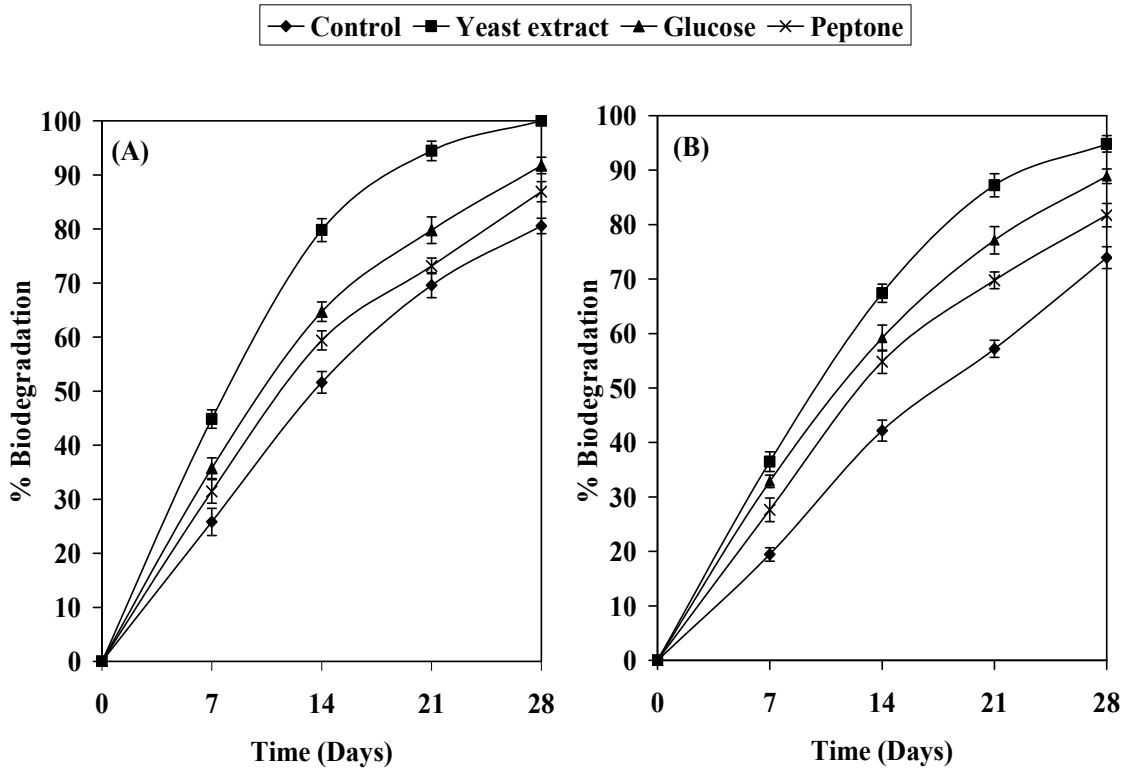


Fig. 5: Effect of different carbon sources on biodegradation of phenanthrene by (A) *P. chrysosporium* and (B) *P. citrinum* (50 ppm).

were supplemented. The results of the present study are similar to organic carbon source supplementation and the presence of co-substrates, which improve the transformation of PAHs, as observed by Hesnawi & Adbeib (2013). In the present study, almost 19 to 20 percent degradation rate was higher with yeast extract than the degradation without the addition of a carbon source. The addition of a carbon source is required for the initial growth of microorganisms as the energy required for microbial growth is not provided by PAHs alone as a carbon source (Cerniglia & Sutherland 2010).

Biodegradation of PAHs Mixture

Although many organisms degrade individual PAHs, to

be effective in PAH bioremediation, they must metabolize them in the environment as a complex mixture (Haritash & Kaushik 2009). Therefore, it is important to study the effect of PAH degradation in a synthetic liquid medium and artificially spiked soil at optimized conditions with the addition of 5 g.L⁻¹ yeast extract as a carbon source.

The experiments presented here were to measure fungal degradation of a mixture of five PAHs for 28 days incubation period (sampled at days 0, 7, 14, 21, and 28). There were no significant reductions in PAHs with uninoculated and autoclaved killed controls. Only 1 to 2 % total degradation of PAHs by both the control with both fungal strains. All results presented in this study were not corrected with their controls.

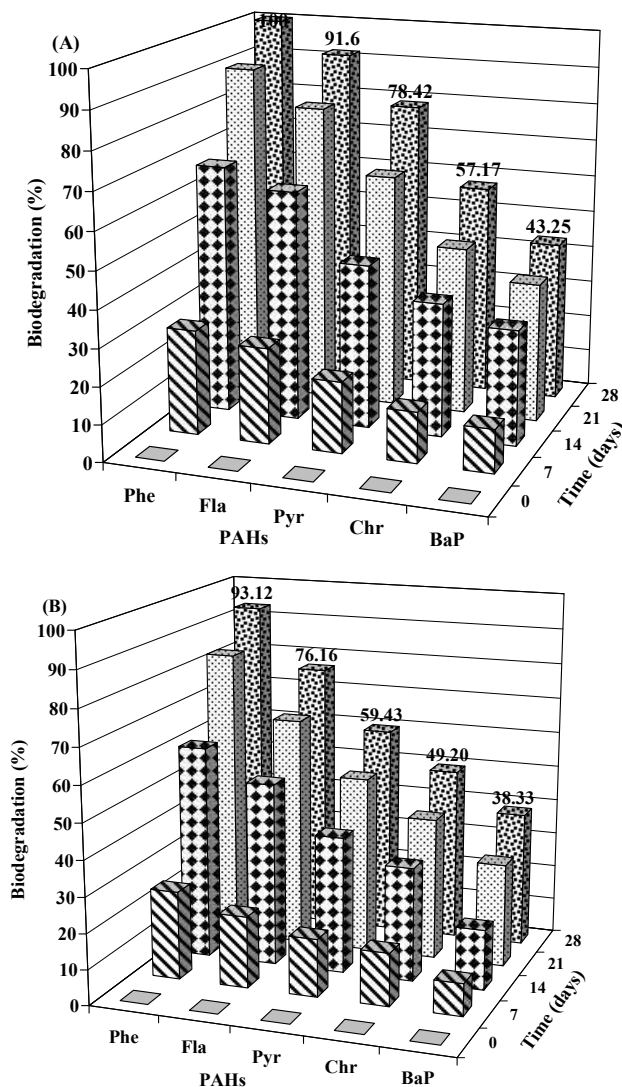


Fig. 6: The percentage biodegradation of individual PAHs in a synthetic mixture in liquid media after 28 days incubation period with (A) *P. chrysosporium* and (B) *Penicillium citrinum* in liquid media. Phen, Phenanthrene; Flu, Fluoranthene; Pyr, Pyrene; Chr, Chrysene; BaP, Benzo(a)pyrene.

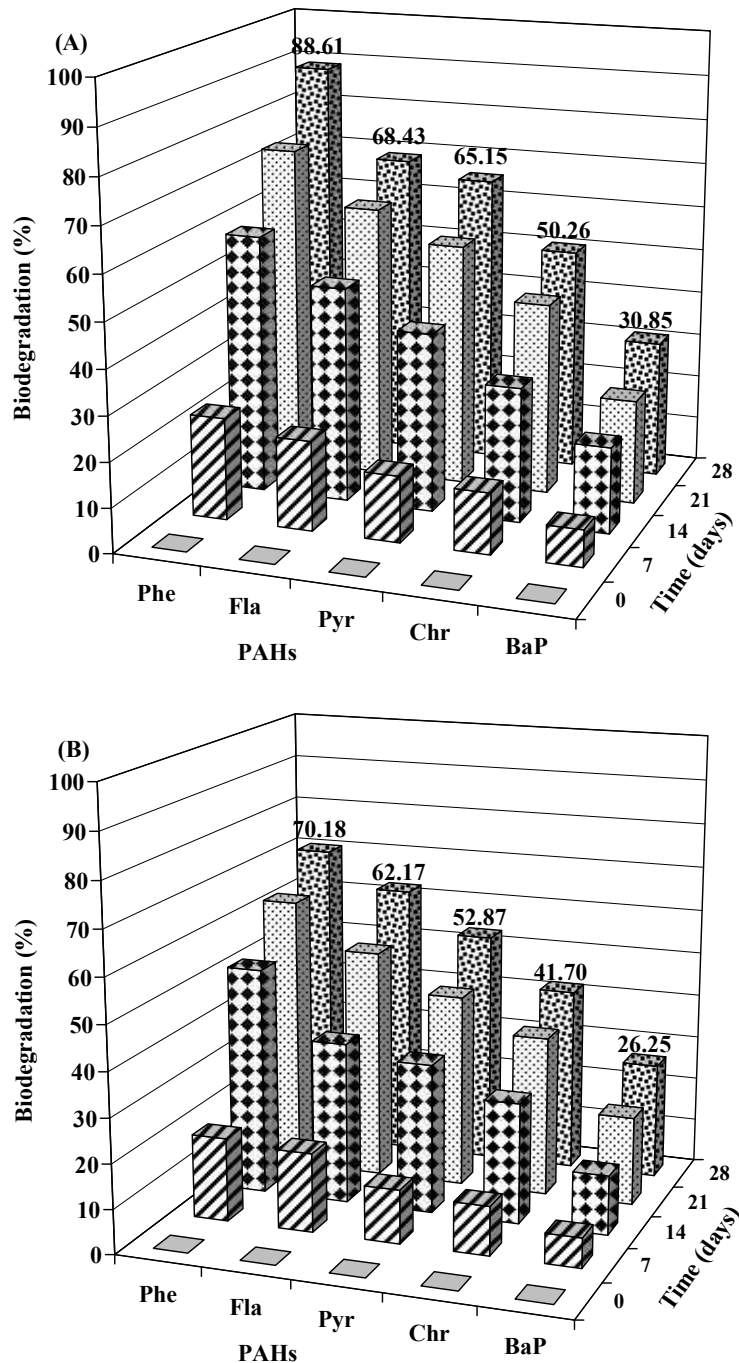


Fig. 7: The percentage biodegradation of individual PAHs in a synthetic mixture in spiked soil after 28 days incubation period with (A) *P. chrysosporium* and (B) *Penicillium citrinum* in spiked soil.

In liquid medium: In liquid medium, the degradation of PAHs mixture with *P. chrysosporium* was 100%, 91.60%, 78.42%, 57.17%, and 43.25% of phenanthrene, fluoranthene, pyrene, chrysene, and benzo(a)pyrene, respectively, as shown by Fig. 6 A after 28 days, indicating the highly

efficient strain. Fig. 6 B showed 93.12%, 76.16%, 59.43%, 49.20%, and 38.33% of phenanthrene, fluoranthene, pyrene, chrysene, and benzo(a)pyrene, respectively, degraded by *P. citrinum* within 28 days. Both fungal strains show less efficiency towards degradation of four to five rings PAHs

(chrysene and benzo(a)pyrene). PAHs of higher molecular weight have lower aqueous solubility, which in turn reduces the bioavailability (Ghosal et al. 2016), thus lowering the biodegradation potential. Pyrene was more rapidly degraded than benzo(a)pyrene with *Trichoderma sp.*, *Aspergillus niger*, and *Fusarium sp.* (Wang et al. 2008). Quintero et al. (2008) observed 42% degradation of γ -HCH in a liquid medium while 8 to 17% degradation in sandy soil using *B. adusta*. The biodegradation of higher molecular weight PAHs is slower than low molecular weight PAHs might be due to their low water solubility, lower uptake into the cell, not induction of degradative enzymes, and insufficient energy yield required for microbial growth (Cerniglia & Sutherland 2010).

In spiked soil: The experiment was carried out in a liquid medium, and optimal conditions were used to ascertain the potential of biodegradation and the influence of different factors such as pH and temperature. However, it is difficult to extrapolate the results of such studies to the field because of strong ecological competition from soil microflora and variable environmental conditions (Diplock et al. 2009, Kadri et al. 2017). To better simulate field conditions, while retaining experimental control, microcosm can be used. These generally comprise small bioreactors, usually jars or Erlenmeyer flasks, where fungal strains grown on a mixture of soil are artificially or naturally contaminated with additional nutrient sources (Canet et al. 1999).

In this study, firstly, the degradation rate of PAHs in liquid media was carried out, followed by spiked soil samples having a mixture of phenanthrene, fluoranthene, pyrene, chrysene, and benzo(a)pyrene. Fig. 7 A, B showed that *P. chrysosporium* was more efficient than *P. citrinum* in removal of five PAHs: 88.61 and 70.18% phenanthrene, 68.43 and 62.17% fluoranthene, 61.15% and 52.87% pyrene, 50.26% and 41.70% chrysene and 30.85 and 26.25% benzo(a)pyrene, respectively (initial concentration = 100% of individual PAH in the soil for experiment). Within 14 days, the removal of phenanthrene was 67.15 and 60.31% with *P. chrysosporium* and *P. citrinum*, respectively, after the degradation rate was slowed down. Phenanthrene degradation was more with both isolates in both cases because in the adaptation experiment, individual microbial culture was enriched with phenanthrene for three months and then with a combination of the five PAHs for another next three months. Similarly, Yuan et al. (2002) reported faster degradation of phenanthrene as compared to other PAHs due to the enrichment of consortium in phenanthrene for three years and in combination with other PAHs for one year. The degradation of chrysene and benzo(a)pyrene was less might be due to their low water solubility.

The degradation pattern was very interesting as in the first two weeks removal rate of PAHs was high, followed by lower

removal rates in the coming two weeks in all experiments of this work. The percent degradation of PAHs increased with increasing incubation time, but the rate of degradation decreased. This might be due to nutrient limitations as one possibility for a decreased rate of removal. Kalantary et al. (2014) reported the bacterial degradation of phenanthrene in soil was enhanced by the addition of a suitable combination of mineral nutrients in the system. In the present study, more PAH is eliminated in a liquid medium than in soil. This might be due to different mass transfers between soil and liquid. As a result of this, PAH showed a much lower rate of metabolism in soil than in liquid media (Wang et al. 2009). Bioavailability is one of the critical factors involved in the bioremediation of hydrophobic pollutants as they tend to sorb on mineral surfaces and organic matter (Ghosal et al. 2016). This results in a reduction in bioavailability of pollutants, thus limiting their bioremediation in soil. The present study indicated that mineralization of phenanthrene was higher in liquid media as compared to soil and biodegradability might be reduced due to sorption of PAHs.

CONCLUSION

This study was conducted to investigate the ability of isolated fungal strains for PAH removal from liquid and spiked soil. Favorable conditions for the development of microorganisms and the addition of carbon sources play a significant role in PAH degradation. Results showed that variations influence phenanthrene biodegradation in pH, temperature, substrate concentrations, and the supplementation of carbon sources. The optimal conditions for PAH biodegradation were determined as pH 7.0 and 30°C. The addition of all three carbon sources enhanced the degradation rate, but yeast extract showed promising results. *P. chrysosporium* showed higher degradation potential than *P. citrinum*. The maximum degradation rate was obtained in liquid medium than spiked soil.

ACKNOWLEDGEMENTS

The authors are delighted to express their gratitude and sincerest thanks to the Dean of the Central Instrumentation Laboratory (CIL) at Guru Jambheshwer University of Science and Technology, Hisar, for the cartography unit.

REFERENCES

- Abdel-Shafy, H.I. and Mansour, M.S.M. 2016. A review on polycyclic aromatic hydrocarbons: source, environmental impact, effect on human health and remediation. Egypt. J. Petro., 25: 107-123. <https://doi.org/10.1016/j.ejpe.2015.03.011>
- Al-Hawash, A.B., Alkoorenee, J.T., Zhang, X. and Ma, F. 2018. Fungal degradation of polycyclic aromatic hydrocarbons. Int. J. Pure App. Biosci., 6(2): 8-24. doi: <http://dx.doi.org/10.18782/2320-7051.6302>

- Alekseev, I. and Abakumov, E. 2021. Polycyclic aromatic hydrocarbons, mercury, and arsenic content in soils of Larsemann Hills, Pravda Coast, and Fulmar Island, Eastern Antarctica. *Bull. Environ. Contam. Toxicol.*, 106(2): 278-288. doi: 10.1007/s00128-020-03063-w.
- Babu, A.G., Reja, S.I., Akhtar, N., Sultana, M., Deore, P.S. and Ali, F.I. 2019. Bioremediation of Polycyclic Aromatic Hydrocarbons (PAHs): Current Practices and Outlook. In Arora P. (ed), *Microbial Metabolism of Xenobiotic Compounds. Microorganisms for Sustainability*, Springer, Singapore, pp. 46-80. Online ISBN 978-981-13-7462-3. 10.1007/978-981-13-7462-3_9
- Bishnoi, K., Sain, U., Kumar, R., Singh, R. and Bishnoi, N.R. 2009. Distribution and biodegradation of polycyclic aromatic hydrocarbons in contaminated sites of Hisar (India). *Indian J. Exp. Biol.*, 47: 210-217.
- Bishnoi, K., Kumar, R. and Bishnoi, N.R. 2008. Biodegradation of polycyclic aromatic hydrocarbons by white rot fungi *Phanerochaete chrysosporium* in sterile and unsterile soil. *J. Sci. Indust. Research.*, 67: 538-542.
- Bishnoi, N.R., Mehta, U. and Pandit, G.G. 2006. Quantification of polycyclic aromatic hydrocarbons in fruits and vegetables using high-performance liquid chromatography. *Indian J. Chem. Technol.*, 13: 30-35.
- Bright, A., Li, F., Movahed, M., Shi, H. and Xue, B., 2023. Chronic exposure to lowmolecular-weight polycyclic aromatic hydrocarbons promotes lipid accumulation and metabolic inflammation. *Biomolecules*, 13:196. <https://doi.org/10.3390/biom13020196>
- Canet, R., Lopez-Real, J.M. and Beck, A.J. 1999. Overview of polycyclic aromatic hydrocarbon biodegradation by white-rot fungi. *Land Contam. Reclam.*, 7: 191-197.
- Cerniglia, C.E. and Sutherland, J.B., 2010. Degradation of Polycyclic Aromatic Hydrocarbons by Fungi. In Temmis, K.N. (ed), *Handbook of Hydrocarbon and Lipid Microbiology*, Springer Berlin, Heidelberg, pp 2079-2110.
- Diplock, E.E., Mardlin, D.P, Killham, K.S. and Paton, G.I. 2009. Predicting bioremediation of hydrocarbons: Laboratory to field scale. *Environ. Pollu.*, 157: 1831-1840. <https://doi.org/10.1016/j.envpol.2009.01.022>
- Etim, E.U., Ola, M.I. and Owode, R.O. 2022. Bioremediation of total polycyclic aromatic hydrocarbon contaminated soil using nitrified sawdust and *Pseudomonas aeruginosa*. *J. Environ. Protect.*, 13: 427-43. 10.4236/jep.2022.136027
- Ghosal, D., Ghosh, S., Dutta, T.K. and Ahn, Y. 2016. Current state of knowledge in microbial degradation of polycyclic aromatic hydrocarbons (PAHs): A review. *Front. Microbiol.*, 7: 1369. <https://doi.org/10.3389/fmicb.2016.01369>
- Gu, H., Yan, K., You, Q., Chen, Y., Pan, Y., Wang, H., Wu, L. and Xu, J. 2021. Soil indigenous microorganisms weaken the synergy of *Massilia* sp. WF1 and *Phanerochaete chrysosporium* in phenanthrene biodegradation. *Sci. Total Environ.*, 781: 146655. <https://doi.org/10.1016/j.scitotenv.2021.146655>
- Gupta, H. and Kumar, R. 2020. Distribution of selected polycyclic aromatic hydrocarbons in urban soils of Delhi, India. *Environ. Technol. Innovat.*, 17(7): 100500. 10.1016/j.eti.2019.100500
- Haritash, A.K. and Kaushik, C.P. 2009. Biodegradation aspects of polycyclic aromatic hydrocarbons (PAHs): A review. *J. Hazard. Mater.*, 169: 1-15. <https://doi.org/10.1016/j.jhazmat.2009.03.137>
- Hesnawi, R. and Adbeib, M. 2013. Effect of nutrient source on indigenous biodegradation of diesel fuel contaminated soil. *APCBEE Proceed.*, 5: 557-561. <https://doi.org/10.1016/j.apcbee.2013.05.093>
- Ibrahim, M., Makky, E.A., Azmi, N.S. and Ismail, J. 2018. Optimization parameters for Mycobacteria confluents biodegradation of PAHs. *MATEC Web Confer.*, 150: 06035. <https://doi.org/10.1051/mateconf/201815006035>
- Jacques, R.J.S., Okeke, B.C., Bento, F.M., Teixeira, A.S., Peralba, M.C.R. and Camargo, F.A.O. 2008. Microbial consortium bioaugmentation of polycyclic aromatic hydrocarbons contaminated soil. *Biores. Technol.*, 9(7): 2637-43. doi: 10.1016/j.biortech.2007.04.047.
- Kadri, T., Rouissi, T., Brar, S.K., Cledon, M., Sarma, S. and Verma, M. 2017. Biodegradation of polycyclic aromatic hydrocarbons (PAHs) by fungal enzymes: A review. *J. Environ. Sci.*, 51: 52-74. <https://doi.org/10.1016/j.jes.2016.08.023>
- Kalantary, R.R., Mohseni-Bandpi, A., Esrafil, A., Nasser, S., Ashmogh, F.R., Jorfi, S. and Ja'fari, M. 2014. Effectiveness of biostimulation through nutrient content on the bioremediation of phenanthrene contaminated soil. *J. Environ. Health Sci. Engg.*, 12(1): 24. DOI:10.1186/2052-336X-12-24
- Liu, S.H., Zeng, G.M., Niu, Q.Y., Liu, Y., Zhou, L., Jiang, L.H., Tan, X.F., Xu, P., Zhang, C. and M. Cheng 2017. Bioremediation mechanisms of combined pollution of PAHs and heavy metals by bacteria and fungi: A mini-review. *Biores. Technol.*, 224: 25-33. <https://doi.org/10.1016/j.biortech.2016.11.095>
- Malik, A., Verma, P., Singh, A.K. and Singh, K.P. 2011. Distribution of polycyclic aromatic hydrocarbons in water and bed sediments of the Gomti River, India. *Environ. Monit. Assess.*, 172(1-4): 529-545. doi: 10.1007/s10661-010-1352-4.
- Masih, A., Saini, R., Singhvi, R. and Taneja, A. 2010. Concentrations, sources, and exposure profiles of polycyclic aromatic hydrocarbons (PAHs) in particulate matter (PM₁₀) in the north-central part of India. *Environ. Monit. Assess.*, 163: 421-431.
- Mineki, S., Suzuki, K., Iwata, K., Nakajima, D. and Goto, S. 2015. Degradation of polyaromatic hydrocarbons by fungi isolated from soil in Japan. *Polycycl. Aromat. Compd.*, 128-120 :(1)35. <https://doi.org/10.406638.2014.937007/10.1080>
- Okere, U.V. and Semple, K.T. 2012. Biodegradation of PAHs in pristine soils from different climatic regions. *Bioremed. Biodegrad.*, 3: 1-11. doi: 10.4172/2155-6199.S1-006.
- Paris, A., Ledauphin, J., Poinot, P. and Gaillard, J.L. 2018. Polycyclic aromatic hydrocarbons in fruits and vegetables: Origin, analysis, and occurrence. *Environ. Pollut.*, 234: 96-106. <https://doi.org/10.1016/j.envpol.2017.11.028>
- Qi, Y., Wang, C., Lv, C., Lun, Z. and Zheng, C. 2017. Removal capacities of polycyclic aromatic hydrocarbons (PAHs) by newly isolated strain from oilfield-produced water. *Int. J. Environ. Res. Pub. Health*, 14(2): 215. doi: 10.3390/ijerph14020215.
- Quintero, J.C., Moreira, M.T., Feijoo, G. and Lema, J.M. 2008. Screening of white rot fungal species for their capacity to degrade lindane and other isomers of hexachlorocyclohexane (HCH). *Cien. Inv. Agr.*, 35(2): 159-167. <http://dx.doi.org/10.4067/S0718-16202008000200005>
- Saraswathy, A. and Hallberg, R. 2002. Degradation of pyrene by indigenous fungi from a former gasworks site. *FEMS Microbiol. Lett.*, 210(2): 227-232. 10.1111/j.1574-6968.2002.tb11185.x.
- Sawulski, P., Boots, B., Clipson, N. and Doyle, E. 2015. Differential degradation of polycyclic aromatic hydrocarbon mixtures by indigenous microbial assemblage in soil. *Lett. Appl. Microbiol.*, 61(2):199-207. doi: 10.1111/lam.12446.
- Shankhar, A.K. and Paliwal, R.2021. Fungi in bioremediation of soil: Mycoremediation of PAHs compounds. In Sharma, V.K., Shah, M.P., Parmar, S. and Kumar, A. (eds), *Fungi Bio-Prospects in Sustainable Agriculture, Environment and Nano-technology*. Academic Press, Cambridge, MA, pp. 157-170. doi:10.1016/B978-0-12-821925-6.00008-3.
- Singh, P. and Tiwary, B.N. 2017. Optimization of conditions for polycyclic aromatic hydrocarbons (PAHs) degradation by *Pseudomonas stutzeri* P2 isolated from Chirimiri coal mines. *Biocata. Agri. Biotechnol.*, 10: 20-29. <https://doi.org/10.1016/j.bcab.2017.02.001>
- Sonwani, R.K., Giri, B.S., Singh, R.S. and Rai, B.N. 2019. Studies on optimization of naphthalene biodegradation using surface response methodology: kinetic study and performance evaluation of a pilot scale integrated aerobic treatment plant. *Process Saf. Environ. Prot.*, 132: 240-248. doi:10.1016/j.psep.2019.10.004

- US EPA 2002. Polycyclic Organic Matter. Retrieved January 20, 2021, from <http://www.epa.gov/ttn/atw/hlthef/polycycl.html>.
- Thacharodi, A., Hassan, S., Singh, T., Mandal, R., Chinnadurai, J., Khan, H.A., Hussain, M.A., Brindhadevi, K. and Pugazhendhi, A., 2023. Bioremediation of polycyclic aromatic hydrocarbons: An updated microbiological review. *Chemosphere*, 328: 138498. <https://doi.org/10.1016/j.chemosphere.2023.138498>
- Ting, W.T.E., Yuan, S.Y., Wu, S.D. and Chang, B.V. 2011. Biodegradation of phenanthrene and pyrene by *Ganoderma lucidum*. *Int. Biodeterior. Biodegrad.*, 65: 238-242. doi: 10.1016/j.ibiod.2010.11.007.
- Wang, H., Lou, J. and Xu, J. 2016. Efficient biodegradation of phenanthrene by a novel strain *Massilia sp.* WF1 isolated from PAH-contaminated soil. *Environ. Sci. Pollut. Res.*, 23(13):13378-88. doi: 10.1007/s11356-016-6515-6.
- Wang, C., Sun, H., Li, J., Li, Y. and Zhang, Q. 2009. Enzyme activities during degradation of polycyclic aromatic hydrocarbons by white rot fungus *Phanerochaete chrysosporium* in soils. *Chemos.*, 77(6): 733-738. <https://doi.org/10.1016/j.chemosphere.2007.0075>.
- Wang, X. X., Gong, Z., Li, P., Zhang, L. and Hu, X. 2008. Degradation of pyrene and benzo(a)pyrene in contaminated soil by immobilized fungi. *Environ. Engg. Sci.*, 25: 677-684. <https://doi.org/10.1089/ees.2007.0075>.
- Yuan, S.Y., Shiung, L.C. and Chang, B.V. 2002. Biodegradation of polycyclic aromatic hydrocarbons by inoculated microorganisms in soil. *Bull. Environ. Contam. Toxicol.*, 69(1):66-73. doi: 10.1007/s00128-002-0011-z.
- Zhong Y., Luan T., Lin L., Liu H. and Tam N. 2011. Production of metabolites in the biodegradation of phenanthrene, fluoranthene, and pyrene by the mixed culture of *Mycobacterium sp.* and *Sphingomonas sp.* *Biores. Tech.*, 102(3):2965-72. doi: 10.1016/j.biortech.2010.09.113.



Sustainable Water Conservation and Management Practices: A Perception Survey of the Farmers of Haryana, India

Manika Kohli and Vinakshi Grover†

Mehr Chand Mahajan DAV College for Women, Sector-36 A, Chandigarh-160036, India

†Corresponding author: Vinakshi Grover; vinakshigrover@gmail.com

Nat. Env. & Poll. Tech.
Website: www.neptjournal.com

Received: 03-09-2023

Revised: 26-10-2023

Accepted: 03-11-2023

Key Words:

Modern irrigation

Sustainability

Water conservation

Water management practices

ABSTRACT

In order to ensure water sustainability, alarming levels of water scarcity across the globe is a critical issue warranting urgent address. The present study aims to bring to light the perception of farmers regarding water conservation and management practices from the selected five districts of the Haryana region of India. By analyzing the responses of 125 farmers, collected through a self-administered questionnaire, the impact of socio-demographic factors, current irrigation system, and cost-benefit perception of the farmers was studied on water conservation and management practices. Using ordinal regression analysis, the study revealed that the cost-benefit perception of the farmers, viz. willingness to pay an additional price for canal water and an increase in the availability of water due to canal lining, are the major factors responsible for undertaking conservation and sustainability measures. Further, socio-demographic variables such as age and education also influence water conservation behavior. The study recommends vital policy reforms and initiatives for efficient water use and management to resolve the grave concern of scarcity of usable water. The present study is unique in its suggestion of a comprehensive water conservation and management framework.

INTRODUCTION

Water is the elixir of life for all beings, may it be flora, fauna, or humans (Ravish et al. 2018). Freshwater is a natural resource that is indispensable for the life and well-being of humans and the ecosystem. Yet, the future availability of this valuable resource is less than certain. As reported by the United States Geological Survey, around 97 percent of water is present in the oceans, which is not potable (Water Science School 2018). Only the remaining 3 percent of water is fresh. Freshwater is distributed among icecaps and glaciers (68.7 percent), surface water (0.3 percent), and groundwater (30.1 percent). Out of the surface water, 87 percent is in the lakes, and the rest in rivers and swamps. This means that a mere one percent of the total water on earth is usable by human beings. In practice, only 0.007 percent of the water on earth is available to serve its 7.8 billion people (United States Census Bureau 2021).

With the growing population and economic activities, the need for this prime natural resource is also surging (Garg & Hassan 2007, Brown 2017, Ghosh 2021). The wasteful expense of this valuable natural resource often undermines the significance of water. The growing urbanization and industrial activity coupled with climate change have resulted in an alarming level of water shortage globally. Nearly one-

fifth of the world's population lives in areas of physical water scarcity (Xiao-Jun et al. 2014, Manju & Sagar 2017). Among the 17 countries facing extreme water stress, the emerging economy of India ranks 13th in number (Hofste et al. 2019). In addition to the surface water resources (rivers, lakes, and streams), even the groundwater resources of the country have been severely overdrawn, mainly for providing water for irrigation. According to World Resources Institute, groundwater stress is more pronounced in the northern part of India, where the groundwater tables have experienced an annual decline at an alarming rate of more than 8 centimeters from 1990-2014 (Hofste et al. 2019). Thus, India is facing worrisome groundwater stress. Despite the depleting water resources of the country, with increasing population water demand is on a constant upsurge (Gupta et al. 2016). India has more than 18 percent of the world's population but only 4 percent of the world's renewable water resources (National Water Mission 2021). Keeping in view the ferocity of the situation, the Haryana region of India, which falls in the north-western part of the country (between 27 degrees 37' to 30 degrees 35' latitude and between 74 degrees 28' to 77 degrees 36' longitude and with an altitude of 700-3600 ft above sea level) has been selected for the present study (Haryana Tourism Corporation Limited 2020). Further, this area is characterized by low and erratic

rainfall, which makes it a perfect milieu to carry out this research.

Given the erratic rainfall and water scarcity in Haryana, the building of canals has been a popular way of irrigating the agricultural fields in this region (Yadav 1987). Through irrigation, canal water is supplied to the fields. The performance of irrigation systems is thus of vital importance to the farmers for better crop yield and earning a decent livelihood (O'Keeffe et al. 2018). Haryana, often called the 'agricultural hub of India,' contributes 6.9 percent of India's food grain production (Tripathi & Gupta 2021). Thus, efforts to strengthen the irrigation infrastructure are of utmost significance, as water stress in Haryana poses a nationwide food security threat (Grewal et al. 2021). In view of the significance of agricultural activities, irrigation channels hold the utmost significance in this region, given the scant rainfall. These channels, however, are in a dismal state and call for rehabilitation/repair. To add, there is huge water loss due to mismanagement and the poor state of the canals. Considerable seepage loss is a major factor contributing to low water-use efficiency when water is conveyed to the fields by an irrigation system. This seepage loss not only reduces the water efficiency of the canal system but also reduces the quality of groundwater through soil salinization and waterlogging (Han et al. 2020).

Urgent remedial measures are, therefore, imperative in the direction of conservation to desist from the current situation of extreme water stress in the country. The suggestion of sustainable water conservation and management practices is thus a major concern that the present study aims to address. From this, the following secondary objectives have further been framed. First, to assess the impact of socio-demographic factors on water conservation and management practices. Second, to discern the impact of the current irrigation system on water conservation and management practices. Third, to study the impact of cost-benefit perception on the adoption of water conservation measures. Fourth, to suggest likely sustainable initiatives for water conservation and management.

Given the deficient water supply in the southwestern region of Haryana, canal irrigation is a preferred medium for agricultural activities. Therefore, the present study has been undertaken to study the perception of the farmers and suggest improvement measures in the overall irrigation system to ensure judicious use and conservation of water. This study contributes to the literature in several ways. First, there is a dearth of empirical evidence suggesting a holistic framework for designing efficient water conservation and management practices in irrigation. The present study aims to fill this gap in the literature. Second, first-hand responses from farmers of

Haryana obtained for the present study provide a unique data set for the implementation of technology-based reform in the agriculture and irrigation sector. Third, the study provides rare evidence of the impact of socio-demographic variables, current irrigation system, and cost-benefit perception of the farmers on water conservation and management through robust statistical analysis. Overall, the present research will be of vital significance for the practitioners, policy-makers, and the public at large.

Literature Review and Hypothesis Development

Keeping in view the objectives of the study, relevant literature has been classified into the following three sub-strands: impact of socio-demographic factors on water conservation and management practices, impact of current irrigation system on water conservation and management practices, and impact of cost-benefit perception of farmers on water conservation and management practices.

Impact of socio-demographic factors on water conservation and management practices: In designing efficient water conservation policies, many studies have explored the role of the socio-demographic profile of the respondents. For instance, Verdugo et al. (2006) established that age and gender significantly impact the water conservation viewpoints of the respondents by studying the responses of 300 individuals (140 males and 160 females) from randomly selected 100 Mexican households. Accordingly, older people and females were found to be more inclined towards conserving water. Similarly, Fan et al. (2014), taking a sample of 776 households across 16 villages in the rural Wei River Basin, found that gender and education determine the perception of water consumption by individuals. In this study, males/younger population underestimated their water consumption, whereas women and the elderly could accurately estimate this pattern.

Recently, Jaafar & Kharroubi (2021), in a study of 678 farmers in Lebanon, established that a significant role is played by socio-demographic factors, like age, nationality, and geographical area, in determining the use of smart irrigation mobile applications. Accordingly, young farmers, as compared to the older ones, were more likely to adopt smart irrigation technology. The level of education, however, exerted no influence on the adoption of smart irrigation technology in this study. Contrary to these findings, Garcia et al. (2014), through a face-to-face survey of 234 Spanish households, established that water conservation campaigns should be targeted towards more educated groups by the authorities to increase the level of awareness of water scarcity. The majority of the related literature, thus, reiterated the general theoretical supposition regarding the impact

of socio-demographic factors on water conservation and management (e.g., Verdugo et al. 2006, Jaafar & Kharroubi 2021). From this, the following may be hypothesized:

H1: There is a significant impact of socio-demographic factors on water conservation and management practices

Impact of current irrigation system on water conservation and management practices: The impact of the current irrigation system on water conservation and management efficiency has often been deliberated on in literature (Lecina et al. 2010, Ahmadzadeh et al. 2016). In India, the current canal irrigation system needs a major overhaul (Afroz & Singh 2007, Shah 2011). In a survey of 10 major canal command areas in India, Singh et al. (2004) found that an alarming proportion of respondents (44 percent) had unfavorable attitudes toward canal irrigation. Various reasons were stated for this dissatisfaction, like the faulty alignment of canals resulting in water scarcity during crucial periods of the year, water logging during the rainy season, poor maintenance and upkeep of the canal water distribution system, lack of proper monitoring by the officer concerned, and the like. These reasons were attributed to the inefficient performance of irrigation administration, low orientation towards operations and maintenance, and the institutional gap with respect to the maintenance of minor canals. Amarsinghe et al. (2021) further emphasized that low water-use efficiency and productivity, as well as the expanding gap between irrigation potential used and irrigation potential created, are important challenges in canal irrigation performance in India.

One of the most critical repercussions of this deterioration in the canal irrigation system is the establishment of a pump irrigation economy, which has caused damage to groundwater resources (Shah 2011). Furthermore, the replenishment rate of groundwater is not in sync with its depletion rate (Jakeman et al. 2016). In this context, Johansson et al. (2002) pointed out that while it is difficult to apportion surface water to competing consumers, draining groundwater has an impact on resource accessibility for future generations. Declining quality is another stark feature, making groundwater unfit for agricultural use (Bhala 2007). Gebremeskel et al. (2018), in a study conducted in the semi-arid Tigray region in Northern Ethiopia, further exclaimed that using more and more groundwater for irrigation increases the salinity of the soil, thereby reducing agricultural productivity. Therefore, increasing the use of groundwater may be expensive. In addition, Barmakova et al. (2022) conducted a study in the Karatal district of the Republic of Kazakhstan. They established that well-managed irrigation practices like monitoring water quality are vital for maintaining groundwater quality.

Jaafar & Kharroubi (2021) furthermore established that while the majority of participants (about 69 percent) preferred

groundwater for irrigation, others showed a preference for canal water (around 12 percent); a faint minority (nearly 7 percent) preferred a combination of both or other irrigation sources. The study highlighted that one of the most important factors that can help farmers optimize their water use is irrigation timing (Jaafar & Kharroubi 2021). It is thus essential to understand the current availability of water in the canal irrigation system and study its impact on conservation practices (e.g., Lecina et al. 2010, Hrozencik et al. 2022). A variety of opinions of the theorists about different sources require an assessment of the current pattern of irrigation in the region of the study to suggest an optimal channel for irrigation. Therefore, the following may be hypothesized:

H2: There is a significant impact of the current irrigation system on water conservation and management practices

Impact of cost-benefit perception of farmers on water conservation and management practices: Among others, farmers' perceptual stance has a major implication on their water conservation and management initiatives (Singh et al. 2004). Knox, Kay & Weatherhead (2011), in a perception study of farmers from the temperate region of England, asserted that efficient use of water resources not only enhances farmers' value (financial benefits) but also helps build sustainable rural communities. The authors suggested the use of this pathway for efficient water use to achieve better irrigation management. A recent example has, further been presented by Han et al. (2020) in their study of the arid region of the Renmin branch canal irrigation district. The study clearly shows that building and regular service of canal lining is vital for reducing seepage loss. As compared to no lining, an interesting finding of the study was that building canal lining using concrete and geomembrane results in a considerable (86 percent) reduction in water loss due to seepage.

Furthermore, the need for smooth delivery of canal water to the fields cannot be overemphasized (Flynn & Marino 1987, Tyagi 2019). Delivery structures, thus, play a vital role in improving water conveyance efficiency. According to the study conducted by Singh et al. (2006) in Hisar (district of Haryana), 34-43 percent of the canal water is lost due to seepage from the conveyance system. In conjunction, Sultan et al. (2014), in a comparative analysis of developing nations, found the water conveyance loss in lined water courses to be lesser than that in unlined ones. Thus, the type of canal lining is a crucial factor for ensuring better water use efficiency. Accordingly, rehabilitation and development of the canals and water courses are required to ensure sustainable water use.

Expressing a corollary view, Singh et al. (2004), through a perception survey of 100 farmers (selected through stratified random sampling) of the command area of Odisha, found that

the majority of the respondents (56 percent) had a favorable outlook towards the role of canal irrigation in cultivation. A major portion (70 percent) of the 50 farmers selected from the non-command areas also reiterated the need for canal irrigation for better yield and income. Further, according to Morita (2021), the quantity and quality of water distributed to farmers should be optimally managed by means of effective irrigation scheduling and implementation of appropriate irrigation technologies on suitable soils. However, the high cost of infrastructure changes, a lack of storage dams, and the unjust water distribution system in irrigation schemes restrain farmers from being more efficient (De Clercq et al. 2021). Water utilization for agricultural output in water-scarce regions, thus, necessitates innovative and long-term research as well as suitable technology transfer (Jaafar & Kharroubi 2021, Lecina et al. 2010). From the above, we hypothesize:

H3: There is a significant impact of the cost-benefit perception of farmers on water conservation and management practices

MATERIALS AND METHODS

Data Collection

The data for the present study has been collected through a survey of the farmers of the Haryana region of India from October 2021 to February 2022. The southwestern region of the Haryana state faced severe droughts/famines during 1966, 1968, and 1987. The solution to counter water scarcity in the region was addressed by the construction of the Jawahar Lal Nehru (JLN) Feeder. JLN Feeder is currently the main channel stretching over 104 kilometres (RD 0 to 343100), which off-takes from Khubru Head at RD 145250/R of Delhi Parallel Branch. JLN Feeder is the lifeline of Southern Haryana, catering to the irrigation and drinking water needs of Rohtak, Jhajjar, Rewari, Narnaul, and Bhiwani districts, having a discharge capacity of 3541 Cs. at the head. The five districts (Rohtak, Jhajjar, Rewari, Narnaul, and Bhiwani) to which the JLN Feeder caters have been identified as five distinct strata, and respondents fulfilling the pre-specified criteria have been randomly selected from each stratum. The Ethical Clearance Certificate before conducting the survey was obtained from the Institutional Ethics Committee of the affiliated institution of the authors.

For the present study, the perception of the farmers has been studied using two potent techniques: focused group discussions and self-administration of questionnaires. One-to-one interaction enabled the observation of the perception of the farmers on canal lining as a water conservation and management measure. Focused group discussions, moreover,

enabled the identification of certain latent constructs that are of significance from a water conservation point of view. To investigate the perceived and expected impact of lining by the population, focus group discussions were conducted. Focus group research involves formal discussions with a selected group of people to address a specific issue. To facilitate the exchange of opinions, the groups should be as homogeneous as possible. These discussions are considered a suitable method to investigate various perceptions and values of groups of people about a certain topic. A trained local facilitator, along with the first author, conducted ten focus group discussions with 5–10 participants each, men and women separately. Discussions were held across 5 different district locations within the state of Haryana served by the JLN Feeder. The topics of discussion were current water availability, expected or actual consequences of irrigation canal lining, and perception and valuing of possible changes and training for the conservation of water.

A structured questionnaire was self-administered to 200 respondents, out of which 125 usable responses could be obtained. The sample was drawn equally from each district. The respondents selected for the present study either owned their farms or worked on rented farms on a sharing basis. For participating in the survey, the following riders were used to select the respondents (farmers) for the present study. First, the farmers below 18 years of age were excluded from the purview of the study. Second, given their small landholding, farmers who reported owning land less than 1 hectare were excluded from the study. Third, only farmers capable of reading, understanding, and interpreting the survey instrument were included in the study. Those with any mental disability were excluded from the study. Fourth, for inclusion in the survey, the respondent must be familiar with either English or Hindi language. Consent of the farmers, who met the premeditated research criteria, was obtained after explaining to them all relevant information (study objectives, potential risks, and benefits of participation in the survey) regarding the survey. The willing and informed participation of the sample respondents was, thus, obtained to depict a true and fair view of the farmers' perception of water conservation and management practices. Farmers meeting the above-specified criteria were thereafter randomly selected for the present study.

Survey Instrument

Data for the present study was collected by the first author, accompanied by field investigators in a private setting. Two field investigators, well-versed in the local language/dialect of the inhabitants of the region, were appointed to facilitate data collection. This ensured effective communication and

better observation of various latent constructs. Selected farmers filled out a multi-dimensional questionnaire during a personal interview session of 10-30 minutes. Initially, the questionnaire was developed in English. Subsequently, it was translated into Hindi (since the majority of the respondents were well-versed in the Hindi language). Thereafter, to check whether the questionnaire qualified for parallel-form reliability, it was re-translated into English. Disagreement, if any, in the re-translated version was corrected to enhance the efficiency of the instrument in capturing the views of the respondents. At the time of the interview, both Hindi as well as English versions were used depending upon the preference of the respondents.

The survey instrument was bifurcated into various sections. Section 1 on the demographic profile of the respondents included questions such as age, gender, district, education, etc. Section 2 aimed to evaluate the current irrigation system. Questions like the type of canal lining in the area, major crops sown by them, and their current use of groundwater were delved into in this section of the questionnaire. Section 3 gauged the cost-benefit perception of the respondents. Response to questions like willingness to pay the additional amount for better access to canal water throughout the year and impact on the availability of water and area under irrigation after building concrete lining of the canal was obtained.

Further, questions on perceived change in water use efficiency and conveyance efficiency were also asked. The last section studied the water conservation measures and management practices preferred by the respondents. In the majority of the questions, a five-point Likert scale was used to obtain the degree of agreement and disagreement where 1, strongly disagree and 5, strongly agree. A pilot study was conducted on a sample of 15 farmers to test the consistency and clarity of the survey instrument. The value of Cronbach's Alpha was further examined to assess the internal consistency of the instrument. The coefficient alpha estimates were found to be within the high-reliability category (i.e., greater than 0.70). The scale was thus considered appropriate to be used for the study.

Conceptual Model and Framework for Analysis

The conceptual framework to study the impact of socio-demographic variables, the current irrigation system in the region, and the cost-benefit perception of farmers on water conservation and management practices has been demonstrated in Fig 1. Socio-demographic variables (gender, education, district, and age), current irrigation system (current use of groundwater, preference of canal water over groundwater), and cost-benefit perception of farmers (willingness to pay additional charges, increase in availability of water, benefit crop yield, improvement in economic status, and increase in water conveyance and water

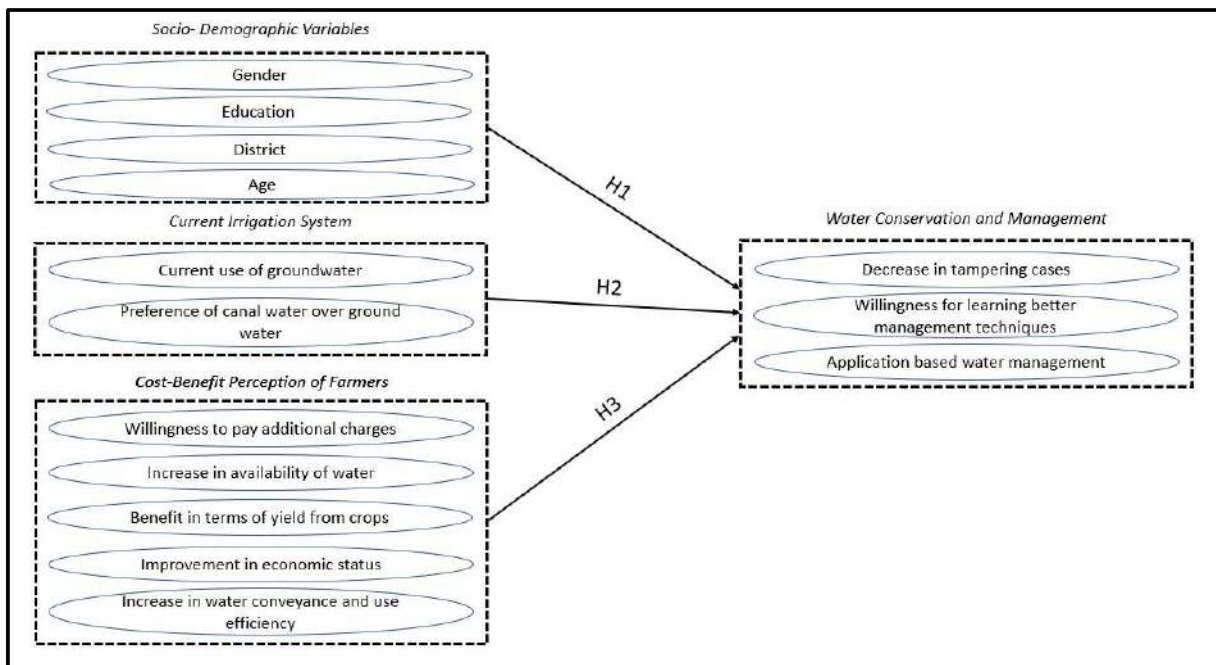


Fig. 1: Conceptual Framework and Hypotheses.

Table 1: Description of Variables.

Measure	Variable	Symbol	Description
Panel A: Dependent Variables			
Water Conservation and Management	Decrease in tampering cases	<i>DTAMP</i>	Impact on tampering cases with regards to the canal irrigation water
	Willingness to learn better management techniques	<i>WLT</i>	Evaluation of willingness of respondents to learn (e.g., undertaking training) better water management techniques for sustainable water use
	Application-based water management	<i>ABWM</i>	The willingness of respondents to use application-based water management techniques
Panel B: Independent Variables			
Socio-Demographic Variable	Age	<i>AGE</i>	Age of the respondents in years
	Gender	<i>GENDER</i>	The gender of the respondents
	Education	<i>EDU</i>	The level of education of the respondents
	District	<i>DIST</i>	Districts of respondents in which the survey was administered
Current Situation of Irrigation System	Groundwater Use	<i>GWU</i>	Current usage level of groundwater in the region of respondent
	Preference of Canal Water over Groundwater	<i>PCW</i>	The preference of respondents for canal water over groundwater for irrigation
Cost-Benefit Perception of Farmers	Willingness to pay additional charges	<i>WPAC</i>	Willingness to pay for additional charges for canal irrigation
	Increase in the availability of water.	<i>IAW</i>	Perception of availability of water in the respondent's region due to canal lining
	Benefit crop yield	<i>BCY</i>	The benefit of the lining of canal/water courses on yield from crops
	Improvement in economic status	<i>ECOSTAT</i>	Whether there has been an improvement in economic status due to canal lining
	Increase in water conveyance efficiency and water use efficiency	<i>IWCUE</i>	Perception of water use efficiency in the region due to canal lining

use efficiency) have been taken as independent variables. Three separate models with dependent variables: willingness to learn better management techniques, decrease in tampering cases, and application-based water management denoting water conservation and management practices have been formulated. The variables have been defined in Table 1. After establishing a basic association between the variables through correlation analysis, the hypothesized relationship will be ascertained through ordinal regression analysis. The respondents (farmers) did not influence the design, conduct, or reporting of the survey.

RESULTS AND DISCUSSION

Focused Group Discussions

The discussions with the farmers helped analyze the cropping pattern followed in the region. The following findings have been derived:

- The current use of groundwater was discussed, and it was concluded that the groundwater in the region is saline, leading to irrigation-related issues for the farmers. The CC irrigation system is likely to bring better water conveyance efficiency and ultimately help in water conservation.

- Farmers demonstrated interest in receiving training in modern agriculture technology and an app-based system for monitoring irrigation in the fields, which is also a stepping stone for sustainable agriculture.

It was, therefore, apparent that farmers are willing to seek assistance from agricultural officers and extension workers on the employment of better irrigation technologies. Through water users' associations and regular meetings on the use of modern technologies and water-saving methods to combat the problems of waterlogging and salinity in the command area, better irrigation systems can thus be put in place.

Table 2 presents the descriptive statistics of the variables under consideration for the present study. The table provides the mean and standard deviation of the key variables. As reported, the average decrease in tampering cases (*DTAMP*) has been observed to be 4.52, which denotes that the water conservation and management measures are in place. The mean value of other dependent variables (*WLT* and *ABWM*) also portrays the willingness of the farmers to undertake water conservation and management practices. Amongst the independent variables, *GWU* having a mean value of 4.59 signifies a high use of groundwater in the region of the study. While there is high current usage of groundwater, preference for canal water is yet clearly highlighted by the

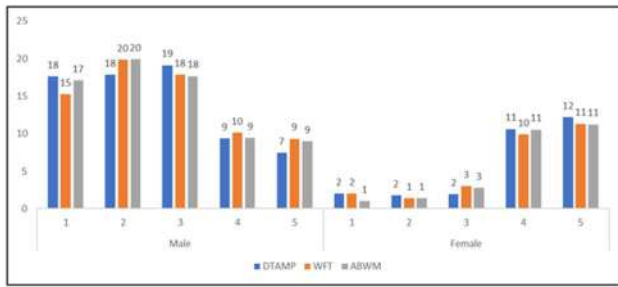


Fig. 2a: District-wise perception of farmers on water conservation and management on the basis of the gender (in %)

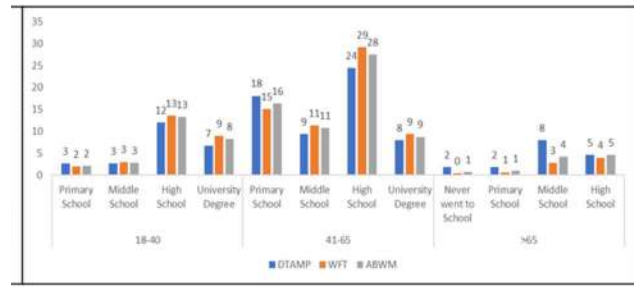


Fig. 2b: Perception of farmers on water conservation practices on the basis of the age and education (in %)

Table 2: Descriptive Statistics

Variables	Mean	Stdeviation
DTAMP	4.520	0.947
WLT	4.030	1.492
ABWM	3.490	0.989
DIST	3.000	1.420
GENDER	1.270	0.447
AGE	1.930	0.624
EDU	2.460	1.051
GWU	4.590	0.742
PCW	4.110	1.259
WPAC	4.030	1.170
IAW	4.280	1.209
BCY	4.230	1.033
ECOSTAT	2.740	0.556
IWCUE	4.500	0.997

Source: Author’s analysis.

Note: Data of 125 respondents' has been presented in the table.

mean value of 4.11 for PCW. Additionally, the mean results demonstrate the expectation of an increase in the availability of water (IAW= 4.28) and increased crop yield (BCY= 4.23). Similarly, the average value of IWCUE observed to be 4.50 indicates a perception of farmers on improvement in water conveyance and use efficiency as a result of the rehabilitation of canal lining.

As shown in Fig. 2a, the male population from the 1st, 2nd, and 3rd districts demonstrated greater vigor for the adoption of water conservation and management practices compared to their female counterparts in other districts. Further, as shown in Fig. 2b, farmers who went to high school and are in the age group of 41-65 years showed higher interest in undertaking water conservation and management measures.

Bivariate correlation coefficients of Spearman’s rho and Kendall’s tau-b have been reported in Table 3. These correlation coefficients establish the strength of the

relationship between variables with rank orders. Statistically significant correlations with a very high correlation coefficient have been observed between ECOSTAT and DTAMP, as well as between IWCUE and DTAMP. Furthermore, statistically significant associations with high correlation coefficients have been observed between variables IAW and BCY, ECOSTAT and IAW, ECOSTAT and BCY, IWCUE and IAW, and IWCUE and BCY.

Further, significant correlations have been observed between IWCUE and ECOSTAT. This is a cause of concern for the computation of the regression models as the correlation coefficient is higher than the acceptable limit (as per the rule of thumb) of 0.50. The problem of multicollinearity arises due to such high correlations. Variance inflation factors (VIFs) have been further utilized as a formal measure of multicollinearity. The VIFs were found to be within the limit of 10 (Mansfield & Helms 1982). Nonetheless, the variables IWCUE and ECOSTAT were included one at a time in the regression models to obtain robust results.

The results have been obtained through ordinal regression analysis. Variables with a ratio or ordinal scale are used as covariates, while variables with categorical responses are taken as factor variables. The impact of socio-demographic factors, current irrigation system, and cost-benefit perception has been regressed on water conservation and management practices. This impact has been analyzed using ordinal regression coefficients by formulating Model 1, Model 2, and Model 3.

The results obtained from the model fitting information of regression analysis, as reported in Table 4, show significant chi-square statistics in all the models. This implies that all models are a significant improvement over the intercept-only model. Thus, the model has better prediction power than a mere guess.

Analysis of the Impact of Socio-Demographic Factors on Water Conservation and Management Practices

Table 5 presents the results of the regression analysis.

Table 3: Non-Parametric Correlations.

	DTAMP	WLT	ABWM	DIST	GENDER	AGE	EDU	GWU	PCW	WPAC	IAW	BCY	ECOSTAT	IWCUE
Kendall's tau_b	DTAMP	1.000	-0.025	-0.016	0.078	-0.028	-0.079	0.016	0.532**	0.612**	0.641**	0.689**	0.920**	0.921**
	WLT	-0.025	1.000	0.812**	0.080	-0.109	-0.477**	-0.064	-0.043	0.067	-0.120	-0.102	-0.091	-0.088
	ABWM	-0.016	0.812**	1.000	0.070	-0.086	-0.441**	0.371**	-0.090	0.051	-0.092	-0.085	-0.060	-0.073
	DIST	0.078	0.080	0.070	1.000	0.478**	-0.040	-0.002	-0.152*	-0.058	-0.004	0.133	0.038	0.064
	GENDER	-0.028	-0.109	-0.086	0.478**	1.000	0.043	-0.094	0.008	-0.139	-0.115	0.038	-0.048	-0.029
	AGE	-0.079	-0.477**	-0.441**	-0.040	0.043	1.000	-0.274**	-0.038	-0.043	-0.215**	-0.011	-0.014	-0.055
	EDU	-0.046	0.405**	0.371**	-0.002	-0.094	-0.274**	1.000	0.007	-0.068	0.010	-0.019	-0.083	-0.081
	GWU	0.016	-0.064	-0.005	-0.075	0.008	-0.038	0.007	1.000	-0.026	-0.082	0.020	0.015	-0.002
	PCW	0.532**	-0.043	-0.090	-0.152*	-0.139	-0.043	-0.068	-0.026	1.000	0.627**	0.617**	0.454**	0.584**
	WPAC	0.612**	0.067	0.051	-0.058	-0.115	-0.215**	0.010	-0.082	0.627**	1.000	0.641**	0.528**	0.601**
	IAW	0.641**	-0.120	-0.092	-0.004	-0.101	-0.011	-0.019	0.020	0.617**	0.641**	1.000	0.688**	0.714**
	BCY	0.689**	-0.102	-0.085	0.133	0.038	-0.014	-0.083	0.015	0.454**	0.528**	0.688**	1.000	0.733**
	ECOSTAT	0.920**	-0.091	-0.060	0.038	-0.048	-0.052	-0.067	-0.002	0.584**	0.601**	0.714**	0.733**	1.000
	IWCUE	0.921**	-0.088	-0.073	0.064	-0.029	-0.055	-0.081	0.046	0.568**	0.617**	0.705**	0.750**	0.964**
Spearman's rho	DTAMP	1.000	-0.026	-0.017	0.088	-0.029	-0.085	0.018	0.594**	0.673**	0.699**	0.750**	0.950**	0.951**
	WLT	-0.026	1.000	0.863**	0.094	-0.116	-0.525**	-0.069	-0.048	0.080	-0.133	-0.116	-0.098	-0.095
	ABWM	-0.017	0.863**	1.000	0.080	-0.089	-0.478**	0.426**	-0.102	0.061	-0.102	-0.093	-0.064	-0.078
	DIST	0.088	0.094	0.080	1.000	0.534**	-0.046	-0.001	-0.187*	-0.078	-0.007	0.152	0.044	0.074
	GENDER	-0.029	-0.116	-0.089	0.534**	1.000	0.045	-0.103	0.008	-0.149	-0.107	0.041	-0.049	-0.030
	AGE	-0.085	-0.525**	-0.478**	-0.046	0.045	1.000	-0.315**	-0.040	-0.049	-0.243**	-0.013	-0.056	-0.060
	EDU	-0.052	0.466**	0.426**	-0.001	-0.103	-0.315**	1.000	0.008	-0.078	0.010	-0.023	-0.074	-0.089
	GWU	0.018	-0.069	-0.005	-0.087	0.008	-0.040	0.008	1.000	-0.030	-0.091	0.021	-0.019	0.048
	PCW	0.594**	-0.048	-0.102	-0.187*	-0.149	-0.049	-0.078	-0.030	1.000	0.690**	0.676**	0.528**	0.620**
	WPAC	0.673**	0.080	0.061	-0.078	-0.124	-0.243**	0.010	-0.091	0.690**	1.000	0.708**	0.599**	0.675**
	IAW	0.699**	-0.133	-0.102	-0.007	-0.107	-0.013	-0.023	0.021	0.676**	0.708**	1.000	0.733**	0.747**
	BCY	0.750**	-0.116	-0.093	0.152	0.041	-0.015	-0.095	0.019	0.528**	0.599**	0.733**	1.000	0.795**
	ECOSTAT	0.950**	-0.098	-0.064	0.044	-0.049	-0.056	-0.074	-0.002	0.632**	0.655**	0.753**	0.769**	0.972**
	IWCUE	0.951**	-0.095	-0.078	0.074	-0.030	-0.060	-0.089	0.048	0.620**	0.675**	0.747**	0.795**	1.000

** Correlation is significant at the 0.01 level (2-tailed).

* Correlation is significant at the 0.05 level (2-tailed).

Table 4: Model Fitting Information.

Dependent Variable	Model	Model	-2 Log Likelihood	Chi-Square	d.f.	Sig.
DTAMP	(a) $DTAMP = f(AGE, GENDER, EDU, DIST, GWU, PCW, WPAC, IAW, BCY, ECOSTAT)$	Intercept Only	193.376			
		Final	122.673	70.703	13.000	0.000
	(b) $DTAMP = f(AGE, GENDER, EDU, DIST, GWU, PCW, WPAC, IAW, BCY, IWCUE)$	Intercept Only	193.376			
		Final	54.510	138.866	13.000	0.000
WLT	(a) $WLT = f(AGE, GENDER, EDU, DIST, GWU, PCW, WPAC, IAW, BCY, ECOSTAT)$	Intercept Only	253.725			
		Final	159.319	94.406	13.000	0.000
	(b) $WLT = f(AGE, GENDER, EDU, DIST, GWU, PCW, WPAC, IAW, BCY, IWCUE)$	Intercept Only	253.725			
		Final	160.119	93.606	13.000	0.000
ABWM	(a) $ABWM = f(AGE, GENDER, EDU, DIST, GWU, PCW, WPAC, IAW, BCY, ECOSTAT)$	Intercept Only	230.927			
		Final	174.946	55.981	13.000	0.000
	(b) $ABWM = f(AGE, GENDER, EDU, DIST, GWU, PCW, WPAC, IAW, BCY, IWCUE)$	Intercept Only	230.927			
		Final	174.887	56.040	13.000	0.000

Link function: Logit

In Model 1, the results obtained by regressing socio-demographic variables (*AGE* and *EDU*) on *DTAMP* exhibited a negative impact. However, the insignificance of these results precludes reliance, and thus, *H1* is rejected in the case of Model 1 (A) and (B). The results highlight that *AGE* and *EDU* variables have no bearing on the decrease in the number of tampering cases in the region. In the case of Model 2, *AGE*, however, has a highly significant negative impact in both the models (Model 2(A): *Coeff.* = -1.880, $p < 0.01$; Model 2(B): *Coeff.* = -1.859, $p < 0.01$). This negative impact implies that with an increase in age, farmers' willingness to undertake training decreases. Additionally, *EDU* has a highly significant positive impact in the case of Model 2 (Model 2(A): *Coeff.* = 1.283, $p < 0.01$; Model 2(B): *Coeff.* = 1.234, $p < 0.01$). So, with an increase in the level of education, the farmers demonstrated a higher willingness to undertake training. Overall, from the results of Model 2, *H1* stands accepted, implying thereby that both *AGE* and *EDU* play a vital role in determining farmers' willingness to undertake training for water conservation and management. Similar results have been obtained by testing the impact of socio-demographic variables *AGE* (*Coeff.* = -1.135, $p < 0.01$) and *EDU* (*Coeff.* = 0.868, $p < 0.01$) on *ABWM* through Model 3 (B). *H1* is thus accepted in the given case. On the contrary, Model 3 (A) demonstrated insignificant estimates, and thus, *H1* is rejected for this model. In sum, the results demonstrate that with increasing levels of education, farmers' willingness to adopt water conservation and management measures improved. However, with an increase in age, the resistance to adopting water conservation and management practices also saw a surge in the present study. These results are in consonance with that of Jaafar & Kharroubi (2021).

Analysis of the Impact of Current Irrigation System on Water Conservation and Management Practices

From the results of Model 1 and Model 2, the impact of the current irrigation system in use on water conservation and management practices is statistically insignificant, thus leading to the rejection of *H2* in the case of both these models. This implies that the current usage of the irrigation system in the region does not influence the adoption of water conservation and management practices (*DTAMP* and *WLT*). On the contrary, a significant negative influence of *GWU* (*Coeff.* = -0.006, $p < 0.01$) and *PCW* (*Coeff.* = -0.031, $p < 0.01$) on *ABWM* has been observed under Model 3 (A). *H2* thus stands accepted in the case of Model 3. It can be inferred that the current pattern of groundwater usage for irrigation and preference for canal water over groundwater demonstrate a negative impact on the application-based water management methods for water conservation.

Further, it signifies that the farmers currently rely highly on groundwater for irrigation, and those who prefer canal water over groundwater demonstrated a negative interest in application-based water management. Likewise, Jaafar & Kharroubi (2021), in their study on smart irrigation apps, demonstrated that the majority of the participants in their study used groundwater for irrigation, followed by canal water and a combination of groundwater and canal water. They emphasized that one of the critical factors for farmers to optimize water use was irrigation scheduling. Further, in a study on the adoption of modern irrigation methods by Gebremeskel et al. (2018), it was found that earlier experience with the use of irrigation systems is a critical factor for the adoption of new systems in the region of the study.

Table 5: Regression Results of the Impact of Socio-Demographic Characteristics, Current Irrigation System and Cost-Benefit Perception of Farmers on Water Conservation and Management Practices.

Independent variables	Model 1				Model 2				Model 3			
	DTAMP				WLT				ABWM			
	A	B	Coefficient	Std. error	A	B	Coefficient	Std. error	A	B	Coefficient	Std. error
Dependent Variable												
1	-3.938***	0.881	-11.728***	2.275	-3.460***	0.742	-3.454***	0.738	-3.994***	0.747	-3.985***	0.747
2	-2.997***	0.822	-8.626***	1.782	-1.355**	0.626	-1.347**	0.621	-1.248**	0.548	-1.235**	0.549
3	-1.256*	0.749	-3.205**	1.427	-1.003	0.619	-0.997	0.614	-0.963*	0.542	-0.95*	0.543
4	-1.016	0.744	-0.725	1.237	-0.440	0.614	-0.444	0.608	5.065***	0.831	5.075***	0.831
Covariate Variables												
AGE	-0.039	0.291	-0.253	0.495	-1.880***	0.350	-1.859***	0.349	-1.131	0.271	-1.135***	0.271
EDU	-0.050	0.274	0.063	0.435	1.283***	0.282	1.234***	0.277	0.876	0.241	0.868***	0.242
GWU	0.057	0.273	-0.114	0.407	-0.561	0.360	-0.482	0.350	-0.006**	0.244	0.000	0.242
PCW	-0.032	0.551	0.395	0.877	0.472	0.500	0.426	0.500	-0.031***	0.471	-0.038	0.468
WPAC	0.707	0.490	0.675	0.725	1.104**	0.537	1.268**	0.538	0.649	0.474	0.681	0.478
IAW	-0.476	0.561	-0.435	0.800	-1.027*	0.596	-1.197**	0.593	-0.198	0.524	-0.217	0.515
BCY	0.604	0.571	1.329	0.857	0.132	0.588	0.161	0.619	-0.338	0.507	-0.298	0.531
ECOSTAT	1.514***	0.570	-	-	-1.127*	0.604	-	-	-0.195	0.500	-	-
IWCUE			2.878***	0.873			-1.066*	0.624			-0.241	0.534
Factor Variables												
District												
District=1	-0.399	0.899	-0.258	1.414	-2.268**	1.040	-2.266**	1.035	-0.912	0.816	-0.908	0.816
District=2	0.357	1.021	3.337*	1.903	-1.002	1.065	-1.085	1.053	-0.269	0.829	-0.249	0.833
District=3	0.504	0.908	1.298	1.540	-0.102	1.065	-0.022	1.070	-0.045**	0.812	-0.010	0.822
District=4	0.648	1.014	3.308*	1.958	1.498*	0.880	1.537*	0.881	0.616	0.742	0.645	0.747
District=5	0.000	.	0.000	.	0.000	.	0.000	.	0.000	.	0.000	.
Gender												
Gender=1	-0.057	0.744	0.179	1.241	2.104**	0.833	2.028**	0.823	0.897	0.623	0.890	0.622
Gender=2	0.000	.	0.000	.	0.000	.	0.000	.	0.000	.	0.000	.
Negelkerke Pseudo R-squared (%)	54.900		85.200		60.300		59.900		42.500		42.500	
Test of Parallel Lines												
Chi square	67.494***		54.510*		35.841		48.888		107.686***		108.289***	
Pearson's Goodness of Fit												
Chi square	901.810***		237.139		512.077***		479.139*		748.385***		744.651***	

Note: (1) Regression estimates have been computed for a sample of 125 respondents. (2) *, **, ***, respectively, indicates significant at the 10 percent, 5 percent, and 1 percent levels. Source: Author's analysis.

Analysis of the Impact of Cost-Benefit Perception of Farmers on Water Conservation and Management Practices

In the case of Model 1 (A), the results of the impact of cost-benefit perception of farmers on water conservation and management practices depicted that *ECOSTAT* exerted a highly significant positive impact ($Coeff.= 1.514, p<0.01$) on *DTAMP*. Similarly, in Model 1 (B), *IWCUE* exerted a highly significant positive impact ($Coeff.= 2.878, p<0.01$) on *DTAMP*. On the contrary, the variables *ECOSTAT* ($Coeff.= -1.127, p<0.1$) and *IWCUE* ($Coeff.= -1.066, p<0.1$) have a negative impact on *WLT* as reflected by the results of Model 2 (A) and (B). This implies that as the perception of economic status improves and the water conveyance and use efficiency increases, the willingness to undertake training takes a toll. Furthermore, *WPAC* exerted a significantly high positive impact on *WLT* (Model 2(A): $Coeff.= 1.104, p<0.05$; Model 2(B): $Coeff.= 1.268, p<0.05$). This demonstrates that the farmers who are willing to pay additional charges are also supportive of undertaking training to learn modern technology in irrigation. Contrarily, a significant negative influence of *IAW* has been observed on *WLT* as reported in Model 2 (Model 2(A): $Coeff.= -1.027, p<0.10$; Model 2(B): $Coeff.= -1.197, p<0.05$). This reflects that with an increase in the availability of water in the region, the farmers' willingness to undertake training for better management techniques decreases. Nevertheless, *H3* stands accepted for both Model 1 and Model 2 due to the significance of the present results. On the other hand, none of the variables has shown a significant impact in the case of Model 3, implying thereby that the cost-benefit perception of farmers has no impact on *ABWM*. This leads us to reject *H3* in this case. Overall, *H3* is accepted in the case of *DTAMP* and *WLT*, which signals that farmers believe that there has been a decline in tampering cases post-canal construction and are willing to undertake training for better conservation and management. Like the present study, Burt & Styles (1999), in a study of modern water control and management practices, also recommended that there exists greater potential to

improve water management through increased conveyance and use efficiency as well as by undertaking optimized delivery measures.

In total, *H1* postulating a significant impact of socio-demographic variables on water conservation and management practices has been accepted as per the results of Models 2 (A), 2 (B), and 3 (B). This, therefore, signifies the direct influence of *AGE* and *EDU* on the willingness to undertake training and adoption of application-based water management techniques by the farmers. Further, *H2* has been accepted only in the case of Model 3 (A), thereby implying that the current irrigation system exerts a major impact only on the perceptual use of application-based water management techniques. Finally, *H3* stands accepted in a majority of the models under investigation, viz., Model 1 (A), 1 (B), 2(A), and 2 (B). Thus, the high influence of the cost-benefit perception of farmers can be established in the decrease in tampering cases and farmers' willingness to undertake training. The overall results of the study have been summarized in Table 6.

Robustness Tests

Several measures to establish the robustness of the results have been undertaken. First, Cox & Snell (in the range of 36.1-67.1%) and McFadden (in the range of 23.6-71.8%) pseudo R squares were computed in addition to Nagelkerke R square for the likelihood estimation measures in ordinal regression. Comparable results have been deduced using these alternative R square measures. Secondly, multiple linear regression with bootstrapped standard errors has been computed as an alternative measure of analysis. Broadly similar inferences have been derived using this alternate specification. For the sake of brevity, the results obtained have not been elaborated here.

CONCLUSION

The present study highlights the importance of steps required in the direction of sustainable water conservation and

Table 6: Overall results.

Hypotheses	Description	Results					
		Model 1 DTAMP		Model 2 WLT		Model 3 ABWM	
		A	B	A	B	A	B
H1	There is a significant impact of socio-demographic factors on water conservation and management practices.	Reject	Reject	Accept	Accept	Reject	Accept
H2	There is a significant impact of the current irrigation system on water conservation and management practices.	Reject	Reject	Reject	Reject	Accept	Reject
H3	There is a significant impact of the cost-benefit perception of farmers on water conservation and management practices.	Accept	Accept	Accept	Accept	Reject	Reject

management practices. Concrete canal lining is deemed an appropriate measure for sustainable irrigation along with other modern technology-driven practices, such as app-based monitoring and irrigation control, that help in efficient water management. The results of the study demonstrated that socio-demographic variables play a key role in the acceptance of modern irrigation practices and willingness to adopt water conservation practices. Further, the farmers also demonstrated a willingness to pay additional charges for canal water. The respondents also believed that by undertaking training there is a likelihood of an increase in the availability of water in the region by efficient management of irrigation practices. The results further point out that there is an expectation of a decrease in the number of tampering cases in the region. Additionally, an increase in the economic status and an increase in water conveyance and use efficiency are envisaged, which will ultimately lead to water conservation.

With the increasing problem of depleting water tables on account of excessive usage and changing properties due to groundwater irrigation in the Haryana region, it is important to spread awareness amongst the farmers about water conservation practices. The findings of the study, thus, have recommendations for the academicians, government, non-profit institutions, society at large, and the environment in general. First, the research provides a backdrop for the evaluation of the current irrigation practices in the selected region. It suggests designing appropriate strategies for increasing water conveyance efficiency and thereby ensuring sustainable water use. Second, keeping sustainable development in perspective, non-governmental agencies can collaborate with governmental institutions to initiate training and education programs for the farmers for better management of irrigation sources. Third, corporate/industrial participants can step in to develop modern technologies, such as the use of app-based water management, which is essential in today's world to enhance farm productivity and conserve water. Fourth, industry participants/engineers can aid in the development of materials and construction technologies for canal lining so as to improve water use efficiency. Finally, the increased awareness about the pertinence of environmental conservation is gaining traction among international agencies (e.g., United Nations Sustainable Development Goal 13- Climate Action). Economies are thus required to take immediate remedial actions for the preservation of the environment for future generations, with water being one of its most essential components.

Given the prominence of water in both farm and non-farm activities, the study carries important implications for determining practical ways and means of efficient water management. The study ignites a sense of realization that

this extremely valuable resource must be utilized judiciously with the intent to save it for future generations. India has been grappling with water scarcity, which calls for investment in efficient water management technologies such as micro-irrigation. There is also a need for private sector participation in resource augmentation and efficiency. This strongly calls for strict implementation of remedial measures for the steady wherewithal of the irrigation system. For instance, maintenance works and rehabilitation of the canal lining are some such imperative measures.

The present study has the following contributions to the implementation of efficient water conservation and management practices. First, to create awareness about the benefits of sustainable use of water and its impact on the environment. The study suggests undertaking large-scale public awareness programs so as to improve water conservation consciousness among the masses in general and the farmers in particular. Secondly, the study emphasizes the role of policy-makers in bringing change in irrigation practices through the training of farmers and propagating technology-based irrigation management. Thirdly, the study is expected to offer insights to industrial corporations about the willingness of farmers to undertake training and adoption of modern technology for irrigation. This will help them to develop modern application-based systems of irrigation and appropriately assist the farmers.

The study is, however, limited in scope on account of the study of perception in restricted geographical areas in the state of Haryana, India. On account of the same, the views of the present sample of farmers cannot be generalized for all regions across the world as this might vary based on the conditions of the area. Further, the water conservation attitudes presented by the farmers cannot be used for actual behaviors. Though the questionnaire was iterated in the regional language and utmost care has been taken while translation of the same, yet gap in understanding and interpretation may have resulted in some distortion in the results. The study mainly focuses on practices farmers can adopt for water conservation and sustainability; however, technical parameters for the efficiency of transportation of the irrigation water and canal lining cannot be commented upon.

Future research endeavors can attempt to explore the technicalities of the shape and materials of canal lining. The present study restricts socio-demographics, current irrigation systems, and cost-benefit perceptions of farmers; however, factors such as the conjunction of various water conservation techniques applied together in different proportions along with the lining of the water courses can provide interesting insights. Furthermore, the study may be replicated in another

geographical jurisdiction to establish the region-specific perceptual differences.

ACKNOWLEDGEMENTS

We thank Dr. Nisha Bhargava, Principal, Mehr Chand Mahajan DAV College for Women, Chandigarh (Principal Investigator, Minor Research Project titled 'Impact of Concrete Canal Lining on Water Conservation: A Socio-Economic Evaluation of the JLN Feeder Rehabilitation Project') for her valuable comments and suggestions.

REFERENCES

- Afroz, A. and Singh, P.P. 2007. Assessment of environmental impacts of Sarda Sahayak Canal irrigation project of Uttar Pradesh, government, India. *International Journal of Environmental Studies*, 28(2-3): 123-130.
- Ahmadzadeh, H., Morid, S., Delavar, M. and Srinivasan, R. 2016. Using the SWAT model to assess the impacts of changing irrigation from surface to pressurized systems on water productivity and water saving in the Zarrineh Rud catchment. *Agric. Water Manag.*, 175: 15-28.
- Amarsinghe, U.A., Sikka, A., Mandave, V., Panda, R.K., Gorantiwar, S., Chandrasekharan, K. and Ambast, S. K. 2021. A re-look at canal irrigation system performance: a pilot study of the Sina irrigation system in Maharashtra, India. *Water Policy*, 23(1): 114-129.
- Barmakova, D.B., Rodrigo-Illari, J., Zavaley, V.A., Rodrigo-Clavero, M.E. and Capilla, J.E. 2022. Spatial analysis of the chemical regime of groundwater in the Karatol irrigation massif in south-eastern Kazakhstan. *Water*, 14(3): 285.
- Bhala, P. 2007. Impact of declining groundwater levels on acreage allocation in Haryana. *Economic and Political Weekly*, 42(26): 2701-2707.
- Brown, K.P. 2017. Water, water everywhere (or, seeing is believing): The visibility of water supply and the public will for conservation. *Nature Culture*, 12(3): 219-245.
- Burt, C. and Styles, S. 1999. *Modern Water Control and Management Practices in Irrigation*. FAO, Rome.
- De Clercq, W., De Witt, M. and Laker, G. 2021. Challenges and opportunities for water conservation in irrigated agriculture in South Africa. *South Afr. Journal of Plant and Soil*, 38(3): 238-246.
- Fan, L., Wang, F., Liu, G., Yang, X. and Qin, W. 2014. Public perception of water consumption and its effects on water conservation behavior. *Water*, 6(6): 1771-1784.
- Flynn, L.E. and Marino, M.A. 1987. Canal design: optimal cross-sections. *J. Irrig. Drain. Eng.*, 113(3): 335-355.
- García, X., Llausàs A. and Ribas A. 2014. Landscaping patterns and sociodemographic profiles in suburban areas: Implications for water conservation along the Mediterranean coast. *Urban Water J.*, 11(1): 31-41.
- Garg, N.K. and Hassan, Q. 2007. Alarming scarcity of water in India. *Curr. Sci.*, 93(7): 932-941.
- Gebremeskel, G., Gebremicael, T.G., Hagos, H., Gebremedhin, T. and Kifle, M. 2018. Farmers' perception towards the challenges and determinant factors in the adoption of drip irrigation in the semi-arid areas of Tigray, Ethiopia. *Sustain. Water Resour. Manag.*, 4(3): 527-537.
- Ghosh, P. 2021. Water stress and water crisis in large cities of India. *Sustain. Climater Manag.*, 11: 131-138.
- Grewal, S.S., Lohan, H.S. and Dagar, J.C. 2021. Potential agricultural practices in saline waterlogged areas of Haryana and their impact on socio-economic conditions of farmers—A synthesis. *J. Soil Sal. Water Qual.*, 13(1): 109-133.
- Gupta, A., Mishra, S., Bokde, N. and Kulat, K. 2016. Need for smart water systems in India. *Int. J. Appl. Eng. Res.*, 11(4): 2216-2223.
- Han, X., Wang, X., Zhu, Y., Huang, J., Yang, L., Chang, Z. and Fu, F. 2020. An experimental study on concrete and geomembrane lining effects on canal seepage in arid agricultural areas. *Water*, 12(9): 2343.
- Haryana Tourism Corporation Limited. 2020. Climate. <https://haryanatourism.gov.in/climate> (Accessed November 26, 2021).
- Hofste, R.W., Reig, P. and Schleifer, L. 2019. 17 Countries, Home to One-Quarter of the World's Population, Face Extremely High Water Stress. <https://www.wri.org/insights/17-countries-home-one-quarter-worlds-population-face-extremely-high-water-stress> (Accessed: January 15, 2022).
- Hrozencik, R.A., Potter, N.A. and Wallander, S. 2022. A national estimate of irrigation canal lining and piping water conservation. Working Paper No. w30123. National Bureau of Economic Research, Cambridge, MA.
- Jaafar, H. and Kharroubi, S. A. 2021. Views, practices, and knowledge of farmers regarding smart irrigation apps: A national cross-sectional study in Lebanon. *Agric. Water Manag.*, 248: 106759.
- Jakeman, A.J., Barreteau, O., Hunt, R.J., Rinaudo, J.D., Ross, A., Arshad, M. and Hamilton, S. 2016. Integrated groundwater management: an overview of concepts and challenges. *Integr. Groundwater Manag.*, 16: 3-20.
- Johansson, R. C., Tsur, Y., Roe, T. L., Doukkali, R. and Dinar, A. 2002. Pricing irrigation water: A review of theory and practice. *Water Policy*, 4(2): 173-199.
- Knox, J.W., Kay, M.G. and Weatherhead, E.K. 2011. Water regulation, crop production, and agricultural water management: Understanding farmer perspectives on irrigation efficiency. *Agric. Water Manag.*, 108: 3-8.
- Lecina, S., Isidoro, D., Playán, E. and Aragüés, R. 2010. Irrigation modernization and water conservation in Spain: The case of Riegos del Alto Aragón. *Agric. Water Manag.*, 97(10): 1663-1675.
- Manju, S. and Sagar, N. 2017. Renewable energy integrated desalination: A sustainable solution to overcome future fresh-water scarcity in India. *Renew. Sustain. Energy Rev.*, 73: 594-609.
- Mansfield, E.R. and Helms, B.P. 1982. Detecting multicollinearity. *Am. Statist.*, 36 (3a): 158-160.
- Morita, M. 2021. Past trends in water productivity at the global and regional scale. *Curr. Direct. Water Scarcity Res.*, 3: 99-118.
- National Water Mission. Base Line Studies of Irrigation Project. 2021. <http://nwm.gov.in/?q=base-line-studies-irrigation-project-0> (Accessed November 26, 2021).
- O'Keeffe, J., Moulds, S., Bergin, E., Brozović, N., Mijic, A. and Buytaert, W. 2018. Including farmer irrigation behavior in a sociohydrological modeling framework with application in North India. *Water Resour. Res.*, 54(7): 4849-4866.
- Ravish, S., Setia, B. and Deswal, S. 2018. Groundwater quality in urban and rural areas of north-eastern Haryana (India): A review. *ISH J. Hydraul. Eng.*, 27(2): 1-11
- Shah, T. 2011. Past, Present, and Future of Canal Irrigation in India. *International Water Management Institute, Colombo*, pp. 69-89.
- Singh, R., Ghosh, S., Kundu, D.K., Kannan, K. and Verma, H.N. 2004. Farm-Level Constraints to Efficient Use of Canal Water in Coastal Orissa and Some Technological Interventions to Enhance Crop Production. WTCER, Publication No. 18. ICAR, Bhubaneswar, India.
- Singh, R., Kroes, J.G., Van Dam, J.C. and Feddes, R.A. 2006. Distributed ecohydrological modeling to evaluate the performance of irrigation system in Sirsa district, India: I. Current water management and its productivity. *J. Hydrol.*, 329(3-4): 692-713.
- Sultan, T., Latif, A., Shakir, A.S., Kheder, K. and Rashid, M.U. 2014. Comparison of water conveyance losses in unlined and lined watercourses in developing countries. *Univ. Eng. Technol. Taxila. Tech. J.*, 19(2): 23.
- Tripathi, S. and Gupta, S. 2021. Haryana. In: *Groundwater Law and Management in India*, pp. 173-187.
- Tyagi, N.K. 2019. Rehabilitation of the delivery system to improve irrigation water management beyond the canal outlet. *Arid Lands Today Tom.*, 11: 205.

- United States Census Bureau. Population Clock. 2021. <https://www.census.gov/newsroom/stories/world-population-day.html> (Accessed August 28, 2021).
- Verdugo, V.C., Sing, B.F. and Pinheiro, J.Q. 2006. Sustainable behavior and time perspective: present, past, and future orientations and their relationship with water conservation behavior. *Interam. J. Psychol.*, 40(2):139-147.
- Water Science School. 2018. Where is Earth's Water? <https://www.usgs.gov/special-topic/water-science-school/science/where-earths-water?> (Accessed: August 28, 2021).
- Xiao-Jun, W., Jian-Yun, Z. and Shahid, S. 2014. Catastrophe theory to assess water security and adaptation strategy in the context of environmental change. *Mitig. Adapt. Strateg. Glob. Change*, 19: 463-477.
- Yadav, D. 1987. Impact of irrigation on the crops of Haryana. *GeoJournal*, 14(1): 115-118.

ORCID DETAILS OF THE AUTHORS

Manika Kohli: <https://orcid.org/0000-0002-2777-6779>

Vinakshi Grover: <https://orcid.org/0000-0002-6652-8583>



Hydrogen Sulfide Oxidizing Microbiome in Biogas-Stream Fed Biofilter in Palm Oil Factory

Siriorn Boonyawanich*, Peerada Prommeenate***, Sukunya Oaew***, Nipon Pisutpaisal*(**) and Saowaluck Haosagul**† 

*Department of Agro-Industrial, Food and Environment Technology, Faculty of Applied Science, King Mongkut's University of Technology North Bangkok, Bangkok, Thailand

**Biosensor and Bioelectronics Technology Centre, King Mongkut's University of Technology North Bangkok, Bangkok 10800, Thailand

***Biochemical Engineering and System Biology Research Group, National Center for Genetic Engineering and Biotechnology, National Science and Technology Development Agency at King Mongkut's University of Technology Thonburi, Bang Khun Thian, Bangkok, 10150, Thailand

†Corresponding author: Saowaluck Haosagul; h_saowaluck@hotmail.com

Nat. Env. & Poll. Tech.
Website: www.neptjournal.com

Received: 07-08-2023

Revised: 30-09-2023

Accepted: 10-10-2023

Key Words:

Hydrogen sulfide

Biofilter

Palm oil factory

Sulfur oxidizing bacteria

16S rRNA gene

ABSTRACT

Hydrogen sulfide (H_2S) is highly corrosive to electric generators, which is the main problem of biogas utilization. The industrial scale of the biofilter system relies on the performance of sulfide-oxidizing bacteria (SOB) via the activity of sulfur oxidation (*soxABXYZ*) and flavocytochrome sulfide dehydrogenase (*fccAB*) enzymes to reduce to a concentration below 100 ppm before using in industrial machinery. The main purpose of this research is to investigate the SOB community in full-scale H_2S removal and their gene expression (*fccAB* and *soxABXYZ*) associated with H_2S elimination efficiency. In this study, SOB communities were obtained from 2 sampling sites of the full-scale biofilter of palm oil factory (PPG), comprising starting sludge (PPG1) and recirculating sludge (PPG2). The abundance of SOB strains was examined by next-generation sequencing analysis (NGS) based on the 16S rRNA gene. The changes in the expression of genes involved in sulfur oxidation, namely *soxABXYZ*, and *fccAB*, between the 2 sampling sites were evaluated by using a comparative genomic hybridization (CGH) microarray. The results indicate that the high abundance of SOB genera that could play a vital role in biofilters belonged mainly to *Sulfurovum*, *Paracoccus*, *Acidihalobacter*, *Acidithiobacillus*, *Thioalkalispira*, *Thiofaba*, *Caldisericum*, *Bacillus*, were rapidly increased in the biofilter tank. Interestingly, expressions of *soxABXYZ* gene cluster at PPG2 were increased in *Paracoccus pantotrophus* J40 and *Paracoccus alkenifer* DSM 11593 for 1.1188 and 1.0518-fold, respectively, while in *Acidihalobacter prosperus* F5, the expression of *fccAB* genes was up to 1.3704 fold in comparison with PPG1. Increasing both relative abundance and gene expressions at PPG2 were correlated with 95% H_2S removal efficiency. Hence, stabilization of the SOB microbiome is vital to H_2S removal in industrial-scale biogas applications.

INTRODUCTION

Palm oil is the 5th most important economic crop in Thailand. It occupies more than 70% of the acreage in Southern Thailand (Giz Agriculture and Food Cluster Thailand 2021). In 2020, palm oil production was approximately 3.78 million tonnes/yr., which accounts for 2.8% of the world market (United States Department of Agriculture 2021). Palm oil consumption is forecast to continue to increase by 5% in 2022. Apart from being used for consumption, palm oil has also been incorporated into the petroleum industry, diesel oil in particular. In order to comply with the circular economy

plan, the palm oil industry in Thailand has to adopt a new policy on waste utilization along with energy efficiency. The wastewater from the palm oil industry is rich in biodegradable organic compounds that are suitable for biogas production. According to the Department of Alternative Energy Development and Efficiency (DEDE) has prepared the 10-year Alternative Energy Development Plan (AEDP 2012-2021), biogas can be used as a renewable energy source for electricity and heat power. Biogas is typically composed of 50-70% methane (CH_4), 30-40% carbon dioxide (CO_2) and 1-2% hydrogen sulfide (H_2S) (Elshiekh et al. 2016). H_2S is harmful to humans and can be toxic to methanogen,

especially during anaerobic digestion. It can cause severe corrosion to boilers and engines, which is the main problem of biogas utilization. To overcome these limitations, it is necessary to reduce the concentration of H_2S to less than 100 ppm before being used in industrial machinery (Tilahun et al. 2018). Several biological processes such as biofilter, biotrickling filter, and bioscrubber have been used to treat H_2S without causing secondary pollution. In this case, it is known that the H_2S elimination process is driven by sulfur oxidation enzyme (encoded by *soxABXYZ* genes) and flavocytochrome c sulfide dehydrogenase (encoded by *fccAB* genes) produced from sulfur-oxidizing bacteria (SOB) (Friedrich et al. 2005, Sander et al. 2006, Chan et al. 2009, An et al. 2016).

A number of studies have focused on the diversity of the SOB community in bioreactors and their ability to oxidize thiosulfate and H_2S in biogas. Omri et al. (2013) developed a biofilter to treat H_2S (inlet H_2S of 0.2-1.3 ppm) from wastewater odor. The dominant SOB in the biofilter were identified as heterotrophic bacteria that belong to the genus *Bacillus*, *Pseudomonas*, and *Xanthomonas*, with the highest removal efficiencies of 99%. Zhou et al. (2015) reported the predominant chemoautotrophic SOB in biotrickling filters, which include the genus *Thiothrix*, *Acidithiobacillus*, *Thiomonas*, *Sulfurimonas*, *Halothiobacillus* and *Thiobacillus* which play an important role in treating H_2S (inlet conc. 2000-7,800 ppm) and enhance methane content in biogas. In the steady state of the anaerobic biotrickling filter system, H_2S concentrations between 2,500 to 10,000 ppm were removed with 100% efficiency by activities of phylum

Proteobacteria and Actinobacteria (Quijano et al. 2018). However, many researchers have mainly investigated the SOB populations based on 16S ribosomal RNA genes only in laboratory or pilot scales. The profile of SOB in full-scale H_2S removal coupled with the change of gene expression associated with H_2S elimination was rarely observed.

Hence, the purpose of this research is to study the abundance and diversity of SOB strains in a full-scale biofilter, which is used to treat H_2S in biogas from palm oil factories using 16SrRNA together with next-generation sequencing. The changes in the expression of flavocytochrome c sulfide dehydrogenase (*fccAB*) and Sox multi-enzyme (*soxAXBYZ*), the key enzymes for sulfide/thiosulfate oxidation, were also investigated.

MATERIALS AND METHODS

The Full-Scale Biofilter System and Samples Collection

The full-scale biofilter system consists of a packed column of pall ring media, which motivates biofilm growth through humidifying biogas that is pumped into the system. In the biofilter system, microbes are coated on porous media in the form of biofilm, and H_2S in biogas will be adsorbed on the porous media and interact with a biofilm of sulfur-oxidizing bacteria (SOB). Biodegradation processes occur in both the biofilm area and the porous media (Fig. 1). The portable H_2S detector can sense the H_2S inlet concentration in the range of 2,500-3,000 ppm, and the H_2S outlet concentration was observed at ~150 ppm. The H_2S removal efficiency was over 95%. Therefore, the SOB was collected from the

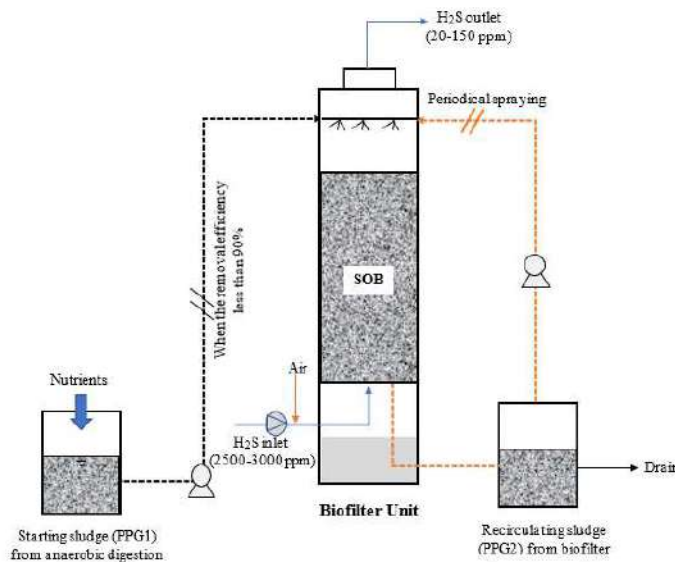


Fig. 1: Schematic diagram of the biofilter system in the PPG factory.

starting sludge (PPG1) and recirculating sludge (PPG2) of the full-scale biofilter tank (under a stable operation period of ~3 months) at Palm Power Green Company (Prachuap Khiri Khan, Thailand). Sludge samples were transported to the laboratory and transferred to a centrifuge bottle (250 mL). Bacteria cells were settled by centrifugation at 10,000g for 15 min. The pellet was kept in a 20°C freezer before the genomic DNA (gDNA) extraction.

DNA Extraction and Purification

Samples from starting sludge (PPG1) and recirculating sludge (PPG2) were defrosted at room temperature. For gDNA extraction, cells were lysed with 600 µL of the extraction buffer (100 mM Tris-HCl, 100 mM EDTA, 1.5 M NaCl) and 600 µL of lysozyme (10 mg/L). The mixture was shaken at 180 rpm at 37°C for 1 h (Dezhbord et al. 2019). Next, 100 µL of sodium dodecyl sulfate (20% w/v) was added and incubated at 65°C for 30 min. DNA precipitation was carried out with the addition of 0.6 volume of isopropanol and then subsequently washed with 1 mL of cold ethanol (-20°C) 2 times. The precipitated DNA was dried at room temperature and dissolved in 30 µL of elution buffer (10 mM Tris-HCl, pH 8.5 at 25°C). Finally, the DNA was purified using the GenepHlow™ Gel/PCR Kit (Geneaid) as described in Haosagul et al. (2020). DNA was extracted from three duplicate samples per sampling site and then merged for further study. DNA purity was evaluated using both gel electrophoresis and the A₂₆₀/A₂₈₀ ratio. The gDNA is considered to be pure if A₂₆₀/A₂₈₀ > 1.8 and A₂₆₀/A₂₃₀ > 1.0. The purified DNA (50 ng/µL) was stored at -20°C for NGS analysis.

Next-Generation Sequencing

In this analysis, next-generation sequencing (NGS) is used to infer the phylogenetic relationships among the phyla and species in the same genus. The gDNA was used as a DNA template for PCR amplification. The specific primer, 515F806-R, was used to target the V4 region of the 16S rRNA gene. PCR reactions were carried out in the 19 µL of PCR Master Mix (1U/µL of *Taq* DNA polymerase, 0.02 mM of dNTPs, 3 mM of MgCl₂, 1X PCR buffers), 0.5 µM of forward and reverse primers, and 1 µL of 10 ng template DNA. The PCR condition was carried out as previously reported (Haosagul et al. 2020). The PCR products were examined in 0.8% (w/v) of agarose gel electrophoresis in 1x TAE (Tris 40 mM, Acetate 20 mM, EDTA 2 mM) buffer and stained with 0.5 µg/mL of ethidium bromide. The NEB Next® Ultra™ II DNA Library Prep Kit for Illumina was used to generate a sequencing library. The sequencing reactions were performed using Illumina HiSeq 2500. The low-quality sequences in raw data were removed using QIIME

(Version 1.7.0). The remaining sequences at 97% identity were clustered into the same operational taxonomic units (OTUs). Species richness was identified using Chao1 and ACE estimators. Community diversity was identified using Shannon and Simpson indexes. The sequencing result was characterized by Good's coverage. These alpha diversity metrics were calculated by QIIME.

Expression of the Sulfur Oxidation Gene

The comparative genomic hybridization (CGH) microarray probes with 61,788 spots were designed for the detection and identification of SOB species in the palm oil factory. Database of genes related to sulfur oxidation (*soxAX*, *soxYZ*, *soxB*, and *fccAB*), including genome sequences of SOB species, were compiled from PATRIC and NCBI databases (Haosagul et al. 2021). The raw signal intensities from the microarray were calculated into log-2 ratios of PPG2/PPG1. The expression of sulfur oxidation genes between the recirculating sludge (PPG2) and starting sludge (PPG1) was investigated. Gene expression related to H₂S oxidation of SOB in the biogas was also studied.

RESULTS AND DISCUSSIONS

Quality of gDNA and NGS Analysis

The genomic DNA band of starting sludge (PPG1) and recirculating sludge (PPG2) were successfully extracted and separated on the agarose gel. gDNA concentrations of PPG1 and PPG2 were found in the range of 462.45–761.08 ng·µL⁻¹, and with the DNA purity (A₂₆₀/A₂₈₀) greater than 1.8, which indicated the absence of protein, phenol, and other contaminants in the samples (Brescia et al. 2012, Hashemipetroudi et al. 2018). The 250 bp PCR products that appeared in lanes 3 and 4 represent the 16S rRNA gene, as shown in Fig. 2. While in lane 1, there is no band on the agarose gel, indicating some contamination during the PCR reaction. Therefore, both samples were subjected to sequencing using the Illumina HiSeq 2500 platform. The sequence analysis was performed using Uparse software version 7.0.1001 (Edgar 2013). A total of 139,348 NGS reads, and 1,846 OTUs were obtained from 2 sampling sites of the palm oil factory. According to the alpha diversity analysis, the observed species, community diversity, and species richness at PPG1 are more diverse than at PPG2 (Table 1). A number of readable sequences encompassed almost 100% of the entire population of bacteria in the sample according to Goods coverage of 0.997. These results indicated that bacterial communities in PPG2 have less bacterial strain diversity, which is possibly due to the anaerobic strains in PPG1 (e.g., Methanogen, SRB) being unable to resist O₂ and H₂S concentrations in the biofilter system.

Diversity of Bacterial Community

Analysis of the microbial population's diversity showed that the majority of microorganisms found in a full-scale biofilter system from the palm oil factory belong to phylum Firmicutes, Proteobacteria, and Euryarchaeota (Fig. 3A), which account for 24-28%, 19-20%, and 11-22% of the total microbial community, respectively. The populations of phylum Firmicutes and Euryarchaeota were significantly decreased in the recirculating sludge (PPG2). In contrast, phylum Proteobacteria and Spirochaetes were found to increase by about 1.6-2.0-fold of the starting sludge (PPG1), which comprise 3 main classes: Epsilonproteobacteria (14.14%), Deltaproteobacteria (6.11%), and unidentified_Spirochaetes (3.74%) (Fig. 3B). The high abundance of the Proteobacteria phylum was observed to degrade H₂S in biogas (Quijano et al. 2018, San-Valero et al. 2019, Haosagul et al. 2020) while phylum Firmicutes were commonly detected in activated sludge fed to biogas reactor (Schnürer et al. 2016, Schnürer & Jarvis. 2018). Gammaproteobacteria and Epsilonproteobacteria were detected on biofilm surfaces that were fed with H₂S in a bioreactor and contained various phenotypes (Konishi et al. 2013). Interestingly, Clostridiales was the dominant order of the phylum Firmicutes found at PPG1 (23.91%) and PPG2 (20.64%) (Fig. 3C). Westerholm et al. (2016) also reported that Clostridiales

and Methanosarcinales dominated the anaerobic microbial community of biogas production. Relative abundance analysis indicated that Helicobacteraceae, a family of Epsilonproteobacteria, was the stable member in the biofilter system, while the Methanosaetaceae, a family of Methanomicrobia, was the unstable major member over time (Fig. 3D).

The outstanding 35 genera that work together in the biofilter system of palm oil factory are shown in an abundance heatmap (Fig. 4A). The following genera were dominated in biofilter at the PPG factory, *Sulfurovum*, *Sphaerochaeta*, *Syntrophomonas*, *Methanosaeta*, *Mesotoga*, Christensenellaceae which could play a vital role. They are members of ammonia-oxidizing bacteria (AOB), nitrite-oxidizing bacteria (NOB), methanogenic bacteria (MB), sulfur-reducing bacteria (SRB), and sulfur-oxidizing bacteria (SOB). These results indicate that the variation in bacterial communities in the biofilter depends on nutrients and operating conditions that affect growth and proliferation. For example, *Methanosaeta* was the predominant Archaeal community that prefers low acetate/COD concentration in anaerobic digesters (Pavlostathis 2011, Tang et al. 2015).

The horizontal bar graph (Fig. 4B) shows the percentage of relative abundance between starting sludge (PPG1) and recirculating sludge (PPG2). SOB was found to be the most

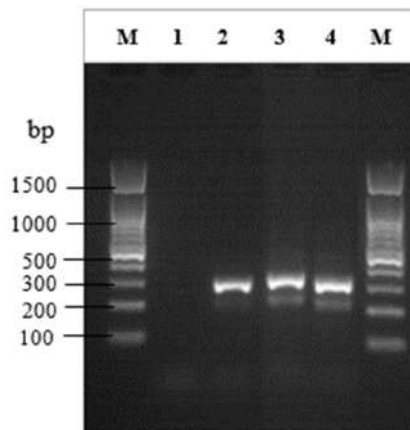


Fig. 2: The PCR products (approximated size 250 bp) were run on 0.8%TAE agarose gel. Lane M was 100bp DNA ladder, and lanes 1 and 2 were negative control (no DNA template) and positive control (*E. coli*), respectively. Lanes 3 and 4 were the amplified products from starting sludge (PPG1) and recirculating sludge PPG2), respectively.

Table 1: Community diversity and species richness.

Sample name	Observed Species	Community diversity		Species richness		Goods Coverage
		Shannon	Simpson	Chao1	ACE	
PPG1	1597	6.317	0.947	1788.482	1826.687	0.997
PPG2	1530	6.026	0.938	1747.562	1772.613	0.997

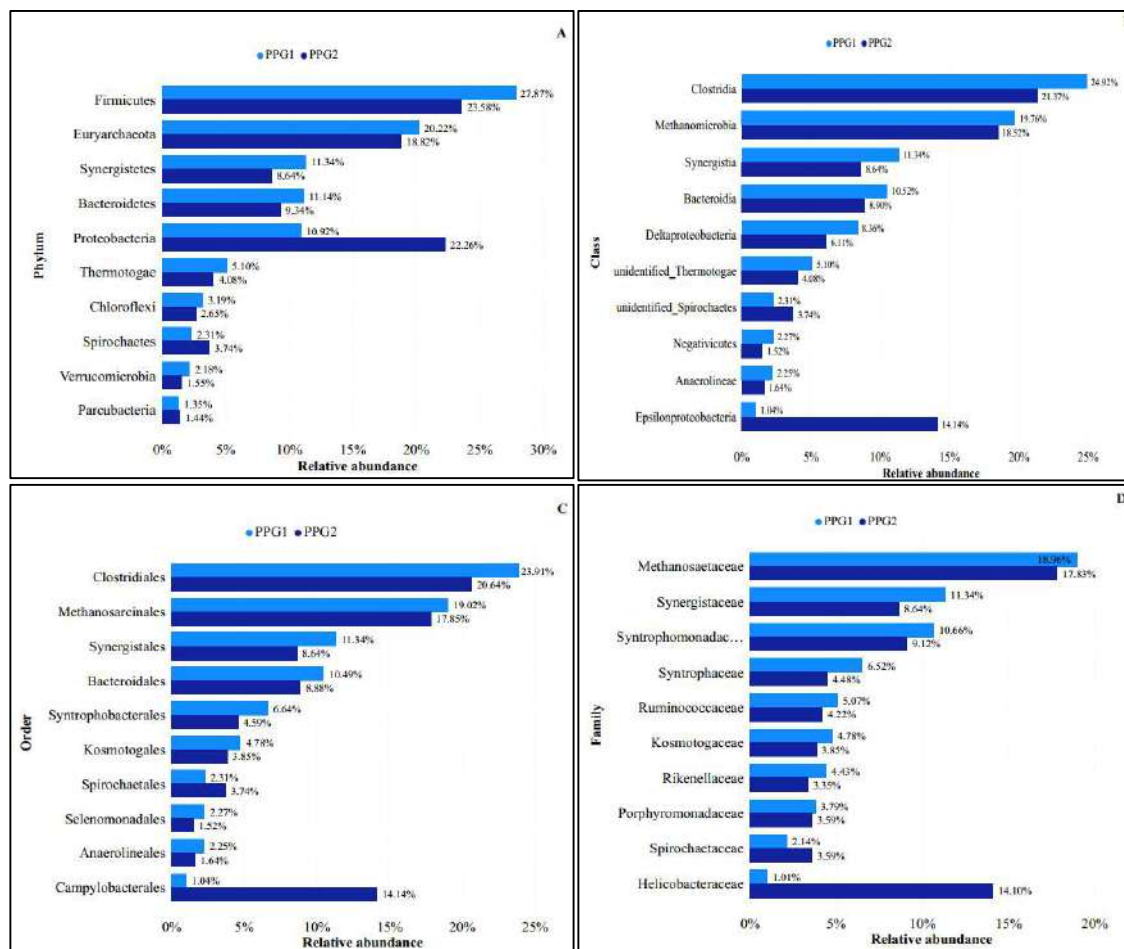


Fig. 3: (A) phylum, (B) class, (C) order, and (D) family of bacterial community in the biofilter system of palm oil factory.

abundant group covered in both sampling sites. They comprise mainly *Sulfurovum* (94.1%), *Acidithiobacillus* (91.0%), *Thioalkalispira* (95.7%), *Thiofaba* (90.9%), *Caldisericum* (100%), and *Bacillus* (100%), were rapidly increased at PPG2. On the contrary, the bacteria belonged to the *Synechococcus* (94.3%), *Acinetobacter* (100%), *Aquaspirillum* (100%), *Chlorobium* (100%), *Pararhodospirillum* (100%), and *Thiothrix* (100%) were commonly found at PPG1. The high abundance might indicate their significant function for the utilization of inorganic/organic compounds as an energy source and CO₂ as the carbon source of obligately/facultative chemoautotrophic bacteria found in the communities. Kovács et al. (2015) reported that *Bacillus* strains, which naturally display the ability to digest protein, were applied to enhance the hydrolysis during biogas production. Furthermore, the concentration of H₂S is a main factor that affects the variation of SOB communities, especially at the H₂S exposure site (Dong et al. 2017). For example, genus *Sulfuritalea*, *Thiobacillus*, *Sulfurovum*, *Sulfuricurvum*, *Sulfurimonas*,

and *Sulfuricella* were typically found at a low H₂S site, while *Acidithiobacillus*, *Sulfobacillus*, *Sulfurospirillum*, *Thiomonas*, and *Halothiobacillus* were presented at a high H₂S site.

Correlation of Expressed Genes Profile in SOB Species-Strain with H₂S Elimination in Biogas Treatment System

The SOB communities are responsible for the sulfide/thiosulfate oxidation process and are of great importance for treatment system optimization in H₂S biological degradation. Many species of SOB contained the thiosulfate oxidizing multienzyme gene subunits (*soxB*, *soxAX*, and *soxYZ*) and the flavocytochrome c sulfide dehydrogenase genes (*fccA* and *fccB*) for sulfide oxidation and related to the diversity of species-strains of SOB. The involvement of these pathways in sulfide/thiosulfate oxidation by sulfur oxidation bacteria (SOB) was described in Haosagul et al. (2021a). Expression of sulfide/thiosulfate oxidation genes of SOB species-

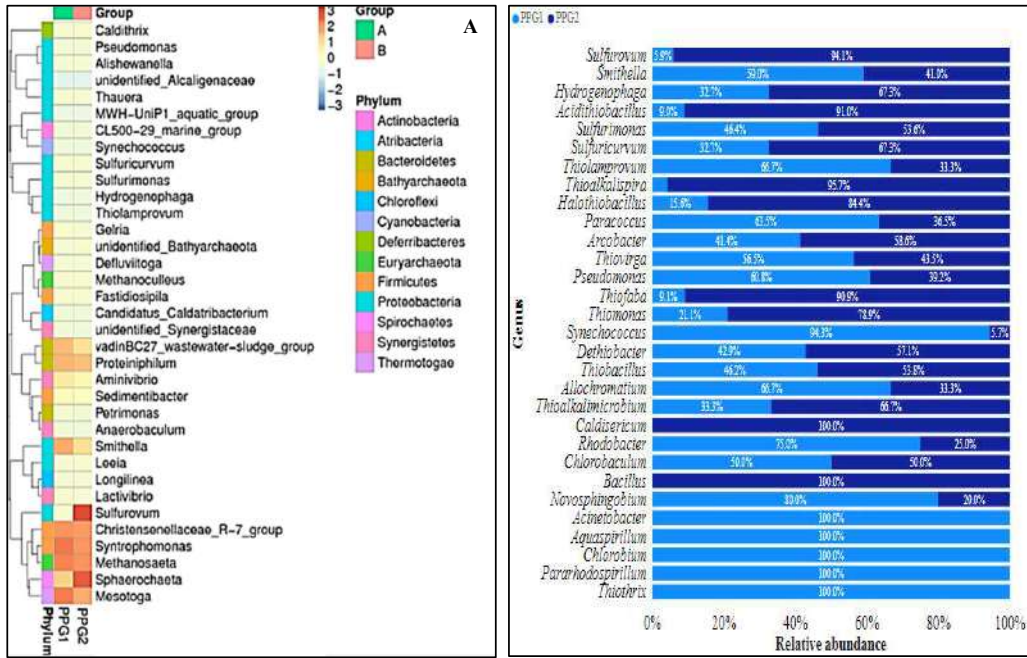


Fig. 4: (A) The abundance heatmap depicting the dominance of the top 35 genera in the biofilter, (B) A comparative horizontal bar graph between starting sludge (PPG1) and recirculating sludge (PPG2).

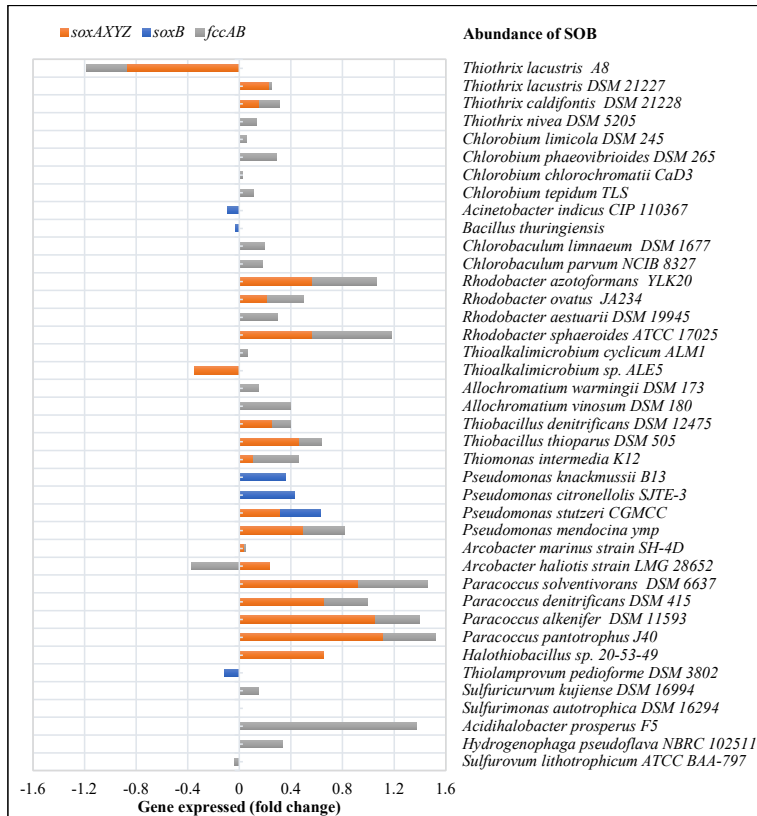


Fig. 5: Abundance of SOB species based on sulfide/thiosulfate oxidation gene expression.

strains was detected as shown in Fig. 5. We found that both *soxAXYZ* and *fccAB* genes predominantly expressed in the palm oil factory belong to *Thiothrix* sp., *Chlorobium* sp., *Rhodobacters* sp., *Thioalkalimicrobium* sp., *Allochroamatium* sp., *Thiobacillus* sp., *Thiomonas* sp., *Pseudomonas* sp., *Arcobacter* sp., *Paracoccus* sp., *Halothiobacillus* sp., *Thiolamprovum* sp., *Sulfuricurvum* sp., *Sulfurimonas* sp., *Acidihalobacter* sp., *Hydrogenophaga* sp. and *Sulfurovum* sp., which correlated well with the H₂S removal efficiency of over 95%. A variety of electron donors (e.g., sulfide, sulfur, thiosulfate, sulfite) and acceptors (e.g., oxygen nitrate nitrite) play a pivotal role in the presence of SOB species in biofilter tank, including fold change of gene copy number variation that observed between the 2 sampling sites (Haosagul et al. 2021b).

Especially, the expression of the *soxAXYZ* gene cluster of *Paracoccus pantotrophus* J40 and *Paracoccus alkenifer* DSM 11593 has been increased by 1.1188 and 1.0518-fold, respectively. In contrast, the expression of *fccAB* genes was up to 1.3704-fold in *Acidihalobacter prosperus* F5 at PPG2, in agreement with their relative abundance study. The expression of six genes (*soxX*, *soxY*, *soxZ*, *soxA*, *soxB*, and *soxCD*) of *P. pantotrophus* GB17 involved with H₂S biodegradation was confirmed by Ramadhani et al. (2017). It has been reported that the halotolerant acidophile *Ac. prosperus* F5 revealed the industrial potential applicability in bioleaching. Catalyzing the dissolution of sulfide minerals (Dopson et al. 2017, Khaleque et al. 2017) and obtaining energy source from sulfide oxidation to sulfur by sulfide cytochrome c reductase (EC:1.8.2.3). Rana et al. (2020) reported the potential for odors elimination due to the release of undesirable H₂S from wastewater using the following species; *C. limicola*, *A. ferrooxidans*, *T. thiolates*, *T. denitrificans*, *P. putida*, and *F. thiosulatoophilum*. These microorganisms, at low microbial counts, can oxidize H₂S with a high removal rate at ambient temperature and neutral pH. In-depth aspects, the ortholog groups containing genes related to sulfur/sulfide/thiosulfate oxidation in all strains could be found in the Kyoto Encyclopedia of Genes and Genomes, KEGG database (M00595-M00596, K17229-17230) (KEGG GENES 2022).

CONCLUSIONS

This study successfully demonstrated the correlation between SOB strains' abundance and the expression of sulfide and thiosulfate oxidation genes in a full-scale biofilter treating H₂S in biogas from palm oil factory sites. The high abundance of SOB genera that play a vital role in biofilters belonged mainly to *Sulfurovum*, *Paracoccus*, *Acidihalobacter*, *Acidithiobacillus*, *Thioalkalispira*, *Thiofaba*, *Caldisericum*, *Bacillus* that appear both *soxAXYZ*

and *fccAB* genes in the metabolic pathway. The results also confirmed that the stability of the SOB microbiome is vital to H₂S removal in industrial-scale biogas applications. The data collection of SOB species-strains and genes associated with sulfide oxidation in this research can be further applied to many issues, for example, biogas purification, evaluation of system efficiency, selection of microbial species in the start-up stage, reduction of clogging problem on the media, and helping save maintenance costs, etc. The limitations of the study also lacked a link between other genes that promote the activity of *sox* and the *fcc* gene to eliminate H₂S.

ACKNOWLEDGEMENTS

This research was funded by the Research and Researchers for Industries (Grant No. PHD60I0028) and King Mongkut's University of Technology North Bangkok, Thailand (KMUTNB-64-KNOW-37).

REFERENCES

- An, D., Dong, X., An, A., Park, H.S., Strous, M. and Voordouw, G. 2016. Metagenomic analysis indicates Epsilonproteobacteria as a potential cause of microbial corrosion in pipelines injected with bisulfite, *Front. Microbiol.*, 7: 28.
- Brescia, P., Banks, P. and Voloshin, A. 2012. Multi-Volume Analysis of Nucleic Acids Using the Epoch™ Spectrophotometer System, *Наука та інновації*.
- Chan, L.K., Rachael, M., Morgan-Kiss, R.M. and Hanson, T.E. 2009. Functional analysis of three sulfides: quinone oxidoreductase homologs in *Chlorobaculum tepidum*, *J. Bacteriol.*, 191: 1026-1034.
- Dezhbord, M., Lee, S., Kim, W., Seong, B.L. and Ryu, W.S. 2019. Characterization of the molecular events of covalently closed circular DNA synthesis in de novo Hepatitis B virus infection of human hepatoma cells, *Antiviral Res.*, 163: 11-18.
- Dong, Q., Shi, H. and Liu, Y. 2017. Microbial character-related sulfur cycle under dynamic environmental factors based on the microbial population analysis in the sewerage system, *Front. Microbiol.*, 8: 64.
- Dopson, M., Holmes, D.S., Lazcano, M., McCredden, T.J., Bryan, C.G., Mulrone, K.T. and Watkin, E.L. 2017. Multiple osmotic stress responses in *Acidihalobacter prosperus* result in tolerance to chloride ions, *Front. Microbiol.*, 7: 2132.
- Edgar, R.C. 2013. UPARSE: highly accurate OTU sequences from microbial amplicon reads, *Nat. Methods*, 10: 996-998.
- Elshiekh, T.M., Elmawgoud, H.A., Khalil, S.A. and Alsabagh, A.M. 2016. Optimum injection dose rate of hydrogen sulfide scavenger for treatment of petroleum crude oil, *Egypt. J. Pet.*, 25: 75-78.
- Friedrich, C.G., Bardischewsky, F., Rother, D., Quentmeier, A. and Fischer, J. 2005. Prokaryotic sulfur oxidation, *Curr. Opin. Microbiol.*, 8: 253-259.
- Giz Agriculture and Food Cluster Thailand. 2021. Sustainable and Climate-Friendly Palm Oil Production and Procurement (SCPOPP) in Thailand. Retrieved from <https://www.asean-agrifood.org/palm-oil-thai>.
- Haosagul, S., Oaew, S., Prommeenate, P., Sawasdee, V., Boonyawanich, S. and Pisutpaisal, N. 2021a. Profile of sulfur-oxidizing bacteria in full-scale Biotrickling filter to remove H₂S in biogas from in cassava starch industry, *Energy Rep.*, 7: 677-685.
- Haosagul, S., Oaew, S., Prommeenate, P., Sawasdee, V. and Pisutpaisal, N. 2021b. DNA microarray for detection and identification of sulfur-oxidizing bacteria in Biogas Clean-up System, *Energy Rep.*, 7: 559-568.

- Haosagul, S., Prommeenate, P., Hobbs, G. and Pisutpaisal, N. 2020. Sulfur-oxidizing bacteria in full-scale biogas cleanup system of the ethanol industry, *Renew. Energy*, 150: 965-972.
- Hashemipetroudi, S.H., Nematzadeh, G., Ahmadian, G., Yamchi, A. and Kuhlmann, M. 2018. Assessment of DNA contamination in RNA samples based on ribosomal DNA, *J. Vis. Exp.*, 131: e55451.
- KEGG GENES. 2022. Database. https://www.kegg.jp/dbget-bin/www_bget?ec:1.8.2.3. (Accessed 21 Jan 2022).
- Khaleque, H.N., Corbett, M.K., Ramsay, J.P., Kaksonen, A.H., Boxall, N.J. and Watkin, E.L. 2017. Complete genome sequence of *Acidihalobacter prosperus* strain F5, an extremely acidophilic, iron-and sulfur-oxidizing halophile with potential industrial applicability in saline water bioleaching of chalcopyrite, *J. Biotechnol.*, 262: 56-59.
- Konishi, M., Watsuji, T.O., Nakagawa, S., Hatada, Y., Takai, K. and Toyofuku, T. 2013. Effects of hydrogen sulfide on bacterial communities on the surface of galatheid crab, *Shinkaia crosnieri*, and in a bacterial mat cultured in rearing tanks, *Microbes Environ.*, 28: 25-32.
- Kovács, E., Wirth, R., Maróti, G., Bagi, Z., Nagy, K., Minárovits, J. and Kovács, K.L. 2015. Augmented biogas production from protein-rich substrates and associated metagenomic changes, *Bioresour. Technol.*, 178: 254-261.
- Omri, I., Aouidi, F., Bouallagui, H., Godon, J.J. and Hamdi, M. 2013. Performance study of biofilter developed to treat H₂S from wastewater odor, *Saudi J. Biol. Sci.*, 20: 169-176.
- Pavlostathis, S.G. 2011. Kinetics and modeling of anaerobic treatment and biotransformation processes, *Comprehensive Biotechnol.*, 1: 385-397.
- Quijano, G., Figueroa-González, I. and Buitrón, G. 2018. Fully aerobic two-step desulfurization process for purification of highly H₂S-laden biogas. *J. Chem. Technol. Biotechnol.*, 93: 3553-3561.
- Ramadhani, A., Kawada-Matsuo, M., Komatsuzawa, H. and Oho, T. 2017. Recombinant Sox enzymes from *Paracoccus pantotrophus* degrade hydrogen sulfide, a major component of oral malodor, *Microbes Environ.*, ME16140.
- Rana, K., Rana, N. and Singh, B. 2020. Applications of sulfur-oxidizing bacteria, *Physiol. Biotechnol. Aspects Extremophiles*, p.131-136.
- Sander, J., Sabine, E.S. and Christiane, D. 2006. Importance of the DsrMKJOP complex for sulfur oxidation in *Allochromatium vinosum* and phylogenetic analysis of related complexes in other prokaryotes, *Arch. Microbiol.*, 186: 357-366.
- San-Valero, P., Peña-Roja, J.M., Álvarez-Hornos, F.J., Buitrón, G., Gabaldón, C. and Quijano, G. 2019. Fully aerobic bioscrubber for the desulfurization of H₂S-rich biogas, *Fuel*, 241: 884-891.
- Schnürer, A., Bohn, I. and Moestedt, J. 2016. Protocol for start-up and operation of CSTR biogas processes. *Hydrocarb. Lipid Microbiol. Protoc.*, 54:171-200.
- Schnürer, A. and Jarvis, Å. 2018. *Microbiology of the biogas process*, Swedish Univ. Agric. Sci., 11: 221-229.
- Tang, Y.Q., Shigematsu, T., Morimura, S. and Kida, K. 2015. Dynamics of the microbial community during continuous methane fermentation in continuously stirred tank reactors, *J. Biosci. Bioeng.*, 119: 375-383.
- Tilahun, E., Sahinkaya, E. and Çalli, B. 2018. A hybrid membrane gas absorption and bio-oxidation process for the removal of hydrogen sulfide from biogas, *Int. Biodeterioration Biodegradation*, 127: 69-76.
- United States Department of Agriculture. 2021. Thailand: Oilseeds and Products Annual, Retrieved from <https://www.fas.usda.gov/data/thailand-oilseeds-and-products-annual-5>.
- Westerholm, M., Crauwels, S., Van, G.M., Dewil, R., Lievens, B. and Appels, L. 2016. Microwave and ultrasound pre-treatments influence microbial community structure and digester performance in anaerobic digestion of waste-activated sludge, *Appl. Microbiol. Biotechnol.*, 100: 5339-5352.
- Zhou, Q., Liang, H., Yang, S. and Jiang, X. 2015. The removal of hydrogen sulfide from biogas in a microaerobic biotrickling filter using polypropylene carrier as packing material. *Appl. Biochem. Biotechnol.*, 175: 3763-3777

ORCID DETAILS OF THE AUTHORS

Saowaluck Haosagul: <https://orcid.org/0000-0002-9448-5840>



Circular Economy as an Important Lever to Reduce Greenhouse Gas Emissions: Case of an Electricity Distribution Company in Morocco

Salma El Majaty†, Abdellatif Touzani and Youssef Kasseh

Laboratoire de Géophysique Appliquée, Géologie Géotechnique, L'Ingénieur et L'Environnement (L3GIE)
École d'ingénieurs Mohamedia 10200, Rabat, Maroc

†Corresponding author: Salma El Majaty; salma.elmajaty@gmail.com

Nat. Env. & Poll. Tech.
Website: www.neptjournal.com

Received: 17-08-2023

Revised: 30-09-2023

Accepted: 12-10-2023

Key Words:

Circular economy

Greenhouse gas

Electricity

Energy efficiency

ABSTRACT

This article discusses the major challenges related to greenhouse gas (GHG) emissions in the electricity sector and their impact on global climate change. The electricity sector is responsible for about a quarter of total global GHG emissions. To address these challenges, Life Cycle Assessment (LCA) is used to measure the environmental impact of different energy sources and electricity generation and distribution processes. The circular economy is presented as a promising approach to reducing the carbon footprint of the electricity sector. By optimizing the use and value of materials throughout their life cycle, this approach contributes to waste minimization and resource efficiency. Morocco is committed to reducing its GHG emissions and has adopted policies and regulatory frameworks to combat climate change. This study aims to calculate the climate change impacts of electricity distribution phases by applying a life-cycle approach to the case of an electricity distribution company in Morocco. This assessment makes it possible to identify significant contributors from each area. In the context of this company, it is a question of demonstrating how the application of the principles of the circular economy concepts contributes to the reduction of greenhouse gas emissions, in particular, that of scope 3. This study may be useful for other similar companies.

INTRODUCTION

Greenhouse gas (GHG) emissions are one of the major challenges to addressing global climate change issues and promoting sustainable development in the electricity sector. Globally, the electricity sector is responsible for emitting approximately 13.7 gigatons of CO₂ equivalent (GtCO₂) each year, or nearly one-quarter of total GHG emissions (Chanda & Bose 2020).

To develop effective and cost-effective strategies, it is imperative to measure GHG emissions in the electricity sector. The use of environmental assessment tools, such as Life Cycle Assessment (LCA) applied to different energy sources and electricity production and distribution processes, provides a better understanding of the environmental impact of these activities (Kiss et al. 2020).

The electricity industry also faces the challenge of effectively managing “scope 3” of GHG emissions, which includes indirect emissions from upstream and downstream activities of the company, such as the production and transportation of fuels used to generate electricity. According to the Carbon Disclosure Project (CDP) (Ott et al. 2017),

indirect “scope 3” emissions represent, on average, 80% of a company’s total electricity-related emissions). Reducing these indirect emissions requires a holistic approach involving collaboration between different stakeholders in the energy supply chain.

The concept of circular economy has attracted increasing interest in recent times due to its great potential to significantly reduce the carbon footprint, including through waste minimization and resource efficiency (Al-Hamrani et al. 2021). For an electricity distribution company, the circular economy offers an innovative approach to optimizing the use and value of materials throughout their life cycle while actively contributing to waste minimization.

In Morocco, the electricity sector is booming. It plays a crucial role in the economic and social development of the country. However, due to its dependence on fossil energy sources, it is also one of the main contributors to greenhouse gas (GHG) emissions in the country. These emissions include both direct emissions from electricity generation and indirect emissions from inputs and activities upstream of the company’s value chain.

Morocco's direct greenhouse gas emissions reached 85,224 Gg CO₂e (gigagrams of CO₂ equivalent). The energy sector was the largest emitter, contributing 47,890 Gg CO₂e, accounting for 63.5% of net national emissions in 2020 (Khan et al. 2022).

Morocco has adopted a proactive policy in the fight against climate change since its participation in the Rio Conference in 1992. The country has put in place regulatory frameworks, such as the National Greenhouse Gas Inventory System (SNIGES), and developed national strategies for sustainable development and adaptation to climate change (Schilling et al. 2012).

In terms of mitigation, Morocco has pledged to reduce its greenhouse gas emissions by 17% by 2030, with the possibility of raising this target to 42%, depending on international support (Okpanachi et al. 2022).

This study aims to calculate the climate change impacts of electricity distribution phases by applying a life-cycle approach to the case of an electricity distribution company in Morocco. This assessment makes it possible to identify significant contributors from each area. In the context of this company, it is a question of demonstrating how the application of the principles of the circular economy concepts contributes to the reduction of greenhouse gas emissions, in particular, that of scope 3. This study may be useful for other similar companies.

In China, Song et al. (2023) assessed the carbon footprint of the electricity sector using the life cycle assessment approach. The study identified coal-fired power plants as the main source of emissions in the electricity sector. To reduce this carbon footprint, the researchers recommended adopting renewable energy sources such as solar, wind, and hydropower, as well as developing carbon capture and storage technologies to minimize emissions from coal-fired power plants.

In the Netherlands, (Moretti et al. (2022) assessed the carbon footprint of the electricity sector using the national inventory approach. The study found that coal and natural gas power plants were the main sources of emissions. To address these emissions, the researchers advocated for the increased use of renewable energy sources, such as offshore wind and biomass, as well as the implementation of energy storage systems to promote the integration of renewables into the electricity grid.

In Nigeria, Oluseyi et al. (2016) assessed the carbon footprint of the oil and gas sector using the life cycle assessment approach. The study identified gas flaring and oil spills as the main sources of emissions. To mitigate these emissions, the researchers recommended the

adoption of renewable energy sources, such as solar and biomass, as well as environmental remediation measures to minimize the impacts of oil and gas activities on the environment.

The circular economy is based on several key principles, such as designing durable and easy-to-repair products, promoting the functional economy where services are privileged over property ownership, and optimizing waste management systems to recover and recover end-of-life materials. This economic model is emerging as a promising approach to addressing environmental challenges, such as climate change, by reducing greenhouse gas emissions and conserving natural resources (Deutz 2020).

In the electricity sector, the circular economy offers significant potential to reduce its carbon footprint. By integrating circular practices such as the use of renewable energy sources, the optimization of logistics flows, and the reuse of equipment, electricity distribution companies can not only reduce their indirect emissions but also contribute to a transition to a more sustainable and climate-resilient energy model (Chishti et al. 2023).

Geissdoerfer et al. (2017) explored the concept of the circular economy as a new sustainability paradigm. Researchers highlighted the importance of the circular economy in reducing GHG emissions by promoting the design of sustainable products and services, extending the life of products through reuse and recycling, and optimizing supply chains. The article also highlighted the potential economic and environmental benefits of the circular economy in the electricity sector.

Ghisellini et al. (2016) offered an in-depth analysis of the circular economy with a focus on the balance between environmental and economic systems. The study explored how the circular economy can reduce GHG emissions by promoting more efficient use of resources, minimizing waste, and promoting the regeneration of materials. The article also highlighted the political, economic, and social implications of the transition to a circular economy.

Yin et al. (2023) reviewed circular economy practices, guidelines, frameworks, and standards. They examined how these instruments can be applied in the electricity sector to reduce GHG emissions and improve environmental sustainability. The article also identified the challenges and opportunities associated with adopting the circular economy in the specific context of the electricity sector.

The literature review confirms the need to integrate the circular economy to act on scope 3 of the carbon footprint of the electricity sector and thus reduce GHG emissions from this sector.

The case study subject of this research proposes EC's concrete actions to act on scope 3 of the carbon footprint of an energy distribution company in Morocco.

Life Cycle Assessment (LCA) is the main tool used to assess the potential environmental impacts of products or services throughout their life cycle, from the extraction of raw materials to their disposal or recycling (Halvaei Khankahdani et al. 2023). LCA follows a four-step iterative model defined by the International Organization for Standardization (Keiser et al. 2023). These steps include defining the purpose and scope of the analysis, inventory analysis to collect data on materials and energy used, assessing environmental impacts throughout the life cycle, and finally, interpreting the results obtained.

The studies highlight the importance of adopting circular practices and promoting renewable energy sources in the electricity sector to reduce the carbon footprint.

MATERIALS AND METHODS

As shown in the methodology, Fig. 1 is carried out in several stages.

The greenhouse gases (GHGs) considered in this study are those defined by the Kyoto Protocol (Pata & Ertugrul 2023), which include carbon dioxide (CO₂), methane (CH₄), nitrous oxide (N₂O), sulfur hexafluoride (SF₆), hydrofluorocarbons (HFCs), hydrochlorofluorocarbons (HCFCs) and nitrogen trifluoride (NF₃) [29] (Chanda & Bose 2020)

Emission elements are classified according to three fields of application: scope 1, which includes the energy consumption of buildings; scope 2, which includes direct GHG emissions from stationary and mobile sources, such as fuel for light- and heavy-duty vehicles and other fuels and hydrocarbons; and scope 3, which includes other indirect emissions such as the purchase of undistributed water (losses), the purchase of works and services, the purchase of goods and chemicals, fixed assets (buildings, vehicles, IT), employee commuting and other energy-related emissions

(excluding combustion). To assess the GHG emissions associated with each element of the organization's activity, emission factors are used. An emission factor is a measure of the mass of GHGs (measured in kgCO₂eq) emitted per unit of an activity input.

Scope of the Greenhouse Gas Emissions Inventory

The company is a public service operator that manages the distribution of electricity in a major city in Morocco. In addition to its main activity, emissions associated with the administrative management of the company and the procurement of goods and services are also taken into account.

Program Categories

Emission elements are classified into three domains. Scopes are a method of classifying the greenhouse gas (GHG) emissions of a business or activity. They are defined by the Kyoto Protocol and widely used to assess a company's environmental impact and develop emission reduction plans.

- Scope 1 encompasses all direct GHG emissions generated by a business or activity, such as emissions from fuel combustion for vehicles and stationary equipment. Emissions related to the production of energy from fuel sources, such as power plants, are also included in this category.
- Scope 2 includes indirect GHG emissions generated by the energy supply of a company or activity, such as electricity, heat, or cold consumption. It also includes electrical losses that occur during the transmission and distribution of energy.
- Scope 3 is a broader category and includes all other indirect emissions generated by a company or activity, such as supplier emissions, production of raw materials, purchases of goods and services, emissions related to product use, and emissions related to employee commuting.

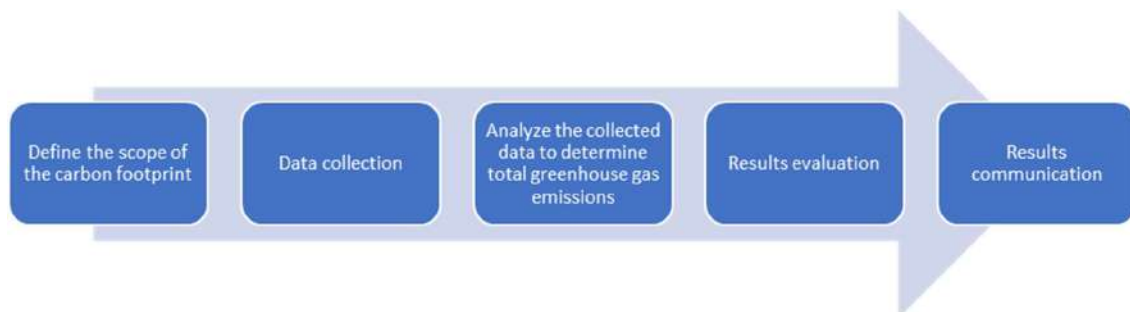


Fig. 1: Methodology.

Table 1: List of activity data and source.

Data	Entities
Number of employees by type of job and activity	Human Resources Branch
Electricity consumption of buildings	HR Department
Water supply and sanitation operations	Logistics Department
Electrical and street lighting operations	Operations Department
Process fuel consumption	Operations Department
Electricity and street lighting	Operations Department
Number and area of buildings	Department of Water and Sanitation Operations
Department of Information Systems of Computer Assets	Logistics Department
Purchase of paper	IT Department
Chemical procurement	Logistics Department
Water and sanitation operations	Operations Department
Purchase of goods and services	Operations Department
Fleet	Procurement Department
Employee commuting	Department of Logistics
Drinking water system losses	Estimate based on the number of employees and a survey on travel patterns in Morocco
Quantity of sludge produced	Water and sanitation
Electricity grid losses	Operations Department
Office waste	Operations Department

The data necessary for the development of the carbon footprint were collected from the departments concerned. Where data were not available, a number of assumptions were used to estimate them from existing data. Table 1 summarizes the data collected for the carbon footprint and its sources: either the department that provided it or the assumptions used to estimate it.

Data Source

The data necessary for the preparation of this study were collected from the departments concerned. Where data were not available, a number of assumptions were used to estimate them from existing data. Table 1 summarizes the data collected for the carbon footprint and its sources: either the department that provided it or the assumptions used to estimate it.

RESULTS AND DISCUSSION

Total emissions amount to 375,000 TeqCO₂ (with an uncertainty of about 12%). The electricity distribution activity accounts for more than 50% of this balance (Fig. 2 and Fig. 3).

Table 2 shows the distribution of emissions by scope. 80% of emissions are related to electricity consumption. These emissions (Fig. 4 to Fig. 6) associated with electricity are mainly classified in Scope 2 (73% of emissions), with the exception of upstream emissions related to fuel extraction, which are included in Scope 3. Direct scope 1 emissions represent only 1% of total emissions. Scope 3 accounts for 26% of emissions, which are mainly based on the purchase of products and services and emissions related to fuel extraction and transportation.

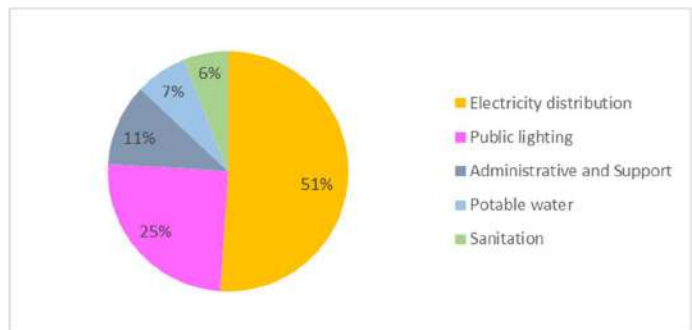


Fig. 2: Breakdown of total GHG emissions by activity.

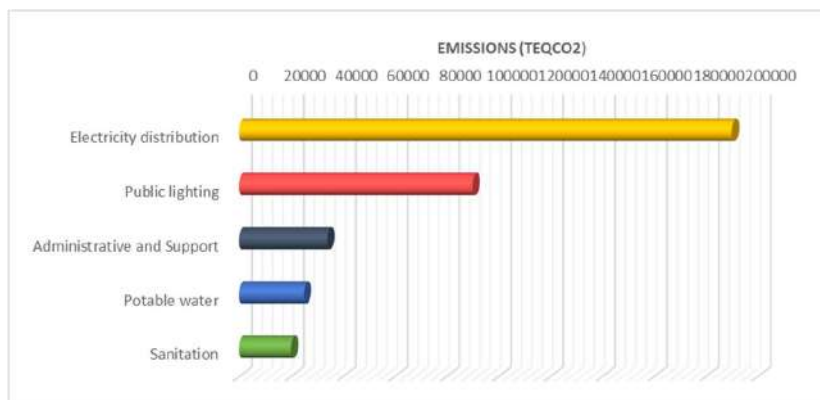


Fig. 3: Volume of GHG emissions by activity.

Table 2: Breakdown of GHG emissions by scope and category.

Program categories	No.	Issuance stations	Potable water	Sanitation	electricity	Public lighting	Admin and Support	Total	%
Direct GHG emissions	1	Direct emissions from stationary combustion sources		14				14	0%
	2	Direct emissions from mobile heat engine sources	451	607	576	158	2 210	4 002	1%
	3	Direct emissions from non-energy processes						-	
	4	Fugitive direct emissions						-	
	5	Emissions from biomass (soils and forests)						-	
		Subtotal	451	620	576	158	2 210	4 016	1%
Indirect emissions associated with energy	6	Indirect emissions related to electricity consumption	11 074	11 291	164 731	83 308	-	270 403	72%
	7	Indirect emissions linked to the consumption of steam, heat, or cold						-	
		Subtotal	11 074	11 291	164 731	83 308	-	270 403	72%
Other indirect GHG emissions	8	Energy-related emissions not included in items 1 to 7	1 146	1 214	15 295	7 697	641	25 993	7%
	9	Purchases of products or services	11 792	7 861	7 249	2 010	33 698	62 611	17%
	10	Capital assets	2 051	2 698	3 220	716	1 395	10 080	3%
	11	Waste	21	33	24	8	367	453	0%
	12	Upstream freight transport						-	
	13	Business trips						-	
	14	Upstream leased assets						-	
	15	Investments						-	
	16	Transportation of visitors and customers						-	
	17	Downstream goods transport						-	
	18	Use of products sold						-	
	19	End of life of products sold						-	
	20	Downstream deductible						-	
	21	Downstream leasing						-	
	22	Home-to-work travel	96	131	122	34	564	947	0%
23	Other indirect emissions						-		
		Subtotal	15 106	11 938	25 910	10 465	36 665	100 083	27%
Total			26 631	23 849	191 216	93 931	38 875	374 502	100%

Circular Economy Strategy to Reduce Emissions

Morocco’s ambition to reduce its GHG emissions and develop renewable and recovery energies should lead

the Moroccan electricity mix to evolve in the coming years. However, more than 81% of the company’s emissions are attributable to the electricity mix distributed on the grid. A “greening” of electricity production in

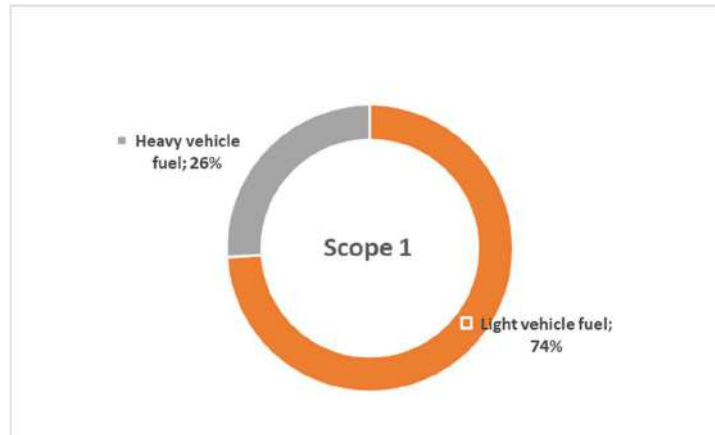


Fig. 4: Scope 1 of GHG emissions.

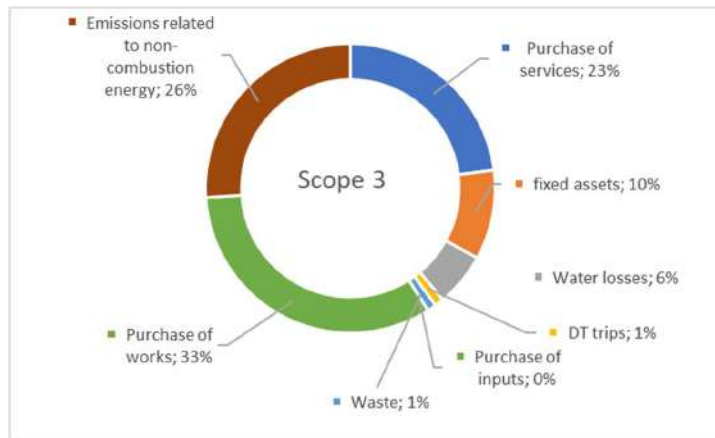


Fig. 5: Scope 2 of GHG emissions.

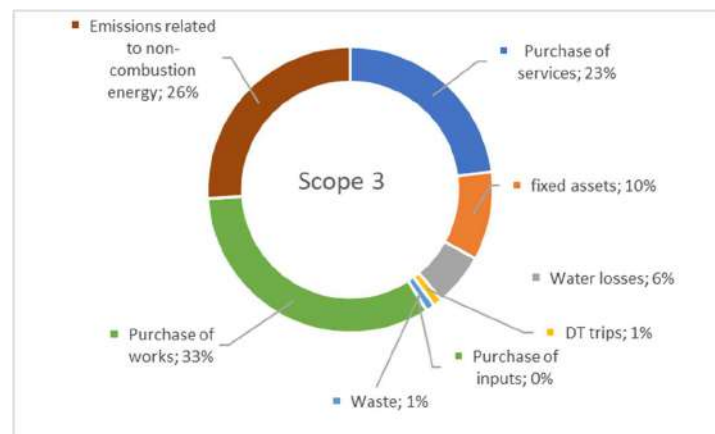


Fig. 6: Scope 3 of GHG emissions.

Morocco would, therefore, have a positive impact on the reduction of GHG emissions from this company's balance sheet.

The objective set by Morocco is to reach by 2030 a share of renewable energy in electricity production of 52% in installed capacity. In 2020, it was estimated at 36.80%, below

the national target of 42%. In 2018, it was 34% in installed capacity, for a real share in electricity production of 19% (11% wind, 4% solar, 4% hydro). The emission factor given by ADEME for electricity distributed on the Moroccan grid was 0.718 kgCO₂/kWh (Ourya et al. 2023).

Assuming a share of renewable energies in electricity production that would increase proportionally to the installed capacity (according to the national target), i.e., +53% between 2018 and 2030, the emission factor of the Moroccan electricity mix in 2030 would be about 0.63 kgCO₂/kWh.

This estimate is deliberately conservative to avoid overestimating the impact of renewable energy development over the next decade. However, it can be assumed that this emission factor is likely to be lower than this Fig. If we assume that the electricity purchased by the company will

follow this same trend, the GHG emissions associated with consumption or the loss of 1 kWh on the grid would lead to 12% lower emissions in 2030.

To take into account this probable evolution of the energy mix, it was decided to determine the following:

A conditional trend trajectory A conditional reduction scenario, which corresponds respectively to the trajectory of “normal business” emissions until 2030, assuming that the Moroccan electricity mix improves, and to the objectives that the company sets itself to achieve in 2026 and 2030, assuming that the Moroccan electricity mix improves.

Following the estimation of the evolution of the activity and the evolution of the Moroccan electricity mix, the trend trajectory and the conditional trend trajectory can be defined in the following Table 3.

Table 3: Trend in GHG emissions.

Trajectory	Total GHG emissions (teqCO ₂)		
	2022	2026	2030
Trend trajectory	375 000	387 000	393 000
Conditional trend trajectory (taking into account the development of renewable energies in the Moroccan electricity mix)	375 000	362 000	355 000
Lower emissions are related to the improvement of the electricity mix compared to the trend trajectory.		-6,5%	-9,8%

Table 4: Objectives scope by scope.

Scope	Objective	Comment
Scope 1	-46%	The targets are based on a -46% trajectory of scope 1 emissions compared to the trend trajectory. As the trend trajectory is based on 2022 emissions, this corresponds to a -46% decrease in scope 1 emissions between 2022 and 2030.
Scope 2	-29%	The targets are based on a trajectory of -29% of scope 2 emissions compared to the trend trajectory. Scope 2 is particularly heavy since it counts emissions related to electrical losses on the network and those related to public lighting. It is directly linked to the deployment of an essential service for the city's population, which explains why it is more complex to reduce, even if orientations 1 and 2 have significant potential for reduction.
Scope 3	-16%	The targets are based on a 16% decrease in scope 3 emissions compared to the trend trajectory in 2030 (i.e., a 15% decrease in scope 3 emissions compared to the initial situation in 2019).

Table 5: Evolution of emissions between 2022 and 2030, according to the trend trajectory and the reduction target, and comparison of emissions in 2030, by item. Emissions are in thousands of teqCO₂.

Post	Emissions 2022	Emissions 2030 (trend trajectory)	2030 emissions (reduction target)	Emissions lower than trend if targets are met
Electrical losses	175	162	118	-27%
Public lighting	91	112	76	-32%
Electricity consumption	30	40	25	-36%
Fuel	5	5	3	-46%
Water loss	6	7	6	-14%
Shopping	57	57	46	-19%
Other travel	1	1	1	-19%
Fixed assets	10	10	10	-6%
Rubbish	0,5	0,5	0,3	-30%
Total	375 000	393 000	284 933	-28%

Taken scope by scope, the objectives correspond to the following evolution (Table 4).

The GHG emissions reduction target would reduce its annual emissions by nearly 110,000 teqCO₂ by 2030, and avoid emissions of nearly 600,000 teqCO₂ over the decade 2020-2030. Table 5 shows the expected emission reductions on the various items.

Estimation of Reduction Potential By Orientation

The purpose of the action plan is not to set a specific GHG emission reduction target at the action level since GHG emissions are not a directly measurable indicator for monitoring the implementation of an action. The evaluation of the emission reduction impact of each action, therefore, serves, above all, the overall vision (Fig 7): to identify an order of magnitude of reduction in order to determine the achievable objectives. It can also be used to estimate the reduction potential associated with each of the identified orientations. It is thus a question of highlighting the prioritization of orientations.

RECOMMENDATIONS

Encourage the Supply of Renewable Energies to the Grid

Law 13.09 obliges the distributor to buy back electricity from renewable sources from medium-voltage producers (Fritzsche et al. 2011). Bill 40.19 aims to allow network operators to obtain supplies from renewable energy production facilities connected to the MV grid to compensate

for the energy used for network management and technical losses (Hawila et al. 2014) within the limit of 7% of the total annual volume distributed (i.e., nearly 300 GWh for the company) the possibilities that the evolution of the legal framework allows it to increase the share of RE on its network.

Responsible Low-carbon Procurement Policy

Many researchers are developing green and sustainable supply chain networks to diminish greenhouse gas release (Abbasi & Ahmadi Choukolaei 2023). The following actions were recommended to identify the main purchasing items requiring further study and identify during workshops the main impacts of energy consumption, resource conservation, and biodiversity protection, review scoring grids to request minimum requirements on environmental criteria. Involve standardization management, act first on the energy performance of equipment, then on its eco-design, and identify relevant labels and certifications to be required.

It is also important to educate buyers about environmental issues. Sustainable development training has already taken place with buyers and should be renewed regularly and provided to each newcomer.

Support suppliers in their transition. As an important economic player in the industry of the city, the company has a role to play in the evolution of the practices of its ecosystem. To support immature suppliers, the first steps can be taken, starting with reporting and transparency requirements.

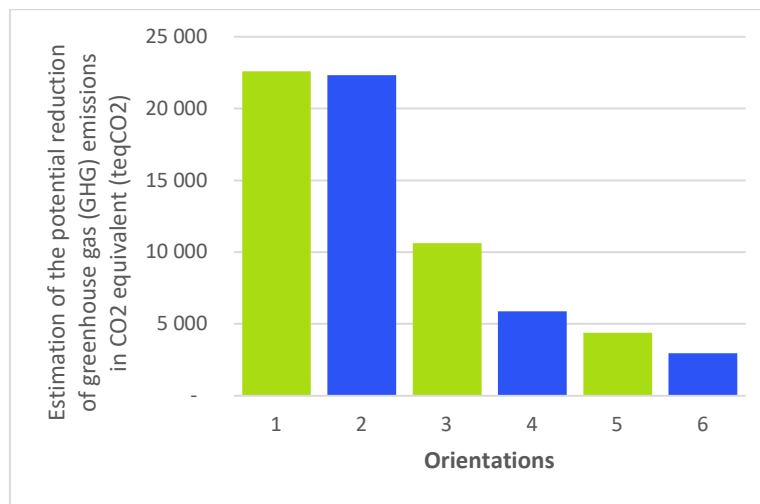


Fig. 7: Estimated GHG emission reduction potential.

Orientation 1: Reducing emissions from electrical losses, Orientation 2: Performance of public lighting, Orientation 3: Responsible low-carbon procurement policy, Orientation 4: Business Process Performance, Orientation 5: Management of buildings and sites, Orientation 6: Reducing travel-related GHG emissions, Orientation 7: Anchoring the DD/environment reflex internally

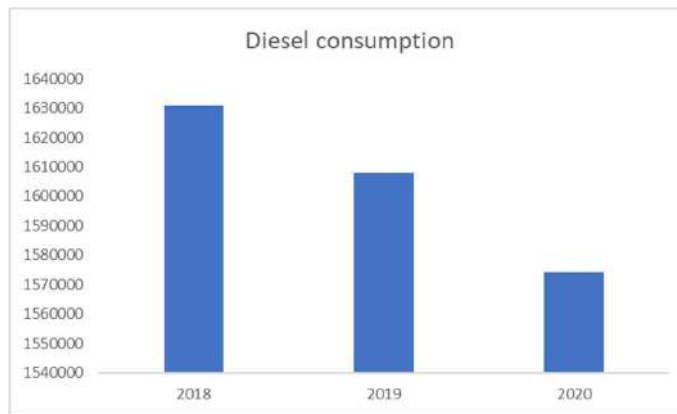


Fig. 8: Diesel Consumption.

Work for the implementation of centralized and automatic reporting of activity data (energy consumption, energy production, number and type of air conditioners, water consumption, vehicles, materials, waste). A dashboard for monitoring energy or even environmental data would be an effective decision-making tool.

Reducing Travel-Related GHG Emissions

One of the primary goals of the current program is centered around enhancing the energy efficiency of the vehicle fleets. An assessment of the fuel consumption of the fleet and a corresponding action plan featuring suggestions to curtail environmentally detrimental emissions have been formulated. The transport energy audit serves as a valuable opportunity to comprehend the energy usage of the company's vehicle fleet and the financial outlay linked to this usage and to pinpoint strategies for streamlining energy consumption (such as adopting eco-friendly driving practices and maintaining tires properly).

To further refine fleet optimization, particularly from an economic standpoint, a comprehensive evaluation of the vehicle fleet was conducted. The objective was to evaluate the appropriateness of vehicle usage in relation to the company's requirements. This evaluation provided a basis to advocate for the incorporation of alternative mobility solutions (like electric vehicles and electric-assisted bicycles) or the reduction in the number of vehicles by embracing shared alternatives (such as car-sharing and bicycle-sharing).

As indicated in Fig. 8, the consumption of diesel fuel exhibited fluctuations, decreasing from 1,630,723 liters in 2018 to 1,607,909 liters in 2019, and further down to 1,574,135 liters in 2020. This translates to reductions of approximately 1% and 2% for the respective years, with a cumulative change of around -1.4% and -2.1% in 2020.

It was recommended to encourage alternative modes of transport for commuting and between sites, conduct a travel survey to know the modes of transport of employees, propose solutions for greening travel (carpooling applications, partnership with the public transport organization, bicycle subsidy...), promote the geographical mobility of agents for more coherence between the place of life and the workplace, lead a reflection on teleworking, and the use of videoconferencing instead of inter-site travel for short meetings and encourage initiatives around new modes of travel. Thus, a test of electric vehicles was carried out. If this technology appears for the moment as expensive and immature, this type of initiative is to be encouraged (hybrid vehicles, CNG trucks, multi-trip optimization software, etc.) in order to identify potentially interesting solutions.

CONCLUSION

In conclusion, the article highlights the urgent need to decarbonize the energy sector to mitigate the adverse effects of climate change. Morocco has implemented various measures to transition to renewable energy sources and improve energy efficiency. However, reducing the carbon footprint of the energy sector remains a major challenge, especially in the electricity distribution sector, which contributes significantly to greenhouse gas emissions. The case study of the Moroccan electricity distribution company provides useful information on strategies that can be implemented to reduce carbon emissions. The energy transition offers significant economic and environmental opportunities for countries like Morocco.

REFERENCES

- Abbasi, S. and Ahmadi Choukolaei, H. 2023. A systematic review of green supply chain network design literature focusing on carbon policy. *Decis. Analytics J.*, 6: 100189. <https://doi.org/10.1016/j.dajour.2023.100189>

- Al-Hamrani, A., Kim, D., Kucukvar, M. and Onat, N. C. 2021. Circular economy application for a Green Stadium construction towards sustainable FIFA World Cup Qatar 2022TM. *Environ. Impact Assess. Rev.*, 87: 106543. <https://doi.org/10.1016/j.eiar.2020.106543>
- Chanda, C.K. and Bose, D. 2020a. Challenges of Employing Renewable Energy for Reducing Greenhouse Gases (GHGs) and Carbon Footprint. Elsevier, The Netherlands, pp. 346-365. <https://doi.org/10.1016/B978-0-12-803581-8.11170-1>
- Chishti, M. Z., Dogan, E. and Zaman, U. 2023. Effects of the circular economy, environmental policy, energy transition, and geopolitical risk on sustainable electricity generation. *Util. Policy*, 82: 101585. <https://doi.org/10.1016/j.jup.2023.101585>
- Deutz, P. 2020. Circular economy. In *Int. Encycl. Human Geogr.*, p. 193-201. Elsevier. <https://doi.org/10.1016/B978-0-08-102295-5.10630-4>
- Fritzsche, K., Zejli, D. and Tänzler, D. 2011. The relevance of global energy governance for Arab countries : The case of Morocco. *Energy Policy*, 39(8): 4497-4506. <https://doi.org/10.1016/j.enpol.2010.11.042>
- Geissdoerfer, M., Savaget, P., Bocken, N.M.P. and Hultink, E.J. 2017. The circular economy: A new sustainability paradigm? *J. Clean. Prod.*, 143: 757-768. <https://doi.org/10.1016/j.jclepro.2016.12.048>
- Ghisellini, P., Cialani, C. and Ulgiati, S. 2016. A review on circular economy : The expected transition to a balanced interplay of environmental and economic systems. *J. Clean. Prod.*, 114: 11-32. <https://doi.org/10.1016/j.jclepro.2015.09.007>
- Halvaei Khankahdani, Z., Ghazimoradi, M.M. and Abdollahi, M. 2023. Life cycle assessment. In *Ref. Module Biomed. Sci.*, p. B9780128243152007000. Elsevier. <https://doi.org/10.1016/B978-0-12-824315-2.00735-1>
- Hawila, D., Mondal, M.D., Kennedy, S. and Mezher, T. 2014. Renewable energy readiness assessment for North African countries. *Renew. Sustain. Energy Rev.*, 33: 128-140. <https://doi.org/10.1016/j.rser.2014.01.066>
- Keiser, D., Schnoor, L.H., Pupkes, B. and Freitag, M. 2023. Life cycle assessment in aviation : A systematic literature review of applications, methodological approaches, and challenges. *J. Air Transp. Manag.*, 110: 102418. <https://doi.org/10.1016/j.jairtraman.2023.102418>
- Khan, Y., Oubaih, H. and Elgourami, F.Z. 2022. The effect of renewable energy sources on carbon dioxide emissions : Evaluating the role of governance and ICT in Morocco. *Renew. Energy*, 190: 752-763. <https://doi.org/10.1016/j.renene.2022.03.140>
- Kiss, B., Kácsor, E. and Szalay, Z. 2020. Environmental assessment of future electricity mix – Linking an hourly economic model with LCA. *J. Clean. Prod.*, 264: 121536. <https://doi.org/10.1016/j.jclepro.2020.121536>
- Moretti, C., Hoefnagels, R., Van Veen, M., Corona, B., Obydenkova, S., Russell, S., Jongerius, A., Vural-Gürsel, I. and Junginger, M. 2022. Using lignin from local biorefineries for asphalts : LCA case study for the Netherlands. *J. Clean. Prod.*, 343: 131063. <https://doi.org/10.1016/j.jclepro.2022.131063>
- Okpanachi, E., Ambe-Uva, T. and Fassih, A. 2022. Energy regime reconfiguration and just transitions in the Global South : Lessons for West Africa from Morocco's comparative experience. *Futures*, 139: 102934. <https://doi.org/10.1016/j.futures.2022.102934>
- Oluseyi, P.O., Babatunde, O.M. and Babatunde, O.A. 2016. Assessment of energy consumption and carbon footprint from the hotel sector within Lagos, Nigeria. *Energy Build.*, 118: 106-113. <https://doi.org/10.1016/j.enbuild.2016.02.046>
- Ott, C., Schiemann, F. and Günther, T. 2017. Disentangling the determinants of the response and the publication decisions : The case of the Carbon Disclosure Project. *J. Account. Public Policy*, 36(1): 14-33. <https://doi.org/10.1016/j.jaccpubpol.2016.11.003>
- Ourya, I., Nabil, N., Abderafi, S., Boutammache, N. and Rachidi, S. 2023. Assessment of green hydrogen production in Morocco, using hybrid renewable sources (PV and wind). *Int. J. Hydrogen Energy*, 03: 898. <https://doi.org/10.1016/j.ijhydene.2022.12.362>
- Pata, U.K. and Ertugrul, H.M. 2023. Do the Kyoto Protocol, geopolitical risks, human capital, and natural resources affect the sustainability limit? A new environmental approach based on the LCC hypothesis. *Resour. Policy*, 81: 103352. <https://doi.org/10.1016/j.resourpol.2023.103352>
- Ray, A. and De, S. 2020. Renewable Electricity Generation – Effect on GHG Emission. In S. Hashmi & I. A. Choudhury (Eds.), *Encyclopedia of Renewable and Sustainable Materials*, p. 728-735. Elsevier. <https://doi.org/10.1016/B978-0-12-803581-8.11015-X>
- Schilling, J., Freier, K.P., Hertig, E. and Scheffran, J. 2012. Climate change, vulnerability, and adaptation in North Africa with a focus on Morocco. *Agric. Ecosyst. Environ.*, 156: 12-26. <https://doi.org/10.1016/j.agee.2012.04.021>
- Song, M., Zhang, L., Gao, Y. and Li, E. 2023. Spatiotemporal evolution and influence mechanism of the carbon footprint of energy consumption at the county level in the Yellow River Basin. *Sci. Total Environ.*, 883: 163710. <https://doi.org/10.1016/j.scitotenv.2023.163710>
- Yin, S., Jia, F., Chen, L. and Wang, Q. 2023. Circular economy practices and sustainable performance : A meta-analysis. *Resour. Conserv. Recycl.*, 190: 106838. <https://doi.org/10.1016/j.resconrec.2022.106838>



Moss Bags as Active Biomonitorers of Air Pollution: Current State of Understanding, Applications and Concerns

Sriroop Chaudhuri  and Mimi Roy

Center for Environment, Sustainability and Human Development (CESH), Jindal School of Liberal Arts and Humanities, O.P. Jindal Global University, Sonapat-131001, Haryana, India

†Corresponding author: Sriroop Chaudhuri; schaudhuri@jgu.edu.in

Nat. Env. & Poll. Tech.
Website: www.neptjournal.com

Received: 31-08-2023
Revised: 26-10-2023
Accepted: 02-11-2023

Key Words:

Moss bag
Urban sustainability
Metal and PAH monitoring
Air quality assessment
Environmental indicators
Parameterization

ABSTRACT

Dual concerns involving the rise in airborne pollutant levels and bulging need to protect-preserve human health have propelled the search for innovative means for air quality monitoring to aid in evidence-based decision-making (pollution prevention-mitigation). In this regard, *moss bags* have gathered a great deal of attention as *active* biomonitorers. In this reflective discourse, we systematically review the world literature to present a bird's eye view of moss bag applications and advances while highlighting potential concerns. We begin with a brief note on mosses as biomonitorers, highlighting the advantages of moss bags over the *passive* technique (native moss), other living organisms (lichens, vascular plants), and instrument-based measurements. A major strand of moss bag research involves urban ecosystem sustainability studies (e.g., street tunnels and canyons, parks), while others include event-specific monitoring and change detection (e.g., SARS-CoV-2 Lockdown), indoor-outdoor air quality assessment, and change detection in land use patterns. Recent advances include biomagnetic studies, radioisotopic investigations, and mobile applications. Efforts are currently underway to couple moss bag results with a suite of indicators [e.g., relative accumulation factor (RAF), contamination factor (CF), pollution load index (PLI), enrichment factor (EF)] and spatially map the results for holistic appraisal of environmental quality (*hot spot* detection). However, while moss bag innovations and applications continue to grow over time, we point to fundamental concerns/uncertainties (e.g., lack of concordance in operational procedures and parameterization, ideal species selection, moss vitality) that still need to be addressed by targeted case studies, before the moss results could be considered in regulatory interventions.

INTRODUCTION

Worldwide surges in air quality-induced public health disorder in the recent past have prompted research to devise novel air quality monitoring techniques (Kumar & Chaudhuri 2022a, b, Kumar and Chaudhuri, 2021) to aid in more informed regulatory decision-making (pollution prevention-mitigation). In the process, an emerging strand of research is devoted to the exploration of various biomonitor species, including vascular plants (trees) (Chaudhuri & Kumar 2022), lichens (Malaspina et al. 2018), and mosses (Vuković et al. 2014, Capozzi et al. 2019, Ștefănuț et al. 2019, Chaudhuri & Roy 2023). Biomonitoring, with the strategic use of living organisms as natural markers of environmental conditions, has been a growing interest among the world research community (Guarino et al. 2021). In this regard, mosses as biomonitorers of ambient air quality have attracted a great deal of attention (Zechmeister et al. 2006, Świsłowski et al. 2022).

Moss-based biomonitoring comes under two main types: passive and active. While the former involves natively occurring species (Chaudhuri & Roy 2023), the latter uses moss transplant in specially constructed bags, exposed over a certain period for natural interception of airborne pollutants (Urošević et al. 2017). Moss bags have been used in a variety of applications involving metals and metalloids (Shvetsova et al. 2019; Zechmeister et al. 2006), polycyclic aromatic hydrocarbons (PAHs) (Di Nicola et al. 2013), atmospheric microfibers (Bertrim & Aherne 2023), and radionuclides (Isidora et al. 2015). In this reflective article, we systematically scan the moss bag literature, using a universally recognized method -the PRISMA (Preferred Reporting Items for Systematic Reviews and Meta-Analyses) (Parakh & Chaudhuri 2023, Adithyalakshmanan et al. 2022), to present a summary view of the experiences and advances using moss bags alongside the concerns and potential future research directions.

We initiate the article by reflecting on the advantages of mosses as biomonitors, followed by a comparative overview of moss bags as against naturally occurring moss (passive techniques) and other organisms (lichens, trees), as well as traditional, instrument-based air quality measurements. Next, we highlight applications of moss bags in various domains of air quality monitoring and assessment. However, an implicit idea in envisioning this study was also to highlight the uncertainties/ambiguities around moss bag research. To that end, in the final sections, we point to certain areas that will require targeted research in days ahead for moss bags to be included in formal regulatory mechanisms. Overall, an implicit motive to present this narrative was to invite process-level discourses to discover newer avenues to expand the reach of moss bags as active biomonitors of ambient air quality. An additional motivation to imagine this research came from our belief that observations made in this narrative may even contribute to the growing research areas of several of the UN sustainable Development goals (UN SDGs) tied to air quality - Good Health and Well Being (SDG 3), Sustainable Cities (SDG 11), Life on Land (SDG 15), Partnership building (SDG 17), to name a few. Collectively, we expect, strategic and well-informed use of moss bags may become a widely adopted regulatory tool to align with climate combat interventions (SDG 13), especially for nations challenged by multidimensional financial-infrastructure shortcomings to install traditional sensor-based monitoring networks.

MATERIALS AND METHODS

We identified relevant literature using the multi-stage PRISMA methodology (*Preferred Reporting Items for Systematic Reviews and Meta-analyses*) (Chaudhuri et al. 2021). The PRISMA literature search and selection methodology comprises four main stages:

- I. **Initial Document Identification:** The search is initiated by using the search words/phrases (listed below) in a variety of search engines, including SCOPUS, PubMed, Science Direct, Springer Lin, Blackwell, and Social Citation Index, Web of Science (WoS), EconLit, JSTOR, and complemented with Google Scholar. This stage of PRISMA identified 84 documents.
- II. **Screening/Exclusion:** Documents selected by the previous stage were subjected to further checks using certain pre-established rules (or norms), such as duplication of results, abstract-only documents, and documents published in foreign languages, to name a few. 21 documents were excluded from the initial selection.
- III. **Eligibility Test:** To further refine and eliminate articles, 18 documents did not meet the eligibility criteria, such

as objectives not aligning adequately with the present study, too many confounding variables, research methodology not clearly outlined, lack of process-level interpretations, no discussion on limitations and/or on future research directions.

- IV. **Final Inclusion:** At the final stage of PRISMS, 46 documents were retained to be considered for review in the main body of the research

Search words/phrases were divided into 5 categories:

Category I: 'active biomonitor*', 'moss bag.'

Category II: 'species,' 'Sphagnum,' 'Hypnum,' 'Pleurozium.'

Category III: 'trace metal,' 'heavy metal,' 'PAH,' 'polycyclic *,' 'pollutant*.'

Category IV: 'clean*', 'wash*', 'dry*', 'shape', 'mesh *', 'pack*', 'exposure *'

Category V: 'standardize*', 'meteorological *'

For each category between II and IV, the term moss bag and/or active biomonitoring was added as a suffix or prefix. The asterisk symbol (***) was used as a wildcard to expand the search horizon. In the final step, 104 documents were retained to be included in the review (Chaudhuri et al. 2020).

General Observations

Why moss: A confluence of physiological traits makes mosses ideal air quality sensors (Chakraborty & Paratkar 2006, Chaudhuri & Roy 2023), including their ubiquitous geographic occurrence lack of real root system (only supporting pseudo roots), which means that nutrient uptake by mosses is not from mineral substrates (soil) but solely from ambient air; high surface-to-volume ratio; high cation exchange capacity (mainly due to presence of large number of organic functional groups) that increases pollutant interception efficiency. Pollutant uptake/interception by mosses occurs via three broad mechanisms: (a) as an aqueous solution, gas, or solid particles and can adhere to the moss cells' surfaces (*intercellular fraction*); (b) outer walls (via ion exchange process) (*extracellular fraction*), and/or (c) be included into cells (via passive or active transport) (*intracellular fraction*) (Popovic et al. 2010, Fernández et al. 2013).

Moreover, the lack of waxy cuticles on moss leaves (single-layered) further facilitates *direct* pollutant interaction through dorsal and ventral surfaces. Another unique attribute is their slow and long growth cycle coupled with a low degree of differentiation (Gao et al. 2023). The growth points at the tips of stems and branches usually stimulate the continuous and periodic division of cell groups in the lower parts of

mosses, which make them evergreen and, in turn, suitable for seasonal assessment of pollutants (Kromar et al. 2007).

Certain studies even identify mosses as better biomarkers of air quality than trees (vascular plants) and/or lichens (Di Nicola et al. 2013). In a study to assess heavy metal (Fe, Zn, Mn, Cu, Ni, Cd, Pb) pollution due to industrial activities (Harjavalta Cu-Ni smelter, Finland), Saleema et al. (2004) observed the highest metal concentrations in mosses, followed by lichens and lowest in vascular plants. In another comparative assessment between the epiphytic moss *Scorpiurum circinatum* and the epiphytic lichen *Pseudevernia furfuracea*, involving a suite of heavy metals (Al, As, Cd, Co, Cr, Cu, Fe, Mn, Mo, Ni, Pb, Ti, V, and Zn), Basile et al. (2008) found that the *Scorpiurum* sp. had the highest bioaccumulation capacity for all metals and showed a more constant and linear accumulation trend than the lichen. In another study involving 14 different moss and lichen species near the Sivas-Tokat motorway, Turkey, Mendil et al. (2009) found higher bioaccumulation capacity in mosses for several trace and heavy metals (Fe, Mn, Pb, Ni, Cr, Cu, and Cd). Moreover, in comparison with lichens, mosses are more geographically extensive in their distribution, more commonly occur in urban areas, and are more convenient to use by employing passive and active accumulators (Sun et al. 2009, Jiang et al. 2018).

Moreover, unlike traditional instrument-based sensors, mosses can offer an integrated profiling of the ambient element pollution over a certain period (Urošević et al. 2017). Due to their continuous accumulation of elements, mosses offer information about the sources of pollution long after the pollution episode itself took place (Golubev et al. 2005). Other advantages of moss-based biomonitoring include uniformity of receptor surface and exposure period, year-round availability, well-defined background concentrations of contaminants, non-destructive sampling, and greater collection efficiency of most elements (Shotyk et al. 2015).

Why moss bags: Compared to the passive technique (natively growing moss), moss bags appear more controllable as most parameters are known and could be conveniently pre-set as per the research requirements (Ares et al. 2012). Moss bags reduce the high degree of variability in the uptake of contaminants, which is a common case with native moss (Giordano et al. 2009, Adamo et al. 2007).

A unique advantage of moss bags is locational flexibility, which means they can be installed anywhere and everywhere, allowing a dense monitoring network with wider area coverage (Limo et al. 2018, Capozzi et al. 2016). This improves pollutant monitoring efficacy, for example, by generating high-resolution spatial maps to facilitate improved regulatory decision-making (Kosior et al. 2015,

Aničić et al. 2009). The locational advantage is particularly advantageous for point-source pollution monitoring (e.g., industrial emissions) (Makholm & Mladenoff 2005) by placing the bags at strategic locations as per the research requirement. Moreover, as moss bags can be placed at different elevations, they help in vertical profiling of pollutant species (atmospheric stratification patterns) (Ares et al. 2012). This is useful in pollution dispersion studies (e.g., long-range pollutant transport mechanisms).

Other advantages of using mosses include simplicity in operations, lack of the need for a power supply, or regular maintenance (calibration-validation, repair-replace). Moss bags offer better opportunities for temporal assessment of air pollutant patterns as the initial concentrations of target pollutants within moss tissues are known, and the *exposure periods* are fixed (Zechmeister et al. 2006, Aničić et al. 2009). In general, moss literature recommends the use of the passive technique for long-term studies (e.g., decadal assessment, as observed in the European Moss Survey (EMS; 1990-present) (Chaudhuri et al. 2023) with larger spatial dimensions (e.g., national to transnational), while moss bags serve better for micro-environments (e.g., urban habitats) over shorter periods (Gribacheva et al. 2021). However, an often-overlooked aspect of the moss bag approach is, as Zechmeister et al. (2020) pointed out, relatively small increments of pollutant accumulation over time, as compared to the pre-exposure concentrations. Moreover, mosses for the bag should be collected from background areas (unpolluted), which, in recent times, has become quite hard to find (Meier et al. 2015). Therefore, increments in pre-exposure concentrations can only be observed after long exposure periods or at high pollution levels. However, there could be several issues of bag wear and tear when exposed over a prolonged period (rain, storm, human intervention)

Applications and Experiences

Urban sustainability studies: A prime focus of moss bag applications is urban sustainability studies (Table 1). Moss bags are deemed particularly useful for urban/per-urban habitats where natively growing mosses are rare, where occurrences of native mosses are low due to lack of natural environment and rather the predominance of built-up surfaces (paved, walled, artificially landscaped) (Adamo et al. 2007, Urošević et al. 2017, Milicevic et al. 2017, Sorrentino et al. 2021a). To that end, a rich body of research explores moss bag applications in urban street canyons (Vuković et al. 2015, De Nicola et al. 2013, Zechmeister et al. 2006), parks (Shvetsova et al. 2019), and/or parking garages (Vuković et al. 2014). Along that line, moss bags have been used in more specialized urban applications to meet regulatory decision making. For example, In Belgrade, Siberia, Urošević et al.

Table 1: Selected applications of moss bags in urban air quality monitoring and assessment. (Authors' own compilation from various moss bag literature).

Reference	Experimental Design	Observations
Isidora et al. (2015)	<ul style="list-style-type: none"> • Location: Belgrade • Target Pollutant (s): Lead radioisotopes (^{204}Pb, ^{206}Pb, ^{207}Pb, ^{208}Pb) • Environment: Street canyon • Moss: <i>Sphagnum girgensohnii</i> 	<ul style="list-style-type: none"> • Generation of Kohonen self-organizing map (SOM) based on Pb-isotope concentrations in moss tissues • Identification of distinct spatial clusters to aid in regulatory decision-making: <i>delineating pollution hot spots</i> • Detection of small differences in samples that apparently are very similar
Di Nicola et al. (2013)	<ul style="list-style-type: none"> • Place: Naples, Italy • Target Pollutant(s): 11 Metals and 15 Polycyclic Aromatic Hydrocarbons (PAHs) • Environment: Urban street canyon • Moss: <i>Hypnum cupressiforme</i> 	<ul style="list-style-type: none"> • Efficient markers for metals and PAHs at a fine spatial scale • Process-level insights: <ul style="list-style-type: none"> • Poorer air quality was on one side of the canyon due to (i) variations in wind directions and (ii) localized air circulation resulting in differential exposure to vehicular emissions • Moss bag outputs corroborated well with a numerical prediction model (<i>Atmospheric Dispersion Modelling System (ADMS)-Road</i>)
Zechmeister et al. (2006)	<ul style="list-style-type: none"> • Place: Vienna, Austria • Target Pollutant(s): 16 PAHs and heavy metals (Al, Ba, Ca, Co, Cr, Cu, Fe, Ni, Mo, Pb, V, Hg, Cd, S, Sb, Zn) • Environment: Street tunnel • Moss: <i>Hylocomium splendens</i> 	<ul style="list-style-type: none"> • Significantly higher pollutant levels in urban street tunnels (negative health implications) • Process-level insights: <ul style="list-style-type: none"> • Various vehicular processes (e.g., abrasion, diesel combustion) • No dilution effect (rain and/or wind) due to localized air circulation within closed tunnel space • Efficient multi-element air quality monitoring
Salo et al. (2016)	<ul style="list-style-type: none"> • Place: Turku, Finland • Target Pollutant(s): Al, Cr, Fe, Na, Ni, Pb, Cd, As, Zn, V, Hg • Environment: urban parks, courtyards, kindergarten, school yards, streets • Moss: <i>Sphagnum papillosum</i> 	<ul style="list-style-type: none"> • Ability to distinguish seasonal air quality changes (<i>road dust</i> period and summer) • Lower pollutant loadings in parks/courtyards than in urban streets • Spatially representative dataset for air quality monitoring and modeling investigations
Rivera et al. (2011)	<ul style="list-style-type: none"> • Place: Girona, Spain • Target Pollutant(s): NO₂ and metals (Al, As, Cd, Cr, Cu, Mo, Pb, Sb, Sn, Zn) • Environment: High-trafficked urban street • Moss: <i>Hylocomium splendens</i> 	<ul style="list-style-type: none"> • Negative impacts of vehicular emissions on air quality • Process-level insights: <ul style="list-style-type: none"> • Metal concentrations were influenced by traffic intensity (<i>e.g., the number of bus lines in the nearest street</i>) • NO₂ levels were influenced by a combination of local emissions (<i>street traffic</i>) and pollutant transport/dispersion from neighboring areas • Metal levels were more spatially variable than NO₂.
Bertrim & Aherne (2023)	<ul style="list-style-type: none"> • Location: Southern Ontario, Canada • Target Pollutant(s): Microplastics (<5 mm) • Environment: Street canyon • Moss Species: <i>Pleurozium schreberi</i> 	<ul style="list-style-type: none"> • Efficient tools for microplastic detection and characterization in the urban atmosphere (<i>fiber types, dimensions</i>) • A strong influence of urban intensity (population density) on microplastic levels • Identification of spatial changes in microplastic types and concentrations
Van Lateen et al. (20202)	<ul style="list-style-type: none"> • Location: Gena, Central Germany • Target Pollutant(s): Al, Ca, Fe, K, Mg, Mn, Na, P, S, Si, Sr, Ti, Ag, As, B, Ba, Cd, Co, Cr, Cs, Cu, La, Li, Mo, Nb, Ni, Pb • Environment: Railroad lines, motorway • Species: <i>Hypnum cupressiforme</i> 	<ul style="list-style-type: none"> • Efficient multi-element pollutant detection and assessment • Ability to distinguish between natural and anthropogenic sources • Suitable for long-term air quality monitoring and assessment over larger spatial dimensions
Swisłowski et al. (2021a)	<ul style="list-style-type: none"> • Location: Poland • Target Pollutant(s): Polycyclic Aromatic Hydrocarbons (PAHs) • Moss Species: <i>P. schreberi</i>, <i>S. fallax</i>, <i>D. polysetum</i> 	<ul style="list-style-type: none"> • Efficient natural markers of PAH distribution patterns in urban environments • Ability to characterize seasonal variations • Comparable efficiency with instrument-based monitoring • Potential threats of environmental stressors on long-term moss vitality (physiological functions)

(2017) investigated the applicability of moss bags (*Hypnum cupressiforme*) to establish the baseline air quality, taking a botanical garden for control (lower traffic activity). Results indicated significantly different trace metal signatures for the garden (low metal concentrations) in comparison to adjoining streets. However, despite lower values, metal

concentrations in the garden appeared significantly higher, posing health threats.

Event-specific air quality monitoring and change detection: Recent advances demonstrate that moss bags could be useful for short-term air quality monitoring for change detection. In Prószków, Poland, Świsłowski et al.

(2021b) *Pleurozium schreberi* to assess short-term changes in the atmospheric aerosol pollution with selected heavy metals (Ni, Cu, Zn, Cd, Hg, and Pb), in 2019/2020 and 2020/2021. Results demonstrated the negative impacts of New Year fireworks on local air quality, realized by elevated concentrations of all metals. In addition, the authors also observed that the SARS-CoV-2 lockdown in 2020 had an ameliorating effect on air quality (lower metal concentrations). Mao et al. (2021) conducted a moss bag study (*Taxiphyllum taxirameum*) in Xinchang City, China, to monitor short-term changes in air quality (between April 2019 and 2020) involving 12 heavy metals (Al, Cr, Fe, Cu, Ni, Pb, Mn, Hg, Zn, V, As, Ba). Results indicated that due to the lockdown restrictions to stall the SARS-CoV-2 virus spread pandemic, as the vehicular emission levels were cut down alongside tourism, it led to significant drops in ambient air concentrations of several heavy metals (e.g., Pb). However, as a downside, a drop in vehicular emissions triggered atmospheric oxidation events, giving rise to various secondary particulate matter.

Indoor-outdoor air quality: While the need for robust and long-term indoor air quality monitoring has emerged as a critical need for public health experts worldwide (WHO 2018), suitable instrumental facilities are yet limited (Zechmeister et al. 2020). Moreover, with the latter, a main constraint is that these technical devices last only for a few hours to days. In this regard, a small body of literature has used moss bags to record concentrations of various trace and heavy metals (Motyka et al. 2013). Major sources of indoor air pollutants may broadly include tobacco smoke, cooking, candles, emissions from furniture, batteries, walls, and water pipes (WHO 2010). Identifying the sources and intensity of pollutant production from them is critical to devising medical interventions. Using the *Hylocomium splendens* moss variety, exposed for 49 days in an office environment (Czech Republic), Motyka et al. (2013) found that moss bags are efficient bioaccumulators of several heavy metals (Sb, Cu, Hg, Pb, Si), occurring in particulate phases.

In this regard, a rapidly evolving area of moss bag research involves the differentiation between indoor and outdoor air quality. In a cross-country tabulation, Sorrentino et al. (2021a) performed a multi-metal assay in Italy (Ca, Mg, Co, Cr, Sr, Ti, U) and Belgium (Ag, As, Cd, Mo, Pb, and Sb) at 20-paired indoor-outdoor locations, exposing using *Hypnum cupressiforme* moss bags (12 weeks exposure period). Results indicated poorer outdoor air quality. Determination of the Indoor/Outdoor ratios, computed by moss-based metal concentrations (mostly lower than 0.75), indicated indoor air quality is strongly influenced by outdoor pollution. However, certain species have typical

indoor origins (e.g., Al, Ag, Cd, Co). In a similar approach, using the *Hypnum cupressiforme* moss bags in 12 coupled indoor/outdoor exposure sites, Capozzi et al. (2019) observed significantly different air quality statuses between the outdoor and the indoor environments. For example, certain species (As, B, Ca, Co, Cr, Cu, Mn, Mo, Ni, Sb, Se, Sn, Sr, V, Zn) were more abundant in the outdoor environment, while certain others (As, B, Cr, Mo, Ni, Se, V) registered elevated concentrations in the indoors as well. The latter was largely sourced to heating and cooking-related emissions, types of building material, and family lifestyle. Using chemical and magnetic analyses, the authors, however, identified that while B, Mo, and Se were enriched mostly outdoors, Ni, Cr, and V were specifically abundant indoors.

In another similar experiment, Świsłowski et al. (2022) used moss bags to assess air quality due to car workshop activities. Results indicated significantly elevated levels of Al, Cr, Fe, and Ba in the parking garage (indoors) than outdoors (traffic emissions), thus posing greater health risks to the workshop personnel (car mechanics). In a novel effort, Zechmeister et al. (2020) exposed *Pleurozium schreberi* moss bags for 8 weeks indoors and outdoors in 20 households in the city of Girona, Spain, to evaluate concentrations of Al, Cr, Cu, Zn, Sn, Cd, Pb, Mo, and Sb. Results indicated (i) different elements of metal enrichment in indoor and outdoor environments, (ii) stronger intercorrelations between metals in the outdoor environment, (iii) lower correlation for the indoors may arise due to more 'diffused' sources of metals, (iv) for certain metals, the indoor: outdoor ratio was far from unity indicating different sources and intensities (Sb, Sn, Cr, Mo) while for some others (Cd, Zn, NO₂), the ratio was close to unity indicating an equilibrium state between indoor and outdoor. Overall, the study showed that moss bags could be a promising tool to assess indoor air quality.

Land use patterns: In Campania, southern Italy, Capozzi et al. (2016) used moss bags (*Hypnum cupressiforme* Hedw) to evaluate the rural-urban structure for ambient air quality. Investigating spatial patterns for 39 metals and 20 PAHs, the authors observed that moss bags were efficient in discriminating between the agricultural (higher metal loads) and urban sites. Main drivers at the agricultural sites included resuspension of soil dust, fertilizer applications, unregulated (and illicit) electronic waste disposal activities, and heavy-duty traffic movement. Moreover, the authors noted a significant accumulation of higher molecular weight species, such as 4-ring and 5-ring PAHs, in moss tissues. Based on the species abundance and comparing with similar studies, the authors identified potential PAH sources, such as coal and wood combustion (Dvorská et al. 2011), oil combustion (Larsen & Baker 2003), and diesel exhausts (Yunker et al. 2002).

Innovations and Opportunities

Growing concerns over air quality degradation and associated public health hazards have triggered research groups around the world to seek newer avenues of moss bag application to bolster and diversify existing air quality monitoring networks. In the following sections, we briefly highlight certain examples:

- Mobile Systems
- Bio-magnetic studies
- Radioisotope assessments
- Integrated Environmental Assessment
- Early Warning systems

Mobile air quality monitoring systems: A recent innovation came with the ‘mobile’ moss bag experiment, carried out by Sorrentino et al. (2021b) to distinguish between land use patterns by attaching moss bags (*Hypnum cupressiforme* species) to bicycles (Antwerp, Flanders region, northern Belgium). The study involved two experimental designs:

- I. Six volunteer cyclists with three moss bags each on their bicycles through urban areas for 50 days
- II. A single volunteer on four routes with three moss bags, cycling around the city for 22 days, through four routes (a heavily trafficked urban motorway; an industrial route with a non-ferrous metallurgical plant and a cement industry; a green route through agricultural and green areas; composite route (including all three above))

A combined chemical and magnetic analysis revealed that the elemental load and fluxes along the four routes followed the order: industrial > urban > composite > green, with significant Ag, As, Cd, and Pb enrichment in the industrial route. Interestingly, a comparison with ‘static’ moss bags revealed better efficacy of the mobile system in pollutant monitoring - elemental fluxes for As, Cu, Fe, Pb, and V for the mobile system were several folds higher than for fixed monitoring positions, which could be due to the wind effect, as maintained by Garcia-Seoane et al. (2019), which largely influences the moss metal uptake capacity/efficiency.

Moss bio-magnetic investigations: A small but growing body of moss research is involved in the biomagnetic characterization of emission-related particulate matter (Capozzi et al. 2019, Sorrentino et al. 2021a). Magnetic techniques are considered rapid and easy tools to identify spatial structures in environmental quality and changes therein (Salo & Mäkinen 2014). These studies rely on the identification of ferrimagnetic species (magnetite, maghemite, heavy metals) associated with particulate matter and gases in traffic- and/or industrial emissions. Recent studies even recommend biomagnetic monitoring of ambient air quality

as a more cost-effective and non-destructive means (Hofman and Samson 2014) than the traditional methods (Li et al. 2017) to assess airborne heavy metals. In the city of Turku, Finland, Limo et al. (2018) used *Sphagnum papillosum* bags to investigate and evaluate the impacts of stop-and-go traffic emissions on air quality. Moss bags were placed alternately at the traffic light crossings (n = 19) and midway areas between the crossings (n = 29) along four street transects and one separate traffic light crossing. Coupled use of mass-specific magnetic susceptibility (χ), hysteresis parameters, and multi-elemental assays revealed that particulate matter was mainly composed of fine-grained pseudo-single-domain (PSD) magnetite and traffic light crossings have significantly higher χ , Cu, Mo, Sb concentrations than the midway street transects. The elements Ba, Cu, Fe, Mo, Ni, Pb, Sb, and Ti showed moderate to high accumulation and correlated strongly with χ and saturation magnetization (MS). Overall, the study indicated the production of low-coercivity ferrimagnetic particles (magnetite and haematite) and heavy metals due to stop-and-go traffic patterns (e.g., brake, tire, asphalt wear), which is a major source of particulate matter, especially along highly trafficked streets. However, a word of caution for adopting a moss-magnetic approach is to be cognizant of the influences of local climatic, geographical, and environmental conditions while interpreting the results as the composition and abundance of the magnetic mineral phases are largely governed by these factors (Salazar-Rojas et al. 2023).

Salo et al. (2012) deployed moss bags in an urban and industrial site in southwest Finland using magnetic profiling of heavy metals in ambient air. While vehicular emission was the main source of heavy metals at the urban site, it was emissions from the Cu-Ni smelter at the industrial site. At both sites, the ambient particulate matter chemistry revealed a distinct magnetite-like phase. Mass magnetic susceptibility (χ) profiling revealed a high enrichment of magnetic elements closer to the sources at both sites, which tapered off with increasing distance from the sources. Overall, both studies indicated that moss bags could be strategically and efficiently used to identify broad mineralogical compositions (hematite and magnetite) of anthropogenic origin (industrial and vehicular combustion products) with spatially distinct air quality patterns.

In a study in Belgrade, Vuković et al. (2015) exposed *Sphagnum girgensohnii* moss bags to distinguish pollution patterns in different urban microenvironments (street canyons, city tunnel, parking garages). Determination of the ferromagnetic particulate fraction in moss samples by Saturated Isothermal Remanent Magnetization (SIRM) revealed different metal signatures - highest SIRM in the tunnel (most polluted), minimum in the garages. Moreover,

a significant correlation ($R > 0.90$) between the moss SIRM values and traffic flow indicated vehicular emissions as the main sources. Additionally, there was a high degree of correlation between the moss SIRM values and Al, Ba, Co, Cr, Cu, Fe, Ni, and Pb concentrations. Results demonstrated that moss bags can be effectively applied for biomagnetic monitoring of the spatio-temporal distribution of road traffic and vehicle-derived pollutants in urban areas.

Radioisotope Measurements

Capozzi et al. (2016) tested three species (*Sphagnum palustre*, *Hypnum cupressiforme*, and *Hypnum plumaeforme*) to assess airborne radiocesium activities (^{134}Cs and ^{137}Cs), eight years in the aftermath of the nuclear meltdown-fallout event in the Fukushima-Daichi Nuclear Power Plant, Japan. In Belgrade, Serbia, Popovic et al. (2010) found that *Sphagnum girgensohnii* moss bags were efficient tools for source detection: ^{137}Cs (fission products) and ^{40}K and ^{210}Pb (naturally occurring). The study detected lower levels of ^{40}K and ^{137}Cs , while high ^{210}Pb loadings in urban atmosphere, attributable to anthropogenic activities.

Integrated environmental quality: A particular strand of moss bag research involves process-level interpretation of environmental changes by coupling the results with

various indicators (Table 2). In Wuxi, China, Hu et al. (2018) computed the relative accumulation factor (RAF) and contamination factor (CF) based on *Sphagnum junghuhnianum* moss bags for a variety of heavy metals (Cr, Cu, Pb, V, Zn). Results indicated considerable enrichment of Cr, Cu, and V ($\text{RAF} > 1$) in the ambient atmosphere and potential environmental health threats. Moreover, the RAF revealed a distinct seasonal pattern of air quality: higher pollutant loadings in winter than summer, most likely to be caused by lack of precipitation in the former (lower wash-off/dilution). Determination of CAF revealed a moderate degree of air pollution due to Cr, while slight contaminations due to other heavy metals. Significant correlations observed between the heavy and between the metals and traffic volume in both seasons helped in pollutant source detection: traffic intensity.

In the Donetsk region, Ukraine, Sergeeva et al. (2021) used *Ceratodon purpureus* and *Brachythecium campestre* moss bag results to compute various indicators. The RAFs helped identify significant enrichment of rare earth elements (REEs: Ce, La, Tb, Sm, Yb, Hf, Th, U, Zr) in the ambient atmosphere, while the EF indicated higher REE enrichment potential of *Ceratodon purpureus* than the *Brachythecium* sp. The La, Ce, Nd, Sm, Yb, Hf, and Th were sourced

Table 2: Various environmental indicators computed using information from moss bags. (Authors' own compilation from various moss bag literature).

Indicator Name	Indicator Development	Significance
Relative Accumulation Factor (RAF)	$\text{EF} = \frac{C_{t1} - T_{t0}}{C_{t0}}$ <p>C_{t0}: Concentration of the pollutant species after exposure period C_{t1}: Concentration of the same after exposure period</p>	RAF > 1 = Significant Accumulation within moss tissues
Contamination Factor (CF)	$\text{CF} = \frac{C_i}{C_B}$ <p>C_i: Concentration of pollutant species within moss tissue C_B: Background concentration of the same</p>	CF < 1 = Slight Contamination CF 1-3 = Moderate Contamination CF 3-6 = Considerable Contamination CF > 6 = High Contamination
Enrichment Factor (EF)	$\text{EF} = \frac{C_i C_x}{C_B C_{bi}}$ <p>C_i: Observed concentration of pollutant species in moss C_x: Concentration of conservative reference element in a moss sample C_B: Background metal concentration at the site C_{bi}: Concentration of conservative reference element in reference</p>	EF ≤ 1 = No Enrichment EF 1-3 = Minor Enrichment EF 3-5 = Moderate Enrichment EF 5-10: Moderately Severe Enrichment EF ≥ 10 = Severe Enrichment
Pollution Loading Index (PLI)	$\text{PLI} = \sqrt[n]{\prod_{i=1}^n \text{CF}}$ <p>where, CF = Contamination Factor n = Total number of pollutant species</p>	PLI < 1 = Non Polluted PLI 1 ≤ PLI < 2 = Slight Polluted PLI 2 ≤ PLI < 3 = Moderately Polluted PLI > 3 = Highly Polluted

to anthropogenic origins ($EF > 1.5$), such as windblown road and/or coal mine dust. Computation of the PLI values indicated high pollution loadings. Overall, recent studies indicate that coupling moss bag outputs with established environmental indicators can not only offer a holistic view of the type/degree of air quality degradation and the overall status of environmental conditions in the region of interest but also may provide insights into the pollution sources and drivers. These indicators can be used to generate high-resolution spatial maps to identify the hot spots of contamination. For example, in the Donetsk region, Sergeeva et al. (2021) were able to delineate three distinct zones with slight ($CAF < 1$), moderate (CF 1-3), and considerable (CF 3-6) pollution for all heavy metals.

Developing early warning systems: Using strategically placed moss bags (*Hylocomium splendens*) across Romania (142 monitoring stations), Stefanaut et al. (2019) found that ambient air concentrations of several heavy metals (Cd, As, Pb, Ni) exceeded the established standards, indicating substantial public health risks. In the process, the authors developed a specialized tool, namely BioMonRo, as an early warning system to notify the regulatory authorities about potential air quality degradation. Along that line, the tool generated high-quality spatial maps of heavy metal pollution and reports, which could be automatically disseminated among multiple parties engaged in similar research. Overall, the results demonstrated that the system could be adopted by national authorities to (i) raise general awareness regarding the risks represented by atmospheric emissions and (ii) as an efficient and cost-effective monitoring

device for the long-term appraisal of airborne heavy metals.

Concerns and Future Directions

Despite the myriad advantages of moss bags, and matched by a growing number of applications and advances through the recent past, there are yet concerns regarding their meaningful and strategic use to assess ambient air quality.

Ideal Species Selection

Before others, a fundamental puzzle for the regulatory for the regulatory authorities is to identify an ideal moss variety, which is keyed to the pollutant uptake capacity of the moss (Fig. 1). A major consideration in this regard is solid understanding of the ion exchange process that takes place on most surfaces – types and proportions of various reactive functional groups (e.g., phosphodiester, carboxyl, phosphoryl, amine, sulfhydryl, and polyphenols) that determine the pollutant binding affinity. However, another consideration is how the pollutant species interact with the surficial binding sites (Fernández et al. 2013). For example, using *Hypnum cupressiforme* moss bags in an oil refinery area of Sardinia (Italy), Cortis et al. (2016) observed a sequence of metal affinity by following the order: $Pb > Co > Cr > Cu, Cd, Mo, Ni, V > Zn > As$ (Cortis et al. 2016). However, this sequence could vary by moss species and environmental conditions, which calls for more species-specific, process-level research. Along that line, some research could also be devoted to understanding the pollutant apportionment process within moss cells (as inter-, extra-, or intra-cellular fractions).

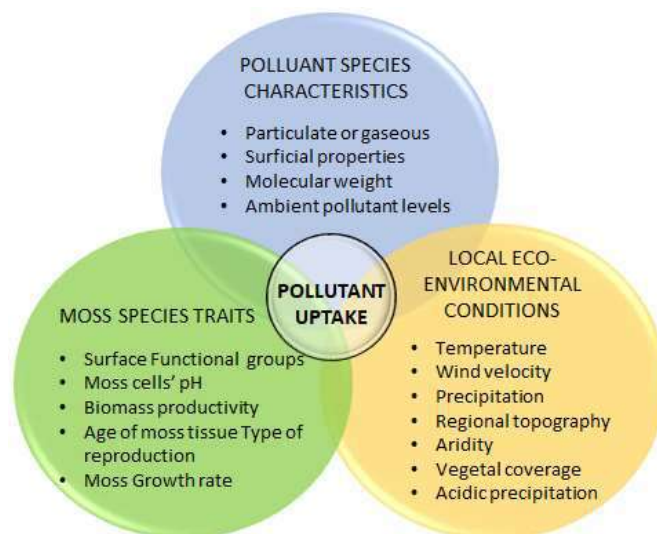


Fig. 1: Potential regulatory consideration for selecting an ideal moss variety (Authors' own illustration).

[NOTE: The considerations depicted herein are of largely 'generic' nature. Besides these, the regulatory authorities might need to think about the context-specific traits (e.g. types of air pollutants, intensity of pollution, distribution of pollutants) to include others]

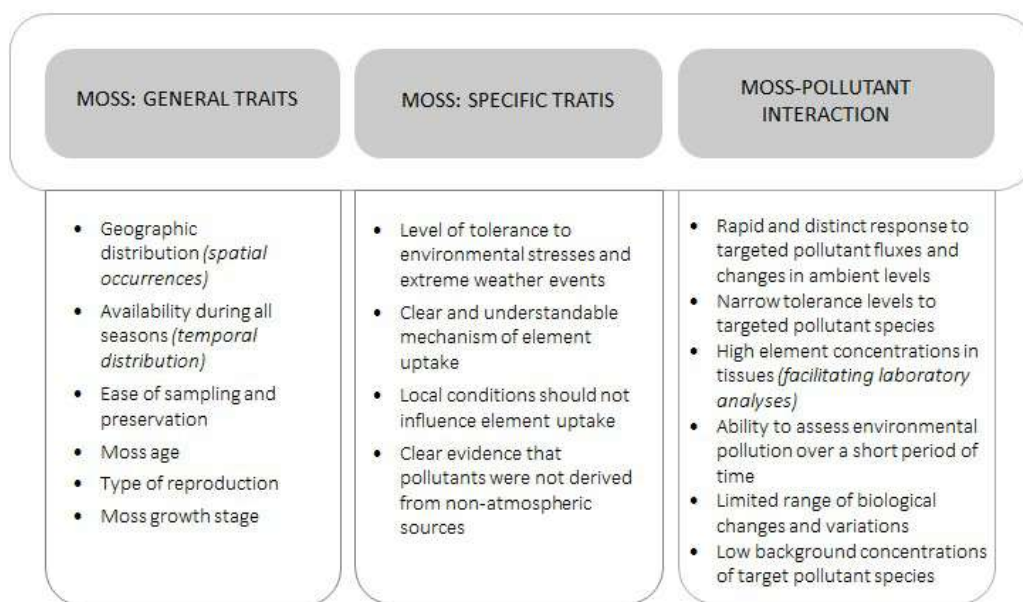


Fig. 2: Overall considerations for identifying the ideal moss variety as found in various moss bag literature (Authors' own illustration).

Table 3: Process-level significance of selected moss bag parameters. [NOTE: Included are broad recommendations for the regulatory authorities, as found in from moss bag literature; Authors' own compilation].

Design Factors	Process-level Significance and Best practice
Bag Material	<ul style="list-style-type: none"> • Plastics and glass fiber are recommended • Non-plastic materials are not recommended as they may interfere with the pollutant uptake process.
Bag Mesh Net Dimension	<ul style="list-style-type: none"> • Inappropriate selection of the mesh size may lead to the loss of large amounts of moss due to wind and/or rain events. • Mesh size should be determined as a compromise between maximization of the interception of aerial deposition and minimization of the risk of loss of material.
Bag Shape	<ul style="list-style-type: none"> • The idea should be to maximize the surface area of moss exposed to the atmosphere. • The 3-D bag shape allows for uniform pollutant capture from all directions; it also allows sample collection by gravitational sedimentation.
Moss Amount and Packing	<ul style="list-style-type: none"> • Even though sufficient moss amounts should be placed in the bag, moss should be loosely packed in thin layers to reduce compaction. • Caution should be practiced to avoid moss layer overlapping and compression, which collectively reduces chances of even exposure to the contaminants (e.g., when shoots overlap, concentrations may decrease gradually)
Exposure Period	<ul style="list-style-type: none"> • Should be guided by research objective • Sufficient time to intercept pollutants • Enough time to 'equilibrate' with ambient conditions • Minimize risks of potential 'leaching' losses (rain events) and/or windblown losses (storm events)
Bag Exposure Elevation	<ul style="list-style-type: none"> • Should be guided by research objective • Entrap pollutant sources close to the ground (e.g., vehicular emissions, storm dust) • Potential risks involve undesirable human interventions (curious citizens, children, etc.) that may tamper with the bag.

Overall, the moss bag literature reveals preference for the Sphagnum variety (Gonzalez & Pokrovsky 2014), partly owing to their ubiquitous geographic occurrence (availability). More process-level reasons include (i) abundance of surficial proton exchange sites and thus, high cation-exchange capacity of the Sphagnum (better pollutant interception/binding capacity); (ii) large area/volume ratio (higher amount of exchange sites exposed to

pollutants); (iii) high permeability of tissues to water, coupled with high water retention capacity (resistant to drought/hydric stresses) (Aničić et al. 2009, Fernández et al. 2009). However, in the absence of Sphagnum, other moss varieties are noted in the literature as well, including *Pleurozium schreberi*, *Hypnum cupressiforme*, and *Pseudoscleropodium purum*. Overall, for best outcomes, the species selection process might want to consider the following in the least

(Fig. 2): Availability, Moss Characteristics, and Moss Data.

Constructional Artefacts

A frequently raised concern about moss bags is the diversity of practices and, thus, lack of concordance in constructional details – there are yet no universally accepted protocols for bag parameterization (Ares et al. 2012, Capozzi et al. 2016). A moss bag embodies a multitude of parameters, including the bag shape (circular, flat), dimension, bag material (nylon, polythene), mesh net sizes, moss amount, moss packing within the bag, ratio between moss weight to bag volume, bag exposure period, bag elevation (Ares et al. 2014). However, moss bag literature documents differences even in the moss ‘preparation’ details, that is before the moss is placed within the bag. It ranges from moss sampling protocols (Capozzi et al. 2017) to washing-cleaning procedures (Ares et al. 2014), to drying (Giordano et al. 2009), and homogenizing (Milicevic et al. 2017). Such differing approaches, however, make comparisons between moss bag results difficult (Świsłowski et al. 2021d). To develop a viable moss bag construct (reliable, replicable), the first need is to understand the process-level significance of each parameter and how they may influence the chemical analysis results (Table 3). To that end, we envision more targeted action in the days ahead to standardize the moss bag protocols.

Moss Vitality

A prime issue about moss bags is the vitality and functional quality of the moss. It owes to the observation that relocation from their natural habitat entails changes in their original environmental and meteorological conditions (Świsłowski & Rajfur 2021c), which may result in hydric and photo stress, affecting the moss viability in the long run (Urošević et al. 2017). Moreover, sustained exposure to high pollutant levels in the ambient atmosphere could alter various physiological parameters in the moss, such as loss of pigmentation due to a drop in chlorophyll contents, which needs to be further researched (Sun et al. 2009). In their study in Sardinia, Italy, Cortis et al. (2016) observed that elevated concentrations of various heavy and trace metals (Cr, Cu, Ni, Zn, Cd, Pb) led to significant proteomic changes in moss cells. For example, 15 gel spots exhibited differential expression profiles between the moss samples collected at the study site and the control site. 14 spots showed a decrease in protein expression, of which nine were associated with ribulose-1,5-bisphosphate carboxylase/oxygenase (RuBisCO) and proteins of the light-harvesting complexes of photosystem (PS) II, while three were associated with protein synthesis, and three with stress-related proteins.

However, on the brighter side, strategic monitoring of such physiological/structural disorders and deformities in moss samples can also help the air quality regulators as the onset of air quality degradation events, for example, an *early warning system*, to devise pre-emptive pollution prevention and remediation mechanisms.

CONCLUSION

With the rise of air quality degradation-induced health hazards around the world, the need to expand the monitoring network has never been so imperative. In the process, moss bags have emerged as cheaper, eco-friendly, and efficient biomonitors, capable of offering denser spatial coverage than the traditional, instrument-based sensors (highly capital and infrastructure intensive) and/or lichens and/or vascular plants. In the present context, we present a bird’s eye view of the current global experiences around moss bags in a variety of applications, including urban sustainability studies, bio-magnetic investigations of particulate matter, land use structure, indoor-outdoor air quality assessment, and short-term change detection, to name a few. More novel applications of moss bags include mobile systems, radioisotopic investigations, and integrative environmental quality assessment with indicator variables. Computation of various environmental indicators. Despite several advantages, however, moss bag literature reveals that much research needs to be done before moss bags can be meaningfully used for regulatory purposes (pollution control-prevention). Future areas of research may include but are not limited to, moss morphological-physiological investigations to aid in species selection, developing a standardized/harmonized protocol for moss bag preparation and parameter optimization, and improving our understanding of the potential influences of environmental-meteorological stressors on moss health.

REFERENCES

- Adithyalakshmanan, K. Kaur, H. and Chaudhuri, S. 2022. Unpacking land degradation neutrality (LDN), an emerging paradigm to conserve land systems’ sustainability in the 21st century? Meta-analysis of Challenges and Opportunities. *Nat. Environ. & Poll. Tech.*, 21(1): 91-100.
- Aničić, M., Tasić, M., Frontasyeva, M.V., Tomašević, M., Rajšić, S. and Strelkova, L.P., Popović, A. and Steinnes, E. 2009. Active biomonitoring with wet and dry moss: a case study in an urban area. *Environ. Chem. Lett.*, 7(1): 55-60.
- Ares, A., Fernández, J.A., Carballeria, A. and Aboal, J.R. 2014. Towards the methodological optimization of the moss bag technique in terms of contaminants concentrations and replicability values. *Atmos. Environ.*, 94: 496-507.
- Ares, A., Aboal, J.R., Carballeira, A., Giordano, S., Adamo, P. and Fernández, J.A. 2012. Moss bag biomonitoring: A methodological review. *Sci. Total Environ.*, 432: 143-158.
- Arndt, J. and Planer-Friedrich, B. 2018. Moss bag monitoring as a screening technique to estimate the relevance of methylated arsine

- emission. *Sci. Total Environ.*, 610-611: 1590-1594.
- Basile, A., Sorbo, S., Aprile, G., Conte, B. and Cobianche, R.C. 2008. Comparison of the heavy metal bioaccumulation capacity of an epiphytic moss and an epiphytic lichen. *Environ. Pollut.*, 151(2): 401-407.
- Bertrim, C. and Aherne, J. 2023. Moss bags as biomonitors of atmospheric microplastic deposition in urban environments. *Biology*, 12(2): 149. DOI:10.3390/biology12020149
- Capozzi, F., Di Palma, A., Adamo, P., Sorrentino, M.C., Giordano, S. and Spagnuolo, V. 2019. Indoor vs. outdoor airborne element array: A novel approach using moss-bags to explore possible pollution sources. *Environ. Pollut.*, 249: 566-572.
- Capozzi, F., Giordano, S., Di Palma, A., Spagnuolo, V., De Nicola, F. and Adamo, P. 2016. Biomonitoring of atmospheric pollution by moss bags: Discriminating urban-rural structure in a fragmented landscape. *Chemosphere*, 149: 211-218.
- Castello, M. 2007. A comparison between two moss species used as transplants for airborne trace element biomonitoring in NE Italy. *Environ. Monit. Assess.*, 133(1-3): 267-76.
- Chakraborty, S. and Paratkar, G.T. 2006. Biomonitoring of Trace Element Air Pollution Using Mosses. *Aero. Air Qual. Res.*, 6(3): 247-258.
- Chaudhuri, S. and Roy, M. 2023. Global ambient air quality monitoring: Can mosses help? A systematic meta-analysis of literature about passive moss biomonitoring. *Environ. Monit. Assess.*, 15: 304. DOI: 10.1007/s10668-023-03043-0.
- Chaudhuri, S. and Kumar, A. 2022. Urban greenery for air pollution control: A meta-analysis of current practice, progress, and challenges. *Environ. Monit. Assess.*, 194(3): 1-30.
- Chaudhuri, S., Roy, M., McDonald, L.M. and Emendack, Y. 2021. Coping behaviors: A review of perceived social and health outcomes of food insecurity on women and children. *Food Security*, 13: 1049-1068.
- Chaudhuri, S., Roy, M., McDonald, L.M. and Emendack, Y. 2020. Reflections on farmers' social networks: A means for sustainable agricultural development? *Environ. Dev. Sustain.*, 23: 2973-3008.
- Cortis, P., Vannini, C., Cogoni, A., De Mattia, F., Bracale, M., Mezzasalma, V. and Labra, M. 2016. Chemical, molecular, and proteomic analyses of moss bag biomonitoring in a petrochemical area of Sardinia (Italy). *Environ. Sci. Pollut. Res.*, 23: 2288-2300.
- De Nicola, F., Murena, F., Castagliola, M.A., Alfani, M.A., Alfani, A., Baldantoni, D., Prati, M.V., Sessa, L., Spagnuolo, V. and Giordano, S. 2013. A multi-approach monitoring of particulate matter, metals, and PAHs in an urban street canyon. *Environ. Sci. Pollut. Res.*, 20: 4969-4979.
- Dvorská, A., Komprdová, K., Lammel, G., Klánová, J. and Plachá, H. 2012. Polycyclic aromatic hydrocarbons in background air in central Europe—seasonal levels and limitations for source apportionment. *Atmospheric Environment*, 46: 147-154.
- Fernández, J.A., Pérez-Llamazares, A., Carballeira, A. and Aboal, J.R. 2013. Temporal variability of metal uptake in different cell compartments in mosses. *Water Air Soil Pollut.*, 224: 1481. DOI:10.1007/s11270-013-1481-9.
- Fernández, J.A., Ares, A., Rey-Asensio, A., Carballeira, A. and Aboal, J.R. 2009. Effect of growth on active biomonitoring with terrestrial mosses. *J Atmos Chem.*, 63(1): 1-11.
- Gao, G., Zeng, H. and Zhou, Q. 2023. Biomonitoring Atmospheric Pollution of Polycyclic Aromatic Hydrocarbons Using Mosses. *Atmosphere*, 14: 26. DOI:10.3390/atmos14010026.
- García-Seoane, R., Fernández, J.A., Chilà, A. and Aboal, J.R. 2019. Improving the uptake of pollutants in moss-bags: The wind effect. *Ecol. Ind.*, 107: 1055.
- Golubev, A.V., Golubeva, V.N., Krylov, N.G., Kuznetsova, V.F., Mavrin, S.V., Aleinikov, A., Yu Hoppes, W.G. and Surano K.A. 2005. On monitoring anthropogenic airborne uranium concentrations and ²³⁵U/²³⁸U isotopic ratio by Lichen-bio-indicator technique. *J. Environ. Radioact.*, 84(3): 333-342.
- Gonzalez, A.G. and Pokrovsky, O.S. 2014. Metal adsorption on mosses: Toward a universal adsorption model. *J. Colloid Interf. Sci.*, 415: 169-178.
- Giordano, S., Adamo, P., Monaci, F., Pittao, E., Tretiach, M. and Bargagli, R. 2009. Bags with oven-dried moss for the active monitoring of airborne trace elements in urban areas. *Environ. Pollut.*, 157: 2798-2805.
- Guarino, F., Improta, G., Triassi, M., Castiglione, S. and Ciatelli, A. 2021. Air quality biomonitoring through *Olea europaea* L.: The study case of "Land of pyres." *Chemosphere*, 282: 131052. DOI:10.1016/j.chemosphere, 2021.131052
- Gribacheva, N., Gecheva, G., Zhiyanski, M., Pavlova-Traykova, E. and Yaneva, R. 2021. Active and passive moss biomonitoring of trace elements in urban and mountain areas, Bulgaria. *Forest. Ideas*, 27(2-62): 309-317.
- Hofman, J. and Samson, R. 2014. Biomagnetic monitoring as a validation tool for local air quality models: a case study for an urban street canyon. *Environ. Int.*, 70: 50-61.
- Hu, R., Yan, Y., Zhou, X., Wang, Y. and Fang, Y. 2018. Monitoring heavy metal contents with *Sphagnum junghuhnianum* moss bags in relation to traffic volume in Wuxi, China. *Int. J. Environ. Res. Public Health*, 22: 15(2): 374. DOI:10.3390/ijerph15020374.
- Isidora, D., Davor, A., Gordona, V., Aničić, U.M., Milica, T., Aleksandra, Perić-Grujić, and Mirjana, R. 2015. Lead spatio-temporal pattern identification in urban microenvironments using moss bags and the Kohonen self-organizing maps. *Atmos. Environ.*, 117: 180-186.
- Jiang, Y., Fan, M., Hu, R., Zhao, J. and Wu, Y. 2018. Mosses are better than leaves of vascular plants in monitoring atmospheric heavy metal pollution in urban areas. *Int. J. Environ. Res. Public Health*, 15(6): 1105. DOI:10.3390/ijerph15061105.
- Kosior, G., Klanova, J., Vankova, L., Kukucka, P., Chropenova, M., Brudzinska-Kosior, A., Samecka-Cymerman, A., Kolon, K. and Kempers, A.J. 2015. *Pleurozium schreberi* as an ecological indicator of polybrominated diphenyl ethers (PBDEs) in a heavily industrialized urban area. *Ecol. Indic.*, 48: 492-497.
- Krommer, V., Zechmeister, H.G., Roder, I., Scharf, S. and Hanus-Illyar, A. 2007. Monitoring atmospheric pollutants in the biosphere reserve Wienerwald by a combined approach of biomonitoring methods and technical measurements. *Chemosphere*, 67: 1956-1966.
- Kumar, A. and Chaudhuri, S. 2022a. Improving urban air quality monitoring in New Delhi, India: Reflections on low-cost air quality sensors (LCAQS) and participatory engagement. *Environ. Urban. Asia*, 13(2): 265-283.
- Kumar, A. and Chaudhuri, S. 2022b. Post SARS-CoV-2 Urban India: Computing air quality health indicators (AQHI) for Gurugram city to assess imminent threats to public health. *Ecol. Environ. Conserv.*, 28: S185-S193.
- Kumar, A. and Chaudhuri, S. 2021. Is COVID-19 only but a short-term respite? A case study of urban air quality in Kolkata, a mega-city in India. *Poll. Res.*, 40: S162-S172.
- Larsen, R.K. and Baker, J.E. 2003. Source apportionment of polycyclic aromatic hydrocarbons in the urban atmosphere: a comparison of three methods. *Environmental Science and Technology*, 37(9): 1873-1881.
- Li, H., Wang, J., Wang, Q., Tian, C., Qian, X. and Leng, X. 2017. Magnetic properties as a proxy for predicting fine-particle-bound heavy metals in a support vector machine approach. *Environ. Sci. Technol.*, 51(12): 6927-6935.
- Limo, J., Paturi, P. and Maniken, J. 2018. Magnetic biomonitoring with moss bags to assess stop-and-go traffic-induced particulate matter and heavy metal concentrations. *Atmos. Environ.*, 195: 187-195.
- Makhholm, M.M. and Mladenoff, D.J. 2005. Efficacy of biomonitoring (moss bag) technique for determining element deposition trends on a mid-range (375 km) scale. *Environ. Monit. Assess.*, 104: 1-18.

- Mao, H.T., Wang, X., Wu, N., Chen, L., Yuan, M., Hu, J. and Chen, Y. 2021. Temporal and spatial biomonitoring of atmospheric heavy metal pollution using moss bags in Xichang. *Environ. Sci. Technol.*, 44(8): 82-90.
- Meier, R., Eeftens, M., Phuleria, H., Ineichen, A., Corradi, E., Davey, M., Fierz, M., Ducret-Stich, R., Aguilera, I., Schindler, C.R., Probst-Hensch, T.N., Tsai, M.Y. and Künzli, N. 2015. Differences in indoor versus outdoor concentrations of ultrafine particles, PM_{2.5}, PM absorbance, and NO₂ in Swiss homes. *J. Expo. Sci. Environ. Epidemiol.*, 25(5): 499-505.
- Mendil, D., Celik, F., Tuzen, M. and Soylak, M. 2009. Assessment of trace metal levels in some moss and lichen samples collected from near the motorway in Turkey. *J. Hazard. Mater.*, 166(2-3): 1344-1450.
- Milicevic, T., Anicic-Urošević, M., Vukovic, G., Skrivanj, S., Relic, D., Frontasyeva, M.V. and Popovic, A. 2017. Assessment of species-specific and temporal variations of major, trace, and rare earth elements in vineyard ambient using moss bags. *Ecotoxicol. Environ. Saf.*, 144: 208-215.
- Motyka, O., Maceckova, B. and Seidlerova, J.T. 2013. Indoor biomonitoring of particle related pollution: trace element concentration in an office environment. *Environ. Monit. Assess.*, 17: 354.
- Parakh, D. and Chaudhuri, S. 2023. Groundwater markets in South Asia: A bibliometric assessment of challenges and opportunities for sustainable irrigation development. *J. Sou. Asi. Dev.*, 18(2): 265-294.
- Rivera, M., Zechmeister, H., Medina-Ramón, M., Basagaña, X., Foraster, M., Bouso, L., Moreno, T., Solanas, P., Ramos, R., Köllensperger, G., Deltell, A., Vizcaya, D. and Künzli, N. 2011. Monitoring of heavy metal concentrations in home outdoor air using moss bags. *Environ. Pollut.*, 159: 954-962.
- Salazar-Rojas, T., Cejudo-Ruiz, F.R. and Calvo-Brenes, G. 2023. Assessing magnetic properties of biomonitors and road dust as a screening method for air pollution monitoring. *Chemosphere*, 310: 136795. DOI:10.1016/j.chemosphere.2022.136795
- Saleema, M., Derome, J., Helmissaari, H., Nieminen, T. and Vanha-Majamaa, I. 2004. Element accumulation in boreal bryophytes, lichens, and vascular plants exposed to heavy metal and sulfur deposition in Finland. *Sci. Total. Environ.*, 324(1-3): 141-160.
- Salo, H. and Mäkinen, J. 2014. Magnetic biomonitoring by moss bags for industry-derived air pollution in SW Finland. *Atmos. Environ.*, 97: 19-27.
- Salo, H., Bučko, M.S., Vaahtovuori, E., Limo, J., Mäkinen, J. and Pesonen, L.J. 2012. Biomonitoring of air pollution in SW Finland by magnetic and chemical measurements of moss bags and lichens. *J. Geochem. Explor.*, 115: 69-81.
- Sang, T.M.N., Hong K.L. and Nguyen, S. 2021. Comparison of moss bag and native moss technique in monitoring airborne particulate and toxic elements. *Sci. Technol. Dev. J.*, 24(2): 1967-1974.
- Saxena, D.K., Srivastava, K. and Singh, S. 2008. Biomonitoring of metal deposition by using moss transplant method through *Hypnum cupressiforme* (Hedw.) in Mussoorie. *J. Environ. Biol.*, 29(5): 683-688.
- Sergeeva, A., Zinicovscaia, I., Grozdov, D. and Yushin, N. 2021. Assessment of selected rare earth elements, HF, Th, and U, in the Donetsk region using moss bags technique. *Atmos. Pollut. Res.*, 12: 101165. DOI:10.1016/j.apr.2021.101165.
- Shotyk, W., Kempter, H., Krachler, M. and Caludio, Z. 2015. Stable (²⁰⁶Pb, ²⁰⁷Pb, ²⁰⁸Pb) and radioactive (²¹⁰Pb) lead isotopes in 1 year of growth of Sphagnum moss from four ombrotrophic bogs in southern Germany: Geochemical significance and environmental implications. *Geochim. Cosmoch. Acta*, 163: 101-125.
- Shvetsova, M.S., Kamanina, I.Z., Frontasyeva, M.V., Madadzada, A.I., Zinicovscaia, I.I., Pavlov, S.S., Vergel, K.N. and Yushin, N.S. 2019. Physics of particles and nuclei letters. *Chemosphere*, 16(6): 994-1003.
- Sorrentino, M.C., Wuyts, K., Joosen, S., Mubiana, V.K., Giordano, S., Samson, R., Capozzin, F. and Spagnuolo, V. 2021a. Multi-elemental profile and enviromagnetic analysis of moss transplants exposed indoors and outdoors in Italy and Belgium. *Environ. Pollut.*, 298: 117871. DOI:10.1016/j.envpol.2021.117871
- Sorrentino, M.C., Capozzi, F., Wuyts, K., Joosen, S., Mubiana, V.K., Giordano, S., Samson, R. and Spagnuolo, V. 2021b. Mobile biomonitoring of atmospheric pollution: A new perspective for the moss-bag approach. *Plants*, 10: 2384. DOI:10.3390/plants10112384
- Stefanaut, S., Öllerer, K., Manole, A., Ion, M.C., Constantin, M., Banciu, C., Maria, G.M. and Florescu, L.I. 2019. National environmental quality assessment and monitoring of atmospheric heavy metal pollution: A moss bag approach. *J. Environ. Manag.*, 248:109224. DOI: 10.1016/j.jenvman.2019.06.125
- Świsłowski, P., Vergel, K., Zinicovscaia, I., Rajfur, M. and Waclawek, M. 2022. Mosses as a biomonitor to identify elements released into the air as a result of car workshop activities. *Ecol. Indic.*, 138: 108849. Doi: 10.3390/jerph19084706.
- Świsłowski, P., Hrabák, P., Waclawek, S., Liskova, K., Antos, V., Rajfur, M. and Zabkowska-Waclawek, M. 2021a. The application of active biomonitoring with the use of mosses to identify polycyclic aromatic hydrocarbons in an atmospheric aerosol. *Molecules*, 26: 7258. DOI:10.3390/molecules26237258.
- Świsłowski, P., Zienmbik, Z. and Rajfur, M. 2021b. Air quality during New Year's Eve: A biomonitoring study with moss. *Atmosphere*, 12(8): 975. DOI:10.3390/atmos12080975.
- Świsłowski, P., Nowak, A. and Rajfur, M. 2021c. The influence of environmental conditions on the lifespan of mosses under long-term active biomonitoring. *Atmos. Pollut. Res.*, 12: 101203. DOI: 10.1016/j.apr.2021.101203.
- Świsłowski, P., Kosior, G. and Rajfur, M. 2021d. The influence of preparation methodology on the concentrations of heavy metals in *Pleurozium schreberi* moss samples prior to use in active biomonitoring studies. *Environ. Sci. Pollut. Res. Int.*, 28(8): 10068-10076.
- Sun, S.Q., Wang, D.Y., He, M. and Zhang, C. 2009. Monitoring of atmospheric heavy metal deposition in Chongqing, China-based on moss bag technique. *Environ. Monit. Assess.*, 148: 1-9.
- Tretiac, M., Adamo, P., Bargagli, R., Baruffo, L., Carletti, L., Crisafulli, P., Giordano, S., Modenesi, P., Orlando, S. and Pittao, E. 2007. Lichen and moss bags as monitoring devices in urban areas. Part I: Influence of exposure on sample vitality. *Environ. Pollut.*, 146: 380-391.
- Urošević, A., Vuković, G., Jovanović, P., Vujičić, M., Sabovljević, A., Sabovljević, M. and Tomašević, M. 2017. Urban background of air pollution: Evaluation through moss bag biomonitoring of trace elements in Botanical Garden. *Urban Forest. Urban Green.*, 25: 1-10.
- Van Laaten, N., Merten, D., Von Tümpling, W., Schäfer, T. and Pirrung, M. 2020. Comparison of spider web and moss bag biomonitoring to detect sources of airborne trace elements. *Water Air Soil Pollut.*, 231: 512. DOI:10.1007/s11270-020-04881-8.
- Vuković, C., Aničić Urošević, M., Tomašević, M., Samson, R. and Popović, A. 2015. Biomagnetic monitoring of urban air pollution using moss bags (*Sphagnum girgensohnii*). *Ecol. Indic.*, 52: 40-47.
- Vuković, G., Aničić Urošević, M., Razumenić, I., Kuzmanoski, M., Pergal, M., Škrivanj S. and Popović, A. 2014. Air quality in urban parking garages (PM₁₀, major and trace elements, PAHs): Instrumental measurements vs. active moss biomonitoring. *Atmos. Environ.*, 85: 31-40.
- WHO 2018. Burden of disease from the joint effects of household and ambient Air pollution for 2016. World Health Organization. https://www.who.int/airpollution/data/AP_joint_effect_BoD_results_May2018.pdf
- Yunker, M.B., Backus, S.M., Pannatier, E.G., Jeffries, D.S. and Macdonald, R.W. 2002. Sources and significance of alkane and PAH hydrocarbons in Canadian arctic rivers. *Estuarine, Coastal and Shelf Science*, 55(1): 1-31.

Zechmeister, H.G., Rivera, M., Kollensperger, G., Marrugat, J. and Kunzli, N. 2022. Indoor monitoring of heavy metals and NO₂ using active monitoring by moss and Palmes diffusion tubes. *Environmental Sciences Europe*, 32(156). DOI:10.1186/s12302-020-00439-x.

Zechmeister, H.G., Dullinger, S., Hohenwallner, D., Riss, A., Hanus-
Illnar, A. and Scharf, S. 2006. Pilot study on road traffic emissions
(PAHs, heavy metals) measured by using mosses in a tunnel

experiment in Vienna, Austria. *Environ. Sci. Pollut. Res. Int.*, 13(6):
398-405.

ORCID DETAILS OF THE AUTHORS

Sriroop Chaudhuri: <https://orcid.org/0000-0002-0380-6128>



Surface Runoff Estimation Using SCS-CN Method for Kurumballi Sub-watershed in Shivamogga District, Karnataka, India

Govindaraju†, T. Y. Vinutha, C. J. Rakesh, S. Lokanath and A. Kishor Kumar

Department of Applied Geology, Kuvempu University, Jnanasahyadri, Shankaraghatta-577451, Karnataka, India

†Corresponding author: Govindaraju; drgov@yahoo.com

Nat. Env. & Poll. Tech.
Website: www.neptjournal.com

Received: 20-09-2023

Revised: 10-11-2023

Accepted: 28-11-2023

Key Words:

Surface-runoff

Curve number

Hydrological soil group

Kurumballi subwatershed

ABSTRACT

SCS-curve number (CN) is one of the most well-liked and commonly applied methods for estimating surface runoff. The present study aims to calculate surface runoff using SCS-CN watershed-based calculation and geospatial technology in the Kurumballi sub-watershed Shivamogga District of Karnataka, India. The study area covers about an area of 47.67 sq. km. The union of land use/land cover classification with hydrological soil groups (HSG) yields the runoff estimation by the SCS-CN curve approach. This method calculates the runoff volume from the land surface flows into the river or streams. Moreover, the study area's delineation of runoff potential zones was done using the thematic integration method. Different thematic layers were used, including lithology, geomorphology, soil, slope, land use and land cover, drainage, surface water bodies, groundwater contour, and isohyetal maps. Furthermore, associating it with the SCS-CN technique, the total surface runoff volume of the study area was estimated. The total surface runoff volume in the study area is 21065849.7 m³. To this study, thematic integration with the SCS-CN approach to estimate runoff for watersheds is valuable for improving water management and soil conservation.

INTRODUCTION

The process of hydrological modeling is vital for water resource management. One of the significant challenges in this field is the analysis of surface runoff based on rainfall. This analysis is crucial for developing, planning, and managing water resources. Observing water quantity through hydrological models is a challenging and scientific task, especially in semi-arid regions (Gajbhiye et al. 2015, Perez-Sanchez et al. 2019, Karunanidhi et al. 2020). Water movement over the land surface and into a defined channel is classified as overland flow. If water infiltrates and moves horizontally close to the soil surface before ultimately reaching a channel, it is known as interflow (Fitts 2002). When groundwater contributes to the overall flow of a stream, it is referred to as base flow, while the collective flow of the stream is known as runoff (Fetter 2001). Typically, water flow is measured in terms of surface runoff, a momentary flow that combines with other waterways to create a watershed (Rao et al. 2010). When determining the volume of surface runoff in an ungauged basin during a rainfall event, the SCS curve number model is a commonly used method. This model employs runoff curve numbers developed by the USDA Soil Conservation Service (SCS 1985), considering various factors such as soil type, land use/treatment, surface condition, and antecedent moisture conditions.

The SCS-CN model is a well-established and recognizable approach known for its stability and ability to incorporate various factors contributing to runoff, including both spatial and non-spatial data sets, such as monthly precipitation, land use/land cover, soil, slope, hydrology, and antecedent moisture conditions (AMC) are used with multi-temporal datasets (Shi et al. 2009, Tejram et al. 2012, Viji et al. 2015, Matej et al. 2016, Shah et al. 2017, Al-Juaidi et al. 2018, Arya et al. 2020). Moreover, the above-mentioned parameters, along with the drainage density, topography, watershed size, and shape, the quantity of direct surface runoff is determined (Agarwal et al. 2014; Tailor & Shrimali, 2016). An essential advantage of this method is its seamless integration with geographic information system (GIS) techniques, as the model's required parameters are predominantly geographical. Researchers have made numerous efforts to approximate surface runoff using the SCS-CN method. This approach involves integrating remote sensing data to evaluate the hydrological characteristics of a given watershed. The SCS-CN model is implemented by utilizing high-resolution satellite datasets, which allow for the mapping of impervious surfaces (Mondal et al. 2009, Ansari et al. 2016). Additionally, the SCS-CN model is utilized in conjunction with the Universal Soil Loss Equation (USLE) to determine the sediment yield of a given watershed

during rainstorms (Mishra et al. 2006). The SCS-CN model was utilized for this study, classified as an empirical model. It is the most widely recognized and trusted method among hydrologists (Williams & LaSeur 1976, Bondelid et al. 1982, Voda et al. 2019, Verma et al. 2020). The model relies on four catchment features: hydrologic soil group, land use, surface condition, and antecedent moisture condition (AMC) (Bansode & Patil 2014).

The SCS-CN method is frequently utilized to assess the seasonal variation of rainfall-surface runoff, which is instrumental in developing resource management protocols involving vegetative and engineering measures (Muthu & Santhi 2015, Anubha et al. 2015) employing GIS techniques to determine a watershed's annual surface runoff depth. Meanwhile, Joy, 2016 utilized the NRCS-CN method to evaluate the surface and average runoff depth. GIS is a commonly utilized tool amongst researchers in conjunction with the curve number approach, as it has demonstrated efficacy in estimating runoff quantities in an efficient and precise manner (Devia et al. 2015). The curve numbers are assigned based on soil type and its infiltration capacity for water across different land use categories. Soil is classified into four hydrological classes: A, B, C, and D. The curve numbers differ depending on land use, soil type, and hydrological variables (Amutha & Porchelvan 2009). Antecedent moisture conditions predict the direct runoff volume for a specified rainfall event by applying the SCS-CN runoff model (Satheeshkumar et al. 2017). We use a curve number to measure the amount of rainfall that becomes surface runoff versus the amount absorbed into the soil (McCuen 1982). A high curve number indicates heavy runoff and low infiltration usually in urban environments. In contrast, a low curve number indicates low runoff and high infiltration most common in dry land (Sayl et al. 2019).

The CN factor values were obtained from different soil, land use, and land management circumstances. However, if available, evaluating the CN value using recorded rainfall-runoff data is better (Liu & Li 2008, He 2003). Previous studies have shown that CN values derived from recorded data vary consistently with the depth of the rainfall, so it is recommended to determine a single CN value (Mishra et al. 2013). In identifying optimal locations for water collection or underground water recharge, Geographic Information Systems (GIS) and Remote Sensing (RS) are indispensable tools. These modern and efficient technologies have surpassed traditional approaches (Khaddor et al. 2017). They are crucial in gathering data on various land use and soil types, which are used to determine curve numbers that play a significant role in runoff estimation (Bo et al. 2011). Consequently, hydrological studies can be conducted with

precision through GIS and RS technology, making them increasingly popular for natural resource management, planning, and development purposes. GIS is also valuable in decision-making by integrating multiple data sets and performing spatial analysis (Jasrotia et al. 2002).

Therefore, this study focuses on utilizing the SCS-CN model in the Kurumballi subwatershed to model runoff via Remote Sensing and Geographic Information System with aiming to achieve the following objectives 1. To prepare and map the thematic layers that influence the surface runoff, 2. To estimate the surface run-off using a combined SCS-CN method and thematic integration, and 3. To determine the volume of run-off using rainfall intensity and depth.

STUDY AREA

Kurumballi sub-watershed is located in the Shivamogga district and covers an average area of 47.67 sq. km. The mini-watershed can be found between latitude 13°59' 24.95" N and longitude 75°21'36.35" E, covered in a survey of India toposheets of 48 N/8 and 48 O/5. Throughout the year study region experiences a temperate environment. June through October sees the majority of the southwest monsoon's rainfall. The Kurumballi Sub-watershed averages 99.804 millimeters of annual precipitation and 21.8°C on average for minimum and 31.8°C on average for maximum temperatures. The location map of the study area is shown in Fig. 1.

GEOLOGICAL SETTING

The study area is well known that the Gneissic complex surrounding the main schist belt is replete with remnants of high-grade metamorphic rocks which are concordant to the fabric of the enclosing gneissic complex lithologically, which represents Archean Migmatites & Granodiorite-Tonalitic Gneiss, Quartz Chlorite Schist with OrthoQuartzite and older Granites.

MATERIALS AND METHODS

The Survey of India toposheets 48 N/8 & 48O/5 on a scale of 1:50,000 were used to create the base map and delineate the Kurumballi subwatershed. In addition, this study gathered secondary datasets and remote sensing data from several governmental organizations. The current study involved the production of rainfall maps using rainfall data from the Department of Statistics in Bangalore. Monthly rainfall data spanning 2011 to 2022 were acquired. The generation of isohyets was accomplished by utilizing ArcGIS. Using ArcGIS software (v. 10.4), all data items were digitally transformed and georeferenced with the UTM and WGS-84 projection/coordinate system (Karunanidhi et al. 2020).

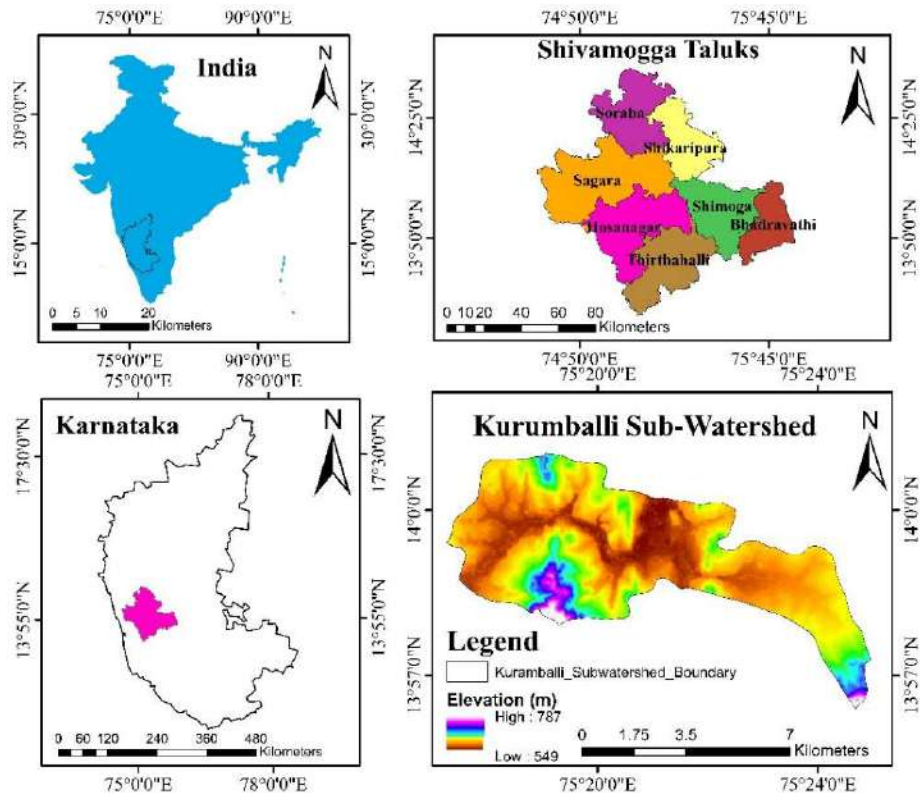


Fig. 1: Location Map of the Study Area.

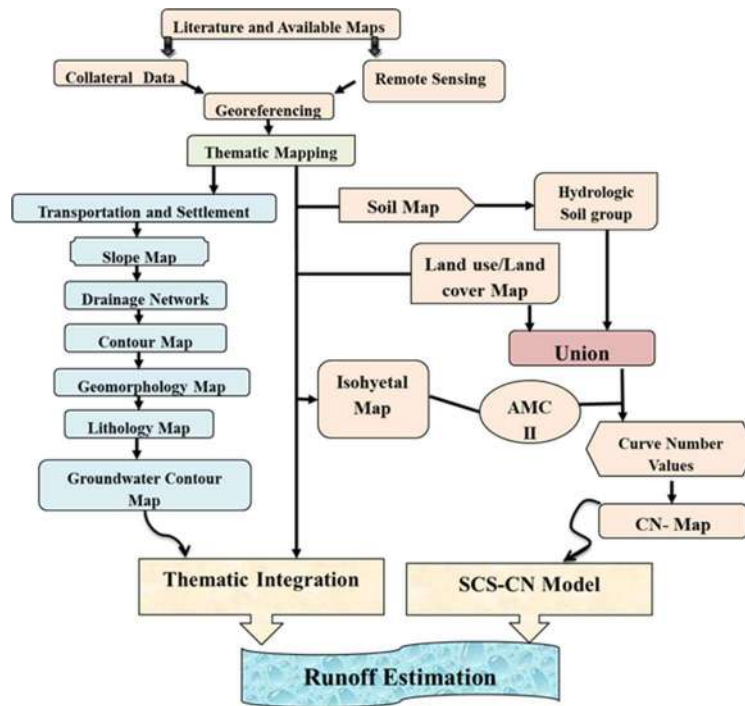


Fig. 2: Flow chart showing the methodology adopted for this investigation.

The soil map of the study area was collected from NBSS/LUP Bangalore. The resulting soil texture map was then used to delineate hydrological soil groups (HSG). Satellite imagery Sentinel II-A 2022 was used to create a land use/land cover (LULC) map, which was then spatially intersected to assign a Curve Number (CN) to each respective polygon in a GIS environment. Finally, all polygons were assigned CN values, further area-weighted method was used to calculate the CN value for each polygon. Following the SCS-CN method (SCS 1985), the runoff potential was estimated using various combinations of HSG, land use, and antecedent moisture condition (AMC) classes (Al-Ghobari et al. 2020, NageswaraRao 2020), the conceptual flowchart of the methodology has depicted in Fig. 2.

SCS Curve Number Method

The soil conservation service curve number (SCS-CN) method was developed by the United States Department of Agriculture's (USDA) soil conservation service (now known as the Natural Resource Conservation Service) in 1954 and is described in section 4 of the National Engineering Handbook (NEH-4) published in 1956. The SCS-CN approach is based on two fundamental principles and the water balance equation. The first hypothesis contrasts the ratio of actual direct surface runoff (Q) to total precipitation (P) (or maximum potential surface runoff) (S) with the ratio of prospective maximum retention (P) to actual maximum infiltration (F) because the second hypothesis connects potential maximum retention (PMR) and initial abstraction (I_a).

The infiltration losses are combined with external storage by the relationship shown below. (Karunanidhi et al. 2020)

$$Q = \frac{(P-I_a)^2}{(P-I_a+S)} \quad \dots(1)$$

Therefore, 'Q' is the direct surface runoff depth (mm), 'P' is the rainfall depth (mm), and 'I_a' is the initial abstraction before surface runoff begins (mm), which includes the surface storage, interception, and infiltration concerning overflow of the watershed. Finally, 'S' is the potential maximum retention after the surface runoff begins (mm). For the Indian condition, 'S' is the potential maximum retention, which is denoted by (Karunanidhi et al. 2020, NageswaraRao, 2020)

The US Soil Conservation Service has found equation 2 by experience, i.e.,

$$I_a = 0.2S \quad \dots(2)$$

Substituting equation (2) for equation (1), the surface runoff equation is depicted below.

$$Q = \frac{(P-0.2S)^2}{(P+0.8S)} \quad \dots(3)$$

For $P > I_a$ (0.2S)

S = the potential infiltration after runoff begins, as calculated by the equation below. (Jaysukh et al. 2015)

$$S = \frac{25400}{CN} - 254 \quad \dots(4)$$

According to Eq. (4), CN (Curve number) is a dimensionless parameter with a range of 1 (minimum runoff) to 100 (Maximum runoff) (Rawat & Singh 2017, Karunanidhi et al. 2020).

Antecedent Moisture Condition (AMC)

Antecedent moisture conditions (AMC) can significantly affect runoff volume as a measure of a watershed's wetness and the soil's capacity to store moisture before a storm (Rawat et al. 2017). Three levels of AMC are essential for the SCS-CN model's execution, and they are listed in Table 1. The total amount of rainfall over the previous five days determines the AMC classification's limitations, which are divided into two categories: the first (growing season) and the second (winter season, dormant season). AMC II is the average moisture condition used in this study (Cronshey 1986). Runoff Curve Numbers (CN) for various LULC categories are obtained for average moisture condition (AMC II) and dry condition (AMC I) or wet condition (AMC II, AMC III) (Table 2). Equation. (5) And (6) are used to calculate the Curve Number for AMC I and AMC III as follows.

$$CN(I) = \frac{CN(II)}{2.281 - 0.0128CN(II)} \quad \dots(5)$$

$$CN(III) = \frac{CN(II)}{0.427 + 0.00573CN(II)} \quad \dots(6)$$

In the preceding equations, CN (II) is the average condition curve number, CN (I) is the dry condition curve number, and CN (III) is the wet condition curve number (Karunanidhi et al. 2020; Taylor et al. 2016)

Area Weighted Curve Number Method

The spatial input maps of soil and land use/land cover are superimposed. These intersection maps represent new polygons called the soil-land map. The value of the curve

Table 1: Classification of antecedent soil moisture condition (AMC).

AMC Group	Soil characteristics	Five-day antecedent rainfall in mm	
		Dormant season	Growing season
I	Dry condition	<13	<36
II	Average condition	13-28	36-53
III	Heavy rainfall/Wet condition	>28	>53

Table 2: Runoff Curve Numbers (AMC II) for Land Use/Land Cover classification are calculated based on the hydrologic soil type. (Source TR55, 1986).

S. No.	Land use Land cover patterns.	Hydrologic Soil Group			
		A	B	C	D
1.	Forest Plantation	25	55	70	77
2.	Plantation	45	53	67	72
3.	Degraded Forest	45	66	77	83
4.	Scrub Forest	33	47	64	67
5.	Encroachment	72	81	88	91
6.	Kharif	64	75	82	85
7.	Settlement	57	72	81	86
8.	Waterbody	97	97	97	97

number varies according to the land use and land cover classes. The obtained results were used to compute the total weighted curve number for the AMC II condition for each polygon of the land area:

$$CNw = \frac{\sum_{i=1}^n (CN_i * A_i)}{\sum_{i=1}^n A_i} \dots(7)$$

In the preceding Eq. (7), ‘CNw’ denotes the weighted curve number; ‘CN_i’ denotes the curve number for a specific land area; ‘A_i’ denotes the area of ‘CN_i’, and A is the total area of the watershed. (Karunanidhi et al. 2020, Taylor et al. 2016, Rawat et al. 2017).

RESULTS AND DISCUSSION

Land Use/Land Cover Pattern

Land use and land cover (LULC) are frequently used to manage the environment sustainably (Karunanidhi et al. 2020). The LULC map was prepared using sentinel satellite data in a GIS environment. The LULC features were identified in the current study using supervised image classification and skilled visual interpretation methodologies. Hence, Scrub forests, Forests, degraded forests, settlements, plantations, forest plantations, and water bodies are the main LULC types identified in the study area (Fig. 3). Most residents in this area work in agriculture, and more than 75% have marginal or very tiny holdings of less than 2 ha. Paddy is the main crop; however, it is also common to see rain-fed crops like maize, Finger Millet, and Ginger in a few isolated locations. Overall, the most critical factors influencing agricultural activity are rainfall and water availability from springs and streams. Arecanut, coconut, cashew, and other plantations are primarily found in mountainous terrain, slopes, and valley floor areas. A total of 27.36% of the area comprises Kharif land, 6.40% of the area comprises forest encroachment, 2.56% of the area comprises Settlement and Forest land includes Plantation (5.46%), Forest Plantation (22.54%) degraded forest (29.46%), and scrubs (4.03%). Forest alteration has been severe due to overgrazing

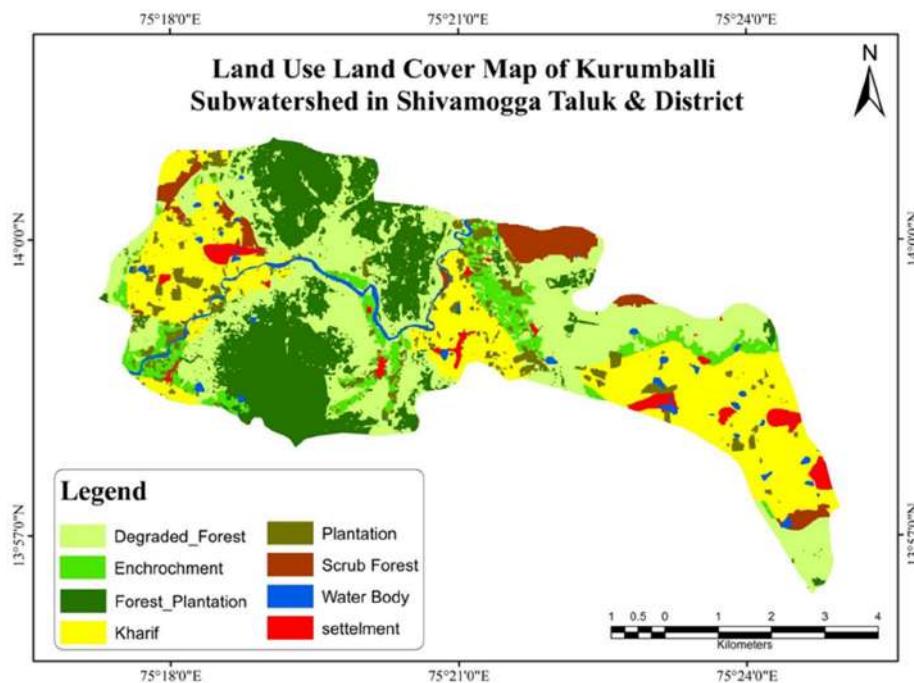


Fig. 3: Land use Land cover map of the study area.

Table 3: Hydrologic soil group for different soil textures (Source USDA-SCS).

HSG	Soil Texture	Type of Soil	Runoff Potential	Remarks
A	Sand, Loamy sand, or Sandy loam	Deep, well-drained sands and gravels	Low	High rate of water transmission
B	Silt loam or loam	Moderately deep, well-drained with moderately fine to coarse textures	Moderate	Moderate rate of water transmission
C	Sandy clay loam	Clay loams, shallow sandy loam, soils with moderately fine to fine textures	Moderately high	Moderate rate of water transmission
D	Clay loam, silty Clay loam, Sandy clay, Silty clay, or Clay	Clay soils that swell significantly when wet, heavy plastic, and soils with a permanent high water table	High	Low rate of water transmission

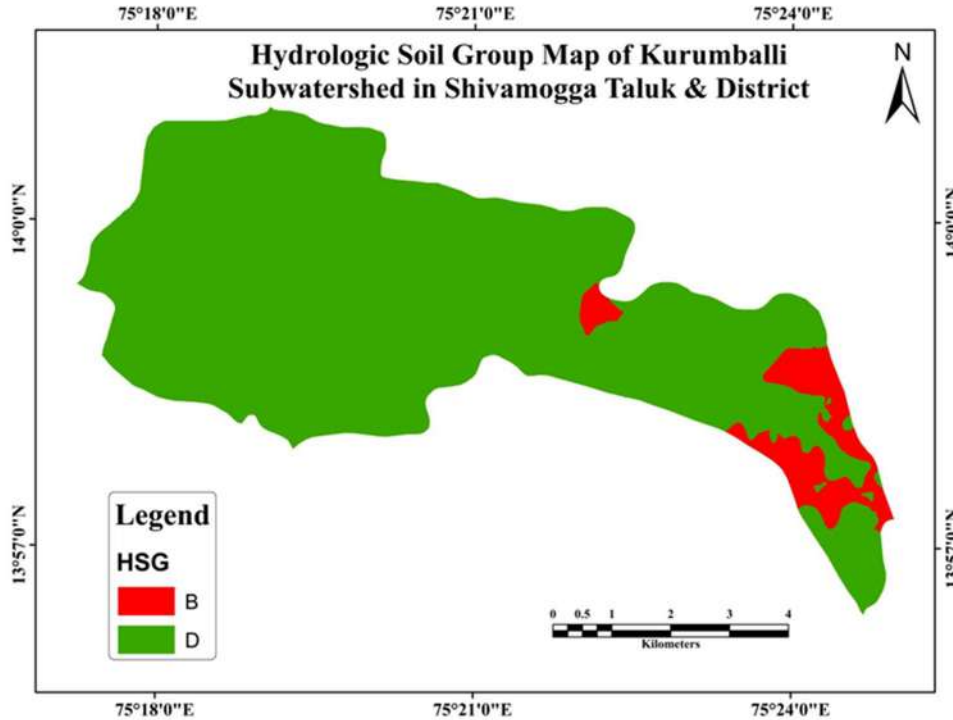


Fig. 4: Hydrologic soil group map of the study area.

and clearing of land for agriculture and development. (NageswaraRao 2020)

Hydrologic Soil Group (HSG)

The hydrological soil group (HSG) is one of the main components used to calculate the curve number (CN). Using the SCS-CN soil classification method, soils were classified into various hydrological groups. Soils are classified into four hydrologic soil groups based on their characteristics: A, B, C, or D tabulated in Table 3. (Tailor et al. 2016). Hydrological soil groups were identified for the Kurumballi sub-watershed based on the USDA-Soil Conservation Service (SCS) guidelines. The HSG classification of soil mainly depends on the infiltration rate of each soil texture category (Karunanidhi et al. 2020). Based on the map of soil textures (Fig. 5), the soil of the Kurumballi sub-watershed

was classified into two HSGs: B and D, as shown in Fig. 4. (Al-Ghobari et al. 2022). Group 'D' soil has high runoff potential with prolonged infiltration rates when thoroughly wetted. Moreover, primarily impervious, Group 'B' soil with moderate infiltration rates when thoroughly wetted. (Karunanidhi et al. 2020, Parvez & Inayathulla 2019)

The criteria mentioned in Table 3 are used to calculate HSG based on the soil's surface texture.

Generating Curve Number (CN)

The curve number is a parameter for catchment retention (S) or perviousness. The soil and land use maps were transferred to the Arc GIS to create the CN map. Following the union of two maps with new polygons reflecting the combined soil-land map, the soil map and land use map were chosen for a union. Each polygon on the soil-land map was given the

Table 4: The Weighted CN values obtained for a variety of preceding moisture conditions (AMC).

AMC	Weighted CN value	Potential maximum retention (s)	P > 0.2 S
I	65.14	135.90	27.18
II	81.12	59.12	11.82
III	90.90	25.44	5.09

proper CN value (Fig. 6) (Gajbhiye 2015). The curve number method (USDA 1972) is also known as the hydrologic soil cover complex method, and it is primarily used for estimating surface runoff (Karunanidhi et al. 2020). The CN has the potential to estimate runoff under the same precipitation conditions, and low CN values indicate that the surface has a high potential to retain water (Rawat et al. 2017); in contrast, high values indicate that the land surface can only store a

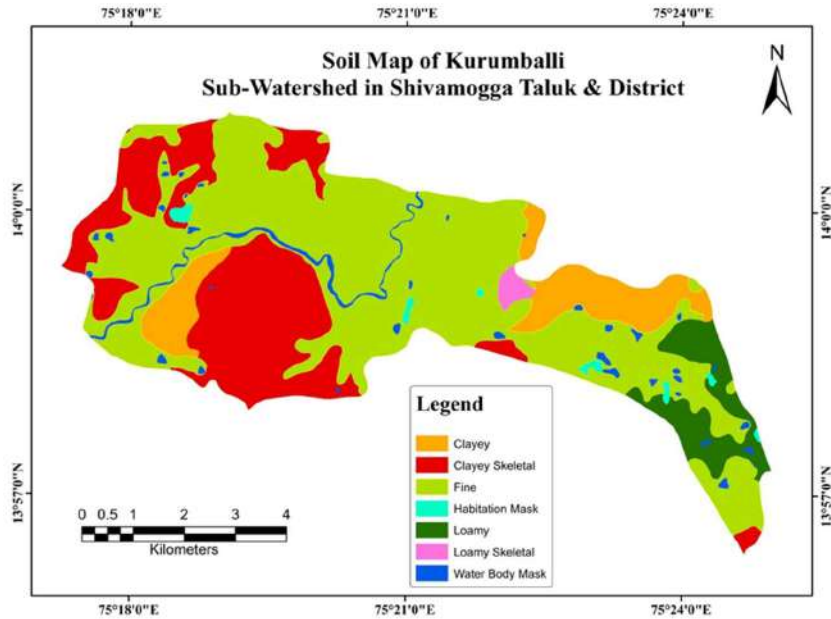


Fig. 5: Soil map of the study area.

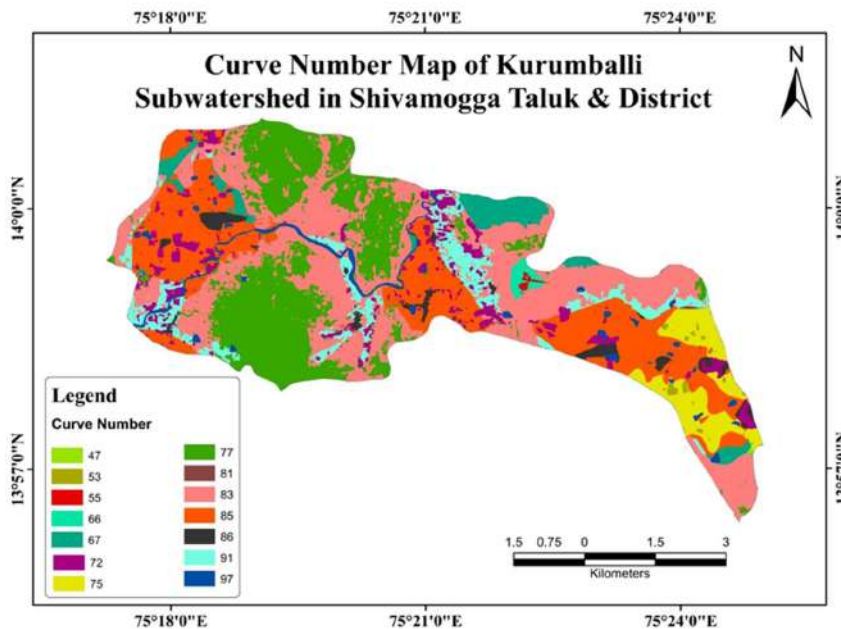


Fig. 6: Curve number map of the study area.

Table 5: Result of Rainfall-Runoff.

Years	Rainfall in mm	Runoff in mm
2011	102.9	54.97
2012	88.4	42.97
2013	112.0	62.75
2014	138.6	86.12
2015	75.9	33.14
2016	73.0	30.89
2017	96.3	49.43
2018	108.4	59.67

small amount of rainfall. As a result, areas with a high CN value will generate a large amount of direct runoff (Rawat et al. 2017). The Weighted CN values obtained for a variety of preceding moisture conditions (AMC) are shown in Table 4.

Data on daily precipitation from the years 2011 to 2018 have been examined. For the years 2011 to 2018, the Kurumballi sub-watersheds yearly rainfall and runoff are displayed in Table 5. The maximum predicted runoff for the watershed was 0.68 mm in 2014, and the minimum was 0.51 mm in 2016, as depicted in Fig. 7 and Table 5 (Tailor & Shrimali 2016). Moreover, the calculation of surface runoff

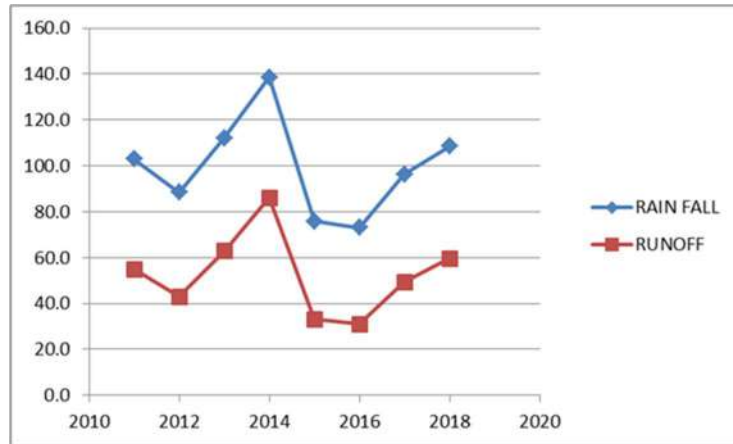


Fig. 7: Graphical plot showing the yearly variation of rainfall and runoff.

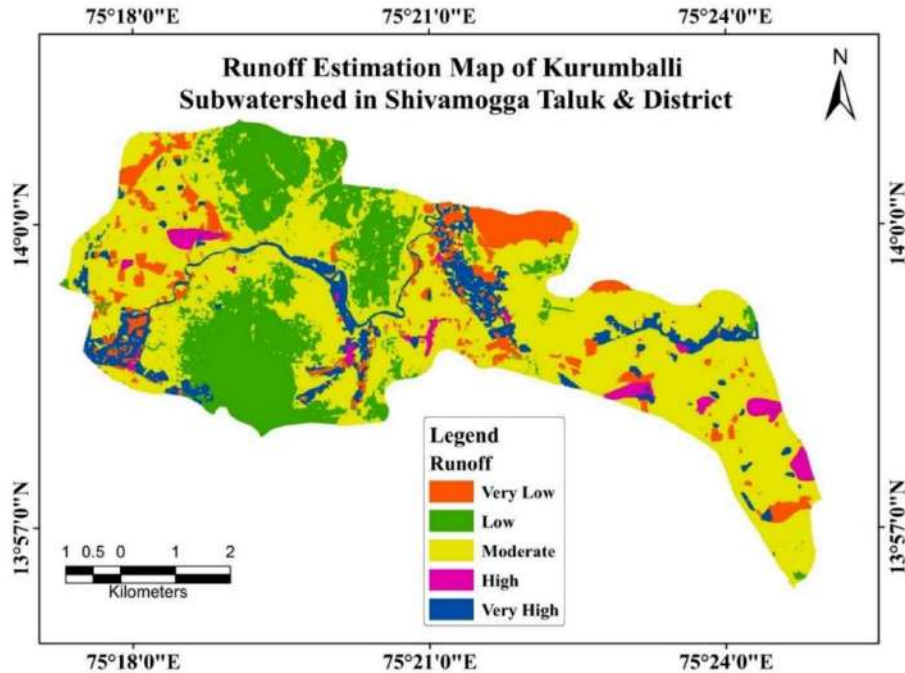


Fig. 8: Runoff estimation map using SCS-CN method.

using the SCS-CN method for the study area is summarized in Table 6.

Calculation of Surface Runoff Using SCS-CN Method

After performing calculations using formulas 5, 6, and 7, we could precisely estimate the amount of runoff in the study area. This estimation was done using the SCS-CN method,

Table 6: Runoff estimation of the study area using the SCS-CN Method.

Different Land use classes	Soil type	HSG	CN	Area Sq. km	% Area	% Area * CN	Weighted CN	Specific retention	Runoff depth	Runoff Volume in m ³
Kharif	Waterbody Mask	D	85	0.377	0.79	67.10	83	52.02	56.51	2693961.18
	Fine	D	85	8.513	17.82	1515.09				
	Clayey Skeletal	D	85	1.111	2.33	197.73				
	Clayey	D	85	0.219	0.46	38.98				
	Loamy	B	75	2.573	5.39	404.05				
	Habitation Mask	D	85	0.2528	0.53	44.99				
Encroachment	Waterbody Mask	D	91	0.101	0.21	19.22	91	25.12	74.92	3571537.54
	Fine	D	91	2.275	4.76	433.47				
	Clayey Skeletal	D	91	0.299	0.63	56.97				
	Clayey	D	91	0.355	0.74	67.65				
	Loamy	B	81	0.020	0.04	3.36				
	Habitation Mask	D	91	0.002	0.0046	0.42				
Forest Plantation	Waterbody Mask	D	77	0.032	0.07	5.17	77	75.87	44.62	2127248.61
	Fine	D	77	5.462	11.44	880.61				
	Clayey Skeletal	D	77	4.573	9.58	737.34				
	Clayey	D	77	0.601	1.26	96.88				
	Loamy	B	55	0.062	0.13	7.08				
	Habitation Mask	D	77	0.001	0.0011	0.09				
Plantation	Waterbody Mask	D	72	0.113	0.236	16.99	71	104.26	34.02	1621805.98
	Fine	D	72	2.045	4.283	308.34				
	Clayey Skeletal	D	72	0.258	0.539	38.83				
	Clayey	D	72	0.015	0.031	2.22				
	Loamy	B	53	0.151	0.315	16.70				
	Habitation Mask	D	72	0.013	0.027	1.94				
Scrub forest	Waterbody Mask	D	67	0.023	0.048	3.25	67	126.119	27.71	1321139.34
	Fine	D	67	1.294	2.710	181.57				
	Clayey Skeletal	D	67	0.342	0.716	47.98				
	Clayey	D	67	0.232	0.485	32.52				
	Loamy	B	47	0.017	0.036	1.68				
	Habitation Mask	D	67	0.001	0.0011	0.09				
Settlements	Waterbody Mask	D	86	0.061	0.128	11.01	83	50.553	57.36	2734469.32
	Fine	D	86	0.693	1.451	124.81				
	Clayey Skeletal	D	86	0.087	0.182	15.64				
	Clayey	D	86	0.046	0.097	8.32				
	Loamy	B	72	0.277	0.580	41.78				
	Habitation Mask	D	86	0.328	0.688	59.13				
					3.126	260.70				

Table Cont....

Different Land use classes	Soil type	HSG	CN	Area Sq. km	% Area	% Area *	Weighted CN	Specific retention	Runoff depth	Runoff Volume in m ³
Degraded Forest	Waterbody Mask	D	83	0.212	0.444	36.83	82.06	53.27	55.81	2660335.37
	Fine	D	83	4.260	8.919	740.32				
	Clayey Skeletal	D	83	6.927	14.504	1203.83				
	Clayey	D	83	3.409	7.138	592.47				
	Loamy	B	66	0.005	0.011	0.73				
	Loamy Skeletal	B	66	0.293	0.614	40.50				
	Habitation Mask	D	83	0.018	0.038	3.12				
					31.668	2617.79				
Waterbody	Waterbody Mask	D	97	0.242	0.507	49.19	97	7.86	90.26	4336010.50
	Fine	D	97	0.739	1.547	150.09				
	Clayey Skeletal	D	97	0.048	0.101	9.75				
	Clayey	D	97	0.021	0.043	4.20				
	Loamy	B	97	0.060	0.126	12.23				
	Habitation Mask	D	97	0.005	0.010	0.95				
						2.334	226.41			

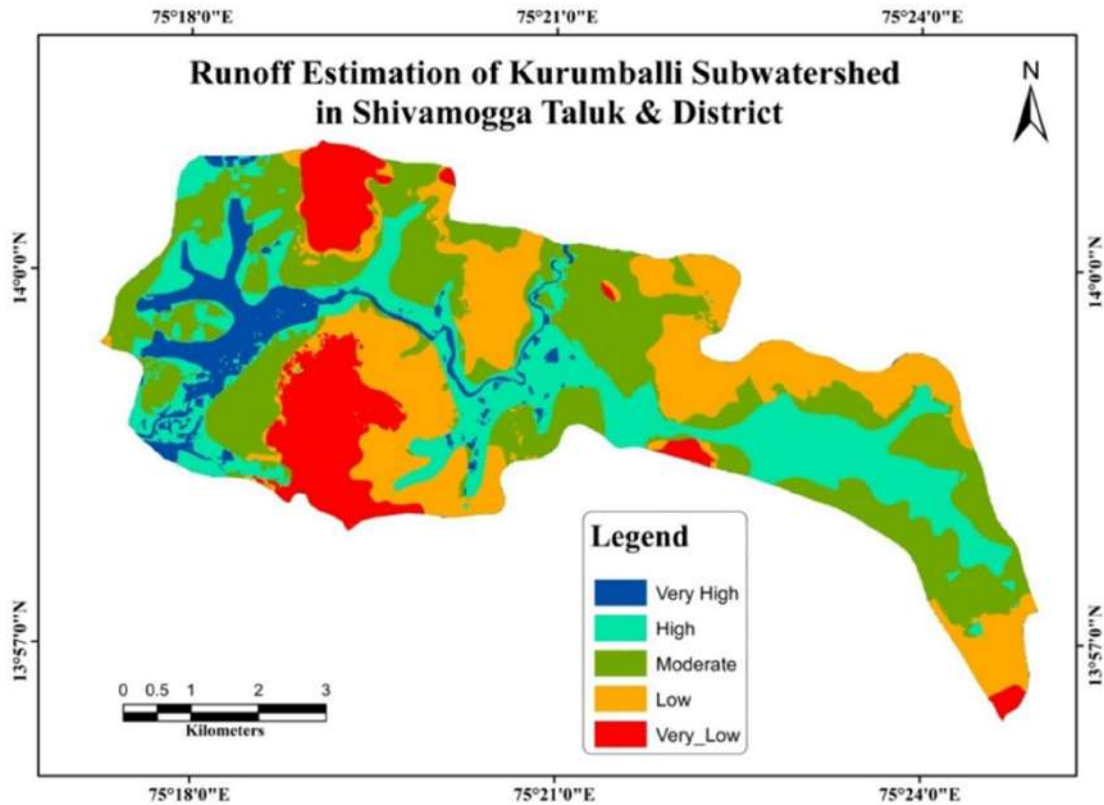


Fig. 9: Runoff potential zonation map using Thematic-integration.

slope, land use, drainage, surface water bodies, groundwater contour, and isohyetal maps. These thematic layers were combined using the ArcGIS 10.4 program to delineate probable zones (Fig. 9). The weights of the various themes were allocated based on their impact on the runoff potential.

Weights were given to various aspects of each topic based on how much of an impact they had on the runoff potential. Based on this assessment, several aspects of the classes were assessed as Very high (7%), High (24%), Moderate (33%), Low (25%), and Very Low (11%). All thematic layers were

then combined after weighting to demarcate potential runoff zones.

CONCLUSIONS

The runoff generation process is highly complex, nonlinear, and dynamic, with numerous interconnected physical factors influencing it. Therefore, precise runoff estimation is carried out for efficient water resource management and growth. There are numerous methods for estimating runoff from rainfall; however, the SCS-CN method remains the most popular, fruitful, and widely used method. The SCS-CN method relies on runoff curve number (CN), determined by land use/land cover (LULC), soil type, Antecedent Moisture condition, and Hydrological soil group. In this study, the SCS runoff curve number for the Kurumballi sub-watershed is estimated using the SCS runoff curve number method, which involves a GIS-based union of the land use land cover map and the hydrologic soil group. First, soil classification results classified the study area into two HSGs (B and D). Group D was the dominant HSG. After that, the estimated curve number is validated using rainfall-runoff data. The total volume of surface runoff in the study area is 21065849.7 m³. Runoff estimation was also performed using thematic layers such as Lithology, Geomorphology, Soil, Slope, Land Use and Land Cover, drainage and Surface water bodies, Groundwater Contour, and Isohyet maps for the delineation of runoff Potential Zones for the study area, which is more accurately correlates with the SCS-CN method. The present study shows that the combination of SCS-CN number and weighted overlay analysis methods is most suitable and accurate for surface runoff potential assessment.

ACKNOWLEDGMENTS

The authors are grateful to the Chairman, Department of Applied Geology, Kuvempu University, Shankaraghatta, for their inspiration to carry out the present work. We want to express our sincere gratitude to everyone who helped and supported this Work and to the editor and reviewers for their valuable comments.

REFERENCES

Al-Ghobari, H., Dewidar, A., & Alataway, A. 2020. Estimation of surface water runoff for a semi-arid area using RS and GIS-based SCS-CN method. *Water*, 12(7), 1924. <https://doi.org/10.3390/w12071924>

Al-Juaidi, A.E. 2018. A simplified GIS-based SCS-CN method for the assessment of land-use change on runoff. *Arab. J. Geosci.*, 11(11): 269. <https://doi.org/10.1007/s12517-018-3621-4>

Amutha, R. and Porchelvan, P. 2009. Estimation of surface runoff in Malattar sub-watershed using SCS-CN method. *J. Indian Soc. Remote Sens.*, 37: 291-304. <https://doi.org/10.1007/s12524-009-0017-7>

Ansari, T.A., Katpatal, Y.B. and Vasudeo, A.D. 2016. Spatial evaluation

of impacts of increase in impervious surface area on SCS-CN and runoff in Nagpur urban watersheds, India. *Arab. J. Geosci.*, 9: 1-15. <https://doi.org/10.1007/s12517-016-2702-5>

Arya, S., Subramani, T. and Karunanidhi, D. 2020. Delineation of groundwater potential zones and recommendation of artificial recharge structures for augmentation of groundwater resources in Vattamalaikarai Basin, South India. *Environ. Earth Sci.*, 79: 1-13. <https://doi.org/10.1007/s12665-020-8832-9>

Bansode, A. and Patil, K.A. 2014. Estimation of runoff by using SCS curve number method and arc GIS. *Int. J. Sci. Eng. Res.*, 5(7): 1283-1287.

Bo, X., Qing-Hai, W., Jun, F., Feng-Peng, H. and Quan-Hou, D. 2011. Application of the SCS-CN model to runoff estimation in a small watershed with high spatial heterogeneity. *Pedosphere*, 21(6): 738-749. [https://doi.org/10.1016/S1002-0160\(11\)60177-X](https://doi.org/10.1016/S1002-0160(11)60177-X)

Bondelid, T.R., McCuen, R.H. and Jackson, T.J. 1982. Sensitivity of SCS models to curve number variation I. *JAWRA J. Am. Water Resour. Assoc.*, 18(1): 111-116. <https://doi.org/10.1111/j.1752-1688.1982.tb04536.x>

Cronshey, R. 1986. *Urban hydrology for small watersheds* (No. 55). US Department of Agriculture, Soil Conservation Service, Engineering Division.

Devia, G. K., Ganasri, B.P. and Dwarakish, G.S. 2015. A review of hydrological models. *Aqua. Proced.*, 4: 1001-1007. <https://doi.org/10.1016/j.aqpro.2015.02.126>

Fetter, C.W. 2001 *Applied Hydrogeology*. Prentice Hall, Upper Saddle River, NJ

Fitts, C.R. 2002. *Groundwater Science*. Elsevier, The Netherlands.

Gajbhiye, S. 2015. Estimation of surface runoff using remote sensing and geographical information system. *International J. Serv. Sci. Technol.*, 8(4): 113-122. <http://dx.doi.org/10.14257/ijunesst.2015.8.4.12>

He, C. 2003. Integration of geographic information systems and simulation model for watershed management. *Environ. Model. Software*, 18(8-9): 809-813. [https://doi.org/10.1016/S1364-8152\(03\)00080-X](https://doi.org/10.1016/S1364-8152(03)00080-X)

Jasrotia, A.S., Dhiman, S.D. and Aggarwal, S.P. 2002. Rainfall-runoff and soil erosion modeling using remote sensing and GIS technique—a case study of tons watershed. *J. Indian Soc. Remote Sens.*, 30: 167-180. <https://doi.org/10.1007/BF02990649>

Karunanidhi, D., Aravinthasamy, P., Roy, P. D., Praveenkumar, R. M., Prasanth, K., Selvapraveen, S. and Srinivasamoorthy, K. 2020a. Evaluation of non-carcinogenic risks due to fluoride and nitrate contaminations in the groundwater of an urban part (Coimbatore region) of south India. *Environ. Monit. Assess.*, 192: 1-16. <https://doi.org/10.1007/s10661-019-8059-y>

Karunanidhi, D., Anand, B., Subramani, T. and Srinivasamoorthy, K. 2020b. Rainfall-surface runoff estimation for the Lower Bhavani basin in south India using SCS-CN model and geospatial techniques. *Environ. Earth Sci.*, 79(13): 1-19. <https://doi.org/10.1007/s12665-020-09079-z>

Khaddor, I., Achab, M., Soumali, M. R. and Alaoui, A.H. 2017. Rainfall-runoff calibration for semi-arid ungauged basins based on the cumulative observed hyetograph and SCS Storm model: Application to the Boukhalef watershed (Tangier, North Western Morocco). *J. Mater. Environ. Sci.*, 8(10): 3795-3808.

Mishra, S., Gajbhiye, S. and Pandey, A. 2013. Estimation of design runoff curve numbers for Narmada watersheds (India). *Journal of Applied Water Engineering and Research*, 1(1): 69-79. <https://doi.org/10.1080/23249676.2013.831583>

Li, C., Liu, M., Hu, Y., Shi, T., Zong, M. and Walter, M.T. 2018. Assessing the impact of urbanization on direct runoff using improved composite CN method in a large urban area. *Int. J. Environ. Res. Public Health*, 15(4): 775. <https://doi.org/10.3390/ijerph15040775>

Liu, X. and Li, J. 2008. Application of SCS model in estimation of runoff from the small watershed in Loess Plateau of China. *Chinese Geogr. Sci.*, 18: 235-241. <https://doi.org/10.1007/s11769-008-0235-x>

- McCuen, R.H. 1982. A guide to Hydrologic Analysis Using SCS methods. Prentice-Hall, Inc., NK.
- Mishra, S.K., Tyagi, J.V., Singh, V.P. and Singh, R. 2006. SCS-CN-based modeling of sediment yield. *J. Hydrol.*, 324(1-4): 301-322. <https://doi.org/10.1016/j.jhydrol.2005.10.006>
- Muthu, A.L. and Santhi, M.H. 2015. Estimation of surface runoff potential using SCS-CN method integrated with GIS. *Indian J. Sci. Technol.*, 8(28): 1-5. <https://dx.doi.org/10.17485/ijst/2015/v8i28/83324>
- NageswaraRao, K. 2020. Analysis of surface runoff potential in the ungauged basin using basin parameters and SCS-CN method. *Appl. Water Sci.*, 10(1): 1-16. <https://doi.org/10.1007/s13201-019-1129-z>
- Parvez, M.B. and Inayathulla, M. 2019. Estimation of surface runoff by soil conservation service curve number model for upper Cauvery Karnataka. *Int. J. Sci. Res. Multidisc. Stud.*, 5: 11.
- Rao, K.N., Narendra, K. and Latha, P.S. 2010. An integrated study of geospatial information technologies for surface runoff estimation in an agricultural watershed, India. *J. Indian Soc. Remote Sens.*, 38: 255-267. <https://doi.org/10.1007/s12524-010-0032-8>
- Rawat, K.S. and Singh, S.K. 2017. Estimation of surface runoff from semi-arid ungauged agricultural watershed using SCS-CN method and earth observation data sets. *Water Conserv. Sci. Eng.*, 1(4): 233-247. <https://doi.org/10.1007/s41101-017-0016-4>
- Satheeshkumar, S., Venkateswaran, S. and Kannan, R. 2017. Rainfall-runoff estimation using SCS-CN and GIS approach in the Pappirepatti watershed of the Vaniyar sub-basin, South India. *Model. Earth Syst. Environ.*, 3: 1-8. <https://doi.org/10.1007/s40808-017-0301-4>
- Sayl, K.N., Muhammad, N.S. and El-Shafie, A. 2019. Identification of potential sites for runoff water harvesting. *Water Manag.*, 172(3): 135-148. <https://doi.org/10.1680/jwama.16.00109>
- Shah, M., Fazil, S.M., Ali, S.R., Pandey, Y., Faisal, S. and Mehraj, I. 2017. Modeling of runoff using curve expert for Dachigam-Telbal catchment of Kashmir valley, India. *J. Curr. Microbiol. Appl. Sci.*, 6(11): 3822-3826. <https://doi.org/10.20546/ijcmas.2017.611.449>
- Shi, Z.H., Chen, L.D., Fang, N.F., Qin, D.F. and Cai, C.F. 2009. Research on the SCS-CN initial abstraction ratio using rainfall-runoff event analysis in the Three Gorges Area, China. *Catena*, 77(1): 1-7. <https://doi.org/10.1016/j.catena.2008.11.006>
- Songara, J.C., Kadivar, H.T., Joshipura, N.M. and Prakash, I. 2015. Estimation of surface runoff of Machhu Dam III Catchment Area, Morbi, Gujarat, India, using curve number method and GIS. *Int. J. Sci. Res. Dev.*, 3(3): 2038-2043.
- Mondal, M.S., Pandey, A.C. and Garg, R.D. 2008. Groundwater prospects evaluation based on hydrogeomorphological mapping using high-resolution satellite images: a case study in Uttarakhand. *J. Indian Society Remote Sens.*, 36: 69-76. <https://doi.org/10.1007/s12524-008-0007-1>
- Tailor, D. and Shrimali, N.J. 2016. Surface runoff estimation by SCS curve number method using GIS for Rupen-Khan watershed, Mehsana district, Gujarat. *J. Indian Water Resour. Soc.*, 36(4): 1-5.
- Verma, S., Singh, P.K., Mishra, S.K., Singh, V.P., Singh, V. and Singh, A. 2020. Activation soil moisture accounting (ASMA) for runoff estimation using the soil conservation service curve number (SCS-CN) method. *J. of Hydrol.*, 589: 125114. <https://doi.org/10.1016/j.jhydrol.2020.125114>
- Viji, R., Rajesh Prasanna, P. and Ilangovan, R. 2015. Gis-based SCS-CN method for estimating runoff in Kundahpalam watershed, Nilgries District, Tamilnadu. *Earth Sci. Res. J.*, 19(1): 59-64. <https://doi.org/10.15446/esrj.v19n1.44714>
- Voda, M., Sarpe, C.A. and Voda, A.I. 2019. Romanian river basins lag time analysis. The SCS-CN versus RNS comparative approach was developed for small watersheds. *Water Resources Management*, 33(1): 245-259. <https://doi.org/10.1007/s11269-018-2100-8>
- Williams, J.R. and LaSeur, W.V. 1976. Water yield model using SCS curve numbers. *J. Hydraul. Div.*, 102(9): 1241-1253. <https://doi.org/10.1061/JYCEAJ.0004609>

ORCID DETAILS OF THE AUTHORS

Govindaraju: <https://orcid.org/0000-0002-0119-4826>



Coal Mining and MSME: Is it Mutually Beneficial?

S. Bintariningtyas[†] , T. Mulyaningsih  and Y. Purwaningsih 

Department of Economics and Business, Sebelas Maret University, Surakarta 57126, Indonesia

[†]Corresponding author: S. Bintariningtyas; selfia.bintari@staff.uns.ac.id

Nat. Env. & Poll. Tech.
Website: www.neptjournal.com

Received: 07-08-2023

Revised: 06-10-2023

Accepted: 13-10-2023

Key Words:

Coal mining

Corporate social responsibility

MSME

Environmental damage

ABSTRACT

The existence of a coal mining company in the vicinity of the community is something to be feared related to environmental damage due to coal mining. On the other hand, coal mining can have a positive impact on the economy of communities around the mine through corporate social responsibility programs. The problem in this research is that MSMEs need help to improve their performance. Therefore, this research aims to examine how the role of mining companies through corporate social responsibility (CSR) programs can contribute to the development of MSMEs in communities around mining areas. The company provides promotional assistance, funding, and capacity building. This research conducted surveys and interviews with respondents, namely MSMEs, around mining locations. The findings show that corporate social responsibility programs in coal mining companies have a positive impact on empowering MSMEs in communities around the mine. By providing training and promotion facilities to MSMEs, mining companies can also improve MSME performance compared to providing access to financial assistance programs. The company not only takes advantage of mining and focuses on its environmental impact but also the company's role in empowering MSMEs.

INTRODUCTION

The existence of coal mining companies around the community is something to be afraid of related to the environmental damage due to coal mining. According to (Coelho et al. 2022), the community around the mining site is dissatisfied with the impacts caused by mining companies. The community around the location also considers the landscape's influences to be severe, aside from the effect on air, water, and health, while the community feels the economic and social benefits at a lower intensity level. On the other side, coal mining impacts regions like no other industry. Revenues generated by that industry are substantial and contribute to local economic development. Coal mining also offers numerous high-paying jobs in regional areas where other employment options are often scarce. Unfortunately, the coal mining benefits are primarily limited in time, highly dependent on foreign demand for coal, and may not systematically result in sustained regional development in the long run (De Valck et al. 2021). In addition to impacting the environment, coal mining can impact the community, including conflicts in the community, declining quality of public health, changes in community life patterns, and social structures that tend to change. However, coal mining is expected to impact the community's economy around the mine positively. For this reason, coal mining companies

must contribute to the community through a corporate social responsibility (CSR) program to improve the surrounding community's living standards and alleviate poverty.

Moreover, the mining sector, especially coal mining, significantly increases Indonesia's exports. It was proven in 2019 that coal production had the highest contribution compared to other mining products. Statistical data on non-oil and gas mining published by BPS also reported that coal production is still the prima donna, where the total production reached 565,640,928 tons in 2020, and this value was the highest among the production of other mineral mining goods.

CSR investments have been proven to contribute to the company's capacity to influence governmental actors and, therefore, for its expansion projects to go through (Carmona & Jaramillo 2020). Besides, many mining companies stated they have carried out their CSR activities aimed at sustainable and community development with various approaches. Mining companies have also highlighted the financial investments and their contributions to local community development focused on sustainable development (Wilson 2022). Furthermore, to improve the economy, the government's main priority is fostering and empowering MSMEs. This MSME coaching program is not only carried out by the government but the involvement of companies or the private sector is expected to contribute to developing

MSMEs. It is done by a company in its social responsibility to the community, especially around the mining company.

One of the company's community empowerment programs is assisting in creating creative and innovative businesses through MSMEs. Micro, small, and medium enterprises, commonly referred to as MSMEs, are businesses with a considerable role in the Indonesian economy. When viewed from a national scale, MSME economic activities significantly contribute to Indonesia's total Gross Domestic Product (GDP). MSMEs also have a massive role in the economy since they can be a driving force for economic revival, as evidenced by the many challenges faced in the globalization and free trade eras and the downturn during the COVID-19 pandemic.

Specifically, according to (ELTI 2013), East Kalimantan has 17 PKP2B (Coal Mining Concession Work Agreements) companies with a total production in 2020 of 114,293,563.23 tons. In this case, Paser Regency is one of the regencies in East Kalimantan province with immense potential for mining resources. As reported (Paser 2017), 275 companies in mining, plantation, forestry, banking, telecommunications, hotels, and restaurants exist in Paser Regency.

Mining activities pose serious risks to the communities involved and the environment as a whole (Quarm et al. 2022). Mining has a negative impact on surrounding agriculture (Dibattista et al. 2023). An important factor in determining the Company's actions in determining compensation by providing incentives to stakeholders (Bhaskar et al. 2023). Only a few people say that the social impacts that occur due to mining require the implementation of a community participation process. CSR can identify and understand how to strengthen quality partnerships in its performance (Neto & Mallett 2023). Companies that implement and follow CSR strategies will gain many benefits, not only economic benefits but also social benefits (Diaye et al. 2023). The company carries out its business activities around where people live. They not only get economic benefits but also provide benefits to the surrounding community. The company fosters and develops MSMEs as a form of corporate social responsibility in contributing to developing MSMEs. MSMEs that are located around mining sites far from the city center. This results in MSMEs being less capable of increasing their sales. MSMEs need companies to be able to provide assistance to improve their performance. Therefore, this research examines whether mining companies help MSMEs to improve performance. MSMEs need assistance that suits their needs.

Corporate Social Responsibility in Mining Companies

Majer (2013) explained that mining activities significantly disrupt the lives of local communities and cause mining

damage. Hence, it is worth analyzing the mining company's approach to maintaining positive relationships with local communities and governments by CSR principles, considering the applicable laws or codes of conduct developed in this area and the potential differences.

The way to do in conducting modern mining operations for the impact that occurs on all aspects of the environment and society. This can be done by planning projects carefully, implementing control measures, exercising control over the impacts of mining and rehabilitating post-mining land, as well as the coal industry and the impact of these activities on the surrounding community, the surrounding environment, and land sustainability capabilities (Dontala et al. 2015). It is more interesting to note that the effectiveness of Corporate Social Responsibility activities can be influenced by the dynamics of social, cultural, and power structures in the communities around mining (Wilson 2022).

In Indonesia, programs as a form of corporate social responsibility are very much spread in various regions. In the scope of corporate social responsibility, the programs cover the fields of economy, education, health, socio-culture, and infrastructure (Nirmaya et al. 2014). Not only large-scale companies but several small companies take part in providing social responsibility to the community.

Moreover, corporate social responsibility is a well-known concept widely used in implementing large and small mining companies. The vital role of CSR in mining companies is to ensure that businesses are responsible for reducing and lowering potential risks arising from work safety problems and possible negative environmental impacts, as well as to make employees better and gain acceptance from the local community. However, the CSR activities' scope and function depend not on the company's profile and size but on the area where they carry out mining operations, so CSR functions are sometimes less than optimal in developing countries (Wirth et al. 2016). Several mining companies have also implemented policies to provide social responsibility to communities around mining sites. Not only that, but they have also carried out activities and programs to empower the community to be economically and financially independent.

MSMEs (Micro, Small and Medium Enterprises)

MSMEs are community businesses that can provide socio-economic welfare. MSMEs, which can be said to be micro, small, and medium enterprises, are the spearheads of the community's economy. Of all businesses, 99% of them can provide 60% employment. They also contribute to a country's sustainable and inclusive economic growth. In addition, people who are transforming globalization and digitalization can be supported by the existence of MSMEs.

(Noviarto & Samputra 2021). MSMEs in developing countries still face several obstacles in increasing sales and technological delays (Mantri & Mishra 2023).

In this case, micro-enterprises are productive businesses owned by one or more persons or individual business entities that meet the criteria for micro-enterprises (PP Republik Indonesia 2021). The criteria for MSMEs included in micro-enterprises are that they have a business capital of up to a maximum of IDR 1 billion and do not include land and buildings for the place of business. Then, small businesses have a business capital of more than IDR 1 to IDR 5 billion, excluding land and buildings for business. In comparison, medium enterprises have a business capital of IDR 5 to IDR 10 billion, excluding land and buildings for business premises. Besides, following the definition of MSMEs according to government regulation, MSMEs are classified from business capital and sales results in one year. Small businesses that adopt and use business management to increase revenue will maximize the resources they have (Lemańska-Majdzik & Okręglińska 2015).

Furthermore, creative human resources are an effort to increase a person's or organization's value, especially MSMEs. They are essential to a country's economy, especially in Indonesia. In realizing this, the creativity of human resources requires support in the form of protection that ensures that intellectual works are safe from misuse and counterfeiting (Nurani, Fahmi, and Fauzi 2021). In addition, MSMEs have a very strategic role in the economic development of a country. Their role is vital to distributing a country's production and playing a role in economic growth and employment. Therefore, if there is a financial crisis, it does not affect MSMEs (Gunawan et al. 2019).

MATERIALS AND METHODS

This research was conducted in Paser Regency, East Kalimantan. The Paser Regency area consists of 10 sub-districts, 5 sub-districts, and 139 villages. Paser Regency is one of the regencies with several companies and foreign investments. Paser Regency also has 275 companies in mining, plantation, forestry, banking, telecommunications, hotels, and restaurants (Humas 2017). In addition, one of the PKP2B mining companies is located in Paser Regency. However, not all companies had CSR programs; only a few companies, especially coal mining companies, had a corporate social responsibility (CSR) program.

MSMEs assisted by coal mining companies through CSR amounted to 986 fostered MSMEs around the mining sites of Paser Regency. The sample used in this research used a probability sampling method with a proportional sampling technique. The formula calculation uses Slovin, with the

population used being MSMEs assisted by coal mining companies. So, the sample uses the following formula:

$$n = \frac{N}{1 + Ne^2}$$

Information:

N = sample size

N = known population size

e = percent allowance for inaccuracy due to sampling error, the desired precision is 10%.

The Slovin formula calculates samples with an error rate of 10% so that minimal sample data is obtained. To facilitate calculations, 100 samples were taken. Next, data collection uses a questionnaire containing questions for the coached MSME actors. This research conducted tests with STATA 14 by analyzing the influence of the variables Promotion and Marketing Assistance (X1), Capital Assistance (X2), and Training Assistance (X3) on the performance of MSMEs (Y).

Questionnaires given to respondents were then measured using the Likert scale measurement method. The Likert scale was utilized to measure the role of CSR in the fostered MSMEs (Sugiyono 2009). The Likert scale is a scale or measurement used to measure the attitudes, opinions, or perceptions of a person or group of people regarding an event and social phenomenon based on the operational definition that the researcher has determined. Therefore, to facilitate data collection in the field, this research uses a Likert scale.

RESULTS

The increasingly stringent development of the business world requires strategies to face competition. MSMEs and industries need strategy and technology to run their business (Gani et al. 2022). Small businesses never get support from other actors to develop innovation activities (Larios-Francia & Ferasso 2023). There are many things companies can do to help communities around mines. The relationship between CSR and MSME performance is not directly related but rather through an environmentally friendly innovation process, thus providing support for the moderated mediation model (Achi et al. 2022). Business actors to improve their performance requires budgeting and also need training assistance (Ragoobur et al. 2023). CSR can identify and understand how to strengthen quality partnerships in its performance (Erdiaw-Kwasie et al. 2023).

The main focus of mining corporate social responsibility is on leading international actors, with particular attention paid to the situation in developing countries (Majer 2013). Partnerships are carried out through corporate social responsibility (CSR)-based programs regulated by applicable

government regulations. Companies gain profits by still paying attention to the surrounding environment. Companies are obliged to address environmental impacts and improve community welfare. Hence, companies should run CSR programs to reduce and lower their impacts and make MSMEs around companies independent and professional (Ghassani 2015).

Sustainable MSMEs need support and socially responsible activities as a unit. As such, a partner provides a conducive opportunity for MSMEs to adopt collective social responsibility, which will serve the needs of various stakeholders, such as workers, communities, and the environment (Tewari & Pathak 2015).

Data in Table 1 show that gender for men with an undergraduate education is only 1% and 4% for women with an undergraduate education. This shows that for women with a bachelor's degree, it is preferable to be self-employed and become MSME actors. This can also illustrate that the absorption of male workers in mining companies requires more male workers than female workers for Bachelor graduates. Most MSME actors have a high school education, namely 50% of men and 34% of women. Whereas for MSME actors who have elementary school equivalent education, there are still 6 men.

The low level of education does not prevent MSME actors from continuing to develop their businesses in order to

improve the welfare of their families. We can also assume that becoming an MSME actor does not require higher education. It indicates that even though they had higher education in college, MSME actors still wanted to become entrepreneurs. Related to that, the theory of limited rationality explains that rationality is limited when individuals, namely MSMEs, decide by considering the decision problem, limitations regarding cognitive thinking, and the time available to make a decision (Noviarto & Samputra 2021). Women entrepreneurs can develop their companies in an integrative and sustainable manner (Hendratmi et al. 2022).

MSMEs that receive guidance from coal mining companies have various fields, namely workshops, culinary, fishery, plantation, and agriculture. Table 2 shows that most of the MSMEs in Legai Village have businesses in the Plantation sector, 41%. This is because most Legai villages have large areas of oil palm land, which are used by the local community to own oil palm businesses. As for Culinary, it has 33% of the total MSMEs, and most of them occupy Batukajang village. Batukajang is an area with a large population. It can be said that the need for food will also be high. This is what attracts business actors to be able to develop MSMEs in the culinary field in Batukajang village. The data also shows that for the agriculture sector, it is only 4%, considering that the land in the area is peat land, which is not suitable for agriculture. Still, there are

Table 1: Education level and gender of fostered MSME actors.

Gender	Education					Amount
	College S-1	College D-3	Senior High School	Junior High School	Elementary Level	
Man	1	1	50	3	6	61
Woman	4	1	34	0	0	39
Amount	5	2	84	3	6	100

Source: obtained from primary data

Table 2: Business fields and villages of MSME.

Village	Business Fields					Amount
	Workshop	Culinary	Fishery	Plantation	Agriculture	
Batu Kajang	4	33	0	0	0	37
Biu	0	0	0	0	2	2
Kuaro	0	0	5	0	0	5
Legai	1	0	0	41	0	42
Pndong	0	0	10	0	0	10
Samuranggau	0	2	0	0	0	2
Songka	0	0	0	0	1	1
Sungai Terik	0	0	0	0	1	1
Amount	5	35	15	41	4	100

Source: obtained from primary data

Table 3: Internet use of fostered MSME actors.

Use the Internet	Production needs	Promotion	Not Use	Amount
No	0	0	41	41
Yes	25	34	0	59
Amount	25	34	41	100

Source: obtained from primary data

several methods of managing agriculture that are suitable for this area.

Along with the times, the increasing sophistication of human needs for technology. Humans need technological sophistication in order to carry out their activities, both production activities and consumption activities. MSMEs in carrying out their buying and selling activities, also require technology, namely the use of the Internet. Internet use in SMEs: 59% use the Internet, and 41% do not use the Internet. Of business actors who use the Internet, 25% use the Internet for production purposes and 34% for promotion purposes. Business actors can carry out production with the help of sophisticated technology and the Internet, such as buying raw materials, training, and production information. Not only in the production process but in promoting their products, business actors also use the Internet. By way of promotion, it can increase product sales. MSME actors also use social media to run their business interactions, including WhatsApp, Instagram, and Facebook and employ the marketplace to sell their products.

Moreover, the digital literacy capabilities of the fostered MSMEs are the capital of MSME actors to develop businesses to increase productivity in the current digitalization era. This digital literacy development of a collective awareness of the need to build literacy in the context of the information society. In addition, its international recognition has implied an effort in recent years from organizations, institutions, and governments to that this change into practice (Tejedor et al. 2020).

The use of the Internet for the community needs to be carried out with literacy that can provide learning to MSMEs.

Table 5: Coefficients.

Y	Coef.	Std. Err.	T	P> t	[95% Conf. Interval]	
xPP	0.343846	0.130724	2.63	0.010	0.084361	0.603332
xPM	-0.074498	0.129392	-0.58	0.566	-0.331338	0.182343
xCB	0.241857	0.099075	2.44	0.016	0.045196	0.438519
_cons	1.896540	0.629581	3.01	0.003	0.646832	3.146247

Source: Stata 14.0 (2023)

Table 4: Internet use of fostered MSME actors.

Business License	Percent.
NIB	40
SIUP	15
SIUDes	45
Total	100

Source: obtained from primary data

This is done to increase the ability of business actors to advance technology. Much can be done if the digital literacy skills of business actors increase, for example, by providing knowledge about product information, production processes, financial literacy, innovation, promotion, and interaction with consumers.

Digital literacy is measured by two indicators, namely digital diffusion and digital literacy. Digital diffusion indicators are presented by device ownership to take advantage of the emergence of digital technology (Mulyaningsih et al. 2020). This also happens to MSME actors who take action to increase their sales. The way for MSMEs to increase sales is to carry out sales promotions using digital devices. The most that is done is by utilizing the social media they have. MSME actors who often take advantage of social media are businesses in the culinary or food sector. Business actors or MSMEs hope that when carrying out promotions, there will also be an increase in income.

Each business sector also had a community that became its organization to strengthen its business capabilities. In addition, business permits had been obtained by 40% of MSMEs with already having a Business Identification Number (NIB). Some of them also had village business permits and special permits from agencies. Most of them, 45%, also obtained a trading business license issued by the local government. And the rest obtained a business license from the village government. Business actors need to look for business opportunities amidst the instability of the current business environment (Choi et al. 2022). As an MSME partner, the company will help provide branding and business permits. A business needs branding as an important element in company storytelling (Olivares-Delgado et al. 2016).

Coefficients

Table 5 shows that after testing to determine the effect how are the programs implemented by coal companies on community welfare by developing SMEs, the result is that training assistance or human resource development significantly improves the performance of SMEs. This means that if the company implements social responsibility programs properly by providing capacity building to the assisted MSMEs, it will improve the performance of MSMEs.

Nonetheless, access to financing or capital programs provided to assisted MSMEs does not have an impact on MSME performance. This is because most MSMEs do not fully know how to access financing provided by companies. This lack of understanding is what causes MSME actors to not use the facilities of the company in accessing financing. MSMEs' inability to access funding is hindered by institutional, structural, and non-financial factors (Cruz & Ashley 2023).

MSME players will take action to increase their sales. MSMEs need the role of other parties to increase sales by carrying out sales promotions (Boberg et al. 2023). For testing, the variables of promotion and marketing assistance have a significant relationship to MSME performance and positively influence MSME performance. In other words, if promotion and marketing increase, the performance of MSMEs will increase. This is per the Mining Company Program, which provides a place for MSMEs to carry out promotions and marketing. The company does help carry out promotions and marketing not only offline but also online.

Mining companies provide training programs, financing access assistance programs, as well as promotion and marketing assistance programs to MSMEs. Corporate social responsibility programs affect the performance of MSMEs and, of course, can affect the welfare of the community around mining locations.

DISCUSSION

The role of mining companies in community empowerment, especially for MSMEs, has a significant impact in the long term. In this study, mining companies in Paser Regency implemented CSR programs for MSMEs around the mining area by conducting training programs, assistance programs for access to financing and capital, and promotion and marketing assistance. The analysis results on the assisted MSMEs were more effective in training assistance programs, improving human resource capabilities. In addition, the training assistance program had a positive effect. Therefore, if the company's CSR increases the training program and

promotion facilities, it will enhance the performance of the assisted MSMEs. The role of companies is through Community Empowerment by utilizing resources to increase MSME innovation (Sahi et al. 2023).

Moreover, business development programs may actively consider choosing partnerships for business development. Here, there is a lack of appropriate commercial service providers to develop businesses and provide optimal services to meet the needs of a more significant segment of entrepreneurs in those operating in the micro-enterprise sector and semi-urban and rural areas (Huq & Moyeen 2011).

Specifically, as MSME actors, they must be 'authorized,' while employees must also be 'authorized.' Thus, someone with authority usually uses his authority from internal leadership traits and not only by his power title. In comparison, authority is power with a title given to someone in an organization. It helps develop self-discipline among employees; thus, although leadership is centralized, the balance of power is also decentralized (Khanzode et al. 2021).

Furthermore, the business has changed substantially recently, from being conceived as a field of ruthless people motivated solely by profit to being perceived as an institution with a serious moral responsibility to society. Traditional businesses, whose mission is the profit of their owners, are always in conflict with the remaining elements in the system, i.e., employees, society, environment, and others (Sanchez-Infante et al. 2020). Thus, companies must adapt and focus on social responsibility activities as a cost of running a business. Many countries have also faced challenging economic development, education, health care, and basic infrastructure (Cesar 2021).

CONCLUSION

Although mining companies are said to be damaging the environment, from an economic point of view, mining can have a positive impact on society. Mining companies have tried to provide social responsibility both to the environment and the community, especially around mining areas. Then one of the programs carried out by the company is to empower the community. The company's CSR roles include providing training programs, capital assistance programs, and promotion and marketing programs. The three CSR programs carried out by mining companies have a positive effect on the performance of MSMEs. For this reason, mining companies provide social responsibility to the community through programs to improve community welfare. Support from the government is needed to collaborate with companies to continue to empower communities around coal mines.

RECOMMENDATION

Mining companies have substantial social impacts, and a vital policy solution is to empower local communities. This involves prioritizing the well-being of residents, reducing poverty, and promoting economic independence through targeted community capacity building.

REFERENCES

- Achi, A., Adeola, O. and Achi, F.C. 2022. CSR and green process innovation as antecedents of micro, small, and medium enterprise performance: The moderating role of perceived environmental volatility. *J. Bus. Res.*, 139: 771-81. doi: 10.1016/j.jbusres.2021.10.016.
- Bhaskar, R., Bansal, S., Abbassi, W. and Pandey, D.K. 2023. CEO compensation and CSR: economic implications and policy recommendations. *Econ. Anal. Policy*, 79: 232-56. doi: 10.1016/j.eap.2023.06.016.
- Boberg, P.S., Bövers, J., Bormann, K.C. and Hoon, C. 2023. Identity leadership in family businesses: the important role of nonfamily leaders. *J. Fam. Bus. Strategy*, 14(2). doi: 10.1016/j.jfbs.2022.100517.
- Carmona, S. and Jaramillo, P. 2020. Anticipating futures through enactments of expertise: A case study of an environmental controversy in a coal mining region of Colombia. *Extr. Ind. Soc.*, 7(3): 1086-95. doi: 10.1016/j.exis.2020.06.009.
- Cesar, S. 2021. Corporate social responsibility fit helps to earn the social license to operate in the mining industry. *Resour. Policy*, 74: 101814. doi: 10.1016/j.resourpol.2020.101814.
- Choi, J., Jeong, B. and Yoon, J.. 2022. Identification of emerging business areas for business opportunity analysis: an approach based on language model and local outlier factor. *Comput. Ind.*, 140: 103677. doi: 10.1016/j.compind.2022.103677.
- Coelho, M., de Cavaleiro, Y., Sanjuan de Medeiros, P., Almeida Santos, J. and Lucas, F.C.A. 2022. Perception of environmental impacts of aggregate mining: A case study from the municipality of Ourém., Pará., Brazil. *Resour. Policy*, 78: 414.
- Cruz, D. and Ashley, N. 2023. PROTOCOL: effects of interventions to prove access to financial services for micro-, small- and medium-sized enterprises in low- and middle-income countries: an evidence and gap map. *Campbell Syst. Rev.*, 19(3): 21-31.
- De Valck, J., Williams, G. and Kuik, S. 2021. Does coal mining benefit local communities in the long run? A sustainability perspective on regional Queensland., Australia. *Resour. Policy*, 71: 102009. doi: 10.1016/j.resourpol.2021.102009.
- Diaye, M.A., Lasram, H. and Pekovic, S. 2023. How does CSR affect workers' compensation? An approach by the theory of incentives. *Int. J. Prod. Econ.*, 260(March): 108860. doi: 10.1016/j.ijpe.2023.108860.
- Dibattista, I., Camara, A.R., Molderez, I., Benassai, E.M. and Palozza, F. 2023. Socio-environmental impact of mining activities in Guinea: the case of bauxite extraction in the region of Boké. *J. Cleaner Prod.*, 387: 135720. doi: 10.1016/j.jclepro.2022.135720.
- Dontala, S.P., Reddy, T.B. and Vadde, R. 2015. Environmental aspects and impacts and its mitigation measures of corporate coal mining. *Procedia Earth Planet Sci.*, 11: 2-7. doi: 10.1016/j.proeps.2015.06.002.
- ELTI. 2013. Daftar perusahaan pertambangan mineral dan Batubara Yang Akan Melapor pada laporan EITI Indonesia kedua tahun kalender 2010 dan 2011.
- Erdiaw-Kwasie, M.O., Abunywah, M. and Baah, C. 2023. Corporate social responsibility (CSR) and cognitive bias: A systematic review and research direction. *Resour. Policy*, 86(PA): 104201. doi: 10.1016/j.resourpol.2023.104201.
- Gani, A., James, A.T., Asjad, M. and Talib, F. 2022. Development of a manufacturing sustainability index for MSMEs using a structural approach. *J. Clean. Prod.*, 353: 131687. doi: 10.1016/j.jclepro.2022.131687.
- Ghassani, N. 2015. MSME development partnership (SDT Partnership. PJB (Pembangkit Jawa Bali) Gresik unit, Gresik Regency MSME development). *J. Public Policy Manag.*, 3(2): 142-51.
- Gunawan, H., Sinaga, B. Langgu. and Wp, S.P. 2019. Assessment of the readiness of micro., small, and medium enterprises in using E-money using the unified theory of acceptance and use of technology (UTAUT) method. *Procedia Comput Sci.*, 161: 316-23. doi: 10.1016/j.procs.2019.11.129.
- Hendratmi, A., Agustina, T.S., Sukmaningrum, P.S. and Widayanti, M.A. 2022. Livelihood strategies of women entrepreneurs in Indonesia. *Heliyon*, 8(9): e10520. doi: 10.1016/j.heliyon.2022.e10520, PMID 36119879.
- Humas, P. 2017. Hanya 21 perusahaan peduli CSR 2017 Kabupaten Paser.
- Huq, A. and Moyeen, A. 2011. Gender integration in enterprise development programs. *Womens Stud Int Forum*, 34(4): 320-28. doi: 10.1016/j.wsif.2011.04.007.
- Khanzode, A.G., Sarma, P.R.S., Mangla, S.K. and Yuan, H. 2021. Modeling the Industry 4.0 adoption for sustainable production in micro., small & medium enterprises. *J. Cleaner Prod.*, 279: 123489. doi:10.1016/j.jclepro.2020.123489.
- Larios-Francia, R.P. and Ferasso, M. 2023. The relationship between innovation and performance in MSMEs: the case of the wearing apparel sector in emerging countries. *J. Open Innov. Technol. Mark. Complexity*, 9(1): 100018. doi: 10.1016/j.joitmc.2023.100018.
- Lemańska-Majdzik, A. and Okręglička, M. 2015. Identification of business processes in enterprise management. *Procedia Econ Fin.*, 27(15): 394-403. doi: 10.1016/S2212-5671(15)01011-4.
- Majer, M. 2013. The practice of mining companies in building relationships with local communities in the context of the CSR formula. *J. Sustain. Min.*, 12(3): 38-47. doi: 10.7424/jsm130305.
- Mantri, A. and Mishra, R. 2023. Empowering small businesses with the force of big data analytics and AI: A technological integration for enhanced business management. *J. High Technol. Manag. Res.*, 34(2): 100476. Doi: 10.1016/j.hitech.2023.100476.
- Mulyaningsih, T., Wahyunengseh, R. and Hastjarjo, S. 2020. Poverty and digital divide: A study in urban poor neighborhoods. *J. Ilmu Sosial Ilmu Pol.*, 24(2): 189-203. doi: 10.22146/jsp.52325.
- Neto, P.B. and Mallett, A. 2023. Public participation in environmental impact assessment processes through various channels – can you listen to us now? Lessons from a Brazilian mining case. *Extr. Ind. Soc.*, 13: 101186. doi: 10.1016/j.exis.2022.101186.
- Nirmaya, G.C., Muflikhati, I. and Simanjuntak, M. 2014. The influence of corporate social responsibility (CSR) programs on the welfare of families around the mine. *J. Consum. Family Sci.*, 7(1): 19-29. doi: 10.24156/jikk.2014.7.1.19.
- Noviarto, S. and Samputra, P.L. 2021. MSME's Sustainable Economic Behavior for Struggling Poverty: agency Theory vs. bounded Rationality Theory. *IOP Conf. S. Earth Environ Sci.*, 716(1): 012120. doi: 10.1088/1755-1315/716/1/012120.
- Nurani, N., Fahmi, M.A.B.Z. and Zul Fauzi, M.A.B. 2021. Micro medium and small Aenterprise human resources' creativity in west Java through intellectual property rights (IPR) license in the pandemic Covid-19 situation. *Turk J. Comput. Math Educ.*, 12(4): 684-94.
- Olivares-Delgado, F., Pinillos-Laffón, A. and Benlloch-Osuna, M.T. 2016. An approach to patronymic names as a resource for families and as a variable for family business identification. *Eur. J. Fam. Bus.*, 6(1): 32-45. doi: 10.1016/j.ejfb.2016.06.001.
- Quarm, J.A., Anning, A.K., Fei-Baffoe, B., Siaw, V.F. and Amuah, E.E.Y. 2022. Perception of the environmental., socio-economic, and health impacts of artisanal gold mining in the Amansie West district, Ghana. *Environ. Chall.*, 9: 100653. doi: 10.1016/j.envc.2022.100653.

- Ragoobur, V.T., Seetanah, B., Jaffur, Z.K. and Mooneeram-Chadee, V. 2023. Building recovery and resilience of Mauritian MSMEs in the midst of the COVID-19 pandemic. *Sci Afr.*, 20: e01651. doi: 10.1016/j.sciaf.2023.e01651.
- Sahi, G.K., Modi, P. and Mantok, S. 2023. New product innovations in times of crisis: how did women entrepreneurs survive the COVID-19 crisis? *Ind. Mark. Manag.*, 111: 19-29. doi: 10.1016/j.indmarman.2023.03.004.
- Sanchez-Infante, H., Yañez-Araque, B. and Moreno-García, J. 2020. Moderating effect of firm size on the influence of corporate social responsibility in the economic performance of micro-, small-, and medium-sized enterprises. *Technol. Forecasting Soc. Change.*, 151: 119774. doi: 10.1016/j.techfore.2019.119774.
- Sugiyono. 2009. *Quantitative, Qualitative, and R&D Research Methods*. Bandung.
- Tejedor, S., Cervi, L., Pérez-Escoda, A. and Jumbo, F.T. 2020. Digital literacy and higher education during COVID-19 lockdown: Spain, Italy, and Ecuador. *Publications*, 8(4): 1-17. doi: 10.3390/publications8040048.
- Tewari, R., Pathak, T.S. 2015. Sustainable CSR for micro., small and medium enterprises. *SSRN Electron J.*, 6(1): 34-44. doi: 10.2139/ssrn.2600570.
- Wilson, S.A. 2022. Measuring the effectiveness of corporate social responsibility initiatives in diamond mining areas of Sierra Leone. *Resour. Policy*, 77: 102651. doi: 10.1016/j.resourpol.2022.102651.
- Wirth, H., Kulczycka, J., Hausner, J. and Koński, M. 2016. Corporate social responsibility: communication about social and environmental disclosure by large and small copper mining companies. *Resour. Policy*, 49: 53-60. doi: 10.1016/j.resourpol.2016.04.007.

ORCID DETAILS OF THE AUTHORS

Selfia Bintariningtyas : <https://orcid.org/0000-0002-3212-2884>

Tri Mulyaningsih: <https://orcid.org/0000-0002-1679-4349>

Yunastiti Purwaningsih: <https://orcid.org/0000-0003-4782-4819>



Temperature-related Saccharification of Delignified Sawdust Materials from the Lagos Lagoon in Nigeria

J. B. M. Seeletse*, N. A. Ndukwe** and J. P. H. van Wyk*† 

*Department of Pharmacology and Therapeutics, Sefako Makgatho Health Sciences University, South Africa

**Department of Chemical Sciences, College of Basic and Applied Sciences, Mountain Top University, Magoki, Ogun State, Nigeria

†Corresponding author: J.P.H. van Wyk: bioenergy.res@gmail.com

Nat. Env. & Poll. Tech.
Website: www.neptjournal.com

Received: 01-09-2023

Revised: 26-10-2023

Accepted: 16-12-2023

Key Words:

Sawdust
Cellulose
Cellulase
Delignification
Optimum incubation temperature

ABSTRACT

Sawdust, a product of the forest industry is mostly left untreated as solid waste. This phenomenon is well observed along the Lagos Lagoon in Nigeria where hundreds of trees are cut daily by sawmills to deliver wood for mainly the furniture industry. Different types of trees are utilized in this manner and the massive amounts of sawdust produced as a result of these activities are polluting the environment causing health risks for humans and animals. Cellulose, a glucose bio-polymer is a major structural component of sawdust and could be developed as a renewable energy resource should the cellulose be degraded into glucose, a fermentable sugar. This saccharification was done with *Aspergillus niger* cellulase and to make the cellulose more susceptible for cellulase action the sawdust was delignified with hydrogen peroxide. Both delignified and non-delignified sawdust were treated with the cellulase enzyme at incubation temperatures of 30°C, 40°C, 50°C, and 60°C. Delignification proved to be effective as an increased amount of sugar was released from all delignified sawdust materials relative to the non-delignified materials when saccharified with *A. niger* cellulase. Most of the materials were degraded at an incubation temperature of 40°C and 50°C and the highest percentage saccharification of 58% was obtained during the degradation of delignified cellulose from the tree, *Ricindendron heudelottii*

INTRODUCTION

Sawdust is a major waste product of the wood industry mainly produced by sawmills when cutting trees in forests such as the rain forest on the banks of the Lago Lagoon in Nigeria. Currently, limited economic procedures are in place to deal effectively with this massive amount of wood waste produced annually resulting in this plant material being classified as organic solid waste. Sawdust is mostly used as a feedstock for the production of low value-added applications such as the absorbent for nitro-glycerine or wastewater containing heavy metals, as plastic fillers, wood compost, and cardboard (Dong et al. 2022, Weber et al. 1993).

The accumulated amount of sawdust along the Lagos Lagoon is a great environmental concern as it not only causes soil and water pollution but also has the potential to catch fire which results in air pollution, a major threat to human and animal lives. Airborne sawdust is another health concern especially when inhaled and it is of environmental concern when greenhouse gases are released from decomposed wood waste when left unattended for long periods. With increasing

concerns regarding the effect of fossil fuel consumption on the environment, it is important to identify and develop renewable resources. It is also important to consider the utilization of energy resources with a lower carbon footprint and renewable biomass such as sawdust has emerged as an alternative source of biofuels and bio-based products (Chen et al. 2020).

As a result of the effect of fossil fuel combustion on the environment, the development of a bio-economy is thus an important strategy to counteract this negative phenomenon, and the utilization of nano-based biodegradable polymers is a suitable example of the application of renewable substances (Kargarzadeh et al. 2018). The cellulose component of lignocellulosic material, a glucose-based polysaccharide is not only described as inexhaustible, but it offers a great potential as feedstock when saccharified into glucose a fermentable sugar. Lignocellulosic materials are made up of cellulose (38-50%), hemicelluloses (23-32%), and lignin (15-25%) in a complex structure. Enzymatic hydrolysis is one of the best methods used to convert cellulosic materials into soluble sugars and

requires low energy demand regardless of the difficulty of the low cellulose accessibility due to the strong linkage of cellulose with lignin (Gupta et al. 2011). To increase cellulolytic enzyme activity in terms of speed and efficiency the lignocellulosic materials can be physically and chemically pretreated to remove or modify the lignin and/or hemicellulose thus increasing the pore space and allow more enzyme accessibility to the cellulose micro-fibrils (Raymond & Maazusa 2015).

The cellulose structure is mostly crystalline while hemicellulose exhibits an amorphous composition because of its branched structure. Hemicellulose is therefore relatively easy to hydrolyze to its monomer sugars compared to the degradation of cellulose (Guerra-Rodríguez et al. 2012). In industry, cellulases are used for the preparation of medicines, perfumes, resins, starch, baking, treatment of waste, and mostly for bioethanol production from lignocellulosic biomass (Sudhanshu & Ramesh 2016). Cellulase enzymes have been isolated from various fungal resources such as species from *Aspergillus*, *Trichoderma*, *Penicillium*, and *Neurospora* as well as bacterial resources from species like *Clostridium*, *Cellulomonas*, *Pseudomonas*, and *Ruminococcus* (Sajith et al. 2016). The saccharification action of cellulase on various waste cellulose materials such as paper (Van Wyk & Sibiyi 2016) and kitchen waste (Ga et al. 2015) has been reported.

The current investigation reveals information on *A. niger* cellulase-catalyzed saccharification of sawdust from five different types of trees along the Lagos Lagoon in Nigeria. This research aimed to investigate the possibility of producing fermentable sugars from the cellulose content of sawdust from various trees. To increase the susceptibility of the cellulose to cellulase action the various sawdust materials have been delignified with the Kraft process (Gustafson et al. 1983) as well as hydrogen peroxide treatment (Ndukwe et al. 2009). The amount of sugar released from the delignified sawdust was compared with the extent of sugar formation from the non-delignified materials and the importance of delignifying cellulose from waste cellulose before cellulase-catalyzed saccharification was confirmed.

MATERIALS AND METHODS

Sawdust Substrate and Cellulase Enzyme

Non-delignified and delignified sawdust samples (10 mg) from five different trees along the Lagos Lagoon in Nigeria were transferred in triplicate into test tubes. Names of these sawdust samples are *Erythrophleum suaveolens*, *Symphonia globulifera*, *Ricindendron heudelotii*, *Pterygota macrocarpa*, and *Milicia excelsa*. Commercially obtained *A. niger* cellulase enzyme (0.1g) was dissolved in 0.005 mol.dm⁻³ pH

5.0 tris buffer resulting in an enzyme solution concentration of 2.0 mg.mL⁻¹. This enzyme solution was used to perform the saccharification of the various delignified and non-delignified sawdust samples.

Delignification of Sawdust - Kraft Pulping and Hydrogen Peroxide Treatment of the Wood Sawdust

To ensure a maximum cellulose exposure to the cellulase enzyme the various sawdust materials were delignified by subjecting 2kg of each of the different sawdust materials (2.8-5.0 mm particle size) to 350g of NaOH and 140g NaS₂ during the Kraft pulping process. The Kraft pulping chemicals were dissolved in 8 L water and the delignification of the lignocellulosic materials (sawdust) was carried out in a rotary steel digester at 170°C and a pressure of 200 kPa for 1 h 45 min at cooking liquor to the wood ratio of 4:1. After the Kraft pretreatment, the extracted cellulose fibers were washed in turns with deionized water until they were free of the Kraft reagents (Ndukwe et al. 2009). To remove residual lignin from these Kraft-treated cellulose all these sawdust materials (10 g) were treated with 30 % hydrogen peroxide (60 mL) at 40°C for 25-30 min.

Cellulase Incubation and Sugar Analyses

The weighed sawdust material in the tubes was incubated with the *A. niger* cellulase enzyme solution (200 uL) and Tris buffer solution pH 5,0 (800 uL) for 2h at different temperatures of 30°C, 40°C, 50°C, and 60°C. The concentration of sugars released from the sawdust materials during cellulase-catalyzed degradation was determined from a standard glucose calibration curve constructed with glucose standard solutions at concentrations of 0.50 mg.mL⁻¹, 2.00 mg.mL⁻¹, 4.00 mg.mL⁻¹, 6.00 mg.mL⁻¹ and 8.00 mg.mL⁻¹. The DNS method as described by Miller was used to calculate the concentration of the sugar produced during *A. niger* action on the waste sawdust (Miller 1959).

Calculation of Resultant Amount of Sugar Produced and Percentage Saccharification

The resultant amount of sugar produced from the delignified and non-delignified sawdust was calculated by subtracting the amount of sugar released from each type of sawdust in the absence of cellulase action from the amount of sugar released when the sawdust was treated with the cellulase enzyme. This amount of sugar known as the resultant amount of sugar was released as a result of the cellulase action on each type of sawdust material.

The percentage saccharification of each sawdust material was calculated by dividing the resultant mass of sugars produced through cellulase action by the total mass of the

sawdust incubated multiplied by a hundred. These values indicate to what extent the sawdust was bioconverted into sugars and can also be used to conclude the relative saccharification of the various sawdust materials.

Statistical Analysis

All the experimental analyses were performed in triplicate, and the mean values with standard deviations were determined with Microsoft Excel.

RESULTS AND DISCUSSION

Cellulose a glucose-based biopolymer is an important structural component of plant materials and this substance is described as the most underdeveloped and thus also the greatest under-utilized global renewable energy resource (Fatma et al. 2018). A reason why this bio-compound is not commercially developed as an energy resource could be because fossil fuel technology is well established and the global economy is completely dependent and developed on this energy source (Olson & Lenzmann 2016). Another issue in preventing the use of cellulose as a resource for the development of renewable substances could be the fact that it is classified as waste and the bio-recycling technology is not well developed. With the negative effects of fossil fuel consumption on the environment becoming more evident it will convince more scientific agencies to consider alternative and renewable energy resources as feedstock for the synthesis of many commodities. Currently, waste cellulose is a major structural component of plant-derived materials and is classified as organic waste which is discarded without being considered as a potential clean energy resource. Cellulose, based on its richness in glucose, a fermentable sugar, is a suitable contender to be developed as an energy resource should glucose be freed effectively from the cellulose structure. Glucose obtained from waste cellulose in plant materials could not only be fermented into an energy-rich compound such as bio-ethanol which is environmentally friendly, but the process would also have a positive effect on the environment as the amount of organic solid waste occupying value land could be limited (Kaur et al. 2013).

The saccharification of waste cellulose is a process that can be achieved by strong alkaline (Glaus & Van Loon, 2008) as well as acidic (Zhou et al. 2021) treatments but these processes are not environmentally benign as both used acid and alkaline agents would have also negative effects on the environment. These acidic and alkaline hydrolytic substances need therefore to be neutralized before being released in the environment, mostly in wastewater resources and these steps will further increase the cost of effectively recovering glucose from cellulose. The enzymatic catalyzed

degradation of cellulose employing a hydrolytic enzyme system known as cellulase into glucose is an attractive means of developing waste cellulose as an energy resource in an effective and environmentally clean way (Agostinho et al. 2015). Effective enzymatic catalyzed reactions depend on several catalytic properties such as enzyme concentration (Kaschuk et al. 2019), substrate concentration (Carver 2019), pH (Ye et al. 2017) as well as the effect of reaction temperature (Li et al. 2019). This investigation obtained information on the relative saccharification of different delignified and non-delignified sawdust materials when bioconverted by the *A. niger* cellulase into sugars.

Delignified (10 mg) and non-delignified sawdust (10 mg) obtained from various trees along the Lagos Lagoon have been exposed to different incubation temperatures of 30°C, 40°C, 50°C and 60°C in the absence as well as in the presence of *A. niger* cellulase enzyme. This investigation was to conclude the incubation temperature for the optimum bio-conversion of these waste cellulose materials into glucose. The incubation of sawdust in the absence of the cellulase enzyme served as a control to determine the amount of free sugar released from these materials when not degraded by the enzyme.

Fig. 1 represents the concentration of sugar released from delignified and non-delignified *Erythrophleum suaveolens* sawdust in the absence as well as in the presence of *A. niger* cellulase. The resultant amount of sugar released from the delignified as well as non-delignified sawdust bio-converted with the cellulase enzyme is summarized in Fig. 2.

From the results represented in Fig. 1, it can be concluded that the amount of sugar released from non-delignified sawdust in the absence of cellulase when incubated at all the temperatures resulted in a concentration that varies between 1.2-1.7 mg.mL⁻¹. In the case of the delignified materials, the amount of sugar released when no cellulase was acting on the sawdust at the various incubation temperatures was slightly higher than the amount of free sugar released from the non-delignified sawdust at values varied between 1.8 and 3.3 mg.mL⁻¹. The general trend for sugars released from the non-delignified sawdust when incubated with the cellulase enzyme is higher than the amount of sugars released from the corresponding sawdust materials not treated with the cellulase enzyme and the values varied between 2.6 and 3.9 mg.mL⁻¹ when incubated at the various temperatures. A similar observation was made when the delignified cellulose was treated with the cellulase enzyme and during this incubation at the various incubation temperatures, the sugars produced varied between 3.8 and 6.7 mg.mL⁻¹ when incubated at the various temperatures.

The resultant amount of sugar released from the non-

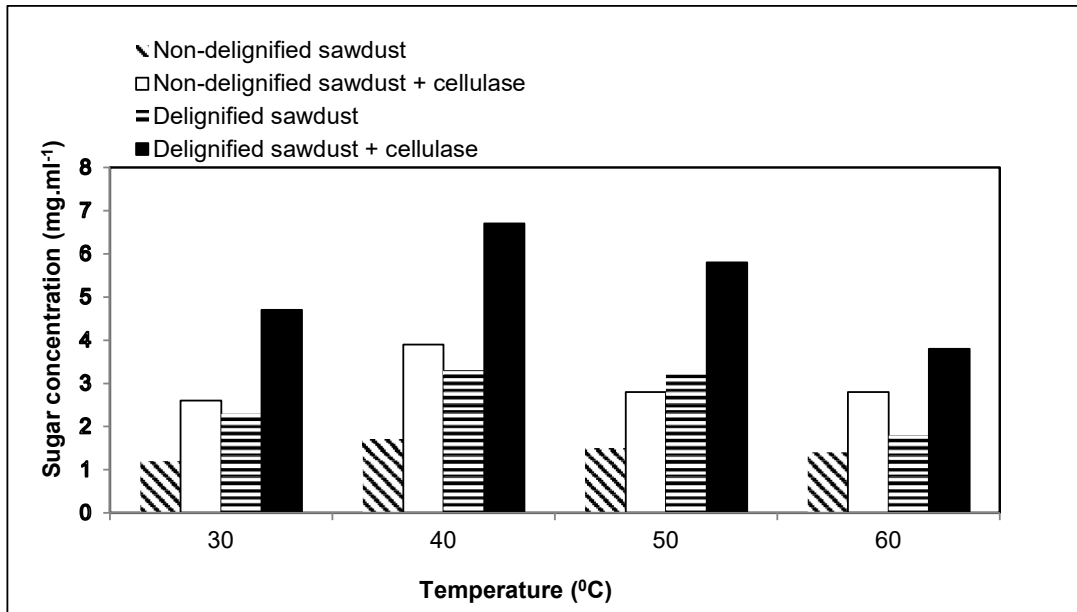


Fig. 1: Amount of sugar released from non-delignified and delignified *Erythropleum suaveolens* sawdust in the absence and presence of *A. niger* cellulase.

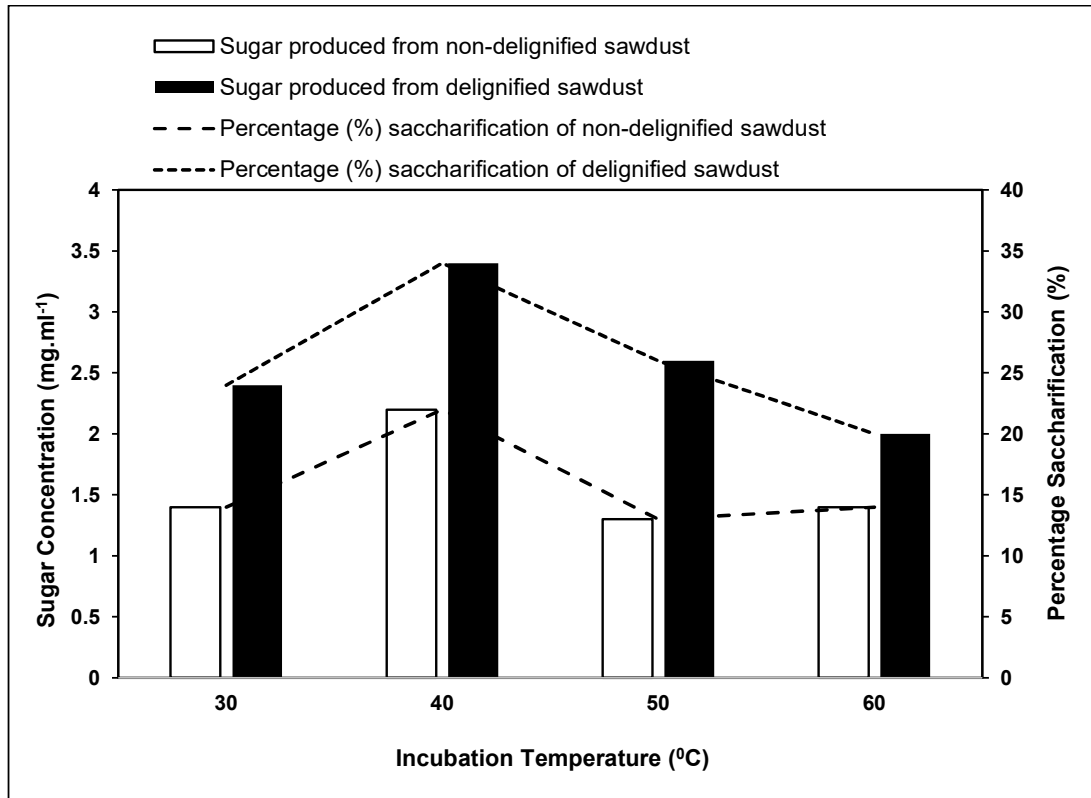


Fig. 2: Resultant amount of sugar produced (mg.mL⁻¹) from non-delignified and delignified *Erythropleum suaveolens* sawdust when bioconverted with *A. niger* cellulase.

delignified and delignified sawdust (Fig. 2) indicates that more sugar was produced from the delignified sawdust at all the incubation temperatures than the concentration of sugars released from the corresponding sawdust not delignified before cellulase catalyzed saccharification. The sugar concentrations obtained from the non-delignified sawdust varied between 1.3 and 2.2 mg.mL⁻¹ whilst the amount released from the delignified sawdust varied between 2.0 and 3.4 mg.mL⁻¹. When the non-delignified material was bio-converted with the *A. niger* cellulase the highest sugar concentration was obtained at a temperature of 40°C which resulted in a sugar concentration of 2.2 mg.mL⁻¹ and a 22% saccharification. The highest degree of saccharification was obtained from the delignified sawdust when it was incubated at a temperature of 40°C producing a sugar concentration of 3.4 mg.mL⁻¹ and 34% saccharification. The amount of sugar produced from the delignified sawdust at the optimum incubation temperature of 40°C was 154% higher than the maximum amount of sugar released from the non-delignified sawdust released when incubated at the optimum incubation temperature of 40°C.

Fig. 3 represents the concentration of sugar released from delignified and non-delignified *Symphona globuifera* sawdust in the absence as well as in the presence of *A. niger* cellulase. The resultant amount of sugar released from the delignified as well as non-delignified sawdust bio-converted with the cellulase enzyme is summarized in Fig. 4.

From the results represented in Fig. 3, it can be concluded

that the amount of free sugar released from non-delignified sawdust (in the absence of cellulase) when incubated at all the temperatures resulted in a concentration that varies between 1.5-2.2 mg.mL⁻¹. In the case of the delignified materials, the amount of free sugar released in the absence of cellulase at the various incubation temperatures was slightly higher than the amount of free sugar released from the non-delignified sawdust at values varied between 1.8 and 2.7 mg.mL⁻¹. The general trend for sugars released from the non-delignified sawdust when incubated with the cellulase enzyme is higher than the amount of sugars released from the corresponding sawdust materials not treated with the cellulase enzyme and the values varied between 3.1 and 4.9 mg.mL⁻¹ when incubated at the various temperatures. A similar observation was made when the delignified cellulose was treated with the cellulase enzyme and during this incubation at the various incubation temperatures, the sugars produced varied between 3.8 and 6.2 mg.mL⁻¹ when incubated at the various temperatures.

The resultant amount of sugar released from the non-delignified and delignified sawdust (Fig. 4) indicates that more sugar was produced from the delignified sawdust at all the incubation temperatures than the concentration of sugars released from the corresponding sawdust not delignified before cellulase catalyzed saccharification. The sugar concentrations obtained from the non-delignified sawdust varied between 1.3 and 3.4 mg.mL⁻¹ whilst the amount released from the delignified sawdust varied between 2.0

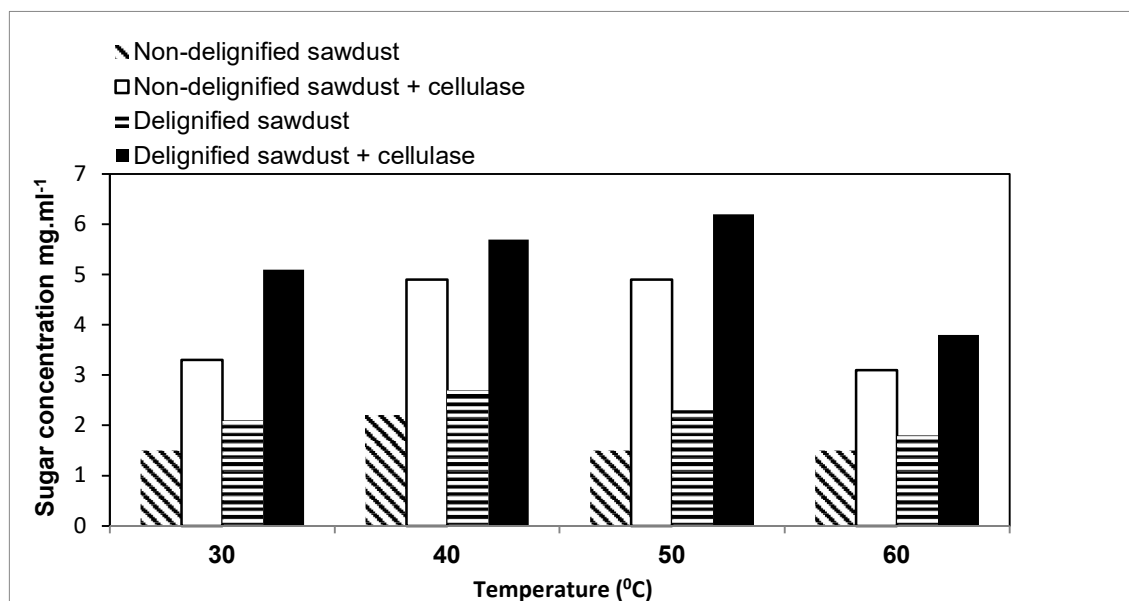


Fig. 3: Amount of sugar released from non-delignified and delignified *Symphona globuifera* sawdust in the absence and presence of *A. niger* cellulase.

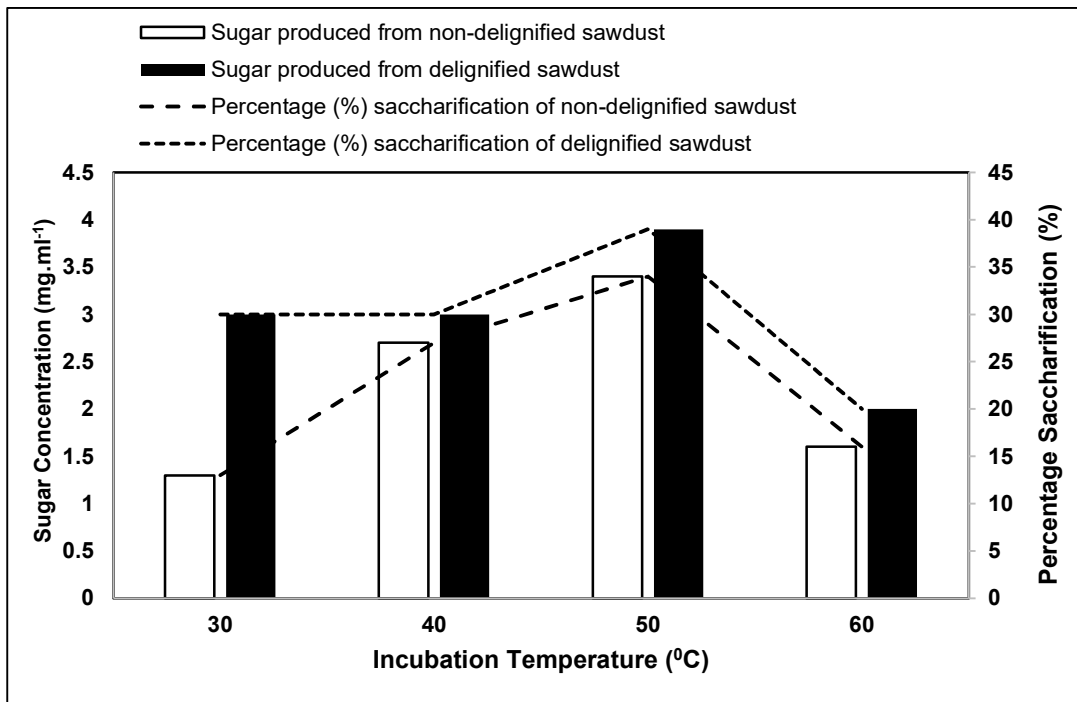


Fig. 4: Resultant amount of sugar produced (mg.mL^{-1}) from non-delignified as well as delignified *Symphona globuifera* sawdust when bioconverted with *A. niger* cellulase.

and 3.9 mg.mL^{-1} . When the non-delignified material was bio-converted with the *A. niger* cellulase the highest sugar concentration was obtained at a temperature of 50°C which resulted in a sugar concentration of 3.4 mg.mL^{-1} and a 34% saccharification. The highest degree of saccharification was obtained from the delignified sawdust when it was incubated at a temperature of 50°C producing a sugar concentration of 3.9 mg.mL^{-1} and 39% saccharification. The amount of sugar produced from the delignified sawdust at an optimum incubation temperature of 50°C was 114% higher than the maximum amount of sugar released from the non-delignified sawdust released when incubated at an optimum incubation temperature of 50°C .

Fig. 5 represents the concentration of sugar released from delignified and non-delignified *Ricindendron heudelottii* sawdust in the absence as well as in the presence of *A. niger* cellulase. The resultant amount of sugar released from the delignified as well as non-delignified sawdust bio-converted with the cellulase enzyme is summarized in Fig. 6.

From the results represented in Fig. 5, it can be concluded that the amount of free sugar released from non-delignified sawdust when incubated at all the temperatures resulted in a concentration that varies between $2.6\text{--}3.4 \text{ mg.mL}^{-1}$. In the case of the delignified materials, the amount of free sugar released at the various incubation temperatures was slightly

higher than the amount of free sugar released from the non-delignified sawdust at values varied between 6.5 and 9.9 mg.mL^{-1} . The general trend for sugars released from the non-delignified sawdust when incubated with the cellulase enzyme is higher than the amount of sugars released from the corresponding sawdust materials not treated with the cellulase enzyme and the values varied between 5.5 and 6.8 mg.mL^{-1} when incubated at the various temperatures. A similar observation was made when the delignified cellulose was treated with the cellulase enzyme and during this incubation at the various incubation temperatures, the sugars produced varied between 10.2 and 13.7 mg.mL^{-1} when incubated at the various temperatures.

The resultant amount of sugar released from the non-delignified and delignified sawdust (Fig. 6) indicates that more sugar was produced from the delignified sawdust at all the incubation temperatures than the concentration of sugars released from the corresponding sawdust not delignified before cellulase catalyzed saccharification. The sugar concentrations obtained from the non-delignified sawdust varied between 2.9 and 3.7 mg.mL^{-1} whilst the amount released from the delignified sawdust varied between 3.5 and 5.8 mg.mL^{-1} . When the non-delignified material was bio-converted with the *A. niger* cellulase the highest sugar concentration was obtained at a temperature of 50°C which resulted in a sugar concentration of 3.7 mg.mL^{-1} and a 37%

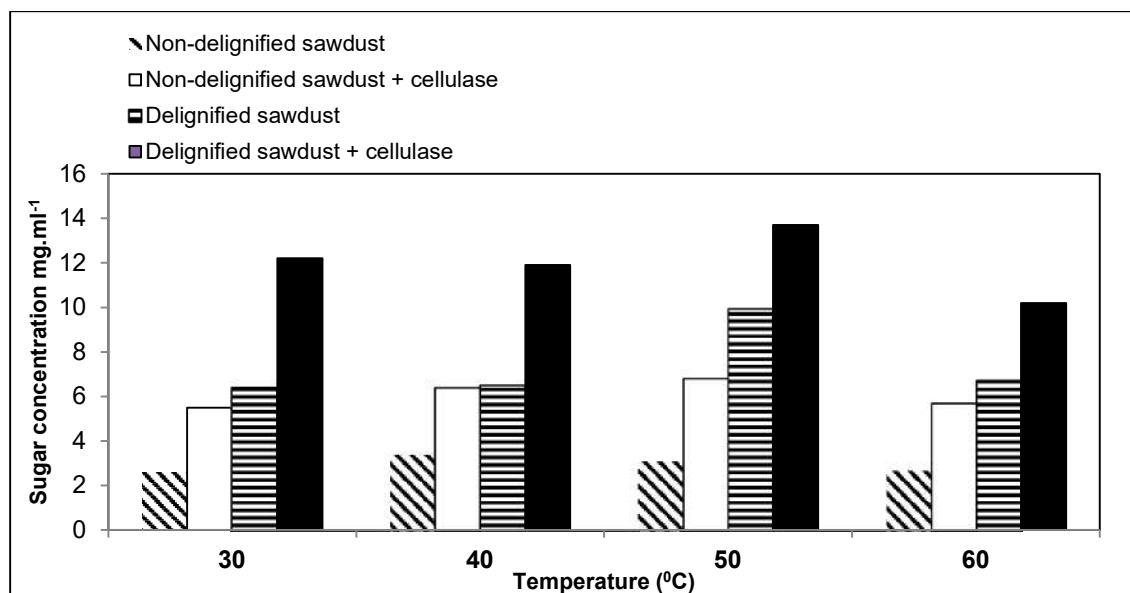


Fig. 5: Amount of sugar released from non-delignified and delignified *Ricindendron heudelotti* sawdust in the absence and presence of *A. niger* cellulase.

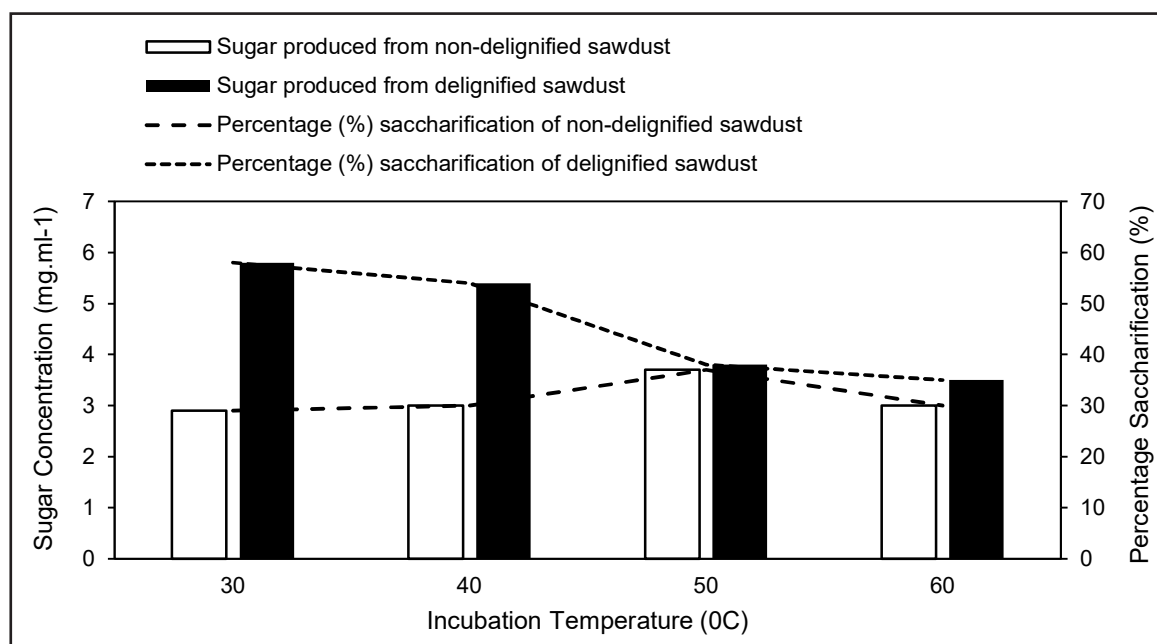


Fig. 6: Resultant amount of sugar produced (mg.mL^{-1}) from non-delignified as well as delignified *Ricindendron heudelotti* sawdust when bioconverted with *A. niger* cellulase.

saccharification. The highest degree of saccharification was obtained from the delignified sawdust when it was incubated at a temperature of 30°C producing a sugar concentration of 5.8 mg.mL^{-1} and 58% saccharification. The amount of sugar produced from the delignified sawdust at the optimum incubation temperature of 30°C was 156% higher than the

maximum amount of sugar released from the non-delignified sawdust released when incubated at the optimum incubation temperature of 40°C.

Fig. 7 represents the concentration of sugar released from delignified and non-delignified *Pterygota macrocarpa* sawdust in the absence as well as in the presence of *A. niger*

cellulase. The resultant amount of sugar released from the delignified as well as non-delignified sawdust bio-converted with the cellulase enzyme is summarized in Fig. 8.

From the results represented in Fig. 7, it can be concluded that the amount of free sugar released from non-delignified sawdust when incubated at all the temperatures in the

absence of cellulase resulted in a concentration that varies between 2.7-2.9 mg.mL⁻¹. In the case of the delignified materials, the amount of free sugar released at the various incubation temperatures was slightly higher than the amount of free sugar released from the non-delignified sawdust at values varied between 3.5 and 8.7 mg.mL⁻¹. The general

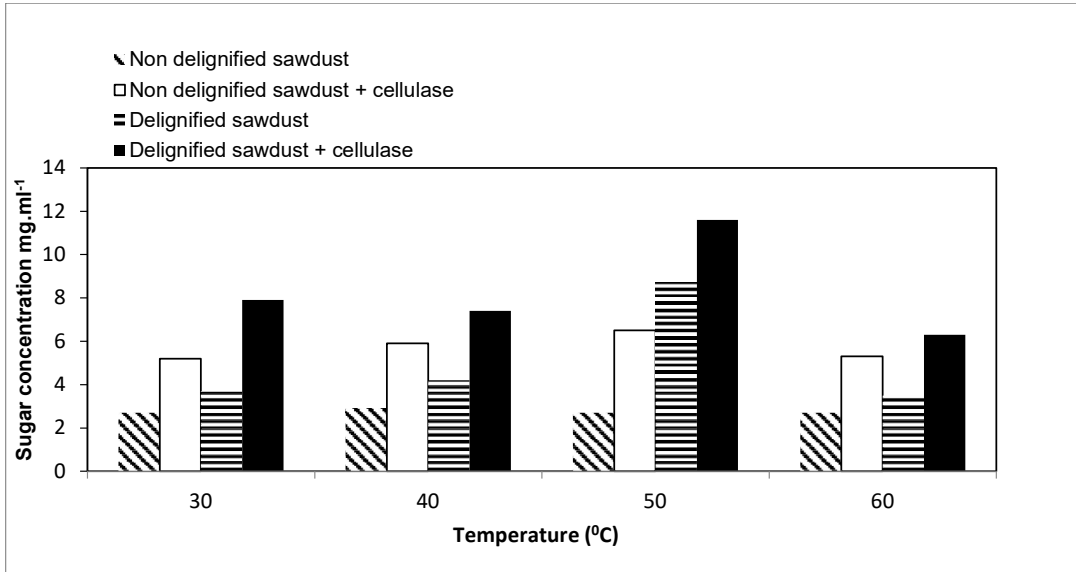


Fig. 7: Amount of sugar released from non-delignified and delignified *Pterygota macrocarpa* sawdust in the absence and presence of *A. niger* cellulase.

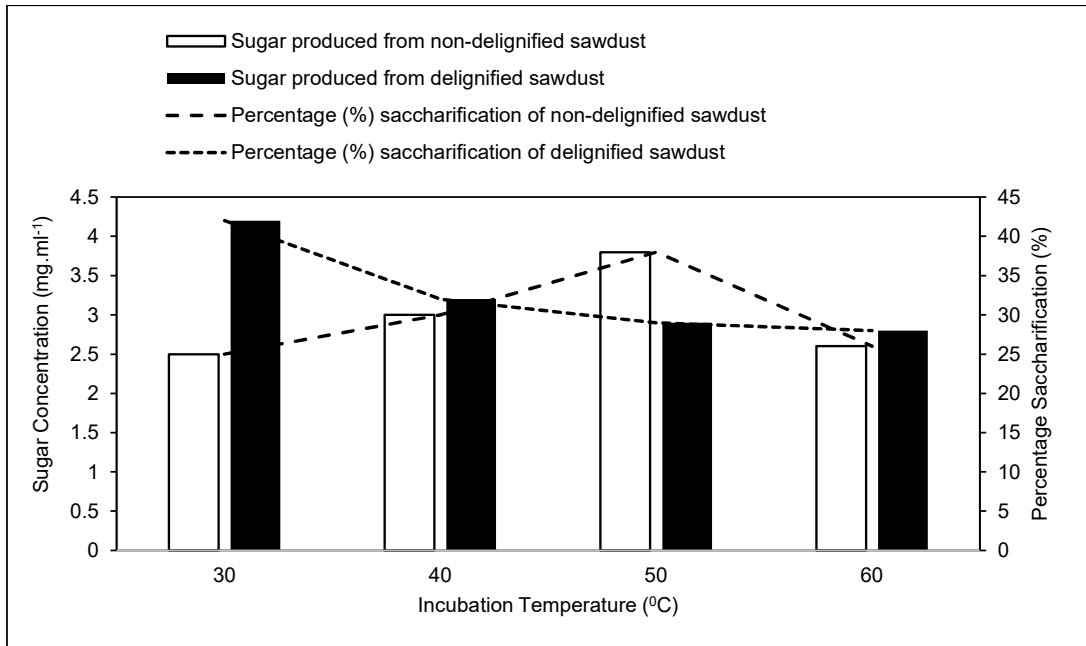


Fig. 8: Resultant amount of sugar produced (mg.mL⁻¹) from non-delignified as well as delignified *Pterygota macrocarpa* sawdust when bioconverted with *A. niger* cellulase.

trend for sugars released from the non-delignified sawdust when incubated with the cellulase enzyme is higher than the amount of sugars released from the corresponding sawdust materials not treated with the cellulase enzyme and the values varied between 5.2 and 6.5 mg.mL⁻¹ when incubated at the various temperatures. A similar observation was made when the delignified cellulose was treated with the cellulase enzyme and during this incubation at the various incubation temperatures, the sugars produced varied between 6.3 and 11.6 mg.mL⁻¹ when incubated at the various temperatures.

The resultant amount of sugar released from the non-delignified and delignified sawdust (Fig. 8) indicates that more sugar was produced from the delignified sawdust at all the incubation temperatures than the concentration of sugars released from the corresponding sawdust not delignified prior to cellulase catalyzed saccharification. The sugar concentrations obtained from the non-delignified sawdust varied between 2.5 and 3.8 mg.mL⁻¹ whilst the amount released from the delignified sawdust varied between 2.8 and 4.2 mg.mL⁻¹. When the non-delignified material was bio-converted with the *A. niger* cellulase the highest resultant sugar concentration was obtained at a temperature of 50°C which resulted in a sugar concentration of 3.8 mg.mL⁻¹ and a 38% saccharification. The highest degree of saccharification was obtained from the delignified sawdust when it was incubated at a temperature of 30°C producing a sugar concentration of 4.2 mg.mL⁻¹ and 42% saccharification. The amount of sugar produced from the delignified sawdust at the optimum incubation temperature of 30°C was 110%

higher than the maximum amount of sugar released from the non-delignified sawdust released when incubated at the optimum incubation temperature of 40°C.

Fig. 9 represents the concentration of sugar released from delignified and non-delignified *Micilia excelsa* sawdust in the absence as well as in the presence of *A. niger* cellulase. The resultant amount of sugar released from the delignified as well as non-delignified sawdust bio-converted with the cellulase enzyme is summarized in Fig. 10.

From the results represented in Fig. 9, it can be concluded that the amount of free sugar released from non-delignified sawdust when incubated at all the temperatures resulted in a concentration that varies between 1.9-2.3 mg.mL⁻¹. In the case of the delignified materials, the amount of free sugar released in the absence of cellulase at the various incubation temperatures was slightly higher than the amount of free sugar released from the non-delignified sawdust at values varied between 5.3 and 6.2 mg.mL⁻¹. The general trend for sugars released from the non-delignified sawdust when incubated with the cellulase enzyme is higher than the amount of sugars released from the corresponding sawdust materials not treated with the cellulase enzyme and the values varied between 3.4 and 4.1 mg.mL⁻¹ when incubated at the various temperatures. A similar observation was made when the delignified cellulose was treated with the cellulase enzyme and during this incubation at the various incubation temperatures, the sugars produced varied between 8.8 and 9.8 mg.mL⁻¹ when incubated at the various temperatures.

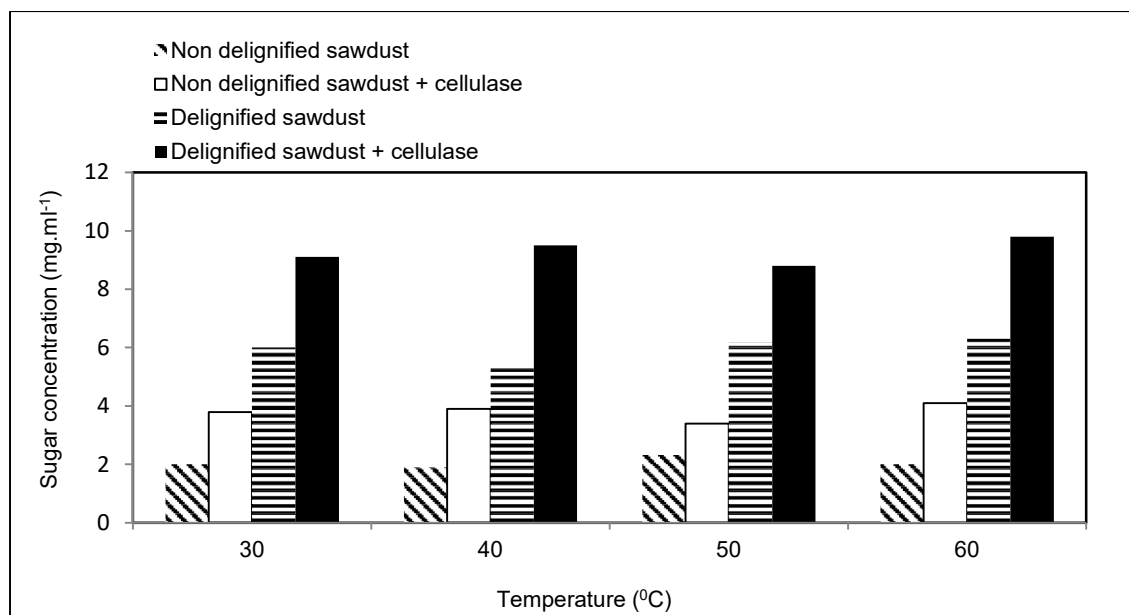


Fig. 9: Amount of sugar released from non-delignified and delignified *Micilia excelsa* sawdust in the absence and presence of *A. niger* cellulase.

The resultant amount of sugar released from the non-delignified and delignified sawdust (Fig. 10) indicates that more sugar was produced from the delignified sawdust at all the incubation temperatures than the concentration of sugars released from the corresponding sawdust not delignified before cellulase catalyzed saccharification. The sugar concentrations obtained from the non-delignified sawdust varied between 1.1 and 2.1 mg.mL⁻¹ whilst the amount released from the delignified sawdust varied between 2.6 and 4.2 mg.mL⁻¹. When the non-delignified material was bio-converted with the *A. niger* cellulase the highest sugar concentration was obtained at a temperature of 60°C which resulted in a sugar concentration of 2.1 mg.mL⁻¹ and a 21% saccharification. The highest degree of saccharification was

obtained from the delignified sawdust when it was incubated at a temperature of 40°C producing a sugar concentration of 4.2 mg.mL⁻¹ and 42% saccharification. The amount of sugar produced from the delignified sawdust at the optimum incubation temperature of 40°C was 200% higher than the maximum amount of sugar released from the non-delignified sawdust released when incubated at the optimum incubation temperature of 60°C.

Cellulase enzymes are biocatalysts responsible for the degradation of cellulose into sugars such as glucose. In case of the destruction of cellulose, the cellulase enzyme is responsible for the breaking of β-1,4-glucosidic bonds between glucose units releasing the glucose units which can further undergo changes such as fermentation by yeast

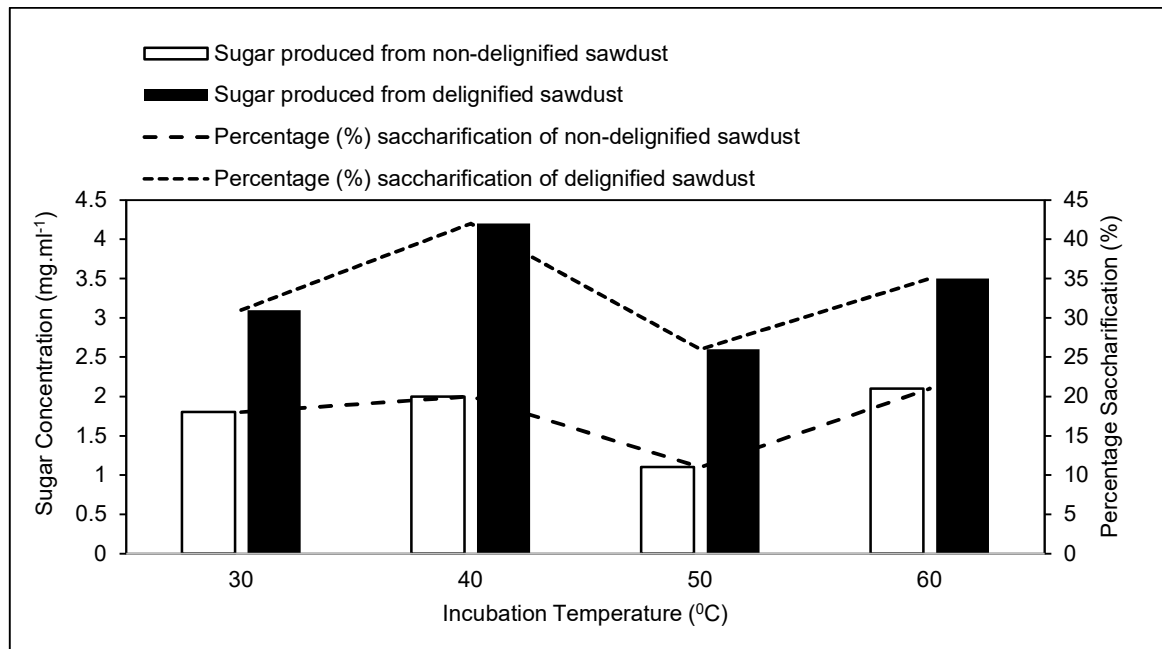


Fig. 10: Resultant amount of sugar produced (mg.mL⁻¹) from non-delignified as well as delignified *Milicia excelsa* sawdust when bioconverted with *A. niger* cellulase.

Table 1: Optimum incubation temperatures and maximum resultant sugar concentrations produced during saccharification of delignified and non-delignified sawdust from different trees along the Lagos Lagoon with *A. niger* cellulase.

Name of tree	Non-delignified cellulose		Delignified cellulose	
	Optimum temperature [°C]	Optimum sugar concentration [mg.mL ⁻¹]	Optimum temperature [°C]	Optimum sugar concentration [mg.mL ⁻¹]
<i>Erythroleum suaveolens</i>	40	2,2	40	3,4
<i>Symphonia globulifera</i>	50	3,4	50	3,9
<i>Ricindendron heudelotii</i>	50	3,8	30	5,8
<i>Pterygota macrocarpa</i>	50	3,8	30	4,2
<i>Milicia excelsa</i>	40	1,8	40	4,2

into environmentally friendly substances such as bioethanol (Zhou et al. 2023). These environmentally friendly procedures will become more in demand especially in cases such as the development of renewable energy resources as the negative effect of fossil fuel combustion will be realized by the global community (Xu et al. 2023). Various potential renewable energy resources such as solar (Khare et al. 2023), wind (Liu et al. 2023), and hydrogen (Khalil & Dincer 2023) are the focus of many development programs, with many already producing positive environmental results. Waste cellulose, which is part of organic waste, has also been identified as a potential energy resource not only for the energy released during combustion but also for its bioenergy potential when developed as a feedstock during the synthesis of bio-chemicals (Yu et al. 2023). To effectively utilize waste cellulose as a resource for bio-energy development needs an environmentally clean process to release glucose from the cellulose structure such as enzymatic catalyzed hydrolysis and incubation temperature is one of the catalytic variables which has to be optimized for maximum cellulase action in releasing glucose from the cellulose material. Another factor that would make the cellulose structure more susceptible to cellulase action and thus produce more fermentable sugar is the pretreatment of cellulose before being hydrolyzed with the cellulase enzyme. Pretreatment methods described as effective in this respect included physical methods such as the milling of cellulose (Hernandez-Varela et al. 2021) as well as chemical procedures (Wang et al. 2023). From the current investigation, it was observed that the hydrogen peroxide delignified sawdust resulted in an increased *A. niger* cellulase-catalyzed saccharification relative to non-delignified sawdust, irrespective of the incubation temperature.

The importance of optimizing the temperature at which the cellulase enzyme is acting on the cellulose structure when saccharifying this bio-polymer has been emphasized by numerous investigations. The optimum incubation temperatures for the bioconversion of both delignified and non-delignified sawdust were observed at mostly 40°C and 50°C, while a few optimal incubations were detected at 30°C. These values compare well with reported optimum cellulase catalytic incubation temperatures of 40°C when *Aspergillus niger* cellulase degrades carboxymethyl cellulose (Sulyman et al. 2020) and 55°C when cellulase from *Aspergillus fumigatus* (Saroj et al. 2022) also acting on carboxymethyl cellulose.

CONCLUSIONS

With the growing global population, the pressure on natural forests will increase as more trees will be needed

for the production of wood-based commodities. During this process, more sawdust will also be produced, which currently is classified and treated as non-manageable solid waste occupying and polluting many water resources and land. The development of the cellulose component of sawdust as a bioenergy resource will not only assist in the production of a clean feedstock for the synthesis of many chemical-related substances but will also help to control environmental pollution. Cellulase-catalyzed bioconversion of cellulose is not only applicable to cellulose from sawdust but could be applied to all plant-based materials such as agricultural, kitchen, and garden waste. Although the cellulase-catalyzed saccharification of waste cellulose is a relatively clean process, its effectiveness in terms of sugar production and percentage saccharification of the cellulose materials depends on the optimization of many catalytic properties, such as incubation temperature. Since cellulose exhibits a complex structural composition, it offers a natural resistance against cellulase action, which seeks the treatment of cellulose before cellulase degradation, rendering it more susceptible to cellulase-catalyzed saccharification. Lignin is a natural component of plant structure that binds the cellulose, and the removal of lignin has a positive effect on the bio-degradation of cellulose. From this investigation, it was concluded that the delignification of cellulose before saccharification with a cellulase enzyme, as well as optimizing the incubation temperature between cellulose and cellulase, does have a positive effect on the extent of sugar production. This also indicates that more bio-products could be synthesized from waste cellulose when delignified and saccharified at optimum temperatures than from non-delignified cellulose or when incubated at a non-optimum incubation temperature.

REFERENCES

- Agostinho, F., Bertaglia, B.B. Almeida, M.V.B. and Giannetti, F. 2015. Influence of cellulase enzyme production on the energetic-environmental performance of lignocellulosic ethanol. *Ecol. Modell.*, 315: 46-56.
- Carver, A.M., Lepisto, R. and Tuovinen, O.H. 2019. Effect of the type and concentration of cellulose and temperature on metabolite formation by a fermentative thermophilic consortium. *Int. J. Hydrog. Energy*, 44(32): 17248-17259.
- Chen, S., Wang, G., Sui, W., Parvez, A.M., Dai, L. and C. Si. 2020. Novel lignin-based phenolic nanosphere-supported palladium nanoparticles with highly efficient catalytic performance and good reusability. *Ind. Crops Prod.*, 145:112164.
- Dong, X., Gan, W., Shang, Y., Tang, J., Wang, Y., Cao, Z., Xie, Y., Liu, J., Bai, L., Li, J., and Rojas, O.J. 2022. Low-value wood for sustainable, high-performance structural materials. *Nat. Sustain.*, 5: 628-635.
- Fatma, S., Hameed, A., Noman, M., Ahmed, T., Shahid, M., Tariq, M., Sohail, I. and Tabassum, R. 2018. Lignocellulosic biomass: A sustainable bioenergy source for the future. *Protein Pept. Lett.*, 25(2): 148-163.

- Ga, W., Chen, Y., Zhan, L. and Bian, X. 2015. Engineering properties for high kitchen waste content municipal solid waste. *Int. J. Rock Mech. Min. Sci.*, 7: 646-658.
- Glaus, M.A. and Van Loon, L.R. 2008. Degradation of cellulose under alkaline conditions: new insights from a 12-year degradation study. *Environ. Sci. Technol.*, 42(8): 2906-2911.
- Guerra-Rodríguez, E., Portilla-Rivera, O.M., Jarquín-Enríquez, L., Ramírez, J.A. and Va'zquez M. 2012. Acid hydrolysis of wheat straw: A kinetic study. *Biomass Bioenergy*, 36: 346-355.
- Gupta, R., Khasa, Y.P. and Kuhad R.C. 2011. Evaluation of pretreatment methods in improving the enzymatic saccharification of cellulosic materials. *Carbohydr. Polym.*, 84: 1103-1109.
- Gustafson, R.R., Sleicher, C.A., McKean, W.T. and Finlayson, B.A. 1983. A theoretical model of the Krafting pulping process. *Ind. Eng. Chem. Process. Des. Dev.*, 22(1): 87-96.
- Hernandez-Varela, J., Chanona-Perez, J.J., Benavides, H.A.C., Sodi, F.C. and Vicente-Flores, M. 2021. Effect of ball milling on cellulose nanoparticles structure obtained from garlic and agave waste. *Carbohydr. Polym.*, 255: 117347.
- Kaschuk, J.J., Lacerda, T.M. and Frollini, E. 2019. Investigating effects of high cellulase concentration on the enzymatic hydrolysis of sisal cellulosic pulp. *Int. J. Biol. Macromol.*, 138: 919-926.
- Kargarzadeh, H., Huang, J., Lin, N., Ahmad, I., Mariano, M., Dufresne, A., Thomas, S. and Galeski, A. 2018. Recent developments in nanocellulose-based biodegradable polymers, thermoplastic polymers, and porous nanocomposites. *Program*, 87: 197-227.
- Kaur, A., Bharti, R. and Sharma, R. 2013. Municipal solid as a source of energy. *Mater. Today Proc.*, 81(2): 904-915.
- Khalil, M. and Dincer, I. 2023. Development and assessment of integrated hydrogen and renewable energy systems for a sustainable city. *Sustain. Cities Soc.*, 98: 104794.
- Khare, V., Chaturvedi, P. and Mishra, M. 2023. Solar energy system concept change from trending technology: A comprehensive review. *E-Prime*, 4: 100183.
- Li, L., Xia, W., Ma, G., Chen, Y. and Ma, Y. 2019. A study on the enzymatic properties and reuse of cellulase immobilized with carbon nanotubes and sodium alginate. *AMB Express*, 9: 112.
- Liu, R., Peng, L., Huang, G., Zhou, Yang, Q. and Cai, J. 2023. A Monte Carlo simulation method for probabilistic evaluation of annual energy production of wind farm considering flow model and wake effect. *ECM*, 292: 117355.
- Miller, G.L. 1959. Use of dinitrosalicylic acid reagent for determination of reducing sugar. *Anal. Chem.*, 31: 426-428.
- Ndukwe, N.A., Jenmi, W.O., Okie, W.O. and Alo BI. 2009. Comparative study of percentage yield of pulp from various Nigerian wood species using the kraft process. *AJEST*, 3(1): 21-25.
- Olson, C. and Lenzmann, F. 2016. The social and economic consequences of the fossil fuel supply chain. *MRS Energy Sustain.*, 3(6).
- Paramjeet, S., Manasa, P. and Korrapati, N. 2023. Biochemical characterization of thermostable carboxymethyl cellulase and B-glucosidase from *Aspergillus fumigatus* 10253. *Appl. Biochem. Biotechnol.*, 194: 2503-2527.
- Raymond, M.T. and Maazuza, Z.O. 2015. Alkali pretreatment and enzymatic hydrolysis of Australian timber mill sawdust for biofuel production. *J. Renew. Energy*, 1-9.
- Sajith, S., Priji, P., Sreedevi, S. and Benjamin, S. 2016. An overview of fungal cellulases with an industrial perspective. *J. Nutr. Sci.*, 6(1): 1-15.
- Sudhanshu, S.B. and Ramesh C.R. 2016. Solid state fermentation for production of microbial cellulases: Recent advances and improvement strategies. *Int. J. Biol. Macromol.*, 86: 656-669.
- Sulyman, A.O., Igunnu, A. and Malomo, S.O. 2020. Isolation, purification, and characterization of cellulase produced by *Aspergillus niger* cultured on *Arachis hypogaea* shells. *Heliyon*, 6(12): e05668.
- Van Wyk, J.P.H. and Sibiyi, J.B.M. 2016. Saccharification of ink-covered office paper by different concentrations of cellulase from *Trichoderma viride*. *J. Chem. Pharm. Res.*, 6(10): 9-17.
- Wang, B., Zanh, X., Li, J., Xu, J., Zeng, J., Li, M., Li, X. and Li, Y. 2023. Efficient preparation of high-purity cellulose from moso bamboo by p-toluene sulfonic acid pretreatment. *Int. J. Biol. Macromol.*, 245: 125395.
- Weber, S., Kullman, G., Petsonk, E., Jones, W., Olenchock, S., Sorenson, W., Parker, J., Marcelo-Baciu, R., Frazer, D. and Castranova, V. 1993. Organic dust exposures from compost handling: case presentation and respiratory exposure assessment. *Am. J. Ind. Med.*, 24: 365-374.
- Xu, J., Zhao, J. and Wen, L. 2023. A comparative study of renewable and fossil fuels energy impacts on green development in Asian countries with divergent income inequality. *Resour. Policy*, 85 (A): 104035.
- Ye, M., Sun, L., Yang, R., Wang, Z. and Qi, K. 2017. The optimization of fermentation conditions for producing cellulase of *Bacillus amyloliquefaciens* and its application to goose feed. *R. Soc. Open Sci.*, 4(10): 1-12.
- Yu, Y., Ahmed, M.S., Shen, B., Li, Y., Ibrahim, M., Bokhari, A. and Klemes, J.J. 2023. Activated waste cotton cellulose as renewable fuel value-added chemicals: Thermokinetic analysis, coupled pyrolysis with gas chromatography and mass spectrometry. *Energy*, 283: 128341.
- Zhou, Z., Jaing, J., Zhao, Q., Wang, Z., Li, L., Gao, Q. and Wang, K. 2023. Performance of high solids enzymatic hydrolysis and bioethanol fermentation of food waste under the regulation of saponin. *Bioresour. Technol.*, 387: 129486.
- Zhou, Z., Liu, D. and Zhao, X. 2021. Conversion of lignocellulose to biofuels and chemicals via sugar platform: An updated review on chemistry and mechanisms of acid hydrolysis of lignocellulose. *Renew. Sust. Energ. Rev.*, 146: 111169.

ORCID DETAILS OF THE AUTHORS

J. P. H. van Wyk: <https://orcid.org/0000-0002-8950-2490>



Assessment of Continuous Growth of Glacial Lakes in the Teesta River Basin Using Semi-Automated Geospatial Approach

A. K. Shukla*†, I. Ahmad*, S. K. Jain** and M. K. Verma*

*Department of Civil Engineering, National Institute of Technology, Raipur, Raipur-492 010, Chhattisgarh, India

**Centre of Excellence in Disaster Mitigation & Management, IIT Roorkee-247667, Uttarakhand, India

†Corresponding author: A.S. Shukla; amitrshukla01@gmail.com

Nat. Env. & Poll. Tech.
Website: www.neptjournal.com

Received: 05-10-2023

Revised: 24-11-2023

Accepted: 28-11-2023

Key Words:

Remote sensing
GIS
NDWI
Glaciers
Glacial lake
Landsat series

ABSTRACT

Global warming is one of the primary causes contributing to melting glaciers and shrinking of glaciers. Because of the glacier retreat, more lakes increase the risk of flooding in people's homes and lives. Several studies on the surging glaciers have been conducted by researchers using various techniques, as well as with the aid of multiple models like the Normalized Differential Water Index (NDWI). The Number of glacial lakes is increasing in the Himalayan region due to climate change (rise of the temperature). Some glacial lakes are potentially dangerous so monitoring is very necessary. It is necessary to evaluate such vulnerable lakes. Therefore, current work is carried out to identify such glacial lakes present in the Teesta River Basin (Eastern Himalaya). Spatiotemporal Landsat data for the last four decades at intervals of ten years from 1990 to 2020 has been considered which was cloud-free and spatial resolution of 30 meters. The dataset mentioned above was used for lake identification and delineation. The findings indicate the presence of lakes with respective areas of 275 (18.90 km²), 337 (24.92 km²), 295 (22.96 km²), and 419 (31.44 km²). It has also been observed that the growth rate is increasing with approximate water spread from 1990 to 2000 (+129%), 2000 to 2010 (+106%), and 2010 to 2020 (+136%). The present study aimed to identify such glacial lakes based on their water spreading area, which is an essential step followed in the study of GLOF (Glacial Lake Outburst Flood) as it will be helpful in the identification of hazardous lakes. In that study, we found that eleven glacial lakes are in the potentially dangerous category situated in the upper Teesta Basin due to the presence of glaciers, which gives a clear reason for the time-to-time assessment of such lakes. By the conducted study it has been observed that the number of glacial lakes has increased, due to which water spread has also increased in the area. It can also be demonstrated that GIS (Geographical Information System), along with remote sensing, is one of the best tools for assessing and monitoring such change detection and differentiation of hazardous glacial lakes in the cryosphere, along with the supporting data.

INTRODUCTION

India's natural border with China is defined by a range of Himalayan Glacier Mountains surrounding it in the north-east. With a combined snow area of around 60000 km², these mountain ranges extend a 2000 km stretch (Kaab et al. 2012, Khadka et al. 2018 & 2019, Maskey et al. 2020). In the Himalayan region, much research found that glaciers and snow areas have decreased in the last few decades. However, with every passing year, these glaciers are retreating by 0.4% per year (Bolch et al. 2012). These glaciers provide food for about 1.3 billion people in Asian nations, which make up about one-fourth of the world's population. In addition, the flow of naturally soured water into the connecting rivers, which are then used for residential, industrial, and irrigating purposes, satisfies the need for water for flora and animals

residing in southern Asia. It has been observed that many glaciers are melting around the world due to climate change. An intergovernmental institute named The International Centre for Integrated Mountain Development (ICIMOD) is an organization that contributes toward conservation and sustainable developments related to the Hindukush Mountain region. ICIMOD has created an inventory of glaciers and glacial lakes for the Himalayan area at regular intervals. It has been revealed that, as the glaciers are thinning and shrinking, the glacier's mouth is receding.

Consequently, depression areas separate from glaciers, and after years, these areas become known as glacial lakes, which are growing both in number and size (Mool et al. 2001). Glacial lakes are formed as the meltwater collects in areas with depressions that are surrounded by moraines

and ice on retreating glaciers. Mainly such glacial lakes are formed in glaciated, and very few of them are found in non-glaciated regions.

The glaciers are receding year after year, which results in the formation and expansion of glacial lakes consistently. Many lakes are considered to be hazardous, as they provide the possibility of catastrophic events. Cryospheric sciences are therefore studied by scholars to broaden their knowledge and contribute to the efforts of the local community, non-governmental organizations, and the government. Many articles are available that explain the mechanism involved in the evolution of these glacial lakes and the factors regulating it (Reynolds 2000, Benn et al. 2012, Thompson et al. 2016). Different researchers have classified Glacial lakes into different types and groups. ICIMOD in the Hindu Kush Himalayan region has classified the lakes into five categories based on their occurrence and process of formation, which is: glacial erosion lake, moraine-dammed lake, ice-blocked lake, Supraglacial Lake, and subglacial lake (Shukla et al. 2018). Glacial erosion lake is the type of lake located at the snout of the retreated glacier formed by the eroded glacier, which is again classified into cirque lake, glacial valley lake, and another glacial erosion lake. Moraine dammed lakes are the type of waterbody that lies between the Moraine ridge and glacier due to the obstruction created by the Moraine. These types of lakes can be divided into three types based on the formation location: End-Moraines, Lateral Moraines, and Moraines Thaw Lake, ice-blocked lakes, including advancing glacier-blocked lakes, and other glacier-blocked lakes, supraglacial and subglacial lake (Dhar et al. 2010). While most glacial lake characteristics can be investigated using remote sensing and GIS techniques, it offers a helpful method for keeping track of all these lakes (Bolch et al. 2012). The primary factors affecting glacial lakes, including the volume and number of lakes and other geometrical aspects like mass, size, length, and width, can be monitored using geospatial data (Reynolds 2000). Numerous studies have shown the significance of remote sensing in monitoring glacier lakes and creating their inventory (Huggel et al. 2002). Remote sensing is typically the sole method that can be used to monitor and map these glaciers. Glacier dynamics and remote sensing have been extensively studied in research. Nevertheless, even though the threshold of NDWI is the most commonly used index for glacial lake mapping, other supporting ground truth verification can be considered important.

The Hindu Kush Himalayan's hydrological conditions at higher altitudes in the catchments can be significantly impacted by these changes in glaciers and snow cover due to climate change (Kargel et al. 2005, Scherler et al. 2011, Brun et al. 2017, Debnath et al. 2018). Additionally, vegetation and

fauna were negatively impacted; ensuing changes in run-off owing to glacier melt will have an indirect or direct impact on approximately a fifth of the world's population (Clague & Evans 2000, Huggel et al. 2004, Garg et al. 2021).

Per one of the research studies, it has been estimated that by the year 2100, 1/3 of the country's whole Himalayan forest will have vanished due to cattle grazing and deforestation (.). The Easter Sikkim Himalayas (Present research work) have to significant rapid growth of glacial lakes and decreases the glacier coverage area (Benn et al. 2012, Khadka et al. 2020). A considerable amount of glaciated area decreases by around 2.5% in the Teesta River basin, and Moraine and debris cover the formation of glacial lakes in the non-glaciated area (Bolch et al. 2012, Basnett et al. 2013, Shukla et al. 2018). Most of the glacial lakes are formed in the upper part of the Sikkim Himalayan because these areas are covered by snow (Nie et al. 2013, Aggarwal et al. 2016). As a result of rising global temperatures brought on by increased global warming, Himalayan glaciers' snow and ice are melting, forming new glacial lakes and increasing the volume of already-existing lakes (Bolch et al. 2012, Veh et al. 2020, Chowdhury et al. 2021), which can be hazardous and result in Glacier Lake Outburst Floods (Abdul et al. 2018, Rajak et al. 2022). This is the main reason for concern GLOF. GLOFs are a serious environmental issue. A glacial lake, often blocked by ice or moraine, releases water suddenly due to glacier melting, landslides, or avalanches. Massive floods in valleys and river basins can threaten human populations, infrastructure, and ecosystems due to rapid water flow downstream. GLOFs are important in glacier-covered regions like the Himalayas and the Andes. A GLOF has long-term socio-economic effects as well as physical impairment. GLOF risk reduction requires glacial lake monitoring and early warning systems. Understanding glacial lake dynamics and taking early steps can improve resilience in sensitive mountainous locations and mitigate climate change's effects on glacial habitats.

The ICIMOD evaluated the glacial lake at the first level for the Indian Himalayan region (Mool & Bajracharya 2003, Budhathoki et al. 2013). According to research from 2003, Sikkim, which has an area of roughly 20.20 km², has about 266 glacial lakes in the eastern Himalayas. They classified a total of 14 glacial lakes as being particularly susceptible. Due to its topographical and lithological features, northern India, along with the Himalayan ranges, experiences disasters like landslides and floods more frequently than other regions (Salerno et al. 2012, Bolch et al. 2012, Basnett et al. 2013, Allen et al. 2016). One similar catastrophe happened in June 2013 in Kedarnath, Uttarakhand; torrential rains caused dam movement that spread to the nearby habitation area, destroying the hamlet and surrounding areas (Dobhal et al. 2013, Martha et al. 2014, Das et al. 2015, Allen et al.

2015, Iwata 2000, Sakai & Fujita 2010, Zhang et al. 2011). Moreover, the frequency of GLOF occurrences suddenly increased in the second half of the 20th century (Bajracharya et al. 2002, Koirala et al. 2017). To analyze these temporal changes using spatial data, which are occurring in the Himalayan glaciers, the current study was carried out (Shrestha & Balla 2011, Koirala et al. 2017). The Teesta basin was delineated for the analysis, primarily covered with high mountain ranges, many glaciers, and lakes. Lakes were indicated for each year of the temporal Landsat series data from 1990 to 2020 (Srivastava et al. 2022), which were then overlaid to analyze the overall regional change (Jain & Mir 2019).

Remote sensing tools/models like the NDWI are often used to measure and keep an eye on the amount of water in different areas (Mitkari et al. 2017, Watson et al. 2018, Jaiswal & Jhariya 2020). NDWI is found by using pictures taken from space or the air since water absorbs light in the near-infrared range and reflects light in the visible range. This measure is very helpful for separating bodies of water, seeing how water levels change, and keeping an eye on trends in aquatic ecosystems. Researchers and environmental scientists use NDWI to look into water flow patterns, track how climate change affects water supplies, and judge the health of wetlands (Magsar et al. 2021). It can be used for more than just monitoring the environment. For example, it can be used to help farmers handle crops by showing how wet the soil is (Gong et al. 2020). NDWI is also very important for crisis management because it helps make maps of areas that are flooded after natural disasters like hurricanes or floods. Additionally, NDWI is a useful and flexible instrument in the field of remote sensing that makes it easier to understand and control water resources around the world.

This study aims to identify the newly formed glacial lakes for the last forty years and demarcate them with the help of spatial datasets. Firstly, differentiation is done using the spatial data available for the required years using the techniques of remote sensing and GIS; once the inventory of lakes is identified, different algorithms, including NDWI and NDSI, are applied for the validation of marked lakes. Finally, the categorization of lakes was done based on the covered area and elevation.

STUDY AREA

The Teesta Basin is situated in the northeast of the country, covering the entire state of Sikkim, a part of the Eastern Himalayan that lies between the boundaries of Nepal and Bhutan (Basnett et al. 2013, Raj et al. 2013). The basin has a total area of about 8141.59 km² with a geographical extent between 27°04'52" and 28°08'26" N latitude and

88°00'57" and 88°55'50" E longitude (shown in Fig. 1). The Teesta River, which is a tributary of the Brahmaputra, originates from Chhombu Chhu. Khangchung Chhu glacial lake is 5281 meters (Abdul Hakeem et al. 2018) in the northeastern corner of Sikkim. Several tributaries, including the Zemu Chhu, Lachung Chhu, Rangyong Chhu, Dik Chhu, Rani Khola, Rangpo Chhu, and Rangit River, then join it. The whole basin lies between 6500 to 813 meters above sea level. Based on a report from the 2011 Census, the overall recorded population of Sikkim was about 610,577, which is an increase of 13% compared to 2001 (Aggarwal et al. 2017). Due to its topographic conditions, glaciers, and other related features, Sikkim is categorized in Zone IV of the Indian seismic chart, which means that it has a high risk of an earthquake with higher intensity (Murthy 2004, Sharma et al. 2012, Aggarwal et al. 2017).

CLIMATE

The climate of Sikkim Himalaya varies with its elevation variation; hence, it can be classified into five types, starting with lower elevation. First comes the subtropical zone, which lies up to 1000 meters. Second comes the warm temperate zone found between the elevation of 1000 and 2000 meters middle Sikkim Himalayan range (2000-25000 meters) comes under the cold temperate zone. The fourth one is the cold zone between 2500 and 4000 meters, and the topmost part of the Himalayas comes under the Frigid Zone with its elevation above 4000 meters (Meetei et al. 2007, Tsering et al. 2019). Sikkim Himalayas has a variety of plant and animal species, and the major glaciated portion of the basin is in the Northern part (SC Mukhopadhyay 1982 and Tsering et al. 2019). It has more than 400 glacial lakes. Out of these, most of them lie above 4500-meter elevation. Mean annual rainfall varies from 2000 to 4000 mm due to altitude (Census, 2011). Precipitation and Melted water are the primary sources of water supply to the Teesta River (SC Mukhopadhyay 1982 and Tsering et al. 2019). Temperature varies from 1.5°C to 9.5°C at a lower altitude, with its maximum temperature recorded during the month of July-Aug (21°C-26°C) and minimum during December to January between 6°C 8°C (Census, 2011).

MATERIALS AND METHODS

Materials

For the present work, Alos Palsar DEM with a resolution of 12.5 meters has been used for watershed delineation and drainage map; the broad basin has been divided into nine sub-basins based on major tributaries. This dataset is freely available to download from <https://search.asf.alaska.edu/>. In

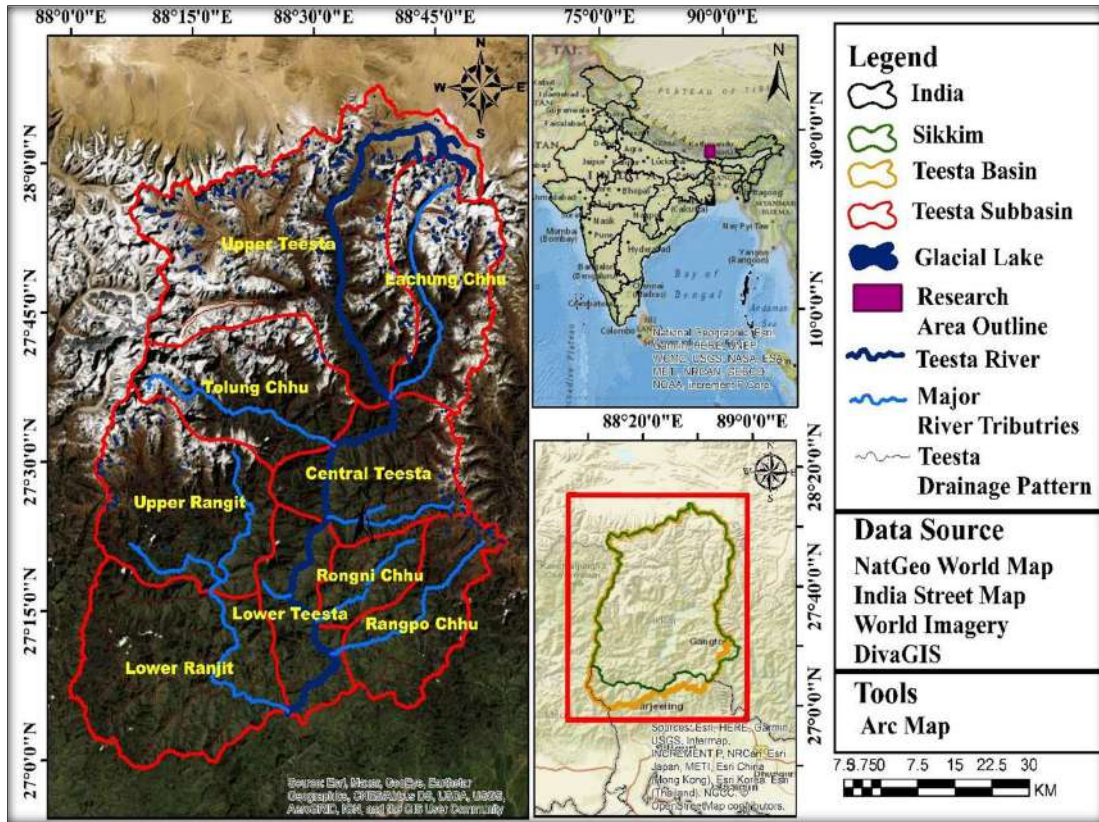


Fig. 1: The study area.

Table 1: List of satellite data used in glacial lake inventory.

Satellite/Sensor	Type of Data	Resolution	Source	Remark
AlosPalsar (Hi-Resolution terrain Data)	DEM	12.5 meter	https://search.asf.alaska.edu/	Watershed delineation and Drainage network
Landsat Series (TM, MSS & OLI/TIRS)	Optical Imagery	Vary from 30 meters to 80 meters	https://earthexplorer.usgs.gov/	Demarcation of glacial lake
Google Earth	Image Landsat/Copernicus	1 meter	https://earth.google.com/	Validate and identify glacial lake

addition, Google Earth images, which are high-resolution data of approximately 1 meter, have been downloaded using SAS Planet software for lake identification. In contrast, Landsat TM, ETM, and OLI/TIRS data with a spatial resolution of 30 and a panchromatic band of 15 meters, respectively, have been downloaded from <https://earthexplorer.usgs.gov/> used as primary data (given in Table 1) for differentiation of lakes for different time series.

Methodology

Geospatial techniques for watershed delineation and investigation of glacial lakes are used by many pieces of research prominently as they allow for the preparation

of a watershed boundary, which includes downloading topographic terrain data and its pre-processing using a predefined algorithm for mosaicking, clipping, and re-projecting. After that, other required steps are done as a part of post-processing with the help of algorithms like r.watershed and r.outlet under QGIS software.

Once the delineation process is completed, different indexes or algorithms are predefined (Wessels et al. 2002, Govindaraj et al. 2013). An index like NDVI and NDWI is being used, which recognizes different objects on the surface based on the reflectance as every object has its properties, which can be classified using for the identification and delineation of

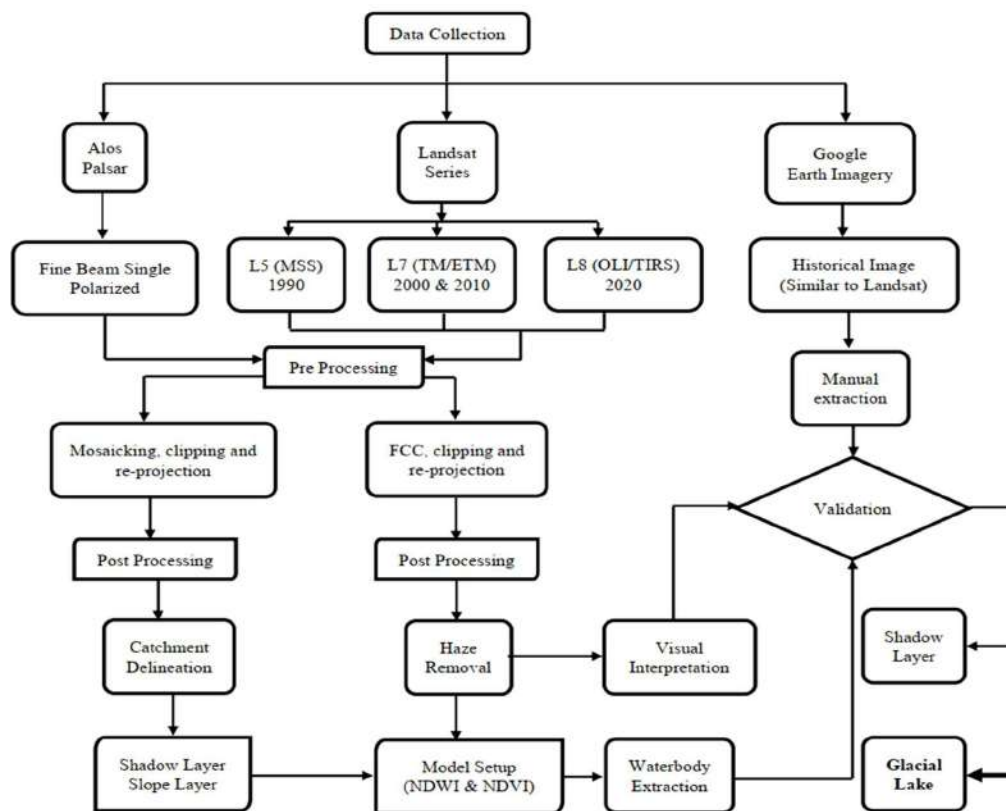


Fig. 2: Flow diagram of methodologies.

glacial lakes. A detailed process adopted is given in Fig. 2.

Identification of Glacial Lakes

The high-resolution Google Earth data allowed for the identification of glacial lakes that are located inside the basin. Through the use of the SAS Planet software, the imagery has been downloaded. After that, the basin was divided into 10 by 10-kilometer grids, and a fishnet was made for the basin, which was then superimposed on the map of the lake that had been downloaded.

Demarcation of Glacial Lakes

Landsat data, which is the most extended time series data available, has been used to demarcate the glacial lakes for the different years 1990, 2000, 2010, and 2020; data for these years has pre-processed, i.e., false-color composite, re-projection, and clip the area of interest, and the lakes were demarcated using the technique of visual interpretation to achieve the maximum accuracy due to variation in the due to the variation of terrain shadow appear which affects the actual pixel value, therefore, resulting in inaccurate digital interpretation.

NDVI

NDVI is the numerical formula for calculating the vegetation cover using the visible bands from satellite imagery (Scanlon et al. 2002, Kunkel et al. 2011). It measures the reflectance value from the leaves and gives the overall vegetation cover on the surface (Malo & Nicholson 1990). Algorithms use NIR and Red band for calculating the vegetation cover where the subtraction of NIR from the red band is divided by the addition of NIR and red. The formula for NDVI is given in Eq.1 (Tucker 1979).

$$NDVI = \frac{NIR - Red}{NIR + Red} \quad \dots(1)$$

Whereas NIR represents the near infrared band, while RED represents the red band. Calculated values from the index range from -1 to +1, where the low values represent there like barren land or rocks, the moderate value represents shrubs or discrete vegetation, while the area with high values shows the maximum vegetation cover (shown in Table 2) (Karaburun 2010, Chouhan & Rao 2011, Xie et al. 2010, Ramachandra et al. 2014, Kumar et al. 2020).

Digital Number (DN) to Spectral Irradiance

Radiance depends on the targeted object; hence, it can be

Table 2: NDVI classification range.

NDVI Range	Feature
-1.0 to 0	Water, Snow, and Cloud
0 to 0.2	Barren land, Built up & Rock
0.2 to 1.0	Vegetation

explained as the ratio of upward flux from the surface to the total incoming flux reaching the surface (Markham & Barker 1987, Govindha Raj et al. 2013, Jaiswal & Jhariya 2020). The value of Top of Atmospheric (TOA) spectral radiance ($L\lambda$) was determined by multiplying multiplicative Rescaling factor OLI bands; $L\lambda$ is proportional to its digital number (DN), which can be computed using the formula (Eq.2) (Markham & Barker 1987, Govindha Raj et al. 2013, Jaiswal & Jhariya 2020).

$$L\lambda = Gain\lambda \times DN\lambda \times Bias\lambda \quad \dots(2)$$

Where,

$L\lambda$ = spectral radiance calculated in ($mW\ cm^{-2}\ sr^{-1}\ mm^{-1}\ counts^{-1}$),

$Gain\lambda$ = calibration coefficient from sensor ($mW\ cm^{-2}\ sr^{-1}\ mm^{-1}\ counts^{-1}$),

$DN\lambda$ = digital number of a pixel in a particular band (counts) and

$Bias\lambda$ = Calibration offset of the sensor band ($mW\ cm^{-2}\ sr^{-1}\ mm^{-1}$).

Spectral Irradiance to Reflectance

Reflectance properties of any object are highly variable and are the ratio of the upward flux reflected energy from the

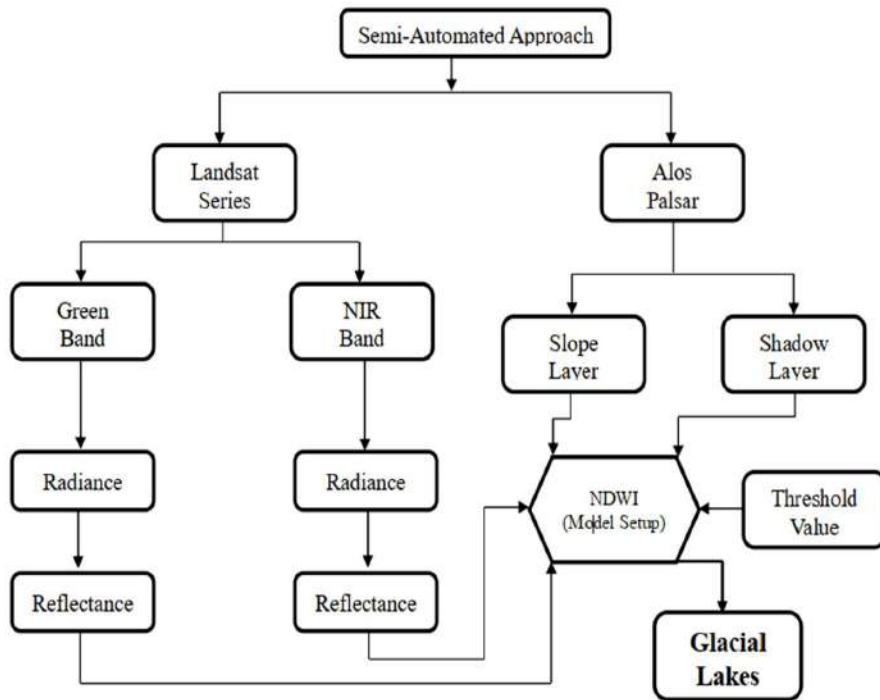


Fig. 3: Semi-automated geospatial approach for extraction of glacial lakes.

Table 3: Earth-Sun Distance in Astronomical Units (Source: L7 Data User Handbook).

Day of Year	Distance	Day of Year	Distance	Day of Year	Distance	Day of Year	Distance	Day of Year	Distance
1	0.98331	74	0.99446	152	1.01403	227	1.01281	305	0.99253
15	0.98365	91	0.99926	166	1.01577	242	1.00969	319	0.98916
32	0.98509	106	1.00353	182	1.01667	258	1.00566	335	0.98608
46	0.98774	121	1.00756	196	1.01646	274	1.00119	349	0.98426
60	0.99084	135	1.01087	213	1.01497	288	0.99718	365	0.98331

surface to the total inward flux reaching the surface (Govindha Raj et al. 2013). For extracting the reflectance values, the converted radiance values will be used; the reflectance is the ratio of the satellite-derived radiance to its equivalent solar radiance (see Fig. 3) (Govindha Raj et al. 2013, Jaiswal & Jhariya 2020). Therefore, spectral reflectance for the dataset was calculated using the formula (See Eq.3).

$$\rho\lambda = \frac{\pi L\lambda d^2}{E_{sun}\lambda \cos\theta_s} \quad \dots(3)$$

Where:

$\rho\lambda$ = Unitlessplanetary reflectance

π = Mathematical constant approximately equal to 3.14159

$L\lambda$ = Spectral radiance at the sensor's aperture (from earlier step)

d = Earth-Sun distance in astronomical units interpolated from values given in (Table 3)

$E_{SUN}\lambda$ = Mean solar exo-atmospheric irradiances (Table 4)

θ_s = Solar zenith angle in degrees

Validation of Glacial Lakes Using NDWI

Normalize Difference water index (NDWI) as used for extracting the water feature, which is done by maximizing the reflectance value of green wavelength and minimizing the reflectance value of NIR (Eq.4) by the water feature, which results in an enhanced water feature with a positive pixel value.

$$NDWI = \frac{Green - NIR}{Green + NIR} \quad \dots(4)$$

Where Green represents the reflectance from the green band (band 3 for Landsat 8), and NIR represents the reflectance from the near-infrared band (band 5 for Landsat 8) using the MINMAX algorithm for the pixel distribution (Radiometric resolution, gray sheds in each band). This index uses the reflectance value from the Green and NIR band, where the wavelength from the

Table 4: ETM+ Solar Spectral Irradiances Source: L7 Data User Handbook).

Band	Watts/(m ² *μm)
1	1970
2	1842
3	1547
4	1044
5	225.7
7	82.06
8	1369

green band is maximized, representing the pixel of water. While the reflectance from NIR is absorbed to minimize the reflectance from the NIR_{band} (Mcfeeters 1996, Sarkar et al. 2020).

When comparing NDWI results with Google Earth or other satellite imagery provided by Google, it's important to note that the accuracy of the match depends on various factors. NDWI is sensitive to atmospheric conditions, sensor characteristics, and the type of surface cover. Google Earth uses a combination of satellite and aerial imagery that may have different resolutions and acquisition times. If the NDWI results match well with the water features visible on Google Earth, it suggests that the index is effectively identifying water bodies in the study area. However, discrepancies can arise due to factors like cloud cover, shadows, or changes in land cover over time. It's always a good practice to validate remote sensing results with ground truth data or additional sources to ensure the reliability of the findings.

RESULTS AND DISCUSSION

Sub-basins were created for the whole Teesta basin coming into India, based on which seven sub-basins were formed. The lakes were identified using the visual interpretation technique, which was then verified using DWI. A description of such inventory lakes is given in Table 5, which signifies the continuous increase in the area of lakes with higher elevation and area. Based on the identified lakes, it can be observed that the upper Teesta sub-basin, located northwest of the upper portion of the basin, has the highest number of lakes because of the higher number of glaciers surrounding the area. In contrast, the Lonchung Basin adjacent to the Upper Teesta Basin is located northeast of the basin and has been observed as the sub-basin with the second-highest number of lakes.

Most glacial lakes were found in the Upper Teesta basin and Lanchhu basin due to glaciers around the sub-basin (Fig. 1 & Fig. 5). The cause behind the formation of such lakes is snowmelt from the surrounding glaciers, which results in increased water quantity in lakes. In contrast, due to retreating glaciers, several new lakes are formed. In addition, the shifting of moraines with the period and nature of the glacier regime also participates in glacial lake formation. Based on the available research done and the obtained result illustrate that there was a significantly smaller number of the glacial lakes found in the lower part of the basin, which was not vulnerable because of it is they are well connected with drains without the moraines obstructing the water flow from the lake into the stream. However, due to the constant melting of glaciers, the number of lakes and the lake area is also increasing, which can be explained by the results, which show the maximum number of lakes present at the altitude

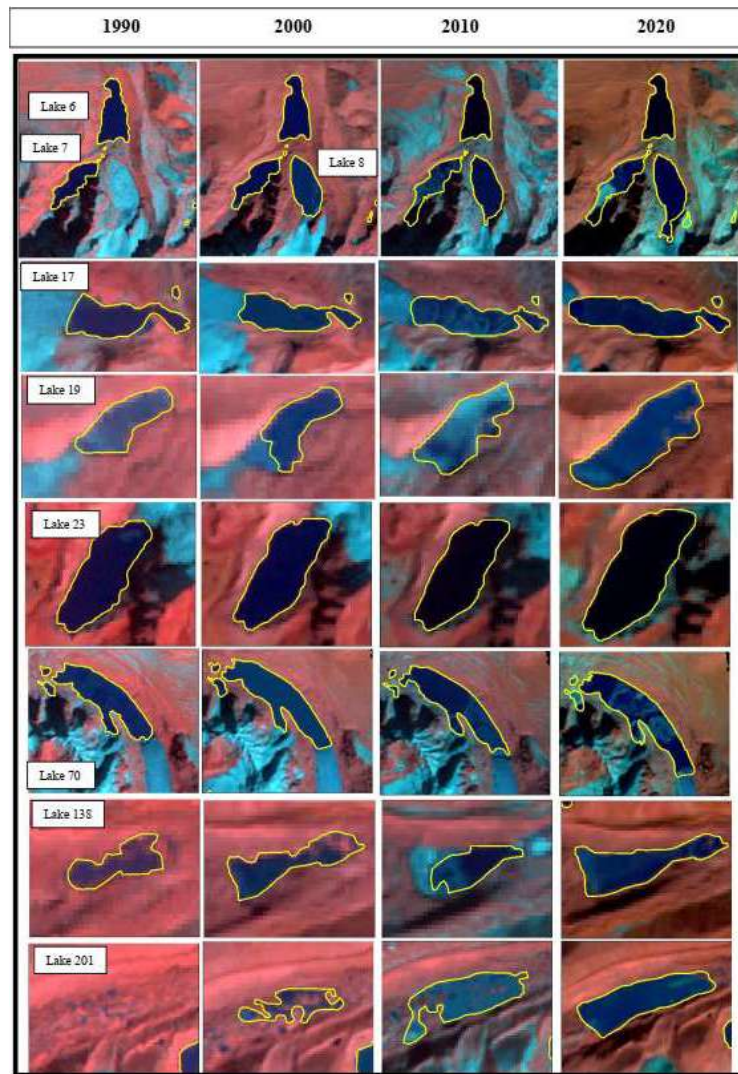


Fig. 4: Glacial Lake from 1990 to 2020.

Table 5: Inventory of Glacial Lake based on water spread area.

Area Range (sqm)	Year 1990		Year 2000		Year 2010		Year 2020	
	No	Area (sqm)	No	Area (sqm)	No	Area (sqm)	No	Area (sqm)
<1000	0	0	4	3523.74	0	0	5	4,805
1000-5000	30	102822	41	141938.71	29	94,986	50	1,64,272
5000-10000	46	3,30,948	45	3,35,816	47	3,26,469	73	5,43,852
10000-50,000	119	29,82,675	154	37,93,760	134	33,72,102	174	43,10,312
50,000-1,00,000	38	28,66,059	38	29,21,080	37	28,33,765	55	40,35,602
1,00,000-5,00,000	35	65,88,200	45	84,60,906	38	70,23,263	51	1,07,59,799
>5,00,000	7	60,35,329	10	88,65,595	10	93,12,357	11	1,16,19,832
Total	275	1,89,06,032	337	2,45,22,619	295	2,29,62,942	419	3,14,38,474

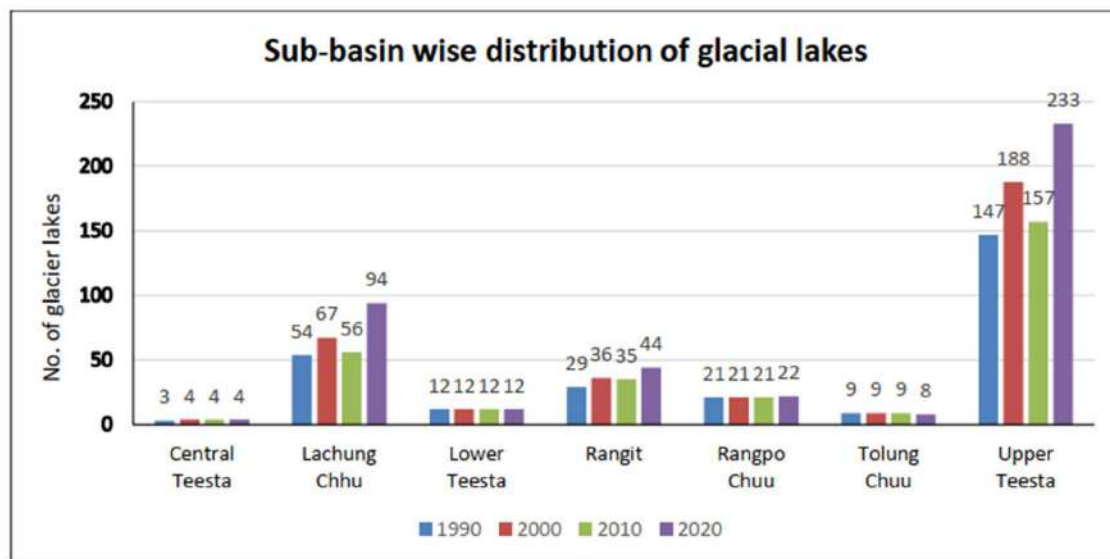


Fig. 5: Sub-basin-wise distribution of glacial lakes.

Table 6: Percentage change of glacial lake.

Lake ID	Year (Area in m ²)				Difference rate 1990-2000	Difference rate 2000-2010	Difference rate 2010-2020
	1990	2000	2010	2020			
6	110673	113423	111709	115627	2.45	1.52	3.45
7	749213	805752	953129	1003817	7.27	16.76	5.18
8	0	106536	112155	129748	--	5.14	14.55
17	411593	476937	437324	476937	14.71	8.67	8.67
19	393589	572566	678492	825073	37.05	16.93	19.50
23	106189	99116	198507	306082	6.89	66.79	42.64
70	569296	593223	579880	598522	4.12	2.27	3.16
138	154501	170099	163917	191009	9.61	3.70	15.27
198	87272	167705	110196	348238	63.09	41.39	103.85
201	0	250273	518487	845961	--	69.78	48.00

Table 7: Elevation zone-wise number of glacial Lake.

Elevation Zone	No. of lake
<3500	3
3500-4000	11
4000-4500	72
4500-5000	104
>5000	229

of 5000 or above with almost 90% of glaciers and glacier mountains. Several glacier lakes are at the snout, which during the summer season, melt as a cause of retreating glaciers. An example of such a glacier lake is Lake No. 23 in 2020 (Fig. 4). Few of the new small glacial lakes are formed near pre-existing lakes due to the melting glaciers; Lake

Number 9 in the year 1990 can be the super-fitted example of such a lake, which has been now separated into a new lake with Lake Number 392 in the year 2020 (Fig. 4). Such lakes formed due to the erosional activity in glaciers are known as glacial erosion lakes. As a result of retreating glaciers, a few new lakes formed between 2000-2020, which were not there in 1990. Other glacial lakes, Lake Number. Also feeds a few lakes. 06 is an example of a lake getting its water from Lakes Number 7 & 8 (see Table 6), which are again glacial erosion lakes located at the snout, and due to the effect of the retreating glacier, they are on the continuous increase for water spread area. Hence, the study demonstrated that glaciers. Retreats are the major reason behind the increasing volume and number of glacial lakes.

By the above-performed study can also be observed that the number of lakes is higher at the higher elevation of 5000 meters (Table 7); an increase in the area of the lake has also been observed, which may be due to the melting glaciers caused majorly due to the human-induced activity. A few lakes had a higher increase rate than others, due to which some of these can be considered vulnerable, depending on other parameters like elevation, depth, volume, and moraines surrounding them, a few of which are shown in Tables 5, 6 & 7.

CONCLUSION

Based on the findings of the research that was conducted, it is feasible to arrive at the following conclusion: the utilization of data received through remote sensing and GIS in conjunction with one another has proven to be very effective in identifying glacier lakes. In addition, using the temporal data that is readily available, it is possible to deduce information relating to historical changes in the glacial lakes, which may then be used effectively to determine which lakes are at risk. To distinguish snow from water and vegetation, the utilization of NDWI and NDVI is of utmost importance. This is because it is extremely challenging to successfully differentiate the features based just on visual perception, as features cast shadows on one another. A study that was conducted over ten years and covered forty years found that glacial lakes in the Upper Teesta basin and the Rongpo basin, which is located in the upper western section of the Teesta basin extension and lies between altitudes of 4500 and 5000 meters, had been expanding at an alarming rate.

As a direct consequence of the climatic regimes in which they are located, the glacial lakes that have been documented display varying rates of area increase. By suggesting that the procedure be carried out on a time basis, it is possible that the remote sensing and GIS approaches that are utilized for GLOF might be utilized more efficiently. This makes it possible to conduct a better assessment as well as an analysis of change detection. As a consequence of this, the information can be utilized to keep track of the variations that are occurring in the quantity and size of these lakes that are forming as a consequence of the development and retreat of glaciers (Table 7). Also, keep an eye on lakes that have a habit of growing their water spread area from year to year while being restricted by things like moraines or other obstacles, and if at all possible, do surveys using an unmanned aerial vehicle (Raaj et al. 2021). In addition, the newly formed lake can be graded according to its vulnerability, which will depend on a variety of circumstances, so that the appropriate preventative

measures can be put into place in the further downstream region.

ACKNOWLEDGMENTS

Authors are highly thankful to those who, knowingly or unknowingly, helped to make this research paper. All authors made equal contributions to this paper.

REFERENCES

- Abdul Hakeem, K., Abirami, S., Rao, V.V., Diwakar, P.G. and Dadhwal, V.K. 2018. Updated inventory of Glacial Lakes in Teesta Basin using remote sensing data for use in GLOF risk assessment. *J. Indian Soc. Remote Sensing*, 46(3): 463-470.
- Aggarwal, A., Jain, S.K., Lohani, A.K. and Jain, N. 2016. Glacial lake outburst flood risk assessment using combined approaches of remote sensing, GIS, and dam-break modeling. *Geomat. Nat. Hazards Risk*, 7(1): 18-36.
- Allen, S.K., Rastner, P., Arora, M., Huggel, C. and Stoffel, M. 2016. Lake outburst and debris flow disaster at Kedarnath, June 2013: hydrometeorological triggering and topographic predisposition. *Landslides*, 13(6): 1479-1491.
- Bajracharya, S.R., Mool, P.K. and Joshi, S.P. 2002. Spatial database development of glaciers glacial lakes in the identification of potentially dangerous glacial lakes of Nepal using remote sensing and geographic information systems. *Remote Sens.*, 5: 46-52.
- Basnett, S., Kulkarni, A.V. and Bolch, T. 2013. The influence of debris cover and glacial lakes on the recession of glaciers in Sikkim Himalaya, India. *J. Glaciol.*, 59: 1035-1046.
- Benn, D.I., Bolch, T., Hands, K., Gulle, J., Luckman, A., Nicholson, L.I. et al. 2012. Response of debris-covered glaciers in the Mount Everest region to recent warming and implications for outburst flood hazards. *Earth Sci. Rev.*, 114: 156-174.
- Bolch, T., Kulkarni, A., Käab, A., Huggel, C., Paul, F. and Cogley, J.G. 2012. The state and glaciers. *Fate of Himalayan Science*, 336: 310-314.
- Brun, F., Berthier, E., Wagnon, P., Käab, A. and Treichler, D. 2017. A spatially resolved estimate of High Mountain Asia glacier mass balances from 2000 to 2016. *Nat. Geosci.*, 10: 668-673.
- Budhathoki, K.P., Bajracharya, O.R. and Pokharel, B.K. 2010. Assessment of Imja Glacier Lake outburst flood (GLOF) risk in DudhKoshi River Basin using remote sensing techniques. *J. Hydrol. Meteorol.*, 7(1): 75-91.
- Chouhan, R. and Rao, N. 2011. Vegetation detection in multispectral remote sensing images: Protective role-analysis of vegetation in 2004 Indian Ocean tsunami. PDPM Indian Institute of Information Technology.
- Chowdhury, A., Sharma, M.C., Kumar De, S. and Debnath, M. 2021. Glacier changes in the ChhombuChhu Watershed of the Tista basin between 1975 and 2018, the Sikkim Himalaya, India. *Earth Syst. Sci. Data*, 13(6): 2923-2944.
- Clague, J.J. and Evans, S.G. 2000. A review of catastrophic drainage of moraine-dammed lakes in British Columbia. *Quat. Sci. Rev.*, 19: 1763-83.
- Debnath, M., Syiemlieh, H.J., Sharma, M.C., Kumar, R., Chowdhury, A. and Lal, U. 2018. Glacial lake dynamics and lake surface temperature assessment along the Kangchengayo-Pahunri Massif, Sikkim Himalaya, 1988-2014. *Remote Sens. Appl. Soc. Environ.*, 9: 26-41.
- Dhar, S., Kulkarni, A.V., Rathore, B.P. and Kalia, R. 2010. Reconstruction of the moraine-dammed lake, based on field evidence and paleo-history, Samudra Tapu Glacier, Chandra Basin, Himachal Pradesh. *J. Indian Soc. Remote Sens.*, 38(1): 133-141.
- Dobhal, D.P., Gupta, A.K., Mehta, M. and Khandelwal D.D. 2013. Kedarnath disaster: Facts and plausible causes. *Curr Sci.*, 105: 171-174.
- Garg, V., Kudekar, A.R., Thakur, P.K., Nikam, B.R., Aggarwal, S.P. and Chauhan, P. 2021. Glacier change studies under changing climate using

- geospatial tools and techniques. *J. Indian Soc. Remote Sens.*, 49(10): 2387-2406.
- Gong, W., Liu, T., Jiang, Y. and Stott, P. 2020. Applicability of the surface water extraction methods based on China's GF-2 HD Satellite in Ussuri River, Tonghe County of Northeast China. *Nat. Environ. Pollut. Technol.*, 19(4): 110.
- Govindha Raj, B.K., Kumar, V.K. and S.N. Remya. 2013. Remote sensing-based inventory of glacial lakes in Sikkim Himalaya: a semi-automated approach using satellite data. *Geomat. Nat. Hazards Risk*, 4(3): 241-253.
- Huggel, C., Haerberli, W., Käab, A., Bieri, D. and Richardson, S. 2004. An assessment procedure for glacial hazards in the Swiss Alps. *Can Geotech.*, 41: 1068-83.
- Huggel, C., Käab, A., Haerberli, W., Teyssie, P. and Paul, F. 2002. Remote sensing based assessment of hazards from glacier lake outbursts: a case study in the Swiss Alps. *Can. Geotech. J.*, 39 (2): 316-330.
- Iwata, S. 2000. Morphological evolution of the debris cover on Khumbu Glacier, Nepal, between 1978 and 1995. *IAHS Publ.*, 264: 3-11.
- Jain, S.K. and Mir, R.A. 2019. Glacier and glacial lake classification for change detection studies using satellite data: a case study from Baspa basin, western Himalaya. *Geocarto Int.*, 34(4): 391
- Käab, A., Berthier, E., Nuth, C., Gardelle, J. and Arnaud, Y. 2012. Contrasting patterns of early twenty-first-century glacier mass change in the Himalayas. *Nature*, 488(7412): 495-498.
- Karaburun, A. 2010. Estimation of C factor for soil erosion modeling using NDVI in Buyukcecece watershed. *Ozean J. Appl. Sci.*, 3(1): 77-85.
- Kargel, J.S., Abrams, M.J., Bishop, M.P., Bush, A., Hamilton, G. and Jiskoot, H. 2005. Multispectral imaging contributions to global land ice measurements from space. *Remote Sens. Environ.*, 99: 187-219. Doi: 10.1016/j.rse.2005.07.004
- Karimi, N., Farajzadeh, M., Moridnejad, A. and Namdari, S. 2014. Evidence for mountain glacier changes in semi-arid environments based on remote sensing data. *J. Indian Soc. Remote Sens.*, 42(4): 801-815.
- Khadka, N., Zhang, G. and Chen, W. 2019. The state of six dangerous glacial lakes in the Nepalese Himalayas. *Terr. Atmos. Ocean Sci.*, 30(1): 63-72.
- Khadka, N., Zhang, G. and Thakuri, S. 2018. Glacial lakes in the Nepal Himalaya: inventory and decadal dynamics (1977–2017). *Remote Sens.*, 10: 1913. <http://dx.doi.org/10.3390/rs10121913>.
- Khadka, N., Chen, X., Yong, N., Thakuri, S., Zheng, G. and Zhang, G. 2020. Evaluation of Glacial Lake Outburst Flood Susceptibility using multi-criteria assessment framework in Mahalangur Himalaya. *Front. Earth Sci.*, 8: 748.
- Koirala, S., Oglethorpe, J., Khanal, K., Dhakal, S., Poudel, K. R., Sharma, K. and Bhandari, K. 2017. Temporal change detection of Kahphuche glacial lake Kaski District, Nepal. *Journal of Nepal Geological Society*, 53: 119-122.
- Kumar, B.P., Babu, K.R., Ramachandra, M., Krupavathi, C., Swamy, B.N., Sreenivasulu, Y. and Rajasekhar, M. 2020. Data on identification of desertified regions in Anantapur district, Southern India by NDVI approach using remote sensing and GIS. *Data Brief*, 30: 105560.
- Kunkel, M.L., Flores, A.N., Smith, T.J., McNamara, J.P. and Benner, S.G. 2011. A simplified approach for estimating soil carbon and nitrogen stocks in semi-arid complex terrain. *Geoderma*, 165(1): 1-11.
- Magsar, A., Matsumoto, T., Enkbold, A. and Nyam-Osor, N. 2021. Application of remote sensing and GIS techniques for the analysis of lake water fluctuations: A case study of Ugii Lake, Mongolia. *Nat. Environ. Pollut. Technol.*, 20(5): 2051-2059.
- Malo, A.R. and Nicholson, S.E. 1990. A study of rainfall and vegetation dynamics in the African Sahel using normalized difference vegetation index. *J. Arid Environ.*, 19(1): 1-24.
- Markham, B.L. and Barker, J.L. 1987. Thematic Mapper bandpass solar exo-atmospheric irradiances. *Int. J. Remote Sens.*, 8(3): 517-523.
- Martha, T.R., Roy, P., Govindharaj, K.B., Kumar, K.V., Diwakar, P.G. and Dadhwal, V.K. 2015. Landslides triggered by the June 2013 extreme rainfall event in parts of Uttarakhand state, India. *Landslides*, 12(1): 135-146.
- Maskey, S., Kayastha, R.B. and Kayastha, R. 2020. Glacial lakes outburst floods (GLOFs) modeling of Thulagi and lower Barun glacial lakes of Nepalese Himalaya. *Prog. Disaster Sci.*, 7:100106.
- McFeeters, S.K. 1996. The use of the normalized difference water index (NDWI) in the delineation of open water features. *Int. J. Remote Sens.*, 17(7): 1425-1432.
- Meetei, L.L., Pattanayak, S.K., Bhaskar, A., Pandit, M.K. and Tandon, S.K. 2007. Climatic imprints in Quaternary Valley fill deposits of the middle Teesta Valley, Sikkim Himalaya. *Quat. Int.*, 159(1): 32-46. doi: 10.1016/j.quaint.2006.08.018.
- Mitkari, K.V., Arora, M.K. and Tiwari, R.K. 2017. Extraction of glacial lakes in Gangotri Glacier using object-based image analysis. *IEEE J. Sel. Top. Appl. Earth Obs. Remote Sens.*, 10(12): 5275-5283.
- Mool, P. K., Wangda, D., Bajracharya, S. R., Kunzang, K., Gurung, D. R. and Joshi, S. P. 2001. Inventory of glaciers, glacial lakes and glacial lake outburst floods. Monitoring and early warning systems in the Hindu Kush-Himalayan Region: Bhutan. *Inventory of glaciers, glacial lakes and glacial lake outburst floods. Monitoring and early warning systems in the Hindu Kush-Himalayan Region: Bhutan.*
- Mool, P. K. and Bajracharya, S. R. 2003. Tista Basin, Sikkim Himalaya: inventory of glaciers and glacial lakes and the identification of potential glacial lake outburst floods (GLOFs) affected by global warming in the mountains of Himalayan region. *International Center for Integrated Mountain Development, Kathmandu, Nepal.*
- Mukhopadhyay, D.K., Chakraborty, S., Treppmann, C., Rubatto, D., Anczkiewicz, R., Gaidies, F., Dasgupta, S. and Chowdhury, P. 2017. The nature and evolution of the Main Central Thrust: Structural and geochronological constraints from the Sikkim Himalaya, NE India. *Lithos*, 16: 282-283: 447-463. doi 10.1016/j.lithos.2017.01.015.
- Murty, C.V.R. 2004. Learning earthquake design and construction, Indian Institute of Technology Kanpur, IITK-BMTPC Earthquake Tip, Kanpur, India.
- Nie, Y., Liu, Q. and Liu, S. 2013. Glacial lake expansion in the Central Himalayas by sat and sat images, 1990-2010. *PLoS ONE*, 8: e83973. doi: 10.1371/journal.pone.0083973.
- Raj, B.K.G., Kumar, V.K. and Remya, S.N. 2013. Remote sensing-based inventory of glacial lakes in Sikkim Himalaya: A semi-automated approach using satellite data. *Water*, 11: 515.
- Rajak, R., Ranjan, R. K., Racoviteanu, A., Lohar, S., Rai, K., Baruah, B. and Gupta, A. 2022. Assessment of glacial lake prone to glacial lake outburst flood using multi-criteria decision analysis (MCDA) in Changme Khangpu basin, Sikkim Himalaya, India.
- Ramachandra, T. V., Bharath, S. and Bharath, A. 2014. Spatio-temporal dynamics along the terrain gradient of diverse landscape. *Journal of Environmental Engineering and Landscape Management*, 22(1): 50-63.
- Reynolds, J.M. 2000. On the formation of supraglacial lakes on debris-covered glaciers. *Glaciers*, 9: 153-164.
- Sakai, A. and Fujita, K. 2010. Formation conditions of supraglacial lakes on debris-covered glaciers in the Himalaya. *Journal of Glaciology*, 56(195): 177-181.
- Salerno, F., Thakuri, S., D'Agata, C., Smiraglia, C., Manfredi, E.C., Viviano, G. and Tartari, G. 2012. Glacial lake distribution in the Mount Everest region: Uncertainty of measurement and conditions of formation. *Global and Planetary Change*, 92: 30-39.
- Scanlon, T.M., Albertson, J.D., Caylor, K.K. and Williams, C.A. 2002. Determining land surface fractional cover from NDVI and rainfall time series for a savanna ecosystem. *Remote Sens. Environ.*, 82(2-3): 376-388.
- Scherler, D., Bookhagen, B. and Strecker, M.R. 2011. Spatially variable response of Himalayan glaciers to climate change affected by debris cover. *Nat. Geosci.*, 4:156. Doi: 10.1038/ngeo1068.
- Shrestha, N.M. and Balla, M.K. 2011. Temporal change detection of LundingTsho glacial lake in Dudh-Koshi basin, Nepal. *J. Environ. Res. Dev.*, 5(3A): 795-800.

- Shukla, A., Garg, P.K. and Srivastava, S. 2018. Evolution of glacial and high-altitude lakes in the Sikkim, Eastern Himalaya over the past four decades (1975-2017). *Front. Environ. Sci.*, 6: 81. Doi: 10.3389/fenvs.2018.00081.
- Srivastava, S., Garg, P.K. and Azam, M. 2022. Seven Decades of Dimensional and Mass Balance Changes on DokrianiBamak and Chhota Shigri Glaciers, Indian Himalaya, Using Satellite Data and Modelling. *J. Indian Soc. Remote Sens.*, 50(1): 37-54.
- Thompson, S., Benn, D.I., Mertes, J. and Luckman, A. 2016. Stagnation and mass loss on a Himalayan debris-covered glacier: processes, patterns and rates. *J. Glaciol.*, 62(233): 467-485.
- Tsering, T., Wahed, M.S.A., Iftekhar, S. and Sillanpää, M. 2019. Major ion chemistry of the Teesta River in Sikkim Himalaya, India: Chemical weathering and assessment of water quality. *J. Hydrol. Reg. Stud.*, 24: 100612.
- Tucker, C.J. 1979. Red and photographic infrared linear combinations for monitoring vegetation. *Remote Sens. Environ.*, 8(2): 127-150.
- Veh, G., Korup, O. and Walz, A. 2020. Hazard from Himalayan glacier lake outburst floods. *Proc. Natl. Acad. Sci.*, 117(2): 907-912.
- Watson, C.S., King, O., Miles, E.S. and Quincey, D.J. 2018. Optimizing NDWI supraglacial pond classification on Himalayan debris-covered glaciers. *Remote Sens. Environ.*, 217: 414-425.
- Wessels, R.L., Kargel, J.S. and Kieffer, H.H. 2002. ASTER measurements of supraglacial lakes in the Mount Everest region of the Himalayas. *Ann. Glaciol.*, 34: 399-407.
- Xie, Y., Zhao, X., Li, L. and Wang, H. 2010, June. Calculating NDVI for Landsat7-ETM data after atmospheric correction using 6S model: A case study. *Geoinformatics*. 1: 1-4.
- Zhang, M., Chen, F., Tian, B., Liang, D. and Yang, A. 2020. High-frequency glacial lake mapping using time series of Sentinel-1A/1B SAR imagery: an assessment for the southeastern Tibetan plateau. *Int. J. Environ. Res. Public Health*, 17(3): 1072.



Elucidating Mycotoxin-Producing *Aspergillus* Species in River Water: An Advanced Molecular Diagnostic Study for the Assessment of Ecological Health and Contamination Risk

R. Ravikiran*, G. Raghu* and B. Praveen**†

*Department of Biochemistry and Plant Physiology, M. S. Swaminathan School of Agriculture, Centurion University of Technology and Management, Paralakhemundi, Gajapati, Odisha, India

**Department of Plant Pathology, M.S. Swaminathan School of Agriculture, Centurion University of Technology and Management, Paralakhemundi, Gajapati, Odisha, India

†Corresponding author: B. Praveen; bpraveen@cutm.ac.in

Nat. Env. & Poll. Tech.
Website: www.neptjournal.com

Received: 22-10-2023

Revised: 14-12-2023

Accepted: 24-12-2023

Key Words:

Aspergillus flavus

Genetic similarity

ITS1 and ITS4 primers

ITS region sequencing

NCBI GenBank

Novel strain gene

Phylogenetic analysis

Water resources conservation

ABSTRACT

The primary goal of this research is to isolate mycotoxin-producing fungus from the Nagavali River. Examining isolated fungi involved analyzing their mycelium growth on culture media and detailed microscopic inspection. We employed PCR analysis utilizing universal primers ITS1 and ITS4 to accurately identify the species. Furthermore, we sequenced the amplified ITS region and rigorously analyzed the sequences using NCBI-BLASTn and the ITS2 database. The analysis found a high 96.38% genetic similarity to the *Aspergillus flavus* strain, resulting in a 600-base pair fragment size. The sequence was given the accession number OR536222 in the NCBI GenBank database. Phylogenetic analysis was performed to ascertain the particular strain of *A. flavus* and its source. Remarkably, this analysis led to the identification of a single new strain gene, which represents a novel discovery in the field of fungal research. These results underscore the vital significance of molecular techniques in promptly and precisely identifying organisms. This research enhances our understanding of mycotoxin contamination in water, providing valuable insights to improve detection and prevention strategies. It accentuates the overarching importance of conserving our water resources and upholding ecological equilibrium, ultimately safeguarding the well-being of both humanity and the environment.

INTRODUCTION

The prevalence of mycotoxin-producing *Aspergillus* species in natural water sources has emerged as a significant ecological and public health issue (Houbraken & Samson 2011). These filamentous fungi, which are frequently connected with agricultural and aquacultural operations, can synthesize mycotoxins, which are a broad collection of secondary metabolites that have been linked to negative effects on human and animal health (Bennett & Klich 2003). Concerns about mycotoxin contamination in aquatic environments have grown in recent years as a result of their possible influence on ecological balance and the safety of water supplies (Brera et al. 2023).

Understanding the genetic variety of *Aspergillus* fungi is critical for understanding their critical ecological roles in the environment and agriculture. With their genetic variety, *Aspergillus* species perform critical roles in nutrient cycling, organic matter decomposition, and mycotoxin synthesis in a

wide range of natural settings, including soil, water bodies, and plant environments. Their remarkable adaptability to diverse environmental conditions, viz., extreme pH ranges, temperature fluctuations, and variable substrate availability, enables them to thrive in disparate ecological niches and engage in intricate interactions with other microorganisms and host organisms (Smith et al. 2023). Additionally, the species genetic diversity among *Aspergillus* holds significant implications for agriculture. These fungi can function as beneficial biocontrol agents, plant partners, or notorious mycotoxin producers, affecting crop quality and food safety negatively. A comprehensive genetic analysis is imperative to harness their potential in sustainable agricultural practices while concurrently mitigating the associated risks of mycotoxin contamination.

Our project, based in Ganagalawanipeta village, Srikakulam, India, aims to thoroughly explore the prevalence of mycotoxin-producing *Aspergillus* species in river water—an ecologically critical reservoir (Gupta et al. 2023).

River water pollution with mycotoxins has been linked to agricultural runoff, aqua cultural waste, and other human activities (Hruska et al. 2019). These contaminants endanger not just aquatic life but also human populations that rely on these water supplies for a variety of functions, including drinking and agriculture. The major goal of this work is to discover and characterize mycotoxin-producing *Aspergillus* species using a molecular diagnostic method centered on the Internal Transcribed Spacer (ITS) region (Samson et al. 2014). In contrast to existing microbiological and chemical tests, which may lack specificity and sensitivity in detecting fungal pollutants, our study provides a PCR-based diagnostic method developed for rapid and accurate identification of toxin-producing fungi across genera (Klich & Pitt 1988).

This research not only raises awareness about the possible health hazards associated with mycotoxin pollution in aquatic environments but also gives critical insights for the development of efficient detection and prevention techniques (Battilani et al. 2016). Water resource conservation and

ecological balance are critical for the well-being of both human populations and the environment (Viegas et al. 2021). Incorporating molecular characterization into our study not only improves the accuracy of our findings but also lays the groundwork for future studies and the development of tailored measures to decrease mycotoxin pollution in aquatic environments. This technique provides us with a thorough understanding of the genetic variety and behavior of mycotoxin-producing *Aspergillus* species, ultimately contributing to larger efforts to protect the environment.

MATERIALS AND METHODS

Study Area

Our investigation was conducted in Ganagalawanipeta village, situated within Andhra Pradesh, specifically in the Srikakulam district (Fig. 1). This area is renowned for its adjacency to the Nagavali River, which flows in a southwest to northeast direction. Characterized by a tropical monsoon



Fig. 1: Study Area and sample collection for fungal isolation.

climate, the region experiences distinct seasonal variations, marked by alternating rainy and dry periods (APHA 1998). The annual precipitation ranges between 900 to 1100 mm, with the highest levels observed typically from June to October (Sparrow 1960).

Sample Collection and Processing

We collected monthly river water samples from three places along the Nagavali River to study seasonal fungal diversity variations. The samples were collected in sterile containers and transferred in a temperature-controlled chain (Fig. 1). At each collection, physicochemical data (temperature, pH, salinity, dissolved oxygen, nutrients) were collected concurrently (Stevens 1974). This stringent technique ensured sample integrity while also providing critical data for the Nagavali River ecosystem fungus diversity and environmental study.

Isolation of Fungi

A serial dilution approach was employed to isolate fungi from water samples (Altschul et al. 1990). We created water dilutions by distributing 100 L of each dilution on Potato Dextrose Agar (PDA) plates using the spread plate method. Plates incubated for up to 7 days at 25°C. For pure cultures, colonies with specific physical characteristics were sub-cultured. The preliminary identification was based on colony features, which were validated by microscopic investigation (Abd-Elaslam et al. 2000). The DRBC (Dichloran Rose Bengal Chloramphenicol) medium, which included 2 micrograms of dichloran and 25 micrograms of rose bengal per mL, significantly limited spreading mold colony growth while recovering more fungal species in greater amounts than previous enumeration media (Manogaran & Lopezh 2017).

The Growth of Fungi in Culture Media

For inoculation, we made a 10^{-6} CFU/mL conidia suspension. The fungal strain was grown in a GMS medium with a 2% sucrose solution and agitation at 150 rpm. After incubation, mycelium was removed using sterile filter paper, weighed, and kept at -80°C for DNA isolation.

Genomic DNA Isolation

The cell disruption process began with rapid freezing using liquid nitrogen and subsequent grinding into a fine powder using a sterile mortar and pestle. For DNA isolations, 100 mg of this disrupted mycelium was used. Genomic DNA isolation, performed in triplicate, included Proteinase K and RNase treatment to remove RNA contaminants. Purified DNA samples were resuspended in Tris-HCl buffer (pH 8.0,

1 mM EDTA) for further analysis. This modified method consisting of 1 M Tris-HCl (pH 8.0), 5 M NaCl, 0.5 M EDTA (pH 8.0), 2% CTAB, and 28.6 mM 2-mercaptoethanol, with the addition of 51DVH (20 mg.mL⁻¹) during homogenization. After incubation and centrifugation, supernatants were mixed with chloroform-isoamyl alcohol, followed by precipitation with cold isopropanol and sodium acetate. DNA pellets were washed, dried, and resuspended in TE buffer.

NanoDrop™ 1000 UV/VIS Spectrophotometer Measurements

We measured absorbance at 260 and 280 nanometers using a Thermo Scientific NanoDrop™ 1000 UV/VIS spectrophotometer. We also estimated the A260/A280 and A260/230 ratios. For accuracy and consistency, we adhered to the manufacturer's methods and requirements.

Electrophoresis of Isolated Genomic DNA

A 2% agarose gel was used to analyze genomic DNA. 1x TBE buffer (0.5 M Tris, 0.5 M Boric acid, 10 mM EDTA) was used to run the gel. Before loading, genomic DNA was combined 1:1 with Fermentas' 6x mass ruler loading dye. Samples were put into different wells. The electrophoresis was performed at 100 V, 50 mA, and a predetermined period. At 254 nm, DNA fragments were evaluated for size and integrity.

Primers and Polymerase Chain Reaction Analysis

Fungal DNA amplification utilized specific primers, ITS 1 (5'-TCC GTA GGT GAA CCT GCG G-3') and ITS 4 (5'-TCC TCC GCT TAT TGA TAT G-3'), strategically designed to align with conserved regions within the 18S (ITS 1) and the 28S (ITS 4) rRNA genes, enabling targeted analysis of the fungal DNA in the ITS region. PCR amplification was carried out using a 5 µL aliquot of the test sample in a total reaction volume of 50 µL. This reaction mixture consisted of PCR buffer (20 mM Tris-HCl [pH 8.4], 50 mM KCl), 0.1 mM of each dATP, dGTP, dCTP, and dTTP, 1.5 mM MgCl₂, 0.3 µM of each primer, and 1.5 U of PlatinumTaq high-fidelity DNA polymerase sourced from TAKARA PrimeSTAR Max DNA Polymerase—fast and high-fidelity PCR. The PCR process included 40 cycles and used an Applied Biosystems™ SimpliAmp™ Thermal Cycler. It began with initial DNA denaturation at 95°C for 4.5 min. Each cycle included denaturation at 95°C for 30 seconds, annealing at 50°C for 30 seconds, and extension at 72°C for 1 min. A final extension step at 72°C for 3 min concluded the cycles. After PCR, the products were stored at 4°C.

The amplicons were stained with ethidium bromide and put on a 1.5% agarose gel with Tris base, acetic acid, and

EDTA buffer for analysis. A 595-bp band demonstrated satisfactory amplification. Clear PCR amplicons were eluted using the NucleoSpin Gel and PCR Cleanup Mini kit according to the manufacturer's instructions. The concentration was assessed using 1.2% agarose gel electrophoresis and NanoDrop readings, and the eluted products were kept at 4°C for sequencing.

DNA Sequencing and Analysis, NCBI GenBank Deposition and Phylogenetic Analysis

The PCR results were immediately forwarded to Barcode Biosciences (<https://www.barcodebiosciences.com/>) for sequencing using particular primers developed for the 18S rDNA region. The sequencing was carried out using an Applied BioSystems Genetic Analyzer 310 and precisely following the manufacturer's instructions. The sequences were meticulously analyzed using Genetyx-Mac10 software when they were obtained. Extensive searches in the DDBJ/EMBL/GenBank nucleotide databases, using BLAST Programmes and the ITS2 database (<http://its2.bioapps.biozentrum.uni-wuerzburg.de/>), verified identity and functioning. This extensive study allowed the sequences to be identified and characterized, providing important insights into the genetic makeup of the fungus. The fungal sequences were then deposited in the NCBI GenBank for easier access and reference.

Multiple alignments of nucleic acid sequences were performed using bioinformatics software (Bio edit version 7.2.5). To identify the fungal *A. flavus* ITS sequences, they were aligned using MEGA 11.0.10 software (<https://www.megasoftware.net/>), and a comparison analysis was performed against the nucleotide sequences available in GenBank. The phylogenetic tree was constructed using the neighbor-joining method described by Saitou & Nei (1987). The species identification was based on calculating the % similarity of the ITS sequences using the criteria given by Higgins and colleagues in 2007. In the phylogenetic study, *Aspergillus terreus* with Accession number EU515150 was used as an out-group, assisting in the contextual placement of the *A. flavus* sequences.

DNA Barcoding and ITS2 Secondary Structure Predictions

In this study, we harnessed the power of the Bio-Rad DNA barcode generator, accessible at <http://biorad-ads.com/DNABarcodeWeb> (accessed on 16 October 2023), to craft precise DNA barcodes for the studied *Aspergillus flavus* specimens. These barcodes were meticulously curated using DNA nucleotide sequences obtained through the application of ITS1 and ITS4 primers. Furthermore, we delved into the

realm of RNA secondary structure predictions, employing nucleotide sequences from the same ITS1 and TS4 primers. This predictive process was facilitated by leveraging the rRNA database hosted on the RNAfoldWebServer v2.4.18 platform, available at <http://rna.tbi.univie.ac.at/cgi-bin/RNAWebSuite/RNAfold.cgi> (accessed on 16 October 2023), following the methodology outlined by Lorenz et al. (2011).

RESULTS AND DISCUSSION

Detecting Mycotoxin-Producing *Aspergillus* species in river water extends beyond scientific inquiry; it represents a critical effort in protecting both the environment and public health. This discovery unveils insights into the distribution, behavior, and potential threats posed by these fungi, particularly their mycotoxin-producing capabilities. By delving into this research, we pave the way for the development of strategies aimed at mitigating these risks and preserving the integrity of water resources, along with the well-being of the communities reliant on them.

Rapid, accurate fungal identification is crucial across fields like agriculture, medicine, and food safety. Traditional methods like morphology are slow and less precise. Our study enhances knowledge of mycotoxin-producing *Aspergillus flavus*, which is vital in agriculture and aquaculture. *A. flavus* presence in these settings raises food safety concerns.

Isolation and Identification of Fungal Isolates and *Aspergillus flavus* Identification

During the six-month study, common *Aspergillus* species like *A. niger*, *A. flavus*, *A. fumigatus*, and *A. terreus* were identified. Differential culture media like CZ, CYA, and MEA were used. Sampling encompassed aquaculture wastewater, agricultural waste areas, and river water. Identification relied on macroscopic and microscopic traits. This comprehensive approach deepened our understanding of *Aspergillus* diversity and its implications for public and environmental health. For *A. flavus*, identification involved analyzing its morphology using specific culture media like AFPA and CDA. AFPA distinguishes *A. flavus* by its distinctive orange colony reverse. Morphological features, including conidia production, further differentiated *A. flavus* from other species. Intriguingly, variations in colony color, structure, and sclerotia formation were observed among *A. flavus* isolates. This highlights the need for molecular techniques to ensure precise identification.

Genetic Characterization

Our modified *A. flavus* genomic DNA extraction method yielded substantial, high-quality DNA confirmed by

nanodrop analysis (Fig. 2). Similar to the Aamir et al. (2015) approach, our method disrupts fungal cells, undergoes RNase treatment and employs phenol: chloroform: Isoamyl alcohol extraction and isopropanol precipitation. It delivers DNA in 1 h, with yields ranging from 60 µg to 230 µg per 200 mg wet fungal mass. This closed system minimizes contamination risks and supports diverse molecular methods, including PCR and RAPD analysis. Compared to Sarkanj et al. (2018) study, our method balances efficiency, cost-effectiveness, and time. It produces pure DNA with favorable ratios and suits downstream applications. Time ranges from 1 hour 15 minutes to 7 h 5 min, with reasonable per-sample costs, ensuring practicality for *A. flavus* genomic DNA isolation and PCR reactions. Our study aligns with Jin et al. (2000) findings, demonstrating the effectiveness and versatility of DNA extraction techniques.

Polymerase Chain Reaction Analysis

Following genomic DNA extraction from *A. flavus* isolates, PCR using ITS1/ITS4 primers produced consistent 600 bp fragments, consistent with Diba et al. (2014) (Fig. 3). This size uniformity suggested genetic similarity among isolates. Electrophoresis and sequencing further confirmed *A. flavus* strain identification. Krulj et al. (2020) study on *A. flavus* from wheat grains also employed PCR amplification and PCR-RFLP with fragment length analysis, yielding similar results. Both studies identified all strains as *A. flavus* through ITS region and β -tubulin gene sequencing. Combining PCR-RFLP with Lab-on-a-chip electrophoresis, as shown by Kurlj et al. (2020), offers rapid *A. flavus* identification. Consistency with Stoll et al. (2003, Mohankumar et al. (2010), and Alrawi and Hussein (2017) highlights PCR's reliability



Sample collection from fish ponds



sample collection from river water



sample collection from Fish catching area

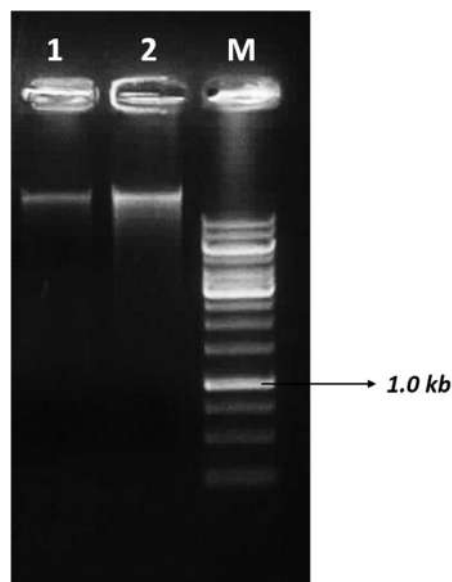


Fig. 2: The 0.8% ethidium bromide-stained agarose gel showing DNA samples after DNA extraction from *Aspergillus* species. Legends: 1- *Aspergillus* species sample as reference (Obtained and stored from previous studies); 2- *Aspergillus flavus* river water sample; M-Molecular Weight Marker; Thermo Scientific™ GeneRuler 1 kb Plus DNA Ladder, ready-to-use.

for *A. flavus* detection using ITS1 and ITS4 primers. Gel electrophoresis, alongside a DNA ladder, confirms the technique's accuracy. These results underscore PCR's value in *A. flavus* identification across various applications.

NCBI BLAST Analysis

The NCBI BLAST analysis of the newly generated sequence revealed compelling results. It exhibited a 100% graphical similarity to *A. flavus*, with 404 BLAST hits on 100 subject sequences, indicating a precise alignment with no gaps and a plus/plus orientation. Taxonomically, 53 out of 103 hits were identified as *A. flavus*, affirming the sequence's affiliation with this species (Fig. 4). Furthermore, the Blast tree view confirmed a match with the *A. flavus* S716A strain, narrowing down the identification to a specific strain within the species. NCBI BLAST tree analysis is vital for the accurate identification and classification of genetic sequences, providing insights into genetic relationships, taxonomy, and potential functions, as demonstrated in this study (Fig. 5).

ITS2 Database Analysis

The BLAST analysis using the ITS2 Database has solidified

the identity of our river water fungi sequence, confirming its alignment with *A. flavus*. Key parameters from the analysis include a Maximum Score of 488, indicating a robust match with a known reference sequence; a Coverage of 81%, signifying significant overlap between the sequences; and an E-Value of 0.0, denoting high biological significance. The ITS2 Database, housing comprehensive data on the ITS2 region of ribosomal RNA genes, enabled this comparison. This result is highly reliable, indicating a close genetic relationship between fungal isolate and *A. flavus*. Moreover, the presence of NCBI GenBank submitted sequences with the accession number OR53622 suggests a novel discovery, indicating that this *A. flavus* species from river water has not been previously reported in India or elsewhere, highlighting the significance of this finding for microbial diversity and ecological studies in water sources.

Sequence Data Analysis

In our study, we successfully isolated Mycotoxin-Producing *Aspergillus* species from river water, and the generated sequence was deposited in the NCBI database with the accession number OR536222. Subsequent NCBI BLAST search analysis revealed a highly significant match with

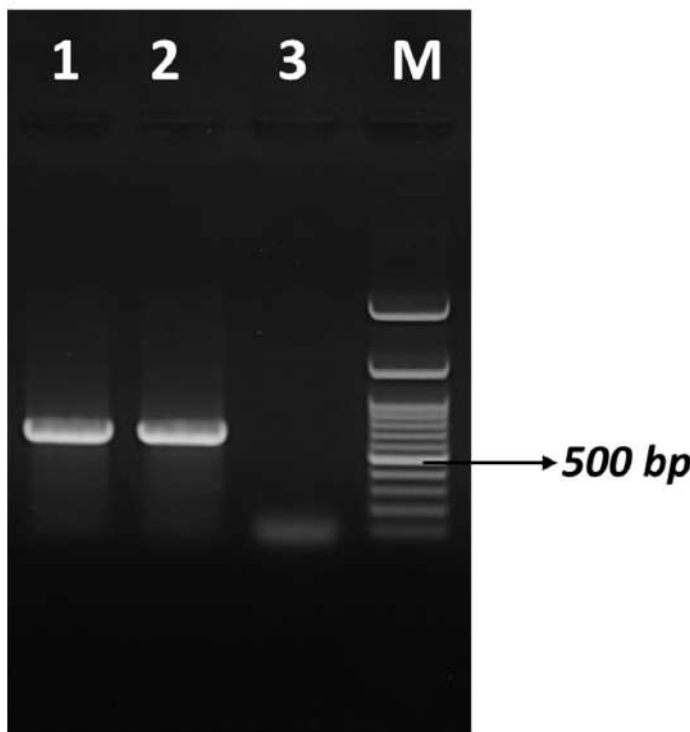


Fig. 3: The PCR of screened 15 different fungal milk samples. The highly conserved region of (ITS) regions of the ribosomal DNA, primers pair ITS1 and ITS4 produced the target band of 600bp, Legends: 1-*Aspergillus flavus* river water sample, 2-Genomic DNA positive control; 3-Genomic DNA negative control; M-Molecular Weight Marker; 100bp DNA ladder (Genedirex).

BLAST® » blastn suite » results for RID-HMETT2XZ016

Job Title: OR536222_Aspergillus flavus_co-occurrence...
 RID: HMETT2XZ016
 Program: BLASTN
 Database: nt_euk
 Query ID: lcl|Query_10075
 Description: OR536222_Aspergillus flavus_co-occurrence of mycotoxin...

Filter Results
 Organism: exclude
 Percent Identity: to
 E value: to
 Query Coverage: to

Reports: Lineage Organism Taxonomy

99 sequences selected

Taxonomy	Number of hits	Number of Organisms	Description
Fungi	102	19	
Leotiomycota	99	17	
Aspergillus	98	16	
Aspergillus subgen. Circumdati	60	2	
Aspergillus flavus	53	1	Aspergillus flavus hits
Aspergillus oryzae	7	1	Aspergillus oryzae hits
Unclassified Aspergillus	27	11	
Aspergillus sp.	17	1	Aspergillus sp. hits
Aspergillus sp. AQGWD 17	1	1	Aspergillus sp. AQGWD 17 hits
Aspergillus sp. AQGSS 10	1	1	Aspergillus sp. AQGSS 10 hits
Aspergillus sp. BAB-4649	1	1	Aspergillus sp. BAB-4649 hits
Aspergillus sp. BAB-4665	1	1	Aspergillus sp. BAB-4665 hits
Aspergillus sp. BAB-4659	1	1	Aspergillus sp. BAB-4659 hits
Aspergillus sp. SV/09-11	1	1	Aspergillus sp. SV/09-11 hits
Aspergillus sp. SZN30	1	1	Aspergillus sp. SZN30 hits
Aspergillus sp. SZN28	1	1	Aspergillus sp. SZN28 hits
Aspergillus sp. SZN23	1	1	Aspergillus sp. SZN23 hits
Aspergillus sp. SZN15k	1	1	Aspergillus sp. SZN15k hits
Aspergillus nomiae	7	1	Aspergillus nomiae hits
Aspergillus tamarii	3	1	Aspergillus tamarii hits
Aspergillus transmontanensis	1	1	Aspergillus transmontanensis hits
Trichoderma viride	1	1	Trichoderma viride hits
fungal sp.	1	1	fungal sp. hits
uncultured fungus	2	1	uncultured fungus hits

Fig. 4: NCBI BLASTn taxonomic analysis of the river fungi isolate sample reveals a significant match with *Aspergillus flavus*, with a total of 53 hits in the database.

NCBI nucleotide accession number KY234271, which corresponds to *A. flavus*. The sequence identity was exceptionally high at 96.38%, with an E-value of 0, indicating a robust and reliable match. Furthermore, the query coverage

reached 100%, reinforcing the accuracy of our identification. These findings emphasize the presence of *A. flavus* in the aquatic environment, highlighting potential concerns related to mycotoxin contamination and underscoring the importance

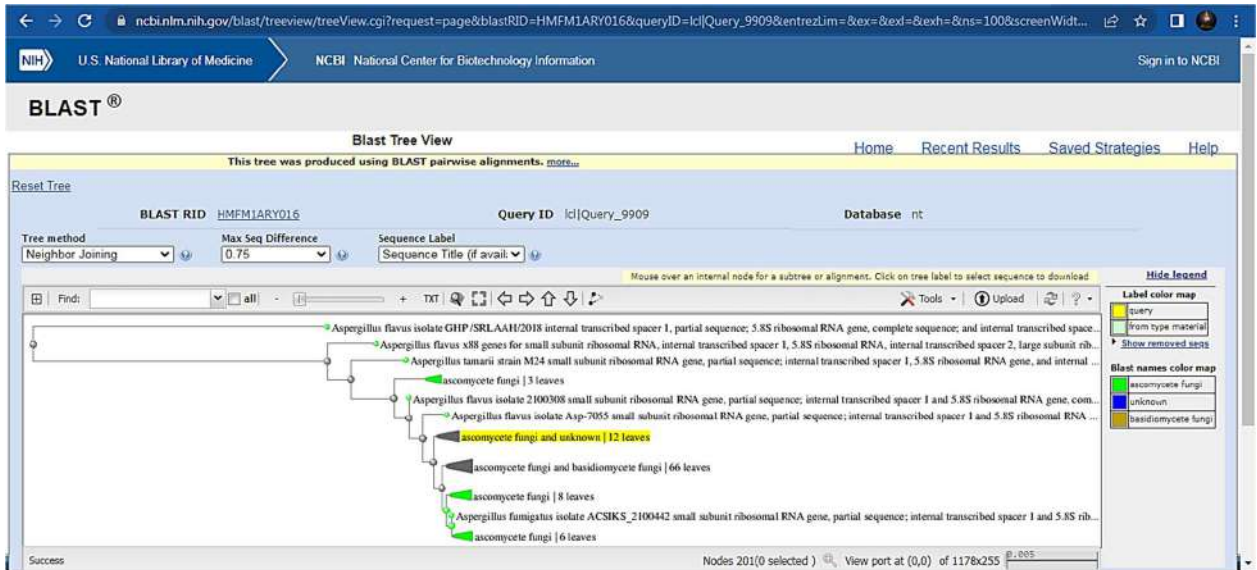


Fig. 5: The NCBI Blast Tree View of *Aspergillus flavus* provides a visual representation of the evolutionary relationships and genetic similarity between our analyzed sample and this particular fungal species.

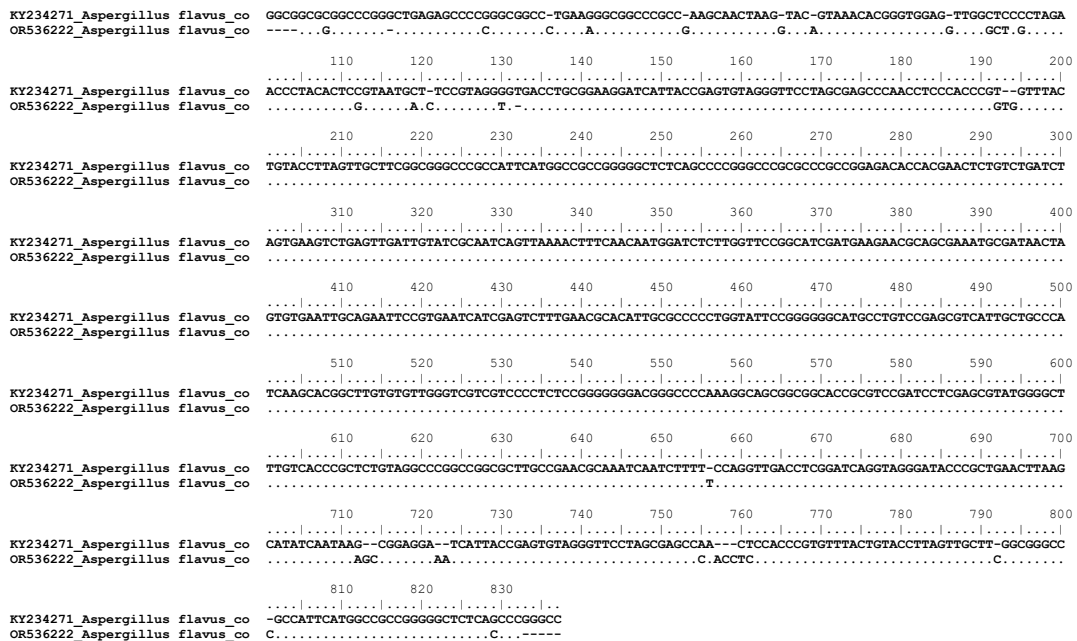


Fig. 6: The multiple sequence alignment compares the genetic sequences of *Aspergillus flavus* isolates from both fish feed (Accession number KY234271) and river water (Accession number OR536222), highlighting their genetic similarity and potential co-occurrence of mycotoxins in these different environments.

of monitoring and addressing such issues in the context of food safety and public health, particularly for smallholder farmers.

The alignment of KY234271_*Aspergillus flavus_co*-occurrence of mycotoxin in fish feed with OR536222_

Aspergillus flavus_co-occurrence of mycotoxins in river water revealed a total of 34 nucleotide variations at specific positions within the sequences (Fig. 6). These variations were observed at positions 9 (C-G), 28 (G-C), 36 (-C), 41 (G-A), 53 (-A), 65 (-G), 69 (-A), 86 (-G), 91 (C-G), 92 (T-

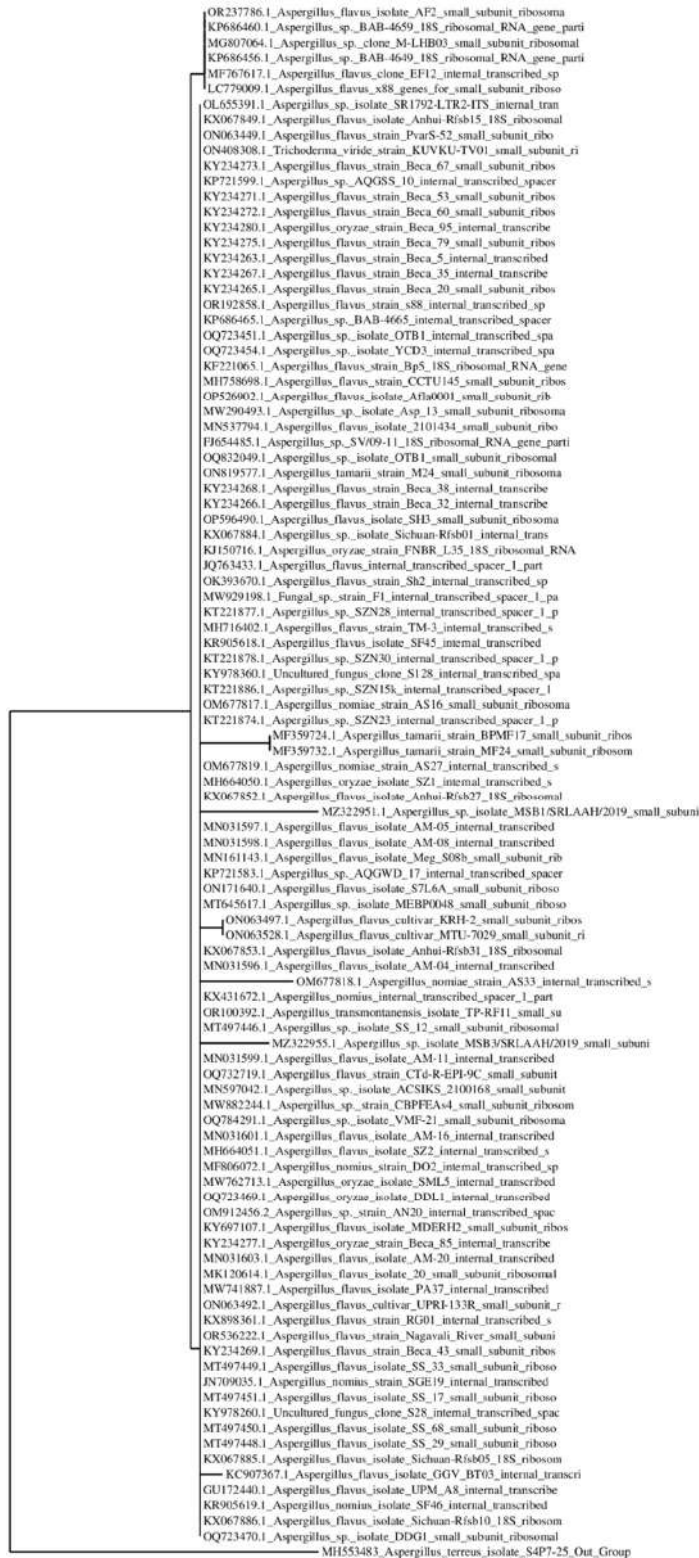


Fig. 7: The phylogenetic tree of specific *Aspergillus flavus* isolates, constructed using Neighbor-Joining methodology with the Tamura-Nei model.

C), 93 (C-T), 95 (C-G), 112 (C-G), 119 (C-A), 121 (-C), 130 (G-T), 192 (T-G), 193 (-T), 195 (-G), 656 (-T), 713 (G-A), 714 (-G), 715 (-C), 721 (-A), 722 (-A), 755 (A-C), 757 (-A), 758 (-C), 759 (-C), 760 (C-T), 761 (T-C), 791 (-C), 801 (-C), and 829 (G-C). The overall nucleotide variation observed in this comparison accounts for approximately 4.062% of the sequences.

It's noteworthy that these variations are primarily distributed in both the 5' and 3' regions of the sequences, while the core sequence remains unchanged. This pattern of variations is a common occurrence in genetic sequences, where certain regions exhibit more variability than others, often due to factors like mutations, insertions, or deletions.

Despite the observed nucleotide variations, the core genetic sequence maintains a consistent and highly similar 96% identity, affirming the fungal isolate's classification as *A. flavus* and reinforcing the accuracy of our identification process. A ClustalW multiple alignment analysis, comparing our river water *Aspergillus flavus* sequence with sequences from diverse sources, including mycotoxin in fish feed, textile industrial effluent, Russia spring water, Egypt canal water, and Turkey magnesite quarries, revealed significant homology within *A. flavus* species. This observation holds ecological and public health significance, as the mycotoxin-producing *Aspergillus* species' presence in natural water sources raises contamination and health concerns. It confirms the strong genetic similarity between the fungal isolate and *A. flavus*, suggesting its taxonomic classification as a strain or variant of this species. These findings enhance our understanding of genetic relatedness, aiding taxonomic classification and emphasizing potential ecological roles in water ecosystems or contamination scenarios.

Phylogenetic Tree Analysis

The clustering pattern in the trees was robustly confirmed through 2,000-replication bootstrap tests using MEGAX and Phylogeny Fr tools during Neighbor-Joining methodology (NJ) tree analysis (Fig. 7). This demonstrated the consistent and reliable clustering of individuals of the same species, primarily guided by the similarity of the ITS sequence of *A. flavus* and *Aspergillus* species. The molecular marker's efficacy in distinguishing closely related fungal species remained uniform regardless of collection site or geographic location, emphasizing the universal applicability of ITS sequencing for species-level identification and phylogenetic analysis, further enriching our comprehension of fungal diversity and evolution.

Antonios Krimitzas et al. (2013) extensive phylogenetic tree work contributed significantly to understanding *Aspergillus* genus relationships, delineating seven well-supported clades using various methods. This research illuminated the evolutionary connections among different *Aspergillus* species.

A related study by Mays et al. (2019) in Diyala Province employed molecular techniques to detect *A. flavus* in milk samples. Using a conventional PCR assay with published primers (ITS1 and ITS4), they confirmed the presence of *A. flavus*, identifying toxigenic isolates through a distinct 600 bp sequence. Phylogenetic analysis pinpointed the specific *A. flavus* strain and its origin, uncovering a novel strain gene added to the Gene Bank database under the accession number MH213344, underscoring its significance in fungal research.

A. flavus River Isolate DNA Barcoding, Secondary Structure Prediction Analysis

The DNA barcode for the *A. flavus* river isolate, derived from the ITS sequences, has provided valuable insights into the genetic variations present, as depicted in Fig. 8A. In this study, the prediction of RNA secondary structures, as depicted in Fig. 8B, was employed to gather crucial information for conducting phylogenetic analyses. The analysis primarily centered on the ITS1 regions, emphasizing the examination of conserved structural elements, including interior loops, hairpin loops, and exterior loops within the *A. Flavus* River isolate. Notably, the assessment of these secondary structures incorporated criteria rooted in free energy minimization, utilizing nearest-neighbor parameters and focusing on Gibbs free energy at 37°C to gauge structural stability. The observed similarities in secondary structure were complemented by resemblances in energy profiles (-ΔG). Nevertheless, variations in nucleotide sequence length contributed to distinctions in the topological features of these structures. This comprehensive approach served to enhance our understanding of the genetic variations and relationships elucidated by the *A. flavus* DNA barcodes derived from the ITS sequences, and it further emphasized the utility of secondary structure prediction in phylogenetic studies.

Thangaraj et al. (2011) study highlighted the significance of RNA transcript secondary structures in systematic fungal studies, as these structures provide valuable information not discernible in primary sequences. The research involved predicting and comparing the secondary structures of the internal transcribed spacer region 1 (ITS1) in four *Aspergillus* species. The examination of these structures revealed a mix of conserved and varied topologies among the species. These

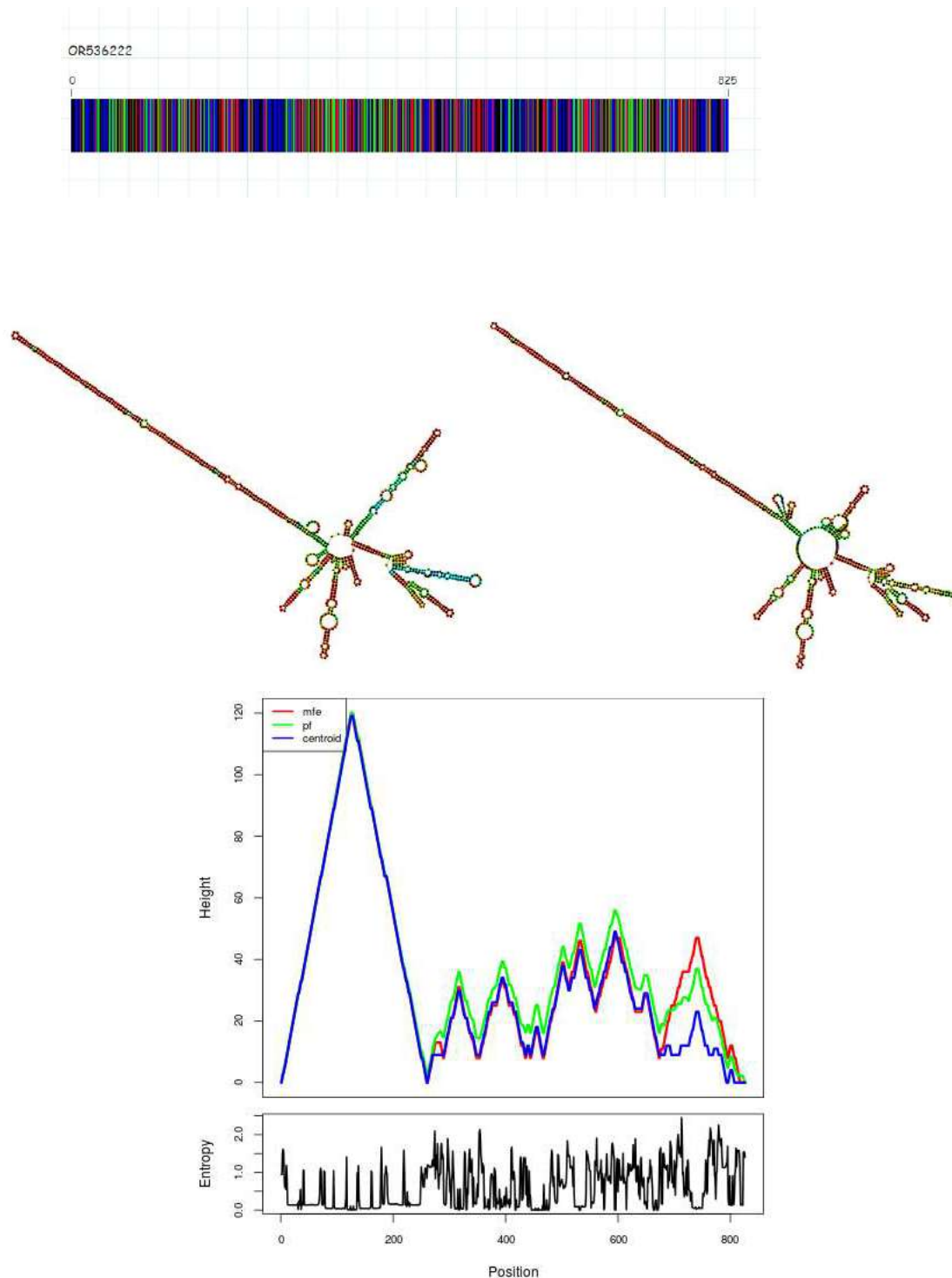


Fig. 8: A comprehensive comparative analysis of the *Aspergillus flavus* river genotype, delving into its genetic and structural characteristics.

distinctive structural characteristics can be employed in generic-level fungal identification. Interestingly, the study found variations in secondary structure topologies, particularly in features like the first stalk and junctions, across different

species. Notably, the phylogenetic trees constructed based on both sequence and secondary structure data exhibited similar cladistics among the four *Aspergillus* species, underscoring the relevance of these RNA structural insights in fungal taxonomy.

CONCLUSION

In conclusion, mycotoxin-producing *Aspergillus* species in natural water sources have significant ecological and public health implications. Molecular methods, including PCR assays, provide rapid and precise species identification. Common *Aspergillus* species were identified using culture media and morphology over six months, with specific *A. flavus* identification based on colony characteristics and specialized media. Genomic DNA extraction from *A. flavus* was efficient. PCR analysis with ITS1/ITS4 primers consistently produced a 600-base pair fragment, confirming genetic uniformity. NCBI BLAST analysis and the ITS2 Database supported *A. flavus* identification. Our study uncovered novel *A. flavus* isolates, underscoring the need for ongoing microbial diversity research. Phylogenetic analysis using ITS sequencing demonstrated its robustness. This approach enhances our understanding of *Aspergillus* diversity and ecological roles, with future research focused on broader diversity exploration and ecological investigations.

ACKNOWLEDGMENTS

The first author extends heartfelt gratitude to the residents of Ganagalawanipeta for their unwavering support and cooperation during this study. Their active participation and invaluable insights have played a pivotal role in shaping the outcomes of this research. Their contributions are deeply cherished and appreciated.

REFERENCES

- Abd-Elsalam, K.A., Khairalla, A.S. and El-Far, M.M. 2000. PCR amplification of rDNA for identification of *Aspergillus* species. *Egypt. J. Microbiology*, 35(1-2): 187-196.
- Aamir, S., Sutar, S., Singh, S.K. and Baghela, A. 2015. A rapid and efficient method of fungal genomic DNA extraction, suitable for PCR-based molecular methods. *Plant Pathol. Quarant.*, 5(2): 74-81. DOI: 10.5943/ppq/5/2/6
- Alrawi, M.A. and Hussein, H.Z. 2017. Molecular identification of fungi *Aspergillus flavus*, which produces a toxin (AFB1) in Iraq. *Pak. J. Biotechnol.*, 14(4): 673-675.
- Battilani, P., Toscano, P. and van der Fels-Klerx, H.J. 2016. Mycotoxin contamination in the EU feed supply chain: A focus on cereal byproducts. *Food Control*, 68: 343-350.
- Bennett, J.W. and Klich, M. 2003. Mycotoxins. *Clin. Microbiol. Rev.*, 16(3): 497-516.
- Brera, C., Catano, C., De Santis, B., Debegnach, F., De Giacomo, M., Mañes, J. and Pogacnik, L. 2023. Emerging mycotoxins in aquatic ecosystems: A comprehensive review. *Environmental Pollution*, 297: 118791.
- Diba, K., Mirhendi, H., Kordbacheh, P. and Rezaie, S. 2014. Development of RFLP-PCR method for the identification of medically important *Aspergillus* species using single restriction enzyme MwoI. *Braz. J. Microbiol.*, 45(2): 503-507. DOI: 10.1590/s1517-83822014000200018
- Gupta, R., Sharma, A. K. and Singh, A. 2023. Ecological and health significance of river water quality. *Environ. Sci. Pollut. Res.*, 30(1): 1-12.
- Hruska, Z., Godoy-Lutz, G., Yao, H., Bai, Y. and Ni, X. 2019. Mycotoxins in aquatic food webs: An underestimated route of exposure to humans? *Environment International*, 129: 158-169.
- Houbraken, J. and Samson, R.A. 2011. Taxonomy of *Penicillium* and *Aspergillus* species used in the food industry. *Food Mycol.*, 7: 107-121.
- Jin, J., Lee, Y.K. and Wickes, B.L. 2004. Simple chemical extraction method for DNA isolation from *Aspergillus fumigatus* and other *Aspergillus* species. *J. Clin. Microbiol.*, 42(9): 4293-4296. DOI: 10.1128/JCM.42.9.4293-4296.2004
- Klich, M.A. and Pitt, J.I. 1988. A laboratory guide to the common *Aspergillus* species and their teleomorphs. CSIRO Division of Food Processing.
- Krimitzas A, Pyrris I, Kouvelis VN, Kapsanaki-Gotsi E, Typas MA. 2013. A phylogenetic analysis of Greek isolates of *Aspergillus* species based on morphology and nuclear and mitochondrial gene sequences. *Biomed Res Int.*, 2013: 260395. DOI: 10.1155/2013/260395
- Krulj, J., Čurčić, N., Stančić, A.B., Kojić, J., Pezo, L., Tukuljac, L.P. and Solarov, M.B. 2020. Molecular identification and characterization of *Aspergillus flavus* isolates originating from Serbian wheat grains. *Acta Aliment.*, 49: 382-389.
- Lorenz, R., Bernhart, S.H., Höner Zu Siederdisen, C., Tafer, H., Flamm, C., Stadler, P.F. and Hofacker, I.L. 2011. ViennaRNA Package 2.0. *Algorithms. Mol. Biol.*, 6: 26.
- Manogaran, G. and Lopez, D. 2017. A survey of big data architectures and machine learning algorithms in healthcare. *J. King Saud Univ.*, 15: 464.
- Mays, J., Khamees, L. and Ahmed, T. 2019. The detection of *Aspergillus flavus* in the milk by molecular method in Diyala Province. *Iraq. J. Biotechnol.*, 18(2): 182-192.
- Mohankumar, M., Vijayasamundeeswari, A., Karthikeyan, M., Mathiyazhagan, S., Paranidharan, V. and Velazhahan, R. 2010. Analysis of molecular variability among isolates of *Aspergillus flavus* by PCR-RFLP of the ITS regions of rDNA. *J. Plant Protect. Res.*, 50(4): 446-451.
- Sarkanj, B., Bosnjak, Z., Peric, M., Kovac, T. and Dzizan, S. 2018. DNA Isolation from *Aspergillus flavus*: optimal method selection. *Food Sci. Technol.*, 10(2): 157-163. DOI: 10.17508/CJFST.2018.10.2.02
- Saitou, N. and Nei, M. 1987. The neighbor-joining method: A new method for reconstructing phylogenetic trees. *Molecular Biology and Evolution*, 4: 406-425.
- Samson, R.A., Visagie, C.M., Houbraken, J., Hong, S.B., Hubka, V., Klaassen, C.H. and Yaguchi, T. 2014. Phylogeny, identification, and nomenclature of the genus *Aspergillus*. *Stud. Mycol.*, 78: 141-173.
- Smith, M. Douhan, G.W., Rizzo, D.M. and Weber, E. 2023. Collecting and voucher documenting fungi for ecological research. *Fung. Ecol.*, 47: 36-41.
- Stoll, M., Piepenbring, M., Begerow, D. and Oberwinkler, F. 2003. Molecular phylogeny of *Ustilago* and *Sporisorium* species (Basidiomycota, Ustilaginales) based on internal transcribed spacer (ITS) sequences. *Canad. J. Bot.*, 81(9): 976-984.
- Thangaraj, M., Bhimba, B.V. and Meenupriya, J. 2011. Phylogenetic relationship in four *Aspergillus* species based on the secondary structure of internal transcribed spacer region of rDNA. *Journal of Advanced Bioinformatics Applications and Research*, 2(3): 200-205.
- Viegas, C., Viegas, S., Jacinto, C., Pádua, M. and Veiga, L. 2021. Fungal contamination in the indoor air of hospital settings. *Microorganisms*, 9(3): 474.



Seasonal Variability of Water Quality for Human Consumption in the Tilacancha Conduction System, Amazonas, Peru

Jaris Veneros^(**) , Llandercita Cuchca Ramos^(***) , Malluri Goñas^(****) , Eli Morales^(*****) ,
Erick Auquiñivín-Silva^(*****) , Manuel Oliva^(*)  and Ligia García^(†) 

*Instituto de Investigación para el Desarrollo Sustentable de Ceja de Selva, Universidad Nacional Toribio Rodríguez de Mendoza de Amazonas, Chachapoyas 01001, Perú

**Department of Ecology, Montana State University, 1156-1174 S 11th Ave, Bozeman, Montana 59715, USA

***Instituto de Investigación en Ingeniería Ambiental (INAM), Universidad Nacional Toribio Rodríguez de Mendoza de Amazonas, Chachapoyas 01001, Perú

****Centro Experimental Yanayacu, Dirección de Supervisión y Monitoreo en las Estaciones Experimentales Agrarias, Instituto Nacional de Innovación Agraria (INIA), Carretera Jaén San Ignacio KM 23.7, Jaén 06801, Cajamarca, Perú

*****Facultad de Ciencias Naturales y Aplicadas, Universidad Nacional Intercultural Fabiola Salazar Leguía de Bagua, Bagua, Perú

*****Facultad de Ingeniería y Ciencias Agrarias, Universidad Nacional Toribio Rodríguez de Mendoza de Amazonas, Chachapoyas 01001, Perú

†Corresponding author: Ligia García; ligia.garcia@untrm.edu.pe

Nat. Env. & Poll. Tech.
Website: www.neptjournal.com

Received: 08-09-2023
Revised: 29-10-2023
Accepted: 08-11-2023

Key Words:

Water quality
Microbiological parameters
Physical parameters
Chemical parameters
Maximum permissible limits

ABSTRACT

This study evaluated the seasonal variability of water quality in the Tilacancha River, the water source that supplies Chachapoyas, and the rural communities of Levanto and San Isidro del Maino of Perú. Eighteen physical, chemical, and microbiological water parameters were evaluated at five sampling points in two seasons (rainy and dry). To determine water quality, the results obtained for the parameters evaluated were compared with the Maximum Permissible Limits (MPL) established in the Regulation on Water Quality for Human Consumption (DS N° 031-2010-SA), approved by the Environmental Health Directorate of the Ministry of Health. In addition, a Pearson correlation was performed to estimate the correlation between the variables evaluated. The results showed that microbiological parameters exceeded the MPLs in both periods evaluated, such as the case of total coliforms (44 MPN.100 mL⁻¹), fecal coliforms (25 MPN.100 mL⁻¹), and *E. coli* (5.45 MPN.100 mL⁻¹), these microbiological parameters reported a positive correlation with turbidity, temperature, total dissolved solids, and flow rate. In addition, aluminum (Al) and manganese (Mn) exceeded the MPL in the rainy (0.26 mg Al.L⁻¹) and dry (1.41 mg.Mn⁻¹.L⁻¹) seasons, respectively. The results indicated that the water of the Tilacancha River is not suitable for human consumption. Therefore, it must be treated in drinking water treatment plants to be used as drinking water.

INTRODUCTION

Population growth and economic development have affected the quantity and quality of the water sources that supply human beings (Tognelli et al. 2016). However, mountain ecosystems represent large water reserves. They are exposed to high human pressure, which threatens the supply of this elemental liquid for its different uses (Wiegandt 2008). Therefore, anthropic activity is one of the main causes of damage to the hydrogeomorphological quality of river systems (Rojas-Briceño et al. 2020). The high vulnerability to water scarcity can lead to the forced migration of millions of people or the overexploitation of these ecosystems, causing

negative impacts on the water resources (Messerli et al. 2004). Therefore, the studies of mountain water systems and the inclusion of the population settled in the lowlands are of great relevance since 7% of these ecosystems provide water resources and 37% other environmental services (Formica et al. 2015). In addition, the alterations that may occur in the headwaters of river basins have repercussions in the lower parts of the basin (Pino et al. 2017) and result in the degradation of water resources, climate, hydrological conditions, ecosystems, and soils, among others (Perez et al. 2018).

The Tilacancha Private Conservation Area (PCA) is home to the Tilacancha and Cruzhuayco sub-basins,

two important sources of water supply, for the city of Chachapoyas, which has a population of approximately 32 589 inhabitants as of 2017 and for the surrounding rural communities (Arellanos 2018, Lucich et al. 2014, Salas et al. 2018). In addition, the Tilacancha PCA provides important ecosystem services related to the provisioning and regulation of water quantity and quality; this provisioning service depends on precipitation, horizontal catchment of remnant forests and grasslands, surface runoff, and aquifers, while quality and quantity regulation services will depend on the soil structures through which water percolates and on the storage capacity of the soil, respectively (Seitz 2015).

The PCA land cover, which is represented by 74.5% grassland, 14.8% forest, 5.2% shrubland, and 4.1% pine forest, is being threatened by deforestation, grassland burning, agriculture, and cattle ranching (CONDESAN 2014) since deforestation rate of 2.06% has been reported in recent years (Salas et al. 2018). In addition, it was reported that the presence of livestock grazing (cattle, horses), wild animals, and land use changes contribute to coliforms and sediments in the river water (Arellanos 2018). In addition, EMUSAP S.R.L (Municipal Company for Drinking Water and Sewerage Services, Chachapoyas, Amazonas) measurements of the amount of water or water flow in recent years report that the rate of water flow has been decreasing (Lucich et al. 2014). Given this scenario, in 2013, EMUSAP, with the support of the National Superintendence of Sanitation Services (SUNASS), developed the Mechanisms of Rewards for Ecosystem Services (MRSE) in the Tilacancha PCA to achieve efficiency in the integrated management of the basin and to serve as a means of compensation through projects and actions for the rural communities of Levanto and Maino, for the conservation of water bodies (Lucich et al. 2014); therefore, EMUSAP S.R.L. has been investing in activities oriented to the implementation of programs aimed at education and training for the conservation of natural resources (SUNASS 2015).

On the other hand, water quality is a key determinant of human well-being and is closely related to health and economic growth (Baque-Miite et al. 2016, Villena 2018). This is essential for countries to establish measures and strategies to achieve sustainable development, taking into account the sanitary situation of the population and the protection of water bodies for their different uses (Villena 2018). Thus, for the quality control of drinking water, several countries have adopted or developed standards and tools based on the determination of concentrations of physical, chemical, and microbiological parameters provided by the World Health Organization (WHO) (Rodriguez-Alvarez et al. 2017). Peru is one of the countries with the greatest

vulnerability to the impacts of climate change on the quantity and quality of water resources. The national government promotes key decisions to counteract these threats to human health, damage to ecosystems, and economic development (Aquino 2017).

Peru also has two regulations for drinking water consumption. The first is the D.S N° 004-2017-MINAM, which approves the Environmental Quality Standards (ECA) for water (MINAM 2017), and the second is the Regulation of Water Quality for Human Consumption D.S N° 031-2010-SA (MINSAs 2010). The first standard establishes the requirements to be met by water bodies according to the category of use designated by the National Water Authority (ANA), while the second establishes the Maximum Permissible Limits (MPL) for microbiological, parasitological, organoleptic, organic and inorganic chemical and radioactive parameters for human consumption water. This standard was promulgated to ensure the safety of water, prevent health risk factors, and promote the health and well-being of the population.

Considering that the quality of water designated for human consumption should be controlled and monitored by measuring physical, chemical, and microbiological parameters (Morales et al. 2019) since they offer multiple advantages as quality indicators due to their ease of quantification (Baque-Miite et al. 2016). This study aimed to determine the seasonal variability of water quality for human consumption, characterizing and comparing 18 physicochemical and microbiological parameters from five sampling points established along the Tilacancha River and the water conduction system to the city of Chachapoyas during the months of February (rainy season) and August (dry season) of 2020.

MATERIALS AND METHODS

Study Area

The Tilacancha PCA is located in the Central Andes of South America, in the Páramo ecoregion of the Cordillera Central, covering the lands of the Levanto and San Isidro del Maino Rural Communities (Fig.1) and this PCA is located at altitudes ranging from 2650 to 3491 meters above sea level and covers an area of 6 800.48 hectares, occupying 4% of the total territory of the Amazon region (Salas et al. 2018). It was recognized as a PCA on July 6, 2010, by Ministerial Resolution N° 118-2010-MINAM, conserving the upper parts of the Tilacancha and Cruzhuayco sub-basins, the mountainous grasslands, the montane forests, and the biological diversity, which contribute to the adequate management and functioning of the Yuyac - Osmal

watershed, guaranteeing ecosystem services over time and contributing to sustainable development (Lucich et al. 2014).

According to the National Meteorological and Hydrological Service of Peru (SENAMHI), the climate of the Tilacancha PCA varies from very humid to cold temperate, generally rainy (Salas et al. 2018), the average annual temperature ranges between 12 °C and 17 °C and the average annual rainfall is 850 mm; however, rainfall records are not regular throughout the year, the months of October to April correspond to a rainy period with an average rainfall of 100 mm/month, while in June to September rainfall decreases to

54 mm/month, with August being the month with the least rainfall (CONDESAN 2014).

Samples and Sampling

Samples were collected in February 2019 and August 2020. For this purpose, five sampling points were established, four of them in the Tilacancha River section, including the catchment, and one at the end of the water conduction line that reaches the city of Chachapoyas (Fig. 1). The selection of the sampling points was carried out taking into account the Protocol for Monitoring the Sanitary Quality

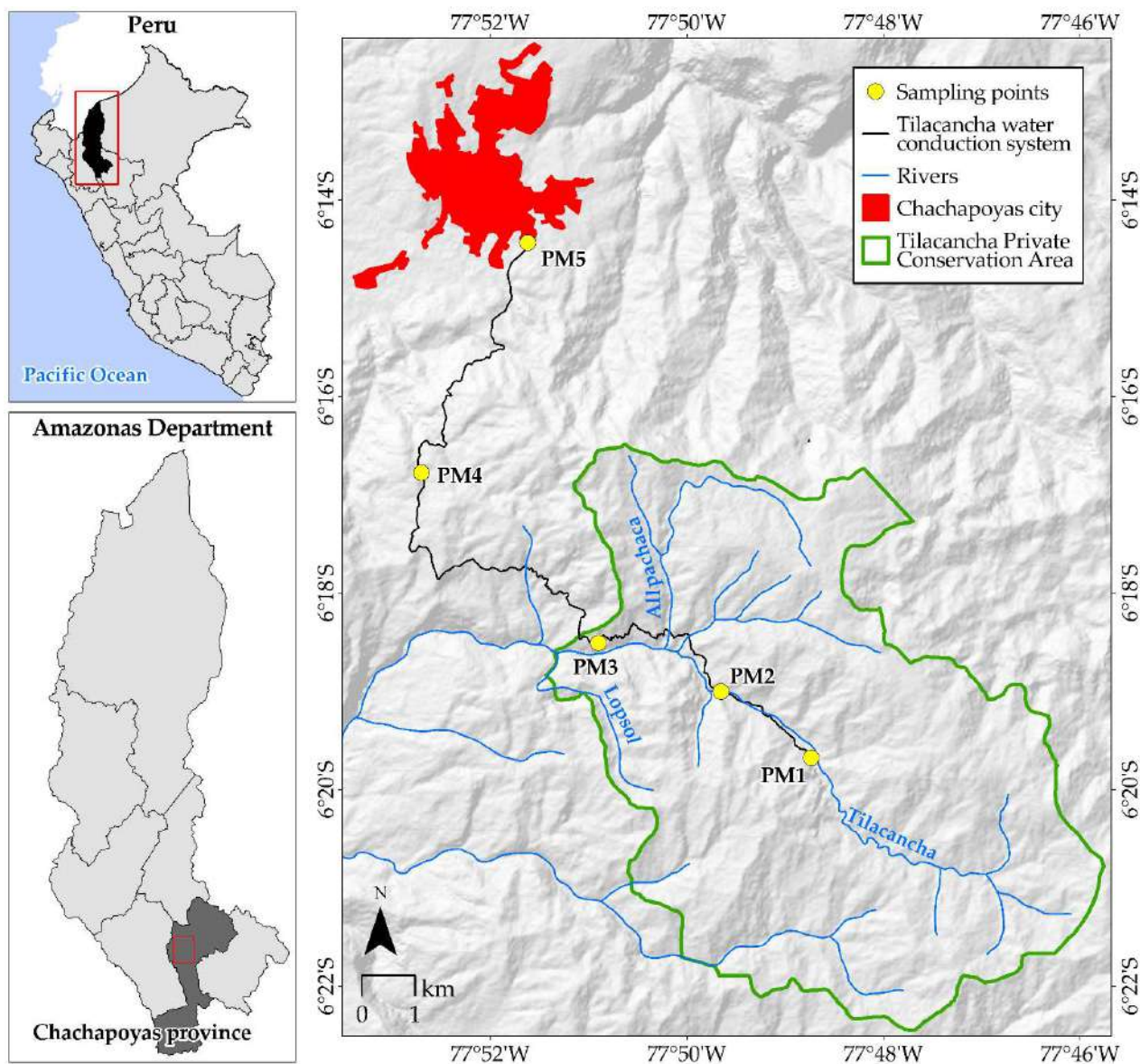


Fig. 1: Tilacancha PCA location.

of Surface Water Resources, Directorial Resolution N° 2254-2007-DIGESA (DIGESA 2007) with appropriate Quality assurance (QA)/quality control (QC) procedures and appropriate standards used for calibration (Konieczka 2007).

In addition, the location of the sampling points was determined according to three criteria: i) Identification: the sites were located so that they were easily identifiable using the Satellite Positioning System (GPS) and recording their UTM coordinates (Table 1); ii) Accessibility: these points were located in places of quick and easy access to collect the samples; iii) Representativeness: taking into account the characteristics of the environment, vegetation cover and the existence of possible factors that influence water quality.

Points PM1, PM2, and PM3 were located along the Tilacancha River, with a minimum separation distance of 1 km (Prat et al. 2012). Point PM4 was located in the water catchment area outside the Tilacacha private conservation area, and point PM5 was located at the end of the water conduction line, located before the entrance to the Chachapoyas Drinking Water Treatment Plant (DWTP) (Table 1).

The samples were collected following the methodology established in the Protocol of procedures for sampling, preservation, conservation, transport, storage, and reception of water for human consumption, as outlined in the Directorial Resolution of the Ministry of Health 160-2015-DIGESA-SA (DIGESA 2015).

Analysis of Physicochemical and Microbiological Parameters

A total of 18 parameters were considered and chosen, taking into of the Supreme Decree DS N° 031-2010-SA (MINSA 2010). The parameters of pH, T° (°C), and EC ($\mu\text{S}\cdot\text{cm}^{-1}$) were measured in the field. They were performed following the Protocol for monitoring the sanitary quality of surface water resources, approved by Directorial Resolution N° 2254-2007-DIGESA (DIGESA 2007). A Multiparameter was used (Hanna, HI 98194), previously inspected to verify its maintenance and calibration. At the time of measurement, surgical gloves were used to avoid direct contact with the

Table 1: UTM coordinates sampling points.

PM	UTM coordinates			Altitude (masl)
	Zone	East	North	
PM1	18	189394	9298678	2939
PM2	18	189112	9299257	2947
PM3	18	188973	9299381	2946
PM4	18	188898	9299661	2941
PM5	18	183468	9309339	2463

sensors and/or contaminate the samples, which could alter the results. For this purpose, the pH sensor also measures the T° at the same time, and the EC was placed in the samples collected in a container previously rinsed directly on the surface of the water of the Tilacancha River; the method recommended in the Protocol for monitoring the sanitary quality of surface water resources approved whit Directorial Resolution N° 2254-2007-DIGESA (DIGESA 2007).

The physicochemical parameters of Total dissolved solids ($\text{mg}\cdot\text{L}^{-1}$), Chlorides ($\text{mg}\cdot\text{Cl}^{-1}\cdot\text{L}^{-1}$), Hardness ($\text{mg}\text{CaCO}_3/\text{l}$), Ammonium ($\text{mg}\cdot\text{N}^{-1}\cdot\text{L}^{-1}$), Iron ($\text{mg}\cdot\text{Fe}^{-1}\cdot\text{L}^{-1}$), Manganese ($\text{mg}\cdot\text{Mn}^{-1}\cdot\text{L}^{-1}$), Aluminum ($\text{mg}\cdot\text{Al}^{-1}\cdot\text{L}^{-1}$), Copper ($\text{mg}\cdot\text{Cu}^{-1}\cdot\text{L}^{-1}$), Zinc ($\text{mg}\cdot\text{Zn}^{-1}\cdot\text{L}^{-1}$), Sodium ($\text{mg}\cdot\text{Na}^{-1}\cdot\text{L}^{-1}$), $\text{mg}\cdot\text{Fe}^{-1}\cdot\text{L}^{-1}$, ($\text{mg}\cdot\text{Mn}^{-1}\cdot\text{L}^{-1}$), Sulfates ($\text{mg}\cdot\text{SO}_4^{-1}\cdot\text{L}^{-1}$), as well as the microbiological evaluation of Total coliforms ($\text{MPN}\cdot 100\text{ mL}^{-1}$ a 35°C), Fecal coliforms ($\text{MPN}\cdot 100\text{ mL}^{-1}$ a $44,5^\circ\text{C}$), *Escherichia coli* ($\text{MPN}\cdot 100\text{ mL}^{-1}$ a $44,5^\circ\text{C}$), were determined according to the methodology by APHA, AWWA, and WEF (American Public Health Association 1999, Walter 1961). For the total dissolved solids, the total dried solids were used. The Turbidity (UNT) was determined with the Nephelometric Method, following EPA specifications (EPA 1970).

Data Analysis

Data analysis was performed by applying the relativization function (Equation 1), transforming the values of the various physicochemical and microbiological parameters to a scale ranging from 0 to 1 (Sepúlveda 2008).

Equation 1

$$f(x) = \frac{x-m}{M-m},$$

Where:

x: Corresponding value of the variable for a given unit of analysis at a given period.

m: Minimum value of the variable in each period.

M: Maximum value of the variable in each period.

This function made it possible to visualize the behavior of the parameters in the rainy and low water seasons concerning the Maximum Permissible Limits established in the regulation by DS N°031-2010-SA. Likewise, a comparison of the averages of each parameter was made with the same regulations and for the same purpose.

In addition, the results of physicochemical and microbiological characteristics were presented in summary tables with mean values and coefficients of variation. The water flow results were subjected to a mean comparison test using Student's t-test to determine the significance of the flow by year of evaluation. Finally, a Pearson correlation was

performed in the R software 4.3.1, which made it possible to evaluate the relationship between the physicochemical and microbiological parameters and the flow rate for the rainy and dry seasons, with significance values of 0.05. The ranges for interpreting the correlation were 0 to 0.3 (0 to -0.3) weak linear relationship, 0.3 to 0.7 (-0.3 to -0.7) moderate linear relationship, and 0.7 to 1 (-0.7 to -1) strong linear relationship (Ratner 2009).

RESULTS

Physicochemical and Microbiological Characteristics of Drinking Water in the Pipeline System as a Function of the Sampling Period

According to Table 2, the results show that none of the physicochemical parameters exceed the MPLs established in the DS N° 031-2010-SA in any of the seasons in which the water samples were taken. As for pH, it is higher during the rainy season (8.38), as is temperature (13.70 °C) and turbidity (3.70 UNT). Electrical conductivity, total dissolved solids, chlorides, and hardness were higher in the dry season with values of 100.70 $\mu\text{S}\cdot\text{cm}^{-1}$, 43.80 $\text{mg}\cdot\text{L}^{-1}$, 7.26 $\text{mg Cl}\cdot\text{L}^{-1}$, and 49.35 $\text{mg CaCO}_3\cdot\text{L}^{-1}$, respectively. Sulfate and ammonium concentrations were also higher in the dry season, with 4.23 $\text{mg SO}_4\cdot\text{L}^{-1}$ and 0.12 $\text{mg N}\cdot\text{L}^{-1}$, respectively.

Concerning to higher concentrations of iron were reported in the rainy season with 0.11 $\text{mg Fe}\cdot\text{L}^{-1}$, and in the dry season, higher concentrations of sodium and zinc were reported with 2.57 $\text{mg Na}\cdot\text{L}^{-1}$ and 0.04 $\text{mg Zn}\cdot\text{L}^{-1}$ respectively, the opposite occurred with copper, which remained stable in both seasons with 0.01 $\text{mg Cu}\cdot\text{L}^{-1}$.

Aluminum (Al) and manganese (Mn) concentrations exceed the MPLs during rainy (0.26 $\text{mg Al}\cdot\text{L}^{-1}$) and dry (1.41 $\text{mg Mn}\cdot\text{L}^{-1}$) periods, respectively, since according to DS N° 031-2010-SA, Al, and Mn concentrations should not exceed 0.2 $\text{mg Al}\cdot\text{L}^{-1}$ and 0.4 $\text{mg Mn}\cdot\text{L}^{-1}$, respectively.

Within the microbiological parameters of the Tilacancha river water in the two study periods, such as total coliforms, fecal coliforms, and *E. coli*, the results exceeded the MPL established in the DS N° 031-2010-SA, and 48.50, 49 and 24 MPN.100 mL^{-1} of water were found, respectively. These values exceed the established in the DS, which determines that it should be less than <1.8 MPN.100 mL^{-1} (Table 3).

Fig. 2 shows the relationship between the values of the physicochemical and microbiological parameters concerning the MPL established in the DS N° 031-2010-SA in the two study stations, using the relativization function (Equation 1); the graph shows that the concentration of microbiological parameters visibly exceeds the LMP whose standardized

Table 2: Physical-chemical characteristics of the water in the drinking water supply system.

Variables	Seasons				MPL
	Rainy		Dry		
	Mean	CV %	Mean	CV %	
pH	8.38	0.02	7.70	0.01	6,5-8,5
T°	13.70	0.06	12.70	0.07	**
Turbidities	1.25	0.60	0.77	0.25	5 NTU
EC	55.40	0.03	89.78	0.03	1500 $\mu\text{S}\cdot\text{cm}^{-1}$
TDS	24.85	0.01	43.80	0.03	1000 $\text{mg}\cdot\text{L}^{-1}$
Chlorides	3.11	0.68	7.26	0.24	250 $\text{mg}\cdot\text{L}^{-1}$
Hardness	33.79	0.07	49.35	0.11	500 $\text{mg CaCO}_3\cdot\text{L}^{-1}$
Sulfates	0.00	0.00	4.23	0.65	250 $\text{mg}\cdot\text{L}^{-1}$
Ammonium	0.02	0.00	0.12	1.76	1.5 $\text{mg N}\cdot\text{L}^{-1}$
Aluminum	0.26*	0.31	0.17	0.19	0.2 $\text{mg}\cdot\text{L}^{-1}$
Copper	0.01	0.48	0.01	0.25	2 $\text{mg}\cdot\text{L}^{-1}$
Iron	0.11	0.11	0.08	0.22	0.3 $\text{mg}\cdot\text{L}^{-1}$
Manganese	0.01	0.34	1.41*	0.50	0.4 $\text{mg}\cdot\text{L}^{-1}$
Sodium	1.90	0.03	2.57	0.16	200 $\text{mg}\cdot\text{L}^{-1}$
Zinc	0.01	0.73	0.04	0.16	3.0 $\text{mg}\cdot\text{L}^{-1}$

* Indicates values that exceed the Maximum Permissible Limits established in the Regulation (DS N° 031-2010-SA).

** The parameter does not apply according to the regulation (DS N° 031-2010-SA).

value is 0, while the other parameters are within the LMP or standard value 1.

Tilacancha River Water Flow Record

Table 4 shows the historical water flow data of the Tilacancha River by EMUSAP S.R.L. for the years 2009 to 2013 (Lucich et al. 2014). In the development of the present investigation, the water flow for the year 2020 was also taken, these data were taken from the same sampling points

Table 3: Microbiological characteristics of the water in the drinking water supply system

Variables	Seasons				MPL
	Rainy		Dry		
	Meam	CV %	Meam	CV %	
Total coliforms	48.5*	0.45	25.6*	0.99	<1.8 MPN.100 mL^{-1}
Fecal coliforms	49*	0.40	25*	1.10	<1.8 MPN.100 mL^{-1}
<i>E. coli</i>	5.45*	0.58	24*	1.10	<1.8 MPN.100 mL^{-1}

* Indicates values that exceed the Maximum Permissible Limits established in the Regulation (DS N° 031-2010-SA).

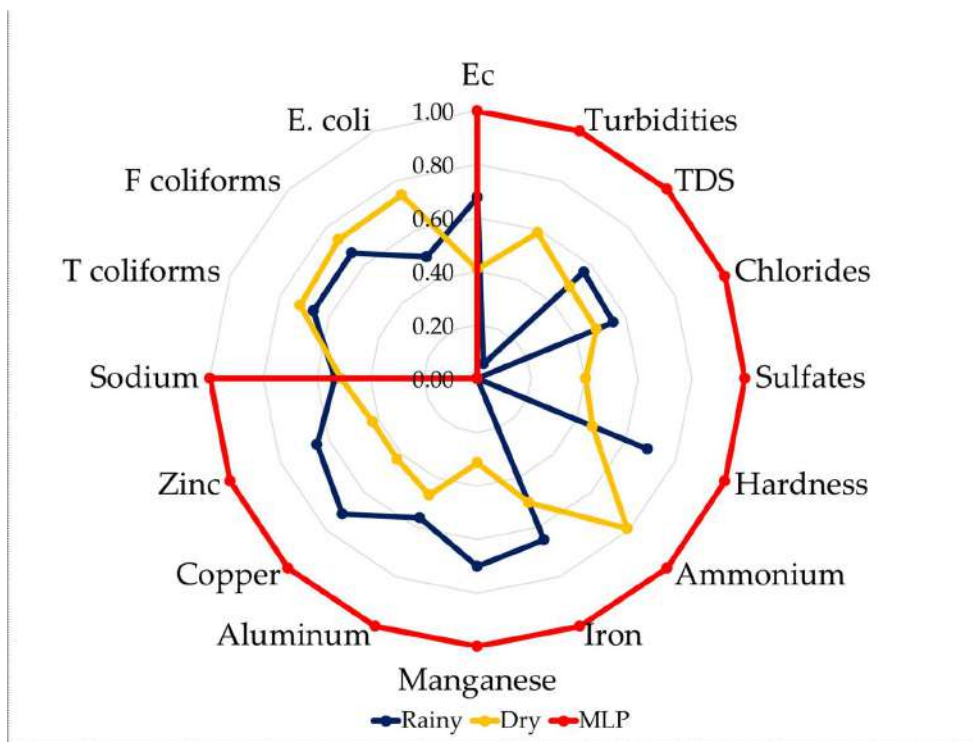


Fig. 2: Level of the relationship of the physicochemical and microbiological parameters concerning the MPLs established in the DS. N° 031-2010-SA

that were found before the treatment plant. The historical water flow of the river reports that in 2009, it had the highest flow ($2.528 \text{ m}^3 \cdot \text{s}^{-1}$), followed by 2011 and 2012 with $1.989 \text{ m}^3 \cdot \text{s}^{-1}$ and $1.727 \text{ m}^3 \cdot \text{s}^{-1}$, respectively. However, there were no significant differences between the years evaluated. On the other hand, for the 2020 year of execution of this research, the lowest water flow value was reported ($0.19485 \text{ m}^3 \cdot \text{s}^{-1}$) for the rainy season (February) with $0.28 \text{ m}^3 \cdot \text{s}^{-1}$ and the dry season (August) with a flow of $0.11 \text{ m}^3 \cdot \text{s}^{-1}$.

Correlation Level of the Physicochemical, Microbiological, and Flow Characteristics of the Tilacancha River

Fig. 3 shows the level of correlation between the physicochemical and microbiological characteristics and the water flow of the Tilacancha River during the rainy season. The pH is strongly positively correlated (blue color and diagonal to the right) with hardness and Na. At the same time, the presence of chlorine has a moderate negative correlation (orange color and diagonal to the left) with the other parameters such as T° , turbidity, EC, TC, FC, *E. coli*, and flow rate, with a strong negative correlation (red color and diagonal to the left).

The temperature (T°) correlated strongly negatively with TDS, TC, FC, Zn, Fe, and Al. Turbidity has a strong

positive correlation with *E. coli* and a moderate correlation with chlorides and a strong negative correlation with Na.

EC was strongly positively correlated with TDS, TC, FC, Al, Cu, Mn, Zn, and flow rate and had a strong negative correlation with *E. coli*. TDS was strongly positively correlated with TC, FC, Al, Cu, Fe, Mn, Zn, flow and negatively correlated with chlorides and *E. coli*. Chlorides had a strong positive correlation only with *E. coli* and a strong negative correlation only with Na. In addition, microbiological parameters such as TC and FC had a strong positive correlation with Al, Cu, Fe, Mn, Zn, and flow rate; *E. coli*, on the other hand, presented a strong negative correlation with Mn, Na, and flow rate. Finally, Aluminum, Copper, Iron, Manganese, Sodium, and Zinc presented a positive correlation between them, generally a strong and moderate one. It should be noted that sulfates and ammonium had values of 0, which means that there is no linear correlation with any of the parameters.

Fig. 4 shows the correlation between the physicochemical and microbiological characteristics and water flow of the Tilacancha River during the low water season. The pH showed a strong correlation and a moderate negative correlation with hardness, sulfates, Cu, Fe, Zn, flow, turbidity, chlorides, ammonium, TC, CF, *E. coli*, and Al. The same was true for T° , which presented a strong negative

Table 4: Tilacancha River flow record for the years 2009-2020.

Months	Caudales [$\text{m}^3 \cdot \text{s}^{-1}$]					
	2009	2010	2011	2012	2013	2020
January	0.338	1.229	1.672	1.316	1.419	
February	2.447	1.808	0.766	2.694	4.341	0.2835
March	2.174	1.261	4.043	2.337	2.532	
April	12.341	1.108	1.874	1.733	0.886	
May	2.434	1.542	8.937	1.495	1.172	
June	1.872	0.945	0.946	6.809	0.978	
July	1.319	0.424	0.700	0.547	0.784	
August	1.211	0.324	0.210	0.279	2.088	0.1062
September	0.795	0.650	0.290	1.051	0.781	
October	1.814	0.494	2.395	1.034	0.639	
November	1.516	0.675	1.308	0.794	0.498	
December	1.074	1.141	0.997	0.639	0.666	
Minimum	0.795	0.324	0.210	0.279	0.498	
Average	2.528 a	0.967 a	1.989 a	1.727 a	1.399 a	0.19485 a
Maximum	12.341	1.808	8.937	6.809	4.341	

Note: The same letters do not report significant statistical differences according to the Student's t-test $p \leq 0.05$.

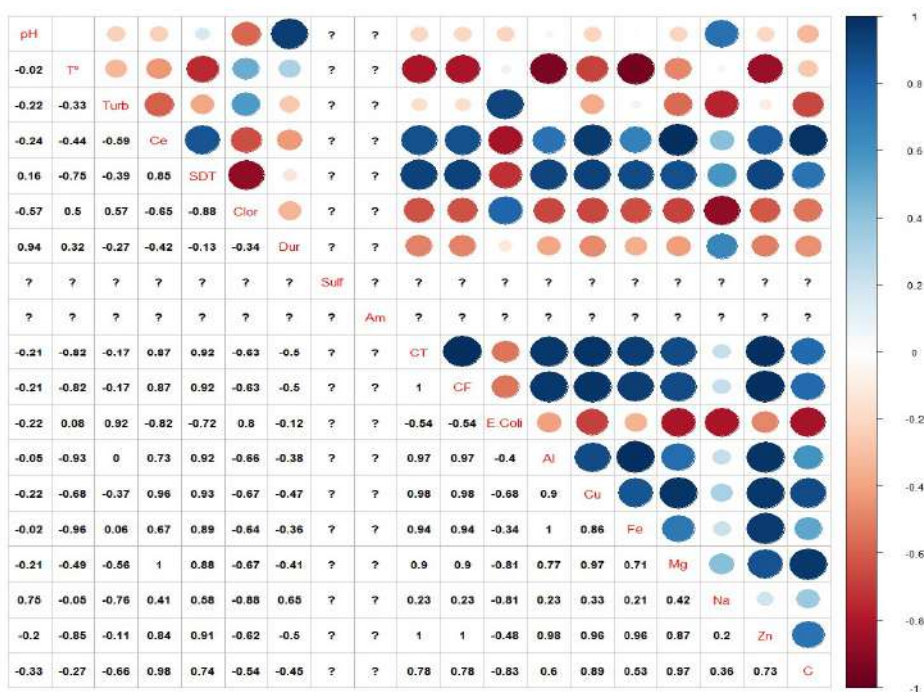


Fig. 3: Correlation of the physicochemical and microbiological characteristics and water flow of the Tilacancha River during the rainy season (? : no data).

correlation with Ce and TDS. Turbidity showed a strong positive correlation with Zn and a negative correlation with Mn. The opposite was true for Ce and TDS, which showed a strong and moderate positive correlation with each other and with TC, CF, *E. coli*, Mn, ammonium, and Fe.

Likewise, chlorides presented a strong and moderate positive correlation with hardness, sulfates, ammonium, Al, Fe, Na, and flow rate, as did hardness, which also presented a strong and moderate positive correlation with sulfates, ammonium, Al, Cu, Fe, and flow rate.

Sulfates, on the other hand, had a strong positive correlation with parameters such as Al, Cu, Fe, Zn, and flow rate and only presented a moderate negative correlation with Mn. Ammonium was strongly positively correlated with all microbiological parameters, Fe, and flow rate. These microbiological parameters (TC, FC, and *E. coli*) were strongly positively correlated with each other and with Fe.

Finally, the Aluminum, Copper, Iron, Manganese, Sodium, and Zinc had a strong positive correlation with Na and flow, as did Cu with Zn and Fe.

DISCUSSION

For sustainable development, water quality is a determining factor that needs to be permanently monitored to avoid possible threats to people’s health (Salvador et al. 2020). Therefore, the study of 18 physicochemical and microbiological parameters of the Tilacancha River and the water conduction line for Chachapoyas in two seasons (rainy and low water) is based on the theory that the use of indicators such as physicochemical and microbiological parameters provide knowledge about the type of water and the various geochemical processes that influence it (Elsayed et al. 2020). In addition to the quantity and physicochemical and microbiological quality of the water, it can be influenced by the climate of the area (Espinal et al. 2013, Morales

et al. 2019) and may be different between rainy and dry seasons (Baque-Miite et al. 2016). This is because rainfall performs different mechanical and chemical processes such as erosion, hydration, hydrolysis, and oxide reduction that promote flooding, runoff, washing of soils, weathering of rocks, and influence the discharge of wastewater (Espinal et al. 2013, Morales et al. 2019). The composition of water, or its physical, chemical, and microbiological constituents, will depend fundamentally on the material through which it flows and with which it comes into contact (Formica et al. 2015, Pino et al. 2017), the seasonal period and sampling depth levels (Leiva-Tafur et al. 2022).

The pH of the water ranged from 8.38 during the rainy season to 7.70 during the dry season, which suggests that there is no notable variation in pH regarding the season, and the values reported are within the range prescribed in the MPLs of DS N°031-2010-SA (between 6.5 to 8.5). If the value is higher than the permitted MPL, it would negatively affect aquatic life, corrosion capacity, and soil alkalinity (Awoyemi et al. 2014).

On the other hand, the values of hardness, total dissolved solids, and electrical conductivity are higher in low water. These results contrast with the theory that suggests that the concentration of these parameters is related to the process of concentration of the flow of this season (Rodriguez-

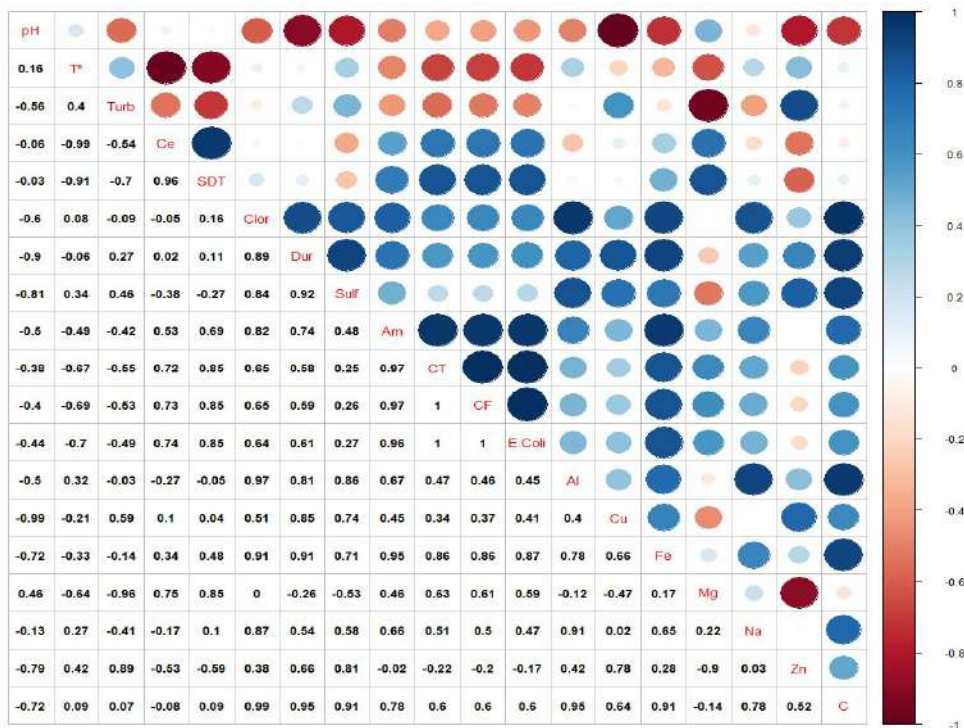


Fig. 4: Correlation of physicochemical and microbiological characteristics and water flow of the Tilacancha River during low water season.

Alvarez et al. 2017). In addition, the electrical conductivity may decrease during wet periods due to the dilution of salts (Akindele et al. 2013). However, the high values of electrical conductivity reflect high values of sodium and chlorides for the dry season, as was found in the results of this research (Awoyemi et al. 2014).

In the case of sulfate and ammonium concentration in the waters of the Tilacancha River, values are within the range of $250 \text{ mg SO}_4\text{.L}^{-1}$ and 1.5 mg N.L^{-1} of the MPL allowed by the DS N° 031-2010-SA were reported; this could be because sulfates in natural waters are found in low concentrations coming from the leaching of sulfide minerals where sulfur is oxidized forming sulfates and increase their concentration when there is contamination, generally due to mining activities. (Awoyemi et al. 2014, Gómez et al. 2004).

On the other hand, concerning the concentrations of microbiological parameters (total coliforms, fecal coliforms, and *E. coli*), exceeding the MPLs makes the Tilacancha River a river with water unfit for human consumption; this may be due to the livestock activities carried out in the area, threatening the conservation of the PCA and contributing pollutants to the water that diminish its quality (Seitz 2015). Microbiological parameters reported higher concentrations in the rainy season or February, which shows that precipitation is the most influential factor for the concentration of coliform bacteria (Seo et al. 2019); as runoff washes soils, washes sediments, and all kinds of pollutants from livestock farming into the rivers (Rodríguez-Alvarez et al. 2017), reasons why water turbidity may also increase during the rainy season. Although the values of physicochemical parameters are lower than the Peruvian regulation DS N° 031-2010-SA, the presence of coliform bacteria alone is a qualitative indicator of contamination, the consequences of which can result in diseases such as gastroenteritis and diarrhea (Seo et al. 2019).

The accumulation and distribution of some physicochemical parameters in freshwater bodies can make them potentially dangerous, producing toxicity when they reach living organisms that make up the food chain (Salas-Mercado et al. 2020). Heavy metal concentrations in the Tilacancha River were reported in the following sequence: $\text{Na} > \text{Al} > \text{Fe} > \text{Cu} > \text{Mn} > \text{Zn}$ in the rainy season and $\text{Na} > \text{Mn} > \text{Al} > \text{Fe} > \text{Zn} > \text{Cu}$. This low concentration of these physicochemical parameters, except for aluminum ($0.26 \text{ mg Al.L}^{-1}$) and manganese ($1.41 \text{ mg Mn.L}^{-1}$) which reported values above the allowed in the LMPs (0.2 mg Al.L^{-1} and 0.4 mg Mn.L^{-1}) in the rainy and dry seasons, respectively, may indicate that there were no significant effects on the suitability of the water for human consumption from the Tilacancha River. The low concentrations of aluminum, copper, iron, manganese, sodium, and zinc in the Tilacancha

River may be because there are no mining and industrial activities in the area, and it is only influenced by the mineralogical characteristics of the soil; the quality of the riparian forest and the heterogeneity of the fluvial habitat is one of the key factors to explain the variability of the water characteristics of the high Andean rivers (Villamarín et al. 2014). In addition, the high concentration of sodium in the Tilacancha River in the two studied periods (1.90 to $2.57 \text{ mg Na.L}^{-1}$ rain and low water, respectively) may be the result of the weathering of silicate minerals in the rocks (1.90 to $2.57 \text{ mg Na.L}^{-1}$ rain and low water, respectively) (Formica et al. 2015), since there is no anthropogenic sodium contamination around the river.

Concerning the metals that exceeded the LMP, such as manganese, with $1.41 \text{ mg Mn.L}^{-1}$ in the dry season, and aluminum, with $0.26 \text{ mg Al.L}^{-1}$ in the rainy season may be due to the soil textural classes of the PCA, where sandy and clay soils predominate (Pereyra-Cachay 2020). In addition, surface waters in contact with sandstone, silicate, limestone, and dolomite rocks accumulate aluminum, manganese, and iron (Ifatimehin & Ojochenemi 2021) because the decomposition of organic matter eliminates dissolved oxygen and generates carbon dioxide, causing manganese and iron to be incorporated as soluble compounds (Chan et al. 2022). In the case of soils, the presence of manganese and aluminum indicates that they have an acid pH, influenced by the fluctuation of climatic factors such as precipitation and evapotranspiration, which cause the dissolution of rocks and minerals (Salinas 1979, Thomas 2015).

The flow of the Tilacancha River during the rainy season was higher than during the dry season, with $0.28 \text{ m}^3\text{.s}^{-1}$ and $0.11 \text{ m}^3\text{.s}^{-1}$, respectively, which may show that the low rainfall of 54 mm/month in August may influence the water level, reducing the flow by between 8 and 14 L.s^{-1} (CONDESAN 2014). However, they may also be due to the impacts of climate change, deforestation, and the periodic burning of forests and grasslands due to a lack of environmental awareness, which may decrease water supply while demand is growing (Lucich et al. 2014).

The positive correlation between turbidity, temperature, total dissolved solids, flow rate, total coliform, fecal coliform, and *E. coli* content indicates that the lower the concentration of turbidity, total dissolved solids, lower temperature, and flow rate in the Tilacancha River water, the better the water quality, as the microbiological load of the water decreases. High water turbidity increases the concentration of microorganisms, affecting drinking water quality (Montoya et al. 2011). The same happens with the water temperature since it determines the concentration of many parameters. If the T° increases, the chemical reactions

also increase. Still, the solubility of gases decreases, and the respiration rate of microorganisms increases, leading to higher consumption of oxygen and decomposition of organic matter (Akindele et al. 2013). Under this scenario, contaminated water requires drinking water treatment before consumption (Baque-Miite et al. 2016). When physical, chemical, and microbiological parameters exceed the MPL, intensive and sectorized monitoring of water sources must be carried out to determine the sources of contamination (Morales et al. 2019).

CONCLUSIONS

According to the 18 physico-chemical and microbiological parameters evaluated, the water from the Tilacancha in the drinking water conveyance system before being treated (at the DWTP) is not suitable for human consumption from the microbiological point of view, both in the rainy and dry seasons, since the bacteria of the Coliform group exceeded the MPLs prescribed in the DS N° 031-2010-SA. There is a dynamic of positive and negative correlations between all parameters, except for sulfates and ammonium, where there is no linear correlation with any of the parameters. These results suggest that the variability of the chemical composition of the water in the different seasons was altered by both anthropogenic and/or natural sources surrounding the water conveyance system. Thus, it is suggested to use this information for water quality management in Tilacancha.

ACKNOWLEDGMENTS

We acknowledge the support given by EMUSAP.

REFERENCES

- Akindele, E., Adeniyi, I. and Indabawa, I. I. 2013. Spatio-temporal assessment and water quality characteristics of Lake Tiga, Kano, Nigeria. *Res. J. Environ. Earth Sci.*, 5(2): 67-77. doi: 10.19026/rjees.5.5640.
- American Public Health Association. 1999. Standard Methods for the Examination of Water and Wastewater. APHA, AWWA, WPCF, Washington.
- Aquino, P. 2017. Water Quality in Peru: Challenges and Contributions for Sustainable Wastewater Management. Law, Environment and Natural Resources (DAR), Lima, Peru.
- Arellanos, E. 2018. Sustainability Scenarios of the Water Service in the Tilacancha River Microbasin based on the Estimated Willingness to Pay with two Econometric Models. Toribio Rodríguez National University of Mendoza de Amazonas.
- Awoyemi, O., Albert A. and Aderonke, O. 2014. The physicochemical quality of groundwater in relation to surface water pollution in the Majidun area of Ikorodu, Lagos State, Nigeria. *Am. J. Water Res.*, 2(5): 126-33. doi: 10.12691/ajwr-2-5-4.
- Baque-Miite, R., Simba-Ochoa, L., González-Ozorío, B., Suatunce, P., Díaz-Ocampo, E. and Cadme-Arevalo, L. 2016. Calidad del agua destinada al consumo humano en un Cantón de Ecuador. *Rev. Cienc. Unemi*, 9(20): 109-117.
- Chan, S. S., Shiong-Khoo, K., Wayne-Chew, K., Chuan-Ling, T. and Loke-Show, P. 2022. Recent advances biodegradation and biosorption of organic compounds from wastewater: microalgae-bacteria consortium - A review. *Bioresour. Technol.*, 344: 126159. doi: 10.1016/j.biortech.2021.126159.
- CONDESAN. 2014. DHR report on the Tilacancha River Microbasin. 64 DIGESA. 2007. Protocol for Monitoring the Sanitary Quality of Surface Water Resources. 21. Ministry of Health.
- DIGESA. 2015. Protocol of Procedures for Sampling, Preservation, Conservation, Transport, Storage and Reception of Water for Human Consumption. 23.
- Elsayed, S., Hussein H., Moghanm F., Khendher, K., Eid, E. and Gad M. 2020. Application of irrigation water quality indices and multivariate statistical techniques for surface water quality assessments in the Northern Nile Delta, Egypt. *MDPI Water*, 12(12): 3-26. <https://doi.org/10.3390/w12123300>.
- Espinal, T., Sedeño, J. and López, E. 2013. Evaluation of water quality in the Yuriria lagoon, Guanajuato, Mexico, using multivariate techniques: A valuation analysis for two periods 2005, 2009-2010. *Rev. Int. Contam. Ambient.*, 29(3): 209-16.
- Formica, S.M., Andrea-Sacchi, G., Agustina-Campodonico, V., Inés-Pasquini, A. and Alejandra-Cioccale, M. 2015. Modeling water quality in mountain rivers with anthropogenic impact. case study: Small mountain range of Córdoba, Argentina. *Rev. Int. Contam. Ambient.*, 31(4): 327-41.
- Gómez, A., Villalba, A., Acosta, G., Castañeda, M. and Kamp, D. 2004. Heavy metals in the surface water of the San Pedro River during 1997 and 1999. *Rev. Int. Contam. Ambient.*, 20(1): 5-12.
- Ifatimehin, O.O. and Ojochenemi, A. 2021. Kogi State : Environment, Society and Development. *Development*, 1: 21. doi: 10.54164/bk.dgev.2021.1.
- Koniczka, P. 2007. The role of and the place of method validation in the quality assurance and quality control (QA/QC) system. *Crit. Rev. Anal. Chem.*, 37(3): 173-90. doi: <https://doi.org/10.1080/10408340701244649>.
- Leiva-Tafur, D., Goñas, M., Culquí, L., Santa Cruz, C., Rascón, J. and Oliva-Cruz, M. 2022. Spatiotemporal distribution of physicochemical parameters and toxic elements in Lake Pomacochas, Amazonas, Peru. *Front. Environ. Sci.*, 10(September). <https://doi.org/10.3389/fenvs.2022.885591>
- Lucich, I., Alvarado, A., Bohorquez, E., Villar, D. and Pineda, R., 2014. Advances in the Regulatory Framework of Remuneration Mechanisms for Hydrological Ecosystem Services: The Case of the Tilacancha Private Conservation Area. NEGRAPATA S.A.C., Lima, Peru
- Messerli, B., Viviroli, D. and Weingartner, R. 2004. Mountains of the world: Vulnerable water towers for the 21st century. *AMBIO J. Hum. Environ.*, 33(13): 29. doi: 10.1007/0044-7447-33.sp13.29.
- Ministerio de Salud (MINSU). 2010. DS N° 031-2010-SA: Reglamento de la Calidad del Agua Para Consumo Humano.
- Ministerio del Ambiente (MINAM). 2017. DECRETO SUPREMO N° 004-2017-MINAM: Aprueban Estandares de Calidad Ambiental (ECA) Para Agua y Establecen Disposiciones Complementarias.
- Montoya, C., Loaiza, D., Torres, P., Cruz, C. and Escobar, J. 2011. Effect of the increase in raw water turbidity on the efficiency of conventional purification processes. *Rev. EIA*, 8(16): 137-48.
- Morales, E., Solano, M., Morales, R., Reyes, L., Barrantes, K., Achí, R. and Chacón, L. 2019. Evaluation of the influence of climatic seasonality on the quality of water for human consumption in a supply system in San José, Costa Rica, period 2017-2018. *Rev. Costarr. Salud Pública*, 28(1): 48-58.
- Pereyra, C., Humberto, C. 2020. Current and future situation of soil water erosion in the ACP Tilacancha, Chachapoyas. Toribio Rodríguez Mendoza Amaz National Univ.

- Perez, D., Segovia, J., Cabrera, P., Delgado, I. and Martins, M. 2018. Land use and its influence on the pressure and degradation of water resources in hydrographic basins. *Rev. Investig. Agraria Ambient.*, 9(1): 41-57. doi: 10.22490/21456453.2089.
- Pino, E., Tacora, P., Steenken, A., Alfaro, L., Valle, A., Chávarri, E., Ascencios, D. and Mejía-Marcacuzco, J.A. 2017. Effect of environmental and geological characteristics on water quality in the Caplina River Basin, Tacna, Peru. *Tecnol. Cienc. Agua*, 8(6):77-99. doi: 10.24850/j-tyca-2017-06-06.
- Prat, N., Rieradevall, M. and Fortuño, V. 2012. Metodología F.E.M para la Evaluación del Estado Ecológico de los Ríos Mediterráneos, pp. 1-44.
- Ratner, B. 2009. The correlation coefficient: its values range between +1/-1, or do they? *J. Target Meas. Anal. Mark.*, 17: 139-42. doi: <https://doi.org/10.1057/jt.2009.5>.
- Rodriguez-Alvarez, M.S., Moraña, L.B., Salusso, M.M. and Seghezze, L. 2017. Spatial and seasonal characterization of drinking water from various sources in a peri-urban town of Salta. *Rev. Argent. Microbiol.*, 20: 6 doi: <https://doi.org/10.1016/j.ram.2017.03.006>.
- Rojas-Briceño, N., Barboza Castillo, E., Gamarra Torres, O., Oliva, M., Leiva Tafur, D., Barrena Gurbillón, M., Corroto, F., Salas López, R. and Rascón, J. 2020. Morphometric prioritization, fluvial classification, and hydrogeomorphological quality in high Andean livestock micro-watersheds in Northern Peru. *Int. J. Geo-Inf.*, 9(5): 305. <https://doi.org/10.3390/ijgi9050305>
- Salas, R., Barboza, E., Rojas, N., Mamani, J. and Rodriguez, N. 2018. Deforestation In the Tilacancha private conservation area: water recharge and water supply zone for Chachapoyas. *Rev. Investig. Agroprod. Sustentable*, 2(3): 54-64. doi: 10.25127/aps.20182.393.
- Salas-Mercado, D., Hermoza-Gutiérrez, M. and Salas-Ávila, D. 2020. Distribution of heavy metals and metaloids in surface waters and on sediments of the Crucero River, Peru. *Water*, 37(4): 185-93. doi: 10.34098/2078-3949.37.4.1.
- Salinas, J.G. 1979. Adaptación de Plantas a Toxicidades de Aluminio y Manganeso En Suelos Ácidos. Bogotá.
- Salvador, D., Caeiro, M., Serejo, F., Nogueira, P., Neves, R. and Neto, C. 2020. Monitoring waterborne pathogens in surface and drinking waters: Are water treatment plants (WTPs) simultaneously efficient in the elimination of enteric viruses and fecal indicator bacteria (FIB)? *MDPI: Water*, 12(10): 2-17. doi: <https://doi.org/10.3390/w12102824>.
- Seitz, G. 2015. Retribuciones Individuales y Colectivas en el Marco de Conformación del Fondo Virtual del Agua de Tilacancha, pp. 1-30.
- Seo, M., Lee, H. and Kim, Y. 2019. Relationship between coliform bacteria and water quality factors at weir stations in the Nakdong River, South Korea. *Water*, 11: 1171. doi: <https://doi.org/10.3390/w11061171>.
- Sepúlveda, Se. 2008. Methodology to Estimate the Level of Sustainable Development of Territories. IICA, San José, Costa Rica.
- SUNASS. 2015. Emusap Invertirá s/. 2.8 Millones para Mejorar Servicio de Agua Potable en Chachapoyas.
- Thomas, M. 2015. PH, aluminum and environmental factors in soils under forests of the Central Cordillera, Dominican Republic. *Rev. Geogr. Venez.*, 56(1): 59-71.
- Tognelli, M. F., Lasso, C. A., Bota-sierra, C. A., Jiménez-segura, L. F. and Neil A. Cox. 2016. Conservation and Distribution Status of Freshwater Biodiversity in the Tropical Andes. Gland, Switzerland, p. 199.
- United States Environmental Protection Agency (US EPA). 1970. Plan de Reordenamiento N° 03 de 1970.
- Villamarín, C., Prat, N. and Rieradevall, M. 2014. Caracterización Física, Química e Hidromorfológica de los Ríos Altoandinos Tropicales de Ecuador y Perú. *Latin American Journal of Aquatic Research*, 42(5): 1072-86. doi: 10.3856/vol42-issue5-fulltext-12.
- Villena, J. 2018. Water quality and sustainable development. *Revista Peruana de Medicina Experimental y Salud Pública*, 35(2): 304. doi: 10.17843/rpmpesp.2018.352.3719.
- Walter, W. G. 1961. Standard Methods for the Examination of Water and Wastewater. Eleventh edition. Springer, New York.
- Wiegandt, E. 2008. Framing the study of mountain water resources: an introduction. *Adv. Glob. Chang. Res.*, 31: 3-13. doi: 10.1007/978-1-4020-6748-8_1.

ORCID DETAILS OF THE AUTHORS

- Jaris Veneros: <https://orcid.org/0000-0001-6981-4078>
Llandercita Cuchca Ramos: <https://orcid.org/0000-0002-2996-2786>
Malluri Goñas: <https://orcid.org/0000-0002-4972-3467>
Eli Morales: <https://orcid.org/0000-0002-8623-3192>
Erick Auquiñivín-Silva: <https://orcid.org/0000-0002-9226-9896>
Manuel Oliva: <https://orcid.org/0000-0002-9670-0970>
Ligia García: <https://orcid.org/0000-0001-7508-7516>



Study on the Technology of Ultrasonic, Chemical and Mechanical Combined Treatment of Oilfield Aging Oil

Le Zhang*†, Jin Hu**, Longlong Yan**, Si Chen*, Yabin Jin*, Huan Zhang***, Zhe Shen* and Tao Yu****

*The Institute of Energy and Architecture, Xi'an Aeronautical Institute, Xi'an 710077, PR of China

**No.10 Oil Production Plant, Changqing Oilfield Company, Oingyang 745100, PR of China

***College of Chemistry and Material, Weinan Normal University, 714099, PR of China

****College of Chemistry and Chemical Engineering, Shaanxi Province Key Laboratory of Environmental Pollution Control and Reservoir Protection Technology of Oilfields, Xi'an Shiyou University, 710065, PR of China

†Corresponding author: Le Zhang: zl_202106011@163.com

Nat. Env. & Poll. Tech.
Website: www.neptjournal.com

Received: 27-09-2023

Revised: 10-11-2023

Accepted: 15-11-2023

Key Words:

Aging oil
Oil recovery rate
Ultrasound treatment
Mechanical dehydration

ABSTRACT

Aging oil is a common pollutant in petrochemical enterprises due to its severe emulsification and flocculation, poor settling performance, low oil recovery rate, and high difficulty in treatment. This article adopts the method of mechanical, ultrasonic, and chemical coupling demulsification to treat aging oil, with the water content and oil recovery rate of the treated aging oil as the inspection indicators. The experiment shows that when the oil-water ratio is 1:4, the heating temperature is 50°C, the stirring speed is 180rpm, the ultrasonic frequency is 25kHz, the power is 40W, the ultrasonic time is 25min, and the pH is adjusted to 3-4. The additional amount of FeSO₄ is 160mg/L, the additional amount of H₂O₂ is 0.11%, and the heating stirring reaction is 40min. When the dosage of cationic PAM with an ion degree of 50 is 35mg/L, the centrifugation speed is 3200rpm. The centrifugation time is 20 min, the crude oil recovery rate after aging oil treatment can reach over 94.6%, and the water content of the treated crude oil is less than 0.5%, meeting the standards for crude oil gathering and transportation in China. The oil content in the water generated after aging oil treatment is about 150 mg.L⁻¹, the suspended solids content is 200 mg.L⁻¹, the oil content in the residue is 6%, and the water content is 53%. By analyzing the appearance of aging oil before and after treatment, it was found that when using this process to treat aging oil, the original spatial cross-linking network structure of the aging oil was broken, allowing the water droplets wrapped in the oil to be released, thereby significantly reducing the water content in the recovered oil and improving the oil recovery rate.

INTRODUCTION

At present, with the extensive application of tertiary oil recovery technology in the mid to late stage of oilfield development, the crude oil recovery rate is constantly improving. At the same time, the emulsification and complexity of the produced liquid are greatly increased (Anisimov et al. 2018). In addition, under the combined action of transportation, standing, temperature, oilfield chemicals, and various mechanical impurities, aging oil with diverse structures and forms, which stably exists in the form of emulsion in all aspects of the entire treatment system, has emerged (Appazov et al. 2021). The source of aging oil is complex, and in the early stages of reservoir development, aged oil mainly comes from the leakage of wellbore, landing crude oil, drilling waste liquid, and emulsified crude oil with a large number of oilfield chemicals added during the oil testing and production process (Hamidi et al. 2021a).

In the process of crude oil production, the aging oil mainly comes from the waste liquid from the workover, the sewage treatment system of the joint station, the bottom oil of the settling tank, and other waste liquid tanks (Chang et al. 2023). The main sources are the following four aspects: (1) Gathering and transportation system: During the oil production process, a large amount of chemical agents, such as demulsifiers, need to be added to the produced liquid (Chen et al. 2022a). Due to the high complexity of the incoming liquid, the compatibility of the agents is not good, resulting in demulsified crude oil re-emulsification. Combined with the solid particles and polymer generated in the environment of the gathering and transportation system, the old oil and residue are formed (Chen et al. 2022b); (2) Waste liquid pool: During drilling and workover operations, most of the waste liquid will eventually accumulate in an open-air waste liquid pool (Coleman 2021). During storage, it will be exposed to sunlight. Under conditions of full contact

with air, the light components will continue to evaporate, resulting in the formation of aged oil due to the floating of crude oil (Dalhat et al. 2022) (3) Ground crude oil: During the process of oil and gas field exploitation, especially during drilling and workover operations, it is inevitable to produce ground crude oil. During the process of recovering ground crude oil, the mixture of crude oil with clay, quartz sand, and other substances causes the stability of the crude oil properties to form aged oil (Deng et al. 2021a); (4) Tank bottom sludge: In the produced liquid treatment system, the settling tank is an important component (Deng et al. 2021b). During the treatment process, a large amount of oily sludge is generated at the tank bottom, and eventually, stable aging oil is produced in the oily sludge treatment plant (Dhote et al. 2018).

The diverse sources of aged oil result in its extremely complex composition, with different sources of aged oil being different (Duan M et al. 2019). The formation of aged oil is closely related to its composition. On the one hand, the extensive use of oilfield chemicals in tertiary oil recovery has led to the joint action of polymers, alkalis, surfactants, and natural surfactants such as resins and asphaltenes in aged oil, increasing the emulsification degree of aged oil (Envelope et al. 2022). On the other hand, aged oil also contains conventional substances such as clay, sediment, mechanical impurities, suspended solids, sulfides, and metal oxide micelles (Gao et al. 2018). Under the combined action of suspended solids and solid particles, metal oxides, and sulfide micelles, the stability of aged oil is further strengthened (Gong et al. 2018).

The hazards of aging oil in oil fields are specifically manifested in the following aspects:

- (1) The properties of aged crude oil are stable, with a density between normal crude oil and water (Hamidi et al. 2021b). It always exists between the dehydrated crude oil and water phase under the action of gravity sedimentation, resulting in a decrease in dehydration efficiency and a significant delay in the separation progress of the oil phase and water phase, increasing sedimentation time and operating costs (Jerez et al. 2022).
- (2) The aging oil emulsion contains a large amount of highly conductive mechanical impurities such as sand and clay, which can easily form short circuits and cause equipment tripping after entering the electric dehydrator, and even cause safety accidents, damaging the electric dehydrator equipment (Khazaal et al. 2021).
- (3) The strong stability of aging oil requires the use of specific demulsifiers during demulsification and

dehydration, and the increased dosage increases economic costs and equipment losses, resulting in a decline in overall economic benefits (Kurilkina et al. 2021).

- (4) During the storage and transportation of aged oil in the dehydration system of the joint station, a large number of sulfate-reducing bacteria will proliferate, and the raw materials and energy for proliferation come from the sulfate in the crude oil (Lee & Jou 2022). During aerobic or anaerobic respiration, sulfate-reducing bacteria generate hydrogen sulfide, corroding metals, and forming ferrous sulfide micelles. The micelles and the flocculent structure of sulfate-reducing bacteria work together to further enhance the stability of aged crude oil (Linhares et al. 2022).

With the continuous development of crude oil extraction, environmental protection is increasingly valued, and the use of green and safe demulsification methods to reduce the harm of aging crude oil has become more significant (Martínez González et al. 2018). Emulsion demulsification is mainly based on two changes: one is to reduce the strength or change the nature of the interfacial facial mask, and the other is to increase the tendency of droplet aggregation and demulsification (Muratova et al. 2022).

At present, the treatment technologies for aged oil at home and abroad mainly include thermochemical dehydration, centrifugal electric dehydration, ultrasonic dehydration, microbial dehydration technology, etc. (Neto et al. 2023). To solve the problem of demulsification and dehydration of aged oil, the article conducted low-cost and rapid demulsification/dehydration technology research experiments on aged oil using a combination of ultrasound, chemistry, and mechanical dehydration methods based on the characteristics of aged oil. This solved the problems of low recovery rate and difficulty in demulsification of aged oil in oil fields.

MATERIALS AND METHODS

Materials

Thermostatic heating magnetic stirrer (MS7-H550-Pro), ultrasonic cleaning instrument (JP030), low-speed centrifuge (H2-16KR), pH meter (pHS-3C), Soxhlet extractor, water separator, electric heating sleeve (250 mL), electric blast drying oven (DHG-9140), infrared oil measuring instrument (HD-HC500) and vacuum circulation pump were used in this experiment.

Analytical grade concentrated sulfuric acid (H_2SO_4), ferrous sulfate ($FeSO_4$), and hydrogen peroxide solution (H_2O_2 , 30%) were used in the experiment. Industrial-grade Cationic polyacrylamide (PAM, Ionization degree 50) was

Table 1: Analysis of Oil and Water Content of Aging Oil.

Project	Oil content [%]	Water content [%]	Solid content [%]
Aging Oil	43.82	52.64	3.54

used in this experiment.

Aging oil samples were taken from the Nanyang Oilfield Oil Mud Reduction Treatment Station of China Petroleum and Chemical Corporation. These samples were stored in a refrigerator at 4°C to minimize biological and chemical reactions as much as possible. The general characteristics of the aging oil samples from the workplace are shown in Table 1.

Experimental Procedure

Take a certain amount of aged oil from a 500 mL beaker, mix it with a certain proportion of water, and place it in a constant temperature heating magnetic stirrer. Start stirring and heating, and heat it to a certain temperature. Take out the beaker, place it in an ultrasonic cleaning device at the same temperature, and activate the ultrasonic function to break the oil-water interface for the first time through the ultrasonic function. After a certain time of ultrasonic treatment, take out the beaker and put it back into the constant temperature heating magnetic stirrer. The mixing and heating functions continue to be turned on. Then add H₂SO₄ solution to the aging oil to adjust the pH of the system to 4~4.5, and then add FeSO₄ and H₂O₂ into the beaker quickly in turn, and continue to stir for a certain time so that the agent can fully contact the aging oil, further break the oil-water interface, and improve the performance of the oil-water interface facial mask. After stirring, the aged oil is subjected to centrifugal dehydration treatment. After centrifugation, the water content in the separated upper oil phase is measured, and the volume of the separated upper oil is measured.

Analytical Methods

The pH of aged oil was measured using a pH meter (PHS-3C, Shanghai Youke Instrument Co., Ltd).

The determination method of water content in oil was in accordance with the method specified in the Determination of Water Content in Crude Oil Distillation Method (GB/T 8929-2006).

The oil recovery rate was calculated by using the following equation:

$$\text{Oil recovery rate: } \varphi = \frac{N}{M} \times 100\%$$

where φ is the oil recovery rate (%), N is the volume of recovered crude oil (mL), and M is the Volume of oil in aged oil (mL).

RESULTS AND DISCUSSION

Mechanical Demulsification Experiment

Oil-water ratio: Due to the high viscosity and poor water dispersibility of aged oil, the effect of directly adding water-soluble demulsifier additives is not ideal (Nezhdbahadori et al. 2018). Consider adding a certain proportion of water to the aging oil to mix it with water, allowing water-soluble demulsifiers to come into full contact with the aging oil to achieve a demulsification effect (Ramirez et al. 2019).

Mix aged oil and water in the proportions of 1:2, 1:3, 1:4, 1:5, and 1:6, respectively. Heat the experimental oil sample with the adjusted oil-water ratio in a 60°C thermostatic magnetic stirrer, and adjust the stirring speed to 200 rpm for 30 min. After stirring, let it stand for another 30 min. Using the water content of the upper oil sample after standing as an indicator, investigate the effect of the oil-water ratio on

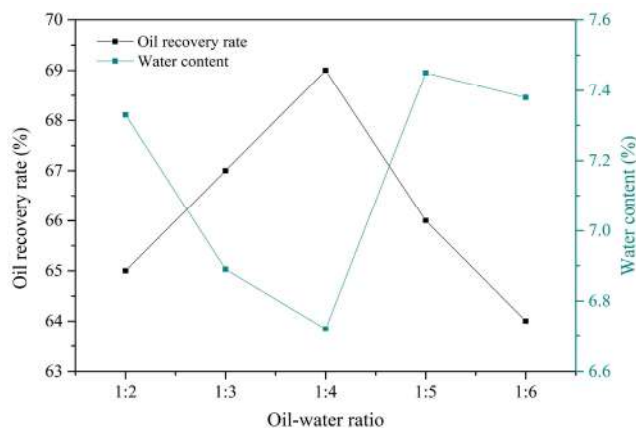


Fig. 1: The effect of the oil-water ratio on the demulsification effect of aged oil.

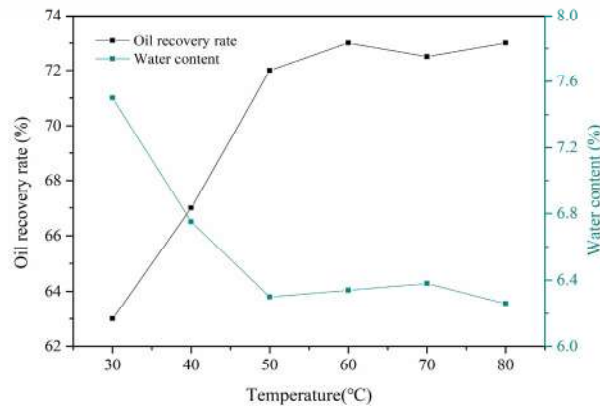


Fig. 2: The effect of heating temperature on the demulsification effect of aged oil.

the demulsification effect. The experimental results are shown in Fig. 1.

When other conditions are constant, as the amount of water added increases, the dispersion effect of the oil phase also increases, and the demulsification effect is obvious. The water content of the treated upper oil sample can be reduced to 7.5%, and the oil recovery rate also increases to 69%, as shown in Fig. 1. But when the water addition ratio exceeds 1:4, the water content of the treated upper oil sample increases with the increase of water content, and the oil recovery rate also decreases. Due to the high water content and unreasonable particle grading in the aging oil system, the demulsification effect of the aging oil will be seriously affected. Therefore, further increasing the water addition ratio will lead to a poor dehydration effect. Therefore, the optimal ratio of oil to water selected is 1:4.

Heating temperature: Due to the significant differences in the flowability of aged oil at different temperatures and the significant impact of temperature on the effectiveness of the agent, selecting the temperature with the best demulsification

effect is one of the key influencing factors (Tessaro et al. 2021).

Mix the aged oil and water in a 1:4 ratio, and heat the experimental oil samples with the adjusted oil-water ratio in a thermostatic magnetic stirrer at 30°C, 40°C, 50°C, 60°C, 70°C, and 80°C, respectively. Adjust the stirring speed to 200 rpm, continue stirring for 30 min, and then let stand for 30min. Using the moisture content of the upper oil sample after standing as an indicator, investigate the influence of temperature on the demulsification effect. The experimental results are shown in Fig. 2.

As the temperature increases, the water content of the upper oil phase gradually decreases after treatment, as shown in Fig. 2. When the heating temperature of the oil sample exceeds 50°C, the water content change of the upper oil phase after treatment is no longer significant. Therefore, the optimal demulsification temperature selected is 50°C. At this time, the water content of the upper oil phase after treatment can be reduced to 6.3%, and the oil recovery rate can reach 73.5%.

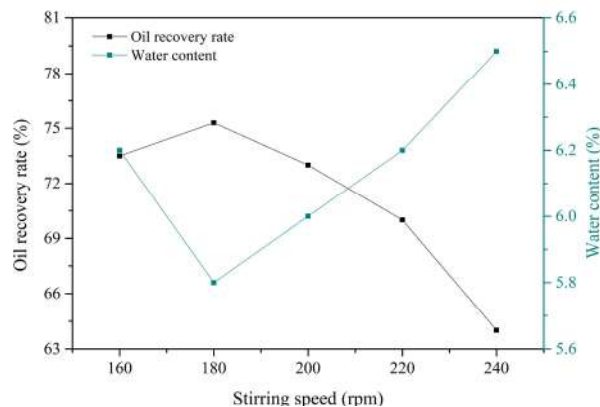


Fig. 3: The effect of stirring speed on the demulsification effect of aged oil.

Stirring speed: Mix aged oil and water in a 1:4 ratio, heat the experimental oil sample with the adjusted oil-water ratio in a 50°C thermostatic magnetic stirrer, and adjust the stirring speed to 160 rpm, 180 rpm, 200 rpm, 220 rpm, and 240 rpm, respectively. Continue stirring for 30min and let it stand for 30 min. Using the moisture content of the upper oil sample after standing as an indicator, investigate the effect of stirring speed on the demulsification effect. The experimental results are shown in Fig. 3.

Both too fast and too slow stirring speeds are not conducive to demulsification. When the stirring speed is below 180 rpm, as the stirring speed increases, the water content of the upper oil phase after treatment gradually decreases. When the speed is higher than 180 rpm, the water content of the upper oil phase shows a significant increase after treatment, as shown in Fig. 3. Due to the emulsification effect of too fast stirring speed, the optimal stirring speed selected is 180 rpm. At this time, the water content of the upper oil phase can be reduced to 5.8% after treatment, and the oil recovery rate can also reach 75.5%. Due to the rapid stirring speed, it will have a re-emulsification effect, which is not conducive to the demulsification of aged oil. Therefore, there will be an increase in water content and a decrease in the oil recovery rate in the treated aged oil.

Ultrasonic Demulsification Experiment

Ultrasound has good conductivity in both oil and water, so the use of ultrasound can improve the demulsification efficiency of aged oil (Wang et al. 2018). When ultrasound with a certain frequency and sound intensity acts on a solution, small bubble nuclei in the liquid are excited under the action of ultrasound, manifested as oscillation, growth, contraction, and collapse of bubble nuclei (Zhang et al. 2018). A series of extreme physical processes such as high temperature, high pressure, luminescence, discharge, shock wave, and jet are generated in the liquid. Under the action of the negative pressure phase of sound waves, cavitation

bubbles are generated and then rapidly collapse under the action of the positive pressure phase of sound waves (Zhao et al. 2019). When cavitation bubbles collapse instantly, local high-temperature and high-pressure zones are generated within a very small space around them. By utilizing the locally generated high-temperature and high-pressure zones, the oil-water interface can be destroyed, leading to the demulsification of aged oil (Hamidi et al. 2021c, Wang et al. 2022).

Ultrasonic frequency and power: Mix aged oil and water in a 1:4 ratio and place them in a constant temperature magnetic stirrer. Stir at a speed of 180 rpm while heating to 50°C. Place the mixed sample in an ultrasonic cleaning device for ultrasonic treatment. This group of experiments studied the effect of ultrasonic frequency and power on the demulsification effect at the same ultrasonic time, using the water content of the upper oil sample after standing as the indicator. Examine the effect of Ultrasonic frequency and power on demulsification efficiency. The experimental results are shown in Fig. 4.

The frequency and power of ultrasound have a significant impact on the demulsification effect of aged oil. As the frequency and power of ultrasound gradually increase, they both exhibit excellent demulsification effects, as shown in Fig. 4. When the frequency reaches 25 kHz, the water content in the aged oil after treatment decreases to a minimum of 5.5%, and the oil recovery rate reaches over 78%. When the power reaches 60W, the water content in the aged oil after treatment decreases to the lowest of 4.8%, and the oil recovery rate reaches over 80%. However, from an energy-saving perspective, when the ultrasonic power increases from 40 W to 60 W, the water content and oil recovery rate in the aged oil after treatment do not change significantly. Therefore, 40 W is chosen as the optimal ultrasonic power.

Ultrasonic time: The experimental conditions in this group are the same as those in 3.2.1, mainly studying the effect of

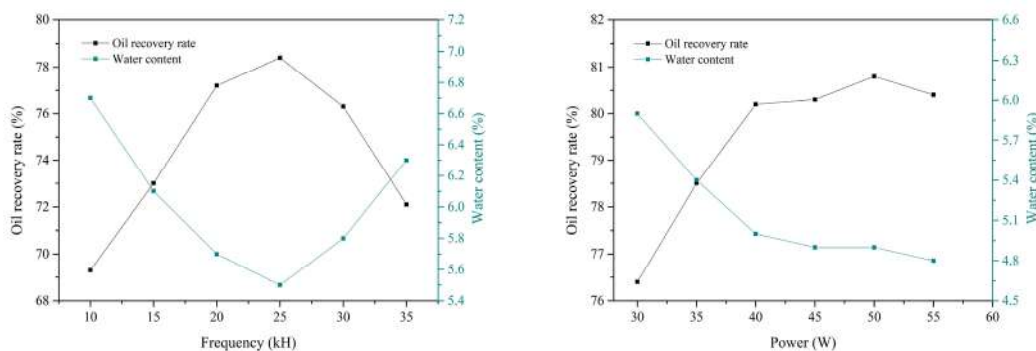


Fig. 4: The effect of ultrasonic frequency and power on the demulsification effect of aged oil.

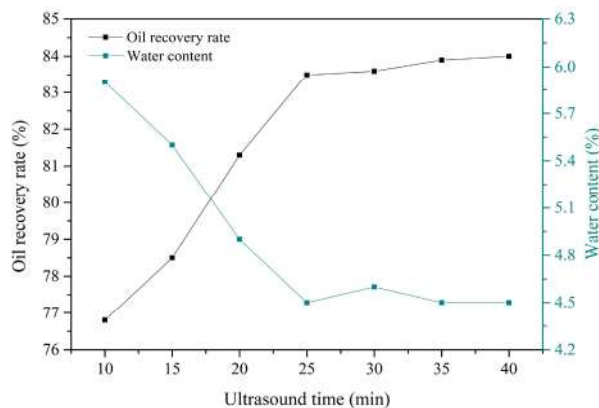


Fig. 5: The effect of ultrasound time on the demulsification effect of aged oil.

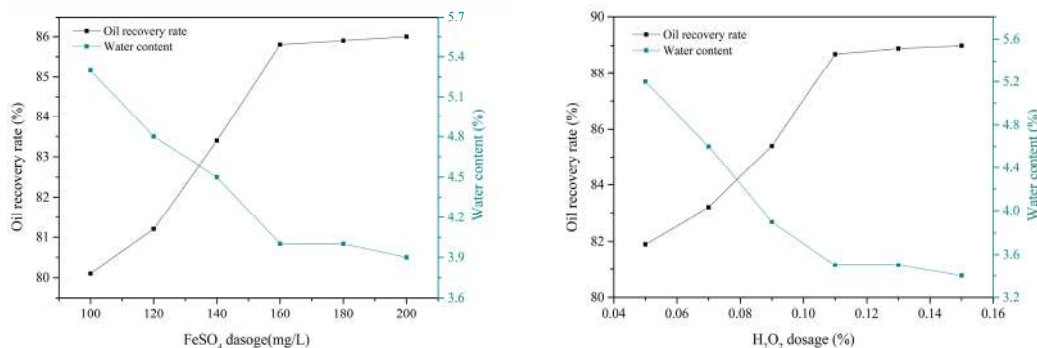


Fig. 6: The effect of reagent dosage on the demulsification effect of aged oil.

different ultrasonic times on the demulsification effect of aged oil at a frequency of 25 kHz and a power of 40W. The experimental results are shown in Fig. 5.

With the extension of ultrasound time, the demulsification effect of aged oil is more obvious, as shown in Fig. 5. When the ultrasound time is 25 min, the optimal demulsification effect has been achieved. At this time, the water content of the aged oil after treatment decreases to 4.5%, and the oil recovery rate reaches 83.5%. When the time exceeds 25 min, the demulsification effect no longer changes significantly. Because the oil-water interface that ultrasound can damage is limited, when the ultrasound time reaches a fixed value, no matter how long the time is extended, the effect of ultrasound no longer significantly increases. It has reached the limit of how ultrasound can handle aging oil.

Chemical Demulsification Experiment

After adding demulsifiers to aged oil, they penetrate the emulsified water droplet protective layer and damage the protective layer (Ramirez et al. 2021). After destroying the original oil-water interface, the tension of the oil-water

interface is reduced. When the surface tension decreases, oil and water droplets continuously collide and coalesce. As the temperature gradually increases, the stability of the oil-water interface decreases, and the kinetic energy of oil-water molecules increases, accelerating the movement of oil and water droplets, ultimately leading to demulsification and precipitation of oil (Duan et al. 2018). This experiment uses the Fenton method for chemical demulsification experiments.

Reagent dosage: The experimental conditions in this group are the same as those in 3.2.2, and the ultrasound time of 25 min is selected. After ultrasonic treatment, the mixed sample is further subjected to chemical demulsification using the Fenton method. Firstly, the pH of the mixed sample is adjusted to 3-4 using a sulfuric acid solution, and then FeSO₄ and H₂O₂ are sequentially added for oxidation treatment. After a certain period of reaction, the water content of the upper oil sample is used as an indicator to investigate the effect of the Fenton reagent on the demulsification effect of aged oil. The experimental results are shown in Fig. 6.

The effect of chemical demulsification is very good, as it can significantly reduce the water content in the aged oil

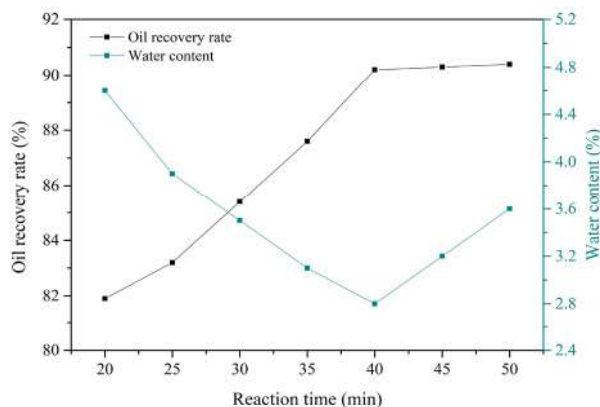


Fig. 7: The effect of chemical reaction time on the demulsification effect of aged oil.

after treatment, as shown in Fig. 6. The experimental results show that the best demulsification effect is achieved when the FeSO_4 dosage is $140 \text{ mg}\cdot\text{L}^{-1}$, and the H_2O_2 dosage is 0.11% . At this time, the water content in the aged oil after treatment can be reduced to 3.5% , and the oil recovery rate can reach 89% . Fenton reagent can exert its strong oxidizing ability to disrupt the oil-water interface of aged oil, thereby releasing most of the water droplets encapsulated in the aged oil, further reducing the water content in the recovered oil.

Chemical reaction time: The experimental conditions of this group are the same as the optimal experimental conditions in 3.3.1. The main focus is to study the effect of chemical reaction time on the demulsification effect of aged oil. The water content of the upper oil sample after different reaction times is used as an indicator to investigate the effect of reaction time on the demulsification effect of aged oil. The experimental results are shown in Fig. 7.

As the reaction time prolongs, the demulsification of aged oil also exhibits good results, as shown in Fig. 7. When the reaction time is 40 min, the demulsification effect is the best.

At this time, the water content of the aged oil after treatment decreases to 2.8% , and the oil recovery rate reaches 90.5% . When the reaction time exceeds 40 min, the water content and oil recovery rate of the aged oil after treatment no longer show significant changes as the reaction time prolongs. Because the oil-water interface that can be broken by chemical demulsification has been completely broken, even adding more chemical agents or longer reaction times cannot improve the effect. That is, when the reaction time is 40 min, all chemical reactions in the aging oil system have been completed.

Dehydration Experiment

Conduct experiments on aged oil under the optimal conditions selected in 3.1, 3.2, and 3.3, and dehydrate the sludge after the experiment. During the dehydration experiment, cationic PAM with an ion degree of 50 needs to be added and then centrifuged for dehydration.

Flocculant dosage: By adding different amounts of PAM for dehydration experiments, the optimal amount of PAM was selected. Using the water content of the upper layer oil

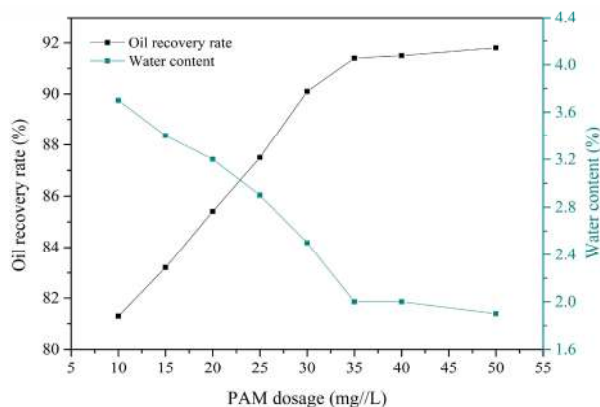


Fig. 8: The effect of flocculant dosage on the demulsification effect of aged oil.

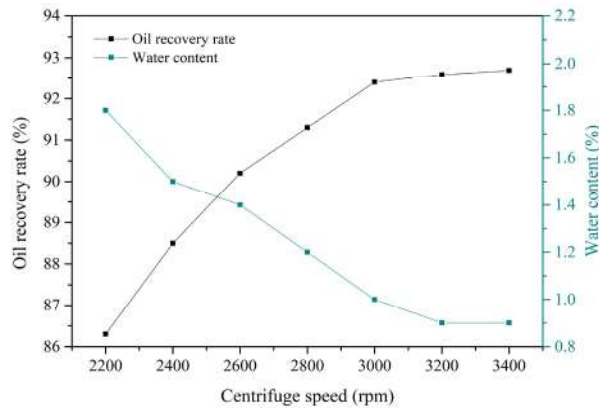


Fig. 9: The effect of centrifuge speed on the demulsification effect of aged oil.

sample after centrifugation as an indicator, investigate the effect of PAM dosage on the demulsification effect of aged oil. The experimental results are shown in Fig. 8.

With the increase in PAM dosage, the water content of the upper oil phase after centrifugal treatment showed a trend of first decreasing and then increasing, as shown in Fig. 8. When the dosage is increased to 35 mg.L^{-1} , the dehydration effect reaches its best. At this time, the water content of the aged oil after treatment can be reduced to 2%, and the oil recovery rate can reach 91.5%. However, further increasing the dosage will result in a worse effect, as excessive addition of PAM will make the aged oil system more dense, which is not conducive to centrifugal dehydration, resulting in a worse effect.

Centrifuge speed: The optimal experimental conditions in this group of experiments are the same as those in 3.4.1. The aged oil is centrifuged at different centrifuge speeds for 10 min, and the water content and oil recovery rate in the upper oil phase after centrifugation are used as indicators to investigate the effect of different centrifuge speeds on the dehydration effect of aged oil. The experimental results are shown in Fig. 9.

As the centrifuge speed continues to increase, the water content of the upper oil phase after centrifugal treatment shows a trend of first decreasing and then increasing, as shown in Fig. 9. When the speed reaches 3200 rpm, the dehydration effect reaches its best. At this time, the moisture

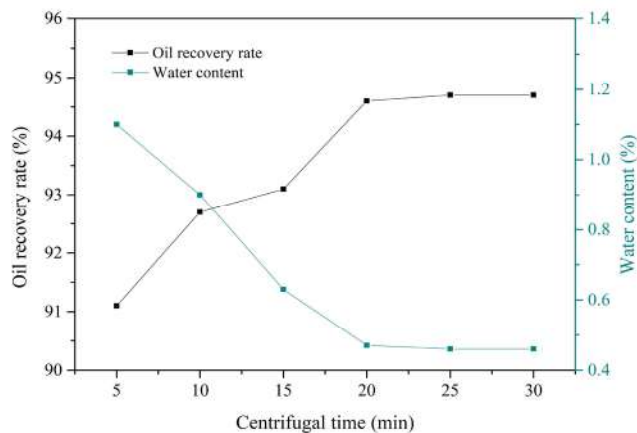

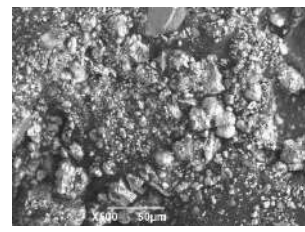

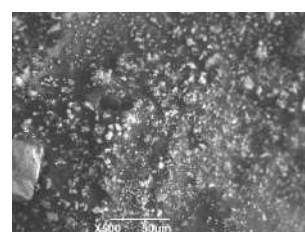

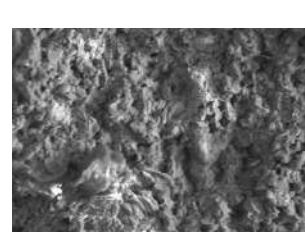



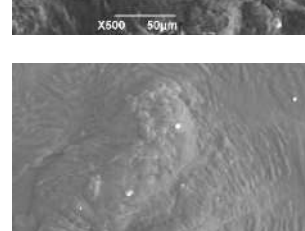

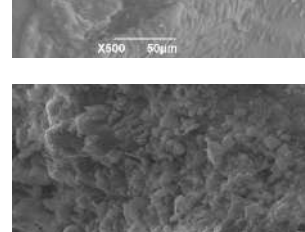


Fig. 10: The effect of centrifugal time on the demulsification effect of aged oil.

Table 2: Analysis of aged oil separation water and solid residue.

Project	Oil content [%]	Water content [%]	Solid content [%]	Oil content [mg.L^{-1}]	Suspend solid [mg.L^{-1}]
Water	-	-	-	150	200
Solid residue	6	53	41	-	-

Table 3: Aging oil characteristics at different stages of the experiment.

Aging oil at different stages	Experimental image	SEM image
Aging oil original sample		
Aging oil sample after mechanical demulsification		
Aging oil after ultrasonic demulsification		
Aging oil after chemical demulsification		
Aging oil after centrifugal dehydration		
Residue after centrifugation		

content of the aged oil after treatment can be reduced to 0.9%, and the oil recovery rate can reach 92.7%. But, as the rotational speed continues to increase, the water content and oil recovery rate of the aged oil after treatment no longer show significant changes. Because at a speed of 3200 rpm, all the free water in the aged oil system has been separated, further reduction of water content requires screening of centrifugation time.

Centrifugal time: The optimal experimental conditions in this group of experiments are the same as those in 3.4.2. The aged oil is centrifuged at a speed of 3200 rpm for different times, and the water content and oil recovery rate in the upper oil phase after centrifugation are used as indicators to investigate the effect of different centrifuge speeds on the dehydration effect of aged oil. The experimental results are shown in Fig. 10.

As the centrifugation time continues to extend, the water content of the upper oil phase after centrifugation treatment shows a trend of first decreasing and then stabilizing, as shown in Fig. 10. When the centrifugation time is 20 min, the water content of the aged oil after treatment can be reduced to 0.47%, and the oil recovery rate can reach 94.6%, fully meeting the requirement of 0.5% water content in China's crude oil gathering and transportation standard.

After screening various influencing factors, the final determined aging oil treatment process is as follows: when the oil-water ratio is 1:4, the heating temperature is 50°C, the stirring speed is 180 rpm, the ultrasonic frequency is 25 kHz, the power is 40W, the ultrasonic time is 25 min, the pH is adjusted to 3-4, the addition amount of FeSO_4 is 160 $\text{mg}\cdot\text{L}^{-1}$, the addition amount of H_2O_2 is 0.11%, the heating stirring reaction is 40 min, the addition amount of cationic PAM with an ion degree of 50 is 35 $\text{mg}\cdot\text{L}^{-1}$, the centrifugal speed is 3200 rpm, and the centrifugal time is 20 min. The crude oil recovery rate after aging oil treatment can reach over 94.6%, and the water content of the treated crude oil is less than 0.5%, meeting the standards for crude oil gathering and transportation in China.

Analysis of Aged Oil Separation Water and Solid Impurities

Under the optimal experimental conditions, the properties of the separated water and residue are shown in Table 2. From the table, it can be seen that the oil content in the effluent after centrifugation is about 150 $\text{mg}\cdot\text{L}^{-1}$, the suspended solids content is 200 mg/L , the oil content in the residue is 6%, and the water content is 53%. After centrifugation, the effluent can be reinjected or reused after simple treatment, and the treated residue is transported to a hazardous waste treatment station for harmless treatment.

Characteristics of Changes During Aging Oil Treatment

This article mainly conducted mechanical demulsification experiments, ultrasonic demulsification experiments, chemical demulsification experiments, and dehydration experiments on aged oil. To better understand the dehydration process of aged oil from a microscopic perspective, this section used scanning electron microscopy to analyze the apparent characteristics of the four stages of aged oil treatment, as shown in Table 3.

The aged oil exhibits a certain cross-linked network structure before treatment, containing a lot of mechanical impurities, and the surface is extremely uneven and irregular, as shown in Table 3. However, with the mechanical, ultrasonic, chemical, and centrifugal processes carried out on the aged oil, there were significant differences in the structure of the aged oil, whether from the experimental sample or the microscopic surface. The small dispersed substances disappeared, the spatial cross-linking network structure of the aged oil was broken, and the water droplets wrapped in the oil could be released, making the surface of the treated aged oil gradually become flat and smooth. Most of the mechanical impurities and encapsulated water in the aged oil have been removed, while the remaining majority are petroleum, with an appearance similar to that of a homogeneous system, exhibiting a flat and smooth surface.

CONCLUSIONS

- (1) In response to the technical challenges of low oil recovery rate and high water content in recovered oil, a mechanical ultrasonic chemical coupling demulsification and dehydration treatment process for aged oil has been developed.
- (2) The final determined aging oil treatment process is as follows: when the oil-water ratio is 1:4, the heating temperature is 50°C, the stirring speed is 180rpm, the ultrasonic frequency is 25kHz, the power is 40W, the ultrasonic time is 25 min, the pH is adjusted to 3-4, the addition amount of FeSO_4 is 160 $\text{mg}\cdot\text{L}^{-1}$, the addition amount of H_2O_2 is 0.11%, the heating stirring reaction is 40 min, the addition amount of cationic PAM with an ion degree of 50 is 35 $\text{mg}\cdot\text{L}^{-1}$, the centrifugal speed is 3200 rpm, and the centrifugal time is 20 min. The crude oil recovery rate after aging oil treatment can reach over 94.6%, and the water content of the treated crude oil is less than 0.5%, meeting the standards for crude oil gathering and transportation in China.
- (3) The oil content in the water generated after aging oil treatment is about 150 $\text{mg}\cdot\text{L}^{-1}$, the suspended solids

content is 200 mg.L⁻¹, the oil content in the residue is 6%, and the water content is 53%. After centrifugation, the effluent can be reinjected or reused after simple treatment, and the treated residue is transported to a hazardous waste treatment station for harmless treatment.

- (4) Through scanning electron microscopy analysis of aged oil at different stages of the treatment process, it was found that when using this process to treat aged oil, the original spatial cross-linking network structure of the aged oil was broken, allowing the water droplets wrapped in the oil to be released, thereby significantly reducing the water content in the recovered oil and improving the oil recovery rate.

ACKNOWLEDGEMENT

This work was supported by the Natural Science Basic Research Program of Shaanxi (Program No. 2021JQ-849), the Special Scientific Research Program of the Education Department of Shaanxi Province (No.22JK0425), and the school-level fund project of Xian Aeronautical University (No. 2021KY1203).

REFERENCES

- Anisimov, A.V., Frolov, V.I., Ivanov, E.V., Karakhanov, E.A., Lesin, S.V. and Vinokurov, V.A. 2018. *Complex Technology of Oil Sludge Processing*. Springer International Publishing, Cham, pp. 617-623.
- Appazov, N.O., Diyarova, B.M., Bazarbayev, B.M., Assylbekkyzy, T. and Dzhiembayev, B.Z. 2021. Rice straw and husk oil sludge for processing through the use of lignosulfonate as a binder with activated charcoal. *Ser. Chem. Technol.*, 2(446): 65-71.
- Chang, X., Li, X. and Ge, S. 2023. Insight into the oil removal mechanism of quaternary ammonium ionic liquid microemulsions for oily sludge treatment. *Sustainable Energy & Fuels*, 6(12): 567-569.
- Chen, X., Zhang, Y., Xu, B. and Li, Y. 2022a. A simple model for estimation of the higher heating value of oily sludge. *Energy*, 9(20): 235-239.
- Chen, Z., Zheng, Z., He, C., Liu, J., Zhang, R. and Chen, Q. 2022b. Oily sludge treatment in subcritical and supercritical water: A review. *J. Hazard. Mater.*, (Jul.5): 433-435.
- Coleman, N. 2021. North Sea newcomers Zennor and Pandion target green shoots in aging oil province. *Platt's Oilgram News*, 5(25): 99-102.
- Dalhat, M.A., Osman, S.A., Mu'Azuz, N.D. and Alagha, O. 2022. Utilization of oil sludge as a rejuvenator in hot-mix-asphalt containing reclaimed asphalt concrete. *Constr. Build. Mater.*, (Jul. 4): 338-340.
- Deng, J., Zhang, H., Yu, B. and Liu, H. 2021a. Research progress on oil sludge treatment in oilfield: A mini-review. *Recent Innov. Chem. Eng.*, 6(5): 14-17.
- Deng, S., Lu, X., Tan, H., Wan, X. and Xiong, X. 2021b. Effects of a combination of biomass addition and atmosphere on combustion characteristics and kinetics of oily sludge. *Biomass Conv. Bioref.*, 6(2): 11-15.
- Dhote, M., Kumar, A., Juwarkar, A. 2018. Petroleum Contaminated Oil Sludge Degradation by Defined Consortium: Influence of Biosurfactant Production. *Proc. Natl. Acad. Sci. India Sect. B Biol. Sci.*, 88(2): 517-523.
- Duan, M., Li, C., Wang, X., Fang, S., Xiong, Y. and Shi, P. 2019. Solid separation from the heavy oil sludge produced from Liaohe Oilfield. *J. Pet. Sci. Eng.*, 172: 1112-1119.
- Duan, M., Wang, X., Fang, S., Zhao, B., Li, C. and Xiong, Y. 2018. Treatment of Daqing oily sludge by the thermochemical cleaning method. *Colloids Surf. A Physicochem. Eng. Asp.*, 554: 272-278.
- Gao, Y., Ding, R., Chen, X., Gong, Z., Zhang, Y. and Yang, M. 2018. Ultrasonic washing for oily sludge treatment in pilot scale. *Ultrasonics*, 90: 1-4.
- Gong, Z., Wang, Z., Wang, Z., Fang, P. and Meng, F. 2018. Study on pyrolysis characteristics of tank oil sludge and pyrolysis char combustion. *Chem. Eng. Res. Des.*, 135: 30-36.
- Hamidi, Y., Ataei, S.A. and Sarrafi, A. 2021a. A simple, fast, and low-cost method for the efficient separation of hydrocarbons from oily sludge. *J. Hazard. Mater.*, 4(23): 134-136.
- Hamidi, Y., Ataei, S.A. and Sarrafi, A. 2021b. A highly efficient method with low energy and water consumption in biodegradation of total petroleum hydrocarbons of oily sludge. *J. Environ. Manage.*, 293: 112911.
- Hamidi, Y., Ataei, S.A. and Sarrafi, A. 2021c. Effect of Dissolution of Extracted Hydrocarbons of Oily Sludge on Petroleum Products. *Chem. Eng. Technol.*, 44(8): 456-458.
- Jerez, S., Ventura, M., Molina, R., Martinez, F., Pariente, M.I. and Melero, J.A. 2022. Application of a Fenton process for the pretreatment of an iron-containing oily sludge: A sustainable management for refinery wastes. *J. Environ. Manage.*, 23(4): 304-307.
- Khazaal, R.M. and Ismail, Z.Z. 2021. Bioremediation and detoxification of real refinery oily sludge using mixed bacterial cells. *Petrol. Res.*, 10(12): 245-250.
- Kurilkina, M.Y., Muslyumova, D.M., Zavyalov, O.A. and Miroshnikov, S.A. 2021. Experience in applying the technology of cavitation treatment of sunflower oil sludge for feeding ruminants. *IOP Conf. Ser. Earth Environ. Sci.*, 624(1): 12110-12116.
- Lee, C.L. and Jou, C.J.G. 2022. Producing Refuse Derived Fuel with Refining Industry Oily Sludge and Mushroom Substrates. *Energies*, 5(8): 15-19.
- Linhaires, V.D.N., De Araujo, L.G., Vicente, R. and Marumo, J.T. 2022. Enhanced removal of radium from radioactive oil sludge using microwave irradiation and non-ionic surfactant. *J. Pet. Sci. Eng.*, 34(5): 211-217.
- Martinez González, A., Silva Lora, E.E., Escobar Palacio, J.C. and Almázan Del Olmo, O.A. 2018. Hydrogen production from oil sludge gasification/biomass mixtures and potential use in hydrotreatment processes. *Int. J. Hydro. Energy*, 43(16): 7808-7822.
- Muratova, A., Lyubun, Y., Sungurtseva, I., Turkovskaya, O. and Nurzhanova, A. 2022. Physiological and biochemical characteristics of *Miscanthus x giganteus* grown in heavy metal-oil sludge co-contaminated soil. *J. Environ. Sci.*, 115: 114-125.
- Neto, O.D.M.M., Silva, I.M., Lucena, L.C.D.F., Lucena, L.D.F.L., Mendonca, A.M.G.D. and Lima, R.K.B.D. 2023. Physical and rheological study of asphalt binders with soybean oil sludge and soybean oil sludge fatty acid. *Waste Biomass Valor.*, 22(10): 657-659.
- Nezhdbahadori, F., Abdoli, M.A., Baghdadi, M. and Ghazban, F. 2018. A comparative study on the efficiency of polar and non-polar solvents in oil sludge recovery using solvent extraction. *Environ. Monit. Assess.*, 190(7): 389-392.
- Ramirez, D., Kowalczyk, R.M. and Collins, C.D. 2019. Characterization of oil sludges from different sources before treatment: High-field nuclear magnetic resonance (NMR) in the determination of oil and water content. *J. Pet. Sci. Eng.*, 174: 729-737.
- Ramirez, D., Shaw, L.J. and Collins, C.D. 2021. Oil sludge washing with surfactants and co-solvents: oil recovery from different types of oil sludges. *Springer Berlin Heidelberg*, 6(5): 123-126.
- Tessaro, A.P.G., Vicente, R., Marumo, J.T., Teixeira, A.C.S.C. and Araujo,

- L.G.D. 2021. Preliminary studies on electron beam irradiation as a treatment method of radioactive oil sludge. *Braz. J. Radiat. Sci.*, 56(8): 211-215.
- Wang, J., Han, X., Huang, Q., Ma, Z., Chi, Y. and Yan, J. 2018. Characterization and migration of oil and solids in oily sludge during centrifugation. *Environ. Technol.*, 39(10): 1350-1358.
- Wang, Z.L., Shi, H., Wang, S.Y., Wang, Z.M., Hao, M.M. and Wang, J. 2022. Theoretical study on the pressurization characteristics of disc-seal single screw pump used in high viscosity oily sludge conveying field. *Petroleum Science*, 23(4): 623-627.
- Zhang, Z.Y., Li, L.H., Zhang, J.S., Ma, C. and Wu, X. 2018. Solidification of oily sludge. *Pet. Sci. Technol.*, 36(4): 273-279.
- Zhao, Y., Yan, X., Zhou, J., Li, R., Yang, S., Wang, B. and Deng, R. 2019. Treatment of oily sludge by two-stage wet air oxidation. *J. Energy Inst.*, 92(5): 1451-1457.



An Overview of Solid Waste Management Practices in Pune, Maharashtra, India

Nilofar Saifi†  and Bandana Jha 

Department of Architecture, School of Planning and Architecture, New Delhi, India

†Corresponding author: Nilofar Saifi; nilofar.phd294arch22@spa.ac.in

Nat. Env. & Poll. Tech.
Website: www.neptjournal.com

Received: 22-10-2023

Revised: 13-12-2023

Accepted: 26-12-2023

Key Words:

Waste management system

SWaCH

Plastic waste

Red dot campaign

E-waste

ABSTRACT

The growing population and rapid urbanization are significant challenges for Indian cities. Pune City generates nearly 2,258 tonnes of waste per day. Pune's informal waste sector has demonstrated remarkable efficiency, cost-effectiveness, and self-sustainability. Moreover, it contributes to favorable economic and social outcomes for the city. With the support of the self-help group SWaCH Seva Sahakari Sanstha Maryadit, Pune, the municipal solid waste management model has successfully achieved a remarkable 95 percent segregation rate. Implementing the Pune municipal solid waste management model showcases the active and efficient engagement of informal waste workers in the collection and resource utilization process. This underscores the possibility of favorable economic, social, and environmental results stemming from collaborations between municipalities and waste pickers. This paper looks at the role of SWaCH in line with Pune Municipal Corporation towards the present waste management system. Primarily reliant on labor, this model accomplishes recycling tasks at a notably lower cost compared to conventional mechanized and centralized waste management approaches. It can also accomplish high recycling levels and relatively considerable plastic waste segregation. Promoting the retrieval of valuable materials, especially plastics, for local and global recycling enterprises actively contributes to the advancement of a circular urban waste management approach. The objective of this research is to explore and provide a realistic understanding of Pune's current status of waste generation, collection, transportation, and disposal. Apart from the SwaCH-PMC model, the paper also focuses on plastic waste recycling, the Red Dot Campaign towards sanitary waste, and household e-waste management in Pune.

INTRODUCTION

Global and Indian concern lies in the current challenges of municipal solid waste management in urban areas, including megacities and smaller villages. Rapid urbanization, economic development, and population growth increase waste generation rates, posing diverse risks to the environment and public health. Municipal authorities struggle to cope with the accelerating pace of waste generation, making solid waste management a vital municipal responsibility. India has a lack of awareness about solid waste management, but it has evolved over the years. The majority of solid waste is not properly treated, with waste segregation being a major obstacle. Factors such as improper collection, transportation unavailability, lack of treatment technologies, and financial shortages contribute to poor waste management practices. Different waste streams have varying hazards, and ranking wastes based on their level of hazards offers economic advantages. MSW is a composite made up of a variety of waste materials produced by residents of the area. MSW is

divided into several fractions, including recyclables and non-recyclable materials that can be composted. The amount and makeup of garbage are influenced by a number of variables, including average income, living standards, population size, social behavior, climate, industrial production, etc. (Bamne & Mhatre 2019).

In the Pune Municipal Corporation (PMC), there are 42 wards and five zones. Also one of the largest Municipal Corporations in Maharashtra. On July 1st, 2021, it underwent a process of delimitation, adding 23 villages to its jurisdiction (Alappuzha 2021). Previously, the city was administered through the P.M.C. through four administrative Zones, each of which was further subdivided into three or four Wards and subsequently into three or four Prabhags. At the most basic level, Kothis are divided into 152 Kothis, 76 Prabhags, 14 Wards, and 4 Zones (Sohkhlet & Nagargoje 2020). Pune Municipal Corporation has used segregation since at least 2008 (Alappuzha 2021). A population of 3.5 million people lives in an area of 244 square kilometers (Kumar & Agrawal, 2020).

SCOPE AND METHODOLOGY OF STUDY

The research objective is to understand the current management of solid waste in Pune, from collection to disposal. This involves analyzing the existing problems, challenges, and potential prospects within the solid waste management systems. The study's methodology is based on qualitative data. To assess the various issues, underlying causes, and negative outcomes related to solid waste management in Pune, secondary data is sourced from diverse outlets such as Research Papers, Annual Reports, Websites, Journals, Government Websites, and publications.

SWaCH: A TRANSFORMATION TOWARDS THE PUNE MUNICIPAL SOLID WASTE MANAGEMENT SYSTEM

Starting from the early 1990s, when Pune, much like numerous cities in India, operated a waste collection system based on communal bins where residents deposited their solid waste every day, and the informal waste pickers to recover recyclables, the city has grappled with escalating amounts of municipal solid waste. The city's underprivileged waste pickers banded together in 1993 to organize their union, known as Kagad Kach Patra Kashtakari Panchayat (KKPKP), to voice their right to dignity and a secure livelihood. They were poor, illiterate, silent, disregarded, and even condemned by some (Le Doze et al. 2018).

The Kagad Kach Patra Kashtakari Panchayat (KKPKP) came up with a sustainable strategy for municipal solid waste management and collaborated with municipal commissioners to advance a decentralized approach. This collaboration was established in conjunction with other civil society organizations dedicated to addressing environmental concerns at the city level (Rode 2011). To convince the Pune Municipal Corporation (PMC) that waste pickers perform essential urban environmental services, Kagad Kach Patra Kashtakari Panchayat (KKPKP) combined research, policy, and political assistance. To obtain official authorization to provide primary garbage collection services, Kagad Kach Patra Kashtakari Panchayat (KKPKP) successfully collaborated with PMC. Given that the PMC's efforts with KKPKP led to Pune becoming one of the first local administrations in India to provide waste pickers with identification cards and health insurance premiums (Le Doze et al. 2018). In the year 2000, public interest litigation over poor municipal solid waste management in major cities resulted in significant changes in national policy, resulting in the National Municipal Solid Waste Law (Management and Handling) Rules 2000 (Rode 2011). These regulations mandate urban authorities to conduct door-to-door waste collection, promote household waste separation, and redirect

waste from landfills to recycling and processing systems. The Kagad Kach Patra Kashtakari Panchayat (KKPKP) implemented a door-step waste collection system for 50,000 properties in the city, backed by the local body through citizen pleas and basic equipment like pushcarts and buckets, to reduce littering and promote waste management. (Le Doze et al. 2018).

In 2007, PMC collaborated with informal waste collectors Kagad Kach Patra Kashtakari Panchayat (KKPKP) to implement the Municipal Solid Waste Rules 2000. Cities were required to submit action plans by December 2007, aiming for 100% door-to-door collection. PMC chose waste picker cooperatives for waste management, with a user fee for door-to-door collection. This prompted the establishment of the PMC-SWaCH cooperative model, resulting in a profound impact on the city's system for managing municipal solid waste (Rode 2011). In 2008, the Pune Municipal Corporation (PMC) granted authorization to SWaCH, India's pioneer cooperative owned by independent waste pickers, to offer doorstep waste collection and waste management services for a duration of five years. The waste pickers are compensated with a service fee and are responsible to both the residents and the PMC.

Waste pickers sort and sell the recyclable materials they collect, and they keep all of the revenue that they make (Alappuzha 2021).

SWaCH, a group of over 80% women, works with representatives from Kothi Councils and the city-level Representatives Council to facilitate workers' participation in decision-making processes, including waste pickers and waste management. At the Kothi level or within neighborhoods, coordinators collect user fees, handle grievances, and offer additional benefits such as composting and the collection of electronic waste. They bridge the gap by recovering reusable waste and supplying essential resources for the official recycling process (Le Doze et al. 2018). In 2013, SWaCH serviced over 390,000 properties in Pune with 2,200 members. The model remained in place without administrative support for two years, with a team of 14 coordinators and staff. PMC renewed the contract in 2016 for five years, and by August 2018, SWaCH had serviced 640,000 properties with 3,076 waste pickers. Therefore, Fig. 1 provides an illustrated timeline of the Pune waste management journey from 1993 to 2018. The revolutionary work of Kagad Kach Patra Kashtakari Panchayat (KKPKP) and the sustainability of the SWaCH model led to the inclusion of a trade union representing informal waste pickers in the Municipal Solid Waste Rules 2016. The incorporation of waste pickers into the municipal solid waste management system, requiring urban areas to provide identity cards

and doorstep collection services, is currently legal (Rode 2011).

SOLID WASTE MANAGEMENT: AN OVERVIEW OF PUNE CITY

According to reports, the city creates almost 2,258 tonnes of garbage every day. Pune believes that biogas cleans the city and is experimenting with ensuring that no trash goes to landfills. With a population of 3.5 million people and an area of 244 square kilometers (Alappuzha 2021). They generate approximately 400 g of solid trash per capita. The city expects trash generation to be 3,255 tons by 2025 and 3600 tons by 2031 and is looking at more intensive technologies such as a biogas plan. An overview of the solid waste management system is shown in the Fig. 2 for Pune. Thermal gasification is used in decentralized vermicomposting, RDFs, recycling, and waste-to-energy systems. Households create over 70% of municipal solid garbage, while hotels,

restaurants, and other commercial entities account for the remaining 30% (Kumar & Agrawal 2020). As per the current studies, Pune City processes about 2,258 tons of waste each day, the majority of which is organic and comes from 70% of the household population. The first municipal-based biogas plant was created in the colony model with a location of 4000 inhabitants around 375 units of energy had enough power to run 250 streetlights and generate 150 tons of compost in 2014; approximately 20 such biogas facilities were operational, with potential increase to 27 or more. Pune Municipal Corporation, PMC, owns models based on public-private partnerships. The operator of the biogas facilities is paid Rs.600,000 per month for maintenance, with an annual increase of 10% - 15%. The facility opened in 2010 at a cost of Rs.60 lakhs (Kumar & Agrawal 2020).

Presently, with the higher price of Rs. 30 lakhs, PMC has paid Rs.1300 to Rs.1400 per tonne for one ferrying of waste to the facility. The collaboration has already begun receiving

1993: Waste pickers in Pune form the Kagad Kach Patra Kashtakari Panchayat (KKPKP) union.
1995: The report of the Planning Commission's High-Power Committee on Solid Waste Management in India recommends incorporating waste pickers, forming cooperatives for door-to-door waste collection, segregation, recovery centres, recycling incentives, and composting for improved waste management.
2000: The Municipal Solid Waste (Management and Handling) Rules mandate doorstep collection, promote trash segregation at the source, dry waste recycling, and waste diversion away from landfills.
2002: Maharashtra government resolution allocates labor for door-to-door garbage collection through user-fee cooperative rubbish pickers.
2006: The Maharashtra Non-Biodegradable Solid Waste (Proper and Scientific Collection, Sorting, and Disposal in Municipal Corporation Areas) Rules establish safe sorting spaces (material recovery facilities) for waste pickers, allowing recyclable items to be diverted through the informal sector.
2007: Maharashtra's Urban Development Department mandates December 2007 deadline for city action plans to implement Municipal Solid Waste Rules 2000, promoting 100% door-to-door collection.
2008: Pune Municipal Corporation authorizes SWaCH cooperative to offer door-to-door waste collection and management services for five years.
2012: Central Ministry mandates waste pickers recognition, identity cards, and personal protective equipment for solid waste management, integrating them into municipal solid waste management systems.
2013: SWaCH and PMC sign a memorandum, ending with over 390,000 properties serviced.
2014 - 2015: Without PMC administrative support, the SWaCH model persists.
2015: The government's drafting committee for the revised Solid Waste Management Rules (due for release in 2016) is comprised of informal waste pickers, who are represented by KKPKP.
2016: Solid Waste Management Rules acknowledge informal waste pickers, collectors, and recyclers as crucial elements of solid waste management, requiring registration, identification, material recovery facilities, and training for waste pickers.
2016: The PMC renews its five-year agreement with SWaCH.
2016: In the government's drafting committee for the 2016 Solid Waste Management Rules, KKPKP represents informal waste collectors.
2018: SWaCH expands to cover 640,000 properties, employing over 3,000 waste-pickers.

Fig. 1: Institutionalizing door-to-door waste collection service in Pune by involving waste pickers: A timeline (Le Doze et al. 2018).

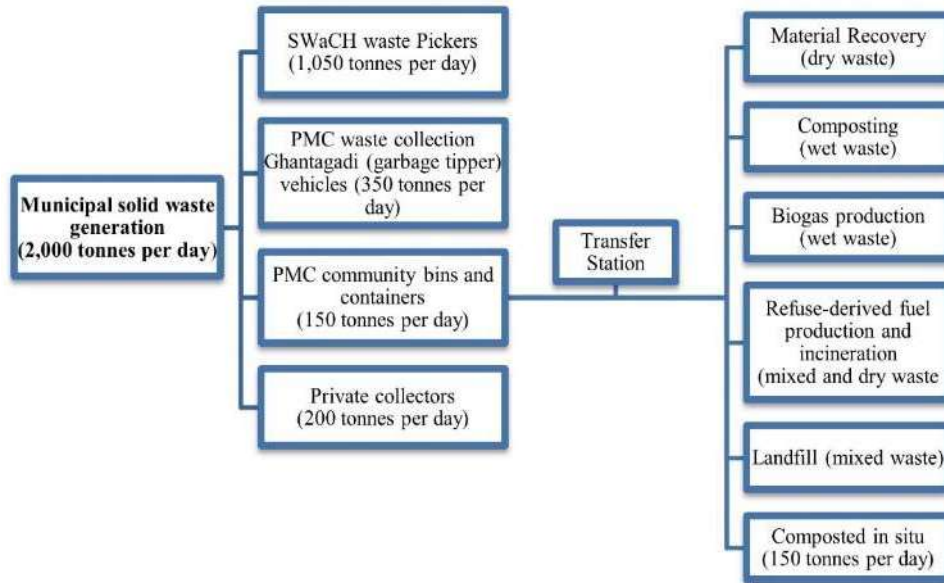


Fig. 2: Municipal solid waste management system in Pune City (Le Doze et al. 2018).

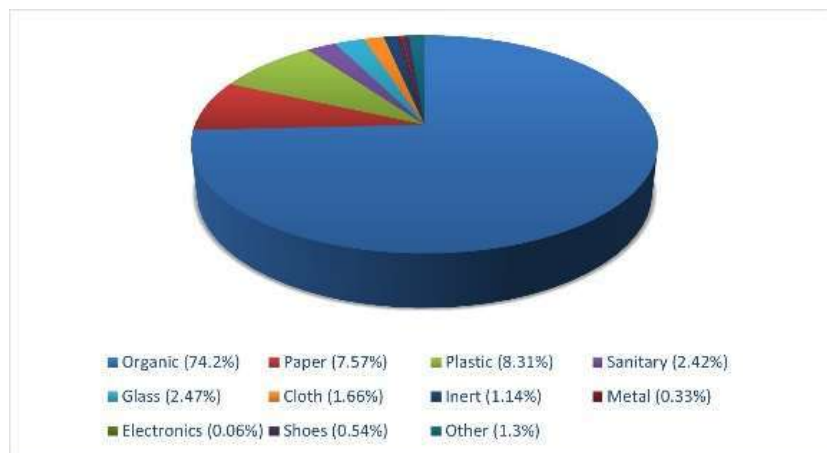


Fig. 3: Municipal Solid Waste Composition in Pune (Alappuzha 2021).

well-managed separated garbage from hotels, which families can directly transfer to the bio-methanation plant (Kumar & Agrawal 2020).

Unsegregated waste generators are likewise subject to the PMC penalty system. A property tax incentive is available to anyone who installs eco-friendly building methods such as solar heaters, rainwater collection, and compost pits. PMC ensures that there is no foul play by doing frequent inspections and rescinding the reimbursement if it is discovered to be nonfunctional. With the support of the self-help group SWaCH Seva Sahakari Sanstha Maryadit, Pune, it has achieved 95 percent segregation (Alappuzha 2021).

Waste Classification and Composition

The Public Health and Sanitation Bye-Laws of 2014 include a comprehensive classification of waste comprising 25 categories. Municipal Solid trash encompasses commercial, residential, and other trash created in a municipal or notified area, except industrial hazardous waste and treated bio-medical waste. The classification is based on the source of trash generation, which can be residential, commercial, educational, public and private gardens, heritage structures, or religious locations. (P.M.C 2014). Fig. 3 illustrates the typical waste composition that is generated.

Biodegradable waste, including tea leaves, eggshells, fruit and vegetable peels, meat and bone fragments, and

animal waste, is considered wet waste. Recyclable waste, including paper, metal, plastic, rubber, and glass, is also known as dry waste. Construction and demolition waste, or “C&D waste,” refers to waste generated during the construction, renovation, maintenance, and demolition of homes and businesses (Alappuzha 2021). E-waste includes information technology, telecommunications equipment, consumer electronics, and related trash, while hazardous components in household cleaners, automobiles, personal care products, and related items are classified as commercial/household hazardous, biomedical, and sanitary waste (P.M.C 2014).

Waste Collection

P.M.C. introduced a standard user charge for door-to-door collections in 2017, tracking management, equipment acquisition, and maintenance expenses (Alappuzha 2021). A hierarchy of waste collection processes is represented below in Fig. 4. Municipal solid waste is collected through primary and secondary methods. Door-to-door services, including Solid Waste Collection and Handling (SWaCH), account for 43% of the total collection. Tipper trucks, also known as “ghantagadi,” collect recyclable and nonbiodegradable waste from building gates via Prabhags, accounting for 12% of the primary collection. Both methods involve unorganized workers and community-based cooperatives (Sohkhlet & Nagargoje 2020).

Pushcart services are available in urban areas that are inaccessible to trucks. After that, the waste gets transported to a station located within each ward. Dumper Placer trucks that additionally transport waste to the transfer station make up 40% of the primary collections. P.M.C. also collects

waste that has been abandoned along roads and streets to be transported to the stations, accounting for 5% of all the primary collections (P.M.C 2017).

Waste is subsequently transported from transfer stations to dry or wet waste processing plants by Bulk Refuse Carriers (BRC) compactors. Currently, C&D garbage is being disposed of directly in low-lying places along waterways (Alappuzha 2021). Out of the 524,778 houses, P.M.C. supplied door-to-door services to 52.70 percent of them in 2010. This suggests that the other 47.3 percent of households dispose of their waste in community bins. 2017 saw a 55% increase in this. SWaCH covered 80.37 percent of premises in Pune’s 41 Prabhags during 2016 and 2017, leaving 19.63 percent of houses unserved and about 100 TPD uncollected (Le Doze et al. 2018).

Waste Disposal

There are currently 50 processing facilities comprising 7 transfer stations, 25 decentralized biogas plants, 14 decentralized biodigesters, and 4 mechanical composting facilities, which together process 30% of garbage. SWaCH diverts 10% of collected garbage. 60% of the remaining waste is sent to the Urali Devachi dump, located 25 kilometers from the city (Sohkhlet & Nagargoje 2020). The landfill site is 43 hectares in size, 15 ha of which are fully utilized and have been permanently sealed off. Both biodegradable and non-biodegradable materials are included in the waste that is disposed of in landfills. The annual cost of collecting, moving, and disposing of waste is projected to be 83.60 crore rupees (11.8 million USD). A landfill receives unprocessed waste (36% of the total waste) (Hemalata 2012). At present, the plants are running at 51% of their installed capacity.

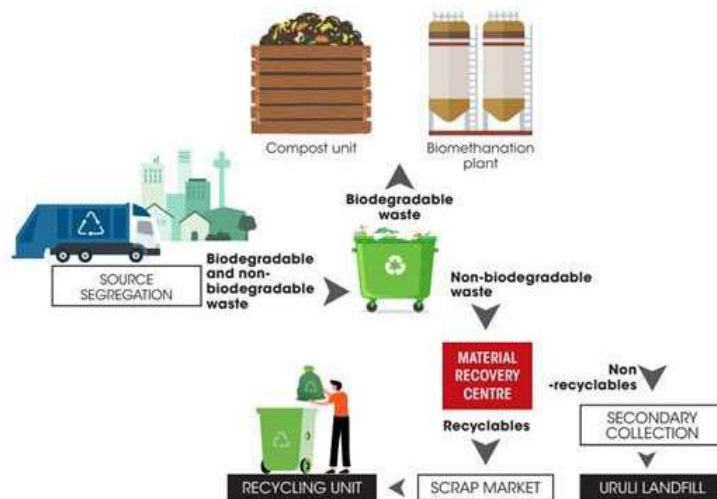


Fig. 4: Process of waste collection in Pune (Alappuzha 2021).

The Clean City Movement and Smart Garbage Management System are initiatives by P.M.C., utilizing GPS and tracking technologies to monitor vehicles and inform citizens. The Katraj Model, a Zero Garbage Ward, aims to reduce landfill waste and promotes the Swachh Awards. 25 decentralized bio-methanation facilities and other composting techniques are operational, and waste-to-energy models using bio-conversion processes generate biogas, promoting sustainable waste management (Sohkhlet & Nagargoje 2020). Pune recently installed a 300 MTD plant capable of producing 11 MW (Le Doze et al. 2018). The Rochem plant, a decentralized waste treatment facility, employs pyrolysis gasification to reduce transportation requirements and promote community engagement. Since 2010, these scientific landfills have been operational, ensuring a reduction in transportation costs and preventing leachate leakage (Kumar & Agrawal 2020). The SWM model in Pune faces challenges due to its size, funding, upgrading, and expertise requirements. Technological solutions like waste incineration and mechanized processing options are vulnerable, causing gaps between processing capacity and actual waste. The current disposal procedures for C&D waste in low-lying areas along rivers also require specific procedures (P.M.C 2017).

PLASTIC WASTE: AN OVERVIEW

The Maharashtra government banned various plastic items, including bags, disposable items, and plastic decorations, on March 23, 2018. The ban applies to individuals and entities, including makers, sellers, and customers. A milk package buy-back scheme and PET bottle buy-back were introduced. Severe penalties apply to those handling or using restricted substances. Although the ban aims to reduce non-recyclable and low-grade plastic in municipal waste streams, it also presents challenges for recycling plastic trash (Le Doze et al. 2018).

Plastic garbage was classified into 30 distinct categories based on how it is handled for recycling/processing. The breakdown of plastic type, generation, and recovery is illustrated in Table 1. In general, 34% of plastics were rigid, while 64% were flexible (single- and multi-layer). Waste pickers recover 37% of plastics.

For recycling, on average. However, the relative recycling rates of different forms of plastic vary significantly. The most recycled plastics are mono-material hard plastics (PET, HDPE, and PR). Transparent, monolayered flexible polymers are more recyclable than colored counterparts in the flexible plastics industry. The recovery rates of multi-layered polymers are the lowest. Instead of being disposed of with organic garbage, compostable plastics are placed in

the flexible plastic stream. (Narayanan & Anantkrishnan 2022).

Plastic Waste: Recycling

Prior to being sent to the end consumers of recovered plastic, who produce new plastic products in India or abroad, small and large plastic recyclers process plastic waste further. They concentrate largely on processing plastic as shown in Fig. 5 (sorting, cleaning, flaking, and pelletizing) (Le Doze et al. 2018). Also, the plastic waste recycling value chain hierarchy Not only is Pune City home to plastic waste processing facilities but Maharashtra state as a whole is also home to numerous such facilities, some of which specialize in certain recycling chain processing operations. There are two types of 'recycling' that materials undergo:

- Closed-loop recycling:** When recycled materials are utilized in applications that are similar to those of the original products, such as the bottle-to-bottle recycling of HDPE plastic granules formed from HDPE bottles into HDPE bottles. The majority of PP and HDPE plastics are recycled in closed-loop systems.
- Open-loop recycling (downcycling):** When products manufactured from recycled materials cannot be recycled themselves and the recycled materials are used for a different use than the original products. The plastic that is recycled the most is PET.

Multi-layered and multi-material plastics are very light in weight and highly voluminous, making them considerably more expensive to handle. They are made of multiple distinct layers and types of plastic, paper, and metal. Because they are largely used for food packaging, these polymers are frequently polluted, which attracts rats and makes them difficult to store.

Even when they are gathered for recovery, recycling them still presents technical difficulties. The combination of plastics and non-plastic materials, such as metal and paper, makes this heterogeneous material difficult to recycle technologically (Narayanan & Anantkrishnan 2022).

A method for collecting multi-layered plastics was established in Pune in 2019 by SWaCH Plus with assistance from ITC Ltd to address this waste management

Table 1: Plastic generation and recovery rates (Narayanan & Anantkrishnan 2022).

Plastic Type	Generation (TPD)	Recovery (%)
Rigid	33.7	69%
Flexible	48.0	22%
Multi-layered	14.7	8%
Compostable	0.0	68%

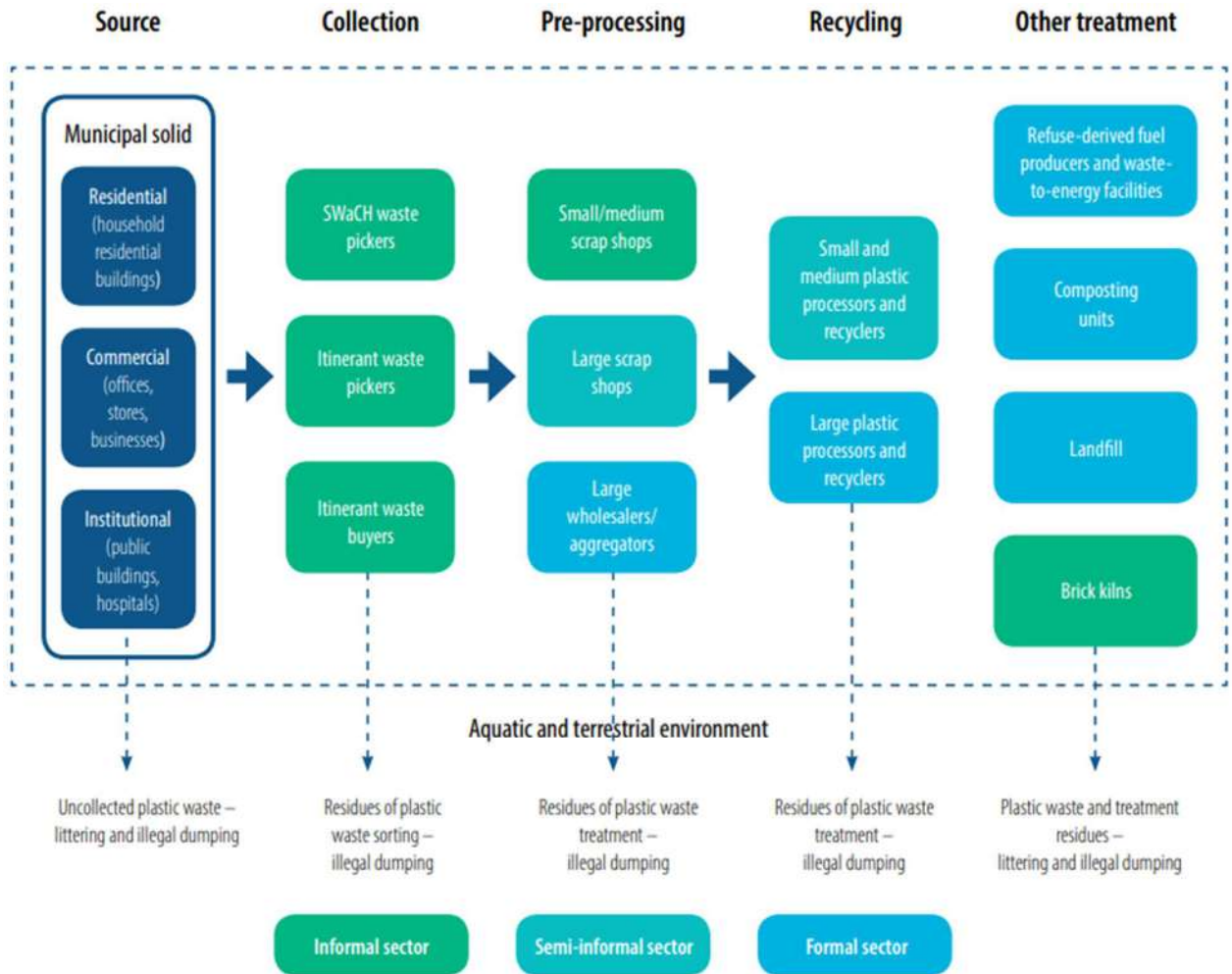


Fig. 5: Plastic waste recycling value chain in Pune (Le Doze et al. 2018).



Fig. 6: SWaCh waste pickers segregating plastics (Narayanan & Anantkrishnan 2022).

and environmental concern. Three tonnes are collected each day at the moment. To prevent overrepresenting the recovery rate for this material using the extrapolation method, data from areas where this system was in operation were separately gathered and excluded in the household

waste audit. Since this approach provides city-level data, it may be combined with the ‘natural’ recovery by waste pickers as shown in Fig. 6 to provide an accurate estimate of the material’s diversion to recycling in Pune (Alappuzha 2021).

As of now, mechanical recycling has received 2200 MT or 70% of the total gathered. The materials gathered by SWaCH Plus are a mixture of mono-layered flexible and multi-layered plastics, as well as multi-layered plastics that have been metalized, colored flexible plastics, and some clear, flexible plastics. The quantity of multi-layered plastics is thought to account for 50% of all plastics handled, according to composition data from SWaCH Plus. It follows that of the 3 tonnes per day collected using this approach, around 1.5 tonnes are made of metalized multi-layered plastic, resulting in an effective recycling rate for multi-layered plastics in Pune of 18% (Supe et al. 2021).

RED DOT CAMPAIGN: AN INITIATIVE TOWARD SANITARY WASTE

As a part of the Information, Education, and Communication (IEC) initiative run by PMC and SWaCH, the campaign was launched in 2016. The motive was to collect sanitary waste separately, with workers collecting waste from door to door. The interactive nature of the campaign led to a better understanding of the issues and approaches of the

citizens (Narayanan & Anantkrishnan 2022). According to the Municipal Solid Waste Management Rules, 2016, and in support of this, PMC encouraged citizens to dispose of their sanitary waste separately (Notification No. S.O. 1357 (e) dated April 8, 2016). Only fifty percent of the residents served by the PMC separated sanitary garbage from other rubbish, according to data obtained by corporation officials. Waste is transported to a feeding station (Fig. 7) by workers who collect it door to door. Each feeder site, which offers waste collection services to 100 to 150 houses, is staffed by five to seven people. A PMC collection van then comes and collects the trash. Waste is transported to the transfer station by the PMC vehicle. Following that, sanitary waste is moved in a red container to the processing plant (Alappuzha 2021).

Collection And Transportation of Sanitary Waste

An average of 1.5 TPD is collected and transported for sanitary waste. Currently, SWaCH staff collect residents' sanitary waste either in a separate plastic bag or a paper cover with a red dot (Fig. 8).

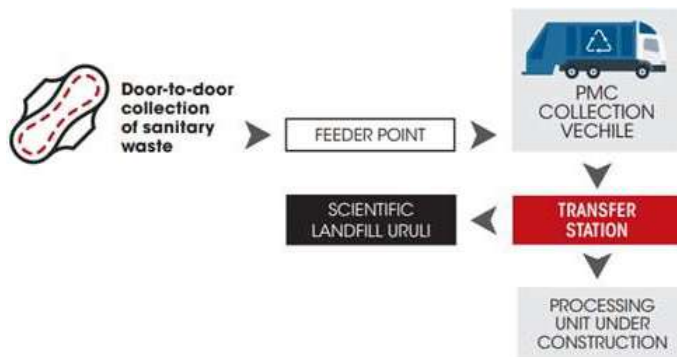


Fig. 7: Process of sanitary waste management in Pune (Alappuzha 2021).



Fig. 8: Sanitary waste collection by waste picker in Pune (Agarwal 2017).

The sanitary waste is then transported to the feeder site using the designated box in the PMC vehicle. Extra bags are utilized and hung separately in the collection vehicle when there is more waste than normal (Agarwal 2017). At the transfer point, sanitary waste is taken out of the PMC vehicle and placed in a red bin. After that, the container is delivered to the research landfill. Every day, all of the sanitary waste is collected. Processing of it is presently underway in Pune's Uruli Scientific landfill (Alappuzha 2021).

Technology

In order to establish a sustainable recycling loop in the sanitary waste industry, an Italian company created a ground-breaking recycling technology that can recycle used absorbent hygiene products, such as baby diapers, feminine hygiene (fem care), and adult incontinence products, to create new products and materials with added value. In Spresiano, northern Italy, the technology is set up and running on an industrial scale (Le Doze et al. 2018). Each year, it can process 10,000 tonnes of spent absorbent hygiene items. Serving a million people would be equivalent to this. The plant is one of a kind and the original in the globe. Using this process, sanitary waste is effectively broken down into plastic, cellulose, and super-absorbent polymers as explained in Fig. 9. These materials can be used to make garden barriers, hard bottle caps for purposes other than food, and viscose clothing.

The sanitary waste processing facility's installation started in 2019, however, because of COVID-19 and a discrepancy in the contractor and PMC's contract, it will take an extra six months to finish. The proposed plant could process ten tonnes of sanitary waste every day. All of the sanitary garbage is picked up each day. It is presently being managed at the scientific landfill near Uruli, Pune (Alappuzha 2021). SWaCH and PMC are working to bring behavioral change to lower-income households through a well-thought-out appeal and plan. However, affluent

households have shown more acceptance and are more accepting of the change, demonstrating their involvement in the system. Workers for the PMC were reluctant to touch or collect sanitary trash at the feeder point (where collected garbage accumulated). When the SWaCH team and PMC management took steps to spread knowledge of the proper treatment of sanitary waste, the PMC employees responded and joined the campaign. One of India's major Information, Education, and Communication (IEC) initiatives is the Red Dot Campaign, which aims to inform people about their duties when handling sanitary waste.

E-WASTE MANAGEMENT: AN OVERVIEW

Global concerns about e-waste volumes, limited treatment infrastructure, illegal trade, and consumer awareness have influenced the development of e-waste management legislation. Informal recycling practices, offering functional comfort and cost advantages, have dominated due to negative environmental and health consequences (Arora 2008). Indian cities, including Pune, face challenges in waste management due to informal sectors, non-segregation, inadequate collection/treatment centers, and lack of e-waste inventory. These factors require an organized approach and adaptable systems for handling e-waste and catering to localities. Solutions should be adaptable and convenient, addressing the interconnected scenario. Pune, a proposed smart city, faces challenges in solid waste treatment due to inadequate sites and infrastructure, with untreated e-waste often remaining in whole or trace form, resulting in environmental impact (Link 2016).

Pune, the cultural hub of India, is renowned for its Zero waste concept and Public-Private Partnership (PPP) strategy, involving Municipal Corporations, NGO organizations, and corporations like Cummins India. This model focuses on e-waste management, involving all sources of e-waste generation. Fig. 10 illustrates several waste sources in the

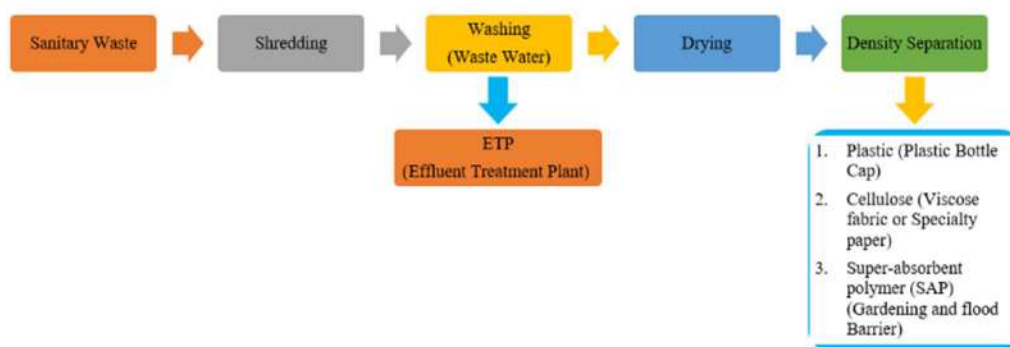


Fig. 9: Processing unit cycle for sanitary waste treatment (Alappuzha 2021).

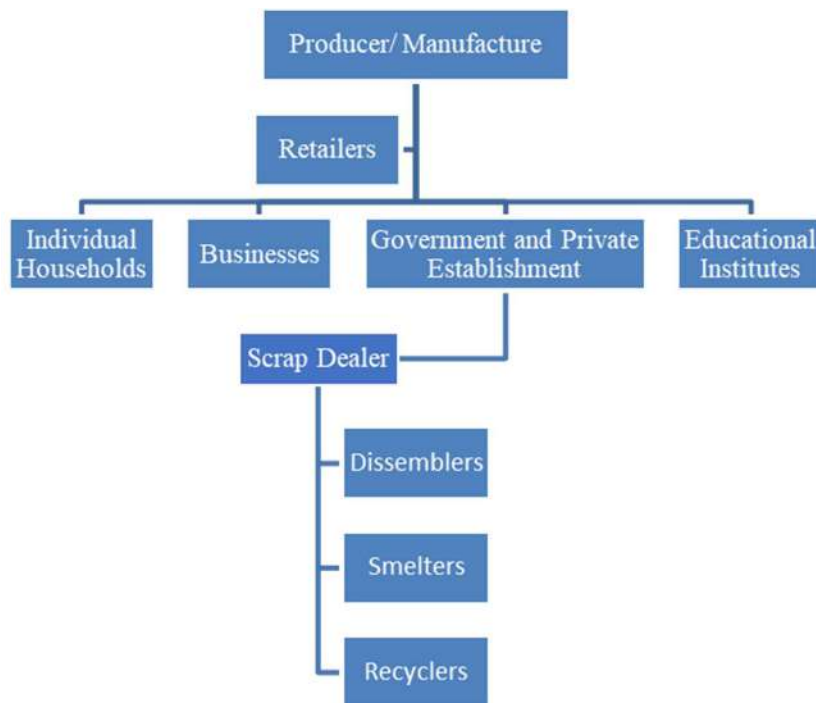


Fig. 10: Stakeholders' hierarchy in E-waste management (Bhat & Patil 2021).

Pune region, illustrating the point of starting to develop an integrated model (Chhura & Kumar 2015).

The government has implemented e-waste rules since 2012, with a shared responsibility model focusing on Extended Producer responsibility. The guidelines outline tasks for bulk consumers, including businesses, government bodies, educational institutions, and producers, excluding households. Government involvement is crucial in managing e-waste, as household usage of e-devices significantly increases volumes over time. Neglectful disposal behavior and environmental pollution result from negligent disposal. To address this, a participatory, structured system and current collection system development are necessary to reduce volumes and achieve economic benefits (Link 2016).

Pune Region Existing Model of E-Waste Management

Pune region generates considerably 10,000 metric tons of e-waste annually in the Pune region, and crucially, all of this operational trash ends up in landfills or scrap markets. The generators and collectors confuse e-waste with municipal solid garbage because they are unaware of the embedded worth of resources in it (Bhat & Patil 2021). Various stages of managing e-waste, including collection, separation, disassembly, reuse, reprocessing restoration, diffusion, and exposed burning/landfilling, are handled by reliable and connected informal sectors (Chhura & Kumar

2015). Therefore, a sketch of the present scenario of e-waste management is shown in Fig. 11. Lack of knowledge combined with a disregard for practical household appliances overlooks the risks that e-waste poses, which encourages irresponsible disposal practices. Despite the fact that homes contribute to the expanding amount of current e-waste, they must be carefully considered in e-waste management.

Pune, the second-largest producer of e-waste in Maharashtra, has been unable to effectively implement e-waste rules in the past four years. The region's proper segregation of dry and wet garbage contributes to proper waste disposal. However, a significant amount of e-waste ends up with informal collectors and recyclers, leading to resource loss and environmental degradation (Bhat & Patil 2021).

Households in the Pune region are significant stakeholders who might influence disposal behavior. Households that are well-informed and knowledgeable aid in the practice of systemic behavior and can aid in the management of sustainable e-waste management systems. Households receive monetary compensation from scrap merchants in exchange for their e-waste; however, products nearing the end of their useful life are diverted to the illegal market for dismantling or reconditioning. When they reach the point when continued use is no longer conceivable, a strong network of informal collectors

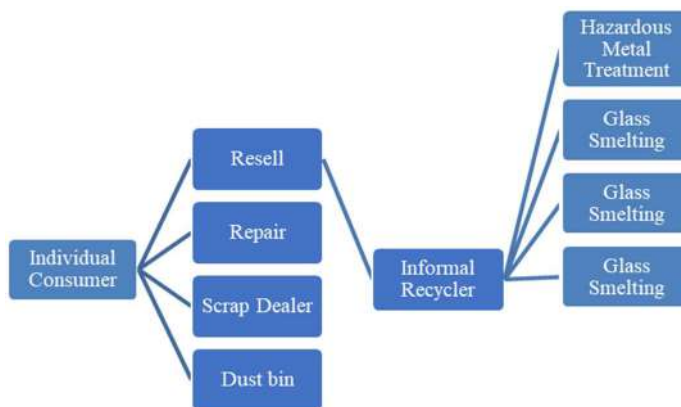


Fig. 11: Present scenario of E-waste management in Pune City (Bhat & Patil 2021).

guarantees their way to the informal recovering plants (Link 2016).

Inadequate collection arrangements by governing bodies have spread to the informal sector, leading to the use of existing e-waste management models. The Pune region model, a PPP model for efficient dry-wet waste management, has a significant gap in its scope, not including e-waste. The Pune region needs an efficient collection system for End-of-Life (EOL) items, with real-time data from generation to treatment and a convenient, accessible collection route. A low-cost method for recovering precious and hazardous metals is also crucial. The authors have developed a simple, low-cost Public-Private Partnership (PPP) model for managing household e-waste, integrating various processes for formal e-waste collection in response to current deficiencies (Bhat & Patil 2021).

CONCLUSION

The success of the Pune Municipal Solid Waste Management and SWaCH Model demonstrates that waste pickers are resourceful and adept at gathering and valuing resources and that partnerships between waste pickers and municipalities can benefit the environment, society, and economy. Pune's collection coverage could be enhanced, but lower-income groups may not be able to afford fees, and the city's structural composition may make it challenging to collect from all corners. Recovering valuable materials (including plastic) for regional and international recycling businesses directly supports a more circular municipal waste management paradigm. If the shift to a more formal circular plastic economy is to incorporate waste pickers and other non-formal actors, then investments must be made in the appropriate infrastructure, competencies, and capacities. The quantity of places and space made available for these decentralized activities closely relates to

how much plastic garbage is collected and recycled in the city. To enhance plastic waste segregation efficiency and improve recyclable materials, municipalities should provide decentralized spaces for sorting and recycling, subsidized scrap shops, recycling hubs, waste collection systems, and locations away from environmental leaks. This will ensure better quality and a more sustainable waste management system.

The Red Dot Campaign is one of the most front-line approaches to sanitary waste segregation. It is easy to replicate the IEC program for sanitary waste separation. The success of PMC in reaching 2.14 million individuals (about 50% of Pune's population) serves as a model for other metropolitan local government entities. In terms of Pune's cleanliness and the dignity of rubbish pickers, citizens demonstrated a readiness to adopt the practice and recognized its significance. Municipal solid garbage is often untreated due to inadequate collection and treatment facilities. This is due to poor collection methods, lack of knowledge, and lack of source segregation. To address this issue, household-generated e-waste needs to be disposed of using a targeted and practical approach. Providing suitable doorstep MSW disposal infrastructure can change this behavior by extending the current segregation paradigm. For all urban local governments, integrating the unorganized sector and creating an organization like SWaCH is the way to go. It would not only assist in bettering waste management in cities but also lift the lowly and marginalized. It is crucial to educate the general people and informal workers about the dangers of disposing of plastic waste in the environment. To increase their sense of responsibility, it would promote an environmental identity inside the industry. As part of their extended responsibility necessities, producers should be urged to promote the improvement of the gray market recycling and scrap trade.

REFERENCES

- Alappuzha. 2021. Waste-wise cities: best practices in municipal solid waste management waste-wise cities. A NITI Aayog-CSE survey 28 cities. Multiple initiatives. Retrieved from www.cseindia.org
- Agarwal, R. 2017. A First-of-a-Kind Campaign in Pune Creates Awareness About Sanitary Waste Segregation. Retrieved from <https://www.downtoearth.org.in/news/waste/a-first-of-a-kind-campaign-in-pune-creates-awareness-about-sanitary-waste-segregation-57033>
- Arora, R. 2008. Best Practices for E-Waste Management in Developing Nations. Research Paper GTZ-ASEM. Europe Aid, EU, pp. 1-25.
- Bamne, P. and Mhatre, S. 2019. Municipal solid waste management in Pune (ms) current challenges and future solutions for development. *J. Emerg. Technol. Innov. Res.*, 6(5): 611-615
- Bhat, V. and Patil, Y. 2021. An integrated and sustainable model for e-waste management for Pune City households. *J. Phys. Conf. Ser.*, 1964(6): 62111. <https://doi.org/10.1088/1742-6596/1964/6/062111>
- Chhura, B. and Kumar Makhija, M. 2015. E-waste: A new challenge and approach for India: An overview. *Int. J. Manag. Technol.*, 2(2): 1-12.
- Hemalata, H.N. 2012. Existing situation of solid waste management in Pune City, India. *Res. J. Recent Sci.*, 1: 348-351
- Kumar, A. and Agrawal, A. 2020. Recent trends in solid waste management status, challenges, and potential for the future Indian cities – A review. *Curr. Res. Environ. Sustain.*, 2: 11. <https://doi.org/10.1016/j.crsust.2020.100011>
- Le Doze, S., Harms, N., Siddique, O., Vougioukas, A., Archer, D., Johnson, O. and Gadgil, M. 2018. Closing the Loop: Pune, India Case Study. <https://www.studocu.com/in/document/united-college-of-engineering-and-research/management-information-systems/closing-the-loop-pune-india-case-study/35984180>
- Link, T. 2016. What India Knows about E-Waste: Report on Awareness Levels of E-Waste amongst Common Citizens in India. Research Reports. Toxic Links, New Delhi
- Narayanan, L. and Anantakrishnan, L. 2022. What we waste: Household waste generation and recovery by waste pickers in Pune. Kashtakari Panchayat. <https://swachcoop.com/pdf/202302-KP-WC-Report-Digital-02.pdf>
- Pune Municipal Corporation (PMC). 2014. Public-Health & Sanitation Bye-laws. Pune Municipal Corporation, Pune.
- Pune Municipal Corporation (PMC). 2017. Solid Waste Management Strategy Plan 2017-2025. Pune Municipal Corporation, Pune.
- Rode, S. 2011. Integrated approach to solid waste management in Pune City. *J. Geogr. Region. Plan.*, 4(8): 492-497.
- Sohkhlet, D. and Nagargoje, S. 2020. Municipal solid waste management: A comparative study between Sydney (Australia) and Pune (India). *E3S Web Conf.*, 170: 4001. <https://doi.org/10.1051/e3sconf/202017004001>
- Supe, G.N., Kshirsagar, K., Mahind, P., Thobde, S., Yalangphale, A. and Professor, A. 2021. Municipal solid waste management system for Pune City. *Int. J. Creative Res. Thoughts*, 9: 41.

ORCID DETAILS OF THE AUTHORS

Nilofar Saifi: <https://orcid.org/0009-0009-6755-5434>
 Bandana Jha: <https://orcid.org/0000-0001-5826-8809>



Transforming Energy Access: The Role of Micro Solar Dome in Providing Clean Energy Lighting in Rural India

R. Karthik*†, Ramya Ranjan Behera**, Uday Shankar***, Priyadarshi Patnaik**** and Rudra Prakash Pradhan*****

*Advanced Technology Development Centre, Indian Institute of Technology, Kharagpur-721302, India

**Rekhi Centre of Excellence for the Science of Happiness, Indian Institute of Technology, Kharagpur-721302, India

***Rajiv Gandhi School of Intellectual Property Law, Indian Institute of Technology, Kharagpur-721302 India

****Department of Humanities and Social Sciences, Indian Institute of Technology, Kharagpur-721302, India

*****Vinod Gupta School of Management, Indian Institute of Technology, Kharagpur-721302, India

†Corresponding author: R. Karthik; karthikee34@gmail.com

Nat. Env. & Poll. Tech.
Website: www.neptjournal.com

Received: 07-11-2023

Revised: 15-12-2023

Accepted: 26-12-2023

Key Words:

Micro-solar dome

Clean energy

Marginalized communities

Renewable energy

Empowerment

ABSTRACT

Access to affordable and reliable energy sources can substantially enhance the lives of marginalized communities in rural areas. Unfortunately, numerous households in these communities rely upon unclean sources of energy such as kerosene to light the house even during daylight. To address this issue, solar off-grid technology - Micro Solar Dome (MSD) was implemented in various states across India, specifically benefiting the scheduled caste and scheduled tribe communities. The study, across the eight selected states, highlights the advantages of adopting off-grid technologies and their roles in promoting awareness of renewable energy solutions. The survey used purposive sampling to collect community members' perceptions of the product's benefits and their awareness of renewable technologies. The results indicated that the utilization of the product not only enhanced illumination levels within households but also contributed to improved safety, increased study hours for children, and facilitated economic activities during the evening hours. Furthermore, the study revealed that education plays a crucial role in adopting solar energy. However, interventions such as awareness programs and hands-on experiences with the products can also greatly enhance awareness and promote adoption in rural areas. Overall, the study provided compelling evidence of the significant and positive impact that small-scale initiatives like the MSD can have on the lives of marginalized communities. It also emphasized the potential of such solutions to empower these communities and improve their overall well-being.

INTRODUCTION

Access to reliable and affordable electricity is essential for improving the quality of life, especially for rural households in India. However, approximately 13.8 million people in rural areas do not have access to grid electricity (World Bank 2021), leaving them reliant on kerosene lamps for lighting, which has significant health and environmental consequences (Pokhrel Amod et al. 2010). The emission from the kerosene lamps usually include black carbon and CO₂, which contributes to global warming. Kerosene lamps emitted about 270,000 tonnes of black carbon, with India accounting for 12% of the emissions (Jacobson et al. 2013). The potential risk of using kerosene-based lights leads to diseases like tuberculosis, a significant health issue in developing countries. Burning candles increased the lead concentration above the ambient standards (Pokhrel Amod et

al. 2010). Using kerosene lamps made women and children more prone to household-based injuries (Sharma et al. 2019).

The Government of India has implemented various vital initiatives to ensure that all areas have access to electricity. One such program, the Deen Dayal Upadhyaya Gram Jyoti Yojana (DDUGJY), designed to provide continuous electricity supply to rural households, agricultural consumers, and industries. This scheme also focuses on improving and upgrading the rural electricity infrastructure. Another significant program is the Pradhan Mantri Sahaj Bijli Har Ghar Yojana (Saubhagya), launched in 2017 to provide free electricity connections to eligible households in rural and urban areas (Malhotra 2022).

According to the International Energy Agency, the country has made the most considerable electrification effort in history, with over 99% of households having

access to electricity as of 2019. Despite these initiatives, frequent power interruptions and poor power quality from the distribution side remain significant challenges (Chamania et al. 2015, Sharma et al. 2019). Additionally, electricity affordability for people in rural areas, particularly marginalized communities, is another critical factor that needs to be considered (Pelz et al. 2021).

In recent years, off-grid solar solutions have emerged as a promising alternative to traditional grid-based electricity, offering clean and reliable electricity that can improve the well-being of households and communities (Akter & Bagchi 2021). Solar technologies such as on-grid solar, solar thermal systems, and off-grid solar systems, including solar home systems, solar lighting systems, mini-grids, and solar lanterns, have the potential to provide sustainable and affordable energy access for rural areas (Mahapatra & Dasappa 2012, Sandwell et al. 2016). Solar lighting systems (SLS) and solar lanterns have garnered attention as promising affordable lighting sources for basic household needs in remote regions (Abdullah-Al-Mahbub et al. 2022). Solar lanterns are particularly suitable for rural areas to ensure basic energy access, as they are a cost-effective, easy-to-use, and sustainable solution. They provide a clean, renewable, and affordable alternative to traditional lighting methods, eliminating dependence on harmful kerosene lamps and contributing to reducing indoor air pollution, benefiting both human health and the environment (Sandwell et al. 2016). The impact of SLS and lanterns must be considered. They provide clean, reliable, and affordable electricity to marginalized communities, improving the quality of life and promoting sustainable development. The United Nations, via its Sustainable Energy for All (SE4ALL) initiative and Sustainable Development Goal 7 (SDG 7), encourages the use of decentralized solar solutions to fulfill the universal energy access target for 2030 sustainably (Banerjee et al. 2013).

This research examined the impact of pico-level solar lighting systems on the quality of life of marginalized rural households. It aimed to explore how improved illumination affects on the quality of life within these communities. Additionally, the research investigated how introducing such technologies can raise awareness of renewable energy, regardless of education level. The findings of this research were expected to provide valuable insights into the potential benefits of pico-level solar lighting systems and help promote the adoption and sustainability of these technologies in marginalized rural households.

BACKGROUND OF THE STUDY

Solar lanterns have become an increasingly popular solution for lighting in rural communities worldwide. While they have

been in use for over a decade, their widespread adoption has accelerated in recent years due to the declining cost of solar technology (Kumar 2015). Governments, NGOs, and private companies have also launched initiatives to promote solar technologies in rural communities. These efforts have helped raise awareness about the benefits of solar energy and make these technologies more accessible to people in remote areas (Wong 2012). Promoting solar technologies in rural areas is essential for providing lighting and has implications for the quality of life in these communities (Rehman et al. 2010). As such, the Quality-of-Life (QoL) concept has received extensive attention in recent decades. The study on quality of life aimed to explore the relationship between various dimensions of well-being, such as health, education, economic insecurity, personal activities, political voice and governance, social connection, environmental conditions, personal insecurity, and energy usage (Seabra et al. 2022).

Solar lanterns are a promising solution to address the issues faced by rural households, particularly in terms of lighting and education. Several studies have shown that using solar lanterns can improve rural households' quality of life while reducing their expenditure on kerosene and candles, as observed in East Timor, Africa (Bond et al. 2010, Kudo et al. 2019). However, a study in Uganda did not show any favorable impact on children's schooling despite using solar lamps for their basic needs (Furukawa 2014).

Nonetheless, the solar light program in Bangladesh found that while there was no effect on academic performance, lighting helped students free from eye irritation, thus improving children's health and ensuring safety from burns (Chamania et al. 2015, Khandker et al. 2014, Kudo et al. 2019). In India, where kerosene lamps were prevalent due to the unreliability of the electricity supply, portable solar lights have been introduced to rural households under the Million Solar Urja Lamp program, increasing study hours for school-going children (Sharma et al. 2019). Therefore, solar lanterns can play a significant role in improving the lives of rural communities, particularly in terms of education and health.

Inadequate lighting is a problem that plagues low-lit areas and severely threatens the safety and well-being of vulnerable groups, especially women. Adequate lighting enhances women's security, mobility, and empowerment (Bose et al. 2021). A recent study on energy initiatives in refugee camps found that while there was no direct link between energy and women's safety, improved lighting could help prevent attacks and improve overall safety (Thorgren & Ghasemi Niavarani 2021). The benefits of solar lanterns were evident in a project in Gujarat's Dahod district, which has significantly aided rural homemakers in their daily

activities and visits to agricultural fields (Agoramoorthy & Hsu 2009). Additionally, a randomized controlled trial in the Barabanki district of Uttar Pradesh demonstrated that solar-powered lighting could substantially improve women’s safety (Aklin et al. 2017). A study conducted in Rwanda found it challenging to quantify the benefits of solar lanterns, yet they enhance domestic productivity and flexibility, leading to more efficient evening activities and improved study conditions, thereby improving household living standards (Grimm et al. 2017).

Finally, Increased awareness about the benefits of solar energy is crucial in promoting its adoption in rural areas (Urmee & Md 2016). Previous studies on solar adoption have found that education strongly affects adoption. For example, a study in Uganda found that non-adopters were more likely to have no formal education than adopters. At the same time, there was no statistically significant difference between non-adopters and adopters with primary education attainment (Aarakit et al. 2021).

In a study of India’s solar lantern program, researchers analyzed the education level of both early and late adopters and found that early adopters generally had higher education (Velayudhan 2003). While education did not significantly influence the adopter categories, it suggested that education plays a role in the early adoption of solar lanterns. Further exploration and understanding of the perceptions of solar energy among marginalized communities are essential to promote sustainable and inclusive development.

CONCEPTUAL FRAMEWORK

The conceptual framework of this study, shown in Fig. 1, addresses two primary challenges prevalent in rural

households of SC /ST communities: reduced illumination levels and a limited understanding of solar energy. The MSD installation represents the introduction of solar lighting solutions in these communities. This intervention is anticipated to bring about improvements in Illumination Enhancement within households’ awareness of solar energy by imparting comprehensive knowledge about solar energy. The outcomes of this framework focus on Improved Quality of Life and Enhanced Solar Adoption.

MATERIALS AND METHODS

India has made numerous efforts to improve the growth of technological innovation to improve energy access and reduce pollution to achieve climate targets. Under Mission Innovation, a global initiative supported by DST, Micro Solar Dome (MSD) to promote clean energy technologies in rural areas (IEA 2020)—in order to increase both awareness and encourage adaptation of solar energy among marginalized rural communities. The project was implemented across 13 states—Assam, Manipur, Tripura, Himachal Pradesh, Jharkhand, Chhattisgarh, Bihar, Rajasthan, Kerala, Odisha, West Bengal, Madhya Pradesh and Nagaland. This project aimed at installing around 44,000 units, specifically focusing on benefiting the Scheduled Castes (SC) and Scheduled Tribes (ST) communities residing in rural areas. The states and villages selected for implementation were identified based on having the highest Scheduled Castes (SC) and Scheduled Tribes (ST) populations, according to the 2011 Census data. Local NGOs assisted in conducting awareness programs on renewable energy in these villages. These programs aimed to educate residents about the benefits and practicalities of the technology. Following these programs, the Micro Solar Domes were installed for individuals who

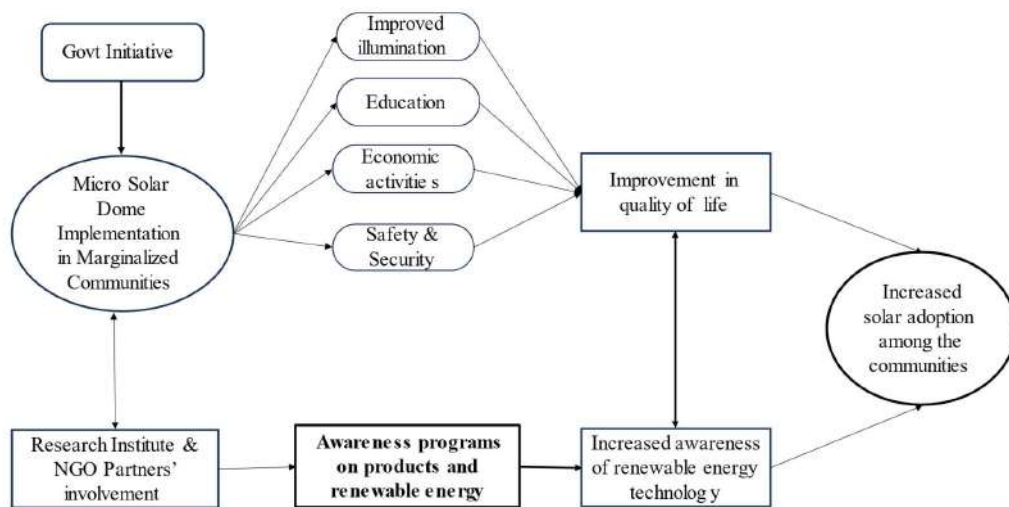


Fig. 1: Conceptual framework of the study.



Fig. 2: Micro Solar Dome.

showed interest and were willing to contribute financially to their installation.

Design of Micro Solar Dome

Fig. 2 shows the Micro solar dome, an innovative and low-cost hybrid product developed by NBIRT, Kolkata, and implemented by IIT Kharagpur.

MSD, a solar lighting system shown in Fig. 3, uses solar panels to convert sunlight into electrical energy through the photovoltaic effect. The electrical energy is then stored as chemical energy in a lithium-ion battery of 4.4 Ah (Ampere hour) with the help of a DC circuit that includes a microcontroller and a battery management system.

The battery management system protects the battery from overcharging and deep discharging. When the switch is operated, it activates a LED in the lower Dome that converts the stored electrical energy into light. Additionally, the device includes a USB port that enables users to charge their mobile phones using the stored electrical energy, and it provides a 2-meter-long charging cable for user convenience.

The system featuring the PCB circuit incorporates an LED indicator that displays the battery's charging status from the solar panels. A provided DC connector allows users to power the LED light from the grid supply directly in cases of insufficient battery power. The battery provides backup lighting for approximately 5-6 h per day. To enhance the

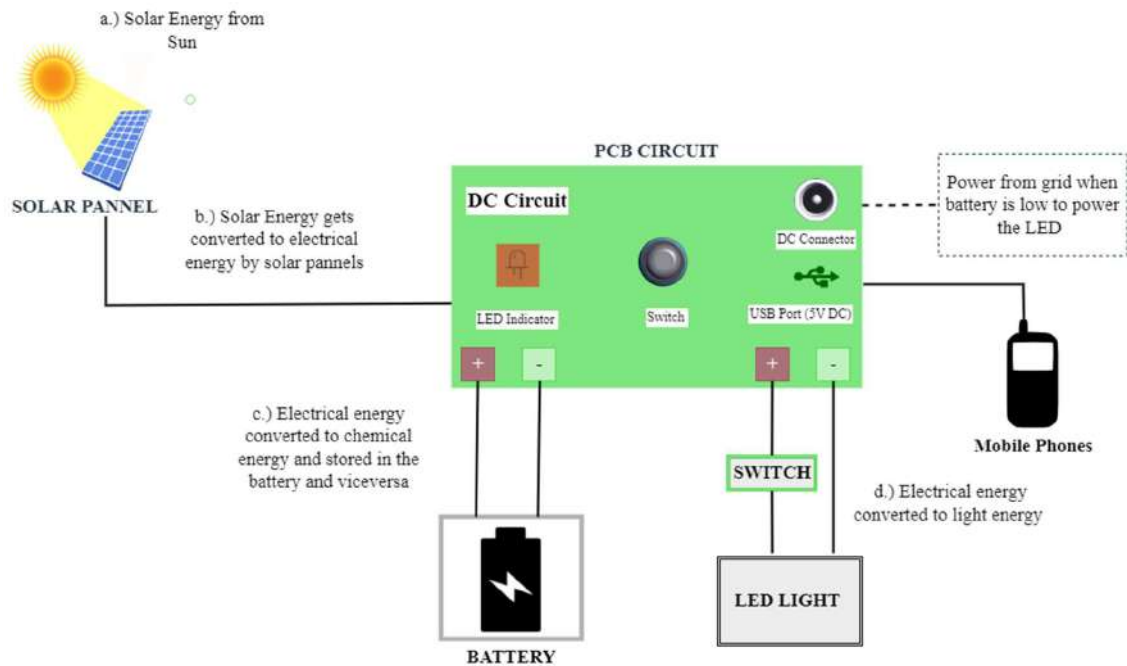


Fig. 3: The working principle of micro solar dome.

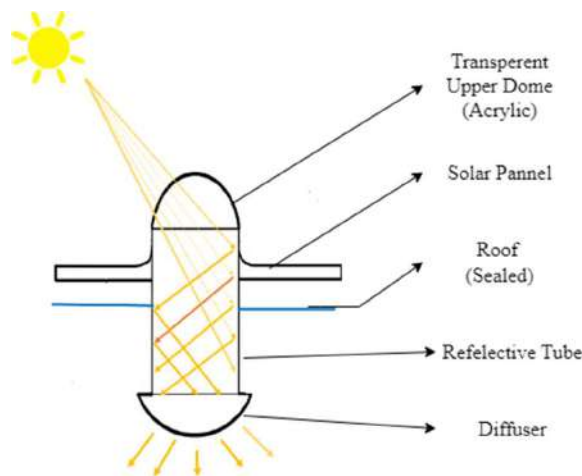


Fig. 4: Working principle of micro solar dome during daytime.

system's effectiveness, users were advised to charge their mobile phones during the day and utilize the stored energy for lighting in the evening.

Light tubes are a design solution for illuminating dark areas within houses where natural light cannot reach. The combination of windows and light pipes can enhance the influx of natural light into a space. The principle of light guiding in tubes relies on multiple reflections. These tubes incorporate highly reflective aluminum alloys. Light pipes transport light to darker sections of a home, and diffusers evenly scatter light, resembling a light source, as shown in Fig. 4. MSD includes a black opaque sheet that prevents light from entering when not required.

Research Methodology

The selection of states West Bengal, Odisha, Rajasthan, Tripura, Assam, Bihar, Manipur, and Kerala was guided by the high percentage of renewable energy installations in these areas.

Beneficiary Demographics: Most respondents engaged as daily wage laborers, primarily focused on agriculture and labor-intensive work. Male family members contributed to their livelihoods through agricultural and daily wage activities, female family members exhibiting versatility engaged in various household businesses. The demographic profile included families with school-going children. Many families resided in remote areas, highlighting the unique challenges faced in such regions.

Sampling strategy: The study adopted an operational research pattern and purposive sampling approach, targeting individuals willing to participate in the survey enthusiastically. The questionnaire incorporated open-ended and closed-ended questions to capture individuals'

perceptions of post-product usage comprehensively. Around 2,500 surveys were conducted, and only 1,718 surveys were used for the analysis after data cleaning. The distribution of surveys across the study regions are (Assam: 291, West Bengal: 674, Kerala: 81, Bihar: 12, Rajasthan: 32, Manipur: 291, Tripura: 19, Odisha: 388).

Time frame considerations: The selected time frame served a strategic purpose from December 2020 to March 2022 after project implementation. Adjustments to the initial plan led to the initiation of data collection when COVID -19 lock downs restrictions eased. Despite changes, the team ensured a substantial timeframe. Respondents were required to use the product for at least six months, allowing for a comprehensive evaluation. The installers recorded demographic details and lighting conditions during installation.

Addressing data collection challenges: As installations commenced, challenges arose from COVID-19 lockdowns. When restrictions eased, community installers played a crucial role. We addressed the initial difficulties of face-to-face interviews for data collection due to strict lockdowns and language barriers by involving local NGOs for support and translation. Emphasizing the importance of community-driven partnerships during unforeseen challenges, local NGOs supported telephonic interviews.

Statistical analysis: Multinomial Logistic Regression (MLR) was chosen for its suitability in handling multiple categorical dependent variables (Rajendran et al. 2007). MLR aids in determining the likelihood of each category or response within the dependent variable. Dependent variables were divided into three groups for education and illumination levels. The analysis considered factors like awareness of renewable energy and quality of life, offering insights into their connections.

Table 1: Basic details about electricity access and kerosene usage.

Baseline questionnaire (n=1718)	Status	N [%]
Beneficiaries having access to electricity	Yes	1537 (89)
	No	181(10.53)
Usage of kerosene/Candle for lighting	Yes	1202(69.96)
	No	516(30.03)
Experienced kerosene-related accidents in past	Yes	19 (1.10)
	No	1699 (98.89)

RESULTS

The study revealed that lighting, driven by grid power availability, emerged as the primary electricity use in rural areas. The results indicated that a majority of the respondents, 89.5%, had access to power, while a minority of 10.5% lacked it. However, the researchers identified various factors contributing to the lack of grid power, such as illegal settlements, inability to pay, and disconnection due to non-payment of bills. Despite having access to electricity, the researchers discovered that power outages were still widespread in rural areas, especially in remote forests and hilly terrains, caused by load shedding, rainstorms, and other natural disasters. As a result, people relied on fossil fuels for lighting, with a staggering 70% of respondents using kerosene lamps, candles, lanterns, and wick lamps during power outages.

Conversely, only a tiny percentage of respondents used battery-powered lights, while others either remained in the dark or faced fewer power interruptions. Unfortunately, using fossil fuel-based lighting came with significant risks, with

around 2% of respondents reporting kerosene light-based accidents. These findings underscore the critical impact of power outages on lighting sources in rural areas and the potential hazards linked to the use of fossil fuels.

Most rural households consisted of kutchra (straw roof and mud walls), semi-pucca (tin-roofed and brick-walled), and pucca houses, with insufficient illumination levels even during daylight hours. The illumination level and the type of house were cross-tabulated for better understanding. Fig. 5 depicts the type of house and illumination levels during the day based on visual observations and perceptions of beneficiaries and surveyors. The findings showed that approximately 59.4% of respondents lived in Kutchra houses, with 79.60% facing deficient illumination levels during the day and 57.4% experiencing dark or average illumination levels. About 37.0% of respondents lived in semi-pucca houses, with 20.1% facing deficient levels of illumination and 40.1% facing dark or moderate illumination levels.

In contrast, only 3.7% of respondents lived in pucca houses, indicating the minority. Those with grid electricity used bulbs or tube lights for daylight illumination, and those with access to grid-supplied electricity were careful to utilize lighting resources within the monthly subsidy. However, those with and without access to the electrical grid resorted to kerosene-based lights for illumination.

Risk Factor Analysis: Multivariate Approach

The frequency graph already depicts the electrification rate, lighting level, and kerosene usage, which may reflect the user's fundamental circumstances. Table 3 illustrates the

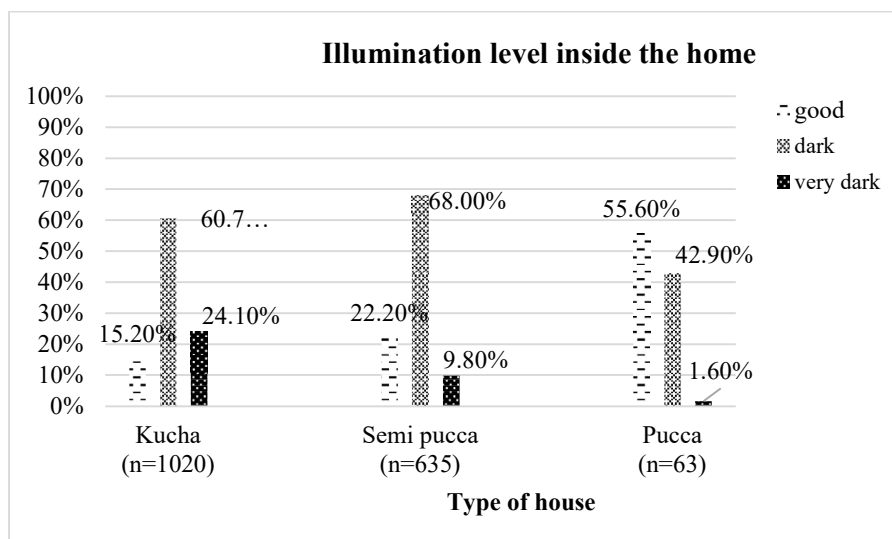


Fig. 5: Illumination level inside the house.

relationship between the risk-dependent variable MSD user education level and user perception variables concerning awareness of renewable energy. The MLR model involves categorical dependent variable (more than two) Y., e.g., three categories of education group and five explanatory (awareness about solar energy) variables X_1, X_2, X_3, X_4 and X_5 (Table 1) and three categories of illumination level inside the house before the MSD installation group and four explanatory (quality of life) variables X_1, X_2, X_3 and X_4 (Table 2).

The exploration of user variables, such as actual illumination level inside the house, safety, increase in education hours of the children, and engagement in economic activities, extended to the user's change in household illumination level after the installation. The categorization included good, dark/average, and very dark illumination levels. The coding for all variables was as follows: 1 for agree, 2 for disagree, and 3 for no knowledge, as presented in Table 2.

It is interesting to note that households with darker illumination conditions experienced a fourfold increase in the expected change in illumination levels after the installation

(3.93(2.16-7.16); $p < 0.001$), indicating that the product was crucial in improving the lighting conditions in households that need it the most. The household with good illumination did not require additional lighting significantly for safety during the dark ($n=331$). The households with dark illumination levels ($n=1016$) have experienced a significant increase in their perception of safety after installing the MSD (6.07(4.03-9.14); $p < 0.001$), demonstrating the significant impact it has had on their lives. In households with good illumination levels, children's education studying hours were drastically increased ($p < 0.001$), and there was no expected change in illumination level ($p < 0.001$) when compared to very dark illumination with each factor. The household having dark illumination perceived a significant increase in time spent on children's education (5.72 (4.01-8.16); $p < 0.001$), providing them with the opportunity to receive a better education, and children also said, "Our eyes are no longer burning".

Awareness Level of Clean Energy Technologies After Installation

The user's education level was explored for other varia-

Table 2: The illumination level's effect on the quality of life.

Illumination level Factors	Status	No [%]	B±SE	Exp(β)95%CI	p-value
Good (n=331)		<i>Intercept</i>			
Productivity	Agree	126 (38.07)	-2.58 ± 0.43		
	Disagree	205 (61.94)	0.93 ± 0.25	2.53(1.57-4.1)	< 0.001
Safety& Security	Agree	187 (56.5)	<i>Reference</i>		
	Disagree	144 (43.51)	-1.02 ± 0.23	0.37(0.23-0.57)	< 0.001
Education	Agree	116 (35.05)	3.69 ± 0.29	39.86(22.69-70.04)	< 0.001
	Disagree	193 (58.31)	5.07 ± 0.41	157.98(71.7-348.1)	< 0.001
	Neutral	22 (6.65)	<i>Reference</i>		
Changes in illumination level	Agree	184 (55.59)	0.03 ± 0.36	1.03(0.51-2.05)	0.951
	Disagree	120 (36.26)	2.01 ± 0.4	7.39(3.39-16.12)	< 0.001
	Neutral	27 (8.16)	<i>Reference</i>		
Dark /Average (n=1078)		<i>Intercept</i>			
Productivity	Agree	377 (34.97)	-2.88 ± 0.37		
	Disagree	701 (65.02)	0.88 ± 0.22	2.4(1.58-3.64)	< 0.001
Safety & Security	Agree	1018 (94.43)	<i>Reference</i>		
	Disagree	60 (5.56)	1.81 ± 0.21	6.07(4.03-9.14)	< 0.001
Education	Agree	495 (45.91)	1.75 ± 0.19	5.72(4.01-8.16)	< 0.001
	Disagree	307 (28.47)	2.9 ± 0.33	18.01(9.51-34.08)	< 0.001
	Neutral	276 (25.60)	<i>Reference</i>		
Changes in illumination level	Agree	747 (69.29)	1.37 ± 0.31	3.93(2.16-7.16)	< 0.001
	Disagree	295 (27.36)	2.45 ± 0.36	11.52(5.78-22.98)	< 0.001
	Neutral	36 (3.33)	<i>Reference</i>		
Very dark (n= 309)		<i>Reference category</i>			

p<0.05 = statistically significant

bles like the importance of off-grid during cyclone/disaster, electricity access equivalent to health care and education, the possibility of off-grid replacement options to grid electricity, and The MSD helping realize the necessities of life. All variables were coded categorically: 1 = agree, 2 = disagree, 3 = no knowledge. The user education was coded as 1= uneducated, 2= primary to higher secondary, and 3=graduation, as shown in Table 3.

Users without any formal education lacked prior knowledge about solar energy ($p < 0.001$) and believed that

access to electricity was equivalent to access to health care and education (3.9 (1.28-11.88); $p < 0.017$). Interestingly, they also firmly believed that MSDs should replace other electrification options in remote areas (29.75(5.9-150.01); $p < 0.001$). On the other hand, respondents with a higher secondary level of education had significantly different beliefs. They considered electricity access to be equivalent to access to health care and education and believed that the Solar Dome could facilitate the realization of basic necessities of life in case of no electricity connectivity

Table 3: Education level on awareness level following the implementation of cleaner technologies.

Awareness factors	Status	No [%]	B±SE	Exp(β)95%CI	p-value
Uneducated (n=1106)					
	Intercept		1.44 ± 0.88		
Electricity is equivalent to access to health care and education	Agree	748(67.64))	1.37 ± 0.57	3.9(1.28-11.88)	0.017
	Disagree	129(11.67))	-0.88 ± 0.6	0.42(0.14-1.33)	0.14
	Neutral	229(20.71))	Reference		
Solar Dome facilitates the realization of necessities of life	Agree	803(72.61))	0.79 ± 0.47	2.19(0.88-5.5)	0.096
	Disagree	132(11.94))	0.03 ± 0.53	1.03(0.38-2.85)	0.961
	Neutral	171(15.47))	Reference		
MSD can help during cyclones/disasters	Agree	578(52.27))	0.12 ± 0.66	1.13(0.32-4.02)	0.861
	Disagree	327(29.57))	1.54 ± 0.89	4.65(0.83-26.15)	0.082
	Neutral	201(18.18))	Reference		
Prior knowledge of solar energy	Agree	157(14.2))	-4.45 ± 0.7	0.02(0.01-0.05)	< 0.001
	Disagree	949(85.81))	Reference		
MSDS should replace other electrification options	Agree	828(74.87))	3.4 ± 0.83	29.75(5.9-150.01)	0.001
	Disagree	178(16.1))	1.8 ± 0.81	6.04(1.25-29.17)	0.026
	neutral	100(9.05))	Reference		
Education (1- 12th)					
	Intercept		1.49 ± 0.88		
Electricity is equivalent to access to health care and education	Agree	390(67.48))	2.35 ± 0.58	10.47(3.37-32.5)	< 0.001
	Disagree	90(15.58))	0.32 ± 0.6	1.38(0.43-4.39)	0.596
	Neutral	98(16.96))	Reference		
Solar Dome facilitates the realization of basic necessities of life	Agree	315(54.5))	0.08 ± 0.48	1.08(0.43-2.72)	0.872
	Disagree	112(19.38))	-0.07 ± 0.52	0.94(0.34-2.58)	0.894
	Neutral	151(26.13))	Reference		
MSD can help during cyclones/disasters	Agree	362(62.63))	0.49 ± 0.67	1.63(0.45-5.92)	0.465
	Disagree	150(25.96))	1.62 ± 0.89	5.04(0.89-28.79)	0.069
	Neutral	66(11.42))	Reference		
Prior knowledge of solar energy	Agree	116(20.07))	-4.02 ± 0.7	0.02(0.01-0.08)	< 0.001
	Disagree	465(80.45))	Reference		
MSDS should replace other electrification options	Agree	397(68.69)	1.72 ± 0.83	5.58(1.12-27.96)	0.037
	Disagree	67(11.6))	0.69 ± 0.81	1.99(0.41-9.62)	0.397
	neutral	114(19.73))	Reference		
Graduation (n=34)			Reference category		

$p < 0.05$ = statistically significant

(10.47(3.37-32.52); $p < 0.001$). Many users had no prior knowledge about solar energy (0.02 (0.01-0.08); $p < 0.001$), and they held a significant belief that MSDs should replace other electrification options like solar energy ($p = 0.037$) in remote areas.

DISCUSSION

Solar energy has revolutionized meeting energy demands and enhancing the quality of life in regions with restricted electricity access. The introduction of solar lanterns has led to significant changes in lighting patterns, with households switching from traditional lighting sources to solar lanterns, resulting in higher levels of satisfaction and economic development opportunities (Adkins et al. 2010). However, despite the many benefits of solar energy, not all studies have shown significant improvements in socioeconomic outcomes. The randomized field trial conducted in Uttar Pradesh's Barabanki area showed that while the provision of solar lights to unelectrified families did not result in significant improvements in development, the research on the socioeconomic and behavioral effects of solar lanterns suggests that they have the potential to provide significant marginal benefits to marginalized populations (Aklin et al. 2017). While solar lanterns may not lead to immediate, measurable socioeconomic improvements, they can still improve the lives of those living in rural communities. As such, future research should continue to investigate the potential benefits of solar lanterns on households' daily behavior, well-being, and perceptions of solar lighting rather than examining the high economic effects (Mahajan et al. 2020). While previous studies extensively examined the impact of solar home systems and off-grid setups in rural areas, only some researchers have prioritized analyzing solar lanterns as the focal point of their investigations. The MSD, used in this study, is a unique product that employs vertical light pipes, one of the most common renewable energy sources used in daylight science and daylighting technology to provide daylight illumination (GhoshThakur et al. 2022). This study has examined the impact of the Micro Solar Dome on economic activities, children's education hours, safety, and awareness of renewable energy technologies.

By focusing on this innovative and versatile product, this research sheds light on a new aspect of solar technology that researchers still need to explore fully. The study's findings showed a concerning situation with lighting in rural homes. It was alarming that these homes did not have enough light even during the day because they kept their windows closed to prevent insects and snakes from coming in. People also restricted electricity use because they feared surpassing the government's free unit allocation. This emphasizes the

significance of seeking alternative solutions to enhance indoor conditions without increasing household energy expenses. The installation of MSDs has effectively addressed this issue. These energy-saving devices have proven effective in providing high luminance flux, resulting in improved lighting conditions inside the home. The installations primarily targeted the kitchen, common room, and cattle-rearing spaces—key areas necessitating consistent daylight illumination. The study further unveiled that approximately 55% of households observed a significant enhancement in illumination following the light pipes' installation. In most households surveyed, women remained at home while male members were involved in agricultural activities or daily wage labor.

With adequate lighting, women felt safer and more secure while doing household chores. However, the grid supply in rural areas was highly intermittent, and power interruptions at night left women feeling vulnerable and forced to rely on kerosene lamps or candles for lighting. The installation of the MSD during the pandemic has been a boon for rural households. It has supported women in carrying out their household chores without any hassles, and the light provided by the MSD has been available from morning until late evening, making them feel safer and more secure, which has been reported in previous studies related to solar technologies (Buragohain 2012, Grimm et al. 2016, Urpelainen 2016). Women often engage in small-scale economic activities such as sewing, weaving, and shopkeeping. However, limited lighting availability has consistently posed an obstacle, constraining their working hours to daylight only. The installation of the MSD has changed this scenario drastically.

Women can now work in the evening, especially in households with low illumination levels, leading to a significant increase in hours spent on economic activities ($p < 0.001$) post-installation. This increase translates into economic benefits for the household and may contribute to women's empowerment. With access to affordable and reliable energy, women can extend their working hours, which reduces gender-related drudgery and enhances their socioeconomic status, as reported in previous studies related to gender implications of energy access (Winther et al. 2018). School-going children have also benefited greatly from the MSD installation. The children's academic performance was not assessed in the study. Still, the increase in education hours has been perceived by the children using it for reading during their late evening hours, which has been reported in previous studies related to solar lanterns and children education (Sharma et al. 2019). Furthermore, with online education becoming the norm during the pandemic, children continued their studies using mobile phones. The installation

of the MSD has enabled them to charge their mobile phones and extend their study hours into the evening.

Empowering Minds: Illuminating Community Awareness

MSD as an alternative to conventional energy sources has garnered significant attention recently. The study aimed to evaluate respondents' perceptions regarding the viability of MSDs as an alternative to traditional electrification options in areas prone to cyclones and natural disasters, along with their views on the importance of electricity access to health and education. The respondents were classified based on their formal education levels. Before the installation of MSDs, many respondents had limited knowledge of solar energy and its potential benefits. However, after the installation, our study revealed a significant increase in awareness of renewable energy among marginalized communities. The MSD facilitates the realization of basic life necessities in the absence of electricity connectivity. Respondents also strongly believed that off-grid products like MSDs could assist them during cyclones and other natural disasters, which often affect coastal areas.

Surprisingly, the level of education did not significantly impact the adoption of solar energy among respondents. While some previous studies have suggested that education plays a significant role in solar adoption. Our findings also align with previous work indicating that other contextual factors, such as social perception of electricity, may be more influential (Etongo & Naidu 2022). MSDs emerge as promising solutions for sustainable advancement, particularly within rural contexts. They replace harmful kerosene lamps, reduce indoor pollution and improving health.

Additionally, these technologies contribute to reducing carbon emissions, aligning with global climate change initiatives. The scope of this initiative extends beyond mere technological implementation, it encompasses key considerations such as prioritizing user-friendliness, ergonomic design, and alignment with local customs as mentioned in the previous studies (Balls 2020). Furthermore, these technologies possess the potential to stoke interest and pave the way for scaling up solar capacity within homes, ultimately fostering a transition toward grid independence. As these dynamic forces coalesce, they chart a trajectory toward a more sustainable and empowered future for rural communities. However, it is essential to also consider the economic, financial, and policy aspects due to their potential to promote economic growth via local entrepreneurship and lower energy costs. These aspects also interact with supportive policies, financial models, and affordability, all contributing to advancing sustainable energy transitions.

Policy Recommendations

This study underscores several key policy recommendations for enhancing the adoption of solar energy solutions in marginalized communities. Foremost among these is promoting community-based solar initiatives, which is vital for fostering a sense of ownership and collaboration. Establishing local support networks can significantly facilitate the collective adoption of solar solutions, making them more accessible and sustainable. Furthermore, the development and deployment of educational and awareness programs are essential. These programs, focusing on raising awareness about the benefits of solar energy, dispelling prevalent myths, and providing practical knowledge on sustainable energy practices, are crucial. Without this foundational awareness and education, merely providing the products would not be as effective. It is vital to ensure that communities are not only equipped with solar technology but also educated about its use and benefits. Lastly, it is crucial to formulate policies specifically tailored to address marginalized communities' unique challenges and needs, thus ensuring equitable access to clean energy resources.

Limitations

While our study has contributed valuable insights into the adoption of solar energy among marginalized communities, it is essential to acknowledge some limitations. Firstly, although the product used in our study was innovative as it could be used both day and night, we could not capture the reduction in kerosene usage as many households still needed firewood stoves for cooking. Additionally, due to COVID-19 restrictions, we could not conduct spot validations in many homes to verify reported increases in income and instead relied on self-reported perceptions. Despite these limitations, our study provides valuable insights into the potential benefits of solar adoption and highlights areas for further research and improvement.

CONCLUSION

The MSD has demonstrated its effectiveness in enhancing the quality of life in rural areas, particularly among marginalized communities. The study has shown that MSD implementation leads to better illumination, increased household safety, extended study hours for children, and expanded economic activities. The positive perception of the people highlights the significant benefits that MSDs offer. A crucial finding of this research is the role of education in fostering the adoption of solar energy technologies, with focus on hands-on experience is critical in enhancing understanding and encouraging the use of solar products. The accessibility of MSDs as affordable and sustainable energy solutions

enables these communities to meet their energy needs independently and reduce reliance on traditional fossil fuels. This research contributes significantly to setting realistic expectations for what can be achieved with basic access to clean energy. It underscores the value of incremental steps towards sustainable energy solutions in rural settings instead of pursuing overly ambitious goals requiring extensive social and economic overhaul. The success of installing MSDs in marginalized communities is a pivotal step in introducing and fostering interest in green energy technologies. In light of these findings, the study advocates for the replication and expansion of similar projects, reinforcing the belief that small-scale, community-centric initiatives can profoundly impact the quality of life in rural households by providing accessible, affordable, and sustainable energy solutions.

ACKNOWLEDGMENT

This work was supported by the Department of Science and Technology, India, with the grant number DST/TMDEWO/COMMITTEE/1/TSP.

REFERENCES

- Aarakit, S.M., Ntaji, J.M., Wasswa, F., Adaramola, M.S. and Ssenono, V.F. 2021. Adoption of solar photovoltaic systems in households: Evidence from Uganda. *J. Clean. Prod.*, 329: 129619. <https://doi.org/10.1016/j.jclepro.2021.129619>
- Abdullah-Al-Mahbub, M., Islam, A.R.M.T., Almohamad, H., Al Dughairi, A.A., Al-Mutiry, M. and Abdo, H.G. 2022. Different forms of solar energy progress: The fast-growing eco-friendly energy source in Bangladesh for a sustainable future. *Energies*, 15(18): <https://doi.org/10.3390/en15186790>
- Adkins, E., Eapen, S., Kaluwile, F., Nair, G. and Modi, V. 2010. Off-grid energy services for the poor: Introducing LED lighting in the Millennium Villages project in Malawi. *Energy Policy*, 38(2): 1087-1097. <https://doi.org/10.1016/j.enpol.2009.10.061>
- Agoramoorthy, G. and Hsu, M.J. 2009. Lighting the lives of the impoverished in India's rural and tribal drylands. *Hum. Ecol.*, 37(4): 513-517. <http://www.jstor.org/stable/40343992>
- Aklin, M., Bayer, P., Harish, S.P. and Urpelainen, J. 2017. Does basic energy access generate socioeconomic benefits? A field experiment with off-grid solar power in India. *Sci. Adv.*, 3(5): e1602153. <https://doi.org/10.1126/sciadv.1602153>
- Akter, S. and Bagchi, K. 2021. Is off-grid residential solar power inclusive? Solar power adoption, energy poverty, and social inequality in India. *Energy Res. & Social Sci.*, 82: 102314. <https://doi.org/10.1016/j.erss.2021.102314>
- Balls, J.N. 2020. Low-cost, adaptable solutions sell: Re-thinking off-grid solar diffusion at the bottom of the pyramid in India. *Energy Res. & Social Sci.*, 70: 101811. <https://doi.org/10.1016/j.erss.2020.101811>
- Banerjee, S.G., Bhatia, M., Azuela, G.E., Jaques, I., Sarkar, A., Portale, E. and Inon, J.G. 2013. *Global Tracking Framework*. Springer, Singapore. Retrieved from : <https://documents.worldbank.org/curated/en/603241469672143906/pdf/778890GTF0full0report.pdf>.
- Bond, M., Aye, L. and Fuller, R.J. 2010. Solar lanterns or solar home lighting systems – Community preferences in East Timor. *Renew. Energy*, 35(5): 1076-1082. <https://doi.org/10.1016/j.renene.2009.10.036>
- Bose, D., Saini, D.K., Yadav, M., Shrivastava, S. and Parashar, N. 2021. Review of sustainable grid-independent renewable energy access in remote communities of India. *Integr. Environ. Assess. Manag.*, 17(2): 364-375. <https://doi.org/10.1002/ieam.4373>
- Buragohain, T. 2012. Impact of solar energy in rural development in India. *Int. J. of Env. Sci. and Dev.*, 3(4): 334.
- Chamania, S., Chouhan, R., Awasthi, A., Bendell, R., Marsden, N., Gibson, J. and Potokar, T.S. 2015. Pilot project in rural western Madhya Pradesh, India, to assess the feasibility of using LED and solar-powered lanterns to remove kerosene lamps and related hazards from homes. *Burns*, 41(3): 595-603. <https://doi.org/10.1016/j.burns.2014.09.001>
- Etongo, D. and Naidu, H. 2022. Determinants of household adoption of solar energy technology in Seychelles in a context of 100% access to electricity. *Discover Sustain.*, 3(1): 38. <https://doi.org/10.1007/s43621-022-00108-4>
- Furukawa, C. 2014. Do solar lamps help children study? Contrary evidence from a pilot study in Uganda. *J. Dev. Stud.*, 50(2): 319-341. <https://doi.org/10.1080/00220388.2013.833320>
- GhoshThakur, R., Basu, A., Haque, Z., Bhattacharya, B., GonChaudhuri, S. and Balachandran, S. 2022. Performance prediction of the micro solar dome in different climatic regions of India from pilot-scale by random forest algorithm. *Sustain. Energy Technol. Assess.*, 52: 102163. <https://doi.org/10.1016/j.seta.2022.102163>
- Grimm, M., Munyehirwe, A., Peters, J. and Sievert, M. 2016. A first step up the energy ladder? Low-cost solar kits and household welfare in rural Rwanda. *World Bank Econ. Rev.*, 31(3): 631-649. <https://doi.org/10.1093/wber/lhw052>
- IEA. 2020. Residential electricity prices in India and selected countries, 2005-2019 Retrieved from Paris: <https://www.iea.org/data-and-statistics/charts/residential-electricity-prices-in-india-and-selected-countries-2005-2019>
- IEA. 2020. India 2020 Energy Policy Review. Retrieved from : <https://www.iea.org/reports/india-2020>
- Jacobson, A., Bond, T.C., Lam, N.L. and Hultman, N. 2013. Black Carbon and Kerosene Lighting: An Opportunity for Rapid Action on Climate Change and Clean Energy for Development. US Department of Energy, Washington, DC. Retrieved from : https://www.brookings.edu/wp-content/uploads/2016/06/04_climate_change_clean_energy_development_hultman.pdf
- Khandker, S.R.A.S., Hussain A.A., Sadeque, Z., Asaduzzaman, K.M.A., Mohammed, A.Y., Mohammad, A.H. and Enamul, A.K.. 2014. Surge in Solar-Powered Homes: Experience in Off-Grid Rural Bangladesh. Directions in Development, Energy, and Mining, World Bank Group, Washington, D.C
- Kudo, Y., Shonchoy, A.S. and Takahashi, K. 2019. Can solar lanterns improve youth academic performance? Experimental evidence from Bangladesh. *World Bank Econ. Rev.*, 33(2): 436-460. <https://doi.org/10.1093/wber/lhw073>
- Kumar, D. 2015. Economic assessment of photovoltaic energy production prospects in India. *Procedia Earth Planet. Sci.*, 11: 425-436. <https://doi.org/10.1016/j.proeps.2015.06.042>
- Mahajan, A., Harish, S.P. and Urpelainen, J. 2020. The behavioral impact of basic energy access: A randomized controlled trial with solar lanterns in rural India. *Energy Sustain. Dev.*, 57: 214-225. <https://doi.org/10.1016/j.esd.2020.04.005>
- Mahapatra, S. and Dasappa, S. 2012. Rural electrification: Optimising the choice between decentralised renewable energy sources and grid extension. *Energy Sustain. Dev.*, 16(2): 146-154. <https://doi.org/10.1016/j.esd.2012.01.006>
- Malhotra, A. 2022. Trade-offs and synergies in power sector policy mixes: The case of Uttar Pradesh, India. *Energy Policy*, 164: 112936. <https://doi.org/10.1016/j.enpol.2022.112936>
- Pelz, S., Chindarkar, N. and Urpelainen, J. 2021. Energy access for marginalized communities: Evidence from rural North India, 2015–2018. *World Dev.*, 137: 105204. <https://doi.org/10.1016/j.worlddev.2020.105204>

- Pokhrel Amod, K., Bates Michael, N., Verma Sharat, C., Joshi Hari, S., Sreeramareddy Chandrashekhar, T. and Smith Kirk, R. 2010. Tuberculosis and indoor biomass and kerosene use in Nepal: A Case-Control Study. *Environ. Health Perspect.*, 118(4): 558-564. <https://doi.org/10.1289/ehp.0901032>
- Rajendran, K., Ramamurthy, T. and Sur, D. 2007. Multinomial logistic regression model for the inferential risk age groups for infection caused by *Vibrio cholerae* in Kolkata, India. *J. Mod. Appl. Stat. Methods*, 6(1): 30. [10.22237/jmasm/1177993740](https://doi.org/10.22237/jmasm/1177993740)
- Rehman, I.H., Kar, A., Raven, R., Singh, D., Tiwari, J., Jha, R. and Mirza, A. 2010. Rural energy transitions in developing countries: a case of the Uttam Urja initiative in India. *Environ. Sci. Policy*, 13(4): 303-311. <https://doi.org/10.1016/j.envsci.2010.03.012>
- Sandwell, P., Chan, N.L.A., Foster, S., Nagpal, D., Emmott, C.J.M., Candelise, C. and Nelson, J. 2016. Off-grid solar photovoltaic systems for rural electrification and emissions mitigation in India. *Sol. Energy Mater. Sol. Cells*, 156: 147-156. <https://doi.org/10.1016/j.solmat.2016.04.030>
- Seabra, C., Almeida, S. and Reis, M. 2022. Quality-of-Life Perception among Young Residents and Visitors: The Impact of COVID-19, 14(23): 16177. <https://doi.org/10.3390/su142316177>
- Sharma, R., Choudhary, D., Kumar, P., Venkateswaran, J. and Solanki, C.S. 2019. Do solar study lamps help children study at night? Evidence from rural India. *Energy for Sustainable Dev.*, 50: 109-116. <https://doi.org/10.1016/j.esd.2019.03.005>
- Thorgren, A. and Ghasemi Niavarani, M. 2021. When darkness falls: Women's safety in refugee camps: A systematic literature review on the role of energy solutions for women (Dissertation). Retrieved from <https://urn.kb.se/resolve?urn=urn:nbn:se:sh:diva-45637>
- Urmee, T. and Md, A. 2016. Social, cultural and political dimensions of off-grid renewable energy programs in developing countries. *Renew. Energy*, 93: 159-167. <https://doi.org/10.1016/j.renene.2016.02.040>
- Urpelainen, J. 2016. Energy poverty and perceptions of solar power in marginalized communities: Survey evidence from Uttar Pradesh, India. *Renew. Energy*, 85: 534-539. <https://doi.org/10.1016/j.renene.2015.07.001>
- Velayudhan, S.K. 2003. Dissemination of solar photovoltaics: a study on the government programme to promote solar lantern in India. *Energy Policy*, 31(14): 1509-1518. [https://doi.org/10.1016/S0301-4215\(02\)00207-0](https://doi.org/10.1016/S0301-4215(02)00207-0)
- Winther, T., Ulsrud, K. and Saini, A. 2018. Solar powered electricity access: Implications for women's empowerment in rural Kenya. *Energy Res. Social Sci.*, 44: 61-74. <https://doi.org/10.1016/j.erss.2018.04.017>
- Wong, S. 2012. Overcoming obstacles against effective solar lighting interventions in South Asia. *Energy Policy*, 40: 110-120. <https://doi.org/10.1016/j.enpol.2010.09.030>
- World Bank .2021. Tracking SDG 7: The Energy Progress Report 2021. World Bank, Washington, DC. <http://hdl.handle.net/10986/38016>



The Stabilization of Copper and Cadmium in The Hydrated CaO-CuO-SiO₂ and CaO-CdO-SiO₂ Composites

A. K. Prodjosantoso*[†] , Y. Febriadi*, A. R. P. Utami** and M. P. Utomo*

*Department of Chemistry, Yogyakarta State University, Depok, Yogyakarta, Indonesia

**Department of Chemistry, Manado State University, Tondano, North Sulawesi, Indonesia

†Corresponding author: A.K. Prodjosantoso; prodjosantoso@uny.ac.id

Nat. Env. & Poll. Tech.
Website: www.neptjournal.com

Received: 05-09-2023
Revised: 26-10-2023
Accepted: 06-11-2023

Key Words:

Stabilization
TCLP
Calcium silicate
Heavy metals
Composites

ABSTRACT

The stabilization of toxic metals in the stable matrices is quite well-known. Research on copper and cadmium stabilization in the CaO-CuO-SiO₂ and CaO-CdO-SiO₂ composites was conducted to study the characteristics of CaO-CuO-SiO₂ and CaO-CdO-SiO₂ composites as well as the Cu and Cd metals stabilization in the hydrated composites. The composites of CaO-CuO-SiO₂ and CaO-CdO-SiO₂ were synthesized by the solid-state reaction method. A stoichiometric amount of CaO, SiO₂, Cu(NO₃)₂, and CdO were calcined at 1050°C for 4 hours. The synthesized compounds were further hydrated in a soaking time of 30, 60, and 90 days. The hydration produced calcium silicate hydrate that can stabilize metals. The Cu and Cd stability in CaO-CuO-SiO₂ and CaO-CdO-SiO₂, respectively, were tested using the Toxicity Leaching Procedure (TCLP) method. The hydrated and hydrated composite characterizations were performed using X-ray diffraction (XRD), Fourier Transform Infra-Red Spectrophotometer (FTIR), and Scanning Energy Microscopy-Energy Dispersive X-ray analyzer (SEM-EDX) and the Atomic Absorption Spectroscopy (AAS) methods. The composites mainly consist of Ca₃SiO₅, Ca₂SiO₄, Ca(OH)₂, SiO₂, and metal oxide of CuO, Cu₂O, and CdO. The composites were able to stabilize ~100% of the heavy metals of Cu and Cd.

INTRODUCTION

Heavy metals can cause environmental pollution. In the environment, gradually heavy metals will be absorbed by and accumulated in living organisms. Bioaccumulation of heavy metals can occur in plants, animals, and humans and cause serious health problems. Some metals that can cause health problems are cadmium (Cd) and copper (Cu) (Hossain et al. 2019).

Copper is toxic to certain levels of the human body. Poisoning of this metal can be acute or through accumulation first. Acute poisoning by Cu causes symptoms such as nausea, vomiting, abdominal pain, hemolysis, nephrosis, seizures, and death. Chronic copper poisoning can occur in the liver, leading to hemolysis (Gaetke et al. 2014). On the other hand, cadmium has negative effects on adult humans, including bone damage, cardiovascular disease, and heart disease. Other effects of cadmium are arthritis, kidney failure, and an increased risk of breast cancer (Chen et al. 2016). Those reasons motivate researchers to stabilize heavy metals to reduce pollution using the stabilization/solidification (S/S) method. The S/S technology is based on stabilizing waste, both physically and chemically. Cement,

lime, and dissolved silica are often used in the S/S process so that the metals do not leak into the environment (Singh & Budarayavalasa 2021).

Composites from a mixture of CaO and SiO₂ can be used to stabilize heavy metals. The reaction between the two compounds will produce calcium silicate compounds. CaO compounds can be obtained from chicken and duck eggshells. This is because eggshells contain 94-97% CaCO₃. The source of CaO compounds can be chosen from eggshells because of their high abundance and priceless. The oxide of SiO₂ can be obtained from nature. Many plants contain silica compounds. Reeds are one of the plants containing silica. However, the use of reeds as a source of SiO₂ is rare (Al-Jubouri et al. 2021).

Hydration is a reaction between certain compounds and water. The reaction can proceed eventually depending on the reactivity of the cation that is substituted (Prodjosantoso 2010). Calcium silicate reacts with water will form calcium silicate hydrate and calcium hydroxide compounds (Schlegel et al. 2015).

One of the main methods for measuring the leaching of heavy metal from the composite is the use of standard

leaching tests. The most used procedure is the Toxicity Characteristic Leaching Procedure (TCLP) of the United States Environmental Protection Agency (USEPA). The TCLP test is needed to determine the absorption rate of copper and cadmium in CaO-CuO/CdO-SiO₂ composites. This test can determine the degree of stabilization of copper and cadmium.

Over the past five years, more than nine hundred articles and journals on heavy metals have been published. This shows how critical the heavy metal problem is. Efforts to stabilize heavy metals with various breakthroughs need to be made. Research by Prodjosantoso and Kennedy (2003) on heavy metals Mg, Cd, Pb, and Ba in the cement phase Ca₃Al₂O₆ states that the change in the cement phase after the inclusion of foreign metals in the structure has a large area for further study with various heavy metals and types of composites.

Based on the description above, the purpose of this study is to determine the amount of metal that is stabilized in composites. This study has a great chance of obtaining the result that heavy metals will not be leached after a certain time of the hydration process.

MATERIALS AND METHODS

Composite Synthesis

The calcium oxide extracted from the powdered eggshell was mixed with the silicon dioxide from the reeds in a crucible. Calcining powder calcium oxide from eggshells and calcining powder silicon dioxide from reed plants were assumed to be pure calcium dioxide (CaO) and pure silicon dioxide (SiO₂). Thus, the molecular mass of these two powders was assumed to be equal to the relative mass of the pure compound. A mixture of these two materials was added with metals (Cu(NO₃)₂·3H₂O and CdO) to form a mixture of 1.8 CaO: 0.2 MO (metal oxide): 1 SiO₂. Then ethanol was added into the mixture and crushed until homogeneous, then dried. Drying was carried out using an oven at 110°C for 4 hours so that a dry mixture was obtained. The dry mixture was calcined at 1050°C for 4 hours and was cooled at room temperature to obtain the CaO-MO-SiO₂ composite. The samples were characterized using XRD, FTIR, and SEM-EDX methods.

Composite Hydration

A total of 5 grams of the composite was soaked in 500 mL of water for 30, 60, and 90 days. After soaking, this mixture was filtered off using a 600 mesh sieve to separate the filtrate from the precipitate. The precipitate was dried using an oven at 105°C for 1 h so that a dry hydrate composite was obtained.

The filtrate was evaluated using AAS to determine the rest of the metal that had not been entangled in the composite. Dry hydrate composites were characterized using FTIR.

Extractor Solution Determination

A total of 0.5 g of dry hydrate composite was put into a 250 mL beaker, added with 9.65 mL of water, and stirred using a magnetic stirrer for 5 min. The homogeneous composite mixture was then filtered off to obtain the filtrate. The pH of the filtrate was measured to determine the type of extractor solution. According to Kumar et al. (2016), two types of extractor solutions can be used. When the pH of the filtrate is < 5, extractor solution #1 of 5.7 mL of glacial acetic acid (98%) and 64.3 mL NaOH 1 N can be used. When the pH is more than 5, extractor solution #2 of 5.7 mL of glacial acetic acid can be nominated. All samples indicated a pH of > 5.

TCLP (Toxicity Characteristic Leaching Procedure)

Two grams of dry hydrated composite was added into a 250 mL Erlenmeyer, and then 40 mL of extractor #2 solution was added and stirred in an incubator for 18 hours at a rate of 60 rpm. The homogeneous mixture was then filtered off using filter paper to separate the filtrate (liquid phase) from the precipitate (solid phase). The liquid phase was characterized using the AAS method to determine the concentration of metal leached from the TCLP process. In contrast, the solid phase was characterized using XRD, FTIR, and SEM methods.

RESULTS AND DISCUSSION

The composite of CaO-CuO-SiO₂ and CaO-CdO-SiO₂ was successfully synthesized (Table 1.). The composites were characterized using the XRD Rigaku MiniFlex 600 operating Cu-K α radiation (1.541874 Å) at 2 θ angle from 2° to 80°.

Table 1: Sample code.

Treatment	Code	
	CaO-CuO-SiO ₂	CaO-CdO-SiO ₂
Composite	Cu.h0	Cd.h0
30-day hydrated composite	Cu.h30	Cd.h30
60-day hydrated composite	Cu.h60	Cd.h60
60-day hydrated composite	Cu.h90	Cd.h90
30-day hydrated composite and TCLP	Cu.h0T	Cd.h30T
60-day hydrated composite and TCLP	Cu.h30T	Cd.h60T
90-day hydrated composite and TCLP	Cu.h90T	Cd.h90T

The XRD diffractogram of unhydrated CaO-CuO-SiO₂ composite (Cu.h0) is described in Fig. 1., indicating that the calcined mixture of eggshell and reeds consists of calcium silicates (Ca₃SiO₅ (30.1%) and Ca₂SiO₄ (59.2%)), calcium hydroxide (Ca(OH)₂ (8.0%)), cristobalite (SiO₂ (2.2%)), copper tenorite (CuO (0.3%)), and unidentified species. Tricalcium silicate (Ca₃SiO₅) is characterized by lines at 2θ° angles of 18.30°; 23.42°; 29.76°; 31.40°; 32.56°; 34.62°; 35.90°; 39.16°; 41.54°; and 43.44°, which are in agreement with COD No. 1540705 data. This is also in accordance with Chen et al. (2007) finding that the XRD diffractogram

of Ca₃SiO₅ is at 2θ° around 23°, 29°, and 31°.

The compound Ca₂SiO₄ is indicated by XRD lines at 2θ° = 23.42°; 29.76°; 32.56°; 34.62°; 41.54°; 43.44°; 44.93°; 46.04°; 47.80°; 48.80°; 51.16°; 53.90°; 56.74°; 58.65°; 60.87°; and 68.52°. These peaks are in accordance with the results of the research of Mei et al. (2020) and COD No. 1546025. The phase of Ca(OH)₂ is indicated by lines at 2θ° about 51.16°, 18.30, and 56.74°, which is in accordance with COD No. 1000045. Samanta et al. (2016) state that Ca(OH)₂ (calcite) is indicated by a line at 2θ° around 51°.

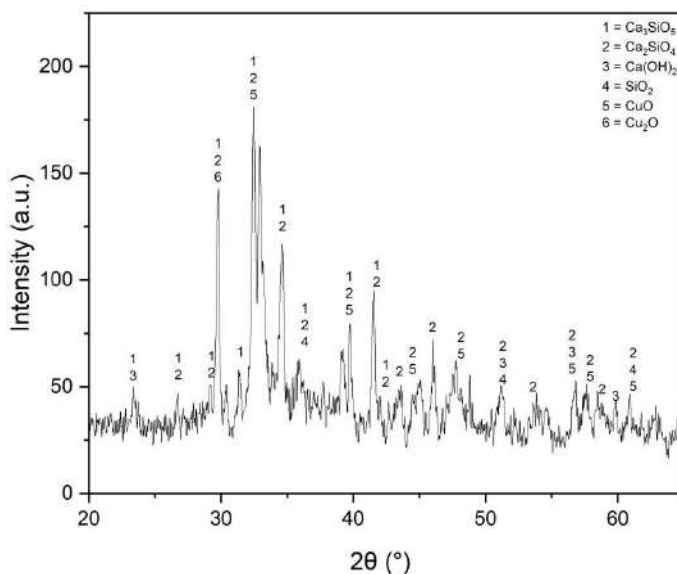


Fig. 1: The XRD diffractogram of Cu.h0 composite.

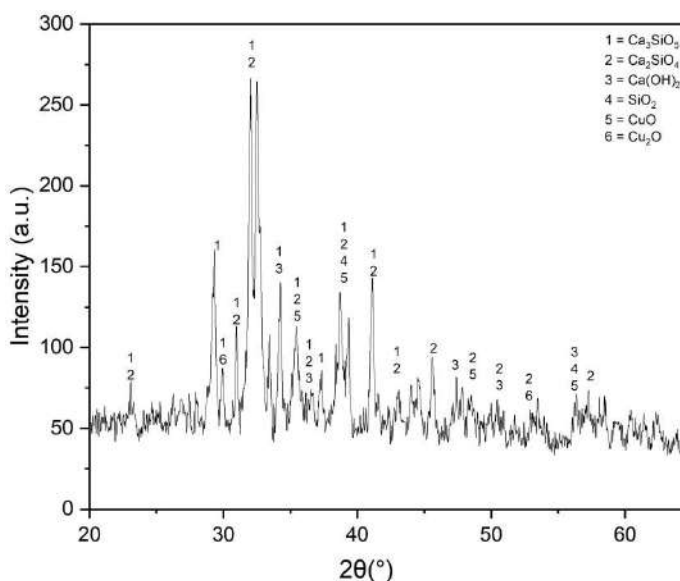


Fig. 2: The XRD diffractogram of Cu.h90T composite.

The compound of SiO_2 is indicated by peaks at $2\theta^\circ$ of 35.90° , 51.16° , and 68.52° . The peaks at 51.16° and 68.52° are in agreement with Geng et al. (2023) for $\alpha\text{-SiO}_2$. Copper compounds of CuO and Cu_2O are observed. The CuO occurs typically at $2\theta^\circ$ angles of 32.48° , 46.04° , 39.16° , 51.16° , 58.65° , and 68.52° , which are in accordance with COD No. 1526990, and Filiz (2020). The Cu_2O cuprite is indicated by the presence of peaks at $2\theta^\circ = 29.76^\circ$, which is in accordance with COD No. 1000063 data (Animasahun et al. 2021).

The Cu.h90T composite is the hydrated sample for 90 days. The XRD diffractogram indicates $2\theta^\circ$ lines at 23.08° ; 29.30° ; 29.95° ; 30.98° ; 32.00° ; 34.22° ; 35.44° ; 36.62° ; 37.32° ; 38.70° ; 41.10° ; and 43.04° (Fig. 2) for Ca_3SiO_5 (COD data No. 1540705). Chen et al. (2007) confirmed that the XRD diffraction peaks of the Ca_3SiO_5 compound are at $2\theta^\circ = 23^\circ$ and 29° . Another silicate, Ca_2SiO_4 compound, is identified by diffraction peaks at $2\theta^\circ = 23.08^\circ$; 30.98° ; 32.00° ; 35.44° ; 36.62° ; 38.70° ; 41.10° ; 43.04° ; 45.60° ; 48.40° ; 50.92° ; 52.97° ; 56.34° ; and 57.28° which is in agreement with COD No. 1546025. $2\theta^\circ$, and the findings of Mei et al. (2020).

XRD lines at $2\theta^\circ = 34.22^\circ$; 36.62° ; 47.40° ; 50.92° ; and 56.34° indicate the presence of Ca(OH)_2 compound (Samanta et al. 2016, COD data No. 1000045). The lines at $2\theta^\circ$ around 38.70° and 56.34° indicate the existence of the SiO_2 compound. The lines at $2\theta^\circ = 29.95^\circ$ and 52.97° indicate the presence of Cu_2O (COD No. 1000063), while the lines at 35.44° , 38.70° , and 48.40° indicate a typical line of CuO (COD No. 1526990, Filiz, 2020). Analyzing using

Match! 3 indicates the presence of Ca_3SiO_5 (20.4%), Ca_2SiO_4 (61.5%), Ca(OH)_2 (4.7%), SiO_2 (5.6%), CuO (7.7%), Cu_2O (0.1%), and an unidentified species (13.5%).

Based on the XRD diffractograms, Cu.h0T and Cu.h90T samples are crystalline phases. In addition, the samples contain Ca_3SiO_5 , Ca_2SiO_4 , Ca(OH)_2 , SiO_2 , CuO , and Cu_2O specieses.

The XRD diffractogram of the Cd.h0 is shown in Fig. 3. The XRD diffractogram of the Cd.h0 sample consisting of several lines indicating the presence of CdO (cadmium oxide monteponite), SiO_2 (cristobalite), Ca_3SiO_5 (alite), Ca_2SiO_4 (silicate), and Ca(OH)_2 .

Based on analysis using Match 3, the percentage of compounds Ca_3SiO_5 is 18.6%; Ca_2SiO_4 27.4%; Ca(OH)_2 40.2 %; SiO_2 13.3%; and CdO 0.2%. The percentage of metal Cd is observed to be very small. This is because Cd evaporated when subjected to heating during the sample treatment (Prodjosantoso & Kennedy 2003).

The diffraction lines at $2\theta^\circ = 32.85^\circ$ and 54.80° indicate the CdO . This is in accordance with the finding of Munawar et al. (2020), showing the XRD lines at $2\theta^\circ = 32^\circ$ and 55° . The SiO_2 XRD lines are observed $2\theta^\circ = 36.10^\circ$; 39.58° ; 41.47° ; 54.80° ; 63.18° ; and 64.78° . Typical lines appearing at $2\theta^\circ = 21.95^\circ$; 23.25° ; 29.56° ; 32.85° ; 34.47° ; 36.10° ; 39.58° ; 41.47° ; 43.29° ; 45.91° ; 47.58° ; 51.25° ; 53.48° ; 54.80° ; 59.85° ; and 63.18° indicate the presence of Ca_2SiO_4 which is in agreement with COD No. 1546025. Lines at $2\theta^\circ = 18.25^\circ$; 21.95° ; 23.25° ; 29.56° ; 32.85° ; 34.47° ; 36.10° ;

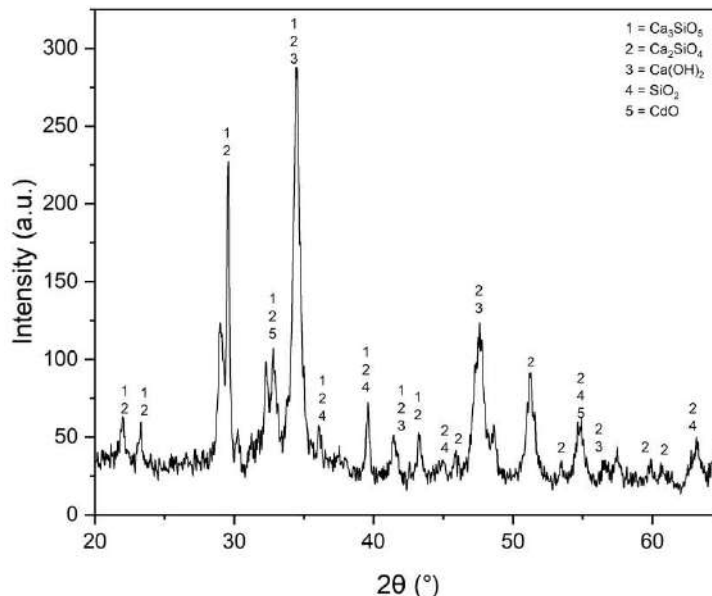


Fig. 3: The XRD diffractogram Cd.h0 sample.

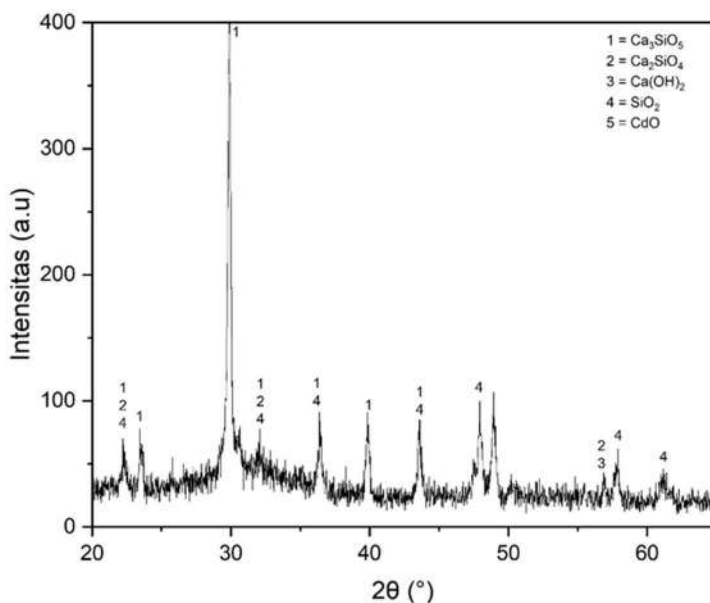


Fig. 4: The XRD diffractogram sample Cd.h90T composite CaO-CdO x-SiO₂ after 90 days of hydration and TCLP.

39.58°; 41.47°; and 43.29° indicate the presence of Ca₃SiO₅ (COD No. 1540705). Chen et al. (2007) state that the XRD lines of Ca₃SiO₅ are about 2θ = 23° and 29°. The lines at 2θ = 18.25°; 34.47°, 47.58°, and 56.59° indicate the Ca(OH)₂ (COD No. 1000045, Samanta et al. 2016).

The XRD diffractogram of Cd.h90T is depicted in Fig. 4. Analysis of the XRD diffractogram of Cd.h90T using Match! 3 indicate the percentage of Ca₃SiO₅ of 58.7%; Ca₂SiO₄ 21.8 %; Ca(OH)₂ 1.0%; SiO₂ 18.3%; CdO 0.1%, and some unidentified peak 17.7%.

The XRD diffraction peaks at 2θ = 22.28°; 23.53°; 29.89°; 32.00°; 36.41°; 39.86°; and 43.58° indicate the presence of Ca₃SiO₅ (COD No. 1540705, Chen et al. 2007). The peaks at 2θ = 18.63°; 22.28°; 32.00°; 56.90°; 65.02°; and 70.66° indicate the presence of Ca₂SiO₄. The line at 2θ = 56.90° indicates the presence of Ca(OH)₂ (COD No. 1000045). The lines are also observed at 2θ = 22.28°; 32.00°; 36.41°; 43.58°; 47.94°; 61.18°; 66.10°; and 70.66° indicating the SiO₂ and at 2θ = 66° indicating the presence of CdO (Munawar et al. 2020).

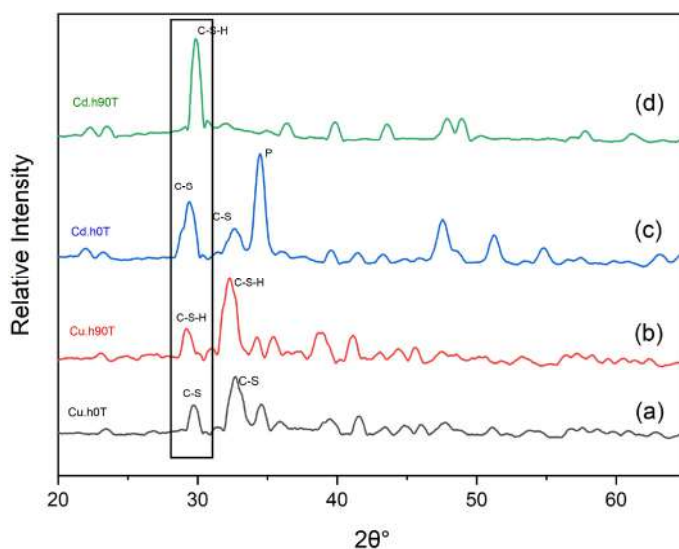


Fig. 5: The XRD diffractogram of (a) Cu.h0, (b) Cu.h90T, (c) Cd.h0, and (d) Cd.h90T samples.

Table 2: The FTIR absorption data of CaO-CuO-SiO₂

Interpretation	Wavenumber [cm ⁻¹]		
	Cu.h0	Cu.h90	Cu.h90T
O-H stretching of Ca(OH) ₂	3625	3627	3595
O-H stretching of H ₂ O	3378	3426	3368
C=O stretching of CO ₂	2359	2360	2357
C-O stretching of CaCO ₃	1405	1414	1419
	1435		
	1477		
Stretching asymmetri Si-O of C-S-H	985	967	996
Ca-O stretching	869	871	872
Si-O-Si group	672	669	668
stretching O-Si-O of SiO ₂	500	495	492

The XRD diffractogram of composite undergoes a shift after the hydration process and TCLP test (Fig. 5). According to Maddalena et al. (2019) the shifts from $2\theta = 29.76^\circ$ to 29.30° and from 29.56° to 29.89° for CaO-CuO-SiO₂ and CaO-CdO_x-SiO₂, respectively, indicate the formation of calcium silicate hydrate (C-S-H).

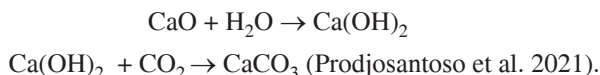
The shifts of the XRD diffractogram are due to the formation of new phases, namely CaO-CuO-SiO₂ and CaO-CdO-SiO₂. In the new phases, the Ca²⁺ ions are partly replaced by copper and cadmium ions in the Cu.h90T and Cd.h90T, respectively. The diameters of the Ca²⁺, Cu⁺, Cu²⁺, and Cd²⁺ ions are 114 pm, 91 pm, 87 pm, and 97 pm, respectively. Thus, due to the ions substituting Ca²⁺ are smaller, the XRD lines are shifted to the right (Fig. 5).

Samples obtained by calcining a mixture of eggshell, reed ash, and metal oxide were analyzed using FTIR to identify the

existence of the functional groups of the compounds in the sample. The vibrations of the samples are listed in Table 2.

The FTIR spectra of Cu.h0, Cu.h90, and Cu.h90T samples are similar (Fig. 6.). The difference is noticeable in the intensity of the peaks spectra, indicating the difference in the quantitative amount of components in the samples.

The O-H vibration at 3200-3600 cm⁻¹ is stronger, along with hydration treatment and TCLP on the samples. The increase in O-H spectra is due to the hydration of CaO-producing Ca(OH)₂. The presence of Ca-O in the Ca(OH)₂ is indicated by absorption at a wavenumber of 800 cm⁻¹. The Ca(OH)₂ readily reacts with CO₂ from air through the following reaction.



The formation of CaCO₃ is supported by the presence of a peak indicating the C-O stretching in the CaCO₃. This peak is weak in the unhydrated sample and is stronger in hydrated and TCLP samples, indicating the increase of CaCO₃ in the unhydrated sample. The increase of CaCO₃ is due to the carbonation of CaO and/or Ca(OH)₂. According to Imani et al. (2022), hydrated CaO reacts with CO₂, producing CaCO₃. The CO₂ in the sample is indicated by the absorption at 2400 cm⁻¹ (Bekhti et al. 2021).

The peak at 900 cm⁻¹ indicates the presence of a Ca-Si-O bond. Hydration treatment causes the absorption of Ca-Si-O to increase in intensity. This is due to the increased amount of C-S-H bonds caused by hydration. The increase in C-S-H is also supported by the presence of free water (H₂O), which is indicated by weak absorption at 3400 cm⁻¹ (Saidani et al., 2018).

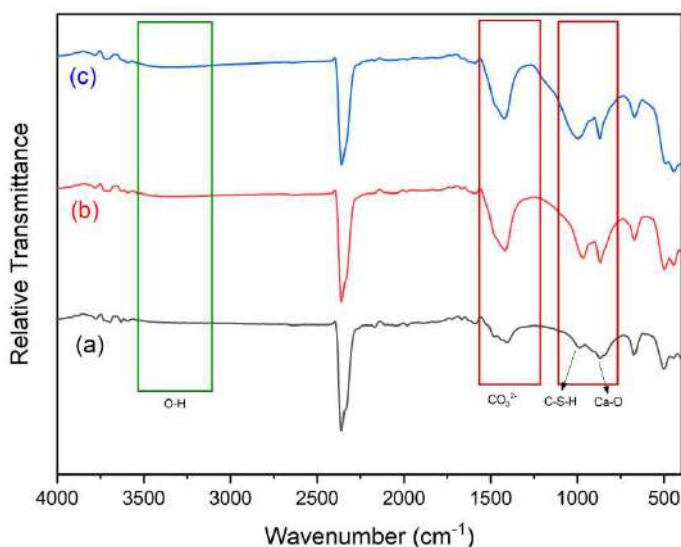


Fig. 6: The FTIR spectra of (a) Cu.h0, (b) Cu.h90, and (c) Cu.h90T.

Table 3: CaO-CdO_x-SiO₂ composite FTIR data absorption.

Interpretation	Wavenumber [cm ⁻¹]		
	Sample Cd.h0	Sample Cd.h90	Sample Cd.h90T
O-H stretching of H ₂ O	3632	3592	3429
O-H stretching of Ca(OH) ₂	3375	3395	3375
C=O stretching of CO ₂	2359	2358	2357 2332
C-O stretching of CaCO ₃	1408	1408	1413
Ca-O-Si	997	966	962
Ca-O stretching	910 873	873	870
Si-O-Si group	706 669	706 666	702 660
O-Si-O stretching of SiO ₂	500	445	443

The FTIR spectra of CaO-CdO₂-SiO₂ are comprised of various absorption peaks (Table 3).

The FTIR spectra of hydrated and unhydrated samples are depicted in Fig. 7. The FTIR spectra differences between Cd.h0 with Cd.h90 and Cd.h90T are observed. The spectra of the hydrated sample observed at 3200-3600 cm⁻¹ are stronger than the unhydrated. This is due to the reaction of CaO with water, forming Ca(OH)₂.

In the C-O absorption area, the asymmetry of CaCO₃ absorption peaks is stronger. This indicates that there is an increase in CaCO₃ after hydration, according to research from Bekhti et al. (2021). Conversely, the Ca-O absorption area at 910-870 cm⁻¹ experienced attenuation of absorption. This is because Ca in CaO is replaced by Cd metal, and then Ca in Ca-Si-O bonds increases in the wavenumber range 1050-

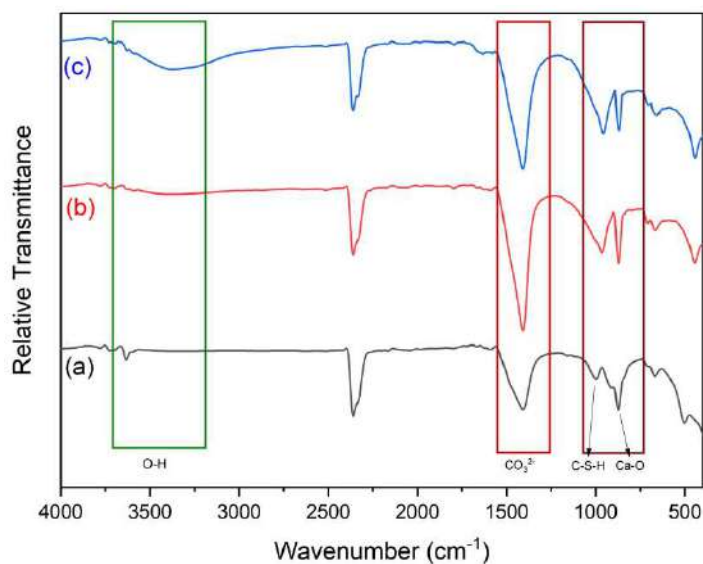


Fig. 7: The FTIR spectra of (a) Cd.h0), (b) Cd.h90, and (c) Cd.h90T.

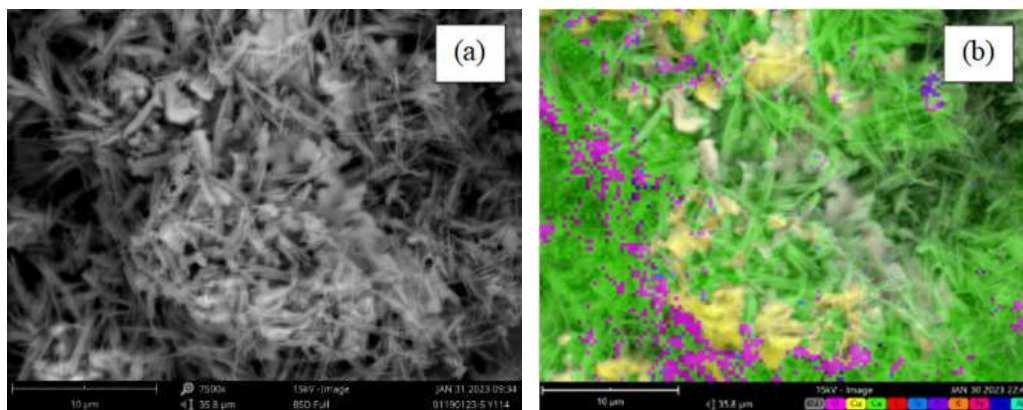


Fig. 8: the surface morphology of Cu.h0 with 7500x magnification (a) and mapping (b).

950 cm^{-1} . This is in accordance with Yang et al. (2022) research.

Selected SEM micrographs of Cu.h0 are presented in Fig. 8. The sample is elongated fibers with a length of about 3 μm . The particles are evenly distributed, and agglomerations are not observed. In addition to observing the surface with SEM, surface analysis was also undertaken using EDX to determine the elements composing the sample (Fig. 8). The distribution of elements is observed to be homogeneous with the dominance of Ca (green). The Cu element is in the middle position, surrounded by other elements.

The EDX analysis of Cu.h0 results in the element composition of the sample (Fig. 9), Ca, Cu, and Si as much as 48.75%; Cu 44.87%; and Si 16.38%, respectively. The tiny amount of other elements detected are K, Fe, Al, and Mg. These elements are in samples as a result of the use of natural material as a precursor. The elements of Al, K, Mg, and Fe were reported to be present in chicken eggshells (Park et al. 2007), and K and Mg are found in

reeds (Butler et al. 2021).

The SEM micrographs of Cu.h90T are shown in Fig. 10. The 90-day hydration and TCLP (Fig. 10.) cause the deformation of the particle. The elongated fibers (Fig. 8.) change to rounded particles having about 1 μm in size. The even distribution of Ca and Si is observed (Fig. 10).

The EDX graph (Fig. 11) describes that the percentages of elements Ca, Cu, and Si are (50.63%), (20.84%) and (16.38%), respectively. The percentage of Cu elements decreases after 90 days of hydration and TCLP. In the sample are also observed, unexpected elements such as K, Al, Mg, and P. These elements can be assumed from eggshells and reeds used as precursors.

The SEM was performed on Cd.h0 samples (Fig. 12). The surface of Cd.h0 is irregular in shape. The surface is dominated by the Ca element, which is characterized by the presence of a dominant green color. The Si elements (purple) are slightly visible, while the cadmium elements are not detected.

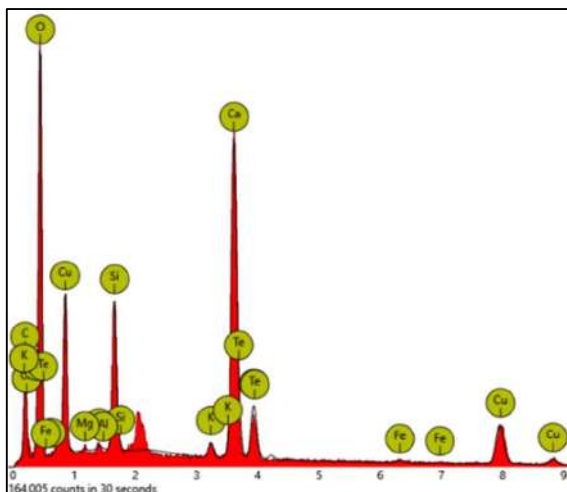


Fig. 9: The EDX of Cu.h0.

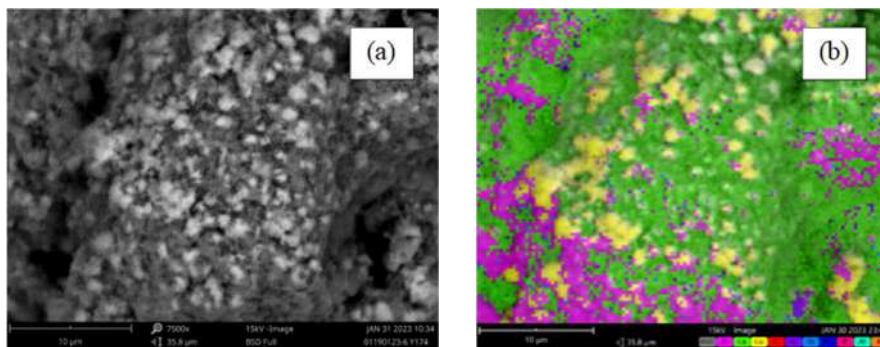


Fig. 10: The SEM micrograph of Cu.h90T.

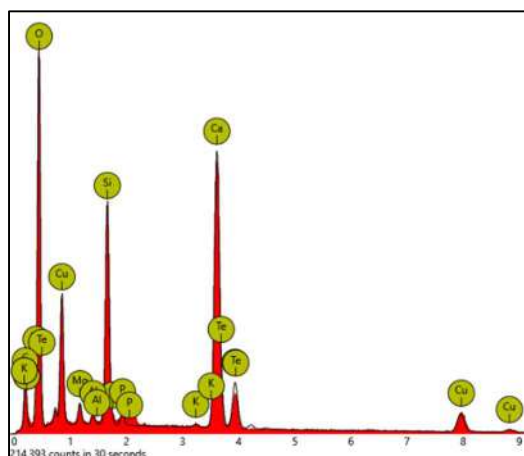


Fig. 11: The EDX graph of Cu.h90T.

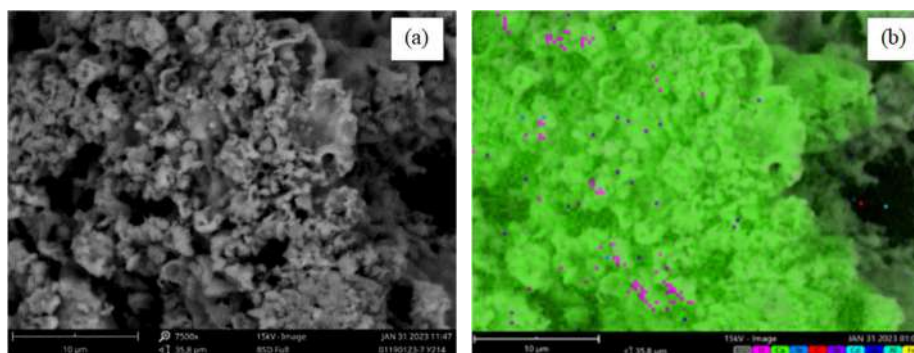


Fig. 12: The surface morphology of Cd.h0.

The SEM micrograph of Cd.h90T can be seen in Fig. 13. The surface of the sample is rough, with no lumps forming. Elemental mapping analysis (Fig. 13. (b)) indicates that the distribution of elements on the sample surface is evenly distributed. The surface is dominated by Ca (green) and the minor of Cd (light blue), which Ca may cover.

The EDX of Cd.h90T (Fig. 14.) shows the percentage

of the main constituents of the sample, i.e., Ca (52.9%), Cd (3.44%), and Si (43.66%). There is a decreasing content of Cd metal after the hydration and TCLP samples. It is believed that Cd evaporates during sample preparation (Prodjosantoso & Kennedy 2003).

For tracing the Cu and Cd metals, the hydration and TCLP filtrate of the samples were analyzed using the AAS method.

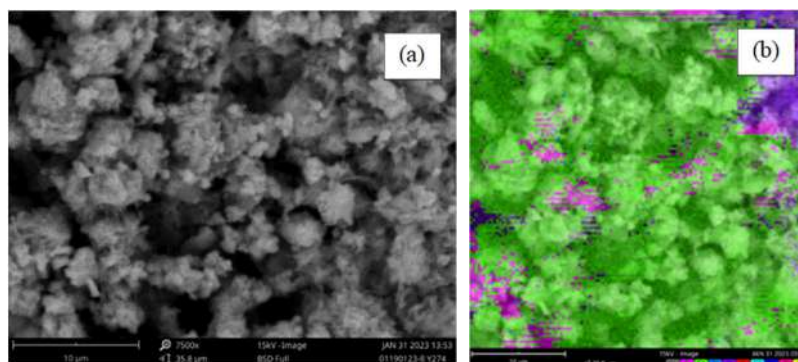


Fig. 13: The surface morphology of Cd.h90T.

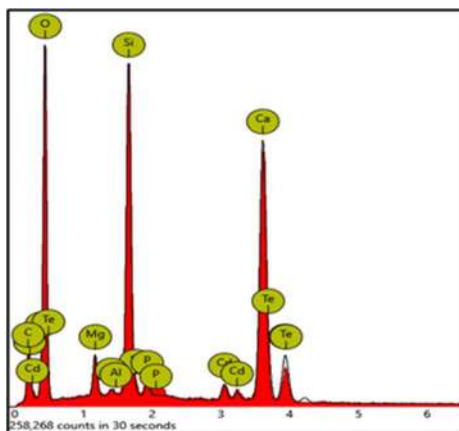


Fig. 14: The EDX of Cd.h90T.

Table 4: The Cu in the hydrated CaO-CuO-SiO₂

Samples	The Cu leached after hydration [mg.L ⁻¹]	The Cu leached after hydration [mole]	Stabilized Cu in samples [mole]	Percentage of Cu in samples [%]
Cu.h30	0.0113	8.9×10^{-8}	0.19999911	99.99995554
Cu.h60	0.0082	6.5×10^{-8}	0.19999935	99.99996774
Cu.h90	0.0062	5.8×10^{-8}	0.19999951	99.99997561

Table 5: The Cu in CaO-CuO-SiO₂ after TCLP.

Samples	The Cu leached after hydration [mg.L ⁻¹]	The Cu leached after hydration [mole]	Stabilized Cu in samples [mole]	Percentage of Cu in samples [%]
Cu.h30T	0.0082	5.2×10^{-9}	0.19999906	99.99999742
Cu.h60T	0.0051	3.2×10^{-9}	0.19999932	99.99999839
Cu.h90T	0.0072	4.5×10^{-9}	0.19999947	99.99999773

Table 6: The Cd in the hydrated CaO-CdO-SiO₂

Samples	The Cd leached after hydration [mg.L ⁻¹]	The Cd leached after hydration [mole]	Stabilized Cd in samples [mole]	Percentage of Cd in samples [%]
Cd.h30	0.1261	5.6×10^{-7}	0.199999439	99.99971955
Cd.h60	0.1296	5.7×10^{-7}	0.199999424	99.99971177
Cd.h90	0.1228	5.5×10^{-7}	0.199999454	99.99972689

Table 7: The Cd in CaO-CdO-SiO₂ after TCLP.

Samples	The Cd leached after hydration [mg.L ⁻¹]	The Cd leached after hydration [mole]	Stabilized Cd in samples [mole]	Percentage of Cd in samples [%]
Cd.h30T	0.1193	4.2×10^{-8}	0.199999397	99.99997877
Cd.h60T	0.1222	4.3×10^{-8}	0.19999938	99.99997826
Cd.h90T	0.1225	4.4×10^{-8}	0.19999941	99.99997820

By doing it, the metals retained in the samples are known.

The AAS analysis of CaO-CuO-SiO₂ samples is presented in Table 4. and Table 5.

The AAS analysis of the samples indicates that both the Cu in the hydrated and TCLP samples are ~100% stabilized. However, the amount of leached metals is observed to be

very small and safe for the environment.

The AAS analysis of CaO-CdO-SiO₂ samples is presented in Table 6. and Table 7.

Similar to the Cu samples, the AAS analysis of the samples indicates that both the Cd in the hydrated and TCLP samples are ~100% stabilized. However, the amount

of leached metals is observed to be very small and safe for the environment.

CONCLUSIONS

Based on the research, it can be concluded that the CaO-CuO-SiO₂ and CaO-CdO-SiO₂ are composed of the main compounds: Ca₃SiO₅ (alite), Ca₂SiO₄ (silicate), Ca(OH)₂ (portlandite), SiO₂ (cristobalite), and metal oxides of CuO (tenorite) and Cu₂O (cuprite), as well as the CdO (mentoponite) for cadmium. The Cu and Cd are stabilized in CaO-CuO-SiO₂ and CaO-CdO-SiO₂ composites by ~100%.

ACKNOWLEDGMENTS

The author would like to thank the Department of Chemistry Education, Yogyakarta State University.

REFERENCES

- Al-Jubouri, S.M., Al-Batty, S.I. and Holmes, S. M. 2021. Using the ash of common water reeds as a silica source for producing high purity ZSM-5 zeolite microspheres. *Micropor. Mesopor. Mater.*, 316: 110953, <https://doi.org/10.1016/j.micromeso.2021.110953>.
- Animasahun, L.O., Taleatu, B.A., Adewinbi, S.A., Bolarinwa, H.S. and Fasasi, A.Y. 2021. Synthesis of SnO₂/CuO/SnO₂ multi-layered structure for photoabsorption: compositional and some interfacial structural studies. *J. Niger. Soc. Physic. Sci.*, 3: 74-81. <https://doi.org/10.46481/jnps.2021.160>.
- Bekhti, H., Boucheffa, Y., Blal, A.H. and Travert, A. 2021. In situ FTIR investigation of CO₂ adsorption over MgO-impregnated NaY zeolites. *Vib. Spectrosc.*, 117: 103313. <https://doi.org/10.1016/j.vibspec.2021.103313>.
- Butler, O.M., Lewis, T. and Chen, C. 2021. Do soil chemical changes contribute to the dominance of blady grass (*Imperata cylindrical*) in surface fire-affected forests? *Fire*, 23 : (2)4. <https://doi.org/10.3390/fire4020023>.
- Chen, C., Xun, P., Nishijo, M. and He, K. 2016. Cadmium exposure and risk of lung cancer: A meta-analysis of cohort and case-control studies among general and occupational populations. *J. Expo. Sci. Environ. Epidemiol.*, 26: 437-444. <https://doi.org/10.1038/jes.2016.6>.
- Chen, Q.Y., Hills, C.D., Tyrer, M., Slipper, I., Shen, H. G. and Brough, A. 2007. Characterization of products of tricalcium silicate hydration in the presence of heavy metals. *J. Hazard. Mater.*, 3(147): 817-825. <https://doi.org/10.1016/j.jhazmat.2007.01.136>.
- Filiz, B.C. 2020. The role of catalyst support on activity of copper oxide nanoparticles for reduction of 4-nitrophenol. *Adv. Powder Technol.*, 9(31): 3845-3859. <https://doi.org/10.1016/j.apt.2020.07.026>.
- Gaetke, L.M., Chow-Johnson, H.S. and Chow, C.K. 2014. Copper: Toxicological relevance and mechanisms. *Arch. Toxicol.*, 11(88): 1929-1938. <https://doi.org/10.1007/s00204-014-1355-y>.
- Geng, C., Mei, Z., Yao, X., Wang, C., Lu, D. and Chen, W. 2023. Effect of the crystalline state of SiO₂ on the compressive strength of cement paste at HTHP. *Constr. Build. Mater.*, 362: 129787. <https://doi.org/10.1016/j.conbuildmat.2022.129787>.
- Hossain, R., Nekouei, R.K., Mansuri, I. and Sahajwalla, V. 2019. Sustainable recovery of Cu and sn from problematic global waste: exploring value from waste printed circuit boards. *ACS Sustain. Chem. Eng.*, 7(1): 4567. <https://doi.org/10.1021/acssuschemeng.8b04657>.
- Imani, M., Tahmasebpour, M., Sánchez-Jiménez, P.E., Valverde, J.M. and Moreno, V. 2022. Improvement in cyclic CO₂ capture performance and fluidization behavior of eggshell-derived CaCO₃ particles modified with acetic acid used in a calcium looping process. *J. CO₂ Util.*, 65: 102207. <https://doi.org/10.1016/j.jcou.2022.102207>.
- Kumar, K.S., Gandhimathi, R. and Baskar, K. 2016. Assessment of heavy metals in the leachate of concrete made with e-waste plastic. *Adv. Civil. Eng. Mater.*, 5(1): 256-262. <https://doi.org/10.1520/ACEM20160003>.
- Maddalena, R., Li, K., Chater, P. A., Michalik, S. and Hamilto, A. 2019. Direct synthesis of a solid calcium-silicate-hydrate (C-S-H). *Constr. Build. Mater.*, 223: 565-554. <https://doi.org/10.1016/j.conbuildmat.2019.06.024>.
- Mei, K., Cheng, X., Pu, Y., Ma, Y., Gao, X., Yu, Y., Zhuang, J. and Guo, X. 2020. Evolution of silicate structure during corrosion of tricalcium silicate (C₃S) and dicalcium silicate (C₂S) with hydrogen sulfide (H₂S). *Corros. Sci.* 163: 108301. <https://doi.org/10.1016/j.corsci.2019.108301>.
- Munawar, T., Yasmeen, S., Hussain, F., Mahmood, K., Hussain, A., Asghar, M. and Iqbal, F. 2020. Synthesis of novel heterostructured ZnO-CdO-CuO nanocomposite: characterization and enhanced sunlight driven photocatalytic activity. *Mater. Chem. Phys.*, 249: 122983. <https://doi.org/10.1016/j.matchemphys.2020.122983>.
- Park, H.J., Jeong, S.W., Yang, J.K., Kim, B.G. and Lee, S.M. 2007. Removal of heavy metals using waste eggshells. *J. Environ. Sci.*, 19(12): -1436 1441. [https://doi.org/10.1016/S1001-0742\(07\)60234-4](https://doi.org/10.1016/S1001-0742(07)60234-4).
- Prodjosantoso, A.K. and Kennedy, B.J. 2003. Heavy metals in cement phases: on the solubility of Mg, Cd, Pb, and Ba in Ca₃Al₂O₆. *Cem. Con. Res.*, 7(33): 1077-1084. [https://doi.org/10.1016/S0008-8846\(03\)00017-6](https://doi.org/10.1016/S0008-8846(03)00017-6).
- Prodjosantoso, A., Widiyati, W., Widyawati, A. and Utomo, M. P. 2021. Cement chemistry: Hydration of Ca_{2-x}Sr_xSiO₄ compound. *Orient. J. Chem.*, 3(37): 589. <https://doi.org/10.13005/ojc/370310>.
- Prodjosantoso, A.K. 2010. *Inorganic Chemical Engineering*. Kanisius, Yogyakarta.
- Saidani, S., Smith, A., El Hafiane, Y. and Tahar, L. B. 2018. Re-examination of β → γ transformation of Ca₂SiO₄. *J. Eur. Ceram. Soc.*, 38(14): -4756 4767. <https://doi.org/10.1016/j.jeurceramsoc.2018.06.11>.
- Samanta, A., Chanda, D. K., Das, P. S., Ghosh, J., Mukhopadhyay, A. K. and Dey, A. 2016. Synthesis of nano calcium hydroxide in aqueous medium. *J Am. Ceram. Soc.*, 99(3): 787-795. <https://doi.org/10.1111/jace.14023>.
- Schlegel, M. L., Pointeau, I., Coreau, N. and Reiller, P. 2004. Mechanism of europium retention by calcium silicate hydrates: An EXAFS study. *Environ. Sci. Technol.*, 16(38): 4423-4431. <https://doi.org/10.1021/es0498989>.
- Singh, R. and Budarayavalasa, S. 2021. Solidification and stabilization of hazardous wastes using geopolymers as sustainable binders. *J. Mater. Cycles. Waste. Manag.*, 23: 1699-1725. <https://doi.org/10.1007/s10163-021-01245-0>.
- Yang, F., Pang, F., Xie, J., Wang, W., Wang, W. and Wang, Z. 2022. Leaching and solidification behavior of Cu²⁺, Cr³⁺, and Cd²⁺ in the hydration products of calcium sulfoaluminate cement. *J. Build. Eng.*, 46: 103696. <https://doi.org/10.1016/j.jobbe.2021.103696>.

ORCID DETAILS OF THE AUTHORS

A. K. Prodjosantoso: <https://orcid.org/0000-0001-7603-5857>



Study of *Chlorella vulgaris* from Different Growth Phases as Biosensor for Detection of Titanium and Silver Nanoparticles in Water

Arularasi Thenarasu^{*(**)}, Mee Kin Chai^{*†} , Yeong Hwang Tan^{* }, Ling Shing Wong^{** },
Ranjithkumar Rajamani^{*** (****) } and Sinouvassane Djearmane^{***** (*****) }

* Institute of Sustainable Energy, Universiti Tenaga Nasional, Jalan Ikram-Uniten, 43000 Kajang, Selangor, Malaysia

**Faculty of Health and Life Sciences, INTI International University, Persiaran Perdana BBN, Putra Nilai, 71800 Nilai, Negeri Sembilan, Malaysia

*** Viyen Biotech LLP, Coimbatore-034, 641015 Tamilnadu, India

**** Department of Biotechnology, Sri Ramakrishna College of Arts and Science, Nava India, Coimbatore, 641006 Tamilnadu, India

*****Department of Biomedical Science, Faculty of Science, Universiti Tunku Abdul Rahman, Kampar, 31900, Malaysia

*****Faculty of Allied Health Sciences, Sri Lakshmi Narayana Institute of Medical Sciences, Puducherry 605502, India

†Corresponding author: Mee Kin Chai, Mkchai@uniten.edu.my

Nat. Env. & Poll. Tech.
Website: www.neptjournal.com

Received: 15-09-2023

Revised: 13-11-2023

Accepted: 15-11-2023

Key Words:

Natural microalgae

Chlorella vulgaris

Nanoparticle pollutants

Fluorescence detection

ABSTRACT

The increased use of metallic nanoparticles has led to concern for environmental contamination and disruption in water quality. Therefore, effective screening of metallic nanoparticles is important for detecting metallic nanoparticles in aquatic environments. Biosensors offer several advantages, including high sensitivity to pollutants, short response time, energy efficiency, and low waste generation. In this study, a whole-cell biosensor was developed using microalgae *Chlorella vulgaris* as a recognition element, and its fluorescence response was used as a measuring parameter for detecting the presence of titanium dioxide (TiO₂) and silver (Ag) nanoparticles in water. The responses of *C. vulgaris* at the lag, exponential, and stationary phases to different concentrations of TiO₂ and Ag nanoparticles were studied. The results showed that in TiO₂ and Ag nanoparticles exposures, the highest fluorescence change (50-150%) was observed at the lag phase, whereas the lowest fluorescence change (40-75%) was observed at the stationary phase. A significant fluorescence change was observed in 15 min. The immobilized *C. vulgaris* under TiO₂ and Ag nanoparticles exposures showed 30-180% higher fluorescence change than the negative control, indicating the potential of *C. vulgaris* as a biosensor for rapid detection of TiO₂ and Ag nanoparticles in water. The mathematical modeling of the responses of *C. vulgaris* to TiO₂ and Ag nanoparticles at 15 min of exposure with high R² indicated that this biosensor is sensitive to the concentration tested (0.010–10.000 mg.L⁻¹). Taken together, these results reveal that, for the first time, it is possible to detect TiO₂ and Ag nanoparticles in water within a very short time using a microalgae-based biosensor. Moreover, no genetic engineering requirement makes this biosensor simple, economical, and free from the restriction on genetically modified microorganisms for environmental applications.

INTRODUCTION

Metallic nanoparticles became popular owing to their unique physicochemical characteristics, such as substantial surface-to-volume ratio, high reactivity, and catalytic activity and use in electronics, energy, biomedicine, and the environment (Khan et al. 2019). The increased use of metallic nanoparticles raised concern over their potential negative environmental effect. Due to the diverse applications of nanoparticles in the

daily production of textiles, cleaning agents, and personal care products, effluent streams receive significant quantities of nanoparticles of diverse compositions and concentrations (Bundschuh et al. 2018). These nanoparticles might bring negative consequences, such as toxicity to underwater organisms and ecosystem disruption (Lead et al. 2018).

Metallic nanoparticles are being observed to increasingly interact with the environment and produce toxic effects. Due

to their small size, metallic nanoparticles can pass through biological barriers, such as cell membranes, and interact with biological macromolecules, causing adverse effects, such as oxidative stress, inflammation, and genotoxicity (Nel et al. 2006). Furthermore, metallic nanoparticles can accumulate in various human organs and tissues, causing harm to essential organs, such as the liver, kidneys, and lungs (Zhang et al. 2012).

Some silver, iron oxide, gold, zinc oxide, and titanium oxide nanoparticles are commonly employed in biomedical, pharmaceutical, and cosmetic industries (Yaqoob et al. 2020). Among these nanoparticles, silver and titanium oxide nanoparticles have gained strong attention among researchers during the last few decades because of their potential hazards to humans and the environment. While small quantities of these nanoparticles do not pose a harmful risk upon exposure, studies have shown that they could gradually accumulate in the brain and intestinal mucosa (Lee et al. 2013). The presence of silver and titanium oxide nanoparticles exerts toxicity once a certain threshold is reached. Moreover, the study proves that titanium dioxide nanoparticles could cause cancer (Baranowska-wójcik et al. 2020). The International Agency for Research on Cancer and the National Institute for Occupational Safety and Health have classified them as possible human carcinogens (Skocaj et al. 2011). Although silver nanoparticles are not classified as a possible human carcinogen, Liao et al. (2019) indicated that even low concentrations of silver nanoparticles ($<6.7 \mu\text{g}\cdot\text{mL}^{-1}$) could induce toxic effects, such as DNA damage and apoptosis of human red blood cells, liver cells, and bronchial epithelial cells. Furthermore, once disposed into the aquatic environment, titanium and silver nanoparticles can bioaccumulate in the human body through the food chain (Asztemborska et al. 2018, Yaqoob et al. 2020). Hence, detecting and monitoring titanium dioxide and silver nanoparticles in water is important to ensure that the water is safe to be discharged and utilized.

In the last two decades, biosensors have emerged as promising tools for detecting metal and other pollutants in environmental matrices (Odobasić et al. 2019). Generally, a biosensor contains three basic elements: biological recognition elements, transducer, and signal processing unit (Nigam & Shukla 2015). Using biosensors in detecting the pollutant of interest is based on the responses of biological recognition elements (Teo & Wong 2014). Upon exposure to metal pollutants, the responses produced by biological recognition elements are converted into detectable signals, such as optical and electrical signals through the transducer (Rocha et al. 2021). Subsequently, the signal is converted into readable information through a signal processing unit (Nigam & Shukla 2015). Biosensor offers several advantages over

conventional analytical methods, including high sensitivity, real-time monitoring, portability, cost efficiency, and high speed (Bereza-Malcolm et al. 2015). Biosensors can also be designed to ideally fulfill the requirement of Sustainable Development Goals (SDG) and operated under very low energy or self-powered using biofuel cells (Grattieri & Minter 2018, Wang et al. 2019), which is more energy-efficient than conventional analytical methods (SDG 7).

Generally, conventional analytical methods entail sample extraction with a high volume of organic solvent and sample before detection (Voon et al. 2022), whereas a biosensor requires trace amounts of reagents and produces less waste, minimizing its environmental impact (SDG 12, 13 and 14). A biosensor is easy to use, making single-person handling possible even without comprehensively understanding the separation and extraction chemistry (Kowalczyk et al. 2023).

In recent years, there has been increased interest in using microorganisms as biological recognition elements in biosensors for detecting metallic particles (Wan Jusoh & Wong 2014). Metallic nanoparticles have been shown to cause changes in growth rate, photosynthetic activity, and enzyme activity in microorganisms (Xiao et al. 2023), which can be used to signal metallic nanoparticles' presence. To date, various algae-based biosensors have been developed to detect different kinds of metallic bulk particles (Berezhetsky et al. 2007, Scognamiglio et al. 2019, Singh & Mittal, 2012). Studies suggested that the metabolic response of microalgae to metal bulk particles and nanoparticles might be similar, probably due to the different mechanisms triggered by bulk particles and nanoparticles (AL-Ammari et al. 2021). Currently, studies concerning algae-based biosensors for detecting metallic nanoparticles, especially silver and titanium metallic nanoparticles, are yet to be developed.

Despite the potential of biosensors in detecting metallic nanoparticles, several issues are still to be addressed. One of the issues is the effect of exposure time on detecting metallic nanoparticles. The exposure time can affect the response of biosensors to metallic nanoparticles (Wan Jusoh et al. 2020). Many studies have focused on the response of the microorganisms to nanoparticles over relatively long exposure times, ranging from hours to days (Amaroa et al. 2014, Hou et al. 2014, Hui et al. 2022).

However, research on the response of microorganisms to nanoparticles over shorter exposure times (below two hours) is lacking. Studying the response of microorganisms to nanoparticles over shorter exposure times could help identify the immediate response of microorganisms to metallic nanoparticles.

Only a few studies have focused on the effect of microorganisms' growth phases on detecting metallic

nanoparticles. In many studies, cells at the exponential phase are often used as test organisms or biological recognition elements in biosensors (Amaro et al. 2011, Cheng et al. 2021, Hazeem et al. 2019). Cells from the lag or stationary phases are rarely used. Utilizing microorganisms from different growth phases might ease the construction of biosensors and the detection of metals. As microorganisms at different growth phases produce different metabolite levels (Canelli et al. 2020, Tiwari & Dhakal 2023), the responses of microorganisms at different growth phases to metallic nanoparticles might also differ.

In this study, immobilized microalga *Chlorella vulgaris* was used as the biological recognition element in the biosensor. The microalgae conduct photosynthesis in the aquatic environment and can produce fluorescence. The presence of metallic nanoparticles induces stress on the microalgae, leading change in fluorescence intensity. This study aims to investigate the response of *C. vulgaris* to the exposure of various concentrations of silver and titanium metallic nanoparticles by measuring the fluorescence intensity change for two hours. The potential for detecting silver and titanium metallic nanoparticles in a short exposure time (15 min to 2 h) was also examined. To the best of our knowledge, this is the first significant effort to detect TiO₂ and Ag nanoparticles in water within 15 min using a microalgae-based biosensor.

MATERIALS AND METHODS

Chemicals and Reagents

Bold-modified Basal freshwater nutrient solution, nanoparticles of titanium oxide (TiO₂), and silver (Ag) were purchased from Sigma-Aldrich (Darmstadt, Germany). The purity of TiO₂ and Ag nanoparticles was $\geq 99.5\%$. The size and surface area of TiO₂ nanoparticles were 21 nm and 35-65 m².g⁻¹, respectively, while the size and surface area of Ag nanoparticles were <100 nm and 5.0 m².g⁻¹, respectively. Both metallic nanoparticles were spherical. The freshwater nutrient solutions were diluted using distilled water before microalgae cultivation. All the glassware used was autoclaved at 121°C for 15 min before use for the experiment.

Microalgae Culture

Chlorella vulgaris was obtained from Universiti Tunku Abdul Rahman, Malaysia. The microalgae were grown and maintained in a conical flask containing 200 mL of Bold's Basal Medium. The culture was maintained at room temperature (25±2°C) and illuminated with 16 hours of cool-white fluorescence light followed by 8 hours of dark period.

Determination of Cell Growth

Growth phases of the cells were determined by cell count using a hemocytometer (Marianela-Superior, Neubauer), light microscope (Eclipse E-100 LED, Nikon), and spectrophotometer (GeneQuant 1300, GE Healthcare Life Sciences) at an optical density of 700 nm.

Immobilization of Microalgae

Before exposure to nanoparticles, immobilization was performed using a 1% (w/v) agarose medium. The volume of 0.5 mL of cells and 0.5 mL of agarose medium were added into a four-sided clear cuvette at 45°C. Then, the cuvette was sealed with plastic paraffin film (Parafilm M, Pechiney Plastic Packaging) and left at room temperature until the mixture solidified.

Exposure of Nanoparticles

The exposure test on nanoparticles is summarized in Fig. 1. The fluorescence was measured using a spectrofluorometer (Promega Glomax Multi Jr., Promega, United States of America). Five concentrations (0.001, 0.01, 0.1, 1.0, and 10 mg.L⁻¹) each of TiO₂ and Ag nanoparticle solutions were prepared using deionized water. A 3 mL of each concentration of nanoparticle solution was added into cuvettes containing the immobilized cells. Each sample was illuminated with light at 490 nm wavelength, and the emitted fluorescence intensity at 680-690 nm wavelength was measured using a spectrofluorometer before and every 15 min after the exposure. The immobilized cells exposed to 3 mL of deionized water were used as the negative control. All exposure tests were conducted in triplicate and repeated using cells in lag, exponential, and stationary phases. The percentage of change in fluorescence intensity after the exposure was determined using the following equation:

$$\text{Change of fluorescence intensity (\%)} = \frac{\text{change of fluorescence for analyte} - \text{change of fluorescence for negative control}}{\dots(1)}$$

Where the change of fluorescence for the analyte is the fluorescence change before and after exposure to metallic nanoparticles, the change of fluorescence for negative control is the fluorescence change before and after exposure to distilled water.

RESULTS AND DISCUSSION

Growth Phase of *Chlorella vulgaris*

The cell density was measured to determine the growth phase of *Chlorella vulgaris*. The growth phase of *C.*

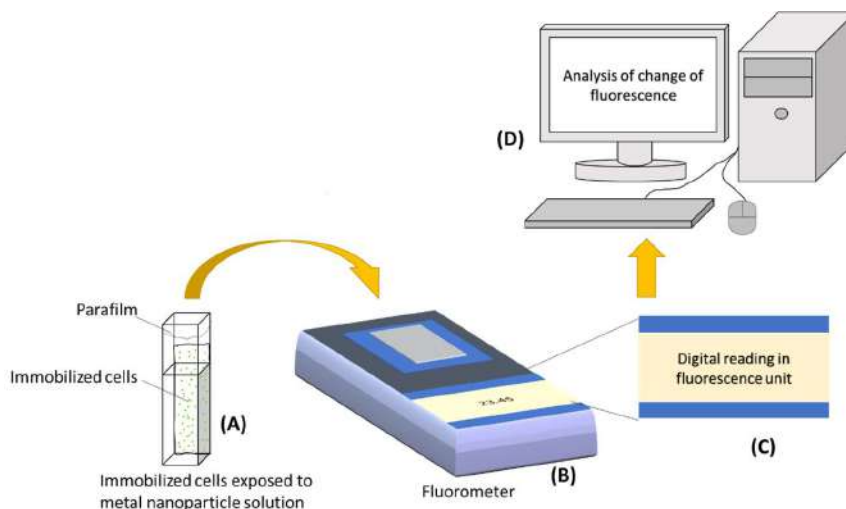


Fig. 1: Summary of exposure test on nanoparticles. Microalga *C. vulgaris* cells were immobilized in the cuvette. Then, 3 mL of the sample was added to the cuvette for the exposure test (A). The cuvette was inserted into the spectrofluorometer (B). The fluorescence intensity of 490 nm was illuminated and emitted fluorescence intensity of 680-690 nm was measured by a spectrofluorometer. The fluorescence intensity was displayed digitally (C) and analyzed using a computer (D).

vulgaris is illustrated in Fig. 2. The cell density of the *C. vulgaris* culture increased slowly in the first 2 days and then rose exponentially from day 2 until day 8. No significant increment in cell density was observed after day 8, where the cell density of 3.82×10^6 cells/mL was determined. Generally, the growth pattern of microalgae involves a lag phase, exponential phase, stationary phase, and death phase (Lee et al. 2015). At the beginning of the culture, which was known as the lag phase, microalgae species were accommodating to a new environment. Therefore, they were growing slowly. After fully accommodating to the new environment, the cells entered the exponential phase in which the cells quickly utilized the nutrients available therefore, the cell density was greatly increased. When the nutrients in the culture medium were depleted, the cells declined to grow with no significant change in cell density. When the nutrient in the medium cannot maintain the microalgal metabolism, the cells die and enter the death phase. The growth phase of *C. vulgaris* in this experiment was similar to other studies in which *C. vulgaris* has a short lag phase and quickly enters an exponential phase (Loh et al. 2021, Yatirajula et al. 2019). In the experiment, lag, exponential, and stationary phases were identified from day 0 to day 2, day 2 to day 8, and day 8 to 13, respectively. No death phase was observed in this experiment, probably due to the short cultivation period. The cells from day 1 (lag phase), day 3 (exponential phase), and day 9 (stationary phase) were chosen for the study of nanoparticle exposure.

The cell density was measured to determine the growth phase of *Chlorella vulgaris*. The growth phase of *C. vulgaris* is illustrated in Fig. 2. The cell density of the *C. vulgaris*

culture increased slowly in the first 2 days and then rose exponentially from day 2 until day 8. No remarkable increment in cell density was observed after day 8, where the cell density of 3.82×10^6 cells/mL was determined. Generally, the growth pattern of microalgae involves the lag, exponential, stationary, and death phases (Lee et al. 2015). At the beginning of the culture, called the lag phase, microalgae species were acclimated to a new environment. Hence, they grew slowly. After fully acclimating to the new environment, the cells entered the exponential phase in which the cells quickly utilized the nutrients available, hence, the cell density was greatly increased. When the nutrients in the culture medium were depleted, the cells declined to grow with no significant change in cell density. When the nutrient in the medium cannot maintain the microalgal metabolism, the cells die, entering the death phase. The growth phase of *C. vulgaris* in this experiment was similar to other studies in which *C. vulgaris* has a short lag phase and quickly enters the exponential phase (Loh et al. 2021, Yatirajula et al. 2019). In the experiment, the lag, exponential, and stationary phases were identified from day 0 to day 2, day 2 to day 8, and day 8 to 13, respectively. No death phase was observed in this experiment, probably due to the short cultivation period. The cells from day 1 (lag phase), day 3 (exponential phase), and day 9 (stationary phase) were chosen for the study of nanoparticle exposure.

Exposure to Ti and Ag Nanoparticles

In this study, *C. vulgaris*, immobilized using agarose gel, was used as a biological recognition element, while the spectrofluorometer was used as a transducer and signal

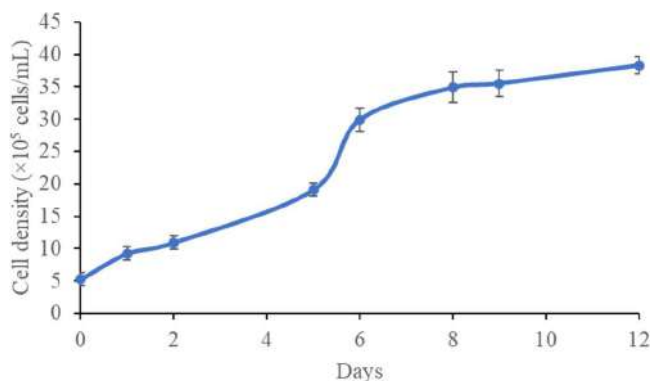


Fig. 2: Growth phase of *C. vulgaris* (n=3).

processing unit. During exposure to nanoparticles, TiO₂ and Ag nanoparticles enter the cells and disrupt the metabolism, including chlorophyll, protein, lipids, and β -carotene, of *C. vulgaris* (Hazeem et al. 2019, Romero et al. 2020). The disruption of chlorophyll content in *C. vulgaris* changed the fluorescence, which the spectrofluorometer can detect and display.

The different growth phases of cells are critical in biosensing because the cells at various growth phases might respond differently to metal nanoparticles (Wong et al. 2018). In this study, the *C. vulgaris* cells at days 1, 3, and 9 were exposed to 0.001–10 mg.L⁻¹ of TiO₂ and Ag nanoparticles.

A significant increase in change of fluorescence intensity compared to negative control was observed in all concentrations of metal nanoparticles from 15 min to 120 min exposure (Fig. 3 and Fig. 4). The overall mean showed that the changes of fluorescence intensity were 84.24–174.08%, 43.59–81.44% and 43.93–64.34% respectively using immobilized *C. vulgaris* at lag, exponential and stationary phases when exposed to TiO₂ nanoparticles. For exposure to Ag nanoparticles, the changes in fluorescence intensity were 53.19–164.60%, 72.41–95.71%, and 43.07–75.09%, respectively, using immobilized *C. vulgaris* at lag, exponential, and stationary phases. Therefore, *C. vulgaris* in the lag phase showed the highest change in fluorescence intensity, whereas *C. vulgaris* in the stationary phase showed the lowest change in fluorescence intensity. The increase in fluorescence intensity detected by spectrofluorometer could be attributed to several reasons. Generally, during the measurement, the spectrofluorometer illuminates a specific wavelength of fluorescence, and it is captured by photosynthetic pigment, especially chlorophyll molecules. After absorbing the specific wavelength of fluorescence, photosynthetic pigments emit another longer wavelength of fluorescence as a byproduct that can be detected by a spectrofluorometer (Huot & Babin 2012). The high

fluorescence intensity detected by the spectrofluorometer may indicate a high concentration of photosynthetic pigments. However, when photosynthetic molecules are harmed or destroyed, they can release more fluorescence than they normally would (Maxwell & Johnson 2000). Consequently, higher fluorescence intensity may be detected.

A significant increase in change of fluorescence intensity compared to negative control was observed in all concentrations of metal nanoparticles from 15 min to 2 hours exposure (Fig. 3 and Fig. 4). The overall mean showed that the changes in fluorescence intensity were 84.24–174.08%, 43.59–81.44%, and 43.93–64.34% using immobilized *C. vulgaris* at the lag, exponential, and stationary phases, respectively, when exposed to TiO₂ nanoparticles. For exposure to Ag nanoparticles, the changes in fluorescence intensity were 53.19–164.60%, 72.41–95.71%, and 43.07–75.09% using immobilized *C. vulgaris* at the lag, exponential, and stationary phases, respectively. Therefore, *C. vulgaris* in the lag phase showed the highest change in fluorescence intensity, whereas *C. vulgaris* in the stationary phase showed the lowest change in fluorescence intensity. The increase in fluorescence intensity detected by the spectrofluorometer could be attributed to several reasons. Generally, during the measurement, the spectrofluorometer illuminates a specific wavelength of fluorescence, and photosynthetic pigments, especially chlorophyll molecules, capture it. After absorbing the specific fluorescence wavelength, the photosynthetic pigments emit another longer fluorescence wavelength as a spectrofluorometer-detectable byproduct (Huot & Babin 2012). The high fluorescence intensity detected by the spectrofluorometer may indicate a high concentration of photosynthetic pigments. However, when photosynthetic molecules are harmed or destroyed, they can release more fluorescence than they normally would (Maxwell & Johnson 2000). Consequently, higher fluorescence intensity may be detected.

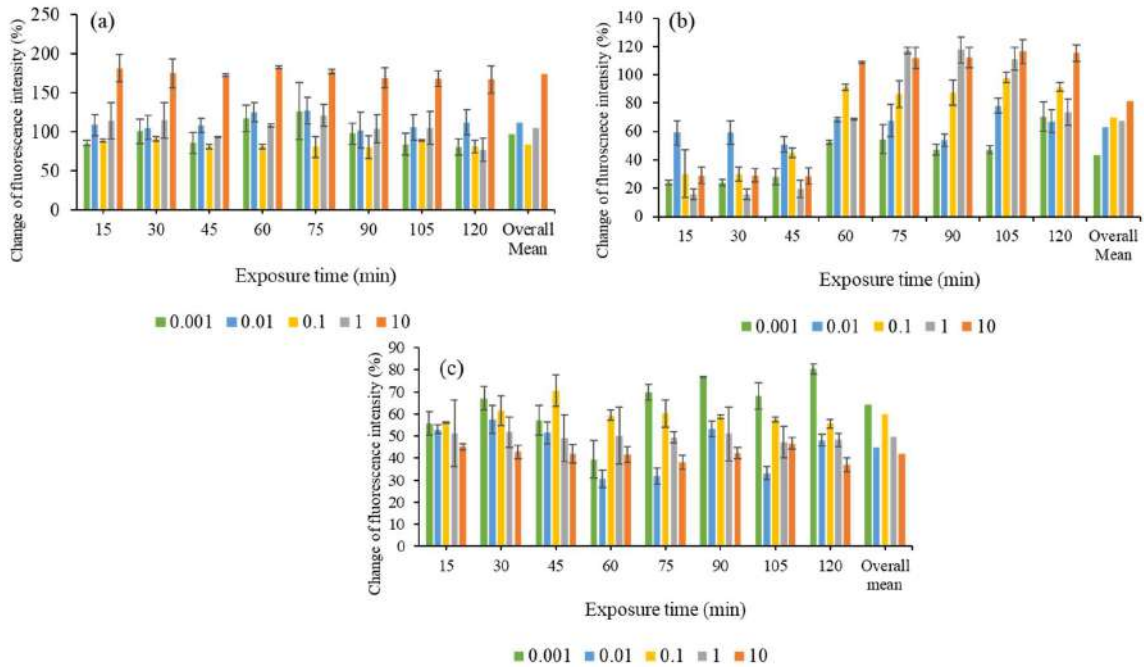


Fig. 3: Responses of *C. vulgaris* to different concentrations of TiO₂ (mg/L) during (a) lag phase (day 1), (b) exponential phase (day 3), and (c) stationary phase (day 9) (n = 3).

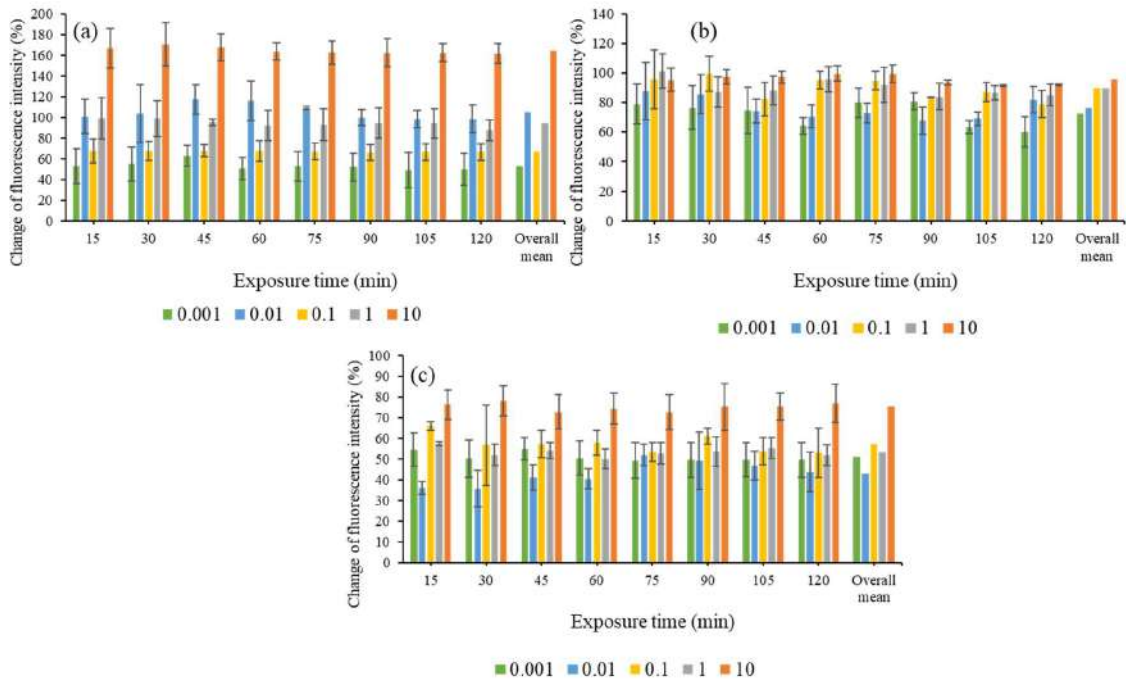


Fig. 4: Responses of *C. vulgaris* to different concentrations of Ag (mg.L⁻¹) during (a) lag phase (day 1), (b) exponential phase (day 3), and (c) stationary phase (day 9) (n = 3).

Previous studies showed that metal nanoparticles such as Ag and TiO₂ could directly decrease the chlorophyll content or induce the production of reactive oxygen species (ROS)

in microalgae, which in turn impairs the photosynthetic pigments and other cellular molecules (Hazeem et al. 2019, Li et al. 2020). To reduce negative impacts caused by damage

to photosynthetic pigments and the production of ROS, microalgae cells can dissipate the excess energy through a non-photochemical quenching mechanism (Quaas et al. 2015). In this mechanism, excess energy is dissipated as heat within a timeframe ranging from seconds to several min (Goss & Lepetit 2015). Besides of non-photochemical quenching mechanism, microalgal photosynthetic pigments also have ROS scavenging systems to minimize the damage (Nowicka 2022). ROS scavenging systems and photochemical quenching mechanisms are affected by the microalgal growth phase (Nowicka et al. 2021). During the lag phase of growth, microalgae grow slowly and have a lower ability for non-photochemical quenching mechanism and synthesis of ROS scavenging systems because of the lower concentrations of photosynthetic pigments and other cellular components. As a result, the highest change in fluorescence intensity was detected during the lag phase. When the microalgae enter the exponential phase or stationary phase, the concentration of photosynthetic pigments and other components is increased, resulting in the greater ability for non-photochemical quenching mechanism and ROS scavenging systems (Sigaud-Kutner et al. 2002, Yusuf & Athirah 2021). Whereas the high cell density in exponential and stationary phases may also reduce the change of fluorescence intensity due to the reabsorption of fluorescence emission by neighboring cells (Wong et al. 2013).

The toxicity of metallic nanoparticles to microalgae depends on concentration, type, and exposure time. Several studies have reported that exposure to TiO₂ and Ag nanoparticles under low concentration can stimulate hormetic response. For instance, studies found that the photosynthetic activity of microalgae exposed to low concentrations of TiO₂ and Ag (<10 mg.L⁻¹) was increased from the beginning of the experiments (Chen et al. 2012, Zhao et al. 2021). This hormetic response in photosynthetic activity might be due to the photosensitizer effect of nanoparticles (AL-Ammari et al. 2021). During exposure, TiO₂ binds to the microalgal cell membrane and helps transfer photo-generated electrons to the thylakoid membrane of chlorophyll, enhancing photosynthesis. However, exposure to high concentrations of TiO₂ and Ag could decrease chlorophyll due to the damage to chlorophyll structure. TiO₂ and Ag nanoparticles bind with photosystem II and induce the production of ROS in chloroplast and mitochondria. These ROS render oxidative stress and damage to the chloroplast molecules, disrupting their ability to capture light energy and potentially inhibiting photosynthesis (Li et al. 2015, Sendra et al. 2017, Thiagarajan et al. 2019). To minimize the damage of nanoparticles, microalgae produce ROS-scavenging enzymes, such as superoxide dismutase and peroxidase, to convert the ROS

into benign molecules (Adochite & Andronic 2021, Hazeem et al. 2019). Most studies determined the response of microalgae after 24 h of exposure to nanoparticles. In this study, the microalgae were exposed to TiO₂ and Ag from 15 to 240 min. No study has explored how the metabolism of microalgae was changed within a very short exposure time to TiO₂ and Ag. This scenario should be further studied.

Besides the aforementioned factors, the size and shape of nanoparticles are also critical factors affecting the toxicity of metallic nanoparticles to microalgae. The studies showed that smaller nanoparticles could induce more censorious toxicity in reducing growth and increasing fluorescence intensity compared to larger nanoparticles during the same cultivation period (He et al. 2019, Ivask et al. 2014, Li et al. 2020). Wang et al. (2019) extrapolated that smaller nanoparticles easily pass through the microalgal cell wall, and cell wall pore sizes larger than the size of nanoparticles lead to toxicity. However, this is not yet proven. The biocomponents on microalgal cell walls can also promote the uptake of smaller nanoparticles into the cells; smaller nanoparticles release more metal ions that facilitate more metal uptake (Zhang & Wang 2019). In addition, as particle size decreases, the surface area per volume increases greatly, rendering them to be reactive with biocomponents in microalgal cells (Abbasi et al. 2023, Zhang & Wang 2019).

Some studies revealed that spherical metallic nanoparticles are more lethal than those of other shapes (Auclair & Gagné 2022). For instance, Wang et al. (2020) found that TiO₂ nanosphere has higher inhibition on microalgal growth and stimulated more ROS production compared to TiO₂ nanotubular. Spherical metallic nanoparticles are smaller and have a high surface-to-volume ratio, which dramatically enhances the dissolution rate of nanoparticles, leading to an abundant release of metal ions 70. The size of TiO₂ and Ag spherical nanoparticles in this study were <100 nm and 21 nm, respectively, resulting in fast uptake of TiO₂ and Ag nanoparticles and remarkable fluorescence intensity change within 15 min.

Analytical Performance of Biosensor

The exposure tests confirmed that *C. vulgaris* responded to all concentrations of TiO₂ and Ag nanoparticles with a more remarkable fluorescence intensity change than the negative control, even in 15 min (Fig. 5). The mathematical modeling in Table 1 indicates the relationship between the responses of *C. vulgaris* (y symbol) at 15 min of exposure and the concentration of TiO₂ and Ag nanoparticles (x symbol). The mathematical modeling with high R² (Table 1) showed that the response of *C. vulgaris* highly correlates to the concentration of TiO₂ and Ag (Wong et al. 2013),

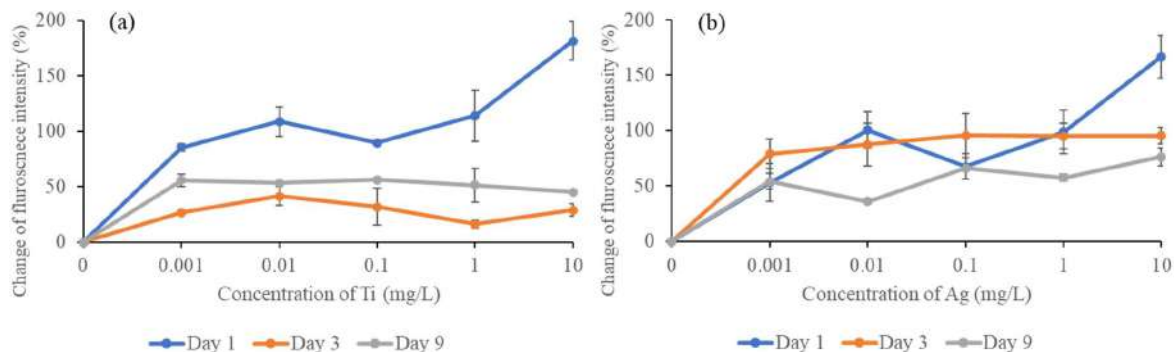


Fig. 5: Responses of *C. vulgaris* to different concentrations of TiO₂ and Ag at 15 min (n = 3).

Table 1: The mathematical modeling and the correlation of the response of *C. vulgaris* to Ti and Ag at different growth phases.

Metals	Growth phase	Detection range [mg.L ⁻¹]	Equation	R ²
TiO ₂	Lag	0.001 – 10.000	$y = -1.173x^2 + 20.459x + 94.057$	0.9444
	Exponential	0.100 – 10.000	$y = 1.741x^2 - 17.674x + 31.927$	1.000
	Stationary	0.001 – 10.000	$y = 0.294x^2 - 3.940x + 55.050$	0.9207
Ag	Lag	0.010 – 10.000	$y = 85.313e^{0.0676x}$	0.8802
	Exponential	0.010 – 1.000	$y = 3.235\ln(x) + 102.030$	0.9931
	Stationary	0.010 – 10.000	$y = 34.478x^3 - 381.55x^2 + 372.09x + 32.427$	1.000

*x represented the concentration of metallic nanoparticle while y represented fluorescence intensity change

indicating the potential of using *C. vulgaris* to anticipate the concentration of metals in unknown samples (Wong et al. 2018). Moreover, the concentration of TiO₂ and Ag allowed in drinking water by water quality monitoring bodies was 0.1 mg.L⁻¹ (Dong et al. 1993, World Health Organization 2021), which is in the detection range of the present developed biosensor.

Table 2 compares the metal ions between a few biosensors and the currently developed biosensors in work. Although the biosensors in other studies can detect a lower concentration of metals than the present developed biosensor, all the listed biosensors in Table 2 can be used to detect the concentration lower than 1.0×10^{-1} mg.L⁻¹, the permission limit allowed in drinking water (Dong et al. 1993, WHO 2021). The microalga *C. vulgaris* in this study can detect TiO₂ and Ag within 15 min, which is faster than in other studies (Table 2). Moreover, the *C. vulgaris* used in this study was derived from nature without any genetic engineering. Genetic engineering on an organism usually involves identifying specific traits, extracting specific genes, inserting specific genes into vector/bacterial plasmid, cloning of plasmid, transforming the transgenic plasmid into a desired organism, and growing of transgenic organism (Liu et al. 2022). More chemicals and complicated processes are required to achieve successful genetic modification. Whereas the method to construct biosensors in this study is simple and

more economical. Using non-genetically modified microalga *C. vulgaris* as a biological recognition element is free from the restrictions on genetically modified microorganisms for environmental applications. Nevertheless, the biosensor used in this work intends to screen the presence of Ag and TiO₂ without identifying specific metals in the water sample.

Several possible strategies are employed to improve the application of currently developed biosensors in work. Besides TiO₂ and Ag nanoparticles, other types of metals, such as copper, zinc, and cadmium, can also disrupt the chlorophyll content of *C. vulgaris*, changing fluorescence intensity (Kondzior & Butarewicz 2018). Therefore, the currently developed biosensor could also detect the presence of these metals. As different metal nanoparticles stimulate various responses, it is indispensable to study their effects on the change of fluorescence intensity of *C. vulgaris* and the growth phase before exposure to real samples. To improve the portability of the currently developed biosensor and the possibility of in situ detection, an electrical-operated spectrofluorometer can probably be replaced by a battery-operated spectrofluorometer (Alarie et al. 1993).

CONCLUSIONS

A microalgae-based biosensor using *Chlorella vulgaris* for detecting TiO₂ and Ag has been successfully developed, with fluorescence emission utilized as a measuring parameter.

Table 2: Comparison of the metal ions (non-nanoparticles) detection using cell-based biosensors and currently developed biosensors in work.

Cell type	Metals	Exposure time [min]	The lowest limit of detection [mg.L ⁻¹]	Reference
Engineered <i>Bacillus megaterium</i> with transformed <i>gfp</i> gene	Cd, Cu (II), and Zn	240	$1.42 \times 10^{-4} - 3.16 \times 10^{-4}$	(Rathnayake et al. 2021)
Engineered <i>E. coli</i> with <i>gfp</i> gene	Cu and Ag	240	$1.27 \times 10^{-3} - 4.30 \times 10^{-3}$	(Martinez et al. 2019)
Engineered <i>E. coli</i>	Hg and Cd	480	$1.34 \times 10^{-3} - 2.59 \times 10^{-3}$	(Hui et al. 2022)
Engineered <i>Tetrahymena thermophila</i>	As Cd, Cu, Zn, Hg, Pb	120	$1.80 \times 10^{-3} - 5.60 \times 10^{-1}$	(Amaro et al. 2011)
Adenine deficient yeast	Ag	120 - 180	8.90×10^{-6}	(Sun & Wang 2022)
<i>C. vulgaris</i>	TiO ₂ and Ag	15	$1.00 \times 10^{-3} - 1.00 \times 10^{-1}$	This work

Microalga *C. vulgaris* at different growth phases responded differently to various concentrations of TiO₂ and Ag nanoparticles. The overall mean showed that the highest responses of TiO₂ and Ag nanoparticles, 84.24-174.08% and 53.19-164.60%, respectively, exposure was obtained during the lag phase, whereas the two lowest responses of TiO₂ and Ag nanoparticles exposure, 43.93-64.34% and 43.07-75.09%, respectively, were observed at the stationary phase. A significant response was observed even within 15 min. The immobilized *C. vulgaris* under TiO₂ and Ag exposure showed 30-180% higher fluorescence change than the negative control, indicating the currently developed biosensor could rapidly detect the presence of TiO₂ and Ag. The biosensor with high R² showed high sensitivity to TiO₂ and Ag nanoparticles, and it could be used to screen TiO₂ and Ag nanoparticles in drinking water. Taken together, these results reveal that, for the first time, it is possible to detect TiO₂ and Ag nanoparticles in water within a very short time using a microalgae-based biosensor. Furthermore, the construction of currently developed biosensors is simple, economical, and free from genetically modified microorganism concerns.

ACKNOWLEDGMENTS

The author would like to acknowledge the Ministry of Higher Education Malaysia (MOHE) (Grant No. FRGS/1/2020/STG03/INTI/01/1) for supporting the project.

REFERENCES

- Abbasi, R., Shineh, G., Mobaraki, M., Doughty, S. and Tayebi, L. 2023. Structural parameters of nanoparticles affecting their toxicity for biomedical applications: a review. *J. Nanopart. Res.*, 25(3): 43. <https://doi.org/10.1007/s11051-023-05690-w>
- Adochite, C. and Andronic, L. 2021. Aquatic toxicity of photocatalyst nanoparticles to green microalgae *Chlorella vulgaris*. *Water*, 13(77). <https://doi.org/10.3390/w13010077>
- AL-Ammari, A., Zhang, L., Yang, J., Wei, F., Chen, C. and Sun, D. 2021. Toxicity assessment of synthesized titanium dioxide nanoparticles in freshwater algae *Chlorella pyrenoidosa* and a zebrafish liver cell line. *Ecotoxicol. Environ. Saf.*, 211: 111948. <https://doi.org/10.1016/j.ecoenv.2021.111948>
- Alarie, J.P., Vo-Dinh, T., Miller, G., Ericson, M.N., Maddox, S.R., Watts, W., Eastwood, D.L., Lidberg, R. and Dominguez, M. 1993. Development of a battery-operated portable synchronous luminescence spectrofluorometer. *Rev. Sci. Instrum.*, 64(9): 2541-2546. <https://doi.org/10.1063/1.1143916>
- Amaro, F., Turkewitz, A.P., Martín-González, A. and Gutiérrez, J. C. 2011. Whole-cell biosensors for detection of heavy metal ions in environmental samples based on metallothionein promoters from *Tetrahymena thermophila*. *Microb. Biotechnol.*, 4(4): 513-522. <https://doi.org/10.1111/j.1751-7915.2011.00252.x>
- Amaro, F., Turkewitz, A.P., Martín-González, A. and Gutiérrez, J.C. 2014. Functional GFP-metallothionein fusion protein from *Tetrahymena thermophila*: a potential whole-cell biosensor for monitoring heavy metal pollution and a cell model to study metallothionein overproduction effects. *Biometals*, 25: 195-205. <https://doi.org/10.1007/s10534-014-9704-0>
- Asztemborska, M., Jakubiak, M., Stęborowski, R., Chajduk, E. and Bystrzejewska-Piotrowska, G. 2018. Titanium dioxide nanoparticle circulation in an aquatic ecosystem. *Water Air Soil Pollut.*, 229(6): 208. <https://doi.org/10.1007/s11270-018-3852-8>
- Auclair, J. and Gagné, F. 2022. Shape-dependent toxicity of silver nanoparticles on freshwater *Cnidarians*. *Nanomaterials*, 12(18): 3107. <https://doi.org/10.3390/nano12183107>
- Baranowska-wójcik, E., Szwajgier, D., Oleszczuk, P. and Winiarska-mieczan, A. 2020. Effects of titanium dioxide nanoparticles exposure on human health- A review. *Biol. Trace Elem. Res.*, 193(1): 118-129. <https://doi.org/10.1007/s12011-019-01706-6>
- Bereza-Malcolm, L.T., Mann, G. and Franks, A.E. 2015. Environmental sensing of heavy metals through whole-cell microbial biosensors: a synthetic biology approach. *ACS Synth. Biol.*, 4(5): 535-546. <https://doi.org/10.1021/sb500286r>
- Berezhetskyy, A.L., Durrieu, C., Nguyen-Ngoc, H., Chovelon, J.M., Dzyadevych, S.V. and Tran-Minh, C. 2007. Conductometric biosensor based on whole-cell microalgae for assessment of heavy metals in wastewater. *Biopolym. Cell*, 23(6): 511-518. <https://doi.org/10.7124/bc.000786>
- Bundschuh, M., Filser, J., Lüderwald, S., McKee, M.S., Metreveli, G., Schaumann, G.E., Schulz, R. and Wagner, S. 2018. Nanoparticles in the environment: where do we come from, where do we go to? *Environ. Sci. Eur.*, 30(1). <https://doi.org/10.1186/s12302-018-0132-6>
- Canelli, G., Neusch, L., Carpine, R., Tevere, S., Giuffrida, F., Rohfritsch, Z., Dionisi, F., Bolten, C. J. and Mathys, A. 2020. *Chlorella vulgaris* in a heterotrophic bioprocess: Study of the lipid bioaccessibility and oxidative stability. *Algal Res.*, 45: 101754. <https://doi.org/10.1016/j.algal.2019.101754>
- Chen, L., Zhou, L., Liu, Y., Deng, S., Wu, H. and Wang, G. 2012. Toxicological effects of nanometer titanium dioxide (nano-TiO₂) on *Chlamydomonas reinhardtii*. *Ecotoxicol. Environ. Saf.*, 84: 155-162. <https://doi.org/10.1016/j.ecoenv.2012.07.019>

- Cheng, W.H., Wong, L.S. and Chong, K.C. 2021. Effect of lead (Pb) exposure towards green microalgae (*Chlorella vulgaris*) on the changes of physicochemical parameters in water. *S. Afr. J. Chem. Eng.*, 37: 252-255. <https://doi.org/10.1016/j.sajce.2021.04.002>
- Dong, S.Z., Chen, C.Z., Li, D.M. and Sun, Y.S. 1993A study of hygienic standards for titanium in the source of drinking water. *Zhonghua Yu Fang Yi Xue Za Zhi*, 27(1): 26-28.
- Goss, R. and Lepetit, B. 2015. Biodiversity of NPQ. *J. Plant Physiol.*, 172: 13-32. <https://doi.org/10.1016/j.jplph.2014.03.004>
- Grattieri, M. and Minter, S. D. 2018. Self-powered biosensors. *ACS Sensors*, 3(1): 44-53. <https://doi.org/10.1021/acssensors.7b00818>
- Hazeem, L.J., Kuku, G., Dewailly, E., Slomianny, C., Barras, A., Hamdi, A., Boukherroub, R., Culha, M. and Bououdina, M. 2019. Toxicity effect of silver nanoparticles on photosynthetic pigment content, growth, ROS production and ultrastructural changes of microalgae *Chlorella vulgaris*. *Nanomaterials*, 9(7): 914. <https://doi.org/10.3390/nano9070914>
- He, X., Xie, C., Ma, Y., Wang, L., He, X., Shi, W., Liu, X., Liu, Y. and Zhang, Z. 2019. Size-dependent toxicity of ThO₂ nanoparticles to green algae *Chlorella pyrenoidosa*. *Aquat. Toxicol.*, 209: 113-120. <https://doi.org/10.1016/j.aquatox.2019.02.003>
- Hou, Q.H., Ma, A.Z., Lv, D., Bai, Z.H., Zhuang, X.L. and Zhuang, G.Q. 2014. The impacts of different long-term fertilization regimes on the bioavailability of arsenic in soil: Integrating chemical approach with *Escherichia coli arsRp::luc*-based biosensor. *Appl. Microbiol. Biotechnol.*, 98(13): 6137-6146. <https://doi.org/10.1007/s00253-014-5656-0>
- Hui, C.Y., Guo, Y., Li, H., Chen, Y.T. and Yi, J. 2022. Differential detection of bioavailable mercury and cadmium based on a robust dual-sensing bacterial biosensor. *Front. Microbiol.*, 13: 1-13. <https://doi.org/10.3389/fmicb.2022.846524>
- Huot, Y. and Babin, M. 2012. Overview of Fluorescence Protocols: Theory, Basic Concepts, and Practice. In: D. J. Suggett, O. Prášil and M. A. Borowitzka (eds.), *Chlorophyll a Fluorescence in Aquatic Sciences: Methods and Applications*. Springer, Dordrecht, pp. 31-73. <https://doi.org/10.1007/978-90-481-9268-7>
- Ivask, A., Kurvet, I., Kasemets, K., Blinova, I., Aruoja, V., Suppi, S., Vija, H., Kaklõinen, A., Titma, T., Heinlaan, M., Visnapuu, M., Koller, D., Kisand, V. and Kahru, A. 2014. Size-dependent toxicity of silver nanoparticles to bacteria, yeast, algae, crustaceans, and mammalian cells in vitro. *PLoS ONE*, 9(7): e102108. <https://doi.org/10.1371/journal.pone.0102108>
- Khan, I., Saeed, K. and Khan, I. 2019. Nanoparticles: Properties, applications, and toxicities. *Arab. J. Chem.*, 12(7): 908-931. <https://doi.org/10.1016/j.arabj.2017.05.011>
- Kondzior, P. and Butarewicz, A. 2018. Effect of heavy metals (Cu and Zn) on the content of photosynthetic pigments in the cells of algae *Chlorella vulgaris*. *J. Ecol. Eng.*, 19(3): 18-28. <https://doi.org/10.12911/22998993/85375>
- Kowalczyk, A., Zarychta, J., Lejman, M. and Zawitkowska, J. 2023. Electrochemical and optical sensors for the detection of chemical carcinogens causing leukemia. *Sensors (Basel, Switzerland)*, 23(7): 1-21. <https://doi.org/10.3390/s23073369>
- Lead, J.R., Batley, G.E., Alvarez, P.J.J., Croteau, M.N., Handy, R.D., McLaughlin, M.J., Judy, J.D. and Schirmer, K. 2018. Nanomaterials in the environment: behavior, fate, bioavailability, and effects-An updated review. *Environ. Toxicol. Chem.*, 37(8): 2029-2063. <https://doi.org/10.1002/etc.4147>
- Lee, E., Jalalizadeh, M. and Zhang, Q. 2015. Growth kinetic models for microalgae cultivation: A review. *Algal Res.*, 12: 497-512. <https://doi.org/10.1016/j.algal.2015.10.004>
- Lee, J.H., Kim, Y.S., Song, K.S., Ryu, H.R., Sung, J.H., Park, J.D., Park, H.M., Song, N.W., Shin, B.S., Marshak, D., Ahn, K., Lee, J.E. and Yu, I.J. 2013. Biopersistence of silver nanoparticles in tissues from Sprague-Dawley rats. *Part. Fibre Toxicol.*, 10(1): 1-14. <https://doi.org/10.1186/1743-8977-10-36>
- Li, F., Liang, Z., Zheng, X., Zhao, W., Wu, M. and Wang, Z. 2015. Toxicity of nano-TiO₂ on algae and the site of reactive oxygen species production. *Aquat. Toxicol.*, 158: 1-13. <https://doi.org/10.1016/j.aquatox.2014.10.014>
- Li, Z., Juneau, P., Lian, Y., Zhang, W., Wang, S., Wang, C., Shu, L., Yan, Q., He, Z. and Xu, K. 2020. Effects of Titanium dioxide nanoparticles on photosynthetic and antioxidative processes of *Scenedesmus obliquus*. *Plants*, 9: 1-13. <https://doi.org/10.3390/plants9121748>
- Liao, C., Li, Y. and Tjong, S. C. 2019. Bactericidal and cytotoxic properties of silver nanoparticles. *Int. J. Mol. Sci.*, 20(2): 449. <https://doi.org/10.3390/ijms20020449>
- Liu, Y., Feng, J., Pan, H., Zhang, X. and Zhang, Y. 2022. Genetically engineered bacterium: principles, practices, and prospects. *Front. Microbiol.*, 13: 1-15. <https://doi.org/10.3389/fmicb.2022.997587>
- Loh, S.H., Chen, M.K., Fauzi, N.S., Aziz, A. and Cha, T.S. 2021. Enhanced fatty acid methyl esters recovery through a simple and rapid direct transesterification of freshly harvested biomass of *Chlorella vulgaris* and *Messastrum gracile*. *Sci. Rep.*, 11: 2720. <https://doi.org/10.1038/s41598-021-81609-6>
- Martinez, A.R., Heil, J.R. and Charles, T.C. 2019. An engineered GFP fluorescent bacterial biosensor for detecting and quantifying silver and copper ions. *BioMetals*, 32(2): 265-272. <https://doi.org/10.1007/s10534-019-00179-3>
- Maxwell, K. and Johnson, G. N. 2000. Chlorophyll fluorescence- A practical guide. *J. Exp. Bot.*, 51(345): 659-668. <https://doi.org/10.1093/jexbot/51.345.659>
- Nel, A., Xia, T., Mädler, L. and Li, N. 2006. Toxic potential of materials at the nanolevel. *Science*, 311: 622-627. <https://doi.org/10.1126/science.1114397>
- Nigam, V.K. and Shukla, P. 2015. Enzyme-based biosensors for detection of environmental pollutants-A review. *J. Microbiol. Biotechnol.*, 25(11): 1773-1781. <https://doi.org/10.4014/jmb.1504.04010>
- Nowicka, B. 2022. Heavy metal-induced stress in eukaryotic algae—mechanisms of heavy metal toxicity and tolerance with particular emphasis on oxidative stress in exposed cells and the role of antioxidant response. *Environ. Sci. Pollut. Res.*, 29(12): 16860-16911. <https://doi.org/10.1007/s11356-021-18419-w>
- Nowicka, B., Zyzik, M., Kapsiak, M., Ogrodzińska, W. and Kruk, J. 2021. Oxidative stress limits the growth of *Chlamydomonas reinhardtii* (Chlorophyta, Chlamydomonadales) exposed to copper ions at the early stage of culture growth. *Phycologia*, 60(4): 303-313. <https://doi.org/10.1080/00318884.2021.1922819>
- Odobašić, A., Šestan, I. and Begić, S. 2019. Biosensors for Determination of Heavy Metals in Waters. In: Rinken, T. and Kivirand, K. (eds.) *Biosensors for Environmental Monitoring*, IntechOpen. <https://doi.org/10.5772/intechopen.84139>
- Quaas, T., Berteotti, S., Ballottari, M., Flieger, K., Bassi, R., Wilhelm, C. and Goss, R. 2015. Non-photochemical quenching and xanthophyll cycle activities in six green algal species suggest mechanistic differences in the process of excess energy dissipation. *J. Plant Physiol.*, 172: 92-103. <https://doi.org/10.1016/j.jplph.2014.07.023>
- Rathnayake, I.V.N., Megharaj, M. and Naidu, R. 2021. Green fluorescent protein-based whole-cell bacterial biosensor for the detection of bioavailable heavy metals in the soil environment. *Environ. Technol. Innov.*, 23: 101785. <https://doi.org/10.1016/j.eti.2021.101785>
- Rocha, D.L., Maringolo, V., Araújo, A. N., Amorim, C.M.P.G. and Montenegro, M. da C.B.S.M. 2021. An overview of structured biosensors for metal ions determination. *Chemosensors*, 9(11): 324. <https://doi.org/10.3390/chemosensors9110324>
- Romero, N., Visentini, F.F., Márquez, V.E., Santiago, L.G., Castro, G.R. and Gagneten, A.M. 2020. Physiological and morphological responses of green microalgae *Chlorella vulgaris* to silver nanoparticles. *Environ. Res.*, 189: 109857. <https://doi.org/10.1016/j.envres.2020.109857>

- Scognamiglio, V., Antonacci, A., Arduini, F., Moscone, D., Campos, E. V. R., Fraceto, L. F. and Palleschi, G. 2019. An eco-designed paper-based algal biosensor for nanoformulated herbicide optical detection. *J. Hazard. Mater.*, 373: 483-492. <https://doi.org/10.1016/j.jhazmat.2019.03.082>
- Sendra, M., Moreno-Garrido, I., Yeste, M.P., Gatica, J.M. and Blasco, J. 2017. Toxicity of TiO₂, in nanoparticle or bulk form, to freshwater and marine microalgae under visible light and UV-A radiation. *Environ. Pollut.*, 227: 39-48. <https://doi.org/10.1016/j.envpol.2017.04.053>
- Sigaud-Kutner, T.C.S., Pinto, E., Okamoto, O.K., Latorre, L.R. and Colepicolo, P. 2002. Changes in superoxide dismutase activity and photosynthetic pigment content during growth of marine phytoplankters in batch-cultures. *Physiol. Plant.*, 114(4): 566-571. <https://doi.org/10.1034/j.1399-3054.2002.1140409.x>
- Singh, J. and Mittal, S.K. 2012. *Chlorella* sp. based biosensor for selective determination of mercury in the presence of silver ions. *Sens. Actuators B: Chem.*, 165(1): 48-52. <https://doi.org/10.1016/j.snb.2012.02.009>
- Skocaj, M., Filipic, M., Petkovic, J. and Novak, S. 2011. Titanium dioxide in our everyday life, Is it safe? *Radiol. Oncol.*, 45(4): 227-247. <https://doi.org/10.2478/v10019-011-0037-0>
- Sun, A. and Wang, W.X. 2022. A yeast-based biosensor for silver nanoparticle accumulation and cellular dissolution. *Biosens. Bioelectron.*, 205: 114082. <https://doi.org/10.1016/j.bios.2022.114082>
- Teo, S.C. and Wong, L. S. 2014. Whole cell-based biosensors for environmental heavy metals detection. *Annu. Res. Rev. Biol.*, 4(17): 2663-2674. <https://doi.org/10.9734/arrb/2014/9472>
- Thiagarajan, V., Natarajan, L., Seenivasan, R., Chandrasekaran, N. and Mukherjee, A. 2019. Tetracycline affects the toxicity of P25 n-TiO₂ towards marine microalgae *Chlorella* sp. *Environ. Res.*, 179: 108808. <https://doi.org/10.1016/j.envres.2019.108808>
- Tiwari, S. and Dhakal, N. 2023. Analysis of variations in biomolecules during various growth phases of freshwater microalgae *Chlorella* sp. *Appl. Food Biotechnol.*, 10(1): 73-84. <https://doi.org/10.22037/afb.v10i1.39796>
- Voon, C.H., Yusop, N.M. and Khor, S.M. 2022. The state-of-the-art in bioluminescent whole-cell biosensor technology for detecting various organic compounds in oil and grease content in wastewater: From the lab to the field. *Talanta*, 241: 123271. <https://doi.org/10.1016/j.talanta.2022.123271>
- Wan Jusoh, W.N.A., Chai, M.K., Wong, L.S., Ong, G.H. and Voon, B.W.N. 2020. Bioindication of heavy metals in aquatic environment using photosynthetic pigments in cyanobacteria. *S. Afr. J. Chem. Eng.*, 34: 78-81. <https://doi.org/10.1016/j.sajce.2020.05.011>
- Wan Jusoh, W.N.A. and Wong, L.S. 2014. Exploring the potential of whole cell biosensor: a review in environmental applications. *Int. J. Chem. Environ. Biol. Sci.*, 2(1).
- Wang, C., Yao, Z., Bai, L., Wang, C. and Jiang, H. 2019. Application of a microbial fuel cell-based biosensor for the energy-saving operation of macrophyte residues bioreactor with low concentration of dissolved organic carbon in effluents. *Chemosphere*, 220: 1075-1082. <https://doi.org/10.1016/j.chemosphere.2018.12.209>
- Wang, F., Guan, W., Xu, L., Ding, Z., Ma, H., Ma, A. and Terry, N. 2019. Effects of nanoparticles on algae: adsorption, distribution, ecotoxicity, and fate. *Appl. Sci.*, 9(8): 1534. <https://doi.org/10.3390/app9081534>
- Wang, Z., Jin, S., Zhang, F. and Wang, D. 2020. Combined toxicity of TiO₂ nanospherical particles and TiO₂ nanotubes to two microalgae with different morphology. *Nanomaterials*, 10(12): 1-11. <https://doi.org/10.3390/nano10122559>
- Wong, L.S., Judge, S.K., Voon, B.W.N., Tee, L.J., Tan, K.Y., Murti, M. and Chai, M.K. 2018. Bioluminescent microalgae-based biosensor for metal detection in water. *IEEE Sens. J.*, 18(5): 2091-2096. <https://doi.org/10.1109/JSEN.2017.2787786>
- Wong, L.S., Lee, Y.H. and Surif, S. 2013. Whole cell biosensor using *Anabaena torulosa* with optical transduction for environmental toxicity evaluation. *J. Sens.*, 2013: 567272. <https://doi.org/10.1155/2013/567272>
- World Health Organization (WHO). 2021. Silver in Drinking Water: Background Document for the Development of WHO Guidelines for Drinking-Water Quality WHO, Geneva, Switzerland.
- Xiao, X., Li, W., Jin, M., Zhang, L., Qin, L. and Geng, W. 2023. Responses and tolerance mechanisms of microalgae to heavy metal stress: A review. *Mar. Environ. Res.*, 183: 105805. <https://doi.org/10.1016/j.marenvres.2022.105805>
- Yaqoob, A.A., Ahmad, H., Parveen, T., Ahmad, A., Oves, M., Ismail, I.M.I., Qari, H.A., Umar, K. and Mohamad Ibrahim, M.N. 2020. Recent advances in metal decorated nanomaterials and their various biological applications: A review. *Front. Chem.*, 8: 1-23. <https://doi.org/10.3389/fchem.2020.00341>
- Yatirajula, S.K., Shrivastava, A., Saxena, V.K. and Kodavaty, J. 2019. Flow behavior analysis of *Chlorella Vulgaris* microalgal biomass. *Heliyon*, 5(6): e01845. <https://doi.org/10.1016/j.heliyon.2019.e01845>
- Yusuf, N. and Athirah, N.M. 2021. Antioxidative responses of *Chlorella vulgaris* under different growth phases. *Squalen Bull. Mar. Fish. Postharvest Biotechnol.*, 17(3): 111-120. <https://doi.org/https://doi.org/10.15578/squalen.692>
- Zhang, H., Zhaoxia Ji, Xia, T., Meng, H., Low-Kam, C., Rong Liu, Pokhrel, S., Lin, S., Wang, X., Liao, Y.P., Wang, M., Li, L., Damoiseaux, R., Telesca, D., Robert, D., Madler, L., Cohen, Y., Zink, J. I. and Nel, A. E. 2012. Use of metal oxide nanoparticle band gap to develop a predictive paradigm for oxidative stress and acute pulmonary inflammation. *ACS Nano*, 6(5): 4349-4368. <https://doi.org/doi:10.1021/nn3010087>
- Zhang, L. and Wang, W.X. 2019. The dominant role of silver ions in silver nanoparticle toxicity to a unicellular alga: evidence from luminogen imaging. *Environ. Sci. Technol.*, 53(1): 494-502. <https://doi.org/10.1021/acs.est.8b04918>
- Zhao, Z., Xu, L., Wang, Y., Li, B., Zhang, W. and Li, X. 2021. Toxicity mechanism of silver nanoparticles to *Chlamydomonas reinhardtii*: photosynthesis, oxidative stress, membrane permeability, and ultrastructure analysis. *Environ. Sci. Pollut. Res.*, 28(12): 15032-15042. <https://doi.org/10.1007/s11356-020-11714-y>

ORCID DETAILS OF THE AUTHORS

- M. K. Chai: <https://orcid.org/0000-0001-9162-7412>
 Y. H. Tan: <https://orcid.org/0000-0001-8290-3366>
 L. S. Wong: <https://orcid.org/0000-0002-5869-0804>
 R. Rajamani: <https://orcid.org/0000-0001-7438-0200>
 S. Djearmane: <https://orcid.org/0000-0002-8251-662X>



Assessment of the Swelling Behavior of NaOH-Contaminated Red Earth in the Visakhapatnam Region of India Using X-ray Diffraction Analysis

Srikanth Satish Kumar Darapu†^{id} and Sai Kumar Vindula

Department of Civil Engineering, GITAM School of Technology,

Gandhi Institute of Technology and Management (GITAM), Deemed to be University, Visakhapatnam, A.P., India

†Corresponding author: Srikanth Satish Kumar Darapu; reach.dssk@gmail.com,

Nat. Env. & Poll. Tech.
Website: www.neptjournal.com

Received: 24-08-2023

Revised: 17-10-2023

Accepted: 01-11-2023

Key Words:

Red earth
Alkali contamination
Swelling behavior of soil
XRD analysis
Zeolites

ABSTRACT

Research on the impact of alkali contamination on the swelling behavior of red earth in the Visakhapatnam region has been notably limited. Therefore, this study aims to investigate the effects of alkali (NaOH) contamination on the swelling characteristics of the region's red earth. The red earth of this region was found to be a well-graded sandy soil with 81% sand and 18% fines. X-ray diffraction studies showed that this region's red earth mainly consists of quartz, kaolinite, and hematite. The soil is inherently non-swelling. However, the free swell tests showed considerable swell under contamination of NaOH solutions of various normalities (0.05, 0.1, 1, 2, and 4N). One-dimensional consolidation tests have shown that the swell increased with the concentration of the NaOH solution and with the duration of the interaction. Red earth exhibited 'an equilibrium swelling' of 5.6, 10, 15, 17, and 20% when contaminated with 0.05, 0.1, 1, 2, and 4N NaOH solutions, respectively. XRD studies revealed that the red earth sample contaminated with even 0.05N NaOH solution and cured for 56 days exhibited the formation of zeolites analcime and natrolite. Silicate minerals like paragonite and ussingite were also formed along with the zeolites. N-A-S-H compounds, hydrosodalites, and zeolites like super hydrated natrolite, zeolite SSZ16, and zeolite ZK-14 were formed at higher normalities of NaOH after a curing period of 56 days, which caused increased swell. The research demonstrated that the formation of zeolites resulting from the alkali contamination led to swelling in the red earth.

INTRODUCTION

Caustic soda (NaOH) is an inorganic pollutant with a highly deleterious impact on the soil (Reddy et al. 2017, Mulyukov 2008, Jozefaciuk 2002, Mal'tsev 1998). Soils can be contaminated by NaOH from the effluents of dyes, paper, pulp, aluminum, ceramic industries, etc., during the operation and due to the effluents (Imran et al. 2015, Sivapullaiah & Manju 2005, Mal'tsev 1998). Non-expansive soils, which were stable, became unstable due to alkali contamination (Chavali et al. 2020, Sruthi et al. 2019, Vindula et al. 2017, Chavali et al. 2017, Vindula et al. 2016). Alkali-related contamination led to foundational and structural deformation, rendering industrial facilities unusable within one to one and a half decades. In the alumina plants, alkali aluminate solutions penetrate the backfill soils causing swelling and damage to the structures, requiring a vast expenditure of material and labor for repairs (Kabanov et al. 1977). Both clayey and sandy soils exhibit swelling under contamination by alkali aluminate solutions used in alumina production. In a three-year case study at Bogoslovskii Aluminum Plant,

the floor in the alumina shop rose from 29 to 133 mm, with cracks exceeding 50 mm. A similar issue was observed at the Acha Alumina Complex, where floors were uplifted more than 80 mm over two years (Kabanov et al. 1977).

One major factor affecting NaOH-contaminated soil's behavior is its dispersion characteristics. The duration of the exposure significantly influenced the behavior of the alkali-contaminated red earth. The more kaolinite in the soil, the more susceptibility to physical, chemical, and mineralogical changes (Sruthi et al. 2019). Chemical contamination changes the pore-fluid properties of the soil and, ultimately, its settlement characteristics (Meegoda & Ratnaweera 1994). The swelling capacity of the alkali-contaminated soil depends majorly on the soil's gradation, mineralogical composition, and clay content (Chunikhin et al. 1988). "Chemical swelling" (Sorochan 1974) or "Chemical heaving" (Sokolovich 1976) increases with increasing content of the mineral alumina (Al_2O_3) and the number of clayey particles ($d < 0.005$ mm) in the soils (Mal'tsev 1998). The process of decomposition of the minerals of the soil

under chemical contamination and subsequent formation of new minerals is termed “artificial lithification” (Voronkevich 1992). RE exhibited abnormal swelling on contamination with 4N NaOH solution (Vindula et al. 2016, Sivapullaiah & Manju 2007). Notably, the heave pressure was 2-3 times the swell pressure (Sokolovich 1995).

Considerable work was done on the swelling nature of alkali-contaminated red earth in regions other than Visakhapatnam (Ma et al. 2022, Chavali et al. 2020, Wang et al. 2020, Liu et al. 2019, Sruthi et al. 2019, Ashfaq et al. 2019, Vidula et al. 2017, Chavali et al. 2017). However, such studies in the Visakhapatnam region are very limited. The RE in the Visakhapatnam region was well-graded sandy soil with a sand content of 81% and fines of 18%. The soil predominantly consists of quartz, kaolinite, and hematite (Fig. 2).

Many industries, like HPCL, Hindustan Zinc Ltd., Coromandel Fertilisers Ltd., Vizag Steel Plant, etc., were established in Visakhapatnam due to the proximity to the natural harbor and seaport, among other reasons. Hence, there is a high probability of alkali contamination in this region (Satyanarayana et al. 2021). Also, as Visakhapatnam is the fastest-growing city in Andhra Pradesh, more and more industrial development is on the cards in the coming decade. Therefore, studying the impacts of alkali contamination on the soil in this region is significant.

The objectives of the research are to analyze the swell properties and mineralogical changes of the red earth in the Visakhapatnam region, contaminated with various concentrations of NaOH solution (0.05, 0.1, 1, 2, and 4N).

MATERIALS AND METHODS

Materials

Red earth (RE), which is found abundantly in the Visakhapatnam region, was collected by open excavation from a depth of 1m from the ground level from the open land opposite Visvesvaraya Bhavan of (Lat. 17.78171705, Long. 83.37515625) of the Visakhapatnam campus of GITAM Deemed to be University. The soil composite was prepared by coning and quartering. Around 50 kg of sample was collected. Approximately 50 kg of samples were gathered, air-dried, sieved through a 425-micron IS sieve, and then stored in an airtight container.

Based on the research works of Sruthi et al. (2019), Reddy et al. (2017), Sruthi & Reddy (2017a), Sruthi & Reddy (2017b), Vindula et al. (2017), Chavali et al. (2017), Vindula et al. (2016), Reddy & Sivapullaiah (2010a), Reddy & Sivapullaiah (2010b), Sivapullaiah & Manju (2007), and Sivapullaiah & Manju (2005), 0.1, 1, 2, 4 normalities of Sodium Hydroxide (NaOH) or caustic soda were selected

as the alkali contaminants. As no research was done on the impacts of 0.05N NaOH, this normality was also included in the study. Sodium hydroxide solutions were prepared using certified ACS-grade sodium hydroxide pellets (CAS: 1310-73-2) with a minimum percent purity of 97.0%, purchased from Fisher Chemical™. These pellets have a density of 2.1 g.cm³, a molar mass of 39.9971 g.mol⁻¹, and a water solubility of 111 g.100 mL⁻¹ at 20°C.

Methods

Free swell tests: Free swell tests were carried out to determine the swell potential of the contaminated samples according to IS 2720: Part 40: 1977 (Reaffirmed Year: 2021) - Methods of test for soils: Part 40 Determination of free swell index of soils. The free swell index was calculated as the percentage increase in the original volume. These tests indicate the possible damage to structures constructed atop due to swelling.

Consolidation tests: One-dimensional consolidation (standard oedometer) tests were conducted under seating load according to IS 2720: Part 15: 1965 (Reaffirmed Year: 2021) - Methods of Test for Soils - Part XV: Determination of Consolidation Properties. These tests provide insights into settlement and swelling characteristics, which help design the ground improvement and remediation methods.

X-ray diffraction (XRD) studies: A PANalytical X-ray diffractometer was used to analyze the mineralogical changes in the NaOH-contaminated RE samples under various curing periods. The samples were grounded in a porcelain crucible, and the material passing through a 75-micron sieve was sent for XRD analysis. The X-ray tube was energized at a voltage of 60 kilovolts (kV) and a current of 55 milliamperes (mA) in conjunction with an X'Celerator ultra-fast detector. Acetone was employed to meticulously eliminate any remnants of prior materials adhered to the mortar and pestle. Subsequently, with thorough attention to detail, the powdered sample was delicately deposited and gently compacted within a rectangular stainless-steel holder. The samples were scanned from a 2θ value of 6° to 70° with a step size of 0.02° using copper k-alpha radiation. Crystal Impact Match! Software based on Crystallography Open Database (COD) was used for identifying mineralogical changes.

RESULTS AND DISCUSSION

Free Swell Tests

The free swell test results presented in Table 1 show that RE exhibited swell even with 0.05N NaOH, and the swell increased with the concentration of the NaOH solutions. This observation is in confirmation of the findings of Sruthi et al. (2019). Thus, it was

preliminarily found that the inherently non-swelling RE exhibited swelling on NaOH contamination. Further, consolidation tests were carried out to study the swelling behavior.

Consolidation Tests

Percentage swell was calculated using the final swell displacements and the original heights of the specimen (Chavali et al. 2017). The Red earth exhibited 'an equilibrium' swelling of 5.6, 10, 15, 17, and 20% (Fig. 1) when contaminated with 0.05, 0.1, 1, 2, and 4N NaOH solutions, respectively. The swell with time was impacted by the concentration of NaOH solution (Reddy & Sivapullaiah 2010b). The alkali-silica reaction, which formed an alkali-silicate gel, was the primary cause of the swell (Sibley & Vadgama 1986).

The higher the concentration of the alkali solution, the faster the reaction between the clay fraction of the soil and the alkali solution. Hence, relative stabilization occurs in a relatively lower period (Kabanov et al. 1977). The higher percentage of swell exhibited by RE at higher concentrations of NaOH can be attributed to the dissolution of the authigenic mineral structure (Vindula et al. 2016) and the formation of the zeolites (Chavali et al. 2017, Sivapullaiah & Manju 2007) which resulted in more significant heave. The formation of zeolites was discussed in the XRD Analysis section. The swelling can also be attributed to the changes in pore-fluid properties (Meegoda & Ratnaweera 1994). The interaction of clayey minerals with alkalis causes mineralogical

decomposition and highly hydrated formations, resulting in the volumetric increase (Sokolovich & Troitskii 1976).

It is significant to note that compaction does not resist the swelling tendency of the foundation soil on interaction with NaOH solution. Prolonged chemical interaction between the spilled caustic soda solution and the kaolinitic red soil from Bangalore (now Bengaluru) district converted the inherently non-swelling soil to soil with high swelling potential (Rao & Rao 1994).

X-Ray Diffraction (XRD) Analysis

XRD tests were conducted, and the resulting graphs were analyzed to identify the new mineral formations influencing the RE's swelling behavior. Microstudies helped understand the interaction of the alkali contaminant (NaOH) with the soil (RE), which further gives an understanding of geotechnical problems like uneven settlements and progressive failures (Sivapullaiah & Manju 2007). Fig. 2 depicts the XRD analysis of RE and the NaOH-contaminated RE samples. The reaction of alkaline contaminants with RE was prolonged. Hence, it is difficult to find the damage in the early stages (Sruthi & Reddy 2017b). At 25°C, kaolinite continues to react with hydroxide ions even after 50 days, and the reaction is irreversible. The reaction of kaolinite and high concentrations of NaOH solution proceeds incongruently, leading to the formation of new minerals, mostly zeolites (Mohnot et al. 1987). Hence, the XRD results were analyzed after a 56-day curing period.

Table 1: Free swell index of NaOH-contaminated RE Samples.

Property	RE + Water	RE + 0.05N NaOH	RE + 0.1N NaOH	RE + 1N NaOH	RE + 2N NaOH	RE + 4N NaOH
Free Swell Index(%)	-	~10	~12	~16	~22	~28

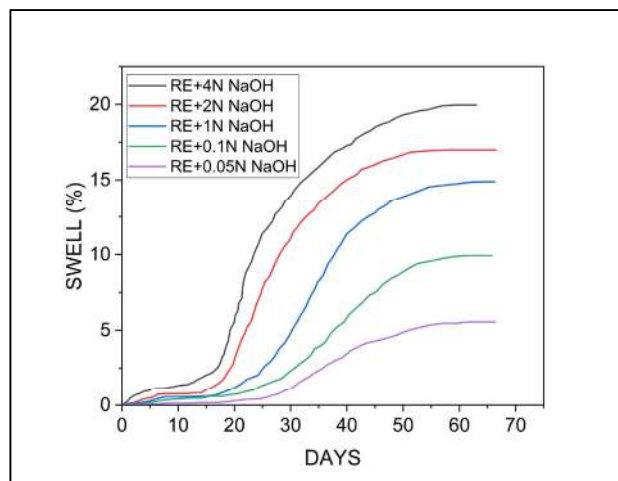


Fig. 1: Variation of swell percentage with duration for red earth contaminated with 0.05, 0.1, 1, 2, and 4N NaOH solutions.

Table 2: X-ray diffraction analysis codes for naoh-contaminated re samples cured for 56 days.

A56	RE + 0.05N NaOH
B56	RE + 0.1N NaOH
C56	RE + 1N NaOH
D56	RE + 2N NaOH
E56	RE + 4N NaOH

XRD pattern (fig. 3) of RE showed the significant peaks of quartz (at 4.21, 3.32, and 1.81 [Å]), kaolinite (at 7.07, 3.54, and 2.27 [Å]), and hematite (at 2.55, 1.67, and 1.45 [Å]). XRD pattern of RE contaminated with even the low concentration of 0.05N NaOH (A56) showed the peaks of zeolites like analcime (at 2.34 [Å]) and natrolite (at 3.57 [Å]). Peaks of ussingite (at 3.83 and 2.99 [Å]) and paragonite (at 2.56, 2.45, and 2.13 [Å]) were also observed. There was an apparent reduction in the quartz and kaolinite peaks, indicating the reaction of NaOH with silica and alumina, which led to the formation of zeolites analcime and natrolite. As the RE in the study area is sandy soil, the formation of silicate minerals like ussingite and paragonite was observed. It is significant to note that even at lower concentrations, zeolites were formed for a curing period of 56 days, indicating the mineralogical changes.

RE contaminated with 1N NaOH (C56) exhibited the peaks of analcime (prominent peak at 2.34 [Å]), natrolite (major peaks at 3.58 and 2.28 [Å]), sodium aluminosilicate hydrate (N-A-S-H) compound (at 2.57 [Å]), ussingite (prominent peak at 3.04 [Å]), paragonite (at 9.94, 4.26, 3.24, and 1.49 [Å]). No kaolinite peaks were observed, indicating the complete reaction of NaOH with the alumina and silica of kaolinite. Peaks of quartz were also reduced. On reacting with 2N NaOH, RE (D56) had shown the peaks of zeolite SSZ16 (at 10.06 [Å]), natrolite (at 4.46, 3.57, and 2.28 [Å]), hydrosodalite (at 2.56, and 2.13 [Å]), N-A-S-H compounds (at 2.88, and 2.45 [Å]), paragonite (at 4.25, 2.52, 1.93, and 1.49 [Å]) and ussingite (at 3.03 [Å]). At 4N NaOH, RE (E56) exhibited peaks of zeolites ZK-14 (at 5.02, 2.13, and 1.82 [Å]), analcime (at 5.57, and 2.80 [Å]), natrolite (at 4.46, 3.58, and 2.28 [Å]), super-hydrated natrolite (at 2.89, and 2.34 [Å]). Peaks of N-A-S-H compounds (at 7.17, 2.56, and 2.46 [Å]), ussingite (at 3.77, and 3.00 [Å]), and paragonite (at 4.25, 3.19, 2.51, and 1.49 [Å]) were also exhibited. Peaks of silica were further reduced, giving rise to new zeolites.

The reaction of Kaolinite and NaOH resulted in the formation of sodium aluminosilicate hydrate (N-A-S-H) compounds. The amount of N-A-S-H formed depends on the clay mineral in the soil, concentration of alkali solution, and interaction time. As the normality increased, the quantity of N-A-S-H compounds also increased. For RE

with less kaolinite, like that in the Visakhapatnam region, the changes in the properties were predominantly due to the formation of N-A-S-H compounds and zeolites (Sivapullaiah & Manju 2005). Changes in the surface charge of alkali-exposed minerals resulted in the formation of new minerals (Jozefaciuk 2002). When the alkali attacked the nucleus of the soil particle, the behavior of the soil was governed by the zeolites (Sruthi et al. 2019).

More aluminous zeolites like analcime are more likely to form in alkaline environments (Ming & Boettinger 2001). Under high pH, kaolinite was converted to water-sensitive analcime. The formation of analcime increased with alkalinity (Zhuang et al. 2018). The reaction of NaOH solution with kaolinite formed Analcime. Analcime is usually formed at lower alkalinity levels (Zhang et al. 2022). Analcime, a microporous zeolite, has a high specific surface area, cation exchange, catalytic capacity, and high adsorption per surface area (Jin et al. 2022, Ma et al. 2015, Atta et al. 2012), and hence influences the swelling behavior and the stability of the soil. Natrolite is a fibrous small-pore zeolite with a total pore volume of 22%. It consists of helical channels of an elliptical section allowing water diffusion (Tsai et al. 2021, Sabylnskii et al. 2016, Paczwa et al. 2016, Demontis et al. 2005, Ibrahim 2004, Line & Kearley 1998, Engelhardt & Michel 1987), which resulted in swelling. Swell caused due to the formation of sodium aluminosilicate hydrate (N-A-S-H) compounds is well documented (Sivapullaiah & Manju 2007), (Sivapullaiah & Manju 2005). N-A-S-H gel is a precursor reaction product to zeolites (Zhou et al. 2022).

Ussingite is a tectosilicate mineral (Williams & Weller 2012) and one of the most apatitic minerals of aluminosilicates. In natural processes, ussingite replaces sodalite (Kotel'nikov et al. 2010). Paragonite is a basic sodium aluminum silicate that belongs to the mica group. It is a rare sodium analog of mica or sodic mica (Gupta & Fareeduddin 2013, Chatterjee 1970). Ussingite and paragonite might not have contributed to the swell. However, their formation, along with the other zeolites, might have increased the swell.

In sample D56 (Table 2), N-A-S-H compounds and natrolite zeolite formation increased. Zeolite SSZ16, a small-pore high-silica zeolite of ABC type, has good adsorption capacity (Lobo 1996). Hydrosodalite is another small-pore zeolite with decent adsorption and high ion exchange capacity (Arasi 2020, Aprea 2014). The formation of these zeolites caused the swell in D56.

In sample E56 (Table 2), along with N-A-S-H compounds, zeolites analcime, natrolite, super hydrated natrolite, and zeolite ZK-14 were also formed. Zeolite ZK-14 is a synthetic chabazite with an open pore structure and stacking faults

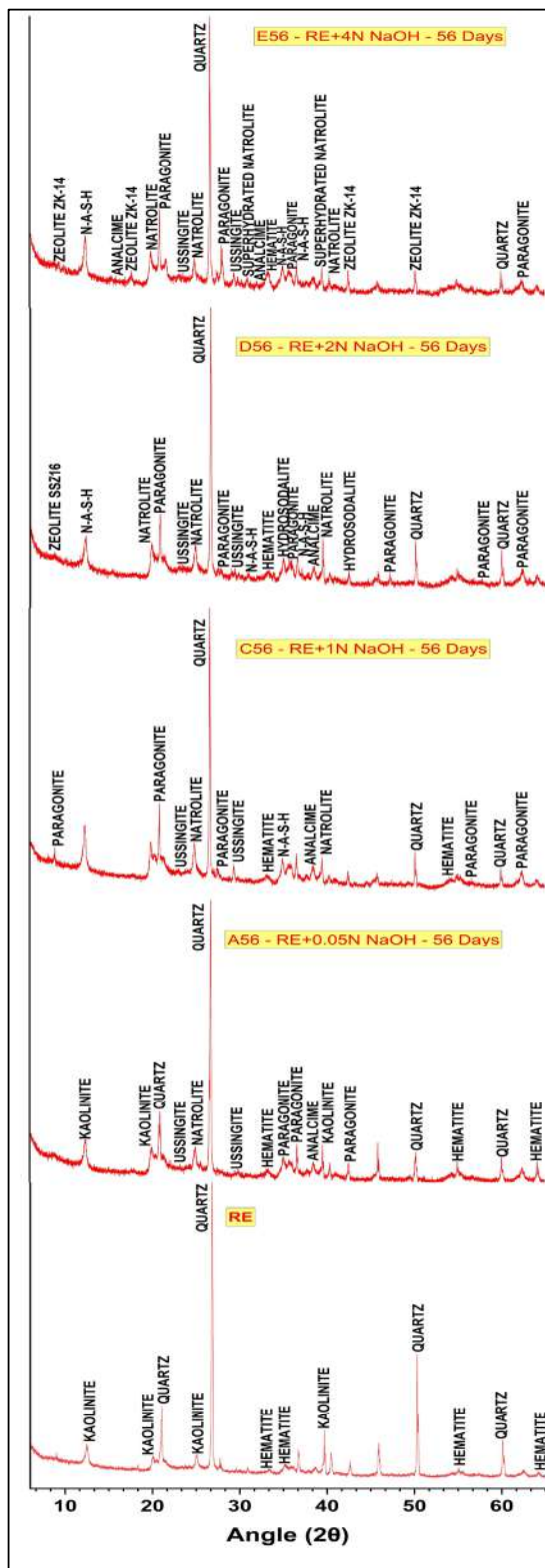


Fig. 2: XRD analysis for RE and RE contaminated with 0.05, 1, 2, and 4N NaOH solutions for a curing period of 56 days.

(Silva et al. 2016, Cartlidge et al. 1983) contributing to the swell. Super hydrated natrolite formed from natrolite by phase transition at 4N NaOH interaction caused anomalous anisotropic swelling in RE due to the selective sorption of NaOH. Superhydrated natrolite contains twice as much water content as that of natrolite. Also, the compressibility of the superhydrated natrolite is more than that of natrolite (IZA n.d.) (Lee et al. 2002, 2001, Belitsky et al. 1992). Hence superhydrated natrolite causes more swell and severe heave than those caused by natrolite.

CONCLUSIONS

- The inherently non-swelling red earth in the Visakhapatnam region underwent swelling when contaminated with NaOH solution, even at 0.05N.
- The swell percentage increased with the increase in the concentration of NaOH solution and the duration of the interaction.
- Red earth exhibited 'an equilibrium' swelling of 5.6, 10, 15, 17, and 20% when contaminated with 0.05, 0.1, 1, 2, and 4N NaOH solutions, respectively.
- RE+0.05N sample exhibited the formation of zeolites analcime and natrolite, along with silicate minerals ussingite and paragonite.
- The RE+1N sample showed the formation of zeolites analcime and natrolite and N-A-S-H compounds, which are precursor reaction products to zeolites.
- In the RE+2N sample, the formation of N-A-S-H compounds and natrolite zeolite increased. Zeolite SSZ16 was formed.
- In the RE+4N sample, super hydrated natrolite and zeolite ZK-14 were formed.
- The formation of the zeolites under the action of various normalities of NaOH solution caused a swell in the naturally non-swelling red earth in the study area.

The study has yielded pivotal findings, offering actionable insights that can be effectively leveraged to mitigate soil contamination issues prevalent in industrial regions where detrimental alkali discharges and effluents are prominent.

REFERENCES

- Alekseeva, T. and Alekseev, A. 1999. Factors affecting the structural stability of three contrasting soils of China. *CATENA*, 38(1): 45-64, ISSN 0341-8162. [https://doi.org/10.1016/S0341-8162\(99\)00055-7](https://doi.org/10.1016/S0341-8162(99)00055-7)
- Apra, P., Caputo, D., Gargiulo, N., de Gennaro, B., Iucolano, F., Liguori, B. and Colella, C. 2014. Ion exchange kinetics and thermodynamics of hydrosodalite, a narrow pore zeolite. *J. Porous Mater.*, 21: 643-651. <https://doi.org/10.1007/s10934-014-9810-y>
- Arasi, M.A., Salem, A. and Salem, S. 2020. Extraction of nanoporous silica from hydrosodalite produced via modification of low-grade kaolin for removal of methylene blue from wastewater. *J. Chem. Technol. Biotechnol.*, 95(7): 1989-2000. <https://doi.org/10.1002/jctb.6387>
- Ashfaq, M., Heeralal, M. and Reddy, P.H.P. 2019. A study on strength behavior of alkali-contaminated soils treated with fly ash. *Lect. Notes Civil Eng.*, 32: 137-143. https://doi.org/10.1007/978-981-13-7017-5_16
- Atta, A.Y., Jibril, B.Y., Aderemi, B.O. and Adefila, S.S. 2012. Preparation of analcime from local kaolin and rice husk ash. *Appl. Clay Sci.*, 61: 8-13. <https://doi.org/10.1016/j.clay.2012.02.018>
- Belitsky, I.A., Fursenko, B.A., Gabuda, S.P., Kholdeev O.V. and Seryotkin, Yu.V. 1992. Structural transformations in natrolite and edingtonite. *Phys. Chem. Miner.*, 18: 497-505, <https://doi.org/10.1007/BF00205264>
- Cartlidge, S., Wessicken, R. and Nissen, H.U. 1983. Electron microscopy study of zeolite ZK-14; a synthetic chabazite. *Phys. Chem. Miner.*, 9: 139-145, <https://doi.org/10.1007/BF00308371>
- Chatterjee, N.D. 1970. Synthesis and upper stability of paragonite. *Contr. Miner. Petrol.*, 27(3): 244-257. <https://doi.org/10.1007/BF00385781>
- Chavali, R.V.P., Vindula S.K., Reddy, P.H.P., Babu, A. and Pillai, R.J. 2017. Swelling behavior of kaolinitic clays contaminated with alkali solutions: A micro-level study. *Appl. Clay Sci.*, 135: 575-582. <https://doi.org/10.1016/j.clay.2016.10.045>
- Chavali, R.V.P., Vindula, S.K., Vydehi, K.V., Reddy, P.H.P. and Moghal, A.A.B. 2020. Effect of acid and alkali contamination on swelling behavior of kaolin clay. *Geo-Congress*, 20: 420. <https://ascelibrary.org/doi/10.1061/9780784482827.024>
- Chunikhin, V.G., Mavrodi, V.K., Kramarenko, O.A. and Dobromil'skaya, N.G. 1988. Effect of leakage of industrial alkali solutions on the construction properties of soils. *Soil Mech. Found. Eng.*, 25: 559-561. <https://doi.org/10.1007/BF01721619>
- Demontis, P., Gullín-González, J., Stara, G. and Suffritti, G. 2005. Structure and dynamics of hydrogen-bonded water helices in high-pressure hydrated phase of natrolite studied by molecular dynamics simulations. *Stud. Surface Sci. Catal.*, 155: 199-211. [https://doi.org/10.1016/S0167-2991\(05\)80149-1](https://doi.org/10.1016/S0167-2991(05)80149-1)
- Engelhardt, G. and Michel, D. 1987. High-resolution solid-state NMR of silicates and zeolites. *Wiley Online Lib.*, 92(9): 1059. <https://doi.org/10.1002/bbpc.198800267>
- Gupta, S. and Fareeduddin. 2013. Occurrence of paragonite in the hydrothermal wall rock alteration zone of G. R. Halli gold deposit, Chitradurga Schist Belt, Western Dharwar Craton, Southern India. *J. Geol. Soc. India.*, 82: 461-473. <https://doi.org/10.1007/s12594-013-0177-5>
- Ibrahim, K. 2004. Mineralogy and chemistry of natrolite from Jordan. *Clay Miner.*, 39(1): 47-55. [doi:10.1180/000985543910119](https://doi.org/10.1180/000985543910119)
- Imran, B., Khan, S.J., Qazi, I.A. and Md. Arshad. 2015. Removal and recovery of sodium hydroxide (NaOH) from industrial wastewater by two-stage diffusion dialysis (DD) and electrodialysis (ED) processes. *Desal. Water Treat.*, 57(17): 7926-7932. <https://doi.org/10.1080/19443994.2015.1048742>
- IZA Commission on Natural Zeolites. (n.d.). iza-online.org
- Jin, Y., Liu, Z., Han, L., Zhang, Y., Li, L., Zhu, S., Li, Z.P.J. and Wang, D. 2022. Synthesis of coal-analcime composite from coal gangue and its adsorption performance on heavy metal ions. *J. Hazard. Mater.*, 423: 127027. <https://doi.org/10.1016/j.jhazmat.2021.127027>
- Jozefaciuk, G. 2002. Effect of acid and alkali treatments on surface-charge properties of selected minerals. *Clays Clay Miner.*, 50: 647-656. <https://doi.org/10.1346/000986002320679378>
- Kabanov, V.M., Lebedeva, G.A., Finkel'shtein, L.I., Tkachenko, G.P. and Shenin, O.S. 1977. Swelling of soils due to wetting with alkali solutions. *Soil Mech. Found. Eng.*, 14 (5): 338-339. <https://doi.org/10.1007/BF02093009>
- Kotel'nikov, A.R., Ogorodova, L.P., Mel'chakova, L.V. and Vigasina, M.F. 2010. Ussingite from the Lovozero Alkaline massif: Calorimetric,

- thermal, and IR spectroscopic study. *Geochem. Int.*, 48: 183-186. <https://doi.org/10.1134/S0016702910020072>
- Lee, Y., Hriljac, J.A., Vogt, T., Parise, J.B. and Artioli, G. 2001. First structural investigation of a super-hydrated zeolite. *J. Am. Chem. Soc.*, 123(50): 12732-12733. <https://doi.org/10.1021/ja017098h>
- Lee, Y., Vogt, T., Hriljac, J.A., Parise, J.B. and Artioli, G. 2002. Pressure-induced volume expansion of zeolites in the natrolite family. *J. Am. Chem. Soc.*, 124(19): 5466-5475. <https://doi.org/10.1021/ja0255960>
- Line, C.M. and Kearley, G. 1998. The librational and vibrational spectra of water in natrolite, Na₂A₂Si₃O₁₀·2H₂O, compared with ab initio calculations. *Chem. Phys.*, 234(1-3): 207-222. [https://doi.org/10.1016/S0301-0104\(98\)00160-8](https://doi.org/10.1016/S0301-0104(98)00160-8)
- Liu, H., Zhang, S.C., Niu, F.J., Shao, Z.S., Niu, Z.L. and Lu, J. 2019. Experimental study on one-dimensional compression characteristics of Q3 loess contaminated by acid or alkali solutions. *Rock Soil Mech.*, 40: 210-216. DOI: 10.16285/j.rsm.2018.1659 [DOI: 10.16285/j.rsm.2018.1659]
- Lobo, R.F., Zones, S.I. and Medrud, R.C. 1996. Synthesis and rietveld refinement of the small-pore zeolite SSZ-16. *Chem. Mater.*, 8(10): 2409-2411. <https://doi.org/10.1021/cm960289c>
- Ma, S., Xiao, H. and Bao, P. 2022. Triaxial test and microstructure analysis of soil from alkali-contaminated sites. *Case Stud. Constr. Mater.*, 17: e01627. <https://doi.org/10.1016/j.cscm.2022.e01627>
- Ma, X., Yang, J., Ma, H., Liu, C. and Zhang, P. 2015. Synthesis and characterization of analcime using quartz syenite powder by alkali-hydrothermal treatment. *Micropor. Mesopor. Mater.*, 201: 134-140. <https://doi.org/10.1016/j.micromeso.2014.09.019>
- Mal'tsev, A.V. 1998. Theoretical and experimental investigations of the effect of aggressive wetting on various types of bed soils. *Soil Mech. Found. Eng.*, 35: 83-86. <https://doi.org/10.1007/BF02465914>
- Meegoda, N.J. and Ratnaweera, P. 1994. Compressibility of contaminated fine-grained soils. *Geotech. Test. J.*, 17(1): 101-112. [doi: 10.1520/GTJ10078J] (doi: 10.1520/GTJ10078J).
- Ming, D.W. and Boettinger, J.L. 2001. Zeolites in soil environments. *Rev. Mineral. Geochem.*, 45(1): 323-345. <https://doi.org/10.2138/rmg.2001.45.11>
- Mohnot, S.M., Bae, J.H. and Foley, W.L. 1987. A study of alkali/mineral reactions. *SPE Res. Eng.*, 2, 653-663. <https://doi.org/10.2118/13032-PA>
- Mulyukov, È.I. 2008. Alkaline swelling and consequences of alkalization of clayey bed soils. *Soil. Mech. Found. Eng.*, 45(5): 182-185. <https://doi.org/10.1007/s11204-008-9026-8>
- Paczwa, M., Sapiga, A.A. and Olszewski, M. 2016. Spin-lattice relaxations study of water mobility in natural natrolite. *J. Struct. Chem.*, 57: 319-324. <https://doi.org/10.1134/S0022476616020116>
- Rao, S.M. and Rao, S.K. 1994. Ground heave from caustic soda solution leakages case study. *Soils Found.*, 34(2): 13-18, https://doi.org/10.3208/sandf1972.34.2_13
- Reddy, P.H.P., Prasad, C.R.V. and Pillai, R.J. 2017. Swelling of natural soil subjected to acidic and alkaline contamination. *Period. Polytech. Civ. Eng.*, 61(3): 611-620, DOI: 10.3311/PPci.8185.
- Reddy, P.H.P. and Sivapullaiah, P.V. 2010a. Mineralogical and morphological changes with alkali treatment of soils. *Indian Geotech. Conf.*, 112: 5641-5651.
- Reddy, P.H.P. and Sivapullaiah, P.V. 2010b. Effect of alkali solutions on the swell behavior of soils with different mineralogy. *Indian Geotech. Conf.*, 199: 2692-2701. DOI: 10.1061/41095(365)273
- Sabylnskii, A.V., Moroz, N.K. and Gabuda, S.P. 2016. Kinetics of self-diffusion of water molecules in natrolite. *J. Struct. Chem.*, 57: 325-329. DOI: 10.1134/S0022476616020128
- Satyanarayana, G.V., Byragi Reddy, T., Srikanth Vemuri, R.S.S., Suryanarayana Rao, K., & Karnena, M.K. 2021. A study on the development of pollution index models and multivariate statistical analysis for heavy metals in the soils of APIIC, Visakhapatnam. *Nat. Environ. Pollut. Technol.*, 20(1): 251-257. DOI: 10.46488/nept.2021.v20i01.027
- Sibley, M.H. and Vadgama, N.J. 1986. Investigation of ground heave at ICI Mond division, Castner-Keller works, Runcorn. *Geol. Soc. Land Eng. Geol. Spec. Publ.*, 2: 367-373. DOI: 10.1144/GSL.1986.002.01.62
- Silva, J.S., Medeiros de Jesus-Neto, R., Fiuza, R.A., Gonçalves, J.P., Mascarenhas, A.J.S. and Andrade, H.M.C. 2016. Alkali-activation of spent fluid cracking catalysts for CO₂ capture. *Micropor. Mesopor. Mater.*, 232: 1-12. DOI: 10.1016/j.micromeso.2016.06.005
- Sivapullaiah, P.V. and Manju. 2007. Induced swelling of Rred earth in alkali solution. *Soils Found.*, 47(1): 59-66. DOI: 10.3208/sandf.47.59
- Sivapullaiah, P.V. and Manju. 2005. Kaolinite - alkali interaction and effects on basic properties. *Geotech. Geol. Eng.*, 23: 601-614. DOI: 10.1007/s10706-004-1661-x
- Sokolovich, V.E. and Troitskii, M.G. 1976. Heaving of a sandy bed as a result of new crystalline-hydrate formations in the latter. *Osn. Fundam. Mekh. Gruntov.*, 6: 5-7.
- Sokolovich, V.E. 1995. Chemical heaving of soils. *Soil Mech. Found. Eng.*, 32(4): 135-137. DOI: 10.1007/BF02336275
- Sokolovich, V.E. and Troitskii, G.M. 1976. Heaving of a sand base as a consequence of the development of secondary crystal hydrate formations. *Soil Mech. Found. Eng.*, 13: 376-378. DOI: 10.1007/BF01706704
- Sorochan, E.A. 1974. Installation of structures on swelling soils [in Russian], Stroizdat, Moscow. *Soil Mech. Found. Eng.*, 11: 421-430.
- Sruthi, P.L., Reddy, P.H.P. and Chavali, R.V.P. 2019. Physico-chemical characterization of alkali-contaminated tropical kaolinitic clays. *Int. J. Geotech. Eng.*, 14(8): 941-955. DOI: 10.1080/19386362.2019.1638045
- Sruthi, P.L. and Reddy, P.H.P. 2017. Physico-chemical behaviour of red earth contaminated with caustic alkalis. *Indian Geotech. Conf.*, 152: 3189-3195.
- Sruthi, P.L. and Reddy, P.H.P. 2017. Characterization of kaolinitic clays subjected to alkali contamination, *Appl. Clay Sci.*, 146: 535-547. DOI: 10.1016/j.clay.2017.07.012
- Tóth, G., Hermann, T., da Silva, M.R. and Montanarella, L. 2018. Monitoring soil for sustainable development and land degradation neutrality. *Environ. Monit. Assess.*, 190(57): 1-4.
- Tsai, Y., Huang, E., Li, Y., Hung, H., Jiang, J., Liu, T., Fang, J. and Chen, H. 2021. Raman spectroscopic characteristics of zeolite group minerals. *Minerals*, 11(167): 1-14, <https://doi.org/10.3390/min11020167>
- Vindula, S.K., Chavali, R.V.P. and Reddy P.H.P. 2016. Role of fly ash in control of alkali induced swelling in red earth: A micro-level investigation, *Int. J. Geotech. Eng.*, 12(1): 46-52, <https://doi.org/10.1080/19386362.2016.1247023>.
- Vindula, S.K., Chavali, R.V.P., Reddy, P.H.P. and Srinivas, T. 2017. Ground granulated blast furnace slag to control alkali induced swell in red earth. *Int. J. Geotech. Eng.*, 13(4): 377-384, <https://doi.org/10.1080/19386362.2017.1359901>.
- Vindula, S.K., Reddy, P.H.P., Prasad, A.S. and Chavali, R.V.P. 2021. Mineralogical and morphological transformations of alkali contaminated red earths. *Mater. Today Proceed.*, 46(1): 263-271. <https://doi.org/10.1016/j.matpr.2020.07.666>.
- Voronkevich, S.D. 1992. Modern problems of engineering geochemistry. *Inzh. Geol.*, 3: 12-25.
- Wang, D., Du, Y., Korkiala-Tanttu, L. and Zhao, Z. 2020. Volume change behavior of natural expansive soils subjected to acid and alkali contamination. *Int. J. Geomech.*, 20(11): [https://doi.org/10.1061/\(ASCE\)GM.1943-5622.0001835](https://doi.org/10.1061/(ASCE)GM.1943-5622.0001835)
- Williams, E.R. and Weller, M.T. 2012. A variable-temperature neutron diffraction study of ussingite; a strong asymmetric hydrogen bond in an aluminosilicate framework. *Phys. Chem. Miner.*, 39: 471-478. <https://doi.org/10.1007/s00269-012-0501-4>
- Zhang, X., Jiang, S., Liu, S., Chen, L. and Tong, L. 2022. Influences of crystallization time and molar composition of hydrogel on the

preparation of sodalite, cancrinite and analcime. Digest J. Nanomater. Biostruct., 17(2): 507-518. doi: 10.15251/DJNB.2022.172.507

Zhou, L., Wang, A. and Li, H. 2022. Effects of curing temperature and water glass modulus on the preparation of hierarchical zeolite precursors. Res. Square, 15: 225-246. <https://doi.org/10.21203/rs.3.rs-2098116/v1>

Zhuang, Y., Liu, X., Xiong, H. and Liang, L. 2018. Microscopic mechanism of clay minerals on reservoir damage during steam injection in

unconsolidated sandstone. Energy Fuels, 32(4): 4671-4681. <https://doi.org/10.1021/acs.energyfuels.7b03686>

ORCID DETAILS OF THE AUTHORS

Srikanth Satish Kumar Darapu: <https://orcid.org/0000-0003-1142-1233>



Eco-Engineered Low-Cost Carbosorbent Derived from Biodegradable Domestic Waste for Efficient Total Chromium Removal from Aqueous Environment: Spectroscopic and Adsorption Study

Vandana Saxena*, Ashish Kumar Singh**, Atul Srivastava*** and Anushree Srivastava*† 

*Department of Applied Science and Humanities, IIMT College of Engineering, Greater Noida, India

**Department of Mechanical Engineering, IIMT College of Engineering, Greater Noida, India

***Centre of Environmental Science, Institute of Interdisciplinary Studies, University of Allahabad, Prayagraj, Uttar Pradesh, India

†Correspondence author: Anushree Srivastava; anushree.srivastava12@gmail.com

Nat. Env. & Poll. Tech.
Website: www.neptjournal.com

Received: 12-10-2023

Revised: 08-12-2023

Accepted: 22-12-2023

Key Words:

Chromium
Bio-adsorption
Biodegradable waste
Groundwater

ABSTRACT

Chromium contamination in water bodies poses severe risks to both the environment and human health. This research introduces an innovative solution to this challenge by creating a vapor-activated carbosorbent from biodegradable household waste. The efficacy of this adsorbent in removing total chromium through batch methods from aqueous solutions was investigated. Surface analysis using scanning electron microscopy (SEM) exhibited a porous structure, while Fourier-transform infrared spectroscopy (FTIR) identified distinct functional groups on the surface. The point of zero charge (PZC), determined at 6.95, revealed the adsorbent's surface chemistry. Impressively, the synthesized carbosorbent exhibited significant adsorption capacities of 23.08 mg.g⁻¹ for Cr(III) and 24.84 mg.g⁻¹ for Cr(VI) under optimal conditions. The Langmuir isotherm model illustrated a monolayer adsorption mechanism aligned with the pseudo-second-order kinetic model, confirming chemisorption. Thermodynamic analysis disclosed favorable and spontaneous chromium adsorption. Negative ΔG° values affirmed the spontaneity, while the exothermic nature of the process was signified by the positive ΔH° value, indicating heat release. Increased randomness at the solid-liquid interface, indicated by the positive ΔS° value, underscored the enhanced affinity between the adsorbent and adsorbate. This study exemplifies the potential of the vapor-activated carbosorbent as an efficient and sustainable remedy for chromium-contaminated water bodies.

INTRODUCTION

Chromium is a potentially toxic element resulting from contemporary anthropogenic activity, which causes direct environmental problems with severe hazards to human beings (Mohanty et al. 2023). Meanwhile, the uncontrolled discharge of chromium into water bodies results in the heavy contamination of aquifers, which are one of the major sources of drinking water (Perraki et al. 2021). The presence of Cr(VI) in groundwater resources must be understood to assess the risks to human health (Vasileiou et al. 2019). In water bodies, chromium exists in two oxidation states, namely trivalent chromium (Cr(III)) and hexavalent chromium (Cr(VI)), and their predominance is majorly dependent upon the pH of the aqueous system). At acidic pH, trivalent chromium occurs as a cation that is dominated by insoluble hydroxide complexes, and hexavalent chromium exists in oxyanions forms of dichromate ($Cr_2O_7^{2-}$) and monovalent chromate

($HCrO_4^-$). However, the alkaline pH supports the existence of divalent chromate ($Cr_2O_4^{2-}$) in water bodies (Anthony et al. 2021). Generally, Cr(VI) is more water soluble and thus more mobile in groundwater. Cr(III) is relatively unstable but still dangerous, while Cr(VI) is very stable and easily oxidized and potentially hazardous to the environment as it is toxic, teratogenic, and carcinogenic by accumulating into cells through easy penetration by cell membranes (Qiu et al. 2020). According to the World Health Organization (WHO), the permissible limit for chromium in drinking water is 50 ppb. At the same time, various parts of the world reported chromium toxicity due to the consumption of contaminated drinking water (Vaiopoulou & Gikas 2020). A variety of technologies can be employed for chromium removal from water bodies, such as reverse osmosis, photodegradation, adsorption, coagulation, electrochemical, biochemical degradation, and ion exchange (Nur-E-Alam et al. 2020,

Karimi-Maleh et al. 2021, GracePavithra et al. 2019). Traditionally, the conversion of hexavalent chromium into trivalent chromium has become the most common method for water treatment (Hackbarth et al. 2016). However, this method is accompanied by the problem of high concentrations of Cr(III) after treatment (Staszak et al. 2023). Adsorption is considered a very simple, economical, and effective technique for the complete removal of total chromium from an aqueous environment (Mallik et al. 2022). Due to their structural heterogeneity, activated carbon and biochar make excellent adsorbents for water remediation. These adsorbents bear different sizes of pores, such as macropores, mesopores, and micropores, which makes them a suitable candidates for the adsorptive removal of pollutants (Islam et al. 2019). Adsorption on activated carbons (AC) is an efficient and most applied technique to treat contaminated water. There are numerous studies reported the application of activated carbons for water treatment (Ugwu & Agunwamba 2020, Yahya et al. 2020, Zhao et al. 2020). Dong et al. (2023) developed a porous biochar using waste collected from the liquor industry in order to decontaminate hexavalent chromium from an aqueous solution. They found that the adsorptive behavior of the alkali activated biochar has $144.5 \text{ mg} \cdot \text{g}^{-1}$ of adsorption capacity at optimum experimental conditions. The study further explained the mechanism of adsorption that suggested multilayer sorption with physical as well as chemical interaction occurring at the surface of the adsorbent (Dong et al. 2023). Another study was conducted by Chakraborty and Das (2023), where they developed a nano silica-coated biochar for the removal of hexavalent chromium from an aqueous solution that showed a maximum adsorption capacity of approximately $80 \text{ mg} \cdot \text{g}^{-1}$. The nanocomposite they prepared was examined at various experimental conditions to understand the mechanism of adsorption. The isothermal modeling and statistical analysis were well utilized in the research work that suggested validation of experimental data obtained during the study (Chakraborty & Das 2023). Similarly, Azaiez et al. studied the adsorptive removal of hexavalent chromium by using biochar, which was modified with zinc chloride. The result revealed an enhanced adsorption capacity of $177.64 \text{ mg} \cdot \text{g}^{-1}$ after modification. The high adsorption efficiency was obtained at extremely acidic conditions, which suggested its applicability to tannery water (Khalifa et al. 2023). However, traditional types of AC can be expensive to synthesize and may not always be energy efficient. Biomaterial-based adsorbents, on the other hand, can be effective and cost-efficient for decontaminating water. Moreover, converting waste biomass into value-added products has gained significant attention due to its renewability, environmental friendliness, and availability. To optimize the preparation of biochar, various methods can be

used, such as physical activation, which involves temperature variation, and vapor activation, which can enhance its pore size distribution and surface area. Additionally, chemical activation using acids, alkalis, and metal oxides can be an effective way to modify the properties of biochar and improve its suitability for water decontamination. Overall, this study aimed to investigate the efficiency of using the prepared carbosorbent for adsorbing Cr(III) and Cr(VI) ions under different conditions, which can be useful for designing effective water treatment strategies

MATERIALS AND METHODS

Characterization of Carbosorbent

The surface morphology of the prepared biochar was examined using a scanning electron microscope (SEM) provided by Philips, Netherlands. Furthermore, to investigate the involvement of functional groups in the adsorption process, an attenuated total reflectance Fourier-transform infrared (ATR-FTIR) spectrometer with a resolution of 4 cm^{-1} , specifically the Nicolet 6700 model from Thermo Scientific in MA, USA, was utilized. This characterization technique allowed for a comprehensive analysis of the functional groups present in the carbosorbent. Further, the point of zero charge (PZC) of the adsorbent was determined by the mass titration method reported by method from the literature. In brief, 25 mL of 0.1 M NaCl solutions were prepared in separate flasks, and their initial pH values were adjusted to a range of pH 3.00 to 11.00 by the addition of suitable quantities of 0.1 M HCl or NaOH solutions. Subsequently, 0.1 g of the carbosorbent was introduced into each flask, followed by continuous stirring for approximately 24 h at room temperature using a shaker. After the 24-hour stirring period, the final pH of each flask was measured, and the difference between the final and initial pH values was recorded. By plotting the ΔpH (difference in pH) against the initial pH, the PZC values were determined.

Adsorption Experiment by Batch Method

The adsorption process of trivalent and hexavalent chromium ions using the prepared carbosorbent was examined using a systematic procedure. To experiment, a 25 mL solution was placed in a 100 mL conical flask containing $10 \text{ mg} \cdot \text{L}^{-1}$ of Cr(III) and Cr(VI) with different pH ranges from 3 to 12 and placed at a magnetic stirrer with a rotation speed of 100 rpm. Additionally, the adsorption tests were performed at room temperature with a contact time of 60 min and an adsorbent dosage of $2 \text{ g} \cdot \text{L}^{-1}$. After each test, the carbosorbent was separated from the solution, and the concentration of the hexavalent and trivalent chromium was estimated. Similarly, the batch adsorption experiments for

under different environments, such as initial concentration ($10\text{--}50\text{ mgL}^{-1}$), adsorbent dosage ($0.25\text{--}2.2\text{ g.L}^{-1}$), contact time ($10\text{--}120\text{ min}$), and temperature ($28\text{--}50^\circ\text{C}$), were performed to evaluate the optimum condition for maximum adsorption capacity of the prepared carbosorbent. The equations (1) and (2) were used to calculate the adsorption efficiency and adsorption capacity for Cr(III) and Cr(VI)

$$\% \text{ Sorption} = \frac{C_i - C_e}{C_i} \times 100 \quad \dots(1)$$

$$q_e \left(\frac{\text{mg}}{\text{g}} \right) = \frac{C_i - C_e}{M} \times V \quad \dots(2)$$

Where C_i and C_e are the initial and final concentrations of the adsorbate, m is the mass of the adsorbent used, v is the volume in liter, and q_e is the maximum adsorption capacity of the developed adsorbent.

A UV-visible spectrophotometer determined the residual concentration of hexavalent chromium. (Systronic 2206) through the diphenyl carbazide method adopted by Kassimu et al. (2022). Briefly, 1 mL of treated solution mixed with 2N sulphuric acid followed by 100 μL of DPC stock solution prepared by dissolving 50 mg of 1,5 diphenyl carbazide in 25 mL acetone. An addition of DPC develops a reddish-violet color by forming a complex with Cr(VI). The intensity of color was examined at 540 nm to calculate the concentration of hexavalent chromium. The calibration curve was obtained with a standard solution of hexavalent chromium having

a concentration of 10 to 50 mgL^{-1} . Meanwhile, trivalent chromium was estimated by determining total chromium with a Flame atomic absorption spectrophotometer (NOAA 350 F-AAS) equipped with acetylene and N_2O gas.

RESULTS AND DISCUSSION

Characterization by SEM, FT-IR, and PZC

The surface morphology of the vapor-activated carbosorbent was analyzed by scanning electron microscope (SEM) and presented in Fig. 1. The surface topography of the material displayed a significant level of heterogeneity with uneven distribution of pores, resulting in a high surface area. An ATR-FTIR study was employed to analyze the stretching and vibration of functional groups present on the surface of vapor-activated carbosorbent and presented in Fig. 2(a). The result revealed variations in the stretching, bending, and ionic vibrations of different functional groups at distinct wavenumbers. The adsorption process is notably affected by the presence of various functional groups, including carboxyl, hydroxyl, sulfate, and amino groups, etc. on the surface of the adsorbent (Bagheri et al. 2020). These functional groups play a crucial role in determining the adsorption capacity and efficiency of the material. The peak detected at approximately 3500 cm^{-1} signifies the presence of OH groups within the sample, while the peak observed in the range of $2900\text{--}2970\text{ cm}^{-1}$ signifies the interaction

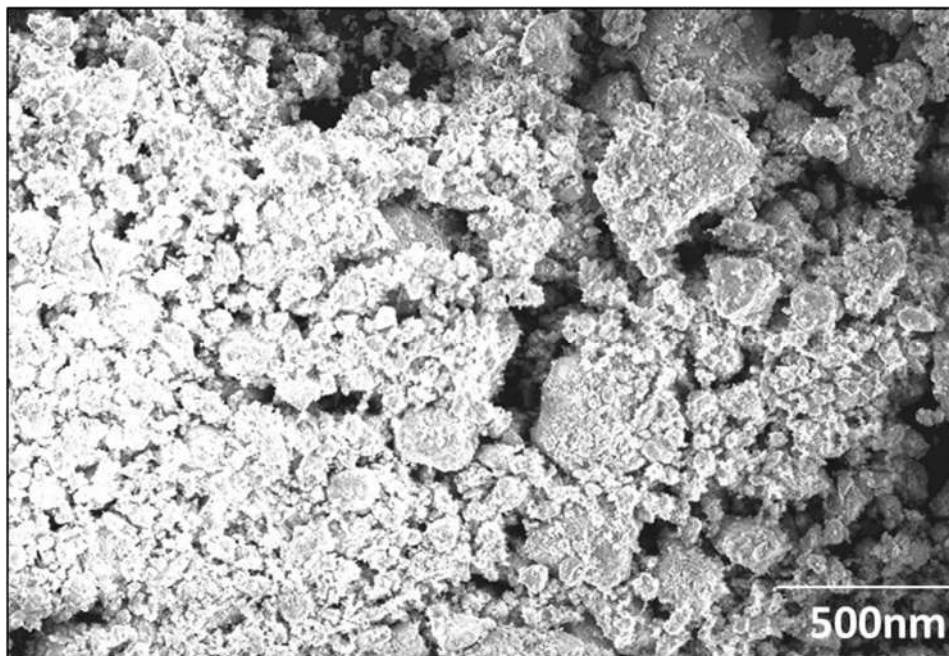


Fig. 1: SEM image of the vapour-activated carbosorbent developed from biodegradable domestic waste.

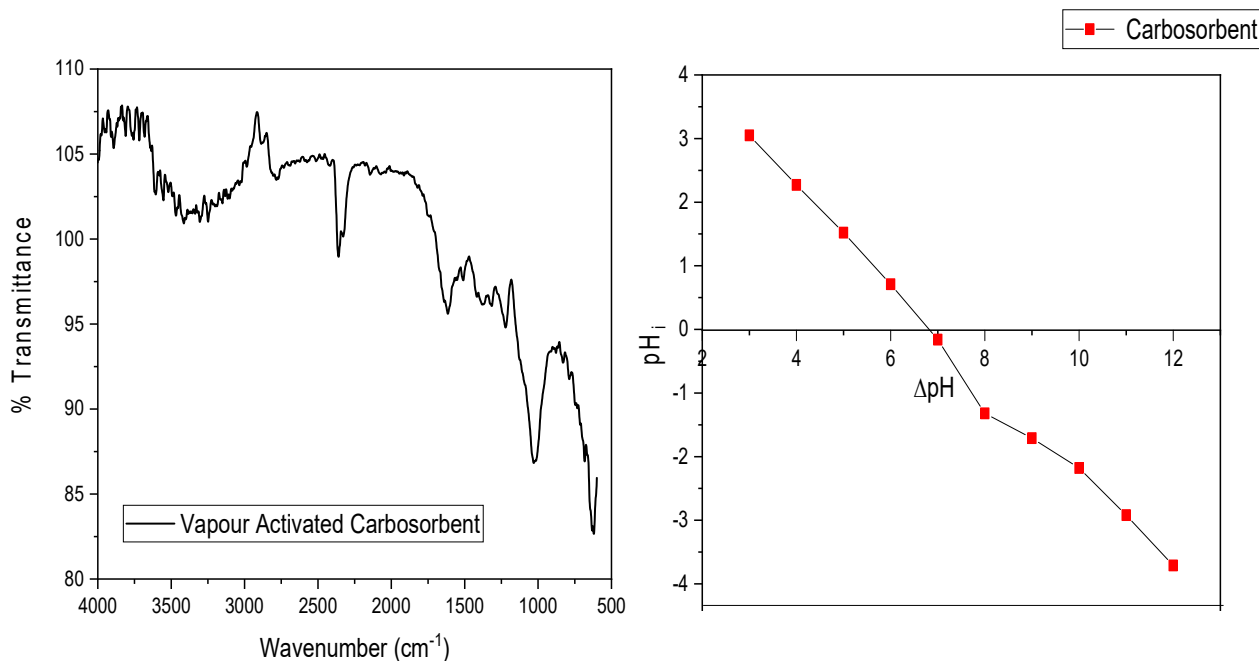


Fig. 2: (a) FTIR spectra of the developed carbosorbent (b) A graph between pH_i versus ΔpH to obtained point of zero charge (PZC).

between C-H bonds and the biochar surface (Zolfi Bavariani et al. 2019). Similarly, the presence of peaks near 1600 cm^{-1} indicates the presence of amides, which can be discerned on the surface of the carbosorbent.

Additionally, the well-defined peak at approximately 1700 cm^{-1} provides evidence for the presence of a carbonyl group (Srivastava et al. 2022a). This peak can be attributed to various functional groups, such as carboxyl groups (-COOH) from organic acids or ester groups (-COOR) from polysaccharides (Adeniyi et al. 2020). Furthermore, the peaks observed around 1200 and 1000 cm^{-1} likely originate from the stretching and vibration involving N-H bonds (Srivastava et al. 2020).

Moreover, peaks in the region of $1000\text{-}1300\text{ cm}^{-1}$ are often observed, which are associated with the stretching vibrations of C-O and C-O-C bonds, indicating the presence of polysaccharides or other organic compounds (Hu et al. 2022). The surface chemistry of the adsorbent was also investigated by measuring the pH at the point of zero charge (pH_{zpc}). A graph plotted between ΔpH versus pH_i where 6.95 of PZC was obtained at section point and presented in Fig. 2(b). The observed neutral pH at the point of zero charges (pH_{zpc}) on the carbosorbent implies the presence of substantial surface groups capable of either consuming or releasing H^+ (Yadav et al. 2023). These groups are likely to be -OH groups, which can exert a notable influence on the adsorptive behavior of the carbosorbent (Andrade et al. 2020).

Effect of pH and Initial Concentration

The pH of a solution exerts a substantial influence on the adsorption of an adsorbate, as it governs critical parameters such as surface charge, ionization degree, and ion speciation. The graph in Fig. 3(a) presents the adsorption data for total chromium removal, specifically examining the impact of pH values ranging from 3 to 9. The experimental setup included using 0.05 g of the adsorbent in a 25 mL test solution with a contact time of 60 to 120 min and a shaking speed of 150 rpm at room temperature. The outcomes of the analysis indicate that the adsorption efficiency of both Cr(III) and Cr(VI) increases concurrently with increasing pH, attaining its peak at pH 7. However, beyond this optimal pH point, a gradual decrease in efficiency is observed. Remarkably, at pH 7, an exceptionally high adsorption percentage of 99.02% was achieved for Cr(III), while Cr(VI) exhibited an even more impressive adsorption rate of 99.18%.

Conversely, an analysis of the adsorption process at the initial pH of 3 revealed significantly inferior efficiency figures of 35.21% (Cr(III)) and 40.75% (Cr(VI)). These findings emphasize that extremely acidic pH conditions negatively impact the adsorption of chromium ions due to electrostatic repulsion between the adsorbate and adsorbent. In a neutral environment, chromium species exist as oxyanions, which release hydrogen atoms as the pH increases (Sarkar et al. 2019). These oxyanions then interact with hydroxyl sites on the adsorbent, resulting in improved adsorption efficiency

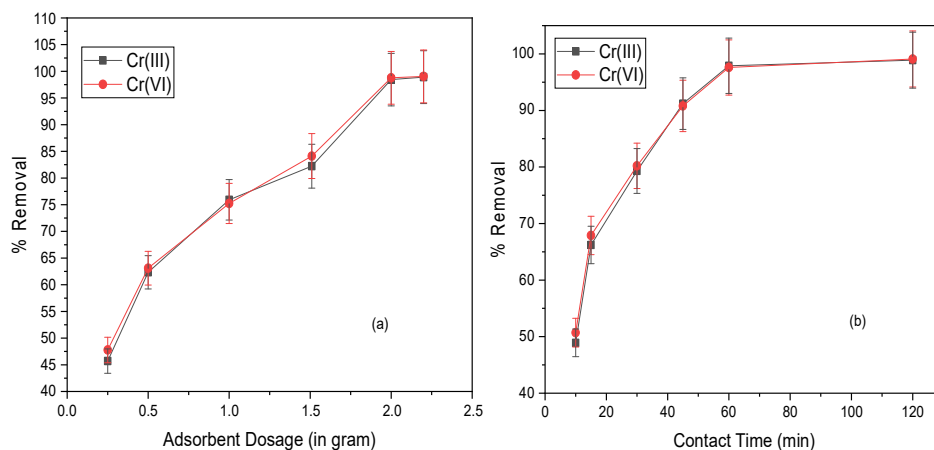


Fig. 3: (a) Effect of pH on the adsorptive removal of trivalent and hexavalent chromium (b) Effect of initial concentration for the removal of total chromium from aqueous solution.

(Chen et al. 2011). However, under alkaline conditions, the presence of competing hydroxide ions reduces adsorption by occupying available sites on the adsorbent surface, thereby hindering the attachment of chromium ions. The observed successive decrease in the percentage removal of Cr ions at lower and higher pH suggests the potential saturation of the binding capacity of the adsorbent (Wan et al. 2023). The findings of this study support previous reports indicating a favorable neutral pH range for chromium removal (Pap et al. 2018, Zhao et al. 2018). However, it is noteworthy that certain researchers have also highlighted the potential of acidic pH levels in effectively removing hexavalent chromium (Gupta et al. 2018, Shakya et al. 2019). The effect of initial concentration on the removal efficiency of total chromium was also examined using a prepared carbosorbent at various predetermined chromium concentrations ranging from 10 to 50 mg.L⁻¹ and presented in Fig. 3(b). Initially, the adsorption and removal rate of chromium solution by the carbosorbent achieved a remarkable 99.3% and 99.5% efficiency for Cr(III) and Cr(VI) ions, respectively. However, as the initial concentration increased, the removal rate declined due to a decrease in available active sites necessary to accommodate higher ion concentrations. In contrast, the adsorption capacity exhibited a rapid increase owing to the intensified adsorption driving force resulting from the higher solution concentration. This facilitated improved contact between the adsorbent and adsorbate. At an initial concentration of 50 mg/L of chromium ions solution, the removal rate of 83.5% and 84.49% for Cr³⁺ and Cr⁶⁺ suggests that the adsorption of chromium ions by the carbosorbent approached equilibrium when the initial concentration reached 50 mg.L⁻¹. Alternatively, this trend could be attributed to the saturation of active sites on the adsorbent at higher chromium concentrations. Consequently,

the decline in the percentage removal of chromium can be ascribed to either the limited binding capacity of the adsorbent or the occupation of active sites by chromium ions (Jamaluddin et al. 2022).

Effect of Adsorbent Dosage and Contact Time

The dosage of adsorbent used for ion uptake played a significant role in adsorption, as illustrated in Fig. 4(a). Under neutral pH conditions and an initial chromium concentration of 10 mg.L⁻¹, a biochar dosage of 2 g.L⁻¹ achieved a remarkable removal efficiency of approximately 99% for total chromium. However, as the mass of biochar increased, both the adsorption amounts and the adsorption per unit mass of adsorbent decreased despite the constant initial concentration of the solution. The initial increase in removal rate with higher adsorbent mass can be attributed to the availability of more binding sites for adsorption. Nevertheless, further increases in adsorbent mass did not impact the removal rate, indicating the saturation of adsorbate sites by chromium ions and their subsequent unavailability (Birhanu et al. 2020). The study also investigated the influence of contact time on the adsorption process and, presented in Fig. 4(b). The result indicated that the adsorption of total chromium increased as the contact time between the carbosorbent and the solution was prolonged. A saturation point was reached after 60 minutes, indicating that further contact time did not lead to significant additional adsorption.

Interestingly, a substantial amount of chromium ions was adsorbed within the initial 30 minutes of contact time, suggesting that a shorter duration may be sufficient for efficient chromium removal using the carbosorbent. Furthermore, the research observed no notable changes in the equilibrium condition beyond the 60-minute mark, up to

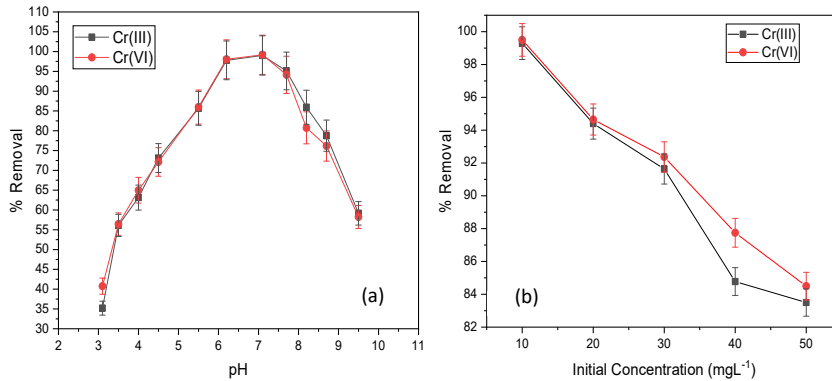


Fig. 4: Effect of adsorbent dosage (a) and effect of contact time (b) on adsorption of trivalent and hexavalent chromium onto vapor-activated carbon sorbent (total chromium⁺, 10mg/L, sorbate concentration: 2g/L at 30°C).

a maximum of 120 minutes. This suggests that the adsorption process achieved equilibrium within the initial 60 minutes of contact time. The reaction rate analysis revealed a rapid initial adsorption process, which can be attributed to the substantial concentration gradient between the adsorbate and the available vacant sites on the surface of the carbosorbent. However, as the experiment continued, the reaction rate gradually decreased. This decline can be attributed to a reduction in the number of vacant sites on the surface of the adsorbent, limiting the adsorption capacity over time (Bai et al. 2020).

Isothermal Modelling

Adsorption isotherms are mathematical models that describe how adsorbate molecules are distributed between liquid phases at various equilibrium concentrations (Dim et al. 2021). The two widely used models are the Langmuir and Freundlich models. In this study, both models were employed to establish the relationship between the number of adsorbed chromium ions and their equilibrium concentration in the solution. The Langmuir model proposes that adsorption takes place on a homogeneous surface with uniformly permeable and efficient regions. Consequently, a monolayer of adsorbate molecules is formed on the surface of the material, effectively saturating the available pores and hindering the mobility of additional molecules (Bedada et al. 2020).

The following formula can be used to define a non-linear expression of the Langmuir isotherm.

$$q_e = q_m K_L \frac{C_e}{1 + K_L C_e} \dots(3)$$

Where,

q_e = the adsorption capacity

C_e = concentration of the adsorbate at equilibrium

K_L = Langmuir Constant ($L \cdot mg^{-1}$), and q_m is the monolayer adsorption capacity in $mg \cdot g^{-1}$

The maximum adsorption capacity of trivalent and hexavalent chromium by the vapor-activated carbosorbent was determined by a nonlinear curve plotted between q_e and C_e and represented in Fig.5(a). The monolayer adsorption capacity was found to be $23.08 \text{ mg} \cdot g^{-1}$ and $24.84 \text{ mg} \cdot g^{-1}$ for Cr(III) and Cr(VI), respectively. The plot also provided a strong correlation coefficient in both cases, denoting the monolayer sorption capacity in units of $mg \cdot g^{-1}$ of the adsorbent. The adsorption energy, indicated by K_L with units of $L \cdot mg^{-1}$, was also analyzed and provided in Table 1.

To assess the shape of the isotherm, a dimensionless constant called the separation factor (R_L) was utilized. The R_L value can be calculated using the following equation:

$$R_L = \frac{1}{1 + K_L C_i} \dots(4)$$

The value of the R_L parameter categorizes the isotherm into the following four types:

Irreversible isotherm ($R_L = 0$): This indicates a complete lack of adsorption, where the solute does not interact with the adsorbent.

Linear isotherm ($R_L = 1$): This suggests a uniform and proportional adsorption process, where the adsorbate concentration is directly related to the amount adsorbed.

Table 1: Comparative values of the parameters calculated for the removal of Cr(III) and Cr(VI) by equilibrium models.

	Langmuir Isotherm		Freundlich Isotherm		
	Cr (III)	Cr (VI)	Cr (III)	Cr (VI)	
$Q_m \text{ [mg} \cdot g^{-1}]$	23.08	24.84	$K_f \text{ [L} \cdot mg^{-1}]$	1.22	1.80
R^2 value	0.957	0.952	R^2 Value	0.93	0.936
$K_L \text{ [L} \cdot mg^{-1}]$	0.63	0.57	1/n Value	0.293	0.281

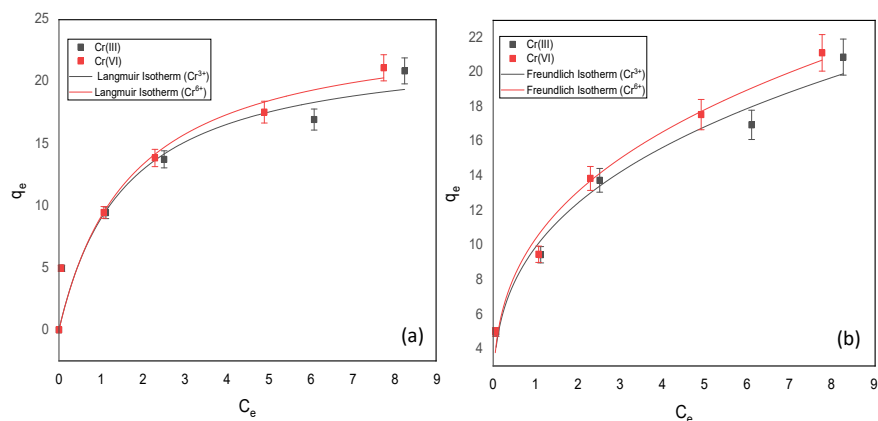


Fig. 5: Langmuir (a) and Freundlich (b) isotherm for adsorption of trivalent and hexavalent chromium onto vapor-activated carbosorbent.

Favorable isotherm ($0 < R_L < 1$): This signifies a favorable adsorption process, where the adsorbent exhibits a preference for the adsorbate. The R_L value between zero and one suggests efficient adsorption with a gradual decrease in the adsorption capacity as the concentration increases.

Unfavorable isotherm ($R_L > 1$): This indicates an unfavorable adsorption process, where the adsorbate faces resistance in interacting with the adsorbent. The R_L value greater than one implies a reduced affinity between the adsorbent and adsorbate as the concentration rises.

The estimated R_L values for Cr(III) and Cr(VI) ions are 0.136 and 0.149, respectively, which are less than one and larger than zero, indicating favorable adsorption (Tangestani et al. 2022). The application of the Freundlich isotherm model was employed to investigate the adsorption of total chromium ions in our research study. This model provides valuable insights into the adsorption process, indicating that it is non-ideal and reversible. It suggests that adsorption occurs through the formation of multilayers of the analyte on a heterogeneous surface with uneven characteristics (Srivastava et al. 2019). The non-linear expression of the isotherm is given as follows.

$$q_e = K_f C_e^{1/n} \quad \dots(5)$$

The Freundlich equation is a widely used empirical model for describing the adsorption process of solute molecules onto a solid adsorbent surface. It incorporates two key parameters: the Freundlich constant (K_f) and the Freundlich exponent (n). The K_f value represents the relative adsorption capacity of the adsorbent, while the exponent (n) provides insight into the intensity of adsorption. Generally, an increase in the K_f value signifies a higher adsorption capacity of the adsorbent. Moreover, when the value of n falls within the range of 1 to 10, it indicates an effective adsorption process. (Dan & Chattree 2018) (Fig. 5b). The n value achieved in

this study is better or equivalent to that of previously reported adsorbents for chromium removal (Jeyaseelan et al. 2021) (Ahmad et al. 2018). By comparing correlation coefficients (R^2), the suitability of isotherm models for the removal study was determined. Table 1 shows that both isotherm models correlate well with experimental data, although Langmuir's isotherm fits best with a higher correlation coefficient than the Freundlich isotherm. The maximum adsorption capacity (q_m) obtained in the present study is better than apple wood biochar where q_m was reported at $7.71 \text{ mg} \cdot \text{g}^{-1}$ (Liu et al. 2020). Another study performed by Amin and Chetpattananondh for the removal of hexavalent chromium by using algal biochar showed $15.94 \text{ mg} \cdot \text{g}^{-1}$ of monolayer adsorption capacity (Amin & Chetpattananondh 2019). Similarly, Rajapaksha et al. examined biochar developed with soybean for the removal of total chromium at acidic pH, where the maximum adsorption capacity was found to be $17.02 \text{ mg} \cdot \text{g}^{-1}$ (Rajapaksha et al. 2018)

Kinetic Modelling

Pseudo-first-order kinetics is commonly used to describe the adsorption process, assuming that the rate of adsorption is proportional to the difference between the saturation concentration and the amount of adsorbate adsorbed on the surface at a given time (Chakraborty et al. 2021).

The mathematical expression for the nonlinear pseudo-first-order kinetic model is:

$$q_t = q_e(1 - e^{-kt}) \quad \dots(6)$$

Where :

q_t is the amount of adsorbate adsorbed at time t

q_e is the amount of adsorbate adsorbed at equilibrium

k_1 is the rate constant of pseudo-first-order kinetics

The pseudo-first-order kinetic model assumes that the

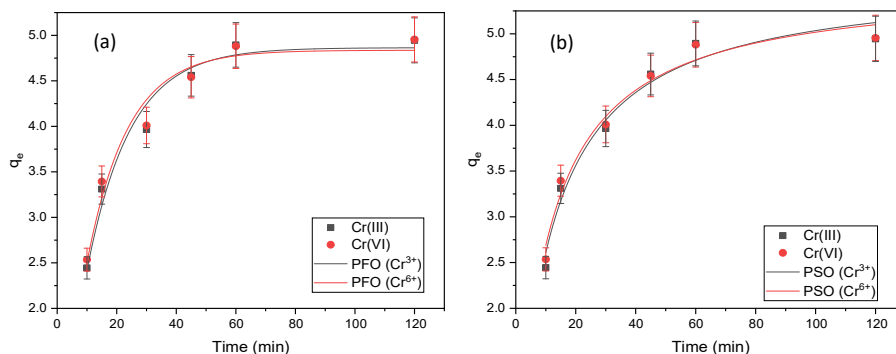


Fig. 6: Adsorption kinetic models for chromium ion uptake (a) pseudo-first-order model, (b) pseudo-second-order model for trivalent and hexavalent chromium onto vapor-activated carbosorbent.

Table 2: Kinetic parameter obtained for adsorption of Cr(III) and Cr(VI) onto vapor-activated carbosorbent.

	Pseudo First Order		Pseudo Second Order	
	Cr (III)	Cr (VI)	Cr (III)	Cr (VI)
$K_1(\text{min}^{-1})$	0.072	0.073	0.010	0.025
R^2 value	0.922	0.925	0.974	0.976
q_e mg/g	4.79	4.81	5.61	5.55

adsorption process is primarily controlled by the external mass transfer and the adsorbate concentration difference between the solution and the adsorbent surface (Revellame et al. 2020). A graph plotted between q_t and time for the adsorption study and presented in Fig. 6a. This model is often used for preliminary analysis or to estimate the rate constant of the adsorption process. However, it is important to note that the pseudo-first-order kinetic model may not always accurately describe the adsorption process. In some cases, the adsorption mechanism may be more complex, involving multiple steps or other factors that are not considered in this simplified model (Benjelloun et al. 2021). To gain a more comprehensive understanding of the adsorption process, it is common to examine the kinetics using the pseudo-second-order model as well. The mathematical expression for the nonlinear pseudo-second-order kinetic model is:

$$q_t = \frac{k_2 q_e^2 t}{1 + k_2 q_e t} \quad \dots(7)$$

Where k_2 is the rate constant of pseudo-second-order kinetics, the pseudo-second-order kinetic model was also plotted with q_t versus t , which provides a more accurate representation of the adsorption process, especially when the pseudo-first-order model fails to describe the experimental data adequately (Srivastava et al. 2021b) (Fig. 6b). The comparative data presented in Table 2 shows that the pseudo-second-order kinetic model exhibits a higher correlation coefficient compared to the pseudo-first-order model for both trivalent and hexavalent chromium. This indicates that

the pseudo-second-order model provides a better fit to the experimental data and offers a more accurate explanation of the sorption kinetic behavior for chromium removal by carbosorbent. The higher correlation coefficient associated with the pseudo-second-order model suggests a stronger linear relationship between the observed and calculated values, indicating a closer agreement between the model and the actual data points (Srivastava et al. 2022b). Furthermore, the pseudo-second-order kinetic model, which represents a single-step rate-limiting process, confirms the chemical nature of the sorption of chromium ions on the carbosorbent.

Thermodynamic Study

To investigate the nature of the sorption process, an adsorption experiment was conducted at different temperatures (25, 34, 42, and 60°C). The objective was to determine the thermodynamic parameters that characterize the reaction occurring during the sorption process. These parameters were determined by evaluating the coefficient of distribution (K_D) at each temperature (Yusuff 2019). The coefficient of distribution (K_D) is a measure of the distribution of an adsorbate between two phases that provides insights into the equilibrium concentration of the adsorbate in each phase at a given temperature (Srivastava et al. 2021a). By performing the adsorption experiment at various temperatures and evaluating the K_D values, it becomes possible to analyze the effect of temperature on the sorption process and determine the corresponding thermodynamic parameters. These parameters can include the standard free energy change (ΔG°), the standard enthalpy change (ΔH°), and the standard entropy change (ΔS°) associated with the sorption reaction.

$$\ln K_D = \left(\frac{\Delta S^\circ}{T}\right) - \left(\frac{\Delta H^\circ}{RT}\right) \quad \dots(8)$$

A graph was constructed to analyze the correlation between the coefficient of distribution (K_D) and inverse of temperature (Fig. 7). This graphical representation allowed

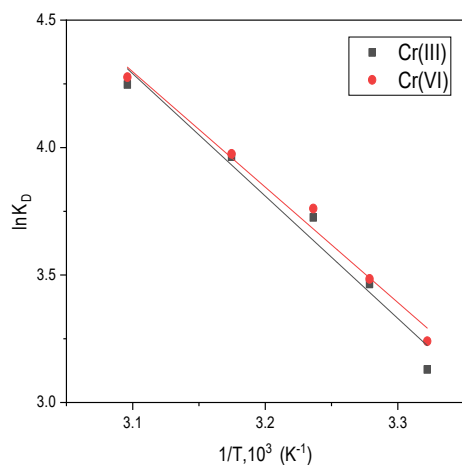


Fig. 7: Plot of $\ln K_D$ Vs. $1/T$ for the estimation of thermodynamic parameters for sorption of total chromium by carbosorbent.

Table 3: Thermodynamic parameters at various temperatures for the adsorption of Cr(III) and Cr(VI).

Temperature (in Kelvin)	Cr(III)	Cr(VI)
301	ΔG° [KJ.mol ⁻¹] -7.831	ΔG° [KJ.mol ⁻¹] -8.108
	$\Delta H^\circ = 33.82$ J.mol ⁻¹	$\Delta H^\circ = 37.57$ J.mol ⁻¹
305	-8.875	-8.836
	$\Delta S^\circ = 159.29$ J.mol ⁻¹	$\Delta S^\circ = 152.31$ J.mol ⁻¹
309	-9.572	-9.661
315	-10.382	-10.41
323	-11.406	-11.48

us to determine the change in Gibbs free energy (ΔG°) at different temperatures, a parameter that indicates the feasibility and spontaneity of the sorption process (Mpelane et al. 2022). The enthalpy change (ΔH°) and entropy change (ΔS°) were also computed using specific equations. These thermodynamic parameters presented in Table 3 shed light on the heat exchange and level of disorderliness occurring at the sorption interface (Jahangiri et al. 2019). The results demonstrated that the sorption process is feasible and spontaneous, as evidenced by the negative ΔG° values. Moreover, as the temperature increased, the sorption process became more favorable. For the adsorption of chromium ions, the process was confirmed to be thermodynamically spontaneous. The positive ΔH° value indicated that the sorption process is endothermic, implying the absorption of heat during the reaction (Abdel-Mohsen et al. 2020). Notably, the calculated enthalpy change (ΔH°) was found to be 39.82 kJ.mol⁻¹ and 37.57 kJ.mol⁻¹ for trivalent and hexavalent chromium, respectively, suggesting a chemical sorption mechanism due to its value exceeding 21 kJ.mol⁻¹. Additionally, the positive ΔS° value indicated an increase in the level of randomness at the solid-liquid

interface during the sorption process (Srivastava et al. 2022c).

CONCLUSION

The vapour-activated carbosorbent developed using biodegradable domestic waste has proven to be effective in removing total chromium from aqueous solutions. The surface characterization of the prepared adsorbent BY SEM revealed its porous structure, while FTIR spectra showed possible functional groups that might play a crucial role in the adsorption process. Additionally, the surface chemistry of the adsorbent is explained by the point of zero charge, which was found to be 6.95. The synthesized carbosorbent exhibited an adsorption capacity of 23.08mg.g⁻¹ and 24.84mg.g⁻¹ for Cr(III) and Cr(VI), respectively, under optimal experimental conditions. The adsorption process followed the Langmuir isotherm model, indicating a monolayer adsorption mechanism, while the pseudo-second-order kinetic model confirmed that the adsorption reaction was of a chemisorption nature. The negative values of ΔG° (standard Gibbs free energy change) indicated that the adsorption process is spontaneous, suggesting favorable adsorption of total chromium onto the adsorbent. In addition, the positive value of ΔH° (standard enthalpy change) suggests an exothermic nature of the adsorption reaction, implying that heat is released during the process. The positive value of ΔS° (standard entropy change) indicates an increase in randomness at the solid-liquid interface during the adsorption of chromium ions, indicating an improved affinity between the adsorbent and the adsorbate. Overall, the combination of a high adsorption capacity, ease of preparation, and the use of low-cost biodegradable domestic waste material makes this material an ideal adsorbent for the removal of total chromium from aqueous solutions. It offers a sustainable and efficient solution for addressing chromium contamination, and its potential as a practical alternative for water treatment is promising.

ACKNOWLEDGMENT

We acknowledge IIMT College of Engineering, Greater Noida, which provided financial support in achieving the various objectives of this research.

REFERENCES

- Abdel-Mohsen, A.M., Jancar, J., Kalina, L. and Hassan, A.F. 2020. Comparative study of chitosan and silk fibroin staple microfibers on the removal of chromium (VI): Fabrication, kinetics and thermodynamic studies. *Carbohydr. Polym.*, 234: 115861. <https://doi.org/https://doi.org/10.1016/j.carbpol.2020.115861>
- Adeniyi, A.G., Ighalo, J.O. and Onifade, D.V. 2020. Biochar from the Thermochemical Conversion of Orange Peel and Albedo: Product

- Quality and Potential Applications. *Chem. Africa*, 3: 439-448. <https://doi.org/10.1007/s42250-020-00119-6>
- Ahamad, K.U., Singh, R., Baruah, I. and 2018. Equilibrium and kinetics modeling of fluoride adsorption onto activated alumina, alum, and brick powder. *Groundw. Sustain. Dev.*, 7: 452-458. <https://doi.org/https://doi.org/10.1016/j.gsd.2018.06.005>
- Amin, M. and Chetpattananonh, P. 2019. Biochar from extracted marine *Chlorella* sp. residue for high-efficiency adsorption with ultrasonication to remove Cr(VI), Zn(II), and Ni(II). *Bioresour. Technol.*, 289: 121578. <https://doi.org/https://doi.org/10.1016/j.biortech.2019.121578>
- Andrade, T.S., Vakros, J., Mantzavinos, D. and Lianos, P. 2020. Biochar obtained by carbonization of spent coffee grounds and its application in the construction of an energy storage device. *Chem. Eng. J. Adv.*, 4: 100061. <https://doi.org/https://doi.org/10.1016/j.cej.2020.100061>
- Anthony, E.T., Alfred, M.O., Saliu, T.D. and Oladoja, N.A. 2021. One-pot thermal synthesis of Ceria/Montmorillonite composite for the removal of hexavalent chromium from aqueous system. *Surf. Interf.*, 22: 100914. <https://doi.org/https://doi.org/10.1016/j.surfint.2020.100914>
- Bagheri, A., Abu-Danso, E., Iqbal, J. and Bhatnagar, A. 2020. Modified biochar from Moringa seed powder for the removal of diclofenac from aqueous solution. *Environ. Sci. Pollut. Res.*, 27: 7318-7327. <https://doi.org/10.1007/s11356-019-06844-x>
- Bai, C., Wang, L. and Zhu, Z. 2020. Adsorption of Cr(III) and Pb(II) by graphene oxide/alginate hydrogel membrane: Characterization, adsorption kinetics, isotherm and thermodynamics studies. *Int. J. Biol. Macromol.*, 147: 898-910. <https://doi.org/https://doi.org/10.1016/j.ijbiomac.2019.09.249>
- Bedada, D., Angassa, K. and Tiruneh, A. 2020. Chromium removal from tannery wastewater through activated carbon produced from *Parthenium hysterophorus* weed. *Energy, Ecol. Environ.*, 5: 184-195. <https://doi.org/10.1007/s40974-020-00160-8>
- Benjelloun, M., Miyah, Y. and Akdemir Evrendilek, G. 2021. Recent advances in adsorption kinetic models: Their application to dye types. *Arab. J. Chem.*, 14: 103031. <https://doi.org/https://doi.org/10.1016/j.arabjc.2021.103031>
- Birhanu, Y., Leta, S. and Adam, G. 2020. Removal of chromium from synthetic wastewater by adsorption onto Ethiopian low-cost Odaracha adsorbent. *Appl. Water Sci.*, 10: 227. <https://doi.org/10.1007/s13201-020-01310-3>
- Chakraborty, R., Verma, R. and Asthana, A. 2021. Adsorption of hazardous chromium (VI) ions from aqueous solutions using modified sawdust: kinetics, isotherm and thermodynamic modeling. *Int. J. Environ. Anal. Chem.*, 101: 911-928. <https://doi.org/10.1080/03067319.2019.1673743>
- Chakraborty, V. and Das, P. 2023. Synthesis of nano-silica-coated biochar from thermal conversion of sawdust and its application for Cr removal: kinetic modeling using linear and nonlinear method and modeling using artificial neural network analysis. *Biomass Convers. Bioref.*, 13: 821-831. <https://doi.org/10.1007/s13399-020-01024-1>
- Chen, X., Lam, K.F. and Yeung, K.L. 2011. Selective removal of chromium from different aqueous systems using magnetic MCM-41 nanosorbents. *Chem. Eng. J.*, 172: 728-734. <https://doi.org/https://doi.org/10.1016/j.cej.2011.06.042>
- Dan, S. and Chatree, A. 2018. Sorption of fluoride using chemically modified *Moringa oleifera* leaves. *Appl. Water Sci.*, 8: 76. <https://doi.org/10.1007/s13201-018-0718-6>
- Dim, P.E., Mustapha, L.S., Termatanun, M. and Okafor, J.O. 2021. Adsorption of chromium (VI) and iron (III) ions onto acid-modified kaolinite: Isotherm, kinetics and thermodynamics studies. *Arab. J. Chem.*, 14: 103064. <https://doi.org/https://doi.org/10.1016/j.arabjc.2021.103064>
- Dong, H., Liang, H. and Yang, L. 2023. Porous biochar derived from waste distiller's grains for hexavalent chromium removal: Adsorption performance and mechanism. *J. Environ. Chem. Eng.*, 11: 110137. <https://doi.org/https://doi.org/10.1016/j.jece.2023.110137>
- GracePavithra, K., Jaikumar, V., Kumar, P.S. and SundarRajan, P. 2019. A review on cleaner strategies for chromium industrial wastewater: Present research and future perspective. *J. Clean Prod.*, 228: 580-593. <https://doi.org/https://doi.org/10.1016/j.jclepro.2019.04.117>
- Gupta, G.K., Ram, M. and Bala, R. 2018. Pyrolysis of chemically treated corncob for biochar production and its application in Cr(VI) removal. *Environ. Prog. Sustain. Energy*, 37: 1606-1617. <https://doi.org/https://doi.org/10.1002/ep.12838>
- Hackbarth, F.V., Maass, D. and de Souza, A.A.U. 2016. Removal of hexavalent chromium from electroplating wastewaters using marine macroalga *Pelvetia canaliculata* as a natural electron donor. *Chem. Eng. J.*, 290: 477-489. <https://doi.org/https://doi.org/10.1016/j.cej.2016.01.070>
- Hu, H., Zhang, J., Wang, T. and Wang, P. 2022. Adsorption of toxic metal ion in agricultural wastewater by torrefaction biochar from bamboo shoot shell. *J. Clean. Prod.*, 338: 130558. <https://doi.org/https://doi.org/10.1016/j.jclepro.2022.130558>
- Islam, M.A., Angove, M.J. and Morton, D.W. 2019. Recent innovative research on chromium (VI) adsorption mechanism. *Environ. Nanotechnol. Monit. Manag.*, 12: 100267. <https://doi.org/https://doi.org/10.1016/j.enmm.2019.100267>
- Jahangiri, K., Yousefi, N. and Ghadiri, S.K. 2019. Enhancement adsorption of hexavalent chromium onto modified fly ash from aqueous solution; optimization; isotherm, kinetic and thermodynamic study. *J. Dispers. Sci. Technol.*, 40: 1147-1158. <https://doi.org/10.1080/01932691.2018.1496841>
- Jamaluddin, N.S., Alias, N.H. and Samitsu, S. 2022. Efficient chromium (VI) removal from wastewater by adsorption-assisted photocatalysis using MXene. *J. Environ. Chem. Eng.*, 10: 108665. <https://doi.org/https://doi.org/10.1016/j.jece.2022.108665>
- Jeyaseelan, A., Katubi, K.M.M. and Alsaiani, N.S. 2021. Design and fabrication of sulfonic acid functionalized graphene oxide for enriched fluoride adsorption. *Diam. Relat. Mater.*, 117: 108446. <https://doi.org/https://doi.org/10.1016/j.diamond.2021.108446>
- Karimi-Maleh, H., Ayati, A. and Ghanbari, S. 2021. Recent advances in removal techniques of Cr(VI) toxic ion from aqueous solution: A comprehensive review. *J. Mol. Liq.*, 329: 115062. <https://doi.org/https://doi.org/10.1016/j.molliq.2020.115062>
- Kassimu, H., Sallau, A.B. and Nzelibe, H.C. 2022. Hexavalent chromium (Cr VI) bioreduction potential of anthocyanins rich extract of watermelon (*Citrullus lanatus*) rind. *Chem. Africa*, 5: 1837-1844. <https://doi.org/10.1007/s42250-022-00504-3>
- Khalifa, E.B., Azaiez, S. and Magnacca, G. 2023. Synthesis and characterization of promising biochars for hexavalent chromium removal: application of response surface methodology approach. *Int. J. Environ. Sci. Technol.*, 20: 4111-4126. <https://doi.org/10.1007/s13762-022-04270-0>
- Liu, N., Zhang, Y. and Xu, C. 2020. Removal mechanisms of aqueous Cr(VI) using apple wood biochar: a spectroscopic study. *J. Hazard. Mater.*, 384: 121371. <https://doi.org/https://doi.org/10.1016/j.jhazmat.2019.121371>
- Mallik, A.K., Muktadir, M.A. and Rahman, M.A. 2022. Progress in surface-modified silicas for Cr(VI) adsorption: A review. *J. Hazard. Mater.*, 423: 127041. <https://doi.org/https://doi.org/10.1016/j.jhazmat.2021.127041>
- Mohanty, S., Benya, A. and Hota, S. 2023. Eco-toxicity of hexavalent chromium and its adverse impact on the environment and human health in Sukinda Valley of India: A review on pollution and prevention strategies. *Environ. Chem. Ecotoxicol.*, 5: 46-54. <https://doi.org/https://doi.org/10.1016/j.eneco.2023.01.002>
- Mpelane, S., Mketi, N., Bingwa, N. and Nomngongo, P.N. 2022. Synthesis of mesoporous iron oxide nanoparticles for adsorptive removal of levofloxacin from aqueous solutions: Kinetics, isotherms, thermodynamics, and mechanism. *Alexandria Eng. J.*, 61: 8457-8468. <https://doi.org/https://doi.org/10.1016/j.aej.2022.02.014>

- Nur-E-Alam, M., Mia, M.A.S., Ahmad, F. and Rahman, M.M. 2020. An overview of chromium removal techniques from tannery effluent. *Appl. Water Sci.*, 10: 205. <https://doi.org/10.1007/s13201-020-01286-0>
- Pap, S., Bezanovic, V. and Radonic, J. 2018. Synthesis of highly efficient functionalized biochars from fruit industry waste biomass for the removal of chromium and lead. *J. Mol. Liq.*, 268: 315-325. <https://doi.org/https://doi.org/10.1016/j.molliq.2018.07.072>
- Perraki, M., Vasileiou, E. and Bartzas, G. 2021. Tracing the origin of chromium in groundwater: Current and new perspectives. *Curr. Opin. Environ. Sci.*, 22: 100267
- Qiu, Y., Zhang, Q. and Gao, B. 2020. Removal mechanisms of Cr(VI) and Cr(III) by biochar supported nanosized zero-valent iron: Synergy of adsorption, reduction and transformation. *Environ. Pollut.*, 265: 115018. <https://doi.org/https://doi.org/10.1016/j.envpol.2020.115018>
- Rajapaksha, A.U., Alam, M.S. and Chen, N. 2018. Removal of hexavalent chromium in aqueous solutions using biochar: Chemical and spectroscopic investigations. *Sci. Total Environ.*, 625: 1567-1573. <https://doi.org/https://doi.org/10.1016/j.scitotenv.2017.12.195>
- Revellame, E.D., Fortela, D.L. and Sharp, W. 2020. Adsorption kinetic modeling using pseudo-first order and pseudo-second order rate laws: A review. *Clean Eng. Technol.*, 1: 100032. <https://doi.org/https://doi.org/10.1016/j.clet.2020.100032>
- Sarkar, A., Ranjan, A. and Paul, B. 2019. Synthesis, characterization, and application of surface-modified biochar synthesized from rice husk, an agro-industrial waste, for the removal of hexavalent chromium from drinking water at near-neutral pH. *Clean Technol. Environ. Policy*, 21: 447-462. <https://doi.org/10.1007/s10098-018-1649-5>
- Shakya, A., Núñez-Delgado, A. and Agarwal, T. 2019. Biochar synthesis from sweet lime peel for hexavalent chromium remediation from aqueous solution. *J. Environ. Manage.*, 251: 109570. <https://doi.org/https://doi.org/10.1016/j.jenvman.2019.109570>
- Srivastava, A., Dave, H. and Azad, S.K. 2021a. Iron Modification of Biochar Developed from *Tectona grandis* Linn. F. for Adsorptive Removal of Tetracycline from Aqueous Solution. *Anal. Chem. Lett.*, 11: 360-375. <https://doi.org/10.1080/22297928.2021.1934113>
- Srivastava, A., Dave, H. and Prasad, B. 2022a. Adsorptive behavior of L-Arginine-silica micro-particles against arsenic and fluoride in aqueous solution. *Environ Nanotechnology, Monit Manag.*, 17: 100636. <https://doi.org/https://doi.org/10.1016/j.enmm.2021.100636>
- Srivastava, A., Dave, H. and Prasad, B. 2022b. Low-cost iron-modified *Syzygium cumini* L. Wood biochar for adsorptive removal of ciprofloxacin and doxycycline antibiotics from aqueous solution. *Inorg Chem Commun.*, 144: 109895. <https://doi.org/https://doi.org/10.1016/j.inoche.2022.109895>
- Srivastava, A., Kumar, S. and Kavita, A. 2022c. Arsenite and arsenate ions adsorption onto a biogenic nano-iron entrapped dual network Fe @ alginate - β - carrageenan hydrogel beads. *Nanotechnol Environ Eng.* <https://doi.org/10.1007/s41204-022-00280-y>
- Srivastava, A., Kumari, M. and Prasad, K.S. 2021b. Hydrogel beads containing ginger extract mediated nano-zirconium as an adsorbent for fluoride removal from aqueous solution. *Int. J. Environ. Anal. Chem.*, 1-15. <https://doi.org/10.1080/03067319.2021.1877282>
- Srivastava, A., Kumari, M. and Ramanathan, A. 2020. Removal of fluoride from aqueous solution by mesoporous silica nanoparticles functionalized with chitosan derived from mushroom. *J. Macromol. Sci. Part A*, 57: 619-627. <https://doi.org/10.1080/10601325.2020.1738896>
- Srivastava, A., Selvaraj, K. and Prasad, K.S. 2019. Nanoparticles Based Adsorbent for Removal of Arsenic from Aqueous Solution. *Asian J. Water, Environ. Pollut.*, 16: 87-93. <https://doi.org/10.3233/AJW-190046>
- Staszak, K., Kruszelnicka, I. and Ginter-Kramarczyk, D. 2023. Advances in the Removal of Cr(III) from Spent Industrial Effluents-A Review. *Materials (Basel)*, 16.
- Tangestani, M., Naeimi, B. and Dobaradaran, S. 2022. Biosorption of fluoride from aqueous solutions by *Rhizopus oryzae*: Isotherm and kinetic evaluation. *Environ. Prog. Sustain. Energy*, 41: e13725. <https://doi.org/10.1002/ep.13725>
- Ugwu, E.I. and Agunwamba, J.C. 2020. A review of the applicability of activated carbon derived from plant biomass in the adsorption of chromium, copper, and zinc from industrial wastewater. *Environ. Monit. Assess.*, 192: 240. <https://doi.org/10.1007/s10661-020-8162-0>
- Vaiopoulou, E. and Gikas, P. 2020. Regulations for chromium emissions to the aquatic environment in Europe and elsewhere. *Chemosphere*, 254: 126876. <https://doi.org/10.1016/j.chemosphere.2020.126876>
- Vasileiou, E., Papazotos, P. and Dimitrakopoulos, D., Perraki, M. 2019. Expounding the origin of chromium in groundwater of the Sarigkiol basin, Western Macedonia, Greece: a cohesive statistical approach and hydrochemical study. *Environ. Monit. Assess.*, 191: 509. <https://doi.org/10.1007/s10661-019-7655-1>
- Wan, Y., Luo, H. and Cai, Y. 2023. Selective removal of total Cr from a complex water matrix by chitosan and biochar modified-FeS: Kinetics and underlying mechanisms. *J. Hazard. Mater.*, 454: 131475. <https://doi.org/10.1016/j.jhazmat.2023.131475>
- Yadav, K., Latelwar, S.R., Datta, D. and Jana, B. 2023. Efficient removal of MB dye using litchi leaves powder adsorbent: Isotherm and kinetic studies. *J. Indian Chem. Soc.*, 100: 100974. <https://doi.org/10.1016/j.jics.2023.100974>
- Yahya, M.D., Obayomi, K.S. and Abdulkadir, M.B. 2020. Characterization of cobalt ferrite-supported activated carbon for removal of chromium and lead ions from tannery wastewater via adsorption equilibrium. *Water Sci. Eng.*, 13: 202-213. <https://doi.org/10.1016/j.wse.2020.09.007>
- Yusuff, A.S. 2019. Adsorption of hexavalent chromium from aqueous solution by *Leucaena leucocephala* seed pod activated carbon: equilibrium, kinetic and thermodynamic studies. *Arab J. Basic Appl. Sci.*, 26: 89-102. <https://doi.org/10.1080/25765299.2019.1567656>
- Zhao, J., Yu, L. and Ma, H. 2020. Corn stalk-based activated carbon synthesized by a novel activation method for high-performance adsorption of hexavalent chromium in aqueous solutions. *J. Colloid Interf. Sci.*, 578: 650-659. <https://doi.org/10.1016/j.jcis.2020.06.031>
- Zhao, N., Yin, Z. and Liu, F. 2018. Environmentally persistent free radicals mediated removal of Cr(VI) from highly saline water by corn straw biochars. *Bioresour. Technol.*, 260: 294-301. <https://doi.org/10.1016/j.biortech.2018.03.116>
- Zolfi Bavariani, M., Ronaghi, A. and Ghasemi, R., 2019. Influence of pyrolysis temperatures on FTIR analysis, nutrient bioavailability, and agricultural use of poultry manure biochars. *Commun. Soil Sci. Plant Anal.*, 50: 402-411. <https://doi.org/10.1080/00103624.2018.1563101>

ORCID DETAILS OF THE AUTHORS

Anushree Srivastava: <https://orcid.org/0000-0003-0056-4511>



Invasive Aquatic Plants as Potential Sustainable Feedstocks for Biochar Production and as an Innovative Approach for Wastewater Treatment

K. M. P. I. Jayathilake*, P.M. Manage* and F. S Idroos†

*Centre for Water Quality and Algae Research, Department of Zoology, University of Sri Jayewardenepura, Sri Lanka

†Corresponding author: F. S Idroos; sumaiyaidroos@sci.sjp.ac.lk

Nat. Env. & Poll. Tech.
Website: www.neptjournal.com

Received: 06-09-2023

Revised: 13-12-2023

Accepted: 22-12-2023

Key Words:

Biochar

Wastewater

Water quality parameters

Invasive aquatic plants

ABSTRACT

Biochar (BC) is a well-established physical treatment method. The high-cost BC limits their use as adsorbents in wastewater. Thus, deriving BC from cheap and locally available waste materials is needed to develop a feasible waste removal technology. Nowadays, BC technology makes it possible to envision a new strategy to manage invasive plants by converting them into value-added products like BC. Hence, the present study was designed to evaluate the potential utilization of BC as an efficient filter medium made by invasive aquatic plants, *Salvinia* spp., and *Eichhornia* spp. A mass of 50 g of prepared activated and nonactivated BC was incorporated in a sand and gravel filter to treat rubber-manufactured wastewater. Wastewater was passed through the filter, and both raw and treated water samples were analyzed for pH, Total Suspended Solids (TSS), Biological Oxygen Demand (BOD₅), Chemical Oxygen Demand (COD), Total Kjeldahl Nitrogen (TKN), Ammoniacal-Nitrogen (NH₃-N), Electrical Conductivity (EC), Total Dissolved Solids (TDS), Total Phosphates (TP), Nitrate (NO₃-N), turbidity and heavy metals (Zinc, Chromium). The control filter was developed only with sand and gravel, excluding BC. Fourier Transform-Infrared Spectroscopy (FT-IR) and Scanning electron microscopy (SEM) were used to analyze BC's chemical and physical characteristics. A brine shrimp lethality assay was carried out for toxicological evaluation. OH stretching (3,550-3,200 cm⁻¹), C=C aromatic stretching (1400-1660 cm⁻¹), and Phenol-O-H bending (1,300-1,400 cm⁻¹) were recorded in all BC samples that involved the adsorption mechanism. Observed images indicated differences in surface morphology of both activated and nonactivated BC were observed under SEM observation. The study concludes that the filter unit incorporated with activated *Eichhornia* spp. Gave the best treatment efficiency when compared to filter units incorporated with other activated and nonactivated BC. The toxicity assay revealed 100% mortality in the control setup and raw wastewater but only 60–70% in the nonactivated BC integrated filters. Activated BC-incorporated filters showed no mortalities. Hence, the study's outcomes suggest a green approach using invasive aquatic plants for sustainable wastewater treatment.

INTRODUCTION

The application of biochar (BC) for the remediation of contaminated water sources may provide a new solution to water contamination issues (Zhang et al. 2013). BC can potentially be applied to decrease and mitigate the bioavailability and leachability of inorganic contaminants like heavy metals and organic contaminants in water sources through adsorption and other physicochemical interactions due to the special properties of BC. BC has been widely used for water conditioning, carbon sequestration, and water remediation. The abundant surface area of BC, the well porosity structure of BC, and the high affinity of functional groups of BCs are reasoned for the proper absorption of heavy metals and aromatic compounds on its surface. Hence,

BC can be applied as a low-cost, suitable adsorbent to remove contaminants from wastewater (Mohan et al. 2014, Inyang et al. 2016).

Biological invasions have a massive number of known and potential impacts on community structure and function of ecosystems and seriously affect the ecological status of water sources (Havel et al. 2015, Leuven et al. 2017). The rapid spreading of invasive plants poses a growing threat to the natural environment throughout all countries. One of the most prominent impacts of invasive species is the direct loss of crops due to infestations. Most invasive plants disturb the scenic beauty of the area and can directly or indirectly create concern and stress among local communities and badly affect the tourism industry (Stiers et al. 2011).

BC is usually produced from various sources, such as crop residues, wood biomass, animal litter, and solid waste (Meyer et al. 2011). However, the resource utilization of invasive plants has become an effective strategy for controlling and managing invasive plants, reducing the cost of prevention and control and turning waste into treasure. (Feng et al. 2021). Recent developments in BC technology make it possible to envision a new strategy to manage invasive plants by converting them into value-added products like BC (Zimmerman et al. 2011).

The high cost of BC limits their use as adsorbents in wastewater treatment and other applications. Presently, researchers pay attention to invasive plants to prepare BC as an environmentally friendly and cheap method for different applications including pollution remediation. Most recently, wastewater treatment using biochar (BC) has become a new technology due to specific characteristics that significantly differ from other alternatives. The physical and chemical properties of BC (surface area, porosity, surface charge, functional groups, and mineral contents) play an important role in adsorption (Zhao et al. 2019). Hence, there is growing interest in using BC as a filter medium (adsorbent) to treat water and wastewater due to its unique properties of BC (Perez-Mercado et al. 2018). The feedstock type and water content of biomass can significantly influence the structure and properties of BC and, hence, its adsorption capacity (Song et al. 2019). The use of invasive aquatic plants as BC feedstocks is more economical and easily available compared to other biomass waste (Feng et al. 2021). Hence, this study used BC produced from *Eichhornia* spp. and *Salvinia* spp. to prepare the filter medium to treat industrial wastewater. This study will help mitigate and manage the aquatic invasive plants' proliferation and enhance the quality of the chemical wastewater released into the environment.

MATERIALS AND METHODS

Sample Collection

Salvinia spp. and *Eichhornia* spp. were collected from the Bellanwila-Nedimala Aththidiya canal, Sri Lanka (6.838037, 79.892105) were used as the biomass for biochar (BC) preparation. Wastewater samples were received from a rubber glove manufacturing plant in Colombo, Sri Lanka. The samples were collected in pre-cleaned plastic containers and transported to the laboratory.

Preparation of BC

BC was prepared according to the method described by Agrafioti et al. (2013) with minor modifications of the pyrolysis process. The *Salvinia* spp. and *Eichhornia* spp. were chopped into small pieces. Feedstock was sun-dried.

Dried samples weighing 250 g were placed in a muffle furnace (Thermolyne, 30400). The feedstock of *Salvinia* spp and *Eichhornia* spp were heated at 300 °C/hour and 350 °C/hour, respectively.

Activation of the BC

A modified approach described by Chen et al. (2017) was used to activate the BC. A weight of 10 g dried BC was activated with 100 mL distilled water containing ZnCl₂ at a final concentration of 0.1 gm.L⁻¹. The mixture was stirred for 1 hour at 50 °C. The sample was aged for 12 hours at room temperature. The mixture was filtered and dried overnight at 105 °C. The impregnated sample was heated to 450 °C, held for 1.5 h under a nitrogen environment in the muffle furnace, and cooled to room temperature with a continuous nitrogen flush. The product was rinsed with 1.0 M HCl and distilled water until it obtained a neutral pH. The sample was then dried in an oven for two hours at 105 °C. The prepared BC was sorted into a size range of 125-250 µm using a sieve set. Both activated and non-activated BC from *Eichhornia* spp. and *Salvinia* spp. were labeled as AE, NAE, AS, and NAS, respectively.

BC Characterization

The microstructures and chemical structure of BC were analyzed using a scanning electron microscope (SEM) (CARL ZEISS EVO 18) and Fourier-transform infrared spectroscopy (FTIR) (Thermo Scientific Nicolet S10). OMNIC Spectra TM, a data-gathering software application, was used to analyze spectral data.

Preparation of the Filter Unit and its Operation

Filter bed was prepared by 6 cm height of sterilized fine sand (0.065- 0.125 mm), 50 g of BC layer (125-250 µm), 2.5 cm height of sterilized coarse sand (2-4 mm), and 2.5 cm height of sterilized gravel layer (4-8 mm), respectively. Control filters were constructed without a BC layer. 1.5 L of raw water sample was passed through the filter unit for the treatment process. The flow rate was kept at 0.3 L.min⁻¹ using a commercially available aquarium pump (NS 160). Each treatment was performed for three hours of retention time.

Analysis of Water Quality Parameters and Selection of the Efficient BC Sample

Water quality parameters such as pH, Electrical Conductivity (EC), Total Dissolved Solids (TDS), turbidity, and Biological Oxygen Demand (BOD₅) were measured using standard meters. Total Suspended Solids (TSS), Chemical Oxygen Demand (COD), Total Kjeldahl Nitrogen (TKN), Ammoniacal Nitrogen (NH₃-N), Total Phosphates (TP), nitrate, and heavy metals (Zinc, Lead, Chromium, and

cadmium) were analyzed using the standard analytical methods. (AOAC, 2000, APHA, 2017). The results were compared with the nationally recommended water quality parameters described by the Board of Investment (BOI) to determine the most effective BC sample.

Bioassay for Toxicity

A brine shrimp lethality assay was carried out for the toxicological evaluation of raw and treated water samples according to the method described by Olowa & Nuneza (2013). Commercially available brine shrimp eggs (Nildiya Aquarium, Wattededara) were purchased and allowed for hatching using 1 L of natural saltwater. Ten newly hatched nauplii were added separately for every 10 mL of raw and treated water samples. The control was created using distilled water. After 24 hours, the dead nauplii were counted. The experiment was carried out in triplicate.

Analytical Statistics

A one-way ANOVA was carried out using SPSS version 21. The Tukey HSD, a multiple comparison test, was applied to find differences between both treatments.

RESULTS AND DISCUSSION

Chemical industrial wastewater consists of numerous inorganic and organic contaminants. At present, biochar (BC) has become a suitable absorbent for wastewater treatment. Hence, in this study BC has been used to treat chemical wastewater. Depending on the industry, different levels of contaminants are released into the environment directly or indirectly through effluent sources (Massoudinejad et al. 2015). In the present study, BC was prepared by two selected invasive plants in Sri Lanka: *Eichhornia* spp and *Salvinia* spp. These invasive aquatic plants pose a serious threat to the ecosystems. Hence, their use in BC preparation will be a sustainable control and management method.

BC Yield

BC conversion rates of selected biomass differed for both plants. Table 1 presents the percentages of BC produced from 250 g of each plant. In this study, the percentage of BC production of *Salvinia* spp. and *Eichhornia* spp was respectively 34.70% and 35.54%. Enaime et al. (2020) have shown that the generally slow pyrolysis process is reasoned to produce 27 – 37% of BC.

Chemical Characterization of Activated and Nonactivated BC

FTIR spectroscopy can provide direct information on the existence of different surface functional groups present in

the organic matter of BC. The adsorption rate of BC also depends on the types and levels of surface functional groups (Qambrani et al. 2017).

In this study (Fig. 1), broadband was found at 3200-3400 cm^{-1} (O-H stretching) in all the BC samples, including AS, AE, NAS, and NAE. This O-H stretching may be attributed to the presence of hydroxyl groups. Similar FTIR spectra were reported by Song et al. (2019) for the rice straw BC with broad bands of 3411 cm^{-1} representing the O-H stretching. Moreover, a sharp band was observed at the 1400-1660 cm^{-1} range (C=C stretching) in all the BC samples. This C=C stretching may be attributed to the presence of aromatic groups. Song et al. (2019) have reported similar FTIR spectra for the pig manure BC with bands 1417 cm^{-1} representing the C=C aromatic stretching.

Qian et al. (2013) have reported that the peaks around 1375 cm^{-1} , corresponding to the O-H bending of phenols, were found in chars derived from red cedar and sorghum. This study found sharp peaks in the 1300-1400 cm^{-1} range, corresponding to phenol O-H bending, in all the BC samples. Similar FTIR spectra were reported by Song et al. (2019) for the rice straw BC with broad bands of 1088.3 cm^{-1} representing the C-O stretching. The peaks in the 1080-1300 cm^{-1} range, corresponding to C-O stretching C-O-C groups and aryl ethers, phenolic C-O associated with lignin, were found in the AE BC sample.

Chen et al. (2017) have reported similar FTIR spectra for tobacco stem BC, with the band in 1057 cm^{-1} representing the C-O-C stretching. Also, in this study, the peaks in the 980-1080 cm^{-1} range, corresponding to C-O-C stretching, were observed in AS and NAE BC samples. Qian et al. (2013) reported that the peaks around 780 cm^{-1} , corresponding to aromatic C-H bending, were clearly visible in red cedar, sorghum, and switchgrass-derived BC. In this study, peaks in the 680-860 cm^{-1} range, corresponding to aromatic C-H bending, were found in the AE BC sample.

More peaks were observed in activated BC samples than in nonactivated BC samples. These peaks represented functions that involve the adsorption mechanisms. These functional groups in activated BC attributed higher water treatment efficiencies compared to nonactivated BC samples. Most peaks could be observed in the AE sample compared with AS, NAS, and NAE samples.

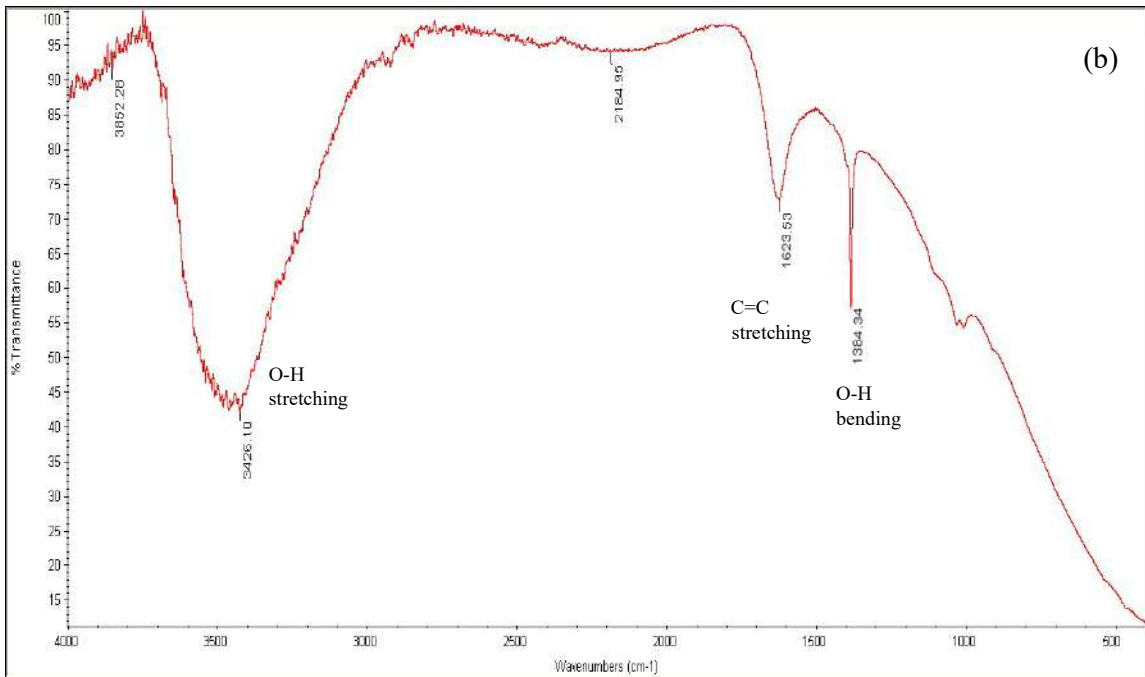
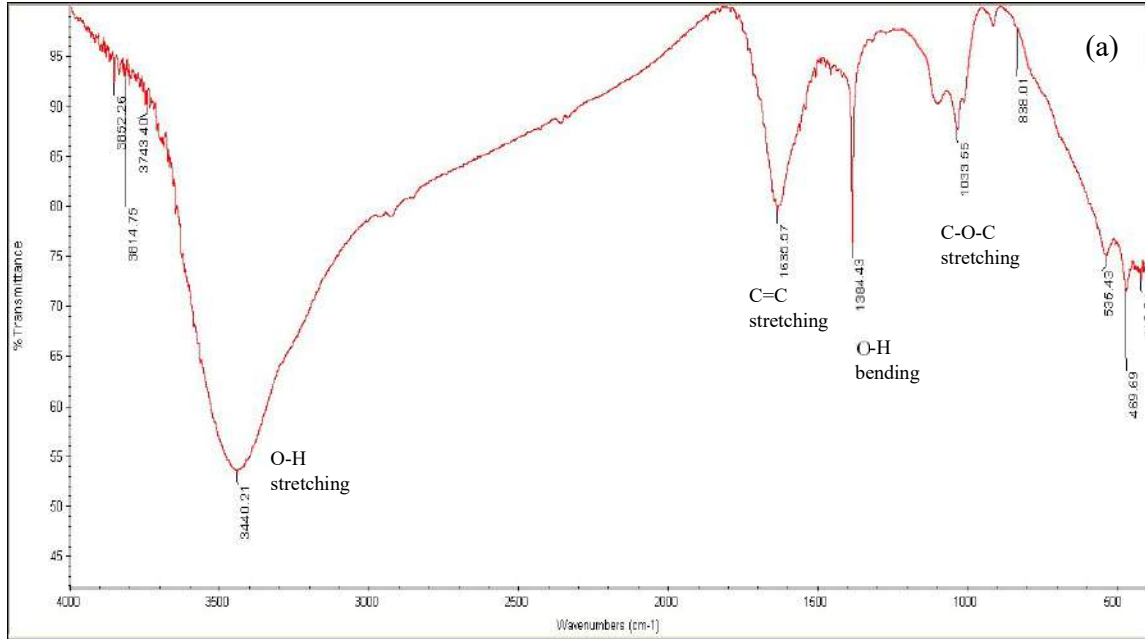
Table 1: Results on percentage biochar production of selected aquatic invasive plants.

Aquatic invasive plant	Initial dry weight before pyrolysis [g]	The weight after pyrolysis [g]	Percentage biochar production
<i>Eichhornia</i> spp.	250.00	88.85	35.54%
<i>Salvinia</i> spp.	250.00	86.76	34.70%

Physical Characterization of Activated and Nonactivated BC

SEM technique was used to observe the surface morphology of nonactivated and activated BC. Fig. 2 shows BC's scanning electron microscope (SEM) images under

(10K ×) magnifications. There are clear differences between the surface morphology of the activated BC samples, and nonactivated BC samples. Cracks, crevices, and some grains of various sizes in large holes appeared on both activated and nonactivated BC samples (Fig. 2). The SEM images of the BC (both activated and nonactivated) revealed a



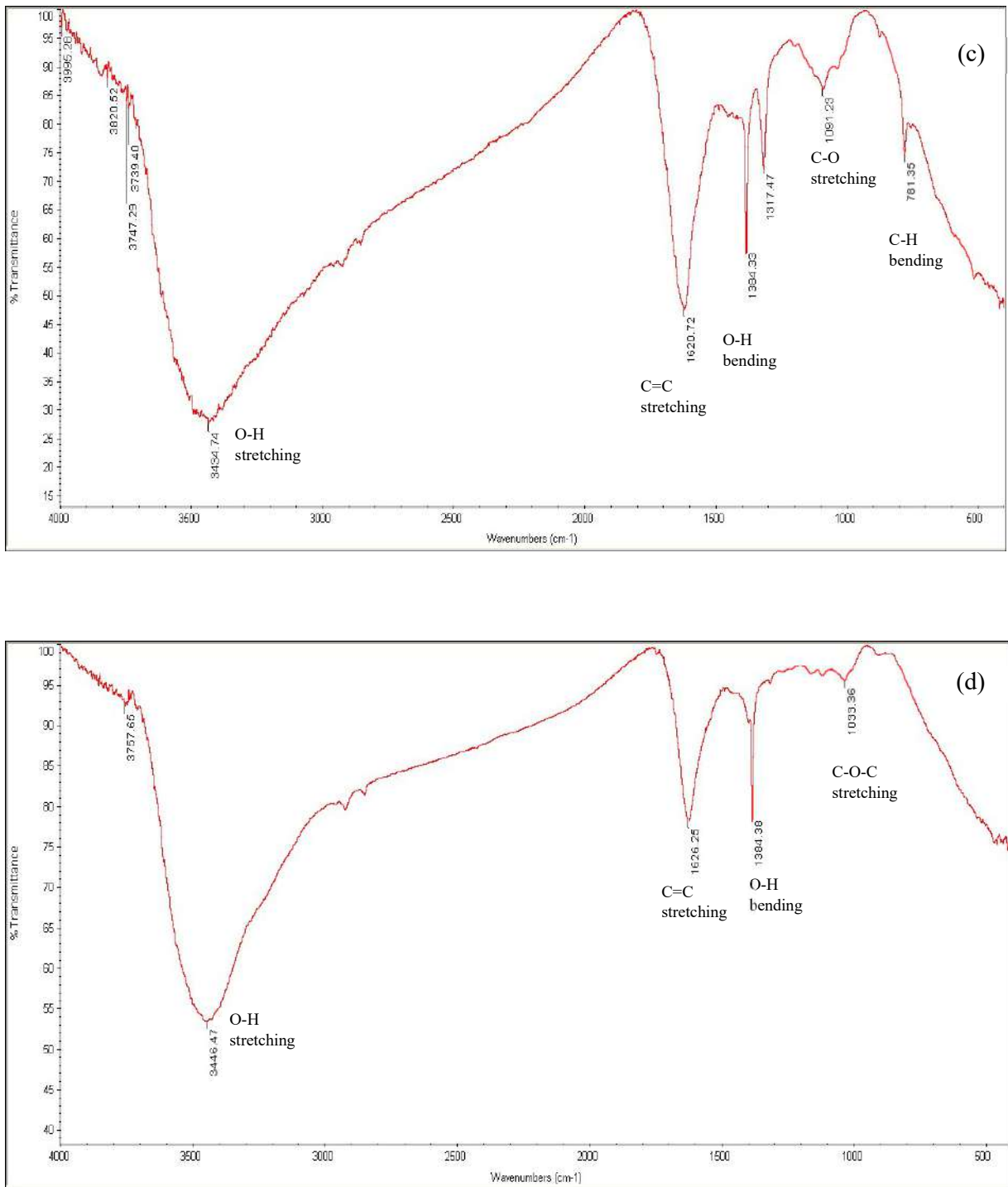


Fig. 1: Fourier-transform infrared spectroscopy (FT-IR) spectra of biochar (a) Activated *Salvinia* spp. (b) Non-activated *Salvinia* spp. (c) Activated *Eichhornia* spp. and (d) Non- Activated *Eichhornia* spp.

random pore structure on the material’s surface and pores that appeared to be distributed all over the BC surface. Pores of various sizes and shapes could be observed. Masto et al.

(2013) have shown that when the biomass is heated under the pyrolysis process, volatile matters are released out of the feedstocks, which make micropores on the surface of BC,

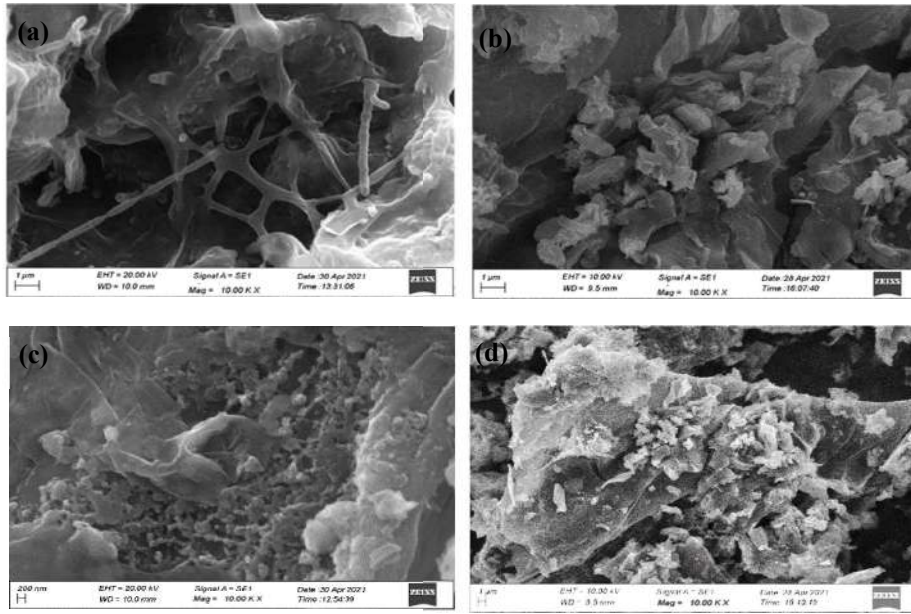
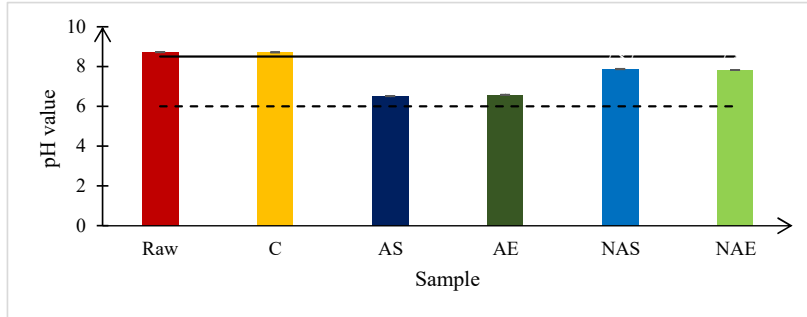


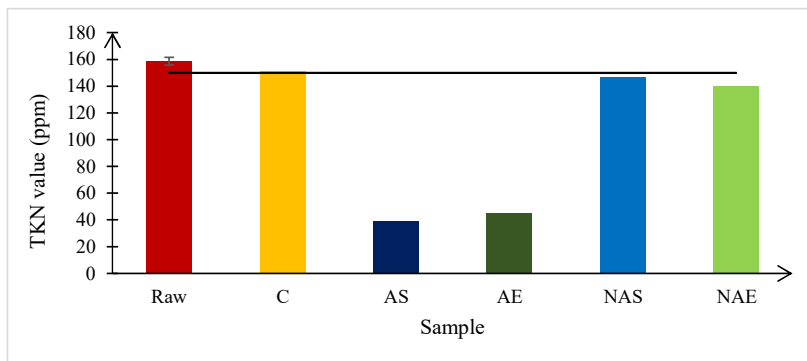
Fig. 2: Scanning electron microscope images of biochar (a) Activated *Salvinia* spp. (10K ×) (b) Nonactivated *Salvinia* spp. (10K ×) (c) Activated *Eichhornia* spp. (10K ×) (d) Non-Activated *Eichhornia* spp. (10K ×).

while the volatiles trapped inside the feedstocks expand the microstructure. Thus, the resulting BC has with high surface area and porosity. These two properties are particularly

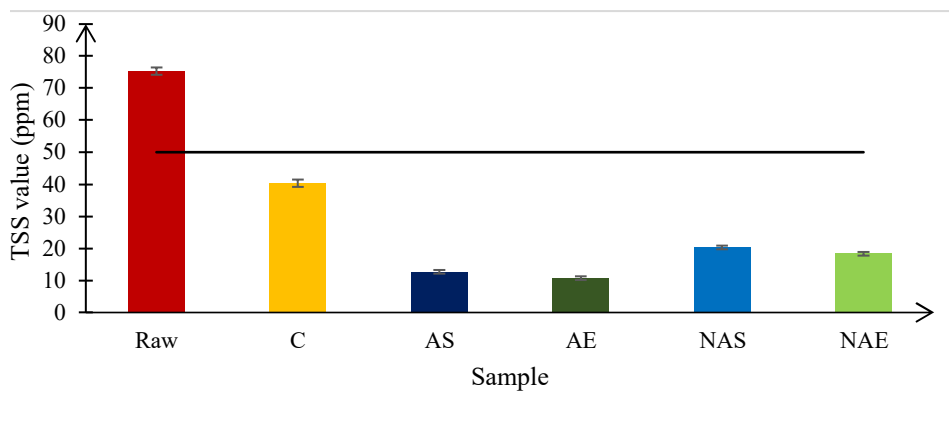
useful for increasing the water holding capacity and are also reasoned for enhancing adsorption mechanisms and capacity by providing huge surface areas (Enaime et al. 2020).



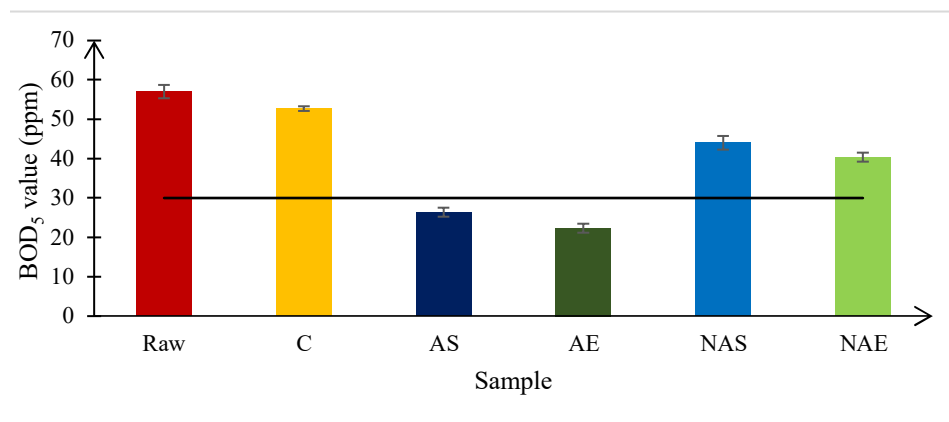
(a)



(b)



(c)



(d)

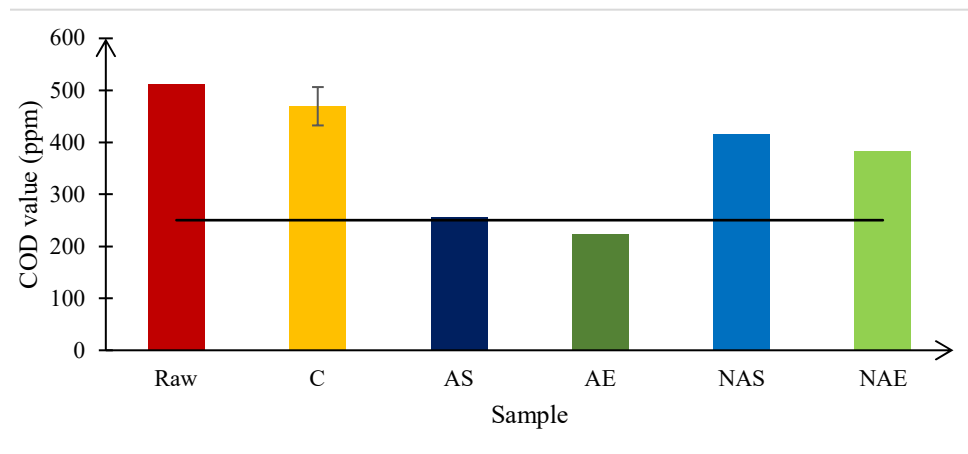
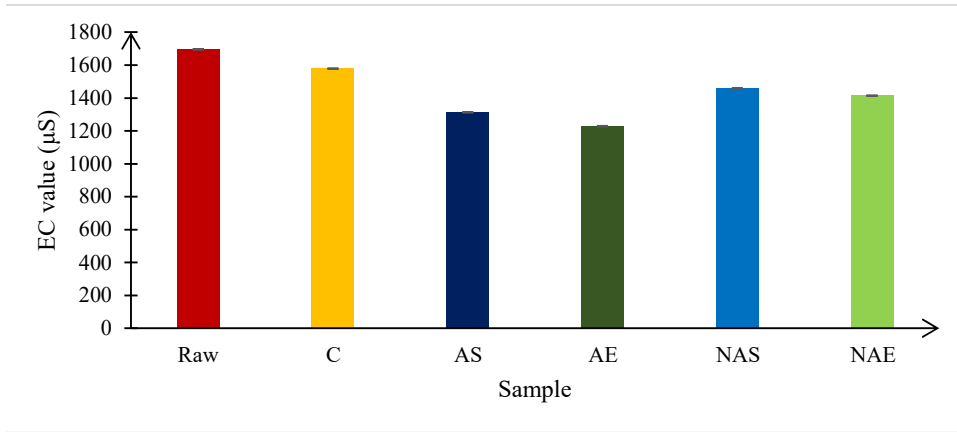
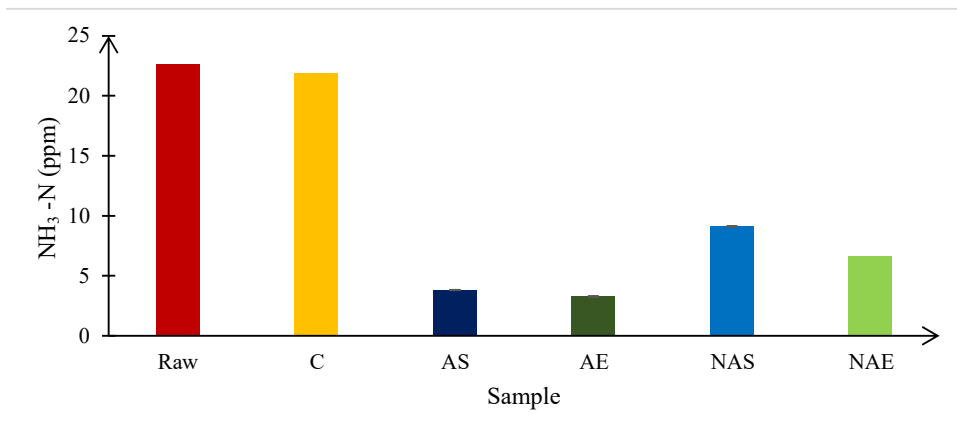


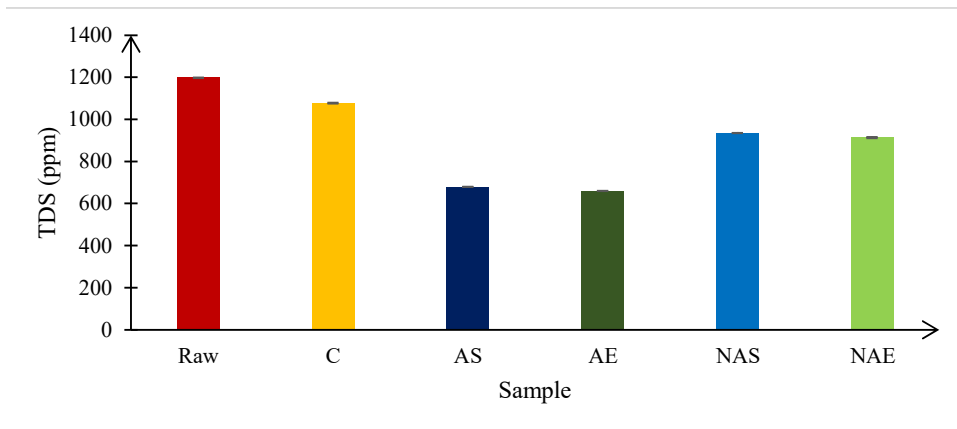
Figure Cont...



(f)

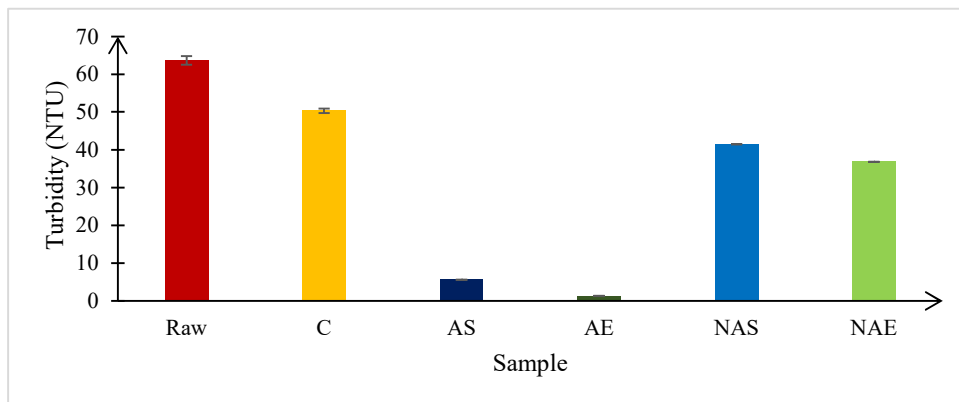


(g)

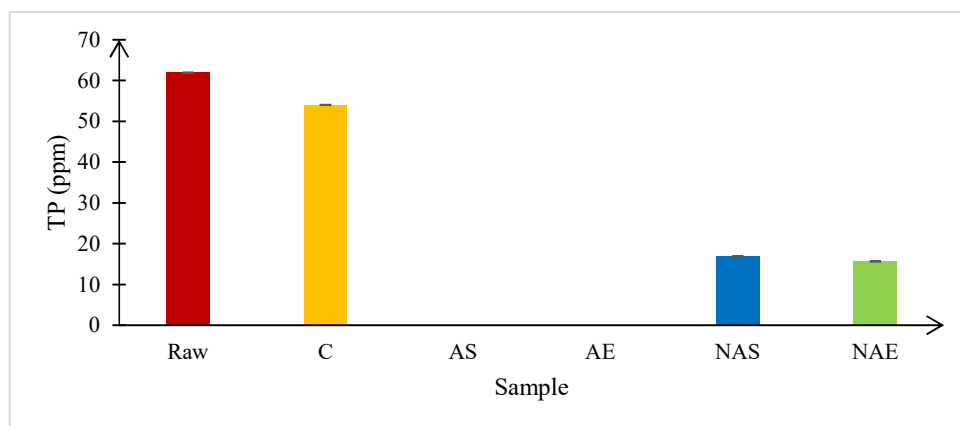


(h)

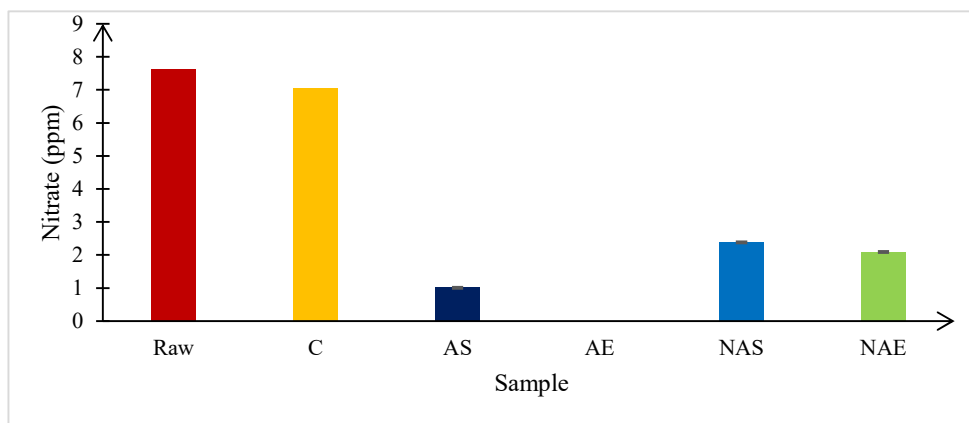
Figure Cont...



(i)

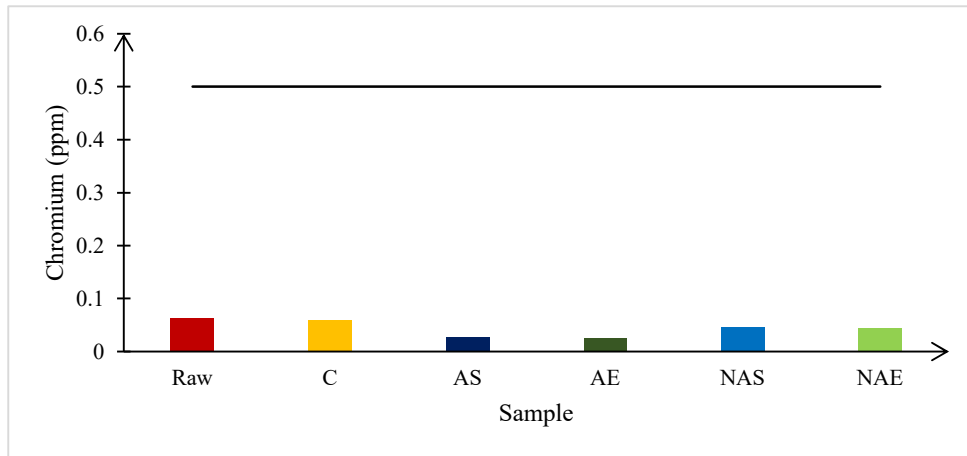


(j)

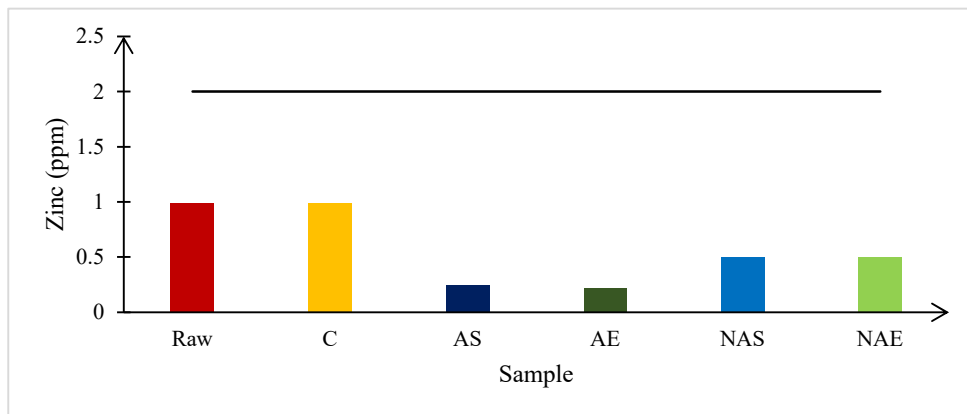


(k)

Figure Cont....



(l)



(m)

----- Minimum BOI standard value ——— Maximum BOI standard value

Fig. 3: Readings of measured water quality parameters of raw sample and treated samples (a) pH (b) Total Kjeldahl Nitrogen (TKN) (c) Total Suspended Solids (TSS) (d) Biological Oxygen Demand (BOD₅) (e) Chemical Oxygen Demand (COD) (f) Electrical Conductivity (EC) (g) Ammoniacal Nitrogen (NH₃-N) (h) Total Dissolved Solids (TDS) (i) Turbidity (j) Total Phosphates (TP) (k) Nitrate (l) Chromium (m) Zinc.

Water Quality Parameters of Treated and Non-Treated Water

The present study forwards a BC-incorporated laboratory sand filter as a treatment option for wastewater. The filter unit was developed using fine, coarse sand, gravel layers, and BC layers (activated and nonactivated BC). The BC layer was placed in between fine and coarse sand layers. The raw water was passed through different filter units to select the best filter media for the effective treatment process. In addition, the control setup was developed incorporating only sand and gravel layers, excluding any form of BC. The measured

water quality parameters before and after treatment through control setup activated BC and nonactivated BC filter units are presented in Fig. 3.

The raw water had a higher pH value (8.72 ± 0.01) than the neutral pH (pH = 7). The recorded pH value of raw water exceeded the national recommended water quality criteria (6.0-8.5). The pH values observed in the treated water obtained from activated and nonactivated BC-containing filter units were close to the neutral pH.

The two traditionally most common oxygen demand measures are the BOD and the COD. The BOD determines

the biodegradable fraction in the wastewater, and the COD measures both the biodegradable and non-biodegradable organic content by oxidizing them in acidic conditions. Previous studies have demonstrated that large specific surfaces and high porosity of BC provide better absorption capacity, which is reasoned for the greater reduction of organic matter than sand. After the initial period dominated by physical and chemical filtration processes, biological activities gradually take over due to the development of a biofilm in BC (Rolland et al. 2009).

In this study, BOD_5 values of raw water (57 ± 1.73) and raw water treated with nonactivated BC samples (37-44 ppm) and control setup (52.67 ± 0.58) exceeded the national recommended water quality criteria. However, BOD_5 values of raw water treated with activated BC samples (14-24 ppm) were lower than the national recommended water quality criteria (30 ppm).

The organic matter removal efficiency is also measured as COD throughout the experiment. Gwenzi et al. (2017) have reported that BC produced from biomaterials has a favorable removal ability for organic contaminants that cause COD. In general, pore-filling, hydrophobic effect, electrostatic interaction, and π - π bond interactions are the main mechanisms of organic contaminants sorption by BC (Gupta et al. 2016; Wang et al. 2020). Pore-filling is an important mechanism for the sorption of organic contaminants in BC. The sorption capacity is directly related to the micropores' surface area (Han et al. 2013). The SEM images of all BC samples have a porous structure, which is one reason for the reduction of COD values in this study. In this study, both activated and nonactivated BC samples have C=C aromatic stretching at 1400 - 1660 cm^{-1} . It represents BC's π - π bond interactions and is reasoned for proper COD removal compared with raw water.

The COD value of water obtained from the AE filter unit (224 ppm) was close to the national recommended water quality criteria (250 ppm). The COD value of water treated with AS filter (256 ppm) exceeded the national recommended water quality criteria. COD values (320-416 ppm) of water obtained from nonactivated filter units were more significant than the national recommended water quality criteria.

The recorded TKN value (158.67 ± 2.89 ppm) in the raw water sample also exceeded the national recommended water quality criteria (150 ppm). However, TKN values of water treated with activated BC filter units (33-45 ppm) showed a clear difference. However, the TKN values of water treated with nonactivated BC (134-147 ppm) were slightly higher than water treated with activated BC. The TKN values (151 ppm) of water obtained from the control setup did not show rapid reduction compared with raw water. Gupta et al.

(2016) reported that the wastewater TKN showed a 58.3% reduction after passing through the BC-containing filter.

The EC value (1578.33 ± 1.53 μS) of water obtained from the control setup has shown little change when compared with raw water (1694 ± 1.73 μS). EC values in water treated with activated and nonactivated filter units ranged from 1220-1460 μS . The EC variation among filter units was quite low compared to raw water's EC value.

The TDS values of water obtained from activated BC filter units showed a two-fold reduction to raw water (1197.33 ± 1.15 ppm). TDS values of water obtained from nonactivated filter units (870-940 ppm) were lower than raw water. However, EC and TDS values of water obtained from the control setup (1076.67 ± 2.31 ppm) did not show clear variation when compared with raw water. Delavernhe et al. (2018) have reported that functional groups like C-H and C-O-C on the BC surface can potentially interact with TDS-causing pollutants, resulting in enhanced removal (Delavernhe et al. 2018). In this study, C-O-C stretching was observed in AS and NAE samples, which is one of the reasons for removing TDS-causing pollutants in these samples.

This study observed higher turbidity (63.67 ± 1.15 NTU) and TSS (75.33 ± 1.15 ppm) in raw water. The recorded TSS value of raw water exceeded the national recommended water quality criteria (50 ppm). However, turbidity and TSS of water treated with activated BC (8-13 ppm) were reduced than water treated with nonactivated BC samples (15-21 ppm). The possibility of TSS concentration reduction upon using BC as an adsorbent was reported by De Rozari et al. (2016) when sewage was treated using BC as the filter media.

BC is also popular in inorganic contaminants removal, which targets the removal of nutrient elements nitrogen and phosphorus that exist in the form of inorganic ions in wastewater (Wang et al. 2020).

This study recorded a higher TP concentration (61.91 ± 0.06) in raw water. But recorded nitrate concentration (7.62 ppm) of raw water is very low. Also, the recorded ammoniacal nitrogen concentration (22.63 ppm) of raw water was lower than the national recommended water quality criteria (50 ppm). However, there are no national recommended water quality criteria for nitrate and TP to discharge industrial effluents into inland surface waters. A clear difference was not observed in ammoniacal nitrogen (21.9 ppm), TP (54.01 ± 0.06 ppm), and nitrate (7.04 ppm) concentrations of raw water treated with the sand and gravel filter unit.

Lou et al. (2016) have reported that BC's high surface area and oxygen functionality are rarely effective for removing phosphate forms and other anions. TP was not

detected in raw water treated with activated BC. The TP concentration of raw water treated with nonactivated BC samples (NAS = 16.86 ± 0.06 ppm, and NAE = 15.63 ± 0.06 ppm) is low comparatively TP concentration of raw water.

Ajmal et al. (2020) have reported the removal efficiency of phosphate from wastewater by BC before and after magnetic modification. Results showed that magnetic BC's sorption efficiency was twice that of unmodified BC. Also, in this study, activated BC was shown to proper removal contaminants compared with nonactivated BC. Ajmal et al. (2020) have shown that phosphate sorption of activated BC occurs due to simultaneous mechanisms like electrostatic attraction, surface precipitation, and complexation, while the phosphate sorption of nonactivated BC is dependent on electrostatic attraction. SEM images obtained in this study showed the porous structure of BC. These porous structures might be the reason for the precipitation mechanisms.

Also, nitrate was not detected in water treated with activated AE BC. Low nitrate concentration (1.01 ± 0.03 ppm) was recorded in raw water treated with AS BC. The nitrate concentration of raw water treated with nonactivated samples is low comparatively nitrate concentration of raw water (NAS = 2.38 ± 0.03 ppm, and NAE = 2.09 ± 0.03 ppm). Viglašová et al. (2018) have demonstrated that multiple interactions, primarily electrostatic attraction and ionic bonds with exchangeable cations from the BC, are reasoned for the nitrate sorption mechanisms based on the sorption study of nitrate by bamboo BC.

Ammoniacal nitrogen concentration in raw water treated with both activated BC samples (AS = 3.82 ± 0.01 ppm and AE = 3.28 ± 0.01 ppm) and nonactivated BC samples (NAS = 9.11 ± 0.02 ppm, and NAE = 6.66 ppm) has very low concentrations comparatively ammoniacal nitrogen concentration of raw water sample (22.63 ppm). Ammoniacal nitrogen concentrations of raw water treated with activated BC samples have low concentrations compared with raw water treated with nonactivated BC. Xiang et al. (2020) have mentioned that precipitation on the surface of BC is the dominant mechanism for the removal of ammonium. Moreover, previous studies have demonstrated that the BC surface is usually negatively charged due to the dissociation of oxygen-containing functional groups like carboxylic, hydroxyl, phenolic(hydroxyl), and carbonyl, which causes electrostatic attraction between BC and positively charged molecules (Ahmad et al. 2014; Qambrani et al. 2017). In this study, FT-IR spectra showed oxygen-containing functional groups like hydroxyl and phenolic in all activated and nonactivated BC samples. These electrostatic interactions due to oxygen-containing functional groups might be involved as a mechanism for ammoniacal nitrogen removal.

BC has been suggested to be used for heavy metal removal from contaminated water. Wang et al. (2020) have shown that removal mechanisms of heavy metals vary depending on the valence state of the target metal at different solution pH. In this study, raw water's concentration of Zinc (Zn) and Chromium (Cr) was high. Lead (Pb) and Copper (Cu) were not recorded in raw water and also treated water because their concentrations were smaller than the minimum detection level (Pb = 0.01 ppm, Cu = 0.01 ppm). These minimum detection level values are even lower than the national recommended water quality criteria values. There is no clear variation in Zinc concentration (0.9867 ppm) of treated water obtained from the control setup compared with raw water samples (0.9886 ppm). Also, there is no clear variation in chromium (0.0585 ppm) concentration of treated water obtained from the control setup compared with raw water samples (0.0625 ppm).

However, after the BC treatment, the initial concentration was decreased in treated water samples of all filter units compared with the raw water sample. This means BC is a suitable material for the sorption of Zinc and Chromium in wastewater. Previous studies have demonstrated that mainly four mechanisms are involved in removing heavy metals from water by BC. Electrostatic attraction between heavy metals and BC surface, ion exchange between heavy metals and alkali or alkaline earth metals or protons on BC surface, complexation with π electron-rich domain or surface functional groups, and co-precipitation to form insoluble compounds (Qian et al. 2015; Tan et al. 2015; Li et al. 2017). Precipitation and electrostatic interactions have been commonly cited as one of the main mechanisms responsible for the immobilization of heavy metals by BC sorbents due to their highest porous structure. According to the FTIR results in this study, all FTIR spectra have shown a peak at $1400\text{-}1660\text{ cm}^{-1}$ range representing the C=C stretching. According to previous studies, it might be a reason for the removal of heavy metals. Pan et al. (2013) reported that the abundance of functional groups in several crop straws BC has been reasoned for the Cr (III) sorption. Previous studies have demonstrated that the Zn (II) sorption mechanism by the BC derived from apple tree branch samples includes surface precipitation, ion exchange, and minor contribution by cation- π interaction (Zhao et al. 2020).

Results of Statistical Analysis

The findings showed no significant difference in pH ($P = 0.708$) between water treated with the control setup and the raw water sample. Significant differences were observed ($P < 0.05$) between the rest of the water quality parameters in the raw water sample and water treated with the control

setup. Moreover, significant differences were also obtained for the water quality parameters ($P < 0.05$) analyzed using one-way ANOVA between the raw water sample and the BC-incorporated filter units (AS, AE, NAS, and NAE). The Turkey HSD, multiple comparison test shows that AE BC is the most effective filter medium for the treatment process.

According to the P values obtained during the statistical analysis, it is clear that treatment of raw water has taken place in all the filter units since during the treatment processes of BC incorporating filter units, all the measured water quality parameters have changed and, in the sand and gravel containing filter treatment process, except for the pH value rest of the parameters have changed. However, most of the measured water quality parameters in the sample treated with sand and gravel were closer to the values of the raw water sample. Interestingly, activated and nonactivated BC-containing sand and gravel filter units (AS, AE, NAS, and NAE) showed higher efficiency than those containing only sand and gravel. Kaetzl et al. (2018) have also shown that over the entire experiment, the removal efficiency of the gravel filter is comparatively low or equal compared with used treated water from BC.

Brine Shrimp Lethality Assay

Brine shrimp was applied as an indicator to assess the toxicity of the final treated water and raw water. Fig. 4 represents the brine shrimp mortalities during the toxicity assay of treated water samples obtained from the filter units composed of sand and gravel, activated and nonactivated BC.

In the brine shrimp toxicity assay, 100% mortality recorded in the non-treated raw water may indicate that the raw water contains higher amounts of chemicals. The treatment with the control setup does not significantly reduce

the toxicity of the water as the sand and gravel were incapable of removing chemicals in the water. In the nonactivated BC-containing filter units, the mortality was lower than the water obtained from the control setup indicating that some amounts of chemicals might be removed through the process. The samples, including nonactivated BC, NAS, and NAE, showed mortalities of 70% and 60%, respectively. There were no mortalities recorded in water samples treated through activated BC. This might be due to the efficient adsorbent of chemicals and toxic substances to the surface layers of the activated BC. Interestingly, Kaetzl et al. (2018) have shown that BC can remove organic and inorganic substances that are caused by the toxicity of wastewater due to the high adsorption capacity.

Among the BC-incorporating filter units, the AE filter unit was given comparatively better water quality parameters than AS, NAE, and NAS units. This was also proved during the Tukey HSD multiple comparison test. Activated BC produced from *Eichhornia* spp. is the most potential adsorbent for industrial wastewater treatment. As a result, the current study has proposed a sustainable strategy for managing invasive aquatic plants and an efficient BC-based filter method to treat industrial wastewater.

CONCLUSION

The low cost of feedstock and physio-chemical properties of biochar (BC) make its application more feasible for wastewater treatment. Porosity, surface area, and functional groups are involved in the adsorption process. Tested activated BC filters suggest that they should have a higher capacity for treating wastewater than nonactivated BC filters, especially activated *Eichhornia* spp. Filter unit. Hence, activated BC is expected to be a highly suitable

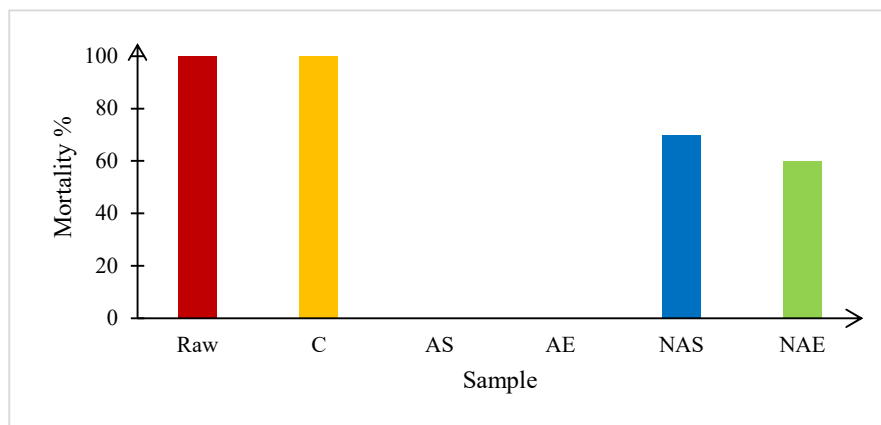


Fig. 4: Mortality of brine shrimp of raw water and treated water samples.

and sustainable material for the improvement of pH, Total Suspended Solids (TSS), Biological Oxygen Demand (BOD₅), Chemical Oxygen Demand (COD), Total Kjeldahl Nitrogen (TKN), ammoniacal nitrogen (NH₃-N), Electrical Conductivity (EC), Total Dissolved Solids (TDS), turbidity, Total Phosphates (TP), nitrate, and heavy metals (Zinc and Chromium). There is no apparent difference between the control setup and the raw water. In conclusion, BC, produced using *Eichhornia* spp., is a promising adsorbent for industrial wastewater treatment. Hence, the present study has forwarded an effective BC-based filter method to treat industrial wastewater and a tangible solution for controlling aquatic invasive plants.

ACKNOWLEDGEMENTS

Instrumental Center at the University of Sri Jayewardenepura would be acknowledged for providing the sample analysis facilities for FTIR, and the Department of Material Science and Engineering at the University of Moratuwa would be acknowledged for providing the sample analysis facilities for SEM.

REFERENCES

- Agrafioti, E., Bouras, G., Kalderis, D. and Diamadopoulos, E. 2013. Biochar production by sewage sludge pyrolysis. *J. Anal. Appl. Pyrolysis*, 101: 72-78.
- Ahmad, M., Rajapaksha, A.U., Lim, J.E., Zhang, M., Bolan, N., Mohan, D., Vithanage, M., Lee, S.S. and Ok, Y.S. 2014. Biochar as a sorbent for contaminant management in soil and water: A review. *Chemosphere*, 99: 19-33.
- Ajmal, Z., Muhmood, A., Dong, R. and Wu, S. 2020. Probing the efficiency of magnetically modified biomass-derived biochar for effective phosphate removal. *J. Environ. Manage.*, 253: 109730.
- AOAC. 2000. Official Methods of Analysis of AOAC International. Seventeenth Edition. AOAC Int., Gaithersburg, MD, USA.
- APHA. 2017. Standard Methods for the Examination of Water and Wastewater. Twenty-Third Edition. American Public Health Association, Washington.
- Chen, R., Li, L., Liu, Z., Lu, M., Wang, C., Li, H., Ma, W. and Wang, S. 2017. Preparation and characterization of activated carbons from tobacco stem by chemical activation. *J. Air Waste Manag. Assoc.*, 67(6): 713-724.
- De Rozari, P., Greenway, M. and El Hanandeh, A. 2016. Phosphorus removal from secondary sewage and septage using sand media amended with biochar in constructed wetland mesocosms. *Sci. Total Environ.*, 569: 123-133.
- Delavernhe, L., Pilavtepe, M. and Emmerich, K. 2018. Cation exchange capacity of natural and synthetic hectorite. *Appl. Clay Sci.*, 151: 175-180.
- Enaime, G., Bacaoui, A., Yaacoubi, A. and Lübken, M. 2020. Biochar for wastewater treatment—conversion technologies and applications. *Appl. Sci.*, 10(10): 3492.
- Feng, Q., Wang, B., Chen, M., Wu, P., Lee, X. and Xing, Y. 2021. Invasive plants as potential sustainable feedstocks for biochar production and multiple applications: A review. *Resour. Conserv. Recycl.*, 164: 105204.
- Gupta, P., Ann, T.W. and Lee, S.M. 2016. Use of biochar to enhance constructed wetland performance in wastewater reclamation. *Environ. Eng. Res.*, 21(1): 36-44.
- Gwenzi, W., Chaukura, N., Noubactep, C. and Mukome, F.N. 2017. Biochar-based water treatment systems as a potential low-cost and sustainable technology for clean water provision. *J. Environ. Manage.*, 197: 732-749.
- Han, Y., Boateng, A.A., Qi, P.X., Lima, I.M. and Chang, J. 2013. Heavy metal and phenol adsorptive properties of biochars from pyrolyzed switchgrass and woody biomass in correlation with surface properties. *J. Environ. Manage.*, 118: 196-204.
- Havel, J.E., Kovalenko, K.E., Thomaz, S.M., Amalfitano, S. and Kats, L.B. 2015. Aquatic invasive species: Challenges for the future. *Hydrobiologia*, 750(1): 147-170.
- Inyang, M.I., Gao, B., Yao, Y., Xue, Y., Zimmerman, A., Mosa, A., Pullammanappallil, P., Ok, Y.S. and Cao, X. 2016. A review of biochar as a low-cost adsorbent for aqueous heavy metal removal. *Crit. Rev. Environ. Sci. Technol.*, 46(4): 406-433.
- Kaetzl, K., Lübken, M., Gehring, T. and Wichern, M. 2018. Efficient, low-cost anaerobic treatment of wastewater using biochar and woodchip filters. *Water*, 10(7): 818.
- Leuven, R.S., Boggero, A., Bakker, E.S., Elgin, A.K. and Verreycken, H. 2017. Invasive species in inland waters: From early detection to innovative management approaches. *Aquatic Invasions*, 12: 269-273.
- Li, H., Dong, X., da Silva, E.B., de Oliveira, L.M., Chen, Y. and Ma, L.Q. 2017. Mechanisms of metal sorption by biochars: Biochar characteristics and modifications. *Chemosphere*, 178: 466-478.
- Lou, K., Rajapaksha, A.U., Ok, Y.S. and Chang, S.X. 2016. Pyrolysis temperature and steam activation effects on sorption of phosphate on pine sawdust biochars in aqueous solutions. *Chem. Speciation Bioavailability*, 28(1-4): 42-50.
- Massoudinejad, M., Mehdipour-Rabori, M. and Hadi Dehghani, M. 2015. Treatment of natural rubber industry wastewater through a combination of physicochemical and ozonation processes. *J. Adv. Environ. Health Res.*, 3(4): 242-249.
- Masto, R.E., Kumar, S., Rout, T.K., Sarkar, P., George, J. and Ram, L.C. 2013. Biochar from water hyacinth (*eichornia crassipes*) and its impact on soil biological activity. *Catena*, 111: 64-71.
- Meyer, S., Glaser, B. and Quicker, P. 2011. Technical, economical, and climate-related aspects of biochar production technologies: A literature review. *Environ. Sci. Technol.*, 45(22): 9473-9483.
- Mohan, D., Sarswat, A., Ok, Y.S. and Pittman Jr, C.U. 2014. Organic and inorganic contaminants removal from water with biochar, a renewable, low cost, and sustainable adsorbent: A critical review. *Bioresour. Technol.*, 160: 191-202.
- Olowa, L.F. and Nuneza, O.M. 2013. Brine shrimp lethality assay of the ethanolic extracts of three selected species of medicinal plants from Iligan City, Philippines. *Int. Res. J. Biol. Sci.*, 2(11): 74-77.
- Pan, J., Jiang, J. and Xu, R. 2013. Adsorption of Cr (III) From acidic solutions by crop straw-derived biochars. *J. Environ. Sci.*, 25(10): 1957-1965.
- Perez-Mercado, L.F., Lalander, C., Berger, C. and Dalahmeh, S.S. 2018. Potential of biochar filters for onsite wastewater treatment: effects of biochar type, physical properties, and operating conditions. *Water*, 10(12): 1835.
- Qambrani, N.A., Rahman, M.M., Won, S., Shim, S. and Ra, C. 2017. Biochar properties and eco-friendly applications for climate change mitigation, waste management, and wastewater treatment: A review. *Renew. Sustainable Energy Rev.*, 79: 255-273.
- Qian, K., Kumar, A., Patil, K., Bellmer, D., Wang, D., Yuan, W. and Huhnke, R.L. 2013. Effects of biomass feedstocks and gasification conditions on the physicochemical properties of char. *Energies*, 6(8): 3972-3986.
- Qian, K., Kumar, A., Zhang, H., Bellmer, D. and Huhnke, R. 2015. Recent advances in the utilization of biochar. *Renew. Sustain. Energy Rev.*, 42: 1055-1064.

- Rolland, L., Molle, P., Liénard, A., Bouteldja, F. and Grasmick, A. 2009. Influence of the physical and mechanical characteristics of sands on the hydraulic and biological behaviors of sand filters. *Desalination*, 248(1-3): 998-1007.
- Song, H., Wang, J., Garg, A., Lin, X., Zheng, Q. and Sharma, S. 2019. The potential of novel biochars produced from invasive aquatic species outside food chain in removing ammonium nitrogen: Comparison with conventional biochars and clinoptilolite. *Sustainability*, 11(24): 7136.
- Stiers, I., Crohain, N., Josens, G. and Triest, L. 2011. Impact of three aquatic invasive species on native plants and macroinvertebrates in temperate ponds. *Biol. Invasions*, 13(12): 2715-2726.
- Tan, X., Liu, Y., Zeng, G., Wang, X., Hu, X., Gu, Y. and Yang, Z. 2015. Application of biochar for the removal of pollutants from aqueous solutions. *Chemosphere*, 125: 70-85.
- Viglašová, E., Galamboš, M., Danková, Z., Krivosudský, L., Lengauer, C.L., Hood-Nowotny, R., Soja, G., Rompel, A., Matík, M. and Briančin, J. 2018. Production, characterization, and adsorption studies of bamboo-based biochar/montmorillonite composite for nitrate removal. *Waste Manage.*, 79: 385-394.
- Wang, X., Guo, Z., Hu, Z. and Zhang, J. 2020. Recent advances in biochar application for water and wastewater treatment: A review. *PeerJ*, 8: e9164.
- Xiang, W., Zhang, X., Chen, J., Zou, W., He, F., Hu, X., Tsang, D.C., Ok, Y.S. and Gao, B. 2020. Biochar technology in wastewater treatment: A critical review. *Chemosphere*, 252: 126539.
- Zhang, X., Wang, H., He, L., Lu, K., Sarmah, A., Li, J., Bolan, N.S., Pei, J. and Huang, H. 2013. Using biochar for remediation of soils contaminated with heavy metals and organic pollutants. *Environ. Sci. Pollut. Res.*, 20(12): 8472-8483.
- Zhao, J., Shen, X.J., Domene, X., Alcañiz, J.M., Liao, X. and Palet, C. 2019. Comparison of biochars derived from different types of feedstock and their potential for heavy metal removal in multiple-metal solutions. *Sci. Rep.*, 9(1): 1-12.
- Zhao, S., Ta, N. and Wang, X. 2020. Absorption of Cu (II) and Zn (II) from aqueous solutions onto biochars derived from apple tree branches. *Energies*, 13(13): 3498.
- Zimmerman, A.R., Gao, B. and Ahn, M.Y. 2011. Positive and negative carbon mineralization priming effects among a variety of biochar-amended soils. *Soil Biol. Biochem.*, 43(6): 1169-1179.



Evaluation of an Electrocoagulation Process Modified by Fenton Reagent

M. A. López-Ramírez†^(**) , O. P. Castellanos-Onorio^{***} , F. Lango-Reynoso^{**} , M. del R. Castañeda-Chávez^{**} , J. Montoya-Mendoza^{**} , M. Díaz-González^{***}  and B. Ortiz-Muñiz^{**} 

*Tecnológico Nacional de México/Instituto Tecnológico Superior de Martínez de la Torre. Camino a Cartago, S/N, 93610, Col. Vega Redonda, Martínez de la Torre, Veracruz, México

**Tecnológico Nacional de México/Instituto Tecnológico de Boca del Río, Veracruz-Córdoba 12, 94290 Boca del Río, Veracruz, México

***Tecnológico Nacional de México/Instituto Tecnológico de Veracruz. Av. Miguel Angel de Quevedo 2779, Formando Hogar, 91897 Veracruz, Veracruz, México

†Corresponding author: M. A. López-Ramírez; miguel.lr@martineztorre.tecnm.mx

Nat. Env. & Poll. Tech.
Website: www.neptjournal.com

Received: 30-10-2023

Revised: 08-12-2023

Accepted: 19-12-2023

Key Words:

Electrocoagulation process

Treatment

Fenton reagent

Electrocoagulation

Advanced oxidation

ABSTRACT

This article is oriented to the degradation of nickel in an ionic state at laboratory level from synthetic water made with nickel sulfate, using the electrocoagulation process with aluminum cathodes and modifying this process by the addition of the Fenton reagent, which results from the combination of hydrogen peroxide (H_2O_2) and ferrous sulfate ($FeSO_4$) being this reagent a catalyst and oxo-coagulant agent. The efficiency of this reagent will be compared with the typical treatment with aluminum sulfate, which is a typical process based on ion exchange/coagulation at the same percentage concentrations as the Fenton reagent. For this purpose, the optimum conditions of the advanced electrocoagulation process were determined, which consisted of determining the concentrations of Fenton's reagent at concentrations of 150 ppm, 300 ppm, and 450 ppm, in addition to the operating variables such as pH of 8 and 10, voltage of 17.5 V and 19 V and their reaction time, which were compared with aluminum sulfate at 300 ppm, 600 ppm, and 900 ppm. The results obtained with respect to the typical treatment were 0% nickel degradation. However, with the advanced oxidation treatment, an average reduction of 97.5% was found at the conditions of 19 V, pH 10, and Fenton 150 ppm in a time of 30 min.

INTRODUCTION

Water is an essential element for the life of all living beings on the planet, and it is also a fundamental human right (Rickert et al. 2016). 97.2% of the water on planet Earth is saline, and only 2.5% corresponds to fresh water; of that 2.5%, 30% is a subway, 68% is in glaciers and other snow layers, and only 1.2% is superficial and found in rivers, lakes and other forms of surface water (Gómez-Duarte 2018), so taking care of it is vital for human development.

Water pollution is a problem that all of us face nowadays since it not only occurs in industrialized or less industrialized countries, but it affects every sector of the population. In addition, many think that this resource that is very indispensable for us will always be there, but the truth is that it is not so since we do not become aware of the acts or activities that we perform with this resource (Guadarrama-Tejas et al. 2016).

Among the main factors that affect ecosystems are heavy metals (HM), which are found in human activities where

mining and smelting operations stand out as the majority among other industrial and urban activities (Malik & Saha 2003), where the water pollution rate can be around 200 million cubic meters per day (Lehmann et al. 1999). This fact leads to a large number of problems both in plant life as these metals end up deposited in soils transported to them by rivers, such as reduced growth or yellowing of leaves (chlorosis) (Kalavathy et al. 2010), as well as in human life where the effects can be skin rashes, stomach upset and ulcers, respiratory problems, weakening of the immune system, kidney and liver damage, lung cancer, heart, bone, testicular, central and peripheral nervous system disorders, cancer or death (Ahmad et al. 2010, Tiemi-Muranaka 2010, Ramírez-Franco et al. 2013).

This growing problem calls for rigorous pollution control and increasingly demanding legislation. In response to this, and given the inability of conventional methods to effectively remove many of the existing pollutants, in recent years, there has been an intense search for new and efficient water treatment technologies (López-Ramírez et al. 2021).

In the last decades, advanced oxidation technologies have been consolidated as an efficient alternative in the destruction of toxic substances, including organic, inorganic, metals, or pathogens. In general, in water treatment, advanced oxidation technologies are used when contaminated effluents have high chemical stability or low biodegradability (López-Ramírez et al. 2021).

Currently, studies are focused on the search for optimum values for the different parameters that affect the oxidation process: pH, temperature, reactor design, nature, and concentration of the pollutant and oxidizing agents that can improve the reaction. In addition, the reaction kinetics, which are generally first order, are studied in detail, among which those shown in Fig.1 stand out:

Among the processes mentioned in Fig. 1, it is observed that heterogeneous processes, with electrical energy, using as central the use of current, is the electro-Fenton, which is a process that is divided into electrochemical oxidation and electrocoagulation that applies the principles of coagulation-flocculation in an electrolytic reactor. This is a vessel equipped with a current source and several electrodes in charge of providing the destabilizing ions of

colloidal particles that replace the functions of the chemical compounds used in conventional treatment, inducing an electric current in the water through metal plates (Caviedes-Rubio et al. 2015).

This electrochemical process has been used for the removal of HM without modification and has obtained remarkable results, which are mentioned in Table 1:

As can be seen, this technique is used for the treatment of wastewater contaminated by HM, mostly from the metallurgical or automotive industries. Since conventional treatments are not very efficient, new technologies must be developed (Alomá-Vicente et al. 2013).

HM is found naturally in the environment, usually in trace amounts. These concentrations are not very harmful to biota in general. Because they are deposited in soils by the decomposition of different minerals (erosion process), they coexist to maintain biogeochemical cycles in both soil and water. However, there is also an anthropogenic enrichment of HM (due to mining, industrial, and agricultural activities, among others), and this process that saturates the natural balance is known as contamination since such concentrations are higher than the geochemical composition of the place.

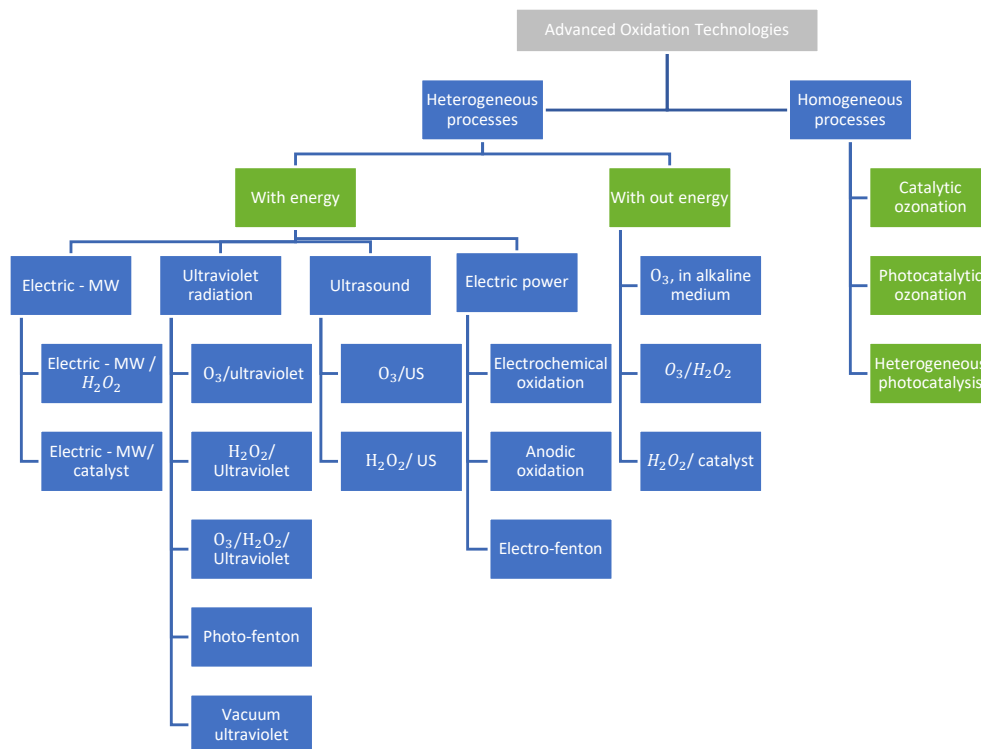


Fig. 1: Classification of advanced oxidation technologies. (Source: Sanz et al. 2013)

Table 1: State of the art of electrochemical processes.

Authors	Year	Results
Abdel-Shafy et al.	2022	They designed an experimental sequence whose purpose was to reduce the amount of Ni, Cu, and Zn in electroplating industry waters.
El-Karamany et al.	2021	Chromium and cadmium solutions from stock concentrations of 560 mg L ⁻¹ chromium and 800 mg L ⁻¹ cadmium were subjected to electrocoagulation.
Chegeni et al.	2021	They planned to perform electrocoagulation in three circumstances. The removal of cyanide and lead, as well as the set of both synthetic and natural water from a gold processing plant.
Sharma et al.	2019	They determined the efficiency of the electrocoagulation process in the removal of Cr (VI) and Pb from the wastewater of an electroplating plant.
Ilhan et al.	2019	The objective was to remove chromium, copper, zinc, nickel, and chemical oxygen demand (COD) from wastewater from the steel industry.
Brahmi et al.	2019	They used aqueous-phase cadmium electrocoagulation first in artificial wastewater and then in real wastewater.

HM such as lead, cadmium, chromium, zinc, mercury, and others are released into aquatic ecosystems as well as soils mainly due to various anthropogenic activities and pose a serious threat to plants, animals, and even humans due to their persistence, bioaccumulation, non-biodegradable property, and toxicity even at low concentrations (Trivedi & Axe 2000, Ahmed et al. 2013). The fact that these metals are found in various ecosystems is of concern since many living things depend on the proper balance in their feeding or living place. How such metals reach the various ecosystems varies depending on the type of activity carried out by man. For example, chromium is a widely used compound in the industry in areas such as plastic plating, metal electroplating for corrosion resistance, leather tanning and finishing, pigments, and wood preservatives (Mohan et al. 2005), other types of metals such as cadmium are used in industry for the manufacture of nickel-cadmium batteries, anti-corrosion agents and pigments (Hamouz et al. 2016). In the case of mercury, six sources of contamination have been identified, which are atmospheric deposition, erosion, human discharges, agricultural materials, mining, and industrial and combustion discharges, as such in natural groundwater and surface water, the content of this metal is below 0.5 µg.L⁻¹, however, in wastewater discharged near local mineral deposits and other contaminated sites the concentration of mercury is much higher. Lead is also released into the environment due to the mining industry and the burning of fossil fuels. It is involved in the manufacture of batteries, ammunition, metal products, and devices for X-ray protection (Mohammad et al. 2017).

As can be seen, the greatest contribution to water pollution by HM is due to wastewater discharges resulting from various anthropogenic activities, mainly of an industrial nature. The degree of contamination of water sources is increasing every day due to the constant use of these metals in industry, which increases the concentration of these metals in water and, therefore, increases the risk to humans

and other living organisms by increasing the probability of being exposed to these metals (Cañizares-Villanueva 2000), as shown in Fig. 2 (García & Moreno 2002).

For wastewater, the HM found in wastewater are arsenic with a generation of 12 842 t.y⁻¹, cadmium 24 319 t.y⁻¹, chromium 61 290 t.y⁻¹, copper with a total of 40 905 t.y⁻¹, mercury with 498 t.y⁻¹, with respect to nickel 60 710 t.y⁻¹, lead approximately 16 470 t.y⁻¹, selenium a total of 5 904 t.y⁻¹, vanadium in wastewater 676 t.y⁻¹ and of zinc 103 715 t.y⁻¹ (Pabón et al. 2020).

The toxicity of HM depends on their mobility in the environment, which, in turn, depends on their chemical speciation, persistence, and tendency to accumulate or bioaccumulate (Kumar et al. 2012).

Within HM, nickel is one of the metals used for metal alloys, electroplating, batteries, and electronics, being one of the most widely used and causing diseases such as dermatitis, nausea, chronic asthma, cough, and carcinogenic effects.

The above and the need to develop new technologies for the treatment of wastewater contaminated with HM, nickel being the object of study.

MATERIALS AND METHODS

The methodology of the present investigation is experimental and quantitative, as shown in Fig. 3, and is centered on 2 experimental stages, the first with a typical process with aluminum sulfate and the second with the electrocoagulation process adding an oxo-coagulant reagent (Fenton). In both experiments, they will be carried out under optimum conditions, and in the case of the reagents, the same quantities will be added. At the same time, each of the experiments will be carried out in triplicate.

Preparation of Solutions

The solutions at 60 ppm of nickel in 500 mL of distilled water

were prepared with 137 mg of nickel sulfate hexahydrate ($\text{NiSO}_4 + 6\text{H}_2\text{O}$) derived from this chemical compound, which has a purity of 98% and a molecular weight of 263 a.m.u. of which nickel weights 58.69 a.m.u.

The procedure for calculating the nickel sulfate required is shown below, starting by determining the percentage of nickel in the compound as expressed in Equations 1 and 2:

$$\frac{RNS}{N} = \frac{Ni_{a.m.u.}}{SN_{a.m.u.}} * \frac{PurE}{100} \quad \dots(1)$$

RNS/N= Ratio of nickel sulfate and nickel

$Ni_{a.m.u.}$ = Molecular weight of nickel

$SN_{a.m.u.}$ = Molecular weight of nickel sulfate

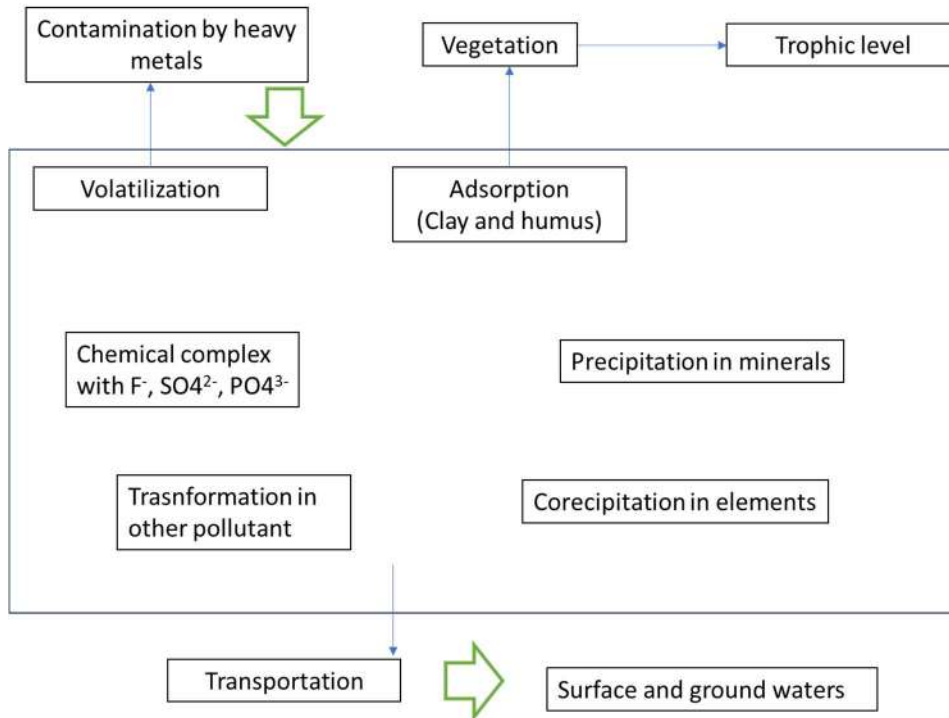


Fig. 2: Dynamics in the heavy metal system. (Source: García et al. 2002)

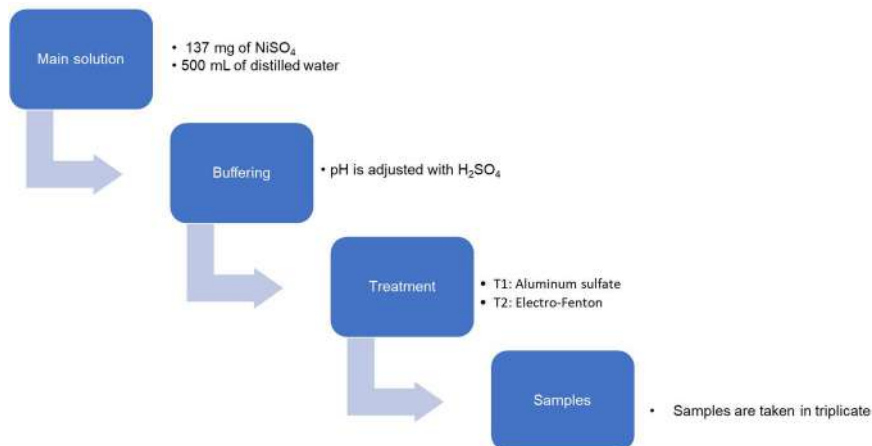


Fig. 3: Process experimentation.

$$\frac{RNS}{N} = \frac{58.69}{263} * \frac{98}{100} = 0.219 \quad \dots(2)$$

Once the ratio of nickel and nickel sulfate is found, we proceed to calculate the necessary amount, remembering that for 500 mL, 30 mg of nickel is needed, so we proceed to calculate the necessary sulfate with equations 3 and 4:

$$Ni = \frac{30 \text{ mg}}{RNS/N} \quad \dots(3)$$

$$Ni = \frac{30 \text{ mg}}{0.219} = 137 \text{ mg} \quad \dots(4)$$

Treatments

Aluminum sulfate treatment: For the titration of aluminum sulfate, the ratios proposed by López-Ramírez et al. (2019) were proposed, which correspond to 30%, 60%, and 90%, which guarantee 3 scenarios, unsaturated, saturated, and supersaturated scenarios, which correspond to 300 ppm, 600 ppm and 900 ppm in 500 mL solutions with an acid pH of 2, 3 and 4 pH.

Electro-Fenton treatment: For the electro-Fenton process, the same methodology of Lopez et al. (2019) is used, which indicates that the Fenton process should be evaluated under the following conditions in Table 2:

According to the electrochemical conditions, Jumpatong (2002) is taken as a reference, which indicates that for electrocoagulation, the following is required (Table 3):

Experimentation and validation of results: For the validation of the data obtained, the Hanna spectrophotometer was used, following the following procedure:

Standard:

1. The low-range nickel method is selected in the spectrophotometer.

Table 2: Fenton reagent concentrations.

Concentration	Compound	Amount	Unit
Fenton 30%	Hierro	75	mg
	Peróxido	0.22	mL
Fenton 60%	Hierro	150	mg
	Peróxido	0.22	mL
Fenton 90%	Hierro	225	mg
	Peróxido	0.22	mL

Table 3: Requirements for electrocoagulation.

Parameter	Compound	Unit
Voltage	17.5 y 19	V
Electrode	Aluminio	-
pH	8 y 10	-

2. A beaker is filled with 25 mL of distilled water, and a packet of reagent A (HI 93740A-0) is added.
3. Add 1 mL of reagent B (HI 93740B-0) and shake to mix.
4. The solution is allowed to stand for 15 min.
5. Reagent C (HI 93740C-0) is added immediately, stirred, and dissolved.
6. The cuvette is filled with 10 mL and this will be the blank, which will be our nickel-free reference value.
7. The cuvette is placed in the cuvette, the hatch is closed, and zero is pressed.
8. At this point, our Hanna equipment is calibrated and ready for samples.

Sample:

1. 1 mL of sample is obtained, and the solution is diluted 1:10, derived that the range of the spectrophotometer covers 0.000 to 1.000 ppm with a minimum resolution of 0.001 ppm, and 2.5 mL of the sample is poured into 22.5 mL of distilled water.
2. A packet of reagent A (HI 93740A-0) is added and shaken until dissolved. It is important to dissolve all the powder since, during the Fenton reaction, Fe3+ is produced, and this element in the ionic state can cause interferences.
3. 1 mL of reagent B (HI 93740B-0) is added, and it is shaken to mix.
4. The solution is allowed to stand for 15 min.
5. Reagent C (HI 93740C-0) is added immediately, stirred, and dissolved.
6. Once dissolved, the cuvette is filled with 10 mL and placed in the Hanna.
7. It is placed in the reader; the hatch is closed, and it is given to read.
8. The reading obtained by our spectrophotometer will be 10 times less than the actual reading, so it should be multiplied by 10. Example: If the Hanna marks a reading of 0.689 ppm, the actual reading will be 6.890 ppm.

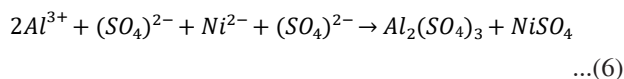
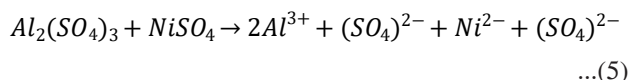
After obtaining the data from the experiments, we proceed to perform the analysis of means by the Tukey method at 95% confidence to have a statistical result that can tell us if there is a difference between the experiments, in addition to the electrocoagulation process, we proceed to perform a full factorial analysis, with 8 runs (24), to visualize the variables that influence the electro-Fenton process, in Minitab 19 (Fig. 4).

Study Area

The present study was carried out in the facilities of the Instituto Tecnológico de Boca del Río since it was conducted with synthetic water and its treatments were at the laboratory level.

RESULTS AND DISCUSSION

The results obtained by the chemical precipitation process are shown in Fig. 5, where we can see that despite varying the concentrations of aluminum sulfate, being this compound is the typical coagulant most used in wastewater treatment processes, its nickel reduction results are null. This is because when aluminum sulfate is dissolved in water, it dissociates and creates the sulfate ion, and with respect to nickel, this only associates with it, creating the nickel sulfate complex, the latter being our reagent for synthetic water. This can be seen in equations 5 and 6, so its use is not suitable in the treatment of water contaminated with nickel.



In the advanced electrocoagulation process, 12 experiments were carried out with a treatment time of 30 min and 60 min. These experiments were carried out in triplicate, and removal averages were obtained as shown in Tables 4 and 5:

According to those interactions, which explain graphically how the variables affect us with respect to the processes, it is observed that for the voltage, the optimum value is 19.0 V; according to the pH, the medium should be found in

10 pH at a concentration of 150 ppm of Fenton reagent and the time with the highest removal for most of the processes is 60 min (Fig. 6 & Fig. 7).

However, it can be observed in Table 4 and Table 5 that in the experiments with voltage 19 V, 10 pH with Fenton concentration of 150 ppm and 300 ppm, in the times of 30 min and 60 min, there is no difference in removal, however, for the validation of this assumption a Tukey test will be performed at 95% with respect to the times, this to determine if the electro-Fenton process.

As shown in Fig. 8 and analyzing both optimum processes, it can be observed that the electrocoagulation process with Fenton at conditions of 150 ppm, 10 pH, and 19 V has no statistically significant change, so we can conclude that, at 30 min of the process, the removal of nickel has reached its maximum removal. There will no longer be a notable advance in this process.

With respect to precipitation with aluminum sulfate, Pinillos 2013 indicates that chemical precipitation, filtration by membranes, electrolytic reduction, extraction by solvents, ion exchange, and adsorption have drawbacks such as low efficiency and applicability, which is demonstrated in this research since the treatment of synthetic water yielded zero efficiency because only ion exchange is present. There is no intermediate process, such as the generation of hydroxyl ions or electrocoagulation.

Rojas-Vargas et al. 2020, obtained similar removal results since these researchers obtained a maximum removal efficiency of 95% in a time of 60 min, and Jumpatong (2002) obtained results close to 98% in a time of 180 min; however, can be observed that this research obtained

Run	C1	C2	C3	C4	C5	C6	C7	C8	C9	C10	C11	C12	C13	C14	C15	C16	C17	C18	C19
1	7	1	1	1	17.5	10	300	64.67											
2	19	2	1	1	17.5	10	150	64.00											
3	13	3	1	1	17.5	8	300	19.90											
4	15	4	1	1	17.5	10	300	64.90											
5	9	5	1	1	17.5	8	150	52.33											
6	1	6	1	1	17.5	8	150	52.17											
7	11	7	1	1	17.5	10	150	53.33											
8	7	8	1	1	19.0	8	150	98.67											

Fig. 4: Minitab 2019.

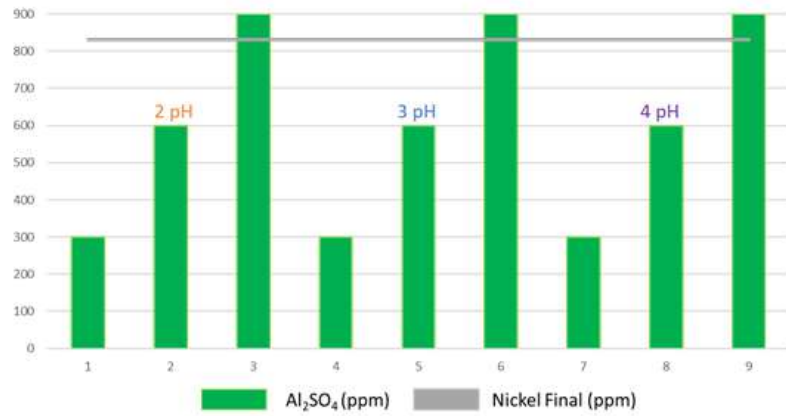


Fig. 5: Results of treatment with aluminum sulfate.

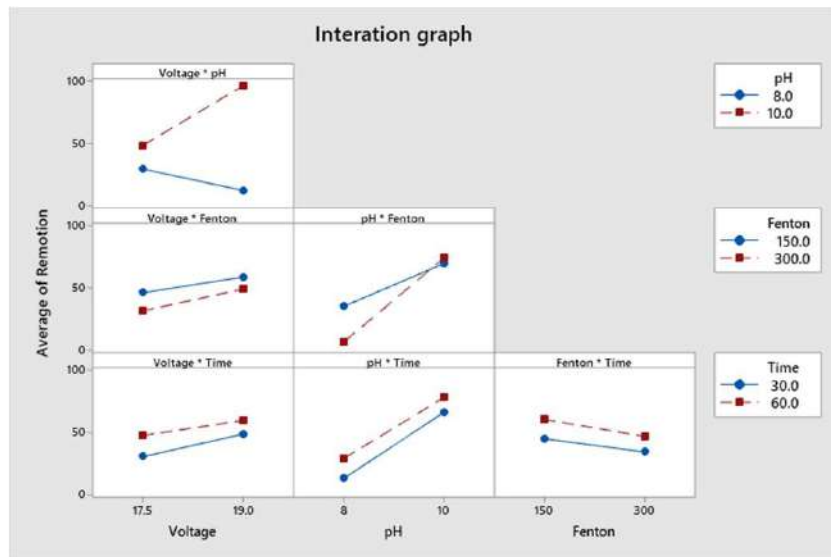


Fig. 6: Interaction graph.

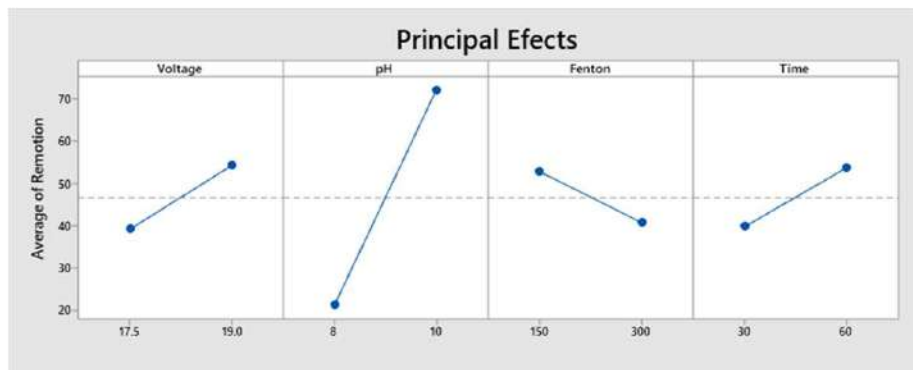


Fig. 7: Effects graph.

Table 4: Average results of advanced electrocoagulation at 30 min.

Voltage [V]	pH	Fenton [ppm]	Average Removal Percentage
17.5	8	150	48.39%
17.5	8	300	0.17%
17.5	8	450	0.61%
17.5	10	150	30.78%
17.5	10	300	42.83%
17.5	10	450	01.22%
19.0	8	150	3.00%
19.0	8	300	0.44%
19.0	8	450	0.39%
19.0	10	150	97.50%
19.0	10	300	93.89%
19.0	10	450	08.00%

Table 5: Average results of advanced electrocoagulation at 60 min.

Voltage [V]	pH	Fenton [ppm]	Average Removal Percentage
17.5	8	150	52.22%
17.5	8	300	17.56%
17.5	8	450	01.22%
17.5	10	150	53.83%
17.5	10	300	66.56%
17.5	10	450	05.06%
19.0	8	150	38.06%
19.0	8	300	08.61%
19.0	8	450	45.94%
19.0	10	150	97.56%
19.0	10	300	94.5%
19.0	10	450	57.17%

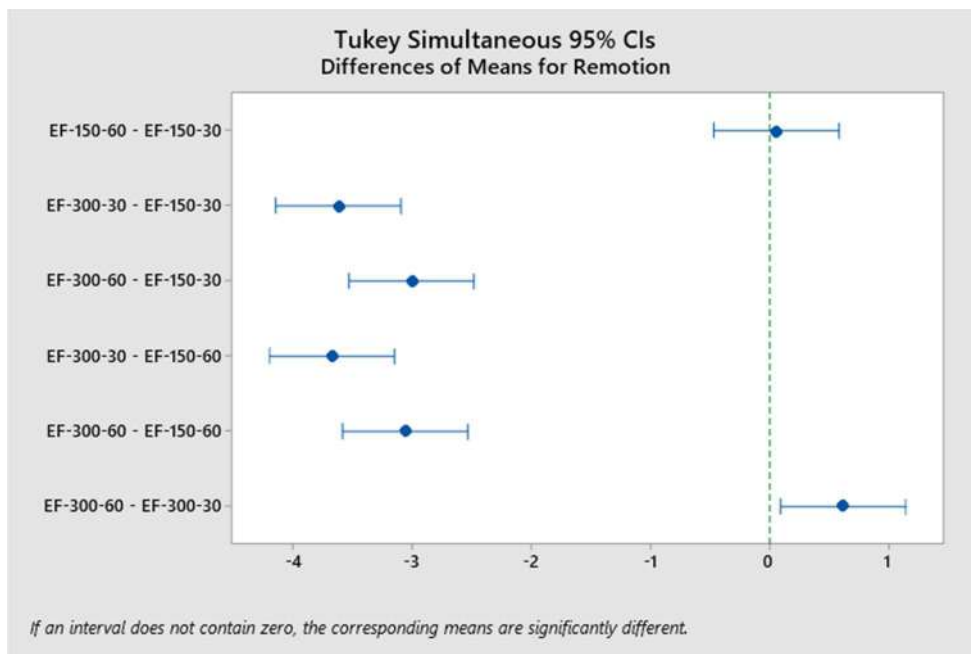


Fig. 8: Test of means with respect to time.

results of 97.50% of nickel removal at 30 min, half the time compared to them.

Martín (2008) mentions that the operating conditions of electrocoagulation depend on the chemistry of the aqueous medium, especially the conductivity, and pH, but also on the particle size, the type of electrodes, the retention time, the spacing between electrodes, and the concentration of the contaminants.

CONCLUSIONS

When comparing the decrease of nickel (II) in the wastewater samples, we can see that the sample treated with aluminum sulfate $[Al_2(SO_4)_3]$ did not have any decrease, so the ion exchange treatment for its reduction or elimination is not adequate; however, the advanced oxidation treatments such as electrocoagulation added with Fenton reagent resulted in an average maximum elimination of 97.56%, reducing from 60 ppm to 1,464 ppm of nickel in our water at 19 V, 150 ppm of Fenton reagent, and 10 pH.

Likewise, with the factorial design, it was corroborated

that the optimal variables for the experimentation are 19 V, 10 pH, a concentration of 150 ppm, and a time of 30 min, as corroborated by a Tukey analysis at 95% confidence.

With respect to time, it is observed that the addition of the Fenton reagent to the electrocoagulation process does affect, since authors such as Roja-Vargas et al. and Jumpatong have obtained results of 95% and 98%, respectively, in times from 60 min to 180 min, being the removal results similar to those presented in the present investigation. However, the times are reduced from 50% to 66% without compromising the percentage of nickel removal in the process.

As a conclusion, the advanced electrocoagulation process (electro-Fenton) is more efficient than traditional methods and even than typical electrocoagulation processes since the same efficiencies are achieved in a shorter time, thus reducing the use of energy. In addition, This process is eco-friendly with the environment since the chemicals discharged into the water to be treated are mostly iron, necessary in the geochemical cycle, and the peroxide, when volatilized and consumed, generates a considerable amount of water, so it is recommended from the environmental point of view.

ACKNOWLEDGMENTS

We are grateful to the Consejo Nacional de Humanidades, Ciencias y Tecnologías, for their support in the development of the project.

REFERENCES

- Abdel-Shafy, H.I., Morsy, R.M.M., Hewehy, M.A.I., Razek, T.M.A. and Hamid, M.A.M. 2022. Treatment of industrial electroplating wastewater for metals removal via electrocoagulation continuous flow reactors. *Water Pract. Technol.*, 17(2): 555-566. <https://doi.org/10.2166/wpt.2022.001>
- Ahmed, M.A., Ali, S.M., El-Dek, S. and Galal, A. 2013. Magnetite-hematite nanoparticles prepared by green methods for heavy metal ions removal from water. *Mater. Sci. Eng. B SolidState Mater. Adv. Technol.*, 178(10):744-751. <https://doi.org/10.1016/j.mseb.2013.03>
- Ahmad, M.A., Amano, Y. and Machida, M. 2010. Adsorption of heavy metals onto activated carbons derived from polyacrylonitrile fiber. *J. Hazard. Mater.*, 180(1-3): 552-560. <https://doi.org/10.1016/j.jhazmat.2010.04.069>
- Al Hamouz, O.C.S., Estatie M. and Saleh, T.A. 2016. Removal of cadmium ions from wastewater by dithiocarbamate functionalized pyrrole-based terpolymers. *Sep. Purif. Technol.*, 177: 101-109. <https://doi.org/10.1016/j.seppur.2016.12.044>
- Alomá-Vicente, I.C., Blázquez-García, G., Calero-de-Hoces, M., Martín-Lara, M.A., Rodríguez-Rico, I.L. and Ronda-Gálvez, A. 2013. General overview of water contamination by nickel. *Biosorption as a treatment technology. Cuban Chem. Mag.*, 15(3): 226-280. <https://goo.su/bgserI>
- Brahmi, K., Bouguerra, W., Hamrouni, B., Elaloui, E., Loungou, M. and Tlili, Z. 2019. Investigation of electrocoagulation reactor design parameters effect on the removal of cadmium from synthetic and phosphate industrial wastewater. *Arab. J. Chem.*, 12(8): 1848-1859. <https://doi.org/10.1016/j.arabjc.2014.12.012>
- Gómez-Duarte, O. 2018. Water pollution in low- and middle-income countries is a global public health problem. *Mag. Facul. Med.*, 66(1): 7-8. <https://doi.org/10.15446/revfacmed.v66n1.70775>
- Cañazares-Villanueva, R.O. 2000. Biosorption of heavy metals through the use of Microbial biomass. *Latin Am. J. Microbiol.*, 42: 131-143.
- Caviedes-Rubio, D.I. Muñoz-Calderón, R.A., Perdomo-Gualtero, A., Rodríguez-Acosta, D. and Sandoval-Rojas, I.J. 2015. Treatments for the removal of heavy metals commonly present in industrial wastewater. A review. *Eng. Reg. Mag.*, 13(1): 73-90. <https://doi.org/10.25054/22161325.710>
- Chegeni, M.K., Shahedi, A., Darban, A.K., Jamshidi-Zanjani, A. and Homaei, M. 2021. Simultaneous removal of lead and cyanide from the synthetic solution and effluents of gold processing plants using an electrochemical method. *J. Water Process. Eng.*, 43: 1-11. <https://doi.org/10.1016/j.jwpe.2021.102284>
- García, C., Moreno, J.L., Hernández-Fernández, M.T. and Polo, A. 2002. Heavy metals and their implications on soil quality. *Sci. Environ.*, 125-138.
- Guadarrama-Tejas, R., Kido-Miranda, J., Rolando-Antunez, G. and Salas-Salgado, M. 2016. Water pollution. *J. Environ. Sci. Nat. Resour.*, 2(5): 1-10.
- Ilhan, F., Ulucan-Altuntas, K., Avsar, Y., Kurt U. and Saral, A. 2019. Electrocoagulation process for the treatment of metal-plating wastewater: Kinetic modeling and energy consumption. *Front. Environ. Sci. Eng.*, 13(73): 1-8. <https://doi.org/10.1007/s11783-019-1152-1>
- Jumpatong, K. 2002. Electrocoagulation of Some Heavy Metals. Tesis de Maestría, Chiang Mai University, Chiang Mai, Tailandia.
- Kalavathy, H., Karthik, B. and Rose-Miranda, L. 2010. Removal and recovery of Ni and Zn from aqueous solution using activated carbon from Hevea brasiliensis: Batch and column studies. *Coll. Surf. B. Biointerf.*, 78(2): 291-302. <https://doi.org/10.1016/j.colsurfb.2010.03.014>
- Kumar, P., Ramalingam, S., Sathyaselvabala, V., Kirupha, S.D., Murugesan, A. and Sivanesan, S. 2012. Removal of Cd (II) from aqueous solution by agricultural waste cashew nut shell. *Korean J. Chem. Eng.*, 29: 756-768. <https://doi.org/10.1007/s11814-011-0259-2>
- Lehmann, M., Zouboulis, A.I. and Matis, K.A. 1999. Removal of metal ions from dilute aqueous solutions: A comparative study of inorganic sorbent materials. *Chemosphere*, 39(6): 81-892. [https://doi.org/10.1016/S0045-6535\(99\)00031-4](https://doi.org/10.1016/S0045-6535(99)00031-4)
- El-Karamany, H., Elbaz, A., Wagdy, R.M. and Mohammed, I.S. 2021. Chromium and cadmium removal from synthetic wastewater by electrocoagulation process. *JETT*, 9(2): 375-382. [https://doi.org/10.47277/JETT/9\(2\)382](https://doi.org/10.47277/JETT/9(2)382)
- López-Ramírez, M.A., Castellanos-Onorio, O.P., Susunaga-Miranda, M.A., Lango-Reynoso, F., Castañeda-Chávez, M.R. and Montoya-Mendoza, J. 2019. Treatment of leachates of a controlled landfill in Veracruz by using the Fenton method. *Nat. Environ. Pollut. Technol.*, 18(1): 1-8.
- López-Ramírez, M.A., Castellanos-Onorio, O.P., Lango-Reynoso, F., Castañeda-Chávez, M.R., Montoya-Mendoza, J., Sosa-Villalobos, C. and Ortiz-Muñiz, B. 2021. Advanced oxidation as an alternative treatment for wastewater. A review. *UTE Appr.*, 12(4): 76-87. <https://doi.org/10.29019/enfoqueute.769>
- Malik, P.K. and Saha, S.K. 2003. Oxidation of direct dyes with hydrogen peroxide using ferrous ions as catalysts. *Sep. Purif. Technol.*, 31: 241-250. [https://doi.org/10.1016/S1383-5866\(02\)00200-9](https://doi.org/10.1016/S1383-5866(02)00200-9)
- Martín, D.A., Rivera, H.M.L., Piña-Soberanis, M. and Pérez-Castrejon, S. 2008. Incidence of the velocity gradient on the efficiency of electrocoagulation to remove arsenic in a plug flow reactor. *Intersci. Technol. Mag.*, 33: 503-509.
- Mohammad, A.M., Salah Eldin, T.A., Hassan, M.A., Hassan, M.A. and El-Anadouli, B.E. 2017. Efficient treatment of lead-containing wastewater by hydroxyapatite/chitosan nanostructures. *Arab. J. Chem.*, 10(5): 683-690. <https://doi.org/10.1016/j.arabjc.2014.12.016>
- Nguyen, T., Ngo, T.H., Guo, W.S., Zhang, J., Liang, S., Yue, Q.Y., Li, Q. and Nguyen, T.V. 2013. Applicability of agricultural waste and

- by-products for adsorptive removal of heavy metals from wastewater. *Bioresour. Technol.*, 148: 574-585. <https://doi.org/10.1016/j.biortech.2013.08.124>
- Mohan, D., Singh, D.K.P. and Singh, V.K. 2006. Trivalent chromium removal from wastewater using low-cost activated carbon derived from agricultural waste material and activated carbon fabric cloth. *J. Hazard. Mater.*, 135(1-3): 280-295. <https://doi.org/10.1016/j.jhazmat.2005.11.075>
- Pabón, S.E., Benitez, R.A., Sarria, R.A. and Gallo, J.A. 2000. Water contamination by heavy metals, analysis methods, and removal technologies. A review. *Bet. Sci. Eng.*, 14(27): 9-18. <https://goo.su/mT9N>
- Pinillo-Torres, J.A. 2013. Removal of Heavy Metals from the Effluents of the Marcapunta Oeste mine. Master's Thesis, National University of Engineering, Lima, Perú.
- Ramírez-Franco, J.H., Martínez Ávila, O.M. and Fernández-Ospina, L.M. 2013. Removal of contaminants in industrial wastewater using activated carbon from patula pine. *Adv. Eng. Res.*, 10(1): 42-49.
- Rickert, B., Chrus, I. and Smocholl, O. 2016. Protecting Surface Water for Health Identifying, Assessing and Managing Drinking Water Quality Risks In Surface-Water Catchments. WHO, Washinton DC.
- Rojas-Vargas, A. Ricardo-Riverón, M. Penedo-Medina and E. Ojeda-Armaignac. 2020. Remoción de níquel por electrocoagulación del sistema Ni (II)-NH₃-CO₂-SO₂-H₂O con electrodos de aluminio. *Tecnol. Chim. Química*, 4(2): 393-412.
- Tiemi-Muranaka, C. 2010. Combinação de adsorção por carvão ativado com processo oxidativo avançado (POA) para tratamento de efluentes contendo fenol. Tesis de Doctorado, Politécnica da Universidade de São Paulo, São Paulo, Brasil.
- Sanz, J., Lombrana, J. and Luis, A. 2013. Estado del arte en la oxidación avanzada a efluentes industriales: nuevos desarrollos y futuras tendencias. *Afinidad. J. Chem. Theoret. Appl. Chem.*, (70)56: 25-33.
- Sharma, D., Chaudhari, P.K. and Prajapati, A.K. 2019. Removal of chromium (VI) and lead from electroplating effluent using electrocoagulation. *Sep. Sci. Technol.*, (55)2: 321-331. <https://doi.org/10.1080/01496395.2018.1563157>
- Trivedi, P. and Axe, L. 2000. Modeling Cd and Zn sorption to hydrous metal oxides. *Environ. Sci. Technol.*, (34)11: 2215-2223. <https://doi.org/10.1021/es991110c>

ORCID DETAILS OF THE AUTHORS

- M. A. López-Ramírez: <https://orcid.org/0000-0001-5841-0668>
O. P. Castellanos-Onorio: <https://orcid.org/0000-0003-3510-2640>
F. Lango-Reynoso: <https://orcid.org/0000-0001-8359-434X>
M. del R. Castañeda-Chávez: <https://orcid.org/0000-0002-9209-0431>
J. Montoya-Mendoza: <https://orcid.org/0000-0002-9281-2190>
M. Díaz-González: <https://orcid.org/0000-0002-2855-9311>
B. Ortiz-Muñiz: <https://orcid.org/0000-0001-5211-9175>



A Comprehensive Study of Remote Sensing Technology for Agriculture Crop Monitoring

R. Sathiya Priya and U. Rahamathunnisa†

School of Computer Science Engineering and Information Systems, Vellore Institute of Technology, Vellore 632 014, TamilNadu, India

†Corresponding author: U. Rahamathunnisa; rahamathu.u@vit.ac.in

Nat. Env. & Poll. Tech.
Website: www.neptjournal.com

Received: 05-10-2023

Revised: 16-11-2023

Accepted: 28-11-2023

Key Words:

Remote sensing satellites

Agriculture

Paddy crop

Spectral indices

ABSTRACT

With the rapid advancement of Remote Sensing Technology, monitoring the agricultural land has become a facile task. To surveil the growth of paddy crops and provide detailed information regarding monitoring soil, drought, crop type, crop growth, crop health, crop yield, irrigation, and fertilizers, different types of remote sensing satellites are used like Landsat 8, Sentinel 2, and MODIS satellite. The main aim of Landsat 8, Sentinel 2 and MODIS satellites is to monitor the land and vegetation area and to provide data regarding agricultural activities. Each of these satellites possesses a different spectral band, resolution, and revisit period. By using the remote sensing spectral indices, different types of vegetation indices are calculated. This survey paper provides comprehensive about Remote Sensing and the major parameters that influence for growth of paddy crops, like soil and water, and the future scope of agriculture and its demand in research is discussed.

INTRODUCTION

A large variety of crops are grown in our country to meet the daily requirements of food. India is one of the fastest-growing populated countries. With the rapid increases in the population, the supply and need in the agro-based industries are getting higher level. The major food crops in India are rice, wheat, maize, and millet. Among all the crops, rice is considered a stable food crop. For the cultivation of the rice soil, temperature, rainfall, and humidity must be maintained at an appropriate level. Rice is the staple crop in India, which is consumed by age people in day-to-day life. The demand for food is always increasing due to population. On an average survey, rice is consumed three times a day, mostly by all the people. However, due to some unpredictable natural disasters, most of the crops are getting destroyed. The early stage of prediction and identifying the problem may help us to store the crops and food. In India, there are three main cropping seasons for agriculture purposes and to cultivate the rice crop, they are known as the Kharif season, Rabi season, and Zaid season. Among these three seasons, Rabi and Kharif are suitable for the cultivation of paddy crops. To improve the productivity and profitability of rice, a structural inequity must be established, and more attention should be focused on technology development (Prasanna et al. 2009).

With the Evolution of Remote Sensing Technology and satellites, we can easily tackle all these problems. Many satellites are developed specifically for monitoring the land and resources that are present on the Earth's surface. Early prediction of the yield, diseases, and insufficient fertilizers helps to take an appropriate step for food management. The satellite information obtained from the image provides a transparency of activities regarding agriculture. The majority of the farmers have adequate knowledge of modern rice cultivation techniques; many different kinds of practices should be reached to the farmers for future generation rice cultivation process they are quality of the seed, spacing between the crops, seedling, time taken for transplanting, maturity of seedling, storing, fertilizer required for the crops, pest control, harvesting, and variety (Uddin et al. 2017). Keeping in mind the increase in population, the need for food is also getting increasing. In upcoming years like 2030, 2040, and 2050, the demand and the supply of the rice will be in a huge manner. India ranks second place in producing rice for food safety and control. Rice plays a vital role, and it remains constant forever (Mondal et al. 2022). Remote sensing plays a major role in agriculture. The satellites that are roaming around the Earth help to obtain information regarding the area that is covered by it. By analyzing and detecting the physical characteristics of changes happening in the area,

we can easily predict upcoming changes. Remote Sensing is used for analyzing and depicting the agricultural crop by using satellite images. Nowadays, remote sensing is used in various fields like forest, transport, Navy, and agriculture also, with the rapid development of these technologies, prediction and decision-making tasking have become facile (Jovanovic et al. 2014).

Remote sensing data is widely used in agricultural areas, like analyzing the nutrient content in the soil, crop production, crop yield, and forecasting (Table 1) (Wojtowicz et al. 2016). With the evolution of Remote Sensing (RS) technologies monitoring agriculture activities has become an easy task.

MATERIALS AND METHODS

Different Remote Sensing satellites are developed to monitor the agriculture, forest, and weather conditions from the regional level to the national level. Each of these satellites has a different bandwidth, resolution, central wavelength, and sensors. Some of the satellites are listed below.

1. Sentinel 2
2. Landsat 8
3. MODIS

Description of Sentinel 2

The Sentinel 2 satellite is integrated with two polar-orbiting satellites, which are placed in the same sun-synchronous orbit and are stepped at 180 degrees to each other's. It is a European-wide swath that has a high resolution. The specification of the Sentinel 2 satellite is it is and twin satellite flying in the same orbit. The revisit period of this satellite is 5 days with cloud-free conditions. The Sentinel 2 satellite provides a variety of services like monitoring the land, agriculture, risk mapping, and disaster

control.

The Sentinel 2 consists of 13 spectral bands from B1 to B12. Each of these has different resolutions, wavelengths, and specific features.

The spectral band's meter ranges from 10 to 60 meter pixel size.

The Sentinel 2 is the Multispectral Imager (MSI).

The Two polar-orbiting satellites provide a high resolution of optical imagery.

The Sentinel 2 data is used to highlight the different parameters for the plant growth like leaf area index, chlorophyll, and water content.

Fig. 1 and Fig. 2 represent the sentinel band details.

The Sentinel 2 dataset is free, and it is openly available for all users.

Description of Landsat 8

The Landsat 8 satellite was developed by NASA and USGC (U.S. Geological Survey) in collaboration. Landsat 8 orbits the Earth in a sun-synchronous, polar orbit at 98.2 degrees. It completes the one-earth orbit for 99 minutes itself. The revisit period and repeat cycle for acquiring data is 16 days one's. Multispectral Image Data is provided for global land mass.

Landsat 8 data is sufficiently consistent in terms of spectral characteristics, data availability, calibration, coverage, and output product quality.

The Landsat 8 satellite consists of two sensors known as

1. Operational Land Imager (OLI)
2. Thermal Infrared Sensor (TIRS)

The Landsat two sensors (OLI, TIRS) provide global landmass coverage at spatial resolutions of 30m, 100m, and

Table 1: Uses of remote sensing.

Application	Remote Sensing Usage
Crop Condition	By using the Normalized Difference Vegetation Index (NDVI) healthy crop area is reflected in green.
Forecasting Crop Production	By using the Remote Sensing technology prediction and yield of the crop production for an estimated field can be done easily. Before the harvest stage, we can detect with the help of remote sensing.
Soil Moisture	The satellite consists of both Active and passive Sensors, these sensors are used to determine the soil moisture content.
Crop stress and damage condition	The withhold capacity of the crop is used to estimate the crop stress condition, and the damaged crop is identified by the reflectance of radiation in the farmland.
Crop Health Analysis	By evaluating the overall crop yield, health analysis is determined for the crops. The fertilizer cost and Time factor are saved.
Water and Drought Monitoring	The remote sensing technology identifies the water content needed for the field crop, and the information is gathered to forecast the rainfall by comparing the rainfall pattern for the given area; the drought is Monitoring.

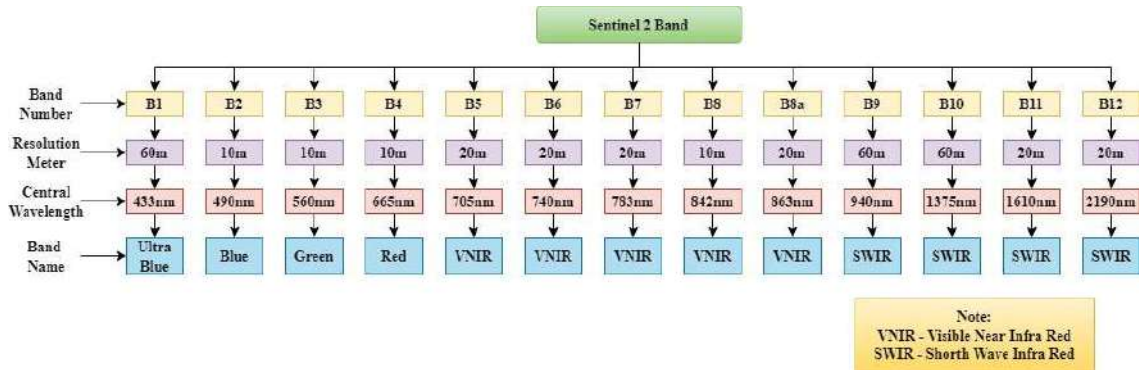


Fig. 1: Sentinel 2 Band details.

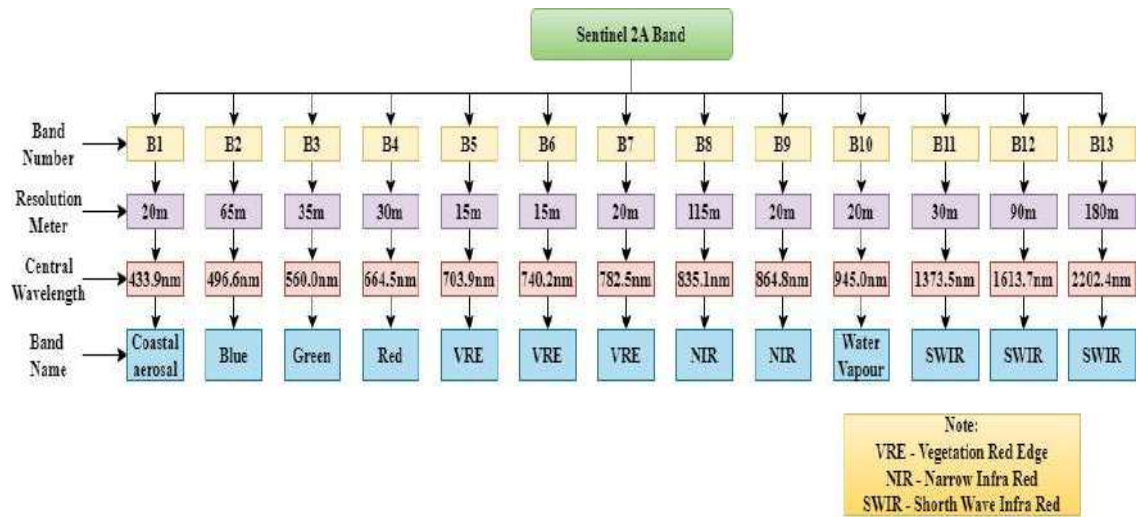


Fig. 2: Sentinel 2A Band.

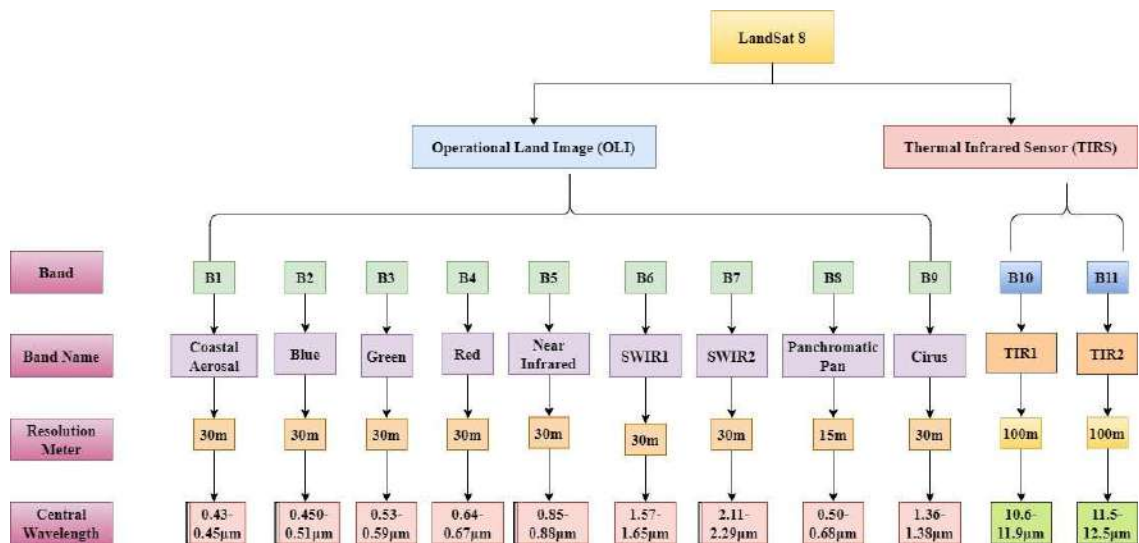


Fig. 3: Landsat 8 Band details.

Table 2: MODIS band details. (Band 1&2 has 250m of spatial resolution, Band (3 to 7) has 500m of spatial resolution, and Band (8 to 36) has 100m of spatial resolution).

Band Number	Band Name	Resolution Meter (m)	Central Wavelength (μm)
B1	VIS	250m	0.620-0.670 μm
B2	NIR	250 m	0.841-0.876 μm
B3	VIS	500 m	0.459-0.479 μm
B4	VIS	500 m	0.545-0.565 μm
B5	NIR	500 m	1.230-1.250 μm
B6	SWIR	500 m	1.628-1.652 μm
B7	SWIR	500 m	2.105-2.155 μm
B8	VIS	1000 m	0.405-0.420 μm
B9	VIS	1000m	0.438-0.448 μm
B10	VIS	1000 m	0.483-0.493 μm
B11	VIS	1000 m	0.526-0.536 μm
B12	VIS	1000 m	0.546-0.556 μm
B13	VIS	1000 m	0.662-0.672 μm
B14	VIS	1000 m	0.673-0.683 μm
B15	VIS	1000 m	0.743-0.753 μm
B16	NIR	1000 m	0.862-0.877 μm
B17	NIR	1000 m	0.890-0.920 μm
B18	NIR	1000 m	0.931-0.941 μm
B19	NIR	1000 m	0.915-0.965 μm
B20	MWIR	1000 m	3.660-3.840 μm
B21	MWIR	1000 m	3.929-3.989 μm
B22	MWIR	1000 m	3.929-3.989 μm
B23	MWIR	1000 m	4.020-4.080 μm
B24	MWIR	1000 m	4.433-4.498 μm
B25	MWIR	1000 m	4.482-4.549 μm
B26	SWIR	1000 m	1.360-1.390 μm
B27	TIR	1000 m	6.538-6.895 μm
B28	TIR	1000 m	7.175-7.475 μm
B29	TIR	1000 m	8.400-8.700 μm
B30	TIR	1000 m	9.580-9.880 μm
B31	TIR	1000 m	10.780-11.280 μm
B32	TIR	1000 m	11.770-12.270 μm
B33	TIR	1000 m	13.185-13.485 μm
B34	TIR	1000 m	13.485-13.758 μm
B35	TIR	1000 m	13.785-14.085 μm
B36	TIR	1000 m	14.085-14.385 μm

Band Name Abbreviations: VIS: Visible, NIR: Near-Infrared, SWIR: Short Wave Infrared, MWIR: Midwave Infrared, TIR: Thermal Infrared

15m. The Landsat 8 consists of 11 bands in which the first nine spectral bands belong to OLI and the last two spectral bands belong to TIRS.

Fig. 3 represents Landsat 8 band details.

The Landsat 8 dataset is free and it's openly available for all users.

Description of MODIS

The MODIS satellite is known as (Moderate Resolution Imaging Spectroradiometer) which was launched by NASA. The swath width of MODIS is 2,330 km which can view the entire Earth's surface in two days. It can able to provide information regarding land, atmosphere, and ocean. The MODIS satellite contains 36 spectral bands and can able to obtain the data at three different spatial resolutions: 250m, 500m, and 1000m.

The MODIS dataset is free, and it's openly available for all users. The MODIS band details are mentioned in Table 2.

Comparison of Different Satellites and Their Parameters

A comparison has been made between MODIS, Landsat 8, and Sentinel 2, which is represented in Fig. 4. which highlights the different features and unique characteristics of each satellite.

Different Types of Spectral Indices

With the help of remote sensing, different kinds of spectral indices are used to evaluate the growth of the crop. When it

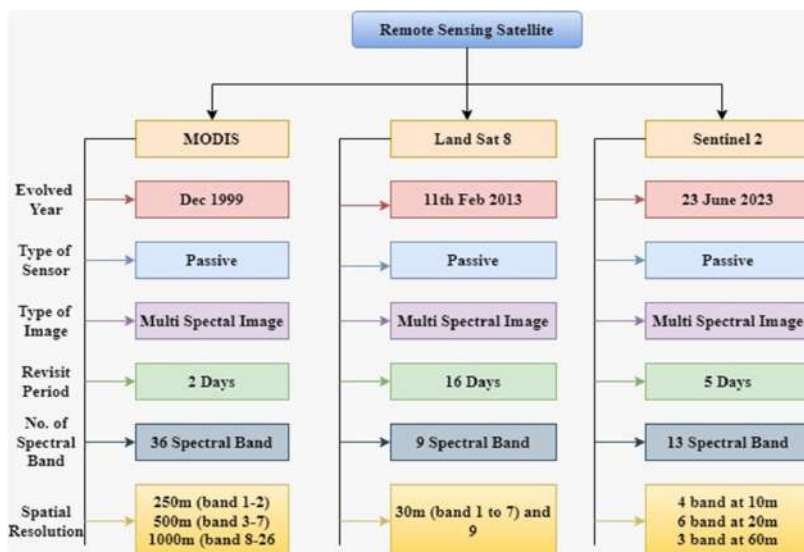


Fig. 4: Satellite features and metrics.

comes to monitoring the crop, the spectral indices which are listed below are the most important things, which include the physical Input like Sunlight, Rainfall, Temperature, and soil.

The spectral indices calculation is done for Landsat 8 and Sentinel 2, and the formula is derived by using the band numbers that are used specifically for the particular satellite.

1. Normalized Difference Vegetation Index(NDVI)
2. Enhanced Vegetation Index(EVI)
3. Advanced Vegetation Index(AVI)
4. Bare Soil Index(BSI)
5. Soil Adjusted Vegetation Index(SAVI)
6. Green Coverage Index(GCI)
7. Normalized Difference Water Index(NDWI)
8. Normalized Pigment Chlorophyll Ratio Index(NPCRI)

Normalized Differences Vegetation Index (NDVI)

The NDVI is computed by using the Red and Near Infrared spectral bands. For identifying the vegetation the NDVI is used. The NDVI can also be used for identifying the crop and its health. Higher the reflectance of Near Infrared implies dense and healthy vegetation.

The standard formula for estimating the

$$NDVI = (NIR - Red)/(NIR + Red)$$

The spectral bandwidth and color differ according to the satellite

Enhanced Vegetation Index (EVI)

EVI is almost familiar with NDVI; the EVI is used to calculate the vegetation greenness and does the atmospheric correction, and the EVI is used to remove the canopy background noise in dense vegetation areas.

The standard formula for estimating the

$$EVI = G * \frac{(NIR-R)}{(NIR+C1*R-C2*B+L)}$$

The spectral bandwidth and color are differed according to the satellite.

Where L denotes the canopy background; C denotes the Coefficient for atmospheric resistance

Advanced Vegetation Index (AVI)

The AVI is used to monitor the crops and forest changes over a period of time. The AVI is also similar to NDVI; by using the multi-temporal combination of both AVI and NDVI we easily identify the types of vegetation, and the crop phenology characteristics are extracted.

The standard formula for estimating the

$$AVI = [NIR * (1 - RED) * (NIR - RED)]^{1/3}$$

The spectral bandwidth and color are differed according to the satellite.

Bare Soil Index (BSI)

The Bare Soil Index (BSI) is used for soil mapping and crop identification by combining NDVI. To identify the soil variation, different combinations of spectral bands are used, like blue, red, near-infrared, and short-wave infrared. To aggregate the mineral composition of the soil short-wave infrared and red spectral bands are used.

The standard formula for estimating the

$$BSI = ((Red + SWIR) - (NIR + Blue))/((Red + SWIR + (NIR + blue)))$$

The spectral bandwidth and color are differed according to the satellite.

LANDSAT 8	SENTINEL 2
$NDVI = (B5 - B4)/(B5 + B4)$	$NDVI = (B8 - B4)/(B8 + B4)$
LANDSAT 8	SENTINEL 2
$EVI = 2.5 * \frac{(B5 - B4)}{(B5 + 6 * B4 - 7.5 * B2 + 1)}$	$EVI = 2.5 * \frac{(B8 - B4)}{(B8 + 6 * B4 - 7.5 * B2 + 1)}$
LANDSAT 8	SENTINEL 2
$AVI = [B5 * (1 - B4) * (B5 - B4)]^{1/3}$	$AVI = [B8 * (1 - B4) * (B8 - B4)]^{1/3}$
LANDSAT 8	SENTINEL 2
$BSI = \frac{(B6 + B4) - (B5 + B2)}{(B6 + B4) + (B5 + B2)}$	$BSI = \frac{(B11 + B4) - (B8 + B2)}{(B11 + B4) + (B8 + B2)}$

Soil Adjusted Vegetation Index (SAVI)

The SAVI is used to strive for the vegetation index by minimizing the soil brightness and its correct the low vegetation area. SAVI is mostly used in arid regions where vegetation cover is low to identify. The standard formula for estimating the SAVI is:

$$SAVI = \frac{(NIR - R)}{(NIR + R + L) * (1 + L)}$$

NIR = pixel values from the near-infrared band

Red = pixel values from the near-red band

L = green vegetation cover, the value of L depends on the following: where

L = 0.5 (Moderate Green Vegetative Cover)

L = 0 (High Vegetation Cover)

L = 1 (No green Vegetation Cover)

The spectral bandwidth and color differ according to the satellite

Green Coverage Index (GCI)

The Green Chlorophyll Index is used to identify the chlorophyll present in different species of plants by which the vegetation state is measured. The chlorophyll value directly reflects the vegetation. The standard formula for estimating the GCI is:

$$GCI = \frac{(NIR)}{(Green) - 1}$$

The spectral bandwidth and color are differed according to the satellite.

LANDSAT 8	SENTINEL 2
$SAVI = \frac{(B5 - B4)}{(B5 + B4 + 0.5) * (1.5)}$	$SAVI = \frac{(B8 - B4)}{(B8 + B4 + 0.428) * (1.428)}$

LANDSAT 8	SENTINEL 2
$GCI = \frac{(B5)}{(B3) - 1}$	$GCI = \frac{(B9)}{(B3) - 1}$

LANDSAT 8	SENTINEL 2
$NDWI = \frac{(B3 - B5)}{(B3 + B5)}$	$NDWI = \frac{(B3 - B8)}{(B3 + B8)}$

LANDSAT 8	SENTINEL 2
$NPCI = \frac{(B4 - B2)}{(B4 + B2)}$	$NPCI = \frac{(B4 - B2)}{(B4 + B2)}$

Normalized Difference Water Index (NDWI)

The NDWI is used to enhance the features of the water bodies in the satellite image. The primary aspect of using the NDWI is to detect the water and monitor the changes in the water bodies. The NDWI uses NIR and SWIR spectral bands.

The following ranges can evaluate the NDWI,

-1 to -0.3 indicates a Drought area

-0.3 to -0.0 indicates Moderate Drought area

0.0 to 0,2 indicate Flooding and Humidity

0,2 to 1 indicate Water Surface Area

The standard formula for estimating the

$$NDWI = \frac{(NIR - SWIR)}{(NIR + SWIR)}$$

The spectral bandwidth and color are differed according to the satellite.

Normalized Pigment Chlorophyll Ratio Index (NPCRI)

Identifying the chlorophyll pigment in the crop is one of the important parameters by which we can determine the physiological changes in the crop. The NPCRI is used to evaluate the chlorophyll content by using the red and blue spectral bands. The information driven by the NPCRI is used to measure chlorophyll and nitrogen. The standard formula for estimating the NPCRI is:

$$NPCRI = \frac{(Red - Blue)}{(Red + Blue)}$$

The spectral bandwidth and color are differed according to the satellite.

An Overview of Remote Sensing and its impact

The land is a gift from nature that the land wants to be preserved, protected, and valued for future generations. The Land that is used for agricultural purposes is known as Cultivable land. The land is the only thing on the Earth that protects all the valuable natural resources like water, soil, forest, and coal. Due to the population increase, the demand and need for food products are getting increasing a lot. The land that is used for production is decreasing day by day due to the Infrastructural development of urban places. In India, 51.09% of the land is only used for cultivation purposes. The Land should reside two important factors which are useful for agriculture purposes known as soil and water.

The Literature survey has been categorized into two different sections. In each of these sections, the different parameters that directly are indirectly influence the growth of the paddy crop are discussed.

Section I: Soil

Soil is an essential part of agriculture. Soil provides formalistic support for agricultural purposes, and it also can be categorized into two different types, physical and chemical based on their properties. Soil health and soil Quality are two major factors that influence the growth of the crop. Soil health represents finite and non-renewable resources. Soil quality represents nutrients, which is held in that healthy soil is identified by the growth of the crops and its nutrition properties. These nutrients are inherited by the crops from the soil and produce nutritious food (Laishram et al. 2012). The soil that is most suitable for agricultural purposes is known as alluvial soil, which is whole and very fertile, and this is the loamy type, which is highly productive for the growth of the crop. The pH of soil ranges from 3.5 to 10. In higher rainfall areas, the pH range of the soil ranges from 5 to 7. Soil quality management will ensure a great impact in guaranteeing agricultural sustainability. Thus we must pay more attention to the land and soil also to ensure the environmental quality will be in a stable position.

The purpose of Soil Moisture Active Passive (SMAP) purpose is to establish high-resolution soil moisture, which has suffered disdainfully due to the failure of the L -the band Synthetic Aperture Radar. To overcome this problem, the author (Entekhabi et al.2010) evaluated the capability of ingesting ISRO's Radar Imaging Satellite-1 (RISAT-1) C-band SAR observation. The SMAP active, passive algorithm obtains the soil moisture at 1, 3, and 9 km over the agricultural region dominant by paddy that experiences seasonal flooding.

A phenology-based algorithm (Li et al. 2020) was developed to identify the unique features of the paddy. One

of the major factors that influence the growth of paddy is soil, and this parameter is considered for the different seasonal paddy crops cultivated. The Normalized Vegetation Index and Soil Vegetation Index are used to highlight the changes in the temporal differences. The growth phase of the paddy based on soil from the initial stage to the heading stage of the paddy is evaluated. For the regional scale estimation, this algorithm is better by comparing the statistical data and Landsat data, where higher accuracy is achieved.

Gasmi et al.2020 propose a new method known as Multilayer Perceptron with Backpropagation Learning Algorithm, which is used to evaluate the soil and the clay prediction by using satellite data. By combining the spectral, temporal, and spatial resolution of the satellite data, a fused image is derived where the prediction of soil obtained a higher accuracy value by adding the soil property to the soil clay map, which is used to derive the spectral index of the satellite image. Since different combinations of satellites are used together to obtain the satellite image, the multispectral bands are one of the most important tools to map the soil parameters.

Jun et al. (2020) proposed a new algorithm for monitoring the paddy soil. It is known as an improved Surface Energy Balance Algorithm for land (SEBALR), and this method is used to identify the paddy field evapotranspiration. This is useful for monitoring and controlling the water management system. An accurate estimate for paddy growth and its evapotranspiration is done by using SEBAL.

Soil is an important factor in the growth of paddy fields. To evaluate the soil Dynamic (Tang et al. 2023), use the CFD-DEM coupling method, which is used to identify the soil characteristics, properties, and resistances with a high accuracy level and to identify the surface energy level of the paddy field. The coupling method is combined with spherical particles Johnson-Kendall-Roberts (JKR) only 10% of the relative error rate is achieved for the soil disturbance characteristics.

Soil plays a massive role in the growth of the paddy crop (Liu et al. 2023). The Mean Residence Time (MRT) of the accumulation of carbon in the soil helps to upland paddy crops, keeping in the aspect of global warming, the accumulation of carbon, can be reduced by paddy. The author of the paper estimates the average percentage of Carbon(C) increases by 7% during the monsoon time in the Asia region.

Section II: Water

Water is one of the most valuable natural resources for agriculture. Plants and crops continuously need water for better yield and growth. Without water, the agriculture

sector can't remain for future generations. In ancient times, agriculture mainly depended on rainfall, but nowadays, many places in India depend on groundwater for agricultural purposes. Water is the most basic thing to produce a healthy crop. In India 17% of GDP is contributed by agriculture, in which the irrigated agriculture serves 20% and the total cultivated land serves 40%. Our Globe is canopied by 71% of water but the availability of fresh water is less than 1%. Efficiently utilizing and managing water resources can lead to the progressive development of our country (Ramasubbu & Rajendran 2020). By increasing agricultural water productivity for future generations, some of the issues can be resolved, like food demand, economic growth impact to reduce poverty, and ensuring the water is available for environmental usage (Molden et al. 2011).

To overcome the shortage of water in agricultural activities NASA develops a Terrestrial Observation and Prediction System (TOPS) for remote sensing satellites like Landsat and MODIS (Melton et al. 2012). The Satellite Irrigation Management Support, when combined with TOPS, provides data regarding water resources, soil moisture, and irrigation, which is useful for the end user, and this framework is also useful for identifying crop water requirements.

Water plays an important role in agriculture. Water management must be done for future generations to improve agricultural activity and supply food based on demand. Different kinds of technologies are effectively involved in this, like IOT, Cloud computing, and Wireless Sensor Networks (Saad et al. 2020). To overcome the drawbacks that we face in traditional methods to and effectively utilize water resources, the current technologies are very useful.

Water Quality (WQ) is the most important factor for all the regular activities present on the surface of the land. Ensuring the quality of the water for water resource management is not an easy task. The author (AI-Sulttani et al. 2021) uses different kinds of Ensemble models like QRF, SVM, RF, GBM, and GBM_H2O to predict the accuracy of the water quality two different feature algorithms like Principal Component Analysis (PCA) and Genetic Algorithm are incorporated with these models in which PCA perform better than Genetic Algorithm.

Using the advanced microwave Scanning Radiometer 2 (AMSR2) (Jiang et al. 2022) proposed a predicting water vapor, but its results in high spatial coverage with low temporal resolution. To overcome this, the Global Navigation Satellite System (GNSS) is used, which results in high temporal resolution and low spatial coverage; by combining these two technologies, a new Back Propagation Neural Network (BPNN) is introduced, which clearly retrieves the

water vapor for global scale. The Global Navigation Satellite System is used to provide data regarding water vapor and to measure the water vapor in spatial resolution within a city limit. The Integrated Water Vapour (IWV) (Marut et al.2022) is used to determine precise changes in the weather model. The GNSS is used to capture the wet and dry changes and their conditions, but the IWV is the first and foremost to analyze the regional scale changes.

For agriculture, ground water is the most important criterion to supply water for the field. Decreases in groundwater lead to depending on the rainfall and other modes of water for the field. To tackle this issue, the author (Leonard et al. 2023) proposes a new concept known as Groundwater Dependent Vegetation (GDV), and this concept is used to identify the groundwater by using Sentinel 2 data. The wet area, which remains green in the dry period, is identified. The hydrogeological parameters are taken into consideration for deriving an accurate result. The vegetation area for agriculture purposes with groundwater is identified as 90% using GDV.

The primary need for agriculture is water based on a good irrigation system. The need and supply of water to the land can be achieved effortlessly. The author (Zhao et al.2023) proposed water-saving Irrigation Technology (WSI), which is known as alternative wetting and Drying Irrigation (AWD). The rainfall after irrigation is considered a waste of natural source water. Collecting the rainfall can be helpful to supply during the demand period, and AWD achieves this. During the Dry period the AWD has achieved excellence in water facility.

Section III: Remote Sensing Impact for Monitoring the Paddy Crop

The primary role of remote sensing in agriculture is to provide information about the physical characteristics of the land, and the sensors which are present that measure the wavelengths of the light absorbed and reflected by green plants. There are various applications of remote sensing like monitoring weather, forestry, agriculture, etc.. In general, remote sensing images are characterized by spectral resolution, spatial resolution, temporal resolution, and radiometric resolution, which is represented in Fig 5.

(Jo et al. 2020) uses three different kinds of deep learning applications to overcome the problems in Paddy for classifying the labeled data. Deep learning applications like data augmentation, semi-supervised classification, and domain-adapted architecture. By using this application, a pixel-based comparison and statistical evaluation is done, which results in the diverse classification of paddy through satellite images.

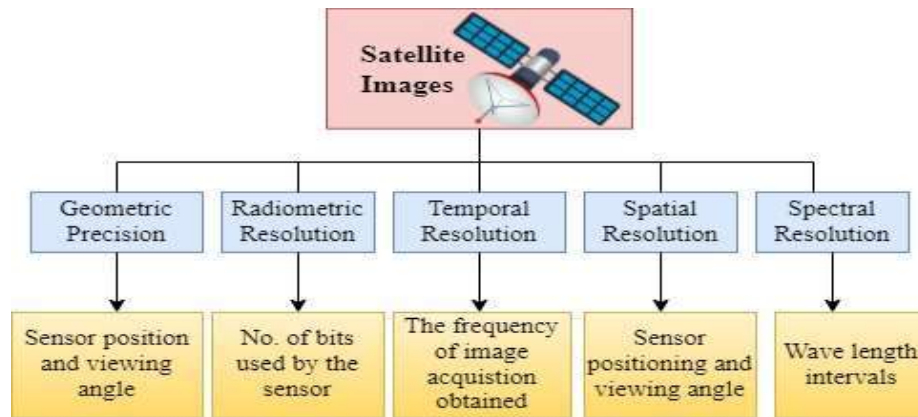


Fig. 5: Parameters influences for the satellite image.

Rice is considered one of the staple crops. Still, its growth and production consist of multifarious activities (Ramadhani et al.2020) that describe various factors that make us understand the shortage of rice production, like water, land, and climate. Accurate mapping of the rice growth stage via satellite image is difficult when it is covered with a cloud. To overcome this problem, an Automatic mapping of rice in real-time with a multitemporal map of the rice growth stage is proposed with the help of remote sensing data like Sentinel 1,2 and Mod13Q1. With this fusion of remote sensing data, good accuracy has been achieved, which helps to map the rice growth at local, national, and regional levels.

A gradient-boosted regression (GBR) is proposed by (Arumugam et al. 2021), which is used to estimate the rice yield from 500m of spatial resolution in India. This approach estimates an accurate crop yield with near real-time estimates.

Remote sensing is a powerful tool for yielding rice estimates from the farm to the regional level. The estimation done by Remote sensing is reliable and more accurate level, (Dela et al. 2021) propose three different models to estimate the rice yield, which are known as the Empirical model, the Semi-empirical model, and the Process-based crop model. The Empirical model is used larger scale in estimating the rice yield. A semi-empirical model is used to estimate the harvest yield, and a Process-based crop model is used to identify crop growth.

To overcome the problem in both spatial semantic information of Landsat and the finest training dataset used to segregate the paddy rice mapping, the author (Lang et al. 2022) proposed a new network known as Full Resolution Network (FR- NET). By using the different band combinations, an excellent performance is achieved in the FR-NET. This FR-NET is most suitable for identifying the

paddy rice mapping in the initial stage and last stage. The Multi-resolution Fusion Unit (MRFU) is used for segmenting the fine data from the Landsat. The FR-NET is composed of multiple MRFUs, which is useful for analyzing more features when compared to any other model. These MRFU are used for maintaining high-resolution stream of this model.

Yang et al. 2022 proposed a Temporal Feature Based Segmentation (TFBS), which is used for classifying paddy rice. This TFBS significantly performs well when compared with LSTM. By using the Synthetic Aperture Radar (SAR), different stages of crop growth are obtained by remote sensing images. The SAR provides the temporal and spatial features of the crop which is relatable for mapping the crop in a large area. The TFBS has achieved high accuracy in multicrop classification, and the best highlighting part of TFBS is the detachment of rice and non-rice features of the paddy crop.

Monitoring the rice at the regional level is not an effortless task (Xin et al. 2022). A new algorithm known as Feature Selection combines the sentinel 1 and sentinel 2 satellite images to predict on a large scale. Using the rice phenology characteristics like water and the color of the paddy helps to recognize the time of harvest. In general, there is a time interval period for the paddy crop to ensure the growth from the planting stage to the heading stage, and by using the rice phenology calendar, the harvest date is estimated. This algorithm is useful for regional-level estimation of paddy and the farmer.

RESULTS AND DISCUSSION

In the production of rice, India ranks second place among the leading countries. The production and the demand for rice are increasing globally since rice is considered an important source of food, and it's economically affordable for all people.

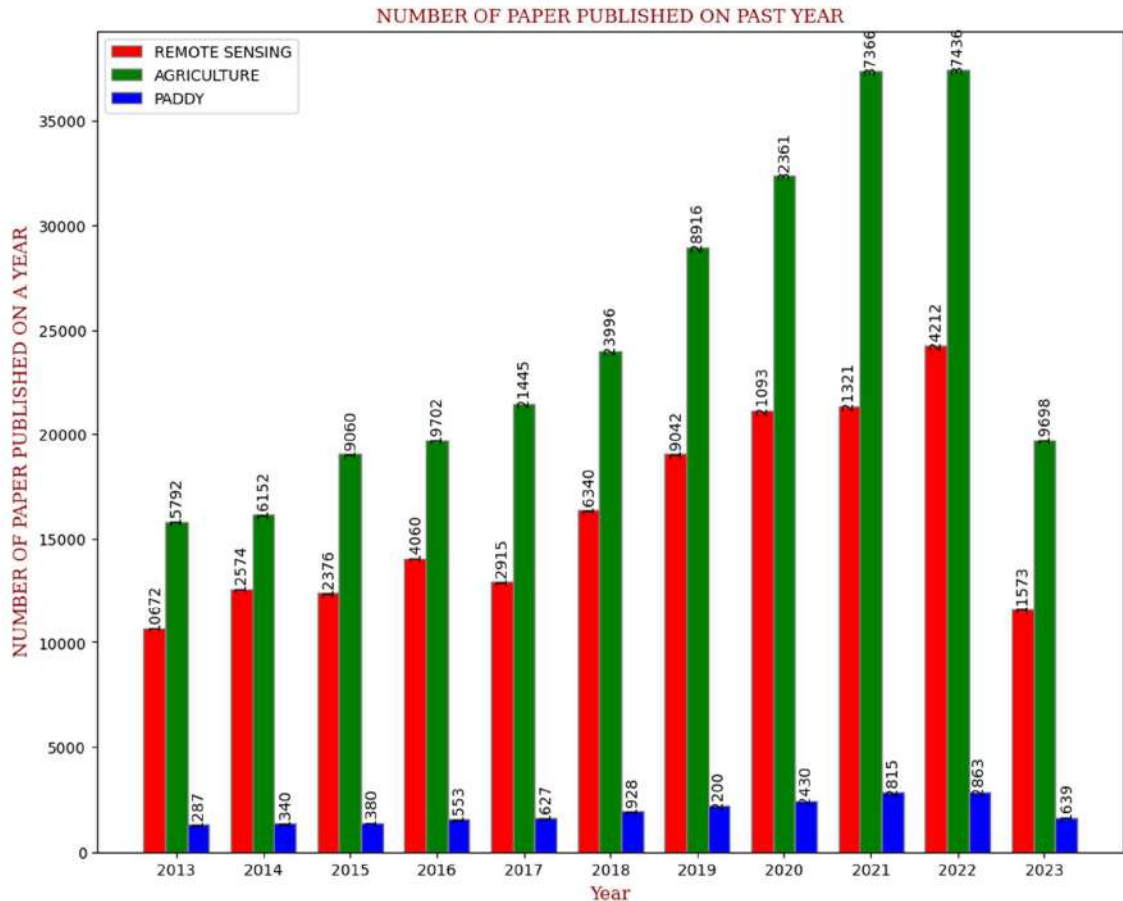


Fig. 6: Number of papers published on remote sensing, agriculture, paddy.

With the development of the Remote sensing technology, monitoring the crops has become an easy task with different methodologies and innovative algorithms for the prediction of crops; its yield forecasting the problems that occur for the crop has also become an effortless task. Different researchers in this field are proposing new ideas, in this decade, the number of papers published in this area is relatively high. A statistical report is taken from the Scopus database by entering keywords like 'Remote Sensing,' 'Agriculture,' and 'Paddy.' The Database retrieves a number of papers published in the last decade; prominent evidence is shown in Fig. 6. Due to the growth of technology and the importance given to agriculture, year by year, the number of papers published in this area is also increasing.

CONCLUSION

This paper has highlighted the importance of rice and the evolution of remote sensing in the agriculture field. With the development of these satellite technologies, monitoring the agricultural land has become an easy task, and monitoring

the early stage of crop growth, crop production, yield, and crop damage helps to take necessary prevention steps for food control. Since rice is a highly consumed food by all genders of people in India, demand for this paddy crop is growing day by day, and equal importance should be given to soil and water because these two greatly influence the growth of the paddy crop.

REFERENCES

- AI-Sultani, A.O., Al-Mukhtar, M., Roomi, A.B., Farooque, A.A., Khedher, K.M. and Yaseen, Z.M. 2021. Proposition of New Ensemble Data-Intelligence Models for Surface Water Quality Prediction. *IEEE Access*, 9: 108527-108541.
- Arumugam, P., Chemura, A., Schauburger, B. and Gornott, C. 2021. Remote Sensing Based Yield Estimation of Rice (*Oryza Sativa* L.) Using Gradient Boosted Regression in India. *Remote Sens.*, 13(12): 2379.
- Dela, D.M., Gao, J. and Macinnis-Ng, C. 2021. Remote sensing-based estimation of rice yields using various models: A critical review. *Geo-spatial Inf. Sci.*, 24: 580-603.
- Entekhabi, D., Njoku, E.G., O'Neill, P.E., Kellogg, K.H., Crow, W.T., Edelstein, W.N., Entin, J.K., Goodman, S.D., Jackson, T.J., Johnson, J., Kimball, J., Piepmeier, J.R., Koster, R.D., Martin, N., McDonald, K.C., Moghaddam, M., Moran, S., Reichle, R., Shi, J.C., Spencer,

- M.W., Thurman, S.W., Tsang, L. and Van Zyl, J. 2010. The soil moisture active passive (SMAP) Mission. Proc. IEEE, 98: 704-716.
- Gasmi, A., Gomez, C., Chehbouni, A., Dhiba, D. and Elfil, H. 2022. Satellite multi-sensor data fusion for soil clay mapping based on the spectral index and spectral bands approaches. *Remote Sens.*, 14(5): 1103.
- Jiang, N., Xu, Y., Xu, T., Li, S. and Gao, Z. 2022. Land water vapor retrieval for AMSR2 using a deep learning method. *IEEE Trans. Geosci. Remote Sens.*, 60: 1-11.
- Jo, H.W., Lee, S., Park, E., Lim, C.H., Song, C., Lee, H., Ko, Y., Cha, S. and Yoon, H. 2020. Deep learning applications on Multitemporal SAR (Sentinel-1) Image Classification Using Confined Labeled Data: The Case of Detecting Rice Paddy in South Korea. *IEEE Trans. Geosci. Remote Sens.*, 58(11): 7589-7601.
- Jovanovic, D., Govedarica, M. and Rasic, D. 2014. Remote sensing as a trend in agriculture. *Res. J. Agric. Sci.*, 46: 32-37.
- Jun, W., Cui, Y. and Luo, Y. 2023. Rice growth period detection and paddy field evapotranspiration estimation based on an improved SEBAL model: Considering the applicable conditions of the advection equation. *Agric. Water Manag.*, 278: 108141.
- Laiashram, J., Saxena, K., Maikhuri, R. and Rao, K. 2012. Soil quality and soil health: A review. *Int. J. Ecol. Environ. Sci.*, 38(1): 19-37.
- Lang, X., Zhao F., Chen J., Yu L., Lu M., Yu Q., Liang S., Fan L., Sun X., Wu W. and Yang P. 2022. A full-resolution deep learning network for paddy rice mapping using Landsat data. *ISPRS J. Photogramm. Remote Sens.*, 194: 91-107.
- Leonard, E.H., De Vita, P. and Conrad, C. 2023. Local identification of groundwater-dependent vegetation using high-resolution Sentinel-2 data – A Mediterranean case study. *Ecol. Indic.*, 146: 109784.
- Li, P., Xiao, C. and Feng Z. 2018. Mapping Rice Planted Area Using a New Normalized EVI and SAVI (NVI) Derived From Landsat-8 OLI. *IEEE Geosci. Remote Sens. Lett.*, 15(12): 1822-1826.
- Liu, Y., Wang P., van Groenigen, K.J., Xu, X., Cheng, K., Zhu, Z., Wang, J., Guggenberger, G., Chen, J. and Luo, Y. 2023. Residence time of carbon in paddy soils. *J. Cleaner Prod.*, 400: 136707.
- Marut, G., Hadas, T., Kaplon, J., Trzcina, E., Rohm, R. and Witold, W. 2022. Monitoring the water vapor content at high spatio-temporal resolution using a network of low-cost multi-GNSS receivers. *IEEE Trans. Geosci. Remote Sens.*, 60: 1-14.
- Melton, F.S., Johnson, L.F., Lund, C.P., Pierce, L.L., Michaelis, A.R., Hiatt, S.H., Guzman, A., Adhikari, D.D., Purdy, A.J., Rosevelt, C., Votava, P., Trout, T.J., Temesgen, B., Frame, K., Sheffner, E.J., Nemani, M. and Ramakrishna, R. 2012. *IEEE J. Sel. Top. Appl. Earth Obs. Remote Sens.*, 5(6): 1709-1721.
- Molden, D., Vithanage, M., Fraiture, C., Faures, J.M., Gordon, L., Molle F. and Peden, D. 2011. *Water Availability and Its Use in Agriculture*, 4: 707-732.
- Mondal, B., Bisen, J., Jambhulkar, N.T. and Rahul R. 2022. Rice supply, demand and exportable surplus in India: Present vis-à-vis thirty years ahead. *Oryza- Int. J. Rice.*, 59: 504-511.
- Prasanna, L., Kumar, S. and Singh A. 2009. Rice Production in India: Implications of Land Inequity and Market Imperfections. *Agric. Econ. Res. Rev.*, 22: 431-442.
- Ramasubbu, B. and Raj, N.R. 2020. Significance of water management and conservation in agriculture. *Pharma Innov. J.*, 9: 174-175.
- Ramadhani, F., Pullanagari, R., Kereszturi, G. and Procter, J. 2020. Automatic Mapping of Rice Growth Stages Using the Integration of SENTINEL-2, MOD13Q1, and SENTINEL-1. *Remote Sens.*, 12(21): 3613.
- Saad, A.E., Benyamina, H. and Gamatié, A. 2020. Water Management in Agriculture: A Survey on Current Challenges and Technological Solutions. *IEEE Access*, 8: 38082-38097.
- Tang, Z., Gong, H., Wu, S., Zeng, Z., Wang, Z., Zhou, Y., Fu, D. and Chuang, L., Cai Y., & Qi L. 2023. Modeling of paddy soil using the CFD-DEM coupling method. *Soil Tillage Res.*, 226: 105591.
- Uddin, M., Billah, K.M., Golam, R., Akanda, P., Mahamud, R.M., Masud, M., Sumon, P. and Antor, N. 2017. Farmers' knowledge of modern rice cultivation techniques at Dumki Upazilla. *Int. J. Adv. Agric. Sci.*, 2(10): 2456-7515.
- Wojtowicz, M., Wójtowicz, A. and Piekarczyk, J. 2016. Application of remote sensing methods in agriculture. *Int. J. Fac. Agric. Biol.*, 11: 31-50.
- Xin, Z., Nishina, K., Akitsu, T., Jiang, L., Masutomi, Y. and Nasahara K. 2022. Feature-based algorithm for large-scale rice phenology detection based on satellite images. *Agric. For. Meteorol.*, 329: 109283.
- Yang, L., Huang, R., Huang J., Lin, T., Wang, L., Mijiti, R., Wei, P., Tang, C., Shao, J., Li, Q. and Du, X. 2022. Semantic segmentation based on temporal features: Learning temporal-spatial information from time-series sar images for paddy rice mapping. *Ieee trans. Geosci. Remote Sens.*, 60: 1-16.
- Zhao, X., Chen, M., Xie, H., Luo, W., Wei, G., Zheng, S., Wu, C., Khan, S., Cui, Y. and Luo, Y. 2023. Analysis of irrigation demands of rice: Irrigation decision-making needs to consider future rainfall. *Agric. Water Manage.*, 280: 108196.



Forensic Identification and Isolation of Pathogenic Bacteria From Raw Vegetables and Fruits

Anuradha Sharma† and Sakshi Manhas

Department of Forensic Science, University Institute of Applied Health Sciences, Chandigarh University, Gharuan, Mohali-140413, Punjab, India

† Corresponding author: Anuradha Sharma; sanu3338@gmail.com

Nat. Env. & Poll. Tech.
Website: www.neptjournal.com

Received: 17-08-2023

Revised: 11-10-2023

Accepted: 13-10-2023

Key Words:

Vegetables

Fruits

Pathogenic bacteria

Forensic microbiology

ABSTRACT

The consumption of contaminated fruits and vegetables is the prime cause of outbreaks of various human diseases. Although fruits and vegetables have high nutritional value, today because of their contamination during handling while performing harvesting and post-harvesting techniques, they are harmful to human health. Most of them are eaten raw without being washed or without providing any treatment. Vegetables and fruits, being rich nutritional sources, can act as carriers or vectors of pathogenic microorganisms, which can create a serious issue for the health of the community targeted. This entire research is based on an emerging field of Forensic Microbiology. Various types of microbial agents can be utilized as bioweapons to conduct the bio crime or bioterrorism through food and water. This research also represents that the identification of microbial agents is very much necessary for the welfare of humans. Identification and isolation of different pathogenic bacteria from raw vegetables and fruits can also shed some light on the terms of the necessity of Forensic Microbiology.

INTRODUCTION

Consumption of fruits and vegetables that are fresh or minimally processed is causing different types of human infections. As some fruits and vegetables are eaten raw, they play the role of hosts for different types of pathogenic microorganisms. Pathogenic microorganisms may be a result of microcolonies spread over plants or plant tissues. The variation in the number of colonies may be due to the soil organisms, exposure of fruits and vegetables to air, dust, and water, along with handling during harvesting and post-harvesting techniques. The reason behind the contamination of fruits and vegetables is the use of untreated wastewater and the manure used for the cultivation of fruits and vegetables. Several types of plant and human pathogens are found in raw fruits and vegetables (Ghazali & Rashid 2019). Several outbreaks due to the consumption of raw fruits and vegetables have gone undetected and unnoticed due to the lack of inspection, supervision, and screening. Various types of causative agents, like *Listeria monocytogens*, *Salmonella* spp, *Shigella* spp, etc., are responsible for the outbreak of illnesses (Hussain et al. 2021). The pathogenic bacteria were found in large amounts in the research conducted on spoiled food products. Their amount of percentage of multi-drug resistant isolates was also high, causing harm to human health and resulting in food-borne illnesses. Microbial forensics has benefit in that its

protocol holds out against the legal investigation. The results obtained from the microbial forensic investigation can also be utilized as proof evidence that might either support or neglect the allegations made in court (Kubba et al. 2021).

This complete research is going to be based on highlighting the techniques of identifying and isolating the microorganisms (Pathogens) present in raw fruits and vegetables, which are very harmful to consume for the human body. Various harmful effects of consuming contaminated raw vegetables and fruits are also going to be entertained by conducting this research.

MATERIALS AND METHODS

The samples of the raw vegetables and fruits were collected, and past years' datasets were also analyzed on behalf of conducting this research. New techniques were explored to achieve better results in identifying pathogens and bacteria on the food products so that the food items could be protected from contamination.

Research Design

The quantitative research design was used in the present study. This type of research design was used based on the analysis of data from past years, which is related to the pathogen's bacteria on the food products.

Study Location

The study was conducted in Nepal considering the collection of 50 samples, 5 of each fresh fruits and vegetables like cucumber, tomato, spinach, cabbage, carrot, apple, guava, grapes, strawberry, and cherry.

Study Population

The dataset of past years is analyzed as secondary data on behalf of conducting this present research.

Data Collection Method

A total of 50 samples, 5 of each fresh fruits and vegetables namely Cucumber (*Cucumis sativus*), tomato (*Solanum lycopersicum*), spinach (*Spinacia oleracea*), cabbage (*Brassica oleracea*), carrot (*Daucus carota*), apple (*Malus domestica*), guava (*Psidium guajava*), grapes (*Vitis vinifera*), Strawberry (*Fragaria ananassa*) and cherry (*Prunus avium*) were collected from 5 different localities, i.e., open market of Kathmandu, Nepal.

Sample Preparation

After collecting the samples, they were taken into the laboratories within an hour. They were washed with 100 mL of distilled water and were diluted fivefold serially. The 10 mL of the washed aqueous solution was mixed with 90 ml of LB (Luria Broth). The incubated mixture (37 degrees Celsius for 24 h) was then utilized for the isolation and identification of bacterial strains using the streaking plate technique (Yeung 2016).

Identification and Isolation of Bacterial Strains

The isolation and identification of bacterial strains were carried out using different selective and non-selective mediums, i.e., Nutrient agar for Total Viable Bacterial Count (TVBC). For *E. coli*, Eosin Methylene Blue (EMB) and for *Salmonella*, Xylose Deoxycholate Agar (XLD) was used. For Identification confirmation, IMViC tests were performed for every species (Zambelli & Brasil 2022).

Bacterial Enumeration

For bacterial enumeration spread plate count technique was used to determine the number of colony-forming units (CFUs).

The list of materials and methods is summarized in Table 1.

RESULTS

Bacterial Load in Fruits and Vegetables

Table 1: List of methods and materials.

Universe	Nepal
Research design	Quantitative research design
Collection of data	Samples are collected
Primary data	Documents, Online journals, datasets, and articles of last years are used as well as analyzed as secondary data.
Duration	45 days

All the samples of fruits and vegetables were examined microbiologically. The results were obtained which gave a huge number of bacterial count, and also *E. coli* and *Salmonella* were detected.

Total Viable Count

The total viable bacterial count is represented in Table 2. Ten different samples were collected from five different locations, and the bacterial load was examined.

From the table, it can be observed that the maximum number of bacteria were found in guava and grapes (TMTC), i.e., too many to count (Fig. 1), followed by carrots. Spinach, cucumber, strawberry, cherry, and tomato were moderately contaminated. Apple was the least contaminated among all the fruits and vegetables.

Selective Culture

Culture of pathogenic bacteria, namely *E. coli* and *Salmonella* was done on selective media (Table 3), i.e., Eosin Methylene Blue (EMB) Agar and Xylose Lysine Deoxycholate (XLD) Agar, respectively. The washed water was first enriched in Luria Broth (LB) for 24 h at 37 degrees Celsius and then was cultured on the selective media respectively. From location 1, samples A, B, C, E, F, G, H, I, and J showed a greenish metallic sheen (Fig. 2), which indicated the presence of *E. coli*, while *Salmonella* was only present in samples B, C, and E, and I and J by formation of black, mucoid colonies as displayed in Fig. 3. Location 2, which was taken from the farm directly showed the formation of a greenish metallic sheen in samples E, F and I while black colonies formation was present in samples E, F, and J. Similarly, the samples obtained from location 3, gave *E. coli* colonies in samples A, B, D, E, H, I, and J while *Salmonella* was only obtained in sample D. For location 4, *E. coli* was present in samples E, F, H and I with Greenish metallic colonies meanwhile sample E, F and J gave black colonies resulting in *Salmonella* formation. Finally, sample A, taken from location 5, gave no growth at all on the plates which concluded in the absence of *E. coli* as well as *Salmonella*. Samples B, C, and D gave a Greenish metallic sheen, confirming the presence of *E. coli*. At the same time, *Salmonella* presence

Table 2: Total viable bacterial count.

Sample	Location 1	Location 2	Location 3	Location 4	Location 5
A (Spinach)	TMTC	2.89*10 ⁸	TMTC	2.52*10 ⁸	2.21*10 ⁸
B (Cucumber)	4.8*10 ⁸	1.64*10 ⁸	TMTC	2.24*10 ⁸	TMTC
C (Cabbage)	2.78*10 ⁸	2.40*10 ⁸	2.13*10 ⁸	2.13*10 ⁸	1.46*10 ⁸
D (Carrot)	1.96*10 ⁸	TMTC	TMTC	2.02*10 ⁸	TMTC
E (Tomato)	1.28*10 ⁸	1.78*10 ⁸	1.74*10 ⁸	2.56*10 ⁸	TMTC
F (Strawberry)	TMTC	2.44*10 ⁸	TMTC	TMTC	1.66*10 ⁸
G (Apple)	1.42*10 ⁸	2.12*10 ⁸	2.15*10 ⁸	1.55*10 ⁸	2.76*10 ⁸
H (Guava)	TMTC	TMTC	TMTC	1.88*10 ⁸	TMTC
I (Grapes)	TMTC	TMTC	TMTC	TMTC	TMTC
J (Cherry)	TMTC	1.83*10 ⁸	1.58*10 ⁸	1.22*10 ⁸	TMTC

Table 3: Selective media and growth.

S. No.	Selective Media	Growth
1.	Eosin Methylene Blue Agar (EMB)	Greenish metallic sheen, shiny colonies
2.	Xylose Lysine Deoxycholate Agar (XLD)	Black, mucoid colonies

was shown by samples B, H and I with black, mucoid colonies.

In addition to culture on selective media, for confirmatory test biochemical test was performed, which includes

Table 4: Various tests performed.

Organism	Gram Staining/ morphology	I (Indole test)	M (MR test)	V (VP test)	C (Citrate test)
Organism 1 (<i>E. coli</i>)	Gram-ve/rod-shaped morphology	Positive	Positive	Negative	Negative
Organism 2 (<i>Salmonella</i>)	Gram-ve/rod-shaped morphology	Negative	Positive	Negative	Negative

the Gram Staining, Indole test, MR/VP test, and Citrate test.

According to Table 4, bacterial strains performing Gram-staining displayed a rod-shaped morphology and exhibited Gram-negative staining. The fruits and vegetables gave a Positive test for the Indole test for the first strain by producing a red ring on the top of the media when Kovach’s reagent was added to it, while it gave a negative Indole test for the second strain. Additionally, both strains tested positive for the MR test as the red color appeared in the tube when methyl red was added. However, both the first

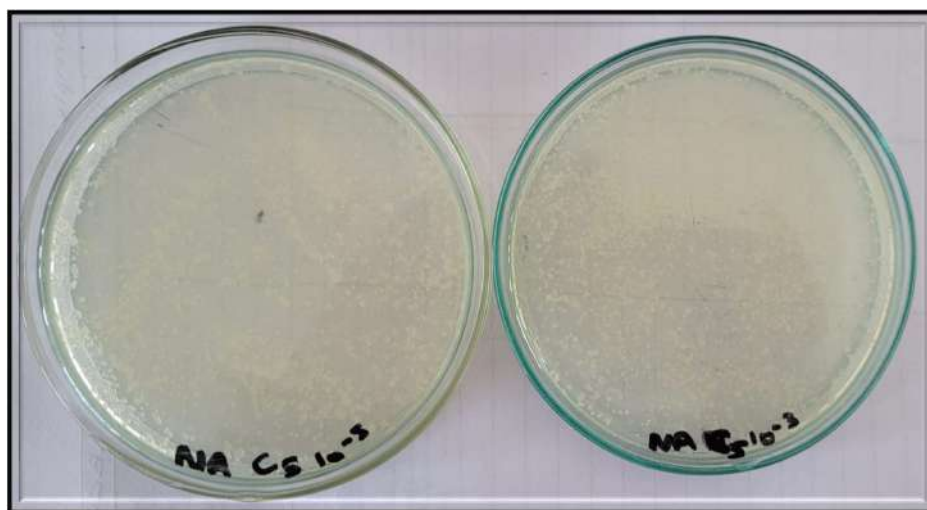


Fig. 1: Total viable bacterial count (TVBC) at different dilutions.

and second strains tested negative for the VP and Citrate tests.

DISCUSSION

The use of different biological and chemical agents in warfare, their production, and their development were recognized in the 1960s (Ranbir et al. 2022). The importance

of microbial forensics along with molecular epidemiology needs to be recognized to answer the legal questions that are related to the anthropogenic incidents affecting society through outbreaks as well as biological attacks (Roselló-Soto et al. 2018). In the year 1984, an outbreak affected almost 751 people in Dalles, Oregon, out of which 45 were also hospitalized because of Salmonella. Similarly, in May 2000,



Fig. 2: Showing a greenish metallic sheen indicating the presence of *E. coli*.

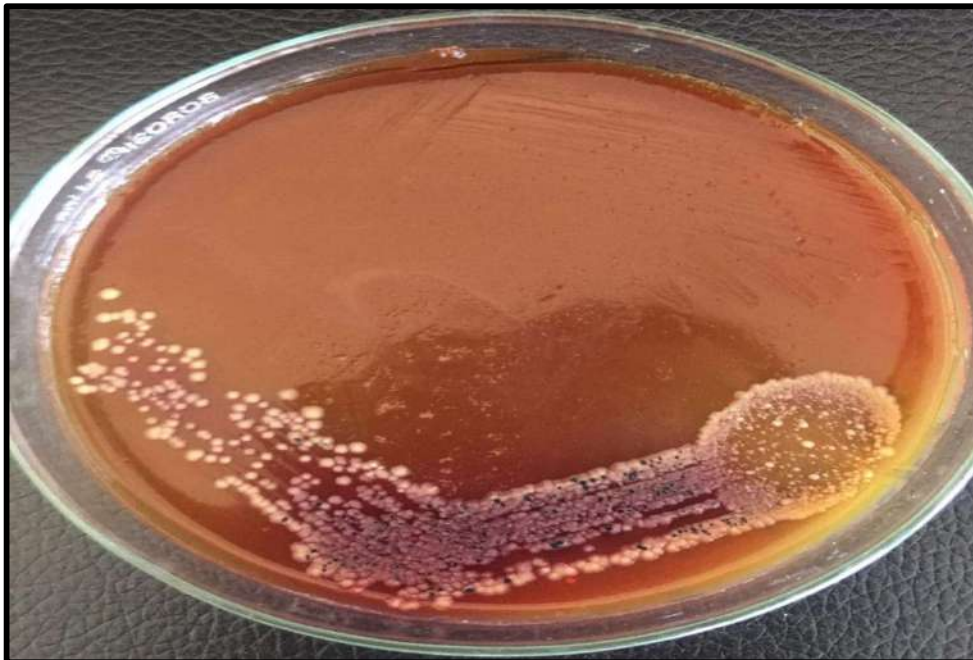


Fig. 3: Showing black colonies indicating the presence of *Salmonella*.

an outbreak due to the *E. coli* strain was identified due to which 2300 cases were reported and 7 deaths were recorded in Walkerton, Canada (Putnik et al. 2018). Microbial forensics was closely associated with the identification of perpetrators involved in biological attacks. Microbial agents can be used as bioweapons to take part in biocrime and bioterrorism (Abd Elkarim et al. 2022). Forensic investigation, with the help of Microbiology, can help to narrow down the type of crime that has taken place using microbial agents and also the person or group that may be involved in the crime (Burcham & Jordan 2017). Hence, to determine the type of crime committed, microbial forensics should be an integral part of a forensic investigation, i.e., bio crime, biowarfare, or bioterrorism. Biocrime is a crime that affects a specific individual using a microbial agent, while bioterrorism is the use of a microbial agent to harm a targeted community (Al-Jassani 2023).

The pathogenic bacteria were found in large amounts in the research conducted on spoiled food products (Venkatramanan et al. 2020). Their percentage of multi-drug resistant isolates was also high, causing harm to human health and resulting in food-borne illnesses (Vidic et al. 2019). Microbial forensics has an advantage: its protocol holds out against legal inquiry (Aljohni et al. 2021). The results obtained from the microbial forensic investigation can be used as evidence that might either support or neglect the allegations made in front of the court. 600 million cases with 4,20,000 deaths per year have been estimated by WHO (Callejón et al. 2015). Around 879 million tons of vegetables and 513 million tons of fruits are produced in Asia. The consumption of raw or partially cooked vegetables and fruits is high in Asian countries. Even though the consumption of organic fruits and vegetables is higher in Asian countries, the rate of contamination is great in organically grown crops, as animal manure is used as fertilizer. Contamination with pathogens can be introduced at different stages of the production of fruits and vegetables (De Giglio et al. 2017).

Different researchers carried out many studies to identify the contamination of fruits and vegetables by pathogenic microorganisms (El Sheikha & Mahmoud, 2016). A study was carried out by Al-Kharousi et al. (2016) to examine the presence of pathogenic bacteria in fresh fruits and vegetables, which concluded that the microbial communities found in the fresh produce of fruits and vegetables can act as opportunistic pathogens and cannot be ruled out instead. It should be provided with better management to improve the microbial quality of the fresh produce (Al-Kharousi et al. 2016).

In developing countries like Nepal, poverty along with poor sanitation is very common, leading to multiple outbreaks of human gastroenteritis caused by of ingestion

of faecally infected food (Shuping & Eloff, 2017). In 2020, conducted research on street food and found that these food items which are inexpensive and easily accessible, contained a large number of pathogenic bacteria, which was causing high health problems in their consumers (Rudhy 2017). From their research, it was concluded that creating food safety and public awareness is very important for reducing foodborne illnesses. As fruits and vegetables are consumed without any thermal treatment, it cause bacterial contamination (Plotka-Wasyłka et al. 2017). A study carried out in 2020, concluded that fresh fruits and vegetables are mostly eaten raw without providing heat treatment or washing them, which act as the best vector for transmitting different pathogenic microorganisms and are having great risk to human health. Hence, different awareness programs should be conducted to provide safety measures for buying and selling fruits and vegetables with hygienic practices (Piombo et al. 2021).

Vegetables and fruits are sold in open markets among which most of them are eaten raw, which allows bacterial contamination, providing a suitable environment (Bwambok et al. 2020). In 2022, research will be carried out to identify bacteria present in vegetable salads found in different local markets (Oliveira et al. 2020). Researchers identified different pathogenic bacteria from the salad, along with the detection of their resistant genes (Vaishnav et al. 2016). Researchers concluded that the safety and the microbial quality of ready-to-eat salads can be challenging for the human population (Asgari 2022). To understand the extent and transmission of the microbial agent across the infected community, the study of outbreak events is required, which will provide light on the emerging field of Forensics, i.e., Microbial forensics, a combination of microbiology and forensics (Umapathi et al. 2022). Identification of accurate microbial agents by applying different physical, biochemical, and molecular tests can help provide information about the person responsible for the attack (Al-Zaidi et al. 2022).

CONCLUSION

It is concluded that the investigation of outbreaks of infectious diseases can be done by identifying the microbial agent. Microbial agent gives us important information about their drug vulnerability, their sources, their transmission routes or pathways, and the factors enhancing their transmission. By determining the presence of microbial agents and their characteristics, it can be estimated whether the contamination of food is intentional and can be redefined as a bio-crime or bioterrorist attack. Samples of fruits and vegetables were examined microbiologically. The results were obtained, which gave a huge number of bacterial count, and also *E. coli* and *Salmonella* were detected. Strain under

investigation compared with reference sources, assumptions made, examined, and the person or group that could have intentionally caused the outbreak can be narrowed down. It can be observed that the maximum number of bacteria were found in guava and grapes (TMTC), i.e., Too Many to Count, followed by carrots. Spinach, cucumber, strawberry, cherry, and tomato were moderately contaminated. Apple was the least contaminated among all the fruits and vegetables. *E. coli* and *Salmonella* displayed rod-shaped morphology and exhibited Gram-negative staining. The fruits and vegetables gave a positive test for the Indole test for the first strain by producing a red ring on the top of the media when Kovach's reagent was added to it, while it gave a negative Indole test for the second strain. Additionally, both strains tested positive for the MR test as the red color appeared in the tube when methyl red was added. However, both the first and second strains tested negative for the VP and Citrate tests. This research can be directly connected with the field of microbial forensics as well as forensic epidemiology.

REFERENCES

- Abd Elkarim, M., Hegazy, E.E. and Zamzam, A. S. A. 2022. Microbiological study of some commonly used foods and drinks in Tanta Al Gharbia Governorate. *Microb. Infect. Dis.*, 3(4): 1032-1043.
- Al-Jassani, M.J. 2023. Evaluation of the antimicrobial potential of phenolic compounds extracted from banana peels (*Musa paradisiaca* L.) against *S. aureus* and *S. typhimurium* In meat and fish. *J. Survey in Fish. Sci.*, 10(3S): 2048-2054.
- Aljohni, A.R.S., Almotiri, T.R., Ibrahim, T., Alhazmy, G.K.S.A. and Mhmodi, F.O.A. 2021. New perspectives on enteric pathogenic bacteria bacterium *Escherichia coli*. *Acta Sci. Microbiol.*, 4(12): 455.
- Al-Kharousi, Z.S., Guizani, N., Al-Sadi, A.M., Al-Bulushi, I.M. and Shaharouna, B. 2016. Hiding in fresh fruits and vegetables: opportunistic pathogens may cross geographical barriers. *Int. J. Microbiol.*, 14: 417. <https://doi.org/10.1155/2016/4292417>.
- Al-Zaidi, Q., Diguľá, C.F., Dopcea, G. and Matei, F. 2022. Conventional versus modern techniques used for the detection of pathogens in food matrices: a review. *Sci. Bull. Ser. F Biotechnol.*, 26(1): 56.
- Asgari, S. 2022. Separation and Detection of Chemical and Biological Contaminants in Fresh Produce by Plasmofluidic Device. Doctoral Dissertation, University of Missouri, Columbia.
- Burcham, Z.M. and Jordan, H.R. 2017. History, current, and future use of microorganisms as physical evidence. *Forensic Microbiol.*, 12: 25-55.
- Bwambok, D.K., Siraj, N., Macchi, S., Larm, N.E., Baker, G.A., Pérez, R.L. and Fakayode, S. O. 2020. QCM sensor arrays, electroanalytical techniques and NIR spectroscopy coupled to multivariate analysis for quality assessment of food products, raw materials, ingredients, and foodborne pathogen detection: Challenges and breakthroughs. *Sensors*, 20(23): 6982.
- Callejón, R.M., Rodríguez-Naranjo, M.I., Ubeda, C., Hornedo-Ortega, R., García-Parrilla, M. C. and Troncoso, A.M. 2015. Reported foodborne outbreaks due to fresh produce in the United States and European Union: trends and causes. *Foodborne Pathog. Dis.*, 12(1): 32-38. <https://doi.org/10.1089/fpd.2014.1821>
- De Giglio, O., Caggiano, G., Bagordo, F., Barbuti, G., Brigida, S., Lugoli, F. and Montagna, M.T. 2017. Enteric viruses and fecal bacteria indicators to assess groundwater quality and suitability for irrigation. *Int. J. Environ. Res. Public Health.*, 14(6): 558.
- El Sheikha, A.F. and Mahmoud, Y.A.G. 2016. Bread Fungal Contamination: Risk of Mycotoxins, Protection of Anti-Fungal, and Need for Fungal Identification. Bread and Its Fortification for Nutrition and Health Benefits. In Rosell, C.M., Bajerska, J. and Sheikha, A.E.E. (eds), *Bread and its Fortification for Nutrition and Health Benefits*, Science Publishers, Inc., New Hampshire; CRC Press, Florida, USA, pp. 150-162.
- Ghazali, N.S.H. and Rashid, N. 2019. Molecular identification of bacterial communities from vegetable samples as revealed by DNA sequencing of universal primer 16S rRNA gene. *Int. J. Med. Sci.*, 4(1): 19-26.
- Hussain, B., Chen, J.S., Hsu, B.M., Chu, I.T., Koner, S., Chen, T.H. and Chan, M.W. 2021. Deciphering bacterial community structure, functional prediction, and food safety assessment in fermented fruits using next-generation 16S rRNA amplicon sequencing. *Microorganisms*, 9(8): 1574.
- Kubba, M.A., Hussein, S.M. and Al-Zaidi, O. S. 2021. The effect of *Allium sativum* (garlic extract) as a prebiotic substance on the activity of probiotic bacteria *Lactobacillus acidophilus* against some local isolates of pathogenic bacteria. *Indian J. Forensic Med. Toxicol.*, 15(2): 387-394.
- Oliveira, M., Mason-Buck, G., Ballard, D., Branicki, W. and Amorim, A. 2020. Biowarfare, bioterrorism, and crime: A historical overview on microbial harmful applications. *Forensic Sci. Int.*, 314: 110366. <https://doi.org/10.1016/j.forsciint.2020.110366>
- Piombo, E., Abdelfattah, A., Droby, S., Wisniewski, M., Spadaro, D. and Schena, L. 2021. Metagenomics approaches for the detection and surveillance of emerging and recurrent plant pathogens. *Microorganisms*, 9(1): 188.
- Plotka-Wasyłka, J., Rutkowska, M., Owczarek, K., Tobiszewski, M. and Namieśnik, J. 2017. Extraction with environmentally friendly solvents. *TrAC Trends Anal. Chem.*, 91: 12-25.
- Putnik, P., Lorenzo, J.M., Barba, F.J., Roohinejad, S., Režek Jambak, A., Granato, D. and Bursać Kovačević, D. 2018. Novel food processing and extraction technologies of high-added value compounds from plant materials. *Foods*, 7(7): 106.
- Ranbir, K.M., Singh, G., Singh, J., Kaur, N. and Singh, N. 2022. Machine learning-based analytical systems: Food Forensics. *ACS Omega.*, 7(51): 47518-47535.
- Roselló-Soto, E., Garcia, C., Fessard, A., Barba, F.J., Muneke, P. E., Lorenzo, J.M. and Remize, F. 2018. Nutritional and microbiological quality of tiger nut tubers (*Cyperus esculentus*), derived plant-based and lactic fermented beverages. *Fermentation*, 5(1): 3.
- Rudhy, R.T. 2017. Isolation, Identification, and Molecular Characterization of Pathogenic Organisms Obtained from Meat Samples (Cooked, Semi-Cooked, and Raw) of Different Areas of Dhaka City. Doctoral Dissertation, BRAC University, Dhaka, Bangladesh.
- Shuping, D.S.S. and Eloff, J.N. 2017. The use of plants to protect plants and food against fungal pathogens: A review. *Afr. J. Trad. Compl. Alt. Med.*, 14(4): 120-127.
- Umapathi, R., Rani, G.M., Kim, E., Park, S.Y., Cho, Y. and Huh, Y.S. 2022. Sowing kernels for food safety: Importance of rapid on-site detection of pesticide residues in agricultural foods. *Food Front.*, 4(3): 666-676.
- Vaishnav, A., Upadhyay, K., Tipre, D. and Dave, S. 2016. Characterization of potent exopolysaccharide-producing bacteria isolated from fruit pulp and potato peels and enhancement in their exopolysaccharide production potential. *J. Microbiol. Biotechnol. Food Sci.*, 6(3): 874.
- Venkatramanan, M., Sankar Ganesh, P., Senthil, R., Akshay, J., Veera Ravi, A., Langeswaran, K. and Shankar, E.M. 2020. Inhibition of quorum sensing and biofilm formation in *Chromobacterium violaceum* by fruit extracts of *Passiflora edulis*. *ACS Omega*, 5(40): 25605-25616.
- Vidic, J., Vizzini, P., Manzano, M., Kavanaugh, D., Ramarao, N., Zivkovic, M. and Gadjanski, I. 2019. Point-of-need DNA testing for detection of foodborne pathogenic bacteria. *Sensors*, 19(5): 1100.
- Yeung, M. 2016. Microbial forensics in food safety. *Microbiol. Spect.*, 4(4): 4-14.
- Zambelli, R.A. and Brasil, I. M. 2022. Molecular techniques for identification applied to food: A review. *Int. J. Agric. Sci Food Technol.*, 8(4): 305-315.



Statistical Performance of Gridded Rainfall Datasets Over Ungauged Jalaur River Basin, Philippines

Christsam Joy S. Jaspe-Santander^{*(**)}†  and Ian Dominic F. Tabañag^{*(***)} 

*School of Engineering, University of San Carlos, Talamban, Cebu City, 6000, Philippines

**College of Engineering, Central Philippine University, Jaro, Iloilo City 5000, Philippines

***Philippine Council for Industry, Energy, and Emerging Technology Research and Development, Department of Science and Technology (DOST-PCIEERD), Bicutan, Taguig City 1631, Philippines

† Corresponding author: Christsam Joy S. Jaspe-Santander; cjjsantander@cpu.edu.ph

Nat. Env. & Poll. Tech.
Website: www.neptjournal.com

Received: 07-09-2023

Revised: 15-12-2023

Accepted: 22-12-2023

Key Words:

Gridded rainfall dataset
Jalaur river basin
Ungauged basin

ABSTRACT

The study presented aims to find the most appropriate climate dataset for the data-scarce Jalaur River Basin (JRB), Iloilo, Philippines, by evaluating the statistical performance of five rainfall datasets (APHRODITE, CPC NOAA, ERA5, SA-OBS, and PGF-V3) with resolutions of 0.25° and 0.5° having a time domain of 1981 to 2005. Bilinear interpolation implemented through Climate Data Operator (CDO) was used to extract and process grid climate datasets with Linear scaling as bias correction to minimize product simulation uncertainties. The datasets were compared to the lone meteorological station nearest to JRB investigated at monthly and annual timescales using six statistical metrics, namely, Pearson's correlation coefficient (r), coefficient of determination (R^2), modified index of agreement (d_r), Kling-Gupta efficiency, Nash-Sutcliffe efficiency (NSE), and RMSE-observations standard deviation ratio (RSR). The results indicate a strong positive correlation with the observed data for both rainfall and temperature ($r > 0.8$; R^2 , $d_r > 0.80$). Although graphical observation shows an underestimation of rainfall, goodness-of-fit values indicate very good model performance (NSE, KGE > 0.75 ; RSR < 0.50). In terms of temperature, variable responses are observed with significant overestimation for maximum temperature and underestimation for minimum temperature. SA-OBS proved to be the best-performing dataset, followed by ERA5 and PGF-V3. These key findings supply useful information in deciding the most appropriate gridded climate dataset for hydrometeorological investigation in the JRB and could enhance the regional representation of global datasets.

INTRODUCTION

High-resolution gridded climate data are necessary input parameters for atmospheric, climatic, hydrological, and ecological studies to establish the hydrological characteristics of a watershed. They are particularly important in modeling and simulation for the evaluation of numerical forecast datasets and impact studies. However, due to the geographical conditions and the shortage of meteorological observations in the Philippines, it is challenging to obtain accurate regional area rainfall amounts in river basins.

The availability of rainfall data is still a major issue in water resource studies (Nassaj et al. 2022, Ang et al. 2022). The quality of rainfall data is critical in the development of a reliable hydrological model to generate streamflow estimates and trends over extended periods (Try et al. 2020). In regions where rainfall data is limited and coarsely distributed, gridded satellite and reanalysis climate datasets

have been widely used to supply the lack of long-term, high-spatial-resolution data (Peralta et al. 2020). However, these datasets vary in spatial resolution and temporal coverage and are highly influenced by their method of production (Ayoub et al. 2020).

Numerous studies have used gridded datasets as an alternate input for gauged data in hydrological modeling applications. Ang et al. (2022) evaluated seven gridded meteorological datasets of rainfall and air temperature covering the data-sparse Tonle Sap Lake Basin in Cambodia. Schumacher et al. (2020) described the performance of five gridded datasets in reproducing rainfall and/or temperature over the complex terrain in the high Chilean Andes, and Try et al. (2020) assessed the performances of various gridded rainfall datasets in rainfall-runoff and flood-inundation modeling of the Mekong River Basin.

This study focused on the statistical evaluation of five

rainfall datasets (APHRODITE, CPC NOAA, ERA5, SA-OBS, and PGF-V3) and four temperature datasets (CPC NOAA, ERA5, SA-OBS, and PGF-V3) to investigate their reliability as alternative climate data source to characterize the climate conditions in JRB. These datasets were compared with the lone ground-based observation station in the basin to identify the most accurate data source that could be used in further evaluation and analysis to characterize the climate condition of the study area.

MATERIALS AND METHODS

Study Area

The Jalaur River Basin (JRB) lies between $10^{\circ}45'$ to $11^{\circ}10'$ North latitude and $122^{\circ}12'$ to $122^{\circ}55'$ East longitude in Panay Island, Philippines. The basin area is 1650 sq km, receiving approximately 2100 mm of rainfall annually. An estimated population of 430,000 reside within the basin, with agriculture as the main source of livelihood. A sizable percentage of land is dedicated for agricultural purposes (45%). The remaining part is classified as grassland/shrubland (39%), woodland/forest (15%) and wetland (1%). Long-term rainfall and temperature data are recorded in the lone meteorological station near the basin, while five (5) flow gauging stations are located along the main river and its tributaries (Fig. 1).

The JRB is projected to be in critical condition in water availability and accessibility by 2025 due to climate and anthropogenic changes. It is crucial to study its hydrologic characteristics and develop a quantitative prediction model to assess its hydrologic response to these changes (Arceo et al. 2018).

Climate Datasets

The observed gauge-based rainfall dataset in the JRB is limited. High-quality daily observation of rainfall and maximum and minimum temperature is available for only one station acquired from the Philippine Atmospheric, Geophysical, and Astronomical Services Administration (PAGASA) dataset for the period 1951-2009. Considering temporal availability and spatial resolution and from previous studies in the Asian region, five rainfall datasets (APHRODITE, CPC NOAA, ERA5, SA-OBS, and PGF-V3) and four temperature datasets (CPC NOAA, ERA5, SA-OBS, and PGF-V3) are investigated (Table 1).

APHRODITE is a long-term daily rainfall and temperature dataset developed by the Research Institute for Humanity and Nature and the Meteorological Research Institute of Japan Meteorological Agency. These rainfall records are produced from dense rain-gauge observation networks covering domains of Monsoon Asia, the Middle East, and Northern Eurasia, available at 0.25° and 0.5° resolutions, and for Japan

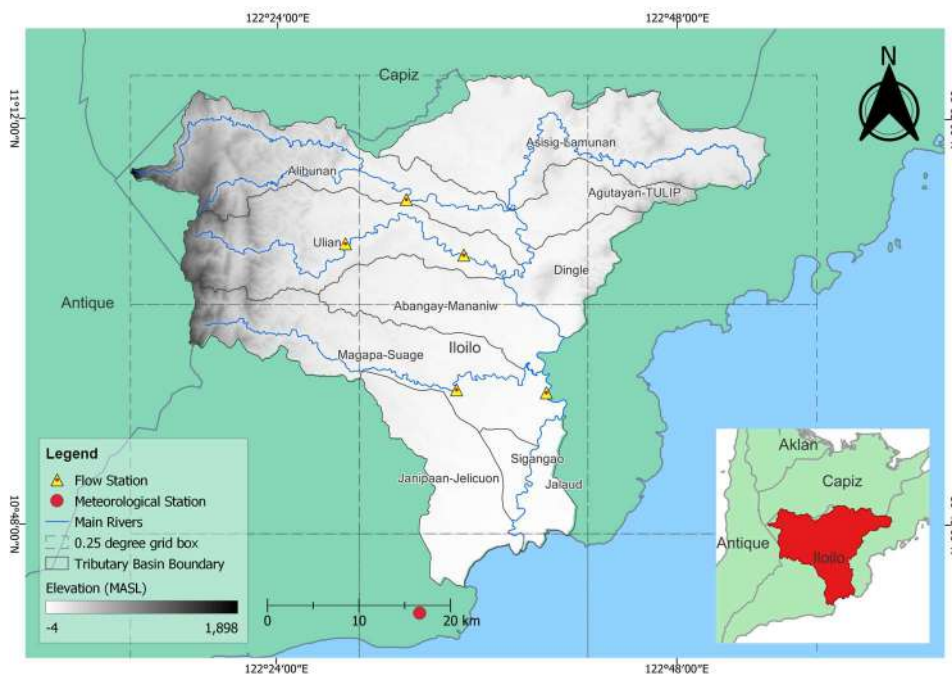


Fig. 1: Location Map of the Jalaur River Basin. The dashed boxes represent $0.25 \times 0.25^{\circ}$ grid cells. The inset indicates the location of the JRB in Panay Island, Philippines.

at 0.05° resolution (Yatagai et al. 2012).

CPC NOAA is a global reanalysis dataset by the American National Oceanic and Atmospheric Administration (NOAA). The Global Telecommunication System (GTS) network’s interpolated station-based observation data records were originally used to create this collection (Fan & Van Den Dool 2008). CPC NOAA is now accessible at 0.5° resolutions from 1948 to the present day and is obtained from over 30,000 gauged data provided by various national and international institutions.

ERA5 or ECWMF Reanalysis v5 is the replacement for ERA-Interim reanalysis. It is an hourly estimate of atmospheric, land, and oceanic climate variables produced by the Copernicus Climate Change Service (C3S). ERA5 uses modeling and data assimilation tools to aggregate enormous volumes of historical information into global estimations. The dataset is available at 0.25° resolutions from 1959 to the present day (Hersbach et al. 2020).

PGF-V3 is a hybrid of observational and reanalysis datasets created by integrating NCEP/NCAR reanalysis data and global observation-based datasets. This dataset, developed by the Department of Civil Engineering, Princeton University, is available at 0.25° resolutions from 1948 to 2016 (Sheffield et al. 2006).

SA-OBS is a high spatial resolution daily gridded data that covers the Southeast Asian region and is based on the station data collated by the Southeast Asia Climate Assessment and Dataset (SACA&D). Meteorological stations throughout Southeast Asia supply these data. The dataset is available at 0.25° and 0.5° resolutions and spans the period 1981 to 2017 (Van Den Besselaar et al. 2017).

Data Processing

The bilinear interpolation method through Climate Data Operators (CDO) was used to extract data to the location of the ground-based meteorological station. This method is

recommended for grid location-based continuous datasets, by calculating the point value using the distance-weighted value of the four nearest points (Schulzweida et al. 2012).

Linear Scaling was applied as a bias correction method (Shrestha 2015). The mean monthly values of the corrected and observed dataset are perfectly matched. The monthly correction factor is developed based on the differences between observed and raw data. The correction factor for rainfall is developed as a multiplier, while the temperature correction factor is an additive.

$$P_{cor,m,d} = P_{raw,m,d} \times \frac{\mu(P_{obs,m})}{\mu(P_{raw,m})} \dots(1)$$

$$T_{cor,m,d} = T_{raw,m,d} + [\mu(T_{obs,m}) - \mu(T_{raw,m})] \dots(2)$$

Where $P_{cor,m,d}$ and $T_{cor,m,d}$ are corrected rainfall and temperature on the d th day of m th month, and $P_{raw,m,d}$ and $T_{raw,m,d}$ are the raw rainfall and temperature on the d th day of m th month. μ represents the correction factor (represents the mean value of observed rainfall at a given month m) (Fang et al. 2015).

Performance Evaluation of Gridded Rainfall and Temperature Datasets

The reliabilities of the rainfall and temperature datasets were evaluated by using the reference gauge method, where the grid climate datasets were directly compared with the observation at the reference gauge (Tian et al. 2021). Statistical and graphical evaluation was conducted in monthly and annual timescales from 1981-2000 for rainfall, and 1995-2000 for air temperature. Data validation for both datasets was done for the period 2001-2005.

Statistical evaluation indices used to assess the reliability of the gridded dataset were based on the evaluation by Legates & McCabe (1999) and Moriasi et al. (2007): Pearson’s correlation coefficient (r), coefficient of determination (R^2) modified index of agreement (d_1), Kling-Gupta efficiency, Nash-Sutcliffe efficiency (NSE), and RMSE-observations

Table 1: Description of rainfall and temperature datasets.

Parameter	Dataset*	Spatial Resolution	Temporal Resolution	Time Domain	Source Institution**
Rainfall	APHRODITE	0.25°	Daily	1951–2015	RISH, Kyoto University
Rainfall & Temperature	CPC NOAA	0.5°	Daily	1979-Present	NCEP/CPC
	ERA5	0.25°	Hourly	1979-Present	
	PGF-V3	0.25°	3-hourly, daily, monthly	1948-2016	Princeton University
	SA-OBS	0.25°	Daily	1981–2017	RNMI

*APHRODITE: Asian Precipitation - Highly-Resolved Observational Data Integration Towards Evaluation, CPC: Climate Prediction Center, ERA5: ECWMF Reanalysis v5, PGF-V3: Princeton Global Forcing v3, SA-OBS: Southeast Asia-Observational

**RISH = Research Institute for Sustainable Humanosphere, NCEP = National Centers for Environmental Prediction, RNMI = Royal Netherlands Meteorological Institute

Table 2: Statistical evaluation indices and their optimal values.

Index	Formula	Value Range	Optimal Value
r	$R = \frac{\sum(P_i - \bar{P})(O_i - \bar{O})}{\sqrt{\sum(P_i - \bar{P})^2 \sum(O_i - \bar{O})^2}}$	-1 to 1	1
R^2	$R^2 = \left[\frac{\sum_{i=1}^N (O_i - \bar{O})(P_i - \bar{P})}{\sqrt{\sum_{i=1}^N (O_i - \bar{O})^2} \sqrt{\sum_{i=1}^N (P_i - \bar{P})^2}} \right]^2$	0 to 1	1
d_1	$d_1 = 1 - \frac{\sum_{i=1}^N (O_i - P_i)}{\sum_{i=1}^N (P_i - \bar{O} + O_i - \bar{O})}$	0 to 1	1
NSE	$NSE = 1 - \left[\frac{\sum_{i=1}^N (O_i - P_i)^2}{\sum_{i=1}^N (O_i - \bar{O})^2} \right]$	$-\infty$ to 1	1
KGE	$KGE = \sqrt{(r - 1)^2 + \left(\frac{\sigma_p}{\sigma_o} - 1\right)^2 + \left(\frac{\bar{P}}{\bar{O}} - 1\right)^2}$	$-\infty$ to 1	1
RSR	$RSR = \frac{\sqrt{\sum_{i=1}^N (O_i - P_i)^2}}{\sqrt{\sum_{i=1}^N (O_i - \bar{O})^2}}$	0 to $+\infty$	0

* P_i and O_i denote predicted and observed, respectively, daily rainfall or temperature of the i^{th} day, \bar{P} and \bar{O} denote predicted and observed, respectively, mean daily rainfall or temperature, σ_p and σ_o denote predicted and observed, respectively, standard deviation for daily rainfall or temperature, and N is the amount of data at daily time series.

Table 3: General performance efficiency ratings for a monthly time step.

Performance Rating	NSE	KGE	RSR
Very Good	$0.75 < NSE \leq 1.00$	$0.75 < KGE \leq 1.00$	$0.00 < RSR \leq 0.50$
Good	$0.65 < NSE \leq 0.75$	$0.50 < KGE \leq 0.75$	$0.50 < RSR \leq 0.60$
Satisfactory	$0.50 < NSE \leq 0.65$	$0.00 < KGE \leq 0.50$	$0.60 < RSR \leq 0.70$
Unsatisfactory	$NSE \leq 0.50$	$KGE \leq 0.00$	$RSR > 0.70$

standard deviation ratio (RSR). Table 2 and Table 3 presents the optimal ranges and benchmarking categories (Moriiasi et al. 2007) of the statistical indices.

Pearson’s correlation coefficient (r) is a statistical test that measures the magnitude of association and direction of relationship between two continuous variables. The values of r range from -1 to 1, with $r = 0$ having no linear relationship. The coefficient of determination (R^2) measures the variance of the grid climate dataset that can be explained by the observed climate data. It quantifies the strength of linear relationship between variables, thus, being called the *goodness of fit model*. The modified index of agreement (d_1) is the modified version of the index of agreement proposed by Willmott (1981) to detect additive and proportional differences in the data. It is used as a standardized measure of the degree of model

prediction error (Ahmed et al. 2019, Willmott 1984). Higher values of R^2 and d_1 , i.e., close to 1, indicate higher accuracy of gridded datasets in estimating rainfall and air temperature.

Nash-Sutcliffe efficiency (NSE) determines the relative magnitude of the residual variance compared to the measured variance. It is used to measure how well a simulation can predict the outcome variable (Nash & Sutcliffe 1970). Kling-Gupta Efficiency (KGE) compares observed data with the grid data, considering the three elements of model error of Nash-Sutcliffe efficiency (NSE), i.e., correlation, bias, the ratio of variances, or coefficients of variation (Gupta et al. 2009). The value of NSE and KGE ranges from $-\infty$ to its optimal value of 1.

Root-mean-square error (RMSE) evaluates the quality of predictions by showing how far the predicted value is

from the measured true values. A model evaluation statistic by Singh et al. (2004) standardizes RSME values using the RMSE-observations standard deviation ratio (RSR). The value of RSR is determined by the ratio of the RMSE and standard deviation of measured data. The values vary from 0, which indicates a perfect model simulation of observed data, to large positive values. Lower RSR values indicate lower RMSE and better climate simulation performance.

RESULTS AND DISCUSSION

Rainfall

The grid-based climate products are evaluated and validated in monthly and annual timescales. The obtained time series are then compared along with the corresponding station-based time series. Scatter plots between the observed and grid rainfall at a monthly time scale, together with statistical indices (r , R^2 , d_f , NSE , KGE , RSR), are shown in Fig. 3. Graphical examination shows an underestimation of grid rainfall datasets for the evaluation period and slight overestimation for the validation period. High values of r , R^2 , and d_f for both periods indicate a high positive correlation between gridded and observed rainfall datasets. Exceptional goodness-of-fit is particularly observed for SA-OBS, followed by PGF-V3 and APHRODITE.

The values of NSE , KGE , and RSR allow us to make explicit interpretations of gridded datasets in estimating rainfall and air temperature. Gridded rainfall products show exceptionally good performance in simulating observed rainfall datasets for the evaluation period. The same can be said for the validation period, except for ERA5 having satisfactory performance with values of $NSE = 0.63$, and $RSR = 0.61$.

Gridded rainfall dataset performance varies for the annual timescale presented in Fig. 2. SA-OBS and PGF-V3 showed

the most acceptable association with the observed rainfall dataset with the lowest RSR values. Although, APH, CPC NOAA, and ERA5 showed good statistical performance when comparing monthly periods, underestimation in high rainfall years and overestimation in low rainfall years can be observed when comparing in annual periods.

Maximum and Minimum Temperature

Scatter plots between the observed and grid maximum and minimum temperature at a monthly time scale, together with statistical indices (r , R^2 , d_f , NSE , KGE , RSR), are shown in Fig. 4 and Fig. 5, respectively. Based on the correlation statistics on the monthly time period, SA-OBS showed exceptional results for both temperature parameters in the evaluation and validation period. The lowest correlation values for maximum temperature can be observed for CPC NOAA ($r=0.89$ $R^2=0.79$, $d_f=0.75$) and ERA5 for minimum temperature ($r=0.78$ $R^2=0.66$, $d_f=0.66$).

SA-OBS showcased exceptional accuracy and prediction performance for maximum temperature ($NSE=0.99$, $KGE=0.97$, $RSR=0.12$) and minimum temperature ($NSE=0.98$, $KGE=0.95$, $RSR=0.14$). CPC NOAA and ERA5 provided the opposite for the same statistical indicators.

The mean annual maximum and minimum temperature variation of the gridded rainfall dataset with the observed temperature is presented in Fig. 6. All datasets follow the annual temperature trend of the observed data, showing significant overestimation starting in 1999 for maximum temperature and underestimation from the same year for minimum temperature.

SA-OBS dataset consistently showed exceptional performance having the highest correlation and prediction power compared to the other datasets and better overall fit to the observed data. Additionally, the SA-OBS dataset

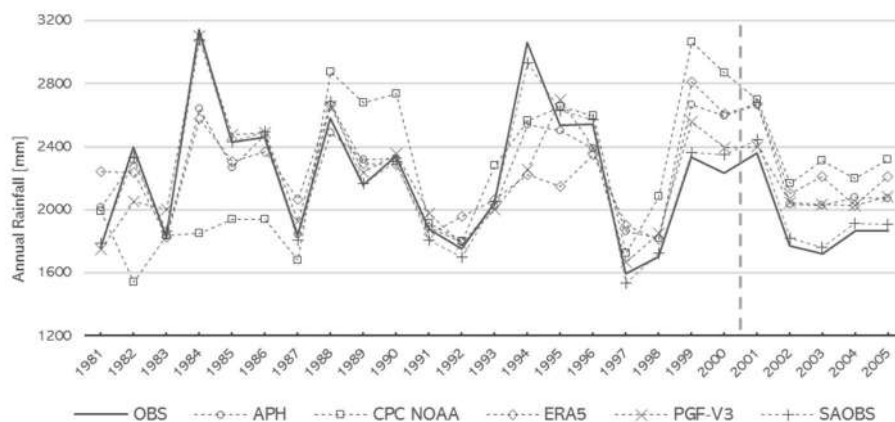


Fig. 2: Mean annual rainfall comparison for the period 1981-2005.

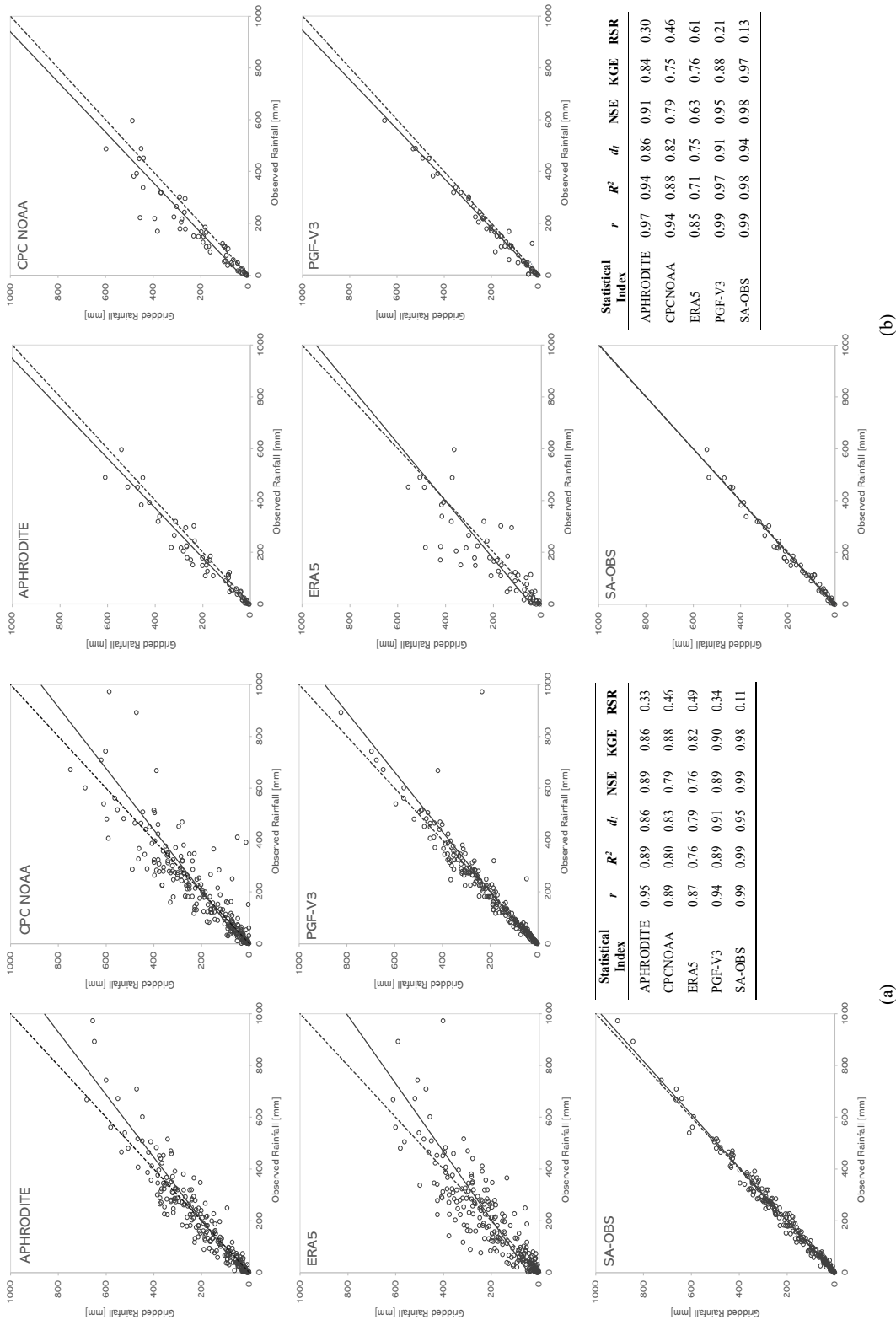


Fig. 3: Scatter plots and statistical indices of observed vs gridded daily rainfall dataset at the JRB for (a) the evaluation period of 1981 to 2000 and (b) the validation period 2001-2005. The dashed lines indicate a 1:1 line and solid lines denote linear regression.

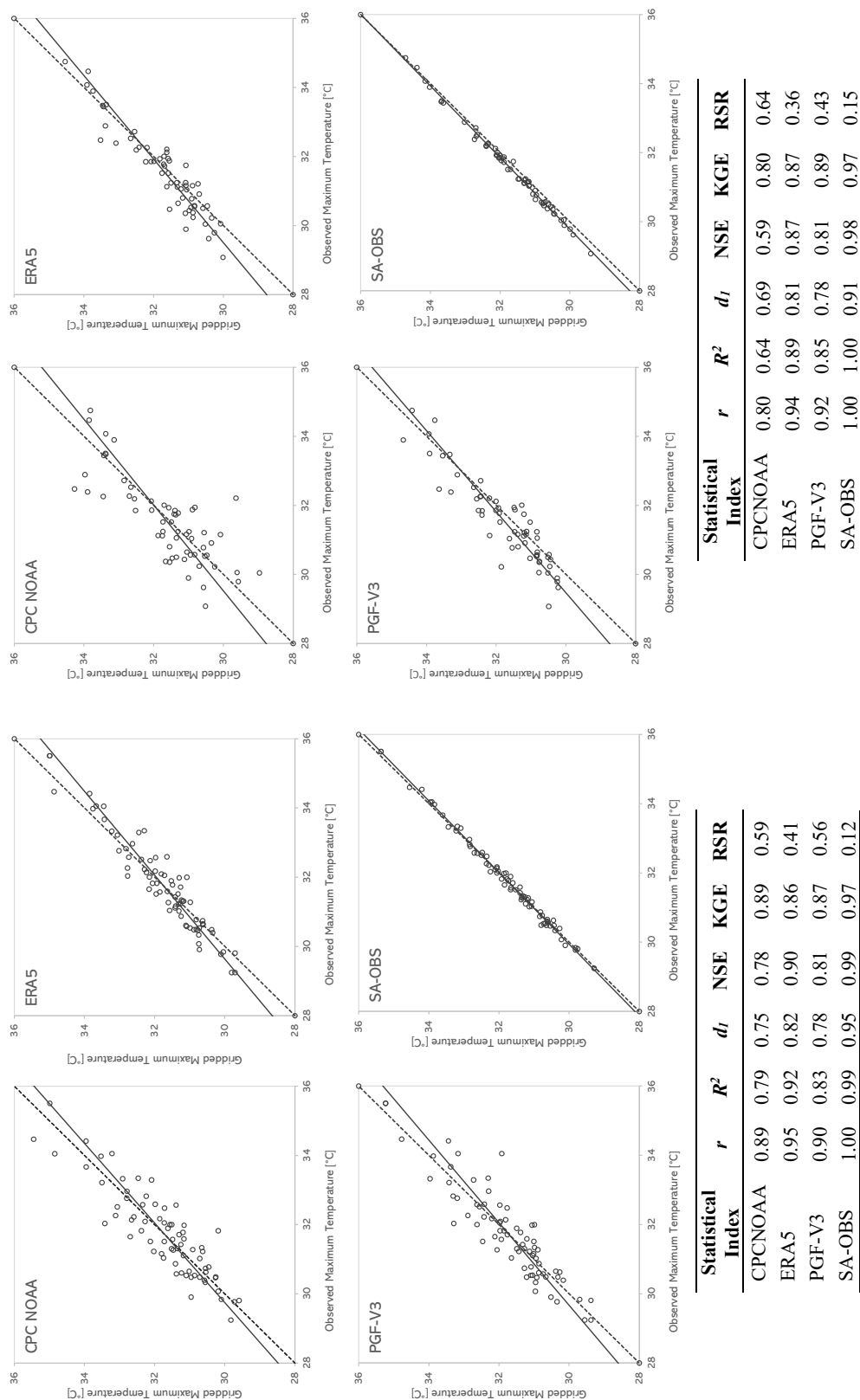
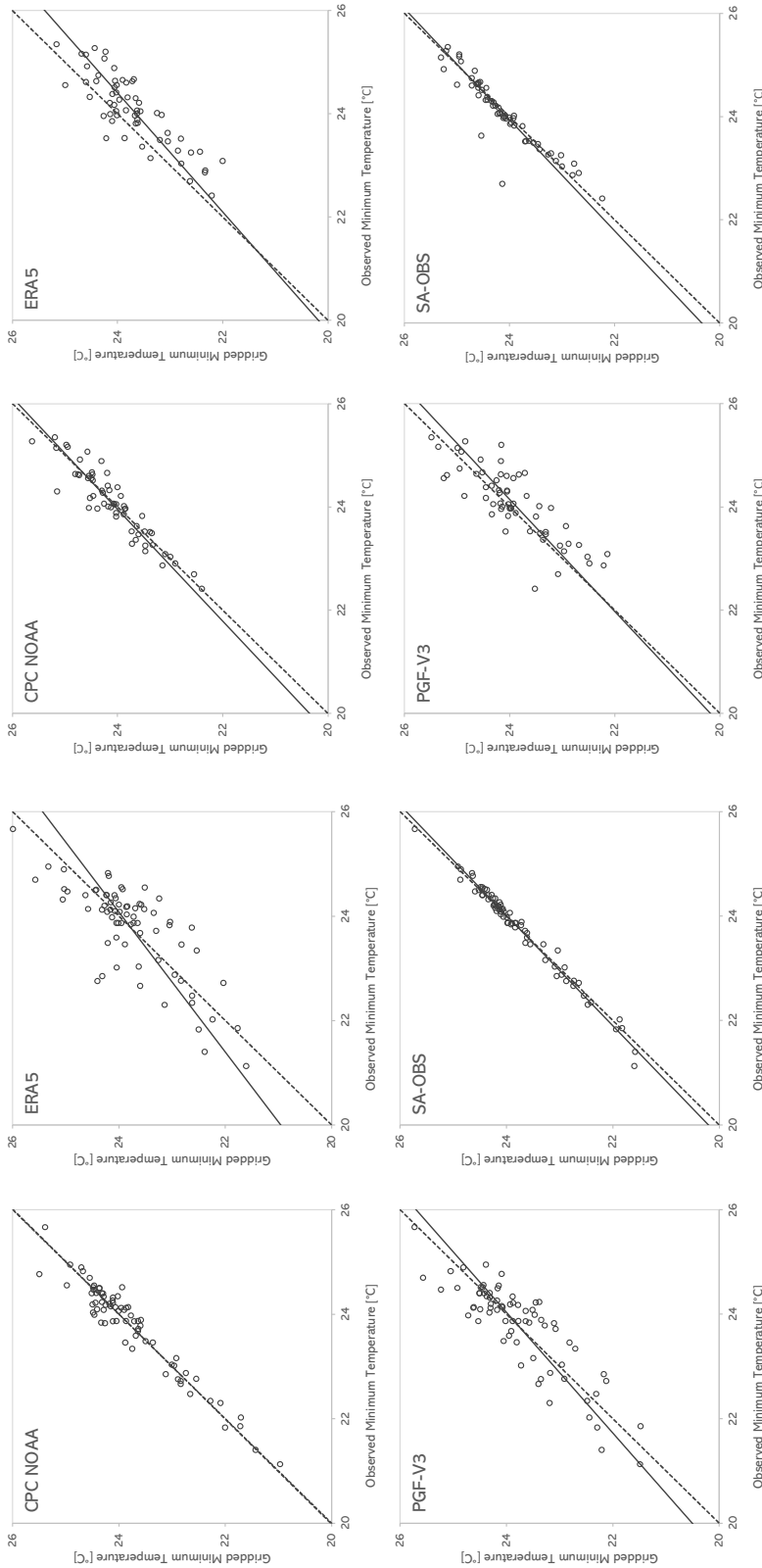


Fig. 4: Scatter plots and statistical indices of observed versus gridded daily maximum temperature at the JRB for (a) the evaluation period of 1995 to 2000; and (b) the validation period 2001-2005. The dashed lines indicate a 1:1 line and solid lines denote linear regression.



Statistical Index	r	R ²	d _I	NSE	KGE	RSR
CPCNOAA	0.91	0.82	0.81	0.80	0.90	0.44
ERA5	0.85	0.71	0.60	0.40	0.84	0.77
PGF-V3	0.83	0.68	0.69	0.55	0.79	0.67
SA-OBS	0.93	0.87	0.87	0.86	0.93	0.38

(b)

Statistical Index	r	R ²	d _I	NSE	KGE	RSR
CPCNOAA	0.97	0.93	0.86	0.93	0.95	0.27
ERA5	0.78	0.66	0.66	0.53	0.77	0.65
PGF-V3	0.87	0.78	0.73	0.73	0.87	0.51
SA-OBS	0.99	0.99	0.93	0.98	0.95	0.14

(a)

Fig. 5: Scatter plots and statistical indices of observed versus gridded daily minimum temperature at the JRB for (a) the evaluation period of 1995 to 2000; and (b) the validation period 2001-2005. The dashed lines indicate a 1:1 line and solid lines denote linear regression.

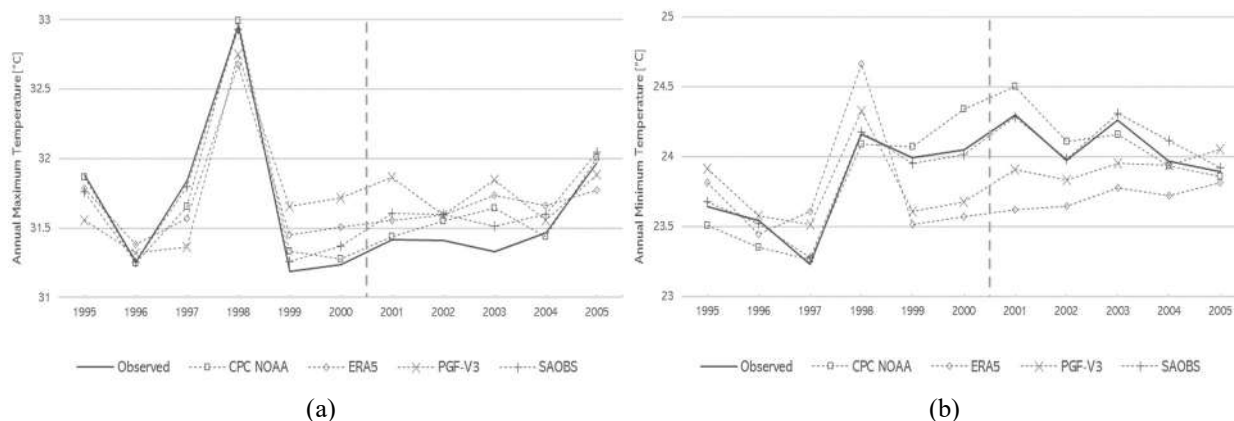


Fig. 6: Mean annual (a) maximum and (b) minimum temperature comparison for the period 1995-2005.

has the lowest RMSE-observation standard deviation ratio, indicating a closer match to the variability of the observed data. Based on the performance efficiency rating presented in Table 3, SA-OBS rated “very good” in all statistical metrics. These results suggest that the SA-OBS dataset performs exceptionally well in capturing the rainfall and temperature patterns in the Jalaur River basin compared to the other gridded datasets.

DISCUSSION

Evaluation and validation studies of gridded climate datasets in the Philippines have been conducted to augment the shortage of data availability in climate research. Salvacion et al. (2018) evaluated raw and downscaled CRU TS monthly gridded climate data in fifty-five meteorological stations throughout the country, concluding that both raw and downscaled gridded datasets showed acceptable performance with respect to rainfall data. Peralta et al. (2020) confirmed four (4) high-resolution gridded rainfall datasets, including APHRODITE, CHIRPSv2, PERSIAN_CDR, and TRMM, that represent the rainfall patterns in the country. Among these datasets, TRMM most accurately replicates the frequency and proportion of rainfall events spatially and temporally. The same dataset was used by Corporal-Lodangco & Leslie (2017) to define the climate zones in the country. However, a countrywide approach is conducted in these studies. Lee & Ahn (2022) recommend a more regional approach in the evaluation of meteorological datasets for future use in regional hydrological models.

A basin-level approach evaluated and validated five grid-based climate products for the Jalaur River Basin in this study. Results show an underestimation of grid rainfall datasets during the evaluation period and a slight overestimation during the validation period. Exceptional goodness-of-fit is observed for

SA-OBS, PGF-V3, and APHRODITE. Except for the ERA5 dataset, gridded rainfall products show good performance in simulating mean monthly observed rainfall datasets. Annual performance varies, with SA-OBS and PGF-V3 showing the most acceptable association with observed rainfall.

The SA-OBS dataset demonstrated exceptional performance in capturing rainfall and temperature patterns, which is consistent with the findings of Ge et al. (2019), where SA-OBS captured spatial distributions and patterns in the Indochina Peninsula, and Ang et al. (2022), where SA-OBS dataset displayed better estimates of seasonal patterns and magnitudes for both minimum and maximum temperatures in the Tonle Sap Basin in Cambodia. Van den Besselaar et al. (2017) observed a similar exceptional simulation of SA-OBS-based rainfall. Compared to other datasets, SA-OBS has been considered one of the more accurate rainfall and temperature estimations in Southeast Asia.

ERA5 rainfall data prove to be valuable in accurately capturing rainfall patterns in Central and East Asia; however, it is highly influenced by topography (Xin et al. 2022, Jiao et al. 2021, Zandler et al. 2020). Lavers (2022) evaluated ERA5 rainfall in the European region, indicating its good overall performance but highlighting the potential underestimation of extreme rainfall events at the daily timescale.

APHRODITE and CPC NOAA underestimated the values of rainfall data for the JRB. Ang et al. (2022) noted an identical tendency of APHRODITE data to underestimate rainfall in the Tonle Sap Lake Basin of Cambodia. Saidah et al. (2019) indicated similar findings for CPC NOAA on the Island of Lombok in Indonesia, further stating that CPC NOAA has poor prediction performance and needs to be calibrated before utilization.

It is important to acknowledge that no gridded dataset can perfectly replicate the actual observation datasets. The

choice of an appropriate dataset for a specific study should be guided by its capability to accurately represent the specific attributes of the data necessary for particular research.

CONCLUSION

This research paper has addressed the critical issue of obtaining accurate and reliable high-resolution climate data for the ungauged Jalaur River Basin in the Philippines. Due to geographical constraints and limited meteorological observations, the study explored the use of gridded rainfall and temperature datasets as alternative sources of climate data. The findings are crucial for various fields, including hydrology, climate modeling, and environmental impact assessments, to better understand the hydrological characteristics of this region and its response to changing climate conditions.

The study evaluated five rainfall datasets (APHRODITE, CPC NOAA, ERA5, SA-OBS, and PGF-V3) and four temperature datasets (CPC NOAA, ERA5, SA-OBS, and PGF-V3) by comparing them with ground-based observations from a single station within the Jalaur River Basin. The statistical analysis employed various indices, including Pearson's correlation coefficient, coefficient of determination, modified index of agreement, Kling-Gupta efficiency, Nash-Sutcliffe efficiency, and RMSE-observations standard deviation ratio. These evaluations were conducted on monthly and annual timescales.

Exceptional goodness-of-fit was observed for SA-OBS, PGF-V3, and APHRODITE in terms of rainfall data, indicating a high positive correlation and accuracy in simulating observed rainfall, especially on a monthly timescale. ERA5 showed satisfactory performance with rainfall data on an annual timescale but was less accurate in capturing high and low rainfall years. For temperature data, SA-OBS consistently demonstrated exceptional performance, with the highest correlation, prediction power, and the lowest RSR values. It provided the best overall fit to the observed data for both maximum and minimum temperatures. CPC NOAA and ERA5 performed less favorably in replicating temperature patterns, particularly maximum temperature, suggesting potential challenges with these datasets in this region.

The results suggest that the SA-OBS dataset is a reliable and accurate source of climate data for this region and is well-suited for further research and analysis. The paper also emphasized that no gridded dataset can perfectly replicate observed data, and the choice of an appropriate dataset should be guided by the specific attributes required for a given research application.

The findings of this study have significant implications

for water resource management and climate research in the Jalaur River Basin. Understanding the reliability of gridded climate datasets is essential for assessing the basin's hydrological response to climate and anthropogenic changes. The study also emphasizes the importance of installing weather stations to improve data collection, especially in major water resources.

In summary, this research contributes to the knowledge and methodology of assessing gridded climate dataset's performance in data-sparse regions, providing valuable insights for future hydrological modeling, climate impact studies, and water resource management efforts in the Jalaur River Basin and similar areas with limited meteorological observations.

ACKNOWLEDGMENT

The authors would like to thank the Philippine Atmospheric, Geophysical, and Astronomical Services Administration for providing the gauged climate data. This research is supported by Central Philippine University and the Department of Science and Technology – Engineering Research and Development for Technology Program of the University of San Carlos.

REFERENCES

- Ahmed, K., Shahid, S., Wang, X., Nawaz, N. and Khan, N. 2019. Evaluation of Gridded Precipitation Datasets Over Arid Regions of Pakistan. *Water*, 11(2): 210.
- Ang, R., Kinouchi, T. and Zhao, W. 2022. Evaluation of Daily Gridded Meteorological Datasets For Hydrological Modeling in Data-Sparse Basins of the Largest Lake in Southeast Asia. *J. Hydrol. Reg. Stud.*, 42: 101135.
- Arceo, M.G.A., Cruz, R.V., Tiban, C., Jr., Balatibat, J. and Alibuyog, N. 2018. Modeling the Hydrologic Responses to Land Cover and Climate Changes of Selected Watersheds in the Philippines Using the Soil and Water Assessment Tool (Swat) Model. *Dlsu Bus. Econ. Rev.*, 28: 84-101.
- Ayoub, A. B., Tangang, F., Juneng, L., Tan, M. L. and Chung, J. X. 2020. Evaluation of Gridded Precipitation Datasets In Malaysia. *Remote Sens.*, 12(4): 613.
- Corporal-Lodangco, I.L. and Leslie, L.M. 2017. Defining Philippine Climate Zones Using Surface and High-Resolution Satellite Data. *Proceed. Comput. Sci.*, 114: 324-332.
- Fan, Y. and Van Den Dool, H. 2008. A Global Monthly Land Surface Air Temperature Analysis For 1948–Present. *J. Geophys. Res.*, 113(D1): 56
- Fang, G., Jian, Y., Chen, Y. and Zammit, C. 2015. Comparing Bias Correction Methods in Downscaling Meteorological Variables For A Hydrologic Impact Study in an Arid Area in China. *Hydrol. Earth Syst. Sci.*, 19(6): 2547-2559.
- Ge, F., Peng, T., Fraedrich, K., Sielmann, F., Zhu, X., Zhi, X., Liu, X., Wei-Wei, T. and Zhao, P. 2018. Assessment of Trends and Variability in Surface Air Temperature on Multiple High-Resolution Datasets Over the Indochina Peninsula. *Theor. Appl. Climatol.*, 135(3-4): 1609-1627.
- Gupta, H.V., Kling, H., Yilmaz, K.K. and Martínez, G. 2000. Decomposition of the Mean Squared Error and NSE Performance Criteria: Implications For Improving Hydrological Modeling. *J. Hydrol.*, 377(1-2): 80-91.

- Hersbach, H., Bell, B., Berrisford, P., Hirahara, S., Horányi, Á., Muñoz Sabater, J., Nicolas, J. P., Peubey, C., Radu, R., Schepers, D., Simmons, A. J., Soci, C., Abdalla, S., Abellan, X., Balsamo, G., Bechtold, P., Biavati, G., Bidlot, J., Bonavita, M. and Thépaut, J. 2020. The Era5 Global Reanalysis. *Q. J. R. Meteorol. Soc.*, 146(730): 1999-2049.
- Ang, R., Kinouchi, T. and Zhao, W. 2022. Evaluation of Daily Gridded Meteorological Datasets for Hydrological Modeling in Data-Sparse Basins of the Largest Lake in Southeast Asia. *J. Hydrol. Reg. Stud.*, 42: 101135.
- Jiao, D., Xu, N., Yang, F. and Xu, K. 2021. Evaluation of Spatial-Temporal Variation Performance of Era5 Precipitation Data In China. *Sci. Rep.*, 11(1): <https://doi.org/10.1038/S41598-021-97432-Y>
- Lavers, D.A., Simmons, A. J., Vamborg, F. and Rodwell, M. J. 2022. An Evaluation of Era5 Precipitation for Climate Monitoring. *Q. J. R. Meteorol. Soc.*, 148(748): 3152-3165. <https://doi.org/10.1002/Qj.4351>
- Lee, D.G. and Ahn, K. H. 2022. Assessment of Suitable Gridded Climate Datasets for Large-Scale Hydrological Modeling Over South Korea. *Remote Sens.*, 14(15): 3535. <https://doi.org/10.3390/Rs14153535>
- Legates, D.R. and McCabe, G. J. 1999. Evaluating The use of "Goodness-of-Fit" Measures in Hydrologic and Hydroclimatic Model Validation. *Water Resour. Res.*, 35(1): 233-241. <https://doi.org/10.1029/1998wr900018>
- Merino, A., GarcíaOrtega, E., Navarro, A., FernándezGonzález, S., Tapiador, F. J. and Sánchez, J.L. 2021. Evaluation of Gridded Rainfall GaugeBased Precipitation Datasets: Impact of Station Density, Spatial Resolution, Altitude Gradient and Climate. *Int. J. Climatol.*, 41(5): 3027-3043. <https://doi.org/10.1002/Joc.7003>
- Moriasi, D.N., Arnold, J.G., Van Liew, M.W., Bingner, R.L., Harmel, R.D. and Veith, T.L. 2007. Model Evaluation Guidelines for Systematic Quantification of Accuracy in Watershed Simulations. *Trans. Asabe*, 50(3): 885-900. <https://doi.org/10.13031/2013.23153>
- Nash, J. and Sutcliffe, J.V. 1970. River Flow Forecasting Through Conceptual Models Part I: A Discussion of Principles. *J. Hydrol.*, 10(3): 282-290. [https://doi.org/10.1016/0022-1694\(70\)90255-6](https://doi.org/10.1016/0022-1694(70)90255-6)
- Nassaj, B.N., Zohrabi, N., Shahbazi, A. and Fathian, H. 2022. Evaluating The Performance Of Eight Global Gridded Precipitation Datasets Across Iran. *Dyn. Atmos. Oceans*, 98: 101297. <https://doi.org/10.1016/J. Dynatmoce.2022.101297>
- Peralta, J.C., Narisma, G. And Cruz, F. 2020. Validation Of High-Resolution Gridded Rainfall Datasets For Climate Applications in the Philippines. *J. Hydrometeorol.*, 21(7): 1571-1587. <https://doi.org/10.1175/Jhm-D-19-0276.1>
- Saidah, H., Saptaningtyas, R.S., Hanifah, L., Negara, I.J. and Widyanty, D. 2020. Noaa Satellite Performance in Estimating Rainfall Over the Island of Lombok. *Iop Conf. Ser.*, 437(1): 012035. <https://doi.org/10.1088/1755-1315/437/1/012035>
- Salvacion, A.R., Magcale-Macandog, D.B., Cruz, P.C.S., Saludes, R.B., Pangga, I.B. and Cumagun, C.J.R. 2018. Evaluation and Spatial Downscaling of Cru Ts Precipitation Data in the Philippines. *Model. Earth Syst. Environ.*, 4(3): 891-898. <https://doi.org/10.1007/S40808-018-0477-2>
- Schulzweida, U.S., Kornblueh, L.K. and Quast, R.Q. 2012. Cdo User's Guide: Climate Data Operators Version 1.5.9. Max-Planck-Institute For Meteorology, Hamburg, Germany.
- Schumacher, V., Justino, F., Fernández, A., Meseguer-Ruiz, Ó., Sarricolea, P., Comin, A.N., Venâncio, L.P. and Althoff, D. 2020. Comparison Between Observations and Gridded Data Sets over Complex Terrain in the Chilean Andes: Precipitation and Temperature. *Int. J. Climatol.*, 40(12): 5266-5288. <https://doi.org/10.1002/Joc.6518>
- Sheffield, J., Goteti, G. And Wood, E.F. 2006. Development Of A 50-Year High-Resolution Global Dataset Of Meteorological Forcings For Land Surface Modeling. *J. Clim.*, 19(13): 3088-3111. <https://doi.org/10.1175/Jcli3790.1>
- Shrestha, M.S. 2015. Linear Scaling Bias Correction. *Int. Cent. Integr. Mountain Dev.*, 6: 41-63.
- Singh, J.S., Knapp, H.V.K. And Demissie, M.D. 2004. Hydrologic Modeling Of The Iroquois River Watershed Using Hspf And Swat. Illinois State Water Survey Contract Report 2004-08. Isws, Illinois, Us.
- Tian, W., Liu, X., Wang, K., Bai, P., Liang, K. And Liu, C. 2021. Evaluation Of Six Precipitation Products In The Mekong River Basin. *Atmos. Res.*, 255: 105539. <https://doi.org/10.1016/J. Atmosres.2021.105539>
- Try, S., Tanaka, S., Tanaka, K., Sayama, T., Oeurng, C., Sovannara, U., Takara, K., Hu, M. And Han, D. 2020. Comparison Of Gridded Precipitation Datasets For Rainfall-Runoff And Inundation Modeling In The Mekong River Basin. *Plos One*, 15(1): E0226814. <https://doi.org/10.1371/Journal.Pone.0226814>
- Van Den Besselaar, E., Van Der Schrier, G., Cornes, R., Iqbal, A. S. And Tank, A.K. 2017. Sa-Obs: A Daily Gridded Surface Temperature And Precipitation Dataset For Southeast Asia. *J. Clim.*, 30(14): 5151-5165. <https://doi.org/10.1175/Jcli-D-16-0575.1>
- Willmott, C.J. 1981. On The Validation Of Models. *Phys. Geogr.*, 2(2), 184-194. <https://doi.org/10.1080/02723646.1981.10642213>
- Willmott, C.J. 1984. On The Evaluation Of Model Performance In Physical Geography. Springer, Singapore, Pp. 443-460. https://doi.org/10.1007/978-94-017-3048-8_23
- Xin, Y., Yang, Y., Chen, X., Yue, X., Liu, Y. And Yin, C. 2022. Evaluation Of Imerg And Era5 Precipitation Products Over The Mongolian Plateau. *Sci. Rep.*, 12(1). <https://doi.org/10.1038/S41598-022-26047-8>
- Yatagai, A., Kamiguchi, K., Arakawa, O., Hamada, A., Yasutomi, N. And Kitoh, A. 2012. Aphrodite: Constructing A Long-Term Daily Gridded Precipitation Dataset For Asia Based On A Dense Network Of Rain Gauges. *Bull. Am. Meteorol. Soc.*, 93(9), 1401-1415. <https://doi.org/10.1175/Bams-D-11-00122.1>
- Zandler, H., Senftl, T. And Vanselow, K. A. 2020. Reanalysis Datasets Outperform Other Gridded Climate Products In Vegetation Change Analysis In Peripheral Conservation Areas Of Central Asia. *Sci. Rep.*, 10(1). <https://doi.org/10.1038/S41598-020-79480-Y>

ORCID DETAILS OF THE AUTHORS

Christsam Joy S. Jasje-Santander: <https://orcid.org/0000-0003-3240-7780>
Ian Dominic F. Tabañag: <https://orcid.org/0000-0002-4049-1073>



Fabrication of Tin and Zinc Gas Diffusion Electrodes for Electrochemical Reduction of Carbon Dioxide

R. M. H. H. Jayarathne*^{id}, A. R. Nihmiya*^{†id}, A. H. L. R. Nilmini**^{id} and P. K. D. D. P. Pitigala***

*Department of Civil and Environmental Technology, Faculty of Technology, University of Sri Jayewardenepura, Homagama, Sri Lanka

**Department of Materials and Mechanical Technology, Faculty of Technology, University of Sri Jayewardenepura, Homagama, Sri Lanka

***Department of Physics, Faculty of Applied Sciences, University of Sri Jayewardenepura, Nugegoda, Sri Lanka

[†]Corresponding author: A.R. Nihmiya; nihmiya@sjp.ac.lk

Nat. Env. & Poll. Tech.
Website: www.neptjournal.com

Received: 27-10-2023

Revised: 08-12-2023

Accepted: 19-12-2023

Key Words:

Electrochemical reduction
Carbon dioxide
Catalyst loading
Current efficiency
Gas diffusion electrodes

ABSTRACT

This study explores the electrochemical reduction of carbon dioxide (CO₂) using tin (Sn) and zinc (Zn) catalyst-loaded gas diffusion electrodes (GDEs). The research explores the influence of electrolytic potential and catalyst loading on the efficiency of CO₂ conversion to valuable chemicals, specifically formic acid and carbon monoxide. The best Sn loading for Sn-loaded GDEs, according to the morphological study, is 7 mg.cm⁻², which results in higher current density (0.33 mA.cm⁻²) and current efficiency (36%). An electrolytic potential of -1.3 V Vs. Ag/AgCl is identified as optimal for Sn GDEs, offering a balance between high current efficiency (35%) and controlled current density. For Zn-loaded GDEs, an optimal loading of 5 mg.cm⁻² yields the highest current efficiency of 19.4% and a peak current density of 0.28 mA.cm⁻² at an electrolytic potential of -1.55 V Vs. Ag/AgCl, in addition to highlighting the crucial role that catalyst loading and electrolytic potential play in enhancing CO₂ reduction efficiency, this research offers insightful information for environmentally friendly CO₂ conversion technology.

INTRODUCTION

The electrochemical reduction of carbon dioxide (ERC) has emerged as a promising and innovative approach to addressing two critical global challenges simultaneously: mitigating the rising levels of atmospheric CO₂ and producing valuable chemicals and fuels sustainably. The process of converting CO₂ to more useful chemicals, particularly “CO₂ neutral fuels,” by using electrical energy is known as the electrochemical reduction of CO₂ (ERC). The ERC process occurs in an electrochemical cell (Fig. 1) at the interface of an electron conductor (cathode) and an ionic conductor (electrolyte). The ERC process involves a water oxidation reaction at the anode and a CO₂ reduction reaction at the cathode. As ERC consumes less energy than traditional chemical reduction processes and can proceed at a moderate temperature and atmospheric pressure, many researchers have proclaimed that ERC in large-scale applications is economically feasible. The economic feasibility of ERC intensely depends on the cathode, including its electrochemical performance and cost (Lu et al. 2014).

Most of the current cathodes for ERC are metal electrodes, and CO₂ is thus provided by sparging in the bulk. Carbon dioxide is introduced into the system by sparging it in the bulk solution. However, the efficiency of the ERC process is limited because CO₂ has low solubility in water at ambient conditions. This limitation arises from the challenge of transferring CO₂ effectively from the bulk solution to the cathode surface. To enhance the efficiency of ERC, gas diffusion electrodes (GDEs) have been developed. A GDE is a porous composite electrode consisting of a gas diffusion layer (GDL), a current collector (CC), and a catalyst layer (CL). The GDL serves the dual purpose of delivering gas and providing waterproofing. The CC is essential for reducing the ohmic losses in the electrode. The CL contains a gas-liquid-solid three-phase interface (TPI), which acts as the site for the ERC reaction.

This electrochemical process involves the use of electrodes and electrocatalysts to drive the conversion of CO₂ into a range of useful compounds, including formic acid (HCOOH), carbon monoxide (CO), methane (CH₄), and ethylene (C₂H₄) (Hori et al. 1989, Hori 2008). Through

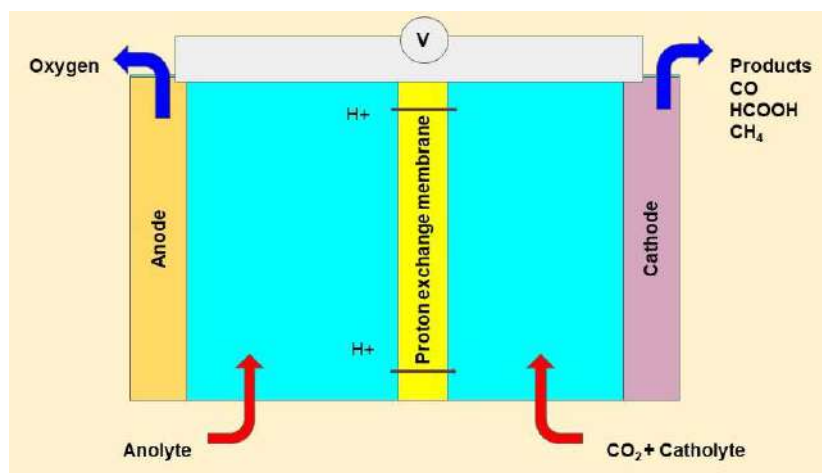


Fig. 1: Electrochemical cell mechanism.

careful control of reaction conditions and catalyst materials, researchers are exploring ways to optimize product selectivity and maximize energy efficiency. The field has witnessed significant advancements in recent years, with the development of novel catalysts, improved reactor designs, and a deeper understanding of reaction mechanisms.

The electrochemical reduction of CO_2 holds immense promise for sustainable energy storage, carbon capture and utilization, and the reduction of greenhouse gas emissions. In this context, this paper explores the fabrication of gas diffusion electrodes, particularly focusing on tin and zinc-based electrodes, as critical components in the electrochemical reduction of carbon dioxide.

Researchers have extensively investigated the use of Sn-based catalysts due to their remarkable activity and selectivity toward formic acid production (Del Castillo et al. 2017, Lei et al. 2018, Wang et al. 2021, Lee et al. 2015). Furthermore, Zn GDEs were also studied by researchers in the conversion of CO_2 to CO (Luo et al. 2019, Luo et al. 2020). Zn is an earth-abundant metal, reducing CO_2 to CO with relatively lower activity than Ag and Au catalysts. Because of the high cost and low abundance, Zn is better than Au and Au as catalysts (Jeanty et al. 2018, Chen et al. 2022, Shi et al. 2020).

A wide range of faradic efficiencies has been reported for formic acid formation on Sn electrodes. By using Sn GDE, Wang et al. (2014) obtained the highest Faradic efficiency of 72.99% and current density of $13.45 \text{ mA}\cdot\text{cm}^{-2}$ with Potassium Bicarbonate (KHCO_3) as the electrolyte. Del Castillo et al. (2017) obtained 70% Faradaic Efficiency and $150 \text{ mA}\cdot\text{cm}^{-2}$ current density with a low catholyte flow rate using Sn/C-GDEs. Luo et al. (2019) obtained 91.6%

CO faradaic efficiency with $200 \text{ mA}\cdot\text{cm}^{-2}$ current density at only -0.62 V vs RHE in a flow cell reactor.

In the ERC, the catalyst loading plays a pivotal role, directly influencing the efficiency and selectivity of the reaction. Researchers have extensively investigated the impact of varying catalyst concentrations, shedding light on the intricate balance between active sites and overcrowding, ultimately shaping the catalytic performance in CO_2 reduction processes. Studies reveal that the performance of Sn-based catalysts is significantly influenced by Sn loading (Wang et al. 2014, Del Castillo et al. 2015).

Understanding the influence of electrolytic potential is paramount in unraveling the complexities of electrochemical CO_2 reduction. Different potential levels profoundly impact the reaction kinetics, driving forces, and selectivity, offering a nuanced insight into the efficiency of CO_2 conversion processes. The effect of the electrolytic potential was studied by many researchers (Kim et al. 2014). Wu et al. (2014) studied about effects of the electrolytic potential for ERC with Sn electrode to obtain a high production for formic acid, and Luo et al. (2019) Studied the effect of electrolytic potential for Zn foil and Porous Zn electrode where CO_2 reduced to CO.

In this comprehensive study, we have delved deep into the intricate world of electrochemical reduction of carbon dioxide using tin (Sn) and zinc (Zn) loaded gas diffusion electrodes. The paper describes the electrochemical process, where CO_2 is transformed into valuable compounds, including formic acid and carbon monoxide, employing specialized electrocatalysts and electrodes. Through a systematic approach, we studied the influence of catalyst loading and electrolytic potential. The performance of electrolysis was evaluated using current density and current efficiency.

MATERIALS AND METHODS

Materials

Vulcan XC 72R Carbon Black Powder, polytetrafluoroethylene (PTFE) Dispersion 30(TE3970 type), Fumasep FAB-PK-130 (anion exchange membrane), EPDM Rubber sheet, were purchased from Fuel Cell Store. Nafion PFSA polymer dispersion D520 (5%), Ethanol, copper mesh, and stainless-steel mesh were purchased from the local market. Distilled water, Potassium Bicarbonate AR, 99.5%, Propan-2-ol 99.8% Tin metal powder pure 99%, and Zinc metal powder, 99% were used.

Methodology

Fabrication of gas diffusion electrodes: First, the mixture of conductive carbon black and ethanol was agitated ultrasonically for 2-3 min. Then polytetrafluoroethylene (PTFE) was added and further agitated ultrasonically and stirred in a hot bath for 10-12 min. Then, the dough was formed and rolled down to a thin film on a stainless-steel mesh to form a gas diffusion layer (GDL). For the preparation of the microporous layer, carbon black loading $25 \text{ mg}\cdot\text{cm}^{-2}$, $5 \text{ mg}\cdot\text{cm}^{-2}$ PTFE and 5 mL of ethanol were used. The size of the GDEs made was $2\times 2 \text{ cm}^2$.

The Sn catalyst ink and Zn catalyst were made by mixing Sn and Zn catalyst particles separately, Nafion ionomer, isopropanol, and deionized water followed by ultrasonication of the mixture for 1 h. The amount of water to isopropanol is 1:1 in the mixture. The catalyst layer of the gas diffusion electrode was prepared by spraying the Sn-catalyst ink and Zn-catalyst on the rolling pressed GDL in several layers using the airbrush and mini compressor. Catalyst ink was

sprayed in different loadings (3,5,7, and $9 \text{ mg}\cdot\text{cm}^{-2}$ with the same fraction of 50% wt. Nafion) on GDLs to make GDEs. The amount of deposited catalyst was detected by weighing.

Characterization of GDEs

Scanning electron microscopy (SEM) images of the GDEs were acquired using the ZEISS EVO 18 Scanning Electron Microscope.

Experimental setup for electrochemical testing:

Electrolysis and EIS were carried out in a Corrtest CS310 Potentiostat/Galvanostat (Wuhan Corrtest Instruments Corp., Ltd., Wuhan, China) electrochemical workstation at room temperature in a three-compartment electrochemical cell. The working electrode was the fabricated GDE, and the copper mesh was the counter electrode, while Ag/AgCl was used as the reference electrode. An anion exchange membrane separated the cathode compartment and anode compartment. The electrolyte was circulated through the compartment using the peristaltic pump (Kamoer Fluid Tech (Shanghai) Co., Ltd). The anion exchange membrane was submerged in KOH solution for 6 to 12 h and then into potassium bicarbonate solution for a period of 48-72 h to fully convert the membrane into bicarbonate form. After rinsing the membrane (which is in the carbonate form) with deionized water or distilled water, it was assembled inside the electrochemical setup for electrochemical CO_2 reduction experiments.

Gas products were collected in gas sampling bags (Aluminum foil gas sampling bags, Guangzhou Huaixing Technology Co., Ltd., China), while liquid products to glass bottles. CO_2 was fed into the gas inlet continuously throughout the experiment. Fig. 1 shows the configuration

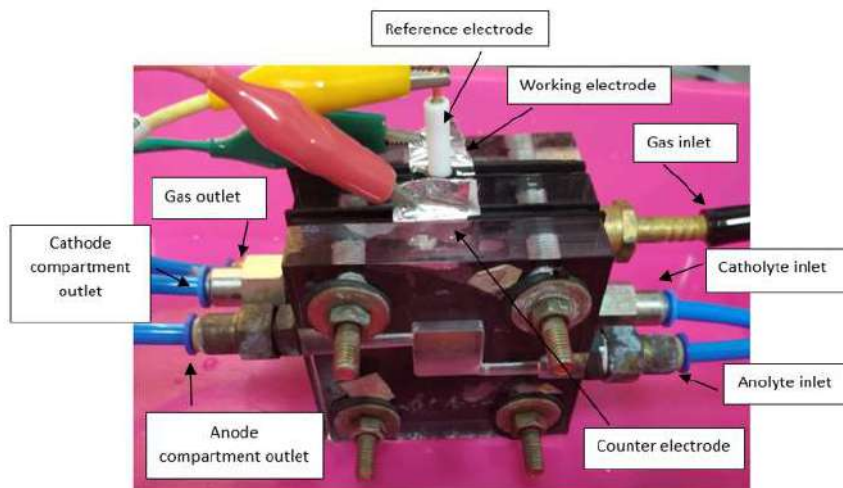


Fig. 2: Three-electrode electrochemical cell.

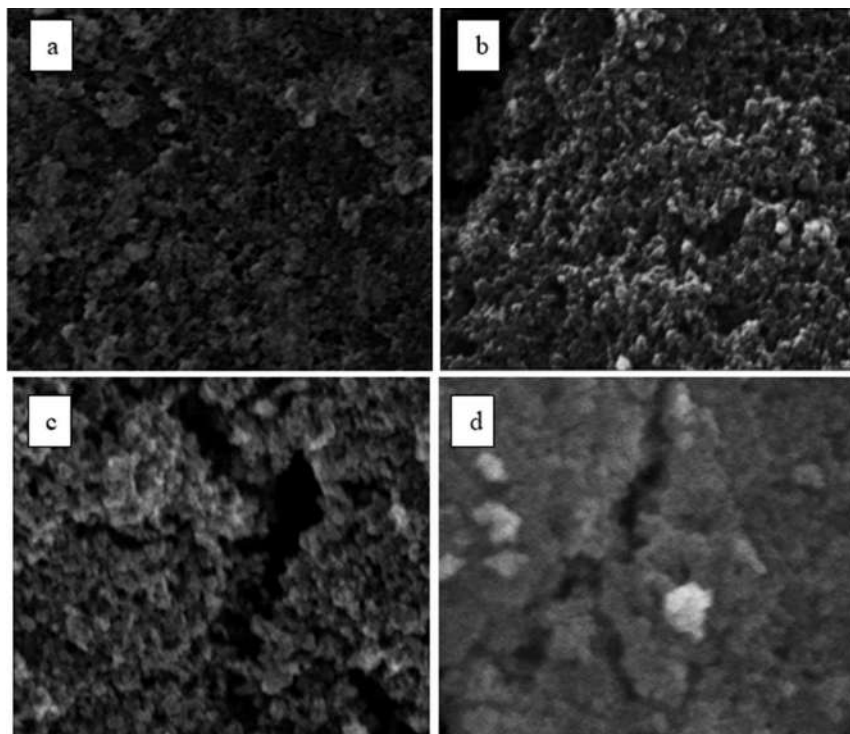


Fig. 3: SEM images of different Sn loadings a) 3 mg.cm⁻² b) 5 mg.cm⁻² c) 7 mg.cm⁻² d) 9 mg.cm⁻².

of the three-electrode electrochemical cell. The gas flow rate was monitored using LCD Display gas flow meter AFM0725 (Warmth Technology Co., Ltd., China). Fig. 2 shows the three-electrode electrochemical cell consisting of three electrodes.

Detection and quantification of the products: To detect and quantify the concentration of produced formic acid, UV-spectroscopy (Thermoscientific Genesys 50) was used. The concentration of formic acid was determined within the wavelength range of 200 to 250 nm, as this interval contains the most significant and characteristic peak for formic acid, which occurs specifically between 200 and 220 nm. Commercially available formic acid (AR 98%) was used as the reference.

For the CO analysis, an Arduino-based gas analyzer was employed. The gas analyzer was interfaced with an Arduino board. The collected gaseous samples were introduced into the gas analyzer in a controlled manner. A gas sensor was housed within a dedicated container, and the gas analyzer was programmed to direct the collected gas through this container. The gas sensor was sensitive to carbon monoxide and provided readings corresponding to the concentration of CO. A series of experimental runs were conducted to gather data on the change in CO(g) concentration before and after passing through the gas sensor. During each run, the

gaseous byproducts collected in the gas sampling bag were introduced into the gas analyzer system for a fixed duration. Multiple experimental runs were conducted to account for variations. The calculated CO(g) concentration differences from each run were averaged to provide a representative measure of the change in CO(g) concentration due to the gas sensor's detection.

Influence of the electrolytic potential: The electrolysis conducted using the Sn GDEs produced only formic acid. No traces of CO were not detected. Conversely, in the ERC experiment done using the Zn GDE, the main product was observed to be CO., and no traces of formic acid were identified. This has good agreement with the literature (Azuma & Watanabe 1990, Hara et al. 1995, Wang et al. 2014).

To investigate the impact of different electrolytic potentials on Sn GDEs, a series of experiments were conducted using potentials of -1.1, -1.3, -1.5, -1.8, and -2 V Vs. Ag/AgCl (+0.197 Vs RHE) reference electrode. To investigate the impact of different electrolytic potentials of Zn GDEs, a series of experiments were conducted using potentials of -1.25, -1.35, -1.45, -1.55, and -1.65 V Vs Ag/AgCl reference electrodes. Each potential was applied for 30 min. The electrolyte used was 0.5 M KHCO₃, and CO₂ was fed at a flow rate of 1 dm³.min⁻¹. The electrolyte was circulated at a constant flow rate of 21 mL.min⁻¹.

RESULTS AND DISCUSSION

Morphological Analysis of Sn GDEs and Current Efficiency Correlation

The morphologies of GDEs with different Sn loadings were observed by SEM (Fig. 3). This figure reveals that when loading increases from 3 mg.cm^{-2} to 7 mg.cm^{-2} , the number of pores between the agglomerated Sn particles has increased. As a result, the increased Sn loading allows for an enhancement in the total area of TPis. However, with further increases in Sn loading, the number of pores decreases, leading to a subsequent reduction in the total area of TPis.

The data presented in Fig. 4 includes the Sn loading on a gas diffusion electrode (GDE) with corresponding current density and current efficiency. As the tin loading on the GDE increases from 3 mg.cm^{-2} to 7 mg.cm^{-2} , the current density also increases. For example, at 3 mg.cm^{-2} , the current density is 0.25 mA.cm^{-2} , while at 7 mg.cm^{-2} , it increases to

0.33 mA.cm^{-2} . This trend suggests that a higher tin loading positively affects the electrochemical reduction of CO_2 by promoting higher current densities.

The increase in current density likely indicates that more active sites are available for the electrochemical reaction, leading to increased CO_2 reduction. Notably, the current efficiency also increases as the Sn loading increases. For instance, at 3 mg.cm^{-2} , the current efficiency is 18%, while at 7 mg.cm^{-2} , it rises to 36%. This implies that the higher current densities achieved at greater tin loadings are associated with higher current efficiencies.

The increase in current efficiency suggests that a larger proportion of the electrons generated during the electrochemical reaction are being utilized for CO_2 reduction. Interestingly, there is a decrease in both current density and current efficiency at an Sn loading of 9 mg.cm^{-2} . This decrease could be attributed to overcrowding of the electrode surface with tin nanoparticles, leading to reduced surface

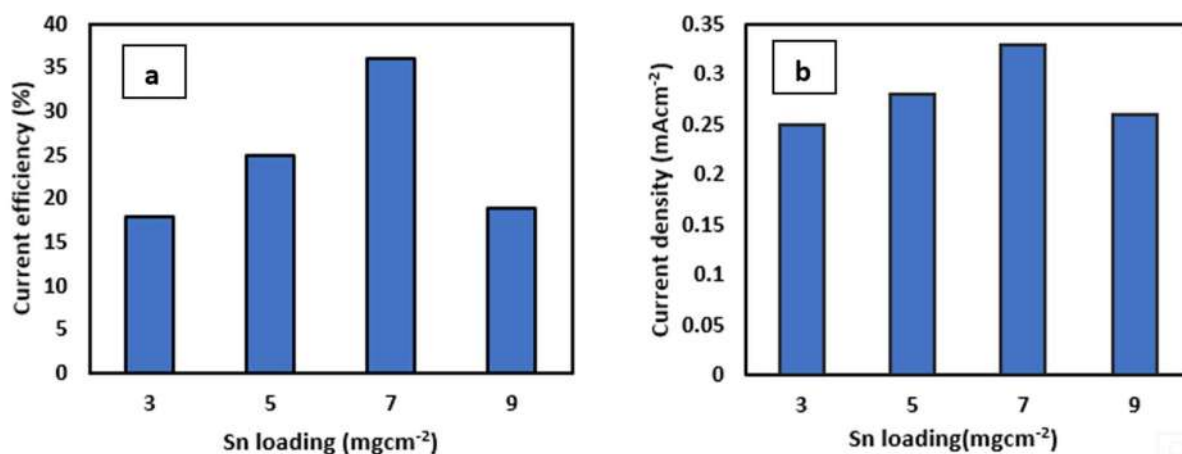


Fig. 4: The graphs of a) Current efficiency Vs. Sn loading, b) Current density Vs. Sn loading.

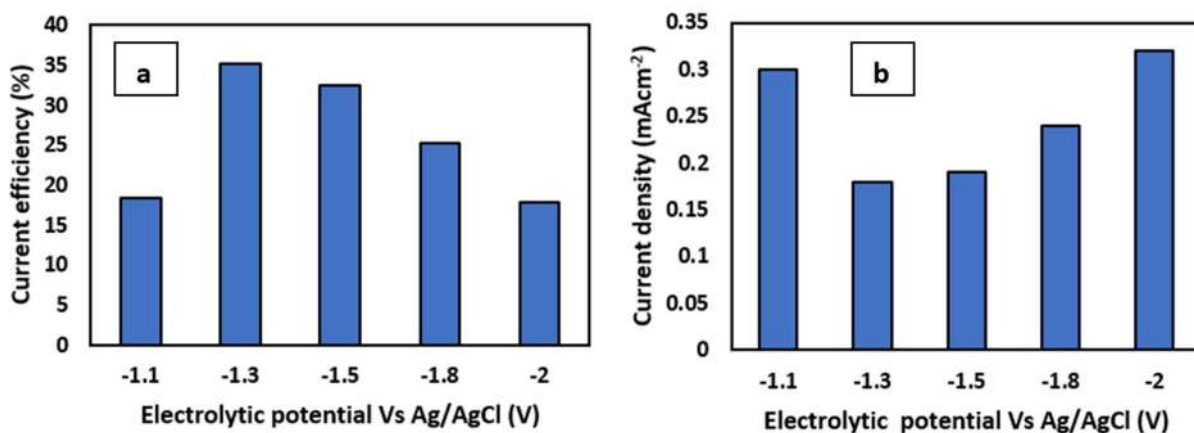


Fig. 5: The graphs of a) Current efficiency vs. electrolytic potential, b) Current density vs. electrolytic potential.

area for electrochemical reactions and potential catalyst deactivation.

Influence of Electrolytic Potential on CO₂ Conversion to Formic Acid

Fig. 5 represents the current efficiency and current density obtained in the conversion of carbon dioxide to formic with different electrolytic potentials.

At -1.1 V, the current efficiency is 14%, which steadily rises to 35% at -1.3 V. The increase in current efficiency with more negative potentials is typical in electrochemical systems. More negative potentials provide a greater driving force for the desired electrochemical reactions, resulting in higher current efficiency. The current efficiency peaks at -1.3 V (35%) and then slightly decreases at -1.5 V (31%), further decreases at -1.8 V (25%), and decreases again at -2 V (18%).

As the potential becomes more negative from -1.3 V to -2 V, the current density generally increases (Fig. 5b). The increase in current density with more negative potentials is expected due to enhanced electrode kinetics at lower potentials. As the potential becomes more negative, the electrode surface becomes more favorable

for electrochemical reactions, leading to a higher rate of electron transfer and, consequently, a higher current density. However, the optimum value was suggested as -1.3 V. Analyzing the experimental data, an electrolytic potential of -1.3 V emerged as a compelling choice for optimization. This potential was suggested as the optimum value due to its combination of the highest current efficiency, the lowest current density, and the potential to minimize competing side reactions. At -1.3 V, the system exhibited exceptional efficiency, effectively channeling a significant portion of the applied current into the desired electrochemical reaction. This high current efficiency indicated a reduced occurrence of wasteful side reactions, underscoring the process's selectivity for the target product. Simultaneously, the observed low current density at this potential implied a controlled rate of electron transfer. Lower current densities can minimize competing side reactions, enhancing the efficiency of the desired electrochemical transformation. This delicate balance between selectivity, controlled electron transfer, and reduced side reactions at -1.3 V represents an optimal configuration. Such a convergence of factors not only improves the efficiency of CO₂ conversion but also extends the lifespan of electrodes, contributing to a more sustainable

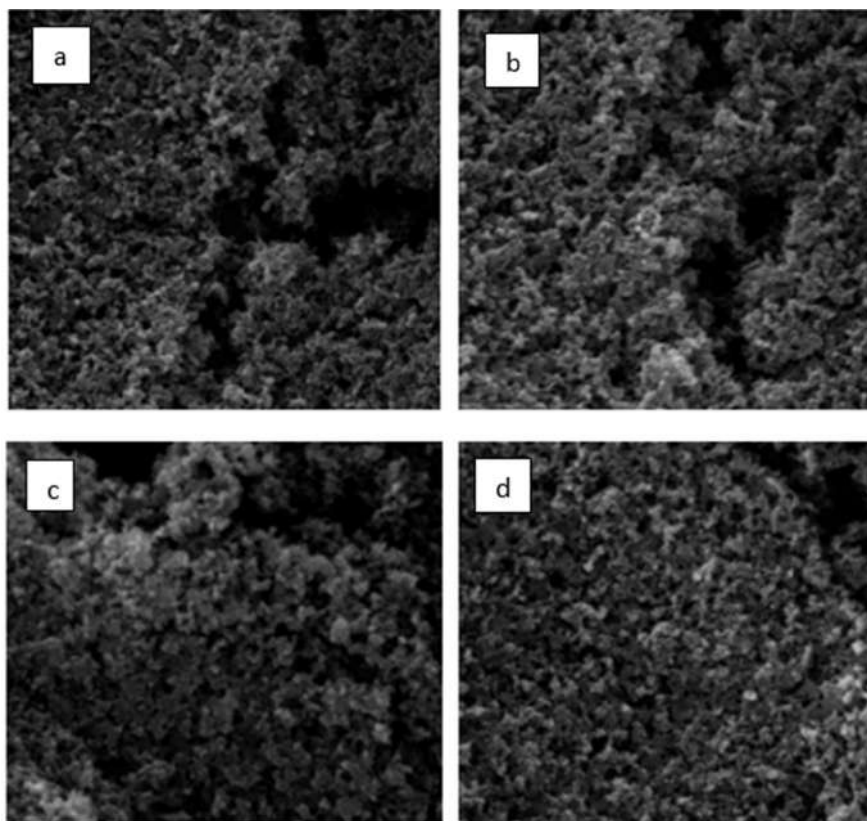


Fig. 6: SEM images of different Zn loadings a) 3 mg.cm⁻² b) 5 mg.cm⁻² c) 7 mg.cm⁻² d) 9 mg.cm⁻².

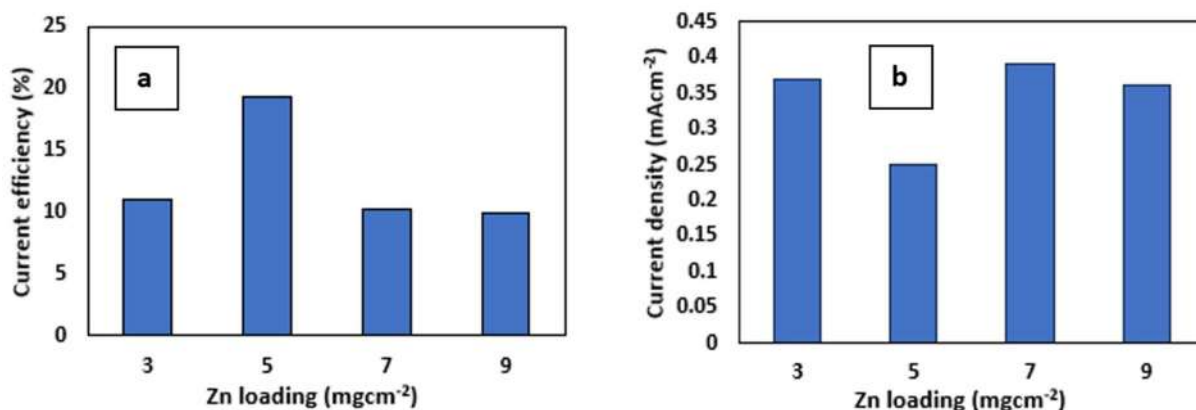


Fig. 7: The graphs of a) Current efficiency Vs. Zn loading and b) Current density Vs. Zn loading.

and cost-effective electrochemical process.

Morphological Analysis of Zn GDEs and Current Efficiency Correlation

The morphologies of GDEs with different Zn loadings were observed by SEM (Fig. 6). This figure shows that when loading increases from 3 mg.cm⁻² to 5 mg.cm⁻², the number of pores between the agglomerated Zn particles increased. As a result, the increased Zn loading allows for an enhancement in the total area of TPIs. However, with further increases in Zn loading (7 and 9 mg.cm⁻²), the number of pores decreases, leading to a subsequent reduction in the total area of TPIs.

The graphs (Fig. 7) illustrate a noticeable trend between zinc loading and current efficiency in the electrochemical system. As Zn loading varies from 3 to 9 mg.cm⁻², the current efficiency demonstrates a non-linear pattern. An optimum point is evident at a loading of 5 mg.cm⁻², where the system achieves the highest current efficiency of 19.4%. At this loading, the electrochemical system maximizes its ability to convert the applied current into the desired reaction, resulting in the highest efficiency. Deviating from this optimal loading, both lower (3 mg.cm⁻²) and higher (7 and 9 mg.cm⁻²) loadings result in decreased current efficiencies, indicating the presence of diminishing returns as loading diverges from the optimum. At higher loadings, mass transport limitations likely hinder the accessibility of reactants to the electrode surface, reducing the efficiency of the desired electrochemical reaction. Similarly, at lower loadings, the limited availability of active sites might lead to underutilization of the applied current, also decreasing efficiency.

The data (Fig. 7b) reveals a distinct trend where current density exhibits variations with changing Zn loading. Current density shows a fluctuating pattern with different Zn loadings. The fluctuations in current density could be attributed to the interplay between multiple factors.

The observed trend in current density can be elucidated through several electrochemical principles. Firstly, at lower Zn loadings, the active surface area available for the electrochemical reactions is limited.

Consequently, the system exhibits a relatively lower current density as there are fewer active sites for the electrochemical reactions to occur. As the Zn loading increases to 5 mg.cm⁻², the active surface area might become more accessible, resulting in a temporary increase in current density. However, beyond this point, the accumulation of Zn particles might start hindering mass transport, limiting the accessibility of reactants to the electrode surface and thereby decreasing the current density. This phenomenon is typical in electrochemical systems where mass transport limitations can significantly influence the observed current densities. The slight increase in current density at a Zn loading of 7 mg.cm⁻² could be attributed to the formation of a particular surface structure that enhances the electrochemical reaction rate at this loading.

Influence of Electrolytic Potential on CO₂ Conversion to Carbon Monoxide

Fig. 8: represents the variation of current efficiency and current density with Electrolytic potential.

As the applied potential to the working electrode becomes more negative, moving from -1.25 V to -1.65 V, a noticeable increase in current efficiency is observed. This trend signifies that at more negative potentials, a higher percentage of electrons are efficiently utilized in the conversion of carbon dioxide to carbon monoxide. The scientific rationale behind this observation lies in the enhanced driving force for the reduction reaction at more negative potentials, reduced overpotential effects, and improved electrode kinetics. The efficiency increased from 1% at -1.25 V to a peak of 18% at -1.55 V before slightly declining to 10% at -1.65 V.

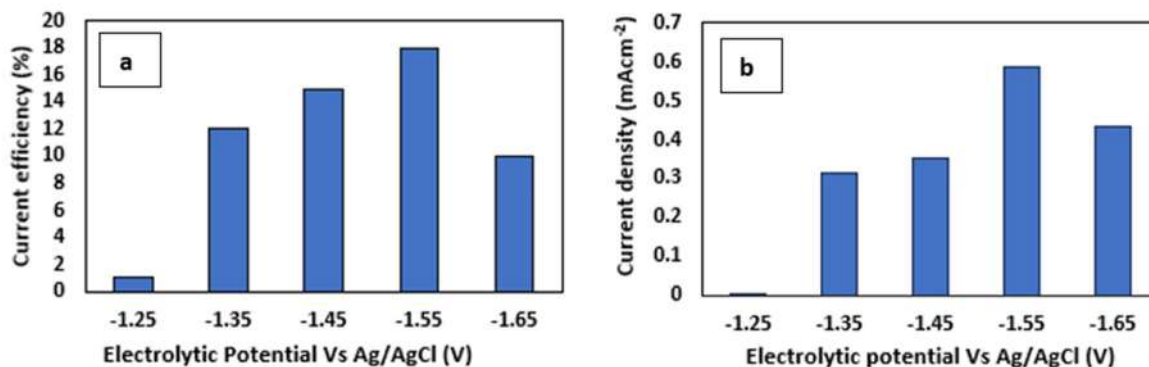


Fig 8: The graphs of a) Current efficiency vs. electrolytic potential, b) Current density vs. electrolytic potential.

The data (Fig. 8b) shows a trend where the current density initially increases with more negative potentials, reaching a peak at -1.55 V, and then decreases slightly at -1.65 V. When the electrolytic potential becomes more negative, it provides a higher driving force for the electrochemical reaction. At a more negative potential, it takes less energy for the reaction to occur, allowing a higher number of electrons to participate. This increased driving force leads to a higher rate of reaction, reflected in the rising current density up to -1.55 V. At -1.55 V, the electrochemical system reaches an optimal balance between the driving force provided by the potential and the kinetic barriers of the reaction. The reaction kinetics are favorable, meaning the reaction proceeds at an efficient rate with a high current density. Furthermore, at -1.55 V, the system achieves the highest current efficiency, indicating that a significant portion of the applied current is being utilized for the desired electrochemical reaction.

CONCLUSION

In conclusion, the experimental investigation into the electrochemical reduction of carbon dioxide to valuable chemicals, namely formic acid and carbon monoxide, has yielded valuable insights into the influence of various parameters on the efficiency of the process. In the case of Sn-loaded Gas Diffusion Electrodes (GDEs), the morphological analysis revealed a delicate balance between Sn-loading and electrochemical performance. Optimal Sn loading was found to be 7 mg.cm⁻², leading to increased current density and efficiency. However, excessive loading of Sn particles (9 mg.cm⁻²) resulted in diminished performance, potentially due to overcrowding of the electrode surface. This balance highlights the importance of controlling the surface area and active sites for maximizing CO₂ reduction efficiency.

Furthermore, the choice of electrolytic potential proved to be a critical factor in determining the efficiency of CO₂

conversion. In the case of Sn GDEs, an electrolytic potential of -1.3 V Vs. Ag/AgCl emerged as the optimal choice, offering a fine-tuned balance between high current efficiency (35%) and controlled current density. This potential provided a significant driving force for the electrochemical reaction while minimizing wasteful side reactions, ensuring a selective conversion of CO₂ to formic acid. Similarly, for Zn-loaded GDEs, an optimal loading of 5 mg.cm⁻² was identified, resulting in the highest current efficiency of 19.4%. Beyond this loading, both lower and higher loadings led to decreased efficiencies, emphasizing the importance of the active surface area in catalyzing the electrochemical reaction effectively. Regarding the electrolytic potential for Zn GDEs, the experiments revealed that a potential of -1.55 V Vs Ag/AgCl struck the perfect balance, resulting in the highest current efficiency of 18%. At this potential, the driving force for the electrochemical reaction was optimal, leading to efficient CO₂ conversion to carbon monoxide.

In summary, this study demonstrates the intricate interplay between catalyst loading, electrolytic potential, current density, and current efficiency in electrochemical CO₂ reduction. Fine-tuning these parameters is crucial for maximizing the efficiency of the process, enabling the sustainable production of valuable chemicals from carbon dioxide. These findings not only advance our fundamental understanding of electrochemical processes but also pave the way for the development of more efficient and environmentally friendly CO₂ conversion technologies.

ACKNOWLEDGMENT

The authors acknowledge the financial assistance provided by the Research Council of the University of Sri Jayewardenepura, Sri Lanka, under grant no: ASP/01/ RE/ FOT/2019/57

REFERENCES

- Azuma, M. and Watanabe, M. 1990. Electrodes in low-temperature aqueous KHCO_3 media. *J. Electrochem. Soc.*, 137(6): 1772-1778.
- Chen, Q., Tsiakaras, P. and Shen, P. 2022. Electrochemical reduction of carbon dioxide: Recent advances on Au-based nanocatalysts. *Catalysts*, 12(11): 1348. <https://doi.org/10.3390/catal12111348>
- Del Castillo, A., Alvarez-Guerra, M., Solla-Gullón, J., Sáez, A., Montiel, V. and Irabien, A. 2015. Electrocatalytic reduction of CO_2 to formate using particulate Sn electrodes: Effect of metal loading and particle size. *Appl. Energy*, 157: 165-173. <https://doi.org/10.1016/j.apenergy.2015.08.012>
- Del Castillo, A., Alvarez-Guerra, M., Solla-Gullón, J., Sáez, A., Montiel, V. and Irabien, A. 2017. Sn nanoparticles on gas diffusion electrodes: Synthesis, characterization, and use for continuous CO_2 electroreduction to formate. *J. CO_2 Util.*, 18: 222-228. <https://doi.org/10.1016/j.jcou.2017.01.021>
- Hara, K., Kudo, A. and Sakata, T. 1995. Electrochemical reduction of carbon dioxide under high pressure on various electrodes in an aqueous electrolyte. *J. Electroanal. Chem.*, 391(1): 141-147.
- Hori, Y. 2008. Electrochemical CO_2 reduction on metal electrodes. In *Modern aspects of electrochemistry*. Springer. pp. 89-189.
- Hori, Y., Murata, A. and Takahashi, R. 1989. Formation of hydrocarbons in the electrochemical reduction of carbon dioxide at a copper electrode in aqueous solution. *J. Chem. Soc. Faraday Trans.*, 85(8): 2309-2326.
- Jeanty, P., Scherer, C., Magori, E., Wiesner-Fleischer, K., Hinrichsen, O. and Fleischer, M. 2018. Upscaling and continuous operation of electrochemical CO_2 to CO conversion in aqueous solutions on silver gas diffusion electrodes. *J. CO_2 Util.*, 24: 454-462. <https://doi.org/10.1016/j.jcou.2018.01.011>
- Kim, H.Y., Choi, I., Ahn, S.H., Hwang, S.J., Yoo, S.J., Han, J., Kim, J., Park, H., Jang, J.H. and Kim, S.K. 2014. Analysis of the effect of operating conditions on electrochemical conversion of carbon dioxide to formic acid. *Int. J. Hydrog. Energy*, 39(29): 16506-16512. <https://doi.org/10.1016/j.ijhydene.2014.03.145>
- Lee, S., Ju, H.K., Machunda, R., Uhm, S., Lee, J.K., Lee, H.J. and Lee, J. 2015. Sustainable production of formic acid by electrolytic reduction of gaseous carbon dioxide. *J. Mater. Chem. A*, 3(6): 3029-3034. <https://doi.org/10.1039/c4ta03893b>
- Lei, T., Zhang, X., Jung, J., Cai, Y., Hou, X., Zhang, Q. and Qiao, J. 2018. Continuous electroreduction of carbon dioxide to formate on tin nanoelectrode using alkaline membrane cell configuration in aqueous medium. *Catal. Today*, 318: 32-38. <https://doi.org/10.1016/j.cattod.2017.10.003>
- Lu, X., Leung, D. Y. C., Wang, H., Leung, M. K. H. and Xuan, J. 2014. Electrochemical reduction of carbon dioxide to formic acid. *Chem. Electro. Chem.*, 1(5): 836-849. <https://doi.org/10.1002/celec.201300206>
- Luo, W., Zhang, J., Li, M. and Züttel, A. 2019. Boosting CO production in electrocatalytic CO_2 reduction on highly porous Zn catalysts. *ACS Catal.*, 9(5): 3783-3791. <https://doi.org/10.1021/acscatal.8b05109>
- Luo, W., Zhang, Q., Zhang, J., Moioli, E., Zhao, K. and Züttel, A. 2020. Electrochemical reconstruction of ZnO for selective reduction of CO_2 to CO. *Appl. Catal. B Environ.*, 273: 119060. <https://doi.org/10.1016/j.apcatb.2020.119060>
- Shi, R., Guo, J., Zhang, X., Waterhouse, G.I.N., Han, Z., Zhao, Y., Shang, L., Zhou, C., Jiang, L. and Zhang, T. 2020. Efficient wettability-controlled electroreduction of CO_2 to CO at Au/C interfaces. *Nat. Commun.*, 11(1): 1-10. <https://doi.org/10.1038/s41467-020-16847-9>
- Wang, Q., Dong, H. and Yu, H. 2014. Fabrication of a novel gas diffusion electrode for electrochemical reduction of carbon dioxide to formic acid. *RSC Adv.*, 4(104): 59970-59976. <https://doi.org/10.1039/c4ra10775f>
- Wang, Q., Wu, Y., Zhu, C., Xiong, R., Deng, Y., Wang, X., Wu, C. and Yu, H. 2021. Sn nanoparticles deposited onto a gas diffusion layer via impregnation-electroreduction for enhanced CO_2 electroreduction to formate. *Electrochim. Acta*, 369: 137662. <https://doi.org/10.1016/j.electacta.2020.137662>
- Wu, J., Sharma, P.P., Harris, B.H. and Zhou, X. D. 2014. Electrochemical reduction of carbon dioxide: IV dependence of the faradaic efficiency and current density on the microstructure and thickness of the tin electrode. *J. Power Sour.*, 258:189-194. <https://doi.org/10.1016/j.jpowsour.2014.02.014>

ORCID DETAILS OF THE AUTHORS

- R. M. H. H. Jayarathne: <https://orcid.org/0009-0009-4347-8112>
A.R. Nihmiya: <https://orcid.org/0000-0003-0903-8753>
A. H. L. R. Nilmini: <https://orcid.org/0000-0001-6983-2831>



Experimental Analysis of Anaerobic Co-digestion: Potential of Fruit Wastes

S. Sathish*, A. Saravanan**, R. Suresh***, K. Saranya****, R. Sarweswaran*, G. Balaji* and S. Seralathan*† 

*Department of Aeronautical Engineering, Hindustan Institute of Technology and Science, Chennai, Tamil Nadu, India

**Department of Chemical Engineering, Hindustan Institute of Technology and Science, Chennai, Tamil Nadu, India

***Department of Mechanical Engineering, Annamalai University, Chidambaram, Tamil Nadu, India

****Department of Physics, Government College of Engineering, Thanjavur, Tamil Nadu, India

†Corresponding author: S. Seralathan; siva.seralathan@gmail.com

Nat. Env. & Poll. Tech.
Website: www.neptjournal.com

Received: 03-10-2023

Revised: 16-11-2023

Accepted: 30-11-2023

Key Words:

Co-digestion
Anaerobic biodigester
Methane
Mango
Papaya peel
Banana peel
Retention time

ABSTRACT

This study focuses on converting fruit waste into usable clean energy by an innovative, cost-effective anaerobic biodigester. The biodigester is designed to anaerobically digest various fruit wastes and starter inoculums of cow dung that are locally obtained. A batch vertical digester of 1000 liters capacity built of fiber with a phonematic agitator positioned in the center is used to improve mixing. The retention time is 30 days with a substrate of banana peels co-digested with mango and papaya peels individually in the ratio of 50:50. The combined wastes generated the biogas and the total quantity of biogas generated for all combined wastes over 21 days varies between 530L/day and 480L/day respectively. In this work, banana and mango peel (waste/water) split 50:50 gives a peak yield of 530L/day. The average ambient temperatures are kept in the range of 25°C to 35°C (i.e., mesophilic range). The pH range of 6.4 to 7.8 is consistently maintained and seems to be stable. Therefore, this proposed anaerobic digester would reduce the disposal of solid waste, and it is cost-effective. After cleaning, it is observed that the combined peels of bananas and papaya contained 91.95% of the estimated biogas and methane, which can be used to solve energy issues such as electricity production and cooking purposes.

INTRODUCTION

Despite being a natural and biodegradable material, fruit waste has the potential to become a significant ecological and environmental issue. The produced market fruit waste needs to be treated carefully as it contains a lot of wasted organic materials, yet it is usually discarded into the environment (Otun et al. 2016). In addition to dietary fiber, juice-seller wastes also contain sizeable amounts of enzymes, vitamins, polyphenols, and carotenoids. To manage food and fruit waste, several bioenergy technologies have been deployed, such as gasification, hydrothermal liquefaction, and biohydrogen production (Sathish & Vivekanandan 2016). The need for hydrocracking, aqueous phase reformation, and high purification were the main challenges faced despite attaining the initial goals (Suelen et al. 2017). The first order and modified Gompertz kinetic models were used to evaluate the biogas and methane production via passion fruit peel, orange, and cashew bagasse (Budiyono et al. 2018). Economically viable methods of treating solid waste, particularly in metropolitan areas of low and low-middle-income nations, were investigated in a bid to minimize

hazards to the environment and public health (Sathish et al. 2018).

Fruit and vegetable wastes are generated in large quantities in markets and are irritants in landfills due to their high biodegradability (Nidhal et al. 2022). Fruit wastes are created in several industries, including wet markets, hotels, restaurants, and housing developments (Teguh et al. 2017). The two primary categories into which fruit waste from various sources can be categorized are pre-consumption and post-consumption food waste. Biogas is produced under anaerobic conditions by bacterial processes involving the biodegradation of organic compounds (Parthiban et al. 2023). Biogas can be produced using municipal solid waste, food waste, manure waste, sewage, green garbage, agricultural, plant, or animal wastes. Methane and biogas are environmentally beneficial green fuels that are used for electricity production, transportation, and heating liquid and solid foods (Divya et al. 2015). Biogas is composed of methane, which makes up the majority of biogas, and carbon dioxide, with traces of moisture and sulfide. The production of biogas, which may be used for heating, cooking, and energy production, is the main advantage of using anaerobic

digestion. Methane and hydrogen, which are produced by the waste from fruits, are the two important gases that can be used to fuel vehicles as well as produce electricity and heat. The major functions of anaerobic digestion are to recover energy from diverse organic materials and to allow for nutrient recycling during the digestion processes (Nathaniel et al. 2020). Anaerobic digestion takes place under well-controlled conditions while sludge fermentation occurs.

Hydrolysis, acidogenesis, acetogenesis, and methanogenesis are the four processes that make up anaerobic digestion. It is thought that during hydrolysis, non-soluble biopolymers become soluble organic molecules. Enzymes that facilitate the reaction are released by the hydrolytic and fermentative bacteria (Muhammad & Shuichi 2014). Long-chain carboxylic acids, glycerol, soluble carbohydrates, and amino acids are by-products of the process. Environmental variables such as pH and high or low temperatures are also some of the key determinants of the final biogas product (Qiangqiang et al. 2022). To create the best conditions for the production of biogas, municipal solid waste, and household waste must be combined (Dieu et al. 2019). Biphasic fermentation with solids content feeds utilizes a solid bed for acid fermentation and subsequent methane production to lessen the inhibition of methane fermentation by organic inputs (Farkad 2016).

Based on the literature reviews, it is understood that biogas can be produced from organic wastes such as fruit waste. This approach is significant as it utilizes one of the

most accessible yet underutilized renewable energy sources in the world to produce biogas. Methane and biogas are produced because of anaerobic co-digestion of fruit wastes. Therefore, the primary goal of this study is to understand how co-digestion of fruit waste, such as banana peel combined with mango peel and banana peel mixed with papaya peel, produces biogas and methane. A floating dome anaerobic digester is used to convert organic fruit waste into biogas, and the parameters such as slurry temperature, daily biogas yield, methane percentage, and slurry pH range are investigated.

MATERIALS AND METHODS

The fresh cow dung was sourced from a local dairy farm, while the fruit trash was procured from the Koyambedu Wholesale Market Complex in the city of Chennai, Tamil Nadu. For this investigation, a one cubic meter anaerobic digester with a range of ambient temperatures was used. The process of anaerobic digestion, which began with fresh cow manure and banana peels, is now being completed using papaya and mango peel, and the waste ratio is 50/50. In the same way that banana peel and mango peel are combined in a 1:1 ratio for digestion, a similar approach is also used for papaya peel and banana peel. The anaerobic digester operates in a temperature range of 30° Celsius to 38° Celsius, and the temperature of the digested slurry is measured every day using a thermocouple linked to a digital thermometer. A pen-type pH redox meter is used to monitor pH during the digesting stages of the thirty-day hydro retention time

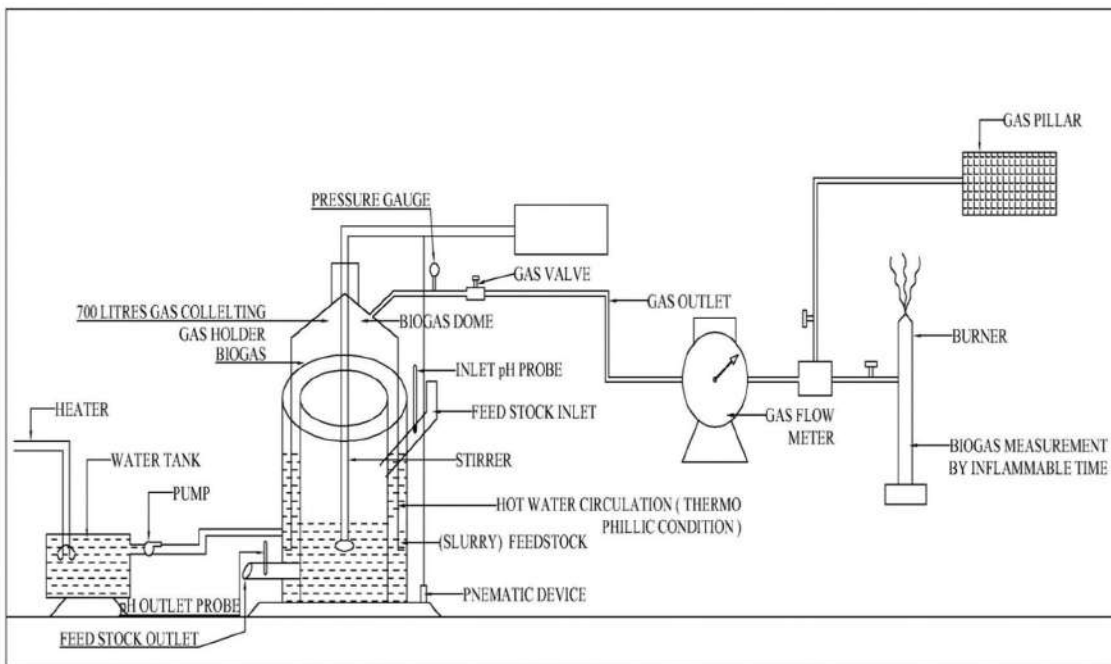


Fig. 1: Schematic experimental setup.

(HRT) tests. The gas chromatography measured methane is examined at Nagapatinam Petrochemical Limited, Tamil Nadu, India.

A pneumatic agitator stirs the digester slurry to raise the percentage of biogas and methane during the digestion periods. The 700-litre gas-holding capacity floating dome anaerobic digester is made of fiber material. The daily biogas amount is determined by using the Albarg gas flow meter, and the digester's gas sample airbags are collected, tested, and evaluated. In the mixing tank, the digester slurry

(a mixture of banana and papaya peels as well as a mixture of banana and mango peels) is made with water in an equal ratio. The prepared slurry is then supplied into the inlet chamber of the digester via the intake pipe. By feeding the new slurry, the old slurry is now pushed from the top of the input chamber into the output chamber. During the digestion time, the slurry is agitated every five minutes to eight minutes inside the digester using the stir agitation device. Fig. 1 shows the schematic view of the experimental setup.

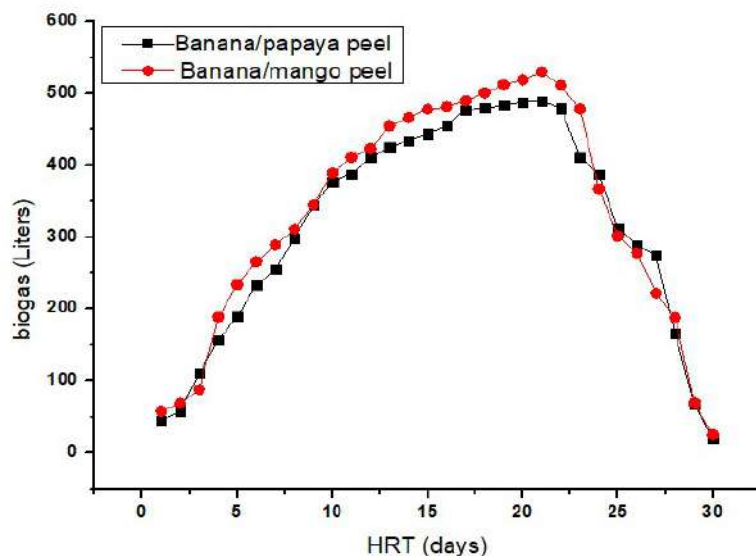


Fig. 2: Hydro retention time with respect to biogas yield.

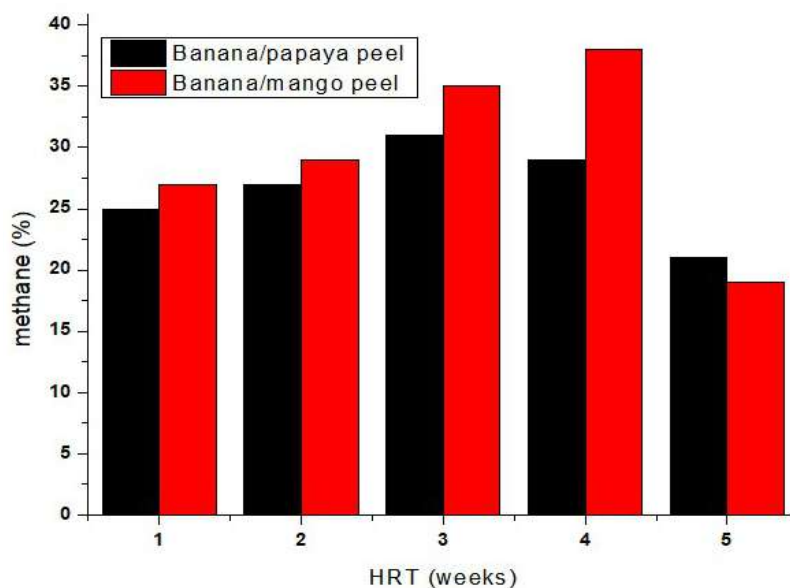


Fig. 3: Hydro retention time with respect to methane.

RESULTS AND DISCUSSION

As a result of the hydrolysis process with banana and mango peel, it is observed that 530 liters of biogas are produced on the 21st day of digestion. Fig. 2 shows the hydro retention time for biogas production. On the same 21st day of digestion, the banana and papaya peels produced 490 liters of biogas. During this time, banana peels had a higher concentration of methanogenesis bacteria. Mango peels' which increased

the carbon/nitrogen ratio is one of the reasons for this combination of ingredients to produce most biogas. On the other hand, the papaya peels' carbon/nitrogen ratio is under 20:1, which has an impact on the generation of biogas during the digestion process.

Bananas mixed with papaya peel and bananas mixed with mango peel have drastically different methane concentrations in biogas. Fig. 3 shows the methane percentage with respect

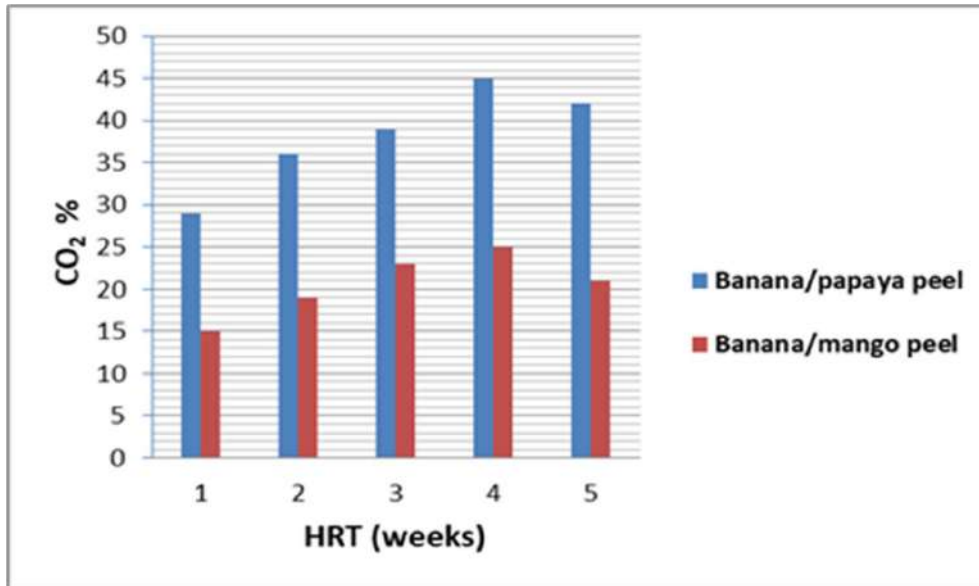


Fig. 4: Hydro retention time with respect to CO₂.

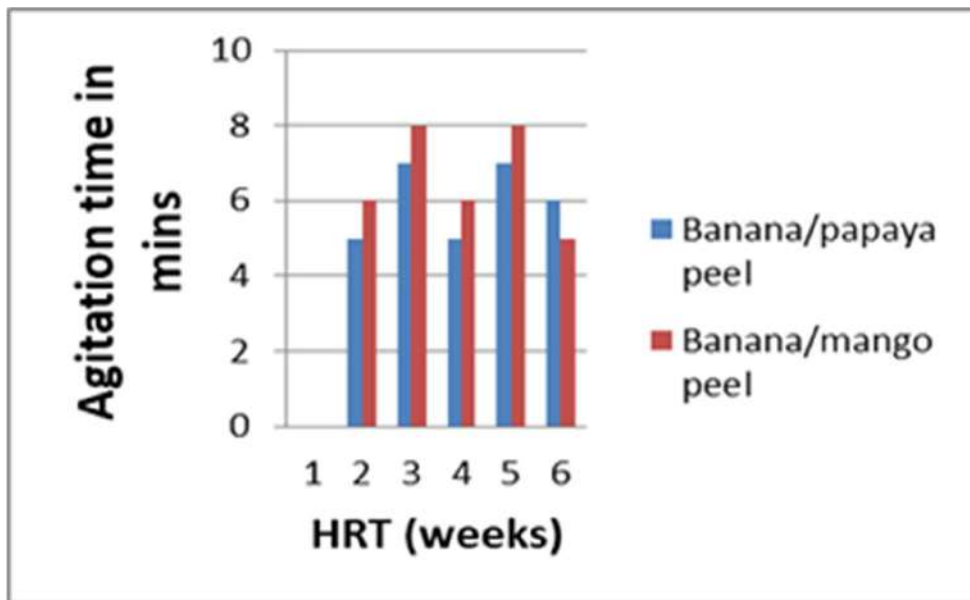


Fig. 5: Hydro retention time with respect to agitation time.

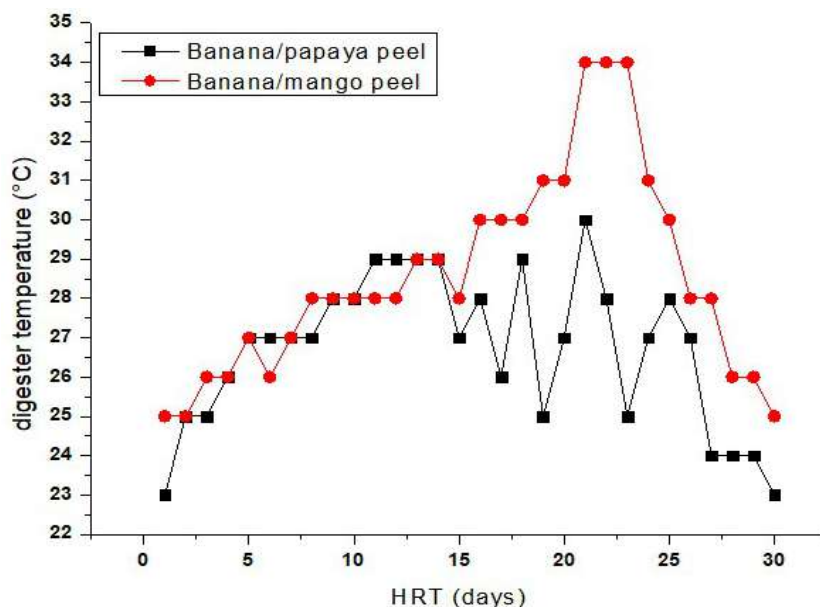


Fig. 6: Hydro retention time with respect to digester temperature.

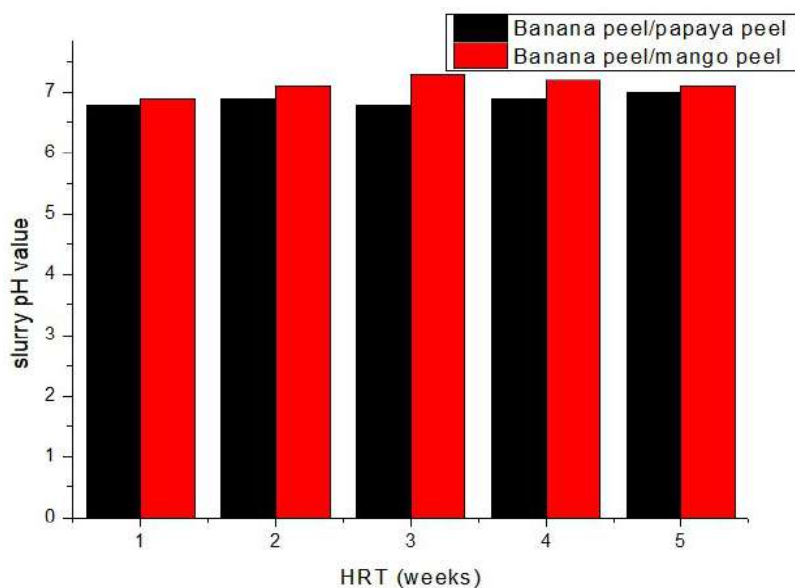


Fig. 7: Hydro retention time with respect to pH range.

to hydro retention time. At the end of the fourth week of digestion, banana mixed with mango peel produced the most methane. According to reports (Otun et al. 2016), mango peel blended with banana peel contains 38% methane. Banana peel with papaya peel has lower methane contents because of the greater alkaline base in this feedstock. Moreover, methane percentages also depend on the acetogenesis of hydrolysis products found in digester slurry.

The levels of carbon dioxide (CO_2) in biogas from banana-mixed papaya peels and banana-mixed mango peels are very different. Fig. 4 illustrates the relationship between carbon dioxide (CO_2) percentage and hydro retention time (HRT). As per the findings, the carbon dioxide levels in the banana mixed mango peels are very low during the periods of digestion. A higher percentage of CO_2 is produced when the banana and papaya peels are mixed. Due to the higher

carbon content of banana and papaya peels, the feedstock produces most of the carbon dioxide.

It is known that to produce biogas and methane, agitation time is a crucial factor. Fig. 5 shows the relationship between the agitation time and hydro retention time. As per the findings, stirring the digester slurry for six minutes results in the highest percentages of biogas and methane compared to other stirrer timing (Seralthan et al. 2023). In an anaerobic digester, agitation encourages homogenization of the substrate, which, on the one hand, improves the contact between substrate and bacteria, speeding up the rate of organic matter degradation, and, on the other hand, prevents the formation of dead volumes, leaving particles in suspension, and which will make it easier for biogas bubbles to move around the digester.

During anaerobic digestion, temperature is one of the key parameters to produce biogas and methane. Fig. 6 illustrates the digester temperature during the digestion periods with respect to hydro retention time. The temperature of the slurry is tracked daily during the 30-day digestion period in this study. During this instance, banana mixed with mango peel produced the most amounts of methane and biogas when the slurry temperature is between 33°C and 34°C with the highest gas production being recorded on the 21st day of digestion. Afterwards, biogas creation is curbed. Previous researchers (Md. Nurul Islam & Zularisam 2018) had found that methanogenesis bacteria do not form at temperatures below 28°C. Due to the low temperature, the production of biogas and methane is impacted during digestion times.

The main causes of acid production are acidogenesis and acetogenesis processes, both of which result in the production of acetic and fatty acids during digestion. Fig. 7 depicts the bio-pH digester's levels being moderated with respect to hydro retention time. In this study, mango peel mixed with banana peel had the highest pH levels of 7.1 to 7.2 during the third week of digestion and produced more biogas than other samples of papaya mixed with banana peels. Under ideal circumstances, volatile acids get converted in an anaerobic digester to methane and carbon dioxide, resulting in a pH of 6.8 to 7.2. The quantity of volatile acids produced in the digester will increase with the quantity of volatile solids fed to it. This will also increase the effect of the digester's alkalinity and pH levels. Sludge with a high volatile content should be moved gently to an anaerobic digester (Sathish et al. 2020). The ability of the reactor mixture to neutralize acids and withstand pH variations is known as the buffering capacity of alkalinity. As a result, process stability and resilience to changes in ambient circumstances are increased by buffering capacity (Vivekanand et al. 2012).

CONCLUSIONS

Based on the experimental results, it can be concluded that the banana peel mixed with mango peel can increase the daily biogas yield. Adding cow dung to fruit substrate enhances the methane and cumulative biogas yield. The process of biogas yield is not merely a source of energy but also used as a source of organic fertilizer. The anaerobic digestion of fruit waste (i.e., banana mixed with mango peels and banana mixed with papaya peels) is also the best method for managing solid waste because it lowers the quantity of waste that must be disposed of in landfills. Based on the study, the following conclusions are made.

- As a result of the hydrolysis process with banana and mango peels, 530 liters of biogas were produced on the 21st day of digestion, whereas the banana and papaya peels produced 490 liters of biogas during the same period.
- At the end of the fourth week of digestion, banana mixed with mango peel produced the most methane, and stirring the digester slurry for six minutes resulted in the highest percentages of biogas and methane.
- Bananas mixed with mango peel produced more quantities of methane and biogas when the slurry temperature is between 33°C and 34°C and the highest gas production is recorded in the 21st stage of digestion.
- Mango peel mixed with banana peel has the highest pH levels of 7.1 to 7.2 during the third week of digestion and produced more biogas than other samples of papaya mixed with banana peels.

Moreover, this approach produces energy in the form of biogas and generates economic benefits if the gas is used internally rather than buying energy from the distributors outside the company.

REFERENCES

- Budiyono, F., Manthia, N., Amalin, H., Hawali, A.M. and Siswo, S. 2018. Production of biogas from organic fruit waste in anaerobic digester using ruminant as the inoculum. *MATEC Web of Conf.*, 156: 03053.
- Dieu, L.H., Chris, D., Henri, C. and Sanderine, N. 2019. Impacts of biogas production on nitrogen flows on Dutch dairy system: Multiple level assessments of nitrogen indicators within the biogas production chain. *J. Ind. Ecol.*, 24(3): 665-680.
- Divya, D., Gopinath, L.R. and Merlin Christy, P. 2015. A review of current aspects and diverse prospects for enhancing biogas production by sustainable means. *Renew. Sustain. Energy Rev.*, 42: 690-699.
- Farkad, A.L. 2016. A study of biogas production from date palm fruit wastes. *J. Clean Prod.*, 139: 1191-1195.
- Md. Nurul, I.S. and Zularisam, A.W. 2018. Achievements and perspectives of anaerobic co-digestion: a review. *Journal of Cleaner Production*, 194: 359-371.
- Muhammad, R.A.M. and Shuichi, T. 2014. Anaerobic co-digestion of cafeteria, vegetable, and fruit wastes for biogas production. *Proceedings*

- of the IEEE 2014 International Conference on Renewable Energy Research and Application (ICRERA), 6 pages.
- Nathaniel, S., Cristina, T., Tilahun, S., Workneh, O. and Olubayo, B. 2020. Design of a household biogas digester using co-digested cassava, vegetable, and fruit waste. *Energy Rep.*, 6(9): 1476-1482.
- Nidhal, B.K., Farkad, A., Lattieff, J.M., Mahdi, M.S., Ghanim, H.S., Muhsin, J. and Narjes, B. 2022. Modeling of biogas production and biodegradability of date palm fruit wastes with different moisture contents. *J. Clean. Prod.*, 375: 134103.
- Otun, T.F., Ojo, O.M., Ajibade, F.O. and Babatola, J.O. 2016. Evaluation of biogas production from the digestion and co-digestion of animal waste, food waste, and fruit waste. *International Journal of Energy and Environmental Research*, 4(4): 8-21.
- Parthiban, A., Sathish, S., Suthan, R., Sathish, T., Rajasimman, M., Vijayan, V. and Jayaprabakar, J. 2023. Modeling and optimization of thermophilic anaerobic digestion using biowaste. *Environmental Research*, 220: 115075.
- Qiangqiang, L., Shiyu, P., Lang, Z., Linchuan, F., Zhenchong, L., Liqin, D. and Yutuo, W. 2022. Improving the biogas potential of rice straw through microwave-assisted ammoniation pretreatment during anaerobic digestion. *BioEnergy Res.*, 15: 21240-1250.
- Sathish, S. and Vivekanandan, S. 2016. Parametric optimization for floating drum anaerobic bio-digester using response surface methodology and artificial neural network. *Alex. Eng. J.*, 55(4): 3297-3307.
- Sathish, S., Chandrasekaran, M. and Parthiban, A. 2018. Effect of co-digestion agricultural-industrial residues: Various slurry temperatures. *Int. J. Amb. Energy*, 39(7): 694-697.
- Sathish, S., Balaji, R., Shafee, S.M. and Mageswaran, C. 2020. Experimental analysis on anaerobic digestion of industrial waste biomass. *AIP Conf. Proceed.*, 2225(1): 060002.
- Seralathan, S., Chenna Reddy, G., Sathish, S., Muthuram, A., Joshuva, A., Narayan, L., Karthikeyan, V., Chatchai, S., Rattapon, N. and Chattariya, S. 2023. Performance and exergy analysis of an inclined solar still with baffle arrangements. *Heliyon*, 9(4): e14807.
- Suelen, P., Luis, E.K., Luciana, P.G. and Luis, A.S.M. 2017. Biogas production from co-digestion of organic fraction of municipal solid waste and fruit and vegetable waste. *Bioresour. Technol.*, 228: 362-367.
- Teguh, A., Rochim, B.C., Abby, V., Stijn, M., Ria, M., Sarto, M. J., Taberzadeh, J. and Siti, S. 2017. Utilization of fruit waste as biogas plant feed and its superiority compared to landfills. *Int. J. Technol.*, 8(8): 1385-1392.
- Vivekanand, V., Vincent, G.H., Eijnsink, M. and Svein, J.H. 2012. Biogas production from the brown seaweed *Saccharina latissima*: Thermal pretreatment and co-digestion with wheat straw. *J. Appl. Phycol.*, 24: 1301-1295.

ORCID DETAILS OF THE AUTHORS

S. Seralathan: <https://orcid.org/0000-0001-6636-7794>



Comparative Analysis of Various Seed Sludges for Biohydrogen Production from Alkaline Pretreated Rice Straw

Pushpa Rani*† , Chhotu Ram** , Arti Yadav*, Deepak Kumar Yadav* , Kiran Bishnoi*** and Narsi Ram Bishnoi* 

*Department of Environmental Science and Engineering, Guru Jambheshwar University of Science and Technology, Hisar, Haryana, India

**Department of Chemical Engineering, College of Engineering and Technology, Adigrat University, Adigrat, Tigray, 7040, Ethiopia

***Department of Environmental Studies, Govt. College for Women, Hisar-125001, Haryana, India

†Corresponding authors: Pushpa Rani, ppvishnoi.in@gmail.com

Nat. Env. & Poll. Tech.
Website: www.neptjournal.com

Received: 14-10-2023

Revised: 06-11-2023

Accepted: 07-11-2023

Key Words:

Rice straw
Alkaline pretreatment
Mixed culture
Anaerobic fermentation
Biohydrogen production

ABSTRACT

The present work studied the effects of alkali pretreatment on the cellulosic biomass of rice straw. The improvement in the cellulose content and reduction in the lignin and hemicellulose percentage was observed with alkali pretreatment. Fourier transformation infrared spectroscopy (FTIR) and Scanning electron microscopy (SEM) analysis confirm the modification in the surface structure of alkali rice straw. Further, the study investigated the potential of different types of seed sludge as inoculum sources for dark fermentative biohydrogen production. In comparison to other sludge samples (beverage industry, food industry, and sewage treatment plant sludge), the mixed culture of sewage treatment plant sludge had the highest cumulative volume of biohydrogen (90.52 mL), as well as the highest hydrogen production yield (0.75 mole_{H₂}/mole) with the substrate utilization of 86.72%. The results provide information on the best sludge source for enhancing biohydrogen production in the dark fermentation method.

INTRODUCTION

Hydrogen is regarded as one of the most promising fuels of the future owing to its significant properties, such as high energy content (142 kJ.g⁻¹) in comparison to hydrocarbon fuels. Presently, most of the hydrogen (50%) is produced by conventional thermo-chemical techniques like thermal or steam reforming of natural gas or petroleum fractions (Sgobbi et al. 2016, Rani et al. 2022, Ram et al. 2023). To promote a more environmentally sustainable fuel, hydrogen production methods should strive to prevent or reduce CO₂ emissions. In recent years, biological hydrogen production has gained a lot of attention among the many hydrogen production techniques (Trchounian et al. 2017). Dark fermentation has become more attractive due to the high hydrogen production rate, no required light source, the use of a variety of potential substrates, and simplicity in construction (Lukajtis et al. 2018, Mohammed et al. 2018). In the dark fermentation process, different types of biomass/substrates such as agricultural waste, fuelwoods, energy crops, livestock residues, algal feedstocks, food waste,

lignocellulosic biomass, municipal solid waste (MSW), dairy waste, industrial waste, etc., could be utilized as a carbon source to the microorganisms (Nasirian et al. 2011). Lignocellulosic biomass is a better option for biohydrogen production due to its massive potential of availability on earth, low price, and enrich in high carbohydrate contents (Kumar et al. 2015, Rani et al. 2023). Rice straw is found to be one of the plentiful, renewable agricultural residues accessible in Haryana, Punjab, Madhya Pradesh, and Uttar Pradesh, India. Rice straw, being an agricultural waste, could be utilized as a raw material for biohydrogen production. The primary components of lignocellulosic biomass are cellulose, hemicellulose, and lignin. The complicated structure of lignocellulosic biomass makes it challenging to use as a feedstock for biofuel production (Sarangi & Nanda 2020, Akubude et al. 2021). Therefore, pretreatment is necessary to simplify the complex structures of this biomass, which further affects the biohydrogen efficiency generation technology. The pretreatment process can partially remove lignin and hemicellulose, reduce cellulose crystallinity, and increase porosity (Saratale et al. 2013, Soares et al. 2020,

Ram et al. 2023). Alkali pretreatment with sodium hydroxide is the most well-known and cost-effective, and it has been frequently used to generate bioenergy from agricultural waste. Alkalis usually attack the lignin-hemicellulose bonds to solubilize the hemicellulose, leading to high delignification and exposing the cellulose to hydrolysis (Zheng et al. 2018, Yadav et al. 2020).

It has been studied that H_2 yield not only upon the type of pretreatment/hydrolysis process but also on the composition and quality of the substrates, type of micro-organisms, either consortium (e.g., anaerobic digested sludge) or pure cultures of mesophilic (e.g., *Clostridium butyricum*) and thermophilic bacteria (e.g., *Caldicellulosiruptor saccharolyticus*), physiological conditions, type of reactor (Rai & Singh 2016). The observation demonstrates that mixed consortia are preferable over pure consortia since they do not require a specific aseptic environment, resulting in simple handling and broad applicability. Further, these cultures are less impacted by the alteration in substrate type and compositions (Łukajtis et al. 2018).

The present research work aims to develop an alternative renewable, sustainable, and cost-effective green approach for biohydrogen production involving the process that utilizes low-cost rice straw waste. The main objective of the study is to investigate the effects of alkali pretreatment on the chemical composition and surface structure of rice straw. Furthermore, the current work aims to compare different sludge types to identify the most suitable one for optimizing biohydrogen production from alkaline-pretreated rice straw.

MATERIALS AND METHODS

Feedstock and Alkaline Pretreatment

Rice straw samples were collected from the rural areas of Fatehabad district (Haryana). The collected samples were washed, dried, and cut into small pieces before grinding and sieved with 80 mm mesh size. The powder samples were oven-dried at 50°C and stored in an airtight bottle for further experiments and subsequent studies.

Alkaline pretreatment was employed to delignify the biomass. Dried rice straw and dilute sodium hydroxide (2% NaOH) were applied to the rice straw. A solid-to-liquid ratio of 5:100 (w/v) was used to make sure that the rice straw powder was completely immersed in the solution. Kept the mixture in the autoclave at 121°C and 15 psi for 60 min. After this, it was allowed to cool. Filter the pretreated rice straw sample from the mixture with muslin cloth and, neutralize the residue by washing it with distilled water, and continue washing till the pH becomes neutral or 7.0.

The pretreated solid was completely dried at a temperature of 50°C.

Seed Sludge

Various sludge samples were collected from different selected sites, such as beverage industry sludge (BS), food industry sludge (FS), and sewage treatment plant sludge (STP), which contains anaerobic bacteria. The samples from different sites were collected in Ziplock polybags, which were sealed and stored at 4°C temperature for the isolation procedure. For the test study, to improve the fermentative microbial flora and get rid of methanogenic and other hydrogen-consuming bacteria that reduce the effectiveness of hydrogen-producing bacteria, the seed sludge was heated at 90°C for 30 min. The following inorganic supplements ($g.L^{-1}$) were present in the feed medium in appropriate amounts: $NaHCO_3$ 6.72, NH_4HCO_3 5.24, $MgCl_2.6H_2O$ 0.1, K_2HPO_4 0.125, $MnSO_4.6H_2O$ 0.015, $FeSO_4.7H_2O$ 0.025, $CuSO_4.5H_2O$ 0.005, and $CoCl_2.5H_2O$ 0.000125 (Endo et al. 1982).

Enrichment of hydrogen-producing mixed cultures was carried out in 125 mL serum vials with a 50 mL working volume following a method described elsewhere (Sivagurunathan et al. 2014). The sterile pre-produced peptone-yeast-glucose (PYG) medium contained the following nutrients (in $g.L^{-1}$): 10, peptone, 10, yeast extract, 0.001, resazurin, 0.5, L-cysteine-HCl, 10, glucose. The pH was adjusted to 7.0 using either 1 N HCl or NaOH before autoclaving. The media was autoclaved at 121°C and 15 psi pressure for sterilization. The PYG medium with inoculum was incubated at 70°C for 10 min for the activation of spores into vegetative cells. After the activation of vegetative cells, serum vials were kept under shaking conditions at 110 rpm at 37°C temperature for 4 days, and anaerobic conditions were maintained to observe the growth of consortia. Freshly grown enriched mixed cultures were used as the inoculum for all the fermentation experiments.

Experimental Design

Batch-mode reactor: The batch tests for biohydrogen production were conducted in 125 mL serum vials with a working capacity of 60 mL containing seed sludge (25 mL), supplement solution (10 mL), and substrate (25 mL). To maintain an anaerobic condition, the nitrogen was first flushed through the vials for five min. The batch reactors were sealed with an airtight stopper with an aluminum cap and incubated at a temperature of 37°C while maintaining an agitation speed of 120 RPM. The initial cultivation pH was adjusted to 7.0 at a temperature of 37°C. All experiment sets were carried out in triplicate to ensure reproducibility,

and the data were reported as mean values. A 25-mL syringe was used to measure the total gas volume using the syringe displacement method. Every 24 hours, the syringe was reset to zero. A needle was injected into the stopper of the syringe to assess the total amount of gas. However, it was observed that the gas pressure within the container could potentially displace the syringe plunger, leading to a quantifiable change in the syringe plunger's volume, which is then recorded as the generated gas volume. A gas chromatograph equipped with a thermal conductivity detector (TCD) was used to measure the hydrogen content.

Analytical Methods

The characteristics of raw rice straw and alkali-pretreated rice straw were tested in the laboratory. The chemical constituents of raw and alkali-pretreated rice straw samples, such as cellulose, hemicellulose, and lignin, were analyzed by the standard method described (Goering & Soest 1970). SEM (Zeiss Sigma500) was used to examine morphological changes in the untreated and alkali-pretreated rice straw. Oven-dried and fine-powdered samples were used to determine the morphology of rice straw. Samples were mounted on the aluminum stubs with the gold coating in a sputter before image analysis. Fourier Transformation Infrared Spectroscopy (FTIR) investigated the various functional groups of the native and alkali-pretreated rice straw samples. FTIR spectra were taken on a Perkin-Elmer Spectrum. The instruments with an absorption wave range between 400 - 4000 cm^{-1} were used for all samples. A trace amount of fine ground sample was mixed with potassium bromide (KBr) to analyze the various spectral lines. A gas chromatograph (5800, Centurion scientific instrument, capillary column, TCD detector) was used to analyze the composition of the biohydrogen gas produced in the reactor. The temperature settings for the column, injector, and detector were 80, 150, and 220°C, respectively. The nitrogen gas was used as a carrier gas, and the flow rate of nitrogen gas was maintained at 20 ml min^{-1} . A pressure-lock gas syringe with a capacity of 1 mL was used for the gas injection. The cumulative biohydrogen production was determined using a mass balance equation (1) (Logan et al. 2002)

$$V_{\text{Hi}} = V_{\text{Hi-1}} + C_{\text{Hi}}(V_{\text{Gi}} - V_{\text{Gi-1}}) + V_{\text{W}}(C_{\text{Hi}} - C_{\text{Hi-1}}) \quad \dots(1)$$

where V_{Hi} and $V_{\text{Hi-1}}$ are cumulative volumes of biohydrogen at the current and previous times. V_{Gi} and $V_{\text{Gi-1}}$ are the total volumes of biogas at the current and previous times,

C_{Hi} and $C_{\text{Hi-1}}$ are the fractions of biohydrogen (%) in the headspace of the bottle at the current and previous time

VW is the cumulative headspace volume within the bottle.

A gas chromatograph (Nucon, 5765) equipped with an FID (flame-ionized detector) was used to measure the volatile fatty acid concentrations (VFAs) at the end of the fermentation process. The temperature settings for the column, injector, and detector were 145, 175, and 185°C, respectively. The initial oven temperature was 95°C and held for 5 min, and further, the temperature was raised to 145°C at 10°C. min^{-1} . Nitrogen was employed as the carrier gas, with a flow rate of 6.0 mL. min^{-1} .

RESULTS AND DISCUSSION

Chemical and Structural Characterization

Table 1 illustrates the percentage of the three major components: cellulose, hemicellulose, and lignin. It was found that the relative proportion of cellulose was increased after alkaline pretreatment as compared to the native rice straw sample. Alkali pretreatment increased the cellulose content from 35.5% in raw rice straw samples to 60.48% by removing amorphous materials from the biomass. Furthermore, alkali pretreatment enhances the accessibility of cellulose, leading to the maximal production of fermentable sugars during enzymatic hydrolysis. The hemicellulose and lignin content were reduced from 24.19% and 13.81% in raw rice straw to 12.28% and 3.38% in alkaline pretreated rice straw, respectively. Alkali pretreatment with sodium hydroxide (NaOH) causes biomass to swell up, which leads to an increase in internal surface area and thereby enhances enzymatic accessibility. Simultaneously, it also decreases the degree of crystallinity of cellulose and disruption of ester bonds between hemicelluloses and lignin. This disruption promotes the solubilization of both lignin and hemicellulose components. Numerous research related to this study also reported similar results (Barman et al. 2012, Zheng et al. 2018).

After sodium hydroxide pretreatment, the surface morphology of rice straw was influenced by the reaction of sodium hydroxide with ester bonds, which led to the removal of lignin and the release of cellulose. The raw rice straw has a smooth, compact surface structure with tightly packed fibers grouped in bundles, as shown by the SEM images (Fig. 1A). The smooth surface indicated that the fibers were covered in lignin. Alkali pretreatment revealed significant changes in the surface morphology of the rice straw sample, which represents the damage to the structure and composition of biomass. The hemicellulose and lignin in the pretreated straw samples were partly removed, fractured, or became loose, exposing interior structures (Kshirsagar et al. 2015). The alkali-pretreated rice straw showed a loose, dispersed, and fragmented fibrous structure containing holes and pits (Fig. 1B). Additionally, it facilitates the breaking up of fiber bundles and movement of

Table 1: Chemical composition of raw rice straw and alkali pretreated rice straw.

Components	Raw rice straw	Alkali pretreated rice straw
Cellulose [%]	35.5	60.48
Hemicellulose [%]	24.19	12.28
Lignin [%]	13.81	3.38

fibrous bundles from one site to another, reducing their cell contents and eliminating other chemical components. The disruption of rice straw components because of dilute alkali pretreatment was also reported by several researchers (Singh et al. 2014, Hartati et al. 2021).

The changes in chemical composition and functional group before and after alkali pretreatment were examined by FTIR. Fig. 2 (A, B) represents the functional bands corresponding to their functional group present in the raw and alkali pretreated rice straw biomass in which the X-axis

(cm^{-1}) symbolizes wavenumber whereas on Y-axis symbolizes transmittance (%T). The FTIR spectrum of rice straw was observed in the region of 500–4000 cm^{-1} .

Table 2 represents the spectrum band and functional group present in raw and alkali-pretreated rice straw. The predominate peaks at 3430.57, 2923.31, 1637.19, 1420.95, 1365.41, 1103.17 in raw rice straw, whereas peaks at 3412.06, 2922.77, 1637.32, 1431.7, 1376.25, 1035.41, 897.1 were observed in alkali pretreated rice straw. It was found that the alkali pretreatment resulted in disappearing of certain peaks and others shifting locations. Furthermore, the alkali pretreatment caused a reduction in the hydroxyl group concentration in the biomass compared to the raw sample, as evidenced by a decrease in the intensity of the O-H absorption band. Table 2 shows peaks and bands that correspond to different functional groups found in raw and alkali-pretreated rice straws.

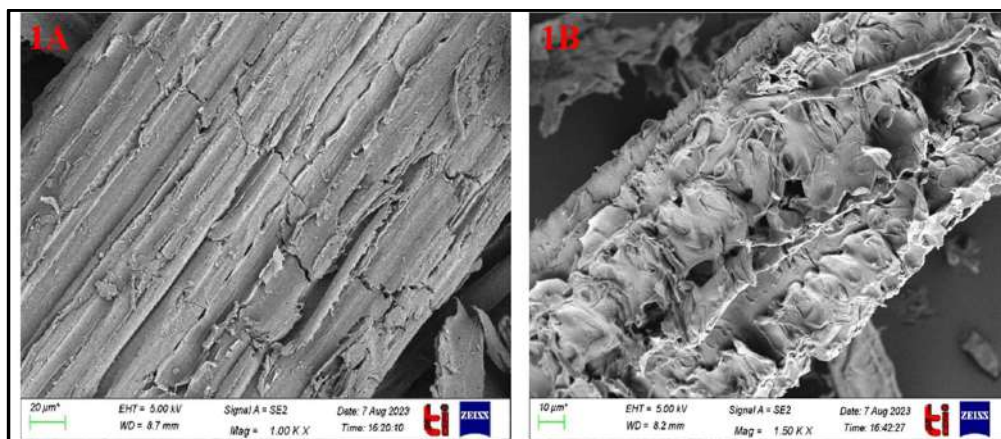


Fig. 1A: SEM images of raw rice straw, 1B: SEM image of alkali pretreated rice straw.

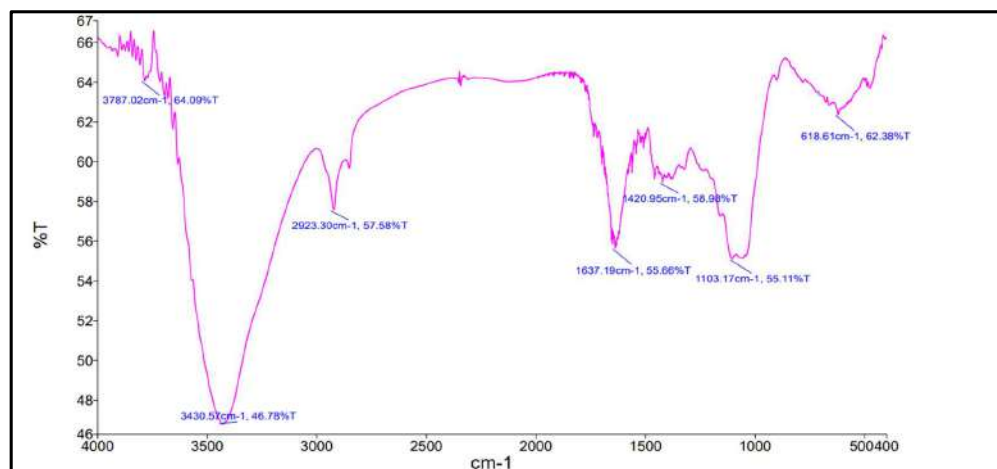


Fig. 2A: FTIR spectrum of raw rice straw.

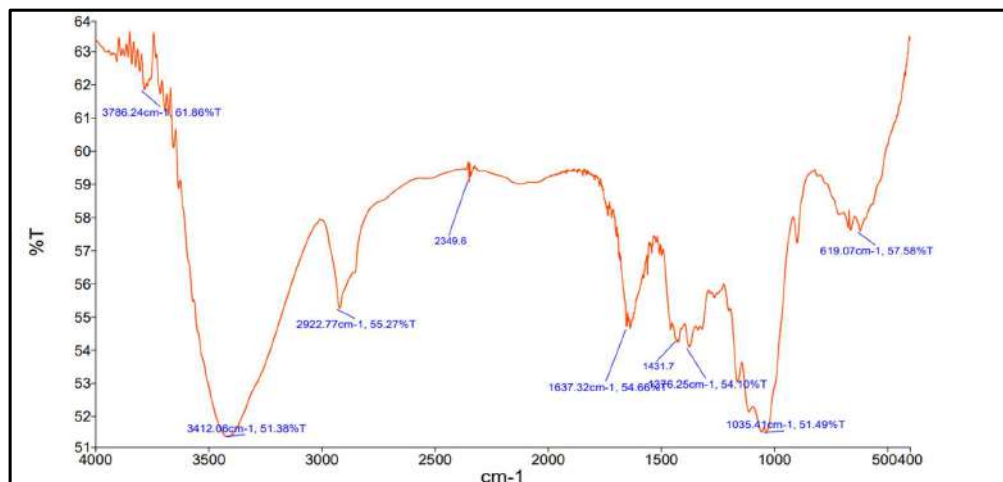


Fig. 2B: FTIR spectrum of alkali pretreated rice straw.

Table 2: FTIR spectrum band and functional groups present in raw and alkaline rice straw.

Frequency (cm ⁻¹)	Functional group	Raw RS	Alkali RS	Band assignment
4000-3000	O-H stretching	3787.02	3786.24	Lignin
		3430.57	3412.06	
2923-2900	C-H stretch	2923.31	2922.77	Cellulose
1650-1630	C=C stretch	1637.19	1637.32	Lignin
1440-1400	C=H bend	1420.95	1431.7	Lignin, Cellulose
1380-1360	C-H deformation	1365.41	1376.25	Cellulose
1332-1330	CH ₂ Wagging	ND	ND	Cellulose
1110-1050	C-O-C& C-O stretch	1103.17	1035.41	Cellulose
898-880	C-H deformation	ND	897.1	Cellulose

Isolation of Bacterial Growth

Sludge samples from different selected sites were collected to isolate the bacterial consortia, which have the maximum capability to degrade the lignocellulosic residue. The sludge samples, such as beverage industry sludge (BS), food industry sludge (FS), and sewage treatment plant sludge (STP), were collected from Haryana. Heat treatment was applied to seed sludge (90°C for 30 min) to obtain dominant microbes for hydrogen production, and hinder the activity of methanogenic bacteria to consume hydrogen. Bacterial isolation was done in two assays i.e., plate as well as liquid assay. For the plate method assay, an agar medium was used to culture the isolates. Liquid method assay, isolates were inoculated into broth medium and kept in an incubator at 110 rpm at 37°C for 4 days.

To observe the growth of mixed consortia, the optical density of each seed sample has been analyzed using a UV-VIS spectrophotometer at the wavelength of 520nm, starting from zero hour to 120 h. Fig. 3 represents the bacterial growth phase of three different seed isolates. It has been observed that

the bacterial growth starts increasing from 10 h of inoculation and reaches a maximum at 48 h. After that, it gradually decreases. The exponential growth of bacteria when the cells are dividing by binary fission and doubling their numbers after each generation time is known as the Exponential or log phase (10-48 h). From zero to 10 h represents the lag phase where the bacteria are metabolically active but not dividing. After the log phase, the stationary phase (48-120 h) is achieved, in which the growth of bacterial cells reaches a plateau as the number of dying cells equals the number of dividing cells. As nutrients become less available and waste products increase, the number of dying cells continues to rise. As a result, bacterial population growth experiences a sharp decline.

From Fig. 3 It has been found that the STP sludge's inoculation showed maximum bacterial growth among the three taken seed sludge.

The Influence of Various Microbial Cultures on Biohydrogen Production

To achieve efficient dark fermentative biohydrogen

production from renewable feedstocks, it is crucial to identify promising mixed microbial communities capable of effectively breaking down and fermenting the biomass to produce biohydrogen. Thus, it is crucial to evaluate seed sludges from various sources that contain microorganisms of various types and activities (Chen et al. 2012). The ability of LCB to produce biohydrogen utilizing various sources of inoculums or sludge was reviewed by Ren et al. (2009). Sivagurunathan et al. (2014) performed research in a threefold combination of mixed cultures comprising cow dung, pig slurry, and sewage sludge to enhance biohydrogen production when utilizing glucose as the substrate. The findings revealed a significant improvement in both hydrogen yield and production rate when using the mixed cultures of pig slurry and sewage sludge, with values of 2.34 moles of H_2 per mole of glucose and 6.76 L per day. This contrasted with the performance of the single culture of pig slurry, which yielded 1.59 moles of H_2 per mole of glucose and 4.43 L per day. Another study reported by Amekan et al. (2018) investigated to assess the impact of different sources of inoculum (fruit waste digester (FW), cow dung digester (CD), and tofu waste digester (TW)), as well as their combinations (FW-CD, CD-TW, FW-TW, and FW-CD-TW), on the production of hydrogen from melon waste. The research demonstrated that the highest cumulative hydrogen production, reaching 743 mL (with a yield of 207.56 mL per gram of volatile solids), was observed with the FW inoculum. However, an even more impressive result was obtained with

the combination of FW-CD-TW, which yielded 1,132 mL of hydrogen (at a rate of 231.02 mL per gram of volatile solids). These findings indicate the significance of microbial diversity and interactions in influencing both the yield and the rate of hydrogen production from melon waste in batch fermenters.

To establish a stable hydrogen production process, it is important to understand the impact of enhanced interactions between microbial diversity and the biohydrogen production process (Sivagurunathan et al. 2014). Hence, in the current work, we investigated the impact of different seed sludge, such as beverage industry sludge (BF), food industry sludge (FS), and sewage treatment plant sludge (STP), on the performance of biohydrogen production, and soluble metabolites accumulation using alkali pretreated RS in the batch test. The data obtained from these three types of seed sludges tested during fermentation of alkali RS (10 g.L^{-1}) into biohydrogen production and fermentation end products are summarised in Table 3.

It was observed from Fig. 4 that the heat-pretreated STP mixed consortia had the highest cumulative volume of biohydrogen (90.52 mL) and hydrogen production yield (0.75 mole H_2 /mole, substrate) among the three mixed cultures. No methane production was observed in any of the three seed sludges after undergoing heat treatment. Earlier research revealed that most of the anaerobic sludge might be improved by thermal enrichment to promote hydrogen generation. Heat

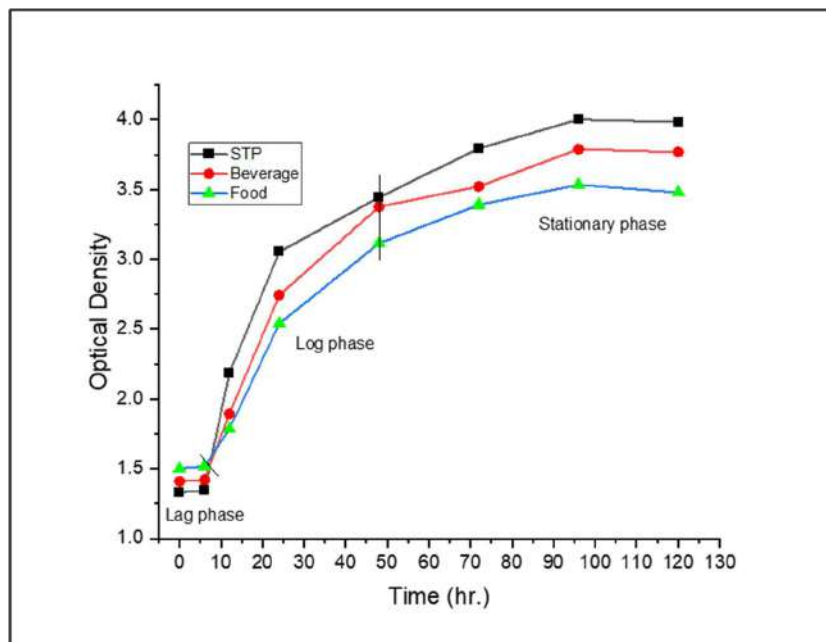


Fig. 3: Bacterial growth phases of three different isolated sludge.

treatment can enrich anaerobic microbes that can produce hydrogen at high temperatures and inhibit other bacteria (Lin et al. 2006, Li & Fang 2007). The maximum biohydrogen was reported at 96th h of fermentation in STP mixed consortia with substrate utilization of 86.72% (Fig. 4). Biohydrogen production ceased after 96 h of fermentation, potentially due to the inhibitory effects of compounds formed during hydrolysis (Srivastava et al. 2017).

Fig. 4 illustrates that the lag phase time (120th h) was prolonged in FS and BS due to decreased bacterial activity of mixed consortia, which resulted in a lower hydrogen yield and substrate utilization rate as compared to STP bacterial consortia. Yang and Wang (2019) studied biohydrogen production by co-fermentation of sewage sludge and grass residue. It was found the efficiency of hydrogen fermentation improved at optimized substrate concentration (10 g.L⁻¹), and the maximum hydrogen yield and VS removal were 45.6 mL/g-VS_{added} and 13.7%, respectively.

Some soluble metabolites, including ethanol and organic acids (acetate, propionate, butyrate), are frequently produced during the hydrogen fermentation process along with hydrogen (Maru et al. 2016). On the one hand, these metabolites are useful indicators for characterizing the performance of the fermentation process. On the other hand, these soluble metabolites can also cause the inhibition of hydrogen production. Table 3 illustrates soluble metabolites end product profiles. As shown in Table 3, the VFAs composition constituted mainly acetate and butyrate

with little production of ethanol. However, the amount of acetate, butyrate, and ethanol varies depending on the type of inoculum employed. In comparison to FS and BS, it was observed that STP microbial consortia comprised maximum VFAs as acetate (1025.71 mg.L⁻¹), butyrate (453.41 mg.L⁻¹), and ethanol (80.19 mg.L⁻¹).

The maximum bacterial growth was observed in STP's sludge inoculation which represents that the STP mixed consortia have maximum capability to degrade the lignocellulosic residue as compared to FS and BS. Further, biohydrogen production potential was also reported maximum in STP bacterial inoculation.

CONCLUSIONS

The current study emphasizes the practical value of utilizing rice straw as a feasible raw material for biohydrogen production through the dark fermentation process. The efficiency of the alkali pretreatment method to break down the lignocellulosic complex structure was confirmed through chemical characterization and SEM and FTIR analysis. Mixed microbial culture plays a significant role in biohydrogen production due to their ability to interact. Mixed cultures can utilize a wider range of substrates, which can increase the efficiency of biohydrogen production. Each microorganism can contribute its unique set of enzymes and metabolic pathways to convert different substrates into hydrogen. Furthermore, maximum cumulative biohydrogen production and high hydrogen yield were observed in

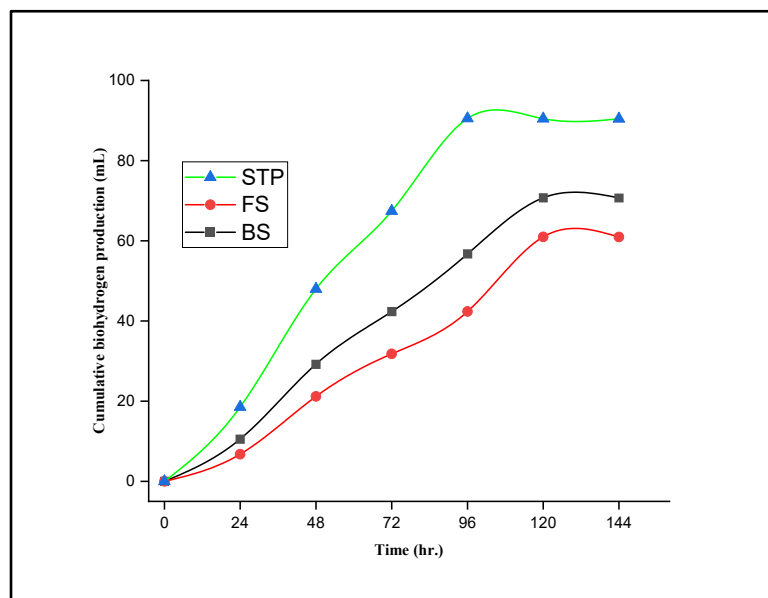


Fig. 4: Cumulative biohydrogen production during fermentation of alkali RS by three seed sludge (STP, FS, BS).

Table 3: Biohydrogen production performance and fermentation end products from alkali pretreated RS (10 g.L⁻¹) using various mixed consortia as seed at initial pH 7.0 and temperature of 37°C.

Seed sludge	Final pH	Cumulative H ₂ [mL]	Hydrogen Yield (mole H ₂ /mole)	Substrate Utilization [%]	Acetate [mg.L ⁻¹]	Butyrate [mg.L ⁻¹]	Ethanol [mg.L ⁻¹]
STP	5.42	90.52	0.75	86.72	1025.71	453.41	80.19
BS	5.67	70.74	0.67	82.07	796.83	348.73	64.39
FS	5.82	60.98	0.56	79.28	614.88	292.81	53.75

sewage treatment plant sludge inoculation as compared with beverage and food sludge. This study showed that mesophilic dark fermentation of alkali-pretreated rice straw with mixed cultures could increase hydrogen yield, hence improving the possibility of biohydrogen production from lignified agricultural residues.

ACKNOWLEDGEMENTS

The authors greatly acknowledge every support from the Department of Environmental Science & Engineering of Guru Jambheshwar University of Science and Technology, Hisar (India).

REFERENCES

- Akubude, V.C., Okafor, V.C., Oyedokun, J.A., Petinrin, O.O. and Nwaigwe, K.N., 2021. Application of Hemicellulose in Biohydrogen Production. Sustainable Bioconversion of Waste to Value Added Products, pp.315-327. DOI: 10.1007/978-3-030-61837-7_19.
- Amekan, Y., Wangi, D.S.A., Cahyanto, M.N., Sarto, S. and Widada, J. 2018. Effect of different inoculum combinations on biohydrogen production from melon fruit waste. Int. J. Renew. Energy Dev., 7(2): 101. DOI: <https://doi.org/10.14710/ijred.7.2.101-109>
- Barman, D.N., Haque, M.A., Kang, T.H., Kim, M.K., Kim, J., Kim, H. and Yun, H.D. 2012. Alkali pretreatment of wheat straw (*Triticum aestivum*) at boiling temperature for producing a bioethanol precursor. Biosci. Biotechnol. Biochem., 76(12): 2201-2207. doi: 10.1271/bbb.120480. Epub 2012 Dec 7.
- Chen, C.C., Chuang, Y.S., Lin, C.Y., Lay, C.H. and Sen, B. 2012. Thermophilic dark fermentation of untreated rice straw using mixed cultures for hydrogen production. Int. J. Hydrog. Energy, 37(20): 15540-15546. <https://doi.org/10.1016/j.ijhydene.2012.01.036>.
- Endo, G., Noike, T. and Matsumoto, J. 1982. Characteristics of cellulose and glucose decomposition in the acidogenic phase of anaerobic digestion. Jap. Soc. Civ. Eng., 325: 61-68. https://doi.org/10.2208/jsej1969.1982.325_61.
- Goering, H.K. and Van Soest, P.J. 1970. Forage Fiber Analyses (Apparatus, Reagents, Procedures, and Some Applications). Technical Paper No. 379. US Agricultural Research Service, Washington, DC.
- Hartati, I., Sulisty, H., Sediawan, W.B., Azis, M.M. and Fahrurrozi, M. 2021. Microwave-assisted urea-based-hydrolytic pretreatment of rice straw: Experimental data and mechanistic kinetic models. ACS Omega, 6(20): 13225-13239. <https://doi.org/10.1021/acsomega.1c01084>.
- Kshirsagar, S.D., Waghmare, P.R., Loni, P.C., Patil, S.A. and Govindwar, S.P. 2015. Dilute acid pretreatment of rice straw, structural characterization, and optimization of enzymatic hydrolysis conditions by response surface methodology. RSC Adv., 5(58): 46525-46533. DOI: 10.1039/C5RA04430H.
- Kumar, G., Bakonyi, P., Periyasamy, S., Kim, S.H., Nemestóthy, N. and Bélafi-Bakó, K. 2015. Lignocellulose biohydrogen: Practical challenges and recent progress. Renew. Sust. Energ. Rev., 44: 728-737. <https://doi.org/10.1016/j.rser.2015.01.042>
- Li, C. and Fang, H.H. 2007. Fermentative hydrogen production from wastewater and solid wastes by mixed cultures. Crit. Rev. Environ. Sci. Technol., 37(1): 1-39. DOI: 10.1080/10643380600729071
- Lin, C.Y., Hung, C.H., Chen, C.H., Chung, W.T. and Cheng, L.H. 2006. Effects of initial cultivation pH on fermentative hydrogen production from xylose using natural mixed cultures. Process Biochem., 41(6): 1383-1390. <https://doi.org/10.1016/j.procbio.2006.01.021>
- Logan, B.E., Oh, S.E., Kim, I.S. and Van Ginkel, S. 2002. Biological hydrogen production was measured in batch anaerobic respirometers. Environ. Sci. Technol., 36(11): 2530-2535. <https://doi.org/10.1021/es015783i>.
- Lukajtis, R., Holowacz, I., Kucharska, K., Glinka, M., Rybarczyk, P., Przyjazny, A. and Kamiński, M. 2018. Hydrogen production from biomass using dark fermentation. Renew. Sust. Energ. Rev., 91: 665-694. DOI: 10.1016/j.rser.2018.04.043.
- Maru, B.T., López, F., Kengen, S.W.M., Constantí, M. and Medina, F. 2016. Dark fermentative hydrogen and ethanol production from biodiesel waste glycerol using a co-culture of *Escherichia coli* and *Enterobacter sp.* Fuel, 186: 375-384. <https://doi.org/10.1016/j.fuel.2016.08.043>.
- Mohammed, A., Abdul-Wahab, M.F., Hashim, M., Omar, A.H., Reba, M.N.M., Said, M.F.M. and Ibrahim, Z. 2018. Biohydrogen production by Antarctic psychrotolerant sp. ABZ11. Pol. J. Microbiol., 67(3): 283-290. doi: 10.21307/pjm-2018-033
- Nasirian, N., Almassi, M., Minaei, S. and Widmann, R. 2011. Development of a method for biohydrogen production from wheat straw by dark fermentation. Int. J. Hydrog. Energy, 36(1): 411-420. DOI: 10.1016/j.ijhydene.2010.09.073
- Rai, P.K. and Singh, S.P. 2016. Integrated dark-and photo-fermentation: Recent advances and provisions for improvement. Int. J. Hydrog. Energy, 41(44): 19957-19971. <https://doi.org/10.1016/j.ijhydene.2016.08.084>.
- Ram, C., Rani, P. and Kumar, A. 2023. Recent developments in biohydrogen production from wastewater: A review. Biocatal. Biotransformation, 1-18. DOI: 10.1080/10242422.2023.2181046.
- Rani, P., Bishnoi, K., Bishnoi, N.R., Kumar, D. and Singh, A. 2022. Biohydrogen production technologies: Past, present, and future perspective. In: Kothari, R., Singh, A. and Arora, N.K. (eds.) Biomass, Bioenergy & Bioeconomy. Microorganisms for Sustainability, Vol 35. Springer, Singapore.
- Rani, P., Yadav, D.K., Yadav, A., Chander, S. and Bishnoi, N.R. 2023. Structural and morphological alteration of wheat straw biomass utilizing alkali Pre-treatment. Ann. Biol., accepted for publication on 13 Feb., 2023.
- Ren, N., Wang, A., Cao, G., Xu, J. and Gao, L. 2009. Bioconversion of lignocellulosic biomass to hydrogen: Potential and challenges. Biotechnol. Adv., 27(6): 1051-1060. doi: 10.1016/j.biotechadv.2009.05.007.
- Sarangi, P.K. and Nanda, S. 2020. Biohydrogen production through dark fermentation. Chem. Eng. Technol., 43(4): 601-612. <https://doi.org/10.1002/ceat.201900452>.
- Saratale, G.D., Saratale, R.G. and Chang, J.S. 2013. Biohydrogen from renewable resources. Biohydrogen, 185-221. DOI: 10.1016/B978-0-444-59555-3.00009-X.
- Sgobbi, A., Nijs, W., De Miglio, R., Chiodi, A., Gargiulo, M. and Thiel,

- C. 2016. How far away is hydrogen? Its role in the medium and long-term decarbonization of the European energy system. *Int. J. Hydrog. Energy*, 41(1): 19-35. <https://doi.org/10.1016/j.ijhydene.2015.09.004>.
- Singh, R., Tiwari, S., Srivastava, M. and Shukla, A. 2014. Microwave-assisted alkali pretreatment of rice straw for enhancing enzymatic digestibility. *J. Energy*, 1-7. <https://doi.org/10.1155/2014/483813>.
- Sivagurunathan, P., Sen, B. and Lin, C.Y. 2014. Batch fermentative hydrogen production by enriched mixed culture: Combination strategy and their microbial composition. *J. Biosci. Bioeng.*, 117(2): 222-228. <https://doi.org/10.1016/j.jbiosc.2013.07.015>.
- Soares, J.F., Confortin, T.C., Toderò, I., Mayer, F.D. and Mazutti, M.A. 2020. Dark fermentative biohydrogen production from lignocellulosic biomass: Technological challenges and future prospects. *Renew. Sust. Energ. Rev.*, 117: 109484. <https://doi.org/10.1016/j.rser.2019.109484>.
- Srivastava, N., Srivastava, M., Kushwaha, D., Gupta, V.K., Manikanta, A., Rameke, P.W. and Mishra, P.K. 2017. Efficient dark fermentative hydrogen production from enzyme-hydrolyzed rice straw by *Clostridium pasteurianum* (MTCC116). *Bioresour. Technol.*, 238: 552-558. doi: 10.1016/j.biortech.2017.04.077
- Trchounian, K., Sawers, R.G. and Trchounian, A. 2017. Improving biohydrogen productivity by microbial dark-and photo-fermentations: Novel data and future approaches. *Renew. Sust. Energ. Rev.*, 80: 1201-1216. DOI: 10.1016/j.rser.2017.05.149.
- Yadav, M., Paritosh, K. and Vivekanand, V. 2020. Lignocellulose to bio-hydrogen: An overview on recent developments. *Int. J. Hydrog. Energy*, 45(36): 18195-18210. DOI: 10.1016/j.ijhydene.2019.10.027.
- Yang, G. and Wang, J. 2019. Biohydrogen production by co-fermentation of sewage sludge and grass residue: Effect of various substrate concentrations. *Fuel*, 237: 1203-1208. <https://doi.org/10.1016/j.fuel.2018.10.026>.
- Zheng, Q., Zhou, T., Wang, Y., Cao, X., Wu, S., Zhao, M. and Guan, X. 2018. Pretreatment of wheat straw leads to structural changes and improved enzymatic hydrolysis. *Sci. Rep.*, 8(1): 1321. DOI: 10.1038/s41598-018-19517-5.

ORCID DETAILS OF THE AUTHORS

- Pushpa Rani: <https://orcid.org/0000-0002-0864-7445>
Chhotu Ram: <https://orcid.org/0000-0002-6914-6070>
Deepak Kumar Yadav: <https://orcid.org/0000-0001-5067-8694>
Narsi Ram Bishnoi: <https://orcid.org/0000-0001-5187-0944>





Effectiveness of Activated Carbon from Nutmeg Shell (*Myristica fragrans*) Waste as Adsorbent for Metal Ions Pb(II) and Cu(II) in Liquid Waste

Ishar*†, Paulina Taba** and Fahrudin***

*Study Program of Environmental Management, Graduate School, Hasanuddin University, Makassar 90245, Indonesia

**Department of Chemistry, Faculty of Mathematics and Natural Sciences, Hasanuddin University, Makassar 90245, Indonesia

***Department of Biology, Faculty of Mathematics and Natural Sciences, Hasanuddin University, Makassar 90245, Indonesia

†Corresponding author: Ishar; izhar77khalqi@gmail.com

Nat. Env. & Poll. Tech.
Website: www.neptjournal.com

Received: 17-11-2023

Revised: 01-01-2024

Accepted: 14-01-2024

Key Words:

Adsorption

SEM

SAA

Nutmeg shell

Pb(II) and Cu(II) ions

ABSTRACT

Various wastes can be utilized to produce activated carbon, one of the wastes that can be utilized is nutmeg shell (*Myristica fragrans*). Activated carbon from nutmeg shells (*Myristica fragrans*) was used in this study to reduce the content of Pb(II) and Cu(II) ions in liquid waste. This research utilized the adsorption method with the batch system to determine the optimum contact time, optimum pH, and adsorption capacity. The characterization of activated carbon was done by Scanning Electron Microscopy (SEM) and Surface Area Analyzers (SAA). The content of Pb(II) and Cu(II) ions in the filtrate after adsorption was analyzed using an atomic absorption spectrophotometer (AAS). The results of SEM analysis showed that the carbon surface was cleaner and had more open pores after the activation process than before activation. The carbon surface area is $19.6243 \text{ m}^2 \cdot \text{g}^{-1}$. From the results of AAS analysis, the optimum time and pH for Pb(II) and Cu(II) ions was 40 min at pH 5 and 70 min at pH 4. With the Freundlich isotherm method, the adsorption capacity of the adsorbent for Pb(II) ions was $9.6028 \text{ mg} \cdot \text{g}^{-1}$ and Cu(II) ions was $0.035 \text{ mg} \cdot \text{g}^{-1}$, and the adsorption effectiveness on liquid waste for Pb and Cu metals was $1.9454 \text{ mg} \cdot \text{g}^{-1}$ and $0.4251 \text{ mg} \cdot \text{g}^{-1}$, respectively. The results showed that activated carbon from the nutmeg shell (*Myristica fragrans*) was able to reduce the levels of Pb(II) and Cu(II) ions in liquid waste.

INTRODUCTION

Environmental pollution due to the discharge of industrial effluents containing heavy metals into water has led to the need to develop effective adsorbents to reduce the content of harmful heavy metals (Xavier et al. 2018, Hayati & Sawir 2017). Porous materials, such as activated carbon (Antika et al. 2019, Saleem et al. 2019), silica (Ouyang et al. 2019, Abuhatab et al. 2020), and zeolite (Hong et al. 2019, Shi et al. 2018), have been widely used as adsorbents. Activated carbon is considered one of the high-efficiency adsorbents due to its low toxicity, large size, rapid adsorption/desorption, good adsorption capacity, high efficiency compared to other materials, and most importantly, easier treatment process, and relatively affordable cost (Wang et al. 2023, Abuelnoor et al. 2021).

The use of activated carbon has a significant ability to reduce the content of heavy metals such as Hg, Cd, Cu, Ni, Pb, and Cr in liquid waste (Abdulrazak et al. 2017, Li et al.

2018) Because some studies only use nutmeg shell (*Myristica fragrans*) to adsorb dyes (Burakov et al. 2018). Activated carbon can be produced from agricultural and plantation waste. One of the wastes that can be utilized is a nutmeg shell (*Myristica fragrans*) (Prasetya et al. 2023). The quality of nutmeg shell (*Myristica fragrans*) activated carbon is very good for use as an adsorbent according to the Indonesian National Standard 06-3730-1995 (Hitijahubessy 2019).

Hazardous metals pose new threats to humans, such as lead and copper that can damage the environment (Thomas & Thalla 2022). These heavy metals are usually present in small amounts, but they are considered to be the most toxic and widespread components in liquid waste effluents (Asiagwu et al. 2017), so systematic and environmentally safe methods are needed. Currently, adsorption is considered an effective and efficient method to remove harmful heavy metal ions from liquid waste effluents. The process is flexible in design and procedure and allows high-quality treated effluent. In addition, in some situations, adsorption is reversible, and

the adsorbent can be regenerated through desorption (Cheng et al. 2019, Idris et al. 2023). Contact time and optimum pH are factors that affect adsorption. The optimum time of adsorption of a metal depends on the type of adsorbent used and its optimum pH, so it will be investigated to determine the optimum conditions for adsorption (Chai et al. 2021).

Therefore, this study aims to analyze the effectiveness of activated carbon from nutmeg shell (*Myristica fragrans*) in reducing Pb(II) and Cu(II) ion levels.

MATERIALS AND METHODS

Tools and Materials

The tools that will be used in this research are glassware commonly used in laboratories, drop pipettes, volume pipettes, Buck Scientific model 205 VPG Atomic Absorption Spectrophotometer (AAS), FTIR (Shimadzu, type: IR Prestige 21), SEM (Hitachi Flexsem 1000) Magnetic stirrer, 100 mesh sieve, Oven (type SPNISOSFD), Hotplate (Ika C MAG Hs 7), Shaker (Oregon KJ-201BD), Analytical Balance (Shimadzu AW220), plastic spray flask, Desiccator. The materials that will be used in this research are nutmeg shell (*Myristica fragrans*), H₃PO₄ 10%, distilled water, aquabides, Pb(NO₃)₂ Merck, CuSO₄.5H₂O Merck, Universal pH paper, Whatman No.42 filter paper, liquid waste.

Sample Preparation, Carbonization, and Carbon Activation

The nutmeg shell waste samples were washed with clean water and dried in the sun. The clean and dry nutmeg shells were broken into small pieces. A total of 3 kg of nutmeg shell was then put into a porcelain cup and heated in a furnace at 400°C for 1 h. This process will produce nutmeg shell carbon. After carbonization, the nutmeg shell carbon was cooled, smoothed, and sieved with a 100-mesh sieve. The sample used is the one that passes the sieve. The carbonization results were then characterized using SEM (Labani' et al. 2015).

During the activation process, nutmeg shell carbon was immersed in a 10% H₃PO₄ activator solution. The volume ratio of 10% H₃PO₄ and carbon mass was 4:1. Soaking lasted for 24 h. The mixture was filtered using a Buchner funnel. Afterward, the precipitate was washed with hot distilled water repeatedly until the pH of the filtrate was close to neutral. After that, the precipitate was heated for 3 h in an oven at 110°C, then cooled in a desiccator. The activation results were characterized using SEM and SAA (Laupa et al. 2019).

Determination of the Optimum Time

Activated carbon 0.5 g was put into nine Erlenmeyers

containing 50 mL of Pb(II) ion solution with a concentration of 10 mg.L⁻¹. Using a shaker, the mixture was stirred for 10, 20, 30, 40, 50, 60, 70, 80 and 90 min. Afterward, the mixture was filtered using the Whatman 42 filter paper, and the concentration of Pb(II) ions in the resulting filtrate was measured by SSA. A blank solution was prepared without adsorbent as previously done. The optimum time was determined from the number of ions adsorbed the most (Tandigau et al. 2018). The concentration adsorbed for each time can be calculated by equation (1).

$$C_{\text{adsorption}} = C_{\text{beginning}} - C_{\text{end}} \quad \dots(1)$$

The amount of metal ions adsorbed (mg.g⁻¹) of adsorbent (nutmeg shell) was determined through equation (2).

$$q_e = \frac{C_0 - C_e}{W} \times V \quad \dots(2)$$

Description:

q_e: amount of metal ions adsorbed (mg.g⁻¹)

C₀: concentration before adsorption (mg.L⁻¹)

C_e: concentration after adsorption (mg.L⁻¹)

V: volume of metal ion solution (L)

W: amount of adsorbent (g)

The same was done for the determination of optimum time on Cu(II) metal ions.

Determination of Optimum pH

Activated carbon 0.5 g was put into five Erlenmeyers, then 50 mL of Pb(II) ion solution, which has a concentration of 10 mg.L⁻¹ at pH 2. After that, the mixture was stirred with a shaker and filtered. An atomic absorption spectrophotometer was used to measure the concentration of Pb(II) ions in the collected filtrate. Then the same way was done at pH 3, 4, 5, and 6 with the same method. A blank solution was made without the addition of activated carbon. The optimum pH is the pH that has the highest number of adsorbed ions (C_{adsorption}) (Tandigau et al. 2018). The same applies to the Cu(II) ion solution.

Determination of Adsorption Capacity

Activated carbon was added to seven Erlenmeyers of 0.5 g each. Next, 50 mL of Pb(II) ion solutions with concentrations of 10, 20, 40, 60, 100, 140, and 200 mg.L⁻¹ were added. Using a shaker, the mixture was mixed at the optimum time and pH obtained previously. The mixture was filtered, and AAS measured the resulting filtrate to determine the concentration of Pb(II). A blank solution was prepared without the addition of activated carbon (Tandigau et al. 2018). The same applies to the Cu(II) ion solution. The adsorption capacity can be determined by the Freundlich equation (Equation 3).

$$[\log(x/m) = \log k + 1/n(\log C)] \quad \dots (3)$$

Or by using Langmuir Equation (4)

$$\frac{C_e}{q_e} = \frac{1}{Q_0 b} + \frac{1}{Q_0} C_e \quad \dots(4)$$

Description:

X: amount adsorbed

m: amount of adsorbent used (g)

C_e : equilibrium concentration (mg.L^{-1})

Q_0 : adsorption capacity (mg.g^{-1})

b: adsorption intensity (L.mg^{-1})

q_e : the amount of substance adsorbed per gram of adsorption (mg.g^{-1})

Determination of Adsorption Effectiveness of Pb(II) and Cu(II) Metal Ions

Activated carbon was put into two Erlenmeyers as much as 0.5 g each. Then, each 25 mL of Pb(II) and Cu(II) solution with a concentration of 10 mg.L^{-1} was mixed in one beaker and homogenized. After that, the solution that has been mixed is pipetted as much as 50 mL and put into an Erlenmeyer that contains activated carbon. The mixture was stirred using a shaker at the optimum time and optimum pH according to the results obtained previously for each solution. The mixture was then filtered, and the filtrate was measured for Pb(II) and Cu(II) using AAS. A blank solution was made without the addition of activated carbon. The same thing was done to determine the effectiveness of adsorption of liquid waste for Pb and Cu metals whose concentrations were unknown.

RESULTS AND DISCUSSION

SEM Characterization

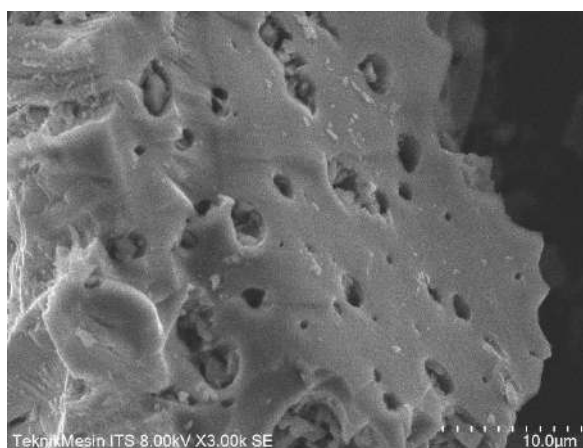
The morphology of nutmeg shell carbon and nutmeg shell activated carbon can be observed by Scanning Electron Microscope (SEM), which provides a detailed picture of the surface morphology of both materials. SEM surface morphology is shown in Fig. 1 (A) and Fig. 1 (B).

The number of pores formed is still small, and there are still pores that have not opened completely, as shown in (Fig. 1a). This is because the carbonization process only removes volatile compounds that cover the carbon, leaving a residue that covers the surface and pores of the carbon. To make the difference on the carbon surface clearer, an activation process is carried out to enlarge and multiply the carbon pores.

This study used 10% H_3PO_4 for the activation process. The carbon was soaked in the activation solution, 10% H_3PO_4 , with a ratio of 1:4 (b/v). This soaking was done to maximize the contact of the carbon-activating solution. (Fig. 1b). Shows the cleaner surface morphology of the carbon compared to the unactivated carbon and the number of pores that appear after activation. The use of 10% H_3PO_4 will open small pores to become larger so that the more pores formed on the surface, the more substances are absorbed. The resulting activated carbon shows that a 10% H_3PO_4 activator is one of the best activators to produce highly porous activated carbon with a high mesopore content. By enlarging the surface area of activated carbon by pores, the adsorption capacity of activated carbon can be increased (Yang et al. 2020, La Hasan et al. 2014).



(a)



(b)

Fig. 1: (a) SEM analysis results of 3000x magnification on nutmeg shell carbon, (b) SEM analysis results of 3000x magnification on nutmeg shell activated carbon.

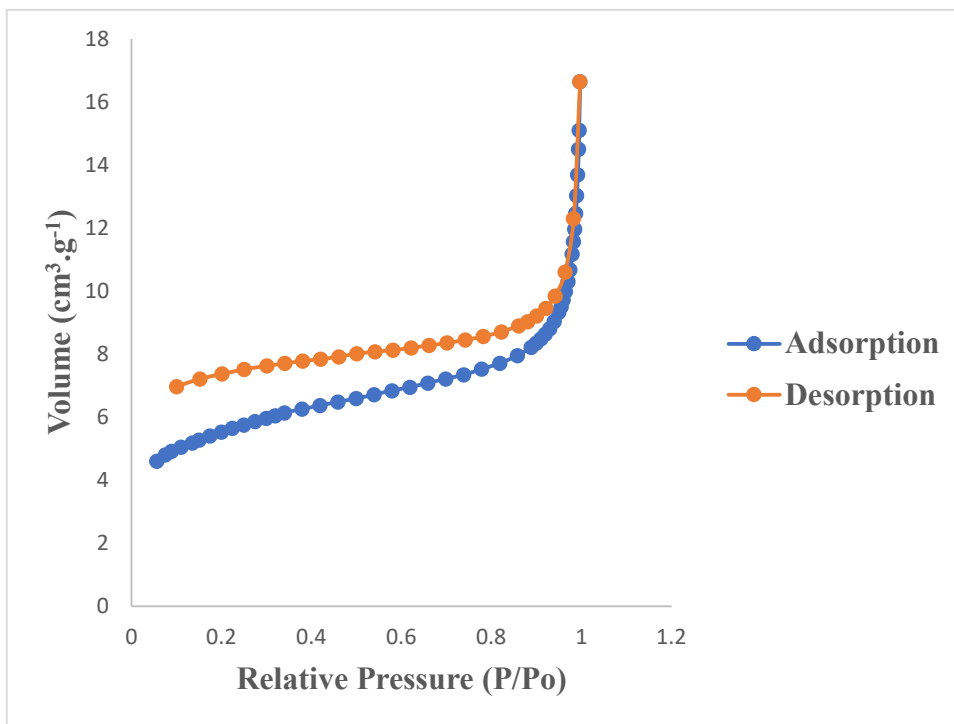


Fig. 2: N₂ Adsorption-desorption isotherm curve on activated nutmeg shell carbon.
(Source: Data Analysis in 2023)

N₂ Adsorption - Desorption Isotherm

N₂ adsorption-desorption characterization was performed to determine the surface area and pore size of the activated carbon material. The surface area was measured by the BET (*Brunauer-Emmet-Teller*) method. This method uses the inert adsorbate gas N₂. Isothermal curves were created by graphing the volume of N₂ adsorbed and desorbed against the relative gas pressure (P/P_0).

The N₂ adsorption isotherm obtained for the activated carbon is shown in Fig. 2. The activated carbon shows an isotherm shape similar to the type IV isotherm based on the *International Union of Pure and Applied Chemistry (IUPAC)* (Bonelli et al. 2001).

Based on the data obtained, the surface area of activated carbon is 19.6243 m².g⁻¹, the pore volume is 0.023665 cm³.g⁻¹, and the pore diameter is 4.8237 nm. Type IV isotherms originate from micro and mesoporous solids, where capillary condensation occurs when gas molecules interact with the mesoporous surface of the adsorbent. The results of the IUPAC type classification show that the activated carbon with the resulting pore diameter belongs to the mesoporous surface type (Bardestani et al. 2019).

The optimum time of adsorption of Pb(II) and Cu(II) metal ions

The optimum time is the time required for the adsorbent to adsorb the largest amount of metal ions observed. Fig. 3 shows the amount of Pb(II) and Cu(II) ions adsorbed by nutmeg shell-activated carbon at different contact times.

The results showed that the amount of Pb(II) and Cu(II) ions adsorbed increased with time. At the 40th and 70th min, the amount of ions adsorbed by the nutmeg shell activated carbon was 0.9718 mg.g⁻¹ and 0.18 mg.g⁻¹, respectively.

The absorbency of nutmeg shell activated carbon to Pb(II) ions increased from the 10th minute to the 40th minute, but after the 50th minute, the absorbency decreased. For Cu(II) ions, the absorbency of nutmeg shell activated carbon increased from the 10th minute to the 70th minute, but after the 80th minute, the absorbency decreased. This is because, in the first minute, the absorbency of Pb(II) ions is relatively increased due to the effective bonding between metal ions and adsorbents. All active sites on the nutmeg shell activated carbon bind to Pb(II) and Cu(II) ions in solution (Li et al. 2017).

The size of the adsorbent affects the adsorption

mechanism, which can lead to a larger interaction surface area. This allows the active side of the adsorbent to interact with Pb(II) and Cu(II) ions very well (Bohli et al. 2017). In the adsorption process, contact time is very important. The longer the contact lasts, the more interactions occur. At a certain point, the number of interactions reaches a high point and then drops. When the adsorbent can no longer adsorb the adsorbed material, it is because the surface is

saturated and uniform desorption occurs. This shows that the physical phenomenon of adsorption occurs, which states that the adsorption process is reversible (Bhatnagar & Sillanpaa 2017).

pH Optimum Adsorption of Pb(II) and Cu(II) Metal Ions

To determine the optimum pH of adsorption of Pb(II) and

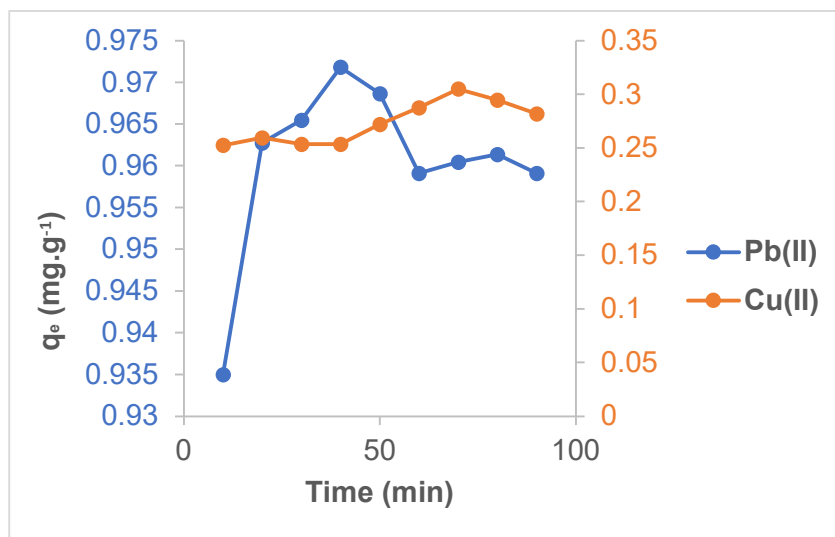


Fig. 3: Effect of contact time on the amount of Pb(II) and Cu(II) metal ions adsorbed by nutmeg shell activated carbon. (Source: Data Analysis in 2023)

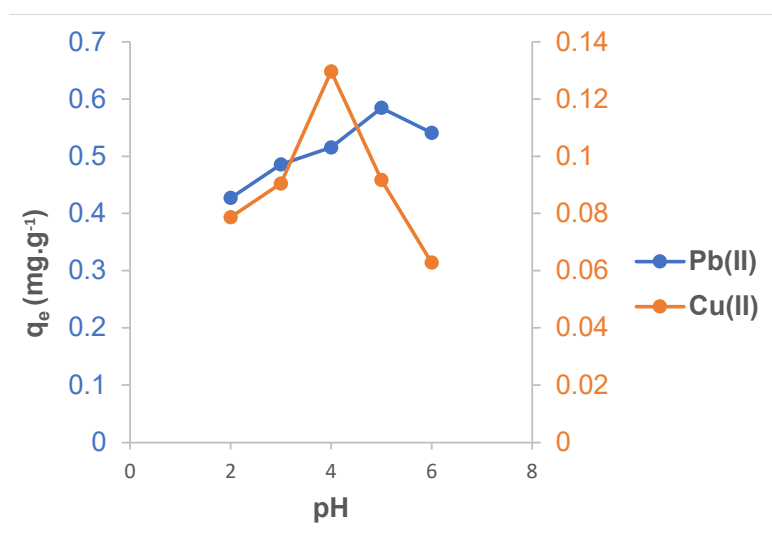


Fig. 4: Effect of pH time on the amount of Pb(II) and Cu(II) metal ions adsorbed by nutmeg shell activated carbon. (Source: Data Analysis in 2023)

Cu(II) ions, the optimum stirring time of Pb(II) ions was 40 min, and Cu(II) ions 70 min was used. The effect of pH on the adsorption of metal ions by nutmeg shell-activated carbon is shown in Fig. 4.

Acidity (pH) is an important parameter that determines metal sorption on activated carbon nutmeg shells of Pb(II) and Cu(II) ions. Changes in pH can affect the chemical and surface properties of the adsorbent, the solubility of metal ions, and the competition of metal ions during the adsorption process (Wang et al. 2015).

Fig. 4 shows that the adsorption process increases with increasing pH but decreases after reaching the optimum pH. pH 2 to 5, the adsorption of Pb(II) ions increases. The amount of ions adsorbed at pH 5 is 0.5845 mg.g^{-1} . While at pH 6 the amount of Pb(II) ions adsorbed decreased to 0.5409 mg.g^{-1} . In Cu(II) ions, the number of adsorbed ions increases at pH 2 to 4. The number of adsorbed ions at pH 4 is 0.1296 mg.g^{-1} . While at pH 5-6, it decreased, the amount of Cu(II) ions adsorbed to 0.0628 mg.g^{-1} .

The low uptake that occurs at pH 6 for Pb(II) ions and at pH 5 for Cu(II) ions is due to several possibilities. First, at low pH, H^+ competes with Pb(II) and Cu(II) ions to interact with functional groups on the surface of nutmeg shell-activated carbon. Second, at low pH, the functional groups on the surface of nutmeg shell activated carbon are surrounded by H^+ ions, thus preventing interaction between Pb(II) and Cu(II) ions with functional groups on the surface of nutmeg shell activated carbon (Tumin et al. 2008). Third, the surface of nutmeg shell activated carbon is positively charged, resulting in

electrostatic repulsion of Pb(II) and Cu(II) ions (Sharma et al. 2009).

The effect of pH on adsorption is very large because it affects the charge of the active site and the charge of metal ions in the solution (Ariyani et al. 2018). Conversely, at pH 5 and pH 4, there is a very strong adsorption of Pb(II) and Cu(II) ions. This is because the number of H^+ ions decreases, and the surface of nutmeg shell-activated carbon releases H^+ ions so that the surface of nutmeg shell-activated carbon becomes negative (Vasu 2008), and electrostatic interactions occur between the surface of nutmeg shell-activated carbon and Pb(II) and Cu(II) ions.

Isotherms and Adsorption Capacity of Pb(II) and Cu(II) Metal Ions

In this study, Pb(II) and Cu(II) metal ions were used for 40 min and 70 min, with pH 5 and 4, respectively. (Fig. 5a) and (Fig. 5b) Shows information about the effect of ion concentration on the amount of Pb(II) and Cu(II) ions adsorbed.

Fig. 5a and Fig. 5b show that the amount of Pb(II) and Cu(II) ions adsorbed increases with increasing concentrations of Pb(II) and Cu(II) ions. In Pb(II) ions with an initial concentration (C_0) of 200 mg.L^{-1} after going through the adsorption process, the final concentration (C_e) becomes 1.5909 mg.L^{-1} , indicating that the number of adsorbed ions is $19.8409 \text{ mg.g}^{-1}$. For Cu(II) ions with an initial concentration (C_0) of 200 mg.L^{-1} after going through the adsorption process, the final concentration (C_e) becomes $51.2222 \text{ mg.L}^{-1}$; this indicates that the number of adsorbed

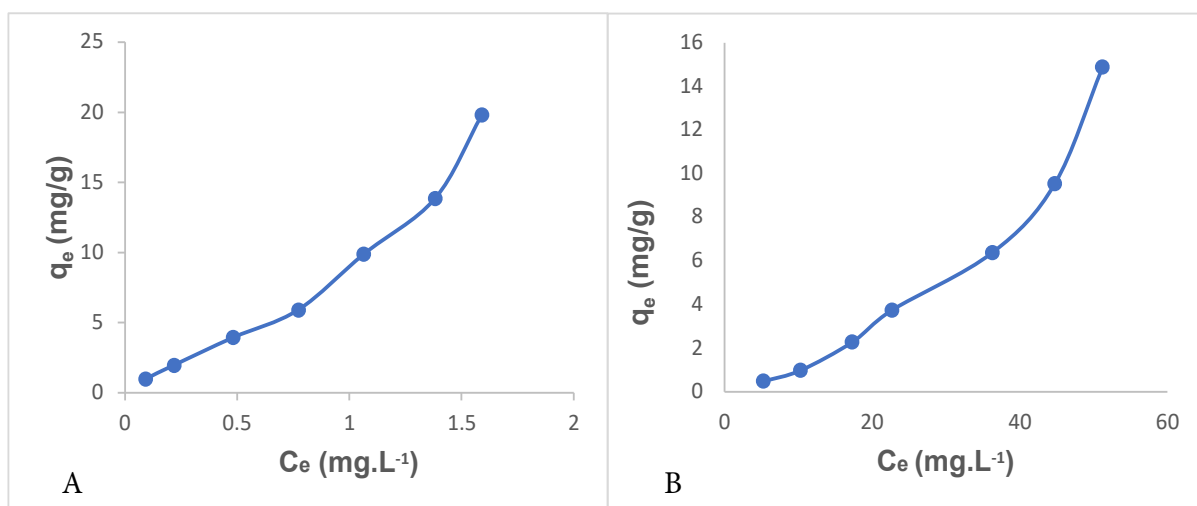


Fig. 5: Graph of concentration effect (a) adsorption of Pb(II) ions by nutmeg shell activated carbon and (b) adsorption of Cu(II) ions by nutmeg shell activated carbon. (Source: Data Analysis in 2023)

Table 1: Adsorption parameter data of Pb(II) ions.

Langmuir Isotherm		Freundlich Isotherm	
Q_0 [mg.g ⁻¹]	90.9090	K_f [mg.g ⁻¹]	9.6028
b [L.mg ⁻¹]	0.0958	n [L.mg ⁻¹]	0.99
R^2	0.1351	R^2	0.9762

Source: Data Analysis in 2023

Table 2: Adsorption parameter data of Cu(II) ions.

Langmuir Isotherm		Freundlich Isotherm	
Q_0 [mg.g ⁻¹]	6.4308	K_f [mg.g ⁻¹]	0.035
b [L.mg ⁻¹]	0.0138	n [L.mg ⁻¹]	0.6746
R^2	0.9003	R^2	0.9884

Source: Data Analysis in 2023

ions is 14.8777 mg.g⁻¹. The ability of nutmeg shell-activated carbon to adsorb Pb(II) ions is greater than that of Cu(II) ions. This occurs due to the nature of Pb, which is more electronegative than Cu so that Pb(II) ions will be more easily adsorbed on the adsorbent surface (Tsai et al. 2016), where most of the adsorbent surface is positively charged due to the presence of functional groups owned by the adsorbent such as hydroxyl, carboxylate, and others. Therefore, the affinity of Pb(II) ions to be adsorbed on the surface of activated carbon nutmeg shells is higher (Winata & Yanti 2020).

The Langmuir and Freundlich adsorption isotherm equations are plotted as linear equilibrium curves to determine the adsorption isotherm. The equilibrium model depends on the largest coefficient of determination (R). The purpose of determining adsorption isotherms is to determine how much Pb(II) and Cu(II) ions are adsorbed on the adsorbent. By using the nature of the adsorption isotherm, it can determine how the adsorbent adsorbs on the surface of the adsorbate (Sahara et al. 2018).

The correlation coefficient (R^2), which is used to determine the role of the variables used, was observed to test whether the isothermal model fits the research data. The closer the R^2 value approaches one, the greater the influence and the better it shows the influence between variables (Fitriansyah et al. 2021). Table 1 and 2 shows the parameter data obtained from the adsorption capacity of nutmeg shell-activated carbon on Pb(II) and Cu(II) ions.

Pb(II) ions follow the Freundlich isotherm, while Cu(II) ions follow the Langmuir and Freundlich isotherms because the R^2 values are both close to 1, but Freundlich is closer. This shows that the whole adsorbent activated carbon nutmeg shell follows the Freundlich isotherm characterized by R^2 values close to 1 against Pb(II) ions and Cu(II) ions. According to the Freundlich equation model, there is more than one surface layer, and the surface is heterogeneous, resulting in

differences in binding energy on the two surfaces (Wijayanti & Kurniawati 2019). Freundlich adsorption isotherms were developed for heterogeneous systems and offer the concept of multilayer adsorption on an absorbent surface.

Freundlich adsorption isotherms assume that adsorption occurs physically, which means that more absorption occurs on the surface of activated carbon. In physical adsorption, the adsorbate is not strongly bound to the surface so that it can move from one surface to another, and another adsorbate can replace the abandoned surface (Jasmal & Ramlawati 2015). If adsorption follows the Freundlich isotherm type, the adsorption takes place by multilayer physisorption. The physisorption mechanism allows for bonding between metal ions in solution, in addition to bonding with the adsorbent. Both bonds are only bound by *Van Der Waals* forces; therefore, the bond between adsorbate and adsorbent is weak. This allows the adsorbate to move freely until, finally, a multilayered adsorption process occurs (Anggriani et al. 2021).

Adsorption Effectiveness of Pb(II) and Cu(II) Metal Ions in Liquid Waste Effluent

The results of the research were conducted with two experiments, namely, making a solution of Pb(II) ions from Pb(NO₃)₂ and Cu(II) ions from CuSO₄.5H₂O with an initial concentration of 10 mg.L⁻¹ each. After that, the solution is mixed into one container. The mixing process of the two solutions aims to see the effectiveness of adsorption that occurs and see the difference between the adsorption results with the mixed solution and the solution without mixing the solution. Adsorption of Pb(II) metal ions and Cu(II) metal ions using activated carbon adsorbent from nutmeg shell (*Myristica fragrans*). The adsorption process is carried out from a solution that has been mixed through a batch system using the optimum time and optimum pH that has been obtained previously and adjusted to each metal ion. Table 3 shows the comparison of the number of ions adsorbed on Pb(II) and Cu(II) ions as well as on Pb and Cu metals from liquid waste.

Second, adsorption of laboratory liquid waste, especially for heavy metal ions Pb and heavy metal ions Cu using activated carbon adsorbent from nutmeg shell (*Myristica fragrans*). Liquid waste was obtained from the waste bin in the Analytical Chemistry Laboratory and Physical Chemistry Laboratory, Department of Chemistry, Hasanuddin University, Makassar. Then, the waste obtained was mixed into one container. The waste that has been mixed is then wet deconstructed using a strong acid, namely nitric acid, which aims as a process of breaking down organic and inorganic compounds into small parts so that they can be analyzed in

Table 3: Amount of ions adsorbed on Pb(II) and Cu(II) ions as well as on Pb and Cu metals from Liquid waste.

Parameters	C ₀ [mg.L ⁻¹]	C _e [mg.L ⁻¹]	W [g]	q _e [mg.g ⁻¹]	Absorbency [%]
Pb(NO ₃) ₂	10	2.0545	0.5	0.7945	79.4545
CuSO ₄ .5H ₂ O	10	5.1148	0.5	0.4885	48.8518
Liquid waste (heavy metal Pb)	42	22.5454	0.5	1.9454	46.3203
Liquid waste (heavy metal Cu)	62.4	58.1481	0.5	0.4251	6.8138

Source: Data Analysis in 2023

certain instruments. Before the adsorption process is carried out, the deconstructed waste is put into 2 Erlenmeyers with a volume of 50 mL each. Then the adsorption process is carried out with a batch system. The time used is the same as in the previous adsorption process on Pb(II) and Cu(II) metal ions, using the optimum time for Pb metal and Cu metal for 40 min and 70 min, respectively. Analysis using AAS was carried out to see the concentration after adsorption through calculation. The results of the calculation resulted in the number of adsorbed ions and the percentage of adsorption for Pb(II) metal ions and Cu(II) metal ions, as well as Pb metal and Cu metal contained in the liquid waste shown in Table 3.

Based on Table 3 shows that the number of adsorbed ions and the percentage of absorption for Pb(II), Cu(II), Pb metal, and Cu metal by nutmeg shell activated carbon are 0.7945 mg.g⁻¹; 0.4885 mg.g⁻¹; 1.9454 mg.g⁻¹ and 6.8138 mg.g⁻¹, respectively. This shows that heavy metal Pb is more easily adsorbed compared to heavy metal Cu due to properties such as electronegativity and hydrolysis constant, with Pb metal being the most electronegative and easily hydrolyzed compared to Cu metal (Vijayaraghavan et al. 2009). The affinity of Pb metal is greater than Cu metal (Futalan et al. 2011). The results obtained show that in the adsorption process using nutmeg shell-activated carbon adsorbent can reduce the concentration of heavy metals from the initial concentration before the adsorption process.

CONCLUSIONS

Based on the results of the study, it can be concluded that the nutmeg shell (*Myristica fragrans*) can be used as an adsorbent for Pb(II) and Cu(II) ions. The optimum contact time required by nutmeg shell activated carbon adsorbent (*Myristica fragrans*) to adsorb Pb(II) and Cu(II) ions occurred in the 40th min and 70th min with an adsorbent mass of 0.5 g each in 50 mL in the Batch system.

The optimum pH required to adsorb Pb(II) and Cu(II) ions using nutmeg (*Myristica fragrans*) shell-activated carbon adsorbent is at pH 5 and pH 4. The adsorption capacity of nutmeg shell activated carbon (*Myristica fragrans*) on Pb(II) and Cu(II) ions tend to follow the Freundlich

isotherm, with maximum adsorbed ions of 9.6028 mg.g⁻¹ and 0.035 mg.g⁻¹, respectively.

The effectiveness of activated carbon on liquid waste in reducing Pb and Cu metal levels is with the number of ions adsorbed at 1.9454 mg.g⁻¹ and 0.4251 mg.g⁻¹ from initial concentrations of 42 mg.L⁻¹ and 62.4 mg.L⁻¹, respectively.

REFERENCES

- Abdulrazak, S., Hussaini, K. and Sani, H.M. 2017. Evaluation of removal efficiency of heavy metals by low-cost activated carbon prepared from African palm fruit. *Appl. Water Sci.*, 7: 3151-3155.
- Abuelnoor, N. Alhajaj, A. Khaleel, M., Vega, L.F. and Abu-Zahra, M.R.M. 2021. Activated carbons from biomass-based sources for CO₂ capture applications. *Chemosphere*, 282: 131111.
- Abuhatab, A., El-Qanni, A., Al-Qalaq, H., Hmoudah, M. and Al-Zerei, W. 2020. Effective adsorptive removal of Zn²⁺, Cu²⁺, and Cr³⁺ heavy metals from aqueous solutions using silica-based embedded NiO and MgO nanoparticles. *J. Environ. Manage.*, 268: 110713.
- Anggriani, U.M., Hasan, A. and Purnamasari, I. 2021. Adsorption kinetics of activated carbon in reducing copper Cu and lead Pb metal concentrations. *J. Kinetics*, 12(02): 29-37.
- Antika, R., Siregar, S.D. and Pane, P.Y. 2019. Effectiveness of corn cob activated carbon in reducing iron Fe and manganese Mn levels in dug well water in Amplas Village, Percut Sei Tuan District, Deli Serdang Regency. *J. Global Health*, 2(2): 81-92.
- Ariyani, D., Cahaya, N. and Mujiyanti, D.R. 2018. Effect of pH and contact time on adsorption of metal Zn II on chitosan-epichlorohydrin modified water hyacinth charcoal composite. *Valency Chem. J.*, 4: 85–92.
- Asiagwu, A.K., Peretomo-Clarke, B.O. and Okposo, M.A. 2017. Sorption kinetics for the removal of methyl violet dye from wastewater using African nutmeg as biomass. *J. Chem. Biol. Phys. Sci.*, 7(1): 097-106.
- Bardestani, R., Patience, G.S. and Kaliaguine, S. 2019. Experimental methods in chemical engineering: Specific surface area and pore size distribution measurements-BET.BJH.DFT. *Can. J. Chem. Eng.*, 97: 2781.
- Bhatnagar, A. and Sillanpaa, M. 2017. Removal of natural matter NOM and its constituents from water by adsorption – a review. *Chemosphere*, 166: 497-510.
- Bohli, T., Ouederni, A. and Villaescusa, I. 2017. Simultaneous adsorption behavior of heavy metals onto microporous olive stones activated carbon: Analysis of interactions. *EuroMediterr J. Environ. Integr.*, 2:19.
- Bonelli, P.R., Rocca, D.P.A., Cerella, E.G. and Cukieman, A.L. 2001. Effect of pyrolysis temperature on composition, surface properties and thermal degradation rates of Brazil nut shell. *Bioresource Technol.*, 76: 15-22.
- Burakov, A.E., Galunin, E.V., Burakova, I.V., Kucherova, A.E., Agarwal, S., Tkachev, A.G. and Gupta, V.K. 2018. Adsorption of heavy metals on conventional and nanostructured materials for wastewater treatment purposes: a review. *Ecotoxicol. Environ. Saf.*, 148: 701-712.
- Chai, W.S., Cheun, J.Y., Kumar, P.S., Mubashir, M., Majeed, Z., Banat,

- F., Ho, S.H. and Show, P.L. 2021. A review of conventional and novel materials towards heavy metal adsorption in wastewater treatment application. *J. Cleaner Prod.*, 286: 126589.
- Cheng, S.Y., Show, P.L., Lau, B.F., Chang, J.S. and Ling, T.C. 2019. New prospects for modified algae in heavy metal adsorption. *Trends Biotechnol.*, 37: 1255-1268.
- Fitriansyah, A., Amir, H. and Elvinawati, M. 2021. Characterization of activated carbon adsorbent from Areca nut (*Areca catechu*) on the adsorption capacity of indigosol blue 04-B dye. *J. Chem. Educ. Sci.*, 5(1): 42-45.
- Futalan, C.M., Kan, C.C., Dalida, M.L., Hsien, K.J., Pascua, C. and Wan, M.W. 2011. Comparative and competitive adsorption of copper, lead, and nickel using chitosan immobilized on bentonite. *Carbohydr. Polym.*, 83(2): 528-536.
- Hayati, U.P. and Sawir, H. 2017. Utilization of cocoa pods as adsorbent for the absorption of chromium VI metal ions in electroplating waste in Bukit Tinggi. *J. Sci. Technol.*, 17(1): 34-41.
- Hitjahubessy, H. 2019. Quality analysis of nutmeg shell activated carbon as adsorption agent. *Rumphius Pattimura Biol. J.*, 1(2): 001-004.
- Hong, M., Yu, L., Wang, Y., Zhang, J., Chen, Z., Dong, L., Zan, Q. and Li, R. 2019. Heavy metal adsorption with zeolites: The role of hierarchical pore architecture. *Chem. Eng. J.*, 359: 363-372.
- Idris, M.O., Yaqoob, A.A., Ibrahim, M.N.M., Ahmad, A. and Alshammari, M.B. 2023. Chapter 1-Introduction of adsorption techniques for heavy metals remediation. *Emerging Techniques for Treatment of Toxic Metals from Wastewater.*, 1-18.
- Jasmal, S. and Ramlawati, L. 2015. Adsorption capacity of palm fiber activated charcoal (*Arenga pinnata*) on Pb²⁺. *J. Sci. At.*, 4(1): 56-66.
- Labbani, A., La Hasan, N. and Maming, M. 2015. Synthesis and characterization of nanoporous carbon from sugarcane bagasse (*Saccharum officinarum*) with ZnCl₂ activator by ultrasonic irradiation as electrochemical energy storage material. *Indones. Chim. Acta.*, 8(1):42-51.
- La Hasan, N., Zakir, M. and Budi, P. 2014. Desilication of rice husk activated carbon as Hg adsorbent in gold processing waste in Buru Regency, Maluku Province. *J. Chim. Acta.*, 7(2): 1-11.
- Laupa, S.A., Alimuddin, A. and Sitorus, S. 2019. Effect of time variation on the adsorption ability of activated carbon from banana stem waste *Musa paradisiaca* L. against benzene. *Atomic J.*, 4(2): 90-95.
- Li, H., Dong, X., da Silva, E.B., de Oliveira, L.M., Chen, Y. and Ma, L.Q. 2017. Mechanism of metal sorption by biochars: Biochar characteristics and modifications. *Chemosphere.*, 178: 466-478.
- Li, J., Xing, X., Li, J., Shi, M., Lin, A., Xu, C., Zheng, J. and Li, R. 2018. Preparation of thiol-functionalized activated carbon from sewage sludge with coal blending for heavy metal removal from contaminated water. *Environ. Pollut.*, 234: 677-683.
- Ouyang, D., Zhuo, Y., Hu, L., Zeng, Q., Hu, Y. and He, Z. 2019. Research on the adsorption behavior of heavy metal ions by porous material prepared with silicate tailings. *Minerals*, 9(291).
- Prasetya, N., Wenten, I.G., Franzreb, M. and Woll, C. 2023. Metal-organic frameworks for the adsorptive removal of pharmaceutically active compounds PhACs: Comparison to activated carbon. *Coord. Chem. Rev.*, 475: 214877.
- Sahara, E., Gayatri, P.S. and Suarya, P. 2018. Adsorption of Rhodamin-B dye in solution by phosphoric acid-activated gumtitir plant stem-activated charcoal. *Indones. E-J. Appl. Chem.*, 6(1).
- Saleem, J., Shahid, U.B., Hijab, M., Mackey, H. and Mckay, G. 2019. Production and applications of activated carbons as adsorbents. *Biomass Convers. Biorefin.*, 9: 775-802.
- Sharma, Y.C., Uma. M. and Upadhyay, S.N. 2009. Removal of a cationic dye from wastewater by adsorption on activated carbon developed from coconut coir. *Energy Fuels*, 23: 2983-2988.
- Shi, J., Yang, Z., Dai, H., Lu, X., Peng, L., Tan, X., Shi, L. and Fahim, R. 2018. Preparation and application of modified zeolites as adsorbents in wastewater treatment. *Water Sci. Technol.*, 2017(3): 621-635.
- Tandigau, S., Nafie, N.L. and Budi, P. 2018. Biosorption of Ni(II) ions by Arabican coffee fruit *Coffea arabica*. *J. Indones. Chem. Acts*, 11(1): 211-220.
- Thomas, T. and Thalla, A.K. 2022. Nutmeg seed shell biochar as an effective adsorbent for removal of Remazol brilliant blue reactive dye: Kinetic, isotherm, and thermodynamic study. *Energy Sources*, 44(1).
- Tsai, W.C., de Luna, M.D.G., Bermillo-Arriego, H.L.P., Futalan, C.M., Colades, J.I. and Wan, M.W. 2016. Competitive fixed-bed adsorption of Pb(II), Cu(II), and Ni(II) from aqueous solution using chitosan-coated bentonite. *Int. J. Polym. Sci.*, 2016: 1-11.
- Tumin, N.D., Chuah, A.L. and Rashid, S.A. 2008. Adsorption of copper from aqueous solution by *Elais guineensis* kernel activated carbon. *J. Eng. Sci. Technol.*, 3(2): 180-189.
- Vasu, A.E. 2008. Surface modification of activated carbon for enhancement of nickel (II) adsorption. *EJ. Chem.*, 5(4): 814-819.
- Vijayaraghavan, K., Teo, T.T., Balasubramanian, R. and Joshi, U.M. 2009. Application of *Sargassum* biomass to remove heavy metal ions from synthetic multi-metal solutions and urban stormwater runoff. *J. Hazard. Mater.*, 164(2-3): 1019-1023.
- Wang, X., Shao, D., Hou, G. and Wang, X. 2015. Uptake of Pb(II) and U(IV) ions from aqueous solutions by the ZSM-5 zeolite. *J. Mol. Liquids*, 207: 338-342.
- Wang, B., Lan, J., Bo, C. and Gong, B. 2023. Adsorption of heavy metal onto biomass-derived activated carbon: Review. *RSC Adv.*, 13: 4275.
- Wijayanti, I.E. and Kurniawati, E.A. 2019. Study of adsorption kinetics of Langmuir and Freundlich isotherms on rubbing ash as adsorbent. *J. Chem. Educ. Sci.*, 4(2): 2502-4787.
- Winata, W.F. and Yanti, I. 2020. Kinetics study of Cu(II) and Pb(II) adsorption using biosorbent from rambutan fruit peel extract polymer. *IJCR-Indones. J. Chem. Res.*, 5(1): 1-7.
- Xavier, A.L.P. Adarme, O.F.H. Furtado, L.M., Ferreira, G.M.D., Silva, L.H.M, Gil, L.F. and Gurgel, L.V.A. 2018. Modeling adsorption of copper(II), cobalt(II), and nickel(II) metal ions from aqueous solution onto a new carboxylated sugarcane bagasse. Part II: Optimization of monocomponent fixed-bed column adsorption. *J. Colloid Interface Sci.*, 516: 431-45.
- Yang, Q., Wu, P., Liu, L., Rehman, S., Ahmed, Z., Ruan, B. and Zhu, N. 2020. Batch interaction of emerging tetracycline contaminant with novel phosphoric acid activated corn straw porous carbon: Adsorption rate and nature of mechanism. *Environ. Res.*, 181: 108899.

ORCID DETAILS OF THE AUTHORS

Ishar: <https://orcid.org/0009-0002-5969-6471>



The Effect of Senegal River Irrigation Water Quality on Soil Salinization: A Study of the Main Canal of the M'Pourie Plain in Mauritania

Mewgef El Ezza dite Hanane Djieh Cheikh Med Fadel*†, B. A. Dick**, E. C. S'Id***, M. B. Ammar**, Ould Sidi Y. M.**, L. S. Mohamed**, Mohamed Iemine Yehdih* and Mohamed Fekhaoui*

*Geo-Biodiversity and Natural Patrimony Laboratory, Scientific Institute, Mohamed V University, Rabat, Morocco, 4 Av. Ibn Batouta, BP 1014 RP, Rabat, Morocco

**Research Unit of the Water, Pollution, Environment, University of Nouakchott, Av. Nouadhibou, BP 880, Nouakchott, Mauritania

***Research Unit: Membrane, Material, Environment and Aquatic Environment (2MEMA)/FST, University of Nouakchott, Av. Nouadhibou, BP 880, Nouakchott, Mauritania

†Corresponding author: M. E. D. H. Cheikh Med Fadel; hananedieh@gmail.com

Nat. Env. & Poll. Tech.
Website: www.neptjournal.com

Received: 25-11-2023

Revised: 10-01-2024

Accepted: 30-01-2024

Key Words:

Senegal river
Irrigation water quality
Soil salinization

ABSTRACT

In this study, the Senegal River, being the main source of water, plays a crucial role in the area's agricultural development. Irrigation on the M'Pourie plain using water from the Senegal River is carried out without any prior sanitation control. An evaluation of the quality of irrigation water and its impact on soil salinization in different agricultural plots soil salinity is crucial for the effective utilization of traditional irrigation water over extended periods. Comprehensive physico-chemical analyses were conducted across nine locations on the M'Pourie plain in Rosso during the dynamic seasons of 2021-2023. Nevertheless, a relatively small number of studies have employed soil salinity indexing methods to examine the consequences of river irrigation on soil salinity. The analysis and interpretation of the results obtained were based both on classic methods (average and correlations) and more advanced techniques such as principal component analysis (PCA) and the Piper diagram which allow characterization and a spatial typology of water. Analysis of the Piper diagram highlights the distinction between two groups of water, weakly and moderately mineralized, ranging from 52.22 $\mu\text{S}\cdot\text{cm}^{-1}$ in the dry season to 72.22 $\mu\text{S}\cdot\text{cm}^{-1}$ in the rainy season, presenting a sodium-potassium bicarbonate facies. The variability of irrigation water supplies, proves to be important in the functioning of an agro-systems. Two modes of operation have become individualized: the dry phase mode, characterized by very strong mineralization of the water linked to a significant load of dissolved elements, and the wet phase mode, whose water quality is poorly mineralized but shows the impact that its irrigation water can represent in the loading of organic and mineral pollution and the need for strict control of these waters upstream before their agricultural use. The results of this study show the absence of risks of soil salinization in relation to the chemical nature of irrigation water and the impact of agriculture on the M'Pourie plain.

INTRODUCTION

The global population is rapidly increasing, and water resources are depleting at an alarming rate, especially in countries where light-textured soils predominate in agricultural areas (Abrisham et al. 2018, Albalasmeh et al. 2022). Water shortages are affecting approximately 700 million people in 43 countries, including regions such as India, the US state of California, the North China Plain, and similar arid and semi-arid areas. Over the last two decades, the annual available freshwater quantity per person has declined by more than 20% (FAO 2020, Khaled et al. 2022).

Vast areas of the world are currently facing challenges related to water availability for agricultural purposes. This predicament is a result of various factors, including climate change, and is expected to worsen in the coming years. In arid zones, soil and irrigation water salinity pose significant environmental constraints on agricultural soils (Alvarez & Sanchez-Blanco 2015, Lakhdhar et al. 2008).

Irrigated agricultural production covers only 4% of Sub-Saharan Africa, in stark contrast to 29% in East Asia and 39% in South Asia (World Bank 2010). Irrigation, the artificial supply of water to cultivated plants to enhance production and foster normal development, is crucial in regions facing

a water deficit due to factors such as insufficient rainfall, excessive drainage, or a decline in the water table. This technique is particularly essential in arid and semi-arid regions (El Asslouj et al. 2007).

Several reasons underscore the paramount importance of water quality in irrigation: it directly impacts crop yields, soil productivity, and environmental protection. Agronomists and economists responsible for land development in arid and semi-arid zones are actively concerned about the effects of irrigation water quality on crops. Freshwater, with irrigation being the primary consumer, is a vital resource. Agriculture allocates approximately 70% of freshwater resources, with industry utilizing around 20% and domestic use accounting for about 10%. It's crucial to note that these proportions vary significantly from one country to another, resulting in notable disparities (Escudier et al. 2019, Ocede 2010).

Successful and sustainable agriculture hinges on effective irrigation water management (Al-Zu'bi, 2007). Excessive salinity adversely affects the rhizosphere, limiting the natural distribution of plants in their habitat. Semi-arid and arid regions, characterized by intense sunlight and scarce rainfall, exacerbate the salinization of irrigated areas, rendering them unsuitable for cultivation (Denden et al. 2005). The high concentration of salt in arid zone soils poses a significant environmental challenge to agriculture (Baatour et al. 2004).

Mauritania, an arid zone with low rainfall, abundant sunlight, and limited water resources, faces the challenge

of managing its scarce water supply. The river's waters are anticipated to be extensively used for both drinking water and irrigation. Despite agriculture contributing only 22.82% to Mauritania's national GDP, the useful agricultural area (UAA) represents less than 0.5% of the national territory, estimated at 502,000 ha (World Bank 2014).

Soil salinization poses a widespread issue in the Senegal River delta, as highlighted by Abidine et al. (2018a) and Ngom et al. (2016). This problem significantly impacts both agricultural production and the quality of irrigation water, as indicated by Abidine et al. (2018b), Asfaw et al. (2018), Elgettafi et al. (2011), Elhag (2016), and Yao & Yang (2010). The indicator widely utilized to assess soil salinity is electrical conductivity. The consequences of salinization include a reduction in arable land and a decline in soil quality, as noted by Gorji et al. (2017), Seyedmohammadi et al. (2016), and Tripathi et al. (2015).

Our study focuses on the M'Pourie plain, located in the upper Senegal River delta at Rosso. Covering an area of 1500 Ha, this pilot farm, established in the 80s for agricultural purposes, includes the main canal. The supply of irrigation water in the main canal of the M'Pourie plain emerges as a decisive factor in agricultural production, influencing both crop intensification and the expansion of irrigated areas.

This study aims to evaluate the impact of irrigation water quality from the Senegal River on soil salinization in the M'Pourie plain by monitoring several chemical tracers at the level of irrigation water and sediments from



Fig. 1: Map of water sampling sites.

several sampling points. A multivariate analysis (principal component analysis) and the Piper diagram were used to confirm the results obtained.

The scientific and socio-economic interest of this study is to verify whether the use of inputs and, more specifically, appropriate irrigation are the main factors that condition the good agricultural use of soil and its impact on agricultural yield.

MATERIALS AND METHODS

Study Area

This study was carried out on the M’Pourie plain in Rosso (Trarza) in southern Mauritania, a pilot farm created in the 1980s and including a machinery department and a pumping station from the Senegal River valley. It covers an area of 1,500 hectares divided into three brigades belonging to the M’Pourie plain and 850 hectares belonging to the cooperatives. The Trarza region lies between latitudes 16°30 and 18°30 and longitudes 14° and 16°, with a surface area of 33,000 km². The M’Pourie Plain is an area of intense agricultural activity. In this study, 9 sampling sites on the main canal along the M’Pourie were selected for irrigation water assessments, and 03 sites for soil assessments (Fig. 1 & 2).

Sampling

Samples were collected on the M’Pourie plain at nine sampling sites on both banks of the main M’Pourie canal,

with four sites in the middle of the canal (SP, CP3, CP2, CP1), four on the left bank (CST3-1-1, CS3-2-1, CS3-1, CS1) and one on the right bank (CS2-1). Sampling sites were located 100 m apart. Soil samples were taken on the M’Pourie plain at flow (S1), in the middle (S2), and at the end (S3). Samples were extracted from the initial 20 cm layer, and the coordinates of each sampling point were captured using a handheld GPS device (Garmin 78). Samples were taken during the last two years, 2021-2023, as follows:

To collect the samples, we used one-liter plastic bottles, which we immersed in the canals to collect a sufficient quantity. The bottles were then hermetically sealed and stored

Main channel 1	CP 1
Main channel 2	CP 2
Main channel 3	CP 3
Secondary channel 1	CS 1
Secondary channel 2	CS 2
Secondary channel 2-1	CS2 1
Secondary channel 3-1	CS3 1
Secondary channel 3 2-1	CS3 2-1
Tertiary, secondary canal 3 1-1	CST3 1-1
Pumping station	SP
Soil1	S1
Soil2	S2
Soil3	S3



Fig. 2: Map of soil sampling sites.

Table 1: Average physicochemical quality at the study site in the wet and dry seasons.

	Dry season			Rainy season			NORMES	
	Min	Max	Moy	Min	Max	Moy	Morocco	FAO
pH	6.9	8.41	7.51	6.61	7.39	7.08	6.5 -8.4	6.5 -8.4
T [°C]	29.1	29.5	29.16	29.8	29.9	29.84	35°C	
Ce [$\mu\text{s.cm}^{-1}$]	50	60	52.22	70	80	72.22	8700	< 750
TDS [mg.L^{-1}]	23.80	28.57	24.86	33.33	38.09	34.38	--	--
Ca ²⁺ [mg.L^{-1}]	3.2	8.81	6.49	24.04	98.30	54.02	--	--
Mg ²⁺ [mg.L^{-1}]	1.91	4.86	3.28	1.94	44.37	10.37	--	--
Cl ⁻ [mg.L^{-1}]	24.85	31.95	28.00	25	32	25.27	350	< 142
NH ₄ ⁺ [mg.L^{-1}]	0.17	0.93	0.41	0.10	0.34	0.20	--	--
SO ₄ ²⁻ [mg.L^{-1}]	4	90	33	12	80	34.22	250	--
N [mg.L^{-1}]	0.35	4.15	1.56	0.20	32	13.36	--	--
HCO ₃ ⁻ [mg.L^{-1}]	42.7	79.3	61	45	80	61.55	518	< 91.5
Na ⁺ [mg.L^{-1}]	18	21	19.44	24	28	25.88	69	--
K ⁺ [mg.L^{-1}]	2	6	4.22	4	8	6.22	--	--
NO ₃ ⁻ [mg.L^{-1}]	1.54	18.26	6.89	0.04	7.27	3.03	50	5.0-30
NO ₂ ⁻ [mg.L^{-1}]	1.15	13.69	5.16	0.06	9.45	3.15	--	--

at 4°C for analysis (Rodier J., 2009). Analyses were carried out in the laboratory of the Water-Pollution-Environment unit of the FST of the University of Nouakchott.

Analytical Methods

Various physicochemical parameters were measured, including temperature (T), hydrogen potential (pH), electrical conductivity (EC), total dissolved solids (TDS), magnesium, sodium, sulfate, potassium, calcium, bicarbonate, chloride, nitrogen, ammonium, nitrate, and nitrite.

The Hanna HI 9024 pH meter was used to measure temperature and hydrogen potential, while the Hanna HI 8733 conductivity meter was employed for electrical conductivity (E.C.) measurements.

To determine chloride (Cl⁻), calcium (Ca²⁺), magnesium (Mg²⁺), and bicarbonates (HCO₃⁻), Mohr's volumetric method was used, as described by P. Jagals et al. (1997).

Nitrates (NO₃⁻), nitrites (NO₂⁻), ammonium (NH₄⁺), and sulfates (SO₄²⁻) were measured using a UV-visible spectrophotometer (WEG 7100). Sodium (Na⁺) and potassium (K⁺) were determined using a Corning-type flame photometer.

RESULTS AND DISCUSSION

Assessment of River Water Quality in the M'Pourie Plain

The results obtained from measuring various quality parameters of irrigation water at M'Pourie are represented in Table 1.

In Mauritania, no established regulations exist outlining water quality standards for irrigation. Consequently, we benchmarked the obtained results against the standards set by Morocco and the Food and Agriculture Organization (FAO). State of average physicochemical quality at the study site in wet and dry seasons as illustrated in Table 1.

During the dry season, the surface waters of the M'Pourie plain exhibit pH values ranging between 6.9 and 8.41. Similarly, in the rainy season, pH varies from 6.61 to 7.39. It is noteworthy that, in all instances, the pH values closely approach neutrality. The seasonal variation in pH does not surpass the standards set by Moroccan or FAO. These findings align with those reported by Bouaroudj et al. (2019). Furthermore, the pH values obtained are lower than those reported by Al-Zu'bi (2007).

The recorded results indicate that the temperature fluctuates between 29.1°C and 29.5°C during the dry season and between 29.8°C and 29.9°C during the rainy season in the studied waters. Notably, there is no significant variation in temperature between these two sampling periods. It is essential to highlight that these results comply with both Moroccan regulations and FAO standards. However, they surpass the temperatures documented in the study conducted by Bouaroudj et al. (2019).

In the M'Pourie plain, surface water displays limited mineralization with electrical conductivity levels ranging from 50 $\mu\text{s.cm}^{-1}$ to 60 $\mu\text{s.cm}^{-1}$ in the dry season and 70 $\mu\text{s.cm}^{-1}$

to $80 \mu\text{s}\cdot\text{cm}^{-1}$ in the rainy season. These conductivity values are lower than those reported by Bouaroudj et al. (2019). Additionally, it is worth noting that conductivity is higher during the rainy season compared to the dry season. An analysis of the temporal distribution of electrical conductivity reveals a specific increase during the rainy period.

Total Dissolved Solids (TDS) values in the dry season fluctuate between $23.80 \text{ mg}\cdot\text{L}^{-1}$ and $28.57 \text{ mg}\cdot\text{L}^{-1}$, while in the rainy season, they range from $33.33 \text{ mg}\cdot\text{L}^{-1}$ to $38.09 \text{ mg}\cdot\text{L}^{-1}$. These readings fall within the established limits of Moroccan and FAO standards and are lower than those documented by Kahimba et al. (2016). This observation suggests that the Senegal River water used for irrigation exhibits relatively low mineralization, indicating a comparatively low mineral content.

Sulfate concentrations in the examined waters vary significantly between the dry and rainy seasons. During the dry season, the waters exhibit sulfate levels ranging from $4 \text{ mg}\cdot\text{L}^{-1}$ to $90 \text{ mg}\cdot\text{L}^{-1}$, while in the rainy season, they fluctuate between $12 \text{ mg}\cdot\text{L}^{-1}$ and $80 \text{ mg}\cdot\text{L}^{-1}$. Researchers (Bouaroudj et al. 2019) documented higher concentrations than those observed in this study. Agricultural activities are likely responsible for the elevated sulfate values observed in the study area, with the primary source of sulfate in the surface waters of the M'Pourie plain being the presence of secondary formations, particularly gypsum. It is noteworthy that these concentrations fall within the acceptable limits established by Moroccan standards.

Chloride values range between $24.85 \text{ mg}\cdot\text{L}^{-1}$ and $31.95 \text{ mg}\cdot\text{L}^{-1}$ during the dry season and between $25 \text{ mg}\cdot\text{L}^{-1}$ and $32 \text{ mg}\cdot\text{L}^{-1}$ during the rainy season. Both Moroccan regulations and the FAO standard comply with these values. The observed bicarbonate values vary between $42.70 \text{ mg}\cdot\text{L}^{-1}$ and $79.30 \text{ mg}\cdot\text{L}^{-1}$ during the dry season and between $45 \text{ mg}\cdot\text{L}^{-1}$ and $80 \text{ mg}\cdot\text{L}^{-1}$ during the rainy season. It should be noted that these values are within the limits set by Moroccan regulations.

This study reports calcium levels of $3.20 \text{ mg}\cdot\text{L}^{-1}$ and $8.81 \text{ mg}\cdot\text{L}^{-1}$ during the dry season and $24.04 \text{ mg}\cdot\text{L}^{-1}$ and $98.3 \text{ mg}\cdot\text{L}^{-1}$ during the rainy season. Good quality irrigation water typically contains calcium concentrations ranging from 20 to $400 \text{ mg}\cdot\text{L}^{-1}$ (Rodier J.2009). Magnesium values are $1.91 \text{ mg}\cdot\text{L}^{-1}$ and $4.86 \text{ mg}\cdot\text{L}^{-1}$ in the dry season, $1.94 \text{ mg}\cdot\text{L}^{-1}$ and $44.37 \text{ mg}\cdot\text{L}^{-1}$ in the rainy season.

In the dry season, sodium and potassium levels respectively measure $18 \text{ mg}\cdot\text{L}^{-1}$ and $21 \text{ mg}\cdot\text{L}^{-1}$, while in the rainy season, they measure $24 \text{ mg}\cdot\text{L}^{-1}$ and $28 \text{ mg}\cdot\text{L}^{-1}$. Additionally, in the dry season, sodium and potassium levels are $2 \text{ mg}\cdot\text{L}^{-1}$ and $6 \text{ mg}\cdot\text{L}^{-1}$, whereas in the rainy season, they are $4 \text{ mg}\cdot\text{L}^{-1}$ and $8 \text{ mg}\cdot\text{L}^{-1}$.

The examination of nitrogen compounds reveals notable concentrations, with some exceeding Moroccan standards. Nitrate levels vary between $1.54 \text{ mg}\cdot\text{L}^{-1}$ and $18.26 \text{ mg}\cdot\text{L}^{-1}$ in the dry season and $0.04 \text{ mg}\cdot\text{L}^{-1}$ to $7.27 \text{ mg}\cdot\text{L}^{-1}$ in the rainy season, aligning with Moroccan regulations. During the dry season, nitrite levels range from $1.15 \text{ mg}\cdot\text{L}^{-1}$ to $13.69 \text{ mg}\cdot\text{L}^{-1}$, and in the wet season, from $0.06 \text{ mg}\cdot\text{L}^{-1}$ to $9.45 \text{ mg}\cdot\text{L}^{-1}$, with the highest values observed in the dry season. Mounjid et al. (2014) documented similar nitrite concentrations.

Ammonium concentrations display seasonal fluctuations, measuring $0.17 \text{ mg}\cdot\text{L}^{-1}$ to $0.93 \text{ mg}\cdot\text{L}^{-1}$ in the dry season and $0.10 \text{ mg}\cdot\text{L}^{-1}$ to $0.34 \text{ mg}\cdot\text{L}^{-1}$ in the rainy season. The elevated concentrations may be attributed to excessive fertilizer use in agricultural regions.

Typology of the Upper Senegal River Delta by ACP

To exploit all the physicochemical results obtained at the study site (Table 2), a multivariate analysis (Principal Component Analysis) was used. The matrix used includes analyses carried out in the wet phase (h) and the dry phase (s).

This method enables the statistical exploration of complex quantitative data by reducing its dimensionality. It transforms the data from a multi-dimensional (more complex) space into a much smaller one, typically two dimensions. The goal is to retain as much information as possible about the dispersion of the data while simplifying its representation (Jolliffe 2002, Besse 1992).

Table 3 and Fig. 3 show the factorial axes deduced from the application of the PCA method. Only the first three factors will be considered. They express 81.3% of the total variance, of which 44.6 % is represented by F1, 25% by F2, and 11.65% by F3.

Fig. 4 shows the projection circle of the variables measured in the F1 and F2 factor space of the PCA. It illustrates the organization of the variables into two main groups. The first group is located in the positive part of F1 and strongly correlated with T, TDS, EC, TU, TH⁻, Ca²⁺, Mg²⁺, and Cl⁻. It defines a mineralization gradient increasing from left to right during the hot season with a significant contribution of chlorides, calcium, and a strong presence of dissolved substances.

The second group is situated in the positive part of F2 correlated with CuT, NH₄⁺, SO₄⁺, and NO₃⁻NO₂⁻. This axis defines a gradient of enrichment in nutrient substances, particularly nitrogenous elements and total copper. It represents an enrichment linked to agricultural activities and the use of fertilizers and a powerful fungicide, copper sulfate.

Table 2: Physico-chemical data matrix for PCA analysis.

code	stations	pH	T	Cs	TDS	Tur	TH	Ca2+	Mg	Cl-	CuF	Mn	NH4+	SO4+	NT	HCO ₃ ⁻	Na+	K+	NO ₃ ⁻	NO ₂ ⁻
			°C	µs.cm ⁻¹	mg.L ⁻¹	NTU	°F	mg.L ⁻¹	mg.L ⁻¹	mg.L ⁻¹	mg.L ⁻¹	mg.L ⁻¹	mg.L ⁻¹	mg.L ⁻¹	Mg.L ⁻¹	mg.L ⁻¹	mg.L ⁻¹	mg.L ⁻¹	mg.L ⁻¹	mg.L ⁻¹
E1s	CP1	7.11	30	70	33	489	14	64	4.4	32	2.3	0.001	0.13	39	10.15	67	25	5	2.3	3.0
E2s	CS1	7.39	30	80	38	54	20	39	4.8	29	0.75	0.02	0.1	19	32	62	27	7	7.3	1.7
E3s	CP2	7.25	30	70	33	681	4	32	9.7	25	2.2	0.11	0.2	37	3	63	26	7	0.7	0.9
E4s	CS2	7.03	30	70	33	649	24	88	4.9	26	0.47	0.03	0.21	15	5.55	65	28	8	1.3	1.7
E5s	CP3	7.17	30	70	33	797	10	34	2.9	29	3.95	0.03	0.34	80	31.2	80	25	5	7.1	9.5
E6s	CS3 1	6.99	30	70	33	837	10	46	2.9	28.5	0.62	0.013	0.32	25	11.1	55	24	4	2.5	3.4
E7s	CS3 2-1	7.14	30	70	33	870	7	24	1.9	29	0.49	0	0.31	16	17.55	55	25	5	4.0	5.3
E8s	CST3 1-1	7.03	30	80	38	383	22	59	17.5	29	4.05	0.021	0.11	65	9.55	62	26	7	2.2	2.9
E9s	SP	6.61	30	70	33	77	149	98	44.4	29	0.26	0.02	0.14	12	0.2	45	27	8	0.0	0.1
E1h	CP1	8.41	29	50	24	107	1.1	1.1	0	0.9	1.25	1.12	0.26	0.26	0.2	67.1	18	2	3.5	2.6
E2h	CS1	7.71	29	60	29	35	1.8	1.1	0	0.8	0.4	0.26	0	17	0	61	19	4	5.5	4.1
E3h	CP2	7.66	29	50	24	104	1.4	0.4	0	0.7	1.3	1.28	0.49	37	0.37	61	18	5	8.6	6.4
E4h	CS2	7.42	29	50	24	30	1.4	0.6	0	0.7	0.28	0.28	0.17	8	0.13	67.1	21	6	1.5	1.2
E5h	CP3	7.37	29	50	24	403	1.4	0.8	0	0.8	2.9	1.32	0.93	90	0.73	79.3	20	5	18.3	13.7
E6h	CS3 1	7.45	29	50	24	36	1.6	0.6	0	0.8	0.42	0.52	0.18	20	0.13	54.9	21	2	1.8	1.3
E7h	CS3 2-1	7.27	29	50	24	26	1.3	0.9	0	0.8	0.3	0.42	0.24	14	0.18	54.9	18	4	3.1	2.3
E8h	CST3 1-1	6.9	29	60	29	289	1.5	0.9	0	0.8	2.95	3.65	0.78	69	0.6	61	21	5	15.0	11.2
E9h	SP	7.41	29	50	24	35	1.4	0.9	0	0.8	0.18	0.16	0.32	4	0.24	42.7	19	5	4.8	3.6

Table 3: Eigenvalues.

	F1	F2	F3
Valeur propre	8.5	4.75	2.21
Variabilité (%)	44.6	25.00	11.65
% cumulé	44.6	69.63	81.29

In the projection of observations from 9 sites and 2 climatic periods onto the F1xF2 factorial plane, two water groups can be distinguished (Fig. 5).

This spatio-temporal typology represents the individualization of two operating models of this agrosystem. During the dry phase, this environment records a very strong

mineralization linked to a drop in water supply, causing solubilization of cations such as calcium and magnesium and anions such as chlorides.

In the phase of a significant supply of water from the river, the environment records a great dilution of the water, causing a drop in mineralization. This decline is accompanied by a water supply of organic nitrogen and mineral pollution, particularly copper, which is generally used as a fungicide.

This presence could represent a risk of an accumulation of this element in the sediments and organisms present in this agrosystem (Eijsackers et al. 2005).

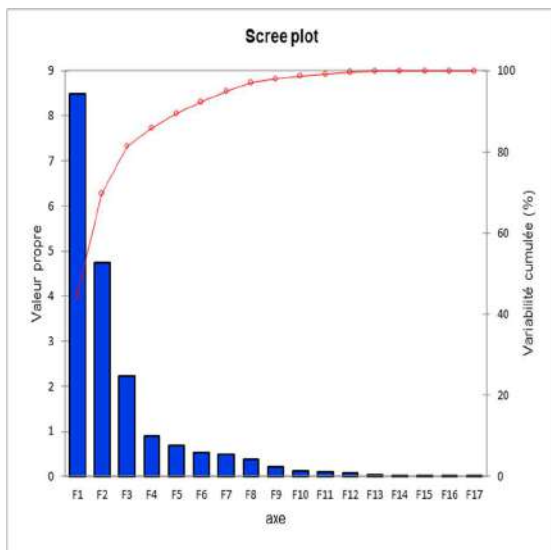


Fig. 3: Distribution of inertia between axes (PCA).

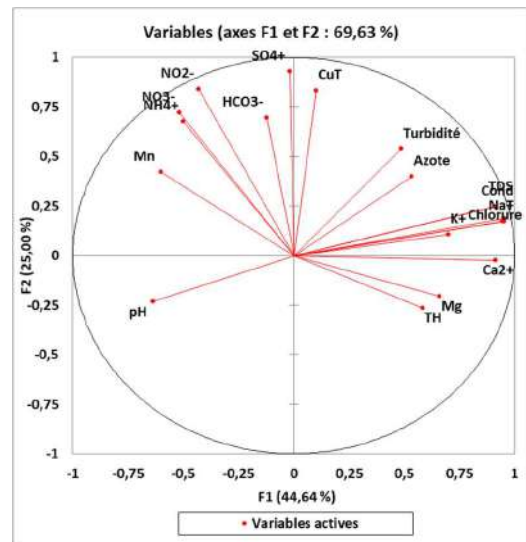


Fig. 4: correlation circle for variables on the F1xF2 factorial axis.

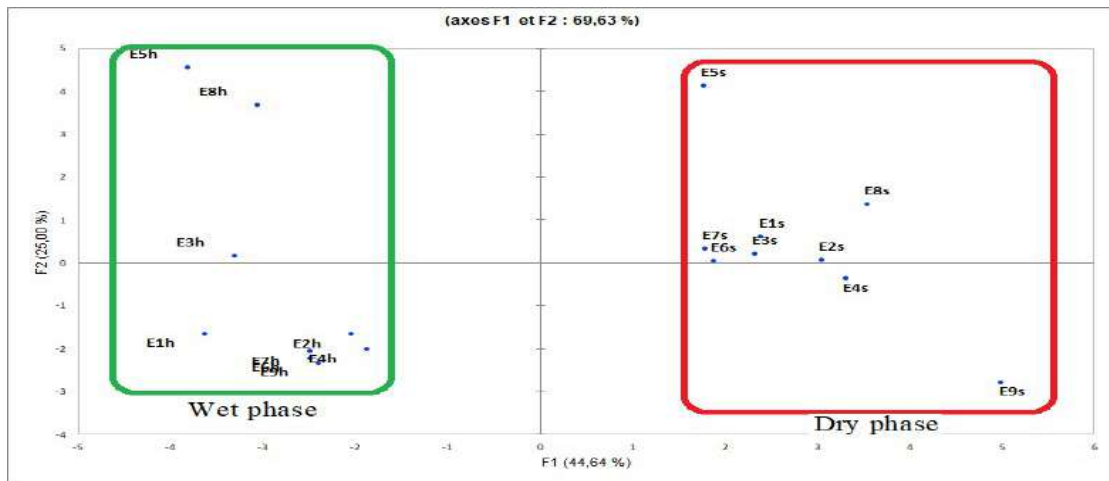


Fig. 5: Projection of individuals on the F1xF2 factorial axis.

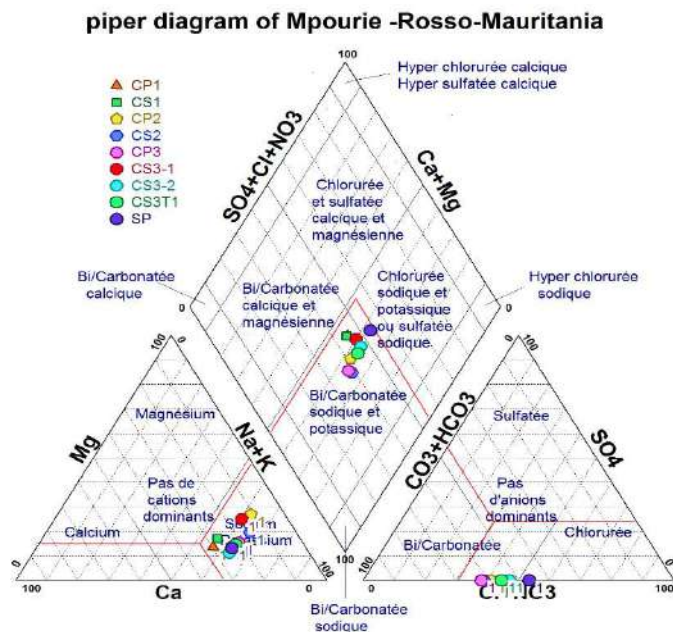


Fig. 6: Piper diagram evaluation in the M'Pourie plain.

Evaluation of the Hydrological Study Using the Piper Diagram

The Piper diagram is a particularly suitable tool for studying the evolution of water facies as a function of increasing mineralization or for comparing different sample groups and highlighting the dominant cation and anion types. The waters of M'Pourie in the Senegal River have low mineralization. Piper used the presentation of these waters as a simulation method to compare river waters and determine the dominant chemical facies at each site and during each climatic season.

The analyses used in the hydrological study originate from the collection of several samples at nine sites spread along the main M'Pourie canal. The results of the analyses for M'Pourie surface water are shown in Fig. 6.

Most of the analyses exhibit sodium-potassium bicarbonate facies, wherein sodium and potassium are the predominant cations, and chloride is the primary anion.

Evaluation of Soil Salinity in the Senegal River

Electrical conductivity (EC) is an essential measure for assessing soil salinity. Soil is generally considered salty

Table 5: Interpretation table for electrical conductivity values (USSL, 2017)

American scale	Unsalted	Lightly salted	Salted	Very salty	Extremely salty
CE mmhos/cm 25°C	<2	2-4	4-8	8-16	>16
Crop reaction	Negligible effects	Harvests of highly sensitive crops are reduced	Harvests of many crops are reduced	Only highly tolerant crops produce results	Only a small number of crops produce harvests

Table 4: Conductivity results on the M'Pourie plain

Website	Conductivity mmhos.cm ⁻¹
S1	0.32
S2	0.34
S3	0.35

when its EC exceeds 4 mmhos.cm⁻¹. The analysis of this parameter at the soil level of the stations considered (Table 4) shows values lower than the salinity threshold tolerated in agriculture (Abidine et al. 2018a). This result is confirmed by the agronomic scale developed by the U.S. Salinity Laboratory (U.S.S.L, 2017), which is graded according to Table 5. This classification places the soil in our environment in the unsalted category and does not present any reaction toward crops.

CONCLUSION

At the end of this study, the importance of climate changes, illustrated in this study by the variability of irrigation water supplies, proves to be important in the functioning of agrosystems. In fact, two modes of operation have become

individualized: the dry phase mode, characterized by a very strong mineralization of the water linked to a significant load of dissolved elements, and the wet phase mode, whose water quality is poorly mineralized but shows the impact that its irrigation water can represent in the loading of organic and mineral pollution and the need for strict control of these waters upstream before their agricultural use.

Irrigation with highly mineralized water can lead to an accumulation of salts in the soil and negatively affect soil structure and nutrient availability to plants. Certain ions, like sodium, can be particularly damaging in the long term.

Furthermore, the results obtained for the soil do not reveal a major impact on the salinization of the latter. However, this problem remains to be verified in the medium and long term by an approach within agricultural fields and with a productivity monitoring of cultivated plants.

REFERENCES

- Abidine, M.M.O., El Aboudi, A., Kebd, A., Aloueimine, B.B., Dallahi, Y., Soulé, A. and Vadel, A., 2018a. Modeling the spatial variability of the electrical conductivity of the soil using different spatial interpolation methods: Case of the Dawling National Park in Mauritania. *GT*, 13: 1-11.
- Abrisham, E.S., Jafari, M., Tavili, A., Rabii, A., Zare Chahoki, M.A., Zare, S., Egan, T., Yazdanshenas, H., Ghasemian, D. and Tahmoures, M., 2018. Effects of a super absorbent polymer on soil properties and plant growth for use in land reclamation. *Arid Land Research and Management*, 32: 407-420.
- Albalasmeh, A.A., Mohawesh, O., Gharaibeh, M.A., Alghamdi, A.G., Alajlouni, M.A., Alqudah, A.M., 2022. Effect of hydrogel on corn growth, water use efficiency, and soil properties in a semi-arid region. *Journal of the Saudi Society of Agricultural Sciences*, 21: 518-524.
- Alvarez, S. and Sanchez-Blanco, M.J. 2015. Comparison of individual and combined effects of salinity and deficit irrigation on physiological, nutritional, and ornamental aspects of tolerance in *Callistemon laevis* plants. *J. Plant Physiol.*, 185: 65-74.
- Al-Zu'bi, Y. 2007. Effect of irrigation water on agricultural soil in Jordan Valley: An example from arid area conditions. *J. Arid Environ.*, 70: 63-79.
- Asfaw, E., Suryabagavan, K.V. and Argaw, M. 2018. Soil salinity modeling and mapping using remote sensing and GIS: The case of Wonji sugar cane irrigation farm, Ethiopia. *J. Saudi Soc. Agric. Sci.*, 17: 250-258.
- Baatour, O., M'rah, S., Ben Brahim, N., Boulesnem, F. and Lachaal, M. 2004. Physiological response of grass pea (*Lathyrus sativus*) to environmental salinity. *Arid Regions Rev.*, 1: 346-358.
- Bouaroudj, S., Menad, A., Bounamous, A., Ali-Khodja, H., Gherib, A., Weigel, D.E and Chenchouni, H. 2019. Assessment of water quality at the largest dam in Algeria (Beni Haroun Dam) and effects of irrigation on soil characteristics of agricultural lands. *Chemosphere*, 219: 76-88.
- El Asslouj, J., Kholtei, S., El Amrani, N. and Hilali, A. 2007. Analysis of the physico-chemical quality of groundwater in the Mzamza community in the vicinity of wastewater. *Africa Sci. Int. J. Sci. Technol.*, 16: 109-122.
- Elgettafi, M., Himi, M., Casas, A. and Elmandour, A. 2011. Hydrochemistry characterization of groundwater salinity in Kert Aquifer, in Morocco. *Geogr. Tech.*, 14(2): 15-22.
- Eijsackers, H., Beneke, P., Maboeta, M., Louw, J.P.E. and Reinecke, A.J. 2005. The implications of copper fungicide usage in vineyards for earthworm activity and resulting sustainable soil quality. *Ecotoxicol. Environ. Safety*, 62: 99-111.
- Elhag, M. 2016. Evaluation of different soil salinity mapping using remote sensing techniques in arid ecosystems. *Saudi Arabia. J. Sens.*, 4: 1-8.
- Food and Agriculture Organization (FAO). 2020. *The State of Food and Agriculture 2020: Overcoming Water Challenges in Agriculture*. FAO, Rome.
- Gorji, T., Sertel, E. and Tanik, A., 2017. Monitoring soil salinity via remote sensing technology under data-scarce conditions: A case study from Turkey. *Ecol. Indic.*, 74: 384-391.
- Jolliffe, I. 2002. *Principal Component Analysis*, Second edition. Springer Verlag, Berlin.
- Escudier, B., Gillery, H., Ojeda, F. and Etchebarne, J.L. 2019. Control of salinity in irrigation water for viticulture. *BIO Web Conf.*, 12: 01010.
- Kahimba, F.C., Ali, R.M. and Mahoo, H.F. 2016. Evaluation of irrigation water quality for paddy production at Bumbwisudi rice irrigation scheme, Zanzibar. *Tanz. J. Agric. Sci.*, 21: 114-119.
- Khaled, I., Kumar, B.A., Roua, A., Juliana, H., Américo-Pinheiro, M. and Farooq, S. 2022. Assessment of three decades treated wastewater impact on soil quality in the semi-arid agroecosystem. *J. Agri. Saudi Soc. Agric. Sci.*, 14: 525-535.
- Lakhdhar, A., Hafsi, C., Rabhi, M., Debez, A., Montemurro, F., Abdely, Jedidi, N., Ouerghi, Z., 2008. Application of municipal solid waste compost reduces the negative effects of saline water in *Hordeum maritimum* L. *Bioresour. Technol.*, 99(15): 7160-7167.
- Denden, M., Bettaieb, T., Alef Salhi, M. and Mathlouthi, L. 2005. Effect of salinity on chlorophyll fluorescence, proline content, and floral production of three ornamental species. *Tropicultura*, 23: 220-225.
- Mounjid J., Cohen N., Fadlaoui S., Belhourri A. and Oubraim S. 2014. Contribution to the evaluation of the physico-chemical quality of the Merzeg watercourse (Suburban Casablanca, Morocco). *Larhyss J.*, 17: 31-51.
- Ngom, F.D, Tweed, S., Bader, J.C., Saos, J.L., Malou, R., Leduc, C. and Leblanc, M. 2016. The rapid evolution of water resources in the Senegal delta. *Glob. Planet. Chang.*, 144: 34-47.
- Ocde, M. 2010. *Sustainable Management of Water Resources in the Agricultural Sector*. OECD Publishing, Paris.
- Jagals, P., Grabow, W. and De Villiers, J. 1997. The effects of supplied water quality on human health in an urban development with limited basic subsistence facilities. *Water Res. Comm.*, 11: 373-378.
- Besse, P.C. 1992. *PCA Stability and Choice of Dimensionality: Statistics & Probability Letters*. Springer, Berlin
- Rodier J. 2009. *Water Analysis: Natural Waters, Waste Water, Sea Water*. Ninth Edition. OECD, Paris.
- Seyedmohammadi, J., Esmaelnejad, L. and Shabanpour, M. 2016. Spatial variation modeling of groundwater electrical conductivity using geostatistics and GIS. *Model. Earth Syst. Environ.*, 2: 1-10.
- Tripathi, R., Nayak, A.K., Shahid, M., Raja, R., Panda, B.B., Mohanty, S., Kumar, A., Lal, B., Gautam, P. and Sahoo, R.N, 2015. Characterizing spatial variability of soil properties in salt-affected coastal India using geostatistics and kriging. *Arab. J. Geosci.*, 8: 10693-10703.
- World Bank. 2014. *Final Report on Support for the Development of the Rural Sector Development Strategy in Mauritania*. World Bank, Washington DC
- World Bank. 2010. *World Development Report 2009: Rethinking Economic Geography*. World Bank, Washington, DC.
- Al-Zu'bi, Y. 2007. Effect of irrigation water on agricultural soil in Jordan Valley: An example from arid area conditions. *J. Arid Environ.*, 11: 63-79.
- Yao, R. and Yang, J. 2010. Quantitative evaluation of soil salinity and its spatial distribution using electromagnetic induction method. *Agric. Water Manag.*, 97: 1961-1970.



A Comparative Review on Bisphenol A Sources, Environmental Levels, Migration, and Health Impacts in India and Global Context

Sugata Datta*(***), Abhishek Chauhan**†, Anuj Ranjan**(*****), Abul Hasan Sardar***, Hardeep Singh Tuli****, Seema Ramniwas*****, Moyad Shahwan*****(*******), Ujjawal Sharma***** and Tanu Jindal**

*Amity Institute of Environmental Sciences, Amity University, Noida Campus, U.P., India

**Amity Institute of Environmental Toxicology Safety and Management, Amity University, Noida, U.P., India

***University of Calcutta, West Bengal, India

****Department of Biotechnology, Maharishi Markandeshwar (Deemed to be University), Mullana, Ambala 12 133207, Haryana, India

*****University Centre for Research & Development, University Institute of Pharmaceutical Sciences, Chandigarh University, Gharuan, Mohali, Punjab, India

*****Department of Clinical Sciences, College of Pharmacy and Health Sciences, Ajman University, Ajman 346, UAE

*****Centre of Medical and Bio-Allied Health Sciences Research, Ajman University, Ajman 346, UAE

*****Academy of Biology and Biotechnology, Southern Federal University, Rostov-On-Don, Russia

*****Department of Human Genetics and Molecular Medicine, School of Health Sciences, Central University of Punjab, Bathinda, India

†Correspondence author: Abhishek Chauhan; akchauhan@amity.edu

Nat. Env. & Poll. Tech.
Website: www.neptjournal.com

Received: 10-10-2023

Revised: 18-11-2023

Accepted: 30-11-2023

Key Words:

Bisphenol A

Health concerns

Environmental levels

Food-contact materials

ABSTRACT

Bisphenol A (BPA) is a widely utilized chemical found in numerous everyday products, including plastic containers, food packaging, and thermal paper. Research has linked BPA exposure to a range of health concerns, encompassing developmental and reproductive issues, cancer, and obesity. Given India's status as one of the world's largest producers and consumers of plastic goods, understanding the potential risks associated with BPA exposure and its health impacts on the Indian population is of paramount importance. This paper conducts a comparative analysis of BPA sources, environmental levels, migration, and health impacts in India in comparison to other countries. By examining data from various nations, we aim to discern overarching trends and patterns in BPA exposure and its associated health effects. This analysis serves as a foundation for the development of policies and regulations designed to safeguard public health. While the Indian government has taken some regulatory steps, such as banning the production, import, and sale of BPA-containing polycarbonate baby bottles, there is a notable absence of specific regulations or bans on BPA in other food-contact materials (FCMs). Studies conducted in India have detected BPA in various food items, underscoring the potential risk of BPA exposure through food consumption. This emphasizes the urgent need for effective monitoring and control of BPA migration in FCMs within India. In conclusion, this comparative review underscores the imperative for ongoing research and rigorous monitoring of BPA exposure and its health impacts in India, as well as in other nations. Safeguarding the health of the general public necessitates a comprehensive understanding of BPA's prevalence, sources, and consequences. By implementing and refining regulations, such as extending bans on BPA in additional FCMs, policymakers can work towards mitigating the risks associated with BPA exposure and ensuring the safety of populations worldwide.

INTRODUCTION

Bisphenol A (BPA) is a carbon-based synthetic compound that belongs to the two hydroxyphenyl groups of diphenylmethane derivatives and has the chemical formula $C_{15}H_{16}O_2$ and a molecular mass of $228.29 \text{ g.mol}^{-1}$. It is an important industrial chemical and is primarily used as an

intermediate in the production of polycarbonate (PC) plastics and epoxy resins. BPA and its derivatives such as bisphenol S (BPS), bisphenol F (BPF), bisphenol E (BPE), bisphenol B (BPB), bisphenol Z (BPZ) and bisphenol AF (BPAF) might be released by the imperfect polymerization of the plastic substances that appears during processing or depolymerization

due to deliberate heating for sterilization or accidental purposes during storage (Lopes-Rocha et al. 2021).

The European Chemical Agency (ECHA) has added BPA to the list of chemicals of very high concern due to its toxicity, and many regulatory authorities have established specific limits on its usage and migration. The World Health Organization (WHO) convened an expert panel and determined that public limits on BPA are premature (World Health Organization 2009). The US Food and Drug Administration (FDA) issued a report highlighting the potential hazards of BPA. Subsequently, it withdrew approval for the use of BPA-based plastics in packaging materials for baby formula or feeding bottles (US FDA 2014). The European Union (EU) and Canada have implemented similar restrictions. The US Environmental Protection Agency (USEPA) has determined that the toxic level of BPA is as high as $50 \mu\text{g}\cdot\text{kg}^{-1}$ of body weight per day, but lower amounts may not be completely safe (European Union 2014). The European Commission (EC) has established a Specific Migration Limit (SML) for BPA in foods of $0.6 \mu\text{g}\cdot\text{g}^{-1}$ of the food substance. In 2010, the Indian government prohibited the manufacture, import, and sale of polycarbonate baby bottles containing BPA, citing concerns about its potential health effects on infants. However, there are no specific regulations or bans on the use of BPA in other food-contact materials (FCMs), such as epoxy resins and polystyrene containers. In 2018, the Food Safety and Standards Authority of India (FSSAI) proposed a draft notification to regulate the use of di-(2-ethylhexyl) phthalate (DEHP) in plastic food packaging materials, which included a maximum limit of $1.5 \text{ mg}\cdot\text{kg}^{-1}$ (FSSAI 2022). The draft notification, however, fails to address the issue of BPA migration from food-contact materials, as it does not make any explicit mention of this concern.

There have been several studies conducted in India that report the migration of BPA from FCMs into food products (Dey 2021, Kumar 2023). These studies have detected BPA in various food items, including canned foods and beverages, baby feeding bottles, and plastic containers used for food storage and microwaving. The levels of BPA migration have been found to vary widely, with some samples containing levels above the regulatory limits set by the authorities. These findings highlight the potential risk of BPA exposure to human health through food consumption and the urgent need for effective monitoring and control of BPA migration in FCMs in India. However, the extent of exposure and associated health risks is still a matter of ongoing research and debate.

Therefore, the purpose of the study holds significant importance for several reasons, as BPA is a widely utilized

chemical that is present in several products, such as plastic containers, food packaging, and thermal paper. The chemical can contaminate the environment by leaching out from these products, thereby resulting in potential health hazards. This has led to growing apprehensions about the likely health impacts of BPA exposure, particularly in vulnerable populations such as pregnant women and children. As India is one of the biggest producers and consumers of plastic products worldwide, with a rapidly growing population and economy, India is expected to experience higher levels of BPA exposure in the future. This comparative review can aid in identifying potential sources of exposure, evaluating the present levels of BPA in the environment, and analyzing the health consequences of BPA exposure in various populations. Through a comparison of data from different countries, researchers can also identify trends and patterns in BPA exposure and its health impacts. This information can help in formulating policies and regulations and is crucial in comprehending the potential risks of BPA exposure, identifying exposure sources, and formulating policies and regulations to safeguard public health.

Major Sources of BPA

BPA is predominantly used in the production of polycarbonate and epoxy resins, accounting for 95% of its industrial use (Hahladakis et al. 2023). The remaining 5% is allocated to a diverse range of applications such as phenoplast resins, phenolic resins, unsaturated polyester resins, can linings, antioxidants, PVC manufacturing and processing additives, ethoxylated BPA, dye developer for thermal paper, polyols, modified polyamide, compounding ingredient for car tires, flame retardants (such as tetrabromo BPA), automotive and transportation equipment, optical media (e.g., DVDs), electronic equipment, construction, linings inside drinking water pipes, thermal and carbonless paper coatings, and foundry casting (Huang et al. 2012). BPA is preferred for its use in the manufacturing of polycarbonate plastics due to its capability to produce durable and rigid plastic materials that exhibit resistance to shattering when exposed to temperature variations, be it heat or cold (Dey et al. 2023). BPA is not only cost-effective but also highly efficient, which accounts for its extensive application in the production of various plastic products, particularly those intended for food and beverage containment. Furthermore, BPA's chemical composition includes phenolic epoxy resins, which find application in the creation of protective coatings for food and beverage containers (Sharma et al. 2023). These coatings play a crucial role in safeguarding the contents of the containers by protecting environmental factors like moisture, heat, and bacteria, ensuring the integrity and safety of the stored food and beverages.

BPA Detected in the Environment

BPA has been detected in the environment, including in air, water, soil, and sediment. It can enter the environment through various sources, such as industrial discharge, landfill leachate, and wastewater treatment plant effluent (Wojnowska-Baryła et al. 2022). BPA has also been found in aquatic organisms, which can accumulate in their tissues through food chain transfer (Kataria et al. 2022). The presence of BPA in the environment is a concern due to its potential adverse effects on human health and the ecosystem. Research is ongoing to better understand the sources, fate, and effects of BPA in the environment and to develop strategies to reduce its environmental impact.

Aquatic Environment: BPA is detected in the aquatic environment (both freshwater and marine waters) due to leaching from BPA-based products and also through effluent from wastewater treatment plants and landfill sites. A large number of peer-reviewed studies have reported specific occurrences and concentrations of BPA in aquatic systems. Table 1 lists BPA levels detected in the rivers in different parts of India. The majority of studies conducted showed that the concentrations of BPA detected in the River Ganga were higher than in the rivers of South India (Mukhopadhyay 2020, Gopal 2021). Compared to riverine locations, coastal waters recorded significantly lower BPA levels, as 49 percent of untreated wastewater from the adjacent districts is directly discharged into the riverine region (Yamazaki 2015, Mukhopadhyay 2020). Freshwater discharge during

the monsoon period dilutes BPA and the plasticizers. Hence lower concentration is reported (Gopal et al. 2021). The concentration of BPA in the upstream section of the Yamuna River (576-603 ng.L⁻¹) was found to be significantly lower than that in the midstream section (10,500-14,800 ng.L⁻¹) (Lalwani et al. 2020). This disparity is likely attributed to the convergence of the Najafgarh drain and 14 other drains located between the Wazirabad barrage and Okhla barrage, which are known to discharge untreated sewage, industrial waste, and other pollutants into the river. The contamination of Vembanad Lake in Kerala by untreated effluents from various sources, including agriculture, domestic, municipal, and industrial sectors, has led to the presence of high levels of iron (11.29 ± 0.39 ppm) and BPA (0.02412 ± 0.0031 µg.mL⁻¹) in the hepatic tissue of edible fish species, particularly *Etroplus suratensis*. The elevated levels of these contaminants have increased hepatic stress markers and distorted hepatic structure in the fish. As a result, consuming contaminated fish from Vembanad Lake is a serious health concern, and effective measures must be taken to mitigate the environmental and health risks associated with pollution in the lake (Pettamanna et al. 2020).

Soil and Sediments: The contamination of sediments in India is largely attributed to the direct discharge of untreated wastewater into rivers, where around 64 percent of the generated wastewater is left untreated. This contamination is further compounded by the disposal of electronic waste, the burning of waste, wastewater discharge, and industrial pollution, which have led to the presence of phthalate esters

Table 1: Concentration of BPA (ng.L⁻¹) in aquatic environment in India.

States/Uts	Location	BPA levels {ng.L ⁻¹ }	References
Tamil Nadu	River Kaveri, River Vellar River Tamiraparani	6.6-136 2.8-6 9.8-36	(Kumar et al. 2014)
Uttarakhand, Uttar Pradesh	Entire stretch of River Ganga	140-4460	(Chakraborty et al. 2021)
West Bengal	Wetlands of Sunderbans	210-2820	
Karnataka	River Arkavathi, a tributary of River Kaveri	49.7 (pre-monsoon) 37.6 (post-monsoon)	(Gopal et al. 2021)
West Bengal	River Hooghly	803 (riverine region) 137.4 (estuarine region)	(Mukhopadhyay et al. 2020)
Tamil Nadu	River Cooum Puzhal Lake River Adyar Buckingham Canal Korttalaiyar Canal	264-628 ND 54-512 835-1950 33	(Yamazaki et al. 2015)
Delhi	River Yamuna	79.6-14,800	(Lalwani et al. 2020)
Tamil Nadu	River Cooum	1,420	
Kerala	Lake Vembanad	24,120-31,000 (hepatic tissues of edible fish <i>Etroplus suratensis</i>)	(Pettamanna et al. 2020)

ND. Not Detected

(PAEs) and BPA in the soil (Mukhopadhyay et al. 2020). Wastewater discharge from industries and homes, as well as the flow dynamics of rivers, has also been identified as principal sources of BPA in surface riverine sediments in the lower stretch of the River Ganga (Mukhopadhyay & Chakraborty 2021). Estuarine sediments from Mumbai showed the presence of BPA within the range of 16.3-35.79 $\mu\text{g.kg}^{-1}$ (Tiwari et al. 2016). Reports have shown similar findings in Zhejiang, China, where farmlands contained BPA, BPF, and BPP (bisphenol P) up to 166, 212.9, and 78.2 ng.g^{-1} dry weight, respectively (Xu et al. 2021). Additionally, landfill leachate in South China showed a total bisphenol content of 32,130 ng/L (Huang et al. 2021). Activated sludge digesters in Shenzhen, China, had BPA concentrations averaging 199.5 ng.g^{-1} dry weight of sludge, suggesting that BPA is the most widely used bisphenol in suspended solids (Qian et al. 2021). BPA concentrations ranging from 82.4-989 ng.g^{-1} of microplastic were found on Hong Kong beaches due to sewage treatment plant discharge (Lo et al. 2021).

ENVIRONMENTAL IMPLICATIONS OF BPA

The widespread use of BPA in various commercial plastic products has resulted in air, water, and soil becoming

potential routes of exposure to this compound. Workers involved in the production of epoxy resin-coated metallic cans, PVC films, and thermal paper are at higher risk of BPA exposure. Furthermore, the plastic industry and thermal paper recycling have led to high levels of BPA leaching into the environment, contaminating soil, air, and aquatic environments (Ramakrishna et al. 2021). Uncontrolled residential trash burning in open bins can produce BPA concentrations and emission rates of up to 58.3 mg.L^{-1} and 9.7 mg.kg^{-1} , respectively (Vasiljevic & Harner 2021). Therefore, it is apparent that anthropogenic sources are the primary contributors to the presence of BPA in the environment.

Plastic pollution in rivers and oceans is a major environmental hazard. Bisphenols, phthalates, polychlorinated biphenyls (PCBs), and polycyclic aromatic hydrocarbons (PAHs) are among the most prevalent contaminants detected in plastics that pollute the aquatic environment. With a high detection rate and concentration, BPA is the most prominent bisphenol analog in wastewater treatment plants, followed by BPS and BPF. The adsorption of BPA on primary and activated sludge in the water treatment process results in higher levels of BPA in anaerobically digested sewage

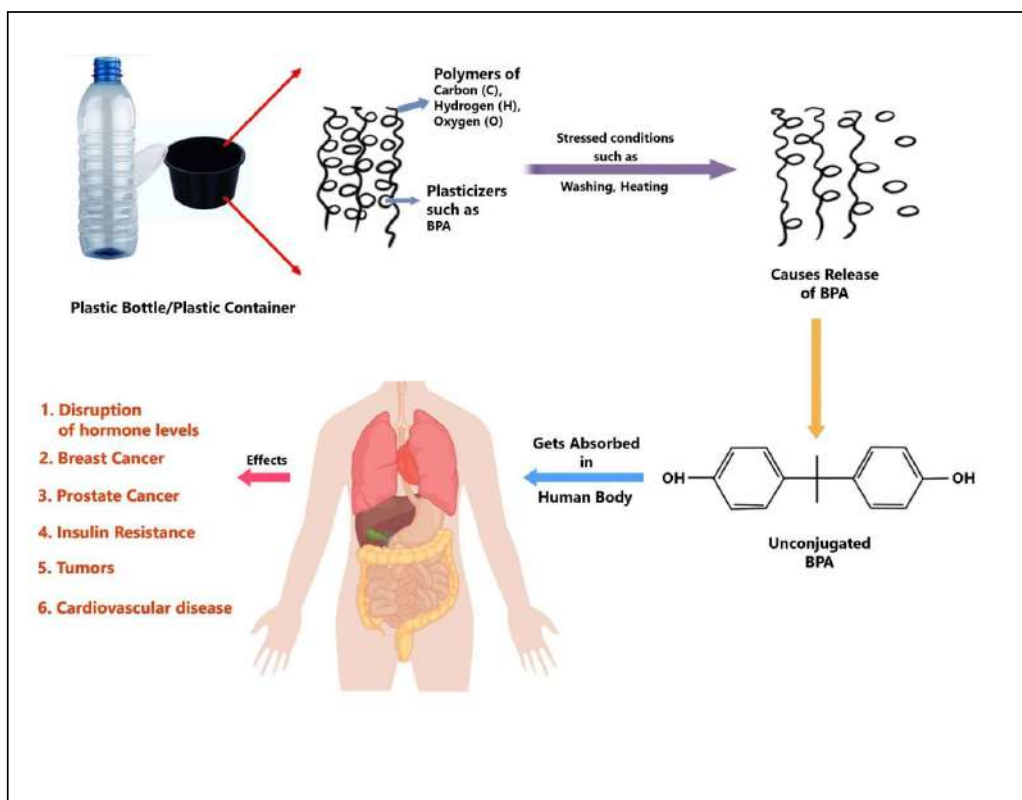


Fig. 1: Mechanism of BPA migration from FCMs and its potential health consequences in humans.

Table 2: BPA leached from FCMs as reported in major countries.

In baby foods				
Location	Food types	BPA content	Types of food containers	References
India	Baby mashed fruit pulp	7.87-61.3 ng.mL ⁻¹	PC baby feeding bottles	(Nepalia et al. 2018)
	Baby cereal rice powder			
	Paper-packaged formula milk			
Egypt	Formula milk	1.65-7.98 ng.mL ⁻¹	Canned	(Shrinithiviahshini et al. 2014) (Karsauliya et al. 2021) (Osman et al. 2018)
	Milk	19 ng.mL ⁻¹	PC baby feeding bottles	
	Powdered infant milk formula	5.46 ng.g ⁻¹	Canned	
	Infant milk formula	87.34-90.95 ng.g ⁻¹	Canned	
	Milk	69.83-125.66 ng.g ⁻¹	PC baby feeding bottles	
Spain	Liquid milk	0.38-547 ng.mL ⁻¹	Plastic packaged	(Molina-García et al. 2012)
	Liquid infant formula milk	1.26-6.31 ng.mL ⁻¹		
	Solid infant formula or powdered milk	ND		
	Infant formula milk	11-12 ng.g ⁻¹		
In other foods				
India	Vegetables and fruits	20-440 ng.g ⁻¹	Canned	(Chauhan & Jindal 2020)
Spain	Meat products	20 ng.g ⁻¹	Canned	(González et al. 2020)
	Fish products	30-40 ng.g ⁻¹	Canned	
Egypt	Vegetables and fruits	7-90 ng.g ⁻¹	Canned	(Osman et al. 2018)
	Meat products	31.02- 724.06 ng.g ⁻¹	Canned	
	Fish products	57.68-168.52 ng.g ⁻¹	Canned	
	Vegetables and fruits	7.24-168.59 ng.g ⁻¹	Canned	
	Dairy products	32.71-90.95 ng.g ⁻¹	Canned	
Italy	Beverages	13.96-14.87 ng.g ⁻¹	Canned	(Cirillo et al. 2019) (Fattore et al. 2015) (Adeyi & Babalola 2019)
	Beer	0.50-0.80 ng.mL ⁻¹	Canned	
	Tuna	5-120 ng.g ⁻¹	Canned	
Southwest	Meat products	ND	Unpackaged (raw)	
Nigeria	Fish products	21.3 ng.g ⁻¹	Canned beef	
		0.78 ng.g ⁻¹	Unpackaged (raw frozen)	
	Dairy products	26.3 ng.g ⁻¹	Canned fish	
		ND	Unpackaged	
		4.8 ng.g ⁻¹	Canned milk	
United States	Vegetables & fruits	ND	Raw fruits and vegetables	(Liao & Kannan 2013)
		0.20 ng.g ⁻¹	Canned vegetables	
		1.11 ng.g ⁻¹	Canned fruits	
		0.235 ng.g ⁻¹	Canned	
		2.55 ng.g ⁻¹	Canned	
Greece	Beverages	1.90 ng.g ⁻¹	Canned	(Tzatzarakis et al. 2017)
	Dairy products	3.23 ng.g ⁻¹	Canned	
	Fats and oils	0.605 ng.g ⁻¹	Canned	
	Fish and Seafood	0.852 ng.g ⁻¹	Canned	
	Cereals	8.99 ng.g ⁻¹	Canned	
	Meat and meat products	0.532 ng.g ⁻¹	Canned	
	Vegetables	0.4-10.2 ng/mL ⁻¹	Plastic	
	Fruits	ND	Tetra pack	
	Beverages (soft drinks)	<0.6 ng.g ⁻¹	Canned	
	Meat products	<0.6 ng.g ⁻¹	Plastic	
China	Fish and Seafood	17.2-30.7 ng.g ⁻¹	Canned	(Cao et al. 2021)
	Vegetables	48.3-66 ng.g ⁻¹	Canned	
	Meat products	100-300 ng.g ⁻¹	Canned	
	Seafood	ND-144 ng.g ⁻¹	Canned	
	Fruit	ND-837 ng.g ⁻¹	Canned	
	Vegetables	ND-102 ng.g ⁻¹	Canned	
	Beverages	2-88 ng.g ⁻¹	Canned	
Korea	Meat products	29.57 ng.g ⁻¹	Canned	(Choi et al. 2018)
	Fish products	33.43 ng.g ⁻¹	Canned	
	Fruits	10.46 ng.g ⁻¹	Canned	
	Vegetables	4.67 ng.g ⁻¹	Canned	
	Beverages	3.79 ng.g ⁻¹	Canned	

ND. Not Detected

sludge. BPA thus accumulates and translocates in agricultural soils after being supplemented with sewage sludge (Hu et al. 2019). BPA leaching or percolation into groundwater from agricultural soils poses a risk to the ecosystem and human health (Mg & Girigoswami 2021). BPA is used as a developing dye for thermal papers; when recycled into toilet paper is transferred to the recycled product and ends up in sewage, where it is partially eliminated during the wastewater treatment process (Hardegen et al. 2021). It has been established that wastewater sludge contains far more BPA than wastewater, and BPA concentrations in sediments in Asia are significantly higher than in Europe and North America (Corrales et al. 2015). The widespread presence of BPA in various environmental media, coupled with its potential adverse effects on human health and ecological systems, underscores the urgency for policymakers and environmental agencies to take prompt and effective measures to mitigate the environmental implications of BPA.

BPA LEACHING FROM FOOD-CONTACT MATERIALS (FCMS)

BPA exposure primarily occurs through dietary intake of food and beverages that have come into contact with these materials (Siddique et al. 2021). Packaged foods have been found to contain the highest levels of BPA, leading to a lowered tolerable daily intake (TDI) by the European Food Safety Agency (EFSA) from 50 to 4 $\mu\text{g}\cdot\text{kg}^{-1}\text{ bw}\cdot\text{day}^{-1}$ (Opinion et al. 2015). BPA, which is incorporated into plastic containers and used in epoxy resin-coated metal cans to improve their durability and protective properties, has the potential to migrate into food and beverages in specific circumstances. These conditions include exposure to heat, repeated washing, or contact with acidic substances (Fig. 1). The prevalence of BPA exposure and its potential health risks make it a significant public health concern, and measures to reduce exposure through dietary sources and regulate its use in FCMS are necessary to mitigate the risk.

Multiple research investigations have revealed that there is a significant rate of BPA migration from FCMS despite the presence of strict regulations (Table 2). These findings highlight the need for continued monitoring and regulation of FCMS to minimize potential health risks associated with BPA.

BPA REGULATION IN MAJOR COUNTRIES

In the European Union, the European Food Safety Authority (EFSA) established a temporary tolerable daily intake (TDI) of 4 $\mu\text{g}\cdot\text{kg}^{-1}\text{ bw}\cdot\text{day}^{-1}$ in risk evaluation of BPA. However, in a re-evaluation of BPA's risk assessment, the EFSA's Panel on Food Contact Materials, Enzymes, and Processing

Aids (CEP) recommended a significantly lower TDI of 0.04 $\text{ng}\cdot\text{kg}^{-1}\text{ bw}\cdot\text{day}^{-1}$. This change was based on scientific studies published between 2013 and 2018 that demonstrated the hazardous effects of BPA, including its ability to impact estrogen receptors and alter immune responses. The EFSA suggested this reduction due to the widespread usage of BPA-based products, as all age groups were found to exceed the previous TDI of 4 $\mu\text{g}\cdot\text{kg}^{-1}\text{ bw}\cdot\text{day}^{-1}$ (Aids 2015).

In the United States, the FDA has calculated estimated daily BPA exposure from its use in FCMS to be 2.42 $\mu\text{g}\cdot\text{kg}^{-1}\text{ bw}\cdot\text{day}^{-1}$ for infants and 0.185 $\mu\text{g}\cdot\text{kg}^{-1}\text{ bw}\cdot\text{day}^{-1}$ for adults. To put this into perspective, the FDA has established a No-Observed-Adverse-Effect Level (NOAEL) for systemic toxicity of BPA based on two multigenerational rat studies, which is 5 $\text{mg}\cdot\text{kg}^{-1}\text{ bw}\cdot\text{day}^{-1}$. This NOAEL is approximately 2000 times higher than the estimated BPA intake from FCMS for infants and a substantial 27,000 times higher for adults, as reported (Shelnutt et al. 2013). Furthermore, USEPA has established a chronic oral Reference Dose (RfD) for BPA at 50 $\mu\text{g}\cdot\text{kg}^{-1}\text{ bw}\cdot\text{day}^{-1}$.

In Canada, the Chemicals Management Plan evaluates and addresses the possible threats that chemical compounds pose to the environment. A Screening Risk Assessment Report for BPA was published in 2008. The conclusion of the report indicated that BPA might be infiltrating the environment, posing a risk to human life or health, as well as having an immediate or long-term negative impact on the environment or biological diversity. BPA was subsequently added to the List of Toxic Substances in Schedule 1 of the Canadian Environmental Protection Act, 1999 (CEPA 1999). Newborns and infants are protected from exposure to BPA by the Canada Consumer Product Safety Act. The Act makes it illegal to manufacture, import, market, or sell PC infant bottles that contain BPA. In 2010, PC baby bottles that contain BPA were forbidden. The enforcement actions of this restriction found only 1 non-compliant sample in 2011 and no non-compliant samples in 2013. As of 2014, Canadian consumers are not expected to find any liquid infant formula products packaged in BPA-containing packaging on the Canadian marketplace.

In other countries, for example, in Japan, food safety regulations are based on the Food Sanitization Law (1947) and Food Safety Basic Law (2003), which aim to protect people's health through food safety. Under Article 18 of this law, in polycarbonates, the BPA level should be $\leq 500\ \mu\text{g}\cdot\text{g}^{-1}$ and $\leq 2.5\ \mu\text{g}\cdot\text{mL}^{-1}$. The Ministry of Health Malaysia (MOH) has banned the importation, manufacture, or sale of any feeding bottles containing BPA since 2012 when they found the rate migration of BPA from PC bottles increased 7-fold when boiling temperature increased from 25°C to 80°C (Tsang 2011). Chinese authorities have banned

BPA in baby feeding bottles as they continue their pitched battle to improve food safety.

In India, there are currently no specific regulations governing the use of BPA in FCMs. However, its usage is regulated under various existing laws such as the Environment (Protection) Act, 1986, the Hazardous Waste (Management, Handling, and Transboundary Movement) Rules, 2016, and the Manufacture, Storage, and Import of Hazardous Chemicals Rules, 1989, due to its hazardous nature. FSSAI introduced the Food Safety and Standards (Packaging) Regulations, 2018 to regulate food contact materials and articles, including a list of packaging materials for certain categories of food and limits on the migration of heavy metals and DEHP (FSSAI 2022). The regulation of baby feeding bottles in India with regards to BPA has undergone amendments over the years, notably through the Infant Milk Substitutes, Feeding Bottles, and Infant Foods (Regulation of Production, Supply, and Distribution) Act 1992, later amended in 2003. However, despite growing concerns internationally and a draft proposal by the Bureau of Indian Standards (BIS) in 2013 aimed at restricting BPA usage in these bottles, no official publication or implementation of this draft by the Indian government has been recorded (Mahamuni & Shrinithiviahshini 2017). There appears to be a lack of specific legal measures governing the permissible levels of BPA in baby feeding bottles within the Indian regulatory framework. In contrast to numerous developed nations where well-established human biomonitoring programs for BPA exist, the involvement and exploration of public health institutions in monitoring BPA as Endocrine Disrupting Compounds (EDCs) and evaluating their health impacts on the broader Indian population have been limited or largely unexplored (Sharma et al. 2022).

The presence of regulations to restrict the usage of BPA in certain products and set maximum limits for BPA migration into food products is noteworthy. However, it is imperative to implement more stringent monitoring and enforcement measures to ensure that these regulations are being adhered to and that BPA levels in food and FCMs remain within safe limits. Rigorous monitoring can help detect any violations or non-compliance, and prompt remedial actions can be taken to prevent harmful exposure to BPA. Furthermore, it is crucial to periodically update and review these regulations based on new scientific evidence to ensure their continued effectiveness in safeguarding public health.

BPA AND ITS EFFECT ON HEALTH

BPA has recently attracted significant attention due to its identification as an EDC (Tarafdar et al. 2022). BPA is characterized as a “weakly estrogenic” substance because

its binding affinity for estrogen receptors is approximately 10,000 times lower than that of natural estrogen (Im & Löffler 2016). Endocrine disruptors work by interfering with normal hormone biosynthesis, secretion, activity, or metabolism, which can adversely affect children’s health, causing “altered neurodevelopment, obesity, and precocious puberty” (Braun & Hauser 2011). Several laboratory investigations and a better knowledge of the mechanisms by which BPA exerts an estrogenic effect have prompted increased attention to the harmful consequences of BPA. In animal experiments, high levels of BPA exposure during pregnancy resulted in preterm birth, reduced fetal and placental weights, slower growth, lower survival due to impairment of uterine spinal arteries, and a prolonged period for offspring to reach puberty (Ma et al. 2019). BPA exposure has also been linked to insulin resistance in animals, with the disruption of the insulin pathway obstructing glucose absorption and affecting the expression of the GLUT4 gene (Cetkovic-Cvrlje et al. 2017). BPA exposure in pregnant OF1 mice was linked to glomerular abnormalities and decreased glomerular development, implying that BPA exposure in pregnant humans may have negative consequences (Nuñez et al. 2018). Other research works have revealed relationships between prenatal or early-life BPA exposure and neurological effects, as well as the development of breast and prostate cancer in adult animals (Santoro et al. 2019). Being lipophilic, BPA can accumulate in adipose tissue, with 50 percent of breast adipose tissue containing BPA (Jain et al. 2020). Urinary BPA levels are also frequently reported to be positively associated with ovarian cancer and infertility in females (Hagobian et al. 2021). Males with higher urinary BPA concentrations displayed a significantly lower sperm count, viability, and motility (Castellini et al. 2020).

The availability of scientific papers reporting on the exposure of BPA in humans in India is limited. However, the presence of EDCs in various body fluids such as urine, blood serum, breast milk, and amniotic fluid is reported by (Shekhar et al. 2017). This study provides insights into the exposure of EDCs, including BPA, among the Indian population, highlighting the need for further research and regulatory measures to protect public health. Additionally, presence of BPA in the urine of patients has also been noted (Muthusamy et al. 2021). The study found that the mean human urine BPA concentrations were significantly higher in the patient group ($5.76 \pm 6.00 \text{ ng.mL}^{-1}$) as compared to the control group ($1.18 \pm 2.11 \text{ ng.mL}^{-1}$). These results suggest that the patients were exposed to higher levels of BPA, which could be a cause for concern. These studies highlight the need for further research to investigate the sources of BPA exposure and its potential impact on human health.

CONCLUSION

This review provides a comparative analysis of BPA sources, environmental levels, migration, and health impacts in India and other countries. Our analysis indicates that BPA is a ubiquitous environmental contaminant with a significant impact on human health. We found that in India, BPA exposure mainly occurs through the consumption of contaminated food and water, as well as occupational exposure in certain industries.

The regulatory landscape concerning BPA in FCMs, particularly in India, reflects a complex interplay between existing environmental and chemical management laws rather than specific guidelines dedicated to its usage. While various laws such as the Environment (Protection) Act, Hazardous Waste Rules, and others acknowledge the hazardous nature of BPA, the absence of stringent, specialized regulations directly addressing its permissible levels in FCMs remains apparent. The Food Safety and Standards (Packaging) Regulations of 2018 brought forth by FSSAI mark an attempt to regulate food contact materials but lack explicit provisions concerning BPA limits. Amendments to regulations governing baby feeding bottles have been proposed, yet formal implementation, as evidenced by the Bureau of Indian Standards' draft proposal in 2013, has not materialized. Notably, compared to developed nations with robust biomonitoring programs for BPA, India appears to have limited involvement from public health institutions in monitoring BPA's impact as an EDC and its broader health implications for the population. Consequently, the existing framework in India reveals a gap in tailored regulations specifically addressing BPA levels in FCMs, highlighting the need for comprehensive guidelines and active involvement of health institutions for effective monitoring and safeguarding of public health.

Our review also highlights the need for further research and regulatory measures to address BPA contamination in India and globally. India, as a rapidly developing country, needs to take proactive measures to reduce exposure to BPA and other environmental contaminants. Future research should focus on identifying the sources of BPA exposure, assessing the extent of exposure, and evaluating the effectiveness of mitigation strategies. Regulatory measures such as the banning of BPA in food-contact materials, as seen in some countries, should be considered in India as well.

In conclusion, the evidence presented in this review underscores the urgent need for action to reduce BPA exposure and mitigate its health impacts in India and globally. We hope that this review will contribute to the ongoing dialogue on environmental health and inform policy decisions to protect public health.

REFERENCES

- Adeyi, A.A. and Babalola, B.A. 2019. Bisphenol-A (BPA) in Foods commonly consumed in Southwest Nigeria and its Human Health Risk. *Scientific Reports*, 9(1): 1-13. <https://doi.org/10.1038/s41598-019-53790-2>
- Aids, P. 2015. Scientific Opinion on the risks to public health related to the presence of bisphenol A (BPA) in foodstuffs. *EFSA Journal*, 13(1): 1. <https://doi.org/10.2903/j.efsa.2015.3978>
- FSSAI 2022. Food Safety and Standards Authority Of India Notification. https://www.fssai.gov.in/upload/notifications/2022/09/631067fe88a44Gazette_Notification_Plastic_01_09_2022.pdf
- Braun, J.M. and Hauser, R. 2011. Bisphenol A and Children's Health. *Curr. Opin. Pediatr.*, 23(2): 233. <https://doi.org/10.1097/MOP.0B013E3283445675>
- Cao, P., Zhong, H. Ning, Qiu, K., Li, D., Wu, G., Sui, H. Xia, M. and Song, Y. 2021. Exposure to bisphenol A and its substitutes, bisphenol F and bisphenol S, from canned foods and beverages on the Chinese market. *Food Control*, 120: 107502. <https://doi.org/10.1016/j.foodcont.2020.107502>
- Castellini, C., Totaro, M., Parisi, A., D'Andrea, S., Lucente, L., Cordeschi, G., Francavilla, S., Francavilla, F. and Barbonetti, A. 2020. Bisphenol A and Male Fertility: Myths and Realities. *Front. Endocrinol.*, 11: 353. <https://doi.org/10.3389/FENDO.2020.00353/BIBTEX>
- Cetkovic-Cvrilje, M., Thinamany, S. and Bruner, K.A. 2017. Bisphenol A (BPA) aggravates multiple low-dose streptozotocin-induced Type 1 diabetes in C57BL/6 mice. *J. Immunotoxicol.*, 14(1): 160-168. <https://doi.org/10.1080/1547691X.2017.1334722>
- Chakraborty, P., Shappell, N.W., Mukhopadhyay, M., Onanong, S., Rex, K.R. and Snow, D. 2021. Surveillance of plasticizers, bisphenol A, steroids, and caffeine in the surface water of River Ganga and Sundarban wetland along the Bay of Bengal: occurrence, sources, estrogenicity screening, and ecotoxicological risk assessment. *Water Res.*, 190: 116668. <https://doi.org/10.1016/j.watres.2020.116668>
- Chauhan, A. and Jindal, T. 2020. *Microbiological Methods for Environment, Food and Pharmaceutical Analysis*. Springer, Cham <https://doi.org/10.1007/978-3-030-52024-3>
- Choi, S.J., Yun, E.S., Shin, J.M., Kim, Y.S., Lee, J.S., Lee, J.H., Kim, D.G., Oh, Y.H., Jung, K. and Kim, G.H. 2018. Concentrations of Bisphenols in Canned Foods and Their Risk Assessment in Korea. *J. Food Prot.*, 81(6): 903-916. <https://doi.org/10.4315/0362-028X.JFP-17-447>
- Cirillo, T., Esposito, F., Fasano, E., Scognamiglio, G., Di Marco Pisciotano, I., Mita, G.D. and Gallo, P. 2019. BPA, BPB, BPF, BADGE and BFDGE in canned beers from the Italian market. *Food Addit. Contam. Part B, Surveill.*, 12(4): 268-274. <https://doi.org/10.1080/19393210.2019.1650835>
- Corrales, J., Kristofco, L.A., Baylor Steele, W., Yates, B.S., Breed, C.S., Spencer Williams, E. and Brooks, B.W. 2015. Global Assessment of bisphenol a in the environment: review and analysis of its occurrence and bioaccumulation. *Publ. Int. Home. Soc.*, 13(3): 1. <https://doi.org/10.1177/1559325815598308>
- Dey, A., Dhupal, C.V., Sengupta, P., Kumar, A., Pramanik, N.K. and Alam, T. 2021. Challenges and possible solutions to mitigate the problems of single-use plastics used for packaging food items: a review. *J. Food Sci. Technol.*, 58(9): 3251-3269. <https://doi.org/10.1007/S13197-020-04885-6/METRICS>
- Dey, S., Veerendra, G.T.N., Babu, P.S.S.A., Manoj, A.V.P. and Nagarjuna, K. 2023. Degradation of Plastics Waste and Its Effects on Biological Ecosystems: A Scientific Analysis and Comprehensive Review. *Biomed. Mater. Devices*, 1: 1-43. <https://doi.org/10.1007/S44174-023-00085-W>

- European Union 2014. Legislation. Official Journal of the European Union. <http://eur-lex.europa.eu/legal-content/EN/TXT/PDF/?uri=OJ:L:2014:015:FULL&from=EN>
- Fattore, M., Russo, G., Barbato, F., Grumetto, L. and Albrizio, S. 2015. Monitoring of bisphenols in canned tuna from Italian markets. *Food Chem. Toxicol.*, 83: 68-75. <https://doi.org/10.1016/j.fct.2015.05.010>
- González, N., Cunha, S.C., Ferreira, R., Fernandes, J.O., Marquès, M., Nadal, M. and Domingo, J.L. 2020. Concentrations of nine bisphenol analogs in food purchased from Catalonia (Spain): Comparison of canned and non-canned foodstuffs. *Food Chem. Toxicol.*, 136. <https://doi.org/10.1016/j.fct.2019.110992>
- Gopal, C.M., Bhat, K., Ramaswamy, B.R., Kumar, V., Singhal, R.K., Basu, H., Udayashankar, H.N., Vasantharaju, S.G., Praveenkumarreddy, Y., Shailesh, Lino, Y. and Balakrishna, K. 2021. Seasonal occurrence and risk assessment of pharmaceutical and personal care products in Bengaluru rivers and lakes, India. *J. Environ. Chem. Eng.*, 9(4): 105610. <https://doi.org/10.1016/j.jece.2021.105610>
- Hagobian, T., Delli-Bovi, Z., Mercado, A., Bird, A., Guy, M. and Phelan, S. 2021. Development and feasibility of randomized trial to reduce urinary bisphenols in women with obesity. *Pilot Feasibility Stud.*, 7(1). <https://doi.org/10.1186/S40814-020-00744-5>
- Hahladakis, J.N., Iacovidou, E. and Gerassimidou, S. 2023. An overview of the occurrence, fate, and human risks of the bisphenol-A present in plastic materials, components, and products. *Integr. Environ. Assess. Manag.*, 19(1): 45-62. <https://doi.org/10.1002/IEAM.4611>
- Hardegen, J., Braeutigam, P., Abendroth, C. and Wichard, T. 2021. Bisphenol A: Quantification in Complex Matrices and Removal by Anaerobic Sludges. *Pollutants*, 1(4): 194-206. <https://doi.org/10.3390/pollutants1040016>
- Hu, Y., Zhu, Q., Yan, X., Liao, C. and Jiang, G. 2019. Occurrence, fate and risk assessment of BPA and its substituents in wastewater treatment plant: A review. *Environ. Res.*, 178. <https://doi.org/10.1016/j.envres.2019.108732>
- Huang, Y.Q., Wong, C.K.C., Zheng, J.S., Bouwman, H., Barra, R., Wahlström, B., Neretin, L. and Wong, M.H. 2012. Bisphenol A (BPA) in China: A review of sources, environmental levels, and potential human health impacts. *Environ. Int.*, 42(1): 91-99. <https://doi.org/10.1016/j.envint.2011.04.010>
- Huang, Z., Zhao, J.L., Zhang, C.Y., Rao, W.L., Liang, G.H., Zhang, H., Liu, Y.H., Guan, Y.F., Zhang, H.Y. and Ying, G.G. 2021. Profile and removal of bisphenol analogs in hospital wastewater, landfill leachate, and municipal wastewater in South China. *Sci. Total Environ.*, 790: 148269. <https://doi.org/10.1016/j.scitotenv.2021.148269>
- Im, J. and Löffler, F.E. 2016. The fate of Bisphenol A in terrestrial and aquatic environments. *Environ. Sci. Technol.*, 50(16): 8403-8416. <https://doi.org/10.1021/ACS.EST.6B00877>
- Jain, J., Gupta, N., Mathur, R., Nimesh, S. and Mathur, S.K. 2020. A study on the impact of BPA in adipose tissue dysfunction (adiposopathy) in Asian Indian type 2 diabetes mellitus subjects. *Indian J. Clin. Biochem.*, 35(4): 451-457. <https://doi.org/10.1007/S12291-019-00843-Y>
- Karsauliya, K., Bhatia, M., Sonker, A. and Singh, S.P. 2021. Determination of Bisphenol Analogues in Infant Formula Products from India and Evaluating the Health Risk in Infants Associated with Their Exposure. *J. Agric. Food Chem.* <https://doi.org/10.1021/ACS.JAFC.1C00129>
- Kataria, N., Bhushan, D., Gupta, R., Rajendran, S., Teo, M.Y.M. and Khoo, K.S. 2022. Current progress in treatment technologies for plastic waste (bisphenol A) in the aquatic environment: Occurrence, toxicity and remediation mechanisms. *Environ. Pollut.*, 315: 120319. <https://doi.org/10.1016/j.envpol.2022.120319>
- Kumar, A., Singh, D., Bhandari, R., Malik, A.K., Kaur, S. and Singh, B. 2023. Bisphenol A in canned soft drinks, plastic-bottled water, and household water tank from Punjab, India. *J. Hazard. Mater. Adv.*, 9: 100205. <https://doi.org/10.1016/j.hazadv.2022.100205>
- Kumar, K., Shanmugam, G., Sampath, S., Larsson, D.G.J. and Rajendran, B. 2014. Ecotoxicology and Environmental Safety GC – MS determination of bisphenol A and alkylphenol ethoxylates in river water from India and their ecotoxicological risk assessment. *Ecotoxicol. Environ. Saf.*, 99: 13-20. <https://doi.org/10.1016/j.ecoenv.2013.09.006>
- Lalwani, D., Ruan, Y., Taniyasu, S., Yamazaki, E., Kumar, N.J.I., Lam, P.K.S., Wang, X. and Yamashita, N. 2020. Nationwide distribution and potential risk of bisphenol analogs in Indian waters. *Ecotoxicol. Environ. Saf.*, 200 (November 2019): 110718. <https://doi.org/10.1016/j.ecoenv.2020.110718>
- Liao, C. and Kannan, K. 2013. Concentrations and profiles of bisphenol A and other bisphenol analogs in foodstuffs from the United States and their implications for human exposure. *J. Agric. Food Chem.*, 61(19): 4655-4662. <https://doi.org/10.1021/JF400445N>
- Lo, H.S., Po, B.H.K., Li, L., Wong, A.Y.M., Kong, R.Y.C., Li, L., Tse, W.K.F., Wong, C.K.C., Cheung, S.G. and Lai, K.P. 2021. Bisphenol A and its analogs in sedimentary microplastics of Hong Kong. *Mar. Pollut. Bull.*, 164 (December 2020): 112090. <https://doi.org/10.1016/j.marpolbul.2021.112090>
- Lopes-Rocha, L., Ribeiro-Gonçalves, L., Henriques, B., Özcan, M., Tiritan, M.E. and Souza, J.C.M. 2021. An integrative review on the toxicity of Bisphenol A (BPA) derived from resin composites used in dentistry. *J. Biomed. Mater. Res. Part B Appl. Biomater.*, 109(11): 1942-1952. <https://doi.org/10.1002/JBMB.34843>
- Ma, Y., Liu, H., Wu, J., Yuan, L., Wang, Y., Du, X., Wang, R., Marwa, P.W., Petlulu, P., Chen, X. and Zhang, H. 2019. The adverse health effects of bisphenol A and related toxicity mechanisms. *Environ. Res.*, 176. <https://doi.org/10.1016/j.envres.2019.108575>
- Mahamuni, D. and Shrinithivihahshini, N.D. 2017. Need for regulatory policies in India on the use of bisphenol A in food contact plastic containers. *Curr. Sci.*, 113(5): 861-868. <https://doi.org/10.18520/cs/v113/i05/861-868>
- Ramakrishna, M., Girigoswami, A., Chakraborty, S. and Girigoswami, K. 2021. Bisphenol A; An overview of its effect on health and environment. *Biointerf. Res. Appl. Chem.*, 12(1): 105-119. <https://doi.org/10.33263/briac121.105119>
- Molina-García, L., Fernández-De Córdoba, M.L. and Ruiz-Medina, A. 2012. Analysis of Bisphenol A in milk by using a multicommuted fluorimetric sensor. *Talanta*, 96: 195-201. <https://doi.org/10.1016/j.talanta.2012.02.021>
- Mukhopadhyay, M. and Chakraborty, P. 2021. Plasticizers and bisphenol A: Emerging organic pollutants along the lower stretch of River Ganga, north-east coast of the Bay of Bengal. *Environ. Pollut.*, 276: 116697. <https://doi.org/10.1016/j.envpol.2021.116697>
- Mukhopadhyay, M., Sampath, S., Muñoz-Arnanz, J., Jiménez, B. and Chakraborty, P. 2020. Plasticizers and bisphenol A in Adyar and Cooum riverine sediments, India: occurrences, sources and risk assessment. *Environ. Geochem. Health*, 42(9): 2789-2802. <https://doi.org/10.1007/s10653-020-00516-3>
- Muthusamy, S., Palanisamy, S. and Ramalingam, S. 2021. Exposure of bisphenol A in breast cancer patients-quantitatively assessed by sensitivity-enhanced high-performance liquid chromatography coupled with fluorescence detection: A case-control study. *Biomed. Chromatogr.*, 35(9): e5137. <https://doi.org/10.1002/BMC.5137>
- Nepalia, A., Singh, A., Mathur, N., Kamath, R. and Pareek, S. 2018. Assessment of mutagenicity caused by popular baby foods and baby plastic-ware products: An imperative study using microbial bioassays and migration analysis. *Ecotoxicol. Environ. Saf.*, 162(June): 391-399. <https://doi.org/10.1016/j.ecoenv.2018.07.002>
- Núñez, P., Fernandez, T., García-Arévalo, M., Alonso-Magdalena, P., Nadal, A., Perillan, C. and Arguelles, J. 2018. Effects of bisphenol A treatment during pregnancy on kidney development in mice: a stereological and histopathological study. *J. Dev. Orig. Health Dis.*, 9(2): 208-214. <https://doi.org/10.1017/S2040174417000939>
- Opinion, S., Panel, E., Materials, FC and Aids, P. 2015. Scientific Opinion

- on the risks to public health related to the presence of bisphenol A (BPA) in foodstuffs. *EfSA J.*, 13(1). <https://doi.org/10.2903/j.efsa.2015.3978>
- Osman, M.A., Mahmoud, G.I., Elgammal, M.H. and Hasan, R.S. 2018. Studying bisphenol A levels in some canned food, feed, and baby bottles in Egyptian markets. *Fresenius Environ. Bull.*, 27(12A): 9374-9381. <https://www.researchgate.net/publication/329963676>
- Pettamanna, A., Raghav, D. and Nair, R.H. 2020. Hepatic Toxicity in *Etroplus suratensis* (Bloch 1790): An Economically Important Edible Fish in Vembanad Fresh Water Lake, Kerala, India. *Bull. Environ. Contam. Toxicol.*, 105(4): 565-571. <https://doi.org/10.1007/s00128-020-02987-7>
- Qian, Y., Jia, X., Ding, T., Yang, M., Yang, B. and Li, J. 2021. Occurrence and removal of bisphenol analogs in wastewater treatment plants and activated sludge bioreactor. *Sci. Total Environ.*, 758: 143606. <https://doi.org/10.1016/j.scitotenv.2020.143606>
- Santillana, M.I., Ruiz, E., Nieto, M.T., Bustos, J., Maia, J., Sendón, R. and Sánchez, J.J. 2011. Migration of bisphenol A from polycarbonate baby bottles purchased in the Spanish market by liquid chromatography and fluorescence detection. *Food Addit. Contam. Part A Chem. Anal. Control Expo. Risk Assess.*, 1618-1610. (11)28. <https://doi.org/10.1080/19440049.2011.589036>
- Santoro, A., Chianese, R., Troisi, J., Richards, S., Nori, S.L., Fasano, S., Guida, M., Plunk, E., Viggiano, A., Pierantoni, R. and Meccariello, R. 2019. Neuro-toxic and Reproductive Effects of BPA. *Curr. Neuropharmacol.*, 17(12): 1109-1132. <https://doi.org/10.2174/1570159X17666190726112101>
- Sharma, B.M., Scheringer, M., Chakraborty, P., Bharat, G.K., Steindal, E.H., Trasande, L. and Nizzetto, L. 2023. Unlocking India's potential in managing endocrine-disrupting chemicals (EDCs): importance, challenges, and opportunities. *Exposure and Health*, 15(4): 841-855. <https://doi.org/10.1007/s12403-022-00519-8>
- Sharma, V., Jain, D., Rai, A.R., Kumari, P., Nagar, V., Kaur, A., Singh, A., Verma, R.K., Pandey, H. and Sankhla, M.S. 2023. Toxicological assessment and concentration analysis of Bisphenol A in food grade plastics: A systematic review. *Mater. Today Proc.*, 16: 545. <https://doi.org/10.1016/J.MATPR.2023.06.336>
- Shekhar, S., Sood, S., Showkat, S., Lite, C., Chandrasekhar, A., Vairamani, M., Barathi, S. and Santosh, W. 2017. Detection of phenolic endocrine disrupting chemicals (EDCs) from maternal blood plasma and amniotic fluid in Indian population. *Gen. Comp. Endocrinol.*, 241: 100-107. <https://doi.org/10.1016/j.ygcen.2016.05.025>
- Shelnutt, S., Kind, J. and Allaben, W. 2013. Bisphenol A: Update on newly developed data and how they address NTP's 2008 finding of "Some Concern". *Food Chem. Toxicol.*, 57: 284-295. <https://doi.org/10.1016/j.fct.2013.03.027>
- Shrinithiviahshini, N.D., Mahamuni, D. and Praveen, N. 2014. Bisphenol is a migration study in baby feeding bottles of selected brands available in the Indian market. *Curr. Sci.*, 106(8): 1081-1084. <https://doi.org/10.18520/CS/V106/I8/1081-1084>
- Siddique, M.A.B., Harrison, S.M., Monahan, F.J., Cummins, E. and Brunton, N.P. 2021. Bisphenol a and metabolites in meat and meat products: Occurrence, toxicity, and recent development in analytical methods. *Foods*, 10(4): 714. <https://doi.org/10.3390/foods10040714>
- Tarafdar, A., Sirohi, R., Balakumaran, P.A., Reshmy, R., Madhavan, A., Sindhu, R., Binod, P., Kumar, Y., Kumar, D. and Sim, SJ 2022. The hazardous threat of Bisphenol A: Toxicity, detection and remediation. *J. Hazard. Mater.*, 423: 127097. <https://doi.org/10.1016/J.JHAZMAT.2021.127097>
- Tiwari, M., Sahu, S.K. and Pandit, G.G. 2016. Distribution and estrogenic potential of endocrine disrupting chemicals (EDCs) in estuarine sediments from Mumbai, India. *Environ. Sci. Pollut. Res.*, 23(18): 18789-18799. <https://doi.org/10.1007/S11356-016-7070-X>
- Tsang, H. 2011. Sgs Consumer Testing Services Safeguards Malaysia Bans Bisphenol-A (Bpa) In Polycarbonate Baby Bottles.
- Tzatzarakis, M.N., Karzi, V., Vakonaki, E., Goumenou, M., Kavvalakis, M., Stivaktakis, P., Tsitsimpikou, C., Tsakiris, I., Rizos, A.K. and Tsatsakis, A.M. 2017. Bisphenol A in soft drinks and canned foods and data evaluation. *Food Addit. Contam. Part B Surveill.*, 10(2): 85-90. <https://doi.org/10.1080/19393210.2016.1266522>
- US FDA. 2014. No Bisphenol A (BPA): Use in Food Contact Application. <https://www.fda.gov/food/food-additives-petitions/bisphenol-bpa-use-food-contact-application%0Ahttp://www.fda.gov/newsevents/publichealthfocus/ucm064437>
- Vasiljevic, T. and Harner, T. 2021. Bisphenol A and its analogs in outdoor and indoor air: Properties, sources and global levels. *Sci. Total Environ.*, 789: 148013. <https://doi.org/10.1016/J.SCITOTENV.2021.148013>
- Wojnowska-Baryła, I., Bernat, K. and Zaborowska, M. 2022. Plastic Waste Degradation in Landfill Conditions: The Problem with Microplastics, and Their Direct and Indirect Environmental Effects. *Int. J. Environ. Res. Public Health*, 19(20). <https://doi.org/10.3390/ijerph192013223>
- World Health Organization. 2009. BISPHENOL A (BPA) - Current state of knowledge and future actions by WHO and FAO. Food and Agriculture Organization of the United Nations, International Food Safety Authorities Network, 5: 1-6. http://www.who.int/foodsafety/publications/fs_management/No_05_Bisphenol_A_Nov09_en.pdf?ua=1
- Xu, Y., Hu, A., Li, Y., He, Y., Xu, J. and Lu, Z. 2021. Determination and occurrence of bisphenol A and thirteen structural analogs in soil. *Chemosphere*, 277: 130232. <https://doi.org/10.1016/j.chemosphere.2021.130232>
- Yamazaki, E., Yamashita, N., Taniyasu, S., Lam, J., Lam, P.K.S., Moon, H.B., Jeong, Y., Kannan, P., Achyuthan, H., Munuswamy, N. and Kannan, K. 2015. Bisphenol A and other bisphenol analogs, including BPS and BPF in surface water samples from Japan, China, Korea and India. *Ecotoxicol. Environ. Saf.*, 122: 565-572. <https://doi.org/10.1016/j.ecoenv.2015.09.029>



Towards a Greener Tomorrow: Exploring the Potential of AI, Blockchain, and IoT in Sustainable Development

Megha Chauhan[†] and Deepali Rani Sahoo

Symbiosis Law School, NOIDA-Symbiosis International (Deemed University), Pune, India

[†]Corresponding author: Megha Chauhan: megha@symlaw.edu.in

Nat. Env. & Poll. Tech.
Website: www.neptjournal.com

Received: 05-10-2023

Revised: 08-12-2023

Accepted: 22-12-2023

Key Words:

Artificial Intelligence
Sustainable development
Blockchain
Internet of things (IoT)
Futuristic approach

ABSTRACT

This article examines the potential for artificial intelligence (AI), blockchain, and the Internet of Things (IoT) to advance sustainability. Through a literature review and critical analysis, the study evaluates the possible advantages, difficulties, and opportunities of utilizing these technologies to support a sustainable future. The research study emphasizes how effective AI is at streamlining resource management, increasing system efficiency, and optimizing energy use. It focuses on the potential of blockchain to improve supply chain accountability and transparency, and it also discusses the game-changing potential of IoT to improve resource management. However, some issues must be resolved, including excessive costs, technological difficulties, data privacy concerns, and social repercussions. The essay advocates creating multidisciplinary research programs, funding R&D, and supporting collaborative relationships. It also suggests creating sustainable implementation plans, prioritizing ethical issues and data governance, and encouraging information exchange and awareness. By accepting these proposals, stakeholders may leverage the promise of green technology and innovation to build a sustainable future. It is also clear that the Internet of Things (IoT) can potentially optimize resource management. Real-time data on a variety of topics, including traffic conditions, air and water quality, and water management, can be provided through IoT-enabled sensors. Cities may reduce traffic, increase energy efficiency, enhance environmental conditions, and encourage sustainable water management techniques by utilizing this data to inform their decisions. However, serious consideration must be given to data privacy, security, scalability, and interoperability issues to ensure IoT solutions' ethical and efficient adoption. Despite their enormous potential, the paper acknowledges the difficulties and constraints in implementing these technologies. Significant obstacles include high implementation costs, complex technical requirements, and the requirement for adequate data privacy and security safeguards. A sustainable and inclusive future also requires resolving ethical issues, including algorithmic prejudice, social fairness, and equitable access to technology. The report recommends encouraging cooperative relationships between academia, business, government, and communities to address these issues. Research and development investments are required to evaluate these technologies' practical use, scalability, and economic viability. In addition, multidisciplinary research initiatives can comprehensively comprehend green technology and innovation's social, economic, and environmental effects. It has been concluded that there is great potential for future technologies, such as AI, blockchain, and IoT, to advance sustainability. Stakeholders can use these technologies' revolutionary potential to build a sustainable future by resolving obstacles, promoting collaboration, and doing additional research. To ensure the ethical and successful application of green technology and innovation for the benefit of the environment and future generations, it is essential to prioritize ethical considerations, establish sustainable implementation strategies, and foster information exchange and awareness.

INTRODUCTION

It took approximately 200,000 years for humankind's intelligence to evolve from natural to artificial, and 10 years to cut the ties with 'earth' to move to the 'cloud' (Garimella & Fingar 2018). The need for sustainable development has become increasingly evident in the face of pressing

environmental challenges. Green technology and innovation have emerged as powerful tools for pursuing a sustainable future. This essay examines the potential of emerging technologies such as artificial intelligence (AI), blockchain, and the Internet of Things (IoT) to contribute to a greener and more sustainable world. We can address critical issues like resource conservation, energy efficiency, waste reduction, and

environmental monitoring by harnessing their capabilities. As it emerges, many industries are shaped by artificial intelligence (AI). For instance, AI is anticipated to impact productivity worldwide (Acemoglu & Restrepo 2018).

According to the Dartmouth Research Project, AI is the issue of “making a machine behave in ways that would be termed intelligent if a human being behaved like this” (McCarthy et al. 1955). AI has altered how information is produced and used for decision-making in general (Mikalef et al. 2017). In several industries that provide more competitive and sustainable goods and services (Govindan et al. 2019, Kuo & Smith 2018, Ding et al. 2019, Garbuio & Lin 2019), AI has transformed business practices (Schneider & Leyer 2019). According to Schneider & Leyer (2019), the interaction between artificial intelligence and human intelligence is based on algorithms that should aid managers in making the best decisions. This leads to a cultural shift in which a significant amount of data, connections, and interactions are incorporated into the regular management of organizations.

ARTIFICIAL INTELLIGENCE (AI) FOR SUSTAINABILITY

Artificial intelligence, with its ability to analyze vast amounts of data and derive meaningful insights, has immense potential to advance sustainability. With various interconnected technologies, such as electric driverless vehicles and smart appliances that can enable demand response in the electricity sector, AI can enable smart and low-carbon cities (International Energy Agency 2017). AI-powered algorithms can optimize energy consumption, enhance resource management, and improve the efficiency of various systems. For instance, AI can enable precision farming techniques in agriculture, minimizing water usage and reducing the need for chemical inputs. Through real-time monitoring and analysis, AI can detect crop diseases, optimize irrigation schedules, and maximize crop yields. These precision farming practices conserve resources and promote sustainable agricultural practices (Idoje et al. 2021). Vinuesa et al. (2020) discovered that AI could facilitate the attainment of 134 targets across all the goals using a consensus-based expert elicitation procedure. However, it can also prevent the achievement of 59 targets.

To get into the depth of the applicability of AI in Sustainable development, varied articles were reviewed. Margaret et al. (2020) discuss the potential of AI techniques, including machine learning and data analytics, in reducing greenhouse gas emissions. It explores various applications, such as energy optimization, transportation management, and intelligent grid systems. Furthermore, it provides insights

into environmental sustainability and AI applications. The author also discusses the potential of AI techniques, including machine learning and data analytics, in reducing greenhouse gas emissions. It explores various applications, such as energy optimization, transportation management, and intelligent grid systems, and concludes that AI has immense potential yet to be unearthed. It has also been observed that by enabling smart grids that partially match energy demand to periods when the sun is shining and the wind is blowing, AI can also aid in integrating variable renewables (International Energy Agency 2017).

Summa et al. (2022) provide an overview of the application of AI techniques in sustainable energy. It examines AI-based solutions for energy optimization, demand response, energy forecasting, and renewable energy integration, discussing their benefits and challenges. Also, Pahwa et al. (2022) examine the potential of AI in addressing environmental challenges. It explores applications of AI in areas such as climate modeling, biodiversity conservation, environmental monitoring, and pollution control. Jan et al. (2022) examine the application of AI in promoting sustainability in supply chain management. It discusses AI applications in demand forecasting, inventory optimization, logistics planning, and reverse logistics.

Moreover, AI can revolutionize energy systems. AI algorithms can balance electricity supply and demand through intelligent grid management, optimize energy distribution and integrate renewable energy sources seamlessly. By analyzing energy consumption patterns, AI can provide insights into optimizing energy usage in buildings, reducing energy wastage and cost savings (Yassine et al. 2021). Furthermore, AI-powered predictive maintenance systems can detect equipment faults in energy infrastructure, enabling timely repairs and minimizing downtime. By facilitating the integration of renewable energy sources, optimizing energy consumption, and ensuring efficient operations, AI plays a crucial role in transitioning to a sustainable and low-carbon energy future. Despite being connected, the Internet of Things (IoT) and Big Data are not the same as artificial intelligence (AI). IoT enables the collection of external data that can be used as an AI input, whereas Big Data encompasses all data that has been collected (Kaplan 2012, Kaplan & Haenlein 2016). Some towns and nations will benefit intellectually and financially from the development of AI, while others will fall behind. The technology's rapid growth has already outpaced the creation and implementation of legal and regulatory frameworks and the mechanisms intended to regulate AI (Munoz & Naqvi 2018, Goralski & Tan 2020). However, present research priorities ignore crucial elements. Regulatory monitoring and knowledge

are required to support AI's rapid progress and promote sustainable development (Margaret et al. 2020). Failure to do so might lead to lapses in ethics, safety, and openness.

BLOCKCHAIN TECHNOLOGY FOR TRANSPARENT AND SUSTAINABLE SYSTEMS

A blockchain system uses encryption to produce, manage, store, and exchange data without a centralized server. By dispersing information storage, blockchain technology increases information transparency and deters information manipulation, challenging modifying previously recorded information (Shin et al. 2020). Blockchains are distributed data structures or ledgers that allow for the secure storage of digital transactions without a central authority. Furthermore, blockchains enable peer-to-peer (P2P) networks to execute intelligent contracts (Swan 2015) automatically. Blockchain, a decentralized and transparent ledger system, has transformative potential across diverse sectors, including supply chains, energy, and waste management (Kouhizadeh & Sarkis 2015). By providing secure and immutable records, blockchain technology enhances transparency, accountability, and traceability, fostering sustainability. In supply chain management, blockchain enables the tracking of products from origin to consumption, ensuring ethical sourcing and reducing environmental footprints (Ehsan et al. 2022). For example, in the food industry, blockchain can provide detailed information about products' origin, production methods, and transportation. This transparency empowers consumers to make informed choices and supports sustainable and ethical practices. Additionally, blockchain can streamline waste management processes by tracking waste streams, ensuring proper disposal, recycling, and reducing illegal dumping (Lin et al. 2021).

In the energy sector, blockchain can facilitate peer-to-peer energy trading, allowing individuals and communities to exchange renewable energy surplus, reducing dependence on traditional centralized grids (Sahebi et al. 2023). Blockchain-based energy platforms can incentivize the adoption of clean energy sources, empowering individuals to participate actively in the renewable energy transition. Moreover, blockchain technology can create energy marketplaces where prosumers can sell excess energy to consumers, fostering a decentralized and resilient energy system (Ying et al. 2022).

INTERNET OF THINGS (IOT) FOR EFFICIENT RESOURCE MANAGEMENT

The Internet of Things (IoT) refers to the network of interconnected devices and sensors that collect and share data (Abbasy & Quesada 2017). Integrating IoT applications can optimize resource management, reduce waste, and enhance

efficiency across various sectors. In smart cities, IoT-enabled systems can optimize transportation networks, monitor air quality, and regulate building energy consumption (Belli et al. 2020). It has also been found that real-time data from IoT sensors can guide urban planning, reducing congestion, lowering emissions, and enhancing residents' quality of life (Harmon et al. 2015). In addition, intelligent traffic management systems can dynamically adjust traffic signals based on real-time traffic conditions, reducing traffic congestion and minimizing fuel consumption (Hossan & Nower 2020).

IoT-based water management systems can detect leaks, monitor water quality, and enable precise agricultural irrigation. By conserving water resources, IoT technologies contribute to sustainable water management and mitigate the impacts of water scarcity (Maroli 2021). Farmers can use IoT sensors to monitor soil moisture levels, weather conditions, and crop health, enabling them to optimize irrigation schedules and minimize water waste (Sinha & Dhanalakshmi 2022).

Green technology and innovation, driven by emerging technologies like AI, blockchain, and IoT, offer immense opportunities to shape a sustainable future. We can address pressing environmental challenges, foster resource efficiency, and promote responsible consumption and production by harnessing their capabilities. Combining AI, blockchain, and IoT creates synergies that enable efficient and sustainable systems in various domains such as energy, agriculture, supply chain management, and waste reduction. However, ensuring these technologies are developed and implemented ethically is crucial, considering privacy, security, and equitable access. Governments, businesses, and individuals must collaborate to unlock the full potential of green technology, foster innovation, and build a sustainable future for generations to come.

To sum up, the following could be the primary objectives related to green technology and innovation in advancing sustainability:

- **Promote Energy Efficiency:** Develop and implement green technologies and innovative solutions to optimize energy consumption, reduce waste, and increase the efficiency of energy systems across various sectors.
- **Foster Sustainable Resource Management:** Utilize emerging technologies such as AI, blockchain, and IoT to enhance resource management practices, including water conservation, waste reduction, sustainable agriculture, and responsible consumption and production.
- **Enhance Environmental Monitoring and Protection:** Leverage technological advancements to monitor and protect the environment, including

- **Enhance Monitoring and Protection:** Leverage technological advancement to monitor and protect the environment, including real-time monitoring of air and water quality, biodiversity conservation, an early warning system for Natural disasters, and sustainable land and ecosystem management.
- **Enable Smart and Sustainable Cities:** Utilize IoT, AI, and blockchain technologies to develop innovative city solutions that enhance urban sustainability, including efficient transportation systems, intelligent grid management, waste management, sustainable infrastructure, and citizen engagement.
- **Support Sustainable Supply Chains:** Implement innovative technologies, such as blockchain, to promote transparency, traceability, and ethical practices in supply chains, including sustainable sourcing, fair trade, responsible manufacturing, and efficient logistics.
- **Empower Renewable Energy Transition:** Accelerate the adoption of renewable energy sources through innovative technologies, AI-driven energy optimization, blockchain-enabled peer-to-peer energy trading, and grid management solutions to achieve a low-carbon and resilient energy future.
- **Promote Environmental Education and Awareness:** Integrate green technology and innovation into educational programs to raise awareness, foster environmental literacy, and equip individuals with the knowledge and skills to contribute to a sustainable future.
- **Foster Collaboration and Partnerships:** Encourage collaboration between governments, businesses, academia, and civil society to foster research and development, share best practices, and drive innovation in green technology and sustainability.
- **Ensure Ethical and Inclusive Technological Development:** Address ethical considerations and data privacy concerns and ensure equitable access to green technologies and innovations, fostering a just and inclusive transition to a sustainable future.
- **Contribute to Global Sustainable Development Goals:** Align green technology and innovation efforts with the United Nations Sustainable Development Goals (SDGs) to address pressing global challenges, including climate action, clean energy, responsible consumption and production, and sustainable cities and communities.

OBJECTIVES OF THE STUDY

These broad objectives provide a framework for advancing

sustainable development through green technology and innovation. They encompass various focus areas, including energy efficiency, resource management, environmental monitoring, sustainable cities, supply chains, renewable energy, education, collaboration, and SDG alignment.

- **Analyze the Potential of Developing Technologies:** Examine how developing technologies like artificial intelligence (AI), blockchain, and the Internet of Things (IoT) could advance sustainability in various industries and fields.
- **Evaluate the Environmental Impact:** Conduct thorough evaluations of the environmental impact of green innovations and technologies to comprehend their potential advantages and disadvantages, including their contributions to lowering greenhouse gas emissions, conserving resources, cutting waste, and protecting ecosystems. **Develop and Improve Sustainable Solutions:** Design, develop, and improve sustainable solutions and systems by integrating green technologies and innovations to address specific challenges, such as energy efficiency, waste management, water conservation, and sustainable agriculture.
- **Investigate Novel Methods for Environmental Monitoring and Management:** Investigate cutting-edge methods for real-time environmental monitoring, early environmental risk detection, effective management of natural resources, and efficient conservation of ecosystems and biodiversity using AI, remote sensing, IoT, and other technologies.
- **Assess Barriers and Challenges:** Identify and analyze technological, regulatory, economic, and social barriers, challenges, and restrictions to the adoption and implementation of green technologies and innovations to create plans for getting around them.
- **Contribute to Policy Development and Decision-Making:** Produce research findings and insights that can support evidence-based policy development, as well as regulations, standards, and frameworks that encourage the adoption and diffusion of green technologies and innovations.

ANALYSIS

The existing literature indicates AI's enormous potential in fostering sustainability across several sectors. Studies have shown that AI-powered algorithms may optimize resource management, increase system efficiency, and reduce energy consumption. For instance, AI-enabled precision farming methods can maximize agricultural yields while minimizing chemical inputs and water use. AI can offer farmers valuable

insights by evaluating data from sensors and satellites, empowering them to decide on irrigation, fertilization, and pest management knowledgeably. This strategy improves agricultural yield while minimizing adverse environmental effects.

Furthermore, sophisticated grid management made possible by AI can transform energy systems. Artificial intelligence (AI) algorithms can efficiently distribute energy, balance supply and demand, and integrate renewable energy sources. Through real-time monitoring and analysis, AI can support demand response systems by altering energy usage by availability and cost. Additionally, AI can enable proactive maintenance of energy infrastructure, reducing outages and enhancing the grid's overall effectiveness and dependability.

The analysis also highlights how blockchain technology has the potential to advance sustainability. Different domains benefit from blockchain's transparency, immutability, and decentralized structure. Blockchain can improve traceability and accountability in supply chain management, ensuring moral sourcing, just commerce, and smaller environmental footprints. Blockchain-based solutions make it possible to validate supply chain transactions, product certifications, and origins, increasing consumer trust and transparency. For instance, in the fashion sector, blockchain may follow a garment's journey from its initial ingredients to its finished product, assuring ethical sourcing, respect for workers' rights, and support for programs for sustainable fashion.

Moreover, the review highlights the transformative capabilities of the Internet of Things (IoT) in optimizing resource management. IoT-enabled systems can enhance transportation networks by providing real-time data on traffic conditions, enabling efficient routing, reducing congestion, and minimizing fuel consumption. In smart cities, IoT sensors can monitor air and water quality, enabling timely interventions to improve environmental conditions. IoT-based water management systems can detect leaks, monitor water quality, and enable precise agricultural irrigation, conserving water resources and promoting sustainable water management practices.

THE POTENTIAL OF EMERGING TECHNOLOGIES

The literature review convincingly demonstrates the significant potential of emerging technologies in promoting sustainability across various sectors. The evidence presented regarding AI applications in optimizing energy consumption, enhancing resource management, and improving system efficiency is compelling. Precision farming techniques powered by AI algorithms have demonstrated substantial water savings and increased crop yields. However, it is

essential to critically examine the scalability, economic viability, and potential unintended consequences of implementing AI on a larger scale. Further empirical evidence and long-term studies are necessary to understand the broader environmental impacts, economic feasibility, and social acceptance of AI applications in different contexts.

Similarly, the existing literature supports the potential of blockchain technology in promoting sustainability through enhanced supply chain transparency and accountability. Blockchain offers a decentralized and immutable ledger that can revolutionize industries such as fashion, ensuring responsible sourcing and fair-trade practices. However, it is crucial to critically evaluate blockchain's scalability, energy consumption, and consensus mechanisms. Further research is necessary to develop sustainable and efficient blockchain solutions that address these limitations while still providing the desired transparency and traceability benefits.

The transformative capabilities of IoT in optimizing resource management, particularly in smart cities and water management systems, are well-documented. IoT-enabled sensors can provide real-time data for improved decision-making, reducing congestion, enhancing energy efficiency, and better water conservation. However, critical examination is needed regarding data privacy and security concerns associated with the large-scale deployment of IoT devices. Additionally, the scalability and interoperability of IoT solutions remain key challenges that require further investigation and innovative approaches to ensure seamless integration and data exchange across different systems and platforms.

Challenges and Limitations

Although the potential advantages of green technology and innovation are substantial, the literature analysis also reveals several difficulties and constraints that must be overcome for practical application. The existing literature effectively points out several difficulties and restrictions related to using green technology and innovation. Widespread adoption of emerging technologies is frequently hampered by their expensive deployment and maintenance costs, especially in regions with limited resources and small and medium-sized businesses (SMEs). Despite the significant potential benefits of these technologies, it is vital to consider their economic viability and cost. These financial obstacles can be overcome, and technological spread can be facilitated by investigating cost-effective implementation solutions, encouraging investment through supportive legislation, and encouraging knowledge sharing and collaboration.

Significant hurdles that must be critically explored include technical complexity and interoperability problems.

Compatibility and standardization are necessary for integrating new technologies into existing systems, but disparate technological architectures, exclusive protocols, and disjointed data ecosystems might hamper these processes. Establishing interoperable frameworks and encouraging open data interchange requires coordinated efforts by industry players, legislators, and standardization bodies to overcome these obstacles. To guarantee seamless integration and leverage the advantages of these technologies, critical analysis and research on interoperability standards, open APIs, and data integration strategies are crucial.

The literature strongly emphasizes the necessity of addressing data privacy and security issues, which are essential for upholding trust in applications of green technology. Privacy protection and cyber threat defense are crucial since AI, blockchain, and IoT depend on massive data. Despite the enormous potential advantages of data-driven applications, it is necessary to consider the moral ramifications and possible dangers of data collecting, storage, and use. Building public confidence and ensuring the responsible use of these technologies requires striking a balance between data collecting for sustainability goals and individual privacy rights and the implementation of strong data protection measures.

- One common challenge is the high costs associated with implementing emerging technologies. The initial investment required for AI systems, blockchain infrastructure, and IoT networks can be substantial. Additionally, ongoing maintenance and updates may require dedicated resources and expertise. Exploring cost-effective implementation strategies and developing scalable solutions that offer a favorable return on investment is crucial to address this challenge.
- Technical complexities and interoperability issues pose additional challenges. Integrating these technologies into existing systems and infrastructures can be complex, requiring compatibility and standardization. Ensuring seamless data exchange and communication between platforms and devices is crucial for effective implementation. Collaborative efforts between technology providers, industry stakeholders, and policymakers are essential to overcome these challenges and establish interoperable frameworks.
- Data privacy and security concerns are significant considerations in green technology and innovation. As AI, blockchain, and IoT involve collecting and analyzing vast amounts of data, safeguarding privacy and protecting against cyber threats become paramount. Developing robust data governance frameworks and implementing strong security measures are essential

to build trust and confidence in these technologies. Additionally, addressing ethical considerations, such as data ownership, consent, and algorithmic biases, is critical to ensure fairness and social equity in applying these technologies.

- Furthermore, green technology and innovation's social and ethical implications should be carefully considered. Ensuring equitable access to these technologies and addressing potential job displacements require proactive measures. It is crucial to ensure that the benefits of green technology are inclusive and do not exacerbate existing inequalities. This may involve providing training and education programs to develop the skills needed for the green economy and considering the social impacts of technology implementation.

CONCLUSIONS AND SUGGESTIONS

The literature review analysis on green innovation and technology reveals the enormous potential of cutting-edge innovations like blockchain, AI, and IoT for furthering sustainability. These technologies present possibilities for improving energy efficiency, supply chain transparency, resource management, and developing innovative, sustainable cities. Cost, technical complexity, data privacy, and societal repercussions are all issues that must be taken into consideration. Future studies must concentrate on social and economic implications, interdisciplinary collaboration, and devising ways to guarantee fair access to and adoption of green technology, in addition to their practical implementation. To reach a sustainable future, we may fully utilize the transformative force of green technology and innovation by solving these issues.

The possibilities and difficulties of new technologies are highlighted by critically analyzing current green technology and innovation. While IoT, blockchain, and AI have great potential to advance sustainability, careful consideration is required to overcome their drawbacks, ensure their ethical and inclusive adoption, and establish long-term viability. Future research should prioritize empirical investigations, interdisciplinary cooperation, and thorough sustainability analyses to advance the discipline. We may aim for more effective and responsible green technology and innovation applications to achieve a sustainable future by critically analyzing current knowledge and filling research gaps. The current body of research shows that AI can potentially optimize resource management and energy usage. However, more study is required to determine its scalability, economic sustainability, and any unforeseen consequences that might arise. Like how blockchain technology can potentially improve supply chain transparency, serious consideration

must be given to scalability and energy use issues. Although IoT may optimize resource management, substantial obstacles must be considered, including data privacy, security, scalability, and interoperability.

In conclusion, the advancement of sustainability is greatly enhanced by green technology and innovation. To address the issues and constraints, guarantee moral execution, and enable evidence-based decision-making, a critical approach is required. We can fully utilize green technology and innovation to build a sustainable future by critically analyzing the current research, controlling research gaps, and encouraging multidisciplinary collaboration. Here are a few ideas that might be put into practice to improve the coordination of the use of AI, Blockchain, and IoT:

- **Foster Collaborative Partnerships:** Collaboration between academia, industry, policymakers, and communities is crucial for successfully implementing green technology and innovation. Encouraging cross-sector partnerships can promote knowledge exchange, facilitate technology diffusion, and address common challenges collectively. Governments and organizations should actively support collaborative initiatives that unite diverse stakeholders to drive innovation and promote sustainable practices.
- **Invest in Research and Development:** Further investment in research and development is needed to address the gaps and limitations identified in the literature review. Governments, funding agencies, and private entities should allocate resources for empirical studies, field trials, and long-term evaluations to assess green technologies' real-world impact, scalability, and economic feasibility. This research should also focus on social and economic implications, including job creation, social equity, and economic viability, to ensure these technologies' inclusive and responsible implementation.
- **Establish Interdisciplinary Research Programs:** Green technology and innovation require interdisciplinary collaboration to tackle complex sustainability challenges. Establishing research programs that bring together experts from various fields, such as engineering, environmental science, social sciences, and economics, can foster a holistic approach to addressing sustainability's social, economic, and environmental dimensions. Encouraging interdisciplinary collaboration can lead to innovative solutions, comprehensive assessments, and a more nuanced understanding of green technologies' potential benefits and limitations.
- **Develop Sustainable and Scalable Implementation Strategies:** Addressing green technology

implementation's high costs and technical complexities is crucial for widespread adoption. Governments, industry leaders, and policymakers should work together to develop sustainable and scalable implementation strategies. This can involve creating incentives for businesses to invest in green technologies, promoting knowledge-sharing and capacity-building programs, and fostering partnerships with technology providers to develop cost-effective solutions. Collaborative efforts should also focus on standardizing protocols, interoperability, and data exchange mechanisms to overcome technical challenges and facilitate the seamless integration of green technologies.

- **Prioritize Ethical Considerations and Data Governance:** Ethical considerations, including data privacy, security, and algorithmic bias, should be at the forefront of green technology and innovation. Governments and organizations should establish robust data governance frameworks that protect individuals' privacy rights while ensuring responsible and transparent use of data. Conducting independent audits, implementing strong cybersecurity measures, and promoting transparency in algorithmic decision-making processes can build trust and address potential ethical concerns. Additionally, attention should be given to ensuring equitable access to green technologies and addressing potential job displacements through targeted policies and skill development programs.
- **Promote Knowledge Sharing and Awareness:** Educating the public, businesses, and policymakers about green technology and innovation's potential benefits and challenges is crucial for their successful adoption. Governments and organizations should invest in awareness campaigns, knowledge-sharing platforms, and capacity-building programs to promote understanding and engagement. Sharing success stories, best practices, and lessons learned can inspire and empower stakeholders to embrace green technologies and drive sustainability initiatives in their respective domains.

By implementing these suggestions, we can create an environment that fosters innovation, addresses challenges, and promotes the responsible and widespread adoption of green technology and innovation. We can work towards a sustainable future driven by transformative technologies with collaborative efforts, interdisciplinary research, and a focus on ethical considerations.

RESEARCH GAPS AND FUTURE DIRECTIONS

There are several research gaps and areas for future green

technology and innovation exploration at this nuance stage. One critical research gap is the need for more empirical studies and case analyses that assess the real-world impact of green technologies and innovations. While ample theoretical knowledge is available, more practical evidence is needed to understand these technologies' effectiveness, scalability, and limitations in different contexts. Conducting field trials, pilot projects, and longitudinal studies can provide valuable insights into their real-world applicability, long-term sustainability, and potential barriers to adoption.

The analysis of the literature review uncovers significant research gaps and areas for future exploration in the field of green technology and innovation. While existing studies provide valuable insights, more empirical research is needed to assess these technologies' real-world impact and scalability. Field trials, pilot projects, and longitudinal studies can help bridge the gap between theory and practice, offering insights into green technology solutions' economic viability, social acceptance, and environmental effectiveness. Critically analyzing the outcomes of such initiatives, examining barriers to implementation, and identifying success factors can guide future efforts and inform evidence-based decision-making.

Additionally, there is a need for interdisciplinary research that examines the social and economic implications of green technology adoption. Understanding the effects on employment, job creation, social equity, and economic viability is crucial for designing inclusive and just transition strategies. Exploring the potential unintended consequences and social acceptance barriers among different stakeholders will inform the development of policies and procedures that foster widespread adoption and mitigate any negative impacts. Critically evaluating green technology and innovation's social and economic dimensions is essential for ensuring long-term sustainability and positive societal outcomes.

Another area for future exploration lies in critically assessing the environmental claims associated with green technology and innovation. While these technologies offer potential benefits, it is essential to critically evaluate their entire life cycle, including the ecological footprint of their production, use, and disposal. Conducting comprehensive life cycle assessments, considering the embodied energy and materials, and evaluating the potential trade-offs associated with different sustainability metrics will enable a more nuanced understanding of their overall sustainability contribution. Critically examining these technologies' environmental impacts, economic viability, and social implications will inform more informed decision-making and sustainable practices. Further research is needed

to understand green technologies' social and economic implications. Investigating their effects on employment, job creation, social equity, and economic viability is crucial to ensure that the benefits of these technologies are inclusive and equitable. Understanding the dynamics of the green job market and identifying strategies to mitigate potential job losses or skill gaps can facilitate a just transition to a sustainable future. Additionally, studying the social acceptance and adoption barriers among stakeholders, including consumers, businesses, and policymakers, can help develop strategies to facilitate widespread implementation.

Interdisciplinary collaboration is another area that requires attention. Green technology and innovation are inherently multidisciplinary, requiring collaboration between academia, industry, policymakers, and communities. Future research should foster cross-sector partnerships, knowledge exchange, and collaborative problem-solving to drive innovation, address challenges collectively, and develop holistic solutions that integrate technological, social, and economic dimensions.

REFERENCES

- Abbasy, M.B. and Quesada, E.V. 2017. Predictable influence of IoT (Internet of Things) in higher education. *Int. J. Edu. Technol.*, 7(12): 914-920.
- Acemoglu, D. and Restrepo, P. 2018. Artificial Intelligence, Automation, and Work. NBER Working Paper No. 24196, National Bureau of Economic Research, Cambridge, MA.
- Belli, L., Cilfone, A., Davoli, L., Ferrari, G., Adorni, P., Di Nocera, F. and Bertolotti, E. 2020. IoT-enabled smart, sustainable cities: Challenges and approaches. *Smart Cities*, 3(3), 1039-1071.
- Ding, Y., Zhang, M. and Duygun, R. 2019. Modeling price volatility based on a genetic programming approach. *Brit. J. Manag.*, 30(2): -328 10.1111/1467-8551.12359 ,340
- Ehsan, I., Muhammad, I.K., Laura, R., Jawaid, I., Amerah, A., Syed, S., Ullah, T. and Alfakih, M. 2022. A conceptual model for blockchain-based agriculture food supply chain system. *Sci. Program.*, 735: 854-860 <https://doi.org/10.1155/2022/7358354>
- Garbuio, N. and Lin, M. 2019. Artificial intelligence as a growth engine for health care startups: Emerging business models. *Calif. Manag. Rev.*, 10.1177/0008125618811931 ,83-59 :(2)61
- Garimella, K. and Fingar, P. 2018. *AI & Blockchain*. Meghan-Kiffer Press, Tampa, FL.
- Govindan, K., Jafarian, A. and Nourbakhsh, V. 2019. Designing a sustainable supply chain network integrated with vehicle routing: A comparison of hybrid swarm intelligence metaheuristics *Comp. Op. Res.*, 10.1016 .235-220 :110/j.cor.2018.11.013
- Harmon, R.R., Castro-Leon, E.G. and Bhide, S. 2015. Smart cities and the Internet of Things. *Manag. Eng. Technol.*, 15: 485-494.
- Hossan, S. and Nower, N. 2020. Fog-based dynamic traffic light control system for improving public transport. *Pub. Transp.*, 12: 431-454.
- Idoje, G., Tasos, D. and Muddesar, I. 2021. Survey for smart farming technologies: Challenges and issues, *Comp. elctr. Eng.*, 92: 107104. <https://doi.org/10.1016/j.compeleceng.2021.107104>.
- International Energy Agency (IEA) 2017. *Digitalization & Energy*. IEA, Paris <https://www.iea.org/reports/digitalisation-and-energy>
- Jan, Z., Ahamed, F., Mayer, W., Patel, N., Grossmann, G., Stumptner, M. and Kuusk, A. 2022. Artificial intelligence for industry 4.0: Systematic

- review of applications, challenges, and opportunities. *Exp. Syst. Appl.*, 54: 119456.
- Kaplan, A.M. 2012. If you love something, let it go mobile: Mobile marketing and mobile social media 4x4 *Bus. Horizons*, 55(2): -129 10.1016/j.bushor.2011.10.009
- Kaplan, A.M. and Haenlein, M. 2016. Higher education and the digital revolution: About MOOCs, SPOCs, social media, and the Cookie Monster *Bus. Horizons*, 59(4): 10.1016/j.bushor.2016.03.008
- Kouhizadeh, M. and Sarkis, J. 2018. Blockchain practices, potentials, and perspectives in greening supply chains. *Sustainability*, 10(10): 3652. <https://doi.org/10.3390/su10103652>
- Kuo, T.C. and Smith, S. 2018. A systematic review of technologies involving eco-innovation for enterprises moving towards sustainability. *J. Clean. Prod.*, 192: 207-220, 10.1016/j.jclepro.2018.04.212
- Lin X., Chang, S.C., Chou, T.H. and Chen, S.C. 2021. Consumers' intention to adopt blockchain food traceability technology towards organic food products. *Int. J. Environ. Res. Public Health*, 18(3): 912. <https://doi.org/10.3390/ijerph18030912>
- Margaret, A., Goralski, T. and Keong, Tan. 2020. Artificial intelligence and sustainable development, *The International Journal of Management Education*, 18(1): 100330, <https://doi.org/10.1016/j.ijme.2019.100330>.
- Maroli, A.A., Narwane, V.S., Raut, R.D. and Narkhede, B.E. 2021. Framework for the implementation of an Internet of Things (IoT)-based water distribution and management system. *Clean Technologies and Environmental Policy*, 23: 271-283.
- McCarthy, J., Minsky, M. L., Rochester, N. and Shannon, C.E. 2006. A proposal for the Dartmouth summer research project on artificial intelligence. *AI Mag.*, 27(4): 12-12. <https://doi.org/10.1609/aimag.v27i4.1904>.
- Mikalef, P., Framnes, V.A., Danielsen, F., Krogstie, J. and Olsen, D. 2017. Big data analytics capability: antecedents and business value. *Inform. Syst.*, 16: 445. <https://aisel.aisnet.org/pacis2017/136>.
- Munoz, J.M. and Naqvi, A. (eds.). 2018. *Business Strategy in the Artificial Intelligence Economy*. Business Expert Press, New York, NY
- Pahwa, M.S., Dadhich, M., Saini, J.S. and Saini, D.K. 2022. Use of Artificial Intelligence (AI) in the Optimization of Production of Biodiesel Energy. *Scrivener Publishing LLC., Salem, MA, USA*. pp. 229-238.
- Sahebi, H., Mohammad, K., Marziye, S. and MirSaman, P. 2023. The benefits of peer-to-peer renewable energy trading and battery storage backup for the local grid. *J. Energy Stor.*, 63: 106970. <https://doi.org/10.1016/j.est.2023.106970>.
- Schneider, M. and Leyer, M. 2019. Adoption of artificial intelligence in the delegation of personal strategic decisions *Manag. Dec. Econ.*, 40(3): 10.1002.231-223/mde.2982 <https://doi.org/10.1016/j.apenergy.2021.116601>.
- Shin, E.J., Kang, H.G. and Bae, K. 2020. A study on the sustainable development of NPOs with blockchain technology. *Sustainability*, 12(15): 6158. <https://doi.org/10.3390/su12156158>
- Sinha, B.B. and Dhanalakshmi, R. 2022. Recent advancements and challenges of Internet of Things in smart agriculture: A survey. *Future Gen. Comp. Syst.*, 126: 169-184.
- Summa, S., Mircoli, A., Potena, D., Ulpiani, G., Diamantini, C. and Di Perna, C. 2022. Combining artificial intelligence and building engineering technologies towards energy efficiency: The case of ventilated façades. *Construct. Innov.*,
- Swan, M. 201. *Blockchain: Blueprint for a New Economy*. O'Reilly Media Inc., New York.
- Vinuesa, R., Azizpour, H., Leite, I., Balaam, M., Dignum, V., Domisch, S. and Nerini, F.F. 2020. The role of artificial intelligence in achieving the sustainable development goals. *Nature Commun.*, 11(1): 1-10. 10.1038/s41467-019-14108-y
- Yassine, H., Khalida, G., Abdullah, A., Faycal, B. and Abbes, A. 2021. Artificial intelligence based anomaly detection of energy consumption in buildings: A review, current trends, and new perspectives, *Appl. Energy*, 287: 16601.
- Ying, W., Yanpeng, W., Halil, C., Juan, C., Vasquez, J. and Guerrero, M. 2022. Towards collective energy Community: Potential roles of microgrid and blockchain to go beyond P2P energy trading. *Appl. Energy*, 314: 119003. <https://doi.org/10.1016/j.apenergy.2022.119003>.

ORCID DETAILS OF THE AUTHORS

Megha Chauhan: <https://orcid.org/0000-0002-5442-3688>
 Deepali Rani Sahoo: <https://orcid.org/0000-0001-6949-7439>



Underlying Anthropogenic Driving Factors of Forest Landscape Degradation in the Kilimanjaro World Heritage Site, Tanzania Using Survey-based Data

E. A. Enoguanbhor*, G.O. Chukwurah**†, E. C. Enoguanbhor***, M.O. Isimah****(*****),
A. E. O. Kosun*****, N. I. Ewurum* and Eike Albrecht*

*Department of Civil Law and Public Law with References to the European Law and Environment,
Brandenburg University of Technology, Cottbus-Senftenberg, Germany

**Department of Urban and Regional Planning, University of Nigeria, Nsukka, Nigeria

***Applied Geoinformation Science Lab, Department of Geography, Humboldt University of Berlin, Germany

****Department of Geography, University of Nigeria, Nsukka, Nigeria

*****Department of Urban and Regional Planning, University of Nigeria, Nsukka, Nigeria

*****Department of Estate Management, University of Nigeria, Nsukka, Nigeria

†Corresponding author: G.O. Chukwurah; gladys.chukwurah@unn.edu.ng

Nat. Env. & Poll. Tech.
Website: www.neptjournal.com

Received: 23-08-2023

Revised: 16-10-2023

Accepted: 29-11-2023

Key Words:

Forest
Landscape degradation
Anthropogenic factors
Policies
Protection

ABSTRACT

This study aimed to investigate the underlying anthropogenic driving factors of forest landscape degradation in the Kilimanjaro World Heritage Sites (WHS), Tanzania using survey-based data. The essence is to support strategic policies for forest landscape protection and natural heritage sustainability. The research employed empirical data using mixed questionnaires of experts and residents to identify various indirect anthropogenic driving factors of forest degradation, analyze rural poverty and causal mechanisms as indirect anthropogenic drivers of forest degradation, and evaluate the level of awareness and community involvement in forest protection. ArcGIS was used to generate the Maps. About 140 sample sizes were utilized for this study. Using purposive and simple random techniques, about 46 and 100 mixed questionnaires were distributed to experts in forest guard and residents, respectively. Data were analyzed using quantitative and qualitative techniques. Findings showed that indirect factors of forest degradation include high tourism demand, poverty, culture and tradition of local communities, lack of forest protection and conservation education, and insufficient land availability. Also, findings showed that rural poverty as an indirect anthropogenic driving factor of forest degradation is attributed to unemployment in rural areas, inadequate land for agriculture, and insufficient productive forestry availability.

Additionally, this study revealed that residents are aware that the forest is under the government's protection, and most people in local communities are not involved in activities for forest protection. Therefore, the study suggests that the locals should be involved in the activities that promote forest protection for effective control and management. Alternative heating methods should also be explored to reduce much pressure on the available forest to improve the natural heritage sustainability of natural WHS found in Sub-Saharan Africa and other parts of the Global South.

INTRODUCTION

Protecting tropical forests from degradation through institutional instruments, including strategic policies and World Heritage Conventions (WHC), is a critical action to be implemented effectively due to the contributions of forests to improving environmental/natural heritage sustainability (Sandstrom et al. 2020, Sahide et al. 2020, Allan et al. 2017, URT 1998a, URT 1998b). In this context, sustainable natural heritage can be regarded as a condition that allows both present and future generations to use the resources of

the natural heritage (e.g., wildlife and eco-tourism) without degrading the healthy state of forest ecosystems

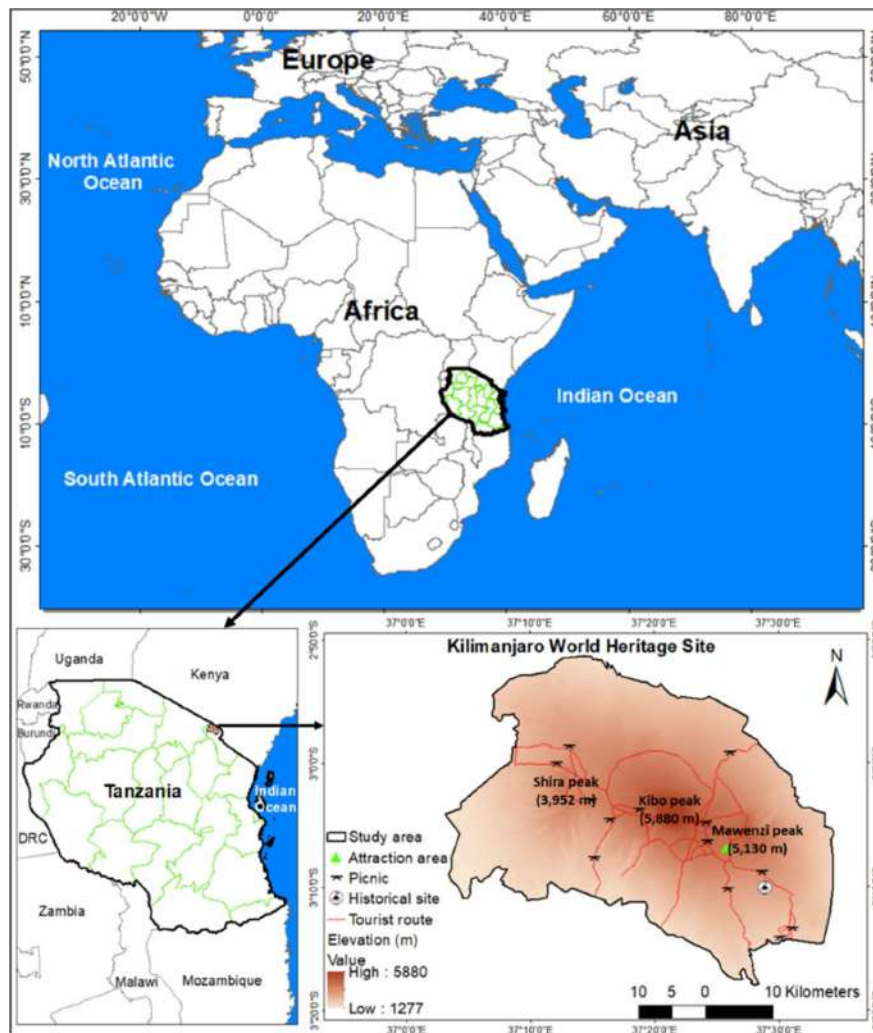
Implementing institutional instruments effectively for forest protection in the Kilimanjaro WHS, Tanzania in particular, and other natural WHS across the World in general, the causes of forest degradation are important to be identified and addressed. Forest degradation is associated with various causes that can be categorized into anthropogenic factors (for example, agriculture, charcoal production, settlement expansion, government policies) and

natural factors, which include topographic elevation and slope, weather/climate (Yahya et al. 2020, Sedano et al. 2020, Shigaeva & Darr 2020). All factors, including anthropogenic factors, can further be categorized into factors used to define the causes of land and environmental dynamics. They include underlying factors that cause the proximate causes and proximate factors that constitute the direct causes, as well as spatial determinants used for geographical explanations of the proximate causes (Abiodun et al. 2017, Meyfroidt 2016).

Regarding the underlying anthropogenic driving factors, which is the focus of the current study, government policies are associated with forest degradation (Saraiva et al. 2020, Kogo & Kumara 2019). According to Khuc et al. (2018), if the population increases by 1%, per capita areas of forest degradation increase by 1.2% in the province of Vietnam.

Additionally, wood-fuel consumption is associated with forest degradation as reported by Sulaiman et al. (2017), that an increase in wood-fuel consumption leads to an increase in forest degradation in Sub-Saharan Africa. Furthermore, the highest and lowest deforestation occurs in the provinces with relatively high and low rates of poverty, respectively, in Vietnam (Khuc et al. 2018). As indirect anthropogenic factors that cause the proximate causes, underlying factors are critical to be neglected. Otherwise, the proximate causes may not be able to be put under control effectively by all institutional instruments for forest protection.

The paper, therefore, aims to use surveys of experts and residents to investigate the underlying anthropogenic driving factors of forest landscape degradation in the Kilimanjaro



Source: Enoguanbhor et al. 2022.

Fig. 1: Maps showing the location of the Kilimanjaro World Heritage Site.

World Heritage Site, Tanzania, using Survey-based Data. Specifically, the study seeks to:

1. Identify various indirect anthropogenic driving factors of forest degradation;
2. Analyze rural poverty and causal mechanisms as indirect anthropogenic drivers of forest degradation and;
3. Evaluate the level of awareness and community involvement in forest protection.

MATERIALS AND METHODS

Study Area

The researchers chose the Kilimanjaro WHS due to the forest degradation over the years (Rutten et al. 2015, Soini 2005) and the forest landscape, particularly the Montane forest, as one of the outstanding universal values of the natural heritage site (UNESCO 2021). The Kilimanjaro WHS (Kilimanjaro National Park) is located in northeast Tanzania and covers 1686.72 km² (Fig. 1). Kilimanjaro National Park was established in 1973 and initially comprised the whole mountain and moorland vegetation above the montane forest. It was inscribed as a natural WHS in 1987 under criteria vii, with the mountain as an outstanding universal value and one of the largest volcanoes in the world (UNESCO 2021, IUCN 2020). In 2005, the Kilimanjaro WHS was extended to include the montane forest (the natural or primary forests that serve as buffer zones and habitats for wildlife) due to human pressure resulting in forest degradation.

The topographic elevation of the mountain ranges from 1277 to 5880 m above sea level at Kibo Peak, which is relatively located at the center of the mountain, as shown in Fig. 1. Other peaks of the mountain include Shira Peak (3,952 m above sea level) and Mawenzi Peak (5,130 m above sea level), peaks located in the northwest and southeast of Kibo Peak, respectively (Fig. 1). As a WHS and a National Park, various strategic actions are taken, including Tanzania National Forest Policy, Tanzania Wildlife Policy, Tanzania National Environmental Policy, Tanzania Tourism Policy, Tanzania National Forest Policy of 1998, Tanzania National Environmental Policy of 1997, WHC of 1972, Wildlife Policy of Tanzania 1998, Tanzania National Park Regulations of 2003, and National Tourism Policy of 1999 (UNESCO 2021, URT 2002).

Data Collection and Analysis

We designed two sets of questionnaires to collect empirical data from experts and residents and the questionnaires comprise open-ended and closed-end (Babbie 2013, Secor 2010). While questionnaires were distributed to experts using

purposive sampling (Babbie 2010), residents' questionnaires were distributed using random sampling (Kothari 2004). The choice of the research respondents and purposive sampling techniques used in this study is because they are the key informants and are more knowledgeable about research interests. 3 researchers administered all questionnaires by hand from 21st February to 8 April 2022. Forestry experts, both males and females, were selected from different Government Departments and Agencies, including the Tanzania Forest Service (TFS), Kilimanjaro National Park (KINAPA), Sokoine University of Agriculture Training Forest (SUATF), and the United Nations Educational, Scientific and Cultural Organization (UNESCO). The expert respondents are adults between the ages of 28 to 40 years with the lowest qualification of a B.sc degree in forestry and related fields. Most of the experts are researchers, and some are forest guards with working experience in various Government departments and Agencies, which include Tanzania Forest Service (TFS), Kilimanjaro National Park (KINAPA), Sokoine University of Agriculture Training Forest (SUATF), and the United Nations Educational, Scientific and Cultural Organization (UNESCO). The total population of the study is 140. Out of 46 questionnaires that were distributed to experts, 26 were retrieved. 100 questionnaires were distributed to residents at Kitowo, Rua, Lyasongoro, and Kokirie settlements, and 66 were retrieved. ArcGIS was used to generate the location of the Kilimanjaro World Heritage Site, land cover transitions, and the degraded primary forest. The sampled respondents and the number of retrieved questionnaires are good enough for the analysis, considering no advanced statistical analysis was done.

Regarding the analysis, we summarized dataset characteristics for closed-ended questions using quantitative(descriptive) analysis by calculating the response

Table 1: Ranking methods for questionnaires' open-ended questions.

Questionnaire	Rank		
	Symbol	Number of times a variable is identified	Description
Experts	*	1-2	Very low
	**	3-4	Low
	***	5-6	Moderate
	****	7-8	High
	*****	9 and above	Very high
Residents	*	1-2	Very low
	**	3-4	Low
	***	5-6	Moderate
	****	7-8	High
	*****	9 and above	Very high

Table 2: Indirect human driving factors of forest landscape degradation in the Kilimanjaro WHS based on experts' surveys.

Driver variables	Ranking
1 High tourism demand	****
2 Poverty in local communities	****
3 Culture and tradition of local communities	**
4 Lack of forest protection and conservation education for local communities	**
5 Insufficient land availability in local communities	*
6 Population growth and pressure	*
7 High dependency	*
8 Lack of sources of energy other than charcoal	*
9 Unemployment	*
10 Environmental degradation in other regions	*
11 Lack of proper security mechanism	*
12 Lack of land use plans	*

Ranking: * = Very low; ** = Low; *** = Moderate; **** = High; and ***** = Very high

frequencies and using qualitative methods of coding, sorting, synthesizing, and ranking for open-ended questions (Bryman 2016, Maxwell 2013). The respondents were asked to identify the various anthropogenic driving factors of forest degradation. The factors were ranked "very low, Low, Moderate High, Very High. We ranked all identified variables based on how many times each respondent identified a variable, as described in Table 1.

RESULTS AND DISCUSSION

The results in Table 2 show the indirect human driving factors of forest landscape degradation in the Kilimanjaro WHS based on experts' surveys. The major factors include high tourism demand and poverty in local communities, with both factors ranked "High." Other factors affecting forest degradation are the culture and tradition of local communities and a lack of forest protection and conservation education for local communities, and both factors are ranked "Low." The factors that are ranked "Very low" include insufficient land availability in local communities, population growth, and pressure, high dependency, a lack of sources of energy other than charcoal, a lack of proper security mechanisms, and a lack of land use plans.

Fig. 2a presents the results of rural poverty contributions to forest degradation in the Kilimanjaro WHS based on experts' surveys. 42.3% of the respondents attributed rural poverty to insufficient job availability in rural areas, and 30.8% attributed it to insufficient land availability for agriculture. 11.5% agreed to insufficient productive forestry availability, and 11.5% attributed it to other factors, including a lack of alternative sources of energy other than charcoal and firewood. The remaining 3.8% could not give their opinion. The results in Fig. 02b show different sources of income based on residents' surveys. While 71.2% of residents earn their incomes from agricultural activities, 22.7% earn from other sources, including small-scale businesses, porting, and construction/building. While 4.5% earn income from tourism

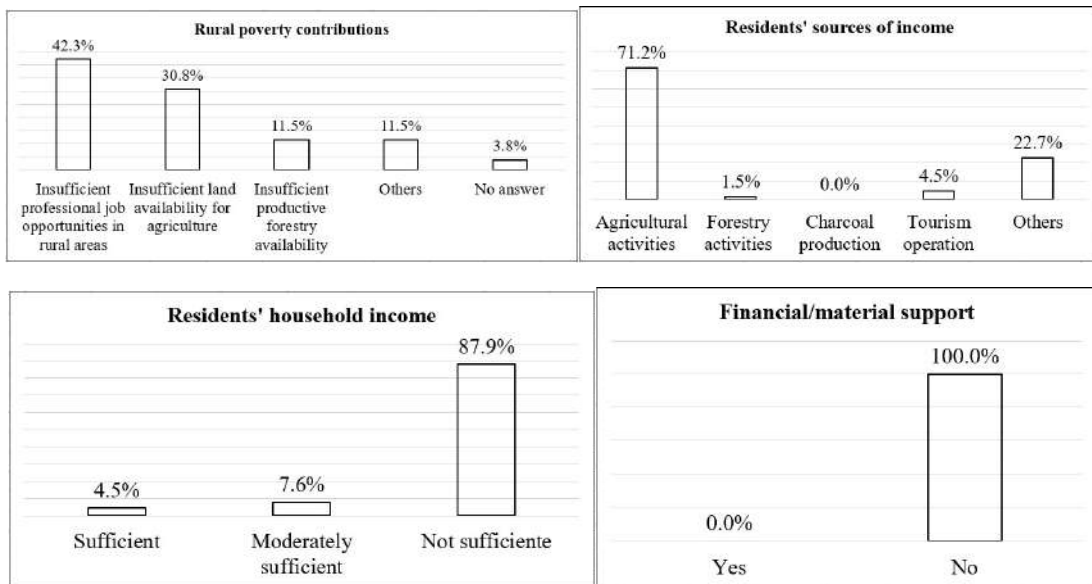


Fig. 2: (a) Rural poverty, (b) sources of income, (c) household income, and (d) financial/material supports as indirect contributions to forest degradation in the Kilimanjaro WHS based on experts' surveys.

operations, 1.5% from forestry activities, and no respondent earns income from charcoal production. Fig. 2c presents the results on the sufficiency of household income based on residents' surveys. 87.9% of the respondents agreed that their incomes are not sufficient for their households, and 7.6% and 4.5% opined that their household incomes are moderately sufficient and (fully) sufficient, respectively. The results in Fig. 2d show government financial/material support for local communities based on residents' surveys. All respondents opined that they receive no financial or/and material support from the government.

Fig. 3a and 3b present the results of awareness of forest protection by the government based on residents' surveys. While 87.9% of respondents are aware that the forest is under the government's protection, 12.1% of them are not aware. The results in Fig. 3b show local communities' involvement in forest protection of the Kilimanjaro WHS based on residents' surveys. While 87.7% of respondents opined that local communities are not involved in the activities for forest protection, 12.3% opined that local communities are being involved.

Our findings on indirect human driving factors of forest landscape degradation in the Kilimanjaro WHS based on experts' surveys (Table 2) show that the major factors include high tourism demand and poverty in local communities, the culture and tradition of local communities, a lack of forest protection and conservation education for local communities, insufficient land availability in local communities, population growth and pressure, high dependency, a lack of sources of energy other than charcoal, a lack of proper security mechanisms, and a lack of land use plans. The findings on high tourism demand and poverty in local communities and insufficient land availability in local communities indicate that the demand for tourism may continue to increase, which may affect forest protection if not managed properly, and poverty and insufficient land availability in local communities may force the people into

the forest for agricultural and illegal logging activities. The findings on population growth and pressure are similar to those of Khuc et al. (2018), who opined that if the population increases by 1%, per capita areas of forest degradation increase by 1.2% in the province of Vietnam. The findings on a lack of sources of energy other than charcoal support the findings from Sulaiman et al. (2017) that an increase in wood-fuel consumption leads to an increase in forest degradation in Sub-Saharan Africa. The finding on poverty in local communities is similar to the finding of Khuc et al. (2018), who reported the highest and lowest deforestation occurs in the provinces with relatively high and low rates of poverty, respectively, in Vietnam.

The findings on rural poverty as an indirect anthropogenic driving factor of forest degradation in the Kilimanjaro WHS based on experts' surveys are attributed to insufficient job availability in rural areas, insufficient land availability for agriculture, insufficient productive forestry availability, and other factors, including a lack of alternative sources of energy other than charcoal and firewood (Fig. 2a). The insufficient professional jobs, land availability for agriculture, and productive forest as a community forest may force most people to exploit the protected forest for human sustenance. The results corroborate the findings of Isieke (2020), who bolstered that indiscriminate exploitation of wood for fuel-wood, unsustainable agricultural practices, mining, bush burning, and infrastructural development are among the drivers of forest degradation. Mores, Jeminiwa et al. (2020) noted that briquettes of charcoal, commercial and subsistence farming, overgrazing, fuel-wood extraction, and population increase contribute to forest degradation.

The findings on different sources of income based on residents' surveys (Fig. 2b) show that most people in local communities earn their incomes from agricultural activities. Their household incomes are not sufficient for their households (Fig. 2c). Also, the people do not receive any financial or/material support from the government (

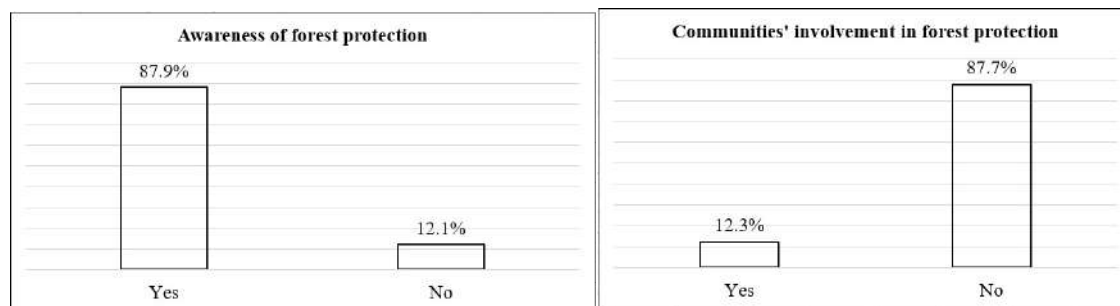


Fig. 3: (a) Awareness of forest protection and (b) local communities' involvement in forest protection based on residents' surveys.

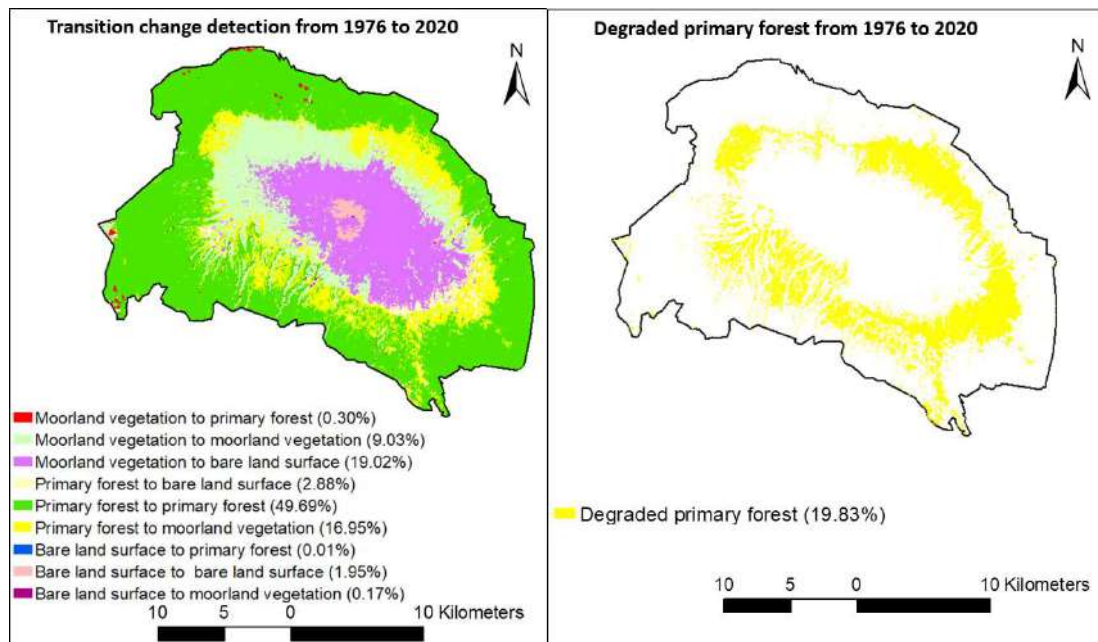
Fig. 2c). These indicate a high level of poverty that may lead to a high level of forest degradation (Khuc et al. 2018). Our finding on awareness of forest protection by the government based on residents' surveys (Fig. 3a) shows that residents are aware that the forest is under the government's protection, indicating possibilities for convincing the people about the necessity for forest protection through conservation education. The findings on local communities' involvement in forest protection of the Kilimanjaro WHS based on residents' surveys (Fig. 3b) show that most people in local communities are not involved in the activities for forest protection. This indicates that the people feel excluded from activities related to their natural heritage, forcing them to resist forest protection, which may lead to a violation.

The implication of the findings can be linked to indirect anthropogenic driving factors of forest degradation, particularly the culture and tradition of local communities and a lack of forest protection and conservation education for local communities. A similar study by Nura and Endris (2020) also confirmed that a lack of community awareness of sustainable use and management of forest resources (44.5%) and a lack of clear understanding of forest laws and regulations among the community (40.4%) contributed to forest deforestation in Jimma Zone, South Western Ethiopia.

From the cultural heritage point of view, the people may be feeling that accessibility and utilization of forest resources

are their fundamental human rights because it is their natural heritage from their ancestors, where their cultural activities (e.g., farming, rearing of animals, harvesting of trees and bees) are to be carried out for human sustenance. The lack of forest protection and conservation education for local communities is worsening the real-world situation because the people ought to be enlightened on the reasons why the forest should be protected for natural heritage sustainability. Despite the awareness of the people that the forest is under protection by the government, if forest protection and conservation education for local communities are not implemented, their culture and tradition would position the minds of the people to resist any form of restrictions from the forest. This may continue to hinder the implementation of the WHC and policies' effectiveness on forest protection and natural heritage sustainability. Additionally, an important implication of the findings can be linked to the living conditions of local communities that have not been able to improve through other institutional instruments for poverty alleviation programs. The main source of income for local communities is agriculture, and the accessibility to lands for agricultural expansion is very low. Their incomes are not sufficient for most people, and they do not receive financial or material support from the government.

Additionally, most people are not involved in the process of forest protection, and unemployment increases. Neglecting



Source: Enoguanbhor et al. (2022).

Fig. 4: Spatial patterns of (a) land cover transitions and (b) the degraded primary forest.

the people in such poor living conditions may continue to affect the effective implementation of the WHC and policies for forest protection and natural heritage sustainability. Thus, a large area of the montane/primary forest landscape has been degraded in the last four decades and has not been able to be regenerated, as shown in Fig. 4.

The information on underlying anthropogenic factors of forest degradation in the study area is essential to supporting the implementation of institutional instruments for forest protection and improving the sustainability of the Kilimanjaro WHS and other natural WHS found in the Global South. Thus, the study contributes to World Heritage Studies and management for natural heritage sustainability. This study is limited by time constraints due to the Tanzanian government bureaucracy while seeking official approval for the field research. Also, most experts were not available for questionnaires' distribution and retrieval. However, the 26 questionnaires retrieved from experts used for the current study can be said to be sufficient, considering no inferential statistics were performed in the current study.

Based on our findings and limitations of the study, we, therefore, recommend the following: First, the culture and tradition of local communities should be evaluated and considered other alternatives which include, through education, re-orient the minds of the people on the need to improve forest protection, attain and maintain forest, and natural heritage sustainability. Second, the living conditions of local communities should be improved through other institutional instruments, for example, poverty alleviation programs. This can be done by creating and improving different sources of income. Third, experts should always try to be available and respond to questionnaires. Finally, future research should apply the same or similar method to investigate the proximate anthropogenic factors of forest degradation.

CONCLUSION

The study used surveys of experts and residents to investigate underlying anthropogenic driving factors of forest degradation in the Kilimanjaro WHS to support strategic policies for forest landscape protection and natural heritage sustainability. Our findings showed that indirect anthropogenic driving factors of forest degradation include high tourism demand and poverty in local communities, the culture and tradition of local communities, a lack of forest protection and conservation education for local communities, and insufficient land availability in local communities. Other factors include population growth and pressure, high dependency, a lack of sources of energy other than charcoal, a lack of proper security mechanisms, and a lack of land use plans. The findings on rural poverty as an

indirect anthropogenic driving factor of forest degradation are attributed to insufficient job availability in rural areas, insufficient land availability for agriculture, insufficient productive forestry availability, and other factors, including a lack of alternative sources of energy other than charcoal and firewood. The findings on different sources of income based on residents' surveys showed that most people in local communities earn their incomes from agricultural activities, and their household incomes are not sufficient for their households. Also, the findings showed that the people do not receive any financial or/ material support from the government (Fig. 2c). The finding on awareness of forest protection showed that residents are aware that the forest is under the government's protection. The findings showed that most people in local communities are not involved in activities.

Therefore, the study suggests that the government, through the authority(s) in charge of a forest, should involve the locals in the activities that promote forest protection for effective control and management. Furthermore, alternative heating methods should be explored to reduce much pressure on the available forest. The findings from our study on underlying anthropogenic factors of forest degradation are crucial to supporting decision-making processes on the implementation of strategic policies and WHC for forest protection and improving natural heritage sustainability in the Global South.

REFERENCES

- Abiodun, O.E., Olaleye, J.B., Olusina, J.O. and Omogunloye, O.G. 2017. Principal component analysis of urban expansion drivers in greater Lagos, Nigeria. *Niger. J. Environ. Sci. Technol.*, 1: 156-168.
- Allan, J.R., Venter, O., Maxwell, S., Bertzky, B., Jones, K., Shi, Y. and Watson, J.E.M. 2017. Recent increases in human pressure and forest loss threaten many Natural World Heritage Sites. *Biol. Conserv.*, 206: 47-55.
- Babbie, E. 2010. *The Practice of Social Research*. Twelfth edition. Wadsworth, Belmont.
- Babbie, E. 2013. *The Practice of Social Research*. Thirteenth edition. Cengage Learning, Madrid, Wadsworth.
- Bryman, A. 2016. *Social Research Methods*. Fifth edition. Oxford University Press, New York, NY.
- Enoguanbhor, E.A., Enoguanbhor, E.C. and Albrecht, E. 2022. Spatial determinants of forest landscape degradation in the Kilimanjaro World Heritage Site, Tanzania. *Cent. Eur. J. Geogr. Sustain. Dev.*, 4(2): 5-23.
- Enoguanbhor, E.C., Chukwurah, G.C., Fotang, C. and Enoguanbhor, E.A. 2023. Integrating GIS and survey-based data to evaluate urban green infrastructural development in the context of urban planning implementation and challenges. *Int. J. Eng. Technol. Innov.*, 5: 111.
- Enoguanbhor, E.C., Gollnow, F., Walker, B.B., Nielsen, J.O. and Lakes, T. 2021. Key Challenges for Land Use Planning and its Environmental Assessments in the Abuja City-Region, Nigeria. *Land*, 10(5): 443.
- Enoguanbhor, E. 2021. *Urban Land Dynamics in the Abuja City-Region, Nigeria: Integrating GIS, Remotely Sensed, and Survey-Based Data to Support Land Use Planning*. Humboldt-Universität zu Berlin, Berlin.

- Enoguanbhor, E., Gollnow, F., Walker, B., Nielsen, J. and Lakes, T. 2022. Simulating urban land expansion in the context of land use planning in the Abuja City-Region, Nigeria. *GeoJournal*, 87: 1479-1497.
- Isieke U. 2020. The Unpopular factors were driving forest, land degradation, and climate change in Nigeria.
- IUCN. 2020. Kilimanjaro National Park - 2020 conservation outlook assessment. <https://worldheritageoutlook.iucn.org/explore-sites/wdpaid/17761>
- Jeminiwa, O.R., Jeminiwa, M.S., Taiwo, D.M., Dauda, M. and Iolaoti-laaro, S.O. 2020. Assessment of forest degradation indices in Mokwa forest reserve, Niger State, Nigeria. *J. Appl. Sci. Environ. Manage.*, 24(8): 1351-1356. DOI: 10.4314/jasem.v24i8.7.
- Khuc, Q.V., Tran, B.Q., Meyfroidt, P. and Paschke, M.W. 2018. Drivers of deforestation and forest degradation in Vietnam: An exploratory analysis at the national level. *Forest Policy Econ.*, 90: 128-141.
- Kogo, B.K. and Kumara, L. 2019. Forest cover dynamics and underlying driving forces affecting ecosystem services in western Kenya. *Remote Sens. Appl. Soc. Environ.*, 14: 75-83.
- Kothari, C.R. 2004. *Research Methodology: Methods & Techniques*. Second edition. New Age Int. (P) Ltd., Publishers, New Delhi.
- Lu, S., Sun, H., Zhou, Y., Qin, F. and Guan, X. 2020. Examining the impact of forestry policy on poor and non-poor farmers' income and production input in collective forest areas in China. *J. Clean. Prod.*, 276: 123784.
- Maxwell, J.A. 2013. *Qualitative Research Design: An Interactive Approach*. Third edition. SAGE Publications, Inc., NJ.
- Meyfroidt, P. 2016. Approaches and terminology for causal analysis in land systems science. *J. Land Use Sci.*, 11(5): 501-522.
- Nura, K.T. and Endris, F.S. 2020. Assessment of levels of community awareness to effects of forest degradation and their environmental management practices in Jimma Zone, South Western Ethiopia. *Int. J. Multicult. Multi-religion. Underst.*, 7(2): 212-228. <https://doi.org/10.18415/ijmmu.v7i2.1501>
- Rutten, G., Ensslin, A., Hemp, A. and Fischer, M. 2015. Forest structure and composition of previously selectively logged and non-logged montane forests at Mt. Kilimanjaro. *Forest Ecol. Manage.*, 337: 61-66.
- Sahide, M.A., Fisher, M.R., Erbaugh, J.T., Intarini, D., Dharmiasih, W., Makmur, M., Faturachmat, F., Verheijena, B. and Maryudi A. 2020. The boom of social forestry policy and the bust of social forests in Indonesia: Developing and applying an access-exclusion framework to assess policy outcomes. *Forest Policy Econ.*, 120: 102290.
- Sandström, C., Kanyama, A.C., Rätty, R., Sonnek, K.M., Nordström, E.M., Mossing, A. and Nordin A. 2020. Policy goals and instruments for achieving a desirable future forest: Experiences from backcasting with stakeholders in Sweden. *Forest Policy Econ.*, 111: 102051.
- Saraiva, M.B., Ferreira, M.D., Cunha, D.A., Daniel, L.P., Homma, A.K. and Pires, G.F. 2020. Forest regeneration in the Brazilian Amazon: Public policies and economic conditions. *J. Clean. Prod.*, 269: 122424.
- Secor, A.J. 2010. Social surveys, interviews, and focus groups. In B. Gomez, and J.P. Jones III (eds), *Research Methods in Geography: A Critical Introduction*. Blackwell Publishing Ltd, West Sussex, pp. 194-205.
- Sedano, F., Lisboa, S., Duncanson, L., Ribeiro, N., Siteo, A., Sahajpal, R., Hurtt, G. and Tucker, C. 2020. Monitoring intra and inter-annual dynamics of forest degradation from charcoal production in Southern Africa with Sentinel-2-2 imagery. *Int. J. Appl. Earth Obs. Geoinform.*, 92: 102184.
- Shigaeva, J. and Darr, D. 2020. On the socio-economic importance of natural and planted walnut (*Juglans regia* L.) forests in the Silk Road countries: A systematic review. *Forest Policy Econ.*, 118: 102233.
- Soini, E. 2005. Land use change patterns and livelihood dynamics on the slopes of Mt. Kilimanjaro, Tanzania. *Agric. Syst.*, 85: 306-323.
- Sulaiman, C., Abdul-Rahim, A.S., Mohd-Shahwahid, H.O. and Chin, L. 2017. Wood fuel consumption, institutional quality, and forest degradation in sub-Saharan Africa: Evidence from a dynamic panel framework. *Ecol. Indic.*, 74: 414-419.
- UNESCO 2021. Convention concerning the protection of the world's cultural and natural heritage. <https://whc.unesco.org/en/conventioncontext>
- URT. 1998. National Forest Policy. Dar Es Salaam: Ministry of Natural Resources and Tourism.
- URT 2002. The Forest Act. Dar Es Salaam: URT.
- URT 1998. The wildlife policy of Tanzania. Dar Es Salaam: Ministry of Natural Resources and Tourism.
- Yahya, N., Bekele, T., Gardi, O. and Blaser, J. 2020. Forest cover dynamics and its drivers of the Arba Gugu forest in the Eastern highlands of Ethiopia during 1986-2015. *Remote Sens. Appl. Soc. Environ.*, 20: 100378.



Optimization of Aviation Biofuel Development as Sustainable Energy Through Simulation of System Dynamics Modeling

Didi Nuryadin*†, Mohammad Nurcholis**, Gita Astyka Rahmanda* and Indra Wahyu Pratama***

*Faculty of Economics and Business, UPN Veteran Yogyakarta, Yogyakarta, Indonesia

**Faculty of Agriculture, UPN Veteran Yogyakarta, Yogyakarta, Indonesia

***Center of Food and Sustainable Development Studies, Yogyakarta, Indonesia

†Corresponding author: Didi Nuryadin, didinuryadin@upnyk.ac.id

Nat. Env. & Poll. Tech.
Website: www.neptjournal.com

Received: 10-08-2023

Revised: 26-10-2023

Accepted: 15-12-2023

Key Words:

Aviation biofuel

Clean energy

Sustainable energy

System dynamics

ABSTRACT

This study aims to optimize the development of aviation biofuel as a sustainable energy source by simulating system dynamics modeling. This study is based on the System Dynamics modeling approach, which is a set of conceptual tools designed to understand the structure and dynamics of complex systems. This study used the system dynamics method specifically designed to analyze complex systems. It has been applied to various sustainability-related issues, including urban area sustainable development modeling, sustainability of water resources, environmental management, and sustainable urbanization. The result obtained using the quantitative modeling showed that the contribution of aviation biofuel to flight intensity in Indonesia is still insignificant. The practical implications of this study are that palm oil has the potential to be a viable raw material for aviation biofuel production in Indonesia, and implementing policies to mitigate negative consequences and optimize land use for aviation biofuel fuel production can contribute to sustainable urban development. The originality of this study lies in its use of System Dynamics modeling to analyze the potential of palm oil as a raw material for aviation biofuel production and identify the various social, economic, environmental, and technological factors that impact it.

INTRODUCTION

The System Dynamics method is a valuable tool for analyzing and predicting the behavior of complex physical, social, and economic systems. This method involves the formulation, simulation, and validation of future developments, making it possible to design and implement effective policy plans that have been applied to a wide range of sustainability issues, including urban area sustainable development modeling (Ab Rasid et al. 2021, Tan et al. 2018, Xing et al. 2019) sustainability of water resources, environmental management (Xiang et al. 2021), and sustainable urbanization (Mishra et al. 2017).

The System Dynamics method was utilized to model and simulate a sustainable management strategy for aviation biofuel development. Historical data from 2014 to 2019 was used to simulate and forecast future developments, and data processing was conducted using the Vensim PLE Software. The dynamic connection between the social, economic, and environmental spheres is intricate. The nature of the relationship is nonlinear, with a feedback loop. Hence, it is very meaningful to simulate the state and scenario of its

development. The results of this study can contribute to guiding a more coordinated and sustainable development.

In this study, a custom model was developed specifically to reflect the unique conditions and characteristics of aviation biofuel development. The construction of this model is based on the mental model of the researchers and respondents, as well as relevant literature and previous studies. Thus, remarkable results were produced, unlike similar studies in other locations. System dynamics modeling depends on the ability of those conducting the study and close sources involved in the model production.

Previous studies showed the operational research methods used in biofuel supply chain planning (Gonzalez et al. 2018). Then, a case study analyzed a method for designing sustainable WEEE management system policies using optimization-based simulation (OBS) (Llerena-Riascos et al. 2021). A study also examined Indonesia's system dynamics approach to biodiesel fund management (Tupa R. Silalahi et al. 2020). The last was about dynamic system modeling of renewable energy diversification as a sustainability university (Arishinta & Suryani 2021). Thus, there was no yet study about aviation biofuel development as sustainable

energy through simulation of system dynamics modeling,

System Dynamics modeling is a set of conceptual tools designed to help understand the structure and dynamics of complex systems. This method involves studying real-world situations to learn about the behavior and structure of a system and then examining the individual components to gain a deeper understanding. The approach is particularly well-suited for studying complex issues such as sustainable development. System dynamics modeling is carried out through four stages: observation of reality, preparation of models (conceptual), interpretation, and utilization of modeling results.

MATERIALS AND METHODS

The System Dynamics method is a valuable tool for analyzing and predicting the behavior of complex physical, social, and economic systems. This approach involves formulating, simulating, and validating future developments by observing the system's behavior, allowing for the design of effective policy plans. The System Dynamics method has been specifically designed for the analysis of complex systems. It has been applied to various sustainability-related issues, including urban area sustainable development modeling (Rusiawan et al. 2015, Strulak-Wójcikiewicz & Lemke 2019, Xing et al. 2019), sustainability of water resources (Kotir et al. 2016), environmental management (Van Oijstaeijen et al. 2020) and sustainable urbanization (Lu & Ke 2018).

The system dynamics in this study were used to model and simulate a sustainable aviation biofuel management strategy. The historical data used were from 2014 to 2019 for simulating and forecasting future developments. Data processing was carried out using Vensim PLE Software. In real terms, the dynamic interaction between social, economic, and environmental is complex. The nature of the relationship is nonlinear, with a feedback loop. Therefore, it is very meaningful to simulate the state and scenario of its development. The results of this study can contribute to guiding a more coordinated and sustainable development.

The model used in this study was built specifically according to the actual conditions in aviation biofuel development. The construction was based on the mental model of those who carried out the study, the respondent, and numerous previous studies. Therefore, the results are unique, and the outputs differ from similar studies in other locations. System dynamics modeling is highly dependent on the ability of those conducting the study and sources involved to produce models as closely as possible to the existing system.

RESULTS AND DISCUSSION

The Potential of Palm Oil in Aviation Biofuel Production

Developing bio-hydrocarbon fuels from vegetable oils is a key national priority in Indonesia. This program aims to achieve a renewable energy mix that includes biofuels, with a target of 23% by 2025. This goal aligns with the National Energy Policy, as the Indonesia National Energy Council (BPDPKS) outlined in 2021.

Indonesia is blessed with a diverse range of natural resources that have the potential to be utilized as sources of biofuels. However, in selecting raw materials for the production of biofuels, particularly aviation biofuels, various considerations must be taken into account, including the technical aspects of the production process, commercial viability, cultivation feasibility, and government policies. Previous research has shown that palm oil is the most promising raw material for the production of aviation biofuel (Siswahyu & Hendarwati 2014). It highlights the importance of considering the technical and commercial viability of potential biofuel sources and the need for further research and development in this area.

The selection of palm oil as the primary raw material for aviation biofuels in Indonesia is due to its technical superiority and suitability for the production process, making it a preferred choice over other potential feedstocks such as biomass, palm kernel, and coconut oil. It is supported by the growing trend of using palm oil as a feedstock for biodiesel in West Africa and Southeast Asia, with Indonesia and Malaysia being major players in the global production of palm oil (Nongbe et al. 2017). As a tropical country, Indonesia has the largest palm oil production potential, as reported in 2015. Indonesia and Malaysia accounted for 83% of global production, with 51% and 34%, respectively (Shigetomi et al. 2020).

Palm oil is a versatile raw material with a high content of medium-chain saturated and monounsaturated fatty acids, making it an ideal choice for producing aviation biofuels (Rutz & Janssen 2014). Palm oil is a perennial crop, unlike soybeans and rapeseed, meaning its oil production is continuous and uninterrupted (Wong et al. 2019). Additionally, palm oil has higher productivity, requiring less fertilizer, water, and pesticides than other crops (Mekhilef et al. 2011). The average world palm oil yield is 3.68 tons/ha/year, significantly higher than soybeans (0.36 tons/ha/year) and rapeseed (0.42 tons/ha/year) (Basiron 2007).

The processing of palm oil produces several derivative products, which include 21.5% Crude Palm Oil (CPO), 5%

Palm Kernel Oil (PKO), and Palm Kernel Cake (PKE), and the remaining waste products, such as fiber, empty fruit bunches, and Palm Oil Mill Effluent (POME) (Wicke et al. 2008). Crude Palm Oil (CPO) is the most commonly used raw material for biodiesel production. In tropical regions, oil palm plantations have the potential to yield 4.27-4.63 tons/ha/year (de Vries et al. 2010). The rapid growth of oil palm plantations in the country, particularly in Sumatra and Kalimantan, is driven by the vast forest areas and favorable climatic conditions (Wulandari et al. 2017). These conditions make Indonesia an important player in the global palm oil and biofuel industries.

Variables Impacting the Use of Palm Oil as Aviation Biofuel

The use of palm oil as a raw material for making aviation biofuels is related to various social, economic, environmental, and technological factors. The linkage can be backward or forward and comprises interrelationships capable of causing causal processes that form a feedback loop. The greater the variables related to the topic of study, the larger the potential loops formed. The variables involved in this study consisted of the following dimensions listed in Table 1.

Causal Loop Diagram of the Development of Biofuels as Sustainable Aviation Biofuels

Causal Loop Diagrams (CLD) are created based on the

Table 1: Aviation biofuel Modeling Variables as Sustainable Biofuels.

Dimension	Principle	Criteria
Social	P1: Respect property and land tenure	C1-Rights of land access
	P2: Social acceptability	C2-National energy security C3-Local prosperity
	P3: Promote responsible work conditions	C4-Health & safety-employees C5-Labor laws
	P4: Prevent alteration to the food supply	C6-Food supply
Political	P5: Relationship between national and international aviation biofuel promotion policies	C7-Agreement national/international aviation biofuel blend-avtur, Subsidy scheme, Advanced aviation biofuel promotion
	P6: National aviation biofuel production consistent with international environmental policies	C8-Biomass is not edible for aviation biofuel production. C9-National amount of land suitable for biomass
	P7: Promote commitment to ethics and transparency	C10-Emission condition GHE
Economic	P8: Economic viability	C11-Influence oil market/aviation biofuel
		C12-Influence diesel market/aviation biofuel
		C13-Production aviation biofuel, Ethical commitment, Land conflicts
		C14-Compliance with local laws
		C15-Influence vegetable oil market/aviation biofuel
		C16-Influence glycerol market/aviation biofuel

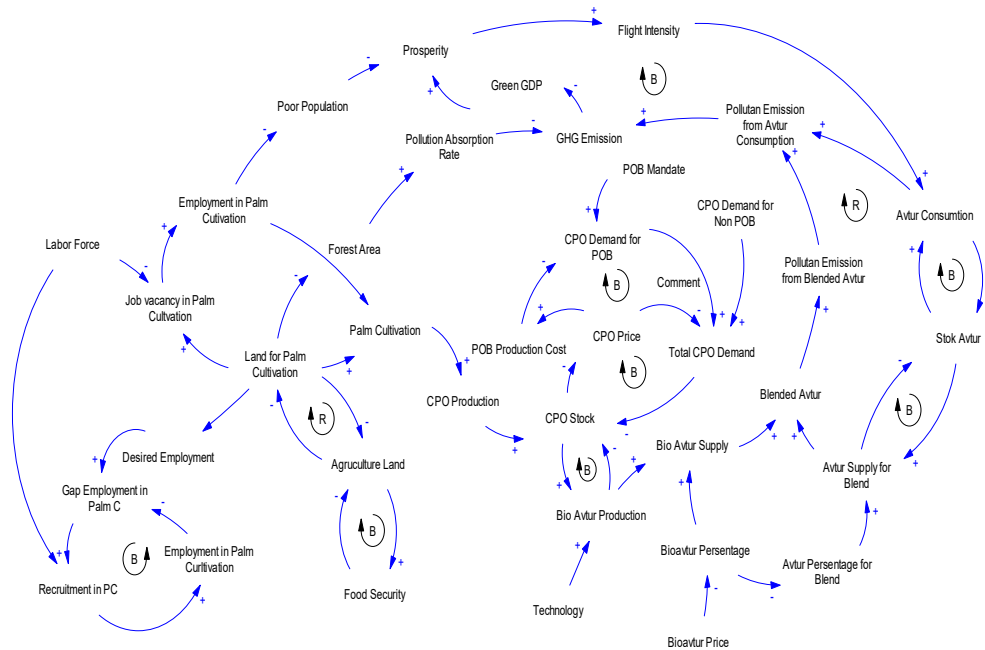
Source: own elaboration

mental model and related references. Meanwhile, the causality relationships between variables are marked with arrows. The CLD analysis results carried out based on the collection of primary and secondary data are shown in Fig. 1.

The development of aircraft fuel in aviation biofuel significantly affects society's economic, social, environmental, technological, and political/regulatory aspects. CLD's Development of Aviation Biofuel as Sustainable Biofuel shows that applying a mixture of aviation biofuels in pure aviation fuel (avtur) affects the decrease in the resulting pollution. It also can reduce the process of global warming in the long run.

The use of aviation biofuels also affects increasing socioeconomic activity macroeconomically, especially in aspects of physical development and sustainable digitization of various industries. This process also increases various community activities, including mobility, by utilizing public transportation in the form of airplanes. Others include a rise in flight intensity not accompanied by increased aviation biofuel production, which reduces the ratio of aviation biofuel mixtures and avtur due to a lack of aviation biofuel stocks. This process potentially increases the production of pollutants from aircraft transportation. In the long run, these conditions hinder the socio-economic activities of the community.

In the environment, producing aviation biofuels



Source: own elaboration.

Fig. 1: CLD of aviation biofuel development as sustainable biofuel.

from sorghum requires special land, which competes with agricultural land and industry needs. The decline in agricultural land can potentially reduce the level of food security and the existence of sorghum land. Therefore, adequate attention must be paid to the regulations and strategies for optimizing sorghum land to ensure sorghum stock is one of the aviation biofuel fuels. On the other hand, the existence of sorghum plantations can absorb labor and contribute to increasing the welfare of the population.

CLD of the Development of Biofuels as Sustainable Aviation Biofuels

Stock and Flow Diagrams (SFD) are built on preconstructed qualitative models and used as a projection tool for the future aviation biofuel management system. SFD also allows for the conduction of simulations on created models. SFD in this study is shown in Fig. 2.

SFD is used to estimate the system's behavior. The development of the number of flights is the main variable observed in this study because it is the main indicator in designing an alternative fuel system. This process is characterized by the increasing availability of fuel and the intensity of flights. The simulation results carried out are shown in Fig. 3.

This research yields simulation results that depict a concerning trend: a decrease in the extent of agricultural and forested land from 2015 to 2030, accompanied by an

expansion of oil palm plantations. The surge in oil palm production is closely linked to the potential expansion of oil palm plantation acreage, which incentivizes the conversion of agricultural and forested land. The implications of this land conversion have been extensively discussed in the scientific literature.

The papers collectively provide evidence that the conversion of forested land into oil palm plantations leads to a loss of biodiversity and contributes to regional climate change. (Koh et al. 2011) shows that the conversion of peat swamp forests to oil palm plantations in Southeast Asia resulted in biodiversity declines and carbon emissions. Vijay et al. (2016) further support this, demonstrating that oil palm expansion in various regions has led to deforestation and threatened biodiversity-rich ecosystems. Koh & Wilcove (2008) confirms that forests are indeed being cleared for oil palm cultivation, resulting in significant biodiversity losses. Finally, (Edwards et al. 2013) highlight the negative impact of forest conversion to oil palm on functional diversity, particularly in terms of dung beetles. These findings collectively emphasize the need for conservation efforts and sustainable land-use practices to mitigate the negative effects of oil palm expansion on biodiversity and climate change.

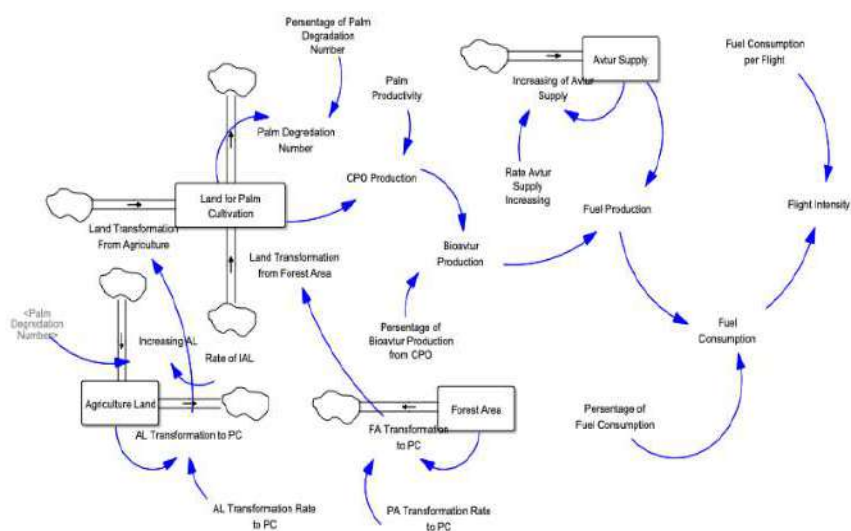
The context provided by the scientific literature underscores the urgency of this issue, as such land conversion can jeopardize invaluable ecosystems and carry significant ecological consequences. Hence, this research

underscores the need for serious attention to the impacts of oil palm plantation growth on agricultural and forested land and emphasizes the importance of implementing the solutions proposed in the scientific literature to maintain a balance between industry needs and environmental sustainability.

Palm oil is one of the high-demand commodities used to produce vegetable oil. The use of palm fruit to produce oil started in the 1980s. The palm species used as the main source of palm oil are *Elaeis guineensis* from Africa and the American palm *Elaeis oleifera*, found in native South and

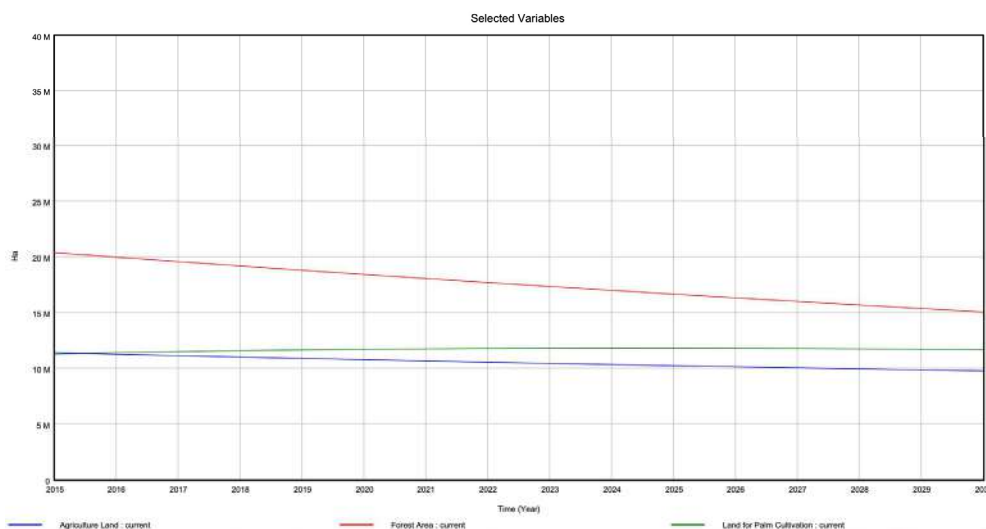
Central America. According to (Affandi & Astuti 2018), ripe palm fruit has a high oil content of 35 to 45%. (Amiruddin 2022) stated that the average oil content of dried mesocarp palm fruit from nine commercial DxP palms in PPKS is 76.3%, while the oil content of dry kernels is between 47.1 to 54.1%. The main purpose of developing oil palm plantations is to produce oil for food. Furthermore, palm oil is also used as a raw material for biofuels in developing technology mixes of renewable fuel and diesel. The government implemented a policy to increase the percentage of biodiesel from palm oil.

This development is faced with the problem of limitations



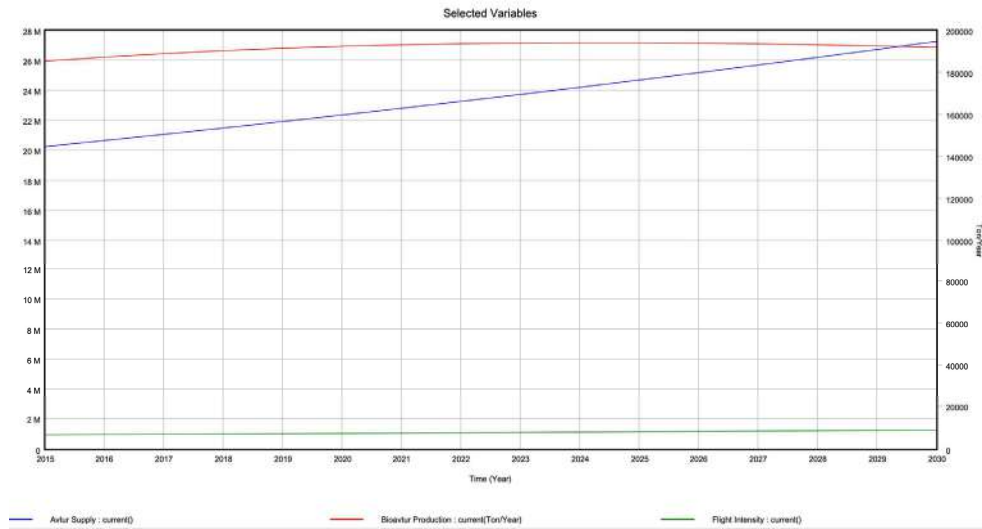
Source: own elaboration.

Fig. 2: SFD of Aviation biofuel development as sustainable biofuel.



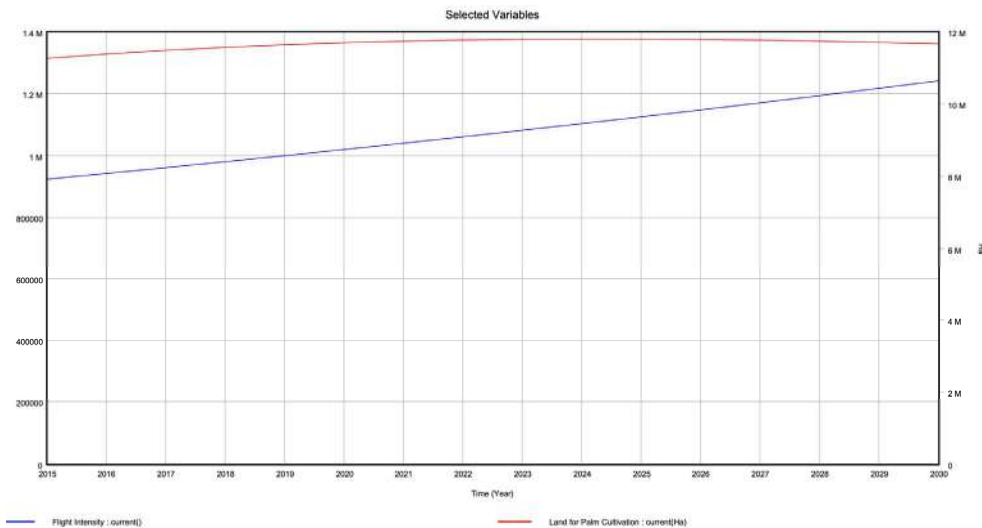
Source: own elaboration

Fig. 3: The Relationship between agricultural land area, forests, and oil palm plantations.



Source: own elaboration.

Fig. 4: The Relationship between avtur production, aviation biofuel, and flight quantity.



Source: own elaboration.

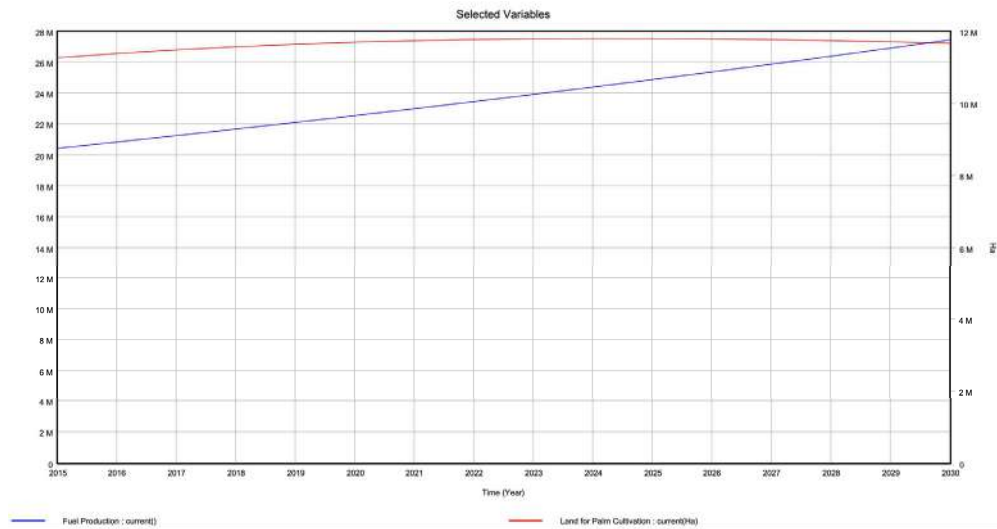
Fig. 5: The Relationship between oil palm plantation area and flight intensity.

and land use change. Land on earth does not increase but decreases because it is mostly intended for development. The development of science led to a cultural change from the old to the modern era. It is in addition to an increase in the type and amount of infrastructure, which requires space. One of the consequences of land is its use to cultivate vegetables and build structures. Another example is the growth of the human population, thereby leading to an additional food supply.

The supply of avtur is projected to continue to increase in line with the development of the aviation industry (Fig. 4).

Conversely, the aviation biofuel offering will form a curve with a maximum production value in 2023. The supply of avtur and the community’s needs drove the increase in flight intensity. The production of aviation biofuels has little impact on flight intensity because the fuel needs of the aircraft are still largely met from conventional aviation fuel.

However, the impact of aviation biofuel production on flight intensity is considered to be minimal because the majority of aircraft fuel needs are still met by conventional aviation fuel. Rising jet fuel prices, potential future emissions legislation, and concerns about fuel security



Source: own elaboration.

Fig. 6: The Relationship between avtur fuel production and oil palm plantation land area.

drive the market development of aviation biofuel. However, the commercialization of aviation biofuels is constrained by high production costs, limited availability of suitable feedstocks, uncertainty surrounding sustainability criteria, and a perceived lack of political and policy support (Gegg et al. 2014). In the EU28, the market penetration of aviation biofuels is currently negligible, but there is potential for growth.

The intensity of aviation continues to rise (Fig. 5). However, on the other hand, the extent of agricultural land fluctuates and begins to decline from the year 2024. This phenomenon is attributed to the fact that aviation fuel is still predominantly derived from fossil energy sources. This indicates that the production of bio-aviation fuel, which is associated with the availability of oil palm plantations, does not exhibit a significant correlation with aviation intensity.

On the Other hand, Nygren et al. 2009) predict a substantial shortage of jet fuel by 2026 due to the decline in crude oil production, making it challenging for the aviation industry to replace it with fuel from other sources. The challenges and perspectives of biomass-derived aviation fuels, emphasizing the need for improved production technology and integration of biology, chemical engineering, and energy crops, are important things to increase the use of aviation biofuel (Wang et al. 2019). Environmental, economic, and social impacts associated with aviation biofuel production in Brazil, including the use of agricultural land and intensive water use (Cremonet et al. 2015).

Generally, the production of avtur fuel is constantly increasing, with a decrease in oil palm agriculture (Fig. 6).

The decline can occur due to competition for the use of oil palm plantation land, food crops, and forest land. However, increasing the need for avtur and decreasing oil palm land shows that the production of both commodities is not significantly correlated.

The potential increase in agricultural land demand for oil palm expansion is due to rising demand for palm oil. Still, it does not directly address the correlation between avtur and oil palm land (Othman 2003). Singh & Bhagwat (2013) highlights the negative environmental impacts of agricultural expansion, including oil palm, but does not specifically address the correlation between avtur and oil palm land. On the other hand, Nasution et al. (2019) compare the income prospects of cocoa and oil palm farming, indicating that oil palm farmers have higher income prospects than cocoa farmers. Still, it does not directly address the correlation between avtur and oil palm land.

CONCLUSIONS

The aviation industry contributes to greenhouse gas emissions, although this contribution is relatively small compared to other sectors. The qualitative modeling results describe the direct and indirect relationships between social, economic, technological, and environmental dimensions in the development system of biofuels as sustainable aviation biofuels. This study used quantitative system dynamics modeling to assess the contribution of aviation biofuels to flight intensity in Indonesia, which was found to be insignificant. However, increasing aviation biofuel production has the potential to reduce the amount of land

used for agriculture and forests, as it would reduce the need for land conversion for oil palm plantations. It would not have a direct impact on flight intensity in Indonesia. To mitigate negative consequences, several policies should be implemented, such as limiting land conversion, regulating palm oil trade schemes, and promoting the use of technology in aviation biofuel production.

ACKNOWLEDGMENTS

The authors are grateful to the Institute for Research and Community Services (LPPM) Universitas Pembangunan Nasional “Veteran” Yogyakarta (UPNYK) for the funding provided.

REFERENCES

- Ab Rasid, N.S., Shamjuddin, A., Abdul Rahman, A.Z. and Amin, N.A.S. 2021. Recent advances in green pre-treatment methods of lignocellulosic biomass for enhanced biofuel production. *J. Clean. Prod.*, 321: 129038. <https://doi.org/10.1016/j.jclepro.2021.129038>
- Affandi, M.I. and Astuti, S. 2018. Development system integration plantation palm oil, cattle and energy in rural areas Lampung Province. The 9th International Conference Rural Research & Planning Group (IC-RRPG) Asian Rural Sustainable Development: Promoting Spiritual, Culture Values and Local Practices, Universitas Mahasaraswati Denpasar, Indonesia, pp. 378-387.
- Amiruddin, M.D. 2022. Field evaluation of oil palm genetic materials for partial resistance in Ganoderma hotspots of tropical peat soil. *J. Oil Palm Res.*, 1: 25. <https://doi.org/10.21894/jopr.2022.0025>
- Arishinta, A. and Suryani, E. 2021. Dynamic system modeling of renewable energy diversification at ITS Surabaya as a sustainable university management effort. *IPTEK J. Proceedings Series*, 6: 195. <https://doi.org/10.12962/j23546026.y2020i6.11093>
- Basiron, Y. 2007. Palm oil production through sustainable plantations. *Eur. J. Lipid Sci. Technol.*, 109(4): 289-295. <https://doi.org/10.1002/ejlt.200600223>
- Cremonez, P.A., Feroldi, M., de Oliveira, C. de J., Teleken, J.G., Alves, H.J. and Sampaio, S.C. 2015. Environmental, economic and social impact of aviation biofuel production in Brazil. *New Biotechnol.*, 32(2): 263-271. <https://doi.org/10.1016/j.nbt.2015.01.001>
- de Vries, S.C., van de Ven, G.W.J., van Itersum, M.K. and Giller, K.E. 2010. Resource use efficiency and environmental performance of nine major biofuel crops, processed by first-generation conversion techniques. *Biomass Bioenergy*, 34(5): 588-601. <https://doi.org/10.1016/j.biombioe.2010.01.001>
- Edwards, F.A., Edwards, D.P., Hamer, K.C. and Davies, R.G. 2013. Impacts of logging and conversion of rainforest to oil palm on the functional diversity of birds in Sundaland. *IBIS*, 155(2): 313-326. <https://doi.org/10.1111/ibi.12027>
- Gegg, P., Budd, L. and Ison, S. 2014. The market development of aviation biofuel: Drivers and constraints. *J. Air Transp. Manag.*, 39: 34-40. <https://doi.org/10.1016/j.jairtraman.2014.03.003>
- Gonzalez, E.D.S., Zhu, J., Zaroni, S. and Maculan, N. 2018. Trends in operational research approaches for sustainability. *Eur. J. Oper. Res.*, 269(1): 1-4. <https://doi.org/10.1016/j.ejor.2017.12.014>
- Koh, L.P., Miettinen, J., Liew, S.C. and Ghazoul, J. 2011. Remotely sensed evidence of tropical peatland conversion to oil palm. *Proc. Natl. Acad. Sci.*, 108(12): 5127-5132. <https://doi.org/10.1073/pnas.1018776108>
- Koh, L.P. and Wilcove, D.S. 2008. Is oil palm agriculture really destroying tropical biodiversity? *Conserv. Lett.*, 1(2): 60-64. <https://doi.org/10.1111/j.1755-263X.2008.00011.x>
- Kotir, J.H., Smith, C., Brown, G., Marshall, N. and Johnstone, R. 2016. A system dynamics simulation model for sustainable water resources management and agricultural development in the Volta River Basin, Ghana. *Sci. Total Environ.*, 573: 444-457. <https://doi.org/10.1016/j.scitotenv.2016.08.081>
- Llerena-Riascos, C., Jaén, S., Montoya-Torres, J.R. and Villegas, J.G. 2021. An optimization-based system dynamics simulation for sustainable policy design in WEEE management systems. *Sustainability*, 13(20): 11377. <https://doi.org/10.3390/su132011377>
- Lu, X. and Ke, S. 2018. Evaluating the effectiveness of sustainable urban land use in China from the perspective of sustainable urbanization. *Habitat Int.*, 77: 90-98. <https://doi.org/10.1016/j.habitatint.2017.10.007>
- Mekhilef, S., Siga, S. and Saidur, R. 2011. A review on palm oil biodiesel as a source of renewable fuel. *Renew. Sustainable Energy Rev.*, 15(4): 1937-1949. <https://doi.org/10.1016/j.rser.2010.12.012>
- Mishra, B.K., Regmi, R.K., Masago, Y., Fukushi, K., Kumar, P. and Saraswat, C. 2017. Assessment of Bagmati River pollution in Kathmandu Valley: Scenario-based modeling and analysis for sustainable urban development. *Sustain. Water Qual. Ecol.*, 9-10: 67-77. <https://doi.org/10.1016/j.swaqe.2017.06.001>
- Nasution, S.K.H., Supriana, T., Pane, T.C. and Hanum, S.S. 2019. Comparing farming income prospects for cocoa and oil palm in Asahan District of North Sumatra. *IOP Conf. Ser.: Earth Environ. Sci.*, 260(1): 012006. <https://doi.org/10.1088/1755-1315/260/1/012006>
- Nongbe, M.C., Ekou, T., Ekou, L., Yao, K.B., Le Grogne, E. and Felpin, F.X. 2017. Biodiesel production from palm oil using sulfonated graphene catalyst. *Renew. Energy*, 106: 135-141. <https://doi.org/10.1016/j.renene.2017.01.024>
- Nygren, E., Aleklett, K. and Höök, M. 2009. Aviation fuel and future oil production scenarios. *Energy Policy*, 37(10): 4003-4010. <https://doi.org/10.1016/j.enpol.2009.04.048>
- Othman, J. 2003. Linking agricultural trade, land demand, and environmental externalities: Case of oil palm in Southeast Asia. *ASEAN Econ. Bull.*, 20(3), AE20-3d. <https://doi.org/10.1355/AE20-3D>
- Rusiawan, W., Tjiptoherijanto, P., Suganda, E. and Darmajanti, L. 2015. Assessment of green total factor productivity impact on sustainable Indonesia productivity growth. *Proced. Environ. Sci.*, 28: 493-501. <https://doi.org/10.1016/j.proenv.2015.07.059>
- Rutz, D. and Janssen, R. 2014. Socio-economic impacts of bioenergy production. *Springer Cham*. <https://doi.org/https://doi.org/10.1007/978-3-319-03829-2>
- Shigetomi, Y., Ishimura, Y. and Yamamoto, Y. 2020. Trends in global dependency on Indonesian palm oil and resultant environmental impacts. *Sci. Rep.*, 1-11. <https://doi.org/10.1038/s41598-020-77458-4>
- Singh, M. and Bhagwat, S. 2013. Tropical agricultural production, conservation, and carbon sequestration conflicts: Oil palm expansion in South East Asia. *Biofuels Econ. Environ. Sustain.*, 72: 420. <https://doi.org/10.5772/52420>
- Siswahyu, A. and Hendarwati, T.Y. 2014. Priority selection of bioavtur raw materials in Indonesia using the Analytical Hierarchy Process (AHP) method. *J. Teknol.*, 6(2): 137-143. <https://doi.org/https://doi.org/10.24853/jurtek.6.2.137-143>
- Strulak-Wójcikiewicz, R. and Lemke, J. 2019. Concept of a simulation model for assessing the sustainable development of urban transport. *Transp. Res. Procedia*, 39: 502-513. <https://doi.org/10.1016/j.trpro.2019.06.052>
- Tan, Y., Jiao, L., Shuai, C. and Shen, L. 2018. A system dynamics model for simulating urban sustainability performance: A China case study. *J. Cleaner Prod.*, 199: 1107-1115. <https://doi.org/10.1016/j.jclepro.2018.07.154>
- Tupa, R. Silalahi, F.M., Simatupang, T. and P. Siallagan, M. 2020. A system dynamics approach to biodiesel fund management in Indonesia. *AIMS*

- Energy, 8(6): 1173-1198. <https://doi.org/10.3934/energy.2020.6.1173>
- Van Oijstaeijen, W., Van Passel, S. and Cools, J. 2020. Urban green infrastructure: A review on valuation toolkits from an urban planning perspective. *J. Environ. Manage.*, 267: 110603. <https://doi.org/10.1016/j.jenvman.2020.110603>
- Vijay, V., Pimm, S.L., Jenkins, C.N. and Smith, S.J. 2016. The impacts of oil palm on recent deforestation and biodiversity loss. *PLoS ONE*, 11(7): e0159668. <https://doi.org/10.1371/journal.pone.0159668>
- Wang, M., Dewil, Raf., Maniatis, K., Wheeldon, J., Tan, T., Baeyens, J. and Fang, Y. 2019. Biomass-derived aviation fuels: Challenges and perspective. *Prog. Energy Combust. Sci.*, 74: 31-49. <https://doi.org/10.1016/j.peccs.2019.04.004>
- Wicke, B., Dornburg, V., Junginger, M. and Faaij, A. 2008. Different palm oil production systems for energy purposes and their greenhouse gas implications. *Biomass Bioenergy*, 32(12): 1322-1337. <https://doi.org/10.1016/j.biombioe.2008.04.001>
- Wong, K.-A., Lam, S.-M. and Sin, J.-C. 2019. Wet chemically synthesized ZnO structures for photodegradation of pre-treated palm oil mill effluent and antibacterial activity. *Ceram. Int.*, 45(2): 1868-1880. <https://doi.org/10.1016/j.ceramint.2018.10.078>
- Wulandari, K., Nurmalina, R. and Tinaprilla, N. 2017. Strategy for developing the bioethanol business unit at PT Perkebunan Nusantara XI using the A'WOT approach. *AGRARIS: J. Agribusiness Rural Dev. Res.*, 3(2). <https://doi.org/10.18196/agr.3247>
- Xiang, X., Li, Q., Khan, S. and Khalaf, O.I. 2021. Urban water resource management for sustainable environment planning using artificial intelligence techniques. *Environ. Impact Assess. Rev.*, 86: 106515. <https://doi.org/10.1016/j.eiar.2020.106515>
- Xing, L., Xue, M. and Hu, M. 2019. Dynamic simulation and assessment of the coupling coordination degree of the economy–resource–environment system: Case of Wuhan City in China. *J. Environ. Manage.*, 230: 474-487. <https://doi.org/10.1016/j.jenvman.2018.09.065>
- Xing, L., Wang, S. and Zhu, L. 2019. Environmental regulation, environmental commitment, sustainability exploration/exploitation innovation, and firm sustainable development. *Sustainability*, 11(21): 6001. <https://doi.org/10.3390/su11216001>



Accumulation and Translocation of Heavy Metals in *Hibiscus cannabinus* Grown in Tannery Sludge Amended Soil

Anita*, Mahiya Kulsoom*, Aneet Kumar Yadav*, Monu Kumar*, Kamla Pat Raw*, Satguru Prasad** and Narendra Kumar**† 

*Department of Environmental Science, Babasaheb Bhimrao Ambedkar University, Lucknow, U.P., India

**Analytical Chemistry Division, IITR-CSIR Lucknow, U.P. India

†Corresponding author: Narendra Kumar; narendrakumar_lko@yahoo.co.in

Nat. Env. & Poll. Tech.
Website: www.neptjournal.com

Received: 09-11-2023
Revised: 19-12-2023
Accepted: 26-12-2023

Key Words:

Hibiscus cannabinus
Tannery sludge
Phytoremediation
Heavy metals

ABSTRACT

Digested sludge wasted by tanneries is rich in nutrients and trace elements however, the presence of toxic metals restricts their use in agriculture. The present study explores the possible application of tannery sludge amendment for the cultivation of an energy crop, *Hibiscus cannabinus*. The toxicity of various sludge amendments (25, 50, 75, and 100%, w/w) was examined during early seedling growth, followed by metal accumulation potential by performing pot experiments. Chemical characterization revealed the presence of Cr (709.6), Cu (366.43), Ni (74.6), Cd (132.71), Pb (454.8) $\mu\text{g.g}^{-1}$ in tannery sludge beside N (2.1%), P 3.8 & K 316.96 (kg.hec⁻¹) respectively. Germination of *H. cannabinus* exposed to sludge extracts ranged between 80 to 95%; Relative seed germination, 81.33 to 84.43%. Relative root growth, 0.9 to 1.16 cm; and germination index, 95 to 110%. It was found that sludge extracts have not caused adverse effects on seed germination and early seedling growth. Heavy metal accumulation was observed as follows: Ni (3.37, 2.38, 1.46 & 0.90 mg.kg⁻¹) > Pb (10.59, 10.15, 5.26, & 2.84 mg.kg⁻¹) > Cu (2.34, 2.24, 0.97 & 0.24 mg.kg⁻¹) > Cd (2.31, 1.19, 1.33 & 1.12 mg.kg⁻¹) > Cr (1458, 1136.12, 601.73 & 211.6 mg.kg⁻¹) in 100, 75, 50, & 25% sludge amended soil, respectively. The bio-concentration pattern of metals was found to be in the order of root > leaf > stem. The findings of the present study give direction for the eco-friendly and cost-effective management of tannery sludge. Further, *H. cannabinus* can be used for the restoration of metal-contaminated agricultural land, however, results need to be corroborated with field trials.

INTRODUCTION

Environmental pollution has become an ever-growing menace encompassing the world for several decades. Different industrial processes are the main causes of significant pollution in the environment. The generation of huge amounts of by-products and waste due to rapid industrialization poses a need to explore economic, eco-friendly, and aesthetically acceptable waste disposable methods (Moshood et al. 2022). Different types of industries discharge ranges of by-products/waste, from relatively simple heavy metals to complex organic compounds that affect plant life, animals, and humans in several ways (Huang et al. 2018). Environmental monitoring and epidemiological surveys have recently shown the amount of metals in the ecosystem and biological tissues, which has raised concerns about metal exposure around the world. (Sugasini & Rajagopal 2015). While certain metals, such as Mn, Cu, Zn, Mo, and Ni, are vital or beneficial micronutrients for microbes, plants, and animals, all metals have potent toxic

effects at high levels and pose a threat to the environment (Małkowski et al. 2019).

In the current era, tanning industries are unavoidable entities around the world and have contributed significantly to economic development (Chiampo et al. 2023). India is the 6th top producer of finished leather in the world, housing more than 3000 tanneries (Rajamani 2023). Goat or sheep skins and cow or buffalo hide are the primary materials used in these tanneries. Tanneries use a lot of water along with significant amounts of both organic and inorganic chemicals. In the process of leather production for one ton of raw hide/skin, on average, about 50 to 100 m³ of wastewater and 45 to 150 kg of solid waste (dried sludge) are produced (Saira & Shanthakumar 2023). Of the solid waste, about 50% is utilized by the manufacturers of poultry feed, gelatine, glue, fish meal, and soap, and the remaining 50% is dumped indiscriminately (Nath et al. 2017). Chrome tanning or mineral tanning is the most common method of leather tanning worldwide. Chromium tanning is relatively

quick and efficient, allowing for a faster production process compared to traditional tanning methods. Considering chromium, the hides and skins absorb roughly 70% of the available amount, with the remaining 30% going into solid waste and effluent wastewater (Ma et al. 2017). Since there are inadequate or non-existent sludge disposal systems, the disposal of solid waste (sludge) is a crucial issue. Before being removed from the drying beds, the dried sludge is carelessly dumped in the industrial area without taking environmental or ecological factors into account (Alibardi & Cossu 2016). This mode of sludge disposal is so far been considered a low-cost solution, but it is extremely harmful to the terrestrial ecosystem, including life forms occupying higher trophic levels (Sunmathi et al. 2022).

Phytoremediation is the use of plants to make soil contaminants nontoxic. Alternative methods for replacing, solidifying, or washing metal-contaminated soil, the concept of employing plants that hyper-accumulate metals to selectively collect and recycle excess soil metals has been investigated as a potentially useful and more affordable method (Chaney et al. 1997). Natural metal hyper-accumulator phenotype is much more important than high yield ability when using plants to remove metals from contaminated soils (Yaashikaa et al. 2022). Remediation of heavy metals from the soil by hyper-accumulator crops needs creative research for practical application. Various researchers have shown that some species of plants grow profusely in soil contaminated by industrial waste and can accumulate potentially toxic elements (PTE), Pb, Cr, Ni, and Cd to levels several degrees higher than in the soil (Zhang et al. 2023). However, the accumulation of PTE may vary from plant to plant and soil to soil. Properties like high biomass, rapid growth, dense root network, resistance to adverse environmental conditions, etc., are required in hyper-accumulator plant species (Ahmad et al. 2023). However, soil properties like pH, organic carbon, cation exchange capacity, stages of growth of plants, and microorganisms around the root zone also influence the process of phytoremediation (Rai et al. 2023).

Kenaf (*Hibiscus cannabinus* L.) is a dicotyledon annual crop characterized by rapid growth, large biomass, strong resistance, and wide adaptability, climates and thrives with abundant solar radiation and high rainfall, minimal fertilizers and pesticides (Coetzee et al. 2008). When the circumstances are right, kenaf can grow up to 5 m tall in 6-8 months and yield up to 30 tons of dry stem material/ha. It is considered an important and multipurpose industrial crop with fibrous stems exploited for building materials, absorbent, and in industries like textile, paper, and pulp. Further, it can be used for the preparation of bio-composites, insulation mats, animal bedding, etc (Falasca et al. 2014). The kenaf has

also been explored for oil production and found to be a potential crop for energy production. The core of kenaf fiber is rich in cellulose and hemicellulose, making it suitable for the production of bio-ethanol second generation (Saba et al. 2015). Kenaf can be a good candidate to restore sites contaminated with industrial waste. Moreover, because of industrial application, the probability of transport of toxicants through the food chain is minimal.

Considering the above-mentioned facts, tannery sludge is examined for physicochemical characteristics, including analysis of potentially toxic elements that accumulate in living tissues and have detrimental effects on plants and animals. The responses of *Hibiscus cannabinus* to various combinations of industrial sludge have been studied in terms of early seedling growth. Further, bio-magnification and bio-translocation of PTE were also evaluated. The overall objective of the study was to explore the application of *Hibiscus cannabinus* in the sustainable usage of tannery sludge and the restoration of agricultural land contaminated by industrial waste.

MATERIALS AND METHODS

Sludge Collection and Sample Preparation

Tannery sludge used for the study was collected from the Common Effluent Treatment Plant (CETP) situated at Leather Technology Park, Banthar, Unnao, U.P. India. Collected sludge was air-dried at ambient room temperature and homogenized by rolling substantial aggregates to remove large slabs of sludge, plastics, etc. The homogenized sludge was brought to a fraction of less than 165 μm by grinding and sieving. Subsequently, the tannery sludge was mixed with garden soil in concentrations of 25, 50, 75, and 100% (w/w) for the pot experiment, whereas garden soil served as a control. Pot experiments were performed in five replicates, and the average were used for further analysis.

Sludge Characterization

The method proposed by Walkley & Black (1934) was used to analyze the organic matter of the soil. The Kjeldahl method (1883) was used to determine total nitrogen content. Whereas the standard Analytical Method (APHA 2005) was followed to determine pH, electrical conductivity, moisture content, total solids, organic carbon, total nitrogen, available phosphorous, and potassium. For analysis of heavy metal in soil and sludge, (1g) of samples were digested with a mixture of HCl: HNO₃ in 3:1 (v/v) (McGrath & Cunliffe 1985) and analyzed by ICP-MS (Perkin Elmer Elan DRC-e).

Phytotoxicity Test

A phytotoxicity test was performed in five replicates with

25, 50, 75, and 100% (w/v) tannery sludge extract following Zucconi et al. (1985) and Visioli et al. (2014). Whereas the corresponding strength of garden soil extract has been served as a control. Tap water has been used as a solvent to obtain sludge/soil extracts. Twenty seeds of *H. cannabinus* were placed for germination in Petri dishes lined with filter paper moistened with 10 mL of sludge/soil extracts. Relative root growth, relative seed germination, and Germination index were calculated after 72 h of germination using the method given by (Hoekstra et al. 2002) as follows:

$$\text{Relativw Seed Germination (\%)} = \frac{\text{number of seeds germinated in test}}{\text{number of seeds germinated in control}} \times 100 \quad \dots(1)$$

$$\text{Relativw Seed Growth (\%)} = \frac{\text{Root length of test plant (cm)}}{\text{Root length of control plant (cm)}} \times 100 \quad \dots(2)$$

$$\text{Germination index (GI)} = \frac{GsLs}{GcLc} \quad \dots(3)$$

Where Gs and Ls denote the seed germination (%) and root elongation (cm), respectively, and Gc and Lc are the corresponding control values. To demonstrate the comparison between different tests, the GI is expressed as a percentage in comparison to the control (100 %). A 1mm emergence of radicle has been considered seed germination.

Pot Experiment

Perforated clay pots containing 5 kg of different sludge amendments were used for pot experiments in five replicates for each sludge-soil combination. Five seeds of *H. cannabinus* were soaked overnight in deionized water before sowing. Tap/groundwater was used in surface irrigation during the plant growth.

Metal Content in Plant Samples

Plant tissues of *H. cannabinus* plants were uprooted after 120 days of exposure. Plant tissues (leaves, stems, and roots) were carefully washed with deionized water to eliminate putative material surface contamination. All plant tissues were oven-dried at 70°C for 72 h. Subsequently, ground into powder using an acid-washed porcelain mortar and pestle. 0.5 g of ground tissue material was digested to determine total metal content using ICP-MS (Perkin Elmer Elan DRC-e).

Each sample underwent digestion using the usual procedure. Using a hot plate (Jeo Tech TM-14SB) at 80°C, a known quantity (0.5 g) of each plant and soil sample was digested by 14 mL concentrated acid mixture (HCL: H₂SO₄ in 3:1 (v/v)) to achieve a transparent solution. The solutions were filtered with Whatman No. 41 filter paper and, further diluted to 25 mL with distilled water and stored at ambient temperature.

Bio-concentration, translocation, and Metal Tolerance Index

The ratio of metal concentration in plant roots or aerial tissues to that in the soil or solution is defined as the bio-concentration factor (BCF). Whereas the potential of plants to move heavy metals from the roots to the shoots is determined by the translocation factor (TF). TF and BCF were calculated as follows (Yoon et al. 2006):

$$\text{Bioconcentration} = \frac{\text{metal concentration in plant (mg/kg)}}{\text{total metal concentration in soil (mg/kg)}}$$

Using the following formula, the percentage of hazardous metals removed from phytoremediation tannery sludge was determined. Ghosh and Singh (2005).

$$\% \text{ of remaining metal } (\alpha) = \frac{\text{metal concentrated in phytoremediated soil (mg/kg)}}{\text{total metal concentration in soil (mg/kg)}} \times 100$$

$$\text{Removal of metals } (\beta)\% = 100 - \alpha$$

RESULTS AND DISCUSSION

Sludge Characterization

Standard methods were used to determine the physicochemical properties of soil and sludge samples. Each sample was evaluated in triplicate. The results are represented as average \pm standard deviation (Table 1). Sludge application increased the total metal concentration in soils. The primary

Table 1: Physico-chemical characteristics of tannery sludge and garden soil.

Parameters	Tannery sludge	Garden soil
pH	8.36 \pm 0.96	8.6 \pm 0.92
Electrical conductivity [μ S cm ⁻¹]	0.21 \pm 0.02	0.18 \pm 0.02
Organic carbon [%]	1.26 \pm 0.8	1.8 \pm 0.26
Total organic matter [mg.kg ⁻¹]	1.36 \pm 0.24	1.53 \pm 0.18
Total nitrogen [%]	2.1 \pm 0.12	1.54 \pm 0.4
Available phosphorus [kg.hec ⁻¹]	3.8 \pm 0.42	13.5 \pm 2.21
Available Potassium [kg.hec ⁻¹]	316.96 \pm 52.74	480.7 \pm 65.18
Available zinc [ppm]	4.66 \pm 0.62	5.81 \pm 0.72
Manganese [ppm]	4.15 \pm 0.62	1.39 \pm 0.18
Sulfur [ppm]	15.78 \pm 2.46	14.6 \pm 2.24
Boron [ppm]	3.03 \pm 0.46	1.9 \pm 0.20
Chromium [μ g.g ⁻¹]	709.6 \pm 15.23	0.9 \pm 0.35
Copper [μ g.g ⁻¹]	366.43 \pm 12.76	0.48 \pm 0.01
Nickel [μ g.g ⁻¹]	74.6 \pm 10.2	0.71 \pm 0.01
Cadmium [μ g.g ⁻¹]	132.71 \pm 20.1	1.1 \pm 0.026
Lead [μ g.g ⁻¹]	454.8 \pm 54.2	6.23 \pm 0.001

determinants of metal availability and uptake in soil are its physico-chemical properties, such as pH, organic matter, organic carbon, CEC, etc. the effect of organic compounds on heavy metal solubility. In addition, considerably hinges on how much of their biologically bound form of organic matter has been humified and how it influences the pH of the soil. The physicochemical characteristics of soil are known to control the fate of the metals through rhizospheric activities and to have a major effect on how plants and soil interact.

Phytotoxicity Test

Seed germination (72 h), along with other early seedling growth parameters, were analyzed at different concentrations of tannery sludge extracts (Table 2). GI less than 50% indicates high phytotoxicity, between 50 to 80% indicates moderate, and more than 80% indicates no phytotoxicity (Zucconi et al. 1985). Research shows that root length is a better indicator compared to while calculating (Bożym et al. 2021). The germination range of *H. cannabinus* was not significantly affected by sludge extract. The average root length of *H. cannabinus* was 0.99 ± 0.005 cm in control. Tap water was taken as control. The highest root length was found in 50% sludge extracts, i.e., 1.166 ± 0.05 cm, whereas the minimum was recorded in 75% concentration 0.9 ± 0.01 cm. Further, 100% concentration has a root length of 0.9133 ± 0.005 cm (Fig. 1), while 25% concentration showed 1.033 ± 0.032 cm. The germination index was found to be more than 80%, which indicates no phytotoxicity. Similar results were reported by Gonçalves et al. (2020) in *Lactuca sativa* exposed to sewage sludge. It might be explained by the increase in mineralization and availability of organic components by sludge extract (Tangredi et al. 2023).

Bio-concentration Factor

A bio-concentration factor (BCF) was calculated to determine the efficiency of *H. cannabinus* to accumulate a heavy metal from the soil. The finding of the bio-concentration factor for metals is presented in Fig. 1. The concentration of Cr was found to be the highest among all the heavy metals, followed by Ni and Cd, whereas the lowest concentration was observed of Pb, followed by Cu. The order of heavy metal uptake was

observed as $Cr > Ni > Cd > Pb > Cu$ in the tannery and garden soil. Further, the bio-concentration factor was found to be highest in plants grown in 50% sludge-amended soil. The results were observed as Cr (76%), Ni (59%), Cd (42%) & Pb (23%). The lowest bio-concentration factor was observed in 100% sludge: Cr (43%), Ni (39%), Cd (28%), Pb (14%) & Cu (12%) (Table 3). The plants' elevated concentration factor highlighted their role in the treatment of tannery sludge wastes with high metal concentrations. The ability of metal accumulation in proportion to plant biomass is referred to as the "bio-concentration factor," and it has been observed for an extensive range of plants (Zhao et al. 2020). A high metal concentration factor led to a reduction in the sludge's metal content and an improvement in the physico-chemical properties of the treated sludge (Ahmad et al. 2016).

Translocation Factor Analysis

Heavy metal distribution in different parts of cultivated plants is observed by multiplying metal concentration with dry matter. The translocation factor in plants cultivated in tannery sludge and garden soil is represented in Fig. 1. Results revealed that accumulation is higher in roots than in aerial parts of plants. Similar findings were reported by Shabani and Sayadi (2012). TF was observed higher in plants cultivated in tannery sludge than those of control soil, which was as $Cd > Cr > Cu > Pb > Ni$ and $Ni > Cr > Pb > Cu > Cd$ in tannery and control, whereas the trend of distribution of heavy metals in plant parts is root > leaf > stem in almost all the concentration of amendment of soil.

Cr was more accumulated than other studied metals. Results revealed that roots have maximum accumulation with values 128.85, 106.66, 77.44 & 32.7 ($\mu\text{g}\cdot\text{g}^{-1}$) further, minimum Cr was translocated to stem, i.e., 72.24, 55.33, 62.12 & 21.34 ($\mu\text{g}\cdot\text{g}^{-1}$) in 100, 75, 50 & 25% respectively. However, accumulation of Cr was found to be higher in leaves than in stem, and the values were recorded as 57.3, 74.13, 33.21 & 14.5 ($\mu\text{g}\cdot\text{g}^{-1}$) in 100, 75, 50, & 25%, correspondingly. Toxicity of Cr affects yield and root growth, further causing a mutagenic impact. Reported toxicity ranges from 10-100 $\text{mg}\cdot\text{kg}^{-1}$ (Kabata-Pendis & Pendias 2011). Results revealed that 100, 75, and 50%

Table 2: Effect of tannery sludge extract on Relative seed germination (RSG), relative root growth (RRG), and germination index (GI) of *H. cannabinus*.

Concentration	Germination [%]	RRG [cm]	RSG [%]	GI [%]
Control	80	100 ± 0.0	100 ± 0.0	100 ± 0.0
100	95 ± 1.13	0.91 ± 0.01	84.43 ± 0.51	87.07 ± 0.94
75	80 ± 1.23	0.9 ± 0.01	82.36 ± 0.55	84.02 ± 1.15
50	90 ± 0.41	1.16 ± 0.05	84 ± 1.52	90.38 ± 1.27
25	80 ± 0.15	1.03 ± 0.03	81.33 ± 1.15	76.21 ± 0.94

Table 3: Total heavy metal accumulation in *H. cannabinus* grown in garden and tannery sludge amended soil ($\mu\text{g}\cdot\text{mg}^{-1}$).

Heavy metals	Cr	Metal removal [%]	Cd	Metal removal [%]	Ni	Metal removal [%]	Pb	Metal removal [%]	Cu	Metal removal [%]
Control	0.9 ±0.35	38	0.31 ±0.026	39	0.71±0.01	71	1.1 ±0.02	29	6.23±0.01	17
Uptake in plant	0.50±0.032		0.096±0.01		0.50±0.01		0.31±0.01		1.04±0.34	
25% Amended soil	120.21±23.2	57	41.21±9.56	42	19.87±2.12	57	128.32±32.1	19	84.2±12.1	29
Uptake in plant	68.5±7.21		17.30±4.32		11.32±3.21		24.3±7.2		23.58±7.81	
50% Amended soil	228.22±42.11	76	88.43±23.11	58	42.4±8.5	59	254.87±32.21	46	168.84±21.1	28
Uptake in plant	173.28±32.91		51.28±7.12		25.01±4.87		58.62±8.42		47.27±9.12	
75% Amended soil	582±88.11	41	103.22±21.1	32	62.11±13.4	45	381.32±43.2	16	284.11±25.1	12
Uptake in plant	236.12±54.7		33.03±6.78		27.9±11.12		61.01±12.11		42.61±12.11	
100% Amended soil	709.6±15.2	37	132.71 ±20.1	28	74.6±10.2	39	454.8±54.2	14	366.43±12.76	12
Uptake in plant	258.03±20.62		37.15±11.12		29.09±6.5		63.67±12.1		43.97±13.9	

concentrations of Cr accumulation were above the toxicity range.

In tannery sludge amended soil, heavy metal Ni was maximum accumulated after Cr. Translocation observed in root were 14.05, 13.97, 11.62 & 5.031 ($\mu\text{g}\cdot\text{g}^{-1}$) in 100, 75, 50, & 25%, respectively. Further minimum translocation was observed in leaves of plants grown in 100 and 75% concentration whereas, in 50 and 25%, it was kept in the stem part with values 9.4 & 4.31, respectively.

Cd was found to be less accumulated than Cr & Ni among the studied metals. Maximum accumulation was observed in the root, i.e., 15.2, 13.3, 27.69 & 7.81 in the concentration of 100, 75, 50 & 25%, respectively. Whereas minimum accumulation was observed in stem 7.60, 14.42 & 5.22 in 100, 50 & 25% sludge amendment. While leaf metal accumulated more than stem at 100 & 25 % with values 6.3 & 5.22 ($\mu\text{g}\cdot\text{g}^{-1}$), whereas accumulation values were equal in 50% concentration, i.e., 9.32 $\text{mg}\cdot\text{kg}^{-1}$, and at 75% sludge strength. Stem accumulated more metal compared to leaf. Cd is a highly toxic element that impacts germination, metabolism, and water status in plants and also causes a reduction in plant biomass. The toxicity range of Cd was reported to be 5-30 $\text{mg}\cdot\text{kg}^{-1}$ (Kabata-Pendias & Pendias 2011, Eid et al. 2016).

Lead was found lesser accumulated than Cr, Ni & Cd. Results revealed that in 100% concentration, metal accumulated maximum in the root (6.5 $\text{mg}\cdot\text{kg}^{-1}$) and minimum in the stem area (14.0 $\mu\text{g}\cdot\text{g}^{-1}$) whereas leaves exhibited accumulation more than the stem, i.e., 18.23 $\mu\text{g}\cdot\text{g}^{-1}$. In 75% sludge amended soil, the values are found to be 25.66 (root), 18.2 (leaf), and 17.2 (stem); similarly, in 50%, it was found to be 26.9 (leaf), 18.1 (root), and 13.2 (stem), further, in 25% it was observed as 11.7 (root), 6.32 (leaf) and 5.01 (stem). Plants absorb Pb, but it is not an essential element for any significant biological function, rather a toxic element for plants if found in a range of 30-300 $\text{mg}\cdot\text{kg}^{-1}$ (Nawab et al. 2015, Kabata-Pendias & Pendias 2011).

Cu was accumulated in a relatively lower amount than other observed metals. Results showed values accumulated in root were 20.3, 19.2, 20.03 & 23.5 $\mu\text{g}\cdot\text{g}^{-1}$ in concentrations of 100, 75, 50 & 25%, respectively, whereas 09.23, 10.58 & 11.19 $\mu\text{g}\cdot\text{g}^{-1}$ was accumulated in leaf and 0.43, 0.53 & 0.25 $\mu\text{g}\cdot\text{g}^{-1}$ accumulated in stem area of plant grown in 100, 75, 50% sludge respectively.

Further, the maximum accumulation of metal in plants cultivated in garden soil was observed in Cd, and a translocation trend of metal was found in the root (0.02) = leaf (0.02) > stem (0.015 $\mu\text{g}\cdot\text{g}^{-1}$). Cu showed less accumulation than Cd, and the trend of translocation is as follows: root (0.44) > leaf (0.33) > stem (0.26) $\text{mg}\cdot\text{kg}^{-1}$. Whereas Pb was

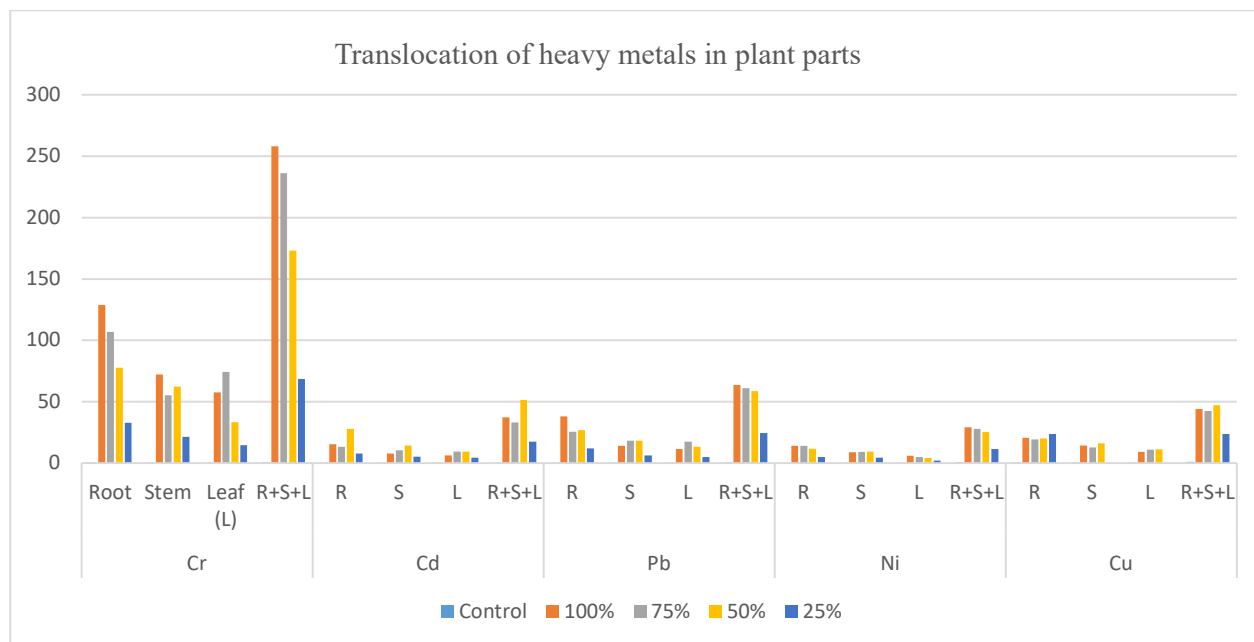


Fig.1: Heavy metal concentration in different parts of plant cultivated in garden and tannery sludge amended soil ($\mu\text{g.kg}^{-1}$).

found to be less accumulated than Cd and Cu, and it was found to be $0.19 > 0.17 > 0.12 \mu\text{g.g}^{-1}$ in root, leaf & stem, respectively. Further, Cr and Ni were found to be minimum accumulated, and values are as follows: $0.13 \text{ \& } 0.19 \text{ (root)} > 0.09 \text{ \& } 0.15 \text{ (leaf)} > 0.14 \text{ \& } 0.09 \mu\text{g.g}^{-1}$ (stem), respectively. Heavy metals are highly leachable; they are more likely to enter the environment and become available for uptake by plants (Kumar et al. 2013).

CONCLUSION

Utilization of tannery sludge in the agricultural field owing to the availability of essential nutrients can be an attractive alternative. However, the study revealed the presence of high levels of Cr (709 mg.kg^{-1}) and other metals (e.g., Cu, Ni, Pb, and Cd), which can be a hindrance. Noticeably, some plants have adapted over time to the locally elevated metal levels. Results exhibited that *H. cannabinus* is tolerant towards tannery sludge leachate during germination and early seedling growth and, consequently, can be grown in tannery sludge-amended soil. Efficient bioaccumulation and translocation of toxic metals from sludge-amended soil to roots and subsequently to aerial parts counteracted in this study gives direction for the application of *H. cannabinus* for reclamation of land contaminated with industrial waste/heavy metals.

ACKNOWLEDGEMENT

The author thankfully acknowledges the financial support received by the University Grant Commission (UGC), New

Delhi, in the form of the National Fellowship for Scheduled Caste Students (UGC-Ref. No.: 210510518471)

REFERENCES

- Ahmad, I., Gul, I., Irum, S., Manzoor, M. and Arshad, M. 2023. Accumulation of heavy metals in wild plants collected from the industrial sites-potential for phytoremediation. *Int. J. Environ. Sci. Technol.*, 20(5): 5441-5452.
- Ahmad, T., Ahmad, K. and Alam, M. 2016. Sustainable management of water treatment sludge through 3 'R' concept. *J. Clean. Prod.*, 124: 1-13.
- Alibardi, L. and Cossu, R. 2016. Pre-treatment of tannery sludge for sustainable landfilling. *Waste Manage.*, 52: 202-211.
- APHA. 2005. *Standard Methods of Water and Wastewater*. 21st Edition, American Public Health Association, Washington, DC.
- Bozym, M., Król, A. and Mizerna, K. 2021. Leachate and contact test with *Lepidium sativum* L. to assess the phytotoxicity of waste. *Int. J. Environ. Sci. Technol.*, 18: 1975-1990.
- Chaney, R.L., Angle, J.S., McIntosh, M.S., Reeves, R.D., Li, Y.M., Brewer, E.P., Chen, K.Y., Roseberg, R.J., Perner, H., Synkowski, E.C. and Broadhurst, C.L. 2005. Using hyperaccumulator plants to phytoextract soil Ni and Cd. *Z Naturforsch C*, 60(3-4): 190-198.
- Chiampo, F., Shanthakumar, S., Ricky, R. and Ganapathy, G.P. 2023. Tannery: Environmental impacts and sustainable technologies. *Mater. Today Proc.*, 56: 111-121.
- Coetzee, R., Labuschagne, M.T. and Hugo, A. 2008. Fatty acid and oil variation in seed from kenaf (*Hibiscus cannabinus* L.). *Industrial Crops and Products*, 27(1): 104-109.
- Gonçalves, M.D.C, de Almeida Lopes, A.C., Gomes, R.L.F., de Melo, W.J., Araujo, A.S.F., Pinheiro, J.B. and Marin-Morales, M.A. 2020. Phytotoxicity and cytogenotoxicity of composted tannery sludge. *Environ. Sci. Pollut. Res.*, 27: 34495-34502.
- Eid, E.M., Shaltout, K.H., Alamri, S.A., Sewelam, N.A. and Galal, T.M. 2020. Uptake prediction of ten heavy metals by *Corchorus olitorius* L. cultivated in soil mixed with sewage sludge. *Food Energy Secur.*, 9(3): e203.

- Falasca, S.L., Ulberich, A.C. and Pitta-Alvarez, S. 2014. Possibilities for growing kenaf (*Hibiscus cannabinus* L.) in Argentina as biomass feedstock under dry-subhumid and semiarid climate conditions. *Biomass and bioenergy*, 64: 70-80.
- Ghosh, S. and Singh, P. 2005. Comparative uptake and phytoextraction study of soil induced chromium by accumulator and high biomass weed species. *Appl. Ecol. Environ. Res.*, 3: 67-79.
- Hoekstra, N.J., Bosker, T. and Lantinga, E.A. 2002. Effects of cattle dung from farms with different feeding strategies on germination and initial root growth of cress (*Lepidium sativum* L.). *Agric. Ecosyst. Environ.*, 93(1-3): 189-196. [https://doi.org/10.1016/S0167-8809\(01\)00348-6](https://doi.org/10.1016/S0167-8809(01)00348-6)
- Huang, J., Guo, S., Zeng, G.M., Li, F., Gu, Y., Shi, Y. and Peng, S. 2018. A new exploration of health risk assessment quantification from sources of soil heavy metals under different land use. *Environ. Pollut.*, 243: 49-58.
- Kabata-Pendias, A. and Pendias, H. 2001. *Trace Elements in Soil and Plants*. Third edition. CRC Press, Boca Raton.
- Kumar, N., Baudh, K., Kumar, S., Dwivedi, N., Singh, D.P. and Barman, S.C. 2013. Extractability and phytotoxicity of heavy metals present in petrochemical industry sludge. *Clean Technol. Environ. Policy*, 15: 1033-1039.
- Ma, H., Zhou, J., Hua, L., Cheng, F., Zhou, L. and Qiao, X. 2017. Chromium recovery from tannery sludge by bioleaching and its reuse in the tanning process. *J. Clean. Prod.*, 142: 2752-2760.
- Malkowski, E., Sitko, K., Zieleźnik-Rusinowska, P., Gieroń, Ż. and Szopiński, M. 2019. Heavy metal toxicity: Physiological implications of metal toxicity in plants. *Plant Metallomics Funct. Omics Syst. Perspect.*, 71: 253-301.
- McGrath, S.P. and Cunliffe, C.H. 1985. A simplified method for the extraction of the metals Fe, Zn, Cu, Ni, Cd, Pb, Cr, Co, and Mn from soils and sewage sludges. *J. Sci. Food Agric.*, 36(9): 794-798.
- Moshood, T.D., Nawadir, G., Mahmud, F., Mohamad, F., Ahmad, M.H. and AbdulGhani, A. 2022. Sustainability of biodegradable plastics: New problem or solution to solve the global plastic pollution. *Curr. Res. Green Sustain. Chem.*, 5: 100273.
- Nath, K., Singh, B.P., Singh, D. and Sharma, Y.K. 2017. Effect of tannery effluent on morphological parameters and metal accumulation in spinach plant. *Res. Environ. Life Sci.*, 2(4): 211-214.
- Nawab, J., Khan, S., Shah, M.T., Khan, K., Huang, Q. and Ali, R. 2015. Quantification of heavy metals in mining-affected soil and their bioaccumulation in native plant species. *Int. J. Phytorem.*, 17(9): 801-813.
- Rai, P.K., Sonne, C. and Kim, K.H. 2023. Heavy metals and arsenic stress in food crops: Elucidating antioxidative defense mechanisms in hyperaccumulators for food security, agricultural sustainability, and human health. *Sci. Total Environ.*, 874: 162327.
- Rajamani, S. 2022. Innovative cleaner leather production process and environmental protection. *Fasc. Text. Leatherwork*, 5: 95.
- Saba, N., Jawaid, M., Hakeem, K.R., Paridah, M.T., Khalina, A. and Alothman, O.Y. 2015. Potential of bioenergy production from industrial kenaf (*Hibiscus cannabinus* L.) based on Malaysian perspective. *Renew. Sustain. Energy Rev.*, 42: 446-459.
- Saira, G.C. and Shanthakumar, S. 2023. Zero waste discharge in tannery industries—An achievable reality? A recent review. *J. Environ. Manage.*, 335: 117508.
- Shabani, N. and Sayadi, M.H. 2012. Evaluation of heavy metals accumulation by two emergent macrophytes from the polluted soil: an experimental study. *Environment*, 32: 91-98.
- Sugasini, A. and Rajagopal, K. 2015. Characterization of physicochemical parameters and heavy metal analysis of tannery effluent. *Int. J. Curr. Microbiol. Appl. Sci.*, 4(9): 349-359.
- Sunmathi, N., Padmapriya, R., Sudarsan, J.S. and Nithiyantham, S. 2022. Optimum utilization and resource recovery of tannery sludge: a review. *Int. J. Environ. Sci. Technol.*, 41: 1-10.
- Tangredi, A., Barca, C., Ferrasse, J.H. and Boutin, O. 2023. Effect of process parameters on phosphorus conversion pathways during hydrothermal treatment of sewage sludge: A review. *Chem. Eng. J.*, 463: 142342.
- Visioli, G., Conti, F.D., Gardi, C. and Menta, C. 2014. Germination and root elongation bioassays in six different plant species for testing Ni contamination in soil. *Bull. Environ. Contam. Toxicol.*, 92: 490-496. DOI 10.1007/s00128-013-1166-5
- Walkley, A. and Black, I.A. 1934. An examination of the Degtjareff method for determining soil organic matter and a proposed modification of the chromic acid titration method. *Soil Sci.*, 37(1): 29-38.
- Yaashikaa, P.R., Kumar, P.S., Jeevanantham, S. and Saravanan, R. 2022. A review on bioremediation approach for heavy metal detoxification and accumulation in plants. *Environ. Pollut.*, 301: 119035.
- Yoon, J., Cao, X., Zhou, Q. and Ma, L.Q. 2006. Accumulation of Pb, Cu, and Zn in native plants growing on a contaminated Florida site. *Sci. Total Environ.*, 368(2-3): 456-464.
- Zhang, M., He, T. and Jin, B. 2023. Effect of mineral additives on pyrolytic characteristics and heavy metal behavior during co-pyrolysis of industrial sludge and hyperaccumulator plant. *J. Anal. Appl. Pyrolysis*, 169: 105827.
- Zhao, M., Zeng, S., Liu, S., Li, Z. and Jing, L. 2020. Metal accumulation by plants growing in China: Capacity, synergy, and moderator effects. *Ecol. Eng.*, 148: 105790.
- Zucconi, F., Monaco, A. and Forte, M. 1985. Phytotoxins during the stabilization of organic matter. In: Gasser J.K.R. Ed.), *Composting of Agric. and other Wastes*. Elsevier Applied Sci. Publ., New York, NY, U.S.A., pp. 73-86.

ORCID DETAILS OF THE AUTHORS

Narendra Kumar: <https://orcid.org/0000-0002-3749-664X>



Beachgoers' Knowledge, Perceptions, and Willingness to Pay for Sustainable Waste Management in Kuakata Sea Beach, Bangladesh

Md. Al Amin*†  and Md. Tanvir Ahmed** 

*Department of Agricultural and Applied Economics, University of Georgia, Athens, GA 30602, United States of America

**Department of Economics, University of Barishal, Barishal-8254, Bangladesh

†Corresponding author: Md. Al Amin; ma99587@uga.edu

Nat. Env. & Poll. Tech.
Website: www.neptjournal.com

Received: 26-10-2023

Revised: 08-12-2023

Accepted: 17-12-2023

Key Words:

Waste management
Logistic regression
Sustainability

ABSTRACT

With rising public awareness and concern for environmental sustainability, calls for nature-friendly marine and beach litter management have grown louder. This study, employing logistic and ordinary least square regressions, explores tourists' knowledge, perceptions, and willingness to pay (WTP) using data ($n = 400$) collected from Kuakata Sea Beach, Bangladesh. Results showed that approximately 99% of the respondents recognize the urgency for further development in the waste management system, while 53% are aware of it. Gender is identified as a statistically significant factor impacting beachgoers' WTP – males are willing to pay more. Besides, visitors with higher incomes demonstrate the willingness to pay more. Additionally, 37% of the respondents think that appropriate information dissemination and raising awareness are critical to confronting this problem, and another 38% recommended proper placement of dustbins on the beach. These outcomes can be very useful in designing any relevant policies for promoting sustainable beach waste management.

INTRODUCTION

Tourism plays a crucial role in generating income and contributes immensely to the economic development of the countries around the globe. Tourism is frequently considered an essential mechanism for a country's economic expansion and societal evolution (Brida & Risso 2009), boosting the economic well-being of the local population (Tang & Tan 2015). Many nations have established tourist hotspots and generated significant foreign currency from tourism earnings, as the World Tourism Organization (UNWTO 2019) reported, accounting for 29% of global service exports and 7% of overall exports of goods and services. Globally, tourism significantly contributed to the economy, accounting for 10.3% of GDP in 2019, the pre-covid time. In recent years, the tourism industry in Bangladesh has shown significant growth, which has boosted the country's economy. The number of foreign tourists visiting Bangladesh increased by 13.6% in 2019, with a total of 2.1 million visitors compared to 1.9 million in 2018 (Bangladesh Tourism Board 2019). The overall contribution of travel and tourism to Bangladesh's GDP was approximately BDT 809.6 billion, equivalent to 4.7% of the country's total GDP. This figure is anticipated to continue to grow annually by 6.4%, reaching BDT 1,596 billion, equivalent to 5% of the total GDP by 2026 (WTTC 2015).

Kuakata Sea Beach, the second longest sea beach in Bangladesh, is considered one of the country's most popular tourist destinations and has seen a significant surge of domestic and international travel enthusiasts, vacationers, and beachgoers recently. Despite its positive economic impact, tourism exerts a huge negative environmental burden on local ecosystems and poses serious threats to environmental sustainability. Tourism's consumption of natural resources in popular destinations can lead to dire social and environmental catastrophes (Camarda & Grassini 2003). With increased tourist activities, a large amount of waste is generated, contributing to global climate changes and public health challenges as the tourism sector acts as a primary source of CO₂ emissions, particularly in low-income countries (Haseeb & Azam 2021). According to research conducted by the UN Environment, the tourism industry's consumption of vital resources, such as water and energy, is increasing in proportion to its production of solid waste, including marine plastic pollution, sewage, greenhouse gas emissions, and biodiversity loss. Due to our addiction to plastics, some of the world's most stunning beaches have encountered dire consequences (UNEP 2021). Numerous beaches in Bangladesh, including Kuakata, have been inundated with piles of plastic waste. Kuakata Beach has been losing its potential as a tourist attraction because of plastic pollution and the disappearance of livestock resulting from

uncontrolled tourism (The Business Standard 2021). The lack of appropriate waste management practices in Kuakata has led to significant environmental deterioration, including the accumulation of solid waste, which can negatively impact the tourism industry and local community. Consequently, waste management has surfaced as a critical issue for sustainable tourism in this area.

Understanding tourists' willingness to pay (WTP) for sustainable waste management at Kuakata Sea Beach can offer valuable insights into the demand for environmental services and the potential for financing sustainable tourism management and promotion. WTP is a metric that gauges the maximum amount of money an individual is willing to spend on a specific good or service, indicating the perceived value of that good or service. Sustainable waste management at Kuakata Sea Beach is an intricate dilemma involving multiple stakeholders, tourists, residents, businesses, and government entities. Unfortunately, the lack of appropriate infrastructure and awareness among tourists and locals has led to greater environmental catastrophes in this area.

Despite extensive global research, there has yet to be research on tourists' WTP for sustainable waste management, specifically in Bangladesh's Kuakata and other sea beaches. This knowledge gap poses a grave challenge for policymakers and stakeholders in developing effective, pragmatic, and nature-friendly regional waste management systems and policies. Therefore, the implementation of sustainable waste management practices at tourist destinations such as Kuakata is crucial for preserving the environment quality and sustaining the tourism industry. In this study, our goal is to identify the factors influencing tourists' attitudes and behaviors towards sustainable waste management in the context of a developing country and provide recommendations for promoting sustainable waste management practices in tourist destinations across Bangladesh. This research delves deeper into tourists' knowledge, perception, and willingness to pay for sustainable waste management at Kuakata Sea Beach in Bangladesh using the Contingent Valuation Method (CVM). Additionally, this study examines various factors influencing tourists' WTP, including demographic characteristics, travel patterns, and environmental literacy, and their implications for fostering sustainable development in the tourism sector in the country.

Never before has the world experienced this kind of precarious environmental challenge. As public awareness and concern for the environment has grown, the issue of marine and beach litter has become more prominent. This type of litter, mainly composed of plastics, originates from various types of waste and can pose considerable dangers to wildlife and humans. Current recycling policies are deemed

insufficient to address this issue, necessitating a global approach to prevent oceanic waste. Studies have highlighted plastics as the primary contaminant in Bangladeshi marine ecosystems, underscoring the significance of coastal management strategies. A sustainable waste management system is increasingly crucial in tourism, especially in renowned tourist destinations like Kuakata Beach Beach, Bangladesh. The impact of waste management approaches on the environment and the tourism experience is explored in a wide range of global studies and reports. Kaza et al. (2018) present an overview of the global solid waste management issue, shedding light on the magnitude of this issue. According to Agyeiwaah et al. (2017), sustainable tourism is defined by key indicators that offer valuable insights into waste management practices.

Moreover, studies conducted by Torres-Delgado & Saarinen (2017) provide us with the frameworks for assessing sustainable tourism development. Furthermore, Budeanu et al. (2016) offer frameworks to evaluate sustainable tourism development and identify the associated challenges and opportunities. Pan et al. (2018) highlight the advancements and hurdles in sustainable tourism, focusing on its contribution to a green economy and offering relevant context. To gain a local perspective, Islam (2015) and Mondal (2017) explore sustainable tourism strategies in Bangladesh. Additionally, studies by Das et al. (2019) and Rodić & Wilson (2017) underscore solid waste management challenges and governance issues, serving the need for researching sustainable waste management practices at Kuakata Sea Beach in Bangladesh.

Liu et al. (2019) find that 80.8% of tourists are willing to pay to safeguard beach tourism resources in Qingdao and China, with factors such as gender and frequency of travel significantly influencing their willingness to pay. The researchers estimate the non-use value of beach tourism resources in the region to be \$0.8 billion. Another study conducted by Halkos & Matsiori (2012) examines various factors that affect people's willingness to pay for enhancing coastal zone quality, such as environmental and recreational activities. The study emphasizes that previous experience of participation in environmental protection programs and individual characteristics, such as Income and age, significantly impact the willingness to pay. According to Rodella et al. (2019), tourists are willing to pay an average of €14.84 per year per user to preserve beach quality on Italian beaches, with natural beaches having the highest value. The study also found that beach typologies, level of urbanization, and lack of knowledge of beach management and related issues influenced tourists' WTP.

Moreover, the findings from contingent valuation and

choice experiment models to evaluate the social costs of marine litter in China demonstrated that visitors' willingness to pay for removing marine litter ranged from USD 0.12-0.20 per person, whereas the social costs of marine litter varied from USD 1.00-1.40 per person, indicating 8-14% of the beach entrance fee. This study highlights the importance of additional entrance fees and environmental strategies that prioritize quality and incentives to encourage volunteerism. The results showed that over 70% of the respondents were willing to pay for environmental preservation, and the amount varied based on beach quality. However, a lack of trust in the fee collection agency and uncertainty about how money will be used can discourage individuals from contributing (Peters & Hawkins 2009). Al-Amin et al. (2021) analyzed wetland ecosystem services in northeastern Bangladesh by studying the perspectives of local experts and the community. They found that these services met the diverse needs of nearby communities. However, only 25% of the respondents expressed an interest in cash payments for conservation, while 45% were willing to contribute through volunteering.

International tourists' perspectives on beach cleanup exercises should be addressed despite their contribution to and impact on beach litter. A total of 685 tourists are surveyed in Ghana to examine their perceptions of beach litter and willingness to participate in cleanup activities. The results show that tourists have negative perceptions of the impact of litter on health, recreation, aesthetics, and the environment. Factors such as age, gender, education, travel party status, and environmental values significantly influence the willingness to participate. This study highlights the need to involve tourists in beach litter management at coastal destinations (Adam 2021). Tourists can influence the sustainability notion of popular tourism attractions significantly. Their knowledge, awareness, and perceptions about sustainable waste dumping practices can deeply shape their actions and expectations towards the destination. For example, a study conducted by Lee and Jan (2015) finds that visitors who have positive experiences in a destination tend to adopt pro-environmental attitudes and biospheric values, meaning that they are more likely to engage in environmentally responsible behavior, like disposing of, recycling, and minimizing their waste in a nature-friendly manner. A separate investigation conducted by Hall et al. (2016) found that tourists' perceptions of sustainable practices within the hospitality and tourism management industry can enormously impact their decision-making activities. For instance, tourists who are aware of the environmental impacts of single-use plastics might be inclined to choose hotels that offer reusable water bottles. Siyambalapatiya et al. (2018) also highlight the importance of green human resource management in advancing

sustainability within the tourism sector, indicating that businesses should hire and train employees who possess a strong understanding of the environmental aspect of their work and are dedicated to sustainable practices.

Iqbal & Hossain (2023) evaluate the extent to which tourists would pay to restore Sundarban mangrove forest ecosystems in Bangladesh, the largest mangrove forest in the world, by collecting data from 607 tourists. The results showed that, on average, tourists were willing to pay BDT 64.54 for the restoration initiatives, which could generate an annual revenue of BDT 11.81 billion. The WTP is affected by tourists' age, monthly Income, and years of schooling. To understand tourists' perceptions of sustainable waste management and willingness to pay (WTP), we conducted this study using the contingent valuation method (CVM). CVM is a survey-based method to estimate the value of non-market goods and services (Orlowski & Wicker 2019). This method involves asking respondents to state how much they would be willing to pay for a particular good or service, even if it is not currently accessible and no market exists for the good. There are several reasons for employing the CVM in our study. Firstly, it is a well-established method used in diverse scenarios (Bennett et al. 2018, Damigos et al. 2016). Secondly, it enables us to capture the full range of values that visitors may place on sustainable waste management, encompassing both use and non-use values (Andersson et al. 2012, Nandagiri 2015). Thirdly, CVM is a cost-effective method to administer (Haab et al. 2013, Weimer et al. 2019, McIntosh 2013). Consequently, CVM is the best way to assess tourists' WTP concerning sustainable waste management at Kuakata Sea Beach, as it allows us to get a direct and unbiased estimation of their willingness to pay without being affected by other factors.

MATERIALS AND METHODS

In this study, we employed a robust methodology to gather comprehensive data from 400 tourists visiting Kuakata Sea Beach. Using the Taro Yamane method, we determined the sample size (n) as follows:

$$n = \frac{N}{1 + N(e^2)}$$

Where N represents the population size (approximately 13500 (The Daily Star 2022)), and e represents the desired precision level (5%). The sample size based on the formula is 388. For convenience, we interviewed 400 individuals to collect the data. We can ensure that having this sample size ensures an adequate representation of the total population and increases the study's reliability.

To ensure the quality and fairness of data collection, we

employed trained enumerators who carried out face-to-face interviews with the tourists by being physically present in the Kuakata sea beach. Enumerators underwent thorough training to reduce the possibility of any biases in data collection, emphasizing the importance of neutrality and consistency in their interactions with the survey respondents.

We structured our questionnaire into three sections to cover various aspects of beachgoers' perspectives, knowledge, and behaviors. Part A was designed to collect data about the tourists' socioeconomic profiles and travel patterns. Part B delved into their knowledge and perceptions regarding sustainable beach waste management, investigating their awareness and attitudes toward this critical issue. Finally, Part C focused on tourists' Willingness to Pay (WTP) for beach litter management and proper disposal.

To assess tourists' WTP for sustainable waste management, we adopted a statistical method using the following logistic regression model, denoted by equation 1.

$$\ln \left[\frac{p}{1-p} \right] = \beta_0 + \beta_1 x_1 + \beta_2 x_2 + \beta_3 x_3 + \beta_4 x_4 + \beta_5 x_5 + \varepsilon \quad \dots(1)$$

Where p is the probability of willingness to pay and $\ln \left[\frac{p}{1-p} \right]$ is the logarithm of odd ratios of individuals' WTP. The regression coefficients $\beta_0, \beta_1, \beta_2, \beta_3, \beta_4$ and β_5 are associated with the intercept, gender, age, educational attainment, occupation, and Income, respectively.

In order to quantify the correlation between beachgoers' willingness to contribute to sustainable waste management and relevant demographic variables financially, we employed an Ordinary Least Squares (OLS) regression analysis, expressed by equation 2.

$$WTP = \beta_0 + \beta_1 \text{Gender} + \beta_2 \text{Age} + \beta_3 \text{Education} + \beta_4 \text{Occupation} + \beta_5 \text{Income} + \beta \quad \dots(2)$$

Where WTP represents beachgoers' willingness to pay for sustainable waste management measured in BDT per day, gender is a binary variable (1 for male and 0 for female). Education is a binary variable indicating whether the individual has graduated (1 for complete and 0 for incomplete). Occupation is a binary variable denoting employment status (1 for employed and 0 for unemployed). Income indicates the monthly Income of the beachgoer in BDT. β_0 is the intercept. $\beta_1, \beta_2, \beta_3, \beta_4,$ and β_5 are the parameters associated with gender, age, education, occupation, and Income.

These models enable us to analyze the relationships between WTP and relevant socioeconomic characteristics, revealing the factors influencing tourists' WTP in effective beach litter management practices. By employing this robust

methodology, we aim to provide valuable insights into tourists' preferences and motivations, contributing to the development of sustainable waste management strategies for Kuakata Sea Beach and similar coastal tourist destinations.

RESULTS AND DISCUSSION

In the context of our study conducted at Kuakata Sea Beach, Bangladesh, a comprehensive analysis of the socioeconomic characteristics of tourists was undertaken to provide a more profound understanding of the socio-demographics of the targeted population. The outcomes of the analysis reveal several noteworthy patterns within the sampled visitors. As shown in Table 1, the gender distribution highlights a clear majority of male respondents, comprising 73.6% of the total sample, while counterparts account for 26.5%. As for the age distribution, the data demonstrate that individuals between the ages of 31 and 65 constitute the largest group, representing 44% of the total, followed by the 19-30 age group at 38.25%. Remarkably, there are no respondents aged above 65 in our sample. In terms of educational attainment, a substantial proportion of beachgoers achieve graduation (34%) and higher secondary education (29%), while only 7.25% of interviewees have completed primary schooling. The distribution of educational background by stream, as depicted in Fig. 1, provides that among seaside visitors, a significant proportion of those with secondary education have backgrounds in science (34.68%), whereas those with higher secondary and graduation-level education are more evenly distributed across Science, Business, and Humanities streams.

Regarding occupation, the majority of participants identified as students (44.75%), followed by the unemployed (27.5%) and employed (16.25%). A smaller fraction identified as retired (9.75%), homemaker (0.5%), or fell into other occupational categories (0.25%). Concerning income levels, the majority of the targeted population (44.5%) report an income of less than BDT20,000, with only a tiny proportion reporting an income exceeding BDT100,000. These demographic statistics offer valuable insights into the composition of the beachgoing population at Kuakata Sea Beach, serving as a foundation for tailored strategies for sustainable waste management initiatives and related undertakings.

The travel pattern of the tourists at Kuakata Sea Beach is analyzed through a set of inquiries outlined in Table 2. The initial inquiry aims at ascertaining whether participants previously visited Kuakata Sea Beach, with 53% answering affirmatively. Among those who had visited before, their frequency of prior visits was analyzed, revealing that 48% visited 1-2 times, 24% came 3-5 times, and 28% toured more

Table 1: Socioeconomic Characteristics.

Socioeconomic Characteristics	Classes	Frequency	Proportion of total [%]
Gender	Male	294	73.6
	Female	106	26.5
Age (years)	<19	71	17.75
	19–30	153	38.25
	31–65	176	44
	>65	0	0
Education	Primary	29	7.25
	Secondary	64	16
	Higher Secondary	116	29
	Graduation	136	34
	Post-Graduation	55	13.75
Occupation	Student	179	44.75
	Employed	69	16.25
	Unemployed	110	27.5
	Homemaker	2	0.5
	Retired	39	9.75
	Others	1	0.25
Income (BDT in thousand per month)	<20	178	44.5
	21-30	72	18
	31-40	82	20.5
	41-50	52	13
	51-70	14	3.5
	71-100	1	0.25
	>100	1	0.25

than 5 times. Respondents were also asked about their travel habits to other sea beaches apart from Kuakata, with 58% acknowledging such travels. In terms of transportation to Kuakata Sea Beach, 14% chose private cars, 73% relied on public buses, 8% opted for motorcycles, and 5% preferred other means. The duration of their typical stay at Kuakata Sea Beach varied, with 11% spending less than a day, 87% staying 1-2 days, and 3% enjoying a 3–5-day visit, while a mere 1% extended more than 5 days. Their trips' primary motive was leisure (87%), with only 3% indicating business purposes, 10% for family gatherings, and a minor 1% for other motivations. Regarding accommodation choices, 96% preferred hotels or resorts, 2% opted for guesthouses or homestays, and 2% made other accommodation arrangements. Regarding daily expenditure, 53% spent less than 1 thousand Bangladeshi Taka, 43% allocated between 1-3 thousand Taka, 3% expended 3-5 thousand Taka, and only 1% exceeded 5 thousand Taka. Additionally, 53% of respondents demonstrated awareness of waste management initiatives at Kuakata Sea Beach, while only 3% had actively participated in beach cleanup activities. These findings provide a valuable understanding of the travel patterns and behaviors of Kuakata's beach visitors, which are essential for comprehending their knowledge, perceptions, and willingness to pay for sustainable waste management initiatives in the region.

Table 3 comprehensively analyzes tourists' knowledge and outlook concerning sustainable waste management at Kuakata Sea Beach, Bangladesh. The data highlights a strong consensus among survey participants, with 99% recognizing

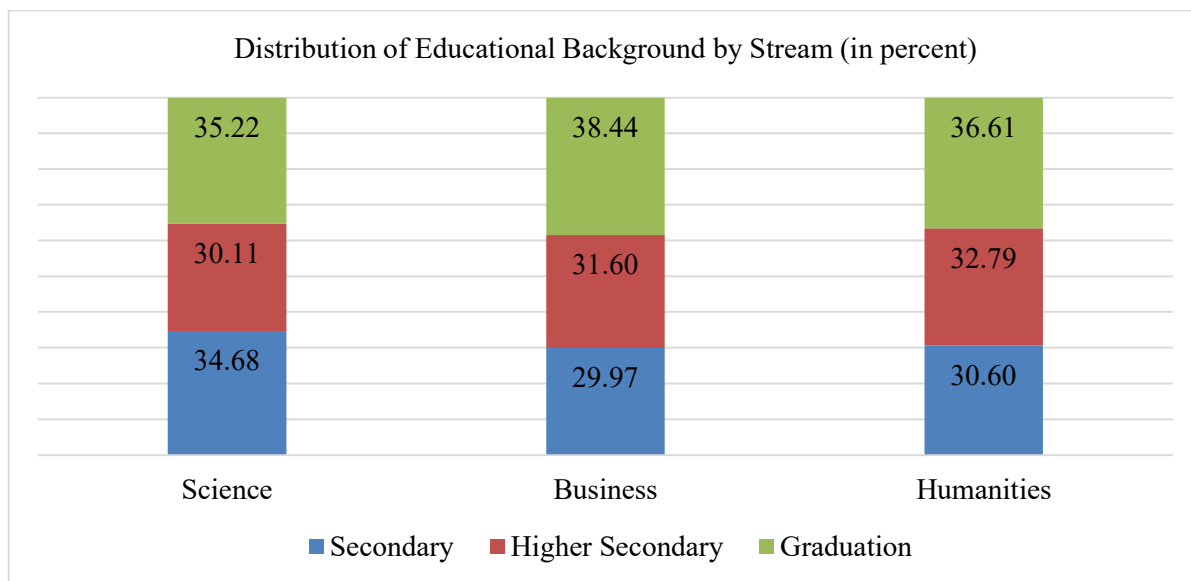


Fig. 1: Educational background.

Table 2: Tourists' travel pattern.

Inquiry	Response	Response Classification [%]			
		1	2	3	4
Have you visited Kuakata Sea Beach before?	1. Yes 2. No	0.53	0.47	-	-
If the answer to the previous question is yes, how many times have you visited Kuakata Sea Beach in the past year?	1.1-2 times 2. 3-5 times 3. More than 5 times	0.48	0.24	0.28	-
Have you traveled to any other sea beaches besides Kuakata?	1. Yes 2. No	0.58	0.43	-	-
How do you usually travel to Kuakata Sea Beach?	1. Private car 2. Public bus 3. Motorcycle 4. Other	0.14	0.73	0.08	0.05
How long is your typical stay at Kuakata Sea Beach (in a day)?	1. <1 2. 1-2 3. 3-5 4. >5	0.11	0.87	0.03	-
What is the main purpose of your visit to Kuakata Sea Beach?	1. Leisure 2. Business 3. Family gathering 4. Other	0.87	0.03	0.10	0.01
How do you usually select your accommodation at Kuakata Sea Beach?	1. Hotel/resort 2. Guesthouse/homestay 3. Others___	0.96	0.02	0.02	-
On average, how much do you spend per day during your stay at Kuakata Sea Beach (in thousand Bangladeshi Taka)?	1. <1 2. 1-3 3. 3-5 4. >5	0.53	0.43	0.03	0.01
Are you aware of any waste management initiatives at Kuakata Sea Beach?	1. Yes 2. No	0.53	0.47		
Have you ever participated in any beach cleanup activities at Kuakata Sea Beach?	1. Yes 2. No	0.03	0.97		

the urgent need for further development in the current waste management situation and an equally resounding 99% expressing their willingness to dispose of waste if suitable dustbins are installed responsibly. Respondents offered a range of perspectives on effective methods for sustainable waste management, with 37% advocating the importance of increasing tourists' awareness, 38% emphasizing the strategic placement of dustbins, 25% underscoring the need for strict government regulations, and only 1% supporting an entry fee for waste management. Moreover, findings demonstrate varying levels of awareness and knowledge among tourists, with 36% confirming their awareness of environmental issues linked to waste management, 54% considering themselves somewhat knowledgeable, and 35% voting for a lack of knowledge on the topic. In terms of satisfaction, 42% of participants expressed satisfaction with existing waste management practices, with an additional 37% reporting general satisfaction. Solid waste pollution was identified as a prominent concern by 34% of respondents, while 51% pointed to air pollution, and 12% specifically noted water pollution, with noise pollution receiving the least attention at 3%. The cleanliness of the beach area during visits was perceived positively, with 46% considering it clean and 43% describing it as moderately clean. Furthermore, 53% showed a willingness to participate in waste management initiatives, and a remarkable 59% expressed being very likely to recommend Kuakata Sea Beach based on its waste management practices, bringing attention to the potential

impact of sustainable waste management on the overall tourist experience and destination promotion.

Table 4 presents an insightful analysis of tourists' willingness to pay for beach litter management and proper disposal at Kuakata Sea Beach, Bangladesh. The data reveals that a noteworthy segment of beachgoers express concern about the presence of litter or waste on the beach, with 37% indicating they are "very concerned" and 41% characterizing themselves as "somewhat concerned." Furthermore, a substantial majority, comprising 68% of respondents, believe that having effective waste management and disposal systems in place is "extremely important." Regarding the willingness to financially support sustainable waste management and litter disposal, 51% of tourists expressed their positive inclination. Additionally, the study found that 63% of those inclined to contribute were open to paying between 26-50 BDT taka daily for this purpose. Moreover, a majority of 71% of respondents who were unwilling to pay cited the belief that it is the government's or local authorities' responsibility as their main reason for not contributing. This research also highlights that 46% of tourists would be more likely to support these initiatives if they were provided with transparent details on the utilization of their payment.

The findings of our logistic regression analysis, as presented in Table 5, shed light on the intricate relationships between tourists' willingness to pay for sustainable waste management in the Kuakata Sea Beach and various household

Table 3: Tourists' knowledge and perception of sustainable beach waste management.

Inquiry	Response	Response Classification [%]				
		1	2	3	4	5
Do you think there is any need for further development of the current situation?	1. Yes 2. No	0.99	0.01			
Are you willing to dump the waste if dustbins are installed on beaches by the appropriate authority?	1. Yes 2. No	0.99	0.01			
What is the most effective method for sustainable waste management, according to you (respondents)?	1. Increasing tourists' awareness 2. Strict government regulation 3. Installing dustbins in frequent places on the beach 4. Entry fee for waste management	0.37	0.25	0.38	0.01	
Are you aware of the environmental issues associated with waste management at Kuakata Sea Beach?	1. Yes 2. I have some knowledge 3. No	0.36	0.51	0.14		
How do you acquire relevant waste management information?	1. TV and newspaper 2. Propaganda and indoctrination 3. Environmental activities 4. Friends and relatives	0.63	0.01	0.08	0.28	
How would you rate your level of knowledge about sustainable waste management practices?	1. Very knowledgeable 2. Somewhat knowledgeable 3. Not knowledgeable at all	0.12	0.54	0.35		
How do you perceive the current waste management practices at Kuakata Sea Beach?	1. Excellent 2. Good 3. Fair 4. Poor	0.10	0.60	0.25	0.06	
Are you satisfied with the current waste management at Kuakata Sea Beach?	1. Very satisfied 2. Satisfied 3. General satisfaction 4. Not satisfied	0.14	0.42	0.37	0.07	
Which kind of environmental pollution do you think is more serious and should be paid more attention to?	1. Water pollution 2. Air pollution 3. Solid waste pollution 4. Noise pollution	0.12	0.51	0.34	0.03	
How would you rate the overall cleanliness of the beach area during your visit?	1. Very clean 2. Clean 3. Moderately clean 4. Dirty 5. Very dirty	0.06	0.46	0.43	0.05	0.00
Are you willing to participate in waste management initiatives at Kuakata Sea Beach?	1. Yes 2. Maybe 3. No	0.11	0.53	0.36		
How likely are you to recommend Kuakata Sea Beach to others based on its waste management practices?	1. Very likely 2. Somewhat 3. Not Likely	0.59	0.39	0.03		

Table 4: Tourists' willingness to pay (WTP) for beach litter management.

Inquiry	Response	Response Classification [%]				
		1	2	3	4	5
How concerned are you about the presence of litter or waste on Kuakata Sea Beach?	1. Very concerned 2. Somewhat concerned 3. Neutral 4. Not concerned 5. Not sure	0.37	0.41	0.11	0.06	0.05
How important do you think it is to have proper waste management and disposal systems on Kuakata Sea Beach?	1. Extremely important 2. Important 3. Neutral 4. Not important 5. Not sure	0.68	0.31	0.01	0.00	0.00
Are you willing to pay an additional fee to support sustainable waste management and proper disposal of beach litter in Kuakata Sea Beach?	1. Yes 2. No	0.51	0.49			
Please indicate the maximum amount (in BDT taka) you would be willing to pay per day for sustainable waste management and proper disposal of beach litter in Kuakata Sea Beach:	1. <25 2. 26-50 3. 51-75 4. 76-100 5. >100	0.63	0.32	0.02	0.03	0.00
If you are not willing to pay an additional fee, please select the reason(s) that apply:	1. I believe it is the responsibility of the government/local authorities. 2. I think the existing fees are already sufficient. 3. I am not convinced that it will make any difference. 4. Other	0.71	0.08	0.16	0.06	
Would you be more likely to support sustainable waste management and proper disposal of beach litter if you were provided with clear information on how your payment would be used?	1. Yes 2. No 3. Not sure	0.46	0.17	0.37		

characteristics. Notably, gender emerges as a significant factor influencing willingness to pay, with a coefficient of 0.53 ($p = 0.04$), indicating that the probability of males' willingness to pay for sustainable waste management is higher than that of females, which is statistically significant at 5%. However, age, education, occupation, and Income do not exhibit statistically significant associations with willingness to pay, as evidenced by their p-values associated with coefficients. These findings emphasize the importance of considering gender-specific strategies when devising sustainable waste management programs to boost beachgoers' participation and support.

Table 6 presents the findings of our OLS regression analysis, illuminating the key factors of beachgoers' financial commitment to sustainable waste management. The constant term, at 26.35 with a p-value of approximately 0, signifies robust baseline support for these initiatives and also indicates that tourists are willing to pay BDT 26.35 per day as compensation for waste management. In terms of significance, Income emerges as a significant determinant, exhibiting a coefficient of 0.35 ($SE = 0.10$, $p < 0.001^{***}$), suggesting that individuals with higher income levels are notably more inclined to allocate resources for this cause. Although the effects of gender, age, educational attainment, and occupation are statistically significant coefficients, their inclusion enriches our understanding of the broader demographic context, providing a comprehensive view of the factors at play in beachgoers' financial support for waste management.

CONCLUSION

In these unprecedented times of global climatic challenges, increasing environmental literacy among the people has led to rethinking the impact of poor beach waste management

Table 5: Logistic regression analysis: Relationships between WTP and household characteristics.

Variables	Coefficient	Stand. Error	P-value	95% conf. interval	
Constant	-1.02	0.51	0.04*	-2.02	-0.03
Gender	0.53	0.26	0.04*	0.01	1.04
Age	0.00	0.01	0.94	-0.02	0.02
Education	0.13	0.10	0.22	-0.08	0.33
Occupation	-0.02	0.14	0.90	-0.28	0.25
Income	0.01	0.01	0.24	-0.01	0.03

Notes: The dependent variable is the beachgoers' WTP for sustainable waste management, indicating 1 for yes and 0 for no. 'Gender' (1 for male and 0 for female), 'Education' (1 for complete graduation and 0 for incomplete), and 'Occupation' (1 for employed and 0 for unemployed) are binary regressors. 'Income' is the beachgoer's monthly Income in BDT. * indicates a 5% level of significance.

Table 6: Relationships between WTP and demographic statistics.

Variables	Coefficient	Stand. Error	P-value	95% conf. interval	
Constant	26.35	5.87	0.00***	14.77	37.92
Gender	-3.77	3.37	0.27	-10.42	2.89
Age	-0.10	0.14	0.50	-0.38	0.19
Education	-0.97	2.78	0.73	-6.45	4.51
Occupation	-2.42	4.92	0.62	-12.12	7.28
Income	0.35	0.10	0.00***	0.15	0.54

Notes: The dependent variable is the beachgoers' WTP for sustainable waste management, measured in BDT per day. 'Gender' is a binary variable, with 1 denoting male and 0 denoting female. 'Education' is also binary, with 1 for complete graduation and 0 for incomplete. Similarly, 'Occupation' is binary, reflecting employment status, where 1 for employed and 0 for unemployed. 'Income' refers to the beachgoer's monthly Income in BDT. *** indicates a 1% level of significance.

on environmental quality. Using a structured questionnaire survey, this study investigated tourists' attitudes, travel patterns, socio-demographic characteristics, and willingness to pay for sustainable beach litter management. Results identified that around half of the respondents (53%) are aware of the threats that poor beach litter management poses to the environment. In comparison, only 3% actively took part in beach cleanup activities in their lifetime. Furthermore, as data showed, 37% of the respondents are very concerned about the current waste management practices in Kuakata Sea Beach. However, 99% of the respondents are willing to dump the waste properly if dustbins are installed and made available in appropriate places on the beach.

Around 50% of the people surveyed are willing to pay for the development of a sustainable beach management system, though almost 71% of the respondents think that it is the primary responsibility of the government or appropriate authorities to maintain and ensure beach cleanliness. Most importantly, level of Income and gender difference act as statistically significant factors for their willingness to pay. A larger portion of the respondents willing to pay for beach cleanliness wants to pay less than BDT 25 per day, which the current poor waste management system of the beach may explain. These results are critical for the concerned policymakers and appropriate beach management authority to investigate this problem. Besides, these results can facilitate introducing and implementing tailor-made policies to address this issue, as the values of these non-market services cannot be determined easily. Last but not least, the focus should be given to raising environmental literacy, the conception of conservation, and sustainability to navigate this problem.

Although this study reflected some valuable insights regarding sustainable beach waste management, it is not

free from some limitations. First of all, a bigger sample size could have generated more precise results. Secondly, a comparative study with other beaches of the country might bring different dimensions of the results found and lead to robust outcomes. Thirdly, an analysis of travel behavior using other methods, such as the Travel Cost Method (TCM), will play a significant role in analyzing beachgoers' willingness to pay. Finally, a cross-country analysis could provide us with a precise understanding of visitors' attitudes, environmental literacy, and WTP from international perspectives. Future research should address these issues to understand better tourists' knowledge, perception, and willingness to pay.

ACKNOWLEDGEMENTS

We extend our deep appreciation to the dedicated team of enumerators who generously volunteered their time and efforts in collecting the invaluable data for this study. Their unwavering commitment and meticulous work played a vital role in the success of this study.

REFERENCES

- Adam, I. 2021. Tourists' perceptions of beach litter and willingness to participate in beach cleanup. *Mar. Pollut. Bull.*, 170: 112591.
- Agyeiwaah, E., McKercher, B. and Sunkul, W. 2017. Identifying core indicators of sustainable tourism: A path forward? *Tour. Manag. Perspect.*, 24: 26-33.
- Al-Amin, A.K.M., Alam, K., Shrestha, U.B., Prodhan, M. H., Hossain, M. A., Sattar, N. and Akhter, T. 2021. Ecosystems, livelihood assets and willingness to pay for wetland conservation in Bangladesh. *Environ. Dev. Sustain.*, 23(12): 17503-17534.
- Andersson, T.D., Armbrrecht, J. and Lundberg, E. 2012. Estimating use and non-use values of a music festival. *Scand. J. Hosp. Tourism.*, 12(3): 215-231.
- Bangladesh Tourism Board. 2019. Bangladesh in ICTM. Retrieved from <http://tourismboard.gov.bd/>
- Bennett, J., Cheesman, J. and Milenkovic, K. 2018. Prioritizing environmental management investments using the Contingent Valuation Method. *J. Environ. Econ. Policy*, 7(3): 244-255.
- Brida, J.G. and Risso, W. 2009. Tourism as a factor of long-run economic growth: An empirical analysis for Chile. *Eur. J. Tourism Res.*, 2(2): 178-185.
- Budeanu, A., Miller, G., Moscardo, G. and Ooi, C.S. 2016. Sustainable tourism, progress, challenges and opportunities: an introduction. *J. Cleaner Prod.*, 111: 285-294.
- Camarda, D. and Grassini, L. 2003. Environmental impacts of tourism. *Mediterr. Series A. Sem.*, 57: 263-270
- Damigos, D., Menegaki, M. and Kaliampakos, D. 2016. Monetizing the social benefits of landfill mining: Evidence from a Contingent Valuation survey in a rural area in Greece. *Waste Manag.*, 51: 119-129.
- Das, S., Lee, S.H., Kumar, P., Kim, K.H., Lee, S.S. and Bhattacharya, S.S. 2019. Solid waste management: Scope and the challenge of sustainability. *J. Cleaner Prod.*, 228: 658-678.
- Haab, T.C., Interis, M.G., Petrolia, D.R. and Whitehead, J.C. 2013. From hopeless to curious? Thoughts on Hausman's "dubious to hopeless" critique of contingent valuation. *Appl. Econ. Perspect. Policy*, 35(4): 593-612.
- Halkos, G. and Matsiori, S. 2012. Determinants of willingness to pay for coastal zone quality improvement. *J. Socio-Econ.*, 41(4): 391-399.
- Hall, C.M., Dayal, N., Majstorović, D., Mills, H., Paul-Andrews, L., Wallace, C. and Truong, V. D. 2016. Accommodation consumers and providers' attitudes, behaviors and practices for sustainability: A systematic review. *Sustainability*, 8(7): 625.
- Haseeb, M. and Azam, M. 2020. Dynamic nexus among tourism, corruption, democracy, and environmental degradation: A panel data investigation. *Environ. Dev. Sustain.*, 23(4): 5557-5575. <https://doi.org/10.1007/s10668-020-00832-9>
- Iqbal, M.H. and Hossain, M.E. 2023. Tourists' willingness to pay for the restoration of Sundarbans Mangrove forest ecosystems: a contingent valuation modeling study. *Environ. Dev. Sustain.*, 25(3): 2443-2464.
- Islam, M.S. 2015. Study on factors influencing tourism: Way forward for sustainable tourism in Bangladesh. *J. Tourism, Hosp. Sports*, 6(1): 1-13.
- Kaza, S., Yao, L., Bhada-Tata, P. and Van Woerden, F. 2018. What a waste 2.0: a global snapshot of solid waste management to 2050. World Bank Publications.
- Lee, T.H. and Jan, F.H. 2015. The effects of recreation experience, environmental attitude, and biospheric value on the environmentally responsible behavior of nature-based tourists. *Environ. Manage.*, 56: 193-208.
- Liu, J., Liu, N., Zhang, Y., Qu, Z. and Yu, J. 2019. Evaluation of the non-use value of beach tourism resources: A case study of Qingdao coastal scenic area, China. *Ocean Coast. Manage.*, 168: 63-71.
- McIntosh, C.R. 2013. Library return on investment: Defending the contingent valuation method for public benefits estimation. *Lib. Inform. Sci. Res.*, 35(2): 117-126.
- Mondal, M.S.H. 2017. SWOT analysis and strategies to develop sustainable tourism in Bangladesh. *UTMS J. Econ.*, 8(2): 159-167.
- Nandagiri, L. 2015. Evaluation of the economic value of Pilikula Lake using travel cost and contingent valuation methods. *Aquat. Proced.*, 4: 1315-1321.
- Orlowski, J. and Wicker, P. 2019. Monetary valuation of non-market goods and services: a review of conceptual approaches and empirical applications in sports. *Eur. Sport Manag. Q.*, 19(4): 456-480.
- Pan, S.Y., Gao, M., Kim, H., Shah, K.J., Pei, S. L. and Chiang, P.C. 2018. Advances and challenges in sustainable tourism toward a green economy. *Sci. Total Environ.*, 635: 452-469.
- Peters, H. and Hawkins, J.P. 2009. Access to marine parks: A comparative study in willingness to pay. *Ocean Coast. Manag.*, 52(3-4): 219-228.
- Rodella, I., Madau, F., Mazzanti, M., Corbau, C., Carboni, D., Utizi, K. and Simeoni, U. 2019. Willingness to pay for management and preservation of natural, semi-urban, and urban beaches in Italy. *Ocean Coast. Manag.*, 172: 93-104.
- Rodić, L. and Wilson, D.C. 2017. Resolving governance issues to achieve priority sustainable development goals related to solid waste management in developing countries. *Sustainability*, 9(3): 404.
- Siyambalapatiya, J., Zhang, X. and Liu, X. 2018. Green human resource management: A proposed model in the context of Sri Lanka's tourism industry. *J. Clean. Prod.*, 201: 542-555.
- Tang, C.F. and Tan, E.C. 2015. Tourism-led growth hypothesis in Malaysia: Evidence-based upon regime shift cointegration and time-varying Granger causality techniques. *Asia Pac. J. Tourism Res.*, 20(1): 1430-1450.
- The Business Standard. 2021. Crabs Die Every Day in Kuakata During Tourist Season: Report. Retrieved from <https://www.tbsnews.net/environment/6000-crabs-die-day-kuakata-during-tourist-season-report-251887>
- The Daily Star. 2022. Kuakata Witnesses Influx of Tourists. Retrieved from <https://www.thedailystar.net/business/economy/news/kuakata-witnesses-influx-tourists-3202981>
- Torres-Delgado, A. and Saarinen, J. 2017. Using indicators to assess sustainable tourism development: a review. *New research paradigms in tourism geography*, 31-47.

- UNEP. 2021. Paradise Lost: Travel and Tourism Industry Takes Aim at Plastic Pollution. Retrieved from <https://www.unep.org/news-and-stories/story/paradise-lost-travel-and-tourism-industry-takes-aim-plastic-pollution-more>
- UNWTO. 2019. Tourism Contribution. Retrieved from <https://www.unwto.org/global/press-release/2019-06-06/exports-international-tourism-hit-usd-17-trillion>
- Weimer, D.L., Saliba, D., Ladd, H., Shi, Y. and Mukamel, D.B. 2019. Using contingent valuation to develop consumer-based weights for health quality report cards. *Health Serv. Res.*, 54(4): 947-956.
- WTTC. 2015. Economic Impact of Travel and Tourism in the Mediterranean. Retrieved from <https://zh.wttc.org/-/media/files/reports/economic-impact-research/regional-2015/mediterranean2015.pdf>

ORCID DETAILS OF THE AUTHORS

Md. Al Amin: <https://orcid.org/0009-0006-3909-7606>

Md. Tanvir Ahmed: <https://orcid.org/0000-0002-6202-9461>



Evaluation of Grid-Based Aridity Indices in Classifying Aridity Zones in Iraq

Wisam Alawadi[†] , Ayman Alak Hassan and Ammar Dakhil

Department of Civil Engineering, College of Engineering, University of Basrah, Basrah, Iraq

[†]Corresponding author: Wisam Alawadi; wisam.abd-ali@uobasrah.edu.iq

Nat. Env. & Poll. Tech.
Website: www.neptjournal.com

Received: 28-10-2023

Revised: 08-12-2023

Accepted: 19-12-2023

Key Words:

Aridity
Aridity index
Dryness
Gridded data
Climate dataset
Climate stations

ABSTRACT

In this study, the aridity index (AI) based on gridded climate data was validated for defining aridity and classifying aridity zones in Iraq through comparison with the results obtained by the station-based aridity index. Gauge-based gridded climate data taken from Climatic Research Unit Timeseries (CRU TS) were used to determine the annual value of four aridity indices (Lang, De Martonne, Ernic and UNEP AI) over the period 1998-2011. The results showed that the aridity distribution maps derived using grid-based aridity indices were reasonably close to those found using station-based ones. The four aridity indices properly identified similar aridity (dryness) classifications in both the station-based and grid-based aridity maps. The area percentage of each aridity class predicted by grid-based AIs was also compared with that obtained by the station-based AIs. The results showed that the variances between the area percentages predicted by grid-based AIs and those estimated using station-based AIs are fairly slight. The Lang AI exhibited the least variance (0.4%) while the De Martonne AI had the biggest variance (-4.8%). Despite these minor variances, it is however possible to conclude that the grid-based aridity index classified the aridity zones of Iraq as properly as the station-based aridity index did.

INTRODUCTION

Aridity, dryness, and drought events caused by climate changes have become major socio-environmental issues in recent years. They have an adverse influence on ecosystems as well as human livelihoods in many different places of the world (Alizadeh et al. 2020). Particularly, aridity poses a significant, continuing challenge to the majority of global regions (Huang et al. 2017). Aridity is defined as a shortage of moisture that is accompanied by a permanent scarcity of rainfall (Agnew & Anderson 1992). Aridity can increase the risk of desertification in areas with dry, hot climates and little precipitation (Costa & Soares 2012). Iraq is one of the countries that is influenced negatively by increasing aridity. To assess the aridity impact, the aridity indices are used for this purpose. An aridity index may be described as a numerical degree of water deficits and dryness at a certain place (Stadler 2005). Since the start of the 20th century, some numerical indices have been provided for measuring the aridity level (Kimura & Moriyama 2019). The indices proposed by Lang (1920) and De Martonne (1926) are the earliest indices that might be still used to explain the aridity (Traore et al. 2020). Those indices applied mean yearly precipitation (in mm) and average annual temperatures (in °C) to measure aridity-humidity in a specific place. Both the indices, in particular De Martonne AI, have been often used

to examine the regional distribution and temporal version of the aridity (Croitoru et al. 2013; Quan et al. 2013; Ashraf et al. 2014; Sarlak and Mahmmod 2018; Pellicone et al. 2019; Nistor et al. 2020 and Ullah et al. 2022).

Using the Lang and De Martonne principle, other kinds of aridity indices have been suggested, but they used different statistic values of the temperature in place of the average temperature. Examples of these indices are Emerger AI, which is derived from annual precipitation and the difference between the largest and lowest temperature of the year. Ernic AI, which used annual precipitation and maximum temperature (Stadler 2005). Also, there are other indices (such as the Köppen AI) that depend on temperature and precipitation, however they are not used as regularly as early aridity indices like Lang and De Martonne (Speich 2019).

In 1992, the United Nations Environment Programme (UNEP) suggested a new approach to measure the degree of aridity as a ratio of the mean yearly precipitation (P) to potential evapotranspiration (PET) (U.N.E.P 1992). UNEP definition reflects the effect of the thermal regime in defining the aridity through incorporated PET which is a good indicator of water loss than temperature (Nastos et al. 2013) The UNEP-AI has been applied by several researchers to measure aridity and classify climates on a regional or worldwide scale (see e.g., Haider & Adnan 2014; Cheval

et al. 2017; Trabucco and Zomer 2018; Derdous et al. 2021).

To calculate the aridity index accurately, meteorological data over a long period required to be accumulated from numerous weather stations distributed homogeneously over the study area. However, in most cases, such information may be inadequate or unavailable. The best alternative way of obtaining the required data is to use the meteorological datasets produced and made accessible online by international climatic organizations. These databases offer gridded, high-resolution data for climate variables including temperature, precipitation, shortwave radiation, vapor pressure, and PET (Harris et al. 2014, Mistry et al. 2019). The data stored within these datasets are usually generated using extensive analyses of meteorological stations and gauge records from all around the world (Werner et al. 2019). Therefore, they could be relied upon to supply the data required for water resources management, and ecological, agricultural, and climate change studies.

The purpose of this research is to evaluate aridity indices calculated based on gridded data in describing the aridity and

classifying the climate in Iraq which is one of the countries suffering increasing dryness. Four aridity indices are used in the study; Lang AI, De Martonne AI, Ernic AI, and UNEP AI. The reason these four indices were chosen over the other aridity indices is because they are commonly used in aridity-related studies. Also, they differ from one another in terms of their data inputs. The results of the aridity mapping and climate classification obtained by grid-based data were compared with those obtained by station-based data to assess the suitability of the gridded data for defining and classifying the aridity in the study area (Iraq).

MATERIAL AND METHODS

Study Area

The study area includes the entire land of Iraq. Iraq is a country located in southwest Asia with a total area of around 435,000 square kilometers. The ground elevation in Iraq ranged from sea level in the south to 3661 meters above sea level in the north (Fig. 1) (Al-Zubedi 2022). In general, the

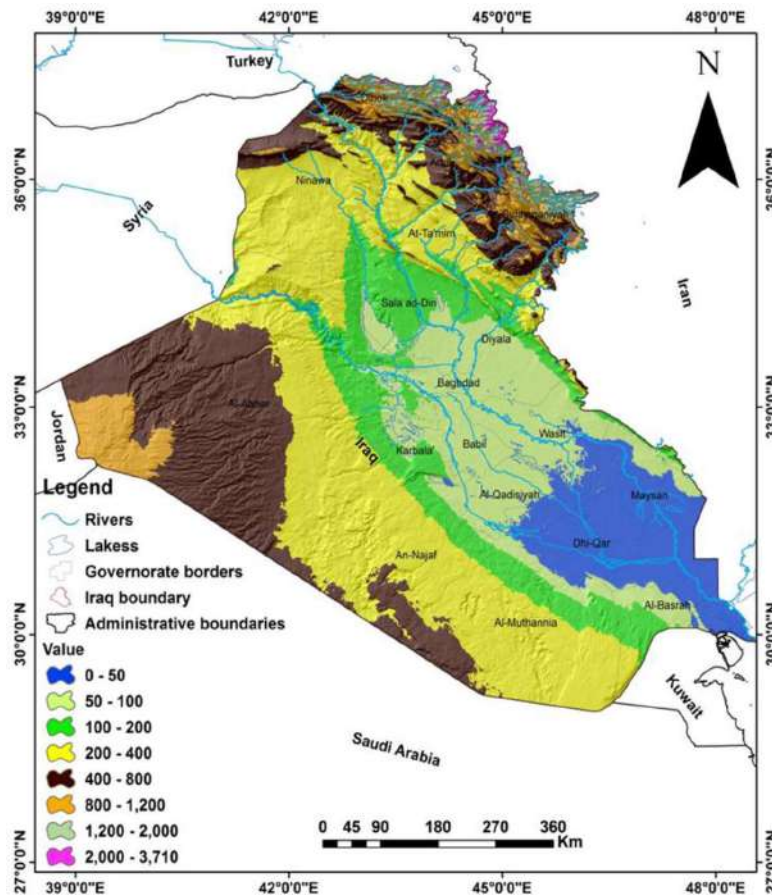


Fig. 1: Location and topographic map of Iraq (Al-Zubedi 2022).

terrain of Iraq is dominated by broad plains, with mountains largely concentrated in the north and northeast (close to the borders with Turkey and Iran).

The climate of Iraq may be described as continental, with an extreme annual temperature range and a relatively small amount of precipitation. The country generally experiences winters that vary between cool and cold, and summers are dry with variations between hot and extremely hot temperatures. The coldest month is January, with temperatures ranging from 5°C to 10°C, while the hottest month is August with temperatures rising up to around 45°C (Salman et al. 2019).

Precipitation falls in Iraq from October to May, with December and February experiencing the largest amount. The mean annual precipitation in Iraq is expected to be between 100 and 180 mm (<https://www.britannica.com/place/Iraq/Climate>). Most of the country receives less than 100 mm/year, however, the highlands (north-eastern regions of Iraq) may receive up to 1200 mm/year of precipitation (Hameed et al. 2018).

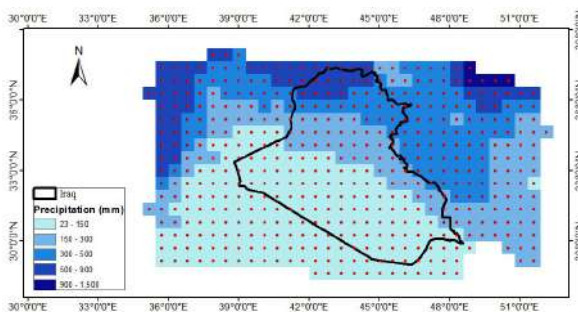
Datasets and Data Processing Methods

The primary inputs required to determine the aridity indices

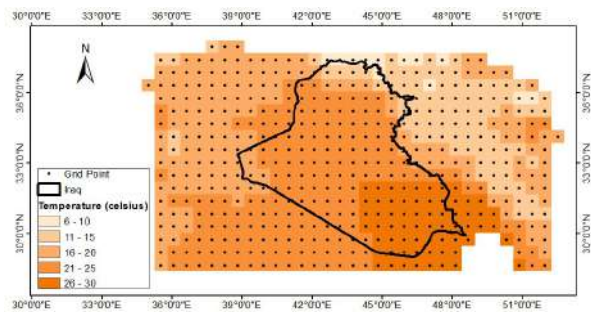
are climatic data such as temperature (T), precipitation (P), and potential evapotranspiration (PET). The required data are often obtained from historical records of the climatic stations distributed across the study region. However, if such station-based data are either unavailable or insufficient, it is possible to collect them from gridded datasets available on weather and climate websites.

Climate Research Time (CRU-TS) was used in this research to generate required metrological data. More than 4000 gridded stations were generated with the aid of CRU-TS with a grid size of 0.5 degrees. Climate change studies are widely using this method around the world. The data generated by CRU-TS were tested by an accurate quality control tactic to make them a common source of data (Harris et al. 2014).

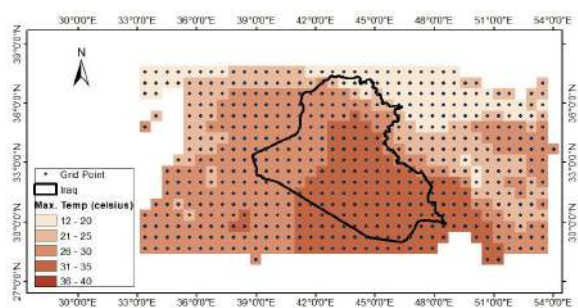
The first step in this method is to download needed gridded data from CRU-TS with a high resolution. These data include the monthly average max temperature, mean and average monthly rainfall, and potential evapotranspiration (PET) for the period from 1998 to 2011. Secondly, spatial processing for the data were done using ArcGIS in order to produce the yearly average for every parameter aforementioned. Fig. 2 shows the annual average layers of



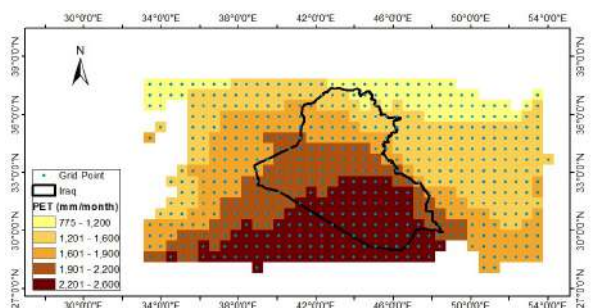
(a) Mean Annual Precipitation



(b) Mean Annual Temperature



(c) Mean Maximum Temperature



(d) Potential evapotranspiration

Fig. 2: Gridded climatology data over the period 1998-2011 was used for calculating aridity indices.

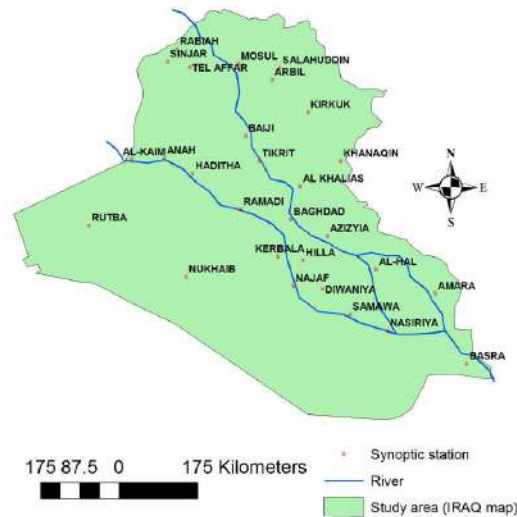


Fig. 3: Location of the meteorological stations in Iraq used by Şarlak and Mahmood 2018.

the max temperature, rainfall, and PET. In the final step, the layers in Fig. 2 were used as input in calculating the aridity index formulas, and four formulas were used (Lang, De Martonne, UNEP, and Ernic).

The station-based values of aridity indices and their distribution were obtained from research conducted by Şarlak and Mahmood in 2018. In their study, the aridity indices of Lang, De Martonne, United Nations Environmental Program (UNEP), and Ernic were computed using historical records of precipitation and temperature from 28 climate stations run by the Iraqi Meteorological Organization and Seismology (IMOS). Fig. 3 illustrates the locations of the meteorological stations utilized in Şarlak and Mahmood's study.

Aridity Index and Its Formulas

As previously mentioned, aridity indices (AI) are usually used to classify aridity zones (dryness-humid regions) according to their degree of dryness. For this purpose, a number of aridity indices have been developed as indicators of dryness and water scarcity. The aridity indices may be broadly classified into two types: those that depend on precipitation and temperature and those that depend on precipitation and potential evapotranspiration (PET) (Quan et al. 2013).

In this paper, four aridity indices had been calculated using gridded climatic data for the period 1998–2011. These indices are Lang, De Martonne, and Ernic index which are based on precipitation-temperature, and UNEP index which are primarily based on precipitation-PET. These indices were frequently utilized in investigating the aridity situations in various regions of the world (Ullah et al. 2022). The equation and inputs required for calculating every aridity index are shown in Table 1.

Based on the magnitudes of the aridity index, the weather of any region may be categorized into different zones in terms of dryness and humidity. Table 2 suggests climate classification recommended for the four aridity indices used in this study. According to the results computed for each aridity index and the related classification scheme, the Iraq areas had been climatically classified and then the spatial distribution for the aridity zones was also obtained.

Table 1: Aridity index formulas and input parameters.

Aridity Index	Formula	Parameters
Lang	$AI = P/T$	P = annual precipitation (mm) T = mean annual temperature (°C).
De Martonne	$AI = P/(T+10)$	P = annual precipitation (mm) T = mean annual temperature (°C).
Ernic	$AI = P/T_{max}$	P = annual precipitation (mm) T _{max} = mean annual max temperature (°C).
UNEP	$AI = P/PET$	P = annual precipitation (mm) PET = potential evapotranspiration (mm).

Table 2: Classification limits of the Aridity Indices used in the study.

Aridity Indices				
Aridity Zone	Lang	De Martonne	UNEP	Ernic
Hyper-arid	---	---	< 0.05	< 8
Arid	< 20	< 5	0.05 – 0.2	8 - 15
Semi-arid	20 - 40	5 - 15	0.2 – 0.5	15 - 23
Sub-humid	----	15 - 30	0.5 – 0.65	23 - 40
Humid	40 - 60	30 – 60	> 0.65	40 - 55
Very Humid	> 160	> 60	---	> 55

RESULTS AND DISCUSSION

Aridity Mapping

To evaluate the effectiveness of the grid-based aridity index in defining aridity and classifying dryness zones in Iraq, the results of the grid-based calculated indices have

been compared to those generated using the station-based indices. Figs. 4 to 7 show the comparison among the aridity distribution maps derived by the four aridity indices (Lang, De Martonne, Ernic, and UNEP AI). The aridity distribution maps were derived from the yearly aridity index values over the duration of 1998-2011 and all selected indices

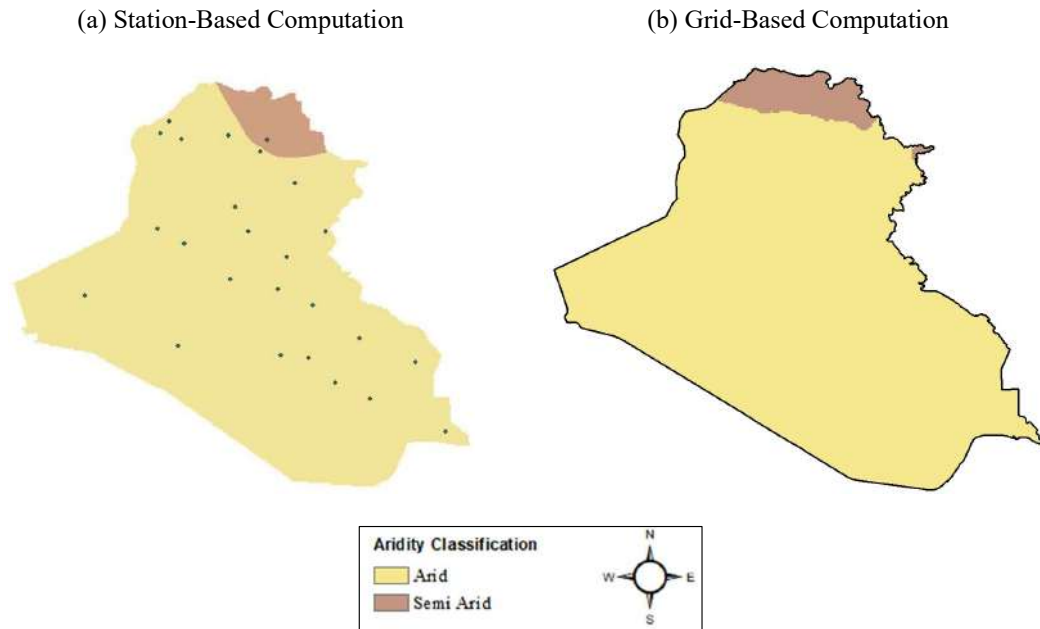


Fig. 4: Aridity distribution maps according to Lang aridity index.

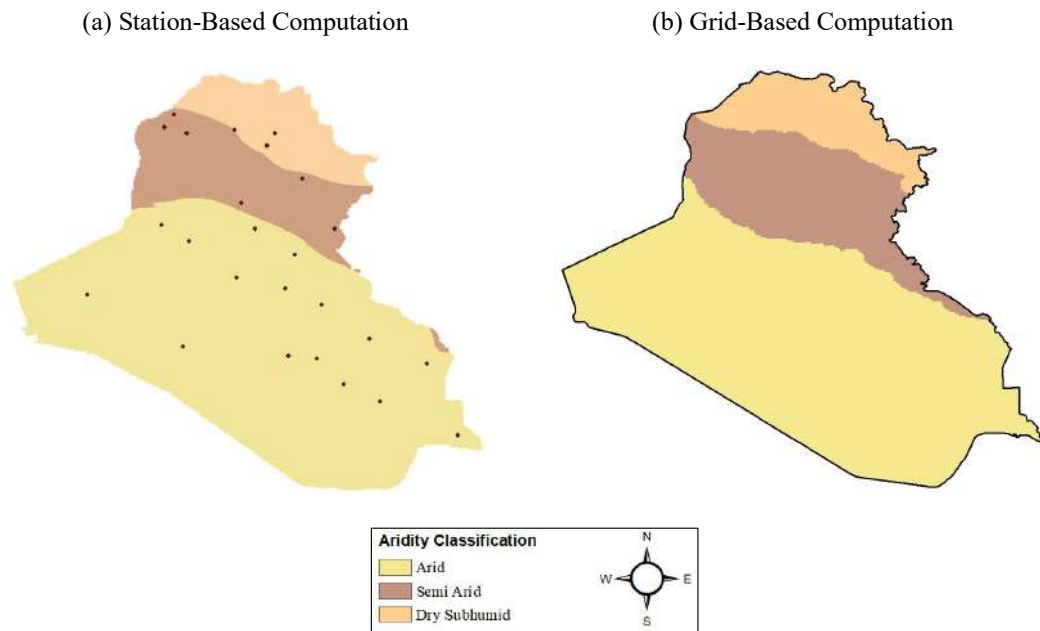


Fig. 5: Aridity distribution maps according to De Martonne aridity index.

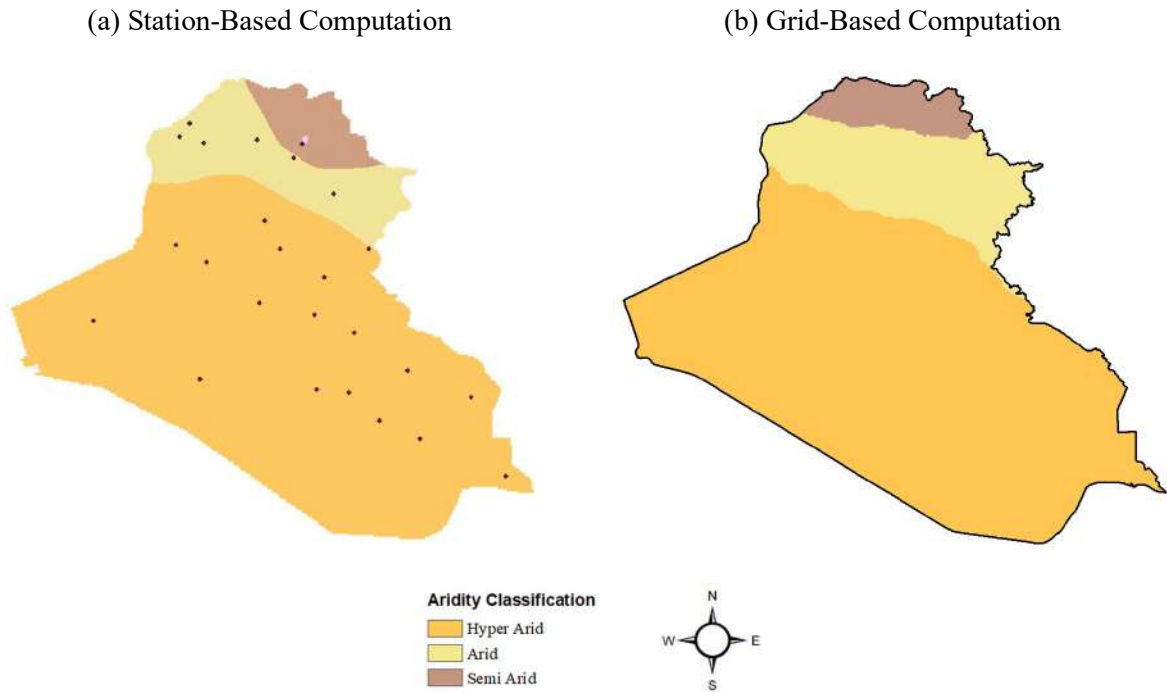


Fig. 6: Aridity distribution maps according to the Ernic aridity index.

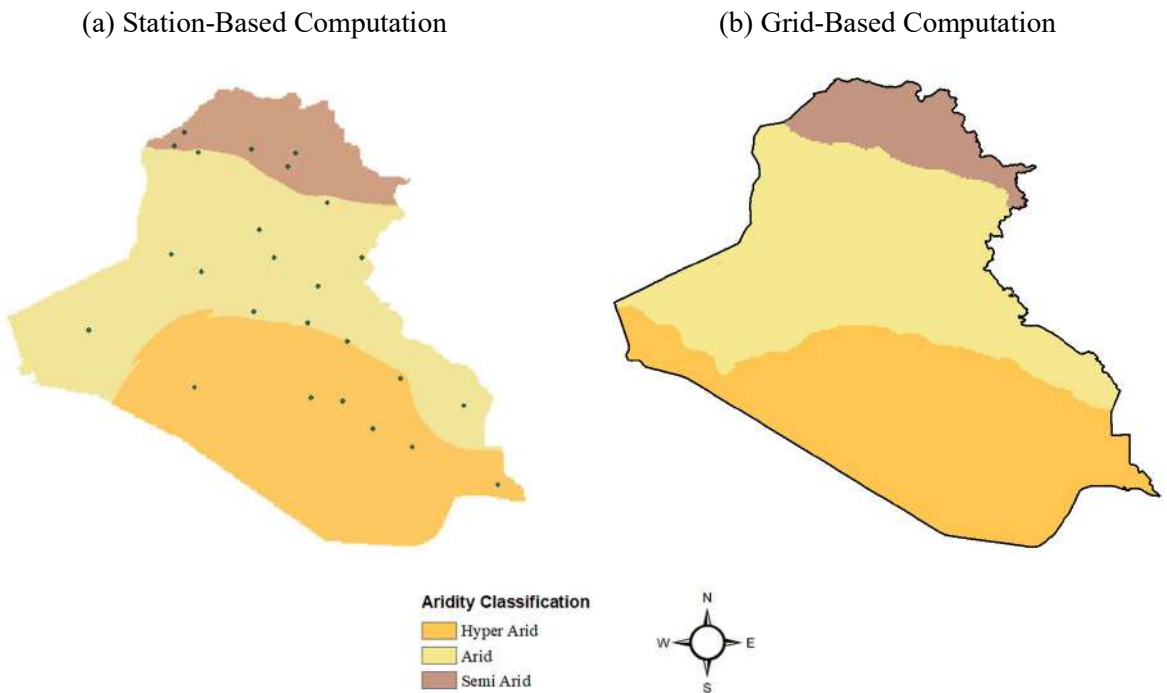


Fig. 7: Aridity distribution maps according to UNEP aridity index.

were computed from gridded and land station weather data. The station-based aridity maps were acquired from a study carried out by way of Şarлак and Mahmood in 2018 while

the grid-based aridity maps were generated using gridded data from CRU-TS. Şarлак and Mahmood (2018) utilized historic records of temperature and precipitation from

28 weather stations dispersed over different areas of Iraq (Fig. 3) to calculate the aridity indices.

The aridity maps displayed in Figs. 4 to 7 generally imply that the aridity zones of Iraq were identified using gridded data with a distribution that is remarkably close to that found using station data. The four aridity indices properly identified similar climatic classifications in both the station-based and grid-based aridity maps. For instance, the Lang AI was able to identify two classes - arid and semi-arid - when utilizing the station data or the gridded data. For the remaining aridity indices, the same aridity zones were also evidently noticeable for both the station and grid-based maps. Furthermore, when comparing the grid-based aridity maps with those produced using station data, the areas of aridity zones appear to be fairly comparable. Regardless of the data source used, the

four aridity indices indicate clearly that the arid climate covers all Iraq regions except a small portion in the north which is classified as sub-humid.

Even though all four aridity indices produced aridity maps and classifications that were closely matched to station-based maps, certain indices appeared to produce results that were more comparable and had less deviation than others. To find out the differences between the grid-based and station-based aridity indices in predicting the aridity classes, the area percentage of each class was calculated and compared as demonstrated in the next section.

Comparison and Variances

To compare quantitatively the grid-based and station-based calculations of the aridity indices, the area percentages of

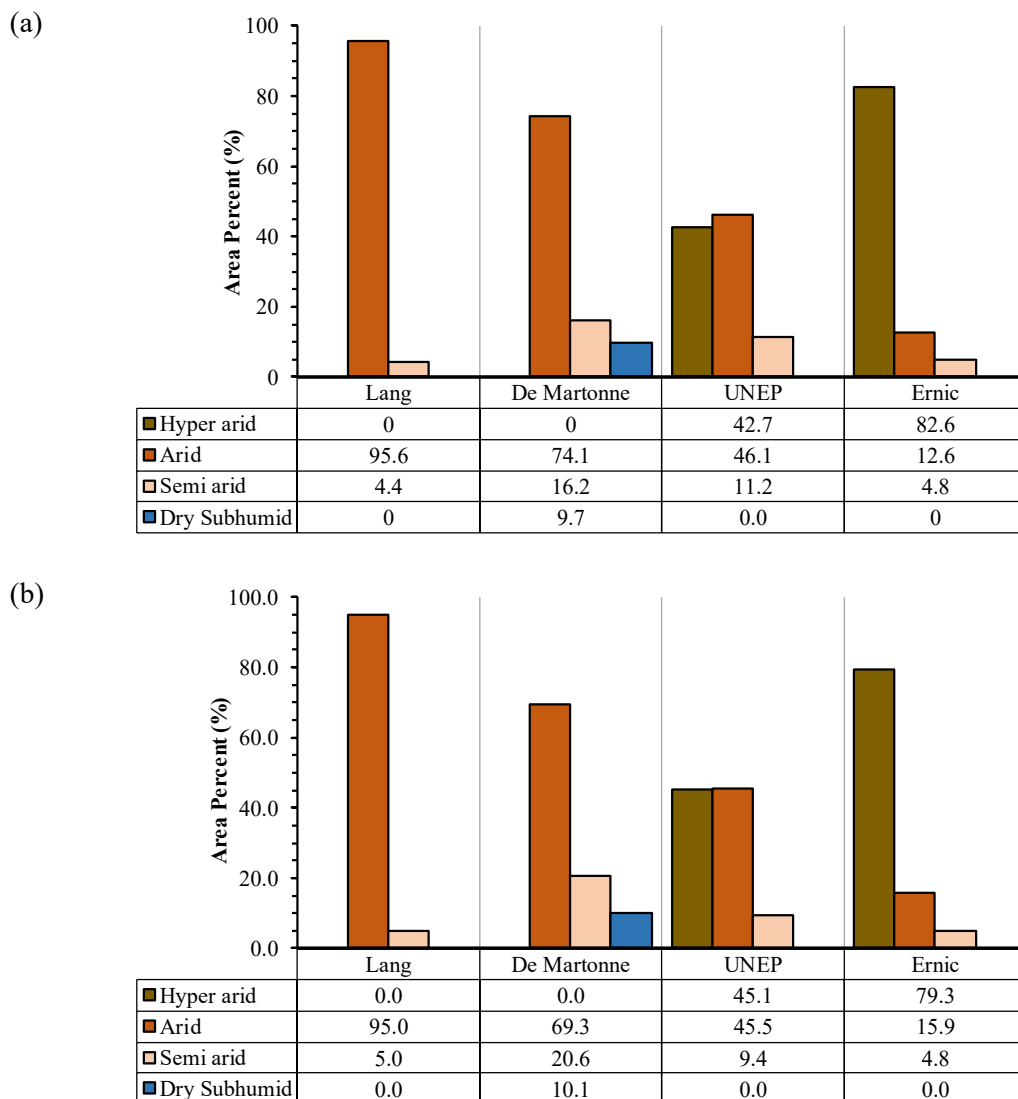


Fig. 8: Area percent for aridity classes according to the four aridity indices computed with (a) Station data and (b) gridded data.

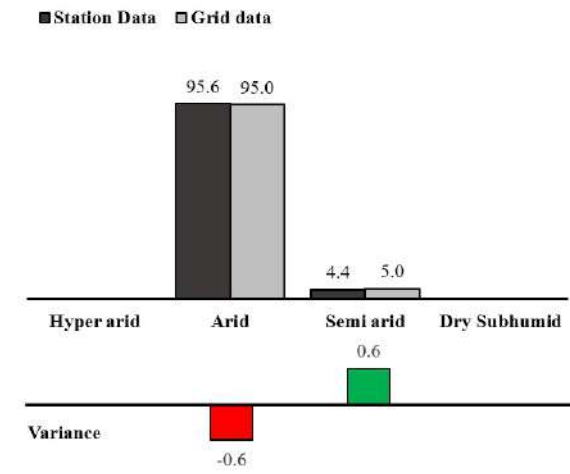
aridity classes derived by the four indices were determined. Fig. 8 shows the area percent for aridity classes according to the four aridity indices computed with (a) station data and (b) gridded data.

The area percentages of any aridity class predicted by grid-based and station-based AI do not differ much. The clear similarity between the two graphs reflects the similarity in the aridity classification obtained by the grid-based and that obtained by the station-based aridity indices. Regardless of the data source, the four aridity indices predicted the same climate classes with areas being nearly equivalent. For example, the highest area percent of the arid class was predicted by the Lang index with values being 95.6% from

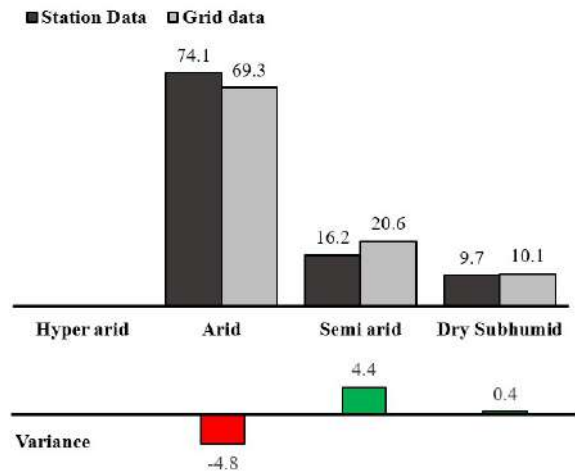
station data and 95% from gridded data (Figs. 8a and b). The dry-subhumid which is the class that was only predicted by De Martonne AI covers the area with percent of 9.7% and 10.1% for gridded and station data respectively.

To give more details onto the differences between the grid and station-based aridity indices, the variance of the area percent for each class were computed. Fig. 9 shows the area percentage variances of the aridity indices computed by station data and gridded data.

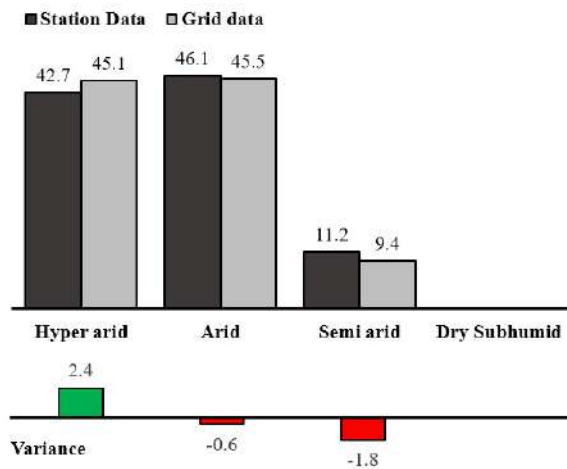
Overall, De Martonne and Ernic's AI gave the highest variances, whereas Lang and UNEP's AI exhibited the lowest values. The variances between the grid-based and station-based classes of the De Martonne AI were -4.8 for the arid



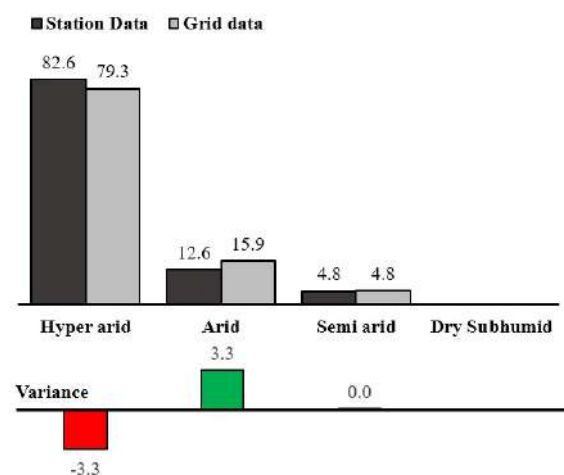
(a) Lang



(b) De Martonne



(c) UNEP



(e) Ernic

Fig. 9: Variances of the aridity indices computed by station data and gridded data in terms of area percentage of each class.

class and 0.4 for the sub-humid class. In the case of Lang AI, the variances were -0.6 for the arid class and 0.6 for the semi-arid class which was the smallest among the aridity indices used in this study. For the UNEP AI, which is dependent on PET and precipitation, the area percent of the climate classes obtained from station data differed marginally when utilizing gridded data. In the case of UNEP AI, the variances were relatively smaller compared to DE Martonne AI with values of 2.4% for hyperarid (the largest variance) and -0.6% for arid (the smallest variance).

The variances between the results of the classifications obtained by the grid and station-based aridity indices may be attributed to different reasons. One of them, is the class limits of the classification scheme applied by each aridity index. When the difference between the lower and upper limits of a class is large, the variance is expected to be less. Other potential causes for the discrepancies between the grid-based and station-based aridity classifications include differences in temperature and precipitation data obtained from gridded datasets and station records. Also, inaccuracies caused by the interpolation technique that was used to distribute the data spatially could be a source for variances in the results. Despite these minor variations, it is however possible to conclude that the grid-based aridity index correctly forecasted the aridity zones of Iraq in a manner that was consistent with the results obtained when station data were employed.

CONCLUSIONS

In this study, gauge-based gridded climate data taken from Climatic Research Unit Timeseries (CRU TS) were used to determine the aridity index (AI) based on four definitions of aridity (Lang, De Martonne, UNEP, and Ernic). The validation of the grid-based aridity index in defining aridity and classifying aridity zones (dryness-humid regions) in Iraq was assessed by comparing the results with those obtained by station-based aridity indices. The station-based aridity distribution results were obtained from a study conducted by Şarlak and Mahmood in 2018. Şarlak and Mahmood (2018) utilized historical records of temperature and precipitation from 28 climate stations distributed throughout different regions of Iraq to calculate the aridity indices.

First, the aridity distribution maps according to the four aridity indices (Lang, De Martonne, Ernic and UNEP AI) were derived from gridded data for a period 1998-2011. The aridity maps generally implied that the aridity zones of Iraq are identified using gridded data with a distribution that is quite close to that found using station data. The four aridity indices properly identified similar aridity classifications in both the station-based and grid-based aridity maps.

Regardless of the data source used, the four aridity indices indicated clearly that the arid climate covers all Iraq regions except a small portion in the north which is classified as a sub-humid.

The area percentage of each climate class predicted by grid-based AIs was also compared with that obtained by the station-based AIs. The findings demonstrated that grid-based predictions of area percentages for every aridity class have some minor differences from those produced by station-based AI. The De Martonne AI demonstrated the largest variance (-4.8%) between the grid-based and station-based classes, and the Lang AI had the smallest variance (0.4%).

Despite these minor variances, it is however possible to conclude that the grid-based aridity index forecasted the dryness zones of Iraq in a manner that was consistent with the results obtained when station data were employed. Therefore, it can be concluded that when gridded data are used, the four aridity indices can effectively determine the degree of dryness and predict aridity zones that are nearly comparable to those generated from station data.

ACKNOWLEDGEMENT

The authors acknowledge the Climatic Research Unit (CRU) for providing the free data that were necessary for carrying out this work and were made accessible by the authors. The authors also thank the University of Basrah for its ongoing support.

REFERENCES

- Agnew, C. and Anderson, W. *Water in the Arid Realm*. Routledge: London. 1992.
- Alizadeh, M.R., Adamowski, J., Nikoo, M.R., AghaKouchak, A., Dennison, P. and Sadegh, M. 2020. A century of observations reveals an increasing likelihood of continental-scale compound dry-hot extremes. *Sci. Adv.*, 6(39): eaaz4571.
- Al-Zubedi, A.S. 2022. *Groundwater in Iraq*. Baghdad.
- Ashraf, B., Yazdani, R., Mousavi-Baygi, M. and Bannayan, M. 2014. Investigation of temporal and spatial climate variability and aridity of Iran. *Theor. Appl. Climatol.*, 118: 35-46.
- Atlas, U.N.E.P. 1992. *World Atlas of Desertification*. UNEP, Nairobi, Kenya
- Cheval, S., Dumitrescu, A. and Birsan, M.V. 2017. Variability of the aridity in the South-Eastern Europe over 1961-2050. *Catena*, 151: 74-86.
- Costa, A.C. and Soares, A. 2012. Local spatiotemporal dynamics of a simple aridity index in a region susceptible to desertification. *J. Arid Environ.*, 87: 8-18.
- Croitoru, A.E., Piticar, A., Imbroane, A.M. and Burada, D.C. 2013. Spatiotemporal distribution of aridity indices based on temperature and precipitation in the extra-Carpathian regions of Romania. *Theor. Appl. Climatol.*, 112: 597-607.
- Derdous, O., Tachi, S.E. and Bouguerra, H. 2021. Spatial distribution and evaluation of aridity indices in Northern Algeria. *Arid Land Res. Manag.*, 35(1): 1-14.
- Haider, S. and Adnan, S. 2014. Classification and assessment of aridity over Pakistan provinces (1960-2009). *Int. J. Environ.*, 3(4): 24-35.

- Hameed, M., Ali, A., and Hamid, M. 2018. Apprehensive drought characteristics over Iraq: Results of a multidecadal spatiotemporal assessment. *Geosciences* 8(2): 58.
- Harris, I.P.D.J., Jones, P.D., Osborn, T.J. and Lister, D.H. 2014. Updated high-resolution grids of monthly climatic observations—the CRU TS3.10 Dataset. *Int. J. Climatol.*, 34(3): 623-642.
- Harris, I., Osborn, T.J., Jones, P. and Lister, D. 2020. Version 4 of the CRU TS monthly high-resolution gridded multivariate climate dataset. *Sci. Data*, 7(1): 109.
- Huang, J., Li, Y., Fu, C., Chen, F., Fu, Q., Dai, A. and Wang, G. 2017. Dryland climate change: Recent progress and challenges. *Rev. Geophys.*, 55(3): 719-778.
- Kimura, R. and Moriyama, M. 2019. Recent trends of annual aridity indices and classification of arid regions with satellite-based aridity indices. *Remote Sens. Earth Syst. Sci.*, 2: 88-95.
- Mistry, M.N. 2019. Historical global gridded degree-days: A high-spatial-resolution database of CDD and HDD. *Geosci. Data J.*, 6(2): 214-221.
- Nastos, P.T., Politi, N. and Kapsomenakis, J. 2013. Spatial and temporal variability of the Aridity Index in Greece. *Atmos. Res.*, 119: 140-152.
- Nistor, M.M., Rai, P.K., Dugesar, V., Mishra, V.N., Singh, P., Arora, A. and Carebia, I.A. 2020. Climate change effect on water resources in Varanasi district, India. *Meteorol. Appl.*, 27(1): e1863.
- Pellicone, G., Caloiero, T. and Guagliardi, I. 2019. The De Martonne aridity index in Calabria (Southern Italy). *J. Maps*, 15(2): 788-796.
- Quan, C., Han, S., Utescher, T., Zhang, C. and Liu, Y.S.C. 2013. Validation of temperature–precipitation based aridity index: Paleoclimatic implications. *Paleogeogr. Palaeoclimatol. Palaeoecol.*, 386: 86-95.
- Salman, S.A., Shahid, S., Ismail, T., Ahmed, K., Chung, E.S. and Wang, X.J. 2019. Characteristics of annual and seasonal trends of rainfall and temperature in Iraq. *Asia-Pac. J. Atmos. Sci.*, 55: 429-438.
- Şarlak, N. and Mahmood Agha, O.M. 2018. Spatial and temporal variations of aridity indices in Iraq. *Theor. Appl. Climatol.*, 133: 89-99.
- Speich, M.J. 2019. Quantifying and modeling water availability in temperate forests: A review of drought and aridity indices. *Forest*, 12(1): 1-16.
- Stadler, S.J. 2005. *Aridity Indexes: Encyclopedia of World Climatology*. Springer, Berlin, pp. 89-94.
- Trabucco, A. and Zomer, R.J. 2018. Global aridity index and potential evapotranspiration (ET0) climate database v2. CGIAR Consort Spat Inf, 10: m9.
- Traore, V., Ndiaye, M., Mbengue, R., Diallo, S., Koita, M., Diaw, A. and Beye, A. 2020. Spatialization of the climate using aridity indices: the case of the agro-ecological zone of peanut basin, Senegal. *J. Mater. Environ. Sci.*, 11: 2106-22.
- Ullah, S., You, Q., Sachindra, D.A., Nowosad, M., Ullah, W., Bhatti, A.S. and Ali, A. 2022. Spatiotemporal changes in global aridity in terms of multiple aridity indices: An assessment based on the CRU data. *Atmos. Res.*, 268: 105998.
- Werner, A.T., Schnorbus, M.A., Shrestha, R.R., Cannon, A.J., Zwiers, F.W., Dayon, G. and Anslow, F. 2019. A long-term, temporally consistent, gridded daily meteorological dataset for northwestern North America. *Sci. Data*, 6(1): 1-16.

ORCID DETAILS OF THE AUTHORS

Wisam Alawadi: <https://orcid.org/0000-0003-4083-3245>



Alleviation of Different Climatic Conditions by Foliar Application of Salicylic Acid and Sodium Nitroprusside and Their Interactive Effects on Pigments and Sugar Content of Maize Under Different Sowing Dates

Priyanka Devi and Prasann Kumar

Department of Agronomy, School of Agriculture, Lovely Professional University, Phagwara-144411, Punjab, India

†Corresponding author: Prasann Kumar; prasann0659@gmail.com

Nat. Env. & Poll. Tech.
Website: www.neptjournal.com

Received: 03-11-2023

Revised: 08-12-2023

Accepted: 24-12-2023

Key Words:

Climate change
Chlorophyll index
Carotenoids content
Salicylic acid
Sodium nitroprusside
Sugar content
Zero hunger

ABSTRACT

The agricultural sector is seriously impacted by climate change, leading to potential risks to food security. In terms of global food production, maize ranks third. As a result, crop production and food security depend critically on assessing the effects of climate change and developing measures to adapt maize. Regarding adaptability, changing planting dates and using different agrochemicals are more effective than other management. Crop models are part of a global decision support system to help farmers maximize yields despite unpredictable weather patterns. To mitigate yield loss and protect the ecosystem, it is essential to use efficient maize-sowing practices in the field. This experiment was carried out to identify the most favorable sowing dates that maximize yield while ensuring the crop's productivity and the integrity of the surrounding ecosystem remain intact. The main aim of this experiment was to mitigate the different climatic conditions by exogenous application of salicylic acid (SA) and sodium nitroprusside (SNP) on pigments and sugar content in maize under different sowing dates. A field experiment was carried out in the School of Agriculture, Lovely Professional University, Punjab, India, during the spring season of 2022. The experiment dealt with various maize crops, PMH-10, sourced from the Punjab Agricultural University (PAU), Punjab. The experiment was conducted in an open-air environment. The experimental setup was laid out in a split-plot design. The results stated that foliar application of salicylic acid and sodium nitroprusside successfully influenced high-temperature tolerance and low temperature at the reproductive phase and initial vegetative stages with other growing climatic conditions of maize in early and late sowings when controlled by increasing the chlorophyll index, carotenoids content, and sugar content of maize.

INTRODUCTION

Food insecurity will excessively affect the world's poor and most vulnerable communities due to climate change (Barbier & Hochard 2018). The last three decades have been the warmest since 1850 (Pachauri et al. 2014). Temperature and precipitation increases occur over the planet, although not equal (Stoker et al. 2013). Several studies (Najali et al. 2018) have examined the possible implications of future climate changes on food production on a global or continental scale. Global production systems are particularly susceptible to the effects of climate change (RK & Meyer 2014; Shafqat et al. 2019). Reduced agricultural productivity is a significant worry for food security, and this is especially true in arid and semi-arid regions (Ahmed et al. 2019). Crop growth, development, and output are already more at risk in dry areas due to the detrimental consequences of increasing temperatures and erratic rainfall patterns (Chattha et al.

2021). The most important discovery from climate change research, in terms of adjustments being made in agricultural production systems, is the variance in climatic projections. Climate change may be seen in various ways, including but not limited to long-term shifts in temperature and rainfall patterns, increases in atmospheric carbon dioxide and other gases, and a rise in the frequency of extreme weather events (Masson et al. 2021, Shafqat et al. 2021). The agricultural value of maize is substantial, especially for the provision of food in developing countries. As its use becomes more commonplace in households, businesses, and factories, the demand for biofuel is expected to continue proliferating (Asseng et al. 2015). However, climate variability makes maize production extremely susceptible to the effects of extreme weather events (Ahmed et al. 2018). The optimal development and reproductive phases can be disrupted by temperature variations, especially under extreme conditions, which can shorten the growing season and reduce crop yield

(Mubashra et al. 2019). Maize's physiological and metabolic systems require favorable environmental conditions to function correctly (Hatfiel & Prueger 2015). Reduced maize output has been linked to variations in the ideal temperature ranges. This loss is exacerbated by both higher daytime and nighttime temperatures.

High heat and dryness put a significant amount of stress on the majority of maize genotypes grown there. It also suggests that planting water-efficient crop cultivars might be an effective solution (Mina et al. 2019). Since the reproductive stages, flowering and grain-filling, are especially vulnerable to increased temperatures, pinpointing the optimal planting time is crucial for increasing productivity and diversifying the current agricultural system to ensure sustainability (Ahmed et al. 2019). Heat stress and the scarcity of critical resources like water and nutrients have become significant obstacles to the efficient production of maize, a widely important cereal crop. Rising temperatures are blamed for these problems (Babel et al. 2019). Increased atmospheric carbon dioxide (CO₂) has been linked to improved plant growth and output. It is important to remember that maize, a C4 crop, may have fewer benefits than other crops regarding photosynthetic accumulation for ultimate biomass output (Mina et al. 2019). The sustainability of maize production in the region is threatened by climate change's possible influence on maize phenology, growth, development, and yield.

Furthermore, it threatens long-term food security. The impact of different sowing dates, plant genetics, and environmental interactions on crop yields may be evaluated using crop growth models (Saddique et al. 2020a, 2020b, 2020c). The capacity of growth regulators, including salicylic acid (SA), ethylene (ET), abscisic acid (ABA), jasmonates (JA), and nitric oxide (NO) donor (SNP) to stimulate development in plants despite times of dormancy and stress has garnered much interest. Particular attention has been paid to how these regulators improve plant resistance to stress (Khan & Khan 2013). Some crops, including wheat, maize, and rice, are particularly vulnerable to high temperatures and heat stress. Scientific investigations (Rai et al. 2018, 2020) corroborate this observation. Salicylic acid (SA) and sodium nitroprusside (SNP), a nitric oxide (NO) donor, are discussed in detail as contributing factors to plant heat tolerance in their study (Prakash et al. 2021).

MATERIALS AND METHODS

Study Site

During the spring season of 2022, a research experiment was conducted at the agricultural area of Lovely Professional

University (LPU), situated in Phagwara, Punjab. The objective of the experiment was to ascertain the optimal timing for maize sowing and identify the appropriate agrochemicals to maximize crop production. A field experiment was carried out in the School of Agriculture, Lovely Professional University, Punjab, India, using a single variety of maize crops, PMH-10, from Punjab Agricultural University (PAU) in Punjab. The experiment used a split-plot design, with two factors: sowing as the main plot and agrochemicals as the sub-plot. The experiment was replicated three times. Salicylic acid at 150 milligrams per liter and Sodium Nitroprusside at 250 micromoles per liter were applied as an exogenous treatment using an appropriate sprayer at different growth stages of maize. The experiment followed the recommended agronomic management practices for maize production in the Punjab area.

Data Collection

Chlorophyll index: Chlorophyll was measured using a SPAD meter at 30, 60, and 90 DAS. Chlorophyll concentration may be determined by measuring the same leaf thrice with the SPAD meter and averaging the results (Arregui 2006).

Carotenoid content (mg.mg⁻¹ fresh weight): Carotenoids are extracted in 80% acetone, and the absorbance is measured at 450 m. The amount of Carotenoids is calculated using the absorbance coefficient described by Jensen (1980).

Total Soluble Sugar content (mg.mL⁻¹): Total soluble sugar in a plant sample may be quickly and easily calculated using the Anthorne reaction. Furfural is produced through the dehydration of carbohydrates in concentrated H₂SO₄. The 630 nm calorimetric measurement of the complex formed when furfural condenses with Anthorne reveals a blue-green (Sadasuvam & Manickam 1992).

Statistical Analysis

All the morphological data were statistically analyzed using variance analysis (ANOVA). Data were assessed by Statistix 10 software with Duncan 's multiple range test (DMRT) with a probability p<0.05.

RESULTS AND DISCUSSION

Chlorophyll Index

The Data presented in Table 1 show the effect of Salicylic acid and sodium nitroprusside on the chlorophyll index of maize when grown under different sowing dates. The results revealed that the chlorophyll index was highly affected by the

application of salicylic acid, with an increase in chlorophyll index by 43.36 and 42.93 in the case of late sowing and early sowing, respectively, at 30 DAS. The results also state that the combined application of salicylic acid and sodium nitroprusside was also able to increase the chlorophyll index by 42.96 at 30 DAS. Similarly, at 60 and 90, DAS application of salicylic increased the chlorophyll index by 47.06, 46.9, and 58.18, 58.02 in late sowing and early sowing, respectively. Salicylic acid mitigated the environmental stress condition by increasing the chlorophyll index, which was created when maize is sown early and late compared to the optimum sowing time. The pigment chlorophyll is responsible for the green coloration of plants. Photosynthesis is essential for plant life because it converts the energy from the sun into the sugars and starches that plants require for survival. Chlorophyll concentration is, therefore, a reliable predictor of plant health. By affecting stomatal closure and the shape of chloroplasts and enzymes involved in photosynthesis, including ribulose 1,5-bisphosphate carboxylase/oxygenase (RuBisCo) and carbonic anhydrase, SA can control photosynthesis in plants. SA can enhance plants' antioxidant enzymes and defense mechanisms and help regulate ion channels and photosynthesis cycles. Enhanced enzyme activity associated with CO₂ absorption at the chloroplast level may be responsible for the higher

photosynthetic rates seen after spray treatments of some phenolic compounds like SA rather than just a rise in stomatal opening. Similarly, it was also reported that foliar sprays of ascorbic acid (AsA), salicylic acid (SA), and hydrogen peroxide (H₂O₂) @ 20 and 40 mg.L⁻¹ were administered to third-leaf stage spring maize seedlings. Increased levels of superoxide dismutase (SOD), chlorophyll, and nutrients were found in plants after foliar treatment, which led to longer shoots and roots (Ahmed et al. 2013) (Table 1).

Where DAS: Days After Sowing, Data is in the form of Mean± at p <0.05, Main Plot- SE- Early, Sowing, S0- Optimum sowing, SL- Late sowing; Subplot- A0- Control, A1- Sodium nitroprusside (250 µM.L⁻¹), A2- Salicylic acid (150 mg.L⁻¹), A3- Sodium nitroprusside (250 µM.L⁻¹) + Salicylic acid (150 mg.L⁻¹)

Total Carotenoid Content

The data presented in Table 2 show the effect of salicylic acid and sodium nitroprusside on the total carotenoid content of maize when grown under different sowing dates at 30, 60, and 90 DAS. In the case of sodium nitroprusside, the total carotenoid range of maize was gradually increased by 41.45 mg.mL⁻¹ in late sown, followed by the application of salicylic acid of 47.02 mg.mL⁻¹ at 30 DAS. However, at 60 DAS, the application of salicylic acid increased the carotenoid content by 57.38 mg.mL⁻¹, followed by sodium nitroprusside by 50.62 mg.mL⁻¹ when grown under optimum sowing. Similarly, at 90 DAS, salicylic acid and sodium nitroprusside increased the carotenoid content by 58.06 and 55.96 mg.mL⁻¹ in the case of optimum sowing, respectively. An increased range of carotenoids will help the plants utilize carotenoids for two primary purposes: they absorb green light energy for photosynthesis and protect chlorophyll from damage caused by sunlight. Most carotenoids are C40 terpenoids; these hydrocarbons are essential in photosynthesis, photomorphogenesis, photoprotection, and plant growth. Additionally, carotenoids are precursors to various apocarotenoids and two plant hormones. As potent antioxidants, carotenoids help plants preserve their high chlorophyll levels by protecting the chloroplasts from damage. Due to their ability to generate significant quantities of heat via photosystems I and II, carotenoids are beneficial for chloroplast membrane protection (Juan et al. 2005). Photosynthetic pigments can be protected from toxic levels of boron by being treated with SA. Because of its beneficial effects on leaf and chloroplast structure, as well as chlorophyll and carotenoid concentration, SA has been suggested as an effective regulator of photosynthesis (Uzunova et al. 2000). Alternatively, SA protects chloroplasts from ROS and boosts chlorophyll stability during synthesis (Fariduddin et al. 2003). In addition to boosting photosynthesis and

Table 1: Effect of salicylic acid and sodium nitroprusside on chlorophyll index of maize grown under different sowing dates at 30, 60, and 90 DAS.

Treatments	Chlorophyll index		
	30 DAS	60 DAS	90 DAS
At different Interval			
Main Plot (Sowing Date)			
SE -Early sowing	39.59	43.15	47.93
S0 -Optimum sowing	40.16	44.97	50.054
SL -late sowing	42.075	45.79	49.935
<u>CV Alpha at 0.05</u>	1.74	3.70	1.63
Sub Plot (Agrochemicals)			
A0- Control	38.144	43.067	42.460
A1-Sodium Nitroprusside [250 µM.L ⁻¹]	39.556	44.078	50.981
A2-Salicylic acid [150mg.L ⁻¹]	42.589	46.667	57.933
A3- Sodium Nitroprusside [250 µM.L ⁻¹] + Salicylic acid [150mg.L ⁻¹]	42.156	44.744	45.200
<u>Alpha at 0.05</u>			
CV (Sowing date and agrochemical)	4.10	2.80	2.82
CD (sowing)	0.79	1.86	0.90
CD (Agrochemicals)	1.64	1.23	1.37
CD (Sowing and agrochemicals)	2.59	2.60	2.24

anthocyanin levels, SA treatment increased phenylalanine ammonia-lyase activity. Possibly due to their free radical scavenging abilities, SNP treatment fostered the development of aerial portions but stunted the growth of roots. A similar result was reported in those sprays of sodium nitroprusside (SNP), a source of nitric oxide (NO), were administered to the leaves either before (control), during (50, 100, 150 M), or after (saline stress) application. Results may suggest that increased activity of antioxidant enzymes like ascorbate peroxidase, peroxidase, H_2O_2 , and the leaf content of proline, chlorophyll content (chlorophyll a & chlorophyll b), and Carotenoid in comparison to the control indicates that exogenous application of sodium nitroprusside (SNP), a NO donor, significantly alleviated the oxidative damage of salinity in rice seedlings (Saroj et al. 2018) (Table 2).

Where DAS: Days After Sowing, Data is in form of Mean \pm at $p < 0.05$, Main Plot- SE- Early Sowing, S0- Optimum sowing, SL- Late sowing; Subplot- A0- Control, A1- Sodium Nitroprusside ($250 \mu M.L^{-1}$), A2- Salicylic acid ($150 mg.L^{-1}$), A3- Sodium Nitroprusside ($250 \mu M.L^{-1}$) + Salicylic acid ($150 mg.L^{-1}$)

Table 2: Effect of salicylic acid and sodium nitroprusside on Total Carotenoids content ($Mg.mL^{-1}$) of maize grown under different sowing dates at 30, 60, and 90 DAS.

Treatments	Total Carotenoids content [$mg.mL^{-1}$]		
	30 DAS	60 DAS	90 DAS
At different Interval			
Main Plot (Sowing Date)			
SE -Early sowing	10.943	38.905	41.548
S0 -Optimum sowing	38.372	50.200	51.749
SL -late sowing	40.474	34.213	33.753
<u>Alpha at 0.05</u>	6.43	0.75	2.34
Sub Plot (Agrochemicals)			
A0- Control	28.668	40.500	40.471
A1- Sodium Nitroprusside [$250 \mu M.L^{-1}$]	33.251	42.729	44.961
A2- Salicylic acid [$150 mg.L^{-1}$]	31.352	44.859	43.651
A3- Sodium Nitroprusside [$250 \mu M.L^{-1}$] + Salicylic acid [$150 mg.L^{-1}$]	26.447	36.337	40.318
<u>Alpha at 0.05</u>			
CV (Sowing date and agrochemical)	3.03	0.97	0.82
CD (sowing)	2.17	0.35	1.12
CD (Agrochemicals)	0.89	0.39	0.34
CD (Sowing and agrochemicals)	2.53	0.68	1.22

Total Soluble Sugar

The data presented in Table 3 show the effect of salicylic acid and sodium nitroprusside on the total soluble sugar of maize at 30, 60, and 90 DAS. The result shows that the application of salicylic acid increased the total soluble sugar of maize by $60.74 mg.mL^{-1}$, followed by sodium nitroprusside by $59.47 mg.mL^{-1}$ in late-sown conditions at 30 DAS, respectively. The results revealed that salicylic acid application was able to mitigate the environmental stress conditions by increasing the sugar content by $67.01 mg.mL^{-1}$, followed by the combined application of salicylic acid and sodium nitroprusside by $66.60 mg.mL^{-1}$ respectively at 60 DAS in early sown conditions. Similarly, at 90 DAS, the application of salicylic acid was able to increase the total soluble sugar content by $49.68 mg.mL^{-1}$ in optimum sowing, and the combined application of salicylic acid and sodium nitroprusside also showed positive results by increasing the sugar content by $45.79 mg.mL^{-1}$ in late sown conditions. An increased range of total soluble sugars activated the plant defense responses, acting as osmotic adjusters or nutritional and metabolic signals. To ensure osmotic adjustment, scavenging of reactive oxygen species, and regulate the cellular energy status through carbon partitioning, sugars play a crucial role in stress sensing and signaling and constitute a regulatory hub for stress-mediated gene expression. Carbohydrate partitioning and critical signal transduction processes in detecting biotic and abiotic stressors are known to be controlled by several sugar transporters. Through photosynthesis, plants can convert inorganic carbon into sugars, meeting their energy needs and those of other heterotrophs (Hennion et al. 2019). Different sugars are assimilated, including glucose and fructose monosaccharides, sucrose, starch, and polyols (Dong & Beckles 2019). Glucose and sucrose are two of the most versatile metabolites, serving as precursors for a wide range of metabolic pathways (including amino acid, sugar alcohol, nucleotide, and lipid biosynthesis), structural building blocks, short- and long-distance signaling molecules, and Osmo protectants in times of stress (Braun et al. 2014). The enzymes amylase, sucrose synthase, and sucrose phosphate synthase (SPS) were all stimulated by SA. Seedlings may develop greater tolerance to NaCl-induced salinity stressors if the extra carbohydrates they get serve as osmotic regulators and improve cellular water absorption and retention. Similarly, it was also reported that the physiological processes of growth and development, photosynthesis, root formation, and germination are regulated endogenously by salicylic acid (Miura & Tada 2014). Root growth is promoted, stomata are closed, and defense genes and secondary metabolites are expressed (Table 3).

Table 3: Effect of salicylic acid and sodium nitroprusside on Total Soluble Sugar ($\text{mg}\cdot\text{mL}^{-1}$) of maize grown under different sowing dates at 30, 60, and 90 DAS.

Treatments	Total Soluble Sugar [$\text{mg}\cdot\text{mL}^{-1}$]		
	30 DAS	60 DAS	90 DAS
Main Plot (Sowing Date)			
SE -Early sowing	8.948	61.698	31.355
S0 -Optimum sowing	54.177	36.800	42.142
SL -late sowing	58.358	30.305	36.648
<u>Alpha at 0.05</u>	5.00	5.71	6.36
Sub Plot (Agrochemicals)			
A0- Control	38.580	36.311	28.336
A1-Sodium Nitroprusside [$250\ \mu\text{M}\cdot\text{L}^{-1}$]	43.724	43.364	36.428
A2-Salicylic acid [$150\text{mg}\cdot\text{L}^{-1}$]	40.624	50.826	43.889
A3- Sodium Nitroprusside [$250\ \mu\text{M}\cdot\text{L}^{-1}$] + Salicylic acid [$150\text{mg}\cdot\text{L}^{-1}$]	39.050	41.23	38.208
<u>Alpha at 0.05</u>			
CV (Sowing date and agrochemical)	8.19	13.36	14.17
CD (sowing)	2.29	2.78	2.64
CD (Agrochemicals)	3.28	5.68	5.15
CD (Sowing and agrochemicals)	5.41	8.94	8.14

Where DAS: Days After Sowing, Data is in form of Mean \pm at $p < 0.05$, Main Plot- SE- Early Sowing, S0- Optimum sowing, SL- Late sowing; Subplot- A0- Control, A1-Sodium Nitroprusside ($250\ \mu\text{M}\cdot\text{L}^{-1}$), A2-Salicylic acid ($150\ \text{mg}\cdot\text{L}^{-1}$), A3- Sodium Nitroprusside ($250\ \mu\text{M}\cdot\text{L}^{-1}$) + Salicylic acid ($150\ \text{mg}\cdot\text{L}^{-1}$)

CONCLUSION

Climate change concerns food security since it is predicted to reduce maize production. The applied agrochemicals were able to mitigate the environmental stress conditions that restrict the growth of maize when grown under different sowing dates compared to optimum sowing. The Salicylic acid and sodium nitroprusside were able to increase the chlorophyll index and carotenoid content, which is directly involved in the photosynthesis process and also protect chloroplast membranes because they can release large amounts of energy in the form of heat through photosystems I and II and also able to increase the total soluble sugar content which helps the maize plant to act as plant defense response by the activation of osmotic adjusters or nutrient and metabolic signals.

ACKNOWLEDGMENT

The authors thank the Department of Agronomy, School of Agriculture, Lovely Professional University, Phagwara, Punjab, India, for providing them with constant moral support and assistance during the research period.

REFERENCES

- Ahmad, I., Basra, S.M., Afzal, I., Farooq, M. and Wahid, A. 2013. Growth improvement in spring maize through exogenous ascorbic acid, salicylic acid, and hydrogen peroxide application. *Int. J. Agric. Biol.*, 15: 95-100.
- Ahmed, I., Rahman, M.H., Ahmed, S., Hussain, J., Ullah, A. and Judge, J. 2018. Assessing the impact of climate variability on maize using simulation modeling under the semi-arid environment of Punjab, Pakistan. *Environ. Sci. Pollut. Res.*, 25: 28413-28430.
- Ahmed, I., Ullah, A., Ur Rahman, M.H., Ahmad, B., Wajid, S.A., Ahmad, A., Ahmed, S. and Hassain, S. 2019. Climate change impacts and adaptation strategies for agronomic crops. *Clim. Chang. Agric.*, 2: 1-14.
- Arregui, L.M., Lasa, B., Lafarga, A., Irañeta, I., Baroja, E. and Quemada, M. 2006. Evaluation of chlorophyll meters as tools for N fertilization in winter wheat under humid Mediterranean conditions. *Eur. J. Agron.*, 24(2): 140-148.
- Asseng, S., Ewert, F., Martre, P., Rötter, R.P., Lobell, D.B., Cammarano, D., Kimball, B.A., Ottman, M.J., Wall, G.W., White, J.W. and Reynolds, M.P. 2015. Rising temperatures reduce global wheat production. *Nat. Clim. Chang.*, 5(2): 143-147.
- Babel, M.S., Deb, P. and Soni, P. 2019. Performance evaluation of AquaCrop and DSSAT-CERES for maize under different irrigation and manure application rates in the Himalayan region of India. *Agric. Res.*, 8(2): 207-217.
- Barbier, E.B. and Hochard, J.P. 2018. The impacts of climate change on the poor in disadvantaged regions. *Rev. Environ. Econ. Policy*, 5: 11-26.
- Braun, D.M., Wang, L. and Ruan, Y.L. 2014. Understanding and manipulating sucrose phloem loading, unloading, metabolism, and signaling to enhance crop yield and food security. *J. Exp. Bot.*, 65(7): 1713-1735.
- Chattha, W.S., Ahmad, H.B., Farooq, M.A., Shafiq, W., Yaseen, M., Ihsan, M.Z., Alghabari, F. and Alzamanan, S.M. 2021. A novel parent selection strategy for the development of drought-tolerant cotton cultivars. *Plant Genet. Resour.*, 19(4): 299-307.
- Dong, S. and Beckles, D.M. 2019. Dynamic changes in the starch-sugar interconversion within plant source and sink tissues promote a better abiotic stress response. *J. Plant Physiol.*, 234: 80-93.
- Fariduddin, Q., Hayat, S. and Ahmad, A. 2003. Salicylic acid influences the net photosynthetic rate, carboxylation efficiency, nitrate reductase activity, and seed yield in *Brassica juncea*. *Photosynthetica*, 41: 281-284.
- Hatfield, J.L. and Prueger, J.H. 2015. Temperature extremes: Effect on plant growth and development. *Weath. Clim. Extremes*, 10: 4-10.
- Hennion, N., Durand, M., Vriet, C., Doidy, J., Maurousset, L., Lemoine, R. and Pourtau, N. 2019. Sugars en route to the roots. Transport, metabolism, and storage within plant roots and towards microorganisms of the rhizosphere. *Physiol. Plant.*, 165(1): 44-57.
- Jensen, N.H., Wilbrandt, R. and Pagsberg, P.B. 1980. Sensitized triplet formation of chlorophyll-a and β -carotene. *Photochem. Photobiol.*, 32(6): 719-725.
- Juan, M., Rivero, R.M., Romero, L. and Ruiz, J.M. 2005. Evaluation of some nutritional and biochemical indicators in selecting salt-resistant tomato cultivars. *Environ. Exp. Bot.*, 54(3): 193-201.
- Khan, M.I.R. and Khan, N.A. 2013. Salicylic acid and jasmonates: Approaches in abiotic stress tolerance. *J. Plant Biochem. Physiol.*, 1(4): e113.
- Masson-Delmotte, V., Zhai, P., Pirani, A., Connors, S.L., Péan, C., Berger, S., Caud, N., Chen, Y., Goldfarb, L., Gomis, M.I. and

- Huang, M. 2021. Climate Change 2021: The Physical Science Basis. Contribution of Working Group I to the Sixth Assessment Report of the Intergovernmental Panel on Climate Change, 2.
- Mina, U., Kumar, R., Gogoi, R., Bhatia, A., Harit, R.C., Singh, D., Kumar, A. and Kumar, A.J.E.I. 2019. Effect of elevated temperature and carbon dioxide on maize genotypes health index. *Ecol. Indic.*, 105: 292-302.
- Miura, K. and Tada, Y. 2014. Regulation of water, salinity, and cold stress responses by salicylic acid. *Front. Plant Sci.*, 5: 4.
- Mubashra, Y., Ashfaq, A., Tasneem, K. and Basra, S.M.A. 2019. Evaluating the impact of thermal variations due to different sowing dates on yield and quality of spring maize. *Int. J. Agric. Biol.*, 21(5): 922-928.
- Najafi, E., Devineni, N., Khanbilvardi, R.M. and Kogan, F. 2018. Understanding the changes in global crop yields through changes in climate and technology. *Earth Future*, 6(3): 410-427.
- Pachauri, R.K., Allen, M.R., Barros, V.R., Broome, J., Cramer, W., Christ, R., Church, J.A., Clarke, L., Dahe, Q., Dasgupta, P. and Dubash, N.K., 2014. Climate Change 2014: Synthesis Report. Contribution of Working Groups I, II and III to the fifth assessment report of the Intergovernmental Panel on Climate Change (p. 151). *Ippc*.
- Prakash, V., Singh, V.P., Tripathi, D.K., Sharma, S. and Corpas, F.J. 2021. Nitric oxide (NO) and salicylic acid (SA): A framework for their relationship in plant development under abiotic stress. *Plant Biol.*, 23: 39-49.
- Rai, K.K., Rai, N. and Rai, S.P. 2018. Salicylic acid and nitric oxide alleviate high temperature induced oxidative damage in *Lablab purpureus* L plants by regulating bio-physical processes and DNA methylation. *Plant Physiol. Biochem.*, 128: 72-88.
- Rai, K.K., Rai, N., Aamir, M., Tripathi, D. and Rai, S.P. 2020. The interactive role of salicylic acid and nitric oxide on transcriptional reprogramming for high-temperature tolerance in *Lablab purpureus* L.: Structural and functional insights using computational approaches. *J. Biotechnol.*, 309: 113-130.
- Saddique, Q., Cai, H., Xu, J., Ajaz, A., He, J., Yu, Q., Wang, Y., Chen, H., Khan, M.I., Liu, D.L. and He, L. 2020a. Analyzing adaptation strategies for maize production under future climate change in Guanzhong Plain, China. *Mitig. Adapt. Strat. Glob. Chang.*, 25: 1523-1543.
- Saddique, Q., Khan, M.I., Habib Rahman, M., Jiatun, X., Waseem, M., Gaiser, T., Mohsin Waqas, M., Ahmad, I., Chong, L. and Cai, H. 2020b. Effects of elevated air temperature and CO₂ on maize production and water use efficiency under future climate change scenarios in Shaanxi Province, China. *Atmosphere*, 11(8): 843.
- Saddique, Q., Li, Liu, D., Wang, B., Feng, P., He, J., Ajaz, A., Ji, J., Xu, J., Zhang, C. and Cai, H. 2020c. Modeling future climate change impacts on winter wheat yield and water use: A case study in Guanzhong Plain, northwestern China. *Eur. J. Agron.*, 119: 126113.
- Saroj, S., Parihar, N.N., Vitnor, S.S. and Shukla, P.K. 2018. Effect of sodium nitroprusside on paddy and maize under different levels of salt stress. *J. Pharmacog. Phytochem.*, 7(1): 266-270.
- Stocker, T.F., Qin, D., Plattner, G.K., Tignor, M.M., Allen, S.K., Boschung, J., Nauels, A., Xia, Y., Bex, V. and Midgley, P.M. 2014. Climate Change 2013: The Physical Science Basis. Contribution of Working Group I to the Sixth Assessment Report of the Intergovernmental Panel on Climate Change.
- Uzunova, A.N. and Popova, L.P. 2000. Effect of salicylic acid on leaf anatomy and chloroplast ultrastructure of barley plants. *Photosynthetica*, 38: 243-250.

ORCID DETAILS OF THE AUTHORS

Priyanka Devi: <https://orcid.org/0000-0002-9066-8279>

Prasann Kumar: <https://orcid.org/0009-0004-4931-7858>



An Appraisal of the Legal Frameworks and Policy Shift in the Nigerian Energy Sector

Michael Otu*, Brian F. I. Anyatang*, Bassey Kooffreh**† and Rose Ohiama Ugbe*

*Faculty of Law, University of Calabar, Nigeria

**Department of Criminal Justice & Legal Studies, University of Mississippi, United States of America

†Corresponding author: Bassey Kooffreh; bekooffr@go.olemiss.edu

Nat. Env. & Poll. Tech.
Website: www.neptjournal.com

Received: 28-09-2023

Revised: 16-11-2023

Accepted: 17-11-2023

Key Words:

Petroleum
Minerals
Electricity
Energy
Policy

ABSTRACT

This paper will explore policy shifts in Nigeria's oil and gas, solar, nuclear, and mineral energy sectors. This policy shift by way of a transition, indigenization, and Nigerianization, has given way to deregulation, decentralization, and de-indigenization of many industries, most notably in the oil and gas sector, through the Petroleum Industry Act (PIA) of 2021 and the Local Content Act of 2010 (LCA). The paper recommends, amongst others, the establishment of a new legal regime that grants resource-based and property rights to resource-bearing communities and incorporates principles of international law, energy diplomacies, International Environmental Law, and international best practices.

INTRODUCTION

The Nigerian national policy on the energy sector has evolved through the colonial, post-colonial, modern, and post-modern eras (Edomah 2021). These policy shifts have been more consistent and recurrent in exploring hydrocarbons. The basis of regulating energy resources in Nigeria is enshrined in the 1960, 1963, 1979, and 1999 Nigerian constitutions. These constitutional provisions were borrowed from the Mineral Oils Ordinances of 1914, 1948, and 1958, which vested mineral resources in all British colonial territories in the Crown. Since independence in 1960, Nigeria has had several legal regimes in the oil and gas sector, mining and minerals, and electricity sector, witnessing a paradigm shift in the ownership, management, and governance of Nigeria's abundant energy and natural resources (Ekhatior 2016). The extant policy, the Petroleum Industry Act (PIA) of 2021 and the Local Content Act of 2010 (LCA), is best described as a liberalization policy.

Many theories have evolved to explain the ownership of energy and natural resources, including qualified ownership, absolute ownership, non-ownership, the domanial system, Islamic ownership, and servitude theories. According to the qualified ownership hypothesis, the landowner has no "title" to the oil and gas in situ but has the exclusive right

to drill and produce from his tract and becomes the owner of the product upon its surface. Since oil and gas cannot be owned until they are captured and reduced into possession, the legal implication is that if oil is found on someone's land, that person does not know such a fact or has done no activity that leads him or her to access such resources, then there is no ownership (Anderson & Kramer 2005).

The non-ownership theory implies nobody can own oil and Gas because of their wandering, fugacious nature (Anderson & Kramer 2005). It is also called the non-qualified ownership theory, meaning nobody owns petroleum until it is explored, exploited, and produced. The person who owns petroleum has the right to explore and exploit it by drilling on the land where the straddle of the crude oil is located. This means there can be no absolute right or title to oil and Gas, which might permeate the strata underlying the land's surface as coal or other solid minerals that form part of the soil because they are fixed to it (Black 2020). The import of the non-ownership theory into the 1960, 1979, and 1999 Nigerian constitutions and the Mining and Minerals Act 2007 makes landowner cannot claim ownership of wild animals on land, air, and sunshine across his land or over his land. He cannot claim ownership over oil and Gas because they are fugacious. This reasoning contradicts the Latin property maxim of *Quicquid plantatur solo, solo credit* which means

that whatever is attached to the land belongs to the land (Denman & Prodana 1972). The triviality of this theory is informed by the fact that oil and Gas that are known to be fugacious have not wandered to every part of Nigeria so that every state can lay claim to them. In developing countries that produce oil and Gas, vest ownership of all minerals is in the Crown or central government to manage and govern. The Crown or central government can explore and exploit its energy and natural resources or grant exploration and exploitation rights to third parties on appropriate contractual terms and conditions.

Islamic ownership theory promotes the oil and gas commons concept. This theory is founded on two pillars: petroleum found under Islamic territory is the common property of the global Islamic community and fairness and justice in the redistribution of common property. This theory emphasizes commonality, communality, and conservation of petroleum and another form of property for the common good (Ghorbani 2017)

Policy Shift in the Petroleum Sector

The colonial era Mineral Oils Ordinances of 1914 and 1948 vested absolute ownership of Nigeria's minerals and mineral oils in the British Crown (Steyn 2009). Oil exploration and production were exclusively granted to British natural and corporate subjects bestowing the monopoly of exploring Nigeria's natural/energy resources only on British subjects. The independence era inherited the British legacies by vesting absolute ownership of Nigeria's energy resources in the federal government through the 1960 and 1963 constitutional provisions. The absolute ownership of energy and natural resources adopted by Nigeria at independence was influenced by the United Nations Resolutions of 1952 and 1962, which stated that countries have "permanent sovereignty over natural resources" within their domains. This resolution, it must be rightly stated, was made only to promote the aspirations of developing countries.

The modern era of Nigeria's energy resources regime was ushered in and dominated by the military government(s). On July 12, 1971, Nigeria made a significant stride by joining the Organization of Petroleum Exporting Countries (OPEC), becoming its eleventh member. This move marked a pivotal moment in Nigeria's relationship with its abundant petroleum resources. The decision aligned with Nigeria's ambition to assert greater control and ownership over its natural wealth. This endeavor was further solidified through legislative actions. Nigeria embraced OPEC's resolution of 1968, which advocated for consolidating the federal government's authority over natural resources. The enactment of the Petroleum Act of 1969 exemplified this

commitment. Under this legislation, the state was vested with complete ownership and control of all petroleum resources within its territory, reshaping the dynamics of the energy sector. The establishment of the Nigerian National Oil Corporation (NNOC) in 1971 underlined Nigeria's growing involvement in the petroleum industry. This entity was later succeeded by the Nigerian National Petroleum Company (NNPC) in 1977, marking a transition to a state-controlled entity overseeing both upstream and downstream activities. Nigeria's ascendancy in the oil market was evident as it reached a production milestone of 2 million barrels per day in 1972, solidifying its position as the seventh major oil producer globally. This achievement paralleled a shift in the industry dynamics, with increased governmental regulation through the NNPC, reducing the dominance of transnational corporations.

The enactment of the Petroleum Act of 1969 marked a significant shift in the government's role in the petroleum sector. This legislation introduced various licenses and agreements, such as oil exploration licenses (OEL), oil mining licenses (OML), oil prospecting licenses (OPL), joint operating agreements (JOA), and production sharing contracts (PSC). Additionally, concessions were reduced from 30 and 40 years to 20 years, with the option of a 5-year renewal term. This change gradually diminished the virtual ownership and control of Nigeria's energy resources by transnational corporations, paving the way for Nigeria's active participation and effective ownership. While transnational corporations continued to contribute to Nigeria's economy by supplying energy, creating employment opportunities, and supporting government revenues and GDP, Nigeria's assertiveness increased. The Federal Military Government further solidified this shift with the introduction of the indigenization policy through the Nigerian Enterprises Promotion Decree of 1972. This policy aimed to promote local ownership by classifying enterprises for Nigerians to own at least 40% equity participation. Notably, the government acquired significant equity interests in oil and gas production and distribution, leading to the establishment of monitoring entities like NNPC and NICON. However, this policy direction saw a reversal with the repeal of the Nigerian Enterprises Promotion Decrees of 1972 and 1977, replaced by the Nigerian Enterprises Promotion (Repeal) Degree No. 7 of 1995. This new act introduced decentralization, deregulation, and de-indigenization of the petroleum sector. Importantly, it emphasized local content policies to increase government participation. The policy shift in Nigeria's petroleum sector between 1969 and 1998 was influenced by various factors. These include the need to change the contractual status quo, pressures from emerging third-world nations for sovereignty over natural resources,

and the imperative for post-civil war reconstruction and rehabilitation programs.

The Local Content Act (LCA), 2010

This legislation was enacted in 2010 to build local capacity to exercise control over the management and governance of petroleum resources in Nigeria, restructure the petroleum sector, and promote sustainable development and use of Nigerian energy resources in the interest of the present and unborn generations. The precursors to this law were the NNOC 1971 and NNPC 1977. From the provisions of the Act, the Nigerian government intends to actualize the first consideration to be given to Nigerian operators in the oil and gas sector and develop Nigeria's capacity in project execution and management of the petroleum industry's upstream, midstream, and downstream sectors. The key innovations introduced by the LCA include the establishment of a Governing Council in Section 71 and Nigerian Content Monitoring Board in Section 69, whose functions are stipulated in Section 70 (a – p) of the Act. The LCA, 2010 provides that for all proposed projects, contracts, subcontracts, and purchase orders estimated by the operator to be in excess of \$1 000,000 (USD), the operator shall provide to the Board for approval, advertisements, pre-qualification criteria, technical bid documents, technical evaluation criteria and the proposed bidders lists under Section 17. Qualified Nigerians are given first consideration regarding employment and training in projects executed in the industry in Sections 28 and 29. Succession plans and Nigerianisation of positions are also provided for under Section 31(1) LCA 2010; the caveat is that a maximum of 5% of management positions must be reserved for expatriates to cater to investor interests. Through the requirements of the succession plan, Nigerians are expected to understudy each incumbent expatriate for a maximum period of 4 years, after which the position would be Nigerianized. Other key innovations include the employment of only Nigerians in junior and intermediate positions and the establishment of the Research and Development Department to take care of research and training as regulated by the minister on standards, facilities, personnel, and technology for training in the industry. The registration of operators and their professional employees in the Nigerian petroleum industry with Nigerian professional associations in Section 42; transfer of technology; utilization of only Nigerian legal, financial, and insurance services by operators in Section 49; establishment of a Joint Qualification System (JQS), an industry data bank that would be used for Nigerian content registration and pre-qualification of contractors in the industry in Sections 55 and 56 and submission of the yearly Nigeria Content Performance Report by operator to the Board

in Section 60, within 60 days of each year. The Act can rightly be described as a piece of legislation that embodies interventionist models with the aim of eventual or ultimate Nigerianisation of the oil and gas industry.

Petroleum Industry Act (PIA) 2021

The Nigerian petroleum industry has undergone a series of complicated experiences, with many attempts being made to effect changes in the sector's policies from the colonial and independence era up until 2021. The industry has also witnessed significant policy redirections, which are intended, in the main, to separate the regulatory, policy, and commercial roles of the Nigerian government agencies in the petroleum sector in anticipation of the passage of the Petroleum Industry Act. The Petroleum Industry Act (PIA) has several primary objectives, including but not limited to the replacement of outdated and archaic legislation within the petroleum sector. It aims to facilitate liberalization and deregulation, streamlining the regulatory environment for greater efficiency. Additionally, the PIA seeks to codify the existing 16 pieces of laws related to oil and gas into a single coherent legislation, thereby enhancing clarity and consistency in governance. Moreover, it aims to address ambiguities in the management and governance of the petroleum sector. To achieve these objectives, the PIA provides comprehensive legal, governance, regulatory, and fiscal frameworks for the Nigerian hydrocarbon sector, alongside initiatives for the development of Host Communities as outlined in Section 2 of the Act. To enhance efficient management and governance of the petroleum industry, the PIA makes adequate provisions for open, competitive, and transparent upstream awards, strict rules for awarding lifting, midstream, and downstream licenses, defines processes for selling shares in Nigerian National Petroleum Company (NNPC) Limited and joint venture operations, increased access to information through an opening of more kinds of documents and data to public scrutiny in Parts II-VII. This will create incentives for effective performance, attract investment and financing, and prevent illegal practices. It clarifies revenue collection concerning rents, royalties, fees, taxes, crude sales, and bonuses. This will likely boost government revenue that can be utilized for development if corruption and embezzlement do not muzzle the buoyant revenues to be derived from these revenue flows. The PIA also provides for better NNPC oversight and governance to enable the sector to attain its full potential through this new NNPC corporate culture of commercial orientation and transparency to be attained through plugging leakages and wastages. This will also stimulate the investing interests of lenders and investors. The preceding would be achieved against the backdrop of governance and institutions, administration, development of

Host Communities, and fiscal framework. Before discussing these provisions, it must be noted that the PIA has 5 Chapters, 319 sections, and eight schedules. The Act ensures efficient management, governance, and fiscal accountability through its proposal to establish a commercially-oriented NNPC Ltd under the Companies and Allied Matters Act and other 14 agencies to ensure a conducive business environment for oil and gas operations in Nigeria. Some agencies are responsible for the technical and commercial regulation of the industry's downstream, midstream, and upstream sectors. The Federal Ministry of Petroleum Resources will also be incorporated.

The Act provides efficient administration to promote the exploration and exploitation of Nigeria's Petroleum Resources to benefit citizens and promote the industry's sustainable development. This will be achieved through: Ensuring safe and efficient transportation and distribution, infrastructure, transparency, and accountability in the management and governance of Nigeria's petroleum resources; By avoiding economic distortions through a competitive market for the sale and distribution of petroleum products and national Gas, as well as eliminating cross-subsidies amongst various consumers; Promoting the development of model licenses and model leases plus a carried interest gives NNPC Ltd the right to participate up to 60% in a contract. The Act provides sustainable development and prosperity within Host communities through 3% of derivation benefits, plus a 3% contribution to the Niger Delta Development Commission. The 6% of funds will be provided by upstream companies annually from their operating expenditures for the Host Communities Development Trust Fund in Sections 234-257. The 3% contribution is too nominal, considering decades of environmental degradation of the Host Communities due to Petroleum exploration and exploitation activities in the communities. The Host communities' Funds will be allocated as follows: 75% for capital projects; 20% for reserve; 5% for administrative expenses. The management of the Fund established by the Petroleum Industry Act (PIA) falls under the purview of a Board of Trustees, to be incorporated with a settler according to Section 235(1), or settlers operating under a joint operating agreement in upstream petroleum operations as per Section 235(2). Failure to adhere to these provisions may result in the revocation of their lease/leases, license, or licenses under Section 238. Additionally, the Act provides for the establishment of a Host Communities Advisory Committee tasked with managing the Host Communities' Development Trust, as outlined in Sections 248-249. This committee is responsible for identifying community development projects and monitoring and reporting on their progress. Moreover, the Act mandates the formation of the Management Committee on the Security of Infrastructure to enhance peacebuilding within communities,

detailed in Sections 250(a - d). Notably, communities risk forfeiting the costs of repairs if they fail to prevent vandalism, sabotage, or other forms of civil unrest leading to damage to petroleum facilities or disruptions of petroleum activities. Furthermore, the funds of the Host Communities Development Trust are exempted from taxation, as stated in Section 256. The fiscal framework provisioned in the Act encompasses a range of measures aimed at ensuring fairness, transparency, and efficiency in the petroleum sector. These measures include rights of pre-emption, incorporation of joint ventures, establishment of a domestic base price and pricing framework, and formulation of pricing formulas for Gas prices for the Gas-based industries, among others, delineated in Sections 258-306. The fiscal framework outlined in the Act is designed to encourage investment in the industry, provide clarity and increased revenues for the government, and ensure a fair return for investors. Taxes specified under the Act, to be collected by the Federal Inland Revenue Service (FIRS), include Hydrocarbon Tax ranging from 15% to 30% on profits from crude oil production, as detailed in Sections 260-261. Additionally, the Act stipulates a Companies Income Tax (CIT) rate of 30%, with an additional 2% Education Tax, with taxes no longer deductible. The Commission is tasked with collecting rents, royalties, and production shares, while the Petroleum Products Regulatory Authority (the Authority) collects gas flare penalties from midstream operations. Penalties are imposed for late filing of tax returns, with fines escalating for subsequent non-compliance. Certain expenses incurred for petroleum operations are exempt from taxation under Section 264. The Act further delineates chargeable tax rates based on the accounting year and the type of operation, with percentages varying for onshore areas, shallow water areas, deep offshore areas, and new licenses, as articulated in Section 267. Provisions are made for additional chargeable taxes under certain circumstances, while measures are in place to deter tax evasion and avoidance, outlined in Sections 269(1-5). Appeals regarding tax matters may be made to the Tax Appeals Tribunal (TAT), according to Section 288. Moreover, the Act imposes Personal Income Tax on companies engaged in upstream, midstream, and downstream operations, while Company Income Tax applies to entities involved in petroleum operations, including concessionaires, licensees, lessees, contractors, or subcontractors, as detailed in Section 302. Operators in the petroleum sector are subject to royalties ranging from 15% for onshore areas to 7.5% for deep offshore and frontier basins, with potential incentives for gas utilization and investment in gas pipelines to reduce gas flaring. Additionally, the Act makes provisions for the abandonment and decommissioning of onshore and deep offshore platforms through environmental management plans, as articulated in Sections 232-233. However,

challenges may arise with the effective implementation, enforcement, and compliance of the legislation, including corruption, lack of political will, leadership and enforcement issues, and inadequate skilled personnel. Despite the aim of the PIA to promote international best practices in Nigeria's petroleum industry, it has faced criticism from various quarters. The Nigerian Governors' Forum has raised concerns about specific sections of the Act, which they believe could diminish their revenue share from the federation account.

Furthermore, challenges in the effective implementation of the Act may impede its intended outcomes. The National Petroleum Policy (NPP), a precursor to PIA 2021, was published in 2017. It seeks to achieve the following objectives: Creation of a market-driven Nigeria's petroleum industry; Maximization of production and processing of hydrocarbons; Moving Nigerian oil from being a source of income to oil as fuel for economic growth; Following hydrocarbon from production to market; Incentives investments in a cost-efficient storage, transportation and distribution systems; Promotion of competition; Maximization of the environmental footprint of petroleum exploration in Nigeria, and manage the balance between depleting petroleum resources and renewable energy. The PIA's comprehensive and extensive provisions have covered all these objectives. PIA and NPP will likely cure regulatory and administrative overlaps, mismanagement, and underproductivity in Nigeria's petroleum sector. This is borne out of the fact that the PIA and NPP need to adequately reflect the international and multi-jurisdictional mechanism of a model energy sector. To tackle gas flaring in Nigeria, the Federal Government implemented the National Gas Policy in 2017, aligning with the country's commitment to the Paris Climate Change Agreement of 2015, which advocates zero tolerance for gas flaring. This policy, titled the "Nigerian Gas Flare Commercialization Programme (NGFCP)," aims to end gas flaring in the near term (within 2-3 years). Its implementation carries several benefits, including the reduction of the long-standing practice of gas flaring in Nigeria and the mitigation of health hazards for Niger Delta communities. Economically, the policy is expected to have a significant impact by tapping into approximately 30 million metric tonnes of gas per annum through the Flare Gas (Prevention of Wastes and Pollution) Regulations of 2018, thus accelerating the development of gas infrastructure. The NGFCP was projected to invest \$3.5 billion by 2020 to reduce gas flaring in Nigeria, according to reports from THISDAY NEWSPAPER in 2018. Furthermore, the NGFCP offers a market-driven solution by making gas bankable for investors and lenders while ensuring no adverse impact on the safety or operational efficiency of gas production and

exploration activities. To operationalize the NGFCP, the Petroleum Industry Act (PIA) includes extensive provisions for the management and governance of gas resources in Nigeria, specifically targeting the reduction of gas flaring, as outlined in Sections 125-173. The Act delineates the rights and responsibilities of gas licensees, suppliers, distributors, and retailers. It also establishes a framework for granting various licenses to gas operators by the regulatory Authority upon payment of prescribed fees. Additionally, the PIA provides for a 5-year tax holiday for investors in gas pipelines to encourage effective implementation of the NGFCP policy and incentivize investment in gas infrastructure development.

Policy Shift in the Minerals and Mining Sector

Before the enactment of the Minerals and Mining Act in 2007, the regulation of minerals in Nigeria was governed by a series of specific laws targeting individual minerals, including the Diamond Trading Act 1990, the Quarries Act 1990, the Gold Trade Act 1990, the Tin Miscellaneous Provision Act 1990, the Tin Production and Development Revolving Loans Act 1990, and the Minerals and Mining Act 1999. These laws lacked comprehensive provisions for reversionary rights in mineral licenses, leaving the federal government's reversionary rights minimally protected. However, the Minerals and Mining Act 2007 ushered in significant changes by stipulating that all lands where minerals are discovered commercially shall be acquired by the federal government. The Act also established the Mining Cadastre Office to administer titles and permissions and prohibited mining exploration and development without proper authorization. Additionally, the Act created Departments of Mines Inspection and Environmental Compliance while granting the Minister authority to establish additional agencies deemed necessary for effective implementation. To incentivize investment in the mining sector, the Act offers various benefits to operators, including the ability to deduct 95% of qualifying expenditure incurred in the year of investment as capital allowance. It also allows deductions for all infrastructure costs and certified exploration costs. Operators enjoy exemptions from customs duties on imported plants, machinery, and equipment for mining operations, as well as quotas for approved expatriates and remittance quotas for expatriate personnel free from any tax on currency transfer out of Nigeria. Furthermore, the Act permits holders of mineral titles to retain a portion of foreign exchange earnings in a foreign exchange domiciliary account for the acquisition of spare parts and necessary inputs. In cases of sale or liquidation due to foreign investment, holders of mining licenses are assured of the free transferability of money for certified foreign loans and repatriation of foreign capital. The Act provides three years of assured tax relief

for investments, with an additional two years available at the investor's discretion. However, holders of mineral rights are obligated to safeguard the environment during exploratory activities and are required to contribute to an Environmental Protection and Rehabilitation Program fund to fulfill their environmental responsibilities. Nonetheless, the Act has been criticized for perpetuating environmental struggles by vesting mineral-bearing lands in the federal government, lacking a clear definition of "fair and adequate compensation" for damage, and imposing relatively low penalties without provisions for environmental remediation for pollution.

Policy Shift in The Electricity Sector

Every country, including Nigeria, seeks to secure energy security by optimizing supply and demand, as energy security constitutes a severe challenge to a country's socio-economic development and economic growth, hence the unbridled attempts by Nigeria to evolve the legal and institutional frameworks to address its energy challenges. There has been a shift in Nigeria's electricity sector policy from the fusion of generation and distribution of electricity to monopolization of generation, transmission, and distribution by a centralized organization, the National Electric Power Authority (NEPA), and Power Holding Company of Nigeria (PHCN), to liberalization and progressive, investor-driven, legal and institutional regulatory frameworks to promote local and foreign investments in the electricity sector. The old Nigerian electricity regime, which spanned from 1896 during the colonial era to 2000, was replete with state monopoly in electricity management and governance, in contrast to the new regime that reflects liberalization of electricity supply, intending to promote competition and radical private sector participation through direct and indirect investments and technical partnerships with the federal government. Under the old electricity regime, electricity governance was effectuated by the colonial government through the establishment of the Nigerian Electricity Supply Company (NESCO) in 1929 under the Electricity Ordinance Act of 1929, the Public Works Department in 1946, and the Electricity Corporation of Nigeria (ECN) established according to the Electricity Corporation Ordinance no 15 of 1950 and Niger Dams Authority (NDA). The post-independence era witnessed the fusion of generation and transmission of electricity on April 1, 1972, with the merging of the two extant electricity organizations, ECN and NDA, into NEPA by National Electric Power Authority Decree No. 4 of 1972. NEPA proved to be ineffective in its governance of electricity generation, transmission, and distribution as a result of its monopoly over the electricity regime. It was unbundled through the commercialization and privatization decree no. 25 of 1988 into 18 new companies and semi-

independent business units under the defunct Power Holding Company of Nigeria (PHCN).

The Nigerian government embarked on electricity reforms in 2000 through the enactment of the Electric Power Sector Reform Act (EPSR Act) 2005. The EPSR Act contains express provisions for liberalization of the electricity regime in Nigeria through the promotion of competition, observation of due process, radical private sector participation through direct and indirect investments, and government technical participation. The new regime, therefore, sharply departs from the old regime of state monopoly in electricity governance in Nigeria. The federal government set targets for Nigeria's power sector through the EPSR Act, which include efficient attainment, safe, affordable and cost-effective generation, transmission, distribution, and marketing in Nigeria, attraction of local and foreign investments, development of a transparent, efficient, and effective regulatory framework for the sector. The EPSR Act also provides for consumer protection and high-performance standards by operators to elicit maximum utility and safety for consumers of electricity in Nigeria. On the contrary, the NEPA Act did not provide for the safety of consumers, efficiency, and safety of cables or appliances of consumers. It forbade any other person or state government from obtaining licenses to operate power plants or generate electricity, therefore, the NEPA Act provisions were inconsistent with the 1999 constitutional provision that places electricity generation transmission and distribution in the concurrent legislative list. The policy shift in the development, management, and governance of electricity and other minerals sectors had needed to be faster since the colonial era when the Electricity Corporation of Nigeria (ECN) was established under the Electricity Corporation Ordinance of 1950. After the fusion of ECN and the Niger Dams Authority (NDA) in 1972 by the National Electric Power Authority Decree No 4, which gave birth to the National Electric Power Authority (NEPA), not much happened in this sector until 2023 when the Electric Power Sector Reform Act (2005) was repealed and re-enacted as the Electricity Act 2023. To attract private sector investments in the Nigerian Electricity Supply Industry (NESI), the Electricity Act 2023 Act introduces a comprehensive legal and institutional framework to guide the operation of a privatized, contract and rule-based competitive electricity market in Nigeria. In accordance with the Constitution of the Federal Republic of Nigeria 1999, as amended, the Electricity Act 2023 expressly recognizes the rights of States to make laws for electricity generation, transmission, distribution, system operation, and the establishment of power stations within its territory. This gives state governments the freedom to operate electricity markets independently from the Nigerian Electricity Regulatory Commission (NERC),

including the ability to issue licenses to private investors for the construction of power plants, the establishment of transmission networks, the operation of mini-grids, and the distribution of power within a state. It is crucial to highlight that NERC will continue to regulate electrical firms in such States until the State has implemented its energy laws and created its electricity market. As the market changes, NERC's role under the Act is to keep it competitive for the sake of consumers and businesses alike. To avoid catastrophic market issues in the NESI, NERC may now intervene to save the licensee firm from bankruptcy. In doing so, NERC can play a more proactive role in regulating the industry and making sure that businesses are functioning efficiently and responsibly. The Act empowers the Federal Ministry of Finance to create tax incentives to encourage and ease the use of renewable energy sources to stimulate the development and use of such sources while striking a balance between possible costs passed on to end-users. Despite these reforms or paradigm shifts in electricity regime policy, electricity demand still constitutes a significant challenge for Nigeria and Nigerians. Nigeria's socio-economic development is still dependent on fixing its energy sector. Persons with access to electricity are still experiencing incessant light shedding and limited electricity supply. Nigeria urgently needs to address its electricity deficit challenge by tapping its abundant renewable energy resources, which can be developed, governed, and utilized from biomass, wind, waves, the sun, hydro-power, bio-fuels, bio-gas, and geothermal sources.

CONCLUSION AND PROPOSALS FOR REFORM

The Nigerian energy sector has experienced significant shifts in policy over the years, but the effective implementation of these policies has often been hindered by various challenges. These challenges, including ambiguous legal provisions, resource mismanagement, and institutional weaknesses, have necessitated urgent reforms to establish a robust energy policy framework. Firstly, there is a pressing need for a new legal regime that grants resource-based and property rights to communities hosting energy resources. This new legislation should not only recognize the rights of these communities but also incorporate principles of international law, energy diplomacy, International Environmental Law, and international best practices. By doing so, Nigeria can ensure fair and sustainable utilization of its energy resources while aligning with global standards and commitments. In addition to legal reforms, strengthening the institutional regulatory frameworks in the energy sector is crucial. This involves addressing issues such as corruption, improving transparency, and recruiting proficient personnel. By

enhancing regulatory effectiveness through proactive enforcement and participatory approaches, Nigeria can ensure that energy sector laws and regulations are consistently adhered to. Another vital aspect of reform is the reconsideration of existing contractual arrangements in the energy sector. Contracts such as risk service contracts, production sharing contracts, and joint ventures have often favored multinational companies, leaving Nigeria primarily as a tax collector. To address this imbalance, Nigeria should prioritize contractual arrangements that safeguard its interests, promote equitable distribution of benefits, and maximize revenue generation from energy resources. Furthermore, sustainable development principles must be explicitly incorporated into energy sector legislation. This includes principles of sustainable development, intergenerational equity, and sustainable resource utilization. By embedding these principles into the legal framework, Nigeria can ensure that energy development activities are conducted in a manner that balances present needs with the interests of future generations. This is particularly crucial in addressing global challenges such as climate change and environmental degradation. Nigeria's potential in nuclear energy remains largely untapped, highlighting the need for investment in this area. This involves recruiting and training skilled personnel in nuclear energy science and technology and reviving relevant legislation such as the Nuclear Safety and Radiation Protection Act. By harnessing its nuclear energy potential responsibly, Nigeria can diversify its energy sources and enhance energy security. Finally, flexible dispute resolution mechanisms are essential for addressing complex energy sector contracts and agreements. Incorporating provisions for choice of law, forum, and mode of settlement in energy sector laws can streamline dispute resolution processes and ensure fair outcomes in commercial disputes between multinational companies and the government. Overall, by implementing these comprehensive reforms, Nigeria can overcome longstanding challenges in its energy sector and establish a more efficient, equitable, and sustainable energy policy framework. This will not only enhance energy security and promote socio-economic development but also position Nigeria as a responsible global energy player in the transition towards a more sustainable energy future.

REFERENCES

- Anderson, O. and Kramer, B. 2005. The Rule of Capture: An Oil and Gas Perspective. *Environmental Law*, 35: 4.
- Anyatang, B., and Kooffreh, B. 2021. Abandonment/decommissioning under Nigerian legal regimes: A comparative analysis. *Environmental Law Review*, 23(2): 110-127. <https://doi.org/10.1177/14614529211006074>.
- Black, B. 2020. *Crude Reality: Petroleum in World History*. Rowman & Littlefield Publishers.

- Denman, D. and Prodano, S. 1972. *Land Use: An Introduction to Proprietary Land Use Analysis* (1st ed.). Routledge. <https://doi.org/10.4324/9781003386667>
- Edomah, N. 2021. The governance of energy transition: lessons from the Nigerian electricity sector. *Energy, Sustainability and Society*, 11: 40. <https://doi.org/10.1186/s13705-021-00317-1>
- Ekhaton, E. 2016. Public Regulation of the Oil and Gas Industry in Nigeria: An Evaluation. *Annual Survey of International & Comparative Law*, 21: 1.
- Ghorbani, E. 2017. Ownership of Petroleum Resources in Islam and The Iranian Law. *Oil, Gas & Energy Law Journal*, 15(3).
- Steyn, P. 2009. Oil Exploration in Colonial Nigeria, 1903–58. *The Journal of Imperial and Commonwealth History*, 37(2): 249-274. <https://doi.org/10.1080/03086530903010376>

ORCID DETAILS OF THE AUTHORS

Rose Ohiana Ugbe: <https://orcid.org/0000-0003-1052-8995>



Heavy Metal Concentration in Fish Species *Clarias gariepinus* (Catfish) and *Oreochromis niloticus* (Nile Tilapia) from Anambra River, Nigeria

E. B. Ogbuene*†, A. M. Oroke*, C. T. Eze***, E. Etuk*, O. G. Aloh****, F. E. Achoru**, J. C. Ogbuka**, O. J. Okolo*, A. V. Ozorme*, C. J. Ibekwe*, C. A. Eze* and S. Akatakpo*****

*Centre for Environmental Management and Control (CEMAC), University of Nigeria, Enugu Campus, Nigeria

**Institute of Maritime Studies, University of Nigeria, Enugu Campus, Nigeria

***Department of Biochemistry, Federal University Oye-Ekiti, Ekiti State, Nigeria

****Department of Geography and Meteorology, Enugu State University of Science Technology ESUT, Enugu, Nigeria

*****Department of Geoscience, University of Texas at Dallas, USA

†Corresponding author: E. B. Ogbuene; ogbuene.emeka@unn.edu.ng

Nat. Env. & Poll. Tech.
Website: www.neptjournal.com

Received: 17-08-2023

Revised: 26-10-2023

Accepted: 10-11-2023

Key Words:

Heavy metals

Contamination

Fish

River pollution

ABSTRACT

Studies have emphasized that the presence of heavy metals in freshwater fish represents a global public health issue. Nigeria, being a developing nation with less emphasis on the quality of seafood consumed by the residents, ranks this study very vital. The policy implication of this study is the advancement of a healthy population in contemporary Nigeria. Hence, this study assessed heavy metal concentration in two fish species, *Clarias gariepinus* (Catfish) and *Oreochromis niloticus* (Nile Tilapia), in the Anambra River. The sample included twenty fishes, of which eighteen were collected from the three sampling locations (the fish ports of Anambra River), namely Otu-nsgube, Otuocha, and Ikemivite) while two control samples were collected from a pond about 200 m away from the river. The levels of heavy metals were determined using Varian AA 240 atomic absorption spectrophotometer (AAS). The results showed that the concentrations of heavy metals (cadmium and arsenic) in the sampled fishes from Anambra River exceeded the joint World Health Organization and Food and Agriculture Organization (FAO/WHO) standard for fish and fish product consumption, while the concentration of chromium, mercury, and lead are within the permissible limit. The study also showed the distribution of the heavy metals in the fish organ varies among fish species. Heavy metals occur higher in *Clarias gariepinus* than in *Oreochromis niloticus*, while tissue preference for heavy metal accumulation is in the order of gill > liver > muscle. It was recorded from this study that the heavy metal concentration in the fish from the pond is generally higher than the fish from the river for some metals. The high level of heavy metals in the sampled fish was attributed to heavy metals contamination of the river as a result of various anthropogenic activities such as mining, burning of fossil fuel and emission from the exhaust of boats/vehicles, overuse of fertilizers and pesticides, discharge of effluent, sewage, and hospital waste. This study concluded that long-term consumption of fish from the river may pose health risks to the consumers due to the possible bioaccumulation of heavy metals, especially cadmium and arsenic. It was recommended that continuous monitoring of heavy metal levels in the fish and water, public awareness, and appropriate legislative provisions should be put in place to ensure that harvested fish and fish products may be safe for human consumption.

INTRODUCTION

Studies have shown that the contamination of aquatic ecosystems by a wide range of pollutants has become a matter of concern over the last few decades. Consequently, there is a need to quantify the heavy metal concentration in fish species from the Anambra River, Nigeria. Fish is an aquatic organism that is widely consumed around the world as a major source of dietary protein. It provides humans with

low saturated fat and omega-3(n-3) fatty acids, including cardio-protective and reproductive benefits. Fish plays a key role in universal food distribution, and its consumption has increased significantly since 1973 (FAO 2004). It is also estimated that over 200 million people, mostly those living in landless communities, depend on fisheries (via fishing, fish processing, marketing, and transportation of fish and fish products) for their livelihood (Sikoki & Otobotekere 1999). However, these numerous benefits of fish may be offset by

the presence of pollutants, especially heavy metals such as (Zn, Cu, Cd, Pb, Hg and Cr). Studies have shown that many of these pollutants originate from various anthropogenic activities such as unsustainable agriculture, industrial activities, and increasing urbanization, which facilitates their entry into rivers, lakes, and oceans (Abou-Arab et al. 1996).

This study aims to quantify the level of concentration of heavy metals (cadmium, lead, mercury, chromium and arsenic) in the tissues (muscles, liver, and gills) of two edible freshwater species of fish: African catfish (*Clarias gariepinus*) and Tilapia fish (*Oreochromis niloticus*) from Anambra River, Nigeria. Anambra River drains into the River Niger at Onitsha, Nigeria. This study is vital considering the high quantities of fish caught in the river. Heavy metals may contaminate these fish.

Evidence has shown that rapid human population growth, anthropogenic activities, urbanization, industrialization, and unsustainable agricultural practices could increase the concentration of heavy metals in the environment above the acceptable threshold, especially in aquatic ecosystems (Maurya & Malik 2018). Fish are conditioned by their environment, and hence, it is obvious that if the growing and harvesting environment of fish is polluted by chemical or microbiological sources, the fish could also be contaminated through the process of bioaccumulation.

It has been established that the heavy metal load of fish reflects the contamination level of their habitat and, thus, is a potential indicator of pollution sinks. At low concentrations, some heavy metals, such as iron, zinc, copper, and manganese, do not pose health concerns but can become toxic agents at higher concentrations. Heavy metals such as lead (Pb), chromium (Cr), mercury (Hg), arsenic (As), and cadmium (Cd) in fish may become toxic at concentrations exceeding the permissible limits. These heavy metals have a high degree of toxicity and rank among the important metals that are of public health concern, thus classified as either “known” or “probable” human carcinogens (United States Environmental Protection Agency 2012). This is a growing issue, especially in developing parts of the world (such as Nigeria), where attention to safety regulations on food is lacking or inadequate.

Evidence has shown that bio-concentration and bio-magnification are capable of leading to toxic effects of metals in fish, even when environmental exposure level is low (Chovanec et al. 2003, Vanderoost et al. 2003). In the context of an empirical review, Maurya and Malik (2018) identified that heavy metal concentration in fish tissues (muscle, gills, and liver) is increasing steadily in the Ganga River. They also demonstrate that the concentration of Pb, Cd, and Cr are higher than the internationally recommended

standard limits of WHO and FAO. In addition, higher concentrations of metals were found in the liver and gills than in muscle. Akpanyungetal (2014) reported on the levels of heavy metals in fish obtained from two fishing sites in Akwa Ibom State, Nigeria, and identified that the levels of Zn and Cu were significantly higher than the maximum recommended levels ($p < 0.05$) at both locations and in all the organs. Ali and Khan (2018) reported concentrations of the heavy metals (Cr, Ni, Cd, and Pb and Ni) but observed that Ni accumulation may pose a potential health risk to fish consumers. Research by Gbogbo et al. (2018) reported that lead and cadmium were below detectable levels in all the fish samples, while Cu was not detected in *B. auritus*. The study maintained that the levels of the remaining metals (mg kg^{-1}) were below FAO/WHO maximum permissible limits in fish and occurred in the rank order $\text{Se (3.5)} > \text{Zn (2.34)} > \text{Cu (0.59)} > \text{As (0.37)} > \text{Hg (0.19)}$ in *C. nigrodigitatus* and $\text{Se (2.97)} > \text{Zn (2.28)} > \text{Hg (0.31)} > \text{As (0.21)}$ in *B. auritus*. In a study on the Bioaccumulation of heavy metals (Zn, Pb, Cd, and Cu) in liver, gills, and flesh in benthic and pelagic fish species collected from Lake Geriyo, it was established that the levels of heavy metals varied significantly among fish species and organs (Bawuro et al. 2018). The flesh possessed the lowest concentration of all the metals, while the liver was the target organ for Zn, Cu, and Pb accumulations. However, Cd exhibited a higher concentration in the gills. Fish species showed an inter-specific variation of metal absorption. These differences were discussed for the contribution of potential factors that affected metal uptake, like age, geographical distribution, and species-specific factors. Similarly, Sobhanardakani et al. (2018), Yaradua et al. (2018), and Adeosun et al. (2014) reported that the level of heavy metals all fall below the USEPA (2012) and WHO/FAO (2015) permissible limit for fish, while Akpanyung et al. (2014) maintained that the levels of Zn, Cu, Pb, Cr and As in the fish at Ibaka were above the standards set by WHO/FAO/UNEP and suggested regular monitoring and assessment of fishing sites in the region for heavy metal contamination. It was noted from the review of literature that most of the environmental monitoring studies have focused primarily on contaminant concentrations in the environment rather than in the biota such as fish (Borgmann et al. 2008). To the best of our knowledge, studies reviewed seldom quantify the level of heavy metal concentration in aquatic biota (fish). Hence, the study quantifies the level of heavy metal concentration in fish samples from the Anambra River. The study is unique because it compares the *Clarias gariepinus* and *Tilapia zilli* sampled together at various sampling stations in Anambra River with heavy metal levels in fish from the pond. The study area is characterized by unsustainable agriculture, which is a serious risk factor for pollution.

MATERIALS AND METHODS

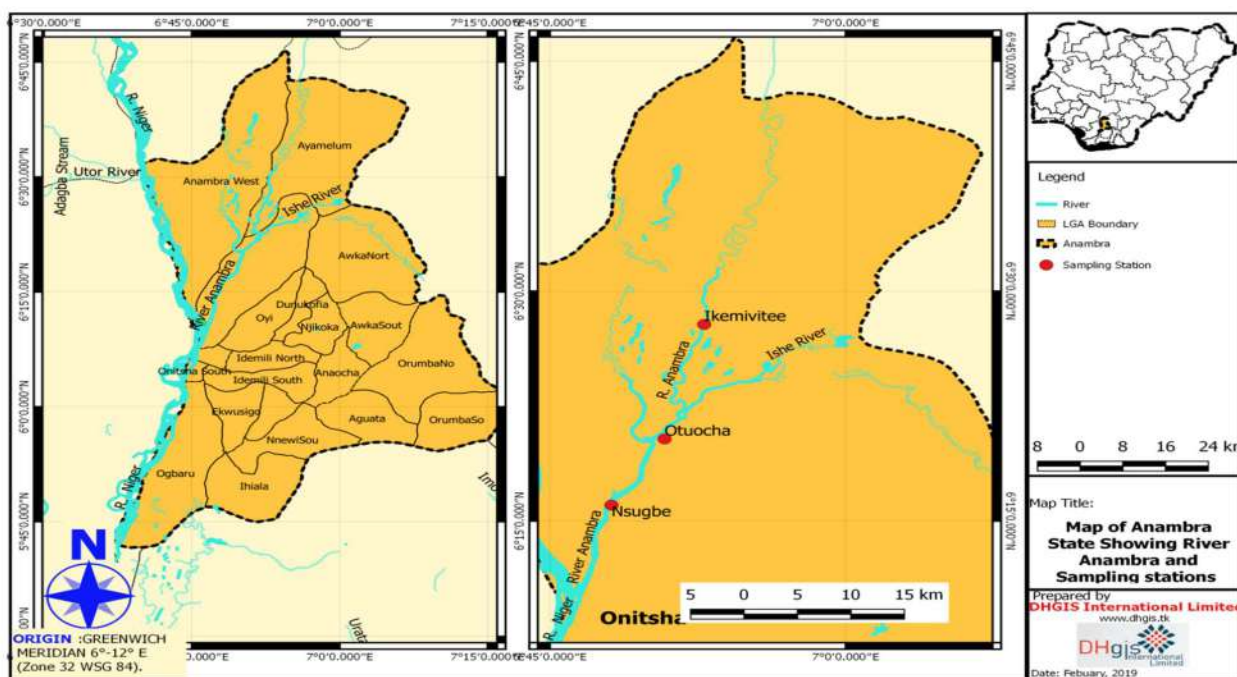
Study Area

The study was carried out in Anambra River, Anambra State, Nigeria. Anambra River is about 230 km in length and has an extensive basin of about 14,010 km². The basin lies between latitude 6°10' and 7°20', longitude 6°35' and 7°40' east of the Niger River into which the Anambra River empties. The Anambra River is the largest tributary of River Niger below Lokoja and is often regarded as a part of the lower Niger lowlands (Awachie & Hare, 1978) in Obiakoret al (2014). The River has a southward course up to the Kogi/Enugu State boundary; it then meanders through Ogurugu to Nando Ikemivite, Otuocha, and Nsugbe, from where it flows down to form a confluence with the Niger River at Onitsha (Fig. 1).

The sampling areas were located around the major fish landing sites of the main river at the adjacent floodplain of Otu-Nsugbe, Otuocha, and Nando Ikemivite. The three stations, Ikemivite, Otuocha and Otu-Nsugbe, with GPS Latitude 6.3500° and Longitude 6.9167°; Latitude 6.3333° and Longitude 6.8500°, as well as Latitude 6.2667° and Longitude 6.8167° respectively, were selected as sampling points. The criteria for selecting these sampling points are based on accessibility, as well as their strategic locations

on the various stretches of the Anambra River, and human activities such as fishing, farming, rice mill industry, market, domestic activities, and refuse dumping. The sample collection involved a total of Twenty (20) life-matured fish samples, comprising 18 experimental (nine samples each) of *Clarias gariepinus* and *Oreochromis niloticus* and 2 control samples, made up of one sample of each fish species. The samples were purchased directly from the fishermen at the three sampling locations (Ikemivite, Otuocha, and Otu-Nsugbe fishing ports) of the Anambra River in September 2022. The control samples were bought from a fish pond that uses borehole water about 200m from the river.

Clarias gariepinus and *Oreochromis niloticus* were chosen because they appear to have great economic value and are readily available in terms of populations, suggesting their ecological importance in the area. Similarly, these species were chosen with consideration for the sensitivity of aquaculture organisms in terms of heavy metals contamination and accumulation. The fish samples caught freshly were thoroughly washed and put in sterile polythene bags and then placed in an icebox to maintain the freshness and transported immediately to the laboratory for dissection. Before dissection, the mean weight and mean length of the fish samples were measured with measuring tape and weighing balance, respectively. The mean weight was 1800 g, while the mean length was 30.5 cm. The taxonomical



(Source: DHGIS Limited, 2019)

Fig. 1: Map of Anambra State, Nigeria, showing Anambra River and sampled stations.

Table 1: Mean Concentration of Heavy metal in Fish samples from Anambra River and Fish pond.

Heavy metals (ppm)	Fish	Otuocha	Otu-Nsugbe	Ikem-Ivite	Fish pond (control)	Joint WHO/FAO standard				
Arsenic	tissues	<i>Clarias</i> <i>garepinus</i>	<i>Oreochromis</i> <i>niloticus</i>	<i>Clarias</i> <i>garepinus</i>	<i>O.</i> <i>niloticus</i>	<i>Clarias</i> <i>garepinus</i>	<i>O.</i> <i>niloticus</i>	<i>Clarias</i> <i>garepinus</i>	<i>O.</i> <i>niloticus</i>	0.26
	Muscle	0.413	0.000	0.105	0.000	0.418	0.000	0.524	0.000	
	Gill	0.000	0.371	0.000	0.000	1.126	0.211	0.693	0.461	
	Liver	0.000	0.000	0.000	0.000	0.131	0.313	0.000	0.000	
Chromium	Muscle	0.000	0.054	0.263	0.057	0.057	0.000	0.106	0.017	1.00
	Gill	0.193	0.028	0.054	0.309	0.061	0.000	0.033	0.077	
	Liver	0.114	0.113	0.021	0.012	0.017	0.014	0.076	0.037	
Mercury	Muscle	0.000	0.146	0.173	0.000	0.000	0.000	0.000	0.000	0.60
	Gill	0.000	0.000	0.324	0.000	0.000	0.000	0.000	0.000	
	Liver	0.000	0.000	0.000	0.000	0.000	0.000	0.000	0.000	
Lead	Muscle	1.061	0.253	0.798	0.299	0.737	0.613	0.814	0.458	1.00
	Gill	0.722	0.535	0.365	0.000	1.730	0.956	1.263	0.350	
	Liver	0.218	0.107	0.630	0.212	0.412	0.175	0.222	0.073	
Cadmium	Muscle	0.428	0.307	1.271	0.329	0.484	0.169	0.438	0.390	0.20
	Gill	0.392	0.276	0.468	0.449	0.361	0.304	0.319	0.297	
	Liver	0.286	0.370	0.389	0.333	0.356	0.279	0.306	0.377	

(Source: Authors' Field Work 2022)

identification of the fish species was done according to the field guide to Nigerian freshwater fishes (Olaosebikan & Raji 1998).

The fish samples were separated according to species and location and stored inside the deep freezer at about -100°C and allowed to thaw. Scales were removed and washed with running tap water to remove dirt before being dissected with sterile scissors. The needed fish tissues (gills, liver, and muscles) were transferred into sterile sample bottles, labeled according to species and location, and kept for digestion and analysis of heavy metals. To avoid contamination, all bottles and glassware used in the preparation of the samples were soaked in nitric acid for 15 min and rinsed with deionized water before being used. The prepared sample was left overnight at room temperature.

Wet digestion of the sample and determination of heavy metals were conducted to digest the samples. The digested samples were poured into auto-analyzer cups, and the concentration of heavy metals (Cadmium, Mercury, Chromium, Arsenic, and Lead) in each sample was determined using a Varian AA 240 Atomic Absorption Spectrophotometer (AAS) according to the method of APHA 1995 (American Public Health Association). The values of the heavy metal concentrations in the tissues were calculated based on dry weights as this discounted the variability due to inner parts differences in the moisture content of organisms. The accuracy and precision were verified using standard reference materials (MA-A-2/TM) provided by the International Atomic Agency (IAEA)

and Zschunke (2013). The absorption wavelengths and detection limits for the heavy metals were noted. The result of the experiment was compared with the Joint WHO/FAO standard for fish consumption. The data collected was analyzed using analysis of variance (ANOVA), and $P < 0.05$ was considered to indicate a statistically significant difference. Means of significant differences were separated using Duncan's Multiple Range Test. Two-way analysis of variance (ANOVA) was used to assess whether the heavy metals concentration in fish varied significantly among the locations and species.

RESULTS AND DISCUSSION

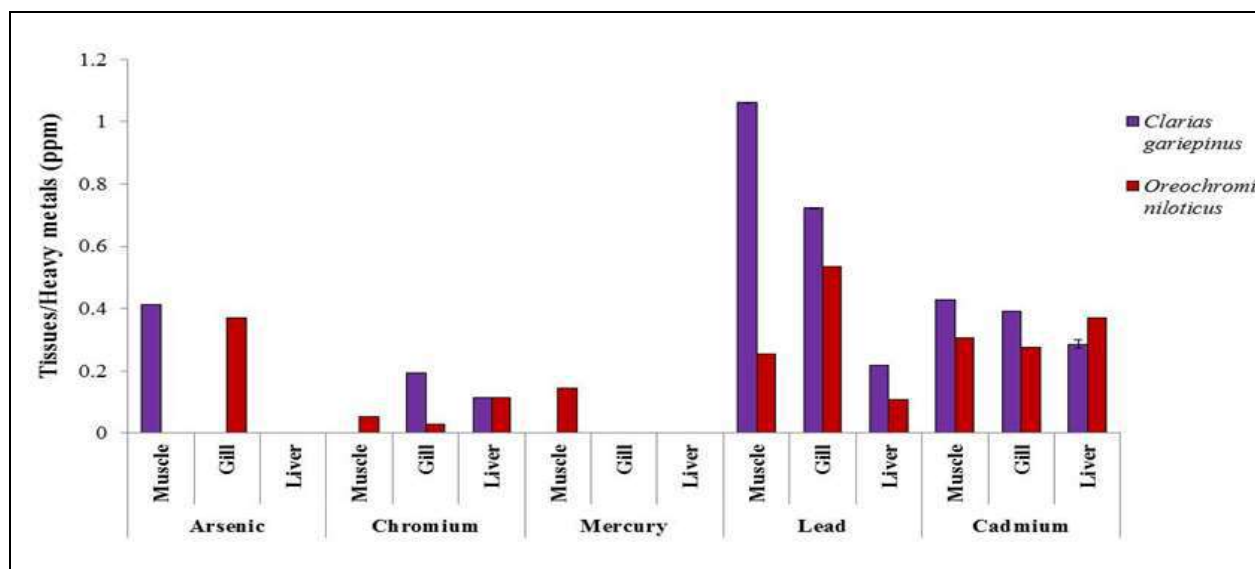
Data in Table 1 shows the level of heavy metal concentration in selected fish samples from the Anambra River. The study quantifies heavy metal concentration in the muscle, gill, and liver of the two species of fish, *Clarias garepinus* (catfish) and *Oreochromis niloticus* (Tilapia fish).

Heavy Metal Concentration in Fish Tissues

The findings of this study showed that the mean concentration of heavy metals in the fish tissues differs significantly amongst the sampled fish species in the Anambra River ($p=0.000$). The variation in the level of heavy was further explained in Table 1. The heavy metal levels in the two species of fish (*Clarias garepinus* (catfish) and *Oreochromis niloticus* (Tilapia fish)) include Arsenic (0.0-0.46ppm), Chromium (0.0-0.309ppm), Mercury (0.0-0.324 ppm), lead (0.0-1.73 ppm) and Cadmium (0.169-0.449 ppm). The fish

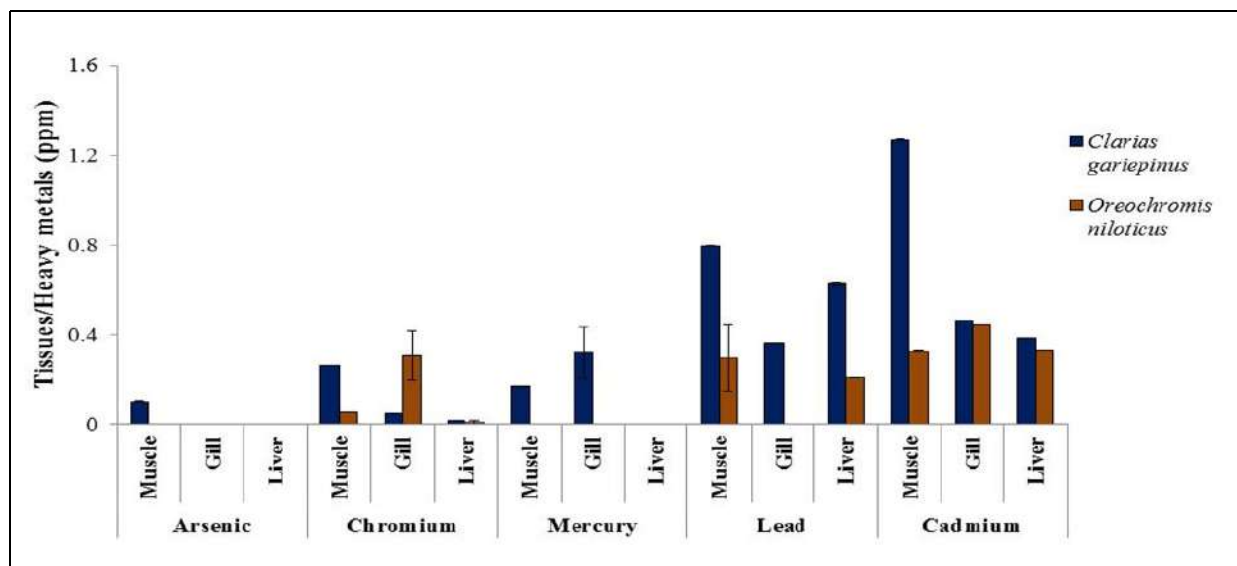
tissue (gill, liver, and muscle) recorded differences in the rate of heavy metal concentrations. The study also established that heavy metal accumulations were higher in the gill, followed by liver and muscle. In the same vein, the level of heavy metals recorded in *Clarias gariepinus* was higher than in *Oreochromis niloticus*. This finding agrees with Maurya and Malik (2018) and Akpanyunget al. (2014). However, their

work was not able to quantify the variation in fish tissue (gill, liver, and muscle). The present study quantifies the disparity in heavy metal accumulation in species-specific factors of fish, with *Clarias gariepinus* recording higher than *Oreochromis niloticus*. The quantity of heavy metal disparity as measured in gill, liver, and muscle are shown in Figs. 2, 3, and 4, respectively.



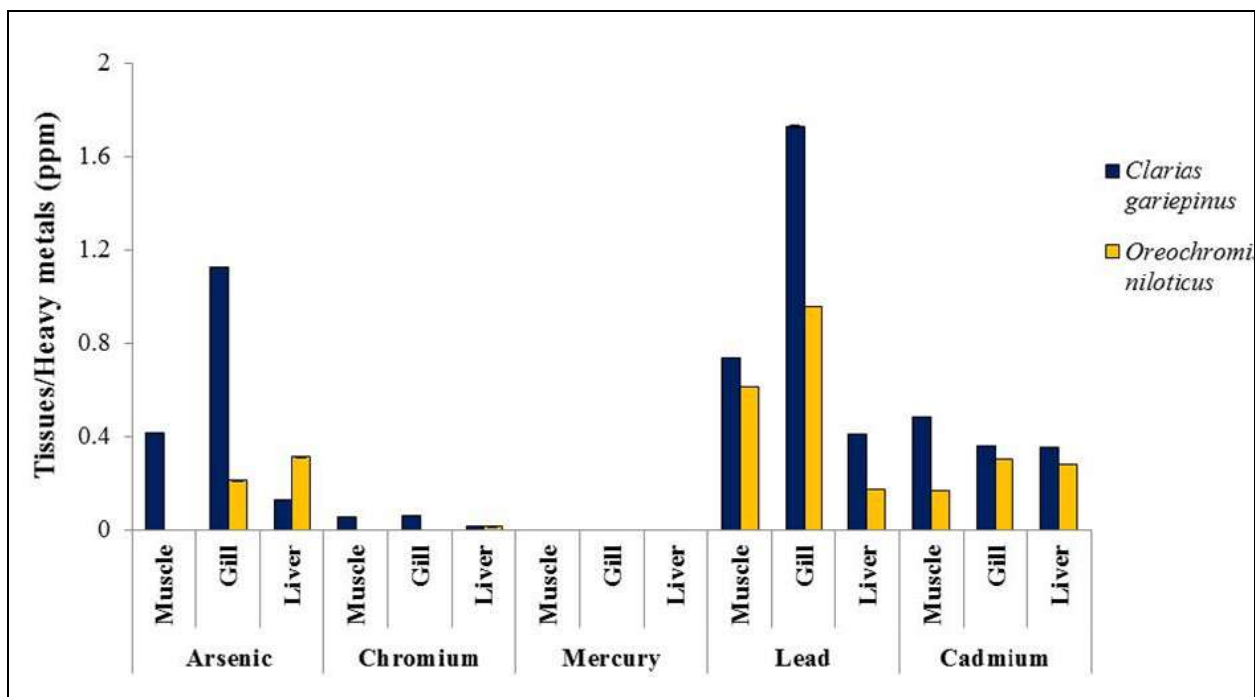
(Source: Result of Researchers' Laboratory Analysis 2022)

Fig. 2: Comparison of heavy metal concentrations in the tissues of *Clarias gariepinus* and *Oreochromis niloticus* at Otuocha in Anambra River, Nigeria.



(Source: Researchers' Laboratory Analysis, 2022)

Fig. 3: Comparison of heavy metal concentrations in the tissues of *Clarias gariepinus* and *Oreochromis niloticus* at Otu-Nsugbe in Anambra River, Nigeria.



(Source: Researchers' Laboratory Analysis 2022)

Fig. 4: Comparison of heavy metal concentrations in the tissues of *Clarias gariepinus* and *Oreochromis niloticus* at Ikem-Ivite in Anambra River, Nigeria.

The disparity in heavy metal accumulation in the fish species studied could be attributed to differences in feeding habits. *Clarias gariepinus* is omnivorous and feeds at all times, while *Oreochromis niloticus* is a carnivore and is typically diurnal. In a similar study carried out by Zhang et al. (2018), they emphasized that metals exhibit various affinities to different organs, and irrespective of the uptake route, gill and liver accumulate high levels of metals and are often used as a good water pollution biomarker.

The differences in metal concentrations can also be attributed to differences in metal uptake, as observed by Hashim et al. (2014) and Adebayo (2017). Other probable reasons include fish size and where fish reside in water. For instance, Adebayo (2017) reported that heavy metal concentrations were higher in omnivorous/herbivore fish such as *Heterotis niloticus* and lower in carnivore fish such as *Clarias anguillaris*. Moreover, Hashim et al. (2014) established that omnivorous fish were detected with elevated concentrations of Cd and Ni, whereas carnivorous fish had the highest concentration of Pb. However, their study was not able to quantify the variation in fish species in different water habitats. Hence, the present study quantifies heavy metal variation in gill, liver, and muscle at different habitats, namely "Otuocha, Otu-Nsugbe, and Ikemivitee" in the Anambra River of Anambra State, Nigeria (Figs. 2 to 4).

The concentration of heavy metals recorded in the fish gill, liver, and muscle could also be attributed to the high influx of heavy metals in the Anambra River from anthropogenic activity.

Differences Between Heavy Metal Concentration in the Experimental and Control Samples

The findings of this study showed that there is a significant difference between heavy metal concentration in the experimental and control samples ($p=0.010$). This finding is further validated by the result in Table 1. The concentration of metals in fish from the pond is generally higher than those from Anambra River except in Chromium and Cadmium, as recorded in *Clarias gariepinus*, and Lead and Chromium, as in *Oreochromis niloticus*. This finding is in line with Zhang et al. (2018), who reported that the concentration proportions of Cd, Cu, and Zn in mixed edible tissues were higher in cultured fish than in wild fish. Akan et al. (2012) identified that sampled wild fish, including *Oreochromis niloticus*, had low values for the heavy metals tested (Cu, Zn, Co, Mn, Fe, Cr, Cd, Ni, and Pb).

The finding of this study further showed that the concentration proportion of lead and cadmium in both pond and river fish was much higher in gill, followed by liver and muscles in both fish species. Thus, we can deduce that organs

like the liver, muscle, and gill were more likely to have higher trace element accumulation abilities in both cultured and wild fish, which differs from other works reviewed.

Similarly, this result agrees with (Ndayisenga & Dusabe 2022), who reported that concentrations of heavy metals values for Fe (0.61 -1.39 ppm) and Mn (0.069-0.186 ppm) for *Tilapia nilotica* and *Clarias gariepinus* reared in fish ponds in 3 districts in Rwanda was above the permissible limit of WHO; However, the study fails to compare heavy metals in fish ponds and River environments.

These findings further revealed that the heavy metal concentration in the aquatic environment may influence cultured fish more than wild fish, probably because the water used in aquaculture does not flow and may be contaminated either through industrial effluents or possible infiltration, thereby increasing the chances of heavy metal bioaccumulation in the fish tissues. In addition, the feeds and chemicals used in culturing the fish may contain heavy metals.

Differences Between Heavy Metal Concentration in the Fish Tissue and Joint WHO/FAO Standard Limit

The findings of this study also indicate that there is a significant difference between heavy metal concentration in the fish tissue and joint WHO/FAO standard limit ($p=0.027$). The finding of the study is validated by the result in Table 1. The heavy metal level in the two species of fish (*Clarias gariepinus* (Catfish) and *Oreochromis niloticus* (Tilapia fish)) ranges as follows: Arsenic (0.0-0.46ppm), Chromium (0.0-0.309 ppm), Mercury (0.0-0.324), Lead(0.0-1.73) and Cadmium (0.169-0.449). These set of values differ from joint WHO/FAO standard limit (arsenic with a value of 0.26 ppm, chromium (1.00 ppm), mercury (0.60 ppm), lead (1.00 ppm), and cadmium (0.20 ppm) as presented in Table 1. The concentration of heavy metals (cadmium and arsenic) in fish samples from Anambra River is higher than the joint FAO/WHO standard for fish diet, except Pb. Cr and Hg, which are within the standard. This indicates that consumption of these fish species at present may be a potential health hazard. This may also pose a health risk to regular fish consumers due to possible bioaccumulation as the concentrations of As and Cd exceed the permissible limit. These findings agree with Adebayo (2017), Maurya and Malik (2018), Mensoor and Said (2018), Hashim et al. (2014), Bawuro et al. (2018) Akpanyung et al. (2014), WHO/FAO/IAEA (1996), Murtala et al. (2012), Oumar et al. (2018) who reported heavy metal concentration above the World Health Organization, Food and Agriculture Organization, the European Commission (EC), USEPA, WHO/FAO, UNEP, (FAO, UNEP, FEPA, and Australian

National Health and Medical Research Council (ANHMRC) standards. It is important to note that some individuals may consume fish more often, and their dietary intake of these heavy metals would further accumulate, which may lead to elevated health risks. Chronic poisoning with heavy metals (Pb) may lead to anemia and brain damage. Research has shown that long-term low-level Lead exposure in children may lead to diminished intellectual capacity and health risks to pregnant women (WHO 1995). It has also been reported that metals such as iron, copper, cadmium, chromium, lead, mercury, and nickel can produce reactive oxygen species. The result of this is lipid peroxidation, DNA damage, and altered calcium homeostasis. Human exposure to cadmium occurs through contaminated food, water, and cigarette smoking, as well as environmental pollutants with acclaimed toxicity at extremely low concentrations. Cadmium and lead are associated with non-carcinogenic and carcinogenic effects, and continuous exposure to heavy metals has been linked to the development of mental retardation, kidney damage, various cancers, and even death in instances of very high exposure in the human body. Similarly, the toxicity of cadmium affects the bone, liver, renal, reproductive, respiratory systems, and DNA repair mechanism, ultimately precipitating diseases such as hypertension, emphysema, and cancer (Ugwuja et al. 2015)

CONCLUSION

This study showed that the heavy metal concentration in various tissues of fish samples differed significantly. While the levels of Cr, Hg, and Pb are within the standard limit set by the joint FAO/WHO (2015), the concentration of As and Cd exceeds the limit. Heavy metal level in the fish at present is a potential hazard, and long-term consumption of the fish from the area may pose a serious health risk to regular fish consumers due to possible bioaccumulation of the heavy metals, especially cadmium and arsenic. To harvest fish and fish products that are safe for human consumption, there should be continuous monitoring of heavy metal levels to prevent bioaccumulation above permissible levels. The water standards and concentrations of heavy metals in the Anambra River should be monitored routinely to ascertain the heavy metal transfer factor to fish from its environment, as well as the sources to enable sustainable aquatic protection and management practices in the area.

The quality of the fish (both wild catch and aquaculture) for human consumption and the health risks associated with the aquatic products need to be given priority. The toxicity of chemicals like antibiotics, feed additives, water treatment products, and other products used in the aquaculture facility or site need to be adequately evaluated

and well documented. Various human activities, such as the location of automobile workshops, dumping of domestic sewage, and other activities that are inimical to the safe use of the river, should be discouraged. Appropriate measures, such as legislative provisions and other tools for effective environmental monitoring, should be mounted and used to protect and enhance the quality of the river.

REFERENCES

- Abou-Arab, A.A., Ayesh, A.M., Amra, H.A. and Naguib, K. 1996. Characteristic levels of some pesticides and heavy metals in imported fish. *Food Chem.*, 57: 478-492.
- Adebayo, I.A. 2017. Determination of heavy metals in water, fish, and sediment from Ureje water reservoir. *J. Environ. Anal. Toxicol.*, 7: 486. doi: 10.4172/2161-0525.1000486.
- Adeosun, F.I., Akinyemi, A.A., Idowu, A.A., Taiwo, I.O., Omoike, A. and Ayorinde, B.J. 2014. The effect of heavy metals concentration on some commercial fish in Ogun Rivers, Opeji, Ogun state, Nigeria. *Afr. J. Environ. Sci. Technol.*, 8 (7): 416-421.
- Akan, J.C., Mohmoud, S., Yikala, B.S. and Ogugbuaja, V.O. 2012. Bioaccumulation of some heavy metals in fish samples from River Benue in Vinikilang, Adamawa State, Nigeria. *Am. J. Anal. Chem.*, 3(11): 78-93.
- Akpangyung, E.O., Ekanemesang, U.M., Akpakpan, E. I and Anadoze, N.O. 2014. The levels of heavy metals in fish obtained from two fishing sites in Akwa Ibom State, Nigeria. *Afr. J. Environ. Sci. Technol.*, 9(4): 365-370.
- Ali, H. and Khan, E. 2018. Assessment of potentially toxic heavy metals and health risks in water, sediments, and different fish species of River Kabul, Pakistan. *Int. J. Hum. Ecol. Risk Assess.*, 24(8): 2101-2118.
- APHA. 1995. 3112B, Cold-Vapour Atomic Spectrometric Method. Standard Methods for the Examination of Water and Waste-Water Twentieth edition, APHA, AWWA.WEF, Washington DC.
- Bawuro, A.A., Voegborlo, R.B. and Adimado, A. A. 2018). Bioaccumulation of heavy metals in some tissues of fish in Lake Geriyo, Adamawa State, Nigeria. *J. Environ. Public Health*, 4: 26-39.
- Borgmann, U., Norwood, W.P. and Dixon, D.G. 2008. Modeling bioaccumulation and toxicity of metal mixtures. *Int. J. Hum. Ecol. Risk Assess.*, 14: 266-289.
- Chovanec, A., Hofer, R. and Schiemer, F. 2003. Fish as bioindicators. *Trace Metals and Other Contaminants in the Environment*, 6: 639-676.
- FAO. 2004. The State of World Fisheries and Aquaculture (SOFIA). Part 1: World Review of Fisheries and Aquaculture, Fishers and Fish Farmers. FAO, Rome
- FAO/WHO. 2015. Codex Alimentarius Commission. Codex General Standard for Contaminants and Toxins in Food and Feed, CODEX STAN 193, 1995; FAO, Geneva, Switzerland.
- Gbogbo, F., Arthur-Yartel, A., Bondzie, J. A., Dorleku, W.P., Dadzie, S. and Kwansa-Bentum, B. 2018. Risk of heavy metal ingestion from the consumption of two commercially valuable species of fish from the fresh and coastal waters of Ghana. *PLoS ONE*, 13(3): 56.
- Hashim, R., Song, T. H., Muslim N. Z. and Yen, T. P. 2014. Determination of heavy metal levels in fishes from the lower reach of the Kelantan River, Kelantan, Malaysia. *Trop. Life Sci. Res.*, 25(2): 21-39.
- Maurya, P.K. and Malik, D.S. 2018. Bioaccumulation of heavy metals in tissues of selected fish species from Ganga River, India, and risk assessment for human health. *Int. J. Hum. Ecol. Risk Assess.*, 7: 47-56.
- Mensoor, M. and Said, A. 2018. Determination of heavy metals in freshwater fishes of the Tigris River in Baghdad. *Fishes*, 3(2): 23.
- Murtala, B.A., Abdul, W.O. and Akinyemi, A.A. 2012. Bioaccumulation of heavy metals in fish (*Hydrocynus forskahlii*, *Hyperopisus bebeoecidentalis*, and *Clarias gariepinus*) organs in downstream Ogun coastal water, Nigeria. *J. Agric. Sci.*, 4: 51.
- Ndayisenga, J.D. and Dusabe, S. 2022. Ponds' water quality analysis and impact of heavy metals on fishes' body. *J. Sustain. Environ. Manag.*, 1(2): 62-72. <https://doi.org/10.3126/josem.v1i2.45334>
- Olaosebikan, B.D. and Raji, A. 1998. Field Guide to Nigerian Fresh Water Fishes
- Oumar, D.A., Flibert, G., Tidjani, A., Rirabe, N., Patcha, M., Bakary T., Ousman A.H., Yves, T. and Savadogo, A.S. 2018. Bioaccumulation in water and Tilapia nilotica fish from Maguite Island of Fitri Lake. *Curr. J. Appl. Sci. Technol.*, 26(2): 1-9.
- Sobhanardakani, S., Tayebi, L. and Hosseini, S. V. 2018. Health risk assessment of arsenic and heavy metals (Cd, Cu, Co, Pb, and Sn) through consumption of caviar of *Acipenser persicus* from Southern Caspian Sea. *Environmental Science and Pollution Research*, 25: 2664-2671.
- Sikoki, F.D. and Otobotekere, A. J. 1999. Fisheries. In Alagoa, E.J. (ed), *The Land and People of Bayelsa State, Central Niger Delta*, Onyoma Research Publications, Port Harcourt, pp. 456-473.
- Ugwuja E.I., Ogbonnaya L.U., Uro-Chukwu H., Obuna J.A., Ogiji E. and Ezenkwa, S.U. 2015. Plasma cadmium and zinc and their interrelationship in adult Nigerians: potential health implications, *Interdiscip. Toxicol.*, 8(2): 77-83. doi: 10.1515/intox-2015-0012.
- USEPA. 2012. Waste and cleanup risk assessment. Retrieved October 10, 2022, from <http://www2.epa.gov/risk/waste-and-cleanup-risk-assessment>.
- Vanderoost, R., Beyer, J. and Vermeulen, N.P. 2003. Fish bioaccumulation and biomarkers in environmental risk assessment: a review. *Environ. Toxicol. and Pharmacology*, 13: 57-149.
- WHO/FAO/IAEA. 1996. Trace Elements in Human Nutrition and Health within the Bradford Beck Catchment, West Yorkshire. WHO, Washington DC.
- Yaradua, A.I., Alhassan, A.J., Kurfi, A.U., Idi, A.A., Muhammad, I.U. and Kanadi, A.M. 2018. Heavy metals health risk index (HRI) in human consumption of whole fish and water from some selected dams in Katsina State Nigeria. *Asian Journal of Fisheries and Aquatic Research*, 1(1): 1-11.
- Zhang, J., Zhu, L., Li, F., Liu C., Qiu, Z., Xiao, M. and Cai, Y. 2018. Comparison of toxic metal distribution characteristics and health risk between cultured and wild fish captured from Honghu City, China. *Int. J. Environ. Resour. Public Health*, 15: 334.
- Zschunke, A. 2013. Reference Materials in Analytical Chemistry: A Guide for Selection and Use. Springer Science and Business Media, Berlin, Germany, p. 25-55.



Presence of Heavy Metals in Purple Crab (*Platyxanthus orbigny*) Tissues in Southern Peru

José L. Ramos-Tejeda[†] , José A. Valeriano-Zapana and Nilton B. Rojas-Briceño

Escuela Profesional de Ingeniería Ambiental, Facultad de Ingeniería y Arquitectura, Universidad Nacional de Moquegua, Pacocha 18610, Peru

[†]Corresponding author: J. L. Ramos; jramost@unam.edu.pe

Nat. Env. & Poll. Tech.
Website: www.neptjournal.com

Received: 30-08-2023

Revised: 11-10-2023

Accepted: 15-10-2023

Key Words:

Beach pollution

Coastal beach

Ilo harbour

Moquegua

Platyxanthus orbigny

ABSTRACT

Heavy metals (iron, copper, and zinc) were quantified in purple crab (*Platyxanthus orbigny*) tissues collected in winter (September 2021), spring (November 2021), and summer (March 2022) at three beaches (Tres Hermanas, Fundición, and El Diablo) in Ilo Harbour (Moquegua), South Peru. The rank order of heavy metal concentrations in purple crab tissues and sediments was similar; iron (Fe) was followed by Copper (Cu), and this last one was followed by Zinc (Zn). The heavy metal concentrations in tissue crabs from the three beaches differed from each other spatially and seasonally. In addition, Fundición Beach was the zone with the highest concentration of those three metals during the summer.

INTRODUCTION

Ocean and sediments naturally present heavy metals (Fe, Zn, Cu, Hg, Ni, and Cd) in their composition as a result of rock weathering, upwelling processes, volcanic activity, river discharge, and atmospheric dust (Krishnaja et al. 1987, Castro & Huber 2019). Some of these metals, in small quantities, such as iron (Fe), zinc (Zn), nickel (Ni), and copper (Cu), are essential for the proper functioning of biochemical and physiological processes in marine life, even humans (Bandara & Manage 2022, Hao et al. 2019). Nevertheless, anthropic activities (e.g., agriculture, local fisheries, petrochemical industry, mining, and domestic activities) dump wastewater in rivers containing heavy metals, which afterward will enter the coastal and marine environments, increasing their concentrations (Bastami & Esmailian 2012, Koski 2012, Patel et al. 2018).

Marine invertebrates (e.g., mollusks and crustaceans) from coastal environments exhibit a variety of feeding habits (e.g., suspension feeding, filtration feeding, and deposit feeding) (Sastre et al. 1999, Jędruch et al. 2019) efficiently adapted to take advantage of nutrients from seawater and sediments, which increase the risk of accumulating heavy metals in their soft tissues and organs (Lu & Wang 2018, Castro & Huber 2019, Raza'i et al. 2022). The organ that

largely bioaccumulates heavy metals is the hepatopancreas, which is in charge of detoxification (Irnidayanti 2015, Liu et al. 2021) and secondarily, muscle tissues, which are the edible part in most marine invertebrates (Lyla & Khan 2011). It has been well documented that heavy metal bioaccumulation has negative effects on different levels of marine invertebrates and represents a potential hazard for humans who consume these organisms (Bat et al. 2020, Gong et al. 2020, Ariano et al. 2021, Tanhan et al. 2023).

Crabs are a diverse group of crustaceans with species on all the coasts of the planet, where they play an important role in the marine food chain (Ruppert et al. 2004, Castro & Huber 2019), as well as in the daily diet of people since they represent a source of proteins of excellent quality and high nutritional value (Hao et al. 2019, Gong et al. 2020, Tanhan et al. 2023). Nonetheless, its feeding habits facilitate heavy metal bioaccumulation in their tissues, which could represent a public health issue (Stoner & Buchanan 1990, Ololade et al. 2011, Laitano et al. 2013, Vogt et al. 2018).

Ilo Harbor, located in the Moquegua region in south Peru, is characterized by a coastline oceanographically influenced by the Humboldt current, which explains its high productivity and biodiversity (Gonzales et al. 2022). However, anthropic activities that dump their wastewater into the ocean are

raising the heavy metal (Pb, As, and Cu) concentrations close to the limit, representing a hazard for benthic species (Boon et al. 2001, Gonzales et al. 2022) and humans (Tanhan et al. 2023). Purple crab (*Platyanthus orbignyi*) is a filter feeder and omnivorous scavenger in juvenile and adult stages, respectively (Oliva et al. 1997), which plays an important role in the marine trophic chain of the Peruvian coasts, being food for octopus, otters, sea lions, sea birds, and fish. Likewise, it represents one of the main items of the artisanal fishery that supplies local markets (Rathbun 1910, Fischer & Thatje 2016, Dillehay 2017, Iannacone et al. 2022).

Several studies performed around the world report the presence of heavy metals in crabs of commercial interest from coastal regions. Liu et al. (2020), for instance, assessing the species *Portunus trituberculatus* in Zhejiang Province (China), found high concentrations of Zn in muscular tissue. A similar study in São Paulo (Brazil) assessing the species *Ulcides cordatu* detected high concentrations of Cu and

Zn (Salvador et al. 2007). Tanhan et al. (2023), studying three crab species from Pattani Bay (Thailand), found high levels of Zn, Cu, and Fe in this order for *Portunus pelagicus* and *Scylla olivacea*, as well as high levels of Zn, Fe, and Cu for *Scylla paramamosain*. Araujo et al. (2021), in a study developed in the protected area of Iguape-Peruíbe (Brazil), evidenced a high concentration of heavy metals in hepatopancreas, suggesting that even protected areas are not exempt from heavy metal pollution. As we see, many crab species of commercial interest from coastal areas are helpful as bioindicators to assess the environmental quality and the possible hazards for human health (Ololade et al. 2011).

This pilot study represents the first work in purple crab (*Platyanthus orbignyi*) from south Peru that identifies the presence of heavy metals in edible muscular tissue. In addition, this work proves the need for implementing long-term monitoring to assess the benthic invertebrate community state to identify possible hazards for the Ilo population in the future.

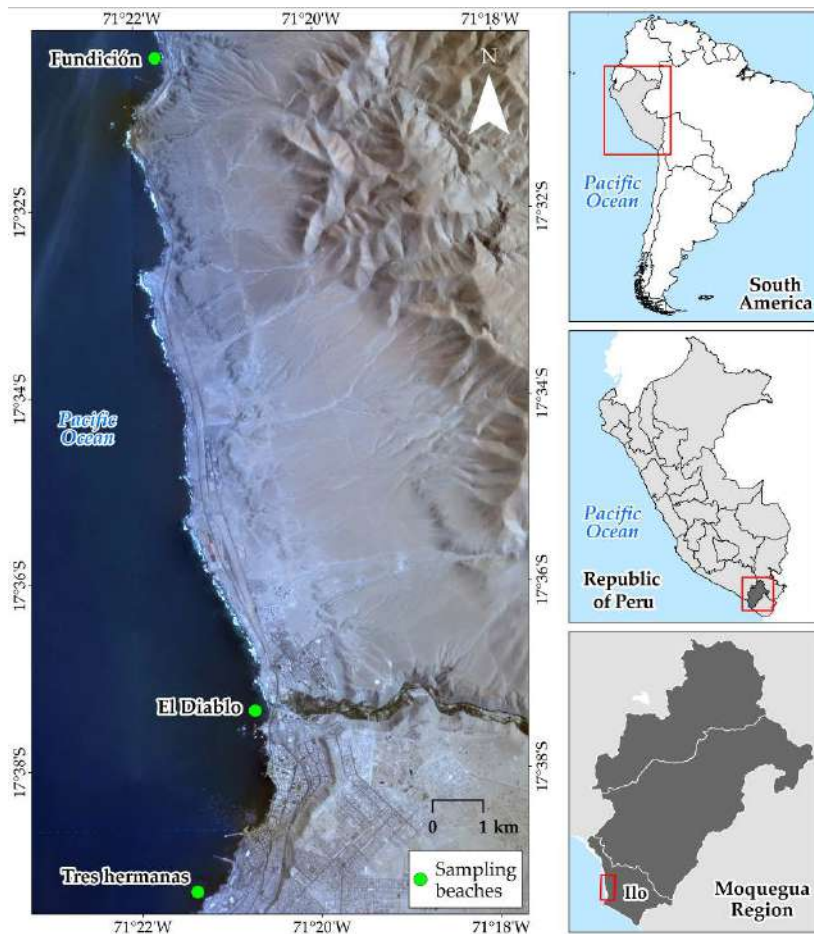


Fig. 1: Map showing the study area and the sampling zones.

MATERIALS AND METHODS

Study Area

This study was performed on three beaches in the Ilo harbor, located on the south coast of Peru: Tres Hermanas Beach (17°39'18" S, 71°21'23" W), El Diablo Beach (17°37'22" S, 71°21'23" W), and Fundición Beach (17°30'22" S, 71°21'45" W) (Fig. 1).

Sampling

A total of 30 commercial-size male purple crab (*P. orbigny*) (70 mm) samples were collected, 10 per beach, by freediving

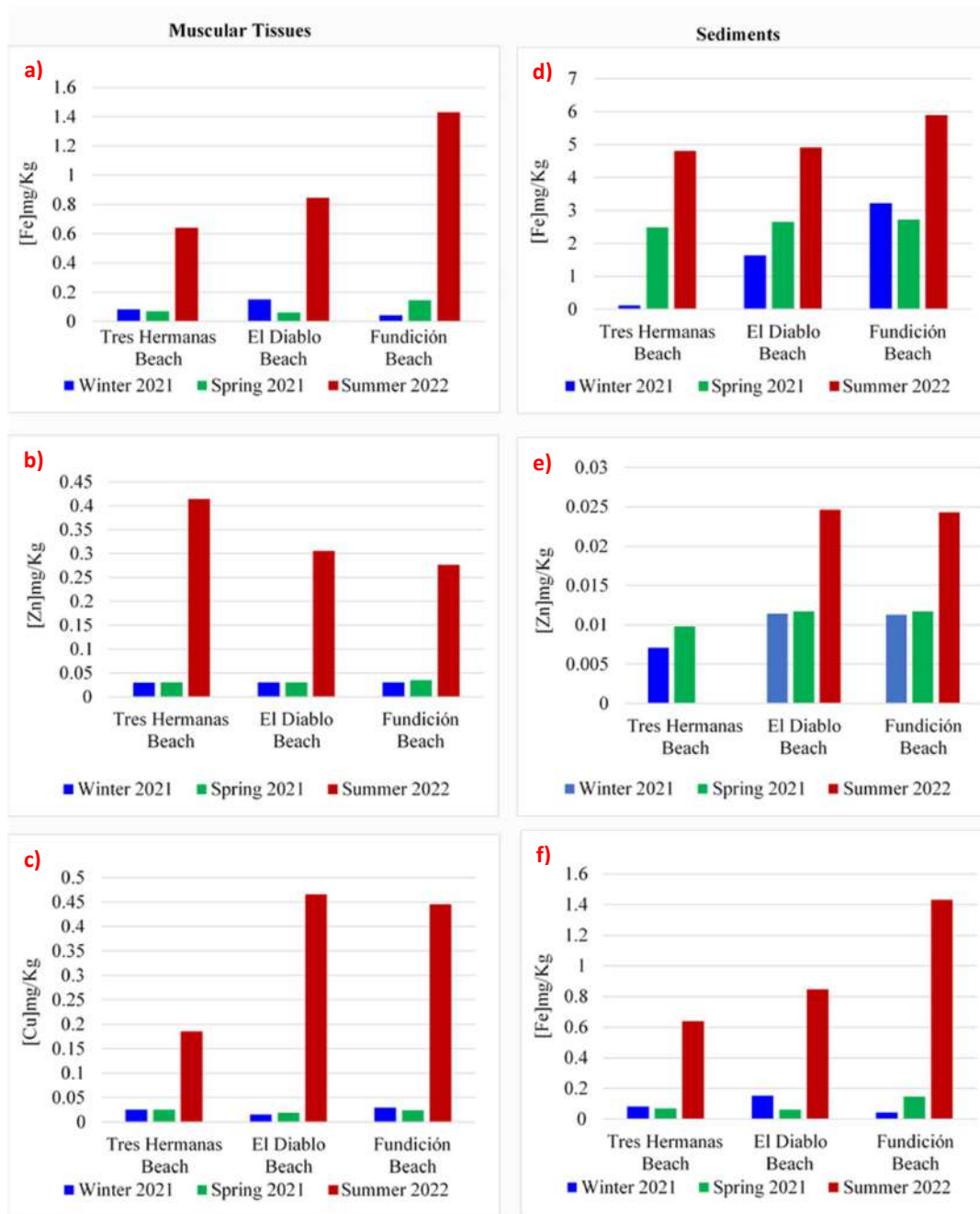


Fig. 2: Levels of heavy metal concentrations (Fe, Zn, and Cu) in samples of muscular tissues (a–c) and sediments (d–f) from Fundición Beach, El Diablo Beach y Tres Hermanas Beach during Winter 2021, Spring 2021, and Summer 2022.

at the end of winter (September 2021), spring (November 2021), and summer (March 2022). In the field, the crab samples were washed with distilled water to remove the sand and other particles from the exoskeleton. The dissection process was done carefully to avoid contamination; after breaking the exoskeleton, muscle tissue samples were removed and weighed until they reached 100g. The tissue samples were packed in Ziplock polyethylene bags, labeled, and transported in coolers at 51°C to be analyzed at the Research and Services laboratory LABINVSERV of the National University of San Agustín. X-ray fluorescence was the technique used by the laboratory for the analysis (Lorber 1986). Moreover, a sediment sample was taken from each beach in the study. In addition, temperature data were taken in each sampling carried out for each season with a HANNA HI98194 multiparameter.

Data Analysis

The results from the laboratory analysis were organized in tables, and the data was analyzed in an Excel program. To visualize the differences between beaches and seasons, the data was represented in bar graphs.

RESULTS AND DISCUSSION

This first pilot study provides evidence of the presence of heavy metals in purple tissue crab and sediments at Ilo Harbour. The results of this study showed that crab tissues bioaccumulate heavy metals in different concentrations, following the rank order of Fe (3.47 mg.kg^{-1}) > Cu (1.23 mg.kg^{-1}) > Zn (1.18 mg.kg^{-1}) (Fig. 2a–c) and it was similarly observed in sediments where the rank order was Fe (28.45 mg.kg^{-1}) > Cu (0.17 mg.kg^{-1}) > Zn (0.11 mg.kg^{-1}) (Fig. 2d–f).

Moreover, it was observed for sediments that iron (Fe) presented a high concentration, which was reflected in the high iron concentration in crab tissues. Nonetheless, for the other heavy metals, copper (Cu) and zinc (Zn), the relationship was opposite. Zaher et al. (2021), studying the bioaccumulation of heavy metals in raw crab from different markets, found a similar pattern to the present study when evaluating Cu and Zn. Those results are coherent with the literature, where it is mentioned that metals such as Fe are present in high concentrations in seafood tissues because this is an essential bioelement for the correct functioning of organisms (Jakimska 2011).

For each season (winter 2021, Spring 2021, and Summer 2022), the temperatures were, respectively, 15.5°C, 15.5°C, and 15.6°C. Sediment samples showed that iron (Fe) was highly concentrated during the summer of 2022 on three beaches, with a predominance at Fundación Beach (Fig. 2d). In the case of zinc (Zn) (Fig. 2e), it was present in

high concentrations during the summer of 2022 at Diablo and Fundación Beaches. Finally, for copper (Cu), high concentrations were evident during the summer of 2022 at Fundación Beach (Fig. 2f). Moreover, high concentrations of iron (Fe), Zinc (Zn), and Copper (Cu) in purple crab tissues were observed at Tres Hermanas Beach, Diablo Beach, and Fundación Beach. In the case of iron (Fe), it was predominant in Fundación Beach (Fig. 2a), unlike zinc (Zn) and copper (Cu), which were superior in Tres Hermanas and Diablo Beach, respectively, during summer 2022 (Fig. 2b and 2c). The high values of heavy metals in those areas can be related to the development of different anthropogenic activities close to the coastal zone, mainly mining. This study shares similar seasonal patterns with other studies, which report high concentrations of heavy metals in crab tissues in the summer. For instance, Çoğun et al. (2017) reported high concentrations of Cu and Zn in soft tissues of *Callinectes sapidus*, and Firat et al. (2008) observed high concentrations of Zn, Cu, and Fe in this rank order for *Charybdis longicollis*. Heavy metals that come from wastewater from domestic and other activities are released into the ocean, where marine organisms take them up through the water column. However, the part that remains free goes down to the bottom, where the sediments act as a reservoir for them and organic matter in general (Bazzi 2014). Purple crabs are benthic organisms that feed on bottom surfaces, eating sediments and other items that facilitate the incorporation and bioaccumulation of heavy metals in their tissue bodies (Laitano et al. 2013, Vogt et al. 2018).

In this sense, the findings in this study are evidence of the importance of implementing long-term monitoring to evaluate the spatiotemporal variability of heavy metals in seafood in general, given that filter feeders such as bivalves (*Aulacomya atra* and *Mesodesma donacium*) are more efficient bioaccumulators of heavy metals than crabs. Despite the lack of robustness in this study, it proves the need to investigate aspects such as the presence and quantification of chemicals in different organs of seafood and the physiological, ecological, and biological impacts on marine biota and humans to prevent future hazards.

CONCLUSIONS

This study provided evidence for the first time of the presence of heavy metals such as iron, copper, and zinc in the muscular tissues of the purple crab and the sediments of three beaches in the port of Ilo, Peru. It was found that iron showed the highest concentrations in both compartments, suggesting the effective bioaccumulation of this metal from the environment by the crab. Likewise, metal levels varied between seasons and locations, being higher during summer

and on beaches closer to anthropogenic activities such as mining. Given its filtering and predatory diet, the purple crab acted as a bioindicator of environmental quality in the area. These findings highlight the need for long-term monitoring of other filtering organisms and the spatiotemporal variability of heavy metal pollution to evaluate potential ecological and physiological impacts and risks to human health derived from the consumption of these marine species. The study serves as a basis for future research that delves deeper into these aspects in the port of Ilo.

FUNDING SOURCES

This project was financed by the Universidad Nacional de Moquegua, through Resolución de la Comisión Organizadora N° 0581-2019-UNAM.

REFERENCES

- Araujo, G.S., Bordon, I.C., Cruz, A.C.F., Gusso-Choueri, P.K., Favaro, D.I.T., Rocha, R.C.C., Saint'pierre, T.D., Hauser-Davis, R.A., Santelli, R.E., Braz, B., Freire, A.S., Machado, W.T.V. and Abessa, D.M.S. 2021. Lead and cadmium contamination in sediments and blue crabs *Callinectes danae* from a Ramsar wetland in southeastern Brazil. *Pan-Am. J. Aqua. Sci.*, 16(2): 161-175.
- Ariano, A., Scivicco, M., D'Ambola, M., Velotto, S., Andreini, R., Bertini, S., Zaccaroni, A. and Severino, L. 2021. Heavy metals in the muscle and hepatopancreas of red swamp crayfish (*Procambarus clarkii*) in Campania (Italy.) *Animals*, 11(7): 1933.
- Bandara, K.R.V. and Manage, P.M. 2022. Heavy metal contamination in the coastal environment and trace level identification. *Intech Open*, 5: 11-16.
- Bastami, A.A., Khoei, J.K. and Esmailian, M. 2012. Bioaccumulation of heavy metals in sediment and crab, *Portunus pelagicus* from Persian Gulf, Iran. *Middle East J. Sci. Res.*, 12(6): 886-892.
- Bat, L., Arici, E., Öztekin, A. and Şahin, F. 2020. Toxic metals in the warty crab in the southern Black Sea: assessment of human health risk. *Marine Biol. J.*, 5(1): 3-11.
- Bazzi, A.O. 2014. Heavy metals in seawater, sediments and marine organisms in the Gulf of Chabahar, Oman Sea. *J. Ocean. Marine Sci.*, 5(3): 20-29.
- Boon, R.G., Alexaki, A. and Becerra, E.H. 2001. The Ilo Clean Air Project: A local response to industrial pollution control in Peru. *Environ. Urban.*, 13(2): 215-232.
- Castro, P. and Huber, M.E. 2019. *Marine Biology. Edition Three*. McGraw-Hill, New York.
- Çoğun, H.Y., Firat, Ö., Aytakin, T.Ü.Z.Ü.N., Firidin, G., Firat, Ö., Varkal, H. and Kargin, F. 2017. Heavy metals in the blue crab (*Callinectes sapidus*) in Mersin Bay, Turkey. *Bull. Environ. Toxicol.*, 829-824 :98.
- Dillehay, T.D. 2017. *Where the Land Meets the Sea: Fourteen Millennia of Human History at Huaca Prieta, Peru*. University of Texas Press, Austin, TX, USA.
- Firat, Ö., Gök, G., Çoğun, H.Y., Yüzereroğlu, T.A. and Kargin, F. 2008. Concentrations of Cr, Cd, Cu, Zn, and Fe in crab *Charybdis longicollis* and shrimp *Penaeus semisulcatus* from Iskenderun Bay, Turkey. *Environ. Monit. Assess.*, 147: 117-123.
- Fischer, S. and Thatje, S. 2016. Temperature effects on life-history traits cause challenges to the management of brachyuran crab fisheries in the Humboldt Current: A review. *Fish. Res.*, 183: 461-468.
- Gong, Y., Chai, M., Ding, H., Shi, C., Wang, Y. and Li, R. 2020. Bioaccumulation and human health risk of shellfish contamination to heavy metals and As in most rapidly urbanized Shenzhen, China. *Environ. Sci. Pollut. Res.*, 27: 2096-2106.
- Gonzales A.G., del, C., Mendez, A.S. and Condori, A.R.M. 2022. Determination of the concentration of heavy metals and oils in seawater in the port of Ilo, Peru. *IOSR-JESTFT*, 16(01): 28-36.
- Hao, Z., Chen, L., Wang, C., Zou, X., Zheng, F., Feng, W., Zhang, D. and Peng, L. 2019. Heavy metal distribution and bioaccumulation ability in marine organisms from coastal regions of Hainan and Zhoushan, China. *Chemosphere*, 226: 340-350.
- Iannacone, J., Príncipe, F., Alvarino, L., Minaya, D., Panduro, G. and Ayala, Y. 2022. Microplastics in the "hairy crab" *Romaleon setosum* (Molina, 1782) (Cancridae) from Peru. *Rev. de Invest. Vet.*, 33(1): e22161.
- Irnidayanti, Y. 2015. Toxicity and traces of Hg, Pb, and Cd in the hepatopancreas, gills, and muscles of *Perna viridis* from Jakarta Bay, Indonesia. *Pakistan Journal of Biological Sciences: PJBBS*, 18(2): 94-98.
- Jakimska, A., Konieczka, P., Skóra, K. and Namieśnik, J. 2011. Bioaccumulation of metals in tissues of marine animals, Part II: metal concentrations in animal tissues. *Pol. J. Environ. Stud.*, 20(5): 1127-1146.
- Jędruch, A., Beldowska, M. and Ziółkowska, M. 2019. The role of benthic macrofauna in the trophic transfer of mercury in a low-diversity temperate coastal ecosystem (Puck Lagoon), southern Baltic Sea. *Environ. Monit. Assess.*, 191(3): 137.
- Koski, R.A. 2012. Metal dispersion resulting from mining activities in coastal environments: A pathways approach. *Oceanography*, 25(2): 170-183.
- Krishnaja, A., Rege, M. and Joshi, A.G. 1987. Toxic effects of certain heavy metals (Hg, Cd, Pb, As, and Se) on the intertidal crab *Scylla serrata*. *Marine Environ. Res.*, 21: 109-119.
- Laitano, M.V., Farías, N.E. and Cledón, M. 2013. Prey preference of the stone crab *Platyxanthus crenulatus* (Decapoda: Platyxanthidae) in laboratory conditions. *Nauplius*, 21: 17-23.
- Liu, Q., Liao, Y., Xu, X., Shi, X., Zeng, J., Chen, Q. and Shou, L. 2020. Heavy metal concentrations in tissues of marine fish and crabs collected from the middle coast of Zhejiang Province, China. *Environ. Monit. Assess.*, 192: 285.
- Liu, X., Jiang, H., Ye, B., Qian, H., Guo, Z., Bai, H., Gong, J., Feng, J. and Ma, K. 2021. Comparative transcriptome analysis of the gills and hepatopancreas from *Macrobrachium rosenbergii* exposed to the heavy metal Cadmium (Cd²⁺). *Sci. Rep.*, 11: 16140.
- Lorber, K. E. 1986. Monitoring of heavy metals by energy dispersive X-ray fluorescence spectrometry. *Waste Manag. Res.*, 4(1): 3-13.
- Lu, G. and Wang, W. 2018. Trace metals and macroelements in mussels from Chinese coastal waters: National spatial patterns and normalization. *Sci. Tot. Environ.*, 626: 307-318
- Lyla, P.S. and Khan, S. 2011. The pattern of accumulation of heavy metals (copper and zinc) in the Estuarine hermit crab *Clibanarius longitarsus* (De Hann). *Indian J. Marine Sci.*, 40: 117-120.
- Oliva, J., Arana, P. and González, A. 1997. Growth and mortality of purple stone crab, *Platyxanthus orbigny*, in the coastal area of Lambayeque, Perú. *Informe del Instituto*, 126: 55-74.
- Ololade, I.A., Lajide, L., Olumekunc, V.O., Ololaded, O.O. and Ejelolu, B.C. 2011. Influence of diffuse and chronic metal pollution in water and sediments on edible seafoods within Ondo oil-polluted coastal region, Nigeria. *J. Environ. Sci. Health Part A*, 46(8): 898-908.
- Patel, P., Raju, N.J., Reddy, B.C.S.R., Suresh, U., Sankar, D.B. and Reddy, T.V.K. 2018. Heavy metal contamination in river water and sediments of the Swarnamukhi River Basin, India: risk assessment and environmental implications. *Environ. Geochem. Health*, 40(2): 609-623.
- Rathbun, M.J. 1910. The stalk-eyed crustacea of Peru and the adjacent coast. *Proc. U.S. Natl. Mus.*, 38: 351-620
- Raza'i, T.S., Thamrin, N., Amrifo, V., Pardi, H., Pangestiansyah Putra, I., Febrianto, T. and Fadhlil Ilhamdy, A. 2022. Accumulation of essential (copper, iron, zinc) and non-essential (lead, cadmium) heavy metals in

- Caulerpa racemosa*, seawater, and marine sediments of Bintan Island, Indonesia. *Research*, 10: 699.
- Ruppert, E.E., Fox, R.S. and Barnes, R.D. 2004. *Invertebrate Zoology: A Functional Evolutionary Approach*. Thomson-Brooks/Cole, Belmont, CA.
- Salvador, M.J., Sawazaki, D.T.A., Vives A.E.S., Hattori, G.Y. and Zucchi, O.L.A.D. 2007. Analysis of crab tissues and the sediment of the estuary from Iguape (São Paulo, Brazil) by total reflection x-ray fluorescence. Santos, SP, Brazil. *Int. Nucl. Atlantic Conf.*, 12: 1456.
- Sastre, M. and Reyes, P. and Ramos, H. and Romero, R. and Rivera, J. 1999. Heavy metal bioaccumulation in Puerto Rican blue crabs (*Callinectes* spp). *Bull. Marine Sci.*, 64: 209-217.
- Stoner, A. W. and B. A. Buchanan. 1990. Ontogeny and overlap in the diets of four tropical *Callinectes* species. *Bull. Mar. Sci.*, 46: 3-12.
- Tanhan, P., Lansubsakul, N., Phaochoosak, N., Sirinupong, P., Yeesin, P., Imsilp, K. 2023. Human health risk assessment of heavy metal concentration in seafood collected from Pattani Bay, Thailand. *Toxics*, 11: 18.
- Vogt, É.L., Model, J.F.A. and Vinagre, A.S. 2018. Effects of organotins on crustaceans: Update and perspectives. *Front. Endocrinol.*, 9: 1-8.
- Zaher, H., Mohamed, A., Hamed, S. and El-Khateeb, A. 2021. Risk assessment of heavy metal bioaccumulation in raw crab and prawn flesh marketed in Egypt. *J. Hum. Environ. Health Promot.*, 7: 6-14.

ORCID DETAILS OF THE AUTHORS

José L. Ramos-Tejeda: <https://orcid.org/0000-0002-2472-0489>

José A. Valeriano-Zapana: <https://orcid.org/0000-0002-5571-0531>

Nilton B. Rojas-Briceño: <https://orcid.org/0000-0002-5352-6140>



The Passive Environmental Effect of the Fungicide Benomyl on Soil Promoting Bacteria and Concentration of Some Important Soil Elements

Zaid Raad Abbas, Aqeel Mohammed Majeed Al-Ezee, Sawsan Hassan Authman and Maan Abdul Azeez Shafeeq† 

Department of Biology, College of Science, Mustansiriyah University, Baghdad, Iraq

†Corresponding author: Maan Abdul Azeez Shafeeq; maanalsalihi@uomustansiriyah.edu.iq

Nat. Env. & Poll. Tech.
Website: www.neptjournal.com

Received: 12-10-2023

Revised: 09-12-2023

Accepted: 16-12-2023

Key Words:

Cyperus rotundus

Fungicide benomyl

Soil promoting bacteria

Soil elements

ABSTRACT

Loam examples were gathered through the 2020-2021 rising periods, and the following measurements were made: Viable bacterial count by reducing root colonization. The outcomes of reviewing the impact of the fungicide Benomyl on development and viable microflora count revealed that the highest microbial count was in Al-Madaein 80×10^3 CFU/mL was recorded, and the lowest count was 60×10^3 CFU/mL for the Aushtar area. The microbial viable count values for the affected microorganisms with Benomyl were decrease to 27×10^3 and 65×10^3 CFU/mL respectively. Those consequences specify that Benomyl has a robust choosiness contrary to microflora, especially when compared to the benomyl effect as folded dose, the microflora I count decreases to 25×10^3 CFU/mL in the Aushtar area and increases to 60×10^3 CFU/mL in Al-Madaein area. Whereas the study estimated the level of eight elements in soil (Mn, Fe, Cu, Zn, NO_3 , P, K, and NH_4) cultured with *Cyperus rotundus* L. Which mentioned the effect of benomyl on these levels after three days of treatment. Mn concentration ranged between 5.96 to 9.11 ppm, while after fungicide benomyl, it decreased to 5.63 -6.53 ppm similar results were observed for other elements. The highest affected element was Mn in the Aushtar area. Those consequences designate that Benomyl has a stout fussiness in contrast to soil nutrients. The greatness of benomyl impacts on loam ingredients and procedures were minor, qualified to impact on mycorrhizal root foundation (reduction through benomyl).

INTRODUCTION

Normal, vigorous bio networks loam nourishing grades are preserved via the nourishing rotation and are moderately unchanging. Agronomic loams, nevertheless, the ability to develop nourishing is scarce as agronomic ecologies are not locked, and nourishing will enduringly exodus the organization as vegetable or animal harvests. In addition to the straight acceptance of nourishing over the roots, numerous florae occupy reciprocally valuable relations with microbes. Roughly florae, beans for specimen, exploit bacteria, for example, rhizobia, to perform organic nitrogen addiction whereby atmospherically nitrogen, which is not straight obtainable to the vegetal, is transformed mad about ammonium nitrate, a method of nitrogen that is obtainable. Another instance is the association of countless florae formulas by mycorrhiza fungi. This connection grants the vegetal distant superior admittance to nourishing than would otherwise be obtainable (Silver et al. 2021). Owing to the incessant usage of pesticides, considerable amounts of them and their dilapidation harvests may amass in the

ecology. Dominant information presented that lone 2-3% of the practical biochemical pesticides spread their goals, although the others remnants in the loam, their extreme usage reasons thoughtful injury to the ecology, earthly in addition to water, and accordingly to the vegetation and animals of the environments (Elslahi et al. 2014). Excessive jeopardy is being modeled on loam microorganisms, and there is intrusion through component sequences and entrance interested in nutriment series. Amongst the insecticides utilized in Sudan, fungicides grade tertiary afterward pesticides and herbicides. Fungicides were originated to have the main suppression outcome on loam microbes (Sherif et al. 2011). The unity of the investigated presented fungicides is Benlate, which is the marketable term for the vigorous element Benomyl or Methyl 1-(butyl carbamoyl) benzimidazole-2-ylcarbamate. It fits into the benzimidazole intimate, an associate of the carbamate collection. It is discriminatory and poisonous to microbes and invertebrates. It is a general extensive range, defensive, and enucleate fungicide utilized for the regulator of numerous vegetable fungal pathogens and chilly stowage decays. The measured fungi are mostly

those causation crumbly molds, Botrytis, Fusarium basic decay, dark patch, and bloom deterioration. Kernel defense and kernel vaccination are regularly mismatched. A single method of permitting the efficacious contamination of pea roots with Rhizobium afterward remediation of kernels through fungicides is to use a fungicide-unaaffected inoculum (Odeyemi & Alexander 1977). A decrease of mycorrhizal relations through remediation of the floras through complete fungicide was revealed to meaningfully recover rudiments translocation from vegetable roots to sprouts and succeeding fundamentals gathering in sprouts (Wong et al. 2007). The impartiality of this research is to examine the poisonousness of the bactericidal outcome of Benomyl on loam-encouraging bacteria and around significant loam essentials.

MATERIALS AND METHODS

Gathering of Soil Samples

Loam specimens were gathered from Aushtar, Al-Wardeia, and Al-Madaein in Iraq, and these places were chosen as sources for the soil in the current research. The soil was cultured with *Cyperus rotundus* L. The samples of the soil were collected in October 2021 because this month, the humidity percentage increased. However, the samples of the soil were gathered at a depth of 35 cm, mixed, and then stored in the lab at room temperature (around 21 °C). The procedure was previously explained by (Dickman et al. 1984). All the tests of soil and the experiments were carried out in Soil and Water Research Center, Ministry of Science and Technology.

Viable Microbial Count

The method of serial dilution was carried out according to (Srinivasulu et al. 2012). 25 g. of the soil was placed in a test tube, and 225 mL of SW (sterilized water) was added and was mixed carefully and thoroughly. After good mixing, the mixture was subjected to a process called Immunomagnetic beads [IMB], as explained by (Han & New 1998). After the IMB, only one mL of the solution was taken and placed in another test tube, and 9 mL of SW was added to complete the volume to 10 mL (dilution process DP). The DP was repeated 10 times of dilution (10 folds in a process called serial dilution). However, the solutions that came out from the serial dilution were plated on Nutrient agar and incubated for 5±2 days at 32±3 °C as described by (Rathore 2014).

Determination of Soil Elements

The determination of the soil elements concentration, which included Magnesium, Iron, Copper, Zinc, Ammonium, and Nitrate, was carried out on both 7850 ICP-MS according to

SFS-EN ISO 17294-2 standard and Shimadzu AA- 6650 Atomic Absorption Spectrophotometer, the protocols were explained by (Sarker et al. 2015).

Application of Benomyl for Suppression of Soil Microflora and Soil Elements

Benomyl preparation: Benomyl (trade name Benlate; DuPont, Canada) is practical as a loam saturate at concentricity prepared by the addition of 10 mL of Benomyl to 10 mL of Sterilized water. However, a significant deliberation after the spread of benomyl to loam for inhibition is that antagonistic impacts on additional loam microflora may happen (Yang et al. 2021).

Treatment procedure: Experimentation is stable to perceive a slightly probable outcome of the Benomyl on loam microflora, and that might impact soil elements accumulation. Therefore experiment was done by measuring the soil microflora viable count before and after three days of treatment with Benomyl. On the other hand, soil elements (Mn, Fe, Cu, Zn, NO₃, P, K, and NH₄) were measured before and after treatment with benomyl.

RESULTS AND DISCUSSION

Floras necessity nutritious with the intention of raise and flourish has possibly directed to an exaggeration of the fundamental complication of the metabolic procedure elaborate in the transmission of indispensable biochemical essentials since the loam obsessed by vegetal matter, the crucial metal nutritious floras acquisition as of the loam are a fair single consistent ingredient in an intimidatingly composite organization of associations and sequences. The defiance to recover and perception of those associations and to drag applied and maintainable agronomic performs since it may fine support those measurements to withstand agronomic output in the upcoming (Silver et al. 2021), the impact of Benomyl on loam essentials was calculated in this investigate.

Viable Micro Floral Count

The comparative function of bacteria and fungi for loam C and N undercurrents ability be evaluated by operating their profusion in loam through the implementation of fungicides and bactericides. The implementation of fungicides and bactericides to loam has developed single of the greatest public procedures to operate microbial communal configuration (Rousk et al. 2008).

The outcomes of research on the stimulus of the fungicide Benomyl on development and viable microflora count are presented in Table 1. The highest microbial count

Table 1: Effect of benomyl on soil Viable count microflora in Iraqi soil (Viable count \pm SE).

Soil samples	Control *10 ³ CFU. mL ⁻¹ (\pm SE)	Benomyl recommended concentration	Benomyl Folded concentration*
Aushtar	60 \pm 51.2	27 \pm 50.2	25 \pm 55.2
Al-Wardeia	75 \pm 50.2	50 \pm 49.2	46 \pm 44.4
Al-Madaein	80 \pm 58.2	65 \pm 51.2	60 \pm 53.6

* (P \leq 0.05) Significantly differences.

was in Al-Madaein, 80 $\times 10^3$ CFU.mL⁻¹ was recorded., and the lowest count was 60 $\times 10^3$ CFU.mL⁻¹ for the Aushtar area. The microbial viable count values for the affected microorganisms with Benomyl were decreased to 27 $\times 10^3$ and 65 $\times 10^3$ CFU.mL⁻¹, respectively. Those consequences elucidate that Benomyl has robust discrimination contrary to microflora, especially when compared to the benomyl effect as folded dose, the microflora l count decreased to 25 $\times 10^3$ CFU.mL⁻¹ in the Aushtar area and decreased to 60 $\times 10^3$ CFU.mL⁻¹ in Al-Madaein area Table 1 and Fig. 1. The statical analysis reveals there is a significant difference (P \geq 0.05).

Benlate, the marketable preparation of the general fungicide benomyl, was practical to a waterlogged sedimentary loam at a concentricity of 5 to 100 $\mu\text{g.g}^{-1}$ vigorous component. At around the farm implementation proportion (S $\mu\text{g.g}^{-1}$), benomyl delayed the reduction in the oxidation-reduction possibilities of the underwater loam. It condensed the accretion of ferric and manganese in resolution (Pal & Sethunathan 1979).

Create discrimination directories fluctuating from 1.496 to 7447.5 meant for the fungicide contrary to diverse microbes (Osman et al. 2012). Create that the fungicide at diverse concentricity of 10- 100 ppm A.I. did not slaughter *Fusarium oxysporum* race CS-20 in the in vitro trial, nevertheless it was greatest poisonous to the fungus and meaningfully compact its development proportion and ending cluster volume at 30 ppm or larger (Fravel et al. 2005). The lowermost venomousness was noted for *Bacillus circulans* and *Azospirillum* sp., while the uppermost noxiousness was documented for *Penicillium* sp. and *Rhizobium* sp. Initiate that the fungicide Benomyl had the greatest impact of the insecticides experienced counter to numerous loam microbiota (Daoud et al. 1990).

Effect of Benomyl on Soil Elements

The outcomes of research on the stimulus of the fungicide Benomyl on soil element concentration are presented in Table 2 and Fig. 2. The study estimated the level of eight elements in soil cultured with *Cyperus rotundus* L., which mentioned the effect of benomyl on these levels after three days of treatment. Mn concentration ranges between 5.96 to 9.11 ppm, while after fungicide benomyl, it decreased to 5.63-6.53 ppm. Similar results were observed for Cu, Zn, NH₄, NO₃, P, and K. The highest affected element was Mn in the Aushtar area. Those consequences specify that Benomyl has a robust discrimination counter to soil nutrients. The static analysis reveals there is a significant difference (P \geq 0.05). Mentioned that benomyl was practical in overpowering mycorrhizae and encouraging component

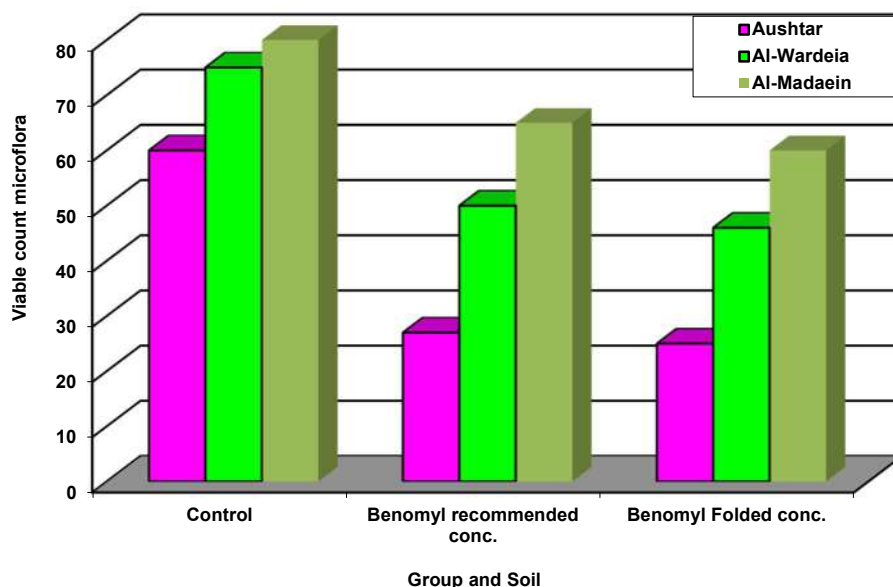


Fig. 1: Effect of benomyl on soil viable count microflora in Iraqi soil.

Table 2: Effect of benomyl on the soil elements concentration in Iraqi areas.

Soil samples	Concentration of soil elements (ppm) *							
Aushtar	Mn	Fe	Cu	Zn	NH4	NO3	P	K
Control	9.11	10.61	3.09	0.66	15.68	29.40	23.50	73.15
Treatment	5.63	8.93	0.36	0.56	20.16	20.72	38.30	60.83
AL-Wardeia								
Control	5.96	9.74	0.43	0.55	22.68	5.88	15.50	67.21
Treatment	5.90	10.17	0.40	0.53	19.60	25.48	32.20	69.05
Al-Madaein								
Control	6.55	9.99	0.42	0.68	22.68	30.8	32.00	89.48
Treatment	6.53	10.27	0.50	0.66	21.84	27.16	35.80	73.62

* ($P \leq 0.05$) Significantly differences.

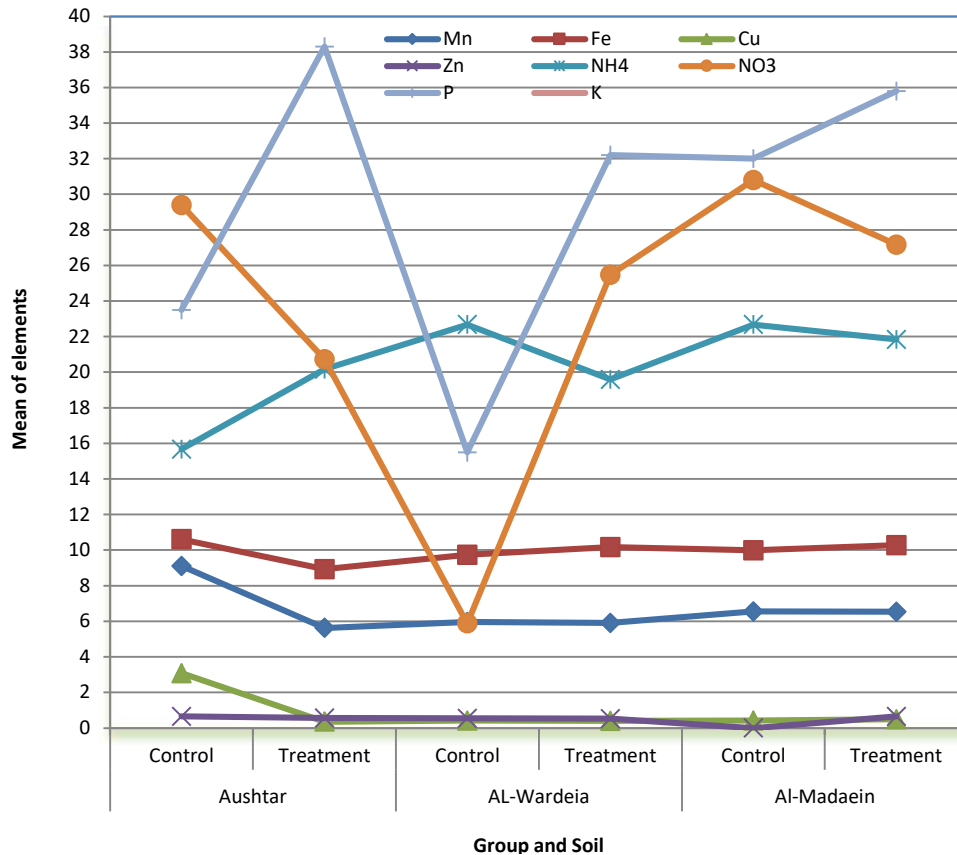


Fig. 2: Effect of benomyl on the soil elements concentration in Iraqi areas.

gathering in vegetable sprouts (Zheljzakov & McNeil 2008). The implementation of benomyl meaningfully augmented phosphate concentration in prickly apple material, nevertheless not in the extra yields. Because fungicides can affect soil microflora, benomyl power then has an impact on element buildup in new growth (Yang et al. 2021). Mycorrhizae's ability to show diverse functions in nutrient acceptance is reliant on the concentration of the nutrient in

loam, and mycorrhizal colonization increased phosphate by vetiver grass (Wong et al. 2007).

Suppression technicality through fungicides and bactericides has been utilized as an easy and inexpensive method to recognize the replies of fungi and bacteria to C- and N- N-rotation procedures. However, for this objective, it is significant to choose appropriate fungicides and bactericides that have a noteworthy impact on goal

microbes and no- or imperfect influence on non-goal microbes. Preceding research has revealed that fungicides and bactericides are not continuously efficient in suppressing the effectiveness of fungi and bacteria, respectively; nonetheless could immediately decrease the efficiency of non-objective microbes also (Bailey et al. 2003, Strickland et al. 2004, Ullah & Dijkstra 2019), the determination that fungicides were softly influenced, while N_2O emanation was decreased via greatest biocides. The implementation of fungicides had unbiased impacts on breathing, NH_4^+ , and ammonification in agroecosystems, nonetheless optimistic impacts in woodlands. Impact volumes of accessible NO_3 and nitrification in rejoinder to bactericides were susceptible to loam pH and C tenor. Our outcomes recommend that maximum fungicides and bactericides suppress microbial growth; nevertheless, they have blended impacts on exhalation and N cycling. Biocides necessary to be judiciously assessed for accidental aspect effectiveness previously, they are utilized in evaluating the function of fungi and bacteria for C- and N- rotation. From the result, it is concluded that the variation in phenolic content might be due to different phenolic constituents present in each plant (Krishnaveni et al. 2020). In the physiological and biochemical, physiological processes of the living system the free radicals (or reactive oxygen species - ROS) are generated (Manasa & Chitra 2020). The study concluded that the residents of villages residing near the bank of the AVM canal face many health-related problems due to pollution of the AVM canal (Delisha et al. 2020). But we hope in the near future, chewing gum can be used as a transport system for different chemical substances, like a medium for applying medicinal drugs (Kopittke et al. 2021). The study of heavy metals (As, Pb, Cu, Ni, Zn) reveals that the concentration level of all these metals is either below the detection limit or well within the prescribed limit of the reported optimum standard of water quality (Saha et al. 2017). The present analysis will help farmers to decide the problems related to soil nutrients and the number of fertilizers to be added to soil to make production economic (Telkapalliwar et al. 2017). It is clearly understood that the samples chosen for the present study are best suited for irrigation purposes (Amaliya & Kumar 2015). The study reveals that water samples have a definite impact on DNA structure as measured by changes in pH (Panda et al. 2012). These increases will certainly have adverse effects on climate as well as health (Kumar & Thambavani 2012). It is concluded that plants can be used as indicators for urban air pollution, and there is a need to protect roadside plants from air pollution (O'Connor et al. 2019).

CONCLUSION

The Benomyl ability to be utilized in connotation through the microbial inoculums and the impacts of benomyl, a general fungicide, were examined in entirely the concentricity utilized instigated worthwhile microflora amount appeared that the maximum bacteriological amount was in Al-Madaein, and the bottommost total in Aushtar zone. The microbial feasible total worth for the influenced microbes through Benomyl was reduced. Those outcomes designate that Benomyl has a robust discrimination contrary to microflora particularly when linked to the benomyl influence as doubled dosage. At the same time, the research assessed the grade of eight essentials in loam cultivated with *Cyperus rotundus* L. Which declared the impact of benomyl on those grades afterward three days of remediation reasons diminished the Mn, Cu, Zn, NH_4 , NO_3 , P, and K concentricity. The maximum influenced component was Mn in the Aushtar region, which mentions that Benomyl has powerful choosiness versus loam. Nutritious. The greatness of benomyl effectiveness on loam ingredients and procedures was minor compared to effectiveness on mycorrhizal root habitation (reduction through benomyl). The benomyl implementation mainly influences mycorrhizal root habitation, by this means circuitously manipulating loam biota and nutritious accessibility. The utilization of fungicides in cultivation to defend florae since loam-accepted pathogens is a prevalent repetition.

ACKNOWLEDGMENTS

The authors would like to thank Mustansiriyah University (www.uomustansiriyah.edu.iq) Baghdad-Iraq for their support in the present work.

REFERENCES

- Amaliya, N.K. and Kumar, S.P. 2015. Status of pond waters for irrigation in Kanyakumari district, Tamilnadu, India. *Asian J. Res. Chem.*, 8(4): 253-256. DOI: 10.5958/0974-4150.2015.00043.7.
- Bailey, V.L., Smith, J.L. and Bolton, H. 2003. Novel antibiotics as inhibitors for the selective respiratory inhibition method of measuring fungal: bacterial ratios in soil. *Biol. Fertil. Soils*, 38: 154-160. DOI: 10.1007/s00374-003-0620-7.
- Daoud, A.S., Qasim, N.A. and Al-Mallah, N.M. 1990. Comparison study on the effect of some plant extracts and pesticides on some phytopathogenic fungi. *Mesopotamia J. Agric.*, 22(4): 227-235. DOI: 10.2478/intox-2014-0002.
- Delisha, A.S., Infant, D.S., Sebastian, M.A. and Chellappan, S. 2020. Common pollutants and health hazards among residents of villages near the bank of AVM canal: A descriptive study. *Int. J. Nurs. Educ. Res.*, 8(3): 337-340. DOI: 10.5958/2454-2660.2020.00075.7.
- Dickman, L.A., Liberta, A.E. and Anderson, R.C. 1984. Ecological interaction of little bluestem and vesicular-arbuscular mycorrhizal fungi. *Can. J. Bot.*, 62(11): 2272-2277. DOI: 10.1139/b84-309.

- Elslahi, R.H., Osman, A.G., Sherif, A.M. and Elhussein, A.A. 2014. Comparative study of the fungicide Benomyl toxicity on some plant growth-promoting bacteria and some fungi in pure cultures. *Interdiscip. Toxicol.*, 7(1): 12. DOI: 10.2478/intox-2014-0002.
- Fravel, D.R., Deahl, K.L. and Stommel, J.R. 2005. Compatibility of the biocontrol fungus *Fusarium oxysporum* strain CS-20 with selected fungicides. *Biol. Control*, 34(2): 165-169. DOI: 10.1016/j.biocontrol.2005.04.007.
- Han, S.O. and New, P.B. 1998. Isolation of *Azospirillum* spp. from natural soils by immunomagnetic separation. *Soil Biol. Biochem.*, 30(8-9): 975-981. DOI: 10.1016/S0038-0717(98)00020-0.
- Kopitke, P.M., Menzies, N.W., Dalal, R.C., McKenna, B.A., Husted, S., Wang, P. and Lombi, E. 2021. The role of soil in defining planetary boundaries and the safe operating space for humanity. *Environ. Int.*, 146: 106245. DOI: 10.1016/j.envint.2020.106245.
- Krishnaveni, M., Sanjana, R., Harinathan, C., Sathyapriya, M., Yazhini, A. and Prakash, K. 2020. Analysis of air pollution tolerance index of plants located at selected sites at Salem and Namakkal District. *Res. J. Pharm. Technol.*, 13(6): 2752-2758. DOI: 10.5958/0974-360X.2020.00489.8.
- Kumar, S.R. and Thambavani, S.D. 2012. Air Quality Index Value of an Ambient Air Pollutants and their Relationship in Urban Area. *Asian J. Res. Chem.*, 5(10): 1242-1250.
- Manasa, K. and Chitra, V. 2020. Evaluation of in-vitro antioxidant activity of camalexin-a novel anti-parkinson's agent. *Res. J. Pharm. Technol.*, 13(2): 578-582. DOI: 10.5958/0974-360X.2020.00109.2.
- O'Connor, D., Müller-Grabherr, D. and Hou, D. 2019. Strengthening social-environmental management at contaminated sites to bolster green and sustainable remediation via a survey. *Chemosphere*, 225: 295-303. DOI: 10.1016/j.chemosphere.2019.03.035.
- Odeyemi, O. and Alexander, M. 1977. Use of fungicide-resistant rhizobia for legume inoculation. *Soil Biol. Biochem.*, 9(4): 247-251.
- Osman, A.G., Sherif, A.M., Elhussein, A.A. and Mohamed, A.T. 2012. Sensitivity of some nitrogen fixers and the target pest *Fusarium oxysporum* to fungicide thiram. *Interdiscip. Toxicol.*, 5(1): 25-29. DOI: 10.2478/v10102-012-0005-6.
- Pal, S.S. and Sethunathan, N. 1979. Effects of benomyl on iron and manganese reduction and redox potential in flooded soil. *J. Soil Sci.*, 30(1): 155-159. DOI: 10.1111/j.1365-2389.1979.tb00973.x.
- Panda, S., Subudhi, M.B. and Garnaik, B.K. 2012. Study of the possible impact of water of Potteru irrigation project on structure of DNA. *Res. J. Pharm. Biol. Chem. Sci.*, 3(4): 612-616.
- Rathore, P. 2014. Isolation, biochemical characterization and inoculation effect of *Azospirillum* on the growth of wheat. *Int J Sci Res*, 3(6): 626-628. Paper ID: 0201427. ISSN (Online): 2319-7064.
- Rousk, J., Demoling, L.A., Bahr, A. and Bååth, E. 2008. Examining the fungal and bacterial niche overlap using selective inhibitors in soil. *FEMS Microbiol. Ecol.*, 63(3): 350-358. DOI: 10.1111/j.1574-6941.2008.00440.x.
- Saha, M., Sengupta, S., Sinha, B. and Mishra, D.K. 2017. Assessment of physico-chemical properties, some heavy metals and arsenic of river Teesta in Jalpaiguri district, West Bengal, India. *Asian J. Res. Chem.*, 10(3): 399-404. DOI: 10.5958/0974-4150.2017.00068.2.
- Sarker, B.C., Baten, M.A., Eqram, M., Haque, U., Das, A.K., Hossain, A. and Hasan, M.Z. 2015. Heavy metals concentration in textile and garments industries' wastewater of Bhaluka industrial area, Mymensingh, Bangladesh. *Curr World Environ.*, 10(1): 61-66. DOI: <http://dx.doi.org/10.12944/CWE.10.1.07>.
- Sherif, A.M., Elhussein, A.A. and Osman, A.G. 2011. Biodegradation of fungicide thiram (TMTD) in soil under laboratory conditions. *Am. J. Biotechnol. Mol. Sci.*, 1(2): 57-68. DOI: 10.5251/ajbms.2011.1.2.57.68.
- Silver, W.L., Perez, T., Mayer, A. and Jones, A.R. 2021. The role of soil in the contribution of food and feed. *Philos. Trans. R. Soc. B*, 376(1834): 20200181. DOI: <https://doi.org/10.1098/rstb.2020.0181>.
- Srinivasulu, M., Mohiddin, G.J., Madakka, M. and Rangaswamy, V. 2012. Effect of pesticides on the population of *Azospirillum* sp. and on ammonification rate in two soils planted to groundnut (*Arachis hypogaea* L.). *Trop. Ecol.*, 53(1): 93-104. ISSN 0564-3295.
- Strickland, T.C., Potter, T.L. and Joo, H. 2004. Tebuconazole dissipation and metabolism in Tifton loamy sand during laboratory incubation. *Pest Manag. Sci.*, 60(7): 703-709. DOI: 10.1002/ps.860.
- Subudhi, M.B. and Panda, S. 2013. Study of Pollution Load of River Potteru and its Possible Impact on Structure of DNA. *Asian J. Res. Chem.*, 6(4): 331-333.
- Telkapalliwari, N.G., Borikar, D.M. and Shivankar, V.M. 2017. Physico-chemical characterization of farmland soil samples of nearby villages of Hingna Taluka, District Nagpur, Maharashtra India. *Asian J. Res. Chem.*, 10(3): 301-304. DOI: 10.5958/0974-4150.2020.00075.9.
- Ullah, M.R. and Dijkstra, F.A. 2019. Fungicide and bactericide effects on carbon and nitrogen cycling in soils: a meta-analysis. *Soil Syst.*, 3(2): 23-38. DOI: <https://doi.org/10.3390/soilsystems3020023>.
- Wong, C.C., Wu, S.C., Kuek, C., Khan, A.G. and Wong, M.H. 2007. The role of mycorrhizae associated with vetiver grown in Pb/Zn contaminated soils: greenhouse study. *Restor. Ecol.*, 15(1): 60-67. DOI: 10.1111/j.1526-100X.2006.00190.x.
- Yang, L.N., Nkurikiyimfura, O., Pan, Z.C., Wang, Y.P., Waheed, A., Chen, R.S., Burdon, J.J., Sui, Q.J. and Zhan, J. 2021. Plant diversity ameliorates the evolutionary development of fungicide resistance in an agricultural ecosystem. *J. Appl. Ecol.*, 58(11): 2566-2578. DOI: 10.1111/1365-2664.13978.
- Zheljzakov, V.D. and McNeil, P. 2008. Comparison of five digestion procedures for recovery of nutrients and trace elements in plant tissue. *J. Plant Nutr.*, 31(11): 1937-1946. DOI: <https://doi.org/10.1080/01904160802402906>.

ORCID DETAILS OF THE AUTHORS

Maan Abdul Azeez Shafeeq: <https://orcid.org/0000-0002-3345-5568>



Study of Temporal Dynamics of Urban Heat Island Surface in Padang West Sumatra, Indonesia

Rery Novio† , Sri Mariya, Widya Prarikeslan and Sophia Aulia Ramon

Department of Geography, Padang State University, Indonesia

†Corresponding author: Rery Novio; rerynovio@fis.unp.ac.id

Nat. Env. & Poll. Tech.
Website: www.neptjournal.com

Received: 24-08-2023

Revised: 26-10-2023

Accepted: 06-11-2023

Key Words:

Urbanization
Urban heat island
Land surface temperature
Temporal dynamics

ABSTRACT

Padang as the capital of the province, is a strategic area and also the center of the economy. Annual population growth affects changes in land use from vegetated land to built-up areas. An increase in barren land will trigger an increase in temperature. SUHI is a temperature phenomenon that occurs on the surface resulting from the increase in temperature. SUHI can be observed through surface temperature data or Land Surface Temperature. This study aims to identify changes in land surface temperature that are affected by changes in land use in the form of building density conditions. In analyzing this using Landsat 7 ETM+ imagery in 2001, 2006, 2011, 2016, and 2020. The building density measurement method LST transformations to measure surface temperature and helps the Surface Urban Heat Island phenomenon. The results of the analysis showed that there was an increase in the building density of the city of Padang over a period of 20 years. This phenomenon affects the surface temperature, indicating that the surface temperature has increased by around 0.47°C. The highest temperature from 2001-2020 occurred in 2016, with the highest temperature of 36°C.

INTRODUCTION

The city, in its place, fulfills its function as a center of human activity, which, compared to its surroundings, develops significantly across various sub-regions in urban areas (Mathewson 2018). Rapid development in urban areas, especially in fast-growing cities, tends to ignore the environmental and social aspects of urban life (Girardet 2008, Lehmann 2010). Various impacts influence the quality of life, which can be observed from physical development as a potential resource. The interaction between villages and cities is very important. The increasing physical development of cities, along with population growth and urban activities, leads to a decrease in vegetated areas, higher pollutant emissions, and the need to comprehensively implement energy-saving and emission-reduction policies. Public activities in urban areas cause changes in the physical appearance of the city, resulting in temperature differences between the central region and its surroundings. Urban growth is most rapid in the developing world, where cities gain an average of five million residents every month in a year (Meenakshi 2012). Thus, “urban sickness” begins to appear, and “urban heat island effect” is one of it. The main cause of “urban heat island” is modification of the land surface by urban development which uses materials which effectively retain heat (Yang 2013).

Solar radiation received from the earth’s surface is absorbed and reflected directly. Hence, the temperature of the urban environment is higher than in rural areas (Effendy 2007). Urban Heat Islands are metropolitan areas that are hotter than surrounding rural areas. It is a feature of hot urban areas compared to surrounding non-urban areas. In general, UHI means an increase in air temperature, but it can also mean the relative heat of the surface and the material above it (Hermawan 2015).

As society develops and urbanization accelerates as a result of development, urban heat islands have grown and negatively impacted air quality conditions, the environment, and energy use, as well as future climate change. An increase in built-up land characterizes a high level of urbanization (Putra et al. 2018). The phenomenon of UHI in urban areas can be divided into types of UHI, namely Surface Urban Heat Island and Atmospheric Urban Heat Island, which have different characteristics in measurement methods, effects, and detection methods (Root 2013).

City Field, the capital of West Sumatra province, is the largest city on Sumatra Island. Its central location and robust economy make it easily accessible and a focal point for community activities and work, leading to population growth. The population of Padang City in the years 2001, 2006, 2011, 2016, and 2020 was 743220, 819740, 844316,

902413, and 909040 individuals respectively (BPS City Padang 2001, 2006, 2011, 2016, 2020).

The increase in population in urban areas is the result of the rate of rural-urban migration, which will create new problems in cities. Along with population growth, the need for housing and infrastructure in the city will also increase (Mariya & Novio 2019). The developments that have occurred have led to an increase in the area of construction land. This affects ecosystem function, biodiversity, and climate (Oktavianingrum et al. 2020). Transitioning from the background behind birth to the problem, two key aspects emerge: 1) Obtaining density area information: Land development in City Padang from 2001 to 2020, and 2) Understanding the consequences: Intensity of the Surface Urban Heat Island resulting from changes in density of developed land.

MATERIALS AND METHODS

Temperature surfaces can counted by subtracting temperature brightness and counting emissivity surface temperature surface data was obtained using Landsat thermal imagery and extracted using the Mono-window method. The processing algorithm for temperature data involves four stages, namely:

- a. Changing digital numbers become radiation for channel thermal (band 6) Landsat 7 ETM.

$$L\lambda = \frac{(L_{max} - L_{min})}{(Q_{calmax} - Q_{calmin})} (Q_{cal} - Q_{calmin}) + L_{min}$$

Information :

$L\lambda$ = Spectral radian at the sensorin
($W/m^2 \cdot srad \cdot \mu m$)

L_{max} = spectral radiance scaled
against $Q_{cal Max}$ ($W/ m^2 \cdot srad \cdot \mu m$)

L_{min} = spectral radiance, Which is scaled
against $Q_{cal Min}$ ($W/ m^2 \cdot srad \cdot \mu m$)

$Q_{CAL Min}$ = calibrated value minimum,
related with L_{min}

$Q_{CAL Max}$ = pixel value calibrated
maximum, with respect to L_{Max}
 $Max = 255$

Q_{cal} = Satellite image pixel value
(DN/Digits number)

- b. Conversion radiance corrected atmospheric to brightness temperature.

The equation used for the calculation of temperature value :

$$Tb = \frac{K2}{\ln\left(\frac{K1}{L\lambda} + 1\right)}$$

Information :

TB = Brightness temperature
satellite(K)

K1 = Calibration constant
spectral radiance

K2 = calibration constant
absolute temperature (K)

$L\lambda$ = Radian Spectral

- c. Surface temperature conversion from Kelvin to Celsius.

$C = T - 273$

Description :

C is degrees Celsius, and T is degrees Kelvin

RESULTS AND DISCUSSION

Analysis of Land Surface Temperature

Processing method temperature Lansat 7ETM+ only uses one band as surface temperature input (Nugraha et al. 2019).

The analysis of the Land Surface Temperature (LST) results shows that the minimum and maximum LST values are located in the city of Padang. The highest LST value, reaching +36°C, was recorded in the year 2016, while the lowest temperature, +8°C, occurred in 2011. This discrepancy impacted the imagery of the research area, with some regions being covered by clouds. Cloud cover poses a challenge in image management, ultimately influencing the accuracy of the classification results. As stated by Sinabutar et al. (2020), clouds obscure areas beneath them, making it difficult to obtain information from those regions and potentially leading to errors in interpretation.

The results of the study on image processing of Landsat 7ETM+ for the years 2001 to 2020 indicate fluctuations in temperature. In 2001, the lowest temperature was recorded at 10°C and the highest at 32°C. Similarly, in 2006, temperatures ranged from 14°C to 32°C. In 2011, temperatures ranged from 8°C to 33°C, while in 2016, temperatures varied from 14°C to 36°C. In 2020, temperatures ranged from 14°C to 32°C.

These findings align with the research conducted by Shrinidi in 2011, which highlighted the variability of

temperatures within cities. Despite Bangalore having a moderate overall temperature, the temperature within the city varies significantly across different geographical locations and land cover types.

The regional analysis of surface temperature processing consistently reveals a pattern wherein lower temperatures are observed on the outskirts of the city while higher temperatures prevail towards the center. This pattern is attributed to the high density of building construction. Specifically, in the case of Padang City, the western part serves as the city center, while the eastern and southern regions are characterized by vegetation.

Distribution SUHI

In the study, the City of Padang is divided into two regions: the western part, classified as urban areas and serving as the city center, and the eastern part, designated as suburban areas. The surface temperature within the city center exhibits warmer conditions compared to the rural areas in the adjacent eastern region of the City of Padang. High surface temperatures are predominant in the central region of the city, whereas lower temperatures prevail in the suburbs. This observation corresponds to the concept of the Urban Heat Island (UHI), wherein urban areas experience higher temperatures than their rural counterparts. Additionally, the temperature gradient indicates that temperatures decrease as the distance from the city center increases (Fawzi 2017).

Analysis SUHI was done to assess the impact of changes in land cover and temperature surface caused by urbanization. SUHI, which is influenced by density building. Enough tall causes enhancement emissivity surface And impacts on enhancement mark LST. Intensity SUHI can be measured with a measure difference mark LST.

On the map distribution UHI (Urban Heat Island) method Threshold, areas that are not exposed to UHI are presented with marks from 0 to negative (≤ 0), whereas areas affected by UHI are classified into 3 classes based on The UHI values are UHI class 1 (UHI range $0-2^{\circ}\text{C}$), UHI class 2 (UHI range $2-4^{\circ}\text{C}$) and UHI class 3 (UHI above 4°C) . the more tall UHI value, the more big the influence of UHI (Jaelani 2020).

By spatial analysis distribution, SUHI City Padang can seen in Figs.1 to 5.

Based on the calculation of the results, 2001 refers to the threshold value limit SUHI (23.39°C), so the obtained mark SUHI highest is 8.78°C and lowest -12.9°C . Viewed from wide. The scope of the area where the phenomenon occurs SUHI in City Padang year 2001, reach 18940 Ha. Meanwhile, 50778 ha is Non-SUHI Because the LST is still on the verge of limit.

Based on the calculation of the results, 2006 refers to the threshold value limit SUHI (23.39°C), so the obtained mark SUHI highest is 8.89°C and lowest -8.91°C . In 2006, the coverage area exhibiting the Urban Heat Island (UHI)

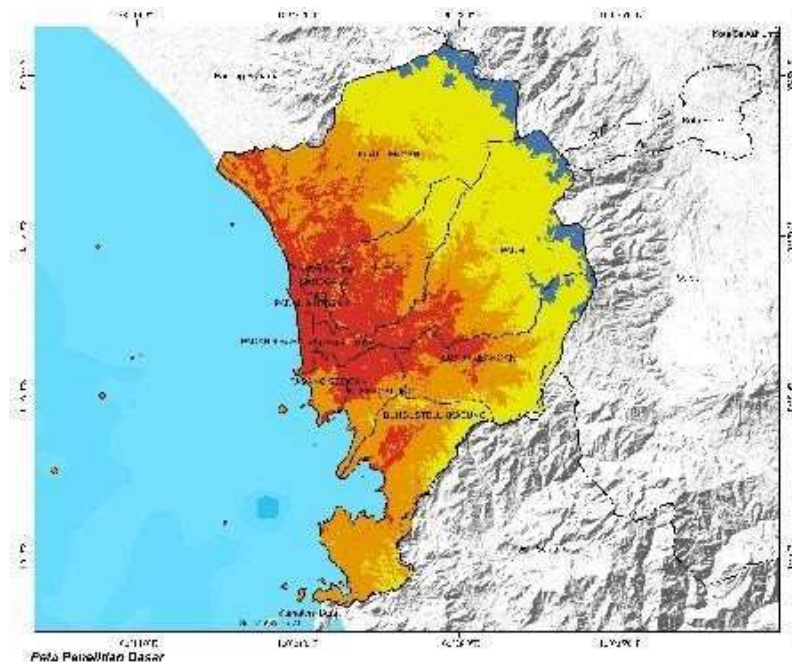


Fig. 1: Map Intensity SUHI Year 2001.

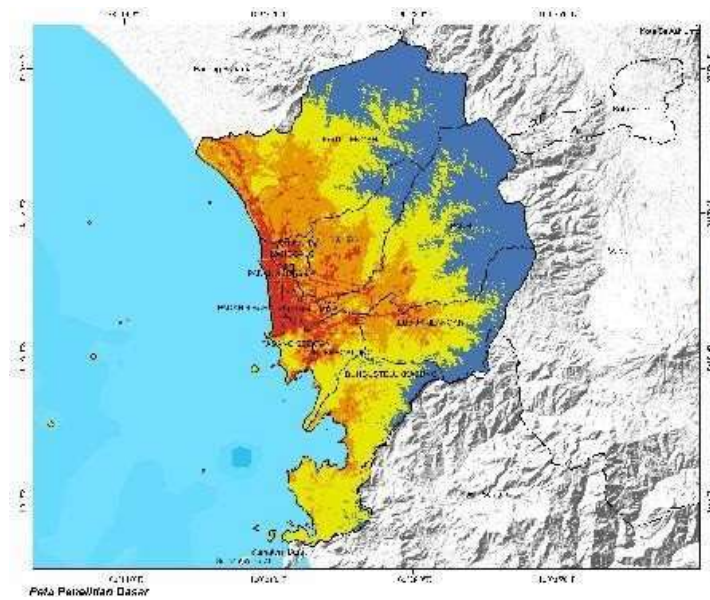


Fig. 2: Map intensity SUHI Year 2006.

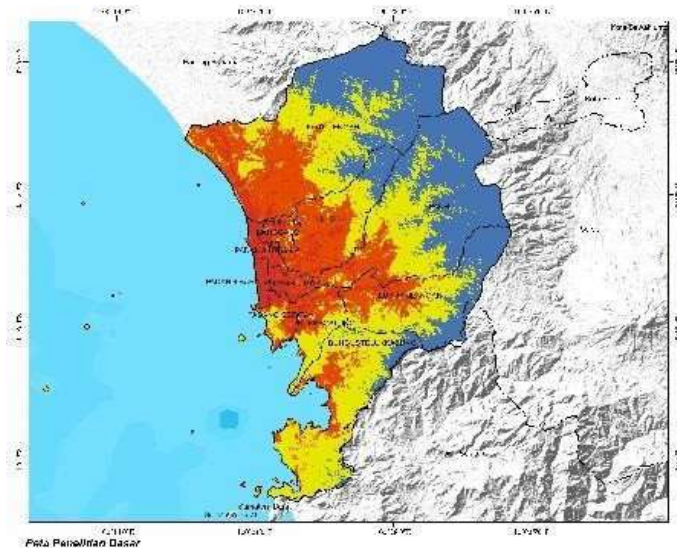


Fig. 3: Map intensity SUHI Year 2011.

phenomenon in the City of Padang reached 21124 Ha, while non-UHI areas covered an extensive area of 48594 ha.

Based on the calculation of the results, 2011 refers to the threshold value limit SUHI (23.51°C), so the obtained mark SUHI is highest at 9.55°C and lowest at -15.41°C . Regarding the coverage area where the SUHI phenomenon occurred in Padang city in 2011, it reached 20019 ha, while 49,687 ha were classified as Non-SUHI areas.

Based on the calculation of the results, 2016 refers to the threshold value limit SUHI (25.95°C), so obtained at 10.89°C

And Lowest -11.02°C . Phenomenon SUHI in the city Field year 2016, reached 17960 ha whereas 51759 Ha is Non-SUHI.

Based on the calculated results, in 2020, the threshold value for the SUHI phenomenon (24.46°C) was determined. Consequently, the recorded highest SUHI value was 8.19°C , while the lowest was -10.08°C . Considering the extent of the SUHI phenomenon in the city of Padang in 2020, it covered an area of 18770 ha, whereas 5,098 ha were classified as non-SUHI areas since the Land Surface Temperature (LST) value remained within the threshold limit.

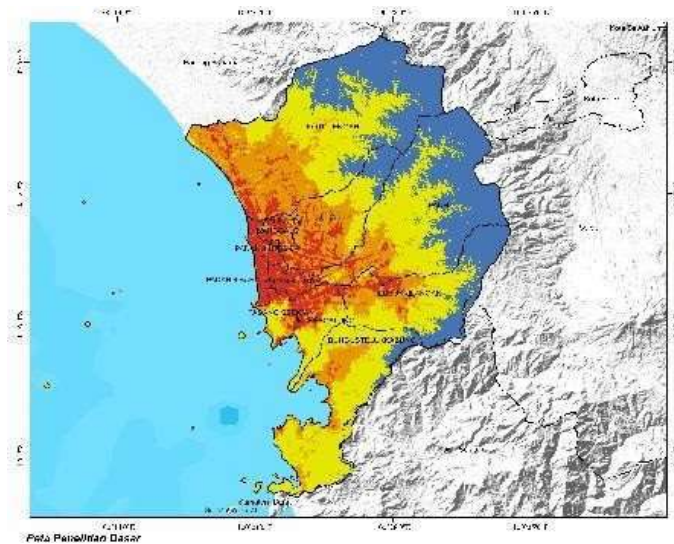


Fig. 4: Map Intensity SUHI Year 2016.

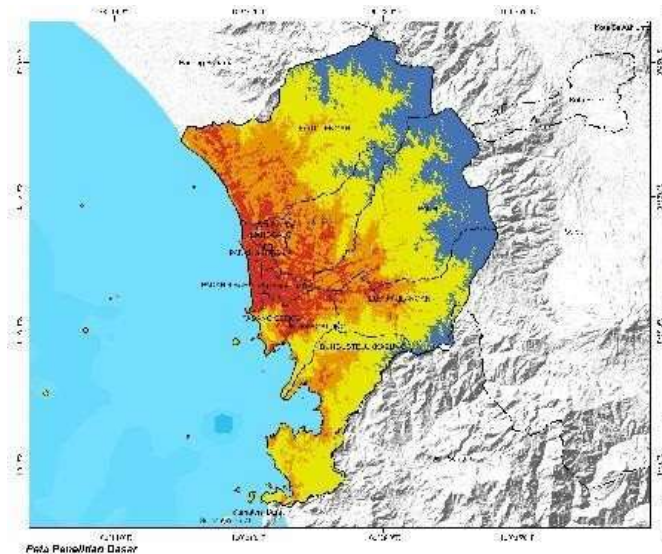


Fig. 5: Map intensity SUHI Year 2020.

The spatial distribution of the urban heat island effect, particularly evident in the center of Padang city with its high and very high temperatures, significantly impacts vegetation density. This distribution is highlighted by the majority of Padang city being characterized by low vegetation density. These observations align with the findings of Wulandari & Sudibyakto (2017), who attributed the UHI phenomenon in urban areas to extensive built-up land and a lack of urban vegetation or forests. Climate change, as emphasized by Prasad and Chakravorty (2015), is an ongoing process with far-reaching implications. Understanding the overall effects of climate change is crucial for accurate diagnosis

and subsequent mitigation efforts. It's imperative to recognize the sensitivity of the climate, which can be adversely affected either by natural phenomena or human interventions. According to Prasad & Chakravorty (2015) and previous studies, climate change is most sensitive to anthropogenic influences, which can directly or indirectly lead to environmental disruptions such as floods, droughts, salinity issues, high temperatures, and more. Additionally, these influences can result in shifts in cropping seasons, alterations in growth and yield patterns, changes in pest and disease dynamics, and modifications in the behavior of pollinating insects.

CONCLUSION

Based on processing data, the study obtained results indicating a change in the density of the building across wider areas. Building density experienced an increase from the year 2001-2020. In 2001, the density of high-rise buildings had an area of 1219 ha. In the year 2020, the density of the building experienced an increase of 2,718 ha to 14152 ha.

The phenomenon of Surface Urban Heat Island (SUHI) in Padang City from 2001 to 2020 exhibits a spatial pattern that remains relatively consistent with urban development. High SUHI areas tend to be concentrated in the central part of the city.

REFERENCES

- BPS City Padang 2001. Padang City in Figure. Padang, Indonesia: Badan Pusat Statistik Badan Pusat Statistik Kota Padang (bps.go.id)
- BPS City Padang 2006. Padang City in Figure. Padang, Indonesia: Badan Pusat Statistik Badan Pusat Statistik Kota Padang (bps.go.id)
- BPS City Padang 2011. Padang City in Figure. Padang, Indonesia: Badan Pusat Statistik Badan Pusat Statistik Kota Padang (bps.go.id)
- BPS City Padang 2016. Padang City in Figure. Padang, Indonesia: Badan Pusat Statistik Badan Pusat Statistik Kota Padang (bps.go.id)
- BPS City Padang 2020. Padang City in Figure. Padang, Indonesia: Badan Pusat Statistik Badan Pusat Statistik Kota Padang (bps.go.id)
- Effendy, S. 2007. The Relationship between Green Open Space and the Urban Heat Island in the Jabotabek Region. Dissertation. School Postgraduate, Inst. Bogor Agriculture, Bogor.
- Fawzi, N.I. 2017. Measuring urban heat island using sensing far away, case in Yogyakarta City. *Sci. Globe Mag.*, 19(2): 195-206.
- Girardet, H. 2008. *Cities People Planet*. Wiley.
- Hermawan, E. 2015. The urban heat island (UHI) phenomenon in some cities big in Indonesia as one impact change global environment. *Citra Widya Edukasi J.*, 7(1): 33-45.
- Jaelani, A.Y. 2020. Analysis of changes in urban heat island (UHI) distribution in the city of Surabaya using multitemporal Landsat satellite imagery. *ITS Eng. J.*, 9(2): 337-350
- Lehmann, S. 2010. *The Principles of Green Urbanism: Transforming the City for Sustainability*. London: Earthscan, pp. 1-15.
- Mariya, S. and Novio, R. 2019. Mapping of slum areas and squatter areas in Padang city. *J. Geogr.*, 8(1): 56-71.
- Mathewson, D.W. 2018. Historic institutionalism and urban morphology in Jakarta: Moving towards building flood planning and development system. *J. Reg. City Plan.*, 29(3): 188-209.
- Meenakshi, S. M. and Sundara, A. 2012. Evaluating environmental land use/land cover change detection in sub urban fringe area around Madurai city using GIS technique. *Nature Environment and Pollution Technology*, 11(4): 595.
- Oktavianingrum, S., Pin, T.G. and Shidiq, I.P.A. 2020. The effect of land cover changes on land surface temperature in South Tangerang in 2005, 2008, 2013, and 2018. *IOP Conf. Ser. Earth Environ. Sci.*, 412(1): 012029.
- Prasad, B.V.G. and Chakravorty, S. 2015. Effects of climate change on vegetable cultivation: A review. *Nat. Environ. and Pollut. Tech.*, 14(4): 923.
- Putra, A.K., Sukmono, A. and Sasmito, B. 2018. Analysis connection change cover land to temperature surface related the Urban Heat Island phenomenon uses image Landsat (Case Study: Surakarta City). *J. Geodesy Undip*, 7(3): 22-31.
- Root, M. (eds). 2013. *Urban Heat Island*. CRC Press/Taylor&Francis Group LLC, NJ, p.149.
- Sinabutar, J.J., Sasmito, B. and Sukmono, A. 2020. Cloud masking studies use band quality assessment, function of mask and multi-temporal cloud masking on images Landsat 8. *J. Geodesy Undip*, 9(3): 51-60.
- Wulandari, R. and Sudibyakto, H.A. 2017. Identification of urban heat islands in the city of Surakarta. *J. Bumi Indon.*, 6(1): 121.
- Yang, L. 2013. Research of urban thermal environment based on digital technologies. *Nature Environment and Pollution Technology*, 12(4): 645.

ORCID DETAILS OF THE AUTHORS

Rery Novio: <https://orcid.org/0000-0003-3542-5095>



Implementation of the AquaCrop Model for Forecasting the Effects of Climate Change on Water Consumption and Potato Yield Under Various Irrigation Techniques

E. E. Salman*†, A. M. Akol*, J. S. Abdel Hamza** and Ahmed Samir Naje*

*College of Engineering, Al-Qasim Green University, Babylon, Iraq

**Soil Science and Water Resources Department, College of Agriculture, University of Al-Qadisiyah, Iraq

†Corresponding author: E. E. Salman; ehsansalaman7@wrec.uoqasim.edu.iq

Nat. Env. & Poll. Tech.
Website: www.neptjournal.com

Received: 11-09-2023

Revised: 18-11-2023

Accepted: 29-11-2023

Key Words:

Climate Change
Irrigation methods
AquaCrop model
Drip Irrigation

ABSTRACT

In this study, the AquaCrop model was employed to analyze the impact of projected future climate changes on the water usage and biomass production of potato crops in Babylon, Iraq, under varying irrigation methods. The irrigation techniques evaluated included sprinkler irrigation, surface drip irrigation, and subsurface drip irrigation at depths of 10 cm and 20 cm. The study involved simulating and forecasting conditions for the year 2050, comparing them to current conditions. The model measured and predicted the evapotranspiration (ET_a) and actual biomass of potato crops for 2050 using the RCP 8.5 scenarios, which outline different trajectories for greenhouse gas emissions. The AquaCrop model was calibrated and validated using statistical measures such as the R², RMSE, CV, EF, and D, achieving a 99% accuracy level in its performance. The findings suggest that using drip irrigation systems and applying the AquaCrop model significantly mitigates the adverse effects of environmental stress on desert soils and enhances sustainable agricultural practices in arid regions.

INTRODUCTION

The potato crop (*Solanum tuberosum* L.) is one of the four most important crops in the world in terms of nutritional importance after wheat, corn, and rice. It tops the tuberous crops. It is believed that the original home of potatoes is the Andes mountains in Bolivia. The southern coast of Chile is its original home. Production is 388,191 million tons worldwide, increasing by 15.5% on an area of 19.303 million hectares (FAO, 2017). Potatoes occupy a large place in global agriculture and contain approximately 80% water, 2% protein, and 18% starch (Qasim et al. 2013). Mohammed et al. (2019) referred to the shift from sprinkler irrigation systems of different types and lawn irrigation to the subsurface drip irrigation system for large areas of corn cultivation in the US. The process has been going on successfully for more than 10 years and production has been increased saving the amounts of water used by 35-55% compared to sprinkler and irrigation systems. In a study conducted by Hassan et al. (2020) to compare the drip irrigation system surface and subsurface, there was a clear effect in the removal of salts from part of the soil parts and keeping it outside the root zone, which contributed to alleviating the effect of osmotic pressure on the plant. It led to an increase in production per unit area and an increase in water use efficiency (Bamohani 2011).

Patel et al. (2010) found that the simulated AquaCrop software with the measured above-ground values after the

main crop growth stages during the period 2009-2010 found that the simulated values above-ground dry biomass are in good agreement with the measured values with a low mean error. The corresponding values of the different coefficients were also well simulated with the measured yield giving correlation coefficients of 0.74 and 0.72. A leaf area index and the use of values of water productivity that are validated to demand atmospheric evapotranspiration and concentration of CO₂ give the model the ability to extrapolate to diverse locations and seasons. Although the model is simple, it pays special attention to the basic processes involved in crop productivity and responses to water, from a perspective of the physiological and agricultural background of the plant. The researcher also obtained a significant response and a good comparison by AquaCrop in simulating the productivity of the potato crop under full irrigation and water deficit (when 80 and 60% of the available water is depleted). In simulating production under extreme water stress, the model had less of an impact (Hassan et al. 2023, Ali et al. 2021, Steduto et al. 2009). It is very helpful for designing and evaluating under-irrigation strategies and water management options, as well as for researching the effects of site, soil type, irrigation management, and seeding history on plant production in semi-digestive and irrigated agriculture because AquaCrop can simulate moderate water stress of a potato crop under dry conditions that occur at different stages of growth. By

utilizing the AquaCrop model, the study aims to assess the canopy cover and its impact on crop growth, water consumption, and overall agricultural productivity in Babylon governorate. This evaluation will provide valuable insights into the suitability of AquaCrop for estimating these variables in this specific region Mohammed et al. (2022).

MATERIALS AND METHODS

Sampling

The field study carried out in the Medhatiya area of Babylon Governorate during the spring of 2021 examined the soil properties of a private plot. Results detailing the soil particle size distribution are presented in Table 1.

Water Consumption

The values of meteorological data can be obtained from the Meteorological Department of the Iraqi Ministry of Agriculture. On land used for agriculture, an experiment

Table 1: Properties of experimental soil during the seasons of 2016 and 2017.

Characteristic		2016	
		Soil depth	
		0-30 cm	30-60 cm
Ece	DSM ⁻¹	2.65	2.7
PH		7.6	7.7
Sand	g.kg ⁻¹	762	705
Silt		137	145
Clay		101	150
CaCO ₃	g.kg ⁻¹	280	291
OM		4.51	2.37
CEC	Cmol.kg ⁻¹	16.31	18.45
N	mg.kg ⁻¹	23.42	19.32
P		12.21	11.72
K		121.32	117.47
Ca ⁺⁺	meq .L ⁻¹	14.62	12.22
Mg ⁺⁺		9.73	8.23
Na ⁺		4.41	5.18
k ⁺		3.24	2.07
SO ₄ ⁻²		14.61	13.25
HCO ₃ ⁻¹		3.19	2.67
Cl ⁻¹		14.30	11.09
Bulk Density		1.39	1.45
Total Porosity	%	47	44
Water Content at 1500 kPa		0.10	
Water Content at 33 kPa	cm ³ .cm ⁻³	0.30	
Available Water		0.20	

was conducted. After that, it was separated into three major sectors, with a 2 m gap between each section. Twelve experimental units, each measuring 4 by 4 meters, were separated into each area. On January 10, 2021, potato seeds were planted, with each tuber being 0.25 m apart and 0.10 m deep. According to the recommended fertilizer amounts of 100 kg P H⁻¹ and 300 kg K H⁻¹, the experimental area was treated with triple superphosphate fertilizer (20% P) before planting. According to the fertilizer guideline of 300 kg N H⁻¹, urea fertilizer (46% N) was added in three batches: the first after 20 days of planting, the second after 30 days, and the third after 25 days of the second batch (Soil Survey Staff, 2016). On December 5, 2021, potato tubers were physically removed.

Statistical Comparison

Five statistical measures were applied to test the performance of the model and compare the simulated and measured results.

First is the root mean square error (RMSE):

$$RMSE = \sqrt{\frac{1}{n} \sum_{i=1}^n (S_i - M_i)^2} \quad \dots(1)$$

Where S_i and M_i are simulated and measured values, respectively, and n is the number of observations.

Second is the coefficient of determination (R²):

$$R^2 = \frac{\sum S_i M_i - \sum S_i + \sum M_i}{\sqrt{\sum S_i^2 - (\sum S_i)^2} \times \sqrt{\sum M_i^2 - (\sum M_i)^2}} \quad \dots(2)$$

Third is the mean bias error (MBE):

$$MBE = \frac{1}{n} \sum_{i=1}^n (S_i - M_i) \quad \dots(3)$$

Fourth is the index of agreement (d):

$$d = 1 - \frac{\sum_{i=1}^n (S_i - M_i)^2}{\sum_{i=1}^n (|S_i - \bar{M}| + |M_i - \bar{M}|)^2} \quad \dots(4)$$

Where: \bar{M} is the mean of the n measured values. The value of d ranges from -∞ to 1.0.

Fifth is the Coefficient of Efficiency (E):

$$E = 1 - \frac{\sum_{i=1}^n (S_i - M_i)^2}{\sum_{i=1}^n (M_i - \bar{M})^2} \quad \dots(5)$$

RESULTS AND DISCUSSION

Predictable Water Consumption of the Potato Crop

When comparing the base period with the period (2050),

Table 2 and Fig. 1 show the actual water consumption of the potato crop and for all study coefficients of difference in irrigation methods according to the two scenarios (RCP 4.5) and (RCP 8.5). There is a significant increase in the consumption values of water for the period when compared with the base period. The actual water used by the potato crop varied from 215 to 326 mm, whereas the water used in the first scenario was between 242 and 380 mm. This represents an absolute difference of 27-54 mm and a relative change of between 12.56% and 16.56% for the scenario (RCP 4.5) when comparing the base period with the period (2050). In comparison to the water consumption of the first scenario, which ranged from 267-433 mm, the actual water consumption values for the potato crop ranged between 215 and 326 mm, with an absolute change ranging between 52 and 107 mm and a relative change ranging from 24.19 to 32.82% for the scenario (RCP 8.5). These results are consistent with previous research (Hassan et al. 2023, Jafaar et al. 2020, 2022, 2023).

Expected Biomass of the Potato Crop

Table 3 displays the actual biomass of the potato crop under various study treatments, comparing different irrigation

Table 2: Water consumption for RCP4.5 and RCP8.5 till 2050.

No.	RCP 4.5					RCP 8.5			
	Treatment	Base period	2020 - 2030	Absolute change	Relative change	Base period	2020 - 2030	Absolute change	Relative change
1	Spr	326	380	54	16.56	326	433	107	32.82
2	Drip S	298	345	47	15.77	298	390	92	30.87
3	Drip Sub1	245	282	37	15.1	245	310	65	26.53
4	Drip Sub2	215	242	27	12.56	215	267	52	24.19

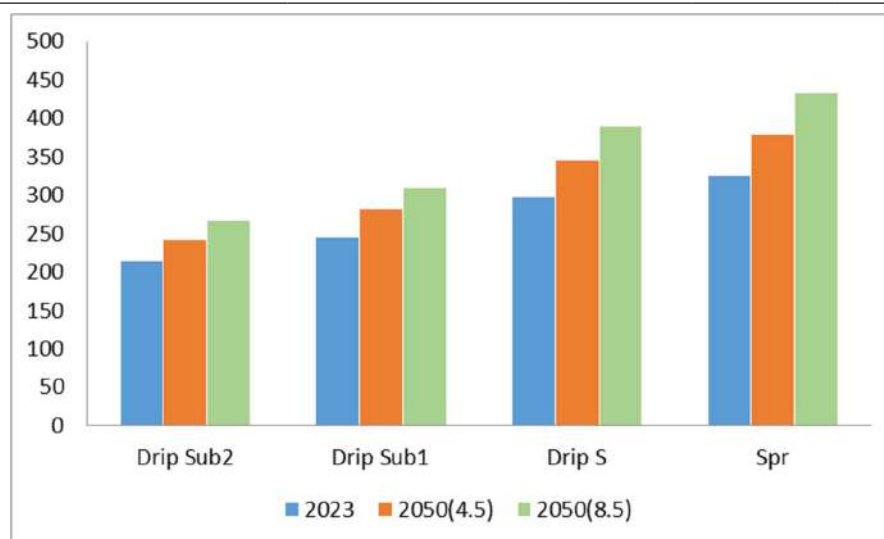


Fig. 1: Water consumption for RCP4.5 and RCP8.5 till 2050.

methods across two scenarios, RCP 4.5 and RCP 8.5, between the baseline period and the year 2050. It is evident from the table that there is a notable reduction in biomass values for the future period compared to the baseline. The actual biomass values of the potato crop ranged between 20.3 and 25.9 tons, compared to the biomass of the first scenario, which ranged between 24.3 and 17.1 tons, with an absolute change ranging between 1.6 and 3.2 tons, and a relative change ranging between 6.15 and 15.76% for the scenario RCP 4.5 when comparing the base period with the period 2050, and the actual biomass values of the potato crop ranged between 25.9 and 20.3 tons compared to the biomass of the first scenario, which ranged between 13.1 and 21.5 tons, with an absolute change that ranged between 4.4 and 7.2 mm and a relative change ranging between 16.99 and 35.47% for the scenario RCP 8.5 when comparing the base period with the period 2050.

The results confirm that the production of the potato crop will decrease in the future (2050), as the potato crop will be affected by climate changes with the temperature rise, which will increase in the flowering stage, which is a sensitive stage, which will lead to an increase in water consumption at this stage. The deterioration of the productivity of yellow

Table 3: Biomass RCP4.5 and RCP8.5 for (2050) compared to the base period.

No	RCP 4.5					RCP 8.5			
	Treatment	Base period	2020-2030	Absolute change	Relative change	Base period	2020-2030	Absolute change	Relative change
1	Spr	20.3	17.1	3.2	15.76	20.3	13.1	7.2	35.47
2	Drip S	22.1	19.5	2.6	11.76	22.1	16.6	5.5	24.89
3	Drip Sub1	24.5	22.3	2.2	8.98	24.5	19.4	5.1	20.82
4	Drip Sub2	25.9	24.3	1.6	6.18	25.9	21.5	4.4	16.99

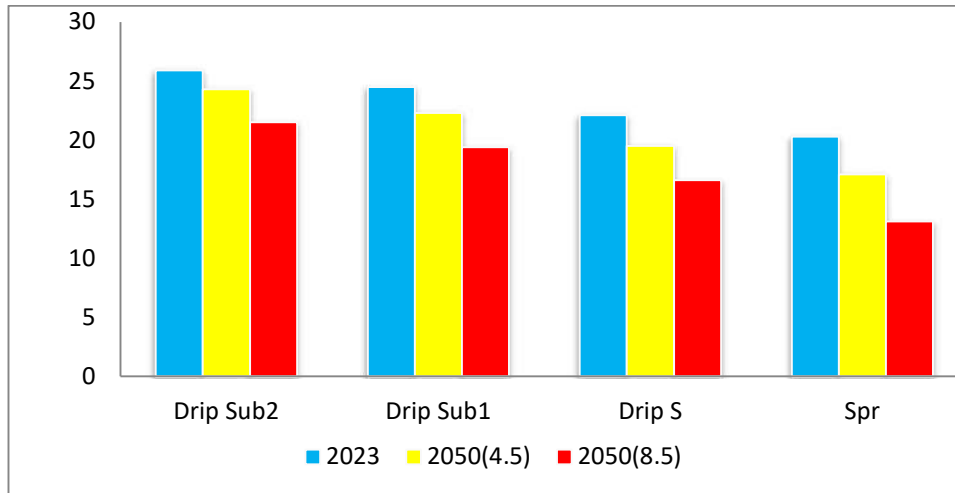


Fig. 2: Biomass for RCP4.5 and RCP8.5 till 2050.

corn is related to several factors, the most important of which is water consumption, which will increase in the future, and requires the availability of additional quantities of water. Therefore, the trend for irrigation methods such as sprinklers and drip will work to reduce the amount of water consumed. It was also noted through the results that the predictions were significantly affected by biomass and water consumption with climate change. It was also found that there are significant differences when comparing the two scenarios, as a decrease in productivity and an increase in water consumption is noted when the concentration of carbon dioxide increases, i.e. in the RCP8.5 scenario compared to the RCP4.5 scenario, and therefore these results confirm that the calibration performance and validity of the (AquaCrop) model for evaluating The effect of climatic changes on the productivity and water consumption of the crop, as it was logical and can predict good crop productivity, water consumption and other characteristics of the crop. The increase in carbon dioxide concentration as a result of climatic effects and depending on the climate change scenarios RCP4.5 and RCP8.5 for future periods had negative effects on biomass and actual water consumption, as the value of water consumption increased and the yield decreased as a result of the impact of climate change compared to the values of the reference period, and this is consistent with

what it was found by Yibrah et al. (2015), Bitri et al. (2014). Water availability and production are important factors in climate change adaptation. To evaluate the effects of climate change and produce outputs, global and regional climate models have been utilized as decision-support tools. Current and future climate data are vital for simulating crop results and assessing the effects of climate change on crop yields, water balance, and food security. Climate change influences water resources by modifying the volume, variability, timing, pattern, and intensity of rainfall. It also influences the water cycle and photosynthesis in plants. Additionally, crop growth can be directly affected by factors such as relative humidity, wind speed, soil temperature, and evapotranspiration, or indirectly through their effects on a plant's physiological processes. The movement of water in the root zone and the soil moisture balance are similarly affected. Crop models, like the AquaCrop model, can be used to assess and simulate soil water balance in different soil strata under varying climatic circumstances and management techniques (Raes et al. 2006, Raes et al. 2011, Akol et al. 2021). Water coming from rain or irrigation is lost as a result of evaporation and transpiration on the soil surface. These models take into account weather factors that directly or indirectly affect the water balance in the soil, as the effects of climate change on the water balance will lead to changes

in soil water storage and water level. groundwater, the level and condition of soil moisture, and can provide some information about irrigation quality, and may reduce the growth period of future crops affecting biomass and actual water consumption (Kang et al. 2009), however the effects of soil moisture resulting from climate change through the practices of modern technologies and the cultivation of varieties resistant to climate change.

Canopy Cover

The RMSE values reached 0.038 for the sprinkler irrigation treatment, 0.028 for the surface drip irrigation treatment, and 0.040 for the treatment, according to the results of the simulated Canopy Cover values and the measured Canopy Cover (Figs. 3 a,b,c,d). Drip irrigation covered a surface area of 10 cm and cost 0.034. The R2 values for all irrigation treatments for the sub-surface drip irrigation treatment

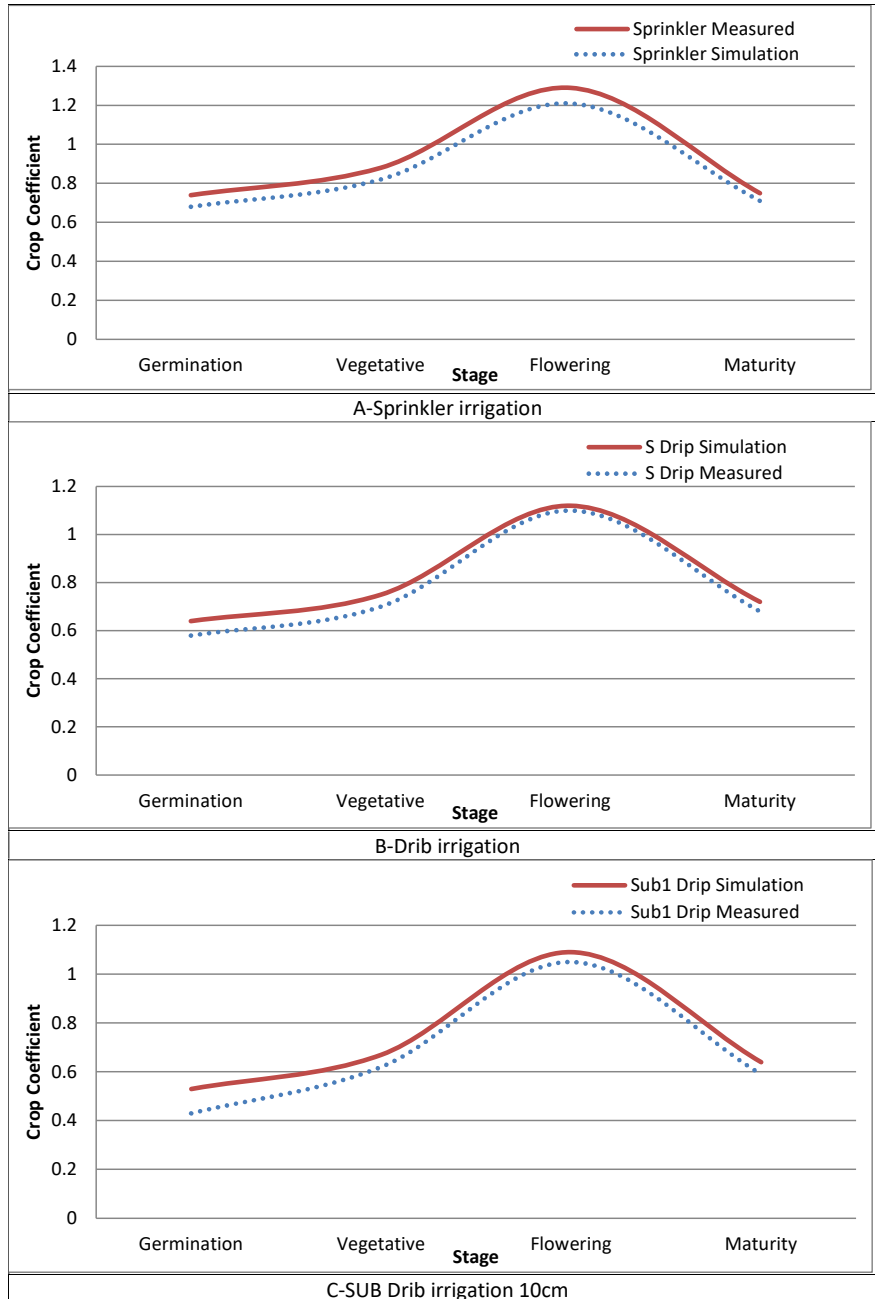


Figure Cont....

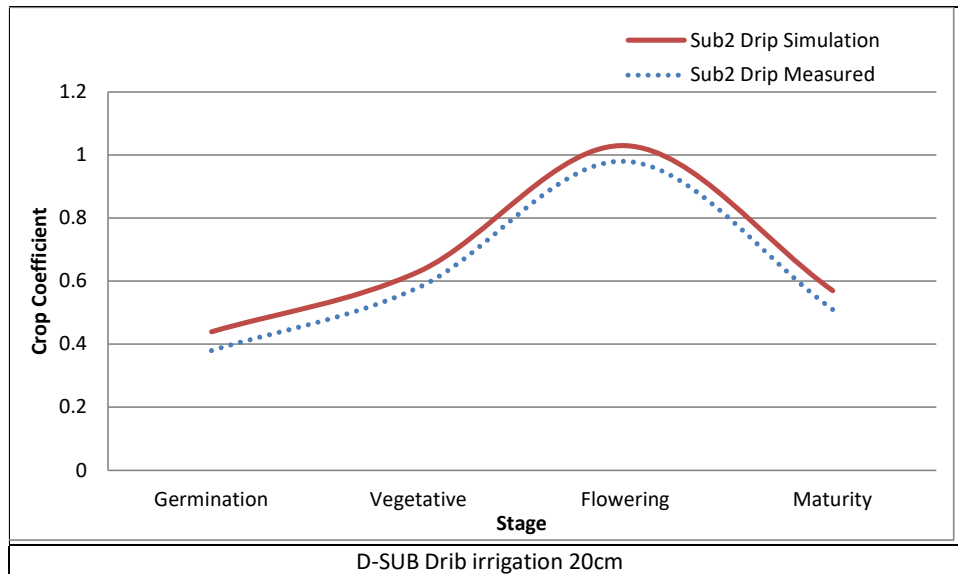


Fig. 3: Crop cover and canopy cover for methods of irrigation.

of 20 cm were 0.99, and the CV values for the sprinkler irrigation treatment were 0.045 and 0.037 for the surface drip irrigation treatment, and 0.060 for the sub-surface drip irrigation treatment of 10 cm and 0.057, respectively for 20 cm of subsurface drip irrigation treatment. For all irrigation treatments, both the EF and d values were 0.99. All irrigation treatments had EF values of 0.99. One of the reasons for the compatibility is that the phenology of potatoes adapts effectively to various climatic situations, with temperature, sun brightness, and growth duration among the major determining elements. As a result, the cultivation environment must change the inputs for vegetative cover (Pawar et al. 2017). The percentage of the soil surface covered by vegetation is measured by the canopy cover index (CC), which varies from a value of (0) when seeds are sown (or when 0% of the soil surface is covered) to a maximum value at the middle of the season, which can reach up to a value of (1) if a cover is achieved. Based on the leaf area index, the entire soil surface is covered by vegetation (100%). AquaCrop tracks the stresses that can arise in the root zone, which can affect the growth of leaves and subsequently the development of vegetation, through the daily computation of soil moisture. Moreover, if these pressures are strong, they may produce plant leaf yellowing. For the model to generate accurate predictions that take into account both the actual evapotranspiration and biomass discovered during the current investigation, this variable must be well-estimated. The AquaCrop model's simulated values for irrigation parameters were compared to measured values using the index (CC) (Greaves and Wang 2016, Ali et al. 2021).

CONCLUSIONS

AquaCrop is employed to increase water production for various irrigation techniques. There is good agreement between the measured and simulated vegetation. This study demonstrates how subsurface irrigation techniques are better than other irrigation techniques. The RCP4.5 and RCP8.5 climate change scenarios show a clear influence of future climatic changes on agricultural output. According to the RCP4.5 scenario and the RCP8.5 scenario, there will be an increase in annual and seasonal rainfall as well as a rise in maximum and minimum temperatures over the two time periods (2030) and (2050) compared to the base period (1985-2005).

REFERENCES

- Akol, A.M., Nassif, N., Jaddoa, K.A., Radhi, K. and Hassan, D.F. 2021. Effect of irrigation methods, tillage systems, and seeding rate on water consumption, biological yield, and harvest index of wheat (*Triticum aestivum* L.). *Int. J. Agric. Stat. Sci.*, 1: 17.
- Ali, Z.A., Hassan, D.F. and Mohammed, R.J. 2021. Effect of irrigation level and nitrogen fertilizer on water consumption and faba bean growth. In: *IOP Conference Series: Earth and Environmental Science*, 722(1): 012043.
- Bamohuni, S. 2011. Design proposal of drip irrigation system for an efficient management of irrigation water for maize improved seeds production in a part of seeds farm of loubmila. *Univ. Stud. Firen. Facol. Agrar.*, 11: 33-40.
- Bitri, M., Grazhdani, S. and Ahmeti, A. 2014. Validation of the aqua crop model for full and deficit irrigated potato production in the environmental condition of Korca Zone, South-eastern Albania. *Int. J. Innov. Res. Sci. Eng. Res. Sci. Eng. Technol.*, 3: 12013-12020.
- FAO. Food and Agriculture Organization of United Nations. *Food Outlook, Need for External Assistance*; June 2017.

- Greaves, G.E. and Wang, Y.M. 2016. Assessment of FAO aqua crop model for simulating maize growth and productivity under deficit irrigation in a tropical environment. *Water*, 8: 557. doi: 10.3390/w8120557.
- Hassan, D., Thamer, T., Mohammed, R., Almaeini, A. and Nassif, N. 2020, November. Calibration and evaluation of aquacrop model under different irrigation methods for maize (*Zea mays* L.) in central region of Iraq. In: Conference of the Arabian Journal of Geosciences, pp. 48-43. Cham: Springer Nature Switzerland.
- Hassan, D.F., Ati, A.S. and Naima, A.S. 2023. Evaluation of the performance of the aqua crop model under different irrigation and cultivation methods and their effect on water consumption. *Iraq. J. Agric. Sci.*, 54(2): 478-490.
- Jafaar, A.A., Mohammed, R.J. and Hassan, D.F. 2022. Effect of phosphorus fertilizer and irrigation level on desert soil management and potato yield. *Int. J. Agric. Stat. Sci.*, 18(2): 609.
- Jafaar, A.A., Mohammed, R.J., Hassan, D.F. and Thamer, T.Y. 2023. Effect of foliar seaweed and different irrigation levels on water consumption, growth and yield of wheat. In: IOP Conference Series: Earth and Environmental Science, 1252(1): 012057.
- Kang, Y., Khan, S. and Ma, X. 2009. Climate change impacts on crop yield, crop water productivity, and food security: a review. *Prog. Nat. Sci.*, 19: 1665-1674.
- Mohammed, R.J., Abdulkadhim, K.A., Hassan, D.F. and Kadhim, T.F. 2019. Effect of wheat straw as organic matter and different water quality on some chemical soil properties and growth of pepper (*Capsicum annum*). In: IOP Conference Series: Earth and Environmental Science, 344(1): 012034.
- Mohammed, R.J., Hameed, I.A. and Thamer, T.Y. 2022. Effect of using different types of well water in Karbala Governorate on soil and plant. *Ecological Engineering & Environmental Technology*, 23.
- Patel, N., Kumar P. and Singh, N. 2010. Performance evaluation of aqua crop in simulating potato yield under varying water availability conditions. *Indian Agric. Res.*, 6: 56-63.
- Pawar, G.S., Kale, M.U. and Lokhande, J.N. 2017. Response of aqua crop model to different irrigation schedules for irrigated cabbage. *Agric. Res.*, 6: 73-81.
- Qasim, M., Khalid, S., Naz, A., Khan, M.Z. and Khan, S.A. 2013. Effects of different planting systems on yield of potato crop in Kaghan Valley: A mountainous region of Pakistan. *Agricultural Science*, 4: 175-179.
- Raes, D., Steduto P., Hsiao, T.C. and Fereres E. 2011. FAO crop water productivity model to simulate yield response to water: AquaCrop version 3.1 Plus.
- Raes, D., Geerts, S., Kipkorir, E., Wellens, J. and Sahli, A. 2006. Simulation of yield decline as a result of water stress with a robust soil water balance model. *Agric. Water Manag.*, 81: 335-357.
- Soil Survey Staff, 2016. Keys to soil taxonomy. USDA, Natural Resources Conservation
- Steduto, P., Hsiao, T.C., Raes, D. and Fereres, E. 2009. Aqua crop: The FAO crop model to simulate yield response to water: I. Concepts and underlying principles. *Agron. J.*, 101: 426-437. doi:10.2134/agronj2008.0139s.
- Yibrah, G., Araya, B. and Amsalu, N. 2015. Performance of aqua crop model in simulating tuber yield of potato (*Solanum tuberosum* L.) under various water availability conditions in Mekelle area, Northern Ethiopia. *J. Nat. Sci. Res.*, 5: 5.



Enhanced Natural Attenuation Technique, Edaphic and Microbiological Changes in Oil-Impacted Soil of Odhiaje Community, Rivers State

P. N. Muonye*† and C. C. Nnaji**

*Department of Civil Engineering, University of Nigeria, Nsukka, Nigeria

**Faculty of Engineering and Built Environment, University of Johannesburg, South Africa

†Corresponding author: P.N. Muonye; engr_muonye@yahoo.com

Nat. Env. & Poll. Tech.
Website: www.neptjournal.com

Received: 29-09-2023

Revised: 02-11-2023

Accepted: 06-11-2023

Key Words:

Bioremediation
Oil spill
Water pollution
Attenuation
Bacteria
Niger Delta

ABSTRACT

Oil spills in the Niger Delta could exert environmental pressures on the soil component. We investigated the impacts of oil spills and the effect of the Enhanced Natural Attenuation (ENA) remediation method on contaminated soil and resident microbial populations in the Odhiaje community in Rivers State, Nigeria. Soil samples for microbiological studies were collected weekly during a 17-week remediation period, while those for edaphic parameters were taken before and after remediation, all at 4 sampling points (SPs). Serial dilution of the oil-impacted soils for microbial density enumeration was carried out according to standard methods. Results revealed that mean concentrations of Total Petroleum Hydrocarbon Contents (THC) (Sig._{value} = 0.009), SO₄²⁻ ions (Sig._{value} = 0.001), and sand compositions (Sig._{value} = 0.045) all differed markedly across the sampling points at p<0.05. Mean levels of EC (Sig._{tvalue} = 0.039) and ΣN (Sig._{tvalue} = 0.058) & K⁺ ions (Sig._{tvalue} = 0.004) differed significantly before and after the remediation exercise at the 95% confidence interval. Application of nutrients was rapidly accompanied by microbial population increases, leading to the consumption of oil contaminants in soils to levels comparable to control over the remediation period. Total Heterotrophic Bacteria counts correlated with pH (r = 0.501) and SO₄²⁻ ions (r = 0.500) (p<0.05), and K⁺ ions (r = -0.800) (p<0.01); Total Heterotrophic Fungi correlated with pH (r = 0.520) (p<0.05), and Mg²⁺ ions (r = 0.820) (p<0.01); Hydrocarbon Utilizing Bacteria correlated with available P (r = 0.530) and silt composition (r = -0.504) (p<0.05), and K⁺ (r = 0.626) and Mg²⁺ ions (r = 0.733) (p<0.01); and Hydrocarbon Utilizing Fungi correlated with K⁺ (r = 0.500) & Mg²⁺ ions (r = 0.506) (p<0.05). Results indicate improvement in C/N ratios and effectiveness of the current cost-effective bioaugmentation technique in the restoration of arable soil productivity in the Odhiaje community.

INTRODUCTION

Crude oil drives the bulk of the Gross Domestic Product (GDP) of Nigeria, as the product currently generates the bulk of the country's foreign exchange and serves as an energy source as well as industrial raw materials used in producing several products and services. The extraction process of this natural resource in the environment of the Niger Delta region of the country could be very damaging. As a result, and over the last decade, oil exploration and exploitation have impacted harmfully on the socio-physical environments of oil-bearing communities in the Nigerian Delta, largely threatening their subsistent peasant economy, the environment, livelihood, and hence the basic survival of the people (Eni & Okpiliya 2011).

Incidence of oil spills in the Niger Delta areas have become rampant, and according to Bob-Manuel & Johnson (2001), they are mainly from fractured pipelines due to

corrosion or company operational errors in the environment, as well as from sabotage of pipelines by locals for economic and political reasons. Further, Ebuehi et al. (2005) have identified other minor causes of spills, including the low level of technological know-how, the weakness of our laws and their feeble enforcement, the callousness of multinational enterprises participating in the oil business in the country, and the carelessness of various personnel within and outside the industry.

Oil spills have impacts, and their effects on the environment on the biota are also diverse. Additionally, widespread spillages on soil in rivers, creeks, ponds, and wells in the riverine areas of the country have rendered arable soils and good drinking water scarce, and many victims of the pollution have suffered from diarrhea and dysentery (Albert et al. 2018). Joseph et al. (2021) reported that the impact has severely degraded borehole water samples in a partially remediated oil spill site. Many products from oil spills are

toxic to wildlife, which, when incorporated into the food chain, will also be poisonous to humans. This knowledge has increased scientific interest in studying the distribution, fate, and behavior of oil and its derivatives in the environment (Semple et al. 2006). Fishing and farming, which are the traditional means of livelihood of the people of the oil-producing communities, are adversely affected. According to (Ogbuagu et al. 2019), deaths of fishes, crustaceans, and other aquatic organisms, which form the main sources of animal protein in the areas, have been reported.

Natural attenuation is the monitoring of natural processes in environmental segments that act without human intervention to reduce the mass, toxicity, mobility, volume, or concentration of contaminants (Jorgensen et al. 2011). It could be utilized as a bioremediation method to treat polluted environments, in which case microorganisms will contribute to pollutant degradation without deliberate human interventions. However, where site evaluations need rapid removal of pollutants, enhanced natural attenuation bioremediation, classified into biostimulation (addition of nutrients and chemicals to stimulate innate microorganisms) and bioaugmentation (inoculation with exogenous microorganisms), can be applied. Of the available remediation techniques, the enhanced natural attenuation is the least expensive in environmental management, because the technique could be practiced with little or no expertise and in a natural environment. The problem of oil spillage in the oil-producing areas of Nigeria has proved as challenging as the inability to recover the spill and remediate the impacted environment. In this regard, Mafiana et al. (2021) reported that over 73% of oil spills are unrecovered. Mafiana et al. (2021) identified non-supplemented in-situ remediation as a potentially cost-effective method for mitigating the impact of oil spillage in oil-producing communities and other impacted sites. Ebuehi et al. (2005) had earlier reported that remediation by enhanced natural attenuation (RENA) with spiking and tilling could be used for the reclamation of oil spill-impacted farm settlements in Rivers State, Nigeria. Chikere et al. (2017) reported successful remediation of oil-impacted soil in Bayelsa State, Nigeria, using enhanced natural attenuation with a significant reduction in total petroleum hydrocarbon (TPH) and polyaromatic hydrocarbon (PAH) as well as a spike in hydrocarbon utilizing bacteria (HUB) during remediation.

The current work evaluated the efficiency of the Enhanced Natural Attenuation (ENA) remediation technique on oil-impacted soil of Odhaje communities in Rivers State, Nigeria. The main focus was on key indicator physicochemical and microbiological parameters of the impacted soil over a timeline. The objectives included the assessment of some edaphic variables in contaminated soil

and population dynamics of relevant resident microbiological organisms before, during, and after the remediation exercise.

STUDY AREA

An Overview of the Study Area

Odhaje community is located at latitudes 0532'11" and 0415'60" N and longitudes 0630'32" and 0625'40" E (Fig. 1) and is within the tropical rainforest zone of Nigeria, with much rainfall and thick vegetation. Presently, the vegetation is dwindling due to population growth, persistent farming, and rapid socio-economic development, including but not limited to mineral exploitation. The climate, typical of the tropics, has an average rainfall of 200 mm, mean ambient temperature of 28°C, and relative humidity of between 88 and 98 % (Shell Petroleum Development Company of Nigeria 2002). The wet season lasts between March and November, while the dry season lasts the remaining four months. The soil is mainly of sandy loam, and economic trees such as *Elaeis guineensis* (oil palm) and *Hevea brasiliensis* (rubber) grow well in the area. Annual crops, mainly cassavas and maize, as well as pineapples, okra, and other vegetables, are also grown extensively in farmlands.

Crude oil exploration and exploitation activities are ongoing in the area, and currently, several oil wells and pipelines are traversing the area. An oil spill incident that occurred in June 2018 at Odhieje Community, Ahoada East Local Government Area in Rivers State of Nigeria, resulted in the discharge of large volumes of crude oil into several hectares of adjoining farmlands and forest. The environmental damages inflicted by this spill alone created environmental stress.

MATERIALS AND METHODS

Field Methods and Sampling Locations

The longitudes and latitudes of four sampling points, including a control where the study was conducted, are presented in Table 1. SP 2 was both the northernmost and easternmost sampling point (SP). Sampling was done according to the method of (Iwegbue 2007) at 0-15 and 15-30cm soil depths and samples were collected with a hand-held stainless auger. However, composite samples were collected for post-remediation assessment of the edaphic variables. Quality assurance procedures were strictly adhered to in sample collections and laboratory analyses.

Soil Remediation Exercise

Oil-impacted soil was excavated up to 0.5 m depth, spread, mixed with plants and animal dung, and plowed to promote

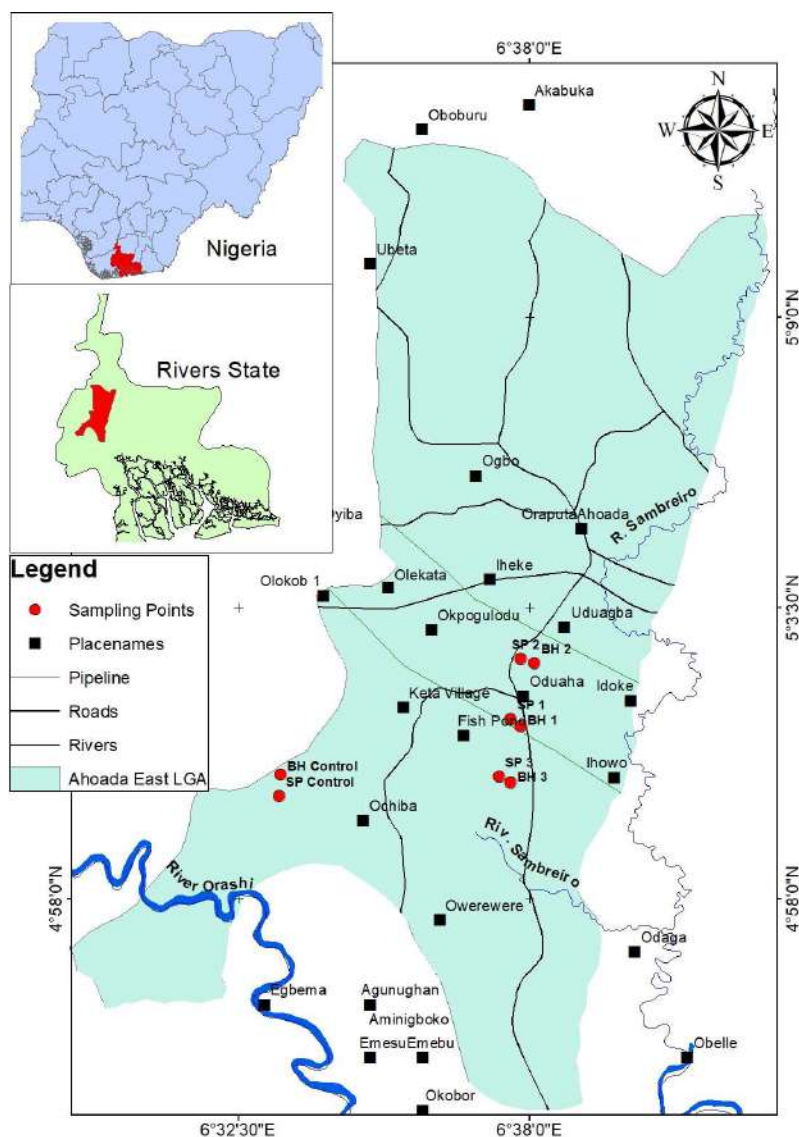


Fig. 1: Map of Odhiaje community and environs in Rivers State, Nigeria, showing the four sampling points (BH 1&SP 1, BH 2&SP 2, BH 3&SP 3, and BH Control/SP Control).

hydrocarbon degradation *in situ*. The procedures of plowing and tilling were done twice with a digger and spade and then homogenized. Composted plants and poultry dung, as well as nitrate-phosphate-potassium (NPK) fertilizer, were added during the homogenization procedure. Ridges (windrows)

were constructed and then leveled severally at alternate times. Soil samples for petroleum hydrocarbons and other edaphic variables assessment were taken before and after a 17-week remediation period.

Laboratory Analyses

This was in keeping with the standard methods of (APHA 2002). THC content was obtained by shaking 10 g of a representative soil sample with 20 mL toluene, and oil was extracted. The extracted oil was determined with absorbance at 420nm wavelength in a Spectronic 21-D spectrophotometer. Concentration was then calculated with reference made to the standard curve that was prepared using

Table 1: Longitudes and latitudes of the sampling locations.

Location	Longitude	Latitude
SP 1	06°37'38.423"E	05°1'22.067"N
SP 2	06°37'50.022"E	05°2'30.607"N
SP 3	06°37'26.824"E	05°0'16.69"N
SP Control	06°33'15.863"E	04°59'57.71"N

a known concentration of hydrocarbons in the extractant. Multiplication was made by the appropriate dilution factor.

To determine the soil pH, Pansu & Gautheyrou (2006) were used. The air-dried soil sample was sieved through a 2 mm sieve, and then 20 g of it was placed in a 50 mL beaker with 40 milliliters of distilled water. A glass rod was used to stir the mixture vigorously and made to stand for 30 min before reading off the pH value on a Corning pH meter (Model 7).

Pansu & Gautheyrou (2006) modified Bougoucos hydrometer method was used to determine textural classifications. A Solution containing sodium carbonate (8 g.L^{-1}) and hexametaphosphate (Calgon 44 g.L^{-1}) were used to disperse the soil samples. The pH of the solution stayed retained at approximately 8.3, and the textural triangular diagram was used to determine the textural classes.

For the exchangeable cations, 1 g sample of soil was put into a digesting tube, followed by an addition of 10 mL conc. HNO_3 . At 96°C , the sample was put in the digester with intermittent stirring for 8 h. When the digestion process was completed, Whatman No. 42 filter papers were used to filter the sample into a 100 mL volumetric flask. The sample was prepared up to the 100 mL mark in the volumetric flask with distilled deionized water. The concentrations of K^+ , Ca^{2+} , Mg^{2+} and Na^+ ions in the supernatant solution were determined using a Varian Spectr-AA 600 Atomic Absorption Spectrophotometer (AAS), with air acetylene flame connected to it.

The sulfate ions presence in the soil sample was confirmed by the monocalcium phosphate extraction method. The soil sample is exposed to the air to become dried and then sieved. 10 g of the dried and sieved sample was put in a 50 mL Erlenmeyer flask. Monocalcium phosphate extracting solution is measured to just 25 mL and added the solution in the Erlenmeyer flask. The solution is shaken for 30 min at a frequency of 200 oscillations per minute. Charcoal measuring 0.25 g was added to each sample, and an extra 3 min of shaking was done. A Whatman No. 42, which is free from sulfate, was used to filter the solution. 10 mL of the filtrate from the extraction process was pipetted and transferred to a 50 mL Erlenmeyer flask. One milliliter of seed was added, and the solution was agitated. Addition of 0.5 g of $\text{BaCl}_2 \cdot 2\text{H}_2\text{O}$ crystals were done, and the solution was put in a steady position for 1 min before a magnetic swirl was used to continuously swirl the flask until the crystals dissolved. HACH DR 2010 UV-visible spectrophotometer at a wavelength of 420 nm was used to read the transmittance at 3-8 min intervals. A linear graph to plot absorbance against the concentration and the absorbance reading was recorded. The concentration of sulfate in 10g of the soil sample was then calculated as:

$$\begin{aligned} \text{MgSO}_4 \text{ - S / kg of soil} &= \frac{\text{mg S/L} \times 0.025\text{L}}{0.010 \text{ kg soil}} = : \\ &= \text{mg S / L} \times 2.5 \end{aligned}$$

For available phosphorus, First, 15 mL of 1M ammonium fluoride and 25 mL of 0.5N HCl were added to 460 mL distilled water to prepare the extracting solution. Then 1g soil sample is air-dried and sieved through a 2mm mesh size. After weighing the dried-up soil sample, it was placed into a centrifuge tube, followed by the addition of extracting solution measuring 7 mL. This mixture stood stirred for 1 minute and then centrifuged. Two milliliters of the clear supernatant were transferred into a 20 mL test tube, and 5 mL of distilled water was added, followed by 2 mL of ammonium solution. 1 mL of chloride solution was added to the mixture. A spectrophotometer at 660 nm wavelength was used to measure the percentage transmittance in 20 min. A standard curve prepared with phosphate in soil standard solution was used in the determination of the amount of available PO_4^{3-} ion in the soil sample.¹¹

The electrical conductivity (EC) of soil samples was determined on the filtrate obtained after filtering the suspension used for pH determination. The Lovibond conductivity meter (Model CM-21 bridge) was used in measuring conductivities in $\mu\text{S.cm}^{-1}$ (Pansu & Gautheyrou 2006).

Total nitrogen was determined by the Macro Kjeldahl method, as described by Pansu & Gautheyrou (2006). A typical soil sample weighing 5 g was shaken with 50 mL of 1N K_2SO_4 . The phenol sulphonic Acid method was employed in determining the nitrogen content using the Aliquot of the resulting extract.

Organic carbon was determined by the wet combustion method of Pansu & Gautheyrou (2006). In duplicate, 2 g of soil sample was put into a 250 mL Erlenmeyer flask after it was weighed. 10 mL of 1N $\text{K}_2\text{Cr}_2\text{O}_7$ solution was added into the flask and swirled gently for the soil to be dispersed. An automatic pipette was used to make a rapid addition of 20 mL conc. H_2SO_4 , directing the stream into the suspension. Instantaneously, the flask was shaken gently, make soil and reagents were mixed. After which it was shaken vigorously for 1 minute. The flask was then made to stand for 30 min on a sheet of asbestos. When thirty min had elapsed, 100 mL of distilled water was added. The addition of Four drops of o-phenanthroline-ferrous indicator and titration with 0.5N ferrous sulfate solution was carried out. The approach to the end-point of titration was marked by the solution changing from a greenish cast to a dark green color. At this point, the ferrous sulfate was added drop-wise until the color changed sharply from blue to red (maroon color) in reflected light against a white background. A blank titration was also made devoid

of soil samples to homogenize the dichromate. The result was computed and organic carbon was expressed in percentage.

Microbial Analysis

Soil samples were air-dried, ground, and sieved through a 2mm mesh size sieve. The oil-contaminated soil samples were serially diluted in ten folds, according to the methods of (Vallabhaneni 2012). Each sample of previously air-dried soil was vigorously shaken in 10 mL of sterile water to prepare a soil suspension. The soil suspension was put into the test tubes, and then, ten-fold serial dilution was done up to 10^{-5} .

In triplicate and from the dilution of 10^{-3} and 10^{-4} of each soil sample, 0.1mL aliquot was aseptically placed against Nutrient (NA) and Sabouraud Dextrose Agar (SDA) plates in clean form by pour plate methods of Brenner et al. (2005) and the spread plates methods of (Vallabhaneni 2012). Incubation of inoculated plates was done at 37°C Centigrade for a duration of 18 to 24 h at ambient temperatures of 48 to 72 h for the details of total heterotrophic bacterial (THB) and fungal (THF) counts, respectively. Colonies that are distinct in incubated plates were counted and then expressed as colony-forming units per gram (cfu.g^{-1}) of the sampled soil.

The Hydrocarbon-Utilizing Bacteria (HUB) and Fungi (HUF) were cultured and enumerated on solid oil agar.

Statistical Analyses

The data analysis was carried out using SPSS v.23.0 and MS Excel 2020 software. Descriptive statistics and plots were employed to express variations in hydrocarbons and soil parameters. To determine variations in concentrations of hydrocarbons and other soil parameters across the locations at $p < 0.05$, The one-way ANOVA test was employed, and mean separation was done with the Duncan Multiple Range test. To explore possible relationships between the

Soil variables and the microbial community in the soil, the Pearson correlation coefficient (r) was utilized.

RESULTS AND DISCUSSION

Edaphic Variability and Oil Spill Remediation

Mean pH changed from 6.0 ± 0.1 , 5.4 ± 0.2 , 4.7 ± 0.01 and 5.7 ± 0.1 before remediation to 5.0 ± 0.1 , 5.5 ± 0.1 , 5.1 ± 0.01 and 5.2 ± 0.1 after remediation at SP 1, SP2, SP3 and the control (Table 2). Electrical conductivity generally increased from 53 ± 2.5 , 54.5 ± 4.0 , 28 ± 2.0 and 33 ± 4.0 at SP1, SP2, SP3 and control point, respectively, before remediation to 85 ± 2.0 , 90 ± 3.5 , 88 ± 2.0 and 86 ± 5.4 $\mu\text{S.cm}^{-1}$ after remediation. Carbon-Nitrogen (C/N) ratios also varied from 16.5 ± 1.6 , 37.5 ± 0.3 , 66.0 ± 2.5 and 9.0 ± 3.0 at SP1, SP2, SP3 and control point respectively before remediation to 26.0 ± 1.1 , 37.5 ± 0.3 , 28.25 ± 2.3 and 60.0 ± 2.7 after remediation.

THC had decreased from 351.77 ± 97.5 before remediation to 161.40 ± 60.5 mg.kg^{-1} after remediation at SP 1; from 5035.30 ± 61.8 before remediation to 2587.30 ± 55.1 mg.kg^{-1} after remediation at SP 2; from 2990.70 ± 37.8 before remediation to 497.40 ± 21.5 mg.kg^{-1} after remediation at SP 3 and from 65.96 ± 9.9 to 67.50 ± 5.5 mg.kg^{-1} at the control point (Table 2). Available phosphorus contents decreased from 13.1 ± 8.2 before remediation to 12.52 ± 3.4 $\mu\text{g.g}^{-1}$ after remediation at SP 1; from 33.95 ± 1.35 before remediation to 10.70 ± 1.1 $\mu\text{g.g}^{-1}$ after remediation at SP 2; from 38.85 7.3 before remediation to 7.5 ± 3.4 $\mu\text{g.g}^{-1}$ after remediation at SP 3 and from 15.80 ± 1.7 before remediation to 11.25 ± 1.0 $\mu\text{g.g}^{-1}$ after remediation at SP Control. Potassium concentration at SP 1, SP 2, SP 3, and the control point decreased from $64.1 \pm 1.3 \pm 71.8$, 7.7 ± 75.6 , 14.1 and 1.3 ± 59.0 $\mu\text{g.g}^{-1}$, respectively, before remediation to 2.51 ± 6.7 , 1.79 ± 4.5 , 1.42 ± 1.0 and 0.87 ± 0.2 $\mu\text{g.g}^{-1}$ respectively after remediation.

Organic carbon content decreased from 3.22 ± 1.24 and $3.62 \pm 0.23\%$ at SP 2 and SP 3, respectively, before

Table 2: Summary of physico-chemical characteristics of impacted soil before and after remediation.

Sample ID	Before Remediation					After Remediation						
	pH	EC [$\mu\text{S.cm}^{-1}$]	THC [mg.kg^{-1}]	Organic C [%]	C/N Ratio	pH	EC [$\mu\text{S.cm}^{-1}$]	THC [mg.kg^{-1}]	Organic C [%]	C/N Ratio		
SP1	5.95	53	351.8	0.97	16.5	5	85	161.4	1.56	26		
SP2	5.4	54.5	5035.3	3.215	63.5	5.5	90	2587.3	1.5	37.5		
SP3	4.7	28	2990.7	3.615	66	5.1	88	497.4	1.13	28.25		
Control	5.7	33	66.0	0.545	9	5.2	86	67.5	1.2	60		
Sample ID	Before Remediation						After Remediation					
	Av. P [$\mu\text{g.g}^{-1}$]	SO_4^{2-} [$\mu\text{g.g}^{-1}$]	K^+ [mg.kg^{-1}]	Na^+ [mg.kg^{-1}]	Ca^{2+} [mg.kg^{-1}]	Mg^{2+} [mg.kg^{-1}]	Av. P [$\mu\text{g.g}^{-1}$]	SO_4^{2-} [$\mu\text{g.g}^{-1}$]	K^+ [mg.kg^{-1}]	Na^+ [mg.kg^{-1}]	Ca^{2+} [mg.kg^{-1}]	Mg^{2+} [mg.kg^{-1}]
SP1	13.1	8.45	64.1	0.75	1.75	1.15	12.52	9	2.51	1.09	1.1	0.3
SP2	33.95	3.3	75.6	1.2	0.75	2.5	10.7	4	1.79	1.08	1.4	0.5
SP3	38.85	5	71.8	0.9	1.15	3.4	7.5	6	1.42	1.13	1.3	0.2
Control	15.8	6.2	59	0.85	0.9	2.05	11.25	5	0.87	1.17	0.8	0.5

remediation to 1.50 ± 1.0 and $1.13\pm 0.1\%$ respectively after remediation, but increased from 0.97 ± 0.22 and $0.55\pm 0.2\%$ at SP 1 and the control point respectively before remediation to 1.56 and $1.2\pm 0.05\%$ respectively after remediation. Sulfate ion concentrations increased from 8.45 ± 0.4 , 3.3 ± 0.3 and $1.0\pm 0.3 \mu\text{g.g}^{-1}$ at SP 1, SP 2, and SP 3, respectively, before remediation to 9.0 ± 0.1 , 4.0 ± 0.1 , $6.0\pm 0.1 \mu\text{g.g}^{-1}$ after remediation. Still, they decreased from 6.2 ± 0.2 before remediation to 5.0 ± 0.1 after remediation at the control point. Magnesium ions decreased from 1.15 ± 0.2 , 2.5 ± 0.1 , 3.3 ± 0.2 and $2.05\pm 0.1 \text{mg.kg}^{-1}$ at SP 1, SP 2, Sp 3, and the control point, respectively, before remediation to 0.3 ± 0.1 , 0.5 ± 0.1 , 0.2 ± 0.1 and 0.5 ± 0.1 respectively after remediation. Total Nitrogen remained fairly unchanged at SP 1 ($0.06\pm 0.001\%$) but decreased from 0.05 ± 0.001 , 0.06 ± 0.001 , $0.06\pm 0.001\%$ at SP 2, SP 3 and the control point, respectively, before remediation to 0.04 ± 0.001 , 0.04 ± 0.001 and 0.02 ± 0.001 respectively after remediation. Sodium concentration increased from 0.08 ± 0.01 , 1.2 ± 0.01 , 0.9 ± 0.02 and $0.9\pm 0.01 \text{mg.kg}^{-1}$ at SP 1, SP 2, SP 3, and the control point, respectively,

to 1.09 , 1.08 ± 0.03 , 1.13 ± 0.001 and $1.17\pm 0.01 \text{mg.kg}^{-1}$. Calcium ions had increased from 0.8 ± 0.02 and $1.2\pm 0.05 \text{mg.kg}^{-1}$ at SP 2 and SP 3, respectively, before remediation to 1.4 ± 0.001 and $1.3\pm 0.02 \text{mg.kg}^{-1}$ after remediation. Still, they decreased from 1.8 ± 0.3 and 1.8 ± 0.02 at SP 1 and the control point, respectively, before remediation to 1.1 ± 0.1 and $0.8\pm 0.001 \text{mg.kg}^{-1}$, respectively, after remediation (Fig. 2).

Of the textural classes, the composition of sand increased very slightly from 49 ± 2 to 51 ± 2 at SP 2. From 64 ± 0.5 to $65\pm 0.2\%$ at SP Control before and after remediation (Fig. 3). However, it decreased from 60 ± 1.5 to $47\pm 1.0\%$ at SP 1 and 74 ± 1.3 to $63\pm 1.0\%$ at SP 3 before and after remediation respectively. Silt composition increased from 17 ± 1.0 to $34\pm 1.0\%$ at SP 1, 0.5 ± 9 to 0.2 ± 26 at SP 3, and 14 ± 0.4 to $28\pm 0.1\%$ at the control point before and after remediation. Clay composition decreased from 23 ± 1.0 to 19 ± 1.0 at SP 1, 25 ± 1.2 to 23 ± 1.0 at SP 2, 17 ± 0.5 to 11 ± 0.2 at SP 3, and 22 ± 0.3 to $7\pm 0.1\%$ at the control point before and after remediation respectively.

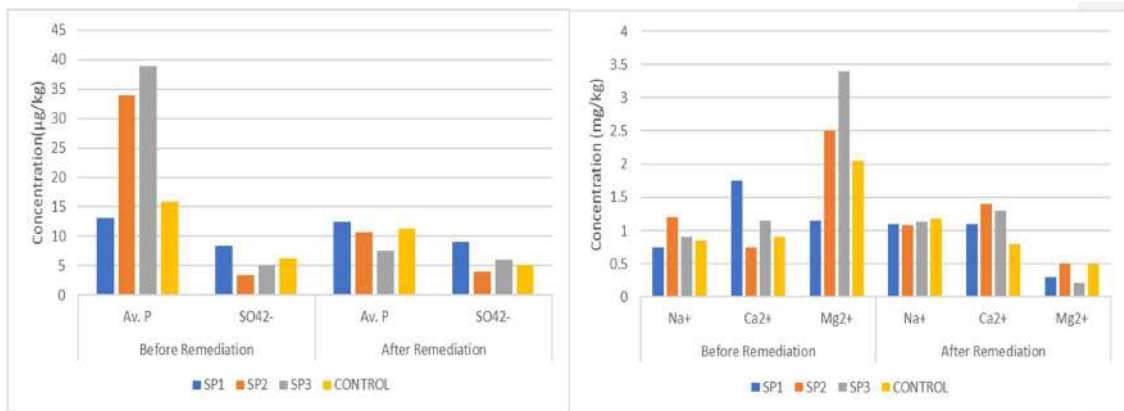


Fig. 2: Attenuation of physico-chemical parameters due to remediation.

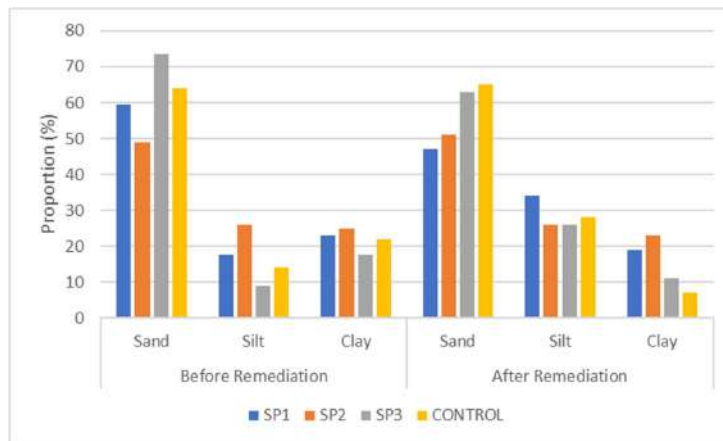


Fig. 3: Variations in soil characteristics before and after remediation.

The One-way ANOVA test revealed that the concentrations of THC (Sig._{value} = 0.009), SO₄²⁻ ions (Sig._{value} = 0.001), and sand compositions (Sig._{value} = 0.045) all differed markedly across the sampling points at p<0.05. A post-hoc mean separation technique with the Duncan Multiple Range test (Table 2) revealed that the observed difference in THCs was between SP 1 = SP Control and SP 2; that in SO₄²⁻ ions was between SP 1 and the rest sampling points, while that in Sand composition was between SP 2 and SP 3. Using the Student's t-test to carry out a pairwise comparison in concentrations of the soil variables showed that mean levels of EC (Sig.tvalue=0.039) and ΣN (Sig.tvalue = 0.058) & K⁺ ions (Sig.tvalue = 0.004) differed significantly before and after the remediation exercise at the 95% confidence interval.

Variations in Microbial Population

The counts of microorganism groups in oil-impacted soil during the 17-week remediation exercise are shown in Tables 4 - 7. For the Total Heterotrophic Bacteria (THB) counts (Table 4), the population of the microorganisms increased in SP 1 from 5.3 × 10⁵ at the commencement of the remediation exercise to 4.0 × 10⁷ cfu.g⁻¹ in week 9. Then, it decreased to 3.5 × 10⁵ cfu.g⁻¹ at the end of the exercise. At SP 2, microorganism counts increased from 6.8 × 10⁶ at

Table 3: Mean separation in edaphic variables impacted by the oil spill in Odhijae community by Duncan Multiple Range (DMR) Test (p<0.05).

Sampling points				
Parameters	SP 1	SP 2	SP 3	SP Control
pH	5.633 ^a	5.433 ^a	4.833 ^a	5.533 ^a
EC	63.666 ^a	66.333 ^a	48.000 ^a	50.666 ^a
THC	288.310 ^a	4219.296 ^b	2159.600 ^{ab}	66.73 ^a
Organic C	1.166 ^a	2.643 ^a	2.786 ^a	0.763 ^a
ΣN	0.060 ^a	0.046 ^a	0.050 ^a	0.046 ^a
C/N ratio	19.666 ^a	54.833 ^a	53.416 ^a	26.000 ^a
Av. P	12.906 ^a	26.200 ^a	28.400 ^a	14.283 ^a
SO ₄ ²⁻	8.633 ^c	3.533 ^a	5.333 ^b	5.800 ^b
K ⁺	43.570 ^a	50.996 ^a	48.340 ^a	39.623 ^a
Na ⁺	0.863 ^a	1.160 ^a	0.976 ^a	0.956 ^a
Ca ²⁺	1.533 ^a	0.966 ^a	1.200 ^a	0.866 ^a
Mg ²⁺	0.866 ^a	1.833 ^a	2.333 ^a	1.530 ^a
Sand	55.333 ^{ab}	49.666 ^a	70.000 ^b	64.333 ^{ab}
Silt	23.000 ^a	26.000 ^a	14.656 ^a	8.666 ^a
Clay	21.666 ^a	24.333 ^a	15.333 ^a	17.000 ^a

Values with the same superscript along the same row are not significantly different at

p<0.05; EC=Electrical conductivity; THC=Total Petroleum Hydrocarbons;

Av. P=Available phosphorus

the commencement of the exercise to 3.1 × 10⁸ cfu.g⁻¹ in week 10 and then decreased to 4.4 × 10⁶ cfu.g⁻¹ at the end.

At SP 3, THB increased from 4.4 × 10⁶ to 2.5 × 10⁸ cfu.g⁻¹ in week 11 and then decreased to 4.1 × 10⁶ cfu.g⁻¹ at the end (Table 4). However, at the control location, microbial populations increased from 4.9 × 10⁶ to 3.5 × 10⁷ cfu.g⁻¹ in week 8 and then decreased to 4.8 × 10⁶ cfu.g⁻¹ at the end of the exercise.

Table 5 shows that the Total Heterotrophic Fungi (THF) counts in the impacted site increased at SP 1 from 7.4 × 10³ to 6.8 × 10⁵ cfu.g⁻¹ in week 10 and then decreased to 2.3 × 10³ cfu.g⁻¹ at the end of the exercise. THF counts also increased at SP 2 from 6.3 × 10³ to 4.5 × 10⁵ cfu.g⁻¹ in week 12 and then decreased to 2.5 × 10³ cfu.g⁻¹ at the end. They increased at SP 3 from 6.4 × 10³ to 5.5 × 10⁵ cfu.g⁻¹ in week 5 and then decreased to 2.5 × 10³ cfu.g⁻¹ at the end of the exercise. At the control location, THF counts increased from 4.5 × 10³ to 3.7 × 10⁴ in week 5 and then decreased to 4.2 × 10³ at the end of the exercise.

The Hydrocarbon-Utilizing Bacteria (HUB) counts increased from 9.9 × 10⁴ to 8.8 × 10⁵ cfu.g⁻¹ in week 10 and decreased to 9.3 × 10³ cfu.g⁻¹ at the end of the exercise in SP 1 (Table 6). At SP 2, it increased from 1.2 × 10⁶ to 1.3 × 10⁸ cfu.g⁻¹ in week 11 and then decreased to 1.9 × 10⁴ cfu.g⁻¹ at the end. They increased from 9.9 × 10⁵ to 7.6 × 10⁷ cfu.g⁻¹ in week 10 and then decreased to 7.4 × 10³ cfu.g⁻¹ at the end of SP 3. HUB counts at the control sampling point also increased from 6.5 × 10³ to 6.1 × 10⁴ cfu.g⁻¹ in week 6 and then decreased to 6.7 × 10³ at the end of the remediation exercise.

Table 7 shows that the Hydrocarbon-Utilizing Fungi (HUF) counts increased from 9.1 × 10² to 8.4 × 10⁴ cfu.g⁻¹ in week 9 and then decreased to 2.1 × 10² cfu.g⁻¹ at the end of the exercise at SP 1. At SP 2, HUF counts increased from 1.1 × 10³ to 1.8 × 10⁴ cfu.g⁻¹ in week 11 and then decreased to 3.0 × 10² cfu.g⁻¹ at the end. At SP 3, counts increased from 9.7 × 10² at the commencement of the experiment to 8.0 × 10⁴ cfu.g⁻¹ in week 11 and then decreased to 2.4 × 10² cfu.g⁻¹ at the end. At the SP Control location, counts increased from 1.1 × 10² to 1.0 × 10³ cfu.g⁻¹ in week 10 and then decreased to 1.1 × 10² cfu.g⁻¹ at the end of the remediation exercise.

Relationships Between Edaphic Variables and Microbial Community in Impacted Soils

Table 8 shows the Pearson's correlation coefficients (r) between the edaphic variables and microbial communities in impacted soils during the remediation period. At p<0.05, THB counts correlated positively with pH (r = 0.501) and sulfate ions (r = 0.500). At p<0.01, it correlated negatively with electrical conductivity (EC) (r = -0.701) and K⁺ ions (r = -0.800). At p<0.05, THF counts correlated positively

Table 4: Total Heterotrophic Bacteria (THB) counts (cfu.g⁻¹) in impacted soils of Odihaaje community during the remediation period.

Sampling Points	Time (Weeks)																
	Wk 1	Wk 2	Wk 3	Wk 4	Wk 5	Wk 6	Wk 7	Wk 8	Wk 9	Wk 10	Wk 11	Wk 12	Wk 13	Wk 14	Wk 15	Wk 16	Wk 17
SP 1	5.3 × 10 ⁵	5.1 × 10 ⁵	5.3 × 10 ⁵	4.5 × 10 ⁶	4.1 × 10 ⁶	4.4 × 10 ⁶	3.1 × 10 ⁷	3.7 × 10 ⁷	4.0 × 10 ⁷	4.8 × 10 ⁶	3.2 × 10 ⁷	3.1 × 10 ⁷	4.5 × 10 ⁶	4.7 × 10 ⁶	4.5 × 10 ⁶	4.8 × 10 ⁵	3.5 × 10 ⁵
SP 2	6.8 × 10 ⁶	6.2 × 10 ⁶	5.0 × 10 ⁷	5.5 × 10 ⁷	6.0 × 10 ⁶	4.1 × 10 ⁷	4.3 × 10 ⁷	4.0 × 10 ⁷	3.0 × 10 ⁸	3.1 × 10 ⁸	6.7 × 10 ⁷	6.4 × 10 ⁷	6.0 × 10 ⁷	5.8 × 10 ⁶	4.8 × 10 ⁶	4.5 × 10 ⁶	4.4 × 10 ⁶
SP 3	4.4 × 10 ⁶	4.4 × 10 ⁶	4.8 × 10 ⁶	3.5 × 10 ⁷	3.0 × 10 ⁷	4.0 × 10 ⁶	3.1 × 10 ⁷	2.5 × 10 ⁸	2.2 × 10 ⁸	2.1 × 10 ⁸	2.5 × 10 ⁸	3.8 × 10 ⁷	4.9 × 10 ⁶	3.0 × 10 ⁷	4.1 × 10 ⁶	4.6 × 10 ⁶	4.1 × 10 ⁶
SP Control	4.9 × 10 ⁶	4.8 × 10 ⁶	4.1 × 10 ⁶	5.1 × 10 ⁶	4.8 × 10 ⁶	4.3 × 10 ⁶	3.1 × 10 ⁷	3.5 × 10 ⁷	5.0 × 10 ⁶	5.1 × 10 ⁶	3.0 × 10 ⁷	4.1 × 10 ⁶	3.1 × 10 ⁷	4.4 × 10 ⁶	4.4 × 10 ⁶	4.1 × 10 ⁶	4.8 × 10 ⁶

Table 5: Total Heterotrophic Fungi (THF) counts (cfu.g⁻¹) in impacted soils of Odihaaje community during the remediation period.

Sampling Points	Time (Weeks)																
	Wk 1	Wk 2	Wk 3	Wk 4	Wk 5	Wk 6	Wk 7	Wk 8	Wk 9	Wk 10	Wk 11	Wk 12	Wk 13	Wk 14	Wk 15	Wk 16	Wk 17
SP 1	7.4 × 10 ³	7.1 × 10 ³	7.2 × 10 ³	6.5 × 10 ⁴	6.1 × 10 ⁴	6.3 × 10 ⁴	6.1 × 10 ⁴	7.0 × 10 ⁴	7.1 × 10 ⁴	6.8 × 10 ⁵	6.0 × 10 ⁵	7.0 × 10 ⁴	6.8 × 10 ⁴	7.0 × 10 ³	4.8 × 10 ³	4.5 × 10 ³	2.3 × 10 ³
SP 2	6.3 × 10 ³	6.4 × 10 ³	7.9 × 10 ²	7.0 × 10 ²	6.8 × 10 ³	6.5 × 10 ³	6.4 × 10 ³	6.1 × 10 ³	5.5 × 10 ⁴	5.2 × 10 ⁴	5.5 × 10 ⁴	4.5 × 10 ⁵	4.1 × 10 ⁵	5.1 × 10 ⁴	6.8 × 10 ³	4.0 × 10 ³	2.5 × 10 ³
SP 3	6.4 × 10 ³	6.4 × 10 ³	6.1 × 10 ⁴	6.5 × 10 ⁴	5.5 × 10 ⁵	5.1 × 10 ⁵	4.8 × 10 ⁵	4.8 × 10 ⁵	4.7 × 10 ⁵	5.5 × 10 ⁴	5.1 × 10 ⁴	5.2 × 10 ⁴	5.6 × 10 ⁴	6.0 × 10 ³	4.1 × 10 ³	2.6 × 10 ³	2.5 × 10 ³
SP Control	4.5 × 10 ³	4.1 × 10 ³	4.0 × 10 ³	4.5 × 10 ³	3.7 × 10 ⁴	4.1 × 10 ³	4.1 × 10 ³	4.0 × 10 ³	4.7 × 10 ³	4.5 × 10 ³	4.1 × 10 ³	4.1 × 10 ³	3.5 × 10 ⁴	4.4 × 10 ³	4.1 × 10 ³	4.0 × 10 ³	4.2 × 10 ³

Table 6: Hydrocarbon Utilizing Bacteria (HUB) counts (cfu.g⁻¹) in impacted soils of Odihaaje community during the remediation period.

Sampling Points	Time (Weeks)																
	Wk 1	Wk 2	Wk 3	Wk 4	Wk 5	Wk 6	Wk 7	Wk 8	Wk 9	Wk 10	Wk 11	Wk 12	Wk 13	Wk 14	Wk 15	Wk 16	Wk 17
SP 1	9.9 × 10 ⁴	9.7 × 10 ⁴	9.7 × 10 ⁴	8.5 × 10 ⁵	8.2 × 10 ⁵	8.4 × 10 ⁵	8.1 × 10 ⁵	8.8 × 10 ⁴	8.4 × 10 ⁵	8.8 × 10 ⁵	8.0 × 10 ⁵	8.2 × 10 ⁵	7.5 × 10 ⁴	7.6 × 10 ⁴	8.7 × 10 ³	8.8 × 10 ³	9.3 × 10 ³
SP 2	1.2 × 10 ⁶	1.3 × 10 ⁶	1.7 × 10 ⁶	1.1 × 10 ⁷	1.3 × 10 ⁷	1.4 × 10 ⁷	1.1 × 10 ⁷	1.0 × 10 ⁸	1.1 × 10 ⁸	1.0 × 10 ⁸	1.3 × 10 ⁸	1.1 × 10 ⁸	1.7 × 10 ⁷	1.9 × 10 ⁶	1.8 × 10 ⁵	1.5 × 10 ⁴	1.9 × 10 ⁴
SP 3	9.9 × 10 ⁵	9.5 × 10 ⁵	9.8 × 10 ⁵	8.4 × 10 ⁶	8.3 × 10 ⁶	8.1 × 10 ⁶	7.2 × 10 ⁷	7.0 × 10 ⁷	7.3 × 10 ⁷	7.6 × 10 ⁷	7.1 × 10 ⁷	8.0 × 10 ⁶	8.5 × 10 ⁶	9.4 × 10 ⁵	9.7 × 10 ⁴	9.1 × 10 ³	7.4 × 10 ³
SP Control	6.5 × 10 ³	6.6 × 10 ³	6.7 × 10 ³	7.1 × 10 ³	7.0 × 10 ³	6.1 × 10 ⁴	6.0 × 10 ⁴	7.8 × 10 ³	7.8 × 10 ³	7.4 × 10 ³	7.3 × 10 ³	7.1 × 10 ³	7.5 × 10 ³	7.0 × 10 ³	6.8 × 10 ³	6.7 × 10 ³	6.7 × 10 ³

Table 7: Hydrocarbon Utilizing Fungi (HUF) counts (cfu.g⁻¹) in impacted soils of Odhrijae community during the remediation period.

Sampling Points	Time (Weeks)																
	Wk 1	Wk 2	Wk 3	Wk 4	Wk 5	Wk 6	Wk 7	Wk 8	Wk 9	Wk 10	Wk 11	Wk 12	Wk 13	Wk 14	Wk 15	Wk 16	Wk 17
SP 1	9.1 × 10 ²	9.3 × 10 ²	9.1 × 10 ²	9.5 × 10 ²	8.7 × 10 ³	8.5 × 10 ³	8.1 × 10 ³	8.5 × 10 ³	8.4 × 10 ⁴	8.1 × 10 ⁴	8.0 × 10 ⁴	8.1 × 10 ³	8.5 × 10 ³	8.7 × 10 ²	5.5 × 10 ²	3.7 × 10 ²	2.1 × 10 ²
SP 2	1.1 × 10 ³	1.2 × 10 ³	1.2 × 10 ³	1.6 × 10 ³	1.7 × 10 ³	2.0 × 10 ³	1.5 × 10 ⁴	1.4 × 10 ⁴	1.5 × 10 ⁴	1.5 × 10 ⁴	1.8 × 10 ⁴	1.6 × 10 ⁴	1.8 × 10 ³	1.5 × 10 ³	3.4 × 10 ²	3.1 × 10 ²	3.0 × 10 ²
SP 3	9.7 × 10 ²	9.5 × 10 ²	8.8 × 10 ³	8.7 × 10 ³	8.5 × 10 ³	8.6 × 10 ³	8.1 × 10 ³	7.5 × 10 ⁴	7.1 × 10 ⁴	7.5 × 10 ⁴	8.0 × 10 ⁴	7.8 × 10 ³	7.3 × 10 ³	4.7 × 10 ²	5.1 × 10 ²	4.5 × 10 ²	2.4 × 10 ²
SP Control	1.1 × 10 ²	1.0 × 10 ²	1.7 × 10 ²	1.2 × 10 ²	1.4 × 10 ²	1.2 × 10 ²	1.8 × 10 ²	1.5 × 10 ²	1.8 × 10 ²	1.0 × 10 ³	1.0 × 10 ³	1.5 × 10 ²	1.2 × 10 ²	1.7 × 10 ²	1.4 × 10 ²	1.7 × 10 ²	1.1 × 10 ²

Table 8: Correlation (r) matrix between the edaphic variables and Microbial groups in oil-impacted soils of the Odhrijae community.

Parameters	pH	EC	THC	THC	Org.C	ΣN	C/N	Av.P	SO ₄ ²⁻	K ⁺	Na ⁺	Ca ²⁺	Mg ²⁺	Sand	Silt	Clay
THB	0.501*	-0.701**	-0.111	-0.174	0.200	-0.270	0.500*	0.024	0.500*	-0.800**	0.123	0.027	0.151	0.072	-0.218	0.283
THF	0.520*	-0.280	-0.134	-0.259	-0.050	-0.267	-0.173	-0.186	-0.173	0.067	-0.053	-0.032	0.820**	0.081	-0.157	0.133
HUB	-0.131	-0.707**	0.436	0.336	0.153	0.349	-0.390	0.530*	-0.390	0.626**	-0.243	-0.429	0.733**	0.347	-0.504*	0.226
HUF	-0.193	-0.538*	0.233	0.254	0.137	0.232	-0.050	0.456	-0.050	0.500*	-0.086	-0.249	0.506*	0.221	-0.324	0.150

*values are significant at p<0.05; **values are significant at p<0.01; THB=Total Heterotrophic Bacteria; THF=Total Heterotrophic Fungi; HUB=Hydrocarbon-Utilizing Bacteria; HUF=Hydrocarbon-Utilizing Fungi; EC=Electrical conductivity; THC=Total Petroleum Hydrocarbons; Org.C=Organic Carbon; C/N=Carbon/Nitrogen ratio; Av.P=Available

with pH (r=0.520), and at p<0.01, they correlated positively with Mg²⁺ ions (r = 0.820). At p<0.05, HUB counts correlated positively with available phosphorus (r = 0.530) and negatively with the composition of silt (r = -0.504). However, at p<0.01, it correlated positively with K⁺ (r = 0.626) and Mg²⁺ ions (r = 0.733) and negatively with EC (r = -0.707). At p<0.05, HUF correlated positively with K⁺ ions (r = 0.500) and Mg²⁺ ions (r = 0.506) and negatively with EC (r = -0.538).

Effect of Remediation on Soil Physicochemical Properties

The current work revealed high concentrations of petroleum hydrocarbons in soil and drastic decreases after remediation, similar to the work of Mafiana et al. (2021) and Chikere (2017) in the Niger Delta area of Nigeria. Soil-oil contaminant generally decreased by up to 50.41% at SP 2 after the 17-week remediation exercise. (Liu et al. 2010) also observed total petroleum hydrocarbon content reduction by 58.2% in treated plots after bioremediation for 360 days. The current work also revealed corresponding and appreciable improvement in the carbon-nitrogen ratio of soil, which got progressively lowered as the remediation proceeded and with the decay and release of more organic nitrogen in the soils. Essien and John (2010) also observed a similar trend in their work in Akwa Ibom State, Nigeria, carried out on the alluvial soils of the coastal plains of the Qua Iboe river wetlands.

By nature, organic carbon in soil is normally derived from flora and fauna, such as peat formation over time, plant fine roots yield, and microbial renewable organic materials from plants, animals, and others (Wang et al. 2013). However, the total organic carbon in the soil might be from crude oil contamination in the oilfield soils. The high concentration of THC in the oil-impacted soil might have resulted in the elevated total organic carbon content recorded. Wang et al. (2010) reported that a significant increase in the total organic carbon contents due to oil contamination is most likely because of the much higher THC concentration in spilled sites.

On a spatial basis, the current work reveals both slight increases and decreases in the pH of soil after the remediation exercise. Previous results from studies on oilfields in China also revealed an increase in soil pH as a result of oil pollution (Wang et al. 2010, Jia et al. 2009). The reason for the higher pH values in crude oil-contaminated soil in this study may be due to two factors: firstly, the hydrophobic nature of crude oil might encourage a potential scarcity in the shallow and underground layers of contaminated soil (Njoku et al. 2009), which could intensify the concentration of salt in the soil, and thereby raising the pH values when matched with the values in the control location. Secondly, the buildup of

exchangeable ions such as Calcium and sodium ions and a decrease in the exchangeable amount of acid and real cation exchange capacity have been revealed to be associated with oil-polluted soil (Osuji et al. 2006, Agbogidi et al. 2007). These mechanisms might also be responsible for the increases in pH values in oil-polluted soil. However, the mechanisms may not have operated in locations where decreases in pH were recorded in the current work.

The levels of petroleum hydrocarbons, SO_4^{2-} ions, and sand composition all differed significantly on a spatial basis. Edaphic properties that showed significant increases in their concentrations after remediation include electrical conductivity, total nitrogen, and K^+ ions. These all contributed to improved soil quality in the area. However, results of a previous study (Wang et al. 2010) showed that oil contamination could decrease available phosphorus concentration in soil by various degrees. A study carried out on the Momoge wetlands of China (Wang et al. 2010) showed a decrease in the concentration of available phosphorus as the time of oil exploration and production increased. Similar decreases were, however, observed in the current work only after remediation. In another experimental oil study, the available phosphorus in crude oil-polluted soil was reduced to as much as 66% in concentration in comparison with the control site as the crude oil content touched 30 mg.kg^{-1} (Eneje et al. 2012). However, Liu et al. (2010) reported that available phosphorus concentrations are not considerably influenced by oil contamination.

From the extant study, lowered available phosphorus concentrations after remediation in all the impacted locations may have been enhanced for two reasons. First, THC in the soil could increase the carbon concentration. This may disturb the balance of soil nutrients. Soil microbes that utilize THC as a carbon source may well consume considerable amounts of available phosphorus when the hydrocarbons are degraded (Wang et al. 2013). Second, phosphorus solubility of phosphorus is exploited at pH near the neutral value, and higher pH values in some locations of the work may have also lowered the available phosphorus concentration when compared with that obtained in the control location. Phosphorus is an important macro-nutrient for plants and soil microorganisms. Decreased available phosphorus concentrations in impacted locations could alter the structural composition of vegetation and microorganisms in the soil, as well as reduce soil ecosystem services and values (Bello & Anobeme 2015).

Effects of Remediation on Microbial Populations

The endpoint and achievement of the oil spill and its bioremediation are dependent on the capability to start and

preserve conditions that help enhance oil biodegradation rates in the contaminated environment. Scientific review that discussed various factors that affect the rate of oil biodegradation, including that by (Das & Chandran 2011), showed that the presence of microorganisms with suitable metabolic capabilities is an important requirement. Optimal rates of growth and biodegradation of hydrocarbon occur when these microorganisms exist. This process can be sustained if the pH is between 6 and 9 and the concentrations of nutrients and oxygen are sufficient. The physicochemical characteristics of the oil and the oil surface area are also vital factors of successful bioremediation. There are two basic approaches to oil spill bioremediation. The first, which was applied in the current study, is bioaugmentation, in which known oil-degrading bacteria are added to supplement the existing microbial population. The second is biostimulation, in which the addition of nutrients or other growth-limiting co-substrates stimulates the growth of indigenous oil degraders. Microbial counts in oil-impacted soils did not show appreciable change over weeks 1-3. Still, they did after week 3 when nutrients, consisting of composted plants and animal dung, as well as nitrate-phosphate-potassium (NPK) fertilizers, were introduced. Generally, counts peaked between weeks 6 and 14 and were least in week 17, marking the end of the remediation exercise in all the sampling points. The hydrocarbon-utilizing bacteria (HUB) counts peaked in week 10, and at week 17, all the microbial communities attained counts comparable to those of their respective control locations.

These exponential increases in microbial population are due to stimulatory effects by the composted plants and animal dungs, as well as NPK fertilizer introduced on the impacted soils. This effect has been explained to be due to the proliferation of microbes in soil, especially in the presence of growth nutrients (Semple et al. 2006, Hollender et al. 2003, Walworth et al. 2007). Findings by Ogbonna et al. (2007) revealed that there is a more rapid bioremediation of crude oil-contaminated soils with a combination of microorganisms, poultry manure, and fertilizers other than microorganisms or fertilizers alone. Selective enrichment of the soil with microbial species that have tolerance for extremely high oil concentrations could spontaneously be caused by the high oil content.

The soil became selectively enriched with very high oil concentration tolerant microbial species due to the excessive petroleum hydrocarbon content of the polluted area.

The general increases recorded in the various microbial community counts also confirm that hydrocarbon pollution does not only enrich the hydrocarbon utilizers but also enriches additional populations that utilize the by-products

that are not intact hydrocarbons, as observed by Walworth et al. (2007). According to (Das & Chandran 2011), bacteria are the most active agents in petroleum degradation, and they work as primary degraders of spilled oil in the environment. Microbial degradation is the major and ultimate natural mechanism by which one can clean up the petroleum hydrocarbon pollutants from the environment. Several bacteria are even known to feed exclusively on hydrocarbons. The hydrocarbon-utilizing bacteria and fungi also increased during the remediation period. These observations are consistent with the knowledge that inputs of hydrocarbon pollutants stimulate increases in microbial numbers (Ogbonna et al. 2007). These categories of microbes utilize hydrocarbons as their sole carbon sources of metabolism. Bello & Anobeme (2015) observed that hydrocarbonoclastic bacteria and fungi as oil degraders are ubiquitous in both the temperate and tropical environments of oil-polluted and unpolluted locations. This also explains the presence of hydrocarbonoclastic microbes even in the control sites. Ramdass & Rampersad (2021) have also reported the presence of a diverse microbial population, including novel oil-degrading filamentous fungi at eight oil-impacted sites in Trinidad.

Interactions of Edaphic variables and Microbial Groups

This study revealed that pH and Mg^{2+} ions had positive effects on the growth of the THF, while EC and K^+ ions appeared to inhibit the growth of the HUF. The recorded decrease in the pH of soil after remediation could be a result of the metabolic activities of the microorganisms, which produced pH-depressing metabolites. The utilization of crude oil by these organisms, which resulted in their population growth, also produced and accumulated acidic metabolites (Essien & John 2010). Electrical conductivity appeared to significantly inhibit the growth of HUF. This observation corresponded with decreases recorded in concentrations of K^+ ions, which usually contribute to the conductivity of soil and water media after the remediation exercise. Potassium and EC also showed inhibitory effects on growths of the THB, HUB, and HUF.

CONCLUSION

The current research set out to employ conventional enhanced natural attenuation techniques in the remediation of oil-impacted soil. This study reveals the effectiveness of bioaugmentation with simple locally-available manure, as well as synthetic fertilizer (NPK), in the restoration of the productivity of arable soil in the Odhaje community in the Delta area of the River Niger, Nigeria. The addition of organic and inorganic nutrients was rapidly accompanied by

microbial population growth in the soil, and this subsequently led to the consumption of the oil contaminant in the soil to comparable levels over a 17-week test period. There was a general decrease in the soil-oil contaminant by up to 50.41% after 17-week remediation, with a corresponding improvement in the carbon-nitrogen ratio of soil.

RECOMMENDATIONS

Enhanced Natural Attenuation (= Landfarming) technique should be recognized as the least expensive of the other bioremediation treatment methods in environmental management. The technique could be practiced with little or no expertise and in a natural environment.

REFERENCES

- Agbogidi, O.M., Eruotor, P.G., Akparobi, S.O. and Nnaji, G.U. 2007. Evaluation of crude oil contaminated soil on the mineral nutrient elements of maize (*Zea mays* L.). *J. Agron.*, 6(1): 188. Doi: 10.3923/ja.2007.188.193.
- Albert. O.N., Amaratunga, D. and Haigh, R.P. 2018. Evaluation of the Impacts of Oil Spill Disaster on Communities and Its Influence on Restiveness in Niger Delta, Nigeria. *Proced. Eng.*, 212: 1054-1061. Doi:10.1016/j.proeng.2018.01.136.
- American Public Health Association (APHA). 2002. Standard Methods for the Examination of Water and Wastewater. Twentieth edition. APHA/AWWA/WEF, Washington DC.
- Bello, O.S. and Anobeme, S.A. 2015. The effects of oil spillage on the properties of soil and environment around the marketing outlets of some petroleum marketing companies in Calabar, Cross River State, Nigeria. *Mayfair J. Soil Sci.*,1(1): 1-14.
- Bob-manual, K.D.H. and Johnson, K.T. 2001. Oil Spill clean-up techniques for sustainable environmental protection in the Niger Delta. *NSE Tech. Trans.*, 36: 2.
- Chikere, C.B., Azubuike, C.C. and Fubara, E.M. 2017. Shift in the microbial group during remediation by enhanced natural attenuation (RENA) of a crude oil-impacted soil: a case study of Ikarama Community, Bayelsa, Nigeria. *Biotech.*, 7: 152. <https://doi.org/10.1007/s13205-017-0782-x>
- Das, N. and Chandran, P. 2011. Microbial Degradation of Petroleum Hydrocarbon Contaminants: An Overview. *Biotechnology Research International*, Article ID 941810, 13 pages. doi:10.4061/2011/941810.
- Ebuehi, O.A.T., Abibo, I.B., Shekwolo, P.D., Sigismund, K.I., Adoki, A. and Okoro, I.C. 2005. Remediation of Crude Oil Contaminated Soil by Enhanced Natural Attenuation Technique. *J. Appl. Sci. Environ. Manag.*, 9(1): 103-106.
- Eneje, R.C., Nwagbara, C. and Uwumarongielori, E.G. 2012. Amelioration of chemical properties of crude oil-contaminated soil using compost from *Calapoignonium mucunoides* and poultry manure. *Int. Res. J. Agric. Sci.*, 2(6):246-251.
- Eni, D.D. and Okpiliya, F.E 2011. Evaluation of on-shore oil spill remediation operations in Port Harcourt, Nigeria. *Int. J. Dev. Manag. Rev.*, 6: 161-171.
- Essien, O.E. and John, I.A. 2010. Impact of crude-oil spillage pollution and chemical remediation on agricultural soil properties and crop growth. *J. Appl. Sci. Environ. Manage.*, 14(4): 147-154.
- Hollender, J., Althoff, K., Mundt, M. and Dott, W. 2003. Assessing the microbial activity of soil samples, their nutrient limitation, and the toxic effects of contaminants using a simple respiration test. *Chemosphere*, 53(3): 269-275.

- Iwegbue, C.M.A. 2007. Heavy Metal and Physio-chemistry of Soils, Sediments, and surface water in the environment of an oil-impacted area of Delta State. M.Phil Thesis. RSUST, Port Harcourt.
- Jia, J., Liu, Y., Li, G. and Zhang, X. 2009. Contamination characteristics and its relationship with physicochemical properties of oil-polluted soils in oilfields of China. *Chem. In. Eng. Soc. China*, 60(3): 726-732.
- Jørgensen, K.S. *Comprehensive Biotechnology*. Science Direct Publications/ Elsevier B.V, The Netherlands.
- Joseph, A., Udofia, U. and Ajang, R. 2021. Evaluation of the water quality of borehole water from a partially remediated oil spill site in Ikot Ada Udo, Akwa Ibom State, South-South Nigeria. *Environ. Technol. Inno.*, 24: 101967.
- Liu, W., Luo, Y., Teng, Y., Li, Z. and Ma, L.Q. 2010. Bioremediation of oily sludge-contaminated soil by stimulating indigenous microbes. *Environ. Geochem. Health*, 32(1): 23-9. Doi: 10.1007/s10653-009-9262-5.
- Mafiana, M.O., Bashiru, M.D. and Erhunmwunsee, F. 2021. An insight into the current oil spills and on-site bioremediation approaches to contaminated sites in Nigeria. *Environ. Sci. Pollut. Res.*, 28: 4073-4094. <https://doi.org/10.1007/s11356-020-11533-1>
- Njoku, K., Akinola, M. and Oboh, B. 2009. Phytoremediation of crude oil contaminated soil: The effect of the growth of *Glycine max* on the physico-chemistry and crude oil contents of soil. *Nature Sci.*, 7(10): 79-87.
- Ogbonna, D.N., Iwegbue, C.M.A., Sokari, T.G. and Akoko, I.O. 2007. Effect of bioremediation on the growth of okra (*Abelmoscus esculentus*) in the Niger Delta. *Environmentalist*, 27:303-309.
- Ogbuagu, D.H., Idewe, M.O. and Nzekwue, K.P. 2019. Bioaccumulation of persistent environmental pollutants (PEPs) in the mud catfishes (*Clarias gariepinus* and *Heterobranchus longifilis*) from the Ogu Creek, Rivers State, Nigeria. *Int. J. Marine Sci.*, 9(7): 54-65.
- Osuji, L.C., Egbuson, E.J. and Ojinnaka, C.M. 2006. Assessment and treatment of hydrocarbon inundated soils using inorganic nutrient (NPK) supplements: II. A case study of Eneka oil spillage in Niger Delta, Nigeria. *Environ. Monit. Assess.*, 115(1): 265-278. Doi: 10.1007/s10661-006-6552-6.
- Pansu, M. and Gautheryou, J. 2006. *Handbook of Soil Analysis: Mineralogical, Organic and Inorganic Methods*. Springer Berlin Heidelberg, New York, p. 995.
- Ramdass, A.C. and Rampersad, S.N. 2021. Diversity and oil degradation potential of culturable microbes isolated from chronically contaminated soils in Trinidad. *Microorganisms*, 9(6): 117. <https://doi.org/10.3390/microorganisms9061167>
- Semple, K.T., Dew, N.M., Doick, K.J. and Rhodes, A.H. 2006. Can microbial mineralization be used to estimate the microbial availability of organic contaminants in soil? *Environ. Pollut.*, 140(1): 164-172.
- Shell Petroleum Development Company of Nigeria (SPDC). 2002. Report on Fourth Quarter 2002-Gaseous Emission Monitoring Report. Quality Environmental Management Company Limited.
- Vallabhaneni, S. 2012. *Soil Microbiology- A Laboratory Manual*. LAMBERT Academic Publishing., NY.
- Walworth, J., Pond, A., Snape, I., Rayner, J., Ferguson, S. and Harvey, P. 2007. Nitrogen requirements for maximizing petroleum bioremediation in a sub-Antarctic soil. *Cold Reg. Sci. Technol.*, 48(2): 84-91.
- Wang, X.Y., Feng, J. and Zhao, J.M. 2010. Effects of crude oil residuals on soil chemical properties in oil sites, Momoge Wetland, China. *Environ. Monit. Assess.*, 161(1): 271-280. Doi: 10.1007/s10661-008-0744-1.
- Wang, Y., Feng, J., Lin, Q., Lyu, X., Wang, X. and Wang, G. 2013. Effects of crude oil contamination on soil physical and chemical properties in Momoge Wetland of China. *Chin. Geogra. Science*, 23(6): 708-715. Doi: 10.1007/s11769-013-0641-6.

... Continued from inner front cover

- The text of the manuscript should run into Abstract, Introduction, Materials & Methods, Results, Discussion, Acknowledgement (if any) and References or other suitable headings in case of reviews and theoretically oriented papers. However, short communication can be submitted in running with Abstract and References. The references should be in full with the title of the paper.
- The figures should preferably be made on a computer with high resolution and should be capable of withstanding a reasonable reduction with the legends provided separately outside the figures. Photographs may be black and white or colour.
- Tables should be typed separately bearing a short title, preferably in vertical form. They should be of a size, which could easily be accommodated in the page of the Journal.
- References in the text should be cited by the authors' surname and year. In case of more than one reference of the same author in the same year, add suffix a,b,c,..... to the year. For example: (Thomas 1969, Mass 1973a, 1973b, Madony et al. 1990, Abasi & Soni 1991).

List of References

The references cited in the text should be arranged alphabetically by authors' surname in the following manner: (Note: The titles of the papers should be in running 'sentence case', while the titles of the books, reports, theses, journals, etc. should be in 'title case' with all words starting with CAPITAL letter.)

- Dutta, A. and Chaudhury, M. 1991. Removal of arsenic from groundwater by lime softening with powdered coal additive. *J. Water Supply Res. Techno. Aqua.*, 40(1) : 25-29.
- Hammer, D.A. (ed.) 1989. *Constructed Wetlands for Wastewater Treatment-Municipal, Industrial and Agricultural*. Lewis Publishers Inc., pp. 831.
- Haynes, R. J. 1986. Surface mining and wetland reclamation. In: Harper, J. and Plass, B. (eds.) *New Horizons for Mined Land Reclamation. Proceedings of a National Meeting of the American Society for Surface Reclamation*, Princeton, W.V.

Submission of Papers

- The paper has to be submitted online in a single WORD file through the online submission portal of journal's website: www.neptjournal.com

Attention

1. Any change in the authors' affiliation may please be notified at the earliest.
2. Please make all the correspondence by e-mail, and authors should always quote the manuscript number.

Note: In order to speed up the publication, authors are requested to correct the galley proof immediately after receipt. The galley proof must be checked with utmost care, as publishers owe no responsibility for mistakes. The papers will be put on priority for publication only after receiving the processing and publication charges.

Nature Environment and Pollution Technology

(Abbreviation: Nat. Env. Poll. Tech.)
(An International Quarterly Scientific Journal)

Published by



Technoscience Publications

A-504, Bliss Avenue, Opp. SKP Campus
Balewadi, Pune-411 045, Maharashtra, India

In association with

Technoscience Knowledge Communications

Mira Road, Mumbai, India

For further details of the Journal, please visit the website. All the papers published on a particular subject/topic or by any particular author in the journal can be searched and accessed by typing a keyword or name of the author in the 'Search' option on the Home page of the website. All the papers containing that keyword or author will be shown on the home page from where they can be directly downloaded.

www.neptjournal.com

©Technoscience Publications: The consent is hereby given that the copies of the articles published in this Journal can be made only for purely personal or internal use. The consent does not include copying for general distribution or sale of reprints.

Published for Proprietor, Printer and Publisher: Mrs. T. P. Goel, A-504, Bliss Avenue, Balewadi, Pune, Maharashtra, India; Editors: Dr. P. K. Goel (Chief Editor) and Prof. K. P. Sharma